THE JOURNAL OF

PHYSICAL CHEMISTRY

Volume 69, Number 7 July 1965

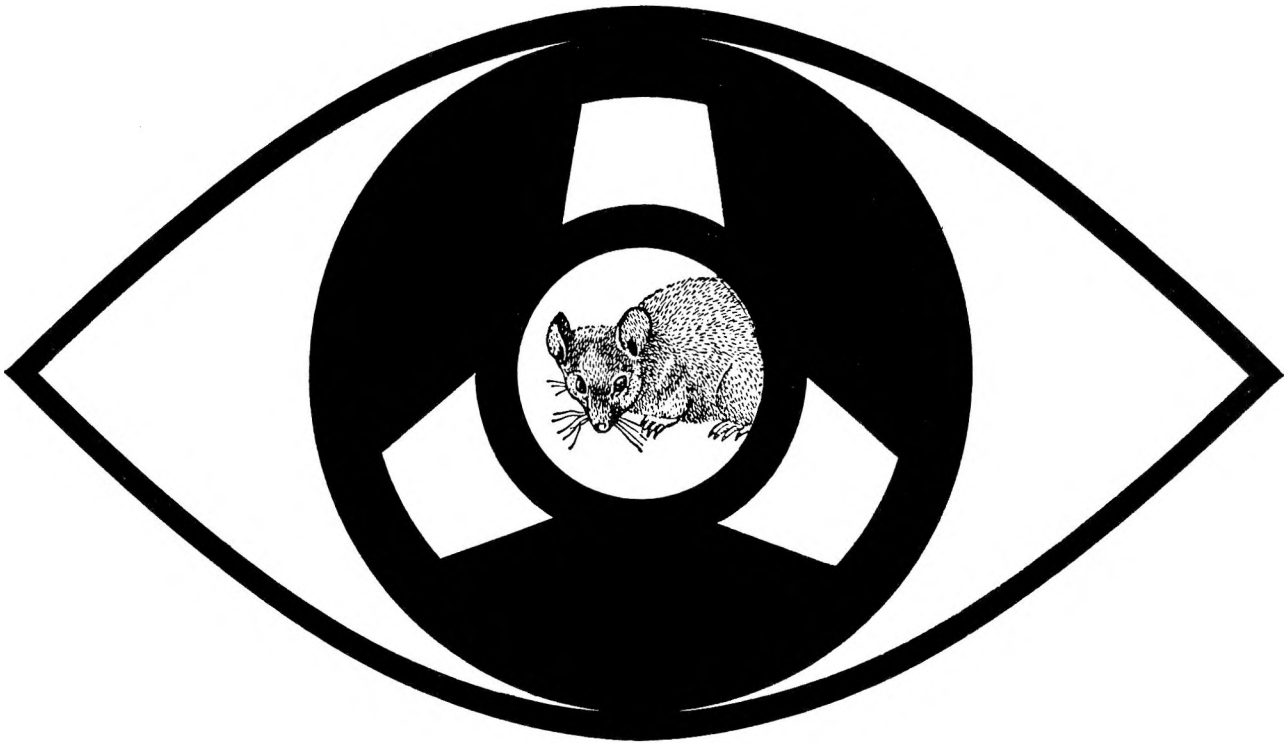

Now you can search Chemical Titles magnetic tapes by computers

Update your information dissemination program through the use of CHEMICAL TITLES Tapes or Custom Searches! These services are being offered for the first time by the Chemical Abstracts Service.

The list of uses to which you can put the tapes, compiled during the production of the printed CT, is almost endless. Indexes for the chemical journals in your company or institutional library which are covered by CT can be generated on an author, selected keyword, or title basis (or any combination of the three). Bibliographies on particular subjects that pertain to your work (reactivity of the phenanthrolines, crystal structure of ternary silicides, metabolism of porphyrins, etc.) can be compiled. Keyword indexes for any number of terms which you may suggest can be generated. Correlative machine searches can be conducted (mice that eat cheese, mice that eat cheddar cheese and Swiss cheese, white mice that eat cheddar cheese but not Swiss cheese, white mice that eat cheddar cheese or Swiss cheese, etc.) to any degree of specificity.

Answers can be in the form of bibliographies, author indexes, keyword indexes or any combination of the three. AND, all of these indexes, bibliographies, etc., can easily be duplicated and distributed to members of your staff at very low cost. No matter how you choose to use the tapes, you are screening a vast amount of unnecessary material from information which is of specific interest to you.

This tape searching service is offered in two forms —CAS will send you tapes on a biweekly basis, along with a user's manual and a searching program for an IBM 1401/1410 system, or CAS will perform the biweekly search of the tapes for you in Columbus.

The subscription price includes a $1,500-per-year base rate plus a use charge of $5 for each scientist at the subscriber's address who will use the service or who will benefit from its use. For searches performed by CAS, the rate is based on one search per set of terms per issue of CT, and an additional charge of $100 per hour for computer use time is made.

Direct inquiries to Mr. E. H. Heilman at CAS, Ohio State Univ., Columbus, Ohio 43210. and direct orders to the ACS, 1155 16th St., N.W., Washington, D. C. 20036.

NOTES

COMMUNICATIONS TO THE EDITOR

AMINCO'S INTEGRATED SYSTEM FOR MATERIALS EVALUATION

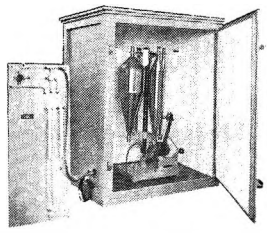

The **PARTICLE-SIZE ANALYZER** physically separates, by means of contamination-free air elutriation, particles ranging in size from 75 to 3 microns.

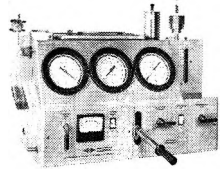

The **POROSIMETER** operates on the mercury intrusion principle. Data yield pore size, volume and distribution. Two models for pores from 0.012 to 100 μ and 0.035 to 100 μ.

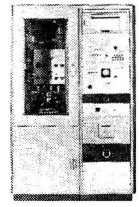

The **ADSORPTOMAT** operates on the classic static BET principle; determines size, volume, distribution and total surface area of pores from 14A to 600A in diameter. Completely automated, the unit produces nitrogen adsorption-desorption isotherms and prints out data in a form suitable for computer application.

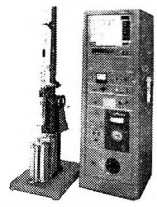

THERMO-GRAV (TGA) An automatic recording thermobalance for studies in vacuum or controlled atmospheres at temperatures to 1000°C. **Modular Thermo-Grav,** provides, at minimum cost, facilities for precise thermogravimetric analysis at programmed heating rates to 1000°C. "Building block" design permits purchase of a core unit and addition of other modules as needs change or funds become available.

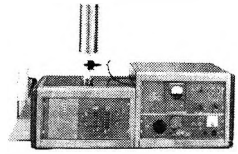

The **DIFFERENTIAL THERMOANALYZER (DTA)** measures enthalpic effects as temperature is varied at a selected heating rate. Operates under vacuum or in controlled atmosphere, to 1500°C.

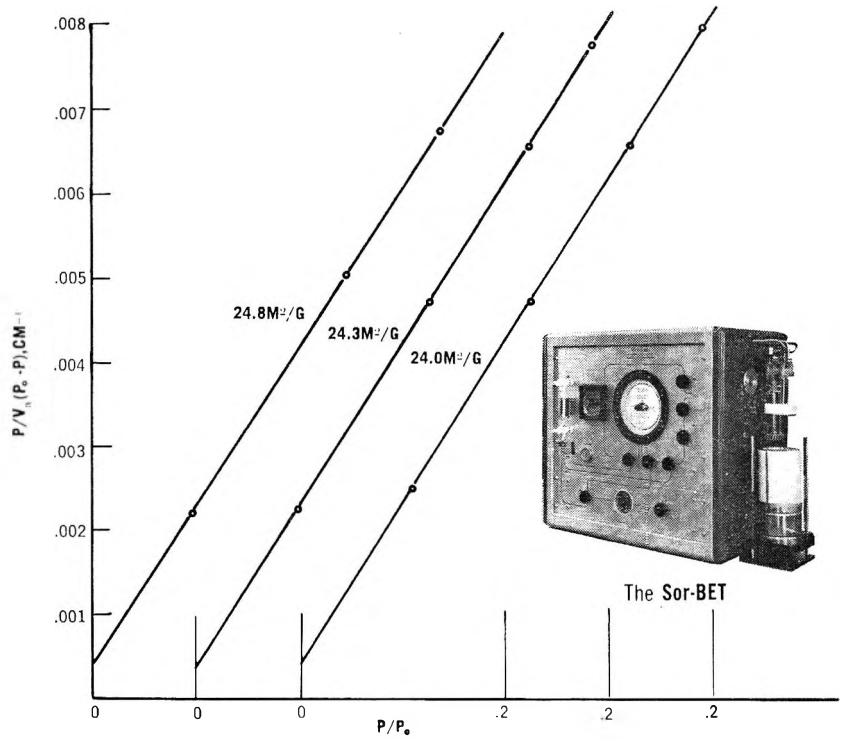

Chart shows results of 3 multi-point tests on silica spheres (NBS Ref. Sample No. 5). The tests were made on a single sample over a period of 4 days with outgassing between runs. The earliest test is on the left, the latest test on the right.

The Sor-BET

for rapid, accurate surface-area measurements on adsorbents, catalysts, etc.

This new instrument performs rapid, accurate BET determinations by the classic procedure of measuring the pressure decrease after adsorption of nitrogen by a sample. It differs from the conventional method in that nitrogen is selectively adsorbed from a binary gas mixture.

Operation is simple and direct, requiring no vacuum, no mercury manometers, no traps. Both the piping and the sample are purged by helium flow.

The unit is compact (35 in. wide x 25½ in. high x 16 in. deep) and self-contained, having a unique recirculating gas pump that cycles a mixture of helium and nitrogen through a sample at liquid nitrogen temperature.

Surface area is determined by the adsorption, at specific pressures, of nitrogen on the sample material. Pressure is measured by means of a 2-cc volume pressure gage, modified for through flow.

Special counter flow sample holders (which are designed to minimize the effects of temperature gradients) permit evaluation of materials with large or small surface areas.

Extensive testing of the new surface-area meter with reference adsorbent samples from the National Bureau of Standards' Bone Char Project produced measurements consistent within the permissible limits of accuracy.

The unit accepts samples from 0.1 to 20 grams or higher (measuring from 0.1 to 1500 m^2/g). Up to 16 three point determinations per day (without data reduction), dependent upon sample characteristics, may be processed.

SEND FOR MATERIALS EVALUATION INSTRUMENTATION PORTFOLIO JPC-7

AMINCO

AMERICAN INSTRUMENT CO., INC.

8030 Georgia Avenue, Silver Spring, Md.

THE JOURNAL OF
PHYSICAL CHEMISTRY

VOLUME 69, NUMBER 7 JULY 15, 1965

The Thermal Isomerization of Trifluoromethyl- and Trifluoroethylcyclopropane[1]

by D. W. Placzek and B. S. Rabinovitch

Department of Chemistry, University of Washington, Seattle, Washington 98105 *(Received March 8, 1965)*

Trifluoromethyl- and trifluoroethylcyclopropane each undergo homogeneous, thermal, unimolecular isomerizations to four isomeric products, trifluorobutene-1, *cis*- and *trans*-butene-2, and isobutene for the former, and trifluoropentene-1, *cis*- and *trans*-pentene-2, and isopentene for the latter. The methyl compound was studied from 445 to 524°; the ethyl compound, from 406 to 542°. The total over-all rates of isomerization are $k_\infty = 4.11 \times 10^{14} \exp(-65.6 \text{ kcal.}/RT) \text{ sec.}^{-1}$ for trifluoromethylcyclopropane and $k_\infty = 2.40 \times 10^{14} \exp(-63.6 \text{ kcal.}/RT) \text{ sec.}^{-1}$ for trifluoroethylcyclopropane. Rate parameters for the individual competitive isomerization processes have also been determined.

Introduction

Much literature has accumulated within the past decade on the study of the structural isomerization of cyclopropane[2] and of substituted cyclopropanes,[2b,c,3] by both thermal and chemical activation methods. Such studies have proven useful for testing the theories of unimolecular reactions; as an adjunct, several workers have aimed at the elucidations of the mechanisms of these reactions.[2c,3g]

Recently, attention has been directed[3f] to fluorine-containing alkylcyclopropanes. These studies had for their purpose the quantitative examination of the effect of quantum statistical weight variations (attendant upon substitution of H by F atoms) upon the elementary microscopic rate constants, k_E. For such a purpose, the substitution of F directly in the ring would have a more drastic effect upon the Arrhenius rate parameters than would be desirable for optimum comparison of theory and experiment[4]; for example, the observed activation energies (kcal. mole^{-1}) for structural isomerization of various cyclopropanes to propylene are: cyclopropane, 65.1[5]; monofluorocyclopropane, 61.0[4c]; and polyfluorocyclopropane, <61.[4] It was thus preferable to restrict the site of

(1) Abstracted in part from the Ph.D. thesis of D. W. Placzek. This work was supported by the National Science Foundation.

(2) (a) T. S. Chambers and G. B. Kistiakowsky, *J. Am. Chem. Soc.*, **56**, 399 (1934); H. O. Pritchard, R. G. Sowden, and A. F. Trotman-Dickenson, *Proc. Roy. Soc.* (London), **A217**, 563 (1953); R. H. Lindquist and G. K. Rollefson, *J. Chem. Phys.*, **24**, 725 (1956); R. E. Weston, *ibid.*, **26**, 975 (1957); E. W. Schlag and B. S. Rabinovitch, *J. Am. Chem. Soc.*, **82**, 5986 (1960); B. S. Rabinovitch, P. W. Gilderson, and A. T. Blades, *ibid.*, **86**, 2994 (1964); (b) J. W. Simons and B. S. Rabinovitch, *J. Phys. Chem.*, **68**, 1322 (1964); (c) D. W. Setser and B. S. Rabinovitch, *J. Am. Chem. Soc.*, **86**, 564 (1964).

(3) (a) M. C. Flowers and H. M. Frey, *J. Chem. Soc.*, 3953 (1959) (1,1-dimethylcyclopropane); 1157 (1962) (1,1-dimethylcyclopropane); *Proc. Roy. Soc.* (London), **A260**, 424 (1961) (1,2-dimethylcyclopropane); (b) J. P. Chesick, *J. Am. Chem. Soc.*, **82**, 3277 (1960) (methylcyclopropane); (c) D. W. Setser and B. S. Rabinovitch, *Can. J. Chem.*, **40**, 1425 (1962) (methylcyclopropane); (d) H. M. Frey and D. C. Marshall, *J. Chem. Soc.*, 3052 (1962) (1,1,2,2-tetramethylcyclopropane); (e) M. L. Halberstadt and J. P. Chesick, *J. Phys. Chem.*, **69**, 429 (1965) (ethylcyclopropane); (f) F. H. Dorer and B. S. Rabinovitch, *ibid.*, **69**, 1952 (1965) (methyl-, ethyl-, propyl-, trifluoromethyl-, trifluoroethyl-, and trifluoropropylcyclopropane); (g) for a review see H. M. Frey, *Progr. Reaction Kinetics*, **2**, 131 (1964).

substitution to a side chain; specifically, a comparative study of the decomposition of chemically activated trifluoromethyl- and of trifluoroethylcyclopropane was made.[3f] In this connection, it was also desirable to carry out a thermal study on these systems and to measure the relevant reaction parameters. The results of the thermal work are now reported.

Experimental

The trifluoromethyl- and trifluoroethylcyclopropanes were prepared by the addition to 3,3,3-trifluoropropene-1 and 4,4,4-trifluorobutene-1 of methylene, derived from the photolysis of ketene, in the gas phase at high pressure. The compounds were purified by gas chromatography until impurities could not be detected.

Reactions were carried out in a 5.2-cc. Pyrex vessel which was seasoned by flushing with a few centimeters of the reactant. This gave reproducible rates of subsequent reaction. The whole gas sample was removed for analysis. The vessel was heated in a vigorously stirred, regulated nitrate salt bath. This arrangement gave a temperature constancy of $\pm 0.25°$ over long periods, with lesser variations for short runs. Temperatures were measured with a chromel–alumel thermocouple calibrated against the melting points of pure zinc and tellurium.

Analyses were performed by g.l.p.c. with a series arrangement of 2,4-dimethylsulfolane and dibutyl phthalate columns. These columns effected adequate separation of all reactants and products except for 5,5,5-trifluoropentene-1 and 2-methyl-4,4,4-trifluorobutene-1, which were not resolved on these columns; the latter were separated on a 12.19-m. dinonyl phthalate column. The analytical columns were calibrated with pure compounds.

All products of the trifluoromethylcyclopropane system could be identified by comparison with the known products studied earlier in chemical activation systems.[3f] The *cis*- and *trans*-trifluorobutene-2 were distinguished with the help of n.m.r. Products of the trifluoroethylcyclopropane system were similarly identified by comparison of retention times and relative rates of production with those for the corresponding known products of the chemical activation trifluoromethylcyclopropane system.[3f]

Results and Discussion

Products of the thermal isomerization of trifluoromethylcyclopropane are similar to those of the isomerization of methylcyclopropane,[3b] and no strange or higher products were found (primed rate quantities will be used to distinguish fluorinated species).

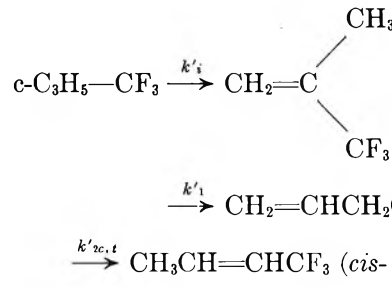

Parallel equations may be written for trifluoroethylcyclopropane

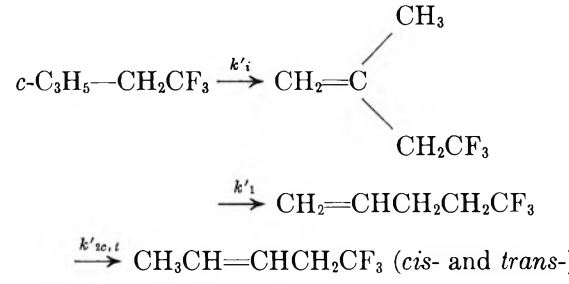

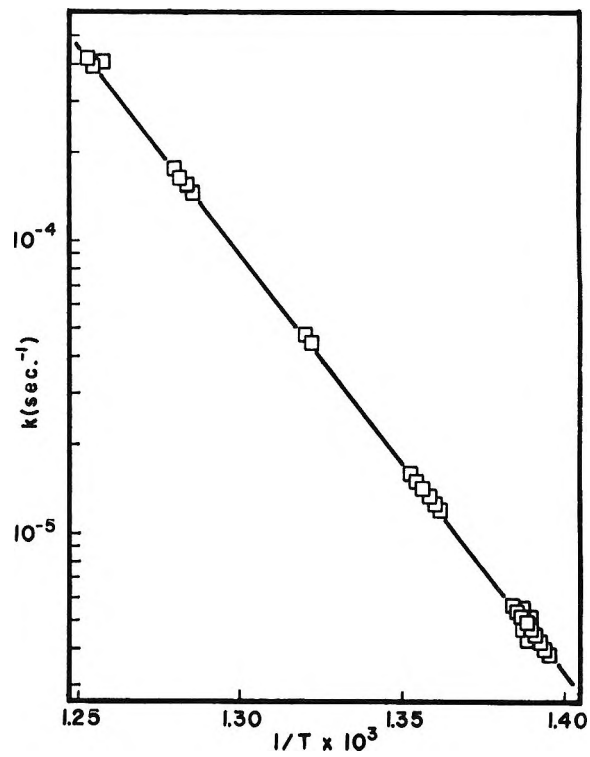

Figure 1. Arrhenius plot for trifluoromethylcyclopropane: over-all isomerization.

(4) (a) A. F. Trotman-Dickenson, Lecture, London, 1963; (b) B. A. Grzybowska, J. H. Knox, and A. F. Trotman-Dickenson, *J. Chem. Soc.*, 746 (1963); (c) F. Casas, J. A. Kerr, and A. F. Trotman-Dickenson, *ibid.*, 3655 (1964).

(5) W. E. Falconer, T. E. Hunter, and A. F. Trotman-Dickenson, *ibid.*, 609 (1961).

Table I: Reaction Parameters for the Isomerizations of Substituted Cyclopropanes

	c-C_3H_5-CF_3[a]		c-C_3H_5-CH_3		c-C_3H_5-CH_2CF_3[b]	
	E_a, kcal. mole^{-1}	A, 10^{14} sec.$^{-1}$	E_a, kcal. mole^{-1}	A, 10^{14} sec.$^{-1}$	E_a, kcal. mole^{-1}	A, 10^{14} sec.$^{-1}$
$(k$ or $k')_i$	69.5	0.75	66.0,[c] 65.1[d]	4.20,[c] 2.16[d]		
$(k$ or $k')_1$	67.3	2.39	64.3,[c] 62.8[d]	8.86,[c] 2.60[d]	63.4	7.52
$(k$ or $k')_{2c}$	65.2	1.48	63.9,[c] 62.7[d]	3.87,[c] 1.76[d]	63.3	6.87
$(k$ or $k')_{2t}$	65.0	0.90	68.1,[c] 65.2[d]	30.8,[c] 3.93[d]	63.1	4.85
$(k$ or $k')_{total}$	65.6	4.11	65.0,[e] 63.2[d] 64.3[c]	28.2,[e] 7.66[d] 17.8[c]	63.6, 61.6[f]	24.0, 25[f]

[a] Runs performed at a pressure of 8.2 cm. ($k'/k'_\infty = 0.98$) and E_a slightly corrected to $p = \infty$ (N. B. Slater, "Theory of Unimolecular Reactions," Methuen and Co., Ltd., London, 1959, p. 163) with use of an assumed value[3b] of $n = 18$. [b] Data for runs at 8.2 cm.; $k'/k'_\infty = 1.0$. Separate values for k'_i and k'_1 were not obtained, but $k'_i/(k'_i + k'_1)$ is only ~0.1 so that these values refer essentially to k'_1. [c] Calculated from the data of ref. 3b, at 10 cm. pressure. [d] See ref. 2c. [e] Original value given in ref. 3b. [f] Data of ref. 3e for c-C_3H_5-CH_2CH_3.

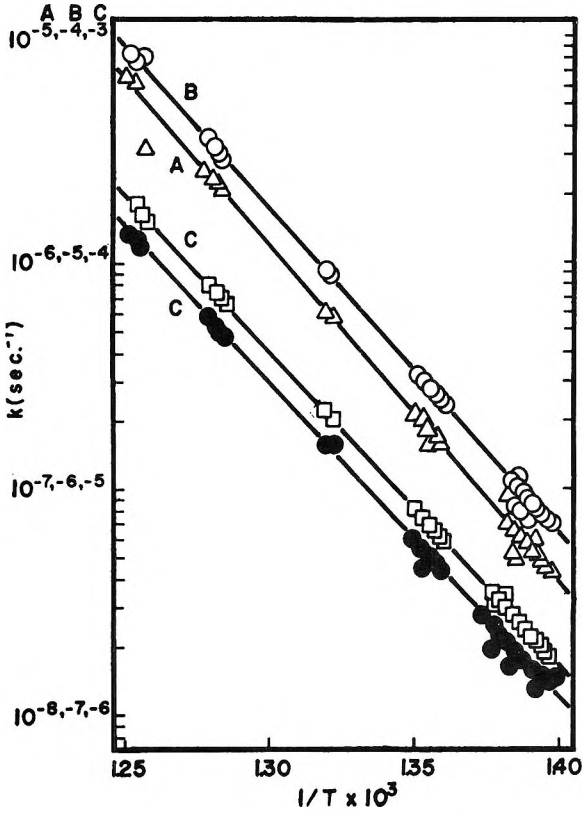

Figure 2. Arrhenius plots for products of trifluoromethylcyclopropane isomerization: △, k'_i; ○, k'_1; □, k'_{2c}; ●, k'_{2t}.

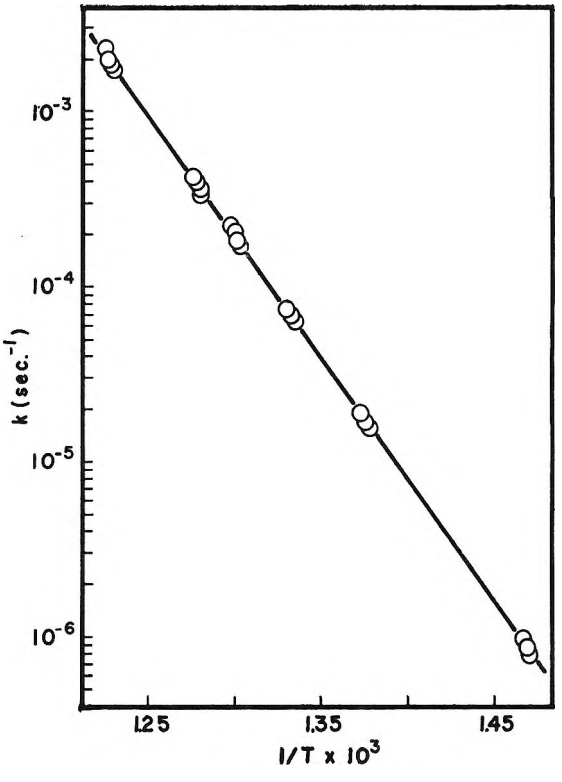

Figure 3. Arrhenius plot for trifluoroethylcyclopropane: over-all isomerization.

The Arrhenius plots for runs performed at 8.2 cm. are given in Figures 1–4. At this pressure, $k'/k'_\infty \simeq 0.98$ for trifluoromethylcyclopropane and $k'/k'_\infty = 1.0$ for trifluoroethylcyclopropane. The least-squares calculation of the pre-exponential factors and activation energies for k_∞ are listed in Table I. Also listed are the available data for methyl- and ethylcyclopropane.

The values for k_{2c} and k_{2t} of Table I do not take explicit account of any subsequent *cis–trans* isomerization of the alkene-2 products. However, in the hydrocarbon cases, the rates of structural isomerization of cyclopropanes[2] and substituted cyclopropanes[2b,c,3a] are greater by an order of magnitude than the rates of geometric *cis–trans* isomerizations of simple alkenes,[6,7] and the listed values should be nearly pure rates. This situation may also obtain for the (unknown)

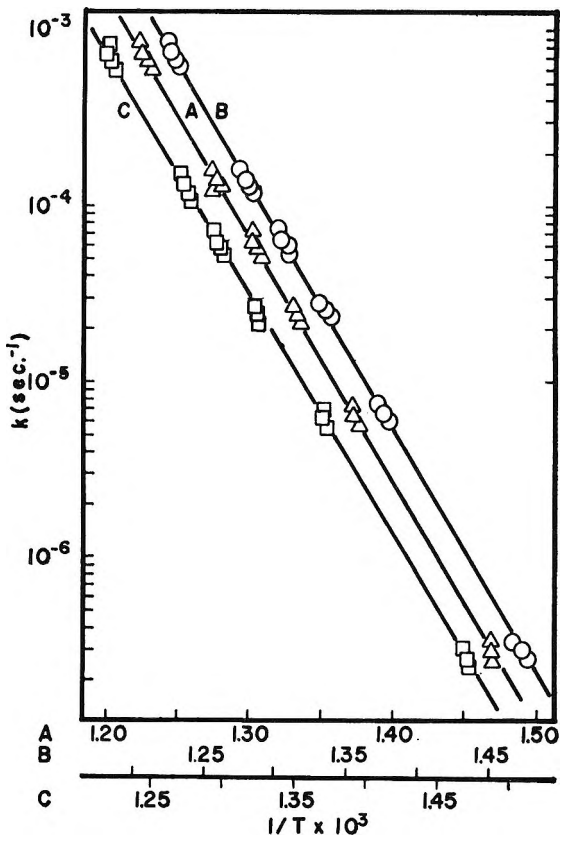

Figure 4. Arrhenius plot for products of trifluoroethylcyclopropane isomerization: O, $k'_1 + k'_i$; △, k'_{2c}; □, k'_{2t}.

rates of trifluorobutene-2 and trifluoropentene-2 isomerization; insofar as it does not, the listed numbers simply represent composite values. This matter is subsequently touched upon again.

The mechanistic effects of fluorine substitution are noteworthy. In the methylcyclopropane system, substitution of the methyl group for an H causes a decrease in the bond strengths of the C–C bonds *adjacent* to the point of substitution. Isobutene, formed by rupture of the bond *opposite* to the point of substitution, is produced in relatively small amounts (Table II); $k_i/(k_1 + k_2) = 0.085$. Fluorine substitution enhances this factor; $k'_1/(k'_1 + k'_2) = 0.013$. The corresponding ratios for ethyl- and trifluoroethylcyclopropane are 0.087, virtually unchanged from the methylcyclopropane system, and 0.029, increased considerably from the trifluoromethylcyclopropane system. Also of note is the ratio k_1/k_2, which indicates preferential transfer of an H atom toward (k_1) or away from (k_2) the substituent group when a bond adjacent to that group is broken. This ratio is unity (1.10,[3b] 0.98[2c]) for methylcyclopropane but only 0.24 for trifluoromethylcyclopropane; the value for ethylcyclopropane ratio is 0.94, again close to unity, and rises to 0.51 for trifluoroethylcyclopropane.

Table II: Relative Rates of Butene Isomer Production (468.0°)

Product	*c*-C_3H_5–CH_3 system[a]		*c*-C_3H_5–CF_3 system
Butene-1	1.00	1.00	1.00
cis-Butene-2	0.63	0.72	2.45
trans-Butene-2	0.28	0.30	1.76
Isobutene	0.16	0.18	0.067

[a] Data of left column from ref. 3b and of right from ref. 2c.

Such ratios appear to do service as an indicator of the magnitude of inductive or field effects, due to fluorine substitution, on the reaction parameters, *i.e.*, of the magnitude of "mechanistic" effects due to substitution. The extensive reduction of the variation within a pair by the intervention of a single methylene group within the trifluoro molecule strongly suggests that the variation would be relatively small for the propyl- and trifluoropropylcyclopropane pair.

An additional result of fluorine substitution is the changed relative rates of production of the *cis*- and *trans*-alkene-2 products. The *cis*:*trans* ratio of ~2 in the thermal methylcyclopropane system[2c,3b] is reduced to ~1.4 in the trifluoro system. The corresponding ratios for thermal ethylcyclopropane systems are ~1.6[3e] and ~1.3. In the methyl- and ethylcyclopropane systems, these ratios are inverted from those that would be expected on the basis of thermodynamic stability. On the other hand, the H_2S-catalyzed thermal isomerization of both *cis*- and *trans*-trifluorobutene-2 yielded mixtures containing an excess of the *cis* form,[8] indicating the greater thermodynamic stability of this configuration. This latter finding has numerous precedents: an eclectic selection of species which demonstrate the greater stability of the *cis* forms of olefins includes 1-bromopropene,[9] crotonitrile,[10] 1-fluoropropene,[11] and 1,2-diiodoethylene.[12] Findings of greater stability of the *cis* compound

(6) J. E. Douglas, B. S. Rabinovitch, and F. S. Looney, *J. Chem. Phys.*, **23**, 315 (1955) (*trans*-ethylene-d_2).

(7) B. S. Rabinovitch and K. W. Michel, *J. Am. Chem. Soc.*, **81**, 5065 (1959); R. B. Cundall and T. F. Palmer, *Trans. Faraday Soc.*, **57**, 1936 (1961) (butene-2).

(8) F. H. Dorer, unpublished results.

(9) K. E. Harwell and L. F. Hatch, *J. Am. Chem. Soc.*, **77**, 1682 (1955).

(10) J. W. Crump, *J. Org. Chem.*, **28**, 953 (1963).

(11) R. A. Beaudet and E. B. Wilson, Jr., *J. Chem. Phys.*, **37**, 1133 (1963).

have been attributed to nonbonded interactions.[11] The 2-alkene products of trifluoromethylcyclopropane are thus isolated in the relative amounts expected from thermodynamic considerations. A plausible contributing factor is simply that *cis–trans* equilibration proceeds further after the formation of the fluoro isomers.

Still another consequence of fluorine substitution is the effect upon the observed Arrhenius activation energies. The activation energies (Table I) for methyl- and trifluoromethylcyclopropane, 63.2[2c] and 65.6, differ somewhat, which is not unexpected. The value reported for ethylcyclopropane, 61.6,[3c] and our value for trifluoroethylcyclopropane, 63.6, also apparently differ. However, the activation energies for other related alkylcyclopropanes, 63.2 for $(CH_3)_2$–*c*-C_3H_4[3a] and 63.3 for *trans*-CH_3–*c*-C_3H_4–CH_3,[3a] are higher than that for ethylcyclopropane and are closely similar to that for trifluoroethylcyclopropane. The thermal ethylcyclopropane system is quite complex, and a true activation energy higher than 61.6 would not be unreasonable. It is expected that the activation energies for propyl- and trifluoropropylcyclopropane are closely equivalent.

Values of critical energies, E_0 may be computed[13] with the use of transition state models described previously[3f]; in general, $E_a - E_0 \simeq 1.8$ kcal. for all species. The models used have been found[3f] to give general agreement with the observed frequency factors of Table I.

(12) R. M. Noyes, R. G. Dickenson, and V. Schomaker, *J. Am. Chem. Soc.*, **67**, 1319 (1945).

(13) S. Glasstone, K. J. Laidler, and H. Eyring, "The Theory of Rate Processes," McGraw-Hill Book Co., Inc., New York, N. Y., 1941, p. 194.

On the Monomer Concentration in Liquid Water

by D. P. Stevenson

Shell Development Company, Emeryville, California *(Received October 31, 1964)*

Three independent lines of evidence that the recent estimates[1,2] of the concentration of nonhydrogen-bonded water molecules in liquid water (0–100°) are at least two orders of magnitude too high are described. Data on the vibrational absorption spectrum of water monomer in CCl_4 solution ($\lambda \leq 2.5\ \mu$) and on the vacuum ultraviolet absorption spectrum ($\lambda \geq 1700$) of water liquid (25–92°) and water vapor are presented.

Introduction

In the recent past, there have appeared three papers dealing with the structure of liquid water. Two of these are theoretical papers in which the Eyring "Significant Structure Theory,"[3] in conjunction with assumptions concerning the structure of liquid water, is employed in the calculation of the thermodynamic properties of the liquid.[1,2] The authors of the theoretical papers infer from their success in reproducing the properties of liquid water that the assumed structure of the liquid is essentially correct. The third paper[4] presents an interpretation of the change in contour of the ~1.2-μ absorption band of liquid water with temperature in terms of changes of relative concentration of structural species and the authors indicate their conclusions to be consistent with the

(1) G. Némethy and H. A. Scheraga, *J. Chem. Phys.*, **36**, 3382 (1962).

(2) R. P. Marchi and H. Eyring, *J. Phys. Chem.*, **68**, 221 (1964).

(3) H. Eyring, T. Ree, and N. Hirai, *Proc. Natl. Acad. Sci. U. S.*, **94**, 683 (1958).

(4) K. Buijs and G. R. Choppin, *J. Chem. Phys.*, **39**, 2035 (1963).

theoretical work.[1] It is the purpose of the present paper to call attention to the fact that certain aspects of the structural implications of these three papers are inconsistent with some of the experimental properties of water. It should be noted that Hornig[5] has criticized certain other aspects of the paper of Buijs and Choppin,[4] who have presented a rebuttal.[6] The present criticisms are independent of those of Hornig.

The structural assumptions of Némethy and Scheraga[1] and of Marchi and Eyring[2] are essentially the same, namely that the water molecules of the liquid are either more or less gas-like monomers or in more or less ice-like aggregates. The monomers engage in no hydrogen bond formation while those in the aggregates tend to engage in four hydrogen bonds. The structural assumptions of Némethy and Scheraga[1] differ from those of Marchi and Eyring[2] in two respects. These are that characteristic fractions of the water molecules associated with the aggregates may engage in fewer than four hydrogen bonds (1, 2, or 3) and that due to the generally polar environment, the rotational motion of the water monomers is free only about the figure axis, degenerating to libration about the two axes at right angles to the figure axis.[1] For the purposes of the present paper, only the assumptions that have been made concerning the gas-like monomer molecules are pertinent.

The partition function for the liquid is written as[1]

$$f_l(T) = \prod_{i=0}^{4} [f_i(T)]^{\alpha_i} \qquad (1)$$

where $f_i(T)$ is the partition function for a molecule engaged in i hydrogen bonds and α_i is the fraction of such molecules. According to Marchi and Eyring,[2] the index i takes only the values 0 and 4, while according to Némethy and Scheraga,[1] $i = 0, 1, 2, 3$, and 4. In order to fit the various thermodynamic properties of liquid water there are found characteristic values for α_0, the fraction of more or less gas-like water molecules in the liquid as a function of temperature as shown in Table I. In the following paragraphs we shall see that three independent operational definitions of the gas-like water molecules that are consistent with the properties of the species assumed by Némethy and Scheraga[1] and by Marchi and Eyring[2] lead to the conclusion that the concentrations of such species in liquid water must be very much smaller than the values shown in Table I.

Table I: Fraction of Gas-Like Water Molecules in Liquid Water

T, °C.	α_0	
	Némethy and Scheraga	Marchi and Eyring
0	0.244	0.018
25	0.307	0.051
50	0.357	0.115
75	0.402	0.221
100	0.437	0.357

Operational Definitions

Inasmuch as the partition function for a species is simply a sum over the energy states available to the species, the manner in which Némethy and Scheraga[1] and Marchi and Eyring[2] write their partition functions for the "gas-like" water monomer species implies that the vibronic energy levels of this species are essentially identical with those of gaseous water molecules. It is well established that, in the absence of specific interaction between solvent and solute, both the vibrational and electronic absorption spectra (which reflect the separation of the accessible energy levels) of the solute molecules are very nearly coincident with those of the vapor spectra. In the case of electronic absorption spectra, for example, those of ammonia and alkyl amines are essentially coincident with their vapor spectra[7,8] in such diverse solvents as isooctane, diethyl ether, and acetonitrile. The nature of the excitation in the case of the amines, $n \rightarrow \sigma^*$, is the same as the lowest electronic excitation process for water,[9] and thus one would expect the longest wave length ultraviolet absorption band of gas-like (*i.e.*, nonbonded) water molecules in liquid water to be very much like that of water vapor.

At a particular temperature, T, and wave length, λ, in the ultraviolet region, the absorptivity of liquid water, $\epsilon_l(\lambda,T)$, can be written as

$$\epsilon_l(\lambda,T) = \sum_{i=0}^{4} \alpha_i(T)\epsilon_i(\lambda) \qquad (2)$$

where the $\alpha_i(T)$ have been defined above, and $\epsilon_i(\lambda)$ are the absorptivities of the water molecules engaged in i hydrogen bonds. From the discussion of the immediately preceding paragraph we conclude that for $\epsilon_0(\lambda)$, the absorptivity of the monomeric molecules, we can substitute $\epsilon_v(\lambda)$, the absorptivity of water vapor at λ. Inasmuch as both $\alpha_i(T)$ and $\epsilon_i(\lambda)$ are by their nature positive quantities, eq. 2 can be rewritten as

(5) D. Hornig, *J. Chem. Phys.*, **40**, 3119 (1964).

(6) K. Buijs and G. R. Choppin, *ibid.*, **40**, 3120 (1964).

(7) D. P. Stevenson, *et al.*, *J. Am. Chem. Soc.*, **83**, 4350 (1961); **84**, 2848 (1962).

(8) E. Tannenbaum, E. M. Coffin, and A. J. Harrison, *J. Chem. Phys.*, **21**, 311 (1953).

(9) A. D. Walsh, *J. Chem. Soc.*, 2260 (1953).

$$\alpha_0(T) \leq \epsilon_l(\lambda,T)/\epsilon_v(\lambda) \quad (3)$$

Equation 3 is our first operational definition of the gas-like water monomer species of liquid water.

The vibration–rotation or infrared absorption spectrum of molecules in a solvent in the absence of specific solute–solvent interaction generally differs from the corresponding vapor spectrum in two respects. These are the loss of fine structure due to collision broadening of the rotational energy levels and a small red shift of the center of gravity of the bands attributed to the polarizability of the medium.[10] Solvents of essentially large polarizability that interact to different degrees with water molecules are carbon tetrachloride and chloroform. We would expect the infrared absorption spectrum of water in CCl_4 solution to be representative of that of a freely rotating H_2O molecule such as that assumed by Marchi and Eyring.[2] For water molecules where rotation is partially hindered by a dipolar field as assumed by Némethy and Scheraga,[1] the infrared spectrum of H_2O in $CHCl_3$ should be representative. The infrared spectra of water in CCl_4 and $CHCl_3$ will be our second operational definition of gas-like water molecules in the liquid.

It has been shown by Powell and Latimer[11] that the entropies and heats of solution of nonpolar molecules in water at 25° increase uniformly with boiling points and molecular sizes, respectively. For the gas-like monomeric water molecules that undergo no specific interaction with the medium, one would expect the heat and entropy of solution in liquid water to be essentially equal to those of a nonpolar molecule of the same polarizability and molecular volume, respectively, where these molecular properties are measured by the van der Waals a and b, respectively. This expectation will be the basis of our third operational definition of the gas-like water molecules of liquid water.

Electronic Absorption Spectrum

The absorption spectrum of water vapor in the vacuum ultraviolet ($1230 \leq \lambda \leq 1850$ Å.) has been reported by Wilkinson and Johnson[12] and by Watanabe and Zelikoff,[13] while measurements of that of liquid water have been reported by Ley and Arends,[14] Barrett and Mansell,[15] and Price and co-workers[16] for $\lambda >$ 1800 Å. The vapor data[12,13] and the liquid data of Barrett and Mansell[15] are reported in the form of rather small graphs, while that of Ley and Arends[14] and of Price and co-workers[16] consist of absorptivities at a very limited number of wave lengths. In view of the fact that no single set of investigators had examined both the liquid and the vapor and that there is virtually no overlap in wave length of the measurements for the two states, we undertook the measurement of both the liquid and vapor spectra to provide a mutually consistent set of $\epsilon_l(\lambda,T)$ and $\epsilon_v(\lambda)$ for use in conjunction with eq. 3.

Our measurements were made with an Applied Physics Corp. Model 15 spectrophotometer operated with continuous nitrogen purge of the monochromater, source, and cell compartments. A specially constructed thermostatic cell holder permits observation of the absorption spectrum at any desired temperature in the range from ~15 to 175°. The observations on water vapor were made on the vapor in equilibrium with (a) 9.8 wt. % and (b) 12.0 wt. % sulfuric acid rather than pure water in order to avoid fogging of the absorption cell windows. The vapor concentration was computed from the cell holder temperature and the vapor pressure was determined by graphical interpolation of the (p,T) tables in the "International Critical Tables."[17] To span the wave length range from 1700- to 1900-Å. cells of 1.00-, 2.50-, and 10.00-cm. length were used and the temperatures ranged from

Table II: The Absorptivity of Liquid Water, Liters/Mole Cm.

λ, Å.	At 23.5°[a]	Lit. values[b]
1750	3.0_3	3.9_7 (30°)[c]
1775	0.83	
1800	0.36_1	
1810	0.23_0	0.18_1 (20°, 16)
1825	0.089_9	0.10_2 (?°, 14)
1850	0.027_4	0.0263 (25°, 15)
1860	0.0168	0.018_1 (20°, 16)
		0.024_0 (?°, 14)
1875	0.00885	0.011_5 (?°, 14)
1900	0.0029_1	
1920		0.0018_1 (20°, 16)
1925	0.0012_8	
1950	0.00055	

[a] This research. [b] References of text indicated in parentheses following temperatures. [c] W. Kaye and R. Poulson, *Nature*, **193**, 675 (1962).

(10) "Infrared and Raman Spectra," G. Herzberg, Ed., D. Van Nostrand and Co., New York, N. Y., 1945, p. 531 ff.

(11) R. E. Powell and W. M. Latimer, *J. Chem. Phys.*, **19**, 1139 (1951).

(12) P. G. Wilkinson and H. L. Johnson, *ibid.*, **18**, 190 (1950).

(13) K. Watanabe and M. Zelikoff, *J. Opt. Soc. Am.*, **43**, 753 (1953).

(14) H. Ley and B. Arends, *Z. physik. Chem.*, **B6**, 240 (1929).

(15) J. Barrett and A. L. Mansell, *Nature*, **187**, 138 (1960).

(16) W. C. Price, *et al.*, *ibid.*, **188**, 45 (1960).

(17) "International Critical Tables," Vol. III, McGraw-Hill Book Co., Inc., New York, N. Y., 1928, p. 303.

Table III: The Absorption of Water Vapor and Liquid under Vacuum Ultraviolet

λ	ϵ_v, l./mole cm.	ϵ_l/ϵ_v 23.5°	25.5°	26.4°	36°	50.6°	64.4°	81.4°	91.8°
1700	1252								
1720	1195								
1740	993								
1750	910	(0.00333)							
1760	812								
1775	623	0.00133							
1780	540								
1800	252	0.00144	0.00127	0.00121	0.00183				
1810	160	0.00144	0.00127	0.00118	0.00184	0.00250			
1820	97.5	0.00121[a]	0.00130	0.00123	0.00170	0.00274	0.00405		
1830	59.5		0.00134	0.00125	0.00192	0.00279	0.00410	0.00637	
1840	37.0		0.00132	0.00121	0.00184	0.00276	0.00409	0.00637	0.08410
1850	22.1	0.00124	0.00132	0.00124	0.00202	0.00290	0.00435	0.00674	0.00902
1860	13.74	0.00122	0.00145	0.00108	0.00191	0.00286	0.00428	0.00671	0.00916
1870	8.59	0.00131[b]	0.00134		0.00181	0.00284	0.00435	0.00679	0.00919
1880	5.35					0.00292	0.00440	0.00681	0.00948
1890	3.28						0.00424	0.00730	0.00971
1900	2.25	0.00129						0.00613	0.00969
1910	1.53								
$\langle\epsilon_l/\epsilon_v \times 10^3\rangle$		1.31 ± 0.09	1.33 ± 0.06	1.20 ± 0.06	1.86 ± 0.09	2.79 ± 0.13	4.23 ± 0.14	6.65 ± 0.36	9.25 ± 0.41

[a] Measurements at 1825 Å.; ϵ_v (1825) = 74.2. [b] Measurements at 1875 Å.; ϵ_v (1875) = 6.78.

24 to 60°. The cell blank was determined from observations on the cells filled with nitrogen. The total repeatibility of measurement, *i.e.*, different acids (a and b), different absorption cells, and different tempera tures, was found to be ±4% for 1740 ≤ λ ≤ 1900 Å.

Measurements on liquid water were made on both the laboratory distilled water and some specially redistilled (block tin condenser) water with indistinguishable results. For these measurements, 0.100- and 1.00-cm. cells were employed with a 0.0100-cm. cell containing the same water at 24° in the reference beam. The balance of the cells (1.00 and 0.100 *vs.* the 0.0100) was checked for λ > 1700 with dry nitrogen in the cells. There are summarized in Table II the results of our measurements at 23.5° along with values from the literature.

There are given in Table III the results of our measurements of the water vapor spectrum along with values of the ratio, $\epsilon_l(\lambda,T)/\epsilon_v(\lambda)$ for various temperatures. Examination of the ratios, ϵ_l/ϵ_v, shown in Table III, indicates that for wave lengths greater than 1800 Å., the ratio is wave length independent at each temperature, and the ratio increases rapidly with temperature.[18] The constancy of the ratio $\epsilon_l(\lambda,T)/\epsilon_v(\lambda)$ at a given temperature is a necessary condition for eq. 3 to be read as an equality, rather than an inequality. The constancy of $\epsilon_l(\lambda,T)/\epsilon_v(\lambda)$ implies that either the absorptivities of water molecules in the polymeric species are proportional to those of water vapor for 1800 ≤ λ ≤ 1900, or negligibly small. Since the latter assumption is the more reasonable one,[8] we will treat eq. 3 as an equality for the wave length range and associate the ratio $\epsilon_l(\lambda,T)/\epsilon_v(\lambda)$ with α_0 the fraction of the monomeric, nonhydrogen-bonded water molecules. Then for the equilibrium

$$\text{ice-like} \rightleftharpoons \text{monomer} \tag{4}$$

(eq. 10 of the paper of Marchi and Eyring[2]) we may write

$$\ln K = \ln \frac{\alpha_0}{1-\alpha_0} = \frac{-3188 \pm 169}{T} + 4.041 \pm 0.52 \tag{5}$$

by a least-squares fit of the average values of $(\epsilon_l/\epsilon_v)/(1 - \epsilon_l/\epsilon_v)$ shown in Table III. The quality of the fit is shown in Table IV, where there are given the ΔH and ΔS for reaction 4. As would be expected from the fact that the ratios ϵ_l/ϵ_v of Table III are two orders of magnitude smaller than the α_0 shown in Table I, the ΔH and ΔS found here cannot both agree with the assignment of Marchi and Eyring.[3] These authors (their Table II) give $\Delta H° = 6.9$ kcal./mole and $\Delta S° = 17.3$ e.u.

The comparison of $\epsilon_v(\lambda)$ of methyl and *t*-butyl alcohol with the $\epsilon_0(\lambda)$ of these alcohols as determined

(18) This increase in the absorptivity of liquid water with temperature has been noted and briefly discussed by Barrett and Mansell.[15]

Table IV: Monomer–Polymer Equilibrium in Liquid Water

T, °C.	Obsd. $\ln \frac{\epsilon_l/\epsilon_v}{1-\epsilon_l/\epsilon_v}$	Calcd.[a]	Obsd. − calcd.
23.5	−6.530 ± 0.076	−6.709	0.179
25.5	−6.623 ± 0.045	−6.632	0.009
26.4	−6.726 ± 0.050	−6.601	−0.125
36.0	−6.287 ± 0.049	−6.272	−0.015
50.6	−5.878 ± 0.047	−5.807	−0.071
64.4	−5.461 ± 0.033	−5.405	−0.056
81.4	−5.007 ± 0.054	−4.952	−0.055
91.8	−4.574 ± 0.044	−4.694	0.120
Standard error	±0.053		±0.110

[a] Calculated from

$$\ln \frac{\epsilon_l/\epsilon_v}{1-\epsilon_v/\epsilon_l} = \frac{-3188 + 169}{T} + 4.041 \pm 0.52$$

liquid: $(H_2O)_{polymer} \rightleftarrows (H_2O)_{monomer}$; $\Delta H = 6.34 \pm 0.33$ kcal./mole; $\Delta S = 8.03 \pm 1.03$ e.u.

from measurements on very dilute solutions in isooctane[19] suggests that our assumption for water, $\epsilon_v(\lambda) \approx \epsilon_v(\lambda)$, is subject to error, of the order of 50%. Such an error would not change the value of ΔH calculated from the temperature coefficient of $\ln \alpha_0/(1-\alpha_0)$, but it would introduce a proportional uncertainty in α_0 taken equal to ϵ_l/ϵ_v and an error of the order of $\pm R \ln 1.5 = \pm 0.8$ e.u. in the estimate of $\Delta S°$. These uncertainties are of no significance as far as our discussion and conclusions are concerned.

Semiempirical Heats and Entropy of Dissociation

Given the heat and entropy changes associated with the solution of unhydrogen-bonded water molecules in liquid water, the heat and entropy changes accompanying reaction 4 can be determined from the known heat and entropy of vaporization of water if one makes the supplementary assumption that the fraction of unhydrogen-bonded molecules in the liquid is small. Within the framework of this operational description of the monomeric species, this latter assumption is subject to *a posteriori* check through the calculation of α_0 (for eq. 4) from the estimated ΔH and ΔS.

From the work of Morrison and co-workers,[20] one finds $\Delta H°$ and $\Delta S°$ of solutions at 25° of methane and the rare gases to be essentially linear in the van der Waals a and b of the gases, respectively, as shown in Figure 1. Taking a and b of water vapor to be 5.464 l.^{2} atm./mole^2 and 30.49 ml./mole, respectively,[21] we find for the process

$$H_2O \text{ (vapor)} \rightleftarrows \text{monomer (liquid)} \qquad (6)$$

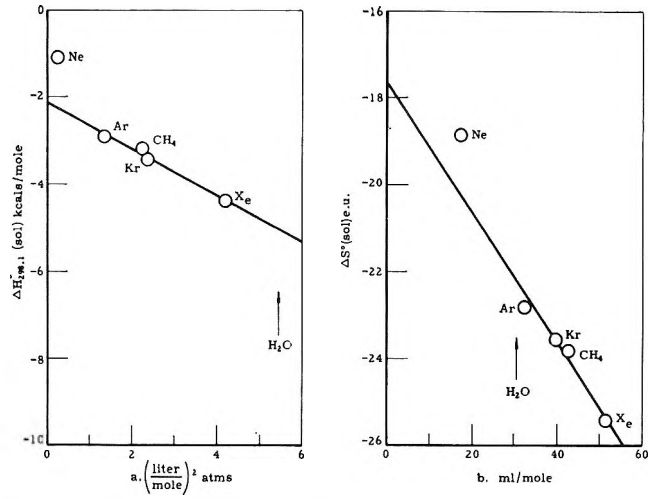

Figure 1. Heats of entropies of solution of gases in liquid water.

$\Delta H° = -5.0$ kcal./mole and $\Delta S° = -22.2$ e.u. at 25°. The heat and entropy of vaporization of water at 25° are 10.52 kcal. and 28.34 e.u., respectively,[22] from which we find for reaction 4

$$\Delta H° = 5.5 \text{ kcal./mole}; \quad \Delta S° = 6.2 \text{ e.u.} \qquad (7)$$

and the corresponding value of α_0 at 25° would be 0.0022. This value is sufficiently small to justify the method of calculation of $\Delta H°$ and $\Delta S°$ for eq. 4 from the vaporization data and monomer solution estimates. This estimate of α_0 differs by less than a factor of 2 from the ϵ_l/ϵ_v of Table III and is again two orders of magnitude less than the estimates quoted in Table I.

Vibration–Rotation Absorption Spectrum

For a variety of reasons, the only portion of the vibration–rotation spectrum of water for which reasonably accurate spectrophotometric measurements can be made for liquid water and its solutions in both CCl_4 and $CHCl_3$ is for the *ca.* 1.9-μ band that has been assigned in the vapor spectrum to the $\nu_2 + \nu_3$ combination band.[23] There is shown in Figure 2 the 1.8–2.0-μ region of the absorption spectra of solutions of water in CCl_4, $CHCl_3$, and of liquid water at 30°. The measurements were made with an Applied Physics Corp. Model 14 spectrophotometer. In the cases of

(19) D. P. Stevenson, unpublished measurements.

(20) T. J. Morrison and co-workers, *J. Chem. Soc.*, 2033 (1948); 3819 (1952); 3411 (1954); 3655 (1955).

(21) The gas constants were taken from the table, pp. 2306–2308 of the "Handbook of Chemistry and Physics," 42nd Ed., Chemical Rubber Publishing Co., Cleveland, Ohio, 1960.

(22) National Bureau of Standards Circular 500, U. S. Government Printing Office, Washington, D. C., 1952, p. 9.

(23) See ref. 10, p. 281.

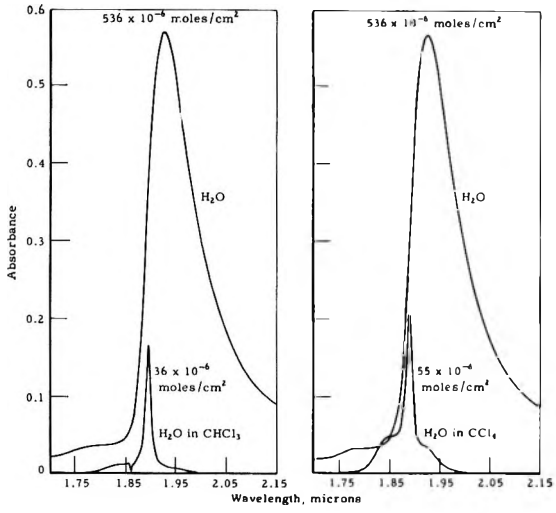

Figure 2. Partial absorption spectrum of liquid water and of H_2O in CCl_4 and $CHCl_3$.

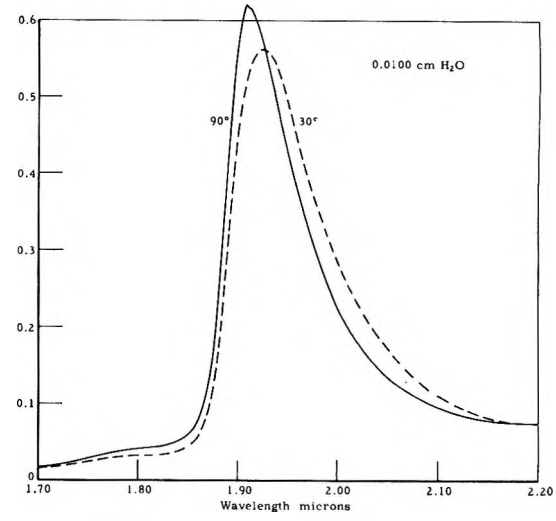

Figure 3. Effect of temperature on the 1.9-μ band of liquid water.

the $CHCl_3$ and CCl_4 solutions, spectral observations were made on approximately saturated solutions (at 24°) and 20:50 dilutions of these in 2.50- and 10.00-cm. cells, respectively. The relative absorbances at the band maximum of the dilutions were 0.39_2 ($CHCl_3$) and 0.40_6 (CCl_4), indicating very little polymeric water to be present in these solutions. The concentration of water in the $CHCl_3$ solution was determined by comparison of the integrated proton magnetic resonance signals of the $C^{13}HCl_3$ line at 5.48 p.p.m. (TMS internal standard) with that of the water line at 1.47 p.p.m. The abundance of C^{13} was taken to be 1.11 mole % (from the mass spectrum of the $CHCl_3$) so that the mole fraction of water in the $CHCl_3$ is given by[24]

$$2X_w = \frac{0.0111}{2} \times \frac{I_{1.47}}{I_{5.48}} \qquad (8)$$

The concentration of water in the CCl_4 solution was determined from the absorbance of the solution at 2.69 μ through the use of the absorptivity, 36.7 l./mole cm., determined by Forbes.[25] The measurements on liquid water were made in a 0.0100-cm. cell.

The integrated intensity of the band for liquid water (1.8–2.1 μ) was found to be 382 (17.8°) and 406 (85.5°) (l./mole cm.) $cm.^{-1}$, while for $CHCl_3$ and CCl_4 (1.8–2.0 μ) there were found 375 and 391 (l./mole cm.) $cm.^{-1}$, respectively. These various integrated intensities may be taken to be equal to one another within their experimental errors.

The general appearance of this 1.9-μ band of liquid water and the manner in which the shape changes with temperature (Figure 3) are both like the observations reported for the 1.2-μ band by Buijs and Choppin.[4] The total lack of structure on the side of the broad band with maximum near 1.89 and 1.90 μ in either the 30 or 90° spectrum indicates that the fraction of gas-like monomeric water molecules in the liquid is certainly less than 0.05 and probably less than the 0.01, *i.e.*, at least an order of magnitude lower than the values quoted in Table I. This result is in accord with that found from the electronic absorption spectrum of liquid water and the semiempirical estimate of ΔH and ΔS for reaction 4.

Although quantitative intensity measurements of the absorption spectrum of water in $CHCl_3$ solution cannot be readily made in the stretching fundamental region (~3700 $cm.^{-1}$), such measurements can be made for CCl_4 solutions of water and for liquid water as are shown in the lowest panel of Figure 4.[26] It will be noted in this Figure 4 that there is no indication of a relatively sharp band near 3700 $cm.^{-1}$ in the liquid water spectrum such as would be expected if 2% or more of the water molecules were unhydrogen bonded.

Because of the potential utility to spectroscopists and analytical chemists, there are also shown in Figure 4 the three principal absorption bands of H_2O in CCl_4 solution that can be observed for $\lambda > 2.5$ μ. In chloro-

(24) The n.m.r. measurements with a Varian A-60 were made by Mr. J. Jungnickel and the mass spectrometer measurements with a CEC 21-103 by Mr. P. A. Wadsworth.

(25) J. W. Forbes, *Anal. Chem.*, **34**, 1125 (1962); measurements by Dr. D. O. Schissler with a Beckman IR-4, 1.00-cm. cell.

(26) The author is indebted to Drs. A. C. Jones and D. O. Schissler for assistance in obtaining these spectra with a Beckman IR-7 spectrophotometer. It should be noted that the apparent absorptivity of H_2O in CCl_4 at the ν_3 maximum (3710 $cm.^{-1}$), 45.9 l./mole cm., is about 30% greater than found with the lower resolution IR-4: see ref. 24.

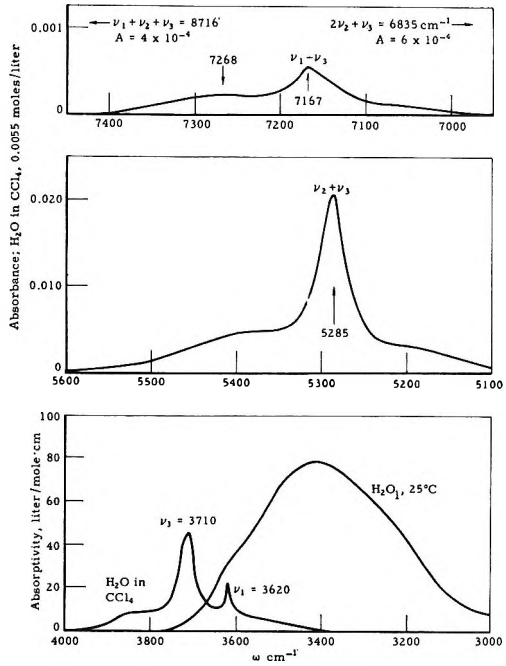

Figure 4. Absorption spectrum of H_2O in CCl_4, and a portion of that of liquid H_2O.

form, the fundamentals shift to 3696 and 3610 cm.$^{-1}$ for ν_3 and ν_1, respectively, while $\nu_2 + \nu_3$ is at 5277 cm.$^{-1}$, $2\nu_2 + \nu_3$ at 6826 cm.$^{-1}$, $\nu_1 + \nu_3$ at 7142 cm.$^{-1}$, and $\nu_2 + \nu_1 + \nu_3$ at 8711 cm.$^{-1}$.

Discussion

The three independent lines of evidence provided by the vacuum ultraviolet absorption spectra of water vapor and liquid, the semiempirically calculated heat and entropy of solution of water monomer in liquid water, and the lack of structure at 1.89–1.90 μ of the broad 1.90-μ band of the near-infrared absorption spectrum of liquid water, all lead to the same conclusion, namely that the concentration of nonhydrogen-bonded water monomer in liquid water at temperatures between 0 and 100° is less than 1% of the molecules of the liquid. The estimates of Marchi and Eyring[2] of ΔH required to convert a tetrahedrally coordinated water molecule to a gas-like water molecule in the liquid is in reasonable agreement with our estimates based on the temperature change of the absorptivity of liquid water (1800–1900 Å.) and semiempirically calculated, as is shown in Table V. The very high value of water monomer concentration computed by Marchi and Eyring[2] is due apparently to overestimation of the entropy increase accompanying monomer formation. The converse situation obtains with respect to the work of Némethy and Scheraga.[1] The latter authors assign an entropy increase that is of the magnitude we find, but their estimate of the energy required for the dissociation is lower by a factor of the order of two.

Table V: Estimates of $\Delta H°$ and $\Delta S°$ for the Reaction Polymer $\rightleftarrows$ Monomer in Liquid Water

	$\Delta H°$, kcal./mole	$\Delta S°$, e.u.
Némethy and Scheraga	2.7[a]	9.5
Marchi and Eyring	6.9	17.3
Vacuum ultraviolet	6.34 ± 0.33	8.0_3 ± 1.03
Semiempirical	5.5	6.2

[a] The $\Delta H°$ = 2.7 is these authors' estimate of the energy difference between four- and zero-coordinated water molecules. The $\Delta S°$ = 9.5 e.u. is that required to fit a Marchi and Eyring like equilibrium, eq. 4 and 5, to the Némethy and Scheraga α_0 at 25°.

Buijs and Choppin[4] assign the 1.2-μ absorption band of liquid water to the superposition of the $\nu_1 + \nu_2 + \nu_3$ bands of water molecules whose protons are engaged in no, one, and two hydrogen bonds on the short wave length tail of the 1.4-μ band due to $\nu_1 + \nu_3$ of these same species. Their interpretation of the change in contour of this absorption band with temperature leads them to the conclusion that the number of hydrogen bonds per water molecule decreases from 1.0 at 0 to 0.8 at 72°. This latter figure would imply that at 72° 20% of the water molecules do not have either electron pair of their oxygen atoms engaged in hydrogen-bond formation. If this were the case, one would expect $\epsilon_l(\lambda,72°)/\epsilon_v(\lambda)$ to be the order of 0.2 rather than 0.005 as found (Table III). This incompatability of the Buijs and Choppin interpretation of the temperature dependence of the contour of the 1.2-μ absorption band with the vacuum ultraviolet absorption spectrum of water indicates there must be a basic error among the postulates of Buijs and Choppin.

It may be further noted that if such species as

$$\begin{matrix} H \\ H \end{matrix}\!>\!O\text{-}(\text{-}H\text{-}O)$$

existed in significant concentration in water one would expect to observe relatively narrow, well-defined absorption bands associated with the excitation of the vibrational modes of the terminal H_2O. That such hydrogen bonding does not markedly perturb the energy levels is attested to by the nature of the absorption spectrum of water in $CHCl_3$ and that of ammonia in water. In both cases the spectra are essentially those of the species (H_2O or NH_3) in inert solvents. Thus begging the question of the origin of the breadth and temperature coefficient of the breadth of the liquid

water absorption bands,[5,6] we can assert with reasonable confidence that the Buijs and Choppin assumption of significant concentration of water molecules with neither hydrogen involved in hydrogen bonds is an untenable one.

In another recent paper, Walrafen[27] interprets his estimates of the integrated relative intensity of the *ca.* 175-cm.$^{-1}$ Raman band of liquid water at various temperatures between 0 and 60° as measures of the fraction of bonded, *i.e.*, more or less ice-like, water molecules in the liquid. He finds for the equilibrium we have written as eq. 4

$$\ln K = \frac{-6309}{T} + 20.918 = \ln \frac{J_{175} - I_{275}}{I_{175}} \qquad (9)$$

(from the equation in his Figure 7). One is forced to the conclusion that an unsuspected large systematic error is involved in his estimates of I_{175} since this eq. 9 implies there to be an entropy increase of 41.5 e.u. accompanying reaction 4, or that the entropy of a mole of "free water molecules" in liquid water is the order of 13 e.u. greater than that of the gas in its standard state. This is to be contrasted with the expectation that the free water molecules should have the order of 20 e.u. less than the gas. In this connection, it should be noted that the change in molal volume requires the entropy of free water molecules in the liquid to be at least $R \ln (25{,}000/18) \sim 14$ e.u., less than that of the gas in its standard state.

In conclusion, it is of interest to note that Mysels[28] has concluded that a large fraction of unbonded water molecules, along with clusters of di-, tri-, and tetrabonded molecules such as postulated by Némethy and Scheraga,[1] is not compatible with the observed excess turbidity of pure liquid water.[29]

(27) G. E. Walrafen, *J. Chem. Phys.*, **40**, 3249 (1964).

(28) K. J. Mysels, *J. Am. Chem. Soc.*, **86**, 3503 (1964).

(29) A reviewer of this paper has suggested a very ingenious alternate explanation of the observation that the liquid water ultraviolet absorption spectrum is parallel to the vapor spectrum (ϵ_l/ϵ_v wave length independent) and that the absorptivity of the liquid increases exponentially with temperature. In essence, this alternate explanation of the observations involves the assumption that in the condensed phase the electronic ground state of the "free water molecules" is stabilized relative to the excited state by an amount approximately equal to a vibrational quantum ($\nu_2 \sim 1600$ cm.$^{-1}$), so that the dominant contribution to the absorption on the long wave length edge of the liquid water spectrum is due to free molecules in the vibrational state (0,1,0) rather than (0,0,0). The room temperature fractional population of (0,1,0) would be the order of 5×10^{-4} and this population would increase exponentially with temperature at a rate equivalent to $\Delta H = 4.6$ kcal./mole. For this explanation to be acceptable, it is necessary that the fraction of free water molecules be of the magnitude calculated by Némethy and Scheraga.[1] The present author believes that the infrared spectral data preclude such a large fraction of monomer and thus render this alternate explanation less believable than that in the text.

Molecular Compounds and Complexes. II. Exploratory Crystallographic Study of Some Donor–Acceptor Molecular Compounds[1]

by J. C. A. Boeyens and F. H. Herbstein

Chemical Physics Group of the National Physical and Chemical Research Laboratories, Council for Scientific and Industrial Research, Pretoria, South Africa (*Received November 9, 1964*)

Exploratory crystallographic results (unit cell dimensions and space groups) are reported for 18 equimolar π-molecular compounds formed between various pairs of the electron donors benzene, naphthalene, anthracene, pyrene, perylene, and diphenyl and the electron acceptors pyromellitic dianhydride (PMDA), tetracyanoethylene (TCE), benzotrifuroxan (BTF), and hexafluorobenzene. Melting point diagrams are given for the systems diphenyl, anthracene, and perylene each with PMDA. An approximate structure is proposed for naphthalene–PMDA which should also hold for other compounds (naphthalene–TCE, anthracene–hexafluorobenzene, and pyrene–hexafluorobenzene) quasi-isomorphous with it. The resemblance between the cell dimensions and postulated molecular arrangements in the C_6F_6 molecular compounds and those in charge-transfer molecular compounds supports the assumption that C_6F_6 is an electron acceptor in these systems. Cell dimensions and space groups are also reported for PMDA and BTF.

The range of crystalline electron donor–acceptor molecular compounds has been appreciably widened during the past few years by the discovery of new electron acceptors. The crystal structures of these newer π-molecular compounds are of interest in their own right as well as for comparison with analogous structures already reported (see part III[2] for partial literature survey). Among the recently reported electron acceptors, we have chosen the strong acceptors pyromellitic dianhydride[3] (PMDA) (I), tetracyanoethylene[4] (TCE) (II), and benzotrifuroxan[5] (BTF) (III) and the weak acceptor hexafluorobenzene,[6] while as electron donors we have used a number of unsubstituted, centrosymmetric aromatic hydrocarbons. The absence of substituents eliminates possible complications due to other interactions such as hydrogen bonding, while centrosymmetrical molecules were chosen in the hope that the molecular compounds formed with the centrosymmetrical acceptors PMDA, TCE, and C_6F_6 would have high crystallographic symmetry with consequent simplifications in the crystal structure analyses planned. These hopes were realized to a large extent.

Preliminary deductions from the exploratory crystallographic results are given in this paper while crystal structure analyses for some of the molecular compounds will be presented in later papers of this series.

Recent work in this laboratory has shown that some of the molecular compounds discussed in this paper have somewhat different crystal structures at room temperature and at lower temperatures. We therefore emphasize that all results given in this paper refer to room temperature (295–300°K.) except where expressly stated otherwise.

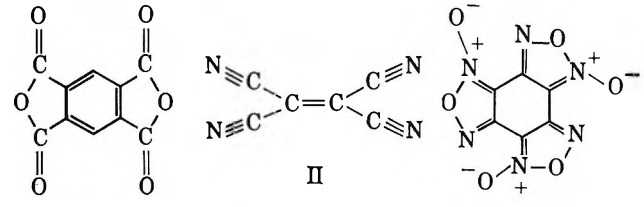

I II III

(1) Part I: G. Gafner and F. H. Herbstein, *J. Chem. Soc.*, 5290 (1964).

(2) Part III: J. C. A. Boeyens and F. H. Herbstein, *J. Phys. Chem.*, **69**, 2160 (1965).

(3) L. L. Ferstandig, W. G. Toland, and C. D. Heaton, *J. Am. Chem. Soc.*, **83**, 1151 (1961).

(4) R. E. Merrifield and W. D. Phillips, *ibid.*, **80**, 2778 (1958).

Experimental

In most instances good crystals of the π-molecular compounds were obtained by slow cooling of hot equimolar mixtures of the components in suitable solvents. Commercially available materials were used except for gifts of BTF from Dr. A. S. Bailey (Oxford) and PMDA from E. I. du Pont de Nemours and Co., Inc. (Wilmington, Del.). We are grateful for this assistance.

As PMDA is easily hydrated, it was necessary to work with dry solvents. Merck 99–100% glacial acetic acid was found to be satisfactory without further drying but the methyl ethyl ketone used had to be dried over $CaCl_2$. The benzene–PMDA molecular compound was prepared by cautiously pouring boiling benzene into a test tube to form a separate upper layer above a solution of PMDA in hot glacial acetic acid; crystals of the molecular compound formed at the interface. This procedure was necessitated by the insolubility of PMDA in benzene. No diphenyl–PMDA molecular compound could be isolated although the melting point diagram (see below) showed that an equimolar molecular compound is formed; in our experiments only a yellow solution was formed which did not yield crystals.

Anthracene gave a green color with TCE in benzene solution but a white addition product soon formed[7] and crystals of the green material could not be obtained.

Crystalline adducts containing a volatile component (*e.g.*, C_6H_6, C_6F_6) often lose this component on exposure to the atmosphere. The residue usually keeps the external shape of the original crystals but is opaque; X-ray photographs show that the second component remains behind as a polycrystalline aggregate. This difficulty was overcome by sealing the crystals together with a little mother liquor into thin-walled glass capillaries. A similar technique was used for perylene–TCE where a chemical reaction (Diels–Alder addition) apparently occurred in crystals which were exposed to the atmosphere during X-ray photography. No reaction took place in crystals sealed into capillaries.

Standard X-ray techniques (oscillation, Weissenberg and precession photography) were used, generally with Cu Kα (Ni filter) radiation. Densities were measured by flotation. Cell dimensions and densities are considered to be accurate to 1–2%. Crystals of most samples were twinned but this was usually obvious on optical examination and the individuals were large enough to be separated with a razor blade. Those crystals which had been sealed into capillaries could not be examined optically and any twinning was detected on analysis of their diffraction patterns.

The melting point diagrams were obtained from measurements made in a Gallenkamp melting point apparatus. The PMDA used for this part of the work was purified by sublimation. The components in the appropriate proportions were ground together in a mortar and then sealed into capillaries for measurement. Liquidus temperatures were determined by noting the temperature at which the last solid disappeared on heating the sample. Repetition of these determinations and the scatter of the results suggest that the liquidus curves are accurate within 2–3°.

Results and Discussion

Melting Point Diagrams. The melting point diagrams for the systems anthracene, diphenyl, and perylene each with PMDA are shown in Figures 1, 2, and 3. Only the equimolar anthracene–PMDA and perylene–PMDA compounds were obtained from solution, despite clear evidence from the melting point diagrams of the existence of diphenyl–PMDA and $(perylene)_2$–PMDA. Equimolar compounds are by far the most common in systems of the type studied here but other molar ratios have been found. For example, Kofler[8] has reported 2:1 molecular compounds of α- and β-naphthylamine with picric acid, there being two molecules of donor to one molecule of acceptor in

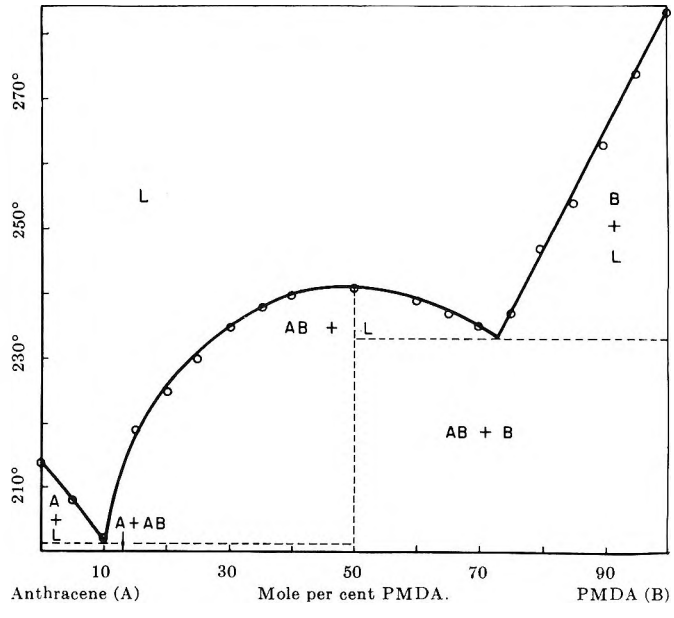

Figure 1. The melting point diagram for the system anthracene–PMDA. Dashed lines were inferred, not determined experimentally.

(5) A. S. Bailey and J. R. Case, *Proc. Chem. Soc.*, 176 (1957); *Tetrahedron*, **3**, 113 (1958).

(6) C. R. Patrick and G. S. Prosser, *Nature*, **187**, 1021 (1960).

(7) H. Kuroda, M. Kobayashi, M. Kinoshita, and S. Takemoto, *J. Chem. Phys.*, **36**, 457 (1962).

(8) A. Kofler, *Z. Elektrochem.*, **50**, 200 (1944)

Table I: Crystallographic and Other Data for Some Equimolar π-Molecular Compounds of PMDA, TCE, BTF, and C_6F_6 and Also for PMDA and BTF

Substance	Solvent	Color	M.p., °C.	a, Å.	b, Å.	c, Å.	β, deg.	Density, g. cm.$^{-3}$ Exptl.	Calcd. from X-ray results	Calcd. as mean of densities of solid components	No. of formula units in unit cell	Space group	Morphology and remarks
PMDA–benzene	Glacial acetic acid	Colorless	...	12.9	6.7	7.68	96	...	1.37	1.38	2	$P2_1/a$	
PMDA–naphthalene	Glacial acetic acid	Yellow	...	9.19	13.0	6.81	104	1.45	1.47	1.43	2	C2, Cm or C2/m	Needles elongated along [001] Bounded by (100), (210)
PMDA–anthracene	Methyl ethyl ketone	Red	240	7.6	10.0	7.3	$\alpha = 105$ $\beta = 115.5$ $\gamma = 101$	1.49	1.48	1.48	1	$P\bar{1}$	Bounded by (100), (010), (210)
PMDA–pyrene	Glacial acetic acid	Red	278	13.9	9.25	7.24	94	1.50	1.49	1.50	2	$P2_1/a$	Rhombs.
PMDA–perylene	Glacial acetic acid	Black	287	13.7	7.16	10.0	94	1.50	1.50	1.52	2	$P2_1/n$	Needles elongated along [010] Bounded by (100), (001), (201)
TCE–naphthalene	Ethyl acetate	Brown	99	7.24	12.8	7.33	94	1.24	1.25	1.23	2	C2, Cm or C2/m	Large rhombs.
TCE–pyrene	Benzene	Black	167	14.2	7.2	7.9	93	1.33	1.36	1.30	2	$P2_1/a$	Needles elongated along [010]
TCE–pyrene				14.58	7.34	8.09	92.4		1.27	...	2	$P2_1/a$	Results from ref 15
TCE–perylene	Chloroform	Green	[a]	15.7	8.19	7.37	96	1.36	1.36	1.33	2	$P2_1/a$	Needles elongated along [010]
BTF–benzene	Benzene	Colorless	...	15.41	7.36	13.75	117	...	1.59	1.44	4	$P2_1/a$	Twinned needles. Pseudo-absence: $0kl$ for $k + l \neq 2n$
BTF–naphthalene	1:4 acetic acid–ethanol	Light yellow	220 dec.	12.6	...	6.92	...	1.50	1.50	1.50	3	R3, $R\bar{3}$, R32 R3m or $R\bar{3}m$	Needles elongated along [00.1]
BTF–anthracene	1:4 acetic acid–ethanol	Orange	194	15.8	17.3	6.8	...	1.53	1.54	1.56	4	$P2_12_12_1$	Needles elongated along [001]
BTF–pyrene	1:4 acetic acid–ethanol	Yellow	240 dec.	20.6	29.6	6.7	111	1.58	1.60	1.57	8	Cc or C2/c	Needles elongated along [001] Bounded by (010), (110)
BTF–perylene	Acetic acid	Red	260 dec.	19.2	6.95	15.6	98	1.56	1.56	1.60	4	$P2_1/a$	Needles elongated along [010]
BTF–diphenyl	1:4 acetic acid–ethanol	Almost colorless	155	7.04	15.1	16.8	...	1.52	1.51	1.52	4	Pbcn	Needles elongated along [100]
C_6F_6–anthracene	C_6F_6	Colorless	...	9.03	12.2	7.26	95	...	1.51	...	2	C2, Cm or C2/m	
C_6F_6–pyrene	C_6F_6	Colorless	...	9.88	13.5	6.98	113	...	1.52	...	2	C2, Cm or C2/m	
C_6F_6–perylene	C_6F_6	Light yellow	...	17.6	7.73	7.31	106	...	1.53	...	2	$P2_1/a$	
PMDA	Glacial acetic acid	Colorless	284	10.7	7.48	10.7	90	1.70	1.71	...	4	$P2_1/n$	Pseudo-tetragonal rhombs. bounded by (100), (001), (101), (110), (011)
BTF	1:4 acetic acid–ethanol	Colorless or pink	195	6.96	19.7	6.58	...	1.86	1.86	...	4	$Pna2_1$	Needles elongated along [001] Bounded by (100), (110)

[a] At 150° it goes over into the yellow Diels–Alder adduct which melts at 265°.

agreement with our results for the perylene–PMDA system. The other well-established ratio of donor to acceptor molecules is 1:2, as in the molecular compounds containing one molecule of 3,4-benzpyrene or coronene and two molecules of 1,3,7,9-tetramethyluric acid.[9] Other ratios such as 2:3 have been reported but confirmatory evidence is lacking; for example, a molecular compound with this ratio of fluorene to 1,3,5-trinitrobenzene was reported by Sudborough,[10] but Kofler[8] found only an equimolar ratio.

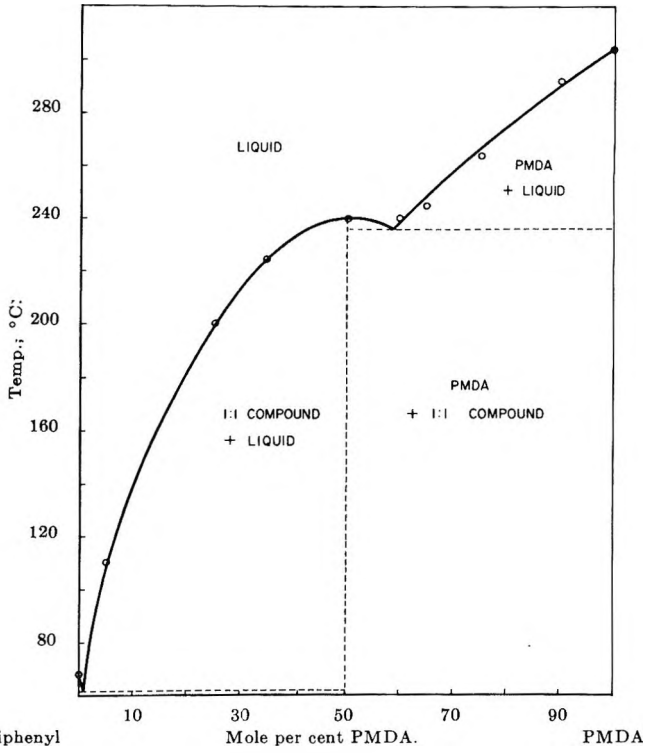

Figure 2. The system diphenyl–PMDA.

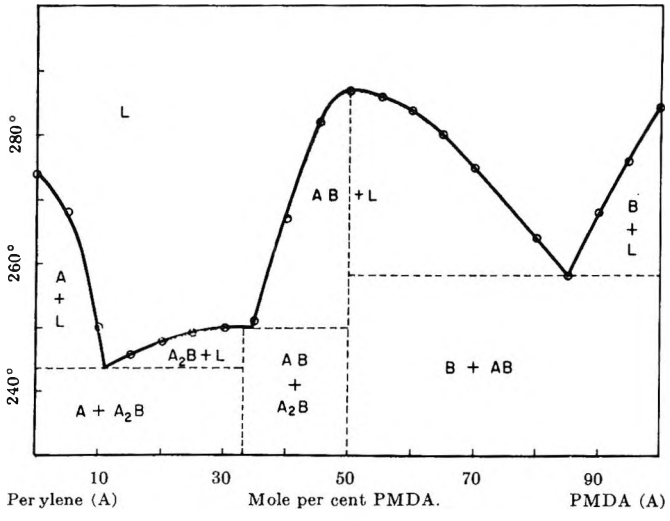

Figure 3. The system perylene–PMDA.

Crystallographic Results. The cell dimensions and space groups of the molecular compounds studied are summarized in Table I, together with other relevant information. In general, the molecular compounds crystallize as needles and oscillation photographs taken with the needle axis as rotation axis show a remarkable similarity in that the repeat distances lie in the range 6.7–7.4 Å.; in addition, the second layer lines often show strong thermal diffuse scattering from planes with spacings of about 3.2–3.5 Å. These features were first observed by Hertel and co-workers,[11–14] who pointed out that they were compatible with structures in which the two components were arranged in alternating array in mixed stacks, the stack axes being parallel to the ~7 Å. repeat direction. Confirmation of the essential correctness of this proposal has come from the crystal structure analyses summarized in part III.[2] Thus oscillation photographs about an appropriate axis will often show whether a particular binary molecular compound has the usual mixed-stack structure with a repeat distance of about 7 Å., or whether the component molecules are segregated into separate stacks as in the molecular complex[1] of hexabromobenzene and 1,2,4,5-tetrabromobenzene (shortest cell dimension 4 Å.). However, it should be noted that it is not always possible to predict stack direction from cell dimensions or crystal morphology alone: for example, in pyrene–TCE, the stack axis is reported to lie along [001] (8.1 Å.) and not along [010] (7.2 Å.).[15] In perylene–TCE (Table I), the needle axis is along [010] (8.2 Å.) which is longer than [001] (7.2 Å.); however, the oscillation photographs about [010] do not show any diffuse scattering and further work will be needed to confirm the direction of the stack axis. Anomalies are not unexpected because of the known sensitivity of morphology to crystallization conditions.

An important feature of the results of Table I is the coincidence of molecular and crystallographic symmetry centers where possible. This will considerably simplify the crystal structure analyses as the problems will be reduced to determination of the orientations of the component molecules. For one group of com-

(9) A. Damiani, P. De Santis, E. Giglio, A. M. Liquori, R. Puliti, and A. Ripamonti, *Acta Cryst.*, **16**, A57 (1963).

(10) J. Sudborough, *J. Chem. Soc.*, **109**, 1339 (1916); *Chem. Abstr.*, **11**, 1131 (1917).

(11) E. Hertel and H. Kleu, *Z. physik. Chem.*, **B11**, 59 (1931).

(12) E. Hertel and G. H. Römer, *ibid.*, **B11**, 77, 90 (1931).

(13) E. Hertel and K. Schneider, *ibid.*, **B13**, 387 (1931).

(14) E. Hertel and H. W. Bergh, *ibid.*, **B33**, 319 (1936).

(15) H. Kuroda and H. Akamatu, *J. Chem. Phys.*, **40**, 3748 (1964).

pounds it is possible to propose a structure directly from symmetry and size considerations and this and other points of interest in the crystallographic results are now discussed.

The Crystal Structure of Naphthalene–PMDA

The molecular compounds naphthalene–PMDA, naphthalene–TCE, anthracene–hexafluorobenzene, and pyrene–hexafluorobenzene all have closely related cell dimensions (Table II) and show the same systematic

Table II: Crystallographic Data for Four Quasi-isomorphous Molecular Compounds

Molecular compound	a, Å.	b, Å.	c, Å.	β, deg.	Z	Space group
Naphthalene–PMDA	9.19	13.0	6.81	104	2	C2, Cm, or
Naphthalene–TCE[a]	7.24	12.8	7.33	94	2	C2/m
Anthracene–C_6F_6	9.03	12.2	7.26	95	2	
Pyrene–C_6F_6	9.88	13.5	6.98	113	2	

[a] Although [100] < [001] the thermal-diffuse scattering indicates that the stack axes lie along [001].

absences. The possible space groups are C2, Cm, and C2/m, of which only the latter is centrosymmetric. In all of these compounds both component molecules are centrosymmetric. As centrosymmetric molecules very rarely[16] or never[17] crystallize in noncentrosymmetric space groups, we may rather reliably assume that C2/m is the correct space group. Structures proposed on the basis of C2/m would not be greatly altered if one of the other possible space groups was in fact correct.

We consider the structure of naphthalene–PMDA in more detail; the other members of this group will have the same distribution of molecules among the special positions of the space group but not necessarily the same molecular orientations. The presence of strong thermal diffuse scattering on the second layer lines of oscillation photographs about [001] shows that the stacks have their axes in this direction. The [001] spacing of 6.8 Å. is just sufficient to accommodate two molecules with their planes approximately normal to [001]. Both component molecules have symmetry D_{2h}-mmm if assumed planar and can therefore be placed at the special positions with (lower) point-group symmetry C_{2h}-2/m. Let the PMDA molecules be placed with centers at positions (a) of the space group, *i.e.*, at (000) and ($^1/_2{}^1/_20$). The long axes of the molecules must then lie either along [010] or in the (010) plane in order to conform to the required point-group symmetry. The first of these possibilities must be rejected as it gives rise to abnormally close intermolecular approaches; the second is quite satisfactory on this score, particularly if the molecular planes are normal to [001]. In order to obtain the familiar mixed stacks, the naphthalene molecules must be centered at positions (c) of the space group, *i.e.*, at ($00^1/_2$) and ($^1/_2{}^1/_2{}^1/_2$). Again, consideration of the distance between naphthalene molecules shows that their long axes must lie in the (010) plane and not along [010]. This structure is shown in Figure 4 in projection down [001].

The above structure would not be greatly changed if one of the other possible space groups were correct. In C2 the molecular centers would be displaced relative to each other along [010] whereas for Cm this displacement would be in the (010) plane. Thus, whatever the true space group, the benzene rings of the two component molecules must be essentially in parallel orientation although not necessarily directly superposed.

PMDA Molecular Compounds. The crystal structures of the molecular compounds of PMDA with anthracene,[2] perylene,[2] and pyrene[18] have been worked out to varying degrees of completeness.

TCE Molecular Compounds. The crystal structure of pyrene–TCE has been determined by Kuroda and

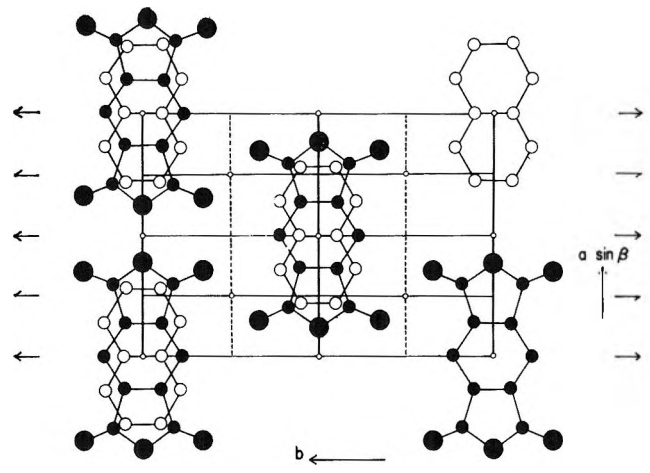

Figure 4. The projection down [001] of the naphthalene–PMDA structure as deduced from cell dimensions and space group. For clarity one molecule of each type has been omitted at the right-hand side of the diagram. The centers of the molecules drawn with full circles are in the plane of the paper while those with open circles are one-half of the [001] translation distance above (or below) the plane of the paper.

(16) F. H. Herbstein and F. R. L. Schoening, *Acta Cryst.*, **10**, 657 (1957).

(17) A. I. Kitaigorodskii, *Soviet Phys. Cryst.*, **3**, 393 (1958).

(18) F. H. Herbstein and J. A. Snyman, unpublished results.

Akamatu[15]; their cell dimensions agree reasonably well with those in Table I although the discrepancy between the two values of a is larger than expected. Details of the structure have not yet been reported.

BTF Molecular Compounds. The structure of BTF itself is not known in detail but there seems little doubt that its molecular formula should be based on that of benzofuroxan. For this molecule both n.m.r.[19-22] and crystal structure[23,24] studies show that the N-oxide formulation IV is correct and not some other formula such as V.[25] The consequent formulation of benzotri-

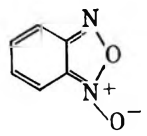

IV

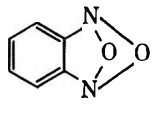

V

furoxan as in III, rather than, say, as hexanitrosobenzene, means that the molecule lacks a center of symmetry. The systematic absences in the diffraction patterns of BTF are compatible with the two space groups $Pna2_1$ and Pnam (see Table I). The latter is eliminated by analysis of the intensity distribution, the $N(z)$[26] test showing conclusively (Figure 5) that the crystals are noncentrosymmetric and thus that the correct space group is $Pna2_1$. As centrosymmetric molecules seldom or never crystallize in noncentrosymmetric space groups,[16,17] this is strong supporting evidence for a noncentrosymmetric molecular structure.

The structure of diphenyl–BTF appears, at first sight, to contradict this conclusion. The space group, which is uniquely defined by the systematic absences, has two sets of fourfold positions, (a) and (b), with point-group symmetry $\bar{1}$ and one set of fourfold positions, (c), with symmetry 2. The only way of arranging the molecules in mixed stacks is to place BTF molecules at positions (a) and diphenyl molecules at positions (b). The stacks then have their axes along [100], the interplanar spacing being about 3.5 Å. If this arrangement is correct than the BTF molecules must be randomly arranged in the crystal in order to simulate the presence of a center in the molecule. This could be achieved by random 60° in-plane rotations of the planar BTF molecules as these have roughly the shape of an equilateral triangle. No diffuse scattering was observed on the photographs, which suggests that there is little correlation between orientations of successive BTF molecules. It is, however, possible that ordering of the BTF molecular orientations occurs at low temperatures with a doubling of the a axis to about 14 Å. Crystals of anthracene–1,3,5-trinitrobenzene[27] have a 14 Å. periodicity along the stack axis due to just such an ordering of the tri-

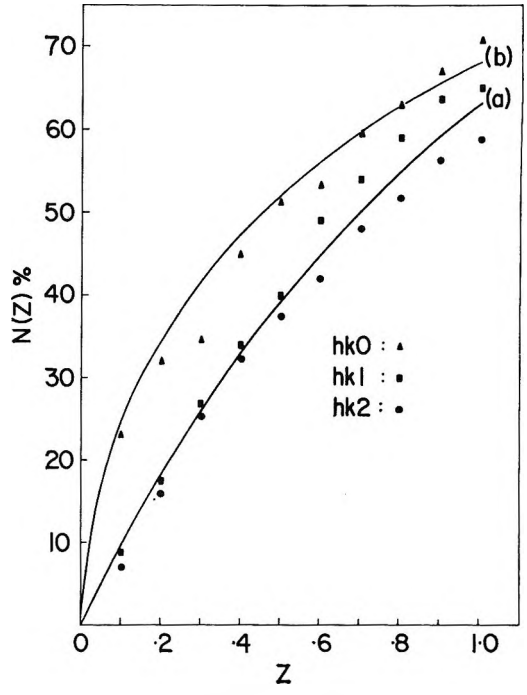

Figure 5. Intensity distribution curves for BTF. Curve a is that calculated for an acentric distribution and curve b that for a centric distribution. The experimental points for the $hk0$ zone follow curve b and those for the $hk1$ and $hk2$ zones follow curve a. This is in accordance with space group $Pna2_1$, but not Pnam.

angular trinitrobenzene molecules. This structure is found both at −173 and 25° while our high-temperature X-ray photographs have shown that it persists up to at least 120°. One would expect the barriers to changes of orientation in the molecular plane to be larger for 1,3,5-trinitrobenzene than for BTF.

(19) F. B. Mallory and C. S. Wood, *Proc. Natl. Acad. Sci. U.S.*, **47**, 697 (1961).

(20) P. Diehl, H. A. Christ, and F. B. Mallory, *Helv. Chim. Acta*, **45**, 504 (1962).

(21) G. Englert, *Z. Elektrochem.*, **65**, 854 (1962).

(22) R. K. Harris, A. R. Katritzky, S. Øksne, A. S. Bailey, and W. E. Paterson, *J. Chem. Soc.*, 197 (1963).

(23) R. Hulme, *Chem. Ind.* (London), 42 (1962).

(24) D. Britton and W. E. Noland, *J. Org. Chem.*, **27**, 3218 (1962).

(25) G. A. Gol'der, Z. V. Todres-Selektor, and S. V. Bogdanov, *J. Struct. Chem.*, **2**, 446 (1962).

(26) E. R. Howells, D. C. Phillips, and D. Rogers, *Acta Cryst.*, **3**, 210 (1950).

(27) D. S. Brown, S. C. Wallwork, and A. Wilson, *ibid.*, **17**, 168 (1964). In our hands an equimolar mixture of anthracene and 1,3,5-trinitrobenzene powders ground together in a mortar melted at 142° to give an *orange* melt. Mixture of equimolar solutions of anthracene and trinitrobenzene yielded *orange* crystals with m.p. 142°. These crystals had the same cell dimensions and space group as those reported by Hertel and Römer[12] and by Brown, *et al.* Hertel and Römer reported their crystals as red with m.p. 164°, in agreement with Sudborough[10] and Kofler.[8] Brown, *et al.*, mentioned that their crystals were orange needles but did not give their melting point. The reason for these differences is not known.

The naphthalene–BTF molecular compound is also disordered but here it is the naphthalene molecules which must take on three different orientations in order to conform to the threefold or higher symmetry demanded by the space group. The diffuse scattering on the photographs suggests a correlation between the orientations of successive naphthalene molecules and it is possible that an ordered phase with [00.1] $\sim 3 \times$ 6.9 Å. will be found at low temperatures.

C_6F_6 Molecular Compounds. Crystalline equimolar molecular compounds are formed by C_6F_6 and aniline (Brooke, *et al.*[28]), benzene, fluorobenzene, mesitylene, 2-methylnaphthalene (Patrick and Prosser[6]), and the aromatic hydrocarbons listed in Table I. Patrick and Prosser suggested that these molecular compounds were of the electron donor–acceptor type, C_6F_6 acting as electron acceptor because of the large negative inductive effect of the fluorine atoms; however, their search for characteristic additional absorption bands in the ultraviolet spectrum of benzene–hexafluorobenzene mixtures was unsuccessful. Although the colors of the molecular compounds of Table I do not differ obviously from those of their components, charge-transfer interactions are indicated by the general resemblance of their unit cell dimensions and symmetries to those of the other molecular compounds of Table I. The lack of color change and the immediate loss of C_6F_6 from these molecular compounds on exposure to the atmosphere both suggest that the charge-transfer interaction is rather weak.

The photographs of the pyrene–hexafluorobenzene molecular compound are noteworthy for very strong diffuse scattering.

Concluding Summary

The crystallographic results obtained for the molecular compounds formed by various aromatic hydrocarbons with the newer electron acceptors pyromellitic dianhydride, tetracyanoethylene, benzotrifuroxan, and hexafluorobenzene show that these must have molecular arrangements similar to those reported earlier from crystal structure analyses of other analogous donor–acceptor molecular compounds. The essential feature common to the molecular compounds of this type studied until now is the arrangement of the two components, plane to plane, in alternating array in mixed stacks. The present exploratory study indicates that the crystals have many features of interest which can only be fully elucidated by detailed crystal structure studies. Some of these will be reported in later papers of this series.

(28) G. Brooke, J. Burdon, M. Stacey, and J. C. Tatlow, *J. Chem. Soc.*, 1768 (1960).

Molecular Compounds and Complexes. III. The Crystal Structures of the Equimolar π-Molecular Compounds of Anthracene and Perylene with Pyromellitic Dianhydride[1]

by J. C. A. Boeyens and F. H. Herbstein

Chemical Physics Group of the National Physical and Chemical Research Laboratories, Council for Scientific and Industrial Research, Pretoria, South Africa *(Received November 9, 1964)*

A full three-dimensional X-ray diffraction analysis (by least squares, with anisotropic temperature factors) has been made of the perylene–pyromellitic dianhydride (PMDA) molecular compound. A limited two-dimensional analysis of the structure of anthracene–PMDA is also reported. Both analyses were of the crystal structures at 300°K. Accurate molecular dimensions were obtained in the first, but not in the second, of these analyses. The dimensions found for the perylene molecule agree well with those in perylene itself and in perylene–fluoranil. The dimensions of the PMDA molecule agree reasonably well with those of benzene and maleic anhydride. The molecular arrangements in both structures are of the mixed stack type familiar from earlier crystal structure analyses of other members of this group of molecular compounds. Within a particular stack the relative disposition of the two components resembles, in both structures, that of adjacent layers in graphite.

Theory[2] predicts and experiment[3-10] confirms that the crystal structures of the π-molecular compounds formed between electron donors such as aromatic hydrocarbons and various electron acceptors have the common feature that the component molecules are arranged, plane to plane, in alternating array in mixed stacks. There is, as yet, no detailed theoretical guide to the relative arrangement of the component molecules *within* the stacks and the experimental results show a variety of mutual orientations. Thus the details of the arrangement within the stacks, which should be helpful in interpreting the interaction between the components, must be determined experimentally. We have therefore analyzed the crystal structures of the equimolar molecular compounds formed between pyromellitic dianhydride[11] (PMDA), a powerful electron acceptor, and the electron donors anthracene and perylene. The relatively high symmetry of the components and the absence of substituents should simplify the theoretical interpretation of the results. The analysis of the anthracene–PMDA molecular compound has only been taken far enough to establish the main features of the molecular arrangement, but the perylene–

(1) Part II: J. C. A. Boeyens and F. H. Herbstein, *J. Phys. Chem.*, **69**, 2153 (1965).

(2) R. S. Mulliken, *J. Am. Chem. Soc.*, **74**, 811 (1952).

(3) *p*-Iodoaniline–1,3,5-trinitrobenzene: H. M. Powell, G. Huse, and P. W. Cook, *J. Chem. Soc.*, 153 (1943).

(4) Hexamethylbenzene–picryl chloride: H. M. Powell and G. Huse, *ibid.*, 435 (1943).

(5) Hexamethylbenzene–chloranil: T. T. Harding and S. C. Wallwork, *Acta Cryst.*, **8**, 787 (1955); N. D. Jones and R. E. Marsh, *ibid.*, **14**, 809 (1962); S. C. Wallwork and T. T. Harding, *ibid.*, **15**, 810 (1962).

(6) Pyrene–1,3,7,9-tetramethyluric acid: P. De Santis, E. Giglio, A. M. Liquori, and A. Ripamonti, *Nature*, **191**, 900 (1961); A. Damiani, P. De Santis, E. Giglio, A. M. Liquori, R. Puliti, and A. Ripamonti, *Acta Cryst.*, **16**, A57 (1963).

(7) Perylene–fluoranil: A. W. Hanson, *ibid.*, **16**, 1147 (1963).

(8) Anthracene–1,3,5-trinitrobenzene: D. S. Brown, S. C. Wallwork, and A. Wilson, *ibid.*, **17**, 168 (1964).

(9) Skatole and indole with 1,3,5-trinitrobenzene: A. W. Hanson, *ibid.*, **17**, 559 (1963).

(10) S. C. Wallwork, *J. Chem. Soc.*, 494 (1961).

(11) L. L. Ferstandig, W. G. Toland, and C. D. Heaton, *J. Am. Chem. Soc.*, **83**, 1151 (1961).

PMDA molecular compound has been the subject of a full three-dimensional least-squares analysis with anisotropic temperature factors. These analyses are both of the room temperature structures of the molecular compounds.

The Crystal Structure of Anthracene–PMDA

Experimental

The equimolar molecular compound of anthracene and PMDA crystallizes as red triclinic needles from methyl ethyl ketone (previously dried with $CaCl_2$). Observation under the polarizing microscope shows these crystals to be twinned macroscopically but single crystals were easily obtained by splitting a twinned needle. Single crystals were elongated along [001] and showed (100), (010), and (210) faces.

Standard X-ray diffraction techniques (oscillation, Weissenberg and precession photography with nickel-filtered Cu Kα radiation) were used throughout this work.

Cell Dimensions and Space Group. Following standard practice,[12] a primitive reduced cell was chosen with $c < a < b$ and $\alpha, \beta, \gamma > 90°$. The value of [001], which lies along the needle axis, was determined directly from an oscillation photograph and a^*, b^*, and γ^* were determined from the corresponding zero-layer Weissenberg photograph. The angles α and β were determined by the method of level offsets,[13] using zero- and first-layer Weissenberg photographs. The remaining dimensions were calculated from standard formulas. The results were: $a = 7.6$ Å., $a^* = 0.1556$ Å.$^{-1}$; $b = 10.0$ Å., $b^* = 0.1103$ Å.$^{-1}$; $c = 7.3$ Å., $c^* = 0.1645$ Å.$^{-1}$; $\alpha = 105°$, $\alpha^* = 67.5°$; $\beta = 115.5°$, $\beta^* = 60°$; $\gamma = 101°$, $\gamma^* = 70°$. The measured density was 1.49 g. cm.$^{-3}$. With one molecule of each component per unit cell, the calculated density is 1.48 g. cm.$^{-3}$, which is also the mean of the densities of the components in crystalline form.

There are no systematic absences and the possible space groups are P1 and P$\bar{1}$. The latter was considered more probable because both components are centrosymmetric (see discussion of space group of naphthalene–PMDA in ref. 1) and this choice was vindicated by the success of the subsequent crystal structure analysis. On this basis the centers of both molecules must lie at crystallographic centers of symmetry; consideration of cell dimensions and molecular shapes suggested that the anthracene molecules were centered at (000) and related positions and the PMDA molecules at (00$^1/_2$) and related positions.

Intensity Measurements. The intensities of 152 $hk0$ reflections (38 with $I_{obsd} = 0$) and 184 $hk1$ intensities (31 with $I_{obsd} = 0$) were measured visually from equi-inclination Weissenberg photographs taken with Cu Kα radiation. The crystal used was approximately cylindrical in shape and was thin enough to warrant neglect of absorption corrections. Corrections for Lorentz, polarization, and spot-shape factors were applied using appropriate computer programs (the computer programs and other relevant information for both structure determinations are summarized below).

Determination and Refinement of Structure

Comparison of the hexagonal distribution of near-in vector peaks in the $hk0$ Patterson projection with the intramolecular vector patterns of the two molecules led to a trial structure which was substantiated using the Fourier transform method.[14,15] The molecular orientations were derived by comparison of the measured unitary structure factors for 51 low-index $hk0$ reflections with values calculated from the transforms of the two molecules. Reasonable agreement for these reflections ($R = 38\%$) supported the postulated structure.

This structure was then refined by Fourier and difference syntheses until $R(hk0) = 21\%$. The Fourier projection at this stage is shown in Figure 1. The positions of all atoms were further refined by least squares, using individual isotropic temperature factors. This reduced $R(hk0)$ to 15%. The z coordinates were calculated on the basis of standard molecular dimensions and refined by a trial and error procedure, R factors for $hk1$ reflections being calculated for a series of tilts of the planar molecules to the (001) plane. The over-all R factor for the best coordinates was 18.5% (336 $hk0 + hk1$ reflections, individual B factors), which was considered adequate to demonstrate that the phase problem had been correctly solved. The atomic coordinates are listed in Table I (see Figure 2) and observed and calculated structure factors are given in Table II. Interatomic distances and angles are reasonable but are not accurate enough to warrant listing here.

Molecular Arrangement

The molecular arrangements in projection down the three principal crystallographic axes are shown in Figure 3. The molecules are arranged in mixed stacks whose axes lie along [001]. These stacks are all

(12) "International Tables for X-Ray Crystallography," N. F. M Henry and K. Lonsdale, Ed. Vol. II, Kynoch Press, Birmingham, England, 1959, p. 106.

(13) M. J. Buerger, "X-Ray Crystallography," John Wiley and Sons, Inc., New York, N. Y., 1942, p. 375.

(14) G. Knott, *Proc. Phys. Soc.* (London), 52, 229 (1940).

(15) H. Lipson and C. A. Taylor, "Fourier Transforms and X-Ray Diffraction," G. Bell and Sons, London, 1958.

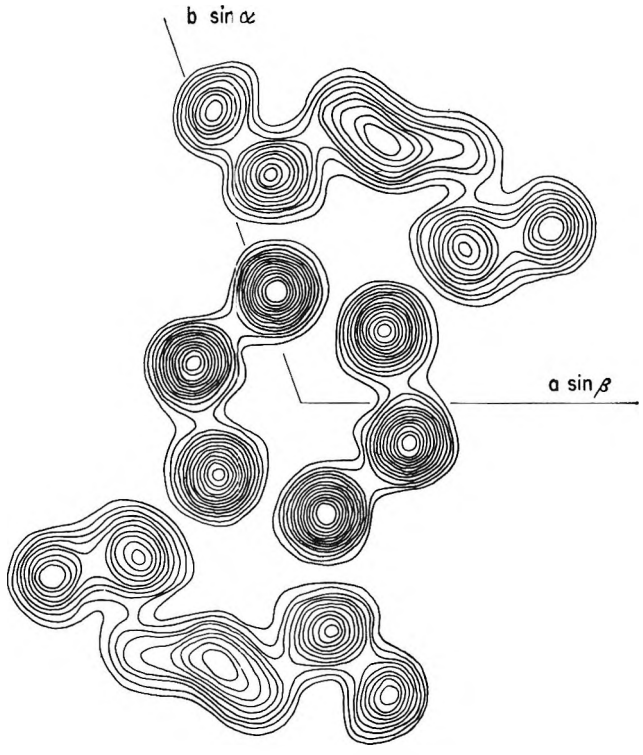

Figure 1. Fourier projection down [001] showing overlapping PMDA and anthracene molecules.

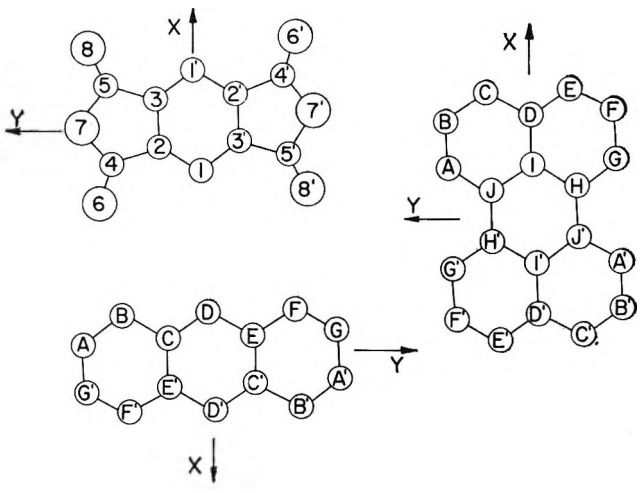

Figure 2. Nomenclature of atoms and molecular axes of PMDA, anthracene, and perylene.

crystallographically identical, with any particular stack being surrounded by six others in quasi-hexagonal array. The inclination of the molecular planes to the stack axes is such that some measure of interleaving occurs.

The molecules were assumed to be planar and parallel, although this is not required by the crystal symmetry. The plane of the anthracene molecule is given by

$$0.6806u + 0.5506v - 0.4834w = 0$$

where u, v, w are orthogonal coordinates (in Å.) related to the *fractional* coordinates x, y, z of the atoms in the triclinic axial system of the unit cell by the equations

$$u = xa + yb \cos \gamma + zc \cos \beta$$

$$v = yb \sin \gamma - zc \sin \beta \cos \alpha^*$$

$$w = zc \sin \beta \sin \alpha^*$$

In the same set of orthogonal axes, the equation of the plane through the PMDA molecule is

$$0.6837u + 0.5483v - 0.4816w = 3.234$$

The small deviations from strict parallelism of the two molecules are due to approximations made in the derivation of the z coordinates of the atoms.

The mean interplanar distance is 3.23 Å., which is compared with other relevant values in Table XI. The molecular arrangement seen in projection onto the plane through the anthracene molecule is shown in Figure 4. No significance should be attached to the deviations from regularity that are evident in this figure; they result from the incompleteness of the refinement. The relative arrangement of carbon atoms of the two adjacent molecules is similar to that in successive sheets of graphite.

Table I: Fractional Atomic Coordinates[a]

Atom	x	y	z
C_D	−0.163	0.055	−0.098
C_E	0.033	0.146	0.134
C_F	0.084	0.301	0.231
C_G	0.272	0.382	0.485
$C_{A'}$	0.440	0.327	0.549
$C_{B'}$	0.405	0.185	0.440
$C_{C'}$	0.204	0.094	0.215
C_1	−0.174	0.049	0.395
C_2	0.022	0.143	0.610
C_3	0.189	0.093	0.738
C_4	0.104	0.299	0.752
C_5	0.365	0.216	0.923
O_6	0.005	0.381	0.756
O_7	0.305	0.335	0.955
O_8	0.545	0.226	0.080

[a] Letter subscripts refer to the anthracene molecule and numeral subscripts refer to PMDA; the system used is shown in Figure 2.

Table II: Observed and Calculated Structure Factors for Anthracene–PMDA

h k l	$\|F_o\|$	F_c
2 -12 0	3.6	-2.8
3	4.5	-3.0
4	6.0	-5.9
0 -11 0	4.4	-3.3
1	2.1	1.5
2	2.2	-1.7
3	2.2	-0.8
4	2.1	-1.4
5	1.9	0.8
6	2.7	-1.3
0 -10 0	2.3	1.5
1	2.5	-1.5
2	3.5	-3.5
3	2.5	-2.5
4	2.4	2.2
5	4.6	-2.4
6	6.9	-4.6
7	4.0	-4.1
1 -9 0	16.1	-16.4
2	7.1	-5.2
3	4.5	-2.5
4	6.7	6.5
5	3.6	0.5
6	3.3	-1.1
7	1.9	-1.2
1 -8 0	6.8	-6.1
2	9.3	6.7
3	20.0	17.6
4	20.7	18.2
5	13.1	11.8
6	2.5	-0.9
7	2.2	-1.4
8	4.0	4.2
1 -7 0	10.7	9.4
2	2.2	-1.0
3	18.2	18.5
4	9.7	8.5
5	2.6	0.7
6	11.1	-11.4
7	5.2	-4.0
8	1.8	2.2
1 -6 0	9.4	-8.8
2	13.7	-11.9
3	8.1	7.5
4	5.8	5.5
5	9.3	-9.7
6	3.6	-3.5
7	4.9	-2.2
8	2.0	1.9
1 -5 0	33.9	-34.8
2	11.9	11.2
3	10.0	7.1
4	4.6	5.1
5	2.3	-1.9
6	2.6	3.3
7	5.7	-3.6
8	2.1	-0.3
1 -4 0	20.9	-17.2
2	1.5	3.9
3	22.0	-18.3
4	16.7	-14.5
5	2.2	-1.0
6	10.5	-13.1
7	2.6	-3.4
8	6.6	-6.1
1 -3 0	14.4	12.0
2	19.5	-21.5
3	17.0	-16.1
4	8.8	-7.3
5	2.2	-0.9
6	3.4	1.4
7	6.8	8.3
8	4.5	-3.2
1 -2 0	8.2	9.9
2	28.5	-25.5
3	12.5	-14.0
4	4.9	-4.0
5	8.4	8.3
6	17.5	22.9
7	2.5	2.0
8	2.0	-1.0
1 -1 0	55.0	64.7
2	12.7	-11.1
3	13.1	12.9
4	12.0	10.5
5	16.2	16.3
6	13.3	12.0
7	3.5	-3.3
8	1.8	-1.8
1 0 0	22.0	24.7
2	15.5	12.3
3	4.0	3.1
4	5.2	6.0
5	9.4	9.8
6	4.5	6.0
7	2.3	3.1
8	2.7	-3.6
0 1 0	25.5	23.8
1	32.5	-34.7
2	10.2	-7.6
3	27.8	-28.0
4	13.1	-17.5
5	9.0	10.6
6	2.5	1.0
7	2.2	-2.0
0 2 0	33.6	-35.7
1	33.2	33.2
2	27.1	-24.6
3	13.1	-12.4
4	8.4	8.5
5	5.1	5.5
6	5.1	-6.3
7	2.0	-2.1
0 3 0	19.7	17.4
1	7.0	5.2
2	9.5	-9.3
3	6.3	5.2
4	2.3	2.5
5	14.7	-16.5
6	2.3	-1.8
7	2.2	-2.2
0 4 0	27.1	-22.9
1	21.0	-25.3
2	1.9	-0.6
3	9.2	-9.6
4	10.2	-12.7
5	7.8	-9.1
6	2.1	0.8
0 5 0	8.9	-4.1
1	3.8	3.6
2	6.7	8.0
3	11.0	11.6
4	2.6	1.3
5	4.6	-4.0
6	2.3	1.7
0 6 0	2.0	1.9
1	3.9	5.9
2	17.6	19.2
3	13.8	14.5
4	3.5	-3.1
5	2.0	-2.8
0 7 0	9.8	-10.1
1	12.1	13.1
2	14.8	15.3
3	3.6	-2.3
4	2.1	-3.5
0 8 0	4.5	-4.0
1	8.3	10.2
2	2.5	2.8
3	2.2	-0.5
0 9 0	3.0	0.6
1	4.3	-1.9
2	2.2	0.3
4 -12 1	3.0	2.0
4 -11 1	1.0	0.2
5	4.0	-2.1
4 -10 1	6.2	4.9
5	1.1	-1.8
6	3.6	2.6
4 -9 1	4.7	-4.3
5	3.7	-3.3
6	1.1	0.2
7	0.8	0.9
4 -8 1	11.0	-11.9
5	7.7	8.6
6	2.2	-0.8
7	1.0	-0.6
3 -7 1	7.9	-7.7
4	7.0	7.2
5	6.2	4.6
6	3.4	-4.6
7	1.0	0.3
3 -6 1	7.6	-6.0
4	4.1	3.4
5	10.6	-13.8
6	4.7	3.4
7	1.6	1.0
3 -5 1	0.9	1.7
4	2.9	1.7
5	4.7	5.7
6	8.1	10.3
7	2.1	-1.7
3 -4 1	3.2	2.0
4	3.7	3.6
5	7.2	6.8
6	2.6	-4.0
7	1.1	-1.6
2 -3 1	20.9	-21.6
3	13.3	12.9
4	10.9	-13.8
5	3.1	-1.0
6	3.2	-3.9
7	1.6	1.0
2 -2 1	17.7	21.3
3	0.8	-0.6
4	2.6	2.6
5	5.2	6.8
6	1.3	1.8
7	1.6	1.5
1 -1 1	10.8	-14.5
2	4.1	6.0
3	17.4	-22.6
4	11.1	11.6
5	9.7	-11.0
6	1.8	-2.7
7	1.0	-0.4
-3 0 1	1.8	0.8
-2	3.6	3.6
1	3.8	4.2
2	4.3	-6.1
3	5.6	6.0
4	4.4	-4.3
5	5.5	-7.4
6	1.2	1.5
7	1.3	0.7
-4 1 1	19.0	21.7
-3	8.7	-8.0
-2	5.4	4.5
-1	8.5	11.1
0	10.7	12.3
1	4.1	4.1
2	3.2	-1.9
3	9.0	10.6
4	11.0	-10.9
5	5.6	5.9
6	3.6	0.8
7	2.2	2.0
-5 2 1	5.7	3.7
-4	15.2	-15.9
-3	13.1	-12.3
-2	13.9	-12.3
-1	8.4	6.2
0	24.8	-31.5
1	5.0	-1.1
2	3.8	-4.6
3	6.3	-6.1
4	1.2	-1.6
5	2.4	0.5
6	1.5	-0.4
-6 3 1	4.2	4.7
-5	8.4	6.4
-4	6.7	-5.0
-3	19.0	20.5
-2	9.0	6.4
-1	2.5	3.3
0	13.9	9.5
1	13.7	14.2
2	4.5	5.1
3	3.7	3.6
4	5.2	6.7
5	3.0	-1.2
6	2.8	2.7
-6 4 1	6.0	-4.7
-5	2.2	1.2
-4	6.7	5.2
-3	15.8	-11.7
-2	7.4	4.8
-1	14.8	-7.4
0	15.2	14.6
1	13.7	-14.6
2	7.4	5.5
3 4 1	1.2	-0.4
4	2.6	-1.7
5	1.1	-1.0
-7 5 1	8.9	-8.0
-6	3.0	2.8
-5	4.1	-2.2
-4	14.6	-12.4
-3	5.6	-5.3
-2	8.3	7.9
-1	6.7	-6.0
0	7.0	-6.9
1	2.2	-3.0
2	6.2	1.7
3	4.2	-3.1
4	1.2	-0.7
5	0.9	1.3
-7 6 1	1.8	1.0
-6	11.5	10.3
-5	9.2	-10.1
-4	9.8	5.7
-3	21.6	17.9
-2	5.1	-5.4
-1	11.7	7.9
0	1.1	-1.3
1	11.7	8.2
2	5.6	-4.6
3	4.5	4.7
4	1.0	1.9
-7 7 1	4.4	4.3
-6	8.2	-8.7
-5	5.7	-3.2
-4	6.6	4.5
-3	14.8	-9.7
-2	10.1	-7.0
-1	4.1	3.7
0 7 1	8.4	-8.3
1	6.4	-5.7
2	2.3	-1.7
3	1.1	-0.1
4	0.8	-1.9
-7 8 1	2.7	1.0
-6	5.7	-5.8
-5	7.4	5.7
-4	7.5	-6.3
-3	1.2	-1.9
-2	10.7	10.4
-1	7.2	-5.9
0	2.4	-1.2
1	1.2	0.3
2	1.1	1.9
3	2.3	-1.9
-7 9 1	1.0	-0.6
-6	1.6	0.5
-5	1.2	-1.0
-4	3.5	1.9
-3	7.3	6.0
-2	3.0	0.9
-1	4.0	-4.4
0	5.6	6.2
1	1.5	-1.0
2	2.0	-1.1
-7 10 1	3.7	-3.8
-6	1.0	1.1
-5	1.1	0.4
-4	1.1	2.3
-3	5.4	-2.1
-2	3.6	-3.3
-1	2.6	2.9
0	1.7	-0.8
1	0.7	-2.3
-6 11 1	3.4	4.0
-5	2.1	2.1
-4	0.9	-0.8
-3	3.9	2.9
-2	1.8	0.4
-1	1.6	3.4

Crystal Structure of Perylene–PMDA

Experimental

The perylene–PMDA molecular compound crystallized from glacial acetic acid as long black needles (m.p. 287°), elongated along [010] and bounded by (100), (201), and (001). The crystals shattered on cooling to 100°K. and thus, despite the large thermal vibration, the present analysis had perforce to be carried out at room temperature.

Accurate cell dimensions were determined from back-reflection Weissenberg photographs (a, c, β) and Mathieson-adaptor rotation photographs (b) using methods described previously.[16] The values and their estimated standard deviations at 20° were found to be (Cu $K\alpha_1$ = 1.54050 Å.; Cu $K\alpha_2$ = 1.54436 Å.): a = 14.613 ± 0.003 Å., b = 7.16 ± 0.01 Å., c = 10.1309 ± 0.0004 Å., and β = 94.67 ± 0.03°. (The difference in the accuracies of a and c is due to a lack of suitable reflections with large h.)

$$\rho_{measd} = 1.50 \text{ g. cm.}^{-3}$$

$$\rho_{calcd} \text{ (for } Z = 2) = 1.504 \text{ g. cm.}^{-3}$$

The space group was uniquely defined by the systematic absences as C_{2h}^5-$P2_1/n$.

The intensities of 1545 hkl reflections (358 with $I_{obsd} = 0$) were measured visually, using equi-inclination Weissenberg photographs taken with Cu $K\alpha$ (nickel filter). The crystal used was approximately cylindrical in shape and was thin enough to warrant neglect of absorption corrections. Lorentz, polarization, and spot-shape corrections were applied using standard computer programs.

(16) F. H. Herbstein, *Acta Cryst.*, 16, 255 (1963).

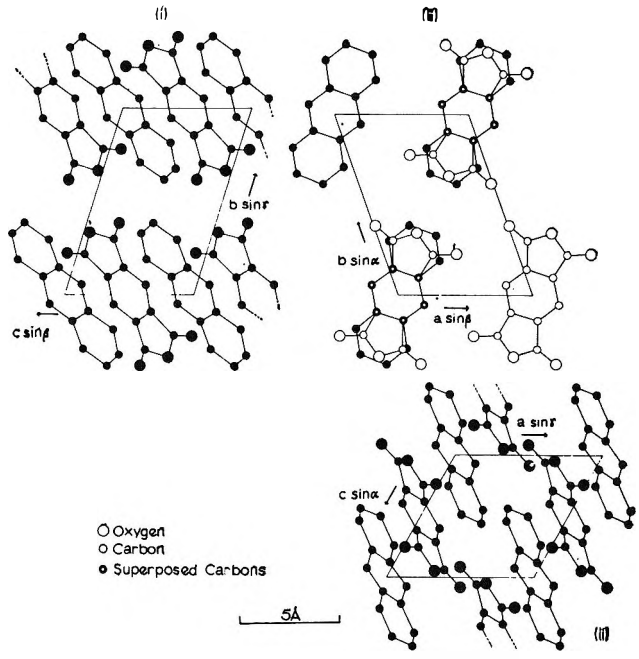

Figure 3. The arrangement of PMDA and anthracene molecules in the unit cell as seen in projection down the three crystallographic axes. In (iii), greater clarity has been obtained by omission of molecules at two of the cell corners. The centers of the molecules drawn with full circles are in the plane of the paper while those with open circles are one-half of the appropriate translation above (or below) the plane of the paper. This convention has also been used in other diagrams in this paper.

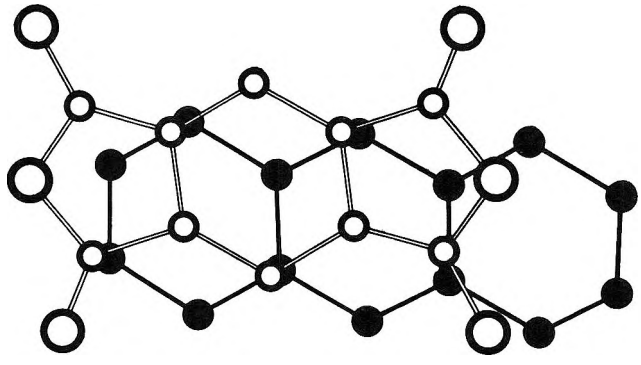

Figure 4. The molecular arrangement in anthracene–PMDA seen in projection onto the plane of the anthracene molecule. The PMDA molecule is 3.23 Å. above the anthracene molecule.

Determination of Trial Structure. The presumption that mixed stacks be formed and the mitations liimposed by the molecular shapes and sizes required that the component molecules be centered at the special positions (000, $^1/_2{}^1/_2{}^1/_2$) and ($^1/_2 0 {}^1/_2$, $0 {}^1/_2 0$) of the space group. The length of b and the presence of strong thermal scattering on the second layer lines of [010] oscillation photographs suggested that the b axis is approximately normal to the molecular planes.

The intramolecular vector pattern of perylene has a well-defined hexagonal arrangement of peaks (Figure 5a) whereas that of PMDA (not shown) is relatively featureless. The hexagonal peak pattern in the Patterson projection down [010] (Figure 5b) thus allowed the orientation of the perylene to be limited to three possibilities but gave no information about the PMDA. The Fourier transforms[14,15] of both molecules were then calculated and unitary structure factor values derived for various molecular arrangements compared with measured values for 32 low-index $h0l$ reflections. The strong reflection ($30\bar{3}$) provided crucial evidence for the orientation of the PMDA molecule, as it was clear from the transform that the perylene contribution to this reflection had to be small. The PMDA orientation was thus determined by the transform method to within a

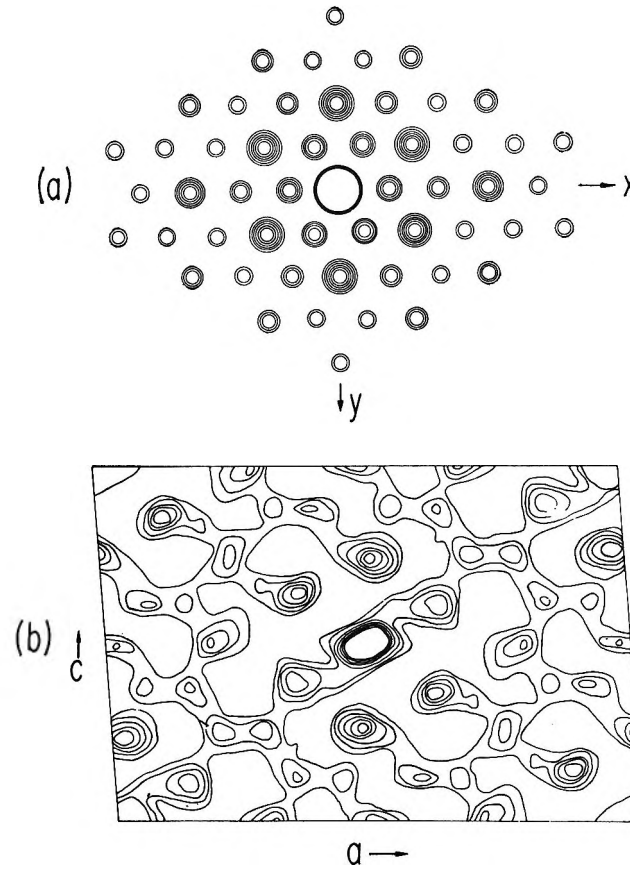

Figure 5. (a) The arrangement of peaks and their relative weights in the intramolecular vector pattern of the (idealized) perylene molecule. (b) The Patterson projection down [010] for perylene–PMDA. Contours are at equal but arbitrary intervals; the origin peak (center of the diagram) has been omitted.

few degrees but three possibilities remained for perylene. Calculation of intermolecular distances showed that only the molecular arrangement shown in Figure 6 (projection down [010]) was acceptable. The initial R factor for the $h0l$ reflections was 30% and this was refined by Fourier and difference syntheses to 25%. The y coordinates of the atoms were calculated assuming standard dimensions for both molecules; the angle between their (parallel) planes and (010) was calculated to be 18°. At this stage structure factors were calculated for all 1545 hkl reflections using $\langle B \rangle$ = 3.9 Å.^{2}, and $R(hkl)$ = 35% was obtained.

Refinement of Atomic Parameters

Further refinement was carried out by least squares, $\Sigma_{hkl} w(F_o - kF_c)^2$ being minimized. The weighing scheme originally suggested by Hughes[17] was used. At first, individual isotropic temperature factors were used for all atoms other than the hydrogens, which were omitted throughout. One cycle of refinement under these conditions reduced $R(hkl)$ to 27%. The diffuse scattering on the photographs suggested that the structure was subject to much thermal vibration and individual anisotropic temperature factors were therefore introduced at this stage. This meant that there were 167 paramerers to be adjusted, whereas the capacity of the 8K IBM 704 at our disposal was only 120 parameters. Accordingly, the refinement was carried out piecewise, three groups of six atoms being chosen at random for each cycle. For each group, the 54 positional and temperature paramerers were refined together with five scale factors. The mean values of the refined scale factors and the new atomic parameters were then used as input data for the next cycle. The values of $R(hkl)$ and $R_1(hkl)$ obtained for a series of cycles are given in Table III. After $R(hkl)$ had fallen to 17.6% all structure factors were printed out and some human errors in the preparation of the input data were

Table III: Variation of $R(hkl) = (\Sigma\Delta F/\Sigma F_o)$ and $R_1 = \sqrt{\Sigma w(\Delta F)^2/\Sigma w F_o^2}$ for a Series of Least-Squares Refinement Cycles with Anisotropic Temperature Factors

Cycle	$R(hkl)$, %	$R_1(hkl)$, %
Start	26.6	33.0
1	21.5	25.7
2	19.0	22.2
3	17.6	20.1
Refinement interrupted (see text)		
Start	15.1	19.2
1	14.5	18.5
2	14.4	18.1

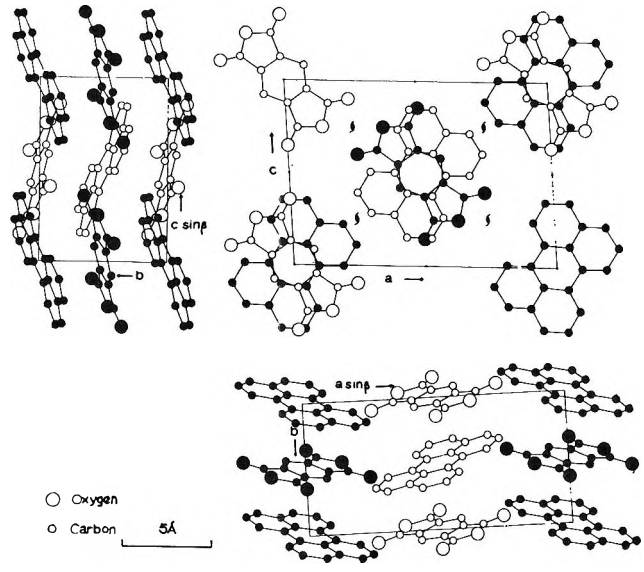

Figure 6. Arrangement of PMDA and perylene molecules in the unit cell as seen in projection down the three crystallographic axes.

corrected. Thirteen reflections suffering from extinction were given zero weight at this stage. An error in the most probable values assigned to the intensities of the 358 reflections with $I_{obsd} = 0$ was also corrected. Use of $^1/_3 I_{min}$ instead of $^1/_2 I_{min}$ led to an appreciable improvement in the agreement between $|F_{obsd}|$ and $|F_{calcd}|$ for these reflections. This change is in satisfying accord with theory.[18]

A three-dimensional difference synthesis was also calculated at this stage. There were no significant features as the excursions of the difference electron density did not exceed 0.3 electron Å.$^{-3}$. Failure to detect the hydrogen atoms can probably be ascribed to the relatively large thermal vibrations.

A new series of refinements was then carried out on the corrected data (lower part of Table III). The final atomic parameters and their standard deviations are given in Table V and observed and calculated structure factors (on an absolute scale) are listed in Table IV. When refinement was stopped, the shifts in atomic parameters were less than one-tenth of their standard deviations. It is noteworthy that the positional parameters changed very little during the refinement, the differences between a set of early coordinates and the final coordinates being summarized in Table VI. Thus the structure was essentially correct at $R \sim 30\%$ and the subsequent refinement to $R \sim 14\%$ consisted primarily in taking the thermal motion into account.

(17) E. W. Hughes, *J. Am. Chem. Soc.*, **63**, 1737 (1941).
(18) W. C. Hamilton, *Acta Cryst.*, **8**, 185 (1955).

Analysis of Thermal Motion. The thermal motion in the crystal was analyzed by the methods described by Cruickshank,[19,20] assuming that the molecules vibrated as rigid bodies and that intramolecular vibrations could be neglected. The translational tensor components T_{ij} and the librational tensor components ω_{ij} derived from the b_{ij} thermal-vibration parameters are given in Table VII. The standard deviations of these components were obtained by comparing observed and calculated values of U_{ij} (Table VIII) and are also given in Table VII. Separate sets of tensor components are given for each molecule and refer, of course, to the two different sets of molecular axes. For both molecules the off-diagonal terms are not significant and therefore the principal axes of the thermal motion coincide with the molecular axes within experimental error.

The translational and librational amplitudes of vibration of the two molecules are summarized in Table IX. The in-plane translations are rather larger than those perpendicular to the molecular planes, but the translational anisotropy is not large. Large errors are attached to the librational amplitudes about X and Y axes and their significance is in doubt. The librations in the molecular plane (*i.e.*, about the Z axis) are well established. As one might expect, the smaller PMDA molecule librates more than perylene. There may well be some interaction between the layer-line scale factors and the temperature factors concerned with vibration in the [010] direction because adjustment of intensities on different layers to an absolute scale was not done experimentally. However, interpretation of the thermal vibrations in terms of rigid-body molecular motions does lead to reasonable physical results. The main importance of this for the present paper is to allow correction of measured bond lengths for thermal libration effects.

Correction of Bond Lengths for Thermal Vibrations. The atomic coordinates of Table V must be corrected for apparent inward displacements due to thermal librations.[21,22] These corrections have been made by Cruickshank's revised method,[23] using a value of $q^2 = 0.1$ Å.^{2} to denote the breadth of the (assumed Gaussian) peaks. This value was taken from Cruickshank's results for anthracene,[21] as appropriate electron-density maps were not calculated during the course of the present structure determination. Uncorrected and corrected bond lengths are given in Table X; the changes are small and of the same size as the estimated standard deviations of the bond lengths. Revised values have not been calculated for the bond angles as allowance for thermal librations does not give improved values.[24]

Summary of Computing Procedures Used. These are listed in ref. 25, to which reference should be made for details. The accession numbers in the "World List" are given in parentheses to facilitate tracing the entries: correction of intensities, Stantec Zebra program by Smits and Boonstra (3017); Fourier-type calculations, IBM 704 program MIFR 1 by Shoemaker and Sly (118); Fourier transform, unpublished IBM 704 program by R. A. Clews; least-squares refinements, IBM 704 program ORXLS by Busing and Levy (12); processing of results, IBM 704 program ORXFE by Busing and Levy (13); best plane, Stantec Zebra program QCDS 10 by Morgan (not listed); atomic scattering factors, the values given by Berghuis, *et al.*,[26] for carbon and oxygen were used.

Results and Discussion

Molecular Dimensions of Perylene. These have been determined recently for perylene itself[27] and for perylene in the perylene–fluoranil molecular compound[7] so that adequate material for comparison with the present results is available. The perylene molecule is necessarily centrosymmetric in both molecular compounds but not in the polymorph[28] of perylene studied by Camerman and Trotter. However, in the latter case the deviations from centrosymmetry are not significant (except perhaps for bonds IH (1.428 ± 0.006 Å.) and I′N′ (1.406 ± 0.006 Å.)) and the dimensions have been averaged for convenience. The three sets of molecular dimensions are shown in Figure 7. The differences among the three sets of results are small, except for bonds CD and DE of the present structure. We have no explanation for this except that it may be due to systematic errors. The measured bond lengths in perylene have been compared[27] with various theoretical estimates.

The perylene molecule in perylene–PMDA is planar

(19) D. W. J. Cruickshank, *Acta Cryst.*, **9**, 747 (1956).

(20) D. W. J. Cruickshank, *ibid.*, **9**, 754 (1956).

(21) D. W. J. Cruickshank, *ibid.*, **9**, 915 (1956).

(22) E. G. Cox, D. W. J. Cruickshank, and J. A. Smith, *Proc. Roy. Soc.* (London), **A247**, 1 (1958).

(23) D. W. J. Cruickshank, *Acta Cryst.*, **14**, 896 (1961).

(24) W. R. Busing and H. A. Levy, *ibid.*, **17**, 142 (1964).

(25) "International Union of Crystallography World List of Crystallographic Computer Programs," 1st Ed., D. P. Shoemaker, Ed., 1962.

(26) J. Berghuis, IJ. M. Haanappel, M. Potters, B. O. Loopstra, C. H. MacGillavry, and A. L. Veenendaal, *Acta Cryst.*, **8**, 478 (1955).

(27) A. Camerman and J. Trotter, *Proc. Roy. Soc.* (London), **A279**, 129 (1964).

(28) J. Tanaka, *Bull. Chem. Soc. Japan*, **36**, 1237 (1963), has reported the crystal structure of another polymorph of perylene in which the molecular symmetry is C_i. However, the molecular dimensions were not determined with sufficient accuracy to warrant comparison with the other available results.

Table IV: Observed and Calculated Structure Factors for Perylene–PMDA

h	k	l	$\|F_o\|$	F_c
0	0	2	30.5	-43.5
3	0	-1	48.1	-72.3
3	0	-3	49.6	60.9
4	0	4	55.3	-74.0
4	0	-4	52.9	-73.2
1	1	-2	36.4	50.9
2	1	-1	32.9	52.5
0	2	1	66.0	-126.2
1	2	1	80.2	138.5
1	2	0	48.7	-69.9
2	2	1	63.0	-109.9
1	4	2	30.9	-72.9
2	4	1	41.5	-52.7
3	4	2	49.7	-65.7
0	0	10	13.7	-14.5
		8	37.2	44.5
		6	20.0	-18.4
		4	29.5	-25.4
1	0	11	1.4	- 0.3
		9	29.2	32.2
		7	18.1	-17.2
		5	4.8	- 3.6
		3	32.5	39.4
		-3	26.7	27.3
		-5	34.9	-27.3
		-7	9.1	-11.0
		-9	12.3	10.2
		-11	4.7	3.3
2	0	12	1.1	- 1.3
		10	12.3	-12.2
		8	30.2	35.6
		6	3.8	3.9
		4	22.7	-24.3
		2	17.6	-20.6
		- 2	37.5	-46.0
		- 4	39.6	-44.7
		- 6	13.2	15.6
		- 8	4.3	3.3
		-10	17.1	-19.7
		-12	3.1	- 2.3
3	0	11	3.6	2.5
		9	18.2	15.9
		7	11.0	- 8.0
		5	5.3	- 5.3
		3	17.3	-13.2
		1	17.0	-13.9
		- 5	46.5	-49.6
		- 7	6.6	- 5.6
		- 9	13.8	-14.6
		-11	6.6	6.1
4	0	12	6.8	- 5.9
		10	1.4	- 0.6
		8	19.2	18.0
		6	17.5	16.3
		2	3.3	1.1
		0	28.8	32.5
		- 2	29.4	24.0
		- 6	5.7	5.1
		- 8	4.0	- 2.3
		-10	7.3	- 5.9
		-12	5.5	- 5.5
5	0	11	1.2	0.3
		9	11.1	9.9
		7	7.8	7.6
		3	20.0	-20.5
		1	11.1	-10.4
		- 1	10.8	-10.4
		- 3	11.3	- 5.3
		- 5	17.0	-13.8
		- 7	1.3	2.2
		- 9	1.4	- 1.4
		-11	5.0	2.7
6	0	12	1.8	- 5.4
		10	1.4	- 0.9
		8	11.5	9.9
		6	13.3	14.0
		4	15.7	-10.3
		2	20.4	-22.1
		0	34.8	-34.8
		- 2	32.4	-24.3
		- 4	17.7	-16.4
		- 6	26.4	24.2
		- 8	10.3	9.2
		-10	6.2	- 7.2
		-12	6.0	- 6.2
7	0	11	1.0	- 1.5
		9	1.4	- 0.4
		7	1.4	0.3
		5	5.6	- 4.3
		3	8.2	- 6.4
		1	21.2	-21.2
		- 1	42.9	-48.9
		- 3	12.3	- 9.8
		- 5	16.7	16.6
		- 7	15.9	15.0
		- 9	10.3	- 9.6
		-11	1.2	- 0.7
8	0	10	2.4	1.8
		8	5.8	- 6.0
		6	4.8	- 5.9
		4	12.6	-12.9
		2	2.0	2.1
		0	5.8	- 4.6
		- 2	21.0	-18.9
		- 4	3.1	- 3.5
		- 6	9.6	9.6
		- 8	11.6	11.1
		-10	4.4	- 4.6
		-12	3.8	- 3.0
9	0	11	0.6	- 3.5
		9	1.3	0.5
		7	7.3	- 8.3
		5	4.8	3.8
		3	4.0	- 3.0
		1	25.9	26.6
		- 1	23.2	-26.0
		- 3	5.3	4.4
		- 5	16.3	17.1
		- 7	17.8	16.1
		- 9	6.1	- 5.3
		-11	3.4	4.4
10	0	10	0.9	- 1.2
		8	3.0	- 6.1
		6	2.8	0.3
		4	21.0	23.9
		2	5.8	4.1
		0	5.2	- 3.1
		- 2	7.5	7.7
		- 4	18.2	18.5
		- 6	20.5	23.5
		- 8	2.7	1.1
		-10	6.1	5.6
11	0	9	2.1	- 1.1
		7	4.9	- 5.1
		5	5.1	4.5
		3	20.0	20.8
		1	6.0	6.2
		- 1	10.1	10.6
		- 3	7.8	6.5
		- 5	21.3	24.8
		- 7	2.8	- 1.1
		- 9	4.3	- 0.6
		-11	3.2	- 2.8
12	0	8	1.1	- 2.9
		6	10.0	- 7.3
		4	7.2	4.5
		2	14.3	13.7
		0	13.0	14.5
		- 2	13.3	13.8
		- 4	11.0	-12.7
		- 6	1.4	0.8
		- 8	3.7	- 3.8
		-10	0.9	- 1.9
13	0	7	1.2	- 0.8
		5	10.3	-10.7
		3	6.0	6.7
		1	14.8	12.6
		- 1	6.4	4.8
		- 3	16.9	-17.1
		- 5	3.9	- 2.8
		- 7	6.0	- 6.8
		- 9	4.2	- 3.6
14	0	8	0.6	- 3.4
		6	2.3	0.9
		4	2.7	- 1.8
		2	4.8	4.7
		0	2.8	- 3.2
		- 2	11.8	-11.1
		- 4	1.4	- 1.7
		- 8	3.5	- 2.5
15	0	7	0.7	- 2.5
		5	1.1	1.0
		3	1.4	2.0
		1	1.4	- 0.2
		- 1	10.3	-10.3
		- 3	2.7	1.2
		- 5	3.7	1.4
		- 7	3.6	- 4.4
16	0	6	0.6	- 1.2
		4	2.1	- 1.8
		2	1.3	- 0.3
		0	1.4	- 0.1
		- 2	2.6	- 0.8
		- 4	4.3	- 1.2
		- 6	5.9	- 7.2
17	0	3	3.6	- 4.5
		1	1.1	- 0.9
		- 1	1.2	- 0.2
		- 3	1.1	- 2.6
		- 5	8.0	- 9.1
18	0	2	2.6	- 4.1
		0	3.1	- 3.7
		- 2	3.1	- 2.6
		- 4	4.2	- 5.1
0	1	12	0.9	0.7
		11	1.1	0.3
		10	10.6	- 9.1
		9	20.8	22.2
		8	13.7	14.6
		7	7.0	5.9
		6	3.3	- 3.6
		5	29.4	29.7
		4	8.5	4.2
		3	19.0	15.5
		2	26.8	-31.9
1	1	12	0.9	0.5
		11	1.1	- 0.2
		10	5.9	7.3
		9	8.1	- 7.3
		8	10.1	10.7
		7	1.1	0.4
		6	21.7	22.5
		5	10.5	- 8.1
		4	3.9	- 1.5
		3	1.7	5.3
		2	27.8	-35.0
		- 3	8.8	- 4.6
		- 4	10.1	9.4
		- 5	16.3	-17.2
		- 6	11.1	10.1
		- 7	5.1	2.7
		- 8	5.5	3.2
		- 9	6.9	- 5.9
		-10	9.3	10.7
		-11	1.2	0.9
		-12	0.9	- 0.3
2	1	12	0.9	- 0.7
		11	2.3	- 0.4
		10	4.2	- 3.0
		9	3.8	4.4
		8	6.4	- 6.6
		7	8.9	7.9
		6	4.8	- 3.4
		5	16.0	-18.0
		4	14.9	-14.8
		3	5.1	- 4.6
		2	43.1	51.1
		1	38.5	-44.2
		0	35.6	-43.4
		- 2	8.0	- 7.0
		- 3	35.4	-36.0
		- 4	24.7	-22.7
		- 5	2.8	0.2
		- 6	3.1	0.3
		- 7	5.8	- 6.1
		- 8	5.6	- 5.3
		- 9	15.8	18.1
		-10	3.5	3.1
		-11	4.0	- 3.6
		-12	0.9	- 0.4
3	1	12	1.7	- 1.4
		11	1.2	0.3
		10	1.2	- 0.4
		9	2.5	- 2.3
		8	6.4	- 7.0
		7	3.7	- 4.4
		6	14.0	-13.5
		5	0.9	0.9
		4	18.4	-14.3
		3	18.6	-15.1
		2	12.1	9.9
		1	31.2	34.5
		0	4.8	4.1
		- 1	11.8	-15.6
		- 2	40.1	-45.7
		- 3	3.0	- 0.1
		- 4	19.5	-20.4
		- 5	0.9	- 0.5
		- 6	4.8	- 4.8
		- 7	5.1	3.1
		- 8	10.8	10.9
		- 9	3.8	- 3.8
		-10	4.1	- 2.5
		-11	1.1	- 0.8
		-12	0.9	- 0.0
4	1	12	1.5	- 2.0
		11	1.1	- 0.7
		10	4.0	3.5
		9	7.0	- 6.4
		8	3.9	- 2.8
		7	9.0	- 8.8
		6	6.9	4.5
		5	16.9	-15.5
		4	0.9	1.1
		3	4.0	- 2.7
		2	22.3	-19.0
		1	18.8	18.3
		0	9.4	9.2
		- 1	21.6	-22.8
		- 2	29.9	26.5
		- 3	7.5	- 8.4
		- 4	21.5	19.6
		- 5	5.4	- 4.4
		- 6	12.7	-11.0
		- 7	10.1	9.4
		- 8	1.2	- 1.2
		- 9	6.6	- 5.8
		-10	1.3	- 1.3
		-11	1.2	- 0.9
		-12	1.8	0.9
5	1	12	1.4	- 2.8
		11	1.1	- 2.6
		10	1.2	0.6
		9	2.5	3.2
		8	13.7	-13.6
		7	2.3	- 1.4
		6	6.9	- 5.3
		5	5.0	2.4
		4	6.7	- 5.7
		3	2.8	- 3.9
		2	11.9	10.8
		1	8.8	8.9
		0	12.4	-12.4
		- 1	6.9	- 2.8
		- 2	25.8	24.3
		- 3	4.0	6.1
		- 4	25.8	23.9
		- 5	12.0	10.7
		- 6	7.5	- 6.5
		- 7	4.8	- 4.4
		- 8	12.6	-13.0
		- 9	6.8	- 7.4
		-10	3.9	- 5.0
		-11	1.2	0.5
		-12	2.5	2.6
6	1	11	1.0	- 0.0
		10	4.2	3.3
		9	11.1	-10.2
		8	6.6	- 6.4
		7	7.6	- 6.0
		6	2.3	- 0.2
		5	1.1	- 1.9
		4	10.4	7.9
		3	4.0	2.0
		2	4.2	4.3
		1	15.2	12.0
		0	8.7	- 9.0
		- 1	4.1	3.7
		- 2	6.9	- 6.2
		- 3	28.7	26.0
		- 4	8.0	- 7.6
		- 5	13.0	-11.6
		- 6	3.0	- 2.3
		- 7	8.8	- 8.2
		- 8	4.2	5.5
		- 9	17.7	-19.5
		-10	5.2	- 5.2
		-11	4.8	4.1
		-12	0.8	- 1.0
7	1	11	0.9	- 1.4
		10	1.1	0.6
		9	6.5	6.5
		8	14.5	-15.7
		7	2.5	- 3.2
		6	2.3	- 2.2
		5	7.6	- 5.6
		4	10.6	6.8
		3	0.9	- 2.0
		2	23.1	25.3
		1	20.2	21.2
		0	30.9	-34.2
		- 1	30.5	-31.7
		- 2	17.1	19.4
		- 3	0.9	- 0.2
		- 4	11.7	-11.8
		- 5	6.9	7.2
		- 6	3.2	- 4.2
		- 7	7.6	4.2
		- 8	23.0	-25.3
		- 9	5.6	- 5.2
		-10	3.3	2.7
		-11	1.1	1.4
		-12	0.8	0.2
8	1	11	2.0	1.4
		10	3.3	3.2
		9	5.7	- 6.8
		8	1.3	- 0.9
		7	1.3	0.4
		6	5.6	6.1
		5	1.1	- 0.1
		4	3.5	- 1.3
		3	11.1	9.2
		2	13.9	-14.1
		1	14.7	-14.2
		0	9.6	5.7
		- 1	4.6	1.5
		- 2	10.2	12.3
		- 3	8.2	- 9.5
		- 4	3.5	0.4
		- 5	13.4	11.6
		- 6	6.1	6.8
		- 7	16.8	-17.9
		- 8	4.1	3.4
		- 9	5.6	- 5.8
		-10	1.2	- 1.6
		-11	2.0	- 1.7
		-12	2.6	- 3.3
9	1	10	3.0	2.5
		9	5.9	5.9
		8	3.5	- 1.6
		7	2.5	- 0.1
		6	4.2	4.5
		5	1.2	- 0.1
		4	12.8	11.9
		3	8.5	8.7
		2	11.9	-10.6
		1	1.0	1.0
		0	11.1	- 8.4
		- 1	0.9	- 1.6
		- 2	13.0	15.2
		- 3	1.1	0.9
		- 4	20.5	20.5
		- 5	15.0	15.7
		- 6	5.4	- 5.9
		- 7	1.3	- 1.0
		- 8	9.2	- 8.7
		- 9	1.2	- 0.7
		-10	1.1	0.6
		-11	0.9	1.1
10	1	10	2.6	- 1.4
		9	1.1	1.6
		8	1.2	- 0.4
		7	5.1	6.9
		6	1.3	- 0.5
		5	9.4	9.8
		4	7.6	7.6
		3	7.7	8.5
		2	7.2	6.3
		1	5.9	- 5.2
		0	5.1	- 3.5
		- 1	16.7	14.5
		- 2	0.9	- 1.2
		- 3	1.1	- 1.2
		- 4	14.9	-15.0
		- 5	23.6	24.8
		- 6	14.4	14.8
		- 7	8.8	- 8.6
		- 8	1.3	1.0
		- 9	3.4	1.9
		-10	1.1	- 0.4
		-11	0.8	- 0.7
11	1	9	0.9	- 0.3
		8	1.1	3.0
		7	1.2	0.3
		6	1.3	1.6
		5	10.0	-11.5
		4	20.5	24.3
		3	14.2	14.6
		2	1.2	- 0.5
		1	3.3	- 3.4
		0	1.1	- 1.8
		- 1	10.0	- 8.9
		- 2	16.0	-16.1
		- 3	11.4	-11.4
		- 4	19.6	23.3
		- 5	6.5	6.2
		- 6	1.3	0.7
		- 7	1.3	- 0.7
		- 8	5.4	5.2
		- 9	1.1	0.5
		-10	4.8	- 4.1
12	1	9	0.7	0.4
		8	2.7	- 2.0
		7	3.3	2.3
		6	3.5	2.6
		5	5.5	5.7
		4	10.0	-10.2
		3	9.6	9.8
		2	1.2	0.8
		1	9.5	-11.3
		0	3.9	- 3.7
		- 1	18.9	-20.6
		- 2	1.2	1.2
		- 3	1.2	1.7
		- 4	5.4	- 6.3
		- 5	12.9	14.2
		- 6	1.3	0.6
		- 7	1.3	3.0
		- 8	1.2	0.9
		- 9	5.9	- 6.8
		-10	2.5	- 3.0
13	1	8	1.6	- 0.9
		7	2.9	- 1.7
		6	2.3	1.3
		5	1.2	- 0.6
		4	4.0	4.9
		3	3.5	- 1.6
		2	10.9	-12.4
		1	1.3	0.9
		0	19.0	-20.7
		- 1	1.2	- 1.8
		- 2	1.3	- 2.1
		- 3	1.3	0.7
		- 4	11.7	13.6
		- 5	1.3	- 0.4
		- 6	5.5	- 3.7
		- 7	3.4	- 3.4
		- 8	4.7	- 3.8
		- 9	0.9	1.1
14	1	8	0.4	- 2.3
		7	0.9	- 0.9
		6	1.1	- 0.9
		5	1.2	1.9
		4	3.4	1.9
		3	6.7	- 5.9
		2	3.5	3.1
		1	11.1	-11.3
		0	5.6	5.2
		- 1	6.7	- 7.2
		- 2	5.6	- 5.9
		- 3	8.1	8.5
		- 4	1.3	- 0.9
		- 5	6.5	- 5.1
		- 6	1.2	- 0.7
		- 7	1.1	- 1.0
		- 8	4.3	3.5
		- 9	2.2	- 1.8
15	1	7	0.6	- 3.3
		6	0.9	- 0.9
		5	1.0	- 1.2
		4	1.1	0.4
		3	5.4	3.8
		2	1.2	- 2.0
		1	4.4	4.2
		0	3.7	- 3.8
		- 1	1.2	- 0.4
		- 2	1.2	- 0.2
		- 3	3.5	- 3.1
		- 4	4.3	- 3.6
		- 5	1.2	1.5
		- 6	1.1	- 0.8
		- 7	0.9	1.0
		- 8	2.3	1.5
16	1	5	0.8	- 0.9
		4	0.9	- 1.5
		3	1.1	0.8
		2	1.1	- 0.0
		1	3.3	2.3
		0	2.4	2.2
		- 1	1.2	- 2.2
		- 2	1.2	1.1
		- 3	1.2	- 2.4
		- 4	1.1	1.6
		- 5	1.0	- 0.1
		- 6	0.9	- 0.9
		- 7	3.8	2.4
17	1	4	1.4	- 1.1
		3	2.4	- 1.9
		2	1.9	0.8
		1	1.0	- 1.2
		0	1.1	0.9
		- 1	1.1	1.8
		- 2	1.0	1.4
		- 3	3.2	3.0
		- 4	1.8	2.0
		- 5	0.8	- 0.2
		- 6	1.2	- 1.2
18	1	2	1.3	- 0.3
		1	0.8	1.0
		0	0.8	0.0
		- 1	2.7	3.4
		- 2	0.8	0.3
		- 3	3.7	4.6
		- 4	0.7	1.3
0	2	12	3.4	- 3.1
		11	7.5	7.5
		10	1.4	0.3
		9	15.8	-18.2
		8	19.1	20.2
		7	21.1	24.9
		6	20.7	-21.2
		5	11.8	10.5
		4	7.8	5.6
		3	14.4	15.5
		2	22.8	24.2
1	2	12	6.0	- 5.8
		11	3.7	- 4.2
		10	9.4	- 9.2
		9	10.4	10.6
		8	18.6	19.4
		7	9.8	10.0
		6	3.2	- 3.1
		5	7.2	- 5.6
		4	4.8	- 6.1
		3	21.1	-22.6
		2	22.2	-21.6
		1	13.7	15.3
		- 1	32.6	-39.2
		- 3	18.0	-13.9
		- 4	29.6	30.2
		- 5	25.8	-25.8
		- 6	1.2	4.9
		- 7	21.0	23.9
		- 8	20.0	-22.4
		- 9	5.4	- 6.0
		-10	4.2	- 3.9
		-11	2.7	- 4.5
		-12	6.4	7.1
2	2	12	5.8	- 5.4
		11	4.5	3.6
		10	9.5	10.3
		9	19.7	-22.9
		8	10.2	9.0
		7	17.0	16.2
		6	8.2	- 7.2
		5	15.3	15.9
		3	23.9	-28.3
		2	16.1	17.3
		0	31.0	34.9
		- 1	26.5	31.9
		- 2	16.4	-17.2
		- 3	22.7	21.9
		- 5	22.1	-20.6
		- 6	19.7	-21.6
		- 7	9.2	- 8.4
		- 8	7.6	6.1
		- 9	8.0	8.5
		-10	5.1	- 5.5
		-11	6.9	- 6.0
		-12	4.6	- 4.4

Table IV (*Continued*)

h	k	l	$\|F_o\|$	F_c
3	2	12	6.3	- 6.2
		11	6.9	- 6.3
		10	5.1	- 5.0
		9	12.8	13.7
		8	12.6	10.7
		7	8.2	6.9
		6	4.3	- 3.6
		5	3.6	2.6
		4	17.7	-17.2
		3	36.2	-42.5
		2	8.3	- 7.4
		1	26.9	30.8
		0	23.1	24.8
		- 1	12.8	-13.7
		- 2	25.2	-30.3
		- 3	3.4	- 3.9
		- 4	26.5	26.3
		- 5	24.1	-22.3
		- 6	13.9	-13.4
		- 7	2.7	1.9
		- 8	1.4	2.1
		- 9	11.4	-12.5
		-10	5.3	- 5.5
		-11	1.3	- 1.5
		-12	8.9	9.1
4	2	12	3.6	- 3.8
		11	1.2	- 1.7
		10	6.1	5.6
		9	10.2	- 9.6
		8	6.6	6.1
		7	7.2	5.8
		6	4.3	3.8
		5	27.3	31.8
		4	13.6	-10.4
		3	23.5	-22.8
		2	14.7	-13.8
		1	10.3	- 9.7
		0	24.7	-25.4
		- 1	8.8	9.7
		- 2	21.1	21.7
		- 3	20.6	24.0
		- 4	32.4	-33.2
		- 5	23.0	-26.1
		- 6	6.8	- 5.0
		- 7	10.4	9.2
		- 8	6.4	- 5.4
		- 9	11.0	10.5
		-10	1.4	1.2
		-11	1.3	- 0.5
		-12	5.7	- 6.0
5	2	11	3.4	- 2.9
		10	4.6	- 4.6
		9	7.0	6.9
		8	1.6	1.5
		7	12.1	10.6
		6	4.5	5.5
		5	14.4	-12.9
		4	15.3	16.2
		3	10.0	- 7.7
		2	3.9	- 3.3
		1	3.7	- 3.6
		0	15.4	-17.2
		- 1	11.2	- 9.1
		- 2	34.7	-33.7
		- 3	31.3	-33.6
		- 4	19.2	20.9
		- 5	7.2	- 4.3
		- 6	11.3	9.8
		- 7	8.0	6.7
		- 8	6.7	7.0
		- 9	1.5	- 0.8
		-10	6.1	- 6.2
		-11	3.5	- 3.9
		-12	5.4	4.6
6	2	11	2.0	- 2.1
		10	2.6	2.7
		9	7.1	- 6.6
		8	4.5	4.0
		7	5.2	- 5.3
		6	2.8	2.4
		5	14.8	13.7
		4	12.7	-12.8
		3	3.0	- 2.0
		2	8.9	- 8.4
		1	12.8	-11.3
		0	11.8	-13.1
		- 1	17.2	-15.3
		- 2	23.2	-21.0
		- 3	9.1	10.7
		- 4	14.9	-13.7
		- 5	9.5	- 8.0
		- 6	9.5	9.0
		- 7	7.5	5.3
		- 8	8.0	7.2
		- 9	4.9	5.1
		-10	1.5	- 2.6
		-11	1.2	- 0.1
		-12	3.7	- 3.6
7	2	11	1.7	- 1.8
		10	1.3	- 1.6
		9	3.9	4.1
		8	4.9	- 3.8
		7	1.6	1.1
		6	6.3	- 6.7
		5	8.5	- 6.6
		4	2.5	- 2.8
		3	12.3	-13.9
		2	8.2	8.9
		1	13.9	-10.3
		0	23.2	24.0
		- 1	18.6	-15.6
		- 2	9.3	- 9.5
		- 3	15.1	-15.7
		- 4	7.8	- 9.0
		- 5	11.7	10.4
		- 6	1.3	- 1.6
		- 7	12.1	10.5
		- 8	8.0	8.6
		- 9	1.5	- 0.8
		-10	4.6	- 3.3
		-11	3.8	- 3.7
		-12	2.0	1.7
8	2	10	3.2	- 1.9
		9	1.4	1.2
		8	1.4	0.0
		7	5.0	- 4.6
		6	4.8	- 5.6
		5	4.6	2.4
		4	1.3	- 1.0
		3	6.7	4.8
		2	8.3	- 7.5
		1	16.0	16.9
		0	9.6	- 6.0
		- 1	13.6	11.1
		- 2	18.2	-16.9
		- 3	1.2	- 0.6
		- 4	7.5	7.3
		- 5	6.2	- 4.9
		- 6	15.3	16.1
		- 7	1.4	1.4
		- 8	4.2	2.7
		- 9	7.6	8.0
		-10	2.6	- 2.4
		-11	3.8	3.3
9	2	10	1.9	- 2.3
		9	2.5	- 2.7
		8	2.8	2.4
		7	4.8	- 5.5
		6	1.6	- 0.7
		5	2.8	- 2.3
		4	12.3	12.4
		3	11.8	12.4
		2	1.3	- 0.7
		1	1.2	0.8
		0	18.2	17.7
		- 1	13.5	-11.6
		- 2	3.8	- 3.3
		- 3	6.0	4.5
		- 4	3.8	3.4
		- 5	12.8	13.0
		- 6	5.2	6.7
		- 7	15.5	15.8
		- 8	7.8	7.4
		- 9	2.8	- 3.4
		-10	2.4	- 2.3
10	2	9	2.2	1.6
		8	2.7	- 3.7
		7	1.4	- 1.3
		6	1.5	- 1.0
		5	6.7	- 4.2
		4	4.0	2.9
		3	12.1	10.7
		2	18.4	19.2
		1	1.3	1.2
		0	7.1	- 5.9
		- 1	7.1	6.0
		- 2	9.3	8.3
		- 3	6.1	5.1
		- 4	10.3	10.4
		- 5	2.8	- 2.7
		- 6	17.8	18.6
		- 7	1.5	0.6
		- 8	2.9	- 3.0
		- 9	1.4	- 1.7
		-10	3.2	2.9
		-11	2.6	2.7
11	2	9	1.9	- 3.0
		8	1.3	2.1
		7	1.4	- 2.3
		6	5.4	- 5.9
		5	4.2	5.0
		4	9.5	-10.8
		3	6.7	5.1
		2	5.1	4.2
		1	9.7	7.7
		0	11.8	11.3
		- 1	10.2	10.0
		- 2	5.8	4.5
		- 3	12.4	12.6
		- 4	16.4	-20.3
		- 5	8.3	7.0
		- 6	1.6	- 2.3
		- 7	1.5	0.7
		- 8	1.4	- 1.9
		- 9	2.4	1.5
		-10	2.0	- 1.9
12	2	8	3.0	- 3.1
		7	1.3	0.6
		6	1.5	0.3
		5	10.3	-10.6
		4	4.2	2.9
		3	5.4	- 5.6
		2	7.0	7.2
		1	6.1	3.7
		0	10.9	10.6
		- 1	2.8	- 2.4
		- 2	5.2	4.6
		- 3	5.2	- 4.9
		- 4	3.0	1.9
		- 5	13.1	-14.1
		- 6	1.5	- 0.5
		- 7	1.4	- 0.5
		- 8	2.6	- 3.5
		- 9	3.6	- 2.6
		-10	3.4	- 2.3
13	2	7	5.0	- 4.6
		6	3.7	3.5
		5	1.4	1.5
		4	7.9	- 7.7
		3	4.8	5.1
		2	6.3	- 3.6
		1	7.0	7.3
		0	5.0	- 5.5
		- 1	5.0	4.4
		- 2	3.0	- 2.0
		- 3	11.0	-11.7
		- 4	6.2	- 5.1
		- 5	1.5	1.1
		- 6	3.9	4.0
		- 7	4.6	- 4.7
		- 8	1.2	- 1.6
		- 9	1.8	- 2.2
14	2	6	5.0	- 5.0
		5	2.6	2.8
		4	1.4	2.8
		3	5.0	- 3.7
		2	5.4	6.1
		1	4.1	- 3.2
		0	1.5	1.4
		- 1	2.9	- 2.8
		- 2	10.2	-11.2
		- 3	6.3	4.5
		- 4	1.4	- 0.9
		- 5	5.2	4.2
		- 6	2.7	- 3.2
		- 7	1.2	- 1.6
		- 8	3.5	- 3.8
15	2	5	2.2	- 1.6
		4	1.3	- 1.9
		3	1.4	1.4
		2	2.8	- 2.5
		1	1.4	- 0.8
		0	4.9	4.9
		- 1	4.0	- 4.6
		- 2	4.0	2.5
		- 3	1.4	- 1.8
		- 4	1.4	0.2
		- 5	1.3	- 2.2
		- 6	1.7	- 1.6
		- 7	3.9	- 4.3
		- 8	2.3	2.3
16	2	4	2.0	- 1.0
		3	3.2	- 3.6
		2	1.3	- 1.8
		1	1.3	0.6
		0	3.7	- 4.4
		- 1	2.7	3.6
		- 2	1.3	- 0.7
		- 3	1.3	- 2.1
		- 4	1.2	- 0.6
		- 5	2.2	- 2.2
		- 6	5.2	- 6.1
17	2	3	2.4	- 2.6
		2	2.8	- 2.7
		1	1.1	- 2.4
		0	2.2	- 1.0
		- 1	2.3	- 2.7
		- 2	3.2	- 1.9
		- 3	2.1	- 1.7
		- 4	1.0	0.8
		- 5	4.3	- 5.5
18	2	- 1	1.7	- 1.5
		- 2	1.6	- 2.3
0	3	12	1.0	1.3
		11	6.3	5.7
		10	8.1	- 8.1
		9	3.2	- 0.8
		8	6.7	6.5
		7	10.5	11.3
		6	6.6	7.0
		5	3.7	3.7
		4	4.3	- 0.7
		3	15.4	14.0
		2	20.9	-22.9
		1	16.9	-19.2
1	3	11	6.8	- 6.1
		10	8.5	9.5
		9	3.2	- 0.5
		8	1.7	- 2.9
		7	10.6	-10.0
		6	11.5	10.0
		5	6.4	- 6.2
		4	5.9	- 7.3
		3	21.1	-21.3
		2	19.5	17.3
		1	11.5	11.5
		0	24.5	-26.4
		- 1	6.8	- 3.0
		- 2	9.9	9.4
		- 3	13.2	-11.1
		- 4	4.6	- 3.0
		- 5	20.4	-19.4
		- 6	1.3	0.9
		- 7	10.3	- 9.8
		- 8	14.6	13.3
		- 9	1.7	- 1.2
		-10	3.1	4.1
		-11	1.3	0.9
		-12	1.0	- 0.1
2	3	11	2.5	2.8
		10	8.1	- 8.9
		9	4.5	4.2
		8	8.5	- 7.6
		7	4.3	1.8
		6	10.0	- 8.3
		5	3.5	- 3.8
		4	13.2	- 9.1
		3	20.8	-20.6
		2	6.5	6.5
		1	18.9	17.3
		0	6.0	- 6.4
		- 1	7.6	5.3
		- 2	8.7	- 9.1
		- 3	1.0	- 2.3
		- 4	27.2	-32.1
		- 5	1.3	0.8
		- 6	1.4	0.7
		- 7	5.3	4.7
		- 8	11.3	-12.2
		- 9	6.8	7.2
		-10	3.1	3.5
		-11	1.3	- 0.6
		-12	1.0	- 1.5
3	3	11	3.4	- 3.7
		10	4.3	3.7
		9	1.6	- 0.7
		8	1.7	0.5
		7	10.8	-11.6
		6	6.8	- 6.0
		5	4.6	- 4.0
		4	6.2	- 6.6
		3	15.1	14.6
		2	32.2	-31.2
		1	10.1	- 8.3
		0	30.5	36.3
		- 1	7.8	- 8.6
		- 2	10.7	-10.0
		- 3	2.0	- 2.1
		- 4	11.0	9.9
		- 5	9.2	9.2
		- 6	7.6	- 7.5
		- 7	7.1	- 7.6
		- 8	13.3	13.3
		- 9	3.2	- 3.3
		-10	5.4	- 6.0
		-11	2.6	- 2.9
		-12	1.0	- 1.8
4	3	11	3.2	- 2.8
		10	1.5	- 1.9
		9	1.6	1.4
		8	4.6	- 3.2
		7	11.7	-11.3
		6	5.2	4.9
		5	7.2	- 5.5
		4	6.3	- 5.0
		3	2.2	1.2
		2	11.2	- 0.9
		1	2.6	3.4
		0	4.6	3.2
		- 1	20.7	-16.6
		- 2	19.4	18.4
		- 3	5.8	4.4
		- 4	16.4	18.3
		- 5	12.3	9.3
		- 6	2.9	- 2.0
		- 7	1.6	- 0.8
		- 8	7.7	- 7.8
		- 9	8.2	- 5.9
		-10	5.3	- 6.2
		-11	2.5	- 2.5
		-12	4.3	4.3
5	3	11	2.1	0.1
		10	2.8	- 3.5
		9	4.5	5.7
		8	8.4	- 7.7
		7	7.0	- 7.3
		6	11.0	-11.5
		5	4.9	3.0
		4	5.3	2.5
		3	5.3	- 4.4
		2	10.0	7.2
		1	15.3	15.8
		0	6.2	4.0
		- 1	4.3	0.9
		- 2	18.0	-17.8
		- 3	15.0	14.4
		- 4	3.4	- 2.3
		- 5	2.7	- 0.9
		- 6	5.1	5.4
		- 7	5.4	- 4.5
		- 8	3.2	- 2.8
		- 9	6.5	- 6.6
		-10	8.8	- 9.9
		-11	2.5	- 2.9
6	3	10	4.6	3.4
		9	1.6	- 1.2
		8	1.7	- 1.8
		7	11.5	-13.1
		6	1.6	1.4
		5	6.6	- 5.5
		4	1.3	- 1.2
		3	12.2	10.2
		2	3.9	2.5
		1	8.1	7.0
		0	6.3	7.5
		- 1	16.0	-15.4
		- 2	21.2	-20.4
		- 3	13.9	14.2
		- 4	5.7	4.1
		- 5	4.9	- 4.8
		- 6	3.0	- 1.4
		- 7	6.2	- 7.2
		- 8	1.7	0.7
		- 9	8.3	- 7.9
		-10	8.0	- 7.9
		-11	1.1	1.3
7	3	10	5.3	- 5.2
		9	7.6	7.4
		8	1.6	- 1.4
		7	5.6	- 5.5
		6	1.6	1.0
		5	3.1	3.8
		4	2.9	- 2.1
		3	1.3	- 0.2
		2	1.3	- 2.1
		1	4.2	4.2
		0	5.6	0.6
		- 1	22.7	-26.8
		- 2	11.4	11.5
		- 3	1.3	4.1
		- 4	6.0	- 5.4
		- 5	6.6	5.1
		- 6	5.4	4.2
		- 7	13.1	14.2
		- 8	11.9	-14.2
		- 9	7.3	- 8.9
		-10	1.4	- 1.6
		-11	2.1	- 0.9
8	3	10	5.6	5.5
		9	3.9	- 2.9
		8	4.3	2.4
		7	3.2	- 1.9
		6	1.7	3.5
		5	6.9	6.9
		4	3.0	- 2.2
		3	16.2	16.3
		2	9.4	8.4
		1	21.6	-19.2
		0	13.0	-12.9
		- 1	9.4	8.8
		- 2	7.7	8.5
		- 3	7.6	8.4
		- 4	5.1	4.0
		- 5	6.8	2.9
		- 6	18.4	21.4
		- 7	13.6	-14.4
		- 8	1.6	- 0.9
		- 9	1.6	0.7
		-10	1.3	- 0.8
		-11	1.0	1.1
9	3	10	3.7	- 3.9
		9	4.1	4.5
		8	3.0	2.1
		7	3.2	2.4
		6	3.2	3.6
		5	4.7	- 1.5
		4	7.3	6.8
		3	9.3	9.5
		2	8.0	7.4
		1	13.4	10.3
		0	1.4	0.6
		- 1	2.8	- 2.7
		- 2	2.9	- 3.1
		- 3	1.5	- 0.8
		- 4	6.8	- 5.8
		- 5	11.0	12.3
		- 6	7.3	6.9
		- 7	11.9	13.6
		- 8	5.3	- 5.3
		- 9	1.5	- 1.9
		-10	1.2	- 1.5
		-11	2.5	- 3.0
10	3	9	2.1	- 0.8
		8	1.4	- 1.4
		7	3.2	1.9
		6	1.6	0.6
		5	4.6	2.3
		4	3.2	2.2
		3	10.7	10.8
		2	15.0	17.4
		1	3.0	- 2.8
		0	7.4	- 8.3
		- 1	1.5	- 1.6
		- 2	7.9	- 7.2
		- 3	1.6	1.3
		- 4	11.0	-10.2
		- 5	1.7	- 1.4
		- 6	16.0	18.9
		- 7	1.6	- 1.1
		- 8	1.6	0.1
		- 9	1.3	2.0
		-10	1.1	1.1
11	3	8	1.2	2.5
		7	2.9	- 2.4
		6	7.5	7.5
		5	4.6	- 5.2
		4	4.6	- 3.9
		3	8.9	9.6
		2	3.2	3.1
		1	5.3	- 4.9
		0	1.6	- 0.7
		- 1	11.0	-11.0
		- 2	7.6	- 7.0
		- 3	18.5	-22.3
		- 4	10.1	9.0
		- 5	13.0	14.4
		- 6	1.6	1.7
		- 7	1.6	- 0.2
		- 8	1.3	0.2
		- 9	1.2	1.1
12	3	8	2.7	- 2.8
		7	2.5	- 0.8
		6	6.8	- 6.5
		5	11.1	12.7
		4	1.6	- 1.1
		3	4.6	- 3.6
		2	3.2	- 1.6
		1	6.6	- 6.2
		0	8.9	- 8.1
		- 1	11.8	-12.8
		- 2	7.8	- 8.2
		- 3	13.6	14.5
		- 4	5.3	- 3.9
		- 5	1.6	1.8
		- 6	1.6	0.7
		- 7	1.6	- 0.8
		- 8	1.3	- 0.7
		- 9	2.9	- 1.8
13	3	7	3.0	- 2.4
		6	1.3	1.5
		5	7.9	- 8.8
		4	6.8	5.9
		3	3.2	3.1
		2	5.4	- 5.3
		1	1.7	1.3
		0	8.4	- 8.9
		- 1	3.2	2.1
		- 2	4.6	- 4.6
		- 3	9.1	-10.6
		- 4	8.9	9.1
		- 5	1.6	0.3
		- 6	1.6	0.6
		- 7	2.7	- 2.8
		- 8	3.2	- 3.4
14	3	6	3.0	- 4.4
		5	2.5	1.8
		4	1.3	- 0.6
		3	1.6	- 2.7
		2	7.2	7.6
		1	7.4	- 7.9
		0	7.5	6.8
		- 1	1.6	- 1.5
		- 2	4.3	- 5.6
		- 3	4.4	3.6
		- 4	4.4	- 3.6
		- 5	2.9	- 1.5
		- 6	1.3	- 2.4
		- 7	2.3	- 1.9
		- 8	4.8	5.3
15	3	5	1.1	- 2.1
		4	3.4	- 3.8
		3	4.3	4.0
		2	4.8	- 5.6
		1	8.1	8.2
		0	1.6	- 2.0
		- 1	1.6	- 2.1
		- 2	4.2	4.2
		- 3	1.5	- 2.6
		- 4	2.8	- 1.9
		- 5	3.6	1.9
		- 6	1.1	0.2
		- 7	2.9	2.4
16	3	4	1.0	1.0
		3	3.7	- 3.1
		2	1.2	1.1
		1	3.6	- 3.9
		0	2.6	2.3
		- 1	1.3	1.9
		- 2	1.3	0.0
		- 3	1.3	1.1
		- 4	3.9	4.8
		- 5	1.1	0.7
		- 6	2.2	- 1.0

Table IV (*Continued*)

h	k	l	$\|F_o\|$	F_c
17	3	2	1.0	0.6
		1	1.1	0.5
		0	1.1	- 1.2
		- 1	1.1	2.5
		- 2	1.1	0.3
		- 3	3.2	4.1
		- 4	2.3	1.7
0	4	11	3.1	- 1.6
		10	4.0	3.3
		9	1.6	- 1.7
		8	4.6	- 5.5
		7	21.8	23.1
		6	1.5	1.4
		5	14.2	-14.9
		4	6.6	6.7
		3	12.2	11.7
		2	12.4	10.3
		1	5.4	- 6.1
1	4	11	5.1	- 5.4
		10	6.6	- 6.9
		9	1.6	- 0.2
		8	1.7	- 0.9
		7	9.6	8.1
		6	16.5	15.4
		5	1.4	- 1.1
		4	12.9	12.9
		3	9.6	-10.6
		1	31.7	33.5
		0	4.7	3.2
		- 1	11.6	10.7
		- 2	1.0	- 0.8
		- 3	15.1	-16.5
		- 4	8.8	8.8
		- 5	6.4	- 6.2
		- 6	25.0	-31.1
		- 7	14.2	16.2
		- 8	5.6	5.8
		- 9	5.5	- 4.9
		-10	4.1	- 3.6
		-11	8.2	- 8.6
2	4	11	9.7	-10.5
		10	10.2	10.2
		9	1.5	0.5
		8	5.6	- 4.9
		7	14.5	13.6
		6	1.5	- 2.1
		5	2.7	- 1.8
		4	5.1	5.2
		3	21.6	-22.9
		2	38.5	42.0
		0	6.4	- 7.0
		- 1	6.9	1.2
		- 2	3.3	3.3
		- 3	7.6	5.3
		- 4	1.3	2.0
		- 5	10.7	11.3
		- 6	5.1	- 4.7
		- 7	25.7	-29.0
		- 8	4.6	- 5.3
		- 9	1.6	2.1
		-10	2.8	2.3
		-11	2.2	1.8
3	4	11	1.0	- 0.4
		10	13.6	-15.3
		9	2.6	2.3
		8	4.5	4.0
		7	7.6	6.0
		6	11.4	10.9
		5	7.0	6.4
		4	13.2	12.5
		3	2.2	0.7
		1	24.1	21.9
		0	8.4	9.9
		- 1	3.7	2.4
		- 2	6.3	5.7
		- 3	20.5	-18.5
		- 4	5.8	3.4
		- 5	10.0	- 9.8
		- 6	17.2	-18.6
		- 7	8.5	7.4
		- 8	10.0	11.2
		- 9	1.6	0.1
		-10	2.8	- 2.4
		-11	7.8	- 8.5
4	4	11	5.6	- 7.1
		10	7.1	7.2
		9	1.6	- 1.4
		8	3.2	- 2.2
		7	5.6	3.3
		6	1.5	0.2
		5	2.9	4.0
		4	8.7	9.3
		3	1.3	1.2
		2	13.3	8.7
		1	3.6	0.5
		0	22.5	-27.0
		- 1	17.1	-23.7
		- 2	18.1	-16.1
		- 3	9.6	7.8
		- 4	4.6	1.4
		- 5	5.7	- 3.9
		- 6	3.2	- 4.6
		- 7	6.4	6.2
		- 8	4.5	- 5.1
		- 9	3.1	2.9
		-10	1.5	3.0
		-11	5.2	4.8
5	4	10	8.7	- 8.9
		9	1.5	1.2
		8	1.6	- 1.6
		7	1.7	0.9
		6	11.4	10.6
		5	6.6	- 4.8
		4	1.4	1.7
		3	7.4	- 6.3
		2	7.7	- 7.2
		1	11.8	-10.8
		0	3.1	- 0.9
		- 1	9.8	7.9
		- 2	4.0	- 2.0
		- 3	32.8	-33.7
		- 4	6.4	- 6.6
		- 5	4.1	- 3.2
		- 6	1.5	2.9
		- 7	1.7	0.9
		- 8	13.9	14.1
		- 9	6.3	6.8
		-10	1.4	0.1
		-11	9.2	- 9.7
6	4	10	3.0	4.0
		9	2.7	- 2.9
		8	3.0	3.3
		7	3.1	- 1.3
		6	14.6	-14.2
		5	8.6	7.1
		4	2.9	- 5.1
		3	5.6	- 4.4
		2	2.6	- 1.7
		1	2.5	- 1.5
		0	4.3	- 4.4
		- 1	7.2	- 5.8
		- 2	17.8	-16.9
		- 3	8.6	8.8
		- 4	6.7	- 6.1
		- 5	3.0	- 2.8
		- 6	3.1	- 2.6
		- 7	7.2	6.6
		- 8	1.6	2.0
		- 9	3.0	2.6
		-10	1.3	1.3
		-11	3.0	2.9
7	4	10	5.3	- 5.4
		9	1.3	2.1
		8	4.3	- 3.2
		7	1.6	1.5
		6	3.2	2.5
		5	11.8	-11.6
		4	5.2	4.3
		3	2.9	- 3.1
		2	2.8	1.3
		1	2.7	- 1.2
		0	5.4	4.6
		- 1	9.5	8.2
		- 2	6.2	7.2
		- 3	16.9	-16.5
		- 4	5.1	- 4.5
		- 5	3.0	2.2
		- 6	3.2	2.6
		- 7	8.7	8.2
		- 8	7.7	7.6
		- 9	5.9	5.7
		-10	1.3	2.3
8	4	9	4.6	- 4.6
		8	2.8	2.7
		7	1.5	- 2.2
		6	6.2	- 5.5
		5	1.7	1.1
		4	3.1	- 2.1
		3	12.9	14.1
		2	2.9	1.4
		1	13.2	13.1
		0	6.3	- 5.3
		- 1	9.1	6.8
		- 2	10.4	- 8.8
		- 3	1.5	- 2.9
		- 4	11.4	12.8
		- 5	1.7	- 1.5
		- 6	10.8	11.2
		- 7	10.4	10.9
		- 8	1.6	2.3
		- 9	1.4	2.5
		-10	2.1	- 2.0
9	4	9	1.1	- 1.5
		8	1.3	- 1.4
		7	1.6	- 1.2
		6	1.6	- 0.6
		5	5.6	- 4.2
		4	1.7	0.8
		3	1.5	1.4
		2	17.1	17.9
		1	5.2	- 4.2
		0	14.9	11.8
		- 1	2.9	- 1.1
		- 2	6.0	4.4
		- 3	8.3	8.2
		- 4	1.7	- 0.6
		- 5	9.1	8.2
		- 6	1.7	- 1.2
		- 7	6.3	5.5
		- 8	8.1	8.4
		- 9	1.3	- 0.9
		-10	1.0	0.7
10	4	8	2.2	- 1.8
		7	1.5	0.3
		6	3.1	- 3.0
		5	1.6	0.5
		4	5.6	- 4.4
		3	6.4	- 7.3
		2	5.6	3.3
		1	16.0	16.5
		0	1.5	0.2
		- 1	9.6	8.0
		- 2	7.3	7.2
		- 3	5.6	3.9
		- 4	7.2	5.8
		- 5	11.8	-11.0
		- 6	6.4	4.0
		- 7	5.4	4.9
		- 8	3.9	- 4.1
		- 9	3.2	- 2.9
11	4	7	1.3	0.2
		6	4.0	- 4.0
		5	1.6	- 0.4
		4	3.2	- 3.4
		3	1.6	- 0.1
		2	3.2	- 2.3
		1	1.7	- 1.1
		0	9.1	8.1
		- 1	8.5	7.6
		- 2	1.7	0.2
		- 3	7.6	8.2
		- 4	9.0	- 8.9
		- 5	1.6	- 1.1
		- 6	7.1	- 7.6
		- 7	1.5	- 1.4
		- 8	2.4	- 2.0
		- 9	1.0	0.6
12	4	7	2.8	- 2.8
		6	4.4	4.7
		5	5.0	- 5.2
		4	3.1	1.2
		3	4.5	- 4.5
		2	1.6	1.4
		1	1.7	3.2
		0	3.2	2.4
		- 1	1.7	- 1.4
		- 2	3.1	3.8
		- 3	14.0	-14.8
		- 4	5.5	4.9
		- 5	7.4	- 6.6
		- 6	1.5	1.5
		- 7	1.3	0.8
		- 8	1.1	- 0.6
13	4	6	5.9	- 6.5
		5	5.8	5.7
		4	4.0	- 3.0
		3	3.0	2.9
		2	1.5	- 1.4
		1	1.6	3.3
		0	4.5	- 4.4
		- 1	1.6	0.9
		- 2	3.1	- 3.4
		- 3	4.3	3.3
		- 4	8.3	- 9.0
		- 5	1.5	1.6
		- 6	2.6	2.9
		- 7	1.2	- 1.7
		- 8	2.7	- 4.0
14	4	5	4.1	- 5.1
		4	3.4	3.8
		3	4.7	- 4.9
		2	1.5	2.8
		1	4.2	- 4.4
		0	5.3	4.6
		- 1	1.6	2.6
		- 2	5.2	- 5.1
		- 3	1.5	- 2.1
		- 4	2.7	1.3
		- 5	2.5	2.1
		- 6	3.1	- 3.4
		- 7	1.7	- 2.2
15	4	4	3.2	- 3.7
		3	2.2	1.9
		2	4.2	- 5.0
		1	1.3	- 0.8
		0	1.4	- 1.0
		- 1	3.8	- 3.4
		- 2	5.3	5.3
		- 3	1.3	- 2.5
		- 4	1.2	0.5
		- 5	3.5	- 3.5
16	4	2	1.9	- 2.4
		1	1.1	0.4
		0	3.7	- 5.3
		- 1	1.1	1.0
		- 2	3.0	- 3.4
		- 3	1.1	- 1.2
		- 4	1.8	- 1.5

to within experimental error, the mean molecular plane being given by

$$0.2163u + 0.9271v - 0.3063w = 0$$

The orthogonal set of coordinates u, v, w are related to the fractional coordinates x, y, z of the atoms in terms of the monoclinic unit cell by

$$u = xa + zc \cos \beta$$

$$v = yb$$

$$w = zc$$

The perylene molecule is essentially planar in perylene–fluoranil, but there are significant deviations from planarity in perylene itself which have been ascribed to intermolecular effects.

Molecular Dimensions of PMDA. The present results are shown in Figure 8. The structures of PMDA itself and of phthalic anhydride have not been determined so that the dimensions of the PMDA molecule found here must be compared with those of benzene[22,29] and maleic anhydride. The correction of the original set of molecular dimensions of maleic anhydride[30] for the effects of thermal libration are described in the Appendix. The bond lengths in the central benzene ring in PMDA are very close to those in benzene itself but two of the three independent bond angles within the ring differ significantly from 120°, the largest difference (5.7°) being at C1. The dimensions of the five-membered rings in PMDA are very similar to those of maleic anhydride (Figure 8). The correspondence between the bond angles is particularly close, the pentagonal rings being nearly regular in both molecules and the C=O bonds being bent outwards in the same way. The pattern of bond lengths is similar but detailed comparison is complicated by (a) the significant differences found between the lengths of symmetry-related C—O and C=O bonds in PMDA, for which no explanation can be offered, and (b) the differences in the two pentagonal rings (ethylenic C=C in maleic anhydride and aromatic C—C in PMDA).

(29) G. E. Bacon, N. A. Curry, and S. A. Wilson, *Proc. Roy. Soc.* (London), **A279**, 98 (1964).

(30) R. E. Marsh, E. Ubell, and H. E. Wilcox, *Acta Cryst.*, **15**, 35 (1962).

Table V: Fractional Atomic Coordinates (before Correction for Effects of Thermal Librations) and Final Thermal Vibration Parameters. (The Anisotropic Temperature Factors of the Atoms Are Given by $T = \exp[-(h^2\beta_{11} + k^2\beta_{22} + l^2\beta_{33} + 2hk\beta_{12} + 2hl\beta_{13} + 2kl\beta_{23})]$. The Standard Deviations Are Given below Each Value)

	u	v	w	β_{11}	β_{22}	β_{33}	β_{12}	β_{13}	β_{23}
C_A	−0.07988	0.06877	0.24042	0.00837	0.00985	0.00781	0.00303	0.00466	0.00200
	0.00043	0.00104	0.00048	0.00036	0.00241	0.00046	0.00067	0.00032	0.00076
C_B	−0.03015	0.14132	0.35060	0.01207	0.02480	0.00595	0.00728	0.00321	0.00217
	0.00056	0.00126	0.00049	0.00056	0.00307	0.00047	0.00096	0.00039	0.00084
C_C	0.06104	0.18038	0.34605	0.00996	0.01936	0.00607	0.00372	−0.00091	−0.00282
	0.00050	0.00119	0.00047	0.00045	0.00277	0.00044	0.00084	0.00034	0.00079
C_D	0.10546	0.15103	0.22546	0.00699	0.01774	0.00863	0.00388	−0.00190	−0.00268
	0.00042	0.00113	0.00052	0.00032	0.00272	0.00051	0.00070	0.00031	0.00088
C_E	0.19630	0.19225	0.21931	0.00678	0.02360	0.01580	0.00410	−0.00300	−0.00357
	0.00046	0.00132	0.00071	0.00035	0.00301	0.00081	0.00078	0.00042	0.00118
C_F	0.23840	0.16038	0.10607	0.00427	0.01866	0.01905	−0.00075	−0.00249	0.00392
	0.00037	0.00121	0.00073	0.00025	0.00283	0.00088	0.00063	0.00037	0.00120
$C_{G'}$	−0.18976	−0.08623	0.00755	0.00533	0.02397	0.01521	0.00166	0.00190	0.00137
	0.00041	0.00128	0.00067	0.00028	0.00290	0.00077	0.00069	0.00036	0.00111
$C_{H'}$	−0.09669	−0.04461	0.00688	0.00346	0.01209	0.00772	0.00162	0.00169	0.00190
	0.00029	0.00093	0.00043	0.00019	0.00217	0.00042	0.00046	0.00022	0.00067
C_I	0.05274	0.07395	0.11168	0.00481	0.00595	0.00613	0.00306	0.00018	0.00062
	0.00032	0.00091	0.00041	0.00022	0.00207	0.00037	0.00048	0.00022	0.00062
C_J	−0.04054	0.03455	0.12336	0.00511	0.01658	0.00441	0.00232	0.00234	0.00184
	0.00032	0.00096	0.00038	0.00023	0.00237	0.00034	0.00053	0.00022	0.00063
$C_{1'}$	0.07774	0.57178	0.08204	0.00381	0.01089	0.00767	0.00123	0.00007	0.00134
	0.00030	0.00093	0.00043	0.00020	0.00224	0.00041	0.00048	0.00022	0.00068
C_2	−0.08267	0.48231	0.04879	0.00283	0.01189	0.00671	0.00093	0.00116	0.00110
	0.00026	0.00086	0.00039	0.00017	0.00218	0.00037	0.00042	0.00019	0.00063
C_3	−0.00894	0.55310	0.12774	0.00457	0.00975	0.00571	0.00182	0.00177	0.00070
	0.00031	0.00092	0.00040	0.00021	0.00211	0.00035	0.00047	0.00022	0.00060
C_4	−0.16138	0.47598	0.12832	0.00475	0.02010	0.01667	0.00382	0.00526	0.00660
	0.00037	0.00116	0.00066	0.00026	0.00277	0.00076	0.00060	0.00036	0.00106
C_5	−0.04079	0.58933	0.25856	0.00985	0.02098	0.00554	0.00547	0.00190	−0.00015
	0.00049	0.00118	0.00046	0.00043	0.00271	0.00044	0.00080	0.00033	0.00077
O_6	−0.23931	0.41709	0.09923	0.00494	0.03164	0.02831	0.00236	0.00577	0.00860
	0.00028	0.00097	0.00061	0.00022	0.00222	0.00094	0.00052	0.00037	0.00108
O_7	−0.13537	0.54484	0.25094	0.00969	0.02258	0.01264	0.00508	0.00837	0.00277
	0.00034	0.00078	0.00041	0.00030	0.00188	0.00047	0.00057	0.00032	0.00071
O_8	−0.00210	0.64979	0.35565	0.01678	0.01908	0.00653	0.00454	0.00195	−0.00478
	0.00044	0.00085	0.00037	0.00050	0.00220	0.00039	0.00075	0.00033	0.00065

Table VI: Summary of Differences in Positional Coordinates between Those for Which $R(hkl) = 30\%$ ($\langle B \rangle = 3.9$ Å.^{2}) and the Final Coordinates

Fractional coordinates	Maximum	Mean
x	0.0069	0.0016
y	0.0039	0.0012
z	0.0045	0.0013

Two comments are, however, warranted. First, the C–C bonds external to the central ring have values only a little shorter than the length of 1.479 Å. proposed for the single bond between two trigonally hybridized carbon atoms.[31] From this we infer that there is not

Table VII: Elements of the Translational (T) and Librational (ω) Thermal Motion Tensors[a] and Their Standard Deviations. The Tensors Are Symmetric; Different Sets of Axes Are Used for the Two Molecules

	Perylene				PMDA			
ij	T_{ij}	$\sigma(T_{ij})$	ω_{ij}	$\sigma(\omega_{ij})$	T_{ij}	$\sigma(T_{ij})$	ω_{ij}	$\sigma(\omega_{ij})$
11	4.89	0.43	6.60	5.27	3.90	0.32	9.86	2.02
22	3.57	0.52	6.97	2.77	2.72	0.24	10.59	4.21
33	2.22	0.81	16.19	1.93	1.93	0.42	33.35	1.30
12	0.58	0.39	−1.38	1.58	0.53	0.23	−1.00	1.01
23	0.29	0.54	−3.31	2.08	0.54	0.25	1.94	1.79
13	0.24	0.46	1.38	2.71	0.01	0.33	1.08	1.38

[a] T_{ij} in 10^{-2} Å.^{2}; ω_{ij} in deg.^{2}.

Table VIII: Observed and Calculated Values (in 10^{-2} Å.^{2}) of Atomic Thermal Vibration Parameters Referred to the Appropriate Molecular Axes. The Calculated Values Are Obtained from the Translational and Vibrational Tensors of Table VII, Thus Assuming That Only Rigid-Body Molecular Motions Occur

	U_{11}		U_{22}		U_{33}		U_{12}		U_{23}		U_{13}	
	Obsd.	Calcd.	Obsd.	Calcd.	Obsd.	Calcd.	Obsd.	Calcd.	Obsd.	Calcd.	Obsd.	Calcd.
A	8.296	7.789	5.196	4.622	2.412	3.828	0.238	2.326	−0.399	0.352	−1.023	0.348
B	9.166	7.858	9.233	7.534	4.868	5.102	5.705	4.032	0.878	0.813	1.252	0.691
C	4.681	5.693	10.329	9.866	4.913	3.221	3.071	2.830	1.119	1.381	0.104	0.630
D	4.283	4.889	8.823	7.679	4.384	3.991	−1.776	0.581	2.019	1.126	0.225	0.238
E	6.074	5.557	5.700	9.975	6.085	5.285	−0.895	−1.487	3.098	1.772	−0.058	−0.242
F	7.411	7.646	8.225	7.827	4.423	5.235	−3.776	−2.844	0.234	1.448	0.119	−0.698
G	8.706	7.794	5.567	4.721	5.943	3.933	−0.344	−1.246	0.712	0.677	−0.139	−0.384
H	5.368	5.663	2.976	3.752	2.701	2.668	0.438	0.115	0.253	0.383	0.093	0.077
I	4.145	4.889	5.028	4.584	1.162	2.659	1.094	0.581	0.902	0.493	−0.124	0.238
J	5.293	5.643	3.485	3.849	3.664	2.642	2.164	1.038	−0.061	0.304	0.709	0.267
1	4.361	3.899	4.444	4.891	2.482	2.616	−0.008	0.545	0.237	0.419	0.167	0.010
2	4.216	5.253	2.741	3.219	2.821	2.534	−0.423	−0.286	0.154	0.543	0.107	0.015
3	5.511	5.304	2.814	3.218	2.344	2.450	0.745	1.370	0.235	0.489	−0.220	−0.084
4	11.271	10.413	3.818	4.116	3.896	4.476	−2.707	−2.478	0.372	0.562	0.321	0.025
5	9.787	10.515	5.278	4.001	4.576	4.112	3.722	3.467	0.716	0.376	0.822	−0.374
6	13.894	12.891	7.334	8.203	6.975	6.747	−5.799	−6.485	0.449	0.453	−0.034	−0.239
7	15.110	15.344	2.448	2.728	5.338	5.328	0.824	0.268	0.462	0.554	−0.908	−0.344
8	12.873	13.400	9.146	7.643	5.719	5.888	7.416	7.373	0.805	0.480	−1.629	−0.695

Table IX: Root-Mean-Square Amplitudes of Translation and Libration in Perylene–PMDA, Referred to Molecular Axes[a]

	R.m.s. amplitudes of vibration	
	PMDA	Perylene
Translation in X direction	0.20 ± 0.02 Å.	0.22 ± 0.02 Å.
Translation in Y direction	0.16 ± 0.02 Å.	0.19 ± 0.02 Å.
Translation in Z direction	0.14 ± 0.02 Å.	0.15 ± 0.03 Å.
Libration about X axis	3.1 ± 1.4°	2.6 ± 2.3°
Libration about Y axis	3.3 ± 2.1°	2.6 ± 1.7°
Libration about Z axis	5.8 ± 1.1°	4.0 ± 1.4°

[a] Note that different axes were used for the two molecules. Estimated standard deviations are also given.

Table X: Bond Lengths (in Å.) before and after Correction for Thermal Libration Effects

Bond	Uncorrected	Corrected
A–B	1.383	1.386
B–C	1.366	1.369
C–D	1.445	1.448
D–E	1.366	1.368
E–F	1.364	1.367
F–G	1.407	1.410
G–H	1.393	1.396
H–I	1.423	1.428
I–J	1.407	1.412
I–D	1.443	1.446
J–A	1.381	1.384
H–J′	1.493	1.498
1–2	1.388	1.396
2–3	1.385	1.393
2–4	1.458	1.462
3–5	1.463	1.467
3–1′	1.390	1.398
4–7	1.362	1.367
5–7	1.414	1.419
4–6	1.228	1.230
5–8	1.176	1.178

much conjugation between central ring and anhydride groups. Secondly, the value of 1.23 ± 0.01 Å. for d(C=O) is at the top of the range of values reported for this distance recently (the largest reported value is 1.237 ± 0.003 Å. in duroquinone).[32] The other value obtained here, 1.18 ± 0.01 Å., is less than the shortest value reported, 1.19 ± 0.01 for maleic anhydride (Figure 8).

The six-membered and five-membered ring systems are not coplanar. The mean plane through the six-membered ring (referred to the same orthogonal coordinate system as was used for perylene) is given by

$$-0.2112u + 0.9286v - 0.3051w = 3.334$$

The deviations of the atoms from this plane are

(31) M. J. S. Dewar and H. N. Schmeising, *Tetrahedron*, **5**, 166 (1959).

(32) F. L. Hirshfeld, D. Rabinovich, G. M. J. Schmidt, and E. Ubell, *Acta Cryst.*, **16**, A57 (1963). We exclude from consideration the value of 1.260 ± 0.004 Å. reported in cytosine monohydrate (G. A. Jeffrey and Y. Kinoshita, *ibid.*, **16**, 20 (1963)) because this carbonyl group is involved in three hydrogen bonds and is thus in a different environment.

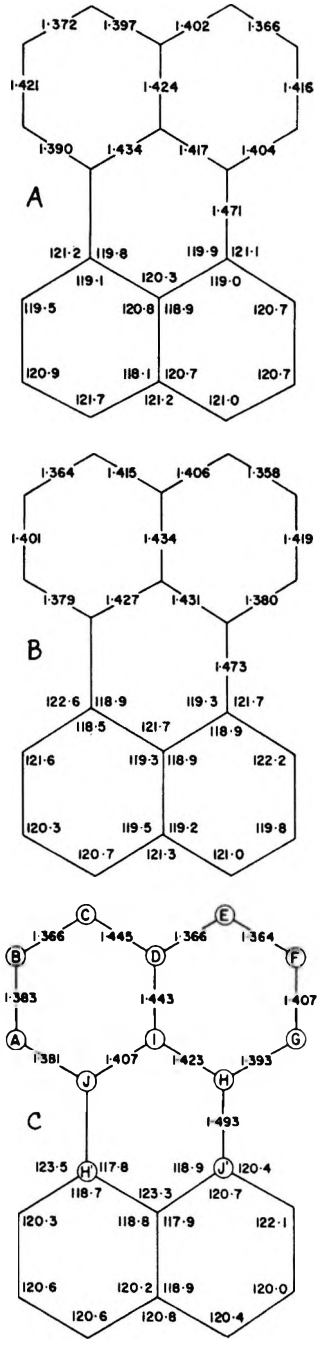

Figure 7. Comparison of the results obtained in three determinations of the molecular dimensions of perylene: (A) Camerman and Trotter,[27] after averaging σ(C–C) ~ 0.005 Å.; σ(C–C–C) ~ 0.4°; (B) Hanson[7]: σ(C–C) ~ 0.005 Å.; σ(C–C–C) ~ 0.5°; (C) present paper: σ(C–C) ~ 0.01 Å.; σ(C–C–C) ~ 0.6°.

shown in Figure 9 and are well beyond experimental error. Their significance is considered below in the discussion of the molecular arrangement, but we note here that the increase in the length of $C_4{=}O_6$ may be due to the fact that it is appreciably bent out of the plane of the rest of the molecule.

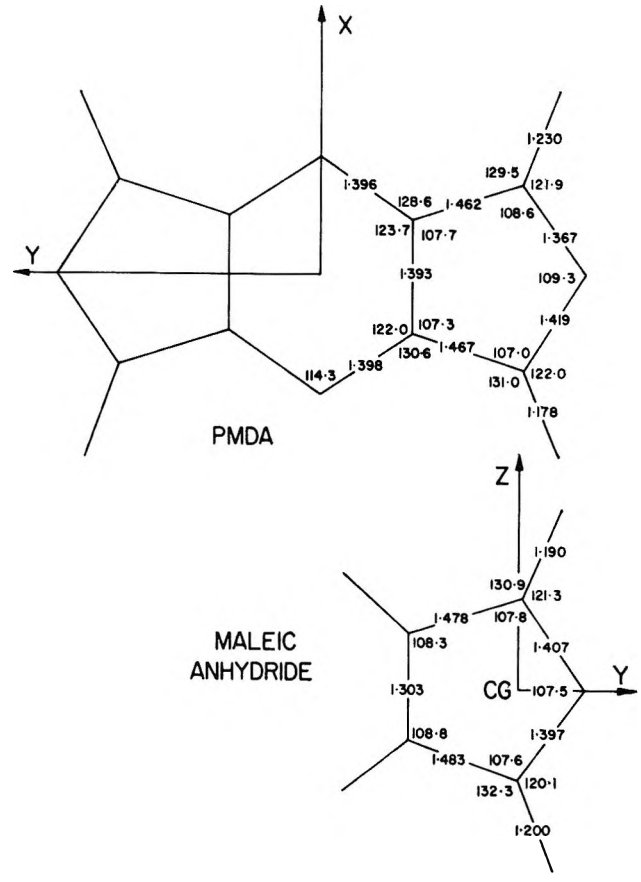

Figure 8. Comparison of molecular dimensions of PMDA with those reported for maleic anhydride (after correction of atomic positions for effects of thermal librations). CG denotes position of molecular center of gravity.

Molecular Arrangement

The two components are arranged in alternating sequence in stacks of almost parallel and almost planar molecules (Figure 6). Similar mixed stacks have been found in all of the crystalline molecular compounds of this general type that have been studied so far. The stack axes lie along [010] and any one stack (*e.g.*, that at ($^1/_2$, —, $^1/_2$)) is surrounded by six others in quasi-hexagonal array. Four of these neighboring stacks (those at (0, —, 0), (1, —, 0), (0, —, 1), (1, —, 1)) are derived from the reference stack by the action of the screw axes parallel to [010], *i.e.*, they are displaced by $^1/_2b$ along the stack axis and differ in orientation. The other two stacks (those at ($^1/_2$, —, $\bar{1}/_2$) and ($^1/_2$, —, $1^1/_2$)) are identical with the reference stack. The shortest C···C and C···O approaches between molecules in different stacks are 3.69 and 3.39 Å., respectively, indicating only van der Waals forces between

Table XI: Interplanar Distances in Some Crystals Containing Molecular Stacks, Layers, or Pairs

Category	Substance	Packing type	Distance between adjacent molecules or molecular layers, Å.	Ref.
(a) One-component crystals	Graphite	Layer	3.35	*a*
	1,12-Benzperylene	Pairs	3.38	*b*
	Coronene	Stacks	3.40	*c*
	Ovalene	Stacks	3.45	*d*
	Perylene	Pairs	3.47	*e*
	α-Phenazine	Stacks	3.49	*f*
	Pyrene	Pairs	3.52	*g*
(b) π-Addition compounds	Perylene–fluoranil		3.23	7
	Anthracene–PMDA		3.23	This paper
	Tetramethyl-*p*-phenylenediamine–chloranil		3.26	10
	Anthracene–1,3,5-trinitrobenzene		3.28	8
	Indole–1,3,5-trinitrobenzene	Mixed stacks	3.29	9
	Skatole–1,3,5-trinitrobenzene		3.30	
	Tetramethyl-*p*-phenylenediamine–bromanil		3.31	10
	Perylene–PMDA		3.33	This paper
	Naphthalene–1,3,5-trinitrobenzene		3.35	10
(c) Various pyrimidine derivatives	Perdeuteriovioluric acid monohydrate	Flat sheets	3.109 ± 0.001	*h*
	Barbituric acid dihydrate	Flat sheets	3.12	*i*
	Dilituric acid trihydrate	Almost flat sheets	3.22	*j*
	Addition complex of 1-methylthymine and 9-methyladenine	Flat sheets	3.276 ± 0.001	*k*

[a] J. B. Nelson and D. P. Riley, *Proc. Phys. Soc.* (London), **57**, 447 (1945). [b] J. G. White, *J. Chem. Soc.*, 1398 (1948). [c] J. M. Robertson and J. G. White, *ibid.*, 607 (1945). [d] D. M. Donaldson and J. M. Robertson, *Proc. Roy. Soc.* (London), **A220**, 157 (1953). [e] D. M. Donaldson, J. M. Robertson, and J. G. White, *ibid.*, **A220**, 311 (1953). [f] F. H. Herbstein and G. M. J. Schmidt, *Acta Cryst.*, **8**, 406 (1955). [g] J. M. Robertson and J. G. White, *J. Chem. Soc.*, 358 (1947). [h] B. M. Craven and Y. Mascarenhas, *Acta Cryst.*, **17**, 407 (1964). [i] G. A. Jeffrey, S. Ghose, and J. O. Warwicker, *ibid.*, **14**, 881 (1961). [j] B. M. Craven, S. Martinez-Carrera, and G. A. Jeffrey, *ibid.*, **17**, 891 (1964). [k] K. Hoogsteen, *ibid.*, **16**, 907 (1963).

different stacks. Perylene–fluoranil[7] has the same space group as perylene–PMDA but the stack axes lie along [001] instead of [010]. Nevertheless, the same quasi-hexagonal arrangement of stacks is found, two neighboring stacks being identical with the reference stack while the other four are shifted by $^1/_2c$ along the stack axis and differ in orientation. The relative shift of neighboring stacks is not always found: for example, in naphthalene–PMDA[1] there is also a quasi-hexagonal arrangement of stacks, two being identical with the reference stack while the other four differ in orientation but are not shifted along the stack axis relative to the reference stack.

The molecular arrangement seen in projection onto the plane of the perylene molecule is shown in Figure 10. The relative arrangement of two successive molecules in a stack is something like that in graphite but the resemblance is not as close as in anthracene–PMDA (Figure 4). Graphite-like arrangements are found in a number of other π-addition compounds (anthracene,[8] skatole, and indole[9] with 1,3,5-trinitrobenzene) but not in perylene–fluoranil[7] and naphthalene–1,3,5-trinitrobenzene.[10] The distance between the two parallel planes describing the perylene molecule and the benzene ring of PMDA is 3.33 Å., which is compared with some other interplanar distances in Table XI and is discussed below.

One anhydride portion of a PMDA molecule is tilted down toward the perylene molecule *below* it so that atoms A and 4 and J and 2 approach to 3.31 and 3.34 Å., respectively (Figure 10). Atoms D and 1′ are 3.35 Å. apart. The other anhydride group of this PMDA molecule is tilted upward (the PMDA molecule is centrosymmetric) toward the perylene molecule *above* it in the stack, the close approaches now being between 4′ and A′ and 2′ and J′. This suggests that the strongest interaction between the two components occurs between the anhydride groups of PMDA, on the one hand, and the region about atoms A and A′ of perylene.

General Discussion

Mulliken[33] has emphasized that theoretical calculations of the relative stabilities of various postulated arrangements of the components of charge-transfer

(33) R. S. Mulliken, *Rec. trav. chim.*, **75**, 845 (1956).

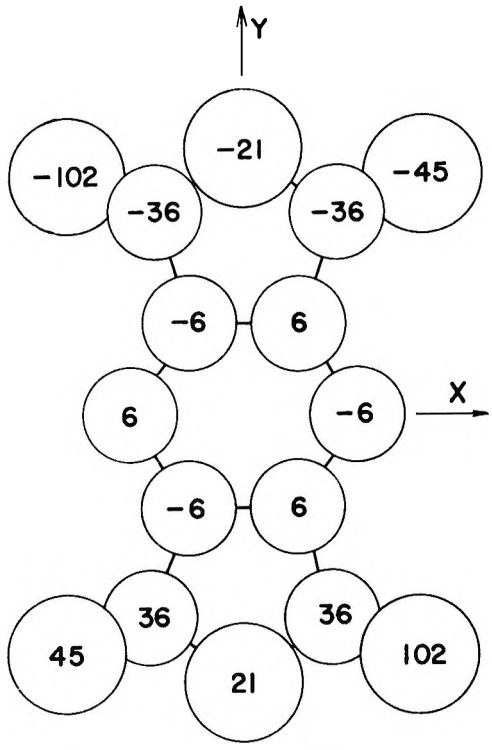

Figure 9. Displacements (in Å. × 10^3) of the atoms in the PMDA molecule from the plane through the central benzene ring. The axial system is the same as in Figures 2 and 8.

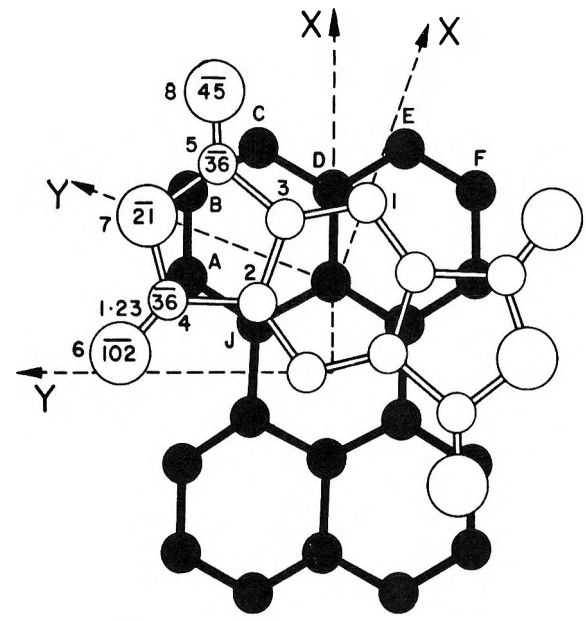

Figure 10. The molecular arrangement seen in projection onto the plane of the perylene molecule. The nomenclature of atoms and axes is the same as in previous figures. The displacements (in Å. × 10^3) of some atoms from the plane through the benzene ring of the PMDA molecule are shown. The PMDA molecule is 3.33 Å. above the perylene molecule.

compounds must include van der Waals and electrostatic contributions to the total interaction energy as well as that due to specific charge-transfer effects. Detailed calculations are likely to be difficult, but one can obtain a qualitative assessment of the relative importance of the latter contribution by comparing the molecular arrangements in the addition compounds with those in one-component systems. Stacking of planar molecules one above the other, with their planes inclined to the stack axis, is found in many one-component crystals. However, the fact that these stacks are mixed in the π-addition compounds, rather than segregated as in the addition complex of hexabromobenzene and 1,2,4,5-tetrabromobenzene,[34] is direct evidence of a special interaction between the components of the π-addition compounds. Further evidence of this interaction is given, as Wallwork[10] has pointed out, by the somewhat shorter interplanar distances that are found in the π-addition compounds compared to graphite and various aromatic hydrocarbons (Table XI). (However, one notes that naphthalene–1,3,5-trinitrobenzene seems anomalous in this respect.) The interactions between superposed molecules in the π-addition compounds seem to be rather weaker than those in various pyrimidine derivatives where rather shorter interplanar distances are found (see Table XI). Electrostatic interactions between superposed molecules are presumably much more important in the latter group than in the π-addition compounds.

One must next inquire what factors determine the relative orientation of adjacent donor and acceptor molecules within a stack. Here one may anticipate contributions both from the variation of the charge-transfer interaction with orientation and from any localized interaction that may occur between the two components. The first type of contribution has had some theoretical attention.[2,35] However, it seems unlikely that the results of Aono's calculations on the hypothetical benzene self-complex will be applicable to π-addition compounds such as those listed in Table XI, where the relative importance of the charge-transfer interactions would be expected to be much greater than in the benzene self-complex. Unfortunately, calculations for actual donor–acceptor pairs are lacking and it is thus not possible at present to assess the role of the delocalized interactions in determining the orientations of the components.

There is some experimental evidence for the occurrence of localized interactions between particular re-

(34) G. Gafner and F. H. Herbstein, *J. Chem. Soc.*, 5290 (1964).
(35) S. Aono, *Progr. Theoret. Phys.* (Kyoto), **20**, 133 (1958).

gions of donor and acceptor molecules, but there have not been any theoretical treatments of this aspect of the problem and quantitative estimates of interaction energies are lacking. The first pointer to the occurrence of localized interactions is that the component molecules in the same stack are not always exactly parallel. This nonparallelism may manifest itself in different ways: for example, in perylene–fluoranil the individually planar molecules are inclined to each other at 1.8°. Hanson[7] comments, "The effect of nonparallelism is to increase the minimum distance of the fluorine atoms from the plane of the overlapping perylene molecule (in the region of overlap) by 0.08 Å. to 3.31 Å. and to decrease the corresponding distance for fluoranil carbon atoms by 0.04 Å. to 3.19 Å. This result is consistent both with F–C repulsion and C–C attraction." In anthracene–trinitrobenzene, the anthracene molecules are inclined by about 8° to the plane of the aromatic ring of the trinitrobenzene, alternate anthracene molecules in a stack being inclined and orientated in directions related by a twofold axis of symmetry. The situation in perylene–PMDA described earlier in this paper is somewhat similar although here it is only the inclinations of the five-membered rings of the PMDA molecules that differ. The second indication comes from the observation that in the molecular compounds of skatole and indole with 1,3,5-trinitrobenzene an unsubstituted carbon atom of the trinitrobenzene molecule lies directly above the nitrogen atom of the second component in both instances, and Hanson[9] has concluded that these carbons and nitrogen atoms "play a decisive role in the intermolecular binding." In the perylene–fluoranil and perylene–PMDA molecular compounds, similar regions of the perylene molecule are involved in the close approaches between the two components and it may be significant that atom A has the highest free valence index of all the atoms of perylene.[36]

Thus it is clear that the newer crystallographic results support earlier conclusions about the existence of a specific (presumably charge-transfer) interaction operating between donor and acceptor molecules in a direction approximately normal to their planes. However, not enough is yet known about the detailed operation of this charge-transfer interaction, nor of possible localized interactions, to explain the experimental results for the relative orientations of component molecules.

A final note of warning is required. The above discussion is entirely in terms of factors affecting the energy of interaction and thus it is tacitly assumed that the relative molecular orientations are the same at room temperature as at absolute zero. This assumption may be invalidated in two ways: polymorphic changes may occur below room temperature or the room-temperature structure may be disordered. Polymorphic changes between 100 and 300°K. have been found for perylene–PMDA (see above) but not for anthracene–PMDA and anthracene–1,3,5-trinitrobenzene.[8] Information is not available for the other addition compounds discussed here nor about the behavior of any addition compounds below about 100°K. An order–disorder transformation has been found[37] in pyrene–PMDA at about 210°K. Below this temperature the pyrene molecules take up two orientations, separated by about 12° of arc, with respect to the PMDA molecules; above 210°K., the pyrene molecules appear to be distributed at random over these two orientations (some minor differences have been ignored in this brief description). Only an average relative orientation of pyrene and PMDA molecules can be inferred from the results of the structure analysis of the disordered phase. The disorder in the room temperature structure manifests itself principally by a particular pattern for the individual temperature factors of the atoms. We have carefully examined our present results for perylene–PMDA for indications of disorder. None have been found. (The individual temperature factors found for anthracene–PMDA are not accurate enough for conclusions to be drawn about possible disorder in this addition compound.) Thus we conclude that we have studied a definite relative molecular orientation in perylene–PMDA but that this is not necessarily the orientation at 0°K. Unfortunately, nothing is known about the crystallography of the low-temperature polymorph of perylene–PMDA as it has not yet been obtained in single-crystal form. Clearly, determinations of crystal structures at appropriately low temperatures will be required before really useful comparisons can be made between theory and experiment.

Appendix

Correction of the Bond Lengths in Maleic Anhydride for Thermal Motion. The anisotropic thermal parameters obtained by Marsh, *et al.*,[30] for maleic anhydride were processed by Pawley[38] in terms of rigid-body thermal motion. In one approach, the origin of the mean-square rotational tensor ω_{ij} was taken at the center of gravity of the molecule and in a second approach this origin was determined by least-squares refinement.

Although the second method gives 2% better agree-

(36) R. D. Brown, *J. Chem. Soc.*, 691 (1950).

(37) F. H. Herbstein and J. A. Snyman, unpublished results.

(38) G. S. Pawley, *Acta Cryst.*, 16, 1204 (1963).

ment between observed and calculated U_{ij} values, the results of the first method indicate a closer coincidence of the main librational directions with the inertia axes of the molecule. The error introduced by putting $\omega_{12} = \omega_{23} = \omega_{13} = 0$ will therefore be less serious if the origin of ω_{ij} is taken at the center of gravity.

This diagonal approximation considerably simplifies the calculation of corrected bond lengths according to Cruickshank's method.[23] The revised bond lengths shown in Figure 8 were obtained by assuming mm symmetry for the molecule and applying the corrections to the molecular parameters of Marsh, *et al.* As in the case of perylene–PMDA, a value for $q^2 = 0.1$ Å.^{2} was assumed.

The System Tetramethylmethane–Tetrachloromethane. Thermodynamics of Mixing in the Plastically Crystalline Region[1]

by Elfreda T. Chang and Edgar F. Westrum, Jr.[2]

Department of Chemistry, University of Michigan, Ann Arbor, Michigan *(Received November 12, 1964)*

Heat capacities of five different compositions (CCl_4 mole fraction of 0.200, 0.334, 0.501, 0.666, and 0.826) of the system tetramethylmethane–tetrachloromethane were determined by adiabatic calorimetry from 5 to 300°K. Thermodynamic functions calculated by integration of the data, together with similar values for the pure components and mixing data for the liquid solutions, yield the excess enthalpies of mixing in the solid state (*i.e.*, for the plastically crystalline solid solution) and the temperature dependence of this quantity. The excess enthalpy of the equimolal solution is compared with the values predicted by theory.

Introduction

During the last two decades a considerable theoretical and experimental endeavor has been devoted to the properties of liquids and liquid mixtures. For example, the cell model, the lattice model, the theory of conformal solutions, the average potential model, etc., have been devised. However, many, if not most, of the quantitative predictions of these theories are not in accord with the existing experimental data. Poor agreement between experiment and theory is due in part to the difficulty of obtaining good experimental mixing data and in part to the imperfection of the present state of development of the theory of fluids.

Several of these theories ascribe a more or less regular structure to the liquid state. Since the solid state has many features in common with the liquid state (*i.e.*, a large number of first neighbors and local order) and, in addition, a determinable lattice structure, measurement of the excess functions of solid solutions should permit, in many instances, a better test of these existing theories of mixtures than is presently possible in the liquid state. With this end in view, a system was sought that forms a continuous series of solid solutions and for which good enthalpy of mixing data were available. To make the experimental chore

(1) Based upon a dissertation submitted to the Horace H. Rackham School of Graduate Studies of the University of Michigan by E. T. Chang in partial fulfillment of the requirements for the degree of Doctor of Philosophy. This work was supported in part by the Division of Research of the U. S. Atomic Energy Commission. Presented at the 146th National Meeting of the American Chemical Society, Denver, Colo., Jan. 1964.

(2) To whom correspondence concerning this paper should be sent.

Table I: Selected Thermodynamic Properties for the System Tetramethylmethane–Tetrachloromethane[a]

	N_{CCl_4}													
	0.000[b] $[C(CH_3)_4]$		0.200		0.334		0.501		0.666		0.826		1.000[c] $[CCl_4]$	
T	C_p	$H^\circ - H^\circ_0$	C_p	$H^\circ - H^\circ_0$	C_p	$H^\circ - H^\circ_0$	C_p	$H^\circ - H^\circ_0$	C_p	$H^\circ - H^\circ_0$	C_p	$H^\circ - H^\circ_0$	C_p	$H^\circ - H^\circ_0$
230	30.39	4862.9	29.54	4970.5	29.43	5076.4	29.75	5118.8	30.55	4991.7	29.46	4960.6	27.97	4883
240									32.29	5859.6				
245	31.77	5329.1	(61.2)	5474.5	34.00	6041.3	33.18	6027.3			31.64	5991.5	29.30	5312
250	32.23	5489.1	34.93	6175.9	34.26	6211.9	33.39	6193.7	32.57	6183.9	31.75	6150.0	29.75	5460
260	36.24	6604.6	35.61	6528.4	34.78	6557.2	33.79	6529.6	32.86	6511.1	31.97	6468.6	31.16	6372
270	37.86	6972.6	36.28	6887.9	35.31	6907.6	34.19	6869.5	33.15	6841.1	32.19	6789.4	31.24	6684
280	38.45	7351.7	36.88	7253.8	35.83	7263.3	34.60	7213.4	33.43	7174.0	32.41	7112.5	31.33	6997
290			37.45	7625.5	36.35	7624.2	35.05	7561.7	33.72	7509.7	32.64	7437.7	31.41	7310
300			38.02	8002.8	36.88	7990.4	35.56	7914.7	34.01	7848.4	32.86	7765.2	31.49	7625
273.15	37.70	7091	36.48	7002	35.47	7019	34.32	6977	33.24	6946	32.26	6891	31.27	6783
298.15			37.92	7929	36.78	7922	35.46	7849	33.95	7786	32.82	7704	31.48	7567

[a] Units: cal., mole of solution, °K. [b] See ref. 7. [c] See ref. 8.

practicable it is essential that equilibrium be achieved at each stage of the process, that "frozen-in" equilibria be avoided in the solid state, and that the time for equilibration be "finite." For these reasons it was considered desirable to make the initial measurements on systems of globular molecules which have approximately the same diameters and which are spherically symmetrical so that the intermolecular forces may be considered central. Such molecules often form plastically crystalline substances, as defined by Timmermans.[3] The calorimetric investigation of the system tetramethylmethane–tetrachloromethane was originally undertaken so that the experimental results, together with existing data on mixing in the liquid phase and heat capacity values for the pure components, would provide an experimental test in the solid state for some of the modern theories of solutions.

Experimental Results

The heat capacities of five compositions of the system tetramethylmethane–tetrachloromethane, with mole fractions of tetrachloromethane (N_{CCl_4}) of 0.200, 0.334, 0.501, 0.666, and 0.826, were measured as described elsewhere.[4,5] Pertinent thermodynamic functions of the compositions studied obtained by digital computer integration are tabulated over the relevant range of temperature (230 to 300°K.) together with those of the pure components in Table I. For more extensive tabulation the detailed paper[5] should be consulted.

Enthalpies of mixing for this system at several temperatures were determined from available enthalpy of mixing data at 0°,[6] the heat capacity data of the pure components,[7,8] and the heat capacity data of this investigation in the following manner. The enthalpy of mixing H^M (or the excess enthalpy, H^E) at temperature T_0 may be expressed as

$$H^E_{T_0} \text{ or } H^M_{T_0} = H_{mix,T_0} - N_A H_{A,T_0} - N_B H_{B,T_0}$$

in which H refers to the relative enthalpy at the temperature T_0, and N refers to the mole fraction. The subscripts mix, A, and B refer to the mixture and to the components. The excess enthalpy at any temperature, T, is therefore

$$H^E_T = H^E_{T_0} + \sum_i^{\pm} \int_{T_0}^{T} N_i C_{p_i}\, dT + \sum_i^{\pm} N_i(\Delta Ht_i \text{ or } \Delta Hm_i)$$

in which the summations are over the components and the solution in the balanced formation reaction, and ΔHt and ΔHm are the enthalpy increments associated with enantiomorphic and melting transitions. Hence

$$H^E_T = H^E_{T_0} + (H_T - H_{T_0})_{mix} - N_A(H_T - H_{T_0})_A - N_B(H_T - H_{T_0})_B$$

For each composition of this system the derived

(3) J. Timmermans, *Phys. Chem. Solids*, **18**, 1 (1961).

(4) E. T. Chang and E. F. Westrum, Jr., *J. Phys. Chem.*, in press.

(5) E. T. Chang, Doctoral Dissertation, University of Michigan, Ann Arbor, Mich., 1962.

(6) A. Englert-Chwoles, Doctoral Thesis, Free University of Brussels, Brussels, 1955.

(7) J. G. Aston and G. H. Messerly, *J. Am. Chem. Soc.*, **58**, 2354 (1936).

(8) J. F. G. Hicks, J. G. Hooley, and C. C. Stephenson, *ibid.*, **66**, 1064 (1944).

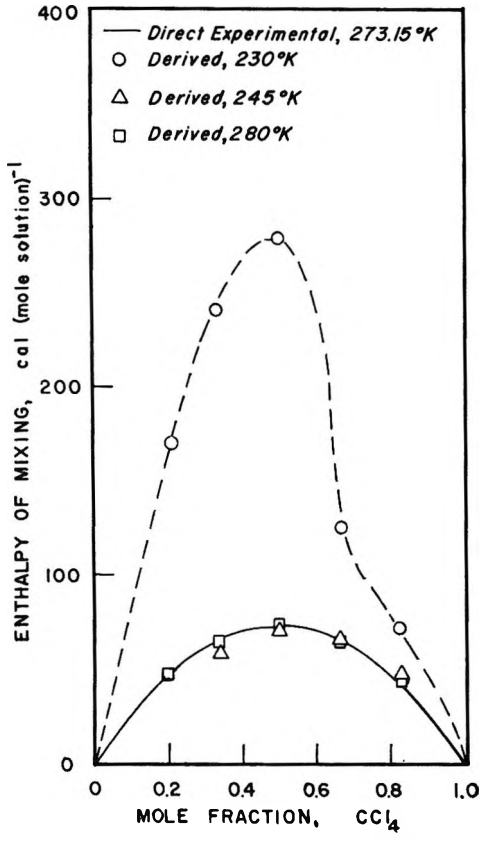

Figure 1. Temperature dependence of the excess enthalpy for the system tetramethylmethane–tetrachloromethane. The uncertainties of all values (occasioned by propagated uncertainties in the work of Englert-Chwoles[6]) is ±5 cal. mole^{-1}.

excess enthalpies and the excess heat capacities at 280, 260, 255, 245, and 230°K. are listed in Table II together with the experimental value of Englert-Chwoles[6] at 273.15°K. upon which the others are based. The excess enthalpy plotted *vs.* temperature is also depicted in Figure 1. It is to be noted that the values for 255°K. are the enthalpies of mixing for *undercooled liquid* tetramethylmethane plus liquid tetrachloromethane forming *liquid* solution; the values for 245°K. are the enthalpies of mixing for the two *undercooled liquid* components forming a *liquid* mixture; and the values for 230°K. are the enthalpies of mixing for the two *solid* components forming a *solid* solution. Values at other temperatures may be derived conveniently by using the relative enthalpy values for the mixtures and the pure components given in Table I.

Discussion

Excess thermodynamic properties of nonpolar liquids have often been selected to test the validity of statistical theories of solutions, *e.g.*, as summarized by

Table II: Temperature Dependence of the Excess Enthalpy and Excess Heat Capacity of the System Tetramethylmethane–Tetrachloromethane[a]

		Temp.					
		280	273.15	260	255[b]	245[c]	230[d]
N_{CCl_4}	Property	Liquid					Solid
0.200	C_p^E	−0.14	+0.07	+0.39	+0.49	...	−0.47
	H^E	47	47	44	42	...	177
0.334	C_p^E	−0.24	−0.08	+0.23	+0.37	+0.64	−0.15
	H^E	65	66	65	63	58	241
0.501	C_p^E	−0.29	−0.16	+0.10	+0.20	+0.39	+0.58
	H^E	73	74	74	74	71	279
0.666	C_p^E	−0.28	−0.18	+0.01	+0.08	+0.22	+1.77
	H^E	65	66	67	67	65	121
0.826	C_p^E	−0.16	−0.13	−0.08	−0.06	−0.02	+1.07
	H^E	44	45	46	46	46	71

[a] Units: cal., mole of solution, °K. [b] Mixing of undercooled liquid $C(CH_3)_4$ with liquid CCl_4. [c] Mixing of undercooled liquids $C(CH_3)_4$ and CCl_4. [d] Mixing of solid $C(CH_3)_4$ with solid CCl_4.

Guggenheim,[9] by Hildebrand and Scott,[10] and more recently by Prigogine[11] and by Rowlinson.[12] Owing to the similarity of the molecular shapes and sizes of the tetramethylmethane and tetrachloromethane molecules, the binary system of these substances has been favored for such purposes. Moreover, the tetrahedral symmetry of the molecules sufficiently approaches spherical symmetry to permit the assumption that intermolecular forces are central.

The excess functions of this system in the liquid state have been well investigated at 273°K. Mathot and Desmyter[13] studied the excess free energy and volume of mixing by measuring the total vapor pressures and densities of several compositions of this system at 273°K. Englert-Chwoles[6] determined the enthalpy and entropy of mixing at 273°K. by adiabatic and isothermal calorimetry. The excess compressibility, $(\partial V^E/\partial P)_T$, was investigated by Jeener,[14] who measured the velocity of sound in liquid solutions of tetramethylmethane and tetrachloromethane. As indicated in the reference cited this system is regular at 273°K., and the respective values of the excess free energy, enthalpy, entropy (expressed as TS^E) and volume at 273°K. ate 76, 74, −2 cal./mole, and −0.5 cm.^{3}, respectively, for the equimolal composition.

(9) E. A. Guggenheim, "Mixtures," Oxford University Press, Oxford, 1952.

(10) J. H. Hildebrand and R. Scott, "Solubility of Non-Electrolytes," Reinhold Publishing Corp., New York, N. Y.; 1950.

(11) I. Prigogine, "The Molecular Theory of Solutions," North Holland Publishing Co., Amsterdam, 1957.

(12) J. S. Rowlinson, "Liquids and Liquid Mixtures," Butterworth Scientific Publications, London, 1959.

(13) V. Mathot and A. Desmyter, *J. Chem. Phys.*, **21**, 782 (1953).

(14) J. Jeener, *ibid.*, **25**, 584 (1956).

The magnitude of the excess volume decreases with increasing pressure.

Theoretically calculated excess functions taken from the references[15–20] cited are compared with the experimental values for this system in Table III. Quantitative agreement between theory and experiment is generally poor. However, in a few cases (*i.e.*, the smooth potential cell model and the average potential model) fair agreement prevails. The best accord at 273°K. (in the liquid phase) is obtained with the average potential model. Lack of accord between the theoretical evaluations are occasioned not only by the differences in the assumptions made concerning the structure of the liquid state and the interactions between species but also on the evaluation of parameters.

Since several of the solution theories are predicated upon a more or less regular structure with many features in common with the solid state, the calorimetric investigation of the system tetramethylmethane–tetrachloromethane was made in part to ascertain whether better agreement between theoretical and experimental excess enthalpies is obtainable for solid solutions.

Table III: Comparison of Calculated Excess Functions with Experiment for the Equimolal Composition of the System Tetramethylmethane–Tetrachloromethane in the Liquid Phase[a]

	T	H^E	TS^E	G^E	V^E
Theory					
Cell model, smooth potential[15]	273	55	−5	60	−0.2
Cell model, Lennard-Jones Devonshire[16]	293	16	−98	...	−3
Average potential model[17]	273	71	−9	80	−1.3[18]
Scatchard–Hildebrand formula[19]	273	...	...	150	...
Random mixture[20]	273	100	12	88	−0.5
Semirandom mixture at fixed volume[20]	273	93	9	84	−0.3
Semirandom mixture at fixed pressure[20]	273	67	5	62	−0.8
Experiment[6]					
	273	74	−2	76	−0.5

[a] Units: cal., mole of solution, °K., cm.³.

The Excess Heat Capacity. The direct method of measuring the heat of mixing using adiabatic or isothermal calorimetry is that commonly used to obtain satisfactory H^E data on liquids. In this method one encounters adiabatic calorimetric concerns, *i.e.*, exchange of heat with surroundings, satisfactory stirring, and rapid and sensitive temperature measurement, plus the further difficulty of ensuring the absence of any appreciable volume of vapor. In practice, measurements of H^E by the direct method may be accurate to about 2% for liquids at room temperature, with lower accuracy at higher temperatures. Measurements of the excess heat capacity, $C_p{}^E$ reveal the temperature dependence of H^E. Very few experimental investigations of $C_p{}^E$ have been made. This neglect has been in part, as Rowlinson[12] stated, "probably due to the fact that even the best theories of solution are not accurate enough to predict reliably the size of the second derivative of the excess free energy with respect to temperature to permit a test of theory." However, in considering a mixture from the standpoint of its excess functions, it is necessary to know the excess free energy and excess enthalpy at the same temperature. Usually G^E is determined at a higher temperature than H^E, and knowledge of the excess heat capacity $C_p{}^E$ of the system is required to correct H^E to the temperature of measurement of G^E. Calculating H^E at one temperature from the experimental value at another demands precise experimental investigation of the heat capacity, for the values of the excess properties are all relatively small, and an error in the heat capacity of the order of 1% would lead to a comparatively large uncertainty in the derived H^E values. Therefore, the derived value of the excess enthalpy is limited by the experimental error of the C_p measurements.

Examination of Table II reveals that the temperature dependence of the excess enthalpy in the liquid range for the system under investigation is comparatively small (*e.g.*, in comparison with that of the system benzene–tetrachloromethane)[5,21] and is slightly negative in the liquid range where both components are liquids and is slightly positive when one or both components are undercooled liquids. The excess enthalpy curve in the liquid solution range tends to be more symmetrical at high temperatures. At lower temperatures within the liquid range the maximum in the curve is shifted slightly to the tetrachloromethane-rich side of the excess enthalpy *vs.* composition diagram (*cf.* Table II and Figure 1). In the plastically crystalline region the derived excess enthalpy curve at 230°K. shows a comparatively large and irregular composi-

(15) I. Prigogine and V. Mathot, *J. Chem. Phys.*, **20**, 49 (1952).

(16) Z. W. Salsburg and J. G. Kirkwood, *ibid.*, **20**, 1538 (1952); **21**, 2169 (1953).

(17) I. Prigogine, A. Bellemans, and A. Englert-Chwoles, *ibid.*, **24**, 518 (1956).

(18) See ref. 11, p. 224.

(19) See ref. 11, p. 231.

(20) See ref. 12, p. 331.

(21) J. R. Goates, R. J. Sullivan, and J. B. Ott, *J. Phys. Chem.*, **63**, 589 (1959).

tion dependence and possibly a discontinuity between the compositions $N_{CCl_4} = 0.5$ and 0.7. Unfortunately, there are insufficient data in this region to elucidate this situation. The existence of phase separations restricts the plastically crystalline region to a relatively short temperature interval[4,5] so that only in the vicinity of 230°K. does the possibility of a continuous series of solid solutions exist. Hence, even in this system, comparison of values of the excess functions is limited to a rather narrow range of temperature.

Comparisons with Theories. The predictions based on the cell model which assumes structures for solutions most closely resembling those of crystals might be expected *a priori* to be especially appropriate for comparison with the excess enthalpy of solid solutions. As Prigogine[22] has suggested, for high densities as in the solid state a harmonic potential approximation for the mean potential may be used. The excess enthalpies for the harmonic oscillator cell model given in Table IV are calculated by the equation[15]

$$\frac{H^E}{N_0 kT} = 0.5 \times 1.435 N_A N_B [(\Lambda_{AA}/kT)^{1/2} - (\Lambda_{BB}/kT)^{1/2}]^2 + 4.83 \frac{V^E}{V^*}$$

in which

$$\frac{V^E}{V^*} = 1.4125[(kT/\Lambda_{AB}) - N_A(kT/\Lambda_{AA}) - N_B(kT/\Lambda_{BB})]$$

Here Λ is the interaction parameter, k is the Boltzmann constant, N_0 is Avogadro's number, and N is the mole fraction. The exact values of physical properties on which Table IV is based are detailed in a separate document.[23]

Since the average potential model gives good agreement with experiment for liquid solutions of this system (*cf.* Table III), a comparison is also made at 230°K. to determine whether the theory is applicable to solid solutions. For the average potential model, H^E in Table IV is calculated from the equation[24]

$$\frac{H^E}{N_A N_B} = [-H_A + TC_{pA}][0.25d^2 + 9\rho^2] - 0.5T^2[dC_{pA}/dT - 0.25dC_{vA}/dT]d^2$$

in which the thermodynamic properties refer only to the configurational part of the properties, and d and ρ are interaction parameters (for which *cf.* discussion by Prigogine[11]).

Finally, the derived experimental excess enthalpy at 230°K. is compared with Hildebrand's theory of solid solutions.[25] Since the difference in the cohesive energies of liquid and solid phases is small, the magnitude of the excess enthalpy in a solid solution may be expected to be nearly the same as that in the corresponding liquid phase. However, a distortion energy due to differences of size and shape must be added to the excess enthalpy which is based upon internal pressure considerations alone (*i.e.*, the excess enthalpy given by the Hildebrand–Scatchard semiempirical formula[10]). The distortion energy is peculiar to the solid phase and is lost on melting; therefore, the part of the excess enthalpy arising from internal pressure differences should be much the same as it is in the liquid phase. The semiempirical excess molal enthalpy formula based on internal pressure considerations[26] is

$$H^E = (N_A V_A + N_B V_B)(\delta_A - \delta_B)^2 \phi_A \phi_B$$

where V refers to the molal volume, δ to the solu-

Table IV: Comparison of Derived Experimental Excess Enthalpies with Calculated Values at 230°K.[a,b]

	N_{CCl_4} 0.200	0.334	0.501	0.666	0.826
	H^E				
Harmonic oscillator cell model					
	43	78	102	101	78
Hildebrand's empirical approach					
Internal pressure considerations	63	88	101	92	61
Distortion energy	34	49	58	53	36
Total	97	137	159	145	97
Average potential model					
$C(CH_3)_4$ as reference	105	146	164	146	94
CCl_4 as reference	111	154	172	154	99
Av.	108	150	168	150	97
Derived experimental					
	177	241	279	121	71

[a] *Cf.* Table ADI-X in ref. 23 for properties used. [b] Units: cal., mole of solution.

(22) See ref. 11, p. 130.

(23) Extensive supplementary tables of experimental data and results including thermodynamic functions at selected temperatures and details and figures delineating the behavior in the transition region have been deposited as a 46-page document, No. 8458, with the ADI Auxiliary Publications Project, Photoduplication Service, Library of Congress, Washington, D. C. A copy may be secured by citing the document number and remitting $6.25 for photoprints or $2.50 for 35-mm. microfilm in advance by check or money order made payable to: Chief, Photoduplication Service, Library of Congress.

(24) See ref. 11, p. 215.

(25) See ref. 10, pp. 302, 304.

(26) See ref. 10, pp. 121, 129.

bility parameter, and ϕ to the volume fraction. The empirical distortion energy formula[27]

$$E^D = \frac{2\delta_A\delta_B(V_AV_B)^{1/2}(V_A - V_B)^2}{(N_AV_A^2 + N_BV_B^2)} N_AN_B$$

holds for a binary solid solution of atoms of different sizes. Since the tetrahedral symmetry of some of the nonpolar organic molecules rather closely approaches spherical symmetry (*e.g.* as do globular molecules by reorientational rotation), a solid solution treatment for atomic lattices would be expected to hold well for approximately spherical molecules.

Examination of the calculated and the derived experimental values of the excess enthalpy in Table IV reveals that the solution is more complex at 230°K. than in the liquid phase. The excess enthalpy values are irregular as well as large, *i.e.*, comparable to RT at the equimolal composition. On the tetrachloromethane-rich side of this system the derived experimental excess enthalpies agree fairly well with the values calculated by the harmonic oscillator cell model, while on the tetramethylmethane-rich side the derived excess enthalpies are more than three times as large as those predicted by this model. The empirical approach of Hildebrand yields excess enthalpies intermediate between those predicted by the harmonic oscillator cell model and the average potential model. Both the harmonic oscillator cell model and Hildebrand's approach predict unsymmetrical excess enthalpy *vs.* mole fraction curves with maxima on the tetrachloromethane-rich side of the system. This contrasts with the derived experimental excess enthalpy curve. The average potential model predicts a symmetrical excess enthalpy curve at all temperatures.

That the situation in the solid state of this system is definitely more complex than in the liquid is further attested by the fact that this system exhibits a minimum in the melting point curve near $N_{CCl_4} = 0.666$. When the deviations from ideality in the solid exceed those in the liquid, a minimum in the melting point curve can be expected. Although no definitive explanation for the irregular behavior of the derived experimental excess enthalpy at 230°K. is offered, a possible explanation is that the large excess enthalpy on the tetramethylmethane-rich side of this system is due to phase separation at this temperature. A rough criterion for immiscibility is a large and positive value of H^E and a G^E exceeding $RT/2$.[28] Moreover, when the difference in molal volume is greater than 20%, the strain energy often occasions separation.[29] However, in this system G^E at 230°K. estimated from the relation $G^E = H^E - TS^E$ is only about 124 cal. mole^{-1} (*i.e.*, less than $RT/2 = 230$ cal. mole^{-1}) for the equimolal composition, and the difference in molal volume is about 12%. A minimum enthalpy of fusion near the equimolal composition[4] is another possible indication of phase separation. This situation might be analogous to that in the system oxygen–nitrogen for which the enthalpy of fusion curve exhibits similar behavior and for which the melting point curve corresponds to a Type V eutectic diagram.[30] The calculated values of the excess enthalpy in solid solution may be used for qualitative comparison only in view of the several approximations used in deriving the values of the properties[23] of the pure components and parameters at 230°K. Moreover, the reliability of the derived experimental excess enthalpies is limited by the ±1% uncertainty in the heat capacity measurements for the pure component tetramethylmethane.[7] It is apparent that even more extensive study of the present system and of other systems of globular molecules that form continuous series of solid solutions is necessary before the validity of this test of solution theory can be fully assessed. Further definitive measurements on properties of solid and liquid solutions in similar systems as well as on their constituents are desiderata for more extensive comparisons.

Acknowledgment. The authors wish to express their sincere thanks to Professor J. G. Aston for his suggestion at Fritzer-Wattens which initiated this interesting project. The partial financial support of the United States Atomic Energy Commission is gratefully recognized.

(27) See ref. 10, p. 304.

(28) See ref. 12, p. 166.

(29) See ref. 10, p. 304.

(30) See ref. 10, pp. 309, 314.

Formation of CO_2^- Radical Ions When CO_2 is Adsorbed on Irradiated Magnesium Oxide

by Jack H. Lunsford and John P. Jayne

Lewis Research Center, National Aeronautics and Space Administration, Cleveland, Ohio
(Received November 30, 1964)

Evidence is presented for the formation of CO_2^- radical ions when CO_2 is adsorbed on ultraviolet-irradiated magnesium oxide. Electrons are thought to be transferred from surface traps to the adsorbed CO_2 molecule and are stabilized in a pseudo-π-antibonding orbital. The e.p.r. spectrum of the radical ($g_z = 2.0017$, $g_x = 2.0020$, $g_y = 1.9974$, $A_z = 230$ gauss, $A_x = A_y = 184$ gauss) is in agreement with the spectrum of the CO_2^- radical that is formed in γ-irradiated sodium formate as described by Ovenall and Whiffen.

Introduction

The application of electron paramagnetic resonance (e.p.r.) spectroscopy to adsorbed molecules has proved the existence of certain radical species that may be intermediates in chemical reactions. The early studies were primarily on adsorbed polynuclear organic compounds.[1-3] An investigation of oxygen on zinc oxide has been reported[4]; however, the particular oxygen radical was not conclusively identified. The formation of surface paramagnetic centers by γ-irradiation of degassed MgO has been recently reported by Nelson and Tench.[5] This type of center, termed an S center, is thought to be an electron trapped at a surface anion vacancy. The S centers, as well as a reddish blue color, are rapidly destroyed upon exposure to oxygen. We have observed a similar phenomenon with MgO following ultraviolet irradiation and, in addition, have observed the spectrum of an oxygen radical ion that is formed on adsorption. This is to be reported separately.[6] It was of interest to see if other gases would also form radical ions when adsorbed on the irradiated surface. In the work reported here we have observed the e.p.r. spectrum of CO_2 adsorbed on ultraviolet-irradiated MgO. The spectrum of adsorbed CO_2 is compared with the e.p.r. spectrum of the CO_2^- radical ion that Ovenall and Whiffen[7] have analyzed in some detail.

Experimental

The MgO used in this experiment was prepared from reagent grade powder. Most of the data were taken on samples that had been impregnated with 0.0035% Fe as $FeCl_3$ or $Fe(NO_3)_3$ and on the original powder that contained about 0.0010% Fe. The powder was boiled in water for several hours, extruded into pellets with a hypodermic syringe, and dried in air at 100°. Degassing was carried out by heating the pellets to 800° under vacuum for several hours. All the samples were then irradiated for 16 hr. by using a low pressure mercury lamp with an intensity of 60 μw./cm.^{2} at 2537 Å.

Electron paramagnetic resonance data were obtained with a Varian spectrometer operating at a cavity resonance frequency of 9100 Mc./sec. A nuclear magnetic resonance (n.m.r.) type gaussmeter was used to monitor the magnetic field continuously. The g values were obtained by comparison with the value for α,α-diphenyl-β-picrylhydrazyl (DPPH) that was placed on the outside of the quartz tube containing the MgO sample. The g value of the DPPH was taken as 2.0036.

After ultraviolet irradiation, the sample was checked for the paramagnetic center and the violet color. When

(1) J. J. Rooney and R. C. Pink, *Proc. Chem. Soc.*, 70 (1961); *Trans. Faraday Soc.*, 58, 1632 (1962).

(2) D. M. Brouwer, *Chem. Ind.* (London), 177 (1961); *J. Catalysis*, 1, 372 (1962).

(3) W. K. Hall, *ibid.*, 1, 53 (1962).

(4) K. M. Sancier and T. Freund, *ibid.*, 3, 293 (1964).

(5) R. L. Nelson and A. J. Tench, *J. Chem. Phys.*, 40, 2736 (1964).

(6) To be published.

(7) D. W. Ovenall and D. H. Whiffen, *Mol. Phys.*, 4, 135 (1961).

these were present, CO_2 was admitted to the sample at a pressure of about 100 torr and at room temperature. A mixture of 57% $C^{13}O_2$ and 43% $C^{12}O_2$ was adsorbed on several samples in an effort to observe the C^{13} hyperfine spectrum that could be used to identify the radical species. The mixture was purified by freezing the CO_2 at 77°K. and pumping off any residual oxygen.

Spectra were also obtained for unirradiated MgO that had been degassed and exposed to CO_2.

Results

After several hours of ultraviolet irradiation, the violet color of the sample begins to appear, and the e.p.r. spectrum shown in Figure 1 was observed. This spectrum of the center, which we will designate an S′ center, has the g values shown in the figure and listed in Table I. The e.p.r. transition can be saturated with a moderate amount of microwave power (approximately 3 mw.). The paramagnetic species is fairly stable through 100°, but heating to 200° for 30 min. reduces the intensity of the derivative curve by 90%. It was further observed that the intensity of the spectrum was enhanced by a factor of 2 by adding the 0.0035% Fe as $FeCl_3$ or $Fe(NO_3)_3$.

Table I: Summary of g Values

	g_z	g_x	g_y	Estd. error
CO_2 on MgO	2.0017	2.0029	1.9974	±0.0003
CO_2^- in γ-irradiated NaCOOH (ref. 7)	2.0014	2.0032	1.9975	±0.0002
S′ center	2.0005	2.0015	1.9990	±0.0003
S center (ref. 5)	2.0007[a]	...	...	±0.0002
F_2 center (ref. 8)	2.0008	...	...	±0.0002

[a] Only one apparent g value was reported for these centers since the anisotropy is of the same magnitude as the line width.

Upon exposure to CO_2, both the S′ center spectrum and the violet color disappear, and the new derivative spectrum shown in Figure 2 appears. The g values of this new spectrum are also listed in Table I. The relative amplitude of the low field shoulder (the first maximum) in relation to the remainder of the CO_2 spectrum varies between doped and undoped samples. This observation indicates that the shoulder belongs to the spectrum of another complex, possibly CO_2 adsorbed in a different manner. Adsorption of CO_2 enriched to 57% C^{13} results in two rather broad hyperfine lines symmetrically disposed on each side of the $C^{12}O_2^-$ spectrum. The amplitude of the hyperfine lines is less than one-tenth of the amplitude of the central line, which is associated with the 43% $C^{12}O_2$.

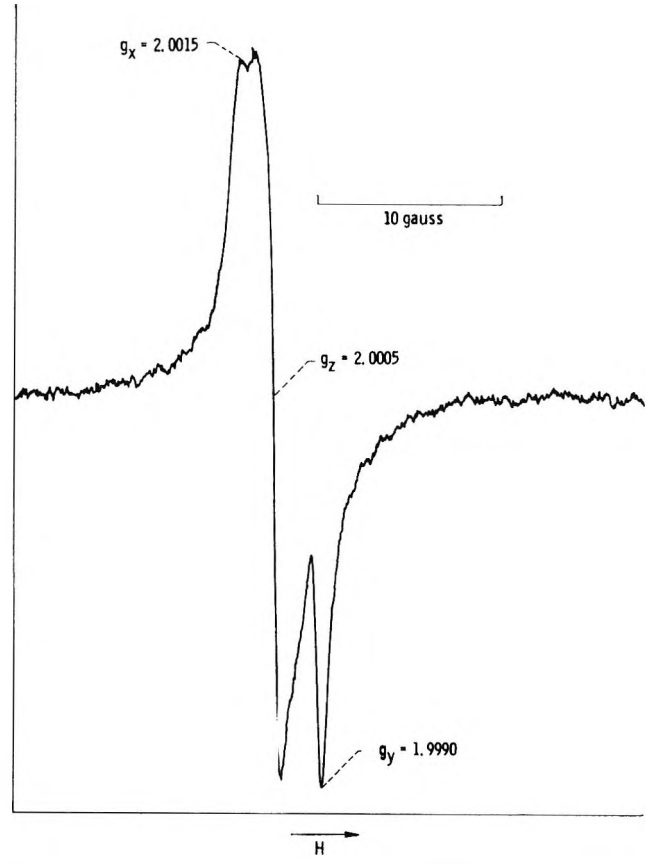

Figure 1. S′ spectrum of ultraviolet-irradiated magnesium oxide.

Values for the hyperfine coupling constants are listed in Table II.

Table II: Hyperfine Coupling Constants

	Hyperfine coupling constants, gauss		
	A_z	A_x	A_y
CO_2 on MgO	230	184[a]	...
CO_2^- in NaCOOH (ref. 7)	195	156	151

[a] In the powder samples it was not possible to resolve A_x and A_y.

The S′ center is destroyed by a partial pressure of oxygen in CO_2 as low as 10^{-3} torr, and no CO_2 spectrum can be detected. One can regenerate the S′ center, however, by again heating the sample to 800° under vacuum and irradiating with ultraviolet light.

Discussion

Ultraviolet light with an energy of 4.9 e.v. apparently promotes electrons into traps that exist on the surface of the degassed MgO. The resulting e.p.r.

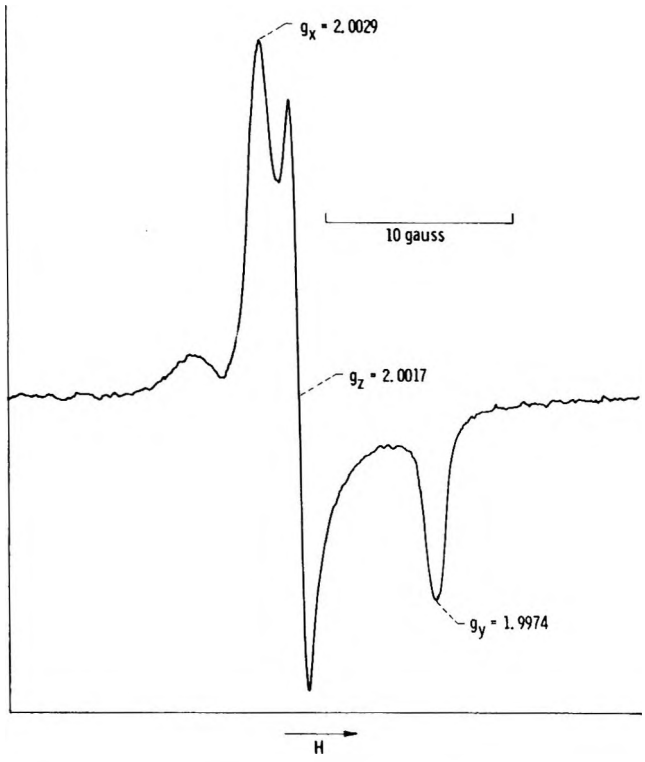

Figure 2. E.p.r. spectrum of carbon dioxide adsorbed on ultraviolet-irradiated magnesium oxide.

spectrum, shown in Figure 1, is characteristic of a center having rhombic symmetry. The similarity in the g value of the S′ center to the g value of the S center[5] and the annealing behavior of the centers indicate that they are related; that is, both centers are electrons trapped at a surface defect. The S center, however, does not have rhombic symmetry. If the S′ center was an electron trapped at an anion–cation vacancy pair existing in the plane of the surface, rhombic symmetry would be satisfied. One symmetry axis would be along the vacancy pair, and the other axis would be perpendicular to the surface. It should be pointed out that the bulk F_2 center (an electron trapped at an anion–cation vacancy pair) reported by Wertz, *et al.*,[8] has a g value of 2.0008 ± 0.0002 and a fairly long relaxation time. We shall assume for this paper that the irradiation-induced paramagnetic center on the surface of the MgO is an electron trapped at an anion–cation vacancy pair in the plane of the surface. The concentration of the cation vacancies is undoubtedly enhanced by the trivalent iron ion through charge compensation,[9,10] but the mechanism by which the anion vacancies are formed is not presently known.

A comparison of the g values for the spectrum of CO_2 adsorbed on ultraviolet-irradiated MgO with the spectrum of CO_2^- radical ions in γ-irradiated sodium formate (NaCOOH) single crystals shows that within experimental error there is complete agreement. As a result of the similarity in the spectra and the analysis by Ovenall and Whiffen of the structure of the CO_2^- radical ion, we conclude that CO_2 adsorbs on irradiated MgO as a nonlinear radical ion. The three g values correspond to three orientations of the magnetic field with respect to the CO_2^- radical: (1) for g_z the magnetic field is parallel to the symmetry axis of the ion; (2) for g_x the magnetic field is perpendicular to the symmetry axis and to the CO_2^- plane; (3) for g_y the magnetic field is perpendicular to the symmetry axis and parallel to the CO_2^- plane. The three different g values support the concept of a bent structure for the radical ion rather than a linear structure. Ovenall and Whiffen use the C^{13} coupling constants to show that the unpaired electron in CO_2^- is primarily in a pseudo-π-antibonding orbital that projects along the external bisector of the O–C–O angle. The magnitude of the coupling constants for the CO_2^- radical ion on MgO is somewhat greater than for CO_2^- in NaCOOH, but the degree of anisotropy is about the same. This indicates that the Fermi contact term, a measure of the s-character of the molecular orbital, is slightly larger for the radical ion on MgO. Overnall and Whiffen further show that the O–C–O angle is 134° in agreement with the O–N–O angle in NO_2, which is an isoelectronic molecule with the CO_2^- radical.

The e.p.r. spectrum of carbon dioxide on unirradiated MgO shows no CO_2^- radical ions. Magnesium oxide is a good electrical insulator, which means that there exists a wide forbidden region, and there are no filled electron or hole traps near the conduction or valence band. The ultraviolet light provides energy for exciting electrons to these intrinsic defects on the surface where the energy is stored as a trapped electron. The adsorption of a CO_2 molecule by a charge transfer offers then a path for some of this stored energy to be released. It will be interesting to see if such radical ions can be detected on the surface of metals where the work function is much lower.

(8) J. E. Wertz, J. W. Orton, and P. W. Auzins, *Discussions Faraday Soc.*, **31**, 140 (1961).

(9) J. H. Lunsford, *J. Phys. Chem.*, **68**, 2312 (1964).

(10) J. White, *Trans. Brit. Ceram. Soc.*, **56**, 553 (1957).

Thermodynamic Properties of Adsorbed Water Molecules and Electrical Conduction in Montmorillonites and Silicas

by J. J. Fripiat, A. Jelli, G. Poncelet, and J. André

Laboratoire de Physico-Chimie Minérale, Institut Agronomique de l'Université de Louvain, Héverlé-Louvain, Belgium *(Received November 30, 1964)*

The relation between some electrical properties and thermodynamic properties of adsorbed water has been studied for two montmorillonites, a silica gel, and a window glass powder at room temperature. A relationship has been found between electrical conduction and the mobility of water molecules in the monolayer. These molecules are immobile on the hydroxylic surface of silica gel and mobile on the oxygen internal surface of montmorillonite. The electrical conduction in the monolayer is believed to be mainly protonic. The dissociation degree of water molecules in this situation seems to be of the order of magnitude of 1%.

I. Introduction

Properties of water molecules adsorbed on ionic surfaces have been extensively investigated by numerous techniques, including calorimetry, infrared spectroscopy, and nuclear magnetic resonance. The influence of water adsorption upon the conductivity and dielectric properties of powders has also been frequently studied.[1-21] However, attempts to relate these electrical characteristics to thermodynamic properties of the adsorbed phase are rather scarce. In this paper, electrical conduction associated with the first and the second adsorbed water layer has been studied in relation to the thermodynamic properties of water molecules and especially to their entropy loss resulting from the adsorption process. Dispersion phenomena will not be considered although dielectric properties obviously affect the measured conductivities.

Three very different materials were chosen. The first one belongs to the class of layer lattice silicates (<2-μ fraction of a Morocco montmorillonite). This crystalline mineral has a large, negatively charged surface, mainly covered by oxygen atoms. The second one is a pure silica gel, the impurity content (Na^+) being as low as 6×10^{-6} Na^+ equiv./g. of SiO_2. The surface is covered by OH groups. The third material is made from an industrial window glass powder. Besides SiO_2, it contains appreciable amounts of Na_2O, CaO, MgO, and Al_2O_3.

Conduction processes in montmorillonite may be assigned either to exchangeable cations balancing the charge of the lattice or to protons coming from the dissociation of adsorbed water molecules. Mortland,

(1) J. Muir, *Trans. Faraday Soc.*, **50**, 249 (1954).
(2) S. Kurosaki, *J. Chem. Soc. Japan*, **73**, 606 (1952).
(3) S. Kurosaki, *J. Phys. Chem.*, **58**, 320 (1954).
(4) S. Kurosaki, S. Saito, and G. Sato, *J. Chem. Phys.*, **23**, 1846 (1955).
(5) M. T. Roll and R. Bernard, *Compt. rend.*, **232**, 1098 (1951).
(6) J. Le Bot and S. Le Montagner, *ibid.*, **233**, 862 (1951).
(7) J. Le Bot and S. Le Montagner, *ibid.*, **236**, 469, 593 (1953).
(8) J. Le Bot and S. Le Montagner, *J. phys. radium*, **16**, 79, 163 (1955).
(9) E. V. Ivanova and N. A. Shalberov, *Chem. Abstr.*, **33**, 2012 (1939).
(10) P. Le Clerc, *Silicates Ind.*, **19**, 237 (1954).
(11) M. A. Cook, R. O. Daniels, and J. H. Hamilton, *J. Phys. Chem.*, **58**, 358 (1954).
(12) B. Rosenberg, *J. Chem. Phys.*, **36**, 816 (1962).
(13) D. C. Freeman and D. H. Stamires, *ibid.*, **35**, 799 (1961).
(14) G. Simkovich, *J. Phys. Chem.*, **67**, 1001 (1963).
(15) M. C. Baldwin and J. C. Morrow, *J. Chem. Phys.*, **36**, 1591 (1962).
(16) K. Dransfeld, H. L. Frish, and H. L. Wood, *ibid.*, **36**, 1574 (1962).
(17) D. M. Young and A. O. Crowel, "Physical Adsorption of Gases," Butterworth and Co., Ltd , London, 1962.
(18) K. W. Wagner, *Arch. Electrotech.*, **2** (9), 371 (1914).
(19) R. W. Sillars, *J. Inst Elec. Eng.* (London), **80**, 378 (1937).
(20) L. K. H. Van Beek, *Physica*, **26**, 66 (1960).
(21) M. Freyman and R. Freyman, *J. phys. radium*, **13**, 589 (1952); **14**, 203 (1953); **15**, 82, 165 (1954).

Fripiat, Chaussidon, and Uytterhoeven[22] have reported that residual water molecules remaining under vacuum in a base-saturated montmorillonite are able to convert NH_3 into NH_4^+. The extent of the transformation suggests that these residual water molecules have a degree of dissociation higher than usual. Therefore, a protonic conduction mechanism would possibly be observed. In the silica gel used here, the amount of impurities is so low that electric conduction by Na^+ seems unlikely at room temperature, and conduction should be protonic. Consequently, if the electrical properties and the behavior of water molecules are similar for these very different adsorbents, the conclusions should be relevant generally to ionic surfaces.

II. Experimental

1. Samples. The *montmorillonite* used in these studies was from Camp Berteau, Morocco. Fractionation of the material for the <2-μ fraction was accomplished by dispersion with NaOH followed by centrifugation at appropriate velocities in accordance with Stokes' law. Saturation of the cation-exchange capacities was made with a large excess of the appropriate chloride followed by dialysis of the clay in distilled water until the resistance of the dialysate approached 1 megohm. It was freeze-dried just before use. The powdered material was used for the accurate adsorption measurements down to very low vapor pressures while, for conductometry and dielectric measurements, pellets (diameter, 9 mm.) were molded in a stainless steel die under high pressure ($4–6 \times 10^3$ kg. cm.$^{-2}$). Measurements of water vapor uptake, conductometric and dielectric measurements were obtained on similar pellets. This procedure has been adopted for each material, and the pellets, as well as the powdered materials, were outgassed overnight at 150° under high vacuum.

Aerogel was obtained according to the procedure described by Imelik[23] and carefully purified by refluxing with HCl solutions and by washing extensively with distilled water.

The third sample was made from the <400 mesh fraction of a ground *window glass*.

The chemical compositions and surface characteristics of these samples are shown in Tables I and II.[24–27]

Table I: Chemical Compositions

Montmorillonite: $[Si^{4+}_8]^{IV}[Al^{3+}_{3.1}\ Fe^{3+}_{0.25}\ Mg^{2+}_{0.67}]^{VI}O_{20}(OH)_4$
Aerogel: $SiO_2 \cdot xH_2O + 6 \times 10^{-6}\ Na^+$ equiv./g. of SiO_2
Glass powder (after calcination at 1000°): SiO_2, 72.77%; Na_2O, 13.97%; TiO_2, 0.03%; K_2O, 0.09%; CaO, 8.17%; MgO, 3.85%; Fe_2O_3, 0.11%; Al_2O_3, 1.01%

Table II: Surface Characteristics of the Samples

	Sodium montmorillonite	Calcium montmorillonite	Aerogel	Glass powder
Surface area, m.^{2} g.$^{-1}$	External, 80[a] Internal, 645[b]	External, 80[a] Internal, 645[b]	135[a]	0.27[c]
Surface area for water,[d] m.^{2} g.$^{-1}$	200	450	201	2.4
Cation-exchange capacity,[e] mequiv./100 g.	95	95		
Surface density of charge,[f] $e/m\mu^2$	0.8	0.8	≤ 0.1	
Hydroxyl surface density, OH/mμ^2			4.2[g]	4.5[h]

[a] N_2 B.E.T. measurements. [b] Ethylene glycol retention.[24,25] [c] Krypton B.E.T. measurements.[26] [d] Obtained from the N_{sm} values quoted in Table IV for the powdered materials assuming a molecular packing of 11 Å.^{2}. [e] NH_4^+ exchange at pH 7. [f] Obtained by dividing the C.E.C. by the surface area and expressed in electron per square millimicron. [g] According to Uytterhoeven and Fripiat.[27] [h] Estimated, Jelli.[26]

For montmorillonite, it is necessary to distinguish between external and internal surface areas. The edges and the upper and lower plane surfaces constitute the external surface while the internal one includes the oxygen 001 planes of the expanding lattice. The edges are probably covered by OH groups. The distance between the silicate sheets increases according to the completion of one, two, etc., adsorbed water layers.[28,29] The opening of each interlayer space occurs at once by introducing the required number of water molecules so that, with increasing pressure, each particle is composed of collapsed, interstratified, and expanded sheets. Upon opening, the *c*-axis spacing of sodium montmorillonite expands from 9.6 to 12.5 Å. for the first water layer and to 15.5 Å. for the second one. Calcium montmorillonite expands to 15.5 Å. because of the higher hydration energy of divalent cations.

For Aerogel and the glass powder, the "surface areas" available to water molecules at complete monolayer coverage seem to be higher than the B.E.T. areas measured with an inert gas (N_2 or Kr). The

(22) M. M. Mortland, J. J. Fripiat, J. Chaussidon, and J. Uytterhoeven, *J. Phys. Chem.*, **67**, 248 (1963).

(23) B. Imelik and Y. Carteret, *Bull. soc. chim. France*, 864 (1951).

(24) S. B. Hendrickx and L. A. Dyal, *Soil Sci.*, **69**, 421 (1950).

(25) J. J. Fripiat, *Bull. Groupe Franc. Argiles*, **9**, 23 (1957).

(26) A. Jelli, Ph.D. Thesis, Laboratoire de Chimie Minérale, Agronomic Institute, University of Louvain, Louvain, Belgium, 1964.

(27) J. Uytterhoeven and J. J. Fripiat, *Bull. soc. chim. France*, in press.

(28) J. Mering, *Trans. Faraday Soc.*, **42**, 205 (1946).

(29) A. G. Keenan, R. W. Mooney, and L. A. Wood, *J. Phys. Colloid Chem.*, **55**, 1462 (1952).

origins of these discrepancies are different in both cases. In Aerogel, it is believed that pretreating under vacuum at 150° provokes a partial surface dehydration while it is likely that a network of very fine pores accessible to water and not to krypton[27] is developed in glass upon grinding.

2. Conductometric and Dielectric Measurements. The apparatus used consists of vacuum lines, conductivity cells, and oil manometers. Details of a conductivity cell are shown in Figure 1. The water uptake is obtained by using quartz helix balances. The Wayne–Kerr a.c. bridge, operated at frequencies from 2×10^2 to 2×10^4 c.p.s., allows one to measure simultaneously the parallel conductance G_p and capacitance X_p of the pellets.

The conductivity σ is derived from G_p according to $G_p = \sigma s/d$, where s and d are the pellet's cross-sectional area and thickness, respectively. The real part ϵ' of the complex dielectric constant obtains from X_p/X_{p_0} where X_{p_0} is the capacitance of the emptied cell; *i.e.*, $X_{p_0} = s/4\pi d$. The imaginary part ϵ'' is derived from the relationship $\epsilon'' = 4\pi\sigma/\omega$. The theoretical aspect of these measurements will be discussed later.

3. Entropy Computations. Entropy data were derived from adsorption isotherms measured at different temperatures. As shown later, this procedure requires a high accuracy at very low pressure. For this reason the adsorption apparatus was equipped with thermostated McLeod gauges and very sensitive mercury manometers, similar to the ones used for krypton adsorption measurements.[30] Water pressures as low as 10^{-4} mm. were detectable.

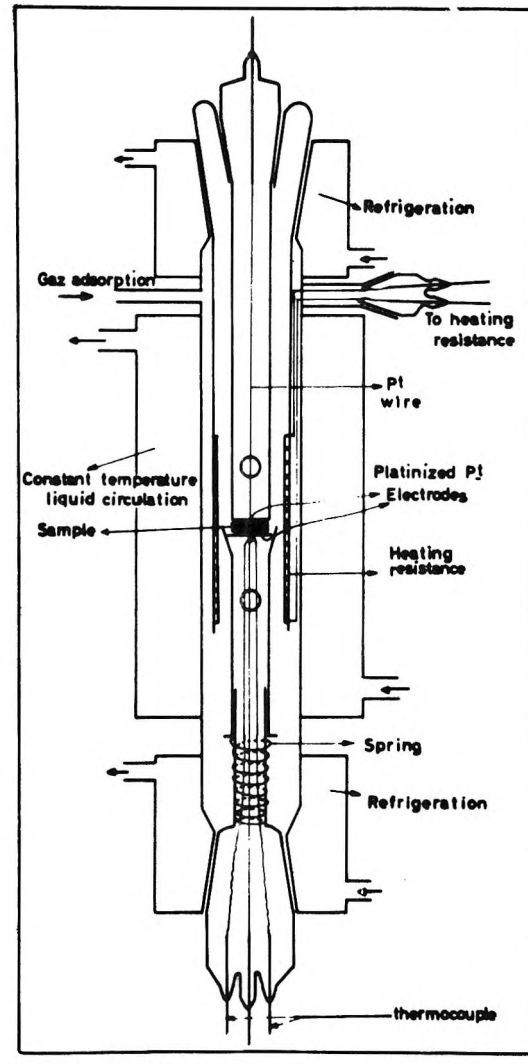

Figure 1. Conductivity cell.

III. Theoretical Considerations

1. Entropy Computations. From the theoretical treatment given by Hill,[31] it follows that

$$\left(\frac{\partial \ln p}{\partial T}\right)_\pi = \frac{\bar{H}_g - \bar{H}_a}{kT^2} = \frac{q_\pi}{kT^2} \qquad (1)$$

or that the partial derivative of the equilibrium pressure p with respect to the temperature T under a constant spreading pressure π is equal to the difference between the average heat contents per molecule, respectively, in the gaseous state ($\bar{H}_g$) and in the adsorbed state ($\bar{H}_a$), divided by kT^2.

The spreading pressure may be calculated by graphical integration of the Bangham relationship. This method of calculation requires the isotherms to be known extremely accurately down to very low pressures.

The Bangham equation should be used with caution because of the stepwise character of the water vapor adsorption by montmorillonite. If it is assumed that the surface area A consists of covered or bare partial surfaces a_i, the number of adsorbed water molecules N_s is

$$N_s = \sum_0^i N_i = \Gamma_i \sum_0^i a_i$$

where i represents the number of swelled silicate sheets and Γ_i the constant surface density of adsorbed molecules. An "apparent" surface concentration can then be defined as

$$\Gamma_{app} = \frac{N_s}{A} = \Gamma_i \frac{\sum_0^i a_i}{A}$$

and the spreading pressure π is then

(30) A. J. Rosenberg, *J. Am. Chem. Soc.*, 78, 2989 (1956).
(31) T. L. Hill, *J. Chem. Phys.*, 17, 120, 520 (1949).

$$\pi = \frac{kT\Gamma_i}{A}\int_0^p \sum_0^i a_i \mathrm{d} \ln p \qquad (2)$$

The integration is usually carried out graphically by plotting the degree of coverage θ divided by the pressure p against p. This procedure may be used for montmorillonite if θ is defined by $\sum_0^i a_i/A$, the relative number of opened lamellae; q_π is deduced at constant π, irrespective of its absolute value, and, hence, determination of π according to (2) is reliable whatever the value of Γ_i. For the other adsorbents, Γ is the Gibbs surface excess. The experimental integral entropy per molecule corresponding to the adsorption process is then obtained from

$$\Delta S_a = \frac{\bar{H}_a - \bar{H}_g}{T} = \bar{S}_a - \bar{S}_g \qquad (3)$$

The experimental ΔS_a are then compared to the theoretical ones deduced from statistical thermodynamic relationships applied to different models of physically adsorbed layers. The consideration of the mobility of adsorbed water molecules is important since they are believed to interact intimately with the electrical charge carriers.

The extreme situations of localized and delocalized (mobile) adsorbed molecules were taken into account.

As far as *localized adsorption* is concerned, it may be assumed that the M adsorption sites are divided into i classes, each of which contains M_i sites. The partition function of N_a adsorbed molecules ($N_a = \Sigma_i N_{ai}$) on M adsorption sites ($M = \Sigma_i M_i$) is then given by

$$Q_{N_a} = \prod_i \frac{M_i!}{N_{ai}!(M_i - N_{ai})!} Q_i^{N_{ai}} e^{-N_{ai}\epsilon_i/kT} \qquad (4)$$

The translation is replaced by three degrees of vibration of the molecule with respect to the solid surface. These degrees of vibration, as well as the internal degrees of freedom of the water molecule, are included in Q_i. The term ϵ_i represents the potential energy of the adsorbed molecule. If the surface is homogeneous, the partition function is

$$Q_a = \frac{M!}{N_a!(M - N_a)!}[Q_i e^{-\epsilon/kT}]^{N_a} \qquad (4')$$

It is necessary to anticipate the experimental results in order to justify the assumption that the surface probably may be considered as homogeneous within *the range of coverage degrees pertinent to the discussion of the conductometric measurements.* Figure 2a shows the equilibrium heat of adsorption, q_π, as a function of the averaged coverage degree, $\bar{\theta}$, for the various adsorbents used in this work.

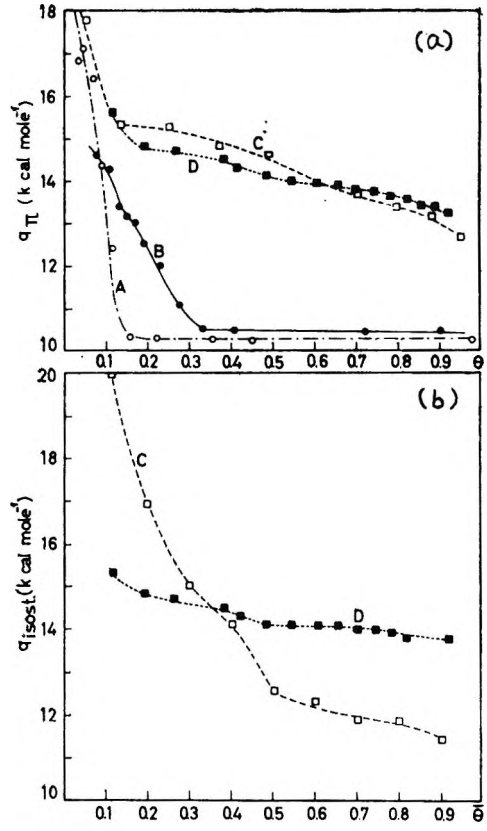

Figure 2. (a) q_π in kcal. mole^{-1} as a function of the averaged coverage degree $\bar{\theta}$: A, calcium montmorillonite at 27°; B, sodium montmorillonite at 27°; C, Aerogel at 35.5°; D, glass powder at 38°. (b) Isosteric heat of adsorption as a function of the averaged coverage degree $\bar{\theta}$: C, Aerogel at 35°; D, glass powder at 38°.

For both sodium and calcium montmorillonites, q_π reaches 10.3–10.5 kcal. mole^{-1} and remains constant for $\bar{\theta} \geq 0.3$. Moreover, the Volmer equation of state for a mobile film[32] is obeyed for $\bar{\theta} > 0.3$. For these montmorillonites, the liquid film is probably composed of mobile molecules, the motion of which is restricted to a bidimensional surface phase. In contrast, the higher q_π values obtained for the Aerogel and the glass powder suggest the occurrence of a localized adsorption. After a sharp variation in the range $0 < \theta < 0.15$, q_π decreases smoothly as θ is increased. In the region of interest for the comparison with conductometric measurements ($\theta \geq 0.2$) the smooth decrease of q_π may be explained as an increasing repulsive effect between adsorbed molecules, without intervention of an heterogeneous distribution of adsorption sites. It

(32) R. Fowler and E. A. Guggenheim, "Statistical Thermodynamics," Cambridge, 1960, p. 444.

is generally accepted that on silica gels pretreated at a moderate temperature, as in our experiments, the primary adsorption sites are hydroxyls groups. The differentiation between hydroxyls must not involve a large spectrum of adsorption energies, the main adsorption sites belonging to one class only.[33,34] Glass surfaces appear to have the same behavior.[26]

Two additional pieces of supporting evidence may be brought in favor of the preceding hypothesis. Figure 2b reproduces, for the two adsorbents on which localized adsorption is believed to occur, the change of $q_{isosteric}$ against $\bar{\theta}$. As usual q_{isost} is defined as $kT^2(\partial \ln p/\partial T)_\theta$. Since q_{isost} represents the differential heat of adsorption, the monotonous decrease of the function q_{isost} $(\bar{\theta})$ is in agreement with the hypothesis of a negligible surface heterogeneity. Moreover, as shown in Figure 3 for the glass powder, the variation of the experimental spreading pressure π against $-\ln(1-\theta)$ fits the equation of state applicable to localized adsorption on a homogeneous surface.[32] The discrepancy observed between the theoretical and experimental data for $\theta > 0.8$ probably arises from the neglected interactions between adsorbed molecules.

As suggested by Figure 2b, the repulsive effects between adsorbed molecules seem to be more active in Aerogel, and consequently the disagreement between the experimental and theoretical π becomes apparent at a lower θ as shown in Figure 3.

In the computation of Q_s according to (4′), it is observed that the frequencies of the fundamental internal modes of vibration are too high to produce an appreciable contribution to the molar entropy. However, slow vibration motions normal and parallel to the surface must be taken into account. Extending Hill's considerations, the frequency of the vibration normal to the surface may be taken as approximately proportional to the square root of the bonding energy D, so that $\nu_s = (a/\pi)\sqrt{D/2\mu}$, where a is the Morse function coefficient and μ, the reduced mass.[31] Hydrogen-bond energy being about 5 kcal. mole^{-1} for water, the corresponding frequency is approximately 6×10^{12} sec.$^{-1}$. This frequency will be used for delocalized adsorption. For Aerogel and the glass powder with an average adsorption energy considered as 10 kcal. mole^{-1}, the increase in the vibrational frequency normal to the surface shifts the theoretical entropy loss of approximately two entropy units towards higher values. This will be considered later in the discussion.

Hill[35] has shown that the frequencies of the vibration parallel to the surface are also proportional to the square root of the adsorption energy. The proportionality coefficient cannot be computed in our case,

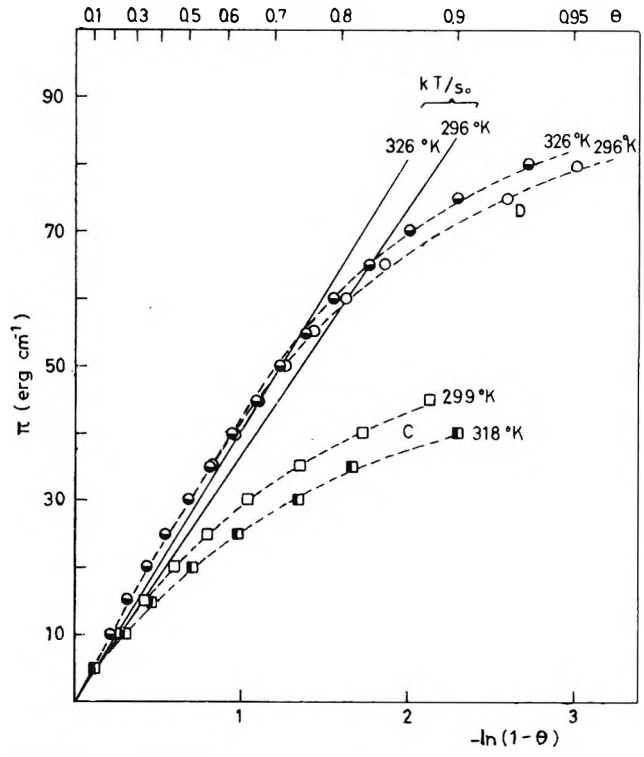

Figure 3. Spreading pressure π against $-\ln(1-\theta)$: dotted lines C, Aerogel; dotted lines D, glass powder; solid lines, kT/s_0.

but the "parallel" frequencies are lower than the "normal" frequency.

Using a "parallel" frequency one order of magnitude smaller than the "normal" frequency would lead to a theoretical entropy loss lowered by approximately 5 e.u. For the sake of simplicity, the parallel frequencies will be taken equal to the normal frequency, but the consequence of this assumption will be discussed later.

The contribution of the rotational partition function to Q_t is easily determined according to classical relationships. In localized adsorption, however, it is very probable that, if any, only one rotation degree around one privileged axis is to be considered. Each hindered rotation degree has, of course, to be replaced by one vibrational degree of freedom with respect to the adsorption site.

For a mobile film (*delocalized adsorption*) the partition function is given by

$$Q_s = \frac{1}{N_s!}\left[\frac{2\pi mkT}{h^2}(A - N_s s_0)Q_t e^{-\epsilon/kT}\right]^{N_s} \qquad (5)$$

(33) A. V. Kiselev and V. I. Lygin, *Colloid J.*, **31**, 561 (1959); *Proc. Intern. Congr. Surface Activity, 2nd, London, 1957*, 2, 179 (1957).

(34) J. J. Fripiat, M. C. Gastuche, and R. Brichard, *J. Phys. Chem.*, **66**, 806 (1962).

(35) T. L. Hill, *J. Chem. Phys.*, **14**, 441 (1946).

The translational contribution $(2\pi mkT)(A - N_s s_0)/h^2$ contains the surface area A of the adsorbent and the area covered by one water molecule (s_0 = 11 Å.^{2}). The rotational partition function is calculated as usual. The internal molecular vibrations are neglected, and the vibrational mode normal to the surface replaces the third translational degree of freedom.

In conclusion, it is believed that the distinction between the mobile and immobile states of adsorbed molecules will not be affected by assumptions made in the computation of the theoretical entropy data to an extent that would invalidate comparison with experimental data within that range of coverage where the conductometric data are of interest.

2. Conductometric and Dielectric Measurements. The equivalent network of the powder pellets is shown in Figure 4, where the electrical parameters characterizing the solid particles (s) and the contact zone (c) are separated.

The parallel conductance G_p and capacitance X_p have the following limiting values at low and high frequency.

$$G_p = \frac{G_s G_c}{G_s + G_c} \qquad X_p = \frac{X_c G_s^2 + X_s G_c^2}{(G_s + G_c)^2} \tag{6}$$

(low frequency)

$$G_p = \frac{X_s^2 G_c + X_c^2 G_s}{(X_s + X_c)^2} \qquad X_p = \frac{X_c X_s}{X_c + X_s} \tag{7}$$

(high frequency)

Huggins and Sharbaugh,[36] who have analyzed such a circuit, have determined that the transition between the low and high frequency conditions occurs around 100 c.p.s. Therefore, high frequency relationships (7) are probably applicable under the conditions used in this work. Moreover, it will be assumed that $G_s > G_c$ and $X_s > X_c$ so that G_s and X_s are effectively measured. This hypothesis is supported by the fact that the contact zone represents only a small proportion of the particle surface area.

The electrical measurements associated with the water adsorption phenomena may then be interpreted according to this hypothesis for conditions where capillary condensation is not significant.

The study of the dispersion of the real and imaginary terms of the complex dielectric constant with respect to the frequency demonstrates that the main phenomenon is the absorption of the electrical energy by free charge carriers. Therefore, the model suggested by Figure 5 may be adopted: charge carriers (ze) have to jump over the potential barrier U in order to move

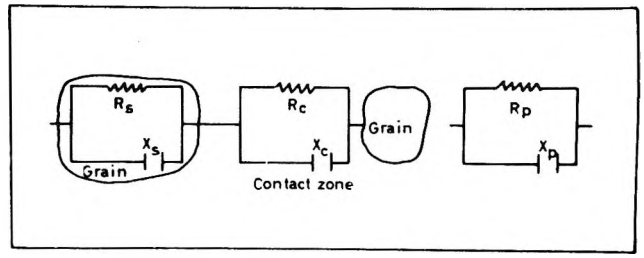

Figure 4. Schematic electrical network of the powder: left, two grains separated by a contact zone; right, equivalent parallel circuit.

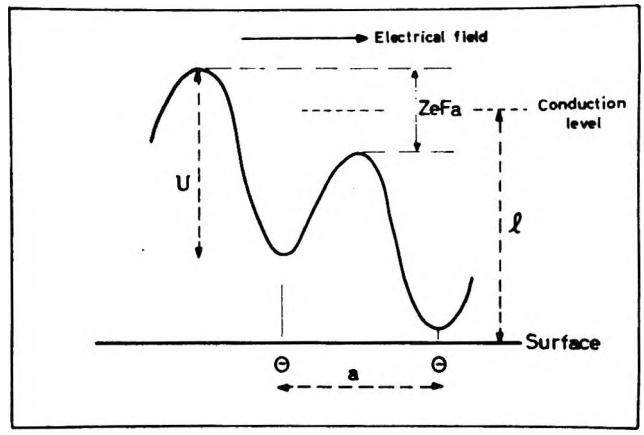

Figure 5. Model adopted for the translation of a charge carrier along the field direction.

from one to the next equilibrium position. The specific conductivity σ is then given by

$$\sigma = n_p \nu \frac{z^2 e^2 a^2}{kT} e^{-U/kT} \tag{8}$$

where n_p is the number of charge carriers per unit volume, ν the number of "jumping attempts" per second, and a the distance between two equilibrium positions.

In the neighborhood of plane electrically charged surfaces, $U = -ze\psi$, where ψ is the electrical potential at the "conduction level." This value may be conveniently expressed either as a function of the surface density of charge χ ($\psi = 4\pi\chi l$) or in terms of the number of charge carriers by volume unit (n_p) since each negative spot must be balanced. Therefore

$$U = -4\pi(ze)^2 l \frac{n_p}{A\rho} \tag{9}$$

where ρ is the density of the sample and A, its surface area. Introducing (9) into (8) leads to

(36) C. M. Huggins and A. H. Sharbaugh, *J. Chem. Phys.*, **38**, 799 (1961).

$$\sigma = n_p \nu \frac{z^2 e^2 a^2}{kT} \exp\left(\frac{4\pi (ze)^2 l n_p}{kTA\rho}\right) \quad (10)$$

and hence to the conclusion that σ is essentially an exponential function of the number of charge carriers per unit volume. It will be experimentally demonstrated that for sections of the adsorption isotherms

$$\sigma = \sigma^*_0 e^{C\theta} \quad (11)$$

and that

$$\epsilon' = \epsilon'_0 e^{K\theta} \quad (12)$$

where C and K are temperature-independent constants and θ, the degree of surface coverage by water molecules. The specific conductivity σ is related to the temperature as

$$\sigma = \sigma_0 e^{-\Delta F^*/RT} \quad (13)$$

where ΔF^* is the activation free energy related to the motion of the carriers. It follows from (13) and (11)

$$\Delta F^* = \Delta F_0^* - CRT\theta \quad (14)$$

$$\Delta S^* = \Delta S_0^* + CR\theta$$

where ΔS^* is the corresponding entropy of activation while ΔF_0^* and ΔS_0^* refer to the dehydrated state.

The comparison among (10), (11), and (12) shows that the number of charge carriers is related to the number of adsorbed water molecules. From relationships 11 and 12, it follows that the tangent of the loss angle is an exponential function of θ.

$$\tan \delta = \frac{4\pi}{\omega} \frac{\sigma^*_0}{\epsilon'_0} e^{(C-K)\theta} \quad (15)$$

It does not depend on the surface coverage for $C \rightarrow K$.

IV. Experimental Results

1. Conductometric and Dielectric Measurements. Exploratory experiments were first made to ensure that the electrical phenomena involved under the adopted experimental conditions were mainly concerned with conduction processes by free charge carriers. For sodium and calcium montmorillonites, it has been observed that ϵ' and ϵ'' decrease rapidly with increasing frequency, the decrease being more pronounced at higher hydration levels; this strongly supports the hypothesis of conduction by free charge carriers.[37] Similar effects were recorded for both Aerogel and the glass powder.

The dielectric and conductometric data were then carefully recorded under various experimental conditions at 1592 hertz, the basic Wayne–Kerr bridge frequency. Some examples of the experimental results are shown in Figure 6.

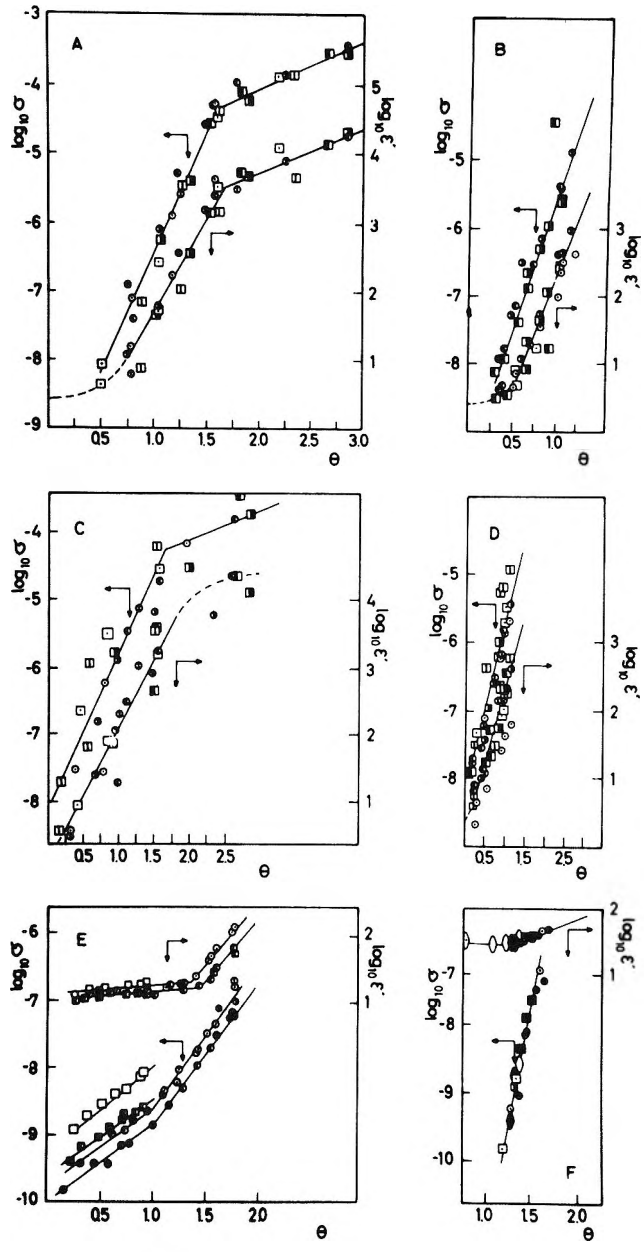

Figure 6. Variation of the logarithm of the conductivity σ (mho cm.$^{-1}$) and of the real part ϵ' of the complex dielectric constant against surface coverage θ. Experiments were duplicated with different pellets. Calcium montmorillonite: A, at 17°; B, at 43°. Sodium montmorillonite: C, at 17°; D, at 42°. The white symbols refer to pellets characterized by porosities approximating 16%; the black ones, to pellets characterized by porosities of about 50%. Aerogel: E, the white circles and squares refer to H_2O adsorption at 20 and 40°, respectively; the black symbols, to D_2O adsorption at the same temperatures. Glass powder: F, white circles, squares, and lozenges refer to H_2O adsorption at 20, 30, and 40°, respectively; black symbols, to D_2O adsorption at the same temperatures.

(37) A. Freyman and M. Scutif, "La spectroscopie hertzienne appliquée à la chimie," Dunod, Paris, 1960, p. 37.

The conductivity σ and dielectric constant ϵ' are expressed in a semilog representation with respect to θ. In some cases, discontinuities are observed which divide the variations of these functions into two linear segments; the corresponding lower and upper limits are indicated in Table III. If the data are expressed by relationships 11 and 12, θ being the ratio of N_s to N_{sm} deduced from the B.E.T. relationship obtained for water adsorption, the C and K coefficients are approximately temperature independent.

Table III: Electrical Parameters Obtained at 1592 Hertz and at Different Temperatures[a]

	Temp., °C.	Sodium montmorillonite Upper limit	Calcium montmorillonite Upper limit	—Aerogel— Lower limit	—Aerogel— Upper limit	—Glass powder— Lower limit	—Glass powder— Upper limit
θ^*	17.0	1.6	1.5				
	20.0			1.1	...	...	...
	26.0	...	1.5				
	37.0	...	...				
	40.0			(1.1)	...	...	...
				Lower linear segment	Upper linear segment	Lower linear segment	Upper linear segment
C	17.0	5.23	7.82				
	20.0			2.56	4.8	...	16.1
	26.0	5.53	8.20				
	37.0	5.20	8.15				
	40.0			2.75	...	...	16.1
Av.	17–40	5.32	8.06	2.65			16.1
K	17.0	4.48	6.40				
	20.0			0.311	4.25	≃0	1.136
	26.0	4.80	6.91				
	37.0	4.45	7.10				
	40.0			0.311	...	≃0	1.136
Av.	17–40	4.57 ± 3%	6.80 ± 4%	0.311		≃0	1.136
C/K Av.	17–40	1.165	1.185	8.5	1.13	...	14.2

[a] C and K coefficients according to relationships 11 and 12; θ^*, surface coverage degrees which delineate the linear segments shown in Figure 6.

Neither the C nor the K coefficient depends on the degree of compaction. For instance, Figure 6 shows that montmorillonite pellets characterized by porosity values covering the range from 16 to 50% give similar results. Such porosities obtain by compressing at pressures ranging from 4.16×10^3 to 6.62×10^3 kg./cm.^{2}. This observation supports the assumption that the measured conductance deals almost exclusively with carriers moving along particle surfaces and not in the interstices. A significant feature of the results is also that the adsorption and desorption data do not differ appreciably.

In some experiments, H_2O has been replaced by D_2O. The ratios of the C coefficients obtained under similar conditions (C_{H_2O}/C_{D_2O}) are slightly higher than 1 but the difference is small.

2. Adsorption Data. The adsorption isotherms have been measured very carefully from approximately 5×10^{-4} to 15 mm. A semilog representation has been adopted to represent the experimental results (Figure 7).

Adsorption by sodium and calcium montmorillonites obviously occurs in two steps, the transition being found for $0.01 < P/P_0 < 0.03$, regardless of the nature of the exchangeable cations. In the case of sodium montmorillonite, the 001 X-ray reflection has been recorded with respect to P/P_0 in a vacuum camera described elsewhere.[38] The change of the 001 spacing with respect to P/P_0 is shown in Figure 8; the comparison of these data with the transition observed in the adsorption isotherm demonstrates that it corresponds to the swelling of the interlamellar space. The nature

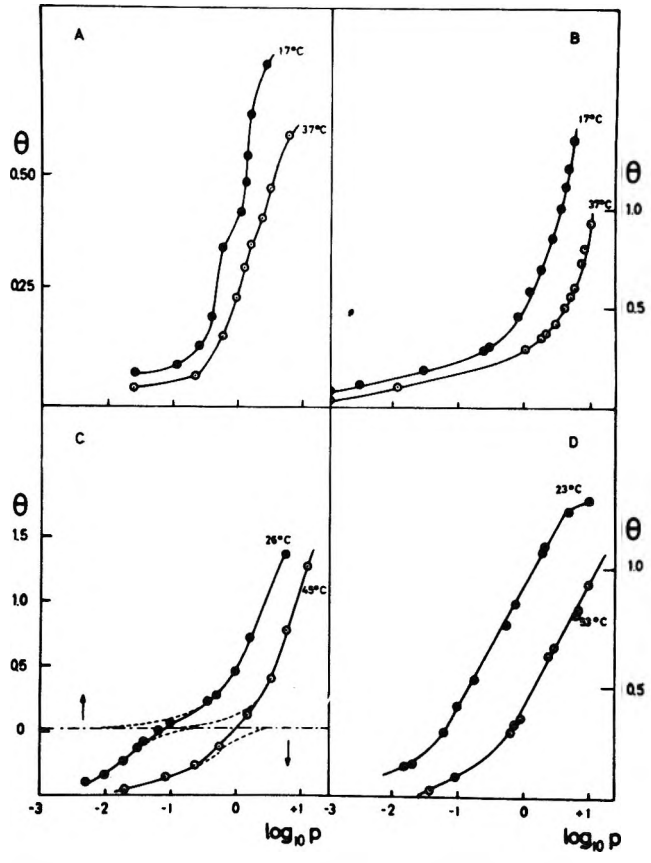

Figure 7. Water adsorption isotherms; θ, *vs.* logarithm of equilibrium pressure (mm.): A, calcium montmorillonite; B, sodium montmorillonite; C, Aerogel; D, glass powder.

(38) J. N. Van Nieuwkerk, *J. Sci. Instr.*, **37**, 172 (1960).

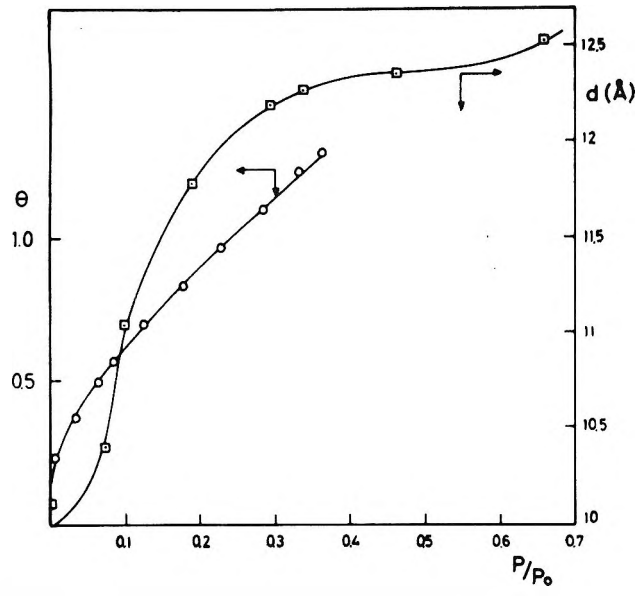

Figure 8. Adsorption isotherm and changes of the 001 spacing of sodium montmorillonite against P/P_0.

of exchangeable cations influences quantitatively the adsorbed volumes and the N_{sm} (B.E.T.) parameters (Table IV). The value obtained for calcium montmorillonite is approximately double that for sodium montmorillonite. X-Ray measurements made possible the use of various models to calculate the theoretical N_{sm} values given in Table IV.

Table IV: N_{sm} B.E.T. Parameters (10^{-3} mole g.$^{-1}$) Obtained for Water on Powders at 25°[a]

	N_{sm}, 10^{-3} mole g.$^{-1}$			
	Sodium montmorillonite	Calcium montmorillonite	Aerogel	Glass powder
Obsd.	3.0	6.85	3.0	0.035
Theoret.	5.5	12.1	...	...

[a] N_{sm} theoretical, calculated for montmorillonites assuming a molecular packing of 11 Å.^{2}, the external and internal surface areas given in Table II, and the adsorption of one or two water layers in the interlamellar space of Na and Ca samples, respectively.

The discrepancy between the experimental and theoretical results might be explained by assuming the superposition of chemical and physical adsorption processes. Exposing partially dehydrated montmorillonites to water vapor provokes a fast chemical adsorption which results from partial rehydration of exchangeable cations located on either external or internal surfaces. The amount adsorbed in this first step is too low to produce a measurable expansion of the lattice parameter c; the presence of less than one water molecule per cation cannot be detected easily by X-ray measurements. Further increase in the water pressure results in a physical adsorption process which affects the external surfaces and, above a given pressure, the internal surfaces. Beyond this limit, changes in c-axis spacings are observed on the X-ray diffraction patterns.

The area available for chemical adsorption around exchangeable cations will depend, of course, upon their charge. It may be appropriate to suggest that from the viewpoint of the water chemisorption process, the area of surface associated with each cation is appreciably less than can be calculated from the surface density of charge. Allowing 90 Å.^{2} to Ca^{2+} and 55 Å.^{2} to Na^+, the surface areas involved in this chemical adsorption should amount to 270 m.^{2} g.$^{-1}$ in calcium montmorillonite and to 330 m.^{2} g.$^{-1}$ in sodium montmorillonite. The areas available for physical adsorption would then be 455 and 395 m.^{2} g.$^{-1}$, respectively; these figures correspond to the observed N_{sm}.

The adsorption isotherms obtained for the glass powder do not require special comments, but the ones obtained for Aerogel are rather surprising. An inflection point occurs in the range of $1 < N_s < 1.2 \times 10^{-3}$ mole g.$^{-1}$, and, below this limit, N_s is proportional to the square root of the pressure as shown in Figure 9. Outgassing at 160° might cause some condensation of surface hydroxyl pairs. Rehydration should then occur at the initial stage of water adsorption. In this adsorption range, accordance with the square-root law indicates that water is dissociated. Thus, for entropy computations it is necessary to split the adsorption isotherms observed for Aerogel into two separate curves related to the dissociation process and to the actual physical adsorption, respectively. This has been done by a sequence of recurrence approximations based on the experimental observation that at low surface coverage the physical adsorption iso-

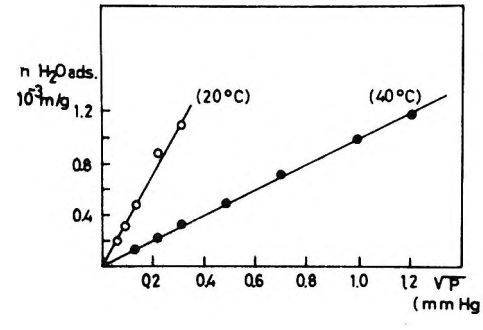

Figure 9. Number of water molecules adsorbed on Aerogel against the square root of equilibrium pressure p (mm.).

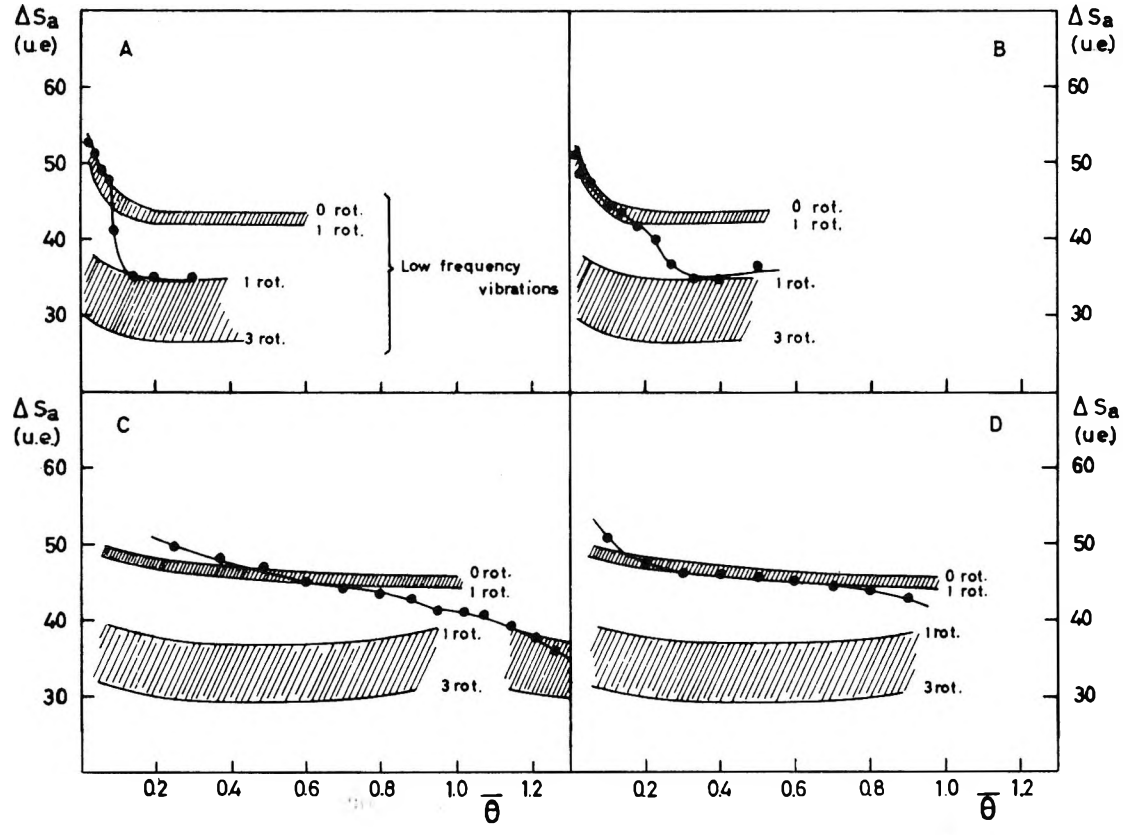

Figure 10. Entropy loss ΔS_a (e.u.) of water molecules as a function of the averaged coverage degree $\bar{\theta}$: black dots, experimental values obtained from relationship 3; upper shaded range, theoretical entropy loss for an immobile film; the upper and lower limits of this range correspond, respectively, to the loss of three and two rotational degrees; lower shaded range, theoretical entropy loss for a mobile film characterized by one (upper limit) and three (lower limit) rotational degrees; A, calcium montmorillonite at 27°; B, sodium montmorillonite at 27°; C, Aerogel at 35.5°; D, glass powder at 38°.

therms are linear; the resulting functions are indicated by the dashed lines in Figure 7C. Therefore, N_{sm} is obtained by substracting 10^{-3} mole g.$^{-1}$ from the value computed according to the B.E.T. theory.

3. Entropy Data. The theoretical entropy losses deduced from relationship 4′ for localized adsorption on a homogeneous surface and from relationship 5 for delocalized adsorption, as well as the experimental data, are shown in Figure 10.

The assumptions made on the vibration frequencies of the adsorbed molecule with respect to the surface do not affect markedly the theoretical data for delocalized adsorption. In the range of interest ($\theta > 0.25$) and for both sodium and calcium montmorillonites, the adsorbed molecules therefore are probably mobile.

For Aerogel and the glass powder, the observed entropy losses are obviously much higher than the corresponding theoretical values for a mobile film so that the translation may, at least, be considered as rather restricted and even probably suppressed in the range of $0.2 < \theta < 1$. The shift of the theoretical data consequently to an overestimation of the frequencies of the vibrational mode parallel to the surface would lower the upper shaded areas of Figures 10C and D and should, therefore, outline still more the immobile character of the adsorbed water molecules. The shift of the theoretical data due to an underestimation of the vibration frequency normal to the surface would elevate the same shaded areas by less than 2 e.u. and would not seriously affect the conclusions.

An eventual heterogeneous character of the surfaces should influence the theoretical calculations in an unpredictable way, but this influence seems to be negligible in the range of coverage degree where comparisons with conductometric data are of interest.

Under these restrictions it may be concluded that the three absorbents used in this work seem to differ considerably from the viewpoint of the mobility of the water molecules belonging to the monolayer. The transition between the immobile and mobile states would take place for the two homoionic montmorillonites at low θ-values; *i.e.*, $\theta = 0.1$ for calcium mont-

Table V: Nature of the Surface, Mobility of Water Molecules, and Electrical Data

Adsorbents	Surface atoms or radicals (O, oxygen; OH, hydroxyls)	θ	Mobility of adsorbed water molecules	C parameter (relationship 11)	K parameter (relationship 12)	C/K
Calcium montmorillonite		$\theta < 0.1$–0.2	Immobile	Not measurable	Not measurable	...
	Internal surface (O)	$0.2 < \theta < 1.5$	Mobile	8.06	6.8	1.185
Sodium montmorillonite		$\theta < 0.2$	Immobile	Not measurable	Not measurable	...
	Internal surface (O)	$0.2 < \theta < 1.6$	Mobile	5.32	4.57	1.165
Aerogel	OH	$\theta < 1$	Immobile	2.65	0.311	8.5
		$\theta > 1$	Mobile	4.8	4.25	1.13
Glass powder	OH	$\theta < 1$	Immobile	Not measurable	0	...
		$1 < \theta <$ undetermined limit	Immobile	16.1	1.136	14.2

morillonite and $\theta = 0.25$ for sodium montmorillonite. For Aerogel the transition between localized and delocalized adsorption appears to occur approximately at $\theta = 1$, while for the glass powder, even at $\theta = 1$, the experimental entropy values are still appreciably higher than the theoretical data characterizing a mobile water film.

From these observations it may be concluded that the physically adsorbed molecules belonging to the monolayer are *mobile* on "oxygen" internal surfaces of montmorillonite and *immobile* on hydroxylic surfaces of Aerogel and of the glass powder.

V. Discussion

The data involved in this discussion are collected in Table V. Exponential relationships between the conductivity and the number of adsorbed molecules have been reported for zeolite–water systems by Stamires,[39] by Barriol, Cabrera, and Robert[40] for silica gel–ammonia systems, and Rosenberg[41] for hydrated proteins. In the first two cases, conduction by exchangeable cations or ammonium ions was assumed while an electronic mechanism was proposed for the hydrated protein system.

As the nature of the charge carriers is not taken into account in deriving the exponential relationships (8–10), it follows that the observed empirical relationships (11) do not permit a distinction to be made between cationic or protonic conduction.

These alternative processes are clearly fundamentally different. Proton migration proceeds following a chain of exchange reactions, $H_3O^+ + H_2O \rightleftarrows H_2O + H_3O^+$, described by Bernal and Fowler[42] and by Conway, Bockris, and Linton.[43] If the adsorbed water layer contains mostly molecules which can rotate but which are unable to move, proton transfer is still possible, provided an adequate distribution of the molecules exists in the surface bidimensional phase. It might be assumed that under these conditions the loss angle would be a function of the surface coverage, as predicted by eq. 15 if the C/K ratio differs appreciably from unity. Actually, in every case where the water molecules are immobile, the C/K values confirm this deduction. If the adsorbed film is composed of molecules with two translational degrees of freedom, proton transfer will not require such a favorable distribution. Experimental results show that the C/K ratios are then very close to unity. Again, according to relationship 15, this would mean that the loss angle does not depend upon the surface coverage.

The relation between the C/K values and the mobility properties of adsorbed molecules should not be as obvious for the cationic as for the protonic conduction.

Moreover the C and K coefficients characterizing the electrical behavior of the *mobile* film on Aerogel and on sodium montmorillonite, for instance, are very close, and, in addition, the absolute values of the *surface conductivities* are similar. For $\theta = 1.5$ and 0.8, these values are 6×10^{-14} mho cm.$^{-3}$ for sodium montmorillonite and 1.6×10^{-14} mho cm.$^{-3}$ for Aerogel; they differ therefore by less than one order of magnitude although the sodium content amounts to 10^{-3} equiv. g.$^{-1}$ in the clay and to 6×10^{-6} equiv. g.$^{-1}$ in the silica gel. This comparison strongly suggests that the charge carriers are not the metal cations.

Numerous questions remain to be solved, especially

(39) D. M. Stamires, *J. Chem. Phys.*, **36**, 3174 (1952).

(40) J. Barriol, C. C. Cabrera, and A. M. Robert, *J. chim. phys.*, **59**, 154 (1962).

(41) B. Rosenberg, *J. Chem. Phys.*, **36**, 816 (1962).

(42) J. D. Bernal and R. H. Fowler, *ibid.*, **1**, 515 (1933).

(43) B. E. Conway, J. O'M. Bockris, and H. J. Linton, *ibid.*, **24**, 832 (1956).

those concerning the basis of the water dissociation process and the explanation of mobility features.

On electrically charged montmorillonite surfaces, it has been shown[22] that the extent of NH_3 conversion into NH_4^+ depends on the strength of the polarizing field of exchangeable cations, which influence the dissociation degree of the water molecules belonging to their hydration shell. Ammonia conversion results in the capture of these protons, the OH^- anions being held by the positive metal ions to maintain the charge balance.

The n.m.r. studies performed by Ducros and Dupont[44] also support the proposed dissociation mechanism and show that the dissociation degree is at least 10^3 times higher than in liquid water. On silica gel surfaces, the force field arising from ionic Si–O bonds should be responsible for similar effects although the degree of dissociation would probably be less pronounced. The somewhat lower conductivity values observed for this material, as compared with montmorillonite, reflects the smaller number of "induced" charge carriers. The chemical adsorption process suggested to explain the early stage of montmorillonite rehydration probably accounts for the production of protons. In Aerogel, the dissociative adsorption reported previously should be related to some extent to the same phenomenon.

The dissociation degree of surface water may be computed from relationships 10 and 11, from which it follows that

$$\alpha = \frac{kTAC}{N_{sm}4\pi e^2 l} \tag{16}$$

α being defined by

$$\alpha = \frac{n_p}{N_s \rho} \tag{17}$$

If l is made equal to 1.5 Å. (*i.e.*, half the monolayer thickness) α is numerically given by $1.12 \times 10^{-2} C/N_{sm}$. For both calcium and sodium montmorillonites, $\alpha \simeq 0.01$ and is of the same order of magnitude for the two other adsorbents. In liquid water at 25°, α is 1.3×10^{-8}, namely, 10^6 times weaker.

A check for the calculated degree of dissociation may be performed by comparing the measured and calculated specific conductivities at $\theta = 1$. From eq. 10, 11, 16, and 17, it follows that

$$\sigma = [\alpha \rho N_{sm} \nu a^2 e^2 \exp(C)]/kT \tag{18}$$

The number of "jumping attempts" per second (ν) and the distance between two potential minima (a) have to be estimated. The distance between two oxygen atoms in close packing may be assumed to represent the latter adequately (3 Å.). According to Zimmerman and Lasater,[45] the lifetime of a hydrogen nucleus (perhaps the water molecule) in the adsorbing phase on silica gel approximates 10^{-3} sec. at $\theta = 0.5$. This provides an order of magnitude for ν, which may be used in computing σ. Hence, the calculated specific conductivities for calcium and sodium montmorillonites at $\theta = 1$ and 20° are 5.6×10^{-8} and 1.4×10^{-6} mho cm.$^{-1}$, respectively. The agreement between these figures and the experimental data shown in Figure 6 supports the value obtained for the dissociation degree of adsorbed water molecules.

The second important fact to be considered concerns the difference in mobility of water molecules on oxygen and hydroxyl surfaces. The formation of hydrogen bonds between the water molecules in the monolayer and surface hydroxyls is probably the reason for localized adsorption in Aerogel and glass powder. The observed differential heats of adsorption are of the order of magnitude expected for such bonds.

Nuclear magnetic resonance measurements (Sears[46]) also confirm the mobility of water molecules associated with the internal oxygen surfaces of montmorillonite and the immobility of water on the hydroxylic external surfaces of kaolinite.

VI. Conclusions

A close correlation has been shown to exist between electrical properties of hydrated silicates and the behavior of adsorbed water molecules on these surfaces.

In the range of water contents investigated here, electrical conductivity is probably mostly protonic. Protons originate from the dissociation of water molecules which is enhanced by surface electrical fields. The degree of dissociation is of the order of magnitude of 10^{-2}.

The loss angle, which is a function of the absorbed electrical energy, depends on the surface mobility of the adsorbed molecules. This angle is strongly influenced by surface coverage for localized adsorption while it is approximately independent of surface coverage for delocalized adsorption.

On hydroxylic surfaces, monolayer water molecules are immobile while on the oxygen surface of montmorillonite they are mobile.

Acknowledgments. We are grateful to Glaverbel S. A. for support given to A. J. and also for permission

(44) P. Ducros and M. Dupont, *Bull. Groupe Franc. Argiles*, T8, 8 (1962).

(45) J. R. Zimmerman and J. A. Lasater, *J. Phys. Chem.*, 62, 1157 (1958).

(46) R. E. J. Sears, *New Zealand J. Sci.*, 3, 127 (1960).

to publish the data obtained for the glass powder. We are also pleased to acknowledge the help provided by Dr. M. Martin (Géopétrole, Paris) for the realization of this work. We wish to thank Dr. J. Chaussidon from C.N.R.A. (Versailles, France) and Prof. H. Laudelout from this university for many helpful discussions. G. P. is indebted to I.R.S.I.A. for a Ph.D. fellowship.

Viscosity of Aqueous Solutions. IV. Chloroammineplatinum(IV) Salts. Influence of Ionic Charge on the Viscosity *B*-Coefficient

by E. R. Nightingale, Jr.,[1] and J. F. Kuecker[2]

Esso Research & Engineering Co., Linden, New Jersey, and University of Nebraska, Lincoln, Nebraska
(Received December 1, 1964)

The viscosities of aqueous solutions of $Pt(NH_3)_6Cl_4$, $[Pt(NH_3)_5Cl]Cl_3$, $[Pt(NH_3)_4NH_2Cl]Cl_2$, and Na_2PtCl_6 have been measured at 20, 25, and 30° in the concentration range 0.005 to 0.1 *m*. The viscosity data have been interpreted in terms of the Jones–Dole equation for strong electrolytes. The viscosity *B*-coefficients for the platinum ions at 25° are calculated to be: $Pt(NH_3)_6^{4+}$, +0.406; $Pt(NH_3)_5Cl^{3+}$, 0.397; $Pt(NH_3)_4NH_2Cl^{2+}$, 0.301; and $PtCl_6^{2-}$, 0.218 l./mole. The ionic activation energies for viscous flow are +370, 290, 480, and −290 cal./mole, respectively. The dependence of the ionic *B*-coefficient on ionic charge has been analyzed as a function of ionic size, structure, and charge type. It is demonstrated that for large ions with hydrophobic surfaces the *B*-coefficient is determined primarily by the size of the ion and is essentially independent of ionic charge. Polyatomic ions with hydrophilic groups such as –Cl, $-NH_2$, or –OH which can more effectively delocalize the ionic charge exhibit diminished *B*-coefficients. For small monatomic ions which are peripherally hydrated, the *B*-coefficient is a function of the electric field about the ion and increases with increasing ionic charge and decreasing crystal radius. The limiting value for the *B*-coefficient is determined by the electric field required to polarize the water molecule to form hydrolytic species $M(OH)_n^{z-n}$.

Previous discussions from our laboratories[3-5] have emphasized that transport processes can provide significant information concerning the nature of ion–solvent interactions and the effective size of hydrated entities. However, transport parameters and infrared spectra indicate that ionic interactions with water are highly specific and greatly dependent upon the charge, size, and structure of the ions. The current contribution is one of a series designed to elucidate the effects of ion parameters on the viscosity of aqueous solutions and also to provide insight into the nature of the ion–solvent interactions which prevail.

The influence of a strong electrolyte upon the vis-

(1) To whom inquiries should be addressed: Esso Research & Engineering Co., P. O. Box 121, Linden, N. J.

(2) Presented in partial fulfillment of the requirements for the M.S. degree, University of Nebraska, 1962.

(3) E. R. Nightingale, Jr., *J. Phys. Chem.*, **63**, 742, 1381 (1959).

(4) E. R. Nightingale, Jr., and R. F. Benck, *ibid.*, **63**, 1777 (1959).

(5) E. R. Nightingale, Jr., *ibid.*, **66**, 894 (1962).

cosity of a polar solvent is given by the Jones–Dole equation[6]

$$\eta/\eta_0 = 1 + A\sqrt{C} + BC \qquad (1)$$

where η/η_0 is the viscosity of a salt solution relative to that of the solvent water, C is the molar concentration, and A and B are constants characteristic of the electrolyte. The A-coefficient represents the contribution from interionic electrostatic forces,[7] and the B-coefficient measures the order or disorder introduced by the ions into the solvent structure. The latter coefficient is a specific and approximately additive property of the ions of a strong electrolyte at a given temperature[8] although no satisfactory theoretical treatment has yet been given. The ionic B-coefficient is proportional to the partial molar entropy of hydration,[3,9] and it recently has been demonstrated that the B-coefficient is also a measure of the radius and, hence, the effective volume of an ion in aqueous solution.[3] While the ionic charge obviously affects the entropy of hydration and effective ionic volume, no previous studies have attempted to explain the role of ionic charge on the viscosity B-coefficient. With the exception of the Cs^+, Rb^+, K^+, Cl^-, Br^-, and I^- ions, all monatomic cations are "positively" hydrated in the sense that the structure of the solution about the ion is more ordered or ice-like than is bulk solution, and the translational motion of the nearest-neighbor water molecules is restricted as compared with that of pure bulk solvent.[10] It is difficult, however, to ascertain the effect of charge for such ions because the ionic size varies widely, and only limited correlations for species of a given radius such as Sr^{2+} and La^{3+} can be obtained. The present study has investigated the effect of ionic charge (and insofar as possible, size and structure) on the viscosity B-coefficient. A necessary condition for this work was that the crystal ionic radius remains sensibly constant throughout a chosen series of ions with varying charge. The substituted chloroammineplatinum(IV) ions were chosen to fulfill this criterion and also to provide a series of ions which were relatively large and minimally hydrated. An additional advantage is that this series of ions is moderately inert to hydrolysis except in very dilute solutions. While in principle it is possible to prepare ions in this series with formal charges from 4+ to 2−, it was feasible to prepare and study the salts of only four of these ions.

The viscosities of the following salts have been investigated: hexaammineplatinum(IV) chloride, $Pt(NH_3)_6Cl_4$; chloropentaammineplatinum(IV) chloride monohydrate, $[Pt(NH_3)_5Cl]Cl_3 \cdot H_2O$; amidochlorotetraammineplatinum(IV) chloride, $[Pt(NH_3)_4NH_2Cl]Cl_2$; and sodium hexachloroplatinate(IV) hexahydrate, $Na_2PtCl_6 \cdot 6H_2O$. The corresponding platinum ions $Pt(NH_3)_6^{4+}$, $Pt(NH_3)_5Cl^{3+}$, $Pt(NH_3)_4NH_2Cl^{2+}$, and $PtCl_6^{2-}$ are designated by their ionic charge and are represented throughout this paper as $Pt(IV)^{4+}$, $Pt(IV)^{3+}$, $Pt(IV)^{2+}$, and $Pt(IV)^{2-}$, respectively. From the known interatomic distances of several of these salts[11] and the van der Waals radii for the chloride and ammonia groups, the crystal ionic radii of these platinum-containing ions are all calculated to be 4.1 ± 0.05 Å.

Experimental

The four platinum salts discussed in the preceding paragraph were prepared and purified according to detailed procedures which, with references, have been published elsewhere.[12] The salts were analyzed for nitrogen, total and ionizable chloride, and in some cases platinum. The salts were dried to a suitable weighing form, and the solutions were prepared on the molal basis with conductivity water. An Ostwald viscometer with flow time of *ca.* 650 sec. was calibrated with water by means of

$$\eta/\rho = Kt - L/t \qquad (2)$$

where η is the absolute viscosity, ρ is the density, and t is the flow time. The characteristic viscometer constants K and L were 1.392×10^{-5} and 0.1237, respectively. The densities and viscosities of the solutions were determined in the same manner as described previously.[4] The absolute viscosities of water at 20, 25, and 30° are 0.01002, 0.008903, and 0.007976 poise, respectively.[13] The densities are 0.99823, 0.99707, and 0.99568 g./ml., respectively.[14]

Results

Five to eight solutions of each salt were prepared in the concentration range 0.005 to 0.1 *m*. The absolute viscosities of the solutions were computed by means of eq. 2, and the data were analyzed graphically and also numerically with an electronic computer using the Jones–Dole equation.[6,15] The viscosity A- and B-

(6) G. Jones and M. Dole, *J. Am. Chem. Soc.*, **51**, 2950 (1929).

(7) H. Falkenhagen and E. L. Vernon, *Physik. Z.*, **33**, 140 (1932).

(8) W. M. Cox and J. H. Wolfenden, *Proc. Roy. Soc.* (London), **A145**, 475 (1934).

(9) H. S. Frank and M. Evans, *J. Chem. Phys.*, **13**, 507 (1945).

(10) O. Y. Samoilov, *Discussions Faraday Soc.*, **24**, 141 (1957).

(11) L. E. Sutton, Ed., "Tables of Interatomic Distances and Configuration in Molecules and Ions," Special Chemical Publication No. 11, The Chemical Society, London, 1958.

(12) J. F. Keucker, M.S. Thesis, University of Nebraska, 1962.

(13) J. R. Coe and T. B. Godfrey, *J. Appl. Phys.*, **15**, 625 (1944).

(14) L. W. Tilton and J. K. Taylor, *J. Res. Natl. Bur. Std.*, **18**, 205 (1937).

coefficients for each salt at the three temperatures are presented in Table I.

Table I: Viscosity A- and B-Coefficients[a] and Activation Energies for the Chloroammineplatinum(IV) Salts

	T, °C.	10^4A, exptl.	10^4A, calcd.	10^3B, exptl.	ΔE^*, kcal.[b]
$Pt(NH_3)_6Cl_4$	20	342		358	
	25	332	350	378	3.51
	30	315		398	
$[Pt(NH_3)_5Cl]Cl_3$	20	237		360	
	25	232	244	376	3.64
	30	224		389	
$[Pt(NH_3)_4NH_2Cl]Cl_2$	20	182		287	
	25	172	158	285	4.05
	30	165		284	
Na_2PtCl_6	20	184		379	
	25	180	183	390	3.76
	30	167		399	

[a] Estimated errors: A-coefficient, $\pm 20 \times 10^{-4}$ (l./mole)$^{1/2}$; B-coefficient, $\pm 15 \times 10^{-3}$ l./mole. [b] $c = 1$ M.

The experimental values for the A-coefficients at 25° agree satisfactorily with those calculated according to the theory of Falkenhagen[7] using the conductance data of Hall and Plowman,[16] Gordon,[17] Walden,[18] and Werner[19] although the temperature coefficient of the A-coefficient was usually greater than predicted by theory. It should be emphasized that, in spite of the fact that the chloroammineplatinum(IV) salts are among the most stable of such complexes, appreciable hydrolysis was observed for solutions more dilute than *ca.* 0.01 m. For this reason, the precision of the A-coefficient is considerably less than for simple salts[4] because the coefficient must be determined by unwonted extrapolation. As indicated in Table I, the measurements of the B-coefficient are likewise less precise than for the common salts. Taking the value of the B-coefficients at 25° for the chloride ion to be −0.007 and for the sodium ion as +0.086,[20] we calculated the magnitude of the B-coefficients for the $Pt(IV)^{4+}$, $Pt(IV)^{3+}$, $Pt(IV)^{2+}$, and $Pt(IV)^{2-}$ ions as +0.406, 0.397, 0.299, and 0.218 l./mole, respectively. These data, together with the ionic activation energies for viscous flow[4] and hydrated radii[3] for the platinum ions, are presented in Table II.

Discussion

Using the results of the previous section, together with those available in the literature,[4,5,20] the variation of the ionic B-coefficient with ionic charge for several series of ions is shown in Figure 1. Curve A illustrates that the ionic B-coefficient for most large ions ($r_x > 4$ Å.) is dependent only upon the ionic radius and independent of the ionic charge. This somewhat surprising result appears to be characteristic of all large ions with hydrophobic surfaces which cannot participate readily in the "flickering clusters" of the water structure.[21] We define such ions as possessing aperipheral[22] hydration.

Table II: Viscosity Parameters of the Chloroammineplatinum(IV) Ions at 25°

	$Pt(IV)^{4+}$	$Pt(IV)^{3+}$	$Pt(IV)^{2+}$	$Pt(IV)^{2-}$
B_{ion}, l./mole	+0.406	+0.397	+0.301	+0.218
ΔE^*_{ion}, cal./mole[a]	+370	+290	+480	−290
$r_{crystal}$, Å.	4.10	4.10	4.10	4.12
r_{Stokes}, Å.	3.41	3.18	3.18	3.12
$r_{hydrated}$, Å.[b]	4.26	4.16	4.16	4.14

[a] See ref. 4. [b] See ref. 3.

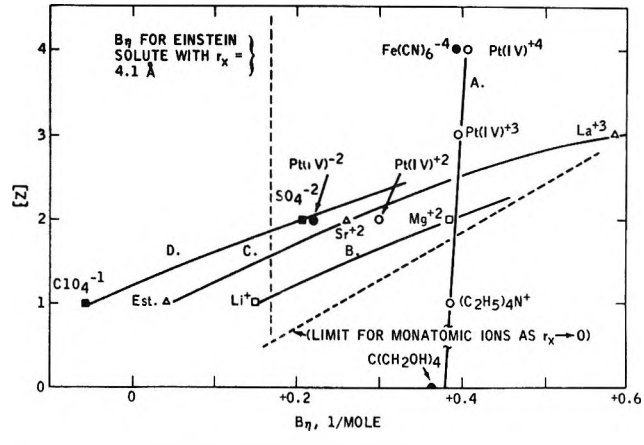

Figure 1. Variation of ionic B-coefficient with ionic charge at 25°: ○, ●, ions with $r_x \sim 4.1$ Å.; □, cations with $r_x \sim 0.6$ Å.; △, cations with $r_x \sim 1.1$ Å.; ■, anions with $r_x \sim 2.9$ Å, and *ca.* 55% π-character in X–O bond.

(15) The computed viscosities for the individual solutions of each of the four salts at three different temperatures are recorded in ref. 12, pp. 17–30.

(16) J. R. Hall and R. A. Plowman, *Australian J. Chem.*, **8**, 158, 168 (1955).

(17) G. C. Benson and A. R. Gordon, *J. Chem. Phys.*, **13**, 473 (1945).

(18) P. Walden, *Z. physik. Chem.*, **2**, 76 (1887).

(19) A. Werner and A. Miolati, *ibid.*, **12**, 54 (1893); **14**, 508 (1894).

(20) M. Kaminsky, *Discussions Faraday Soc.*, **24**, 171 (1957).

(21) H. S. Frank and W. Y. Wen, *ibid.*, **24**, 133 (1957).

Polyatomic ions with hydrophobic surfaces and aperipheral hydration are explicitly assumed not to permit appreciable delocalization of charge onto the ion surface. Hence, they act much like insulated spheres in a conducting continuum (of flickering charges) with the ionic charge more or less concentrated at the center of the ion. However, if the ionic charge is partially delocalized onto the surface, this delocalized charge will serve to melt some of the ice-like structure around the ion. The ionic surface can thus participate more effectively in the cluster fluctuations of the water molecules, and the ion will thus exhibit a smaller B-coefficient than if the solvent structure about the ion was more highly ordered. The decreased magnitude of the ionic B-coefficients for the $Pt(IV)^{2+}$ and $Pt(IV)^{2-}$ ions (Figure 1) arises in the manner just described. The $-NH_2$ and $-Cl$ groups in $[Pt(NH_3)_4NH_2Cl]^{2+}$ and $[PtCl_6]^{2-}$ disperse the ionic charge considerably more effectively than do the NH_3 groups in $Pt(NH_3)_6^{4+}$. This type of behavior is also exhibited by $C(CH_2OH)_4$[23] as compared with the $(C_2H_5)_4N^+$ ion and parallels that discussed previously for the IO_3^- and IO_4^- ions.[4,24]

The essential difference between the IO_3^-/IO_4^- system and that observed in this study is that the transition from IO_3^- to IO_4^- enhances charge localization by increasing the π-bond character in the X–O bond from 21 to 55% and results in a *negative* B-coefficient for IO_4^- in water. In the current work, the delocalization accompanying the substitution of charged Cl^- ions for neutral NH_3 molecules similarly melts the ice-like region about the ion, but, because of the inherent large size of the ion, the B-coefficient remains positive. It is interesting to note that the $PtCl_6^{2-}$ ion acts almost as an Einstein solute, its B-coefficient being only 0.05 unit larger than predicted by the Einsteim volume-fraction relation.[25]

In contradistinction with the large aperipherally hydrated ions, curves B and C in Figure 1 illustrate the variation of the B-coefficient with charge for *small* monatomic ions with crystal radii of 0.6 and 1.1 Å., respectively. For a given radius, the B-coefficient increases with charge because, on the average, a larger number of water molecules are peripherally oriented in the stronger electric field about the surface of the more highly charged ion. For a given charge, the B-coefficient also increases with decreasing size for the same reason. The structure-ordering behavior of such monatomic ions ($B_\eta > 0$) is said to be affected by peripheral solvation. It is interesting to note that an estimate can be made of the maximum value of the B-coefficient for monatomic ions by extrapolating a plot of r_x *vs.* B_η (at constant charge). As shown in Figure 1, the upper limit for monatomic ions is $B \simeq 0.6$, because ions with very intense electrical fields polarize the water molecules sufficiently to form hydrolytic species $M(OH)_n^{z-n}$.

The effect of the smaller polyatomic ions on the solvent structure is also determined primarily by the surface charge density which is never exactly spherically symmetrical. Curve D in Figure 1 illustrates the variation of the B-coefficient for XO_4^{-z} ions with $r_x = 2.9$ Å. and with approximately 50% π-character in the X–O bond.[24] The latter parameter is a necessary criterion for the comparison of such polyatomic ions.

The relation between ΔE^* and dB/dT has been given[4] by

$$\Delta E^* = \frac{R\,d \ln \eta_0}{d(1/T)} + \frac{R}{1 + BC} \times \frac{d(1 + BC)}{d(1/T)} \quad (3)$$

from which it may be seen that the sign of ΔE^* is the negative of that for dB/dT. The *positive* activation energies for viscous flow shown in Table II for the $Pt(IV)^{4+}$, $Pt(IV)^{3+}$, and $Pt(IV)^{2+}$ ions closely approximate that calculated previously for the $(C_2H_5)_4N^+$ ion.[5] As the temperature is increased, the ordered solution structure about these ions is diminished more than is that of the pure solvent, and the relative viscosity and, hence, the B-coefficient decreases. A *negative* activation energy such as is observed for the $PtCl_6^{2-}$ ion has heretofore only been associated with peripherally hydrated ions about which the electric field is sufficiently large to permit a further ordering of the water molecules as the solvent structure is destroyed by an increase in temperature.[4] It is clear that a negative activation energy for an ion with aperipheral hydration implies a condition in which the "apparent" size of the ion (*i.e.*, the B-coefficient) increases with temperature. Since such an ion does not induce extensive "ice-likeness" in the solvent about the ion, it appears that the condition of positive B-coefficients accompanied by negative activation energies can only occur for species with hydrophilic or partially hydrophilic surfaces (*e.g.*, those with surface groups such as $-OH$, $-NH_2$, or $-Cl$). Ions of this type most nearly represent an Einstein solute in that their effect upon the solution viscosity is closely proportional to the volume fraction of the solute.

(22) Literally, "hydrated" *away* from the surface. The behavior of R_4N^+ ions in enhancing the solvent structure *away* from the ion surface has been described by Frank (ref. 21). We shall define "structure ordering" as resulting from *peripheral* (Li^+, F^-, etc.) or *aperipheral* (R_4N^+, $Pt(NH_3)_6^{4+}$, etc.) solvation although ions with aperipheral "hydration" are actually *un*hydrated.

(23) F. J. Kelley, R. Mills, and J. M. Stokes, *J. Phys. Chem.*, **64**, 1448 (1960).

(24) E. R. Nightingale, Jr., *ibid.*, **64**, 162 (1960).

(25) A. Einstein, *Ann. Physik*, **19**, 289 (1906); **34**, 591 (1911).

The Role of the Doublet State in the Photochemistry of Chromium(III) Complexes[1]

by H. L. Schläfer

Institut für physikalische Chemie der Universität, Frankfurt am Main, Germany (*Received December 2, 1964*)

The photochemical behavior of chromium(III) complex ions when aqueous solutions of the respective compounds have been irradiated in the visible and ultraviolet range is discussed. It can be shown that the lowest metastable doublet state in the term system most probably plays an important role with respect to the photochemistry.

It is well known that coordination compounds of chromium(III) are particularly sensitive to light. When exposed to daylight aqueous solutions of these complexes show photochemical conversions which can be partially seen as characteristic changes in visible color. Photochemical reactions have been observed in a number of transition metal compounds. They can be divided in two different types: (1) ligand exchange, isomerization or racemization, reactions, and (2) oxidation–reduction reactions which lead to a change in the oxidation number of the metal ion and finally to a decomposition of the complex ion. Examples for the first type are a photoaquation

$$[MA_6] + H_2O \xrightarrow{h\nu} [MA_5(H_2O)] + A \qquad (1)$$

or a photoracemization

$$d\text{-}M(A\text{–}A)_3 \xrightarrow{h\nu} l\text{-}M(A\text{–}A)_3 \qquad (2)$$

where (A–A) is a bidentate ligand. An example of the second type is the photodecomposition of tris-oxalato complexes of trivalent central ions (M = Co^{3+} and Fe^{3+}).

$$[M(C_2O_4)_3]^{3-} \xrightarrow{h\nu} [M(C_2O_4)_2]^{2-} + C_2O_4^-$$

$$C_2O_4^- + [M(C_2O_4)_3]^{3-} \longrightarrow 2CO_2 + [M(C_2O_4)_2]^{2-} + C_2O_4^{2-} \qquad (3)$$

Chromium(III) complexes are most favorable for photochemical investigations as here only reactions of the first type occur when solutions of these compounds are exposed to light. In the case of cobalt(III) complexes, an analysis of the photochemical behavior is complicated owing to the fact that both types of photoreactions can be observed and also, as Adamson[2] has shown, sometimes in certain spectral regions simultaneously.

In order to initiate a general discussion of the photochemistry of chromium(III) compounds we shall start with a short inspection of the experimental material available today. Then we shall attempt to get some information on the excited states which are possibly responsible for the photoreactions.

Ligand exchange reactions (aquation or other substitution processes) and racemization reactions, those run as dark reactions with a comparatively slow rate ($k \approx 10^{-3}$–10^{-7} sec.$^{-1}$ for first-order reactions, activation energies of ≈15–25 kcal.), go much faster when exposed to light. The final products of the dark and the light reactions are generally the same. Photochemical effects can be produced using light of the wave lengths of all the bands in the visible and ultraviolet region of the respective absorption spectra.

The absorption spectra of chromium(III) complexes of practically octahedral microsymmetry are in general of the type shown in Figure 1. Normally one observes two or (in cases where the ultraviolet slope is at short wave lengths as in $[Cr(H_2O)_6]^{3+}$) three weak bands (I, II, and III in the order of increasing wave numbers) with values of log $\epsilon \approx 2$ and half-widths of ≈1500 to 2000 cm.$^{-1}$. On the long wave length tail of band I generally occurs a very sharp band (J) with

(1) Summary of a paper presented at the Gordon Research Conference on Inorganic Chemistry, New Hampton, N. H., Aug. 10–14, 1964.

(2) A. W. Adamson, *Discussions Faraday Soc.*, **29**, 163 (1960).

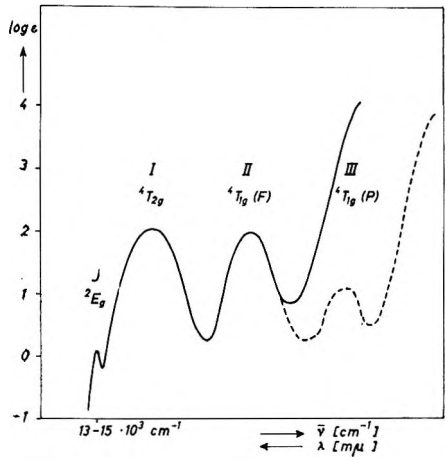

Figure 1. Schematic absorption spectrum of a chromium(III) complex with practically octahedral microsymmetry.

log $\epsilon \approx 0$, half-width when measurable ≈ 100 to 200 cm.$^{-1}$. If one works with great resolution in some cases a typical vibrational structure of J can be seen. At low temperatures in crystalline compounds in this spectral region lines can be observed, for example in the chromium(III) alum. In ruby ($Cr^{III}Al_2O_3$) two lines occur, the so-called "chromium doublet." Whereas the positions of the bands I, II, and III are strongly dependent on the nature of the ligands, the weak sharp band J always holds its position in the spectral region of 13,000 to 15,000 cm.$^{-1}$.

Chromium(III) complexes show photochemical reactions of the first type when exposed to light of the wave lengths of all bands I, II (and III). The quantum yields ϕ are nearly independent of the wave length of the exciting light. One obtains, within experimental error, similar values for ϕ for the different absorption bands. In some cases apparent activation energies obtained from the temperature dependence of the measured quantum yields have been found (*e.g.*, $[Cr(H_2O)_6]^{3+}$ photochemical O^{18} exchange, 13 kcal.[3]; $[Cr(H_2O)_6]^{3+}$ photosubstitution of water for SCN^-, 4 to 8 kcal.[4]). The quantum yields fall in the region 0.45 to 0.015 (Table I).

The excited electronic states of chromium(III) compounds can be characterized using the usual treatment of ligand-field theory. The result is shown in Figure 2. Only the lower part of the term system is given. The different electronic states are classified by their irreducible representation of the group O_h in the nomenclature of Mulliken and their multiplicity. Also the one-electron configurations $d\epsilon^n d\gamma^m$ in the limiting case of the strong ligand field from which these states arise when electron repulsion is taken into account are given in parentheses. Spin-orbit coupling is not considered. The bands I, II, and III in Figure 1 correspond to parity forbidden transitions (→) from the ground state $^4A_{2g}$ to the excited quartet states $^4T_{2g}$, $^4T_{1g}(F)$, and $^4T_{1g}(P)$. The weak sharp band J corresponds to a transition from the quartet ground state to the lowest doublet ^2E_g (- - →). This transition is, in addition, spin forbidden. The band J is therefore an intercombination band with very low intensity.

Table I: Quantum Yields for Different Photochemical Reactions with Chromium(III) and Cobalt(III) Complexes

Compd.	Type of reaction	Quantum yield, ϕ,[a] excitation in the region of quartet → quartet bands	Apparent activation energy, kcal.	Ref.
$[Cr(NH_3)_6]^{3+}$	Aquation	3×10^{-1}		*b*
$[Cr(en)_3]^{3+}$	Aquation	4.5×10^{-1}		*c*
$[Cr(NH_3)_5H_2O]^{3+}$	Aquation	3×10^{-1}		*b*
$[Cr(NH_3)_5(NCS)]^{2+}$	Aquation	1.5×10^{-2}		*d, e*
$[Cr(NH_3)_2(NCS)_4]^-$	Aquation	$\sim 2 \times 10^{-1}$		*d, e*
$[Cr(H_2O)_5(NCS)]^{2+}$	Aquation	2×10^{-4}		*e*
$[Cr(C_2O_4)]^{3-}$	Racemization	4.5×10^{-2}	~ 2	*f*
$[Cr(H_2O)_6]^{3+}$	O^{18} exchange	3×10^{-2}	13	*g*
		Quantum yield, ϕ,[a] excitation in the region of the first singlet → singlet band		
$[Co(NH_3)_6]^{3+}$	Aquation	$<2 \times 10^{-3}$		*h*
$[Co(NH_3)_5SO_4]^{2-}$	Aquation	$\sim 10^{-3}$		*h*
$[Co(NH_3)_5Cl]^{2+}$	Aquation	1.5×10^{-3}		*h*
$[Co(NH_3)_5Br]^{2+}$	Aquation	1.3×10^{-3}	~ 10	*h*
$[Co(C_2O_4)_3]^{3-}$	Racemization	Very small		*f*

[a] The values of $\phi_{(4)}$ for Cr^{III} complexes were obtained by irradiation with light of the wave length of the two (in the case of $[Cr(H_2O)_6]^{3+}$, three) quartet → quartet bands I, II (and III). The quantum yield does not practically depend on the wave length of the exciting light. For Co^{III} complexes only cases were selected where the oxidation–reduction reactions practically play no role; that is, the charge-transfer bands do not extend far to the long wave length region of the absorption spectrum. The above-mentioned yields were measured for ~550 mμ, that is, the first singlet → singlet band ($^1A_{1g} \rightarrow {}^1T_{1g}$). Only in $[Co(NH_3)_6]^{3+}$ also the second singlet → singlet band ($^1A_{1g} \rightarrow {}^1T_{2g}$) was irradiated. The quantum yield is almost the same for both bands. [b] Reference 17. [c] H. L. Schläfer and E. Nikolaiski, unpublished results; E. Nikolaiski, Thesis, University of Frankfurt on the Main, 1962. [d] A. W. Adamson and A. H. Sporer, *J. Inorg. Nucl. Chem.*, **8**, 209 (1958); *J. Am. Chem. Soc.*, **80**, 3865 (1958). [e] Reference 4. [f] A. W. Adamson and S. Spees, Abstracts, International Conference on Coordination Chemistry, London, 1959, p. 90. [g] Reference 3. [h] Reference 2.

(3) R. A. Plane and J. P. Hunt, *J. Am. Chem. Soc.*, **79**, 3343 (1957).
(4) A. W. Adamson, *J. Inorg. Nucl. Chem.*, **13**, 275 (1960).

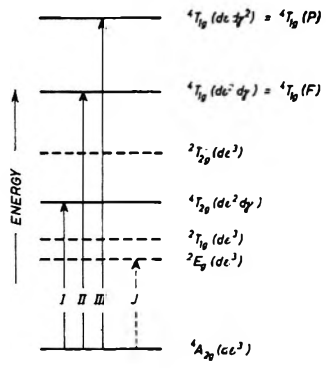

Figure 2. Term system of a chromium(III) complex ion with octahedral microsymmetry (schematic graph): →, parity forbidden; - - - →, parity and spin forbidden.

It is possible to obtain the average radiative lifetime τ_e of the excited states from the respective absorption bands using the usual procedure (Appendix I). For the excited quartet states one gets $\tau_e^{(4)} = k_r^{(4)-1} \approx 10^{-6}$ to 10^{-7} sec. and for ^2E_g $\tau_e^{(2)} = k_r^{(2)-1} \approx 10^{-3}$ sec. k_r is the first-order rate constant for the emission that is equal to A_{ik}, the Einstein coefficient for spontaneous emission.

From this consideration it is clear that the ^2E_g state is a metastable state with comparatively long lifetime. This can be proved by luminescence experiments. It should be mentioned here that one observes, when rigid solutions of chromium(III) complexes at low temperature are irradiated in the region of the quartet → quartet bands, the narrow phosphorescence emission $^2E_g \rightarrow {}^4A_{2g}$ with more or less vibrational structure.[5]

Measurements of this kind by Forster and De Armond[6] on chromium(III) β-diketone chelate compounds yield, calculated from the decay of the phosphorescence, lifetimes in the order of $\tau \approx 0.6$ to 0.04×10^{-3} sec. at 85°K. That means

$$\frac{1}{\tau} = k_r + k_{nr} \approx 10^4 \text{ to } 10^5 \text{ sec.}^{-1}$$

where k_{nr} is the first-order rate constant for the nonradiative transition $^2E_g \rightsquigarrow {}^4A_{2g}$.

Values for τ for ruby were obtained by Maiman, *et al.*[7]: $\tau = 4.3 \times 10^{-3}$ sec. at 77°K. and $\tau = 3 \times 10^{-3}$ sec. at 300°K.

The phosphorescence occurs practically at the same wave length as the intercombination band in absorption. The two corresponding potential energy surfaces have, on first approximation, minima at the same distances of the corresponding normal coordinates.

Now let us discuss the question of the ^2E_g state as an intermediate in the photochemistry of chromium(III) complexes.[8-10] From the two experimental facts that: (i) the quantum yield is nearly independent of the wave length in the spectral region of the quartet → quartet bands, and (ii) the photochemical reaction already has taken place when excitation occurs in the first band I, one can conclude that generally the two upper quartet states $^4T_{1g}$(P) and $^4T_{1g}$(F) are not themselves directly responsible for the reaction. With respect to the well-known facts obtained from various luminescence experiments with molecules it is to be expected that an excitation of the higher quartet terms is instantaneously followed by a very rapid internal conversion to the first excited quartet state $^4T_{2g}$. The first-order rate constant for this nonradiative process is assumed to be of the order $k_{ic} > 10^{10}$ to 10^{11} sec.$^{-1}$. That means that the lifetime of these higher quartet states is very short $\tau < 10^{-10}$ to 10^{-11} sec. For a discussion of the photochemical behavior we have therefore only to look at the $^4T_{2g}$ and the ^2E_g state, the first excited quartet and the lowest doublet[11] (Figure 3).

Besides an emission (k_2), two nonradiative processes can take place from the first excited quartet $^4T_{2g}$: (i) a radiationless transition to the ground state $^4A_{2g}$

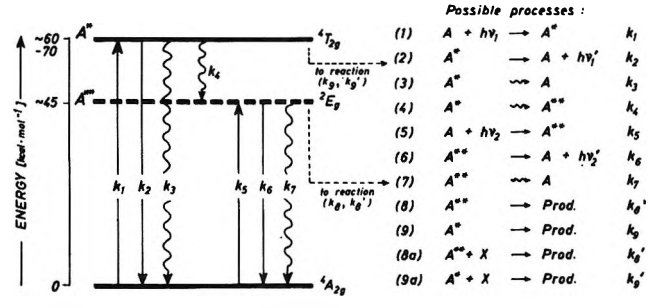

Figure 3. Lowest part of the term system of chromium(III) complexes (schematic graph): radiative transitions, →; nonradiative transitions, ⇝.

(5) (a) G. B. Porter and H. L. Schläfer, *Z. physik. Chem.* (Frankfurt), **37**, 109 (1963); (b) *ibid.*, **38**, 227 (1963); (c) *ibid.*, **40**, 280 (1964).

(6) K. De Armond and L. E. Forster, *Spectrochim. Acta*, **19**, 1687 (1963).

(7) T. H. Maiman, R. H. Hoskins, I. J. Heanens, C. K. Asawa, and V. Evtuhov, *Phys. Rev.*, **123**, 1151 (1961).

(8) H. L. Schläfer, *Z. physik. Chem.* (Frankfurt), **11**, 65 (1957).

(9) H. L. Schläfer, *Acta Chim. Akad. Sci. Hung.*, **18**, 375 (1959).

(10) H. L. Schläfer, *Z. Elektrochem.*, **64**, 887 (1960).

(11) The higher quartert states $^4T_{1g}$(P) and $^4T_{1g}$(F) (Figure 2) can presumably only be regarded as intermediates in photochemical reactions if these reactions are extremely fast. Processes of this kind (besides monomolecular transformations) are protonation and ion-pair formation with rate constants of about 10^9 to 10^{11} M^{-1} sec.$^{-1}$. If the reaction starts from protonated species or ion pairs, then there may be a certain possibility that the higher quartets themselves are involved in the photochemistry, but these cases are expected to be exceptions. In the field of organic molecules, the higher singlet states are normally of minor importance for photochemical reactions.

(k_3), and (ii) another radiationless transition to the metastable state ^2E_g (k_4).

Maiman[12] has determined k_4 for ruby and obtained 2×10^7 sec.$^{-1}$. A theoretically estimated value of Malkin[13] 4.5×10^7 sec.$^{-1}$ is in good agreement. In solutions it is to be expected that k_4 is somewhat greater. So we assume $k_4 > 10^7$ sec.$^{-1}$. k_3 is not known. Forster,[6] from experiments on chromium(III) β-diketone chelates in rigid solutions, concludes from the measured luminescence quantum yields that k_3 has approximately the same order as k_4. With respect to the k_2 value of 10^6 to 10^7 sec.$^{-1}$ obtained from the absorption spectrum (Appendix I) the reciprocal lifetime of $^4T_{2g}$ is

$$\frac{1}{\tau} = k_2 + k_3 + k_4 > 10^7 \text{ sec.}^{-1}$$

which means an average lifetime of $\tau < 10^{-7}$ sec.

From this very crude consideration it follows that a reaction with molecules that populate the first excited quartet state is only possible if the first-order rate constant for such an reaction (for example, an aquation) has an order of magnitude $\gtrsim 10^7$ sec.$^{-1}$ or if the product of the second-order rate constant and the concentration of the substituting molecule or ion has this value.

For the reciprocal lifetime of the doublet state the equation $\tau^{-1} = k_6 + k_7$ holds where k_6 is the rate constant for spontaneous emission, $\approx 10^3$ sec.$^{-1}$, obtained from the intercombination band in absorption (Appendix I). k_7 is the constant for all radiationless transitions to the $^4A_{2g}$ ground state. In ruby $k_6 + k_7 = 3 \times 10^3$ sec.$^{-1}$ (300°K.) according to Maiman, *et al.*[7]; in rigid solutions of Cr^{III} chelates $k_6 + k_7 = 10^4$ to 10^5 sec.$^{-1}$ (85°K.) according to Forster and De Armond.[6] In aqueous solutions at room temperature the k_7 values will probably increase somewhat. We can therefore assume for the reciprocal lifetime $\tau^{-1} = k_6 + k_7 > 10^5$ sec.$^{-1}$. The average lifetime is $\tau \lesssim 10^{-5}$ sec.

The above very rough estimations lead to the conclusion that molecules in the doublet state can undergo a reaction if the first-order rate constant for such a process or the product of the second-order rate constant and the concentration of the substituting molecules is of the order of $\gtrsim 10^5$ sec.$^{-1}$. This point of view gives some evidence that the doublet state is probably the one responsible for the photochemistry as its lifetime is more favorable for an approach of a substituting molecule or ion than is the shorter lifetime of the $^4T_{2g}$ state.

Now we shall attempt to discuss the fact that the rate of the photochemical process is so enormously increased as compared with the dark reaction.

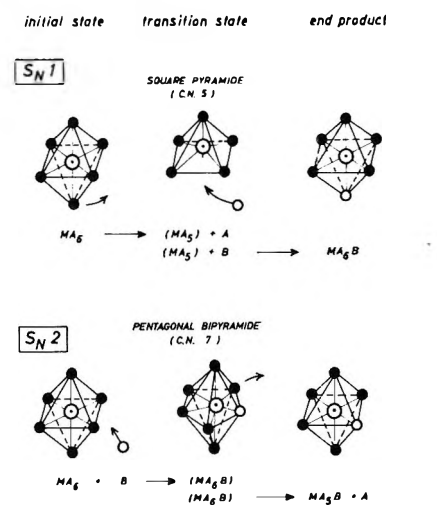

Figure 4. The two limiting cases for a substitution of a ligand A in an octahedral complex by an ion or molecule B (SN1 or SN2 reaction).

It is possible following the treatment of Basolo and Pearson[14] to estimate the ligand-field contribution to the activation energy ΔE_a (Appendix II). In doing this we will use the strong-field approximation dealing with one-electron configurations and assuming for the photosubstitution reaction an SN1 or SN2 path with a transition state of the form of a square pyramid or of a pentagonal bipyramid (Figure 4). Furthermore it is assumed that the transition state, in the case where the reaction starts from the metastable states ^2E_g (Cr^{III}) and $^3T_{1g}$(Co^{III}) has a spin with $S = 3/2$ for Cr^{III} and $S = 0$ for Co^{III}.

It can easily be seen that ΔE_a for a reaction that starts from the ground state $^4A_{2g}$ is positive with $+2Dq$ (for SN1) or $+4.26Dq$ (for SN2) that is roughly about $+14$ or $+30$ kcal. For both excited states ^2E_g and $^4T_{2g}$ the corresponding values (Table II) are negative. That means we have no ligand-field contribution to the activation energy. Chromium(III) complexes in those electronic states behave like complexes with spherically symmetric metal ions and therefore react with much faster rates than chromium(III) species in the ground state.

It is of interest to compare these results with cobalt(III) compounds. The first spin-allowed absorption band of cobalt(III) complexes with octahedral microsymmetry corresponds to the transition $^1A_{1g}(d\epsilon^6) \rightarrow {}^1T_{1g}(d\epsilon^5 d\gamma)$. The intercombination band with the

(12) T. H. Maiman, *Phys. Rev. Letters*, **4**, 564 (1960).

(13) B. S. Malkin, *Fiz. Tverd. Tela*, **4**, 2214 (1962).

(14) F. Basolo and R. G. Pearson, "Mechanisms of Inorganic Reactions," John Wiley and Sons, Inc., New York, N. Y., 1958.

Table II: Estimation of the Ligand-Field Contribution to the Activation Energy

Cr^{III} electronic state	Ligand-field stabilization energy: Initial state E_i	Transition state: E_t SN1	Transition state: E_t SN2	Contribution to the activation energy, $\Delta E_a = E_t - E_i$, for SN1	(Kcal.)	SN2	(Kcal.)
$^4A_{2g}(d\epsilon^3)$	$12Dq$	$10Dq$	$7.74Dq$	$2Dq$	(14)	$4.26Dq$	(30)
$^2E_g(d\epsilon^3)$	$12Dq - P$	$10Dq$	$7.74Dq$	$2Dq - P$	(−31)	$4.26Dq - P$	(−15)
$^4T_{2g}(d\epsilon^2d\gamma)$	$2Dq$	$10Dq$	$7.74Dq$	$-8Dq$	(−56)	$-5.74Dq$	(−40)
Co^{III} electronic state							
$^1A_{1g}(d\epsilon^6)$	$24Dq - 3P$	$20Dq - 3P$	$15.48Dq - 3P$	$4Dq$	(28)	$8.52Dq$	(60)
$^3T_{1g}(d\epsilon^5d\gamma)$	$14Dq - 2P$	$20Dq - 3P$	$15.48Dq - 3P$	$-6Dq + P$	(−2)	$-1.48Dq + P$	(30)
$^1T_{1g}(d\epsilon^5d\gamma)$	$14Dq - 3P$	$20Dq - 3P$	$15.48Dq - 3P$	$-6Dq$	(−42)	$-1.48Dq$	(−10)

lowest wave number that occurs on the long wave length tail of the above singlet → singlet band corresponds to $^1A_{1g}(d\epsilon^6) \rightarrow {}^3T_{1g}(d\epsilon^5d\gamma)$.

Calculations of the same kind as above (Table II) lead to ΔE_a for a reaction that starts from the $^1A_{1g}$ ground state of $+4Dq$ (SN1) or $+8.52Dq$ (SN2) that is about +28 or +60 kcal. These values indicate a very slow rate. A reaction from the $^1T_{1g}$ state has negative values for ΔE_a; this is no ligand-field contribution to the activation energy. One gets a positive contribution $-1.48Dq + P$ for the metastable $^3T_{1g}$ state, assuming an SN2 path, that is about +30 kcal. For an SN1 mechanism one obtains $-6Dq + P$ that is approximately −2 kcal., but with respect to the uncertainty of the value for the spin-pairing energy P this can also mean a slightly positive value of ΔE_a.

Therefore a difference between Co^{III} and Cr^{III} complexes with respect to photosubstitution is to be expected. Whereas chromium(III) complexes easily undergo photoreactions by irradiating in the quartet → quartet bands, this is not so in the case of cobalt(III) compounds by irradiating the singlet → singlet bands. In both cases the metastable states $^2E_g(Cr^{III})$ and $^3T_{1g}$ (Co^{III}) were populated indirectly by internal conversion from the higher quartet or singlet states. Chromium(III) species, present in the doublet, should react very fast. Cobalt(III) complexes existing in the triplet state are expected to react only slowly. The rate will be not very much faster than the rate for molecules in the singlet ground state.

Molecules in the $^1T_{1g}$ state should react with a fast rate. However with respect to the shorter lifetime $\tau < 10^{-7}$ sec, this electronic state is not favorable for photochemical reactions.

This treatment helps to understand why in cobalt(III) compared with chromium(III) complexes photosubstitution reactions are less important and occur only to a comparatively small extent ($\phi < 10^{-3}$, Table I). Observations of this type of photochemical processes in cobalt(III) compounds are complicated due to electron-transfer reactions that occur in some complexes to a certain degree in the region of the d → d ligand-field bands. The reason is that the long wave length slopes of the charge-transfer bands extend under the subsequent ligand-field bands.

It should be emphasized that the activation energy E_a is only one quantity determining the rate. The other is the pre-exponential factor PZ in the Arrhenius equation including entropy effects. In the aforementioned considerations it is tentatively assumed that this term has about the same order for different reactions.

Using the steady-state treatment and assuming absorption only in the quartet bands an expression for the quantum yield of the form

$$\phi_{(4)} = \frac{k_4k_8}{(k_6 + k_7 + k_8)(k_2 + k_3 + k_4)} \qquad (4)^{15}$$

can easily be derived (Appendix III). The constants k have the same meaning as in Figure 3. With the respective values for k (an estimation of their order is given before) one obtains $1 < \phi < 10^{-1}$ (10^{-2}) in qualitative agreement with the experimental values (Table I).

By direct excitation of the ^2E_g state the expression for the quantum yield has the form

$$\phi_{(2)} = \frac{k_8}{k_6 + k_7 + k_8} \qquad (5)^{15}$$

Only the internal conversion processes (k_3, k_4, k_7) and the reaction that starts from the doublet state (k_8, k_8') will depend on the temperature. Whereas the temperature dependence of the nonradiative transitions is normally not important, the reaction from the doublet is expected to have an activation energy.

(15) For a second-order reaction (8a, Figure 3) $k_8'[X]$ stands for k_8.

This explains the observed temperature dependence of ϕ in some cases.

Edelson and Plane[16] very recently obtained support for the mechanism with the ^2E_g state as an intermediate. They determined the quantum yield of the photoaquation of $[Cr(NH_3)_6]^{3+}$ by irradiating in the region of the intercombination band at ≈ 650 mμ. Whereas an irradiation in the quartet → quartet bands gives $\phi \approx 0.3$, at 650 mμ ϕ values of the order of unity are observed.

By direct excitation of the doublet state most of the excited molecules undergo photoaquation whose rate is faster than the internal conversion process $^2E_g \rightsquigarrow {}^4A_{2g}$. Irradiation in the region of the quartet → quartet bands always gives smaller values for ϕ, as the nonradiative processes $^4T_{2g} \rightsquigarrow {}^4A_{2g}$ play an important role and therefore the average number of reactive molecules in the doublet state is smaller.

In those cases where the energy difference ΔE between the electronic states $^4T_{2g}$ and ^2E_g is small (comparable to kT) a thermal back reaction of molecules in ^2E_g to $^4T_{2g}$ is possible, as discussed by Plane and Edelson[17] for $[Cr(H_2O)_6]^{3+}$. Then this process may give an additional activation energy. Qualitatively it can be argued that ϕ should become smaller as the number of molecules in the doublet state is decreased and the nonradiative deactivation process from $^4T_{2g}$ to the ground state is increased. But this argument holds only if one assumes that k_8 (k_8'), the rate constant for the reaction for molecules in the doublet state, is not very different for different complex ions.

The difference in energy, ΔE, which has to be used with respect to the thermal back reaction between the first excited quartet and the doublet is always smaller than the energy difference ΔE_{exp} between the absorption maximum of the broad quartet → quartet band I and the narrow intercombination band J. This is clearly to be seen from a plot of the respective potential energy curves (Figure 5). Whereas the ground state and the doublet state have potential energy surfaces with minima almost at the same internuclear distances (both states belong to the configuration $d\epsilon^3$) the first excited quartet ($d\epsilon^2 d\gamma$) has a surface with a minimum at greater internuclear distance. The length of the vertical arrows indicate, in accordance with the Franck–Condon principle, roughly the position of the respective band maxima.

For example $[Cr(urea)_6]^{3+}$ has $\Delta E_{exp} = 1910$ cm.$^{-1}$. It can be concluded from luminescence experiments[5a] that the zero vibrational levels of ^2E_g and $^4T_{2g}$ are very nearly at the same energy ($\Delta E_0 \approx 0$). The different chromium(III) complexes have ΔE_{exp} values from 1900 to 13,900 cm.$^{-1}$ (for $[Cr(CN)_6]^{3-}$).

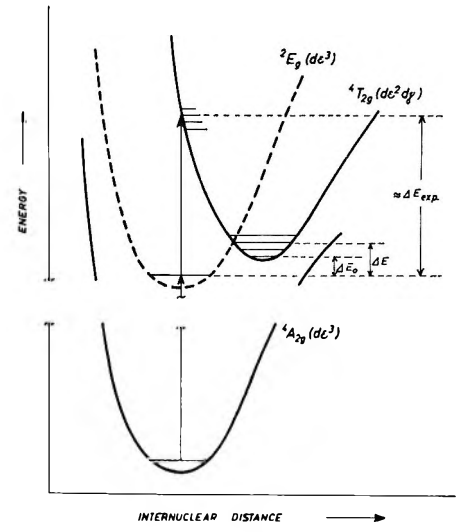

Figure 5. Potential energy curves for the $^4A_{2g}$ ground state and the two excited states ^2E_g and $^4T_{2g}$.

In cases of small ΔE_{exp} and therefore *a fortiori* smaller ΔE the equation for ϕ has to be modified because of the thermal back reaction. Qualitatively ϕ values for reactions where ΔE_{exp} derived from the absorption spectrum is small are of the order 10^{-2} about a factor of 10 smaller than the usual values of 10^{-1} for reactions with greater ΔE_{exp}. But there exists, as Adamson[4] has shown, one exception, that is $[Cr(NH_3)_5(NCS)]^{2+}$ where $\phi = 1.5 \times 10^{-2}$ in spite of $\Delta E_{exp} = 3300$ cm.$^{-1}$.

At last it should be mentioned that no luminescence is observed on solutions of chromium(III) complexes at room temperature which undergo photochemical reactions.

From these considerations it may be seen that there is some evidence that the doublet state can be regarded as an intermediate in the photochemistry of chromium(III) complexes. This does not exclude, in all cases, the possibility that the first excited quartet itself plays a role. But at the present not enough experimental material, especially very accurate measurements on suitable chosen systems, is available to answer this question.

Acknowledgment. The author is very much indebted to Professor Lippert of Stuttgart for critically reading the manuscript.

Appendix I

Calculation of the Average Radiative Lifetime τ_e. τ_e can be calculated by the equation

(16) M. R. Edelson and R. Plane, *Inorg. Chem.*, **3**, 231 (1964).
(17) M. R. Edelson and R. Plane, *J. Phys. Chem.*, **63**, 327 (1959).

$$\tau_e = \frac{1}{A_{ik}} = \frac{g_k N_L}{g_i 8\pi\bar{\nu}_{ik}^2 c \times 10^3 \times 2.30 \int_0^\infty \epsilon(\bar{\nu})d\bar{\nu}}$$

With

$$\int_0^\infty \epsilon(\bar{\nu})d\bar{\nu} \approx 2.1289\epsilon_{max}\delta$$

one obtains

$$\tau_e = \frac{g_k \times 10^9}{g_i 6.15\bar{\nu}_{ik}\epsilon_{max}\delta}$$

A_{ik} is the Einstein probability coefficient of spontaneous emission, g_k and g_i are the degeneracies of the two electronic states, N_L stands for Avogadro's number, $\bar{\nu}_{ik}$ is the wave number in cm.$^{-1}$, ϵ_{max} the molar extinction coefficient of the maximum of the absorption band, c the velocity of light, and δ the half-width of the band ($\epsilon = \epsilon_{max}/2$ for $\bar{\nu} = \bar{\nu}_{max} \pm \delta$).

For the excited quartet states $^4T_{2g}$, $^4T_{1g}(F)$ and $^4T_{1g}(P)$ with $\delta \approx$ 1600–1900 cm.$^{-1}$ and $\epsilon_{max} \approx$ 50–80 l. mole^{-1} cm.$^{-1}$ and with the respective values for $\bar{\nu}_{ik}$ the calculated radiative lifetimes are $\tau_e^{(4)} \approx 1\text{–}5 \times 10^{-6}$ sec.

The $\tau_e^{(2)}$ values for the $^2E_{g1}$ state with $\delta \approx$ 150–200 cm.$^{-1}$ and $\epsilon_{max} \approx$ 0.3–3 l. mole^{-1} cm.$^{-1}$ are $1\text{–}8 \times 10^{-3}$ sec.

Appendix II

Estimation of the Ligand-Field Contribution to the Activation Energy ΔE_a for Cr^{III} and Co^{III} Complexes with Octahedral Microsymmetry When a Substitution Reaction $[MA_6] + B = [MA_5B] + A$ Is Considered. As initial states we take the ground and the two first excited states, that is $^4A_{2g}$, ^2E_g, and $^4T_{2g}$ for Cr^{III} and $^1A_{1g}$, $^3T_{2g}$, and $^1T_{1g}$ for Co^{III}. The ligand-field stabilization energy E_i for the initial states of an octahedral assembly can be calculated in first approximation using the $d\epsilon^n d\gamma^m$ configurations and taking the respective spin-pairing energies into consideration. By the same procedure the ligand-field stabilization energy E_t for the transition states (coordination number 5 = square pyramid, coordination number 7 = pentagonal bipyramid) can be estimated. For this purpose the energy values calculated by Basolo and Pearson[14] were used, that gives the position of the several one-electron d orbitals in terms of the parameter Dq assuming a ratio of $\overline{a^2}/r^4 : \overline{a^4}/r^6 \approx 3:1$ (a = electron–nucleus distance, r = central ion–ligand distance).

For Cr^{III} compounds the calculations were done with a Dq of 7 kcal., that is about the Dq value for $[Cr(NH_3)_6]^{3+}$. The spin-pairing energy P is taken as approximately 45 kcal. Also 7 kcal. is assumed for Dq of Co^{III} complexes that corresponds nearly to the value for $[Co(NH_3)_6]^{3+}$. A crude value for P is 50 kcal. For the transition state the values of S are assumed to be $S = {}^3/_2$ for Cr^{3+} and $S = 0$ for Co^{3+}, also for the case where the reaction starts from the metastable states ^2E_g and $^3T_{1g}$ with $S = {}^1/_2$ and 1.

With these assumptions the values of Table II have been found. The results of these calculations should not be taken too literally, physical significance is only attributed to the statement that ΔE_a is positive or negative, the latter case means no ligand-field contribution to the activation energy.

Appendix III

Calculation of an Expression for the Quantum Yield Assuming a Reaction of Chromium(III) Species in the ^2E_g State. With the notation of Figure 3 and the assumption of a stationary concentration of excited molecules A* and A** in the $^4T_{2g}$ and ^2E_g state, and with respect to the fact that a population of the doublet state takes place only by internal conversion from the first excited quartet ($k_5 = 0$), one obtains

$$\frac{d[A^*]}{dt} = k_1[A] - k_2[A^*] - k_3[A^*] - k_4[A^*] = 0 \quad (A1)$$

$$[A^*] = \frac{k_1[A]}{k_2 + k_3 + k_4} \quad (A2)$$

$$\frac{d[A^{**}]}{dt} = k_4[A^*] - k_6[A^{**}] - k_7[A^{**}] - k_8[A^{**}] = 0 \quad (A3)$$

$$[A^{**}] = \frac{k_4[A^*]}{k_6 + k_7 + k_8} = \frac{k_4 k_1[A]}{(k_6 + k_7 + k_8)(k_2 + k_3 + k_4)} \quad (A4)$$

The quantum yield is defined as

$$\phi = \frac{d(\text{products})/dt}{cQ/dt} = \frac{k_8[A^{**}]}{k_1[A]} \quad (A5)$$

where dQ/dt is the number of quanta absorbed from A per unit time. The result is

$$\phi = \frac{k_4 k_8}{(k_6 + k_7 + k_8)(k_2 + k_3 + k_4)} \approx \frac{k_4 k_8}{(k_7 + k_8)(k_3 + k_4)} \quad (A6)$$

k_6 and k_2 are negligible, as no luminescence is observed in solutions at room temperature that undergo photoreactions.

The value of ϕ depends on the different constants. For these only very crude approximations can be made. Therefore an exact calculation is not possible. Using

the approximate values given before in the text it can be seen that $1 < \phi < 10^{-1}$ (10^{-2}). This is the range in which the experimental values have been found.

When excitation in the higher quartet states occurs, the $^4T_{2g}$ state is populated by internal conversion. Also in this case eq. A6 holds.

Reaction of Boroxine with $BF_3(g)$. Infrared Spectrum and Stability of $HBF_2(g)$[1]

by Richard F. Porter and Satish K. Wason

Department of Chemistry, Cornell University, Ithaca, New York *(Received December 10, 1964)*

Chemical reactions of solid boroxine with gaseous BF_3 have been investigated. Exchange of hydrogen in boroxine for fluorine in BF_3 yields gaseous HBF_2. At ordinary temperatures BF_3 reacts with boroxine more rapidly than with diborane. For the reaction, $^1/_6B_2H_6(g) + {}^2/_3BF_3(g) = HBF_2(g)$, $\Delta H_{298°K} = 3.0 \pm 0.5$ kcal./mole. The heat of formation of $HBF_2(g)$ at 298°K. is -175.7 ± 1.5 kcal./mole. Infrared spectra for HBF_2 and DBF_2 have been analyzed. Five of the six fundamentals of HBF_2 have been assigned with aid of the Teller–Redlich product rule for isotopic shifts in frequencies.

Introduction

Boroxine ($B_3O_3H_3$) has been observed as a gaseous product in a high-temperature reaction of $H_2O(g)$ or $H_2(g)$ with $B–B_2O_3$ mixtures. The reaction proceeds

$$^3/_2H_2(g) + B(s) + B_2O_3(l) = B_3O_3H_3(g) \quad (1)$$

at temperatures near 1400°K. A solid product is isolated by condensing the gas in a trap at liquid nitrogen temperatures. This solid contains B–H bonds and exhibits an infrared spectrum with several features characteristic of the gaseous molecule.[3,4] Although it is known that the solid decomposes at ordinary temperatures,[5,6] little information is presently available on its chemical behavior. In this paper we present results of an experimental study of the reaction of solid boroxine with gaseous BF_3.

Experimental

The apparatus for preparation of solid boroxine is illustrated in Figure 1. A 20-g. mixture of powdered boron and boric oxide in a molar ratio of about 2:1 was heated *in vacuo* to a temperature range between 1355 and 1400°K. Water vapor was then introduced through a glass frit, while the system was continually pumped to remove H_2 which was also a product. Solid boroxine was collected in a bulb maintained in a liquid nitrogen trap. The product appeared as a coating on the interior of the bulb. Under favorable conditions approximately 1 g. of solid could be isolated in a 2-hr. run. After three or four preparations, it was necessary to reload a fresh $B–B_2O_3$ mixture to prevent unreacted water from entering the trap with the product. The bulb containing solid boroxine was fitted with several stopcocks as means of introducing reactants and for withdrawing gaseous samples for spectral analyses. In separate experiments the water source for the high-temperature reaction was replaced by a 48% HF solution to provide a reactant mixture of HF and H_2O gases. The products of the reaction of

(1) Work supported by the Army Research Office (Durham) and the Advanced Research Projects Agency.

(2) (a) W. P. Sholette and R. F. Porter, *J. Phys. Chem.*, **67**, 177 (1963); (b) R. F. Porter and S. K. Gupta, *ibid.*, **68**, 280 (1964).

(3) G. H. Lee, W. H. Bauer, and S. E. Wiberley, *ibid.*, **67**, 1742 (1963).

(4) S. K. Wason and R. F. Porter, *ibid.*, **68**, 1443 (1964).

(5) S. K. Gupta and R. F. Porter, *ibid.*, **67**, 1286 (1963).

(6) L. Barton and D. Nicholls, *Proc. Chem. Soc.*, 242 (1964).

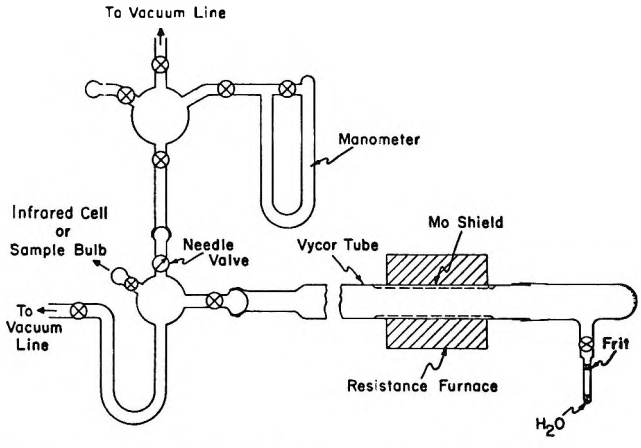

Figure 1. Apparatus for preparation of boroxine.

these gases with B–B_2O_3 mixtures, which may include fluorinated boroxines, were trapped at −196°. The gaseous products from the same reaction were also isolated in a method similar to that described earlier.[4] In these experiments a reactant gas mixture was introduced into the furnace and the reaction was allowed to proceed for about 20 min. The gaseous products were then swept into an infrared cell by flowing argon through the furnace at atmospheric pressure.

Results

In initial experiments BF_3(g) at a pressure of about 30 torr was added to the reaction bulb containing boroxine at room temperature. Diborane, which is produced by partial decomposition of the solid, was removed immediately before the addition of BF_3. The infrared spectrum shows bands due to diborane, BF_3, and at least one product. The new bands were identified as those reported by Coyle, Ritter, and Farrar[7] and by Lynds and Bass[8] for HBF_2(g). The mass spectrum of the product (Figure 2) also confirms this assignment. Ion peaks in the m/e range 40–45, which might be attributed to the hypothetical B_2H_5F, were not observed. A major fraction of the BF_2^+ and HBF^+ ion intensity may be attributed to HBF_2(g). With intensity corrections for BF_3 and a small quantity of BF_2OH,[9] we obtained for the mass spectrum of HBF_2 intensity ratios of $BF_2^+:HBF^+:BF^+ = 100:81:\sim7$. The low intensity of parent ion, HBF_2^+, was anticipated in view of the general behavior of boranes on electron impact.[10] In a separate experiment a mixture of B_2H_6 and BF_3 was added to a bulb containing a sample of boroxine which had been decomposed at 80°. No reaction between B_2H_6 and BF_3 was observed at room temperature. This indicates that HBF_2 is formed by the reaction of BF_3 with solid boroxine and is not

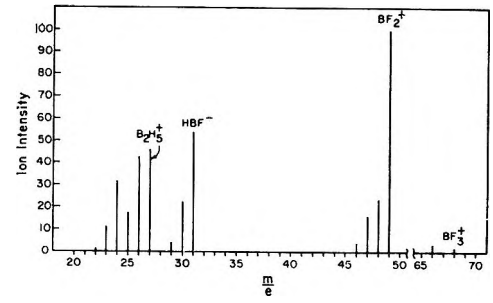

Figure 2. Mass spectrum of products of the reaction of BF_3(g) with boroxine.

formed mainly by a catalytic reaction of B_2H_6 and BF_3 on the surface of the solid. Thus it should be noted that the reaction of BF_3 with boroxine at room temperature is much faster than the reaction of BF_3 and B_2H_6.

Infrared Spectrum of HBF_2(g). In Figure 3 are shown infrared spectra of reaction products containing HBF_2(g). These spectra were recorded on a Perkin-Elmer Model 521 grating infrared spectrophotometer with slit width varying between approximately 2.0 to 1.5 cm.$^{-1}$ in the frequency range 2500–650 cm.$^{-1}$. Figure 3b is a spectrum of gases obtained when the condensed product from the reaction of HF(g) and H_2O(g) with B–B_2O_3 mixture was warmed to room temperature. Heating the solid to 80° resulted in further decomposition to yield B_2H_6, BF_3, and HBF_2. This indicates that the solid prepared by this method is partially fluorinated. The gaseous products of this reaction, which were isolated by sweeping the furnace chamber with argon, have a spectrum illustrated in Figure 3a. The initial spectrum of these products showed, in addition to HBF_2(g), the presence of $B_3O_3H_3$(g) and BF_3(g). However, intensities of these additional species diminished rapidly and the window film at about 1260 cm.$^{-1}$ due to B_2O_3(s) appeared. This suggests that partially fluorinated gaseous boroxines[11] cannot be isolated at ordinary temperature due to the possible reaction sequence

$$B_3O_3H_3(g) + BF_3(g) = B_3O_3H_2F(g) + HBF_2(g)$$

$$B_3O_3H_2F(g) + BF_3(g) = B_3O_3HF_2(g) + HBF_2(g)$$

$$B_3O_3HF_2(g) = HBF_2(g) + B_2O_3(s)$$

(7) T. D. Coyle, J. J. Ritter, and T. C. Farrar, *Proc. Chem. Soc.*, 25 (1964).
(8) L. Lynds and C. D. Bass, *Bull. Am. Phys. Soc.*, [6]9, 661 (1964).
(9) R. F. Porter, D. R. Bidinosti, and K. F. Watterson, *J. Chem. Phys.*, **36**, 2104 (1964).
(10) I. Shapiro, *et al.*, Advances in Chemistry Series, No. 32, American Chemical Society, Washington, D. C., 1961, p. 127.
(11) R. F. Porter and W. P. Sholette, *J. Chem. Phys.*, **37**, 198 (1962).

Table 1: Vibrational Frequency Assignments for $HBF_2(g)$ and $DBF_2(g)$

Fundamental	Symmetry type	Frequency, cm.$^{-1}$ $H^{11}BF_2$	Frequency, cm.$^{-1}$ $D^{11}BF_2$	Description
ν_1	A_1	2620[a]	1965[a]	B–H (B–D) stretch
ν_2	A_1	1165[a]	1127[a]	B–F symmetric stretch
ν_3	A_1	540[a]	540[a]	F–B–F in-plane bend
ν_4	B_1	1401.5 (^{10}B, 1451)[b]	1392.5[b]	B–F asymmetric stretch
ν_5	B_1	...	...	H–B–F in-plane bend
ν_6	B_2	925 ($1^{10}B$, 942)[b]	785 (^{10}B, 805)[b]	Out-of-plane deformation

[a] Band center estimated from band contour. [b] Q-branch measurement.

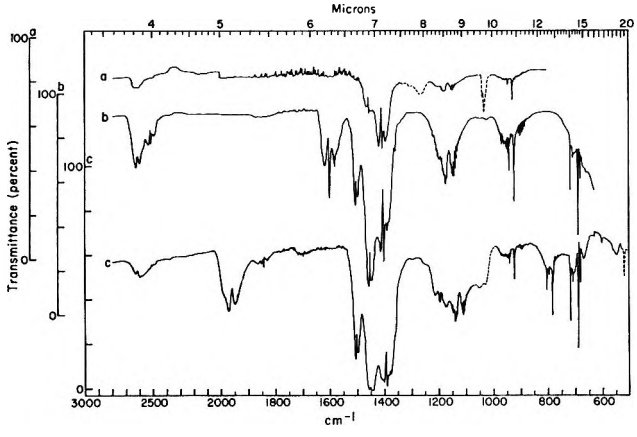

Figure 3. Infrared spectra of: (a) HBF_2 in argon; (b) gaseous products obtained from a high-temperature reaction of HF and H_2O gases with $B–B_2O_3$ mixture (film on the cell windows is shown by dotted lines); and (c) products of the reaction of BF_3 with partially deuterated boroxine (film on the cell windows is shown by dotted lines).

Figure 3a represents a spectrum of nearly pure $HBF_2(g)$ in argon. The spectrum in Figure 3c was obtained with samples prepared by the reaction of $BF_3(g)$ with partially deuterated solid boroxine.

Frequency assignments for $HBF_2(g)$ are given in Table I. Some of the bands have sharp Q branches. In other cases it was necessary to estimate band centers from band shapes. A number of the bands show rotational structure characteristic of a light molecule. For the band at 925 cm.$^{-1}$ the average separation of this structure on the P branch is 4.45 cm.$^{-1}$.

Stability of $HBF_2(g)$. The heat for the reaction

$$^1/_6B_2H_6(g) + {}^2/_3BF_3(g) = HBF_2(g) \qquad (2)$$

was obtained by combining standard free-energy increments with calculated values of $\Delta S°$. Gaseous mixtures of B_2H_6, BF_3, and HBF_2 were prepared by the reaction of BF_3 with solid boroxine. At ordinary temperatures the reaction path to $HBF_2(g)$ does not involve reaction 2 directly. However, as we will note, our observations indicate that the final state of the system is close to equilibrium. Partial pressures of each gaseous species were obtained by an infrared absorption method similar to that used by Lynds and Bass.[12] A series of intensity measurements was taken on samples of pure B_2H_6 and BF_3 over a range of pressures between 3 and 20 torr in a 10-cm. infrared cell. This cell was also used for analysis of mixtures containing the reaction product. Partial pressures of B_2H_6 and BF_3 in a reaction mixture of known total pressure were obtained by comparison of their absorption intensities with those for the standard samples. The partial pressure of HBF_2 was then obtained by difference from the total pressure. Errors in pressures obtained by this procedure are within about $\pm 10\%$. A summary of data for two sets of experimental conditions is given in Table II. Pressures listed in the table relate to conditions within the reaction bulb. To allow for equilibrium the sample prepared at room temperature was held in the reaction bulb for about 3 hr. before analysis.

The entropy of $HBF_2(g)$ was calculated by the usual statistical thermodynamic procedure. The molecule was assumed to have C_{2v} symmetry with B–H and B–F bond distance of 1.20 and 1.29 Å., respectively, and bond angles of 120°. The vibrational partition function was computed from the five frequencies listed in Table I and one frequency for the in-plane H–B–F bend assumed to be 1000 ± 100 cm.$^{-1}$. The calculated entropy of $HBF_2(g)$ at 298°K. is 58.4 cal./mole °K. Entropies for B_2H_6 and BF_3 were taken from the JANAF tables.[13] The calculated heat for reaction 2 (Table II) was combined with heats of formation of $B_2H_6(g)$ and $BF_3(g)$[13] (7.5 and −270.0 ± 2.0 kcal./

(12) L. Lynds and C. D. Bass, *J. Inorg. Chem.*, **3**, 1147 (1964).

(13) "JANAF Thermochemical Data," Thermal Laboratory, Dow Chemical Co., Midland, Mich., 1960.

Table II: Thermochemical Data for the Reaction
$^1/_6B_2H_6(g) + {}^2/_3BF_3(g) = HBF_2(g)$

Temp. of sample prepn. °K.	Initial, P_{BF_3}, atm.	P_{HBF_2}, atm.	$P_{B_2H_6}$, atm.	P_{BF_3}, atm.	K_{eq}	ΔS° (296°K.), entropy units	ΔH° (296°K.), kcal./mole
296	4.8×10^{-2}	1.5×10^{-2}	2.1×10^{-2}	1.4×10^{-2}	0.49	8.7	3.0
360	6.3×10^{-2}	5.1×10^{-2}	2.9×10^{-2}	3.5×10^{-2}	0.85	8.7	2.7

mole, respectively) to give, for the heat of formation of $HBF_2(g)$, -175.7 ± 1.5 kcal./mole at 298°K.

Discussion

The reaction of BF_3 with boroxine can be understood in terms of a mechanism involving substitution of fluorine for hydrogen as in the scheme

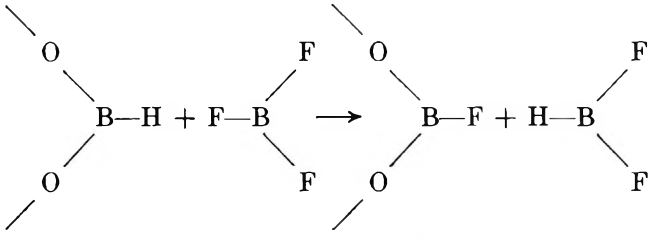

This behavior is analogous to the observations of Coyle and co-workers,[7] who found that $HBF_2(g)$ is formed in a rapid reaction of $BF_3(g)$ with dimethoxyborane. There is also evidence that further substitution of fluorine for hydrogen in boroxine occurs. This was noted from the material balance with respect to the initial amount of BF_3 added to the reaction vessel (see Table II). We observed a total pressure decrease of fluorinated species when the reaction was run at room temperature but we also observed a considerable quantity of diborane in the products. This effect could not be realized in a one-step substitution to produce $HBF_2(g)$. The effect can be accounted for either by subsequent disproportionation of $HBF_2(g)$ or by a further reaction of HBF_2 with the solid to yield diborane. Since the conditions are favorable for a gas–solid reaction, the latter situation seems quite probable. This reaction probably provides the path by which reaction 2 can attain equilibrium. The equilibrium constant obtained from products prepared at 80° and allowed to cool to room temperature (Table II) are higher than those obtained from samples prepared at room temperature. This indicates that, since the endothermic reaction should proceed to a greater extent at high temperatures, the readjustment to equilibrium at room temperature is not rapid. However, under these conditions the solid had been depleted of B–H groups because of the higher reaction temperature.

Calculations of the effect of isotopic substitution on the vibration frequencies in HBF_2 were made with aid of the Teller–Redlich product rule.[14] Moments of inertia for isotopic species of HBF_2 were evaluated from the same molecular parameters as used above for entropy computations. The pertinent equations are

$$\frac{(\nu_1\nu_2\nu_3)_i}{(\nu_1\nu_2\nu_3)_j} = \left\{\left(\frac{m_j}{m_i}\right)\left(\frac{M_i}{M_j}\right)\right\}^{1/2}$$

$$\frac{(\nu_4\nu_5)_i}{(\nu_4\nu_5)_j} = \left\{\left(\frac{m_j}{m_i}\right)\left(\frac{M_i}{M_j}\right)\left(\frac{I_{Zi}}{I_{Zj}}\right)\right\}^{1/2}$$

$$\frac{(\nu_6)_i}{(\nu_6)_j} = \left\{\left(\frac{m_j}{m_i}\right)\left(\frac{M_i}{M_j}\right)\left(\frac{I_{Yi}}{I_{Yj}}\right)\right\}^{1/2}$$

where m_i and m_j are masses of light (H or ^{10}B) and heavy (D or ^{11}B) atoms, respectively; M_i and M_j are molecular weights of difluoroborane species containing light and heavy atoms; I_Z is the moment of inertia taken about an axis perpendicular to the plane of the molecule and I_Y is the moment of inertia taken about an axis perpendicular to a plane passing through the sym-

Table III: Observed and Calculated Products of Frequency Ratios for HBF_2

Isotope substitution	Symmetry type	Product of frequency ratios[a] Calcd.	Found
D for H in ^{11}B species	A_1	1.400	1.378
	B_1	1.365	...
	B_2	1.172	1.178
^{10}B for ^{11}B in hydrogenated species	A_1	1.04	...
	B_1	1.035	...
	B_2	1.019	1.018

[a] Pertains to ratio for light to heavy molecule.

(14) G. Herzberg, "Infrared and Raman Spectra of Polyatomic Molecules," D. Van Nostrand Co., Inc., New York, N. Y., 1945, p. 231.

metry axis. Results of the calculations are given in Table III. For the situations where comparison is possible, the agreement between calculated and observed products is good.

Although there is insufficient experimental data for application of the product rule in the B_1 symmetry type, the band at 1401.5 cm.$^{-1}$ is most probably the asymmetrical B–F stretch. As illustrated in Figure 3a, this band is the strongest in the spectrum and is similar to the band at 1392.5 cm.$^{-1}$ in DBF_2 in relative intensity and band shape. An alternative possibility is to assign the 1401.5-cm.$^{-1}$ band to ν_5,[8] the in-plane B–H bend. On the basis of the latter assignment, a large isotope shift to a lower frequency is expected on deuterium substitution. If such a band is present in DBF_2, it must be considerably weaker than the corresponding band in HBF_2 since most of the band structure in the region between 1050 and 1250 cm.$^{-1}$ (Figure 3c) can be attributed to ν_2 in either HBF_2 or DBF_2. A weak band at ~1200 cm.$^{-1}$ can be attributed to B_2HD_5 impurity.[15] Another factor supporting the ν_4 assignment for the 1401.5-cm.$^{-1}$ band is the magnitude of the isotope shift observed in $H^{10}BF_2$. Of the two frequencies belonging to the B_1 symmetry type, ν_4(B–F stretch) involves the greater participation of the boron motion and is expected to show a larger ^{10}B isotope effect. The product rule (Table III) predicts a maximum shift of about 49 cm.$^{-1}$ toward higher frequencies. The observed shift is 49.5 cm.$^{-1}$. The situation is similar to that in BF_3[16] where the frequency ratio of the asymmetrical B–F stretching vibrations for $^{10}BF_3$ and $^{11}BF_3$ is 1.035. The band at 540 cm.$^{-1}$ did not exhibit a discernable isotope effect on deuterium substitution and was assigned to ν_3, the in-plane B–F bend. In BF_3(g), the in-plane ^{11}B–F bend occurs at about 480 cm.$^{-1}$.[16] The isotopic shift on the band at 1165 cm.$^{-1}$ in HBF_2 to 1127 cm.$^{-1}$ in DBF_2 is about that predicted for ν_2 from application of the product rule for the species of the A_1 symmetry type (Table I). We can rule out the assignment of 1165-cm.$^{-1}$ band to ν_5 since the product rule for the B_1 symmetry type predicts a much larger isotope shift on deuterium substitution.

(15) See ref. 10, p. 139.

(16) L. P. Lindeman and M. K. Wilson, *J. Chem. Phys.*, 24, 242 (1956).

Verification of the Flory Theory of Random Reorganization of Molecular Weight Distribution—Kinetics of Methylsiloxane Polymerization

by Jack B. Carmichael and James Heffel

Basic Polymer Research Laboratory, Dow Corning Corporation, Midland, Michigan
(Received December 11, 1964)

The distributions of linear and cyclic methylsiloxanes were determined by gas–liquid chromatography during acid clay catalyzed reactions of equal molar amounts of D_4 [D = $(CH_3)_2SiO$] and MM [M = $(CH_3)_3SiO_{1/2}$] at 80°. The theoretical and experimental distributions of the linears are compared as a function of time. The relatively large amounts of MD_4M and MD_8M present after 0.5 hr. indicate that D_4 initially enters the linear chains as a unit. Sufficient reorganization has occurred after 0.5 hr. that the distribution of $MD_{10}M$ through $MD_{13}M$ is approximately random. The distribution of shorter chains becomes increasingly random as the reaction proceeds toward equilibrium.

I. Introduction

Kinetic studies of polymerization of dimethylsiloxanes have been performed by many workers. Grubb and Osthoff[1] have shown that the KOH-catalyzed polymerization of D_4 [D = $(CH_3)_2SiO$] is first order by following the change in vapor pressure of the polymerizing system. Many other authors have studied the anionic polymerization of cyclodimethylsiloxanes using LiOH, NaOH, and KOH.[2] In all these studies, some gross parameter of the polymerizing system (*e.g.*, viscosity) was determined for kinetic analysis.

Only Van Wazer and Moedritzer[3] have reported the analysis of reactants and products obtained during polymerization of dimethylsiloxanes. By means of n.m.r. these workers studied the $AlCl_3$-catalyzed reaction of dimethyldichlorosilane with D_4 in a 4:1 molar ratio. Amounts of the molecules $(CH_3)_2SiCl_2$, D_4, and $(CH_3)_2ClSiD_{1-4}Si(CH_3)_2Cl$ were reported as total silicon weight per cent. The formation of large chains or large rings was detected early in the reaction. The collected kinetic data were not analyzed in detail but are probably amenable to the statistical treatment herein applied to the D_4 + MM reorganization [M = $(CH_3)_3SiO_{1/2}$].

Britton and co-workers first reported the use of acid clays to polymerize dimethylsiloxanes.[4] Dimethyldichlorosilane was converted to a hydrolysis mixture by reaction with water, and the hydrolysis mixture was polymerized using a sulfuric acid treated clay (termed Retrol).

Ishzuka and Aihara[5] contributed the pioneering publication to clay-catalyzed siloxane rearrangements. A white clay, terra alba, was treated with sulfuric acid, washed, and dried. A mixture of D_4 and MM was polymerized at 80°, and the viscosity rise with time was determined. The equilibrium viscosity was found to be equivalent to the viscosity from a sulfuric acid catalyzed polymerization. A linear correlation between rate and amount of clay was established. With fixed amounts of D_4 and MM no change in equilibrium viscosity was noted upon changing catalyst concentration or temperature.

Simmler[6] has studied the equilibration of methylsiloxanes using as catalyst sulfuric acid treated Fuller's Earth at 80°. *Via* terminal group analysis he reported the relative reactivities of methylsiloxanes as D_3 >

(1) W. T. Grubb and R. C. Osthoff, *J. Am. Chem. Soc.*, **77**, 1405 (1955).

(2) Z. Laita and M. Jelinek, *Vysokomolekul. Soedin.*, **4**, 1739 (1962), and ref. 1–8 contained therein.

(3) K. Moedritzer and J. R. Van Wazer, *J. Am. Chem. Soc.*, **86**, 802 (1964).

(4) E. C. Britton, H. C. White, and C. Moyle, U. S. Patent 2,460,805 (Feb. 8, 1949).

(5) T. Ishzuka and T. Aihara, *Kogyo Kagaku Zasshi*, **59**, 1198 (1956).

(6) W. Simmler, *Makromol. Chem.*, **57**, 12 (1962).

$D_4 > MM > MM' > M'M' > M''M''$, where M' = $BrCH_2(CH_3)_2SiO_{1/2}$ and M'' = $ClCH_2(CH_3)_2SiO_{1/2}$.

In this study the distributions of cyclic and linear dimethylsiloxanes were determined during the acid clay catalyzed reaction of D_4 and MM at 80°. Reactant and product analyses were by gas–liquid chromatography. This technique was previously described for the determination of cyclic distribution in high molecular weight dimethylsiloxane polymers.[7]

The fit of the data to the Flory theory[8-10] of random reorganization of the linear species was determined as the reaction proceeded.

II. Experimental

Materials. Octamethylcyclotetrasiloxane (D_4) and hexamethyldisiloxane (MM) were distilled for use as the polymerization species. Chromatographic analyses indicated each material was free of other siloxane impurities. A sulfuric acid treated Fuller's Earth was used to catalyze the polymerization. Typical analysis: total free moisture = 1% by weight; total SO_3 = 2.5% by weight.

Polymerization Reactions. Amounts of 59.3 g. of D_4 and 32.5 g. of MM (1:1 molar ratio) were added to a glass polymerization vessel. The vessel was placed in a double-boiler reactor. Refluxing benzene was maintained in the bottom portion to ensure that the temperature was constant at 80°. Dow Corning® 550 Fluid was used as a heat-transfer fluid in which the polymerization vessel was immersed. After 1 hr. of preheating reactants, 0.4687 g. of catalyst was added. Polymers were analyzed periodically after reaction times of 0.5 to 48 hr. Fractions were obtained by opening the top of the reactor and sampling the contents with a hypodermic syringe. The fractions were cooled and filtered through no. 1 filter paper to remove the catalyst. All samples were analyzed by qualitative detection of sulfur. No detectable sulfur wa found in any sample.

Analysis of Polymers. A standard mixture containing accurately known quantities of toluene, D_3 through D_6, and MM through MD_9M was analyzed using gas–liquid chromatography. The weight response factors for each cyclic and linear species in the mixture were calculated. The weight response factors for D_7 through D_9 and $MD_{10}M$ through $MD_{13}M$ were obtained by extrapolation. The composition of the standard mixture and weight response factors are given in Table I. A precise amount of toluene was weighed into each filtered polymer fraction to serve as an internal standard. Area per cents of constituents D_3 through D_9 and MM through $MD_{13}M$ were determined from the chromatograph. Weight per cents were obtained by multiplying the area per cent by the corresponding weight response factor.

Table I: Standard Siloxane Mixture

Component	Wt. %	R^a	
	Linears		
MM	6.29	1.14	
MDM	6.76	1.25	
MD_2M	7.02	1.35	
MD_3M	7.21	1.44	
MD_4M	7.34	1.49	
MD_5M	7.42	1.55	
MD_6M	7.50	1.64	
MD_7M	7.55	1.66	
MD_8M	7.60	1.72	
MD_9M	7.64	1.77	
$MD_{10}M$		1.81	Extrapolated
$MD_{11}M$		1.85	
$MD_{12}M$		1.90	
$MD_{13}M$		1.96	
	Cyclics		
D_3	2.75	1.20	
D_4	7.10	1.35	
D_5	7.89	1.55	
D_6	5.57	1.74	
D_7		1.95	Extrapolated
D_8		2.11	
Toluene	4.367	1.000	

[a] Weight response factors based on toluene

$$\frac{\text{wt. \% toluene}}{\text{area of toluene}} = \left(\frac{\text{wt. \% } x}{\text{area of } x}\right)R$$

Chromatography Conditions. The F & M Model 720 linear temperature programmed gas–liquid chromatograph was used for all analyses. The 0–1-mv. Brown recorder was equipped with a Model 201B Disc integrator. Columns used were a matched set, each being 0.61 m. × 0.64 cm. stainless steel packed with 10% LP-122 (diphenylsiloxane–dimethylsiloxane copolymer) on ST-111 (60–80 mesh Chromasorb P, nontreated). Column temperatures were programmed from 50 to 75° at 2°/min., then 15°/min. to 350°.

III. Experimental Results

The weight percentages of each linear and cyclic species *vs.* time are plotted in Figures 1–6. Analysis of these data makes several observations clear: (1) equilibrium is reached within 3–17 hr.; (2) good analytical

(7) J. B. Carmichael and R. Winger, *J. Polymer Sci.*, Part A, in press.
(8) P. J. Flory, *J. Am. Chem. Soc.*, **58**, 1877 (1936).
(9) P. J. Flory, *ibid.*, **64**, 2205 (1942).
(10) P. J. Flory, *Chem. Rev.*, **39**, 137 (1946).

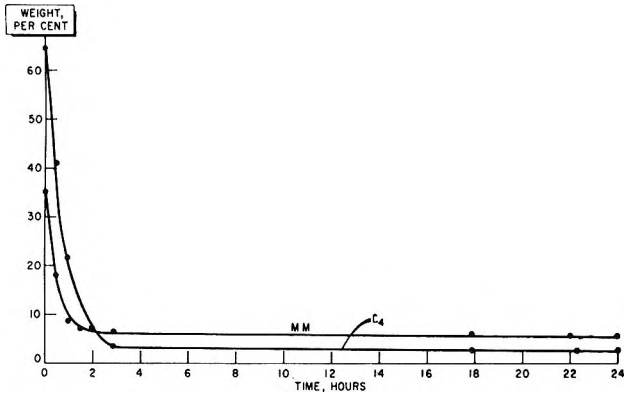

Figure 1. Disappearance of MM and D_4 as a function of time.

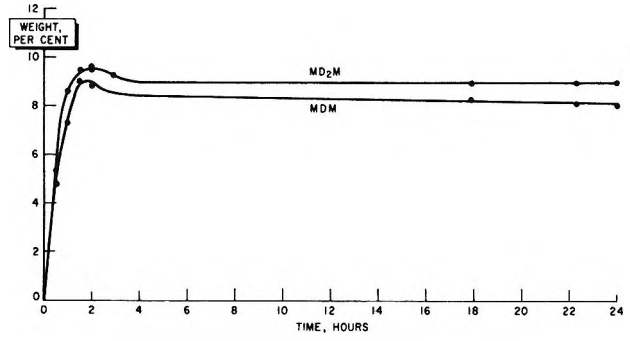

Figure 2. Formation of $MD_{1-2}M$ as a function of time.

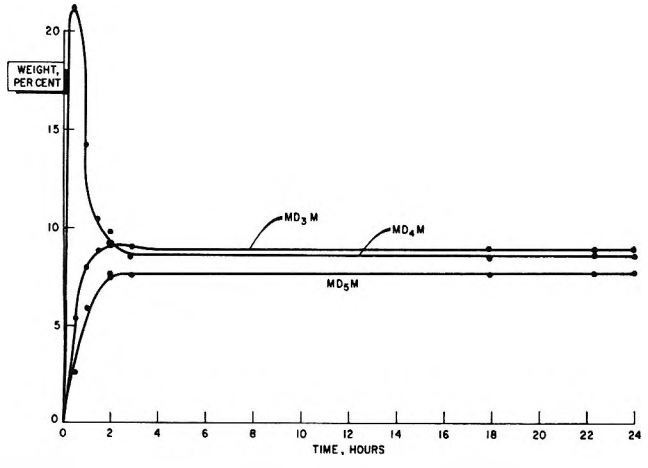

Figure 3. Formation of $MD_{3-5}M$ as a function of time.

precision was obtained; (3) the early and prominent maxima noted for MD_4M and, tc a lesser extent, MD_8M indicate that the following net reactions are initially important

$$MM + D_4 \longrightarrow MD_4M \quad (a)$$

and/or

$$MD_4M + D_4 \longrightarrow MD_8M \quad (b)$$

$$MM + 2D_4 \longrightarrow MD_8M \quad (c)$$

A graphic illustration of the differences between the equilibrium distribution and the kinetically controlled distribution after 0.5 hr. is depicted in Figure 6.

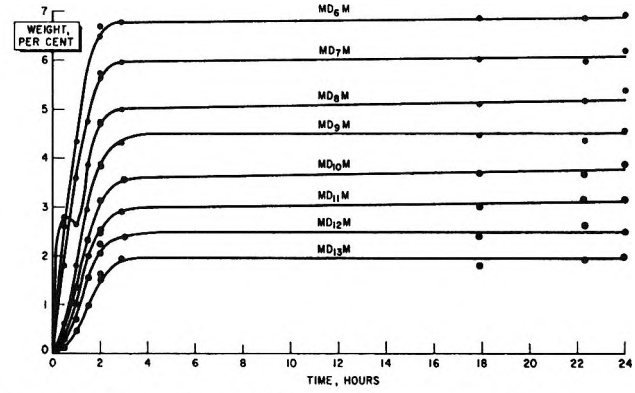

Figure 4. Formation of $MD_{6-13}M$ as a function of time.

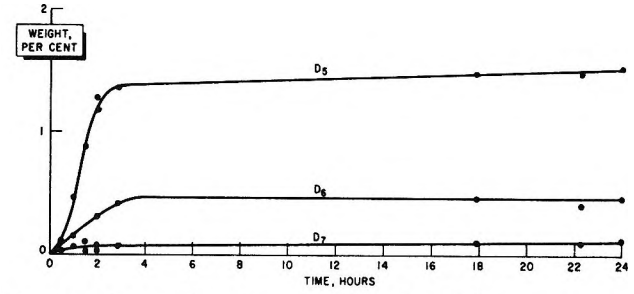

Figure 5. Formation of D_{5-7} as a function of time.

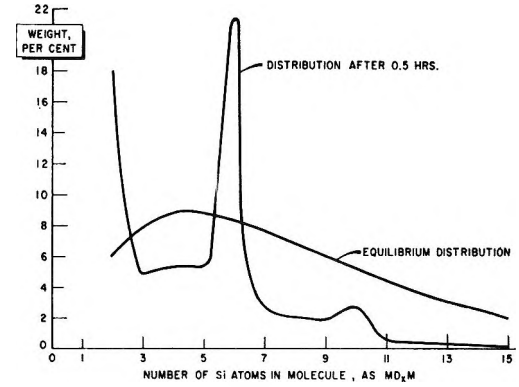

Figure 6. Comparison of equilibrium and kinetically controlled distributions.

IV. Analysis of the Results

Adaptation of the Flory Theory.[9] Consider a polymer wherein interchange may occur freely but in which the average chain length is fixed.

Table II: Comparison of Theory and Experiment—Molecular Weight Distribution (Based on Linear Portion) *vs.* Run Time, Wt. %[a]

Linears	Time,[b] 0.5	Calcd. p = 0.580[c]	% diff.	Time, 1	Calcd. p = 0.645	% diff.	Time, 1.5	Calcd. p = 0.697	% diff.	Time, 2	Calcd. p = 0.735	% diff.	Time, 2.9	Calcd. p = 0.747	% diff.
MM	30.7	17.4	76.4	11.09	12.6	12.0	8.5	9.05	10.0	6.04	7.05	14.3	6.64	6.40	3.8
MDM	8.2	20.6	60.2	9.39	16.4	42.7	10.48	12.80	18.1	9.76	10.35	5.2	8.98	9.60	6.5
MD_2M	9.0	17.8	49.4	11.14	15.7	29.0	10.99	13.40	18.0	10.42	11.4	8.2	9.73	10.65	8.6
MD_3M	9.2	13.80	33.3	10.40	13.50	23.0	10.22	12.50	18.2	10.03	11.4	12.0	9.50	10.70	11.2
MD_4M	36.3	10.00	263.0	18.32	10.95	67.3	12.19	10.80	12.9	10.36	10.4	0.4	8.99	9.90	9.2
MD_5M	4.4	7.00	37.1	7.54	8.45	10.8	7.82	9.10	14.1	8.33	9.00	7.4	8.01	8.90	10.0
MD_6M	3.6	4.70	23.4	5.59	6.35	12.0	6.89	7.35	6.3	7.23	7.70	6.1	7.14	7.80	8.5
MD_7M	3.1	3.10	0.0	4.65	4.70	1.1	5.52	5.90	6.4	6.25	6.55	4.6	6.27	6.65	5.7
MD_8M	4.8	2.00	140.0	3.43	3.40	0.9	4.48	4.60	2.6	5.17	5.40	4.3	5.26	5.60	6.1
MD_9M	1.0	1.30	23.1	2.31	2.45	5.7	3.41	3.60	5.3	4.26	4.40	3.2	4.52	4.65	2.8
$MD_{10}M$	0.7	0.85	17.6	1.75	1.75	0.0	2.68	2.70	0.7	3.44	3.55	3.1	3.72	3.85	3.4
$MD_{11}M$	0.7	0.55	27.3	1.30	1.25	4.0	2.31	2.10	10.0	2.72	2.85	4.6	3.01	3.15	2.5
$MD_{12}M$	0.5	0.35	42.9	0.88	0.85	3.5	1.80	1.60	12.5	2.34	2.25	4.0	2.49	2.50	0.4
$MD_{13}M$	0.2	0.20	0.0	0.58	0.60	3.3	1.10	1.15	4.3	1.71	1.80	5.0	2.04	2.05	0.5

[a] Theoretical values computed by arbitrarily fitting $MD_{13}M$ at each time. [b] Time measured in hours. [c] $W = rp^{r-1}(1-p)^2$ where average degree of polymerization $= (2-p)/(1-p)$.

The weight fraction of x-mer thus obtained is

$$W_x = xp^{x-1}(1-p)^2 \qquad \text{(i)}$$

where p is a parameter related to the average degree of polymerization. For the reaction MM + D_4

$$p = \frac{yz}{1+yz} \qquad \text{(ii)}$$

where y is the average number of D groups in the molecule MD_yM as determined by number-average molecular weight by the original ratio of constituents, and z is the fraction of D groups in the linear portion of the polymerizing mixture (*i.e.*, a correction for the total weight per cent cyclics).

For siloxane polymers, MM represents a 1-mer.

The same equation (i) can be derived in a much simpler manner by considering the random condensation of a difunctional monomer where, once formed, the molecules cannot redistribute.[8]

The Flory theory assumes no cyclization. However, the theory will apply to the linear species as a separate subset of molecules if the reaction has reached equilibrium.[11] Here the system does not reach equilibrium for several hours, and the amounts of cyclics change with time. Therefore the weight per cents of linear species were recalculated as per cent by weight of linear species to the exclusion of cyclic constituents.

Comparison of Theory and Experiment. The recalculated weight per cents of linear species appear in Table II. The comparison of theory with experiment was obtained by arbitrarily fitting the experimental weight per cent of $MD_{13}M$ to the theoretical weight per cent. The theoretical weight per cents of MM through $MD_{12}M$ were then obtained at the same value of p from the curves of weight fractions of x-mer for x = 1–14 as a function of p. Curves for x = 5, 10, and 20 appear in Flory's first paper.[8] The important conclusions include the following.

1. Maxima occur for the weight percentages of MDM, MD_2M, MD_3M, and MD_4M at times of approximately 1.5, 2, 2.5, and 0.5 hr. The maximum at 0.5 hr. for MD_4M has been ascribed to opening of D_4 followed by termination. The maxima for the other species may be examined by considerations of the random theory. For random polycondensation, as the polymerization reaction proceeds, the amount of a particular polymer builds up to a maximum located at $p = (x-1)/(x+1)$ then falls away to approach zero as p approaches unity. For x = 2, 3, and 4 the maxima are predicted to occur at values of p = 0.35, 0.5, and 0.6, respectively. However, the values of p which best describe the experimental data are 0.70, 0.73, and approximately 0.74, respectively. The deviation between the two sets of p values is explained as follows. The initial reaction in the polymer is highly nonrandom and leads to the formation of MD_4M. Therefore p increases rapidly. Rearranged small linear species are then produced. Lesser amounts of MDM, MD_2M, and MD_3M are formed in the early stages of the reaction than if polymerization had occurred by the condensation of $(CH_3)_2Si(OH)_2$.

2. After 0.5 hr. a reasonable fit between theory and

(11) H. Jacobson and W. H. Stockmayer, *J. Chem. Phys.*, **18**, 1600 (1950).

experiment is obtained for MD_6M through $MD_{13}M$ with the exception of MD_8M. This fit means that these large linear species are, to a good approximation, being formed randomly, and their formation is therefore independent of the mechanism of the initiation of the reaction. The overabundance of MD_8M is due to reactions b and c cited earlier.

3. After 1.0 hr. a good fit is obtained for MD_5M through $MD_{13}M$. Note that by this time MD_8M fits the random theory almost exactly.

4. After 1.5 hr. a *reasonable* fit is obtained for all species. The maximum per cent difference is 18.2.

5. After 2.9 hr. a *good* fit is obtained for all species. The maximum per cent difference is 11.2.

V. Conclusions

The large quantities of MD_4M and MD_8M formed during the early stages of the reaction indicate that, when D_4 is cleaved by the acid catalyst, it enters the linear molecules as a unit. Reorganization occurs rapidly, so that after 0.5 hr. the distribution of chains MD_9M through $MD_{13}M$ is approximately random. The distribution of shorter chains becomes increasingly more random as the reaction proceeds until, at equilibrium, the distribution of all linear species is well explained by a random reorganization model. A corollary to the above conclusions is that the rate constant for propagation of dimethylsiloxanes appears to be approximately independent of molecular size.

Acknowledgment. We wish to acknowledge a helpful discussion with Dr. Chi-long Lee. Mr. Donald Mead distilled the octamethylcyclotetrasiloxane used in this study. We thank Dr. John Speier for criticizing the manuscript.

Equilibrium Molecular Weight Distribution of Cyclic and Linear Methylsiloxanes

by Jack B. Carmichael and James Heffel

Basic Polymer Research Laboratory, Dow Corning Corporation, Midland, Michigan
(Received December 11, 1964)

Data are reported for the equilibrium molecular size distributions of cyclic and linear methylsiloxanes in five polymers with number-average molecular weights ranging from 459 to 1348. The distributions of linear species agree with the earlier work of Scott and agree reasonably well with the Flory theory of random reorganization. The amounts of cyclic molecules are sharply dependent on molecular weight. However, the equilibrium constants for cyclic formation for cyclic species with four to eight units are shown to be virtually identical with the equilibrium constants for cyclic formation in high molecular weight polymers reported in a previous publication. For octamethylcyclotetrasiloxane, K_{av} in moles of siloxane units per liter was found to be 0.72 in this study. For high polymers, K_{av} was previously reported to be 0.74.

I. Introduction

Molecular weight distributions of polymers are conventionally determined by indirect methods. The ultracentrifuge, fractional precipitation,[1] turbidimetric titration,[2] and, most recently, gel permeation chromatography[3] have been employed. The important experimental feature of this work is that a direct method employing gas–liquid chromatography is used to measure molecular weight distribution. Gas–liquid chromatography cannot be applied to high polymers but allows direct measurement of individual species in low molecular weight polymers. Using the techniques of this work, molecules containing up to 15 siloxane units have been separated and identified. By knowing the amounts of these individual constituents, a large portion of the molecular weight distribution can be directly constructed. If a function can be determined which will fit the experimentally measured portion of the distribution, the remainder can be extrapolated. This procedure is applied here to the equilibrium distribution of methylsiloxanes.

In a previous publication,[4] gas–liquid chromatography was used to follow the molecular weight distribution during the clay-catalyzed reaction of MM + D_4. M denotes the chain terminating unit, $(CH_3)_3SiO_{1/2}$, and D denotes the difunctional unit, $(CH_3)_2SiO$. There, the initial distribution of linear species was found to be nonrandom. As the reaction progressed, the distribution became increasingly more random, and weight per cents of the linear species agreed well with those calculated from the Flory theory of random rearrangement. We further test the Flory theory for applicability to the linear distributions obtained in this work.

Scott[5] previously reported the molecular weight distribution in low molecular weight dimethylsiloxanes. He used sulfuric acid to catalyze the reaction between MM and D_4 at room temperature. Using fractional distillation, Scott separated linear and cyclic species in an equilibrated mixture of number-average molecular weight 438 ± 20. The largest species Scott separated was MD_6M.

The polymer prepared by Scott was duplicated in this work and analyzed by gas–liquid chromatography for cyclic and linear species. The largest species quantitatively identified using these techniques was $MD_{13}M$.

II. Experimental

The materials and experimental methods used in this work were the same as those reported in the pre-

(1) See P. J. Flory, "Principles of Polymer Chemistry," Cornell University Press, Ithaca, N. Y., 1953, Chapter VII, for a discussion of conventional experimental methods for determination of polymer molecular weights and molecular weight distribution.

(2) W. C. Taylor and J. P. Graham, *J. Polymer Sci.*, **B2**, 169 (1964).

(3) J. C. Moore, *ibid.*, **A2**, 835 (1964).

(4) J. B. Carmichael and J. Heffel, *J. Phys. Chem.*, **69**, 2213 (1965).

(5) D. W. Scott, *J. Am. Chem. Soc.*, **68**, 2294 (1946).

vious publication[4] with the following exceptions. (1) The ratio of MM to D_4 was varied such that the calculated number-average molecular weights ranged from 459 to 1348. (2) No samples of polymers were obtained during the polymerization reaction. (3) The sulfuric acid catalyzed polymer was first placed in a separatory funnel and the excess sulfuric acid layer separated. Ammonia was bubbled through the remaining liquid; 4 g. of Super-Cel was added, and the solution was filtered through a sintered filter with aspirator pressure. The polymer was then washed neutral with water. Sodium sulfate was then added to absorb excess water. The mixture was again filtered, and the resultant polymer was analyzed.

The composition and conditions for each reaction are listed in Table I. Times necessary to reach equilibrium were established in the first publication in this series.[4]

Table I: Polymer Compositions and Properties

Polymer	Compositions: D_4, g.	MM, g.	Acid clay, g.	Reaction time, hr.	Properties: Calcd. mol. wt.[a]	Density,[b] g./ml.
Scott	64.6	35.4	[c]	494	459	0.884
2	59.3	32.5	0.4687	112	459	0.8353
1	64.6	35.4	[c]	494	459	0.8944
3	59.3	32.5	0.4687	112	459	0.8397
4	75.28	16.49	0.4687	143	904	0.877
5	80.71	11.05	0.4687	142	1348	0.892

[a] On basis of monomer ratio. [b] At polymerization temperature. [c] Polymerized at 25° using 1 ml. of concentrated H_2SO_4.

III. Results and Discussion

Table I contains the properties of the polymers prepared in this study. These properties are compared with those of Scott's polymer. The compositions of the equilibrated polymers by concentration are tabulated in Table II.

A. Distribution of Linear Species. Flory's statistical treatment of the equilibria in heterogeneous polymer solutions[6] assumes that the standard free energy change in a reaction

$$x\text{-mer} + y\text{-mer} \rightleftharpoons (x + y)\text{-mer} \qquad (1)$$

is always the same regardless of x and y. We may, after Scott, apply this theory to the siloxane equilibria

$$MD_{x-2}M + MD_{y-2}M \rightleftharpoons MD_{x+z-2}M + MD_{y-z-2}M \qquad (2)$$

The theory assumes that the standard free energy change for a reaction leading to the formation of one siloxane unit is always the same and equal to $\Delta F°$. If

Table II: Composition of Equilibrated Dimethylsiloxane Mixtures by Concentration

Compd.	Scott	Concn., mole/l., in polymer: 1	2	3	4	5
MM	0.354	0.0738[a]	0.3681	0.2818	0.0907	0.0379
MDM	0.325	0.2965	0.3264	0.2790	0.0816	0.0351
MD_2M	0.276	0.2839	0.2796	0.2335	0.0764	0.0353
MD_3M	0.230	0.2286	0.2170	0.1902	0.0695	0.0338
MD_4M	0.160	0.1822	0.1680	0.1519	0.0625	0.0313
MD_5M	0.129	0.1419	0.1301	0.1213	0.0563	0.0298
MD_6M	0.096	0.1106	0.0971	0.0963	0.0507	0.0277
MD_7M		0.0860	0.0758	0.0770	0.0453	0.0254
MD_8M		0.0671	0.0559	0.0601	0.0398	0.0240
MD_9M		0.0517	0.0419	0.0470	0.0358	0.0224
$MD_{10}M$		0.0395	0.0318	0.0369	0.0311	0.0196
$MD_{11}M$		0.0302	0.0233	0.0285	0.0272	0.0185
$MD_{12}M$		0.0233	0.0168	0.0219	0.0234	0.0165
$MD_{13}M$		0.0181	0.0126	0.0171	0.0198	0.0150
D_3			0.002	0.003	0.001	0.001
D_4	0.092	0.0751	0.049	0.0751	0.116	0.131
D_5		0.0379	0.032	0.0437	0.0617	0.0748
D_6		0.0095	0.0073	0.0089	0.0168	0.0204
D_7		0.0018	0.0018	0.001	0.0039	0.0050
D_8		0.0009			0.0011	0.0017

[a] Value in error due to volatilization during work-up.

equilibrium constants are written in terms of the molar concentration of the reactants and products in reaction 2, those equilibrium constants will be unity regardless of the values of x, y, and z. This is because the number of siloxane bonds remains constant on passing from the left to the right of eq. 2. The theory is tested by calculating values of the equilibrium constant, K, for many values of x, y, and z. The results are tabulated in Table III. The average values of K are quite close to 1. The maximum deviation from 1 for all of the K values calculated was 0.27. In no case does the average deviate from 1 by greater than 0.07. Standard deviations are always less than 0.09. We therefore conclude that eq. 2 is a very satisfactory approximation for the equilibria involving the short linear methylsiloxanes considered here.

In the accompanying paper of this study the form of the molecular weight distribution was found to approach the random distribution as the reaction progressed. Applicability of the random molecular weight distribution theory was further tested on the polymers prepared here.

Reaction 2 is satisfied by the relation

$$C_x = Ap^x \qquad (3)$$

(6) P. J. Flory, *J. Chem. Phys.*, 12, 425 (1944).

Table III: Equilibrium Constants for Reactions

$$MD_xM + MD_yM \rightleftharpoons MD_{x+z} + MD_{y-z}M$$

	Polymers				
	1	2	3	4	5
K^a	1.06	1.07	1.07	1.02	1.02
σ	0.09	0.07	0.09	0.03	0.04

[a] Average of 34 combinations of x, y, and z.

where C_x is the concentration of x-mer, A is the normalization constant, and p is the fraction of unreacted end groups and is directly related to the number-average degree of polymerization (see ref. 4).

The data in Table IV are plotted in Figures 1 through 3. A significant deviation below the straight line can be seen in all cases for MM. The deviation decreases for MDM and is almost negligible for MD_2M. This means that the standard free energy of a siloxane linkage in a very short linear chain is higher than the free energy of an isolated siloxane linkage in a long chain. The effect is most pronounced in hexamethyldisiloxane, MM.

Some drift below the best straight line also is seen for the large linear species $MD_{11}M$–$MD_{13}M$. The drift could be due to (1) inaccuracies in the data caused by the necessity of extrapolating weight-response factors past MD_9M and (2) physically meaningful trend of the distribution away from the normal and toward a more narrow distribution. This possibility was explored by calculating the ratio of the weight- to number-average molecular weights. This ratio for the random distribution will be $\bar{M}_W/\bar{M}_N = 1 + p$. Weight-average molecular weights were measured by direct summation of the data for polymers 2 and 3.

The amounts of linears $MD_{14}M$ through $MD_{26}M$ were determined by extrapolating the plots of Figures 1 and 2 for polymers 2 and 3. Weight per cents of cyclic and linear species for these polymers appear in Table IV. Number- and weight-average molecular weights were calculated from the expression $M_n = \Sigma 1/(W_i/M_i)$ and the expression $M_w = \Sigma W_i M_i$ where W_i and M_i refer to the weight fraction and the molecular weight of the ith species. Values of M_n and M_w for only the linear portion of each polymer were determined by recalculating the weight per cents of the linears as per cent by weight of linear species to the exclusion of cyclic species.

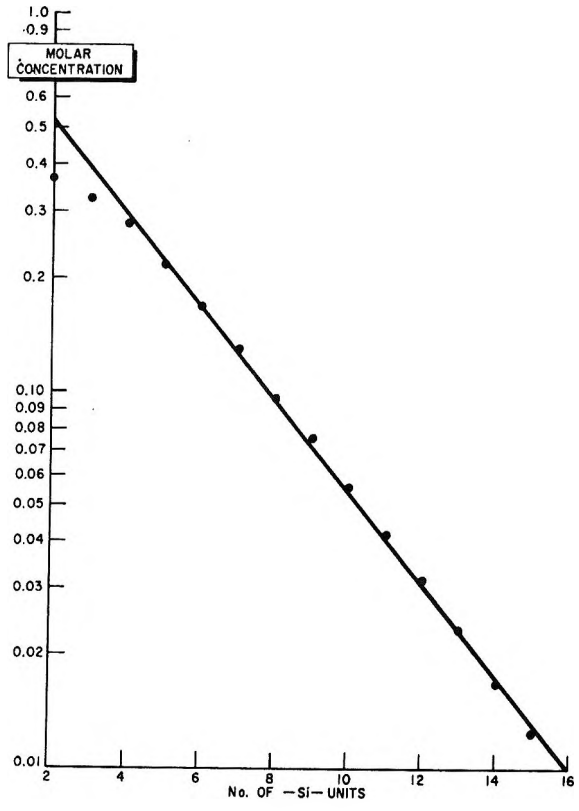

Figure 1. Plot of log (molar concentration) *vs.* number of siloxane units for polymer 2.

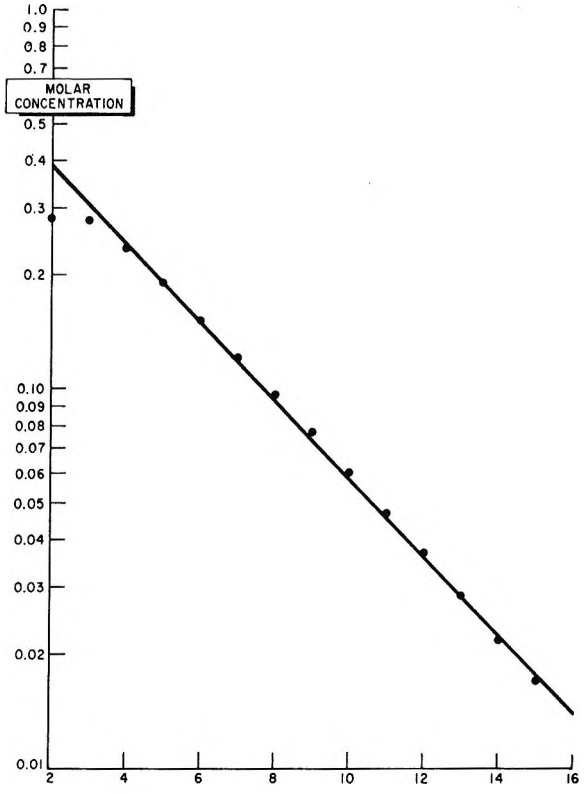

Figure 2. Plot of log (molar concentration) *vs.* number of siloxane units for polymer 3.

Table IV: Composition of Equilibrated Dimethylsiloxane Mixtures by Weight

Compd.	Wt. % in polymer 2	Wt. % in polymer 3	
MM	7.26	5.45	
MDM	9.24	7.86	
MD_2M	10.4	8.64	
MD_3M	10.0	8.72	
MD_4M	9.23	8.30	
MD_5M	8.31	7.70	
MD_6M	7.06	7.00	
MD_7M	6.18	6.25	
MD_8M	5.06	5.41	
MD_9M	4.17	4.65	
$MD_{10}M$	3.42	3.98	
$MD_{11}M$	2.73	3.32	
$MD_{12}M$	2.12	2.75	
$MD_{13}M$	1.70	2.30	
$MD_{14}M$	1.36	1.96	$MD_{14}M$–$MD_{26}M$ extrapolated from Figures 1 and 2
$MD_{15}M$	1.07	1.62	
$MD_{16}M$	0.86	1.36	
$MD_{17}M$	0.68	1.12	
$MD_{18}M$	0.55	0.93	
$MD_{19}M$	0.43	0.77	
$MD_{20}M$	0.34	0.63	
$MD_{21}M$	0.27	0.52	
$MD_{22}M$	0.21	0.43	
$MD_{23}M$	0.17	0.35	
$MD_{24}M$	0.13	0.28	
$MD_{25}M$	0.10	0.24	
$MD_{26}M$	0.08	0.19	
D_3	0.05	0.07	
D_4	1.79	2.65	
D_5	1.44	1.62	
D_6	0.41	0.47	
D_7	0.11	0.05	
Total	96.93	97.57	

For polymer 2, $M_n = 421$ and $M_w = 550$. For the linear portion, $M_n = 408$ and $M_w = 577$.

For polymer 3, $M_n = 486$ and $M_w = 623$. For the linear portion, $M_n = 456$ and $M_w = 654$.

The ratio M_w/M_n is 1.41 and 1.43 for the linear portions of polymers 2 and 3, respectively. The random theory predicts ratios of 1.75 and 1.79 for the two polymers.

The polymers thus appear to be somewhat less disperse than the random distribution. This may be due, in part, to the arbitrary cutoff at $MD_{26}M$ and to the extrapolation procedure itself.

B. Distribution of Cyclic Species. The cyclic distributions determined for the polymers prepared here are plotted by weight per cent in Figure 4. In Figure 4 a plot is shown of the amount of cyclics D_4 through D_6 as a function of molecular weight. Also shown on the graph are the amounts of cyclics present in a polymer

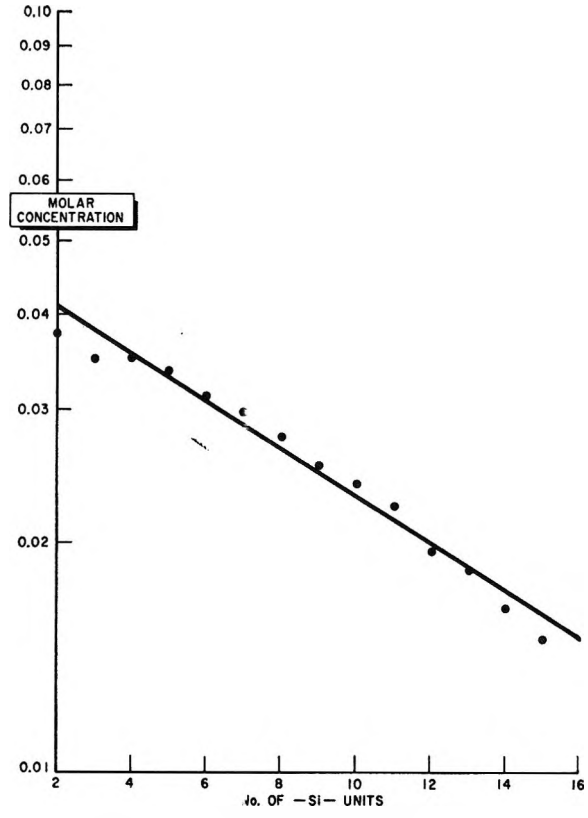

Figure 3. Plot of log (molar concentration) *vs.* number of siloxane units for polymer 5.

of molecular weight of approximately 1,000,000.[7] The increase in total weight per cent cyclics as a function of molecular weight is shown in Figure 4.

The quantities of cyclics present are sharply dependent on molecular weight. Total amounts of cyclics for polymers 1, 2, 3, 4, and 5 are 3.80, 4.70, 4.86, 7.69, and 8.92%, respectively. Previously, the total cyclics were shown to equal 12.8% for a polydimethylsiloxane having an average molecular weight of 10^6. This polymer had been polymerized to an equilibrium state at 110°.[7]

The dependence of quantities of cyclic species on molecular weight will now be interpreted.

Consider the equilibrium between a chain of $n + x$ siloxane units and a chain of n units plus a cyclic of x units.[8]

$$C_{n+x} \rightleftharpoons C_n + R_x \tag{4}$$

Assuming activity coefficients equal to unity

$$K = \frac{[C_n][R_x]}{[C_{n+x}]} \tag{5}$$

(7) J. B. Carmichael and R. Winger, *J. Polymer Sci.*, **A3**, 971 (1965).

(8) H. Jacobson and W. H. Stockmayer, *J. Chem. Phys.*, **18**, 1600 (1950).

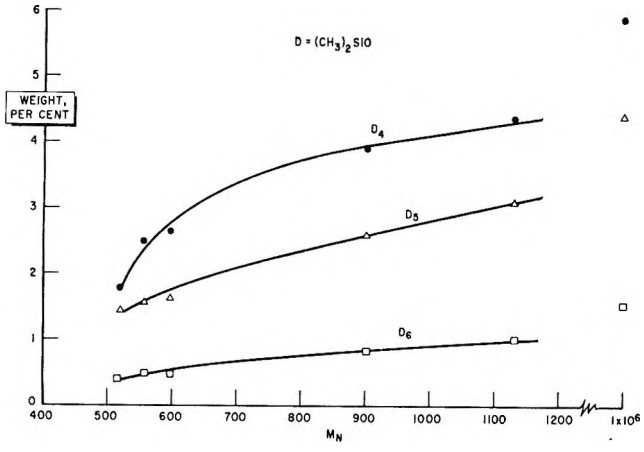

Figure 4. Increase in amounts of D_{4-6} with increasing molecular weight.

For the high molecular weight polymers discussed in a prior publication[7]

$$K \simeq [R_x] \tag{6}$$

The functional form of the ratio $[C_n]/[C_{n+x}]$ must be determined for the low molecular weight polymers prepared in this study in order to calculate K.

From (3), $C_n = Ap^n$ and $C_{n+x} = Ap^{n+x}$. Substituting into (5) one obtains

$$K = \frac{[R_x]}{p^x} \tag{7}$$

The concentrations of cyclics were determined for polymers 1–5 and appear in Table II. The corresponding values of p for these polymers were determined from the slopes of plots of log $[C_n]$ *vs.* n. Three such plots are shown in Figures 1–3. For polymers 1–5 values of p are 0.78, 0.75, 0.79, 0.90, and 0.93, respectively. With these data, we are equipped to calculate K for each cyclic determined in each of five polymers and assess its constancy with variable polymer molecular weight.

If K were not independent of molecular weight for equilibrated dimethylsiloxane polymers, then (1) $C_x \neq Ap^x$ and/or (2) activity coefficients are not unity and the use of concentrations in eq. 5 is not valid.

In Table V the K_n values are calculated for cyclics D_4–D_8 for polymers 1–5. K_4 is calculated for Scott's[4] polymer. Deviations between the K values for polymers 1–5 and K values for high molecular weight polymers are small and random. The average K and the standard deviations are shown for each cyclic. The average K values for low molecular weight polymers are virtually identical with the average K values for high molecular weight polymers for every cyclic analyzed.

Table V: Calculation of K for Cyclic Formation[a]—Comparison with K Determined for High Polymers

	Equil. const., K, mole of -SiO-/l.							Cyclic concn. in high polymers[b]
	Polymer						Std.	
Cyclic	1	2	3	4	5	Av.	dev.	
D_4[c]	0.81	0.61	0.77	0.70	0.70	0.72	0.07	0.74
D_5	0.65	0.67	0.70	0.52	0.53	0.61	0.07	0.55
D_6	0.25	0.24	0.22	0.19	0.19	0.20	0.03	0.20
D_7	0.07	0.10	0.04	0.06	0.06	0.07	0.02	0.05
D_8	0.05	...	...	0.02	0.02	0.03	0.01	0.02

[a] See eq. 7. [b] Average cyclic concentration for $(Me_2SiO)_n$ polymers of $M_v \sim 1 \times 10^6$. See ref. 7. [c] For Scott's polymer, $K = 0.97$ for D_4.

The important conclusions are the following.

1. $C_x = Ap^x$ for low molecular weight equilibrated dimethylsiloxanes.

2. The use of concentrations in eq. 5 is valid. Other logical conclusions (3 and 4) can be extrapolated from the results.

3. The function $C_x = Ap^x$ describes the molecular weight distribution by concentration for equilibrated siloxane polymers of any average molecular weight.

4. The position of equilibrium in a chemical reaction is independent of catalyst. We verify that for this polymerization the distributions of cyclic and linear species are independent of catalyst at equilibrium. The study of high molecular weight polymers in ref. 6 was carried out with potassium silanolate and sulfuric acid catalysts. These catalysts were first shown to give equivalent cyclic distributions. This present study utilized sulfuric acid and acid clay catalysts. These catalysts were herein shown to give equivalent cyclic and linear distributions. Further, when the two studies are compared through determination of equilibrium constants of cyclic formation, results are equivalent.

The two studies thus mesh into a consistent picture of the distributions of cyclic and linear dimethylsiloxane species and the variables upon which these distributions depend.

Acknowledgments. Dr. John Ryan provided helpful criticisms of the manuscript. We are grateful to Mr. K. E. Polmanteer for his critical review of both papers in this series.

Appendix. Alternative Method for Calculating p

The average degree of polymerization of the linear portion, P, can be shown to be related to p from the theory of condensation polymerization.[4]

$$P = \frac{1}{1 - p} \tag{A1}$$

Here P is the number of siloxane bonds − 1 since MM is the smallest species present. $P = 1$ for MM to be consistent with Flory's theory. From the experimentally determined number-average molecular weight the size of the average species present will be MD_zM.

However, we must determine the size of the average *linear* species present, P, from which p can be calculated from (A1).

$$\text{(fraction of linear siloxane bonds)} \equiv z = \frac{\text{(moles of linear –SiO– bonds in D groups)}}{\text{(total moles of –SiO– bonds originally present in } D_4)} \tag{A2}$$

Then the size of the average linear molecule is $MD_{z2}M$. Therefore

$$P = 1 + xz \tag{A3}$$

Substituting (A3) into (A1) and solving for p

$$p = \frac{xz}{1 + xz} \tag{A4}$$

Equations A1–A4 may be applied to calculate p for polymer 4.

From Table I

$$\bar{M}_N = 903 \tag{A5}$$

903 − 162.4 (molecular weight of MM) = 740.6

740.6 = average molecular weight of the middle of the chain (*i.e.*, the D units) (A6)

$$\frac{740.6}{74.13} = 9.99 = x \tag{A7}$$

One may now proceed to calculate z.

total weight per cent cyclics found = 7.69 (A8)

initial charge of D_4 (see Table I) = 82.03 (A9)

converted to initial charge of D_4 + MM = 100 g.

Applying eq. A3

$$z = 1 - \frac{7.69}{82.03} = 0.907 \tag{A10}$$

Combining the results of (A7) and (A10) and inserting into eq. A4 to calculate p one obtains

$$p = \frac{9.99(0.907)}{1 + 9.99(0.907)} \tag{A11}$$

$$p = 0.90 \tag{A12}$$

This value agrees well with the previously calculated p value of 0.90 from the slope of log C_x *vs.* x. Excellent agreement between the two methods is thus obtained for this case.

The calculation method of obtaining p outlined here becomes highly desirable for polymers of much higher molecular weight than those studied here. If $\bar{M}_N$ were of the order of 10,000–50,000, the determination by gas–liquid chromatography of species $MD_{13}M$ would represent only a small fraction of the molecular weight distribution curve of the linear molecules. Also, the amounts of these individual constituents would be extremely small, rendering plots of log C_x *vs.* x virtually useless as tools for calculating p. However, if $\bar{M}_N$ is known and the polymers are polymerized to equilibrium, the calculation method can be immediately applied to yield p. The form of the molecular weight distribution is then immediately known from the relation $C_x = Ap^x$. The molecular weight distribution is equivalently expressed as weight fraction *vs.* molecular size as $W_x = xp^{x-1}(1 - p)^2$, where W_x = weight fraction of x-mer.

Protonic Conduction in the Water I Region

by R. A. Horne and R. A. Courant

Arthur D. Little, Inc., Cambridge, Massachusetts *(Received December 12, 1964)*

The activation energies, E_a, of electrical conduction for aqueous HCl solutions of various concentrations have been determined from precision conductivity measurements over the temperature range -1 to $+10°$. In contrast to "normal" ionic conduction in aqueous solution which exhibits a pronounced maximum in E_a near the temperature of maximum density, E_a for protonic conduction remains fairly constant. Protonic conduction is composed of two components: "normal" ionic conduction whose rate-determining step is "hole"-formation in the solvent water and which presumably can occur in both the "free" and clustered water and conduction whose rate-determining step is the rotation of water molecules and which is confined to the "free," rotatable water monomers between the clusters. Ordinarily, the latter process dominates, but below about 2° the influence of the former becomes appreciable. There also appears to be a tendency of E_a for HCl, as in the case of salts, to decrease with increasing HCl concentration.

Introduction

"Normal" electrical conduction in aqueous solutions of electrolytes such as KCl as believed to involve the formation of a "hole" in the solvent.[1] Protonic conduction, however, proceeds by an "anomalous" mechanism, and the rate-determining step of this process at ordinary pressures involves the rotation of water molecules[2-5] and is confined to the "free" molecules between the water clusters.[6] As temperature is decreased, at about 4° (the temperature of maximum density) water undergoes a partial conversion from the quartz-like structure of water II to the relatively open ice–tridymite structure of water I.[7] As a consequence, at this temperature the activation energy of "normal" electrical conduction for electrolytes such as KCl or NaCl goes through a maximum (see Figure 1) and then as the temperature is further lowered drops down rapidly to values of the same order as the energy required for H-bond rupture in liquid water.[7-9] The relatively open structure of water I evidently facilitates hole formation.

Frank and Wen[10] more recently have proposed a water model which consists of "fluctuating clusters" of more or less rarified ice-like structures immersed in "free" water, and Némethy and Scheraga,[11] have made estimates of the temperature dependence of the size and concentration of these clusters. On the basis of this model, the appearance of a maximum in the density of water can be explained with greater simplicity, without resort to two structural forms, in terms of the dissolution of the relatively rarified clusters superimposed upon normal thermal expansion.

For the sake of convenience, however, we will continue to speak of the water I and water II regions.

Rather surprisingly, there is a paucity of precision

(1) S. Glasstone, K. J. Laidler, and H. Eyring, "The Theory of Rate Processes," McGraw-Hill Book Co., Inc., New York, N. Y., 1941, Chapters IX, X.

(2) R. A. Horne, B. R. Myers, and G. R. Frysinger, *J. Chem. Phys.*, **39**, 2666 (1963).

(3) B. E. Conway, *Can. J. Chem.*, **37**, 613 (1959); *Z. Naturforsch.*, **14**, 841 (1959).

(4) J. D. Bernal and R. H. Fowler, *J. Chem. Phys.*, **1**, 515 (1933).

(5) B. E. Conway, J. O'M. Bockris, and H. Linton, *ibid.*, **24**, 834 (1956); M. Eigen and L. DeMaeyer, *Z. Elektrochem.*, **60**, 1037 (1956); *Proc. Roy. Soc.* (London), **A247**, 505 (1958).

(6) R. A. Horne, "Theory of Electrical Conductance in Acidic, Aqueous Solutions," Arthur D. Little, Inc., Technical Report No. 1, Office of Naval Research, Contract No. Nonr-4424(00), May 15, 1964; *J. Electrochem. Soc.*, in press.

(7) J. D. Bernal and R. H. Fowler, *J. Chem. Phys.*, **1**, 515 (1933).

(8) R. A. Horne and R. A. Courant, *J. Phys. Chem.*, **68**, 1258 (1964).

(9) R. A. Horne and R. A. Courant, *J. Geophys. Res.*, **69**, 1152 (1964).

(10) H. S. Frank and W. Y. Wen, *Discussions Faraday Soc.*, **24**, 133 (1957).

(11) G. Némethy and H. A. Scheraga, *J. Chem. Phys.*, **36**, 3382 (1962).

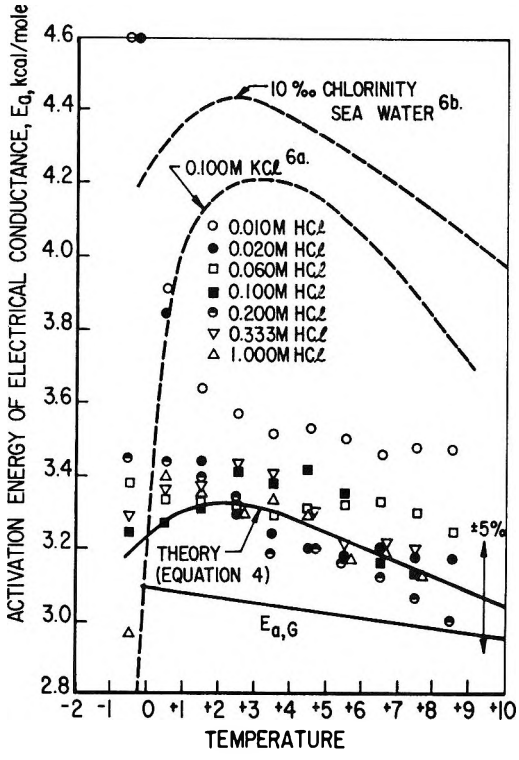

Figure 1. Temperature dependence of the activation energy of protonic electrical conductance in the water I region.

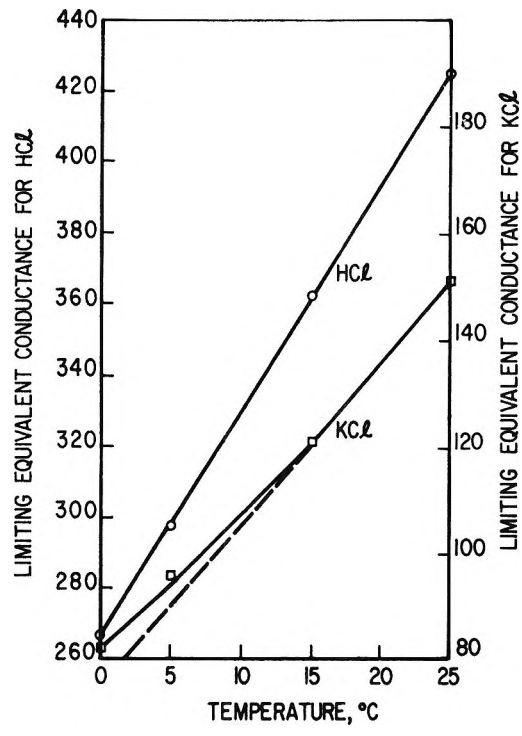

Figure 2. Comparison of temperature dependence of the limiting equivalent conductances of aqueous KCl and HCl solutions.

conductivity measurements on aqueous solutions in the region 0 to +10°, yet even examination of existing data shows differences between KCl and HCl solutions. Figure 2, based on data cited by Robinson and Stokes,[12] shows a very significant dissimilarity in the temperature dependence of the limiting equivalent conductances of HCl and KCl solutions. The curve for the former appears to be linear whereas that of the latter deviates from linearity. A more recent study of 0.100 *M* KCl solutions in the water I region[8] revealed somewhat less of a deviation from linearity than suggested by Figure 2. Inasmuch as the activation energy of conductance depends on the slope of the conductance *vs.* temperature plot, Figure 1 suggests that the activation energy of conduction of protonic solutions, unlike "normal" salt solutions, does not exhibit a pronounced maximum near the temperature of maximum density. The foregoing considerations prompted us to examine the activation energy of protonic conduction in the water I region.

Experimental

The precision conductivity bridge and the thermostatic bath have been described earlier.[8,13] A capillary-type conductivity cell with electrodes constructed of snarls of platinized platinum wire was used. The cell was calibrated at 5° on the basis of the data of Owen and Sweeton[14] for HCl and its constant was 65.80 cm.$^{-1}$. This cell differed from the high pressure capillary cells used earlier[13] inasmuch as the capillary was horizontal rather than vertical and the arms of the cell were more widely spaced. The thermocouple probe, encased in a glass capillary, was placed into the conductivity cell. The aqueous HCl solutions were prepared and standardized by the usual methods. The maximum deviation in the conductance measurements is 0.05%.

Results

The temperature dependence of the specific conductance of aqueous HCl solutions of various concentrations in the range −2 to +10° is shown in Table I. Calculations showed that, over this temperature range, the change in density with temperature has a negligible effect on the conductance (less than 0.01%). Activation energies of electrical conductance, E_a, were calculated at 1° intervals from values read from plots of the

(12) R. A. Robinson and R. H. Stokes, "Electrolyte Solutions," 2nd Ed., Butterworths Scientific Publications, London, 1959, p. 465.

(13) R. A. Horne and G. R. Frysinger, *J. Geophys. Res.*, 68, 1967 (1963).

(14) B. B. Owen and F. H. Sweeton, *J. Am. Chem. Soc.*, 63, 2811 (1941).

Table I: Specific Conductances of Aqueous HCl Solutions

0.010 *M*		0.020 *M*		0.060 *M*		0.100 *M*		0.200 *M*		0.333 *M*		1.000 *M*	
Temp., °C.	Sp. cond., ohm^{-1} cm.$^{-1}$	Temp., °C.	Sp. cond., ohm^{-1} cm.$^{-1}$	Temp., °C.	Sp. cond., ohm^{-1} cm.$^{-1}$	Temp., °C.	Sp. cond., ohm^{-1} cm.$^{-1}$	Temp., °C.	Sp. cond., ohm^{-1} cm.$^{-1}$	Temp., °C.	Sp. cond., ohm^{-1} cm.$^{-1}$	Temp., °C.	Sp. cond., ohm^{-1} cm.$^{-1}$
−0.725	0.002417	−1.130	0.004798	−1.310	0.01442	−1.315	0.02387	−0.623	0.04762	−1.330	0.07574	−0.860	0.2059
+0.920	0.002537	−1.115	0.004803	−0.590	0.01466	−0.720	0.02413	−0.550	0.04768	−1.310	0.07629	−0.860	0.2073
+1.385	0.002567	−0.340	0.004917	−0.417	0.01471	−0.710	0.02414	−0.510	0.04776	−1.280	0.07608	−0.592	0.2081
+1.535	0.002571	−0.310	0.004933	+0.165	0.01487	−0.710	0.02414	+0.396	0.04767	−1.180	0.07645	−0.190	0.2099
+1.725	0.002580	+0.475	0.005046	+0.700	0.01506	+0.110	0.02459	+1.079	0.04943	−0.440	0.07774	−0.140	0.2101
+3.415	0.002688	+0.530	0.005051	+0.925	0.01514	+0.120	0.02461	+1.539	0.05002	−0.240	0.07810	+0.858	0.2147
+3.670	0.002712	+1.295	0.005140	+0.945	0.01520	+0.645	0.02490	+3.470	0.05229	−0.240	0.07813	+0.916	0.2155
+3.855	0.002713	+1.355	0.005147	+1.215	0.01525	+0.650	0.02492	+4.424	0.05319	+0.235	0.07862	+1.125	0.2169
+4.060	0.002726	+1.410	0.005157	+1.295	0.01526	+0.650	0.02493	+4.478	0.05325	+0.253	0.07858	+2.048	0.2203
+5.045	0.002800	+2.130	0.005242	+1.305	0.01528	+1.335	0.02526	+5.090	0.05399	+0.380	0.07926	+2.590	0.2238
+5.555	0.002826	+2.895	0.005314	+1.305	0.01530	+1.460	0.02534	+5.140	0.05396	+0.463	0.07934	+2.770	0.2248
+5.655	0.002834	+2.895	0.005322	+1.510	0.01536	+1.505	0.02537	+5.938	0.05484	+0.655	0.07977	+3.030	0.2256
+6.790	0.002905	+3.595	0.005406	+1.910	0.01555	+2.355	0.02589	+5.938	0.05479	+0.863	0.07968	+3.880	0.2290
+6.970	0.002922	+3.595	0.005411	+3.325	0.01601	+2.450	0.02590	+6.518	0.05553	+1.300	0.08086	+4.650	0.2332
+7.845	0.002981	+3.610	0.005410	+3.890	0.01620	+3.055	0.02624	+6.590	0.05538	+1.842	0.08155	+5.412	0.2376
+8.080	0.002996	+4.345	0.005492	+4.550	0.01642	+3.105	0.02627	+7.590	0.05688	+2.570	0.08313	+6.220	0.2404
+8.205	0.002988	+4.400	0.005504	+5.560	0.01679	+4.395	0.02704	+7.680	0.05688	+3.130	0.08387	+6.845	0.2433
+9.775	0.003108	+4.450	0.005504	+5.870	0.01692	+4.395	0.02708	+7.710	0.05673	+3.130	0.08401	+6.845	0.2435
+9.820	0.003111	+5.930	0.005678	+5.870	0.01692	+5.050	0.02749	+7.750	0.05679	+3.340	0.08432	+6.968	0.2459
+10.600	0.003146	+5.980	0.005681	+5.960	0.01694	+5.805	0.02791			+3.350	0.08422	+7.167	0.2458
+10.670	0.003171	+7.045	0.00580	+8.330	0.01782	+5.820	0.02794	+8.940	0.05827	+3.780	0.08547	+7.350	0.2472
		+7.055	0.005802	+10.675	0.01863	+5.850	0.02796			+4.070	0.08565	+7.543	0.2489
		+8.040	0.005923	+10.775	0.01867	+6.690	0.02840	+8.985	0.05819	+4.675	0.08674	+7.543	0.2490
		+8.055	0.005920			+7.885	0.02909	+9.050	0.05823	+6.040	0.08989	+8.000	0.2495
		+8.080	0.005930			+7.900	0.02910	+9.080	0.05818	+6.190	0.08959	+9.170	0.2561
		+9.125	0.006063			+7.930	0.02915			+6.195	0.08995	+9.250	0.2565
		+9.150	0.006058			+8.565	0.02948			+7.218	0.09164	+9.680	0.2576
										+8.130	0.09327	+9.680	0.2579
										+8.130	0.09365	+10.040	0.2602

data contained in Table I using the integrated form of the Arrhenius equation

$$E_a = (\log K_2 - \log K_1)4.576T_2T_1/\Delta T \qquad (1)$$

where the K's the specific conductances. The values of E_a thus obtained are shown in Table II and in Figure 1. The present values of E_a between 8 and 9° are slightly higher than literature values (see Table III) between 5 and 15° as they should be. The present experimental error in E_a is estimated to be about 5% and is indicated on Figure 1. Again, as in the case of earlier work,[14] this error is large enough to prevent cogent conclusions from being drawn concerning the concentration dependence of E_a. Nevertheless, despite the spread in the values of E_a several significant qualitative generalizations can be drawn from Figure 1. The temperature dependence of E_a of protonic conduction in the region near the temperature of maximum density is clearly different from that for "normal" conduction, in particular, the pronounced maximum found in the case of salts is not observed; E_a of conductance for dilute HCl

Table II: Activation Energies of Electrical Conductivity of Aqueous HCl Solutions

	HCl concn., *M*						
	0.010	0.020	0.060	0.100	0.200	0.333	1.000
Temp., °C.	Activation energy, E_a, kcal./mole						
−0.5	4.60	4.68	3.38	3.24	3.45	3.29	2.97
+0.5	3.91	3.84	3.34	3.27	3.44	3.36	3.40
+1.5	3.64	3.44	3.33	3.31	3.39	3.37	3.35
+2.5	3.57	3.29	3.31	3.41	3.34	3.43	3.29
+3.5	3.52	3.24	3.29	3.38	3.19	3.40	3.33
+4.5	3.53	3.20	3.31	3.42	3.20	3.30	3.29
+5.5	3.50	3.18	3.32	3.35	3.17	3.21	3.17
+6.5	3.46	3.20	3.33	3.16	3.12	3.21	3.20
+7.5	3.48	3.18	3.30	3.13	3.06	3.19	3.13
+8.5	3.47	3.18	3.25	...	3.00	...	...

Table III: Activation Energies of Conduction (in kcal. mole^{-1}) of Aqueous HCl Solutions (Calculated from Data of Owen and Sweeton[14])

	Concn., *m*				
Temp., °C.	0.001	0.010	0.100	1.000	Av.
5–15	3.14	3.10	3.00	2.98	3.05 ± 0.06
15–25	2.76	2.78	2.79	2.77	2.76 ± 0.01
25–35	2.46	2.43	2.43	2.43	2.44 ± 0.01
35–45	2.32	2.29	2.29	2.20	2.27 ± 0.04
45–55	2.14	2.08	1.96	2.02	2.05 ± 0.06
55–65	2.06	1.97	1.90	1.91	1.96 ± 0.05

solutions continues to increase as temperature decreases; and E_a for rather more concentrated solutions exhibits a slight maximum near the temperature of maximum density. Figure 3 is a pictorial summary of what we feel to be the trends evidenced by the data of Owen and Sweeton[14] and Figure 1, yet badly obscured by the scatter in the values.

Discussion

Before examining the present experimental results, it is worthwhile to consider activation energies of conductance calculated on the basis of the earlier published work of Owen and Sweeton[14] and other investigators. Table III shows that the average E_a decreases with increasing temperature by roughly 0.023 kcal. mole^{-1} deg.$^{-1}$ over the range 10 to 50°. The rate of decrease decreases somewhat with increasing temperature. There also appears to be a tendency for E_a at a given temperature to decrease with increasing electrolyte concentration although Table III exhibits exceptions to this rule, and this observation probably does not lie outside the realm of experimental error. Some further E_a values, calculated in the neighborhood of 10°, are shown in Table IV. Notice that E_a for HNO_3 is very close to that for HCl of the same concentration, but

Table IV: Activation Energies of Acidic Conduction

Soln.	Temp., °C.	E_a, kcal./mole	Ref.
Inf. dil. HCl	10	3.12	*a*
0.001 *M* HCl	10	3.14	*b*
0.010 *M* HCl	10	3.10	*b*
0.010 *M* HCl	10	3.20	*c*
0.100 *M* HCl	10	3.00	*b*
0.100 *M* HCl	10	3.15	*c*
0.100 *M* HCl	10	2.97	*d*
1.00 *M* HCl	10	2.98	*b*
0.10 *M* HNO_3	10	3.08	*c*
0.002 *M* $HClO_4$	30	2.48	*e*

[a] Calculated from data in ref. 8. [b] Calculated from data in ref. 14. [c] Calculated from data in 'The International Critical Tables." [d] See ref. 2. [e] Calculated from data of N. Goldenberg and E. S. Amis, *Z. physik. Chem.* (Frankfurt), **30**, 65 (1961).

that E_a for 0.002 *M* $HClO_4$ is significantly less than for 0.001 or 0.010 *M* HCl. We have no explanation for this behavior. The decrease in E_a with increasing temperature in the water II region has been attributed to thermal destruction of the water structure,[1] but this hypothesis should not be applicable to the abnormal component of protonic conduction for that process is largely confined to the "free" or unstructured water between the clusters. Rotation within a water structure appears to be very difficult.[15] That the structure of the clusters is that of ice I remains to be established although such would seem reasonable. Recent n.m.r. studies of single crystals of D_2O ice revealed only small amplitude vibrations of D and *no* hindered rotation or D transfer.[16] Again these findings are difficult to reconcile with certain theories of protonic conduction in ice. We are inclined to the view that the abnormal mechanism is largely confined to the monomeric water, a view based on the correlation between acidic conductivity and monomer concentration,[6] the fact that the rate-determining step involves the rotation of a water molecule (and monomers are easiest to rotate), and the infrequency of small polymers in the "free" water.[11] Present fashion is to represent the proton as $H_9O_4^+$, but we doubt that this species plays an important role in the abnormal mechanism. Robinson and Stokes[17] conclude ". . . the only entity undergoing dipole orientation in water is the simple H_2O molecule." Haggis, Hasted, and Buchanan[18] claim that only 0- and 1-bonded water is free to rotate without bond rupture. At higher fre-

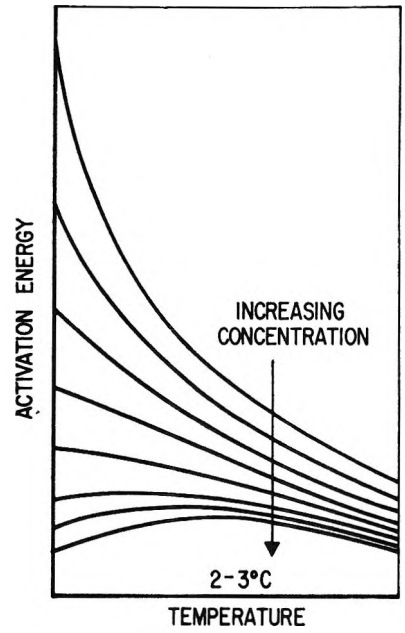

Figure 3. Schematic representation of the effects of concentration and temperature on activation energies of protonic conduction.

(15) F. Heinmets and R. Blum, *Trans. Faraday Soc.*, **59**, 1141 (1963), report an activation energy for proton transfer in pure ice of 24.2 kcal.

(16) P. Waldstein, S. W. Rabideau; and J. A. Jackson, *J. Chem. Phys.*, **41**, 3407 (1964).

(17) Reference 12, pp. 11, 12.

(18) G. H. Haggis, J. B. Hasted, and T. J. Buchanan, *J. Chem. Phys.*, **20**, 1452 (1952).

quencies, however, higher forms might rotate, and their inclusion improves the linearity of Arrhenius plots of dielectric relaxation time and tends to lower the activation energy.[19] Thus, the possibility remains that such higher forms might be responsible similarly for the lowering of E_a of electrical conduction with increasing temperature. In this connection it is worthwhile to notice that, although the concentration of the larger small clusters decreases with increasing temperature, the concentration of 1- and 2-bonded waters increases,[11,18] but most of these waters, it must be remembered, are on cluster surfaces and not in small clusters. Another possible explanation is that even the "free" waters, although not married to their neighbors, are nevertheless aware of their presence and that these forces, which would tend to restrain rotation, become attenuated with increasing temperature, thereby facilitating water rotation and lowering E_a of protonic conduction.

Thermal destruction of this secondary structuring of the "free" water could also facilitate "hole" formation and thus account for the similarity of the temperature dependencies of $E_{a,HCl}$ and $E_{a,KCl}$ in the water II region. The "secondary structuring" may be attributed to electrostatic interaction among the water molecules whereas the primary structuring in the clusters involves stronger interactions with a great deal of covalent character.[20]

The most important difference between protonic and "normal" conductance illustrated by Figure 1 is the absence in the former case (for HCl) of the pronounced maxima observed in the latter (dashed curves for sea water and KCl).[8,9] "Normal" conduction takes advantage of the relatively open ice-like structure of the clusters and occurs in both the clusters and the "free" water, but protonic conduction does not. E_a for abnormal conductance, unlike $E_{a,KCl}$, continues to increase as the temperature is decreased in the water I region, and the slight observed decrease in $E_{a,HCl}$ in the case of more concentrated solutions can be attributed to the increasingly important contribution from the "normal" component of protonic conduction.

Application of the theory of protonic conduction in aqueous solutions recently proposed by Horne[6] is of interest in connection with the results presented by Figure 1. This theory gives the conductance, Λ, by

$$\Lambda = \Lambda^* - \{(1.32 \times 10^3)^2/(1.32 \times 10^3 + 2.39 \times 10^4\sqrt[3]{C}) + 2.39 \times 10^4\sqrt[3]{C}\}e^{-E_{a,h}/RT} \quad (2)$$

where

$$\Lambda^* = \lim_{C \to 0} \Lambda \text{ vs. } \sqrt[3]{C} \quad (3)$$

and $E_{a,h}$ is the activation energy of "hole" formation as given by E_a for "normal" conductance. Values of the activation energies of electrical conduction of aqueous HCl solutions, based on Λ-values from eq. 2 are given in Table V. The theory predicts qualitatively the increase in E_a with decreasing temperature in dilute solutions and the decrease in E_a with increasing concentration. The theory fails in the region in which it is not expected to be applicable, namely, in relatively concentrated solutions below +3° where "normal" conduction is making a significant contribution.

Table V: Protonic Conduction Activation Energies Calculated from Theory

Temp., °C.	Λ^*[a]	$E_{a,h}$,[b] kcal./mole	$E_{a,0.001\ M\ HCl}$, kcal./mole	$E_{a,1.00\ M\ HCl}$, kcal./mole
−1	259	1.40	...	...
+0	265	3.32	16.8	...
+1	271	4.00	5.3	17.4
+2	279	4.21	4.3	8.3
+3	286	4.25	3.7	5.7
+4	293	4.20	3.4	2.7
+5	300	4.13	3.3	2.4
+6	307	4.02	3.1	1.5
+7	313	3.90	3.0	1.2

[a] Interpolated (between +5 and +15°) and extrapolated (from +5 to −1°) from ref. 6. [b] From R. A. Horne and R. A. Courant, *J. Phys. Chem.*, **68**, 1258 (1964).

Often, one of the steps of a multistep process has a much higher activation energy than the others. This step will be rate determining, and the Arrhenius activation energy obtained from the experiment will be that of this step. However, if two or more of the steps have similar activation energies, a mixed activation energy, analogous to a mixed potential, may be obtained. If the fraction of the total protonic conduction by the rotational mechanism, X_G, is taken to be inversely proportional to the activation energy of the process, $E_{a,G}$, then the value of the mixed activation energy, $E_{a,G+N}$, can be estimated.

$$E_{a,HCl} = X_G E_{a,G} + (1 - X_G)E_{a,N} \quad (4)$$

$$X_G = C_G = C_G/E_{a,G} \quad (5)$$

The subscripts G and N indicate the abnormal (water rotation) and "normal" (hole formation) conductive mechanisms, respectively. At 5° the limiting conductance of H^+ is 250 while that of K^+ is 47.[12] This may be interpreted to mean that at this temperature roughly 80% of the protonic conduction is *via* the abnormal mechanism and the other 20% by the "normal" con-

(19) C. H. Collie, J. B. Hasted, and D. M. Ritson, *Proc. Phys. Soc.*, (London), **60**, 145 (1948).

(20) J. Clifford and B. A. Pethica, *Trans. Faraday Soc.*, **60**, 1483 (1964).

ductive mechanism. The composite E_a at 5° is given as 3.20 kcal./mole by Figure 1. The "normal" contribution (the curve for KCl in Figure 1) is 4.20 kcal./mole, thus giving an $E_{a,G}$ of 3.00 kcal./mole. Over the range 20 to 80° $E_{a,HCl}$ varies linearly with temperature with a coefficient of −0.022 kcal./mole deg.[21] $E_{a,G}$ is next calculated on the basis of its value at 5° and the assumption that it has the same temperature coefficient in the 0 to 20° range. $E_{a,N}$ is taken to be equal to $E_{a,KCl}$ and is read from Figure 1. The value of the constant C_G is 2.4 kcal./mole. Calculated values of $E_{a,G+N}$ are shown in Figure 1. The agreement with experiment is satisfactory for so crude an approximation.

As the concentration of protons increases, relative to the water concentration, the "normal" mode of conduction becomes increasingly important below 4°, and the observed E_a is thereby lowered.

Of special importance is the observation that the proton conductivity, despite the allegedly great mobility of protons in an ice lattice,[5] apparently does not utilize the ice-like water I as a conductive path. This behavior is in contrast to that of the "normal" conductive process which appears to be able to take advantage of conductive paths in either the structured clusters of the free water.[22]

The present experimental results cast further doubt on the opinion that protons have very great mobilities in ice.[5] The lattice in that medium, so the argument runs, nicely aligns the water molecules enabling the fast proton flip to occur without the preliminary of a relatively slow and energetic rotation of water molecules along a chain. Conductivity,[23] proton-mobility,[24] and electron-exchange experiments[25] in ice all have failed to substantiate this view. Not only are the activation energies of proton-transport processes much greater in ice than in liquid water,[15,23,26] but also the destruction of order in liquid water by temperature or pressure[2] facilitates rather than hinders proton transfer. In fact, far from providing an easy conductive path, structure in the water is avoided by the protons participating in conductive processes. This is especially striking in the low temperature region below 4° where ice-like forms are present. If the ice structure were conducive to the Grotthuss mechanism, one would expect the protons to avail themselves of this path of least resistance, but the present results give no intimation that they are in the least so inclined. On the contrary, they continue to detour around the growing regions of iciness. As Conway[27] has shown, the mechanism of the rotation of water molecules in ice is different from the liquid and requires more energy.

Unfortunately, the experimental deviation in the present results, as in the case of the earlier work of Owen and Sweeton,[14] obscures the concentration dependence of $E_{a,HCl}$ in the low temperature region, but, again, there seems to be a tendency for $E_{a,HCl}$ to decrease with increasing HCl concentration. In the case of sea water, however, E_a definitely does decrease with increasing chlorinity.[9] This decrease is something of a puzzle for both NaCl and HCl tend to increase the structure of the adjacent water[28] and might, therefore, be expected to increase E_a. A possible explanation might be that, although they increase the water order in their immediate neighborhood, they tend to disorder the more remote water.

We would like to make two further observations concerning the rotational rate-determining step of protonic conduction. The presence of fluoride ion markedly hinders the rotation of water molecules[29]; therefore, the activation energy of acidic conduction should be increased in the presence of F^-. Unfortunately, estimation of this parameter is greatly complicated by the strong association of H^+ and F^- ions. However, $E_{a,HF}$, calculated from limiting conductances at 0 and 25°[30] is 3.08 kcal./mole, whereas $E_{a,HCl}$ similarly estimated is 3.03 kcal./mole. Again E_a values calculated from limiting conductances at 18 and 25°[31] for HF and HCl are 2.77 and 2.75 kcal./mole, respectively. Thus, the ability of the fluoride ion to hinder water rotation is reflected in the activation energies of protonic conduction although the differences are so small that a great deal of significance cannot be attached to them.

Orientation of water molecules in an electric field also entails the rotation of water molecules and should, therefore, require the same energy as the rate-determining step in protonic conduction by the abnormal mechanism. The logarithm of the dielectric relaxation time *vs.* the reciprocal of the absolute temperature departs somewhat from linearity and has a slope corresponding to an E_a of roughly 5 kcal./mole.[19] This

(21) R. A. Horne and E. H. Axelrod, *J. Chem. Phys.*, **40**, 1518 (1964), Figure 1.

(22) "Normal" conduction *via* the structured clusters is responsible for the decrease of $E_{a,KCl}$ with decreasing temperature in the water I region, but the similarity to $E_{a,HCl}$ in the water II region suggests that in that temperature region a large part of the "normal" conduction is *via* the "free" water.

(23) R. S. Bradley, *Trans. Faraday Soc.*, **53**, 687 (1957).

(24) F. Heinmets, *Nature*, **188**, 925 (1960).

(25) R. A. Horne, *J. Inorg. Nucl. Chem.*, **25**, 1139 (1963).

(26) See Table III in ref. 16.

(27) B. E. Conway, *Can. J. Chem.*, **37**, 613 (1959).

(28) R. W. Gurney, "Ionic Processes in Solution," McGraw-Hill Book Co., Inc., New York, N. Y., 1953, Chapter 9.

(29) H. R. Pruppacher, *J. Chem. Phys.*, **39**, 1586 (1963), and the references cited therein.

(30) From International Critical Tables, data.

(31) From data of Robinson and Stokes (ref. 12).

value appears high; only 4.5 kcal./mole are required for the complete separation of two water molecules. In a subsequent paper, Hasted and co-workers[18] corrected the dielectric relaxation time data for triply bound waters and by so doing obtained a linear log ($\eta_3\tau$) *vs.* $1/T$ plot with a slope corresponding to 3 kcal./mole. This value is now in good agreement with that for protonic conduction.

Acknowledgment. This work was supported in part by the Office of Naval Research. The authors are indebted to Mr. D. S. Johnson for assistance with some of the experiments.

The Exclusion of Ions from Charged Microporous Solids[1]

by Lawrence Dresner

Oak Ridge National Laboratory, Oak Ridge, Tennessee *(Received December 12, 1964)*

The exclusion of ions from charged microporous solids has been studied. The microporous solids have been represented either by cylindrical microcapillaries on whose inner surface a fixed, homogeneous electric charge resides or by the space between two charged plates. A rapid graphical procedure is described with which the distribution coefficients describing the partition of the electrolyte between the pore liquid and the external solution may be calculated. The procedure is applicable to salts with a variety of stoichiometric coefficients.

Introduction

If a charged microporous body comes to equilibrium with an external electrolyte solution, the ionic concentrations in the pore liquid differ from the ionic concentrations in the external solution. The cause of these differences is the electric double layer that forms at the pore walls. Owing to the repulsion of coions (ions of the same sign of charge as the fixed charge) from the double layer, the average coion concentration in the microporous solid is less than that of the feed solution; *i.e.*, coions are to some extent excluded from the microporous solid. It is the purpose of this paper to suggest two simple approximate methods for calculating the extent of coion exclusion from charged microporous solids and to compare them with each other and with some exact results.

Interest in coion exclusion first arose in connection with studies of clays and soils. Using the results of Quenouille's calculations of coion exclusion by planar double layers, Schofield[2] calculated the specific surface area of clay lamellae in dilute suspensions from measurements of the coion exclusion (called by him *negative adsorption*). Bolt and Warkentin[3] and later de Haan and Bolt[4] tried to find the positive adsorption of anions on the edges of clay lamellae by correcting the measured net adsorption using calculated values of the negative adsorption. Recently, Kraus and the author[5] looked into the possibility of using charged microporous materials as filters in the purification of salt water; here the coion exclusion largely determines the salt-rejecting capacity of the filter.

Quenouille and Bolt and his co-workers based their calculations on the theory of interacting planar double layers.[6] In their calculations, as in the calculations

(1) Research sponsored by the Office of Saline Water, U. S. Department of the Interior, under Union Carbide Corporation's contract with the U. S. Atomic Energy Commission.

(2) R. K. Schofield, *Nature*, **160**, 408 (1947).

(3) G. H. Bolt and B. P. Warkentin, *Kolloid-Z.*, **156**, 41 (1958).

(4) F. A. M. de Haan and G. H. Bolt, *Soil Sci. Soc. Am. Proc.*, **27**, 636 (1963).

(5) L. Dresner and K. A. Kraus, *J. Phys. Chem.*, **67**, 990 (1963).

presented in this paper, the only departures from ideality that are taken into account in the intermicellar phase are those due to long-range electrostatic effects, which are usually described by the Poisson–Boltzmann equation. In other words, in the actual evaluation of thermodynamic formulas, the activity coefficients that refer to the intermicellar phase are replaced by their respective electrostatic parts. It should be noted that the use of the Poisson–Boltzmann equation itself represents an approximation since the assumption that the average concentration of an ion is related to the average electrical potential through Boltzmann's law is not strictly correct.[7,8] Because elliptic functions appear in the theory of interacting planar double layers used by Quenouille and by Bolt and his coworkers, practical computations of coion exclusion with it are difficult. As previously mentioned, it is the purpose of this paper to suggest two simple approximate methods for calculating coion exclusion.

The first of the approximate methods of calculating coion exclusion from microporous solids is based on the results of two limiting cases. When the feed solution is very dilute, the double layer is very thick, and the region of strong coion exclusion extends completely across the pores. Since in this case coions are strongly excluded from the pores, the electric potential distribution in the pores may be calculated under the assumption that there are no coions whatever in the pores. The latter calculation is relatively simple to carry out. By assuming that the introduction of a small number of coions does not significantly perturb this potential, we may then calculate the distribution coefficient of the electrolyte between the liquid and the external solution. This limiting case will henceforth be referred to as the case of good exclusion.

As the feed solution becomes more concentrated, the double layer becomes thinner, and eventually double layers originating on opposite walls of a pore no longer interact significantly. If the curvature of the pore walls is neglected when this point is reached, coion exclusion may be calculated easily using the relatively simple theory of a *single* planar double layer. This limiting case will henceforth be referred to as the case of poor exclusion.

If the distribution coefficients obtained in these limiting cases are plotted against the concentration of the feed solution on log–log paper, the resulting arcs rather unambiguously define a smooth curve, which then represents a useful estimate of the distribution coefficient as a function of feed concentration for a given pore dimension and surface charge density. Given in the next section are some graphs and a nomogram which allow the procedure just described to be carried out with little effort for cylindrical and lamellar micro capillaries. These numerical data not only apply to symmetrical (or z–z) electrolytes but also to electrolytes of the $3z$–z, $3z$–$2z$, $2z$–z, z–$2z$, $2z$–$3z$, and z–$3z$ types.

The second approximate method of calculating coion exclusion from charged micropores is based on the variational method of solving the Poisson–Boltzmann equation suggested some time ago.[9] The variational method is based on the existence of a functional which is extremized (in the case at hand, minimized) by a solution of the differential equation being solved. What is done in practice is to choose an n-parameter family of trial functions and evaluate the functional in terms of these as yet undetermined parameters. The parameters are then chosen so that the value of the functional is an extremum. This specifies a *best* member of the n-parameter family. With this best trial function, approximate values of the various physical quantities of interest can be evaluated. In general, the better the best trial function is able to approximate the behavior of the true solution, the more accurate will be the approximate values of the various physical quantities.

One of the drawbacks of the variational method is that in the absence of an exact solution of the equation being studied there is no good way to gauge its accuracy except to recalculate the same problem with a sequence of steadily improving trial functions until the results converge. In ref. 9, the mean activity coefficient (but not the distribution coefficient) of a symmetrical salt in a charged cylindrical microcapillary was calculated using as the family of trial functions a family of expressions similar in form to the solution pertaining to the limiting case of very strong coion exclusion. With this family of trial functions, the variational calculations are fairly easy to carry out although the minimization mentioned above must be done numerically. However, there appear to be no other trial functions better than this family that do not render the calculations insuperably difficult. As a result, one has no clear idea about the accuracy of these calculations. In this paper, the variational calculations (with the trial functions of ref. 9) are tested in two ways, namely, by comparison with the results of the method of limiting cases and by comparison with some exact results ob-

(6) E. J. W. Verwey and J. Th. G. Overbeek, "Theory of the Stability of Lyophobic Colloids," Elsevier Publishing Co., Inc., New York, N. Y., 1948.

(7) L. Onsager, *Chem. Rev.*, **13**, 73 (1933).

(8) J. G. Kirkwood, *J. Chem. Phys.*, **2**, 767 (1934); J. G. Kirkwood and J. C. Poirier, *J. Phys. Chem.*, **58**, 591 (1954).

(9) L. Dresner, *ibid.*, **67**, 2333 (1963).

tained by numerical integration of the Poisson–Boltzmann equation.

In the next section, the method of limiting cases is discussed. To assist the reader, this section contains only results, the relevant derivations being found in a series of appendices to the main body of the paper. Since the variational method is described in detail in ref. 9, it will not be discussed further here. The following section of the paper is devoted to a comparison of the exact and the various approximate results. Following that, there are three appendices, one summarizing the thermodynamic relations used in this paper and two covering the limiting cases.

The Limiting Cases

Two kinds of pores are considered in this paper, cylindrical and lamellar; R represents either the radius of the cylindrical pore or the *total* thickness of the lamellar pore. The pore walls are charged, and the pores are imagined to be in equilibrium with a solution of an electrolyte that ionizes into two kinds of ions. The ions with the same sign of charge as the fixed charge are called coions; those with the opposite sign, counterions. If ze is the charge of the counterions expressed as a multiple of the proton charge e, then the charge of the coions expressed in the same way is taken to be $-\rho ze$, this relation defining the positive number ρ. The surface density of charge on the pore walls is written as $-\sigma ze$, again as a multiple of the proton charge. This relation defines the surface density parameter σ, which is also always positive.

When the micropores are in contact with a solution of pure water, the average counterion concentration in them, c_0, will just neutralize the fixed surface charge $-\sigma ze$. It follows from this requirement that

$$c_0 = 2\sigma/R \tag{1}$$

When the micropores are in contact with a solution of electrolyte, some of the electrolyte invades the pore. The distribution coefficient D of the salt is the ratio of its average concentration in the pore liquid to its concentration in the external solution. In this paper, the distribution coefficient of the salt will always equal the distribution coefficient of the coions. The purpose of this paper is to show how to express D in terms of the dimension R, the concentration c_0 (or the surface density parameter σ), and the concentration of the external electrolyte. For the sake of convenience, it is best to specify this latter concentration in terms of the concentration c of *counterions* in the external electrolyte.

These three physical variables may be combined into the following two dimensionless variables, in terms of which we may always express D

$$\xi_R = \left(\frac{z^2e^2c_0}{kT\epsilon}\right)^{1/2} R \tag{2a}$$

$$\Gamma = \frac{c}{c_0} \tag{2b}$$

Here k is Boltzmann's constant, T is the absolute temperature, and ϵ is the dielectric constant of the salt solution, which for practical cases we take to be a concentration-independent constant. To facilitate practical calculations, a nomogram of eq. 2a for the case $\epsilon = \epsilon_{water} = 7.08 \times 10^{-10}$ f.m. and $kT = 0.025$ e.v. ($T = 290°$K.) is given in Figure 1.

In evaluating the formulas of the limiting case of poor exclusion, it was convenient to introduce an additional dimensionless quantity, *viz.*

$$\Lambda = \frac{\xi_R}{4\sqrt{2\Gamma}} \tag{3}$$

The activity coefficient γ_+ of the coions and the activity coefficient γ_- of the counterions in the capillary are given by the formulas

$$\frac{1}{\gamma_-} = 1 + \frac{G(\Lambda)}{\Gamma} \tag{4a}$$

and

$$\frac{1}{\gamma_+} = 1 - \frac{F(\Lambda,\rho)}{2\Gamma\Lambda} \tag{4b}$$

A formula for the function $G(\Lambda)$ and formulas for the function $F(\Lambda,\rho)$ for $\rho = {}^1/_3, {}^1/_2, {}^2/_3, 1, {}^3/_2, 2$, and 3 are given in Appendix 2. They are somewhat complicated, and to aid in practical calculations they have been plotted in Figure 2. D is given in terms of the activity coefficients by the following formula (*cf.* Appendix 1)

$$D = \frac{1}{\gamma_+}\left(\frac{1/\gamma_-}{D + \frac{1}{\Gamma}}\right)^{\rho} (\gamma_\pm')^{\rho+1} \tag{5}$$

Here $\gamma_\pm'$ is the mean activity coefficient of the electrolyte in the external solution phase. Since this formula contains the unknown quantity D on both sides of the equation, D must be found by iteration. If $1/\gamma_+$ is taken as the initial guess for D, the iteration procedure converges rapidly.

The good exclusion theory, which is explained in detail in Appendix 3, applies to the limit in which $D << 1$. In this limit, eq. 5 becomes

$$D = \Gamma^{\rho}\frac{(\gamma_\pm')^{\rho+1}}{\gamma_+\gamma_-^{\rho}} \tag{6}$$

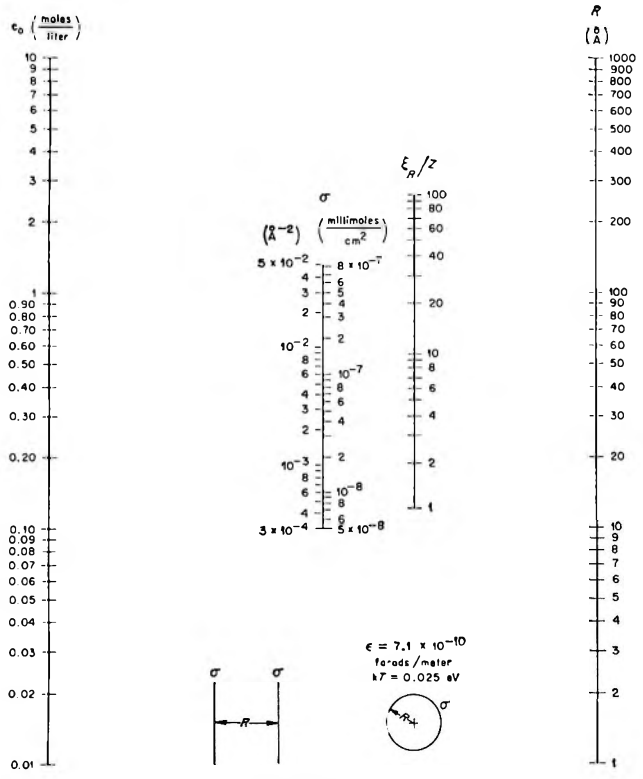

Figure 1. A nomogram relating the variables c_0, σ, ξ_R, and R. (*Cf.* eq. 1 and 2.)

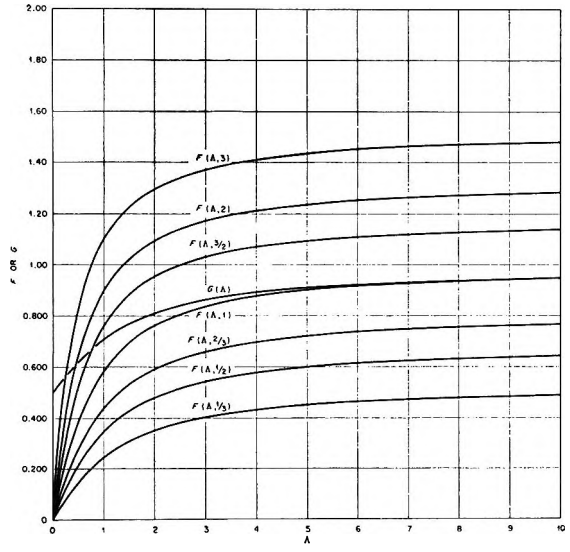

Figure 2. The functions $F(\Lambda,\rho)$ and $G(\Lambda)$. (*Cf.* eq. 4.)

In the good exclusion limit, the quantity $1/\gamma_+\gamma_-^{\rho}$ depends only on ξ_R; shown in Figures 3 and 4, respectively, are its values in cylindrical and lamellar microcapillaries. These values were calculated with the formulas derived in Appendix 3.

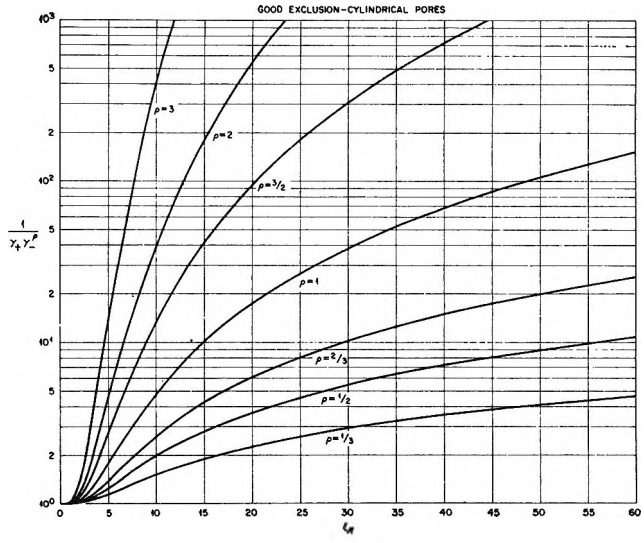

Figure 3. $1/\gamma_+\gamma_-$ as a function of ξ_R for cylindrical pores. (*Cf.* eq. 6.)

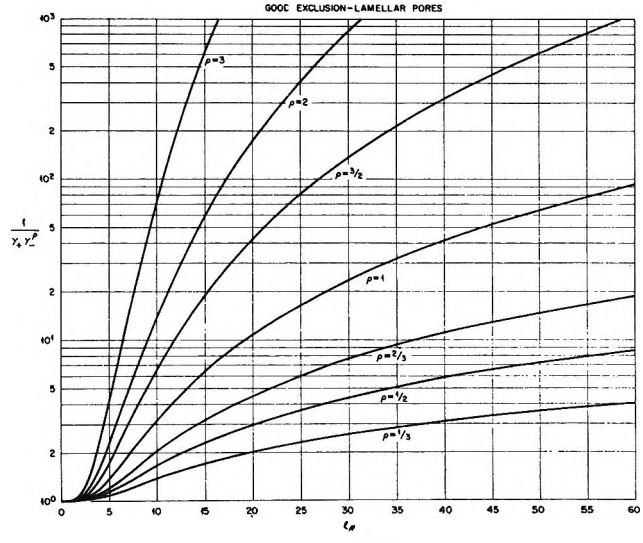

Figure 4. $1/\gamma_+\gamma_-^{\rho}$ as a function of ξ_R for lamellar pores. (*Cf.* eq. 6.)

Comparison of the Variational Method with the Method of Limiting Cases

Figures 5a, b, and c are comparisons of the variational method[9] of calculating D with the method of limiting cases. All three figures refer to a cylindrical microcapillary for which $\xi_R = 12$ but differ in that they refer, respectively, to 1–2, 1–1, and 2–1 electrolytes. $\gamma_\pm'$ has again been taken equal to unity for convenience. The variational results agree fairly well with the results of the limiting cases in both extremes and join them smoothly in a reasonable manner. For smaller ξ_R, the comparison is very similar. For larger

ξ_R, however, the variational results change in nature. The "knee" in the curves sharpens and also rises, ultimately developing into a maximum at which the distribution coefficient exceeds unity (for ξ_R around 20 or larger). Now it is impossible for electrostatic effects alone to make the distribution coefficient larger than unity; therefore, it is clear that the trial function used in the variational calculations is inadequate when ξ_R exceeds 12 by any substantial margin. Furthermore, we might expect from these considerations that the variational method with the trial function of ref. 9 will always overestimate the distribution coefficient. Never-

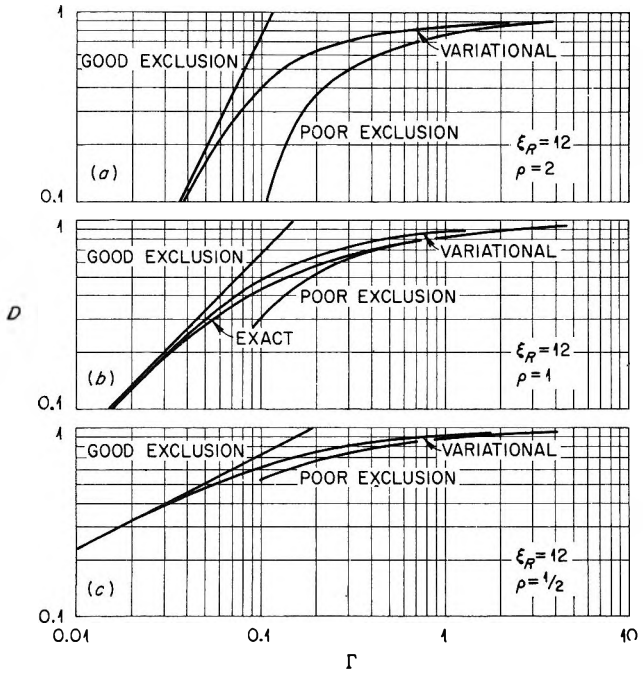

Figure 5. Comparison of the variational method of calculating D with the method of limiting cases and with an exact calculation.

theless, for values of $\xi_R \leq 12$ we might expect the overestimate to be a small one. To test this latter point, some exact values of the distribution coefficient D of a symmetrical electrolyte were calculated by numerical integration of the Poisson–Boltzmann equation for two cylindrical microcapillaries with ξ_R equal to 6 and 12, respectively. The results for $\xi_R = 12$ are shown in Figure 5b; the variational results are about 10% too high in the region of the "knee" and become more accurate in the two extreme regions. For $\xi_R = 6$, the variational and exact results never differ by more than about 2%. Thus, it seems clear that as long as $\xi_R \lesssim 12$ the variational method as described in ref. 9 should give good results.

Appendix 1. Thermodynamic Relationships

Let us consider an electrolyte that ionizes into two kinds of ions, counterions of charge ze and coions of charge z_+e. If c is the concentration of counterions in an ordinary aqueous phase, then the concentration of coions must be $-zc/z_+$ in order to maintain the over-all electroneutrality of the phase. Inside a charged microcapillary, the condition of over-all electroneutrality takes the form

$$zc_- + z_+c_+ - zc_0 = 0 \tag{1.1}$$

where c_+ and c_- are the concentrations of the co- and counterions, respectively. When two such phases are in contact, the condition of thermodynamic equilibrium requires that

$$\left(-\frac{z}{z_+}c\gamma_+'\right)^z(c\gamma_-')^{-z_+} = (c_+\gamma_+)^z(c_-\gamma_-)^{-z_+} \tag{1.2}$$

Here γ_+ and γ_- are the activity coefficients of the co- and counterions, respectively, in the pore liquid, and γ_+' and γ_-' are the respective total activity coefficients in the external phase. If we now set $z_+ = -\rho z$ and eliminate c_- from eq. 1.1 and 1.2, we obtain the equation

$$\frac{c^{1+\rho}}{\rho}\gamma_+'\gamma_-'^{\rho} = c_+(c_0 + \rho c_+)^{\rho}\gamma_+\gamma_-^{\rho} \tag{1.3}$$

The distribution coefficient is defined by the relation

$$D = \frac{\rho c_+}{c} \tag{1.4}$$

Substituting eq. 1.3 into eq. 1.4, we find that

$$D\left(\frac{1}{\Gamma} + D\right)^{\rho} = \frac{\gamma_+'\gamma_-'^{\rho}}{\gamma_+\gamma_-^{\rho}} \tag{1.5}$$

When $\rho = 1$ (symmetrical electrolyte), eq. 1.5 can easily be solved to give

$$D = \sqrt{\left(\frac{1}{2\Gamma}\right)^2 + \frac{\gamma_-'\gamma_+'}{\gamma_-\gamma_+}} - \frac{1}{2\Gamma} \tag{1.6}$$

Otherwise, it can be rearranged in the following form suitable for iterative solution

$$D = \frac{1}{\gamma_+}\left(\frac{1/\gamma_-}{\frac{1}{\Gamma} + D}\right)^{\rho}\gamma'_+\gamma_-'^{\rho} \tag{1.7}$$

Finally, it should be noted that $\gamma_+'\gamma_-'^{\rho}$ equals $(\gamma_\pm')^{\rho+1}$, where $\gamma_\pm'$ is the mean activity coefficient of the electrolyte in the external solution phase.

Appendix 2. The Case of Poor Exclusion

Let us begin by considering a single planar double layer; *i.e.*, let us consider the equilibrium of a solution of a single symmetrical (z–z) electrolyte of bulk concentration c with an infinite charged plane. The Poisson–Boltzmann equation for the electric potential ϕ is then

$$\nabla^2\phi = \frac{1}{\epsilon}(zece^{ze\phi/kT} - zece^{-ze\phi/kT}) \qquad (2.1)$$

Following the now classical theory of Verwey and Overbeek,[6] we introduce the variables

$$\psi = \frac{ze\phi}{kT} \qquad (2.2a)$$

$$\zeta = \left(\frac{2z^2e^2c}{kT\epsilon}\right)^{1/2} x \qquad (2.2b)$$

in terms of which the Poisson–Boltzmann equation becomes

$$\frac{d^2\psi}{d\zeta^2} = \sinh\psi \qquad (2.3)$$

For the purposes of this paper we shall only need to integrate this differential equation once, which we do by first multiplying both sides by $2d\psi/d\zeta$. This converts both sides into perfect differentials, which we can integrate immediately

$$\frac{d\psi}{d\zeta} = -2\sinh\left(\frac{\psi}{2}\right) \qquad (2.4)$$

Here we have used the boundary condition that the potential vanishes at infinity.

According to Marcus[10] (*cf.* also ref. 9), the electrostatic contribution to the activity coefficient γ_i of an ion of charge z_ie in a homogeneous phase occupying the volume V is given by

$$\frac{1}{\gamma_i} = \frac{1}{V}\int_V e^{-z_ie\phi/kT}d^3r \qquad (2.5)$$

Now in a large volume surrounded by a charged surface S, the only place where the potential will differ significantly from zero is close to S. The single double-layer approximation consists of using eq. 2.4 to describe the variation of the potential near the surface S of V. In other words, we take

$$\frac{1}{\gamma_i} = \frac{1}{V}\int_V e^{-z_i\psi/z}dV = 1 - \frac{1}{V}\int_V (1 - e^{-z_i\psi/z})dV = 1 - \frac{S}{V}\int_0^\infty (1 - e^{-z_i\psi/z})dx \qquad (2.6)$$

For the two kinds of capillaries that we shall be considering in this paper, namely, cylindrical and lamellar capillaries, the surface-to-volume ratio S/V is given by $2/R$. If we denote by ζ_R the value of ζ when $x = R$, then we can rewrite eq. 2.6 as

$$\frac{1}{\gamma_i} = 1 - \frac{2}{\zeta_R}\int_{\psi_0}^0 (1 - e^{-z_i\psi/z})\frac{d\psi}{d\psi/d\zeta} = 1 - \frac{1}{\zeta_R}\int_0^{\psi_0}\frac{1 - e^{-z_i\psi/z}}{\sinh(\psi/2)}d\psi \qquad (2.7)$$

where ψ_0 is the value of ψ at the charged plane ($\zeta = 0$). ψ_0 may be found from the boundary condition that applies at $\zeta = 0$. Because there must be over-all charge neutrality in V, the electric field will vanish outside both cylindrical and lamellar capillaries, as we can see by a simple symmetry argument and an application of Gauss' law. Since the surface S bears an electric charge $-z\sigma e$, the component of the electric vector along the outward normal to S just inside the surface S is equal to $\sigma ze/\epsilon$. Written in terms of ψ and ζ this boundary condition becomes

$$\sinh\left(\frac{\psi_0}{2}\right) = -\frac{1}{2}\left(\frac{d\psi}{d\zeta}\right)_{\zeta=0} = -\frac{\zeta_R}{8\Gamma} = -\frac{\xi_R}{4\sqrt{2\Gamma}} = -\Lambda \qquad (2.8)$$

Making the change of variables $\psi = -2y$, we finally find that

$$\frac{1}{\gamma_i} = 1 + \frac{1}{2\Gamma\Lambda}\int_0^{\text{arc sinh }\Lambda} e^{(z_i/z)y}\frac{\sinh\left(\frac{z_i}{z}y\right)}{\sinh y}dy \qquad (2.9)$$

$z_i = z$ for counterions; thus

$$\frac{1}{\gamma_-} = 1 + \frac{1}{2\Gamma\Lambda}\int_0^{\text{arc sinh }\Lambda} e^y dy = 1 + \frac{1}{\Gamma}\frac{\Lambda - 1 + \sqrt{\Lambda^2 + 1}}{2\Lambda} \qquad (2.10)$$

where γ_- is the counterion activity coefficient. For coions z_i has the opposite sign; *i.e.*, $z_i = -z$; thus, the coion activity coefficient γ_+ is given by

$$\frac{1}{\gamma_+} = 1 - \frac{1}{2\Gamma\Lambda}\int_0^{\text{arc sinh }\Lambda} e^{-y}dy = 1 - \frac{1}{\Gamma}\frac{\Lambda - 1 + \sqrt{\Lambda^2 + 1}}{2\Lambda(\Lambda + \sqrt{\Lambda^2 + 1})} \qquad (2.11)$$

If we now substitute the activity coefficients given in the last two equations into eq. 1.6 of Appendix 1 and

(10) R. A. Marcus, *J. Chem. Phys.*, **23**, 1057 (1955).

for convenience set $\gamma_{\pm}' = 1$, we find after some rearrangement that

$$D = 1 - \frac{1}{\Gamma}\frac{\Lambda + 1 - \sqrt{\Lambda^2 + 1}}{2\Lambda} \qquad (2.12)$$

Verwey and Overbeek have pointed out that the coions do not contribute very much to the structure of the double layer since they are excluded from it. Therefore, when the electrolyte is not symmetrical, we calculate the activity coefficients of the ions using in eq. 2.5 the potential ϕ appropriate to a symmetrical electrolyte the charge of whose ions is numerically equal to the charge of the actual counterions. The activity coefficients are therefore given by eq. 2.9. Remembering that for coions $z_i = -\rho z$, we see that if we write the coion activity coefficients in the form of eq. 4 the functions $F(\Lambda,\rho)$ are given by the integrals

$$F(\Lambda,\rho) = \int_0^{\text{arc sinh }\Lambda} e^{-\rho y}\frac{\sinh \rho y}{\sinh y}dy \qquad (2.13)$$

These integrals may be evaluated by making the substitution $v = e^{-y}$. Then

$$F(\Lambda,\rho) = \int_N^1 \frac{v^{2\rho} - 1}{v^2 - 1}dv$$

$$N = e^{-\text{arc sinh }\Lambda} = (\Lambda + \sqrt{\Lambda^2 + 1})^{-1} \qquad (2.14)$$

We find with no trouble

$$F(\Lambda,1) = \int_N^1 dv = 1 - N \qquad (2.15a)$$

$$F(\Lambda,2) = \int_N^1 \frac{v^4 - 1}{v^2 - 1}dv = \int_N^1 (v^2 + 1)\,dv = \frac{4}{3} - N - \frac{N^3}{3} \qquad (2.15b)$$

$$F(\Lambda,3) = \int_N^1 \frac{v^6 - 1}{v^2 - 1}dv = \int_N^1 (v^4 + v^2 + 1)dv = \frac{23 - 15N - 5N^3 - 3N^5}{15} \qquad (2.15c)$$

$$F(\Lambda,{}^1/_2) = \int_N^1 \frac{v - 1}{v^2 - 1}dv = \int_N^1 \frac{dv}{v + 1} = \log\left(\frac{2}{1 + N}\right) \qquad (2.15d)$$

$$F(\Lambda,{}^3/_2) = \int_N^1 \frac{v^3 - 1}{v^2 - 1}dv = \int_N^1 \left(v + \frac{1}{1 + v}\right)dv = \frac{1 - N^2}{2} + \log\left(\frac{2}{1 + N}\right) \qquad (2.15e)$$

When $\rho = {}^1/_3$ or ${}^2/_3$, the integrals are a little more difficult to evaluate. Making the substitution $v = u^3$ we find

$$F(\Lambda,{}^2/_3) = \int_{N^{1/3}}^1 \frac{3u^2(1 + u^2)}{u^4 + u^2 + 1}du = 3[u - \Phi_0(u)]_{N^{1/3}}^1 = 3[1 - N^{1/3} - \Phi_0(1) + \Phi_0(N^{1/3})] \qquad (2.16a)$$

and

$$F(\Lambda,{}^1/_3) = \int_{N^{1/3}}^1 \frac{3u^2}{u^4 + u^2 + 1}du = \frac{3}{2}[\Phi_1(u)]_{N^{1/3}}^1 = \frac{3}{2}[\Phi_1(1) - \Phi_1(N^{1/3})] \qquad (2.16b)$$

where

$$\Phi_0(u) = \frac{1}{4}\log\left(\frac{u^2 + u + 1}{u^2 - u + 1}\right) + \frac{1}{2\sqrt{3}}\text{arc tan}\left(\frac{u\sqrt{3}}{1 - u^2}\right) \qquad (2.16c)$$

and

$$\Phi_1(u) = \frac{1}{4}\log\frac{(u^2 - u + 1)^3}{(u^4 + u^2 + 1)(u^2 + u + 1)} + \frac{1}{\sqrt{3}}\text{arc tan}\left(\frac{u\sqrt{3}}{1 - u^2}\right) \qquad (2.16d)$$

The results obtained above may be compared with the formula published by Schofield[2] in the following way. Schofield was interested primarily in the limit of very large Λ. In this limit, it is easy to see that $1/\gamma_-$ approaches $1 + 1/\Gamma$ while the distribution coefficient D approaches unity. Thus, the term in parentheses on the right-hand side of eq. 1.7 has a value very close to 1, especially if $1/\Gamma$ exceeds unity by any substantial margin. Thus, if we again set $\gamma_{\pm}' = 1$ for convenience, $D \approx 1/\gamma_+$. Furthermore

$$F(\Lambda,\rho) = \int_0^{\infty} e^{-\rho y}\frac{\sinh \rho y}{\sinh y}dy - \int_{\text{arc sinh }\Lambda}^{\infty} e^{-\rho y}\frac{\sinh \rho y}{\sinh y}dy \approx F(\infty,\rho) - \int_{\text{arc sinh }\Lambda}^{\infty} e^{-x}dx \approx F(\infty,\rho) - e^{-\text{arc sinh }\Lambda} \approx F(\infty,\rho) - \frac{1}{2\Lambda} \qquad (2.17)$$

Thus

$$D \approx 1 - \frac{F(\infty,\rho)}{2\Gamma\Lambda} + \frac{1}{4\Gamma\Lambda^2} \qquad (2.18)$$

The numbers $F(\infty,\rho)$ can be obtained from eq. (2.15); they are given in Table I.

Table I

ρ	1/3	1/2	2/3	1	3/2	2	3
$F(\infty,\rho)$	0.536	0.693	0.816	1.000	1.193	1.333	1.533
$q/2$	0.580	0.732	0.845	1.000	...	1.225	1.325

Schofield has obtained from the calculations of Quenouille an equation for D with exactly the same form as eq. 2.18, but with the constant $F(\infty,\rho)$ replaced by another, slightly different constant (called by him $q/2$). The reason for this difference is that Quenouille based his calculations on the correct electric potential rather than the potential appropriate to a suitable symmetrical electrolyte. Also shown in the table are Schofield's values of $q/2$; in most cases they are within 10% of the value of $F(\infty,\rho)$. Bolt and Warkentin[3] also remark on this point.

Since the thickness of the double layer is, at most, a few units of ζ, the single double-layer approach is valid only if R is large when measured in units of ζ, *i.e.*, only if $\zeta_R >> 1$. For convenience, we also note here that $\zeta_R = \xi_R\sqrt{2\Gamma}$ (*cf.* eq. 2.8).

Appendix 3. The Case of Good Exclusion

Let us begin by considering a volume V surrounded by a charged surface S and containing a sufficient number of mobile counterions in its interior just to neutralize the surface charge. The Poisson–Boltzmann equation for the electric potential ϕ in the interior of V is then

$$\nabla^2\phi = -\frac{ze}{\epsilon}\frac{c_0 e^{-ze\phi/kT}}{\frac{1}{V}\int_V e^{-ze\phi/kT}\mathrm{d}^3r} \tag{3.1}$$

The second term on the right-hand side of eq. 3.1 is the local concentration of counterions at any point in the volume V; the integral in the denominator of this term is present in order to normalize the total number of counterions in V to Vc_0. If we integrate eq. 3.1 over the volume V, we obtain from the divergence theorem a relation between the surface integral of the electric field and the concentration c_0, namely

$$\iint\frac{\partial\phi}{\partial n}\mathrm{d}s = -\frac{zec_0V}{\epsilon}$$

To avoid possible confusion, it is worthwhile to point out that this boundary condition is the same as the boundary condition derived in Appendix 2, *viz.*, that the component of the electric vector along the outward normal to S just inside the surface S is equal to $ze\sigma/\epsilon$.

Equation 3.1 can be brought into a form more suitable for solution by introducing the variables

$$\psi = -\frac{ze\phi}{kT} - \log\frac{1}{V}\int_V e^{-ze\phi/kT}\mathrm{d}^3r \tag{3.2a}$$

and

$$\xi = \left(\frac{z^2e^2c_0}{kT\epsilon}\right)^{1/2}\mathbf{r} \tag{3.2b}$$

where $\mathbf{r}$ is the radius vector. In terms of these variables eq. 3.1 becomes

$$\nabla^2\psi = e^{\psi} \tag{3.3}$$

The function ψ obeys the normalizing condition $(1/V)\int_V e^{\psi}\mathrm{d}^3\xi = 1$.

No observable quantity can depend on the choice of zero of the potential ϕ. In other words, any observable quantity must be invariant to the addition of a constant to the potential ϕ. In fact, this must be so simply because eq. 3.1, which determines ϕ, is invariant to the addition of a constant to ϕ and thus only determines ϕ to within an additive constant. The ionic activity coefficients, given by Marcus' eq. 2.5, which we shall also use here, are not themselves invariant to the addition of a constant to ϕ, but neither are they observable quantities. On the other hand, the combination $\gamma_-^{\rho}\gamma_+$ of these activity coefficients, which determines the distribution coefficient (which is observable), is invariant to the addition of a constant to the potential ϕ. This means that, when we evaluate the ionic activity coefficients from Marcus' equation, it will be correct to use the potential given by eq. 3.2a *without the second (constant) term on the right-hand side.* It then follows that

$$\frac{1}{\gamma_-} = \frac{1}{V}\int_V e^{\psi}\mathrm{d}^3\xi = 1 \tag{3.4a}$$

and

$$\frac{1}{\gamma_+} = \frac{1}{V}\int_V e^{-\rho\psi}\mathrm{d}^3\xi \tag{3.4b}$$

In the case of cylindrical microcapillaries, Dresner and Kraus[5] have solved eq. 3.3 and find that ψ is given by

$$\psi = -2\log\left(b - \frac{\xi^2}{8b}\right) \tag{3.5a}$$

where

$$b^2 = 1 + \frac{\xi_R^2}{8} \tag{3.5b}$$

and ξ_R is the value of ξ corresponding to R [*cf.* eq. 2a]. Substituting eq. 3.5a into eq. 3.4b, we obtain

$$\frac{1}{\gamma_+} = \frac{2}{{\xi_R}^2}\int_0^{\xi_R} \xi d\xi \left(b - \frac{\xi^2}{8b}\right)^{2\rho} \tag{3.6}$$

Substituting $x = 1 + ({\xi_R}^2 - \xi^2)/8$, we easily find that

$$\frac{1}{\gamma_+} = \frac{(b^2)^{2\rho+1} - 1}{(2\rho + 1)(b^2 - 1)(b^2)^\rho} \tag{3.7}$$

Since, in the good exclusion theory, D is always very much less than unity, it can be dropped on the right-hand side of eq. 1.7, which then takes the form

$$D = \Gamma^\rho \frac{(\gamma_\pm')^{\rho+1}}{\gamma_+\gamma_-^\rho} = \Gamma^\rho \frac{(b^2)^{2\rho+1} - 1}{(2\rho + 1)(b^2 - 1)(b^2)^\rho}(\gamma_\pm')^{\rho+1} \tag{3.8}$$

In the case of lamellar microcapillaries, we do not have the solution of eq. 3.3 already written down, so we shall have to solve eq. 3.3 *ab initio*. We begin by again converting both sides into perfect differentials by multiplying by $2d\psi/d\xi$. Then we integrate

$$\frac{d\psi}{d\xi} = \sqrt{2(e^\psi - e^{\psi_0})} \tag{3.9}$$

Here ψ_0 is the value of ψ along the midplane of the capillary ($\xi = 0$), where the gradient of the potential ψ vanishes. A second integration yields

$$\xi = \int_{\psi_0}^{\psi} \frac{d\psi}{\sqrt{2(e^\psi - e^{\psi_0})}} = \sqrt{2}e^{-\psi_0/2} \cos^{-1}\left\{e^{(\psi_0 - \psi)/2}\right\} \tag{3.10a}$$

or upon inverting

$$e^{-\psi} = e^{-\psi_0} \cos^2\left(\frac{\xi e^{\psi_0/2}}{\sqrt{2}}\right) \tag{3.10b}$$

By integrating the differential equation (3.3) over the interior of the microcapillary and using the normalization condition for ψ, we see that

$$\frac{\xi_R}{2} = \left(\frac{d\psi}{d\xi}\right)_{\xi_R/2} = \sqrt{2(e^{\psi_w} - e^{\psi_0})} \tag{3.11}$$

where ψ_w is the value of ψ at the capillary wall ($\xi = \xi_R/2$). Substituting eq. 3.10b into 3.11, we find that ψ_0 is determined by the equation

$$\frac{{\xi_R}^2}{8} = \left(\frac{\xi_R e^{\psi_0/2}}{2\sqrt{2}}\right) \tan\left(\frac{\xi_R e^{\psi_0/2}}{2\sqrt{2}}\right) \equiv a \tan a \tag{3.12}$$

Substituting eq. 3.10b into 3.4b, we finally obtain for $1/\gamma_+$ the result

$$\frac{1}{\gamma_+} = \frac{2}{\xi_R}\int_0^{\xi_R/2} e^{-\rho\psi_0} \cos^{2\rho}\left(\frac{\xi e^{\psi_0/2}}{\sqrt{2}}\right)d\xi \tag{3.13a}$$

$$= e^{-\rho\psi_0}\int_0^1 \cos^{2\rho}\left(\theta\frac{\xi_R e^{\psi_0/2}}{2\sqrt{2}}\right)d\theta \tag{3.13b}$$

$$= \left(\frac{\tan a}{a}\right)^\rho \int_0^1 \cos^{2\rho}(a\theta)d\theta \tag{3.13c}$$

Thus

$$\rho = 1: \quad \frac{1}{\gamma_+} = \frac{\tan a}{a}\left[\frac{1}{2} + \frac{1}{2}\cos a \frac{\sin a}{a}\right] \tag{3.14a}$$

$$\rho = 2: \quad \frac{1}{\gamma_+} = \left(\frac{\tan a}{a}\right)^2\left[\frac{3}{8} + \frac{\sin a}{a}\left(\frac{3}{8}\cos a + \frac{1}{4}\cos^3 a\right)\right] \tag{3.14b}$$

$$\rho = 3: \quad \frac{1}{\gamma_+} = \left(\frac{\tan a}{a}\right)^3\left[\frac{5}{16} + \frac{\sin a}{a}\left(\frac{5}{16}\cos a + \frac{5}{24}\cos^3 a + \frac{1}{6}\cos^5 a\right)\right] \tag{3.14c}$$

$$\rho = \frac{1}{2}: \quad \frac{1}{\gamma_+} = \left(\frac{\tan a}{a}\right)^{1/2}\frac{\sin a}{a} \tag{3.14d}$$

$$\rho = \frac{3}{2}: \quad \frac{1}{\gamma_+} = \left(\frac{\tan a}{a}\right)^{3/2}\frac{\sin a}{a}\left[\frac{2}{3} + \frac{1}{3}\cos^2 a\right] \tag{3.14e}$$

The values of $1/\gamma_+$ shown in Figure 4 for $\rho = {}^1/_3$ and $\rho = {}^2/_3$ were calculated numerically by evaluating the trigonometric integral in eq. 3.13c with Simpson's rule.

Pulse Radiolysis Studies. VIII. Kinetics of Formation of Triplet States of Aromatic Molecules in Acetone Solutions[1]

by Shigeyoshi Arai and Leon M. Dorfman[2,3]

Argonne National Laboratory, Argonne, Illinois *(Received December 23, 1964)*

The pulse radiolysis method has been used to identify aromatic triplet states in electron-irradiated solutions. The triplet states of naphthalene, anthracene, and 1,2-benzanthracene were identified from the optical absorption spectra in acetone solutions of these arenes. The energy-transfer process between the solvent and solute molecules was studied by direct observation of the kinetics of formation of the triplet state. The absolute bimolecular rate constants for triplet formation were found to be: $(6.2 \pm 0.6) \times 10^9\ M^{-1}$ sec.$^{-1}$ for anthracene and $(4.5 \pm 0.9) \times 10^9\ M^{-1}$ sec.$^{-1}$ for naphthalene, both at 23° in acetone. The data indicate a half-life greater than 5 μsec. (for a first-order decay) for the precursor in pure acetone. The G value for all three of the triplets observed was found to be between 1 and 2 molecules/100 e.v. The mononegative molecule ion of anthracene was also identified from its absorption spectrum and was found to have a G value of 1.7 ± 0.6 molecules/100 e.v.

Introduction

The formation of electronic triplet states of aromatic molecules in various solutions irradiated with electrons has been established in pulse radiolysis investigations. These observations in both the liquid[4-6] and gaseous[7] phase have identified the triplet state from the ultraviolet absorption bands resulting from triplet–triplet transitions.

In this paper, information on the role of the triplet state in radiation chemistry is presented for naphthalene, anthracene, and 1,2-benzanthracene in acetone solution. In addition to the absorption spectra, the rate constants for the formation reactions have been determined. The times involved have a direct bearing on the possible nature of the precursor of the aromatic triplets. The aromatic anion, which is also formed in these solutions, has been identified from its absorption spectrum.

Experimental

Pulse Irradiation. A 14- to 15-Mev. electron beam from the linear accelerator was used. Pulse lengths of 0.4 and 1 μsec. were used at currents of 3 to 200 ma. A 0.4-μsec. pulse at 100 ma. delivers a dose of approximately 1.4×10^{17} e.v./g. Cylindrical quartz cells were used as before[8-10] with the same electron beam geometry as in previous work. Each solution was degassed by pumping in a cell with side arm, and the cell was then sealed off.

Spectrophotometry. The spectra in the present investigation were all obtained spectrophotometrically from the optical density readings of decay curves for each particular species at about 0.5 μsec. after the electron pulse. In the case of the triplet states the lifetime under our conditions was longer than 4.5 μsec.

(1) Based on work performed under the auspices of the U. S. Atomic Energy Commission.

(2) Department of Chemistry, The Ohio State University, Columbus, Ohio.

(3) To whom requests for reprints should be sent.

(4) J. D. McCollum and W. A. Wilson, ASD Technical Report 61-170, Aug. 1961.

(5) J. M. Nosworthy and J. P. Keene, *Proc. Chem. Soc.*, 114 (1964).

(6) S. Arai and L. M. Dorfman, *J. Chem. Phys.*, **41**, 2190 (1964).

(7) M. C. Sauer, Jr., and L. M. Dorfman, *J. Am. Chem. Soc.*, **86**, 4218 (1964).

(8) L. M. Dorfman, I. A. Taub, and R. E. Bühler, *J. Chem. Phys.*, **36**, 3051 (1962).

(9) G. Czapski and L. M. Dorfman, *J. Phys. Chem.*, **68**, 1169 (1964).

(10) M. C. Sauer, Jr., S. Arai, and L. M. Dorfman, *J. Chem. Phys.*, **42**, 708 (1965).

so that the optical density reading at 0.5 μsec. required no correction for the decay in this time.

A 500-w. Osram xenon lamp, Type XBO 450 W, was used as the continuum source. To avoid any photolysis of the acetone during the experiments, a Corning No. 0–51 filter was interposed between the lamp and the reaction cell. The light was monitored by a 1 P28 photomultiplier over the wave length region below 6000 Å. and by a 7102 photomultiplier over the region above 6000 Å.

A Bausch and Lomb grating monochromator, Type 33-86-25, f/3.5, was used. Grating No. 33-86-01 was used over the region 2000 to 4000 Å. and grating No. 33-86-02 over the region 4000 to 8000 Å. With each of these the exit slit in front of the photomultiplier was set for a band width of 24 Å. In the spectral plotting, points were obtained at wave length intervals of 25 (for the narrower bands, and near the maxima) to 200 Å. Two passes of the analyzing light beam through the cell were used.

Materials. Acetone was reagent grade, obtained from Baker and Adamson Co., and was used without further purification. Anthracene was scintillation grade from Reilly Tar and Chemical Corp.; naphthalene was Baker Analyzed reagent from J. T. Baker Chemical Co.; 1,2-benzanthracene was from Aldrich Chemical Co.

Results and Discussion

Spectra. The transient ultraviolet absorption spectra observed in acetone solutions of anthracene, naphthalene, and 1,2-benzanthracene are shown in Figure 1. These agree within experimental error with the triplet–triplet absorption spectra reported by Porter and Windsor[11] in flash photolysis studies using spectrophotographic methods. The anthracene solutions show a strong maximum at 4240 Å., in precise agreement with the spectrum in flash photolysis[11] and a weaker band at about 4040 Å., compared to 4010 Å. The relative intensity of the bands in our observations is 1.00 to 0.32 compared with 1.00 to 0.34 in the flash photolysis.[11] The naphthalene solutions show a spectrum with a sharp maximum at 4150 Å. and a slightly weaker band at 3900 Å., with a third at 3750 Å. These compare with 4150, 3915, and 3720 Å. in the flash photolysis.[11] The relative band intensities in the present work are 1.00, 0.67, and 0.40, respectively, compared with 1.00, 0.68, and 0.27 in the earlier work.[11] It appears that the peak at 3720 Å. may have an overlapping contribution from other species, such as the naphthalene mononegative ion.[12] The 1,2-benzanthracene exhibits bands at 4850, 4590, and 4280 Å. with relative intensities of 1.00, 0.84, and 0.92. This

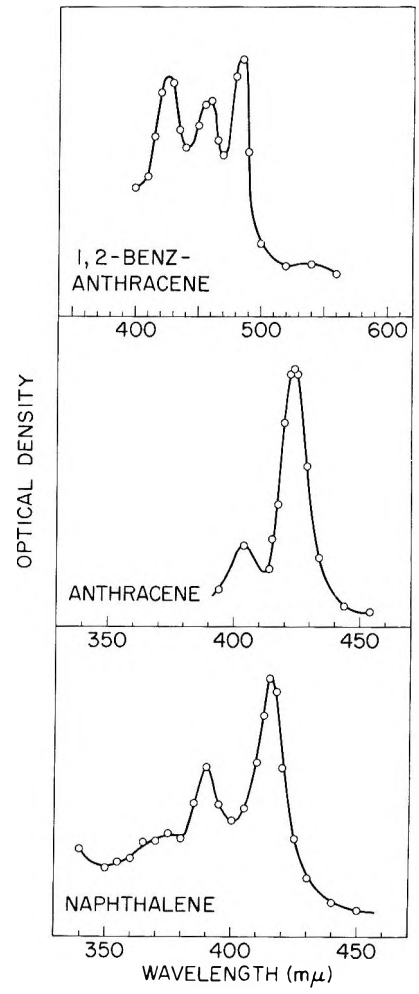

Figure 1. Absorption spectra of triplet states of aromatic molecules in pulse-irradiated acetone solution. The ordinate shows the relative optical density.

compares with[11] 4850, 4610, and 4345 Å., for which the reported intensities[11] are 1.00, 0.84, and 0.53. Again, only the band closest to the ultraviolet region differs, the other two being in good agreement. There can thus be little doubt that our observed spectra may be identified as the triplet–triplet absorption spectra of the respective aromatic molecules. It appears that there is no significant wave length shift for acetone as the solvent in the present work, compared with paraffin oil in the flash photolysis.

In the case of anthracene solutions the mononegative ion of anthracene was identified from the major peak at 7300 Å. and weaker, partially resolved bands at 6600 and 6000 Å., in satisfactory agreement with the earlier

(11) G. Porter and M. Windsor, *Proc. Roy. Soc.* (London), **A245**, 238 (1958).

(12) P. Balk, G. J. Hoijtink, and J. W. H. Schreurs, *Rec. trav. chim.*, **76**, 813 (1957).

work.[12,13] This species has also been observed[6] in the pulse radiolysis of anthracene in ethanol.

Kinetics. At concentrations of the aromatic molecule below about 5×10^{-4} *M* the rate of formation of the triplet state was slow enough to permit the observation of a rate curve which could be used for kinetic analysis. The decay rate of the aromatic triplet is much lower than its rate of formation and decreases with decreasing pulse current. At concentrations of the aromatic molecule above 2×10^{-5} *M* and at sufficiently low current, the formation rate curves exhibit a well-defined plateau.

This is illustrated in the case of anthracene, for which two typical rate curves, obtained at 4240 Å., at low pulse current, are shown in Figure 2a and b. At both concentrations the decay of the triplet may be seen, but a plateau is still defined.

These formation rate curves fit a first-order rate law as may be seen by plotting log $(D_\infty - D_t)$ against time, where D_t and D_∞ are the optical densities of the triplet state at time t and at the rate curve plateau, respectively. Figure 3 shows a typical plot of a first-order rate law test for triplet anthracene formation at an anthracene concentration of 2.7×10^{-4} *M*. Good linearity is generally obtained except at the lowest concentrations where the rate of decay of the triplet is not negligible and at the highest pulse currents. In the case of naphthalene, the effect of a nonnegligible decay rate is somewhat more pronounced since it was necessary to work at higher pulse current.

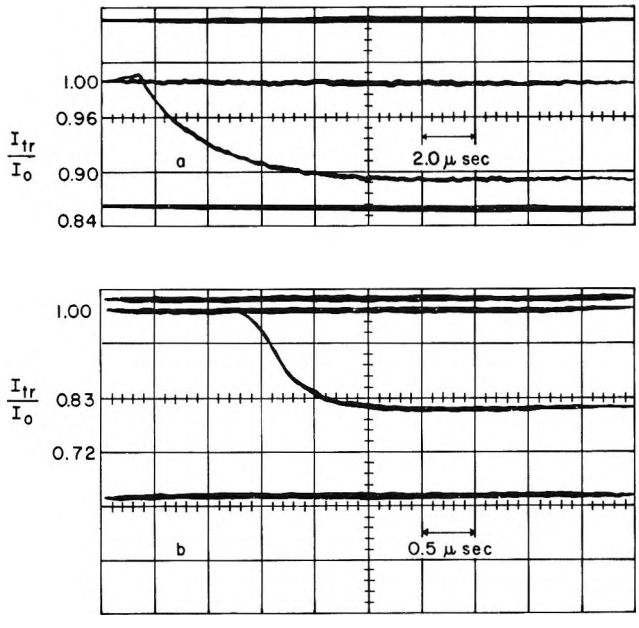

Figure 2. Rate curves for the formation of anthracene triplet state in acetone following a 0.4-μsec. pulse at approximately 10-ma. current. The absorption was monitored at 4240 Å.: a, [anthracene] = 3.9×10^{-5} *M*; b, [anthracene] = 3.5×10^{-4} *M*.

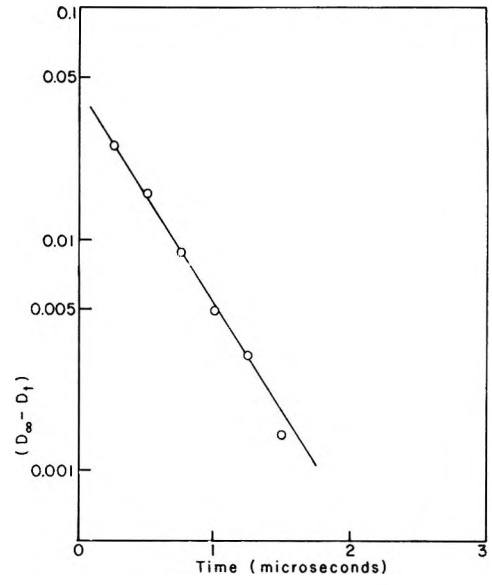

Figure 3. First-order rate law test for rate curve for triplet anthracene formation; [anthracene] = 2.7×10^{-4} *M*.

The absolute rate constant for triplet formation may be obtained from the following analysis of the data. The formation reaction

$$CH_3COCH_3' + \text{anthracene} = {}^3\text{anthracene} \quad (1)$$

involving an unspecified energy state of the acetone, is in competition with the decay of this state

$$CH_3COCH_3' \longrightarrow CH_3COCH_3 \quad (2)$$

As will be seen from the data, k_2, the first-order rate constant for the decay, is comparable to $k_1[\text{An}]$, where An represents anthracene, at the lowest concentrations used in these experiments.

The differential rate expressions are

$$\frac{d[{}^3\text{An}]}{dt} = k_1[CH_3COCH_3'][\text{An}] \quad (\text{I})$$

and

$$\frac{d[CH_3COCH_3']}{dt} = -k_2[CH_3COCH_3'] - k_1[CH_3COCH_3'][\text{An}] \quad (\text{II})$$

Integrating these equations gives

$$2.303 \log (D_\infty - D_t) = -(k_1[\text{An}] + k_2)t + \text{constant} \quad (\text{III})$$

(13) E. de Boer and S. I. Weissman, *Rec. trav. chim.*, **76**, 824 (1957).

The term $k_1[An] + k_2$ is obtained from the first-order plots of the individual rate curves.

For the conditions where a good plateau is not established, an approximate correction for the decay may be made in the following manner by including the reaction

$$^3\text{anthracene} \longrightarrow \text{anthracene} \qquad (3)$$

Assuming the decay curve to be linear over its initial portion, eq. I becomes

$$\frac{d[^3An]}{dt} = k_1[CH_3COCH_3'][An] - k_3 \qquad (Ia)$$

At the steady-state point, $d[^3An]/dt = 0$, and integration leads to

$$2.303 \log \left\{ D_s - D_t + k_3\left(t_s + \frac{1}{k_1[An] + k_2} - t\right)\right\} = -(k_1[An] + k_2)t + \text{constant} \qquad (IV)$$

where D_s is the optical density and t_s the time, both at the steady-state point. The value for $k_1[An] + k_2$ is determined by successive approximation starting with a plot of eq. III. The value obtained from the slope is inserted into eq. IV. The final, limiting value is obtained from the slope by successive plots of the left-hand side of eq. IV against time.

Figure 4 shows a plot of $k_1[An] + k_2$, obtained in this way, against [anthracene] over a ninefold concentration range. The data give $k_1 = (6.2 \pm 0.6) \times 10^9$ M^{-1} sec.$^{-1}$ at 23°. The use of the foregoing correction for triplet decay results in a rather small difference in the case of anthracene. Without applying this correction, the rate constant obtained is approximately 10% higher. From the intercept in Figure 4, at zero concentration of anthracene, we obtain $k_2 = 1.2 \times 10^5$ sec.$^{-1}$. This gives a half-life of 5.8 μsec. for the acetone state in this system in the absence of anthracene.

A similar treatment was applied to data for naphthalene obtained from triplet formation curves observed at 4150 Å. Figure 5 shows a plot of k_1[naphthalene] $+ k_2$ against [naphthalene] over a tenfold concentration range. The data give $k_1 = (4.5 \pm 0.9) \times 10^9$ M^{-1} sec.$^{-1}$ at 23° for naphthalene solutions. If the correction for triplet decay is not applied in this case, the rate constant obtained is approximately 20% higher. From the intercept in Figure 5 we obtain $k_2 = 1.6 \times 10^5$ sec.$^{-1}$ and a half-life of 4.3 μsec. for the acetone precursor. This is in satisfactory agreement with the value determined from the anthracene solutions.

From the magnitude of the bimolecular rate constants for triplet formation in these systems it appears that

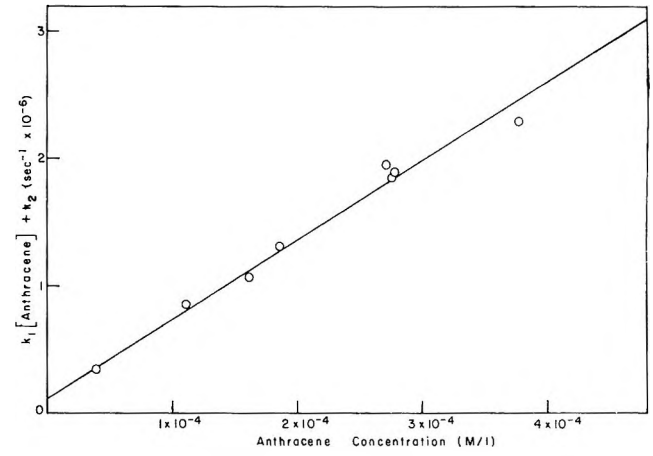

Figure 4. Plot of k_1[anthracene] + k_2 against [anthracene]. The slope gives $k_1 = (6.2 \pm 0.6) \times 10^9$ M^{-1} sec.$^{-1}$ for anthracene and $k_2 = 1.2 \times 10^5$ sec.$^{-1}$ at 23°.

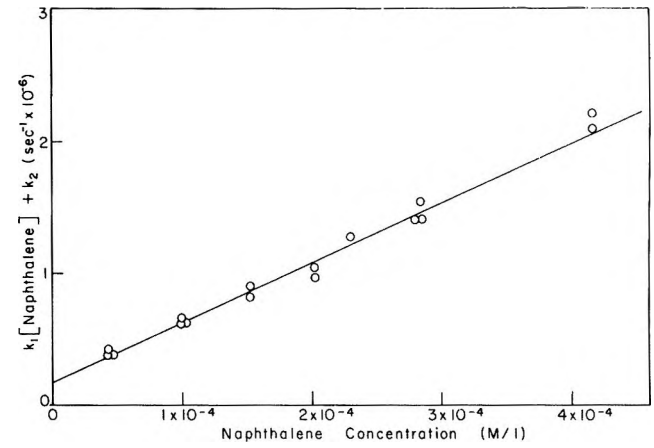

Figure 5. Plot of k_1[naphthalene] + k_2 against [naphthalene]. The slope gives $k_1 = (4.5 \pm 0.9) \times 10^9$ M^{-1} sec.$^{-1}$ for naphthalene and $k_2 = 1.6 \times 10^5$ sec.$^{-1}$ at 23°.

the energy-transfer process involves diffusion-controlled collisional interaction with cross sections of molecular dimensions. However, a full appraisal of this matter requires additional information concerning the activation energies for the reactions.

This half-life of at least 5 μsec. for the acetone state, which is the precursor of the aromatic triplet, suggests that this excited state of the acetone is itself a triplet. The singlet electronic state would appear to be ruled out on the basis of a shorter radiative lifetime. The possibility of the mononegative ion as the precursor is ruled out by the result of simultaneous observation of the anion decay at 7300 Å. and the triplet formation at 4240 Å. This observation shows quite different kinetics for the two species. The possibility of aromatic triplet formation by recombina-

tion of a solvated electron or other negative species with aromatic cation appears to be ruled out from rate considerations. Since the triplet formation is pseudo-first-order, the rate-limiting step would have to be the charge-transfer reaction, and the recombination reaction would have to be very rapid. At the low current of these experiments, a rate constant of even 10^{11} M^{-1} sec.$^{-1}$ for the recombination would give a half-time well over 10 μsec., which is more than an order of magnitude too long to satisfy this condition.

The decay curves were observed for both the anthracene triplet (at 4240 Å.) and the naphthalene triplet (at 4150 Å.) following a 0.4-μsec. pulse. These decay curves were of complex order, fitting a second-order rate law only over the first half of the observed rate curve. In the latter half, the rate became increasingly too high to fit a second-order decay. The half-times for the initial portion were approximately 25 μsec. for an 80-ma. pulse for anthracene and 5 μsec. for a 180-ma. pulse for naphthalene. Since these observed decay curves may have contributions from a number of reactions, such as triplet–triplet annihilation, triplet–radical quenching, and so on, no detailed interpretation is possible at present.

The decay of the anthracene anion was observed at 7300 Å. The decay curve fits a second-order rate law, the slope of the straight line being independent of pulse current. The good second-order fit suggests that the anion may be decaying in reaction with positive species, the initial concentrations of the two species being approximately equal. However, in the absence of more definite information concerning the concentration of positive species, it is not possible to determine the bimolecular rate constant for the reaction.

G Values. We may arrive at a rough estimate of the radiation chemical yield of the aromatic triplet state and, hence, also of its precursor, on the basis of the values of the molar extinction coefficient[11] for the triplet–triplet transition of the aromatic molecule. The value determined will have a large uncertainty since the molar extinction coefficients in the literature[11] have an indicated uncertainty of ±50%. Moreover, there may also be some effect of solvent since the values of ϵ which serve as our reference have been determined in a liquid paraffin of viscosity 30 cp., whereas they are being applied here to acetone solution. It is noteworthy in this connection that no spectral shift is observed.

We have examined the scavenging efficiency of the aromatic molecules for triplet formation over the concentration range 4×10^{-5} to 4×10^{-2} M. The curve for anthracene is shown in Figure 6. There is no further increase in the observed optical density above

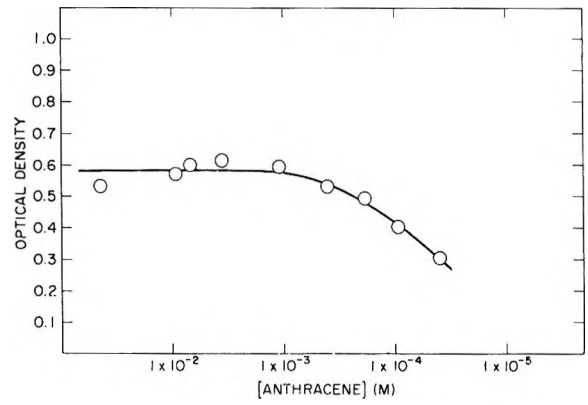

Figure 6. Scavenger efficiency of anthracene in triplet formation. The optical densities shown were taken from rate curves at time extrapolated to the middle of a 0.4-μsec. pulse.

10^{-3} M, indicating complete scavenging of the excited acetone. In the case of naphthalene, a similar curve is obtained, leveling off at about 2×10^{-3} M.

On the basis of the observed optical density for anthracene triplet at 4240 Å., the dose delivered to the solution, and the value[11] $\epsilon_{4240} = 7.2 \times 10^4$ M^{-1} cm.$^{-1}$, we obtain G(³anthracene) = 1.1 molecules/100 e.v. The uncertainty here is about ±0.7 in view of the error limit of ±50% in the extinction coefficient for the triplet state.

Similar measurements with 1,2-benzanthracene taking[11] $\epsilon_{4850} = 2.3 \times 10^4$ M^{-1} cm.$^{-1}$ as the value for the extinction coefficient of the triplet, give G(³benzanthracene) = 1.9 ± 1.0 molecules/100 e.v. The analogous data for naphthalene give only an upper limit for the G value since the extinction coefficient[11] $\epsilon_{4150} \geq 10^4$ M^{-1} cm.$^{-1}$ is only a lower limit. On this basis the data give G(³naphthalene) $\leq$ 3 molecules/100 e.v. It seems probable,[14,15] judging from recent work[15] on triplet–triplet annihilation in the gas phase, that ϵ_{4150} for naphthalene is two to three times the lower limit suggested in the earlier paper. This observed G value of 1 for the aromatic triplet indicates that the G value for the precursor of the triplet is also about 1 if the result of the quenching reaction by the arene is exclusively triplet formation.

The yield of anthracene anion was also determined from the observation of the optical density at 7300 Å., at the midpoint of the pulse by extrapolation of the decay curves. The anthracene anion yield was found to level off at anthracene concentrations above 5×10^{-3} M. The G value was determined from the ratio

(14) G. Porter, private communication.

(15) G. Porter and P. West, *Proc. Roy. Soc.* (London), **A279**, 302 (1964).

of the optical densities at 7300 in ethanol solution of anthracene and in acetone solution of anthracene, the absolute reference value being $G_{e_{sol}^-}^{ethanol} = 1.0$ for the solvated electron in ethanol from our previous work.[16] The use of this ratio

$$G(\text{anthracene}^-) = \frac{D_{7300}^{\text{acetone}}}{D_{7300}^{\text{ethanol}}} \times 1.0 \qquad (V)$$

assumes that the extinction coefficient of the anion in acetone is the same as in ethanol. The data give G (anthracene$^-$) = 1.7 ± 0.6 molecules/100 e.v. Most of the uncertainty originates in the value for $G_{e_{sol}^-}^{ethanol}$.

In pulse-irradiated acetone, without any additive, a weak transient absorption is observed, starting at about 6000 Å. and increasing to about 3200 Å., the transmission limit. The decay is complex, showing the presence of several absorbing species.

Acknowledgments. We are greatly indebted to Mr. Douglas Harter for his technical assistance in this work. The linear accelerator was operated by Mr. B. E. Clifft and Mr. E. Backstrom. We are grateful to Dr. Myran C. Sauer, Jr., with whom we have had frequent discussions.

(16) I. R. Taub, D. A. Harter, M. C. Sauer, Jr., and L. M. Dorfman, *J. Chem. Phys.*, **41**, 979 (1964).

Thermochemistry of Aqueous Aminosulfonic Acids. Sulfamic and Sulfanilic Acids and Taurine

by Harry P. Hopkins, Jr., Ching-Hsien Wu, and Loren G. Hepler

Department of Chemistry, Carnegie Institute of Technology, Pittsburgh, Pennsylvania
(Received December 28, 1964)

Results of calorimetric determinations of heats of solution and of ionization of sulfamic acid, sulfanilic acid, and taurine are presented and used in subsequent thermodynamic calculations. For ionization of the aqueous acids we find ΔH° = 0.25, 4.2, and 9.99 kcal. mole^{-1} and ΔS° = −3.8, −0.7, and −7.95 cal. (deg. mole)$^{-1}$ for sulfamic acid, sulfanilic acid, and taurine, respectively. These small negative values for entropies of ionization provide supporting evidence that the aqueous acids exist in the zwitterion form. We calculate $\bar{S}_2^\circ$ = 56.4 and 48.4 cal. (deg. mole)$^{-1}$ for the standard partial molal entropies of aqueous taurine and the aqueous anion derived from taurine, respectively.

In addition to the inherent biological importance of some aminosulfonic acids, such as taurine, these substances are of interest because of their structural relation to amino acids. Like the amino acids, the aminosulfonic acids can exist in solution as zwitterions. Acidities of the aminosulfonic acids vary widely, sulfamic acid being of special interest because it is an "almost-strong" electrolyte. This paper is concerned with our calorimetric investigations of these acids and subsequent thermodynamic calculations.

Experimental

The calorimeter used is patterned after one previously described,[1] except that a Mueller G-2 bridge and

(1) W. F. O'Hara, C.-H. Wu, and L. G. Hepler, *J. Chem. Educ.*, **38**, 519 (1961).

HS galvanometer have been used with a nickel wire resistance thermometer for temperature measurements. Also, the resistance thermometer and calibration heater are contained in a glass spiral filled with mineral oil rather than wound on a silver cylinder. All of the calorimetric work reported here was carried out with 950 or 960 ml. of water or aqueous solution in the calorimeter with mean reaction temperature of 25.0 ± 0.2°.

Sulfamic acid (HSO_3NH_2) was purified according to the method described by Sisler, Butler, and Audrieth.[2] The crystals were dried in a vacuum desiccator, broken up with a glass rod, dried in an oven at 40° for 4 hr., and replaced in the desiccator.

Certified reagent grade sulfanilic acid monohydrate from Fisher Scientific Co. was recrystallized from water and dried in an oven at 100–105° for 2–3 hr., ground, and returned to the oven for 2–3 hr. The resulting sulfanilic acid (p-$NH_2C_6H_4SO_3H$) was stored for at least 1 week in a desiccator with 98% H_2SO_4 before analysis and use. Titration with standard NaOH indicated a purity of 99.9%.

Taurine, $NH_2CH_2CH_2SO_3H$, received from Fisher Scientific Co. as Highest Purity material, was recrystallized twice from water. Kjeldahl nitrogen analysis indicated that the recrystallized material contained 11.01% nitrogen (theoretical: 11.19%).

Results and Discussion

King[3] has determined pK = 9.0614 for ionization of aqueous taurine as indicated by

$$^+NH_3CH_2CH_2SO_3^-(aq) = H^+(aq) + NH_2CH_2CH_2SO_3^-(aq) \quad (1)$$

Heats of ionization were determined by measuring the heats of reaction of aqueous taurine (HT) with aqueous NaOH to yield water and the anion of taurine (T^-). Samples (10-ml.) of 5.15 M NaOH were mixed with 950 ml. of H_2O containing a known amount of dissolved HT. A reaction equation for this process is

$$HT(aq) + OH^-(concd) = T^-(aq) + H_2O(l) \quad (2)$$

Separate determination of the total heat associated with breaking the bulb containing the concentrated NaOH and diluting the NaOH (our values in agreement with literature values) permitted us to calculate heats for

$$HT(aq) + OH^-(aq) = T^-(aq) + H_2O(l) \quad (3)$$

These values, designated ΔH_n, are listed in Table I. Combination of $\Delta H_n^\circ = -3.35$ kcal. mole^{-1} with $\Delta H^\circ = 13.34$ kcal. mole^{-1} for the heat of ionization of water[4,5] leads to $\Delta H^\circ = 9.99$ kcal. mole^{-1} for the ionization reaction (1). We estimate that the total uncertainty (from possible sample impurities, calorimetric errors, and extrapolation to infinite dilution) is less than ±0.06 kcal. mole^{-1}. The e.m.f. studies of King led to K values at several temperatures from which he calculated that $\Delta H^\circ = 10.00$ or 10.04 kcal. mole^{-1}. Combination of our ΔH° with King's $\Delta G^\circ = 12.36$ kcal. mole^{-1} gives $\Delta S^\circ = -7.95$ cal. (deg. mole)$^{-1}$. King reports $\Delta S^\circ = -7.9$ cal. (deg. mole)$^{-1}$.

Table I: Heats of Neutralization of Aqueous Taurine by Aqueous NaOH

Moles of taurine/950 ml. of H_2O	$-\Delta H_n$, kcal. mole^{-1}
0.009655	3.34
0.013930	3.36
0.016635	3.42
0.020431	3.39
0.021865	3.35

Heats of solution of taurine in water are reported in Table II. The solubility of taurine has been reported[6] to be 0.837 m, but the composition of the solid phase in equilibrium with saturated solution was not specified. Our Kjeldahl nitrogen determination indicates that the solid phase is anhydrous taurine. We have estimated the activity coefficient of aqueous taurine in saturated solution to be 1.32 by analogy with the data for betaine reported by Smith and Smith.[7] For the standard free energy of solution we calculate $\Delta G^\circ = -0.061$ kcal. mole^{-1}. This quantity is combined with our $\Delta H^\circ = 5.78$ kcal. mole^{-1} to yield $\Delta S^\circ = 19.6$ cal. (deg. mole)$^{-1}$ for the standard entropy of solution. From this ΔS° and the standard entropy of crystalline taurine,[8] we calculate $\bar{S}_2^\circ = 56.4$ cal. (deg. mole)$^{-1}$ for the standard partial molal entropy of aqueous taurine.

The preceding entropy of aqueous taurine can be combined with our $\Delta S^\circ = -7.95$ cal. (deg. mole)$^{-1}$ for ionization of aqueous taurine as in eq. 1 to yield $\bar{S}_2^\circ = 48.4$ cal. (deg. mole)$^{-1}$ for the standard partial molal entropy of the aqueous anion of taurine, $NH_2CH_2CH_2SO_3^-(aq)$.

The entropy of ionization of aqueous taurine is considerably less negative than is characteristic of acids

(2) W. C. Fernelius, *Inorg. Syn.*, 2, 178 (1946).

(3) E. J. King, *J. Am. Chem. Soc.*, 75, 2204 (1953).

(4) J. Hale, R. M. Izatt, and J. J. Christensen, *J. Phys. Chem.*, 67, 2605 (1963).

(5) C. E. Vanderzee and J. A. Swanson, *ibid.*, 67, 2608 (1963).

(6) J. B. Dalton and C. L. A. Schmidt, *J. Biol. Chem.*, 109, 241 (1935).

(7) E. R. B. Smith and P. K. Smith, *ibid.*, 117, 209 (1937).

(8) H. M. Huffman and S. W. Fox, *J. Am. Chem. Soc.*, 62, 3464 (1940).

Table II: Heats of Solution of Taurine

Moles of taurine/950 ml. of H_2O	ΔH, kcal. mole^{-1}
0.007166	5.78
0.009470	5.78
0.009608	5.72
0.010790	5.74
0.012951	5.72
0.019194	5.75

$\Delta H^\circ = 5.78 \pm 0.05$

that exist in a neutral rather than zwitterion form in solution, in agreement with King's[3] argument that the ionization process should be described as in eq. 1.

Calorimetric determination of the heat of ionization of aqueous sulfamic acid is necessarily less direct than for weaker acids such as taurine since solutions of sulfamic acid in water contain nonnegligible amounts of hydrogen and sulfamate ions as well as un-ionized sulfamic acid. One approach to the desired ΔH° of ionization makes use of previously reported heats of solution of crystalline sulfamic acid in water while another approach makes use of those data and our newly determined heats of solution of sulfamic acid in aqueous sodium hydroxide.

When crystalline sulfamic acid is dissolved in water, processes represented by both of the following equations take place

$$HS(c) = HS(m') \qquad \Delta H_4 \tag{4}$$

$$HS(c) = H^+(m) + S^-(m) \qquad \Delta H_5 \tag{5}$$

where HS and S^- represent sulfamic acid and sulfamate ion and m and m' indicate their concentrations. The previously reported[9] heats of solution of sulfamic acid can be expressed as

$$\Delta H_{obsd} = \alpha\Delta H_5 + (1 - \alpha)\Delta H_4 \tag{6}$$

where α represents the degree of ionization calculated from the known amount of acid dissolved in a known amount of water and the ionization constant reported by King and King.[10] Activity coefficients used in this calculation are subsequently discussed.

In order to use eq. 6 it is necessary to combine eq.

$$H^+(m) + S^-(m) = H^+(aq) + S^-(aq) \qquad \Delta H_7 \tag{7}$$

7 and ΔH_7 with eq. 5 and ΔH_5 to obtain

$$HS(c) = H^+(aq) + S^-(aq) \qquad \Delta H_8 \tag{8}$$

in which (aq) indicates that the preceding species are at infinite dilution. Equation 6 now becomes

$$\Delta H_{obsd} = \alpha(\Delta H_8 - \Delta H_7) + (1 - \alpha)\Delta H_4$$

which is rearranged to

$$\frac{\Delta H_{obsd} + \alpha\Delta H_7}{\alpha} = \Delta H_8^\circ + \frac{(1 - \alpha)}{\alpha}\Delta H_4^\circ \tag{9}$$

In eq. 9 we have written ΔH_8° to emphasize that this is a standard heat of solution and have assumed that the heat of dilution of the neutral HS(aq) in dilute solution is zero so that $\Delta H_4 = \Delta H_4^\circ$. Heats of dilution represented by ΔH_7 have been taken to be equal to the already known heats of dilution of aqueous hydrochloric acid at the same concentrations.[11] We have followed King and King[10] in taking $\mathring{a} = 3.85$ Å. in the extended Debye–Hückel equation and have used the activity coefficients calculated in this fashion with the ionization constant also reported by King and King for evaluating by successive approximations the values of α needed for use in eq. 9.

A graph of $(\Delta H_{obsd} + \alpha\Delta H_7)/\alpha$ *vs.* $(1 - \alpha)/\alpha$ has been constructed and the slope and intercept used to evaluate $\Delta H_8^\circ = 4.53$ and $\Delta H_4^\circ = 4.33$ kcal. mole^{-1}. The same calculation has also been carried out with activity coefficients of hydrogen and sulfamate ions taken equal to those of aqueous HCl at the same ionic strength leading to $\Delta H_8^\circ = 4.52$ and $\Delta H_4^\circ = 4.35$ kcal. mole^{-1}. Combination of ΔH_8° and ΔH_4° gives $\Delta H_{10}^\circ = 0.19$ kcal. mole^{-1} for the heat of ionization as in

$$HS(aq) = H^+(aq) + S^-(aq) \tag{10}$$

Another method of determining the heat of ionization of aqueous sulfamic acid has made use of the data in Table III for heat of reaction of crystalline sulfamic acid with aqueous NaOH represented by ΔH_{11} and eq. 11. In making use of these data, we also use the pre-

$$HS(c) + OH^-(aq) = S^-(aq) + H_2O \qquad \Delta H_{11} \tag{11}$$

viously reported[9] heats of solution of sulfamic acid in water (already designated ΔH_{obsd} in this paper) and heats of ionization of water (ΔH_w) at ionic strengths corresponding to those of the solutions in our experiments.[4] Combining these ΔH quantities gives us

$$\Delta H_n = \frac{\Delta H_{11} - \Delta H_{obsd} + \alpha\Delta H_w}{1 - \alpha} \tag{12}$$

in which α-values are those appropriate to the solutions that would have been obtained had the amounts of sulfamic acid listed in Table III been dissolved in 960 ml. of water, and ΔH_m refers to $HS(aq) + OH^-(m) = S^-(m') + H_2O$.

(9) C.-H. Wu and L. G. Hepler, *J. Chem. Eng. Data*, **7**, 536 (1962).

(10) E. J. King and G. W. King, *J. Am. Chem. Soc.*, **74**, 1212 (1952).

(11) "Selected Values of Chemical Thermodynamic Properties," National Bureau of Standards, Circular 500, U. S. Government Printing Office, Washington, D. C., 1952.

Table III: Heats of Solution of Sulfamic Acid in 0.050 *M* NaOH

Moles of sulfamic acid/960 ml. of soln.	ΔH_{11}, kcal. mole^{-1}	ΔH_n, kcal. mole^{-1}
0.008126	−8.94	−13.28
0.006472	−8.96	−13.35
0.03126	−8.85	−13.26
0.02791	−8.87	−13.40
0.02613	−8.84	−13.21

The simplest treatment, and all that is justified by the accuracy of the ΔH_n values listed in Table III, is to take an average $\Delta H_n = -13.30$ (av. dev. = 0.08) kcal. mole^{-1} at an average ionic strength of about 0.05 combined with $\Delta H_w = 13.44$ kcal. mole^{-1} at this same ionic strength to give $\Delta H_{10} = 0.14$ kcal. mole^{-1} for the heat of ionization of aqueous sulfamic acid.

Consideration of the possible errors in experimental heats (ref. 9 and Table III) and errors introduced by uncertainties in values of α (based on K and calculated activity coefficients) indicates that our first value ($\Delta H_{10}^\circ = 0.19$ kcal. mole^{-1}) is more certain than our second ($\Delta H_{10}^\circ = 0.14$ kcal. mole^{-1}) for ionization of aqueous sulfamic acid. King and King[10] calculated $\Delta H^\circ = 0.27$ and 0.46 kcal. mole^{-1} from values of K at different temperatures based on two sets of activity coefficients. Precise analysis of uncertainties in these four ΔH_{10}° values (which are not entirely independent of each other) is impossible, but it appears reasonable to select $\Delta H_{10}^\circ = 0.25 \pm 0.15$ kcal. mole^{-1}. Combination of this heat of ionization with the average free energy of ionization ($\Delta G_{10}^\circ = 1.38$ kcal. mole^{-1}) reported by King and King[10] leads to the entropy of ionization $\Delta S_{10}^\circ = -3.8$ cal. (deg. mole)$^{-1}$. This small negative value of the entropy of ionization provides further evidence that undissociated sulfamic acid is largely in the zwitterion form in aqueous solution.

The heat of ionization of sulfanilic acid has also been calculated from calorimetric data. Heats of solution of sulfanilic acid in water are listed in Table IV. These data have been used as in eq. 9 for sulfamic acid in calculating $\Delta H^\circ = 3.6$ kcal. mole^{-1} for the solution of sulfanilic acid to yield un-ionized aqueous sulfanilic acid and $\Delta H^\circ = 7.6$ kcal. mole^{-1} for solution to give ions as in eq. 4 and 8 already written for sulfamic acid. Combination of these heats gives $\Delta H^\circ = 4.0$ kcal. mole^{-1} for ionization of aqueous sulfanilic acid.

A more accurate evaluation of the heat of ionization of aqueous sulfanilic acid has been obtained from combination of the heats listed in Table IV with those for solution of sulfanilic acid in aqueous NaOH listed in Table V. These data have been treated by an equation like (12) and have yielded the ΔH_n values also listed in Table V. The ionization constant at 25° reported by MacLaren and Swinehart[12] has been used in this calculation and also in the calculation discussed in the preceding paragraph.

Table IV: Heats of Solution of Sulfanilic Acid in Water

Moles of sulfanilic acid/950 ml.	ΔH, kcal. mole^{-1}
0.005234	4.72
0.005947	4.62
0.006441	4.60
0.008483	4.52
0.009376	4.47
0.01127	4.41
0.01617	4.35
0.01984	4.26

Table V: Heats of Solution of Sulfanilic Acid in 0.05 *M* NaOH

Moles of sulfanilic acid/960 ml. of soln.	ΔH_{obsd}, kcal. mole^{-1}	ΔH_n, kcal. mole^{-1}
0.008150	−5.65	−9.10
0.01089	−5.63	−9.12
0.01275	−5.61	−9.16
0.01440	−5.64	−9.18
0.01722	−5.63	−9.18

Although there appears to be a dilution effect in the values of ΔH_n listed in Table V, we are not at all sure this effect is real since uncertainties in ΔH_n increase as concentration decreases owing to the increasing value of α and the decreasing magnitude of the actual calorimetrically measured heat. We therefore take an average value of $\Delta H_n = -9.15$ kcal. mole^{-1} and combine with the heat of ionization of water[4] at the same average ionic strength to obtain $\Delta H = 4.3$ kcal. mole^{-1} for ionization of aqueous sulfanilic acid. Estimation of heats of dilution and combination of the resulting $\Delta H^\circ = 4.2$ kcal. mole^{-1} with that of the less accurately known value given earlier in this paper indicates that our "best" value for the heat of ionization is $\Delta H^\circ = 4.2 \pm 0.2$ kcal. mole^{-1}. MacLaren and Swinehart[12] have reported an equation for log K as a function of temperature, from which we have calculated $\Delta H^\circ = 4.29$ kcal. mole^{-1}. We are unable to estimate the uncertainty to be associated with this value.

Combination of our $\Delta H^\circ = 4.2$ kcal. mole^{-1} with the

(12) R. O. MacLaren and D. F. Swinehart, *J. Am. Chem. Soc.*, **73**, 1822 (1951).

Table VI: Thermodynamics of Ionization in Aqueous Solution at 298°K.

	$\Delta G°$, kcal./mole	$\Delta H°$, kcal./mole	$\Delta S°$, cal./(deg. mole)
$^+H_3NSO_3^- = H^+ + H_2NSO_3^-$	1.38	0.25	−3.8
$^+H_3N\text{-}C_6H_4\text{-}SO_3^- = H^+ + H_2N\text{-}C_6H_4\text{-}SO_3^-$	4.41	4.2	−0.7
$^+H_3NC_2H_4SO_3^- = H^+ + H_2NC_2H_4SO_3^-$	12.36	9.99	−7.95

standard free energy of ionization, $\Delta G° = 4.41$ kcal. mole^{-1}, calculated from the reported[12] ionization constant at 25°, gives $\Delta S° = -0.7$ cal. (deg. mole)$^{-1}$ for the standard entropy of ionization of aqueous sulfanilic acid. This small negative entropy value provides supporting evidence for the conclusion of MacLaren and Swinehart[12] that sulfanilic acid in aqueous solution is in the zwitterion form.

A summary of thermodynamics of ionization of sulfamic acid, sulfanilic acid, and taurine is given in Table VI.

Acknowledgments. We are grateful to the National Institutes of Health for financial support of this research and to Professor E. J. King for his helpful comments.

The Nitration of Nitrobenzene with Nitronium Fluoroborate in Hydrogen Fluoride

by Mary L. Kilpatrick, Martin Kilpatrick, and John G. Jones[1]

Department of Chemistry, Illinois Institute of Technology, Chicago, Illinois 60616
(Received December 28, 1964)

In this paper, the nitration of nitrobenzene by solutions of nitronium fluoroborate in hydrogen fluoride is shown to be of the first order with respect to both reactants. The rate constant is enhanced as the ionic strength of the medium rises, and an equation describing this behavior can be based on the Brønsted equation. Activation parameters indicate that the slowness of the nitration compared with its counterpart in sulfuric acid as solvent is due to a higher activation energy not entirely offset by a more favorable entropy of activation. This is explained in terms of solvation.

The investigation here described was begun in 1958, by which time several nitronium salts were known.[2] It was thought a good idea to employ one of these in some ionizing solvent, so as to measure the rate and order of attack of the nitronium ion itself on an aromatic substrate without having to take into account the pre-equilibria which produce nitronium ions from nitric acid.[3] If a suitable salt–solvent system were chosen, one would be able to weigh out nitronium ions directly into solution.

Hydrogen fluoride was chosen as the ionizing solvent because of its low viscosity[4] and high dielectric constant.[5] Handling experience had already been gained,[6] and it was known to be a good solvent for

(1) Taken in part from the Ph.D. Thesis of J. G. Jones, Illinois Institute of Technology, June 1964.

(2) (a) D. R. Goddard, E. D. Hughes, and C. K. Ingold, *Nature*, **158**, 480 (1946); (b) A. H. Woolf and E. J. Emeléus, *J. Chem. Soc.*, 1050 (1950); (c) D. R. Goddard, E. D. Hughes, and C. K. Ingold, *ibid.*, 2559 (1950); (d) M. Schmeisser and S. Elischer, *Z. Naturforsch.*, **7b**, 583 (1952); (e) E. E. Aynsley, G. Hetherington, and P. L. Robinson, *J. Chem. Soc.*, 1119 (1954).

(3) (a) G. M. Bennett, J. C. D. Brand, and G. Williams, *ibid.*, 869 (1946); (b) R. A. Marcus and J. M. Fresco, *J. Chem. Phys.*, **27**, 564 (1957); (c) F. G. Bordwell and E. W. Garbisch, *J. Am. Chem. Soc.*, **82**, 3588 (1960).

ultraviolet spectroscopy, transparent from 220 to 800 mμ.[7]

Nitronium fluoroborate, NO_2BF_4, was chosen as the stable nitronium salt, and we were able to confirm by infrared studies that it existed as NO_2^+ and BF_4^- ions in the solid state.[3b,8] Studies on its solutions in hydrogen fluoride[8] proved it to be freely soluble, up to 1.5 *m* solutions being possible at 25°, and to exhibit the conductance behavior of a strong uni-univalent electrolyte, in a manner very similar to potassium fluoroborate.[9]

After preliminary nitrating experiments with NO_2-BF_4–HF and a variety of aromatic substrates, nitrobenzene was chosen as a convenient substrate because its nitration to *m*-dinitrobenzene proved clear-cut and easy to follow by ultraviolet spectroscopy using fairly conventional apparatus. Nitrobenzene has also been used as a substrate in several key studies of nitration; *e.g.*, it was used by Martinsen[10] in the first successful kinetic investigation of nitration, and also in Westheimer and Kharasch's[11] proof that the nitronium ion is the active nitrating species in sulfuric–nitric acid mixtures. Most recently, Ciaccio and Marcus[12] have used it as substrate in a determination of rates and rate laws of nitration employing nitronium fluoroborate in several solvents, and in the Discussion our results will be compared with theirs.

To our knowledge, this kinetic investigation is the first to be carried out in which hydrogen fluoride acts as solvent alone, rather than as solvent and one of the reactants simultaneously.

Experimental

Hydrogen Fluoride. Hydrogen fluoride from the Harshaw Chemical Co. was purified by condensing it into a Kel-F vessel, freezing it, pumping off hydrogen, and then distilling it through a Kel-F column packed with nickel helices.[13,14] This procedure regularly produced hydrogen fluoride of specific conductance $(3 \pm 2) \times 10^{-5}$ ohm^{-1} cm.$^{-1}$. Assuming that the chief impurity is water, and that in hydrogen fluoride it is entirely converted[15] to $H_3O^+HF_2^-$, and assuming that this latter substance has the same conductance properties in hydrogen fluoride as potassium fluoride,[16] then hydrogen fluoride of our specific conductance should contain *ca.* 10^{-4} mole/l. of water as $H_3O^+HF_2^-$.

Potassium Fluoride. Mallinckrodt analytical grade $KF \cdot 2H_2O$ was dried on a polyethylene sheet in a vacuum desiccator over P_2O_5, with continuous pumping. The crystals crumbled to fine white KF powder, and drying was completed in a drying pistol at 140°. Anhydrous potassium fluoride is deliquescent, so the product was transferred from the drying pistol to glass ampoules in a drybox, and the ampoules were then sealed.

Potassium Fluoroborate. Analytical grade was not obtainable, so a sample was prepared from analytical grade reagents after Van der Muellen and Van Mater,[17] but using polyethylene instead of platinum vessels. The product was dried in a vacuum desiccator and kept in an air-tight polyethylene bottle.

Dinitrogen Pentoxide. This was prepared from Matheson N_2O_4 and ozonized oxygen, after Gibson.[18] The white crystals were stored briefly in a glass bottle kept in a dewar vessel of Dry Ice.

Nitronium Fluoroborate. This was prepared from dinitrogen pentoxide, hydrogen fluoride, and boron trifluoride after Olah, Kuhn, and Mlinko's[19] modification of a method evolved by Schmeisser and Elischer,[20] illustrated by the equations

$$N_2O_5 + HF + BF_3 \xrightarrow{CH_3NO_2} NO_2^+BF_4^-\downarrow + HNO_3$$

$$HNO_3 + 2HF + 2BF_3 \xrightarrow{CH_3NO_2} NO_2^+BF_4^-\downarrow + H_3O^+BF_4^-$$

The preparation was performed in a Kel-F apparatus fitted with Kel-F valves, and at its conclusion surplus hydrogen fluoride and boron trifluoride were pumped

(4) An extrapolation of the data of J. H. Simons and R. D. Dresdener, *J. Am. Chem. Soc.*, **66**, 1070 (1944), gives a value of 2.07×10^{-3} poise at 20° (*cf.* water at 20°, 10.02×10^{-3} poise).

(5) An extrapolation of the data of K. Fredenhagen and J. Dahmlos, *Z. anorg. allgem. Chem.*, **178**, 272 (1928), gives a value of $\epsilon = 67.5$ at 20° (*cf.* water at 20°, 80.0).

(6) *E.g.*, M. Kilpatrick and F. E. Luborsky, *J. Am. Chem. Soc.*, **75**, 577 (1953).

(7) H. H. Hyman and M. Kilpatrick, *ibid.*, **80**, 77 (1958).

(8) M. Kilpatrick, M. L. Kilpatrick, and J. G. Jones, to be published; *cf.* D. Cook, S. J. Kuhn, and G. A. Olah, *J. Chem. Phys.*, **33**, 1669 (1960).

(9) *Cf.* M. Kilpatrick and F. E. Luborsky, *J. Am. Chem. Soc.*, **76**, 5863, 5865 (1954).

(10) H. Martinsen, *Z. physik. Chem.*, **50**, 385 (1904); **59**, 605 (1907).

(11) F. H. Westheimer and M. S. Kharasch, *J. Am. Chem. Soc.*, **68**, 1871 (1946).

(12) L. L. Ciaccio and R. A. Marcus, *ibid.*, **84**, 1838 (1962).

(13) M. Kilpatrick, J. A. S. Bett, and M. L. Kilpatrick, *ibid.*, **35**, 1038 (1963).

(14) M. E. Runner, G. Balog, and M. Kilpatrick, *ibid.*, **78**, 5183 (1956).

(15) S. Kongpricha and A. F. Clifford, *J. Inorg. Nucl. Chem.*, **18**, 270 (1961).

(16) K. Fredenhagen and G. Cadenbach, *Z. physik. Chem.*, **146**, 245 (1930).

(17) P. A. Van der Muellen and H. L. Van Mater, *Inorg. Syn.*, **1**, 24 (1939).

(18) G. Gibson, C. D. Beintema, and J. J. Katz, *J. Inorg. Nucl. Chem.*, **15**, 110 (1960).

(19) G. A. Olah, S. J. Kuhn, and A. Mlinko, *J. Chem. Soc.*, 4257 (1956).

(20) M. Schmeisser and S. Elischer, *Z. Naturforsch.*, **76**, 583 (1952).

off the mush of white nitronium fluoroborate crystals, and the crystals were then freed of $H_3O^+BF_4^-$ in nitromethane by filtration on a sintered glass funnel, in a drybox. The crystals were washed with dry nitromethane and Freon 113, and then transferred to a drying pistol where they were dried *in vacuo* at 140° over P_2O_5. The pistol was opened in the drybox and the free-running small crystals were transferred to glass ampoules which were subsequently sealed. All handling of this very deliquescent salt was performed in a drybox.

Nitrobenzene. Reagent grade nitrobenzene was dried over P_2O_5 and then distilled through a 2-m. Podbielniak fractionating column at a 50:1 reflux ratio. The fraction boiling between 210.6 and 210.8° was collected as an almost colorless liquid; f.p. 5.7°, $n^{20}D$ 1.5526.

m-Dinitrobenzene. Eastman White Label *m*-dinitrobenzene was recrystallized from isooctane as long pale yellow fibrous needles; m.p. (uncor.) 90.0° (lit. 90°).

Conductance Measurements. The HF was distilled directly into a Kel-F conductance cell having a cell constant of 0.09 cm.$^{-1}$, and its conductance was measured on a General Radio Co. bridge (Type 650-A). Conductance was used in the present work merely to monitor the purity of the HF. The conductance or "monitor" cell is shown schematically in Figure 1.

Preparing Nitronium Fluoroborate Solutions. The conductance cell, thoroughly washed with hydrogen fluoride and then evacuated, was weighed, HF was condensed into it, and the cell was weighed again. Then the filled cell, a weighed ampoule of nitronium salt, a special Kel-F valve and mixing chamber (Figure 2), and a diamond-pointed glass cutter were transferred to a drybox, where the sealed ampoule was opened with the glass cutter. Salt was shaken from the ampoule into the mixing chamber, which was then screwed onto the special valve which was in turn screwed onto the valve of the conductance cell; to visualize the assembly ready for the dissolving of the NO_2BF_4, consult Figure 2, and replace the optical cell shown there by the conductance cell of Figure 1. Both valves between the conductance cell and the mixing chamber were then

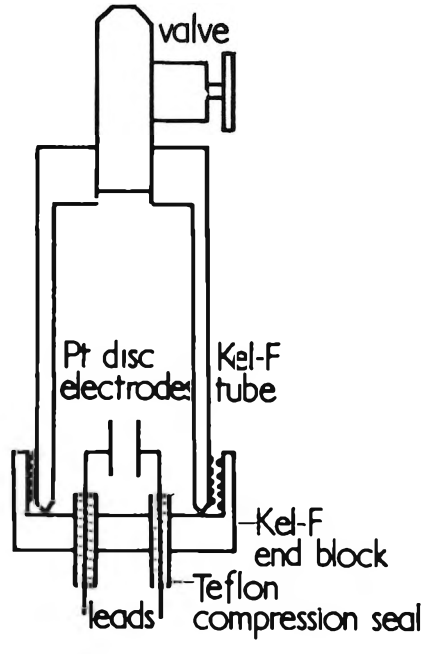

Figure 1. Cell for solution preparation and monitoring of conductance.

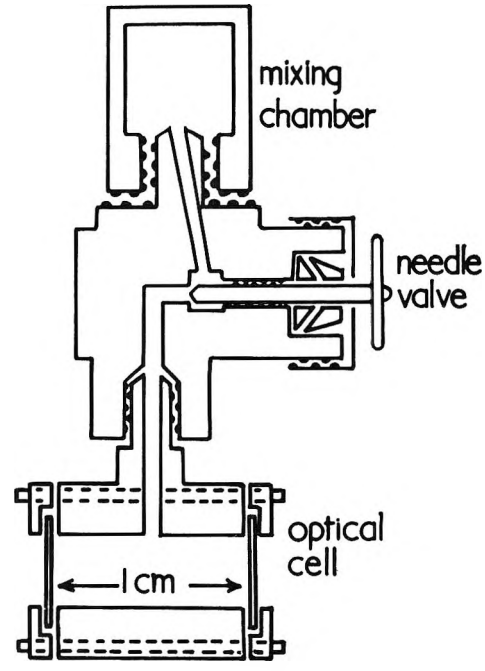

Figure 2. Optical cell and mixing chamber.

opened and hydrogen fluoride was shaken back and forth between the cell and the mixing chamber until all of the solid had dissolved. Finally, the cell, mixing chamber, ampoule, and cutoff ampoule neck were removed from the drybox, the ampoule was resealed with a torch, and the ampoule plus neck weighed.

A similar procedure was used for adding potassium fluoride or potassium fluoroborate to nitronium fluoroborate solutions. Nitronium fluoroborate and potassium fluoride dissolved speedily with the evolution of heat, but potassium fluoroborate could take up to 20 min. to dissolve completely.

The Optical Cells. The cells, 1 cm. in path length, were made of Kel-F with synthetic sapphire windows obtained from the Linde Co. Instead of closing the

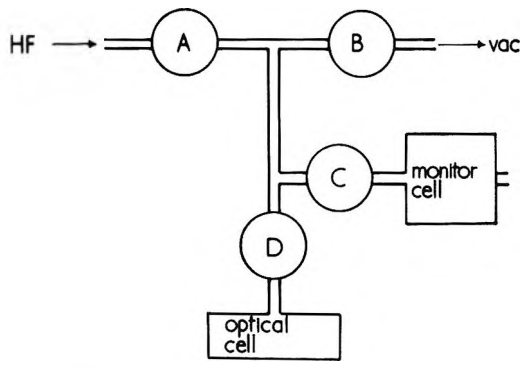

Figure 3. Solution transfer to the optical cell.

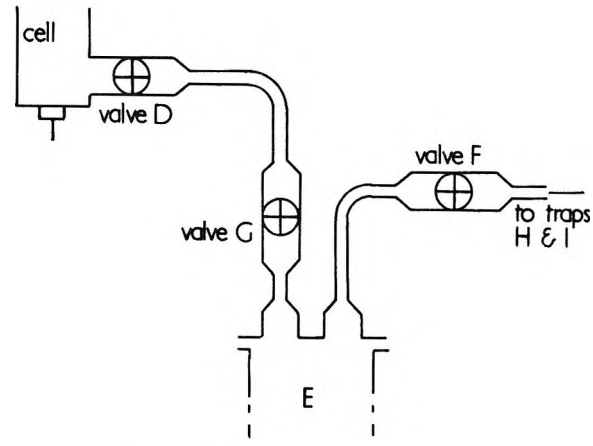

Figure 4. Cell-emptying arrangements.

cell with a polyethylene tube pinched shut,[7] we used a Kel-F valve, as for solution preparation (*cf.* Figure 2).

Filling the Cells. The cells were filled with hydrogen fluoride or with nitrating solution in the absence of air, using the Kel-F apparatus diagrammed in Figure 3. With valves B and D open, the optical cell and all dead space above it were evacuated. Then valve B was closed and valve C opened, allowing solution to flow from the conductance cell to the optical cell. When the latter had filled, valves C and D were closed, and the dead space was evacuated by opening valve B again.

Emptying the Cells. The optical and conductance cells could be emptied in the absence of air in the Kel-F apparatus diagrammed in Figure 4. Vessel E was evacuated, and then with valve F closed, valves D and G were opened, allowing solution to flow into vessel E. Hydrogen fluoride condensed in the traps H and I, while solid residues remained in E.

Dilution. The apparatus just described was particularly useful in diluting solutions made up in the conductance cell because it enabled one to dispose of some solution without contaminating the remainder. In order to effect dilution, the desired amount of solution was discharged into vessel E as described above, and then valves D and G were closed and the conductance cell was taken from the line, weighed, and then filled up by condensing hydrogen fluoride from the fractionating column into it. The cell was weighed again, and knowing the weight of the empty cell, the molality of the diluted solution could be calculated.

The Kinetic Experiments. Before kinetic experiments were performed, two optical cells were filled with hydrogen fluoride and placed in reference and sample compartments of a Cary 11 PM spectrophotometer, and the cells were optically balanced one against the other over the range 220–400 mμ. Then the sample cell was emptied, filled with nitrating solution, and a tiny drop of nitrobenzene placed on top of valve D; a mixing chamber (Figure 2) was screwed on top of the valve and the cell and chamber were replaced in the sample compartment of the spectrophotometer, and a baseline was drawn. Sample and reference compartments were controlled to ±0.05° by pumping water from a thermostat through channels made in their walls, and the temperature of the compartment was measured with a calibrated thermometer. After the lapse of 15 min. for the attainment of thermal equilibrium, the cell containing the nitrating solution was removed from the sample compartment, valve D was opened, and nitrating solution and nitrobenzene were thoroughly mixed by shaking the solution back and forth from the cell to the mixing chamber. Valve D was then closed, the sample cell replaced, and the spectrum of the reacting solution scanned from 220 to 400 mμ. Scanning was repeated at intervals set on a programming device. Because the reaction was slow, the change of temperature on mixing was of little account, since thermal equilibrium was restored well within the first half-life of the reaction.

Results

The spectrum of nitrobenzene in hydrogen fluoride displays a single maximum at 278 mμ, and that of *m*-dinitrobenzene a single maximum at 245 mμ. These maxima are at longer wave lengths than are the maxima of the two nitro compounds in water as solvent (nitrobenzene at 270 mμ,[21] *m*-dinitrobenzene at 242 mμ).[22] The red shift on going from water to hydrogen fluoride as solvent can be explained in terms of Nagakura and Tanaka's[23] theory that the absorption

(21) E. A. Garton, D. Robinson, and R. T. Williams, *Biochem. J.*, **50A**, 228 (1952).

(22) L. Doub and J. M. Vandenbelt, *J. Am. Chem. Soc.*, **71**, 2414 (1949).

(23) S. Nagakura and J. Tanaka, *J. Chem. Phys.*, **22**, 236 (1954).

of nitrobenzene is identified with a $\pi \rightarrow \pi^*$ transition, π-electron density migrating from the benzene ring to the nitro group upon excitation. If the nitro group is hydrogen-bonded to some acid species, then this charge migration will have already occurred to some extent in the ground state, leading to a narrower energy gap between ground and excited states and a subsequent "red shift" in the position of maximum absorption.

It may be asked if there is any evidence for protonation of nitrobenzene in HF as solvent. For instance, Brand[24] found that nitrobenzene absorbs at 285 mμ in 95% H_2SO_4, but protonates in oleums, the protonated species having a new, separate absorption at 350 mμ. Conductance measurements[25] indicate that nitrobenzene is hardly protonated in HF alone, and we have found that addition of NbF_5 to HF will cause the appearance of a new peak at *ca.* 340 mμ, as well as a peak at *ca.* 285 mμ, the former, by analogy with Brand's results, attributable to the protonated and the latter to the unprotonated form of nitrobenzene.

The spectral changes occurring in a kinetic experiment are illustrated in Figures 5 and 6 which present results obtained using a solution 1.364 *m* in NO_2BF_4 and originally *ca.* 10^{-4} *m* in nitrobenzene. As Figure 5 shows, the spectrum of nitrobenzene changes gradually to that of *m*-dinitrobenzene, the nitrobenzene peak at 278 mμ appearing to shift to shorter wave lengths and increase in height during the course of the reaction. When the absorbance at 245 mμ had reached the maximum value no further change was observed. In Figure 6 there is plotted *vs.* *t*, the time elapsed since mixing, either log $(A_\infty - A_t)$, where *A* is the optical density at 245 mμ (curve a), or log $(A_t - A_\infty)$, where *A* is the optical density at 300 mμ (curve b). The absorption spectrum was recorded at 5-min. intervals. The plot shows that the reaction is first order with respect to nitrobenzene. In subsequent experiments, the absorbance at 245 mμ alone was used as an indicator because of the greater change measured at this wave length. The first-order rate constants obtained are collected in Table I, and it will be seen that they decrease as the NO_2BF_4 concentration decreases.[26]

As the reaction becomes so slow at low concentrations of NO_2BF_4, a variant of Swinbourne's method[27] was used in these cases to estimate A_∞ without waiting for completion of the reaction. The suitability of this variant was tested on the run just discussed where $[NO_2BF_4] = 1.364$ *m*. Values of $A_{(t + \Delta t)}$ were plotted against values of A_t where Δt had values of 300 and 900 sec., and in each case the straight line which could be drawn through the A_t, $A_{(t + \Delta t)}$ point-pairs went through the point $A_t = A_{(t + \Delta t)} = A_\infty = 1.60$

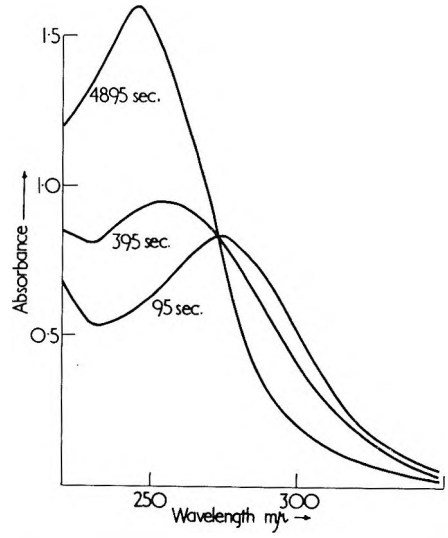

Figure 5. Changes in absorption spectrum during the nitration of nitrobenzene with 1.36 *m* NO_2BF_4–HF solution at 25°.

Table I: First-Order Rate Constants for the Nitration of Nitrobenzene with NO_2BF_4–HF Solutions

Molality of NO_2BF_4	k', sec.$^{-1}$	Half-lives for which followed
	At 25°	
1.45	1.39×10^{-3}	12
1.36	1.38×10^{-3}	10.5
1.07	8.71×10^{-4}	12
0.922	7.10×10^{-4}	8
0.666	3.67×10^{-4}	5
0.637	4.24×10^{-4}	10
0.502	2.27×10^{-4}	5
0.322	1.38×10^{-4}	3.5
0.191	6.95×10^{-5}	2.5
0.144	4.55×10^{-5}	1.2
0.115	5.48×10^{-5}	4
0.110	3.91×10^{-5}	3.5
0.077	2.76×10^{-5}	1.7
0.074	2.79×10^{-5}	4
0.046	1.81×10^{-5}	3.5
0.039	1.25×10^{-5}	2.3
0.018	5.44×10^{-6}	1
	At 12.5°	
1.24	2.76×10^{-4}	12
0.695	9.21×10^{-5}	8
0.441	4.50×10^{-5}	1.6
0.241	2.26×10^{-5}	3
0.110	9.06×10^{-6}	1.6

(24) J. C. D. Brand, *J. Chem. Soc.*, 997 (1950).

(25) L. Quarterman, H. H. Hyman, and J. J. Katz, *J. Phys. Chem.*, 65, 90 (1961).

(26) Quantities of *meta* and *para* isomer too small to affect the spectra significantly would have no effect on the rate constants since they would be formed in constant ratio to the *meta* isomer throughout any given run.

(27) J. Swinbourne, *J. Chem. Soc.*, 2371 (1960).

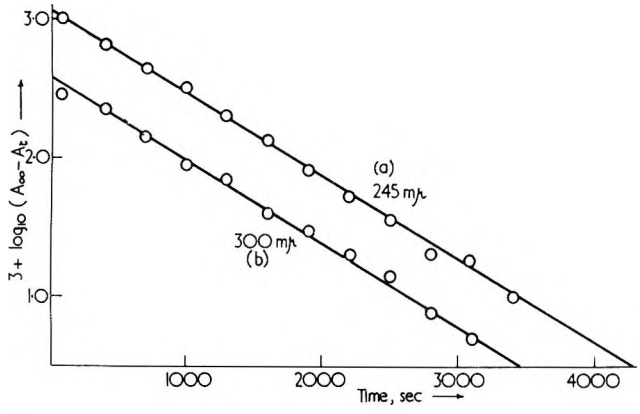

Figure 6. First-order plots for the nitration of nitrobenzene with 1.36 m NO_2BF_4–HF solution at 25°.

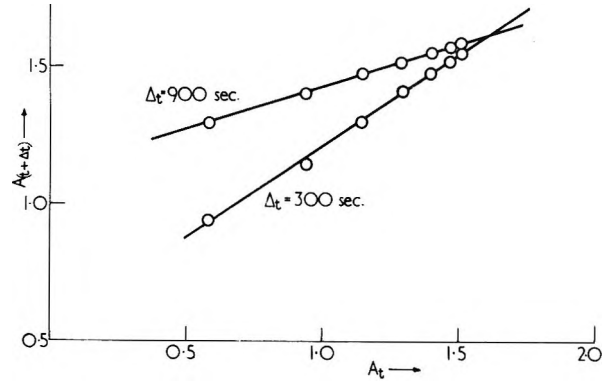

Figure 7. Swinbourne plots for the nitration of nitrobenzene with 1.36 m NO_2BF_4–HF solution at 25°.

(Figure 7). This value of A_∞ was in agreement with that actually observed, and the same was true of other runs used for test purposes. Thus Swinbourne's method is quite satisfactory for estimating A_∞ in our case, a proven first-order reaction. Another feature of Swinbourne's method is that the value of the first-order rate constant (which we designate as k') can be estimated directly from the plot of $A_{(t+\Delta t)}$ *vs.* A_t, which has a slope of $\exp(-k't)$. However, since the rate constant is very sensitive to small changes in slope, we used Swinbourne's method only to evaluate A_∞ and then made a plot, using all of the data, of log $(A_\infty - A_t)$ *vs.* t to obtain k'.

At 25° there are at hand nine values of k' for solutions more dilute than 0.2 m NO_2BF_4, and in Figure 8 it is shown that over this range the first-order constant is directly proportional, within experimental error, to $[NO_2BF_4]$; the line drawn is the least-squares line through the origin. The nitration is therefore of the first order with respect to each reactant, and since nitronium fluoroborate has been shown to be a strong electrolyte in anhydrous HF, the rate law may be written

$$-\mathrm{d}[\mathrm{PhNO_2}]/\mathrm{d}t = k[\mathrm{PhNO_2}][\mathrm{NO_2^+}] \qquad (1)$$

The second-order constant obtained from the slope of the line of Figure 8 is 3.68×10^{-4} 1000 g. of HF/mole sec. at 25°.

For the more concentrated NO_2BF_4 solutions, the values of the first-order constant lie above the continuation of the line of Figure 8, the curvature becoming more pronounced as $[NO_2BF_4]$ increases, and the second-order constant calculated from the individual points, $k = k'/[NO_2BF_4]$, increases threefold over the range of NO_2BF_4 concentration employed.

Since we are dealing with an ion–molecule reaction, the effect of increasing electrolyte concentration upon the rate constant would be given, according to the Brønsted equation, as

$$k = k_0 f_{\mathrm{PhNO_2}} f_{\mathrm{NO_2^+}} / f_{\pm} \qquad (2)$$

where k_0 is the second-order constant at infinite dilution in HF, and the f's are activity coefficients, $f_\pm$ being that for the critical complex or transition state, of charge +1. Setting

$$\ln f_{\mathrm{NO_2^+}} = -A\sqrt{\mu} + (b_{\mathrm{NO_2^+}})\mu$$

$$\ln f_{\pm} = -A\sqrt{\mu} + b_{\pm}\mu$$

$$\ln f_{\mathrm{PhNO_2}} = b_{\mathrm{PhNO_2}}\mu$$

where A is the proportionality constant of the limiting law of Debye and Hückel, and the b's are salting-out coefficients, we obtain

$$\log k = \log k_0 + b\mu \qquad (3)$$

where $b = \{b_{\mathrm{NO_2^+}} + b_{\mathrm{PhNO_2}} - b_\pm\}/2.3$.

If eq. 3 applies, a linear relationship should be found between the logarithm of the observed second-order constant and the ionic strength. The conformity of the data to (3) will be seen from Figure 9. Application of the method of least squares to all of the results except the four where foreign salts were added (for which see below) gives

$$(\text{at } 25°) \quad 4 + \log k = 0.527 + 0.347\mu \qquad (4)$$

$$(\text{at } 12.5°) \quad 5 + \log k = 0.865 + 0.383\mu \qquad (5)$$

The value of the second-order constant at infinite dilution is 3.36×10^{-4} 1000 g. of HF/mole sec. at 25° as calculated from (4), and 7.32×10^{-5} at 12.5° as calculated from (5); the former may be compared with 3.68×10^{-4} found from the dilute solution data alone (*cf.* Figure 8). There is fair agreement between the two values of k_0 at 25°, and since a positive electrolyte effect

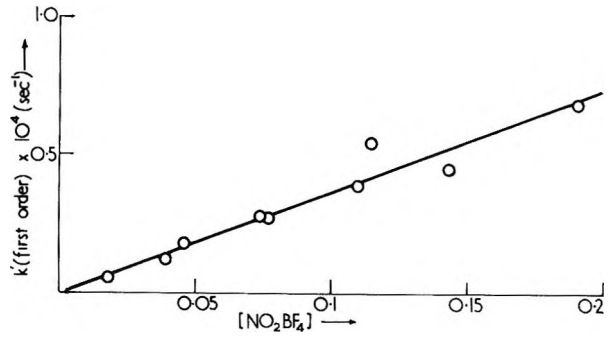

Figure 8. Variation of observed first-order nitration rate constant with nitronium salt concentration in dilute solution at 25°.

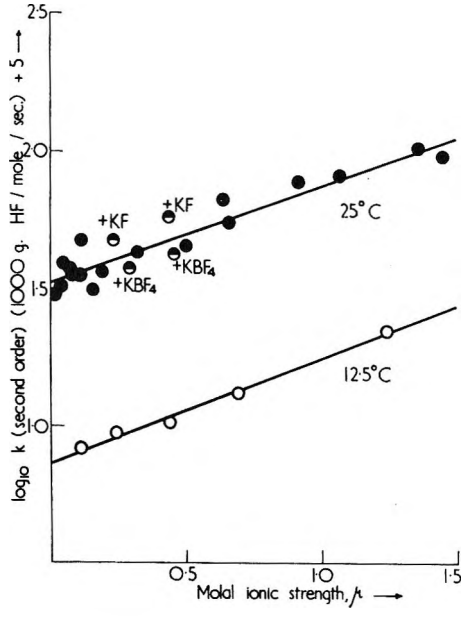

Figure 9. Variation of log k (second order) with ionic strength.

would tend to increase the slope of the line of Figure 8, the value obtained from eq. 4 is considered the more reliable. An error analysis[28] of the least-squares lines of eq. 4 and 5 yields a standard deviation in the rate constant at infinite dilution of 0.13×10^{-4} 1000 g. of HF/mole sec. at 25° and 0.25×10^{-5} at 12.5°.

A few experiments were performed to ascertain if increasing the ionic strength with an electrolyte other than NO_2BF_4 enhanced the rate of nitration. The results are given in Table II and are also shown in Figure 9. Table II shows that KBF_4 and KF both effect rate enhancement, and Figure 9 shows that NO_2BF_4, KBF_4, and KF effect roughly similar degrees of enhancement. These results confirm our supposition that the increase in the second-order rate constant with increase in NO_2BF_4 concentration was an electrolyte effect.

Table II: Effect of KBF_4 and KF on Rate of Nitration

Salt medium	Ionic strength	10^4k at 25°, 1000 g. of HF/mole sec.
0.110 m NO_2BF_4	0.110	3.55
0.110 m NO_2BF_4 + 0.180 m KBF_4	0.290	3.72
0.110 m NO_2BF_4 + 0.340 m KBF_4	0.450	4.10
0.115 m NO_2BF_4	0.115	4.77
0.115 m NO_2BF_4 + 0.095 m KF	0.210	4.82
0.115 m NO_2BF_4 + 0.219 m KF	0.434	5.81

Since measurements have been made at two temperatures and the rate constants at each temperature fitted to a linear function, we can calculate the activation parameters shown in Table III. Standard deviations[28] are given in the table for the parameters calculated from the rate constants at infinite dilution.

Table III: Calculated Activation Parameters

μ	E_a, kcal./mole	ΔH^* at 25°, kcal./mole	log A, 1000 g. of HF/mole sec.	ΔS^*, e.u.
0	20.8 ± 0.7	20.2 ± 0.7	11.77 ± 0.53	−6.6 ± 2.5
1.0	19.6	19.0	11.22	−9.1

Discussion

Our results may be compared directly with those of Ciaccio and Marcus[12] for the nitration of nitrobenzene with NO_2BF_4 in some different solvents at 25°. In all of the cases listed in Table IV, the reaction was of the first order with respect to nitrobenzene and with respect to NO_2BF_4. Although different scales of concentration were used by Ciaccio and Marcus and by us, the value of the second-order constant given for the nitration in HF is that at infinite dilution, and since the density of anhydrous HF is not far from 1 g./ml, the comparison is valid. The main points of difference between our results and those of Ciaccio and Marcus are that their rate constants are greater than ours, and that they find no salt effect. This latter result is perhaps due to the fact that in all cases their salt concentration is below 0.3 M. In the previous section we noted that below a 0.2 m concentration of nitronium fluoroborate we could obtain a second-order rate con-

(28) Y. Beers, "Introduction to the Theory of Errors," 2nd Ed., Sections V and VI, Addison-Wesley, Reading, Mass., 1957.

stant of 3.68×10^{-4} at 25° essentially invariant with salt concentration from 0.02 to 0.2 *m*.

Table IV: The Rate of Nitration of Nitrobenzene with NO_2BF_4 in Various Solvents at 25°

Solvent	Range of concn.[a,b] NO_2BF_4	Range of concn.[a,b] $PhNO_2$	k, M^{-1} sec.$^{-1}$ or m^{-1} sec.$^{-1}$
CH_3SO_3H[a]	0.05–0.15	0.004–0.02	1.8×10^{-2}
H_2SO_4, 0.12 *M* in H_2O[a]	0.05–0.3	0.004–0.02	7.7×10^{-3}
H_2SO_4, 0.18 *M* in SO_3[a]	0.05–0.1	0.004–0.01	5.3×10^{-3}
CH_3CN[a]	0.1–0.2	0.02–0.04	1.8×10^{-3}
HF[b]	0.02–1.45	*ca.* 10^{-4}	3.36×10^{-4}

[a] See ref. 12; concentrations in moles/liter. [b] Present work; concentrations in moles/1000 g. of HF.

In order to explain our lower rate constant we shall refer to our activation parameters. Ciaccio and Marcus found that the rate of nitration of nitrobenzene using mixed nitric–sulfuric acid was almost identical with that obtained using nitronium fluoroborate dissolved in sulfuric acid, and that it was in very good agreement with results of Martinsen's for mixed acids. Now Martinsen found, for 100% sulfuric acid as solvent, that the second-order rate constant for the nitration of nitrobenzene was 6.67×10^{-3} l./mole sec. at 25° and 6.67×10^{-4} at 0°, giving $E_a = 15.0$ kcal./mole, $A = 5.73 \times 10^8$, $\Delta H^* = 14.4$ kcal., and $\Delta S^* = -20.3$ e.u. Thus the nitration of nitrobenzene has a lower heat of activation in sulfuric acid than it has in hydrofluoric acid, but a more unfavorable entropy of activation. Obviously, since the reaction is faster in sulfuric acid, the enthalpy factor is predominant. An explanation for this could perhaps lie in both the nitronium ion and nitrobenzene being more solvated in hydrofluoric acid than they are in sulfuric acid—a reasonable assumption in view of the much smaller size of the hydrogen fluoride molecule. Then in hydrofluoric acid there will be more solvent molecules to push aside before the transition state is formed, accounting for the higher energy of activation. At the same time, during the formation of the transition state more solvent molecules will be liberated, accounting for the more favorable entropy of activation in hydrogen fluoride. Increasing the ionic strength of the nitrating system will tend to take solvent molecules away from the reacting species and should therefore promote the reaction by lowering the activation enthalpy, though making the entropy factor more unfavorable. Both effects are indeed observed, as Table III shows.

Our finding that potassium fluoride and fluoroborate cause similar rate enhancements is interesting and points a way to prove that proton loss is or is not rate-determining during a reaction carried out in hydrogen fluoride as solvent. If proton loss were rate-determining, then potassium fluoride would cause a marked acceleration, more marked than potassium fluoroborate, since the latter is a neutral salt whereas the former is a strong base in the hydrogen fluoride solvent.[7] The fact that in our system about equal small enhancements are shown by both salts indicates that proton loss is not rate-determining in nitration, in agreement with others' experiments.[29,30]

A reading of some physical chemistry textbooks would seem to indicate that salts have little or no effect upon ion–molecule reactions. However, this is not the case in certain instances, *e.g.*, the hydrogen ion catalyzed hydrolysis of acetals. It is true that this is not an ion–molecule reaction in our sense, but involves a pre-equilibrium transfer of a proton to the substrate followed by the rate-determining breakdown of the protonated species,[31] but for such a reaction the Brønsted equation has the same form as for an ion–molecule reaction and so comparison is permissible. As the ionic strength was increased to 0.2 by addition of KCl in the hydrolysis of diethyl acetal, at 0°, Riesch and Kilpatrick[32] found the second-order rate constant to increase by 25% over the value at $\mu = 0$. As the ionic strength was increased to 0.2 we found the second-order constant for the nitration of nitrobenzene by NO_2BF_4, at 12.5°, to increase by 20% over the value at $\mu = 0$ in the high-dielectric solvent hydrogen fluoride.

Acknowledgments. This research was supported in part by a grant from the Petroleum Research Fund administered by the American Chemical Society. Grateful acknowledgment is hereby made to the donors of the fund. J. G. J. is also grateful to Illinois Institute of Technology for the award of a fellowship for 1961–1962.

(29) L. Melander, *Arkiv Kemi*, **2**, 213 (1950).

(30) W. M. Lauer and W. E. Noland, *J. Am. Chem. Soc.*, **75**, 3689 (1953).

(31) M. Kilpatrick, *ibid.*, **85**, 1036 (1963).

(32) L. C. Riesch and M. Kilpatrick, *J. Phys. Chem.*, **39**, 561 (1935)

The Integrated Absorption Intensity of the C=O Stretching Band of Carbon-13-Labeled Benzoic Acid

by S. Pinchas

The Weizmann Institute of Science, Rehovoth, Israel *(Received December 28, 1964)*

The integrated absorption intensity in the C=O stretching region of a very dilute chloroform solution of a sample of about 50% C^{13}-benzoic acid was measured in comparison with the corresponding intensity of normal benzoic acid. The small decrease observed in this integrated absorption is within the experimental error of the theoretically expected value. The reason for the different effect of C^{13} and O^{18} on the C=O band intensity of monomeric benzoic acid is discussed.

Introduction

The estimation of the integrated absorption intensity of various $X=O^{18}$ stretching bands (X = C, P, S, As) in comparison with the absorption intensity of the corresponding $X=O^{16}$ bands has recently been carried out for a number of compounds of various classes.[1-9] It has thus been observed that substituting O^{18} for O^{16} in the X=O group usually changes the absorption intensity of the X=O stretching band by 10–80%. This quite appreciable difference in intensity is rather unexpected, especially since it has been shown, in the case of O^{18} phosphorus oxychloride, not to be compensated by some opposite change in the intensity of another band which belongs to the same species.[10]

Theoretically the sum, $\Sigma A_i/\omega_i^2$, where A_i is the integrated absorption of the ith band of *this* species (A_1) and ω_i is its zero-order frequency, should be an isotopic invariant[11] of phosphorus oxychloride. Hence, since the difference between the $P=O^{16}$ and $P=O^{18}$ stretching frequency in this case is only about 3%, the theoretically expected decrease in the integrated absorption of the $P=O^{18}$ stretching band of a carbon tetrachloride solution of $PO^{18}Cl_3$ amounts to 5–10% while it was observed to be about 24% of the absorption intensity of the corresponding $P=O^{16}$ band.[10]

In the case of monomeric benzoic acid dissolved in chloroform also, the observed decrease in the integrated absorption intensity of the $C=O^{18}$ stretching band,[3] relative to its corresponding $C=O^{16}$ value, is about 10% while the expected difference between these intensities seems to be only 2–4%.

It thus appeared worthwhile to investigate whether this phenomenon is limited only to oxygen-18-labeled compounds or whether it is also shown by molecules labeled with other isotopic elements, *e.g.*, carbon-13, when these form doubly bonded groups. The integrated absorption intensity in the C=O stretching region of the commercially available, *ca.* 50 atom % C^{13}-benzoic acid, in comparison with the intensity of the normal acid, was therefore measured.

Experimental

The labeled benzoic acid sample was a product of the Isotopic Specialties Co., Burbank, Calif., claimed to possess a carbon-13 enrichment of 55–58 atom % and a purity of 99%.

The normal benzoic acid used was a British Drug House highest purity product. The infrared absorption measurements were carried out with a Beckman IR-7 spectrophotometer equipped with the linear ab-

(1) M. Halman and S. Pinchas, *J. Chem. Soc.*, 3264 (1958).
(2) S. Pinchas, D. Samuel, and M. Weiss-Broday, *ibid.*, 1688 (1961).
(3) S. Pinchas, D. Samuel, and M. Weiss-Broday, *ibid.*, 2382 (1961).
(4) S. Pinchas, D. Samuel, and M. Weiss-Broday, *ibid.*, 2666 (1961).
(5) S. Pinchas, D. Samuel, and M. Weiss-Broday, *ibid.*, 3063 (1961).
(6) S. Pinchas, D. Samuel, and M. Weiss-Broday, *ibid.*, 3968 (1962).
(7) A. Lapidoth, S. Pinchas, and D. Samuel, *ibid.*, 1128 (1963).
(8) J. Bernstein, M. Halmann, S. Pinchas, and D. Samuel, *ibid.*, 821 (1964).
(9) I. Laulicht and S. Pinchas, *Israel J. Chem.*, 1, 404 (1963).
(10) I. Laulicht, S. Pinchas, D. Sadeh, and D. Samuel, *J. Chem. Phys.*, 41, 789 (1964).
(11) B. Crawford, Jr., *ibid.*, 20, 977 (1952).

sorbance attachment, using a slit of about 0.3 mm. (corresponding in this region to an optical slit width of *ca.* 0.9 cm.$^{-1}$). The absorbance of an 0.06–0.09 g./l. of chloroform solution of each benzoic acid modification was recorded *vs.* wave number in the 1630–1800-cm.$^{-1}$ region using a 2-cm. thick cell and a scale of 10 cm.$^{-1}$/in. The measurements were made against an iron screen (since the transmission of the pure solvent under these conditions was only about 15%) after the absorbance of the pure solvent in the same cell had been recorded first, similarly, on the same chart paper. Each measurement was usually made in duplicate, its mean value being taken into account. These measurements were repeated at least twice for each modification, on independent solutions.

The estimation of the integrated absorption intensity of a sample in this region was carried out by weighing the chart paper enclosed between the respective absorbance curve of the solution and that of the pure solvent and comparing this weight with that of a rectangle of this paper of known dimensions.

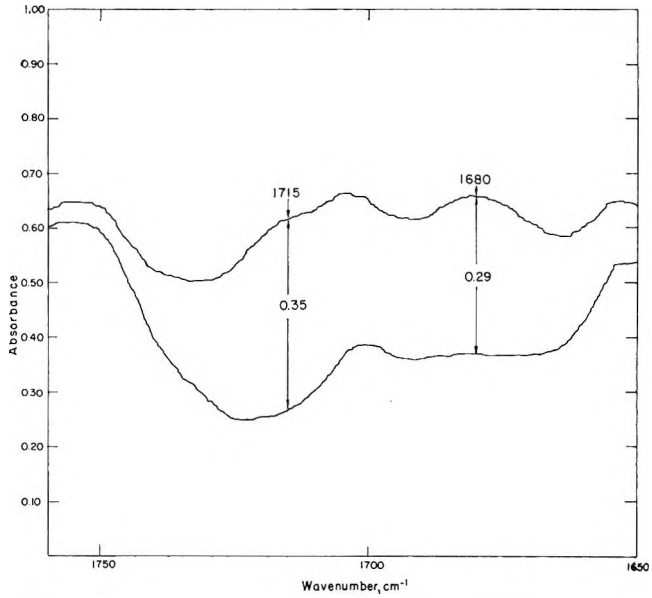

Figure 1. The absorbance of a 0.090-g./l. solution of C^{13}-labeled benzoic acid in chloroform. The upper curve represents the absorbance of the solution in a 2-cm. cell against an iron screen. The lower curve gives the absorbance of the pure chloroform under these conditions.

Results and Discussion

Since benzoic acid remains in the associated form down to quite dilute chloroform solutions,[3] very low concentrations had to be used to obtain its dissociation (0.06–0.09 g./l.); these, however, were suitable only for the observing of the very strong C=O stretching bands but not for the investigation of the whole monomeric benzoic acid spectrum.

The single normal benzoic acid band at[3] 1715 cm.$^{-1}$ was observed to be replaced in the case of the C^{13}-labeled benzoic acid by a doublet. Its somewhat stronger branch, due to the normal benzoic acid content of the labeled sample, appeared at the normal position of 1715 cm.$^{-1}$ while the other branch, due to the C^{13}-benzoic acid, was located at 1680 cm.$^{-1}$ (see Figure 1). That the 1715-cm.$^{-1}$ branch was observed to be stronger than that at 1680 cm.$^{-1}$ seems to suggest that the real enrichment of the sample used for this investigation was somewhat lower than 50 atom % C^{13}, *i.e.*, about 10% less than the enrichment claimed by its supplier.

Beer's law was checked for the normal monomeric benzoic acid and shown to hold within a few per cent for a 100% change in concentration. It is interesting to note that the isotopic shift brought about by the C^{13} labeling of monomeric benzoic acid dissolved in chloroform, equal to 35 cm.$^{-1}$, is appreciably larger than that due to the labeling of benzoic acid with O^{18}, which amounts only[3] to 27 cm.$^{-1}$ for chloroform solutions and 32 cm.$^{-1}$ for carbon tetrachloride solutions. Theoretically, however, one would expect the reverse phenomenon to occur since, assuming Hooke's law to hold, the calculated isotopic shift of a diatomic CO molecule with a 1715-cm.$^{-1}$ stretching frequency is 41 cm.$^{-1}$ for O^{18} labeling[12] but only 38 cm.$^{-1}$ for C^{13} labeling. The close agreement between the last value and the one observed here (35 cm.$^{-1}$) supports the application of Hooke's law in this case.

The half-width of the C^{12}=O stretching band of benzoic acid has now been found to be only 42 cm.$^{-1}$ as compared with the value of 49 cm.$^{-1}$ reported for it previously.[3] This discrepancy is probably to be attributed to the much better resolution of the double monochromator used in this study as compared with that of the ordinary monochromator used in the previous investigation. However, this half-width is still too large, compared with the isotopic shift, to allow an exact estimation of the integrated absorption of each isotopic band separately, from the absorbance curves of an isotopic mixture. The integrated absorption intensity in the *whole* region between 1630 and 1800 cm.$^{-1}$ was therefore estimated for each of the two isotopic samples. The absorption of both these samples beyond these limits is negligible and, in the case of the 1630-cm.$^{-1}$ limit, also not amenable to measurement because of the neighboring 1600-cm.$^{-1}$ absorption band of the chloroform.

The results of these estimations are given in Table I. The experimental errors indicated in the table are

(12) M. Halmann and S. Pinchas, *J. Chem. Soc.*, 1703 (1958).

Table I: The Integrated Absorption Intensity of the Monomeric Isotopic Benzoic Acids in the 1630–1800-Cm.$^{-1}$ Region

Material	Concn., g./l.	Integrated absorption intensity, l. mole^{-1} cm.$^{-2}$
Normal	0.069	17,700
Normal	0.060	18,000
	Mean	17,850 ± 150
Labeled	0.090	17,200
Labeled	0.079	17,250
	Mean	17,200 ± 150
	Difference of means	650 ± 250

the estimated random errors. The possible systematic error is no doubt larger but is not relevant for this study, provided that it is the same for both samples. Table I shows that the difference between the integrated absorption intensity of the normal benzoic acid and that of the *ca.* 50% C^{13}-benzoic acid, in the C=O stretching region, is only 3.6 ± 1.4%.

Benzoic acid monomer belonging to the C_s point group does not fulfil Crawford's conditions,[11] for the invariance of the $\Sigma A_i/\omega_i^2$ sum, for any of its species (since both its A' and its A'' species contain rotations that change the dipole moment of the molecule). It seems however that, since the difference in the moment of inertia between the two isotopic benzoic acids, in respect to every axis of rotation, is small, one can ignore its effect on the intensity of the absorption bands of C^{13}-benzoic acid.

On the other hand, the close agreement between the observed isotopic shift of 35 cm.$^{-1}$ and the value of 38 cm.$^{-1}$, calculated for the expected difference between the C^{12}=O and C^{13}=O stretching frequencies, seems to suggest that the C=O stretching vibration of monomeric benzoic acid is practically limited only to the carbonylic group. Hence, it appears that the change in the intensities and frequencies of the other A' bands of benzoic acid, as a result of labeling it with C^{13}, can also be neglected.

The integrated absorption intensity of the C=O stretching band of C^{13}-benzoic acid may thus still be expected to be approximately related to the corresponding absorption of the normal acid as the squares of the respective frequencies. Since the enrichment of the labeled sample was only about 50%, one therefore gets for the calculated intensity ratio in this case $A_1/A = (1715^2 + 1680^2)/(2 \times 1715^2) = 0.98$.

The observed decrease in the integrated absorption of the *ca.* 50% C^{13}-labeled benzoic acid sample of 3.6 ± 1.4% is thus in rough agreement with the calculated value of about 2% for this sample when due allowance is made for the approximations made during its calculation.

One therefore concludes that, while O^{18} seems to decrease the C=O band absorption of a chloroform solution of monomeric benzoic acid appreciably more than anticipated on the basis of Crawford's sum rule, C^{13} behaves practically as expected. The difference between the isotopic shift of 27 cm.$^{-1}$ for the C=O frequency of O^{18}-benzoic acid in chloroform solution and that of 35 cm.$^{-1}$ for the corresponding C^{13} benzoic acid (although both are calculated to be about 40 cm.$^{-1}$) seems relevant here. This difference appears to support the assumption that the hydrogen bonding between the benzoic acid C=O group and the chloroform molecules is weaker in the case of the C=O^{18} group, relative to that of the C=O^{16} group,[3] since the C=O^{18} isotopic shift would then be expected to be partly counterbalanced by the decrease in hydrogen bonding of the C=O^{18} group. If this is really the case and the C=O^{18} group interaction with the chloroform solvent is in fact weaker than that of the C=O^{16} group, one would also anticipate the integrated absorption intensity of the C=O^{18} stretching band of O^{18}-benzoic acid to be lower from the value expected for it (from the absorption intensity of the *n*-benzoic acid and the difference in the isotopic frequencies) since it is well known that hydrogen bonding increases considerably the integrated absorption intensity of the hydrogen-bonded C=O group of benzoic acid.[13]

In the case of the C^{13}=O^{16} group, however, no such decrease in the strength of the hydrogen bonding to the chloroform solvent seems reasonable. Hence, it appears that the observed difference between the effect of C^{13} and O^{18} on the integrated absorption intensity of the benzoic acid C=O stretching band can be rationalized.

It must be added, however, that no explanation for the existence of such a difference in the hydrogen bond strength of the isotopic C^{12}=O groups can as yet be offered, nor can such a difference in the interaction of the various isotopic X=O groups with the solvent explain all the anomalous data observed so far in this respect.[1-10] It is, *e.g.*, difficult to see how the P=O stretching band intensity of a cyclohexane solution of O^{18} phosphorus oxychloride can be affected materially by a difference in the very weak interaction of the isotopic P=O groups with the solvent.[10] It thus seems more logical to look for some common origin which is at

(13) C. N. R. Rao, "Chemical Applications of Infrared Spectroscopy," Academic Press, New York, N. Y., 1963, p. 209.

the bottom of both the different solvent interaction with the X=O^{18} group and the appreciably different absorption intensities for the X=O^{18} stretching bands.

Acknowledgment. The loan of a Beckman IR-7 spectrophotometer by the National Heart Institute, National Institutes of Health, Bethesda, Md., is gratefully acknowledged. The author also wishes to thank Mr. Joseph Goldberg for technical assistance with the measurements.

The Infrared Absorption of Oxygen-18-Labeled Phenol

by S. Pinchas, D. Sadeh, and D. Samuel

The Weizmann Institute of Science, Rehovoth, Israel *(Received January 28, 1965)*

The absorption spectra of dilute solutions of normal and 74 atom % O^{18}-phenol have been measured in the 4000–220-cm.$^{-1}$ region. A number of hitherto controversial or doubtful assignments of normal phenol bands are examined critically in the light of the results of these measurements. The origin of a number of bands, belonging to monomeric normal phenol and as yet unreported in the literature, is discussed. It was observed that the integrated absorption intensity of the monomeric phenolic O^{18}–H group stretching band is about 20% lower than that of the corresponding O^{16}–H band although the difference in frequency between them is (in agreement with theory) only about 0.3%.

Although the infrared absorption spectra of phenol and deuterated phenol have already been studied, analyzed, and reported several times,[1-6] the assignments of five of their normal vibrations are still in some doubt.[4] Thus, *e.g.*, while Green[2] attributes the 1344-cm.$^{-1}$ band (and a shoulder at 1322 cm.$^{-1}$) observed for a carbon tetrachloride solution of phenol to a Fermi resonance between the combination 502 + 825 = 1327 cm.$^{-1}$ and the ν_{C-C} fundamental (originally at about 1333 cm.$^{-1}$), Wilmshurst and Bernstein[7] assign this fundamental, in the case of toluene, to a band at 1155 cm.$^{-1}$ and Fuson, *et al.*,[8] to a band at 1494 cm.$^{-1}$. Evans,[6] on the other hand, assigns the 1344-cm.$^{-1}$ band of dissolved phenol to a ν_{C-C} mode of vibration with an in-plane O–H bending character.

Also, while Jakobsen[4] attributes the out-of-plane O–H bending fundamental of phenol dissolved in polar solvents to a weak band at about 664 cm.$^{-1}$, the exact location of this vibration in the case of nonpolar solvents is not known.[6]

It has thus been interesting to measure the infrared absorption spectrum of dilute nonpolar solutions of highly enriched (monomeric) O^{18}-phenol, in comparison with similar solutions of normal phenol, in the 4000–220-cm.$^{-1}$ region. Similar measurements were found to be very helpful in the assignment of fundamentals of other oxygen-containing molecules.[9,10] The investigation of the infrared spectrum of O^{18}-phenol seems also

(1) M. Davies and R. L. Jones, *J. Chem. Soc.*, 120 (1954).

(2) J. H. S. Green, *ibid.*, 2236 (1961).

(3) R. Mecke and E. Greinacher, *Z. Elektrochem.*, **61**, 530 (1957).

(4) R. J. Jakobsen, U. S. Department of Commerce, Office of Technical Services, Publication Board Report, 171, 342 (1960).

(5) J. M. Lebas, *J. chim. phys.*, **59**, 1072 (1962).

(6) J. C. Evans, *Spectrochim. Acta*, **16**, 1382 (1960).

(7) J. K. Wilmshurst and H. J. Bernstein, *Can. J. Chem.*, **35**, 911 (1957).

(8) N. Fuson, C. Garrigon-Lagrange, and M. L. Josien, *Spectrochim. Acta*, **16**, 106 (1960).

(9) S. Pinchas, D. Samuel, and M. Weiss-Broday, *J. Chem. Soc.*, 3968 (1962).

Table I: The Absorption Bands of O^{18}- and Normal Phenolic Solutions in the 4000–220-Cm.$^{-1}$ Region

Material	Solvent	Cell thickness, mm.	Concn., g./ml.	Bands, cm.$^{-1}$
Normal	CCl_4	0.2	0.010	3620 (37), 3500 (b, 77), 3108 (sh), 3076 (80), 3046 (71), 3024 (80)
Labeled	CCl_4	0.2	0.011	3610 (39), ~3500 (b, 66), 3077 (69), 3047 (67), 3022 (70)
Normal	CCl_4	1.0	0.006	2950 (vw), 1606 (sh), 1598 (27), 1502 (29), 1472 (31), 1389 (sh), 1344 (27), 1333 (sh), 1313 (vw), 1256 (27), 1182 (8), 1168 (sh), 1152 (24)
Labeled	CCl_4	1.0	0.009	1606 (sh), 1598 (25), 1500 (21), 1480 (20), 1455 (29), 1412 (43), 1342 (30), 1330 (28), 1302 (vw), 1250 (b, 19), 1180 (5), 1155 (sh), 1133 (vw), 1112 (sh)
Normal	CCl_4	0.4	0.019	1072 (46), 1052 (vw, sh), 1026 (51), 1000 (vw), 973 (vw), 884 (52)
Labeled	CCl_4	0.4	0.019	1085 (sh), 1071 (33), 1048 (33), 1028 (sh), 1000 (sh), 974 (b, 34), 918 (34), 884 (vw)
Normal	C_6H_{12}	0.4	0.010	1071 (28), 1044 (28), 1027 (sh), 1000 (41), 971 (vw), 910 (48)
Labeled	C_6H_{12}	0.4	0.012	1070 (35), 1046 (24), 1026 (sh), 1000 (sh), 950 (52), 910 (48)
Normal	C_6H_{12}	0.4	0.010	827 (49), 812 (33), 751 (2), 688 (10)
Labeled	C_6H_{12}	0.4	0.012	841 (43), 823 (vw), 802 (32), 751 (20), 716 (vw), 688 (35)
Normal	CCl_4	0.5	0.085	608 (33), 536 (35), 510 (29), 458 (65), 415 (61)
Labeled	CCl_4	0.5	0.088	604 (16), 574 (19), 530 (31), 506 (25), 416 (61)
Normal	C_6H_{12}	2	0.013	400 (42), 320 (7), 272 (32), 252 (48), 235 (57), 226 (48)
Labeled	C_6H_{12}	2	0.010	389 (52), 315 (13), 277 (31), 253 (40), 233 (54), 224 (59)

to be of importance in connection with the problem of the qualitative and quantitative analysis of labeled phenol.

The infrared absorption of dilute carbon tetrachloride or cyclohexane solutions of *ca.* 74 atom % O^{18}-phenol was therefore measured in comparison with similar solutions of normal phenol, the results of these measurements being reported here.

Results

The frequencies of the absorption bands observed for the two isotopic modifications of phenol are collected in Table I. The per cent transmission is usually added in parentheses after the corresponding frequency. All the solutions used for the measurements reported in Table I, except their most concentrated representatives of *ca.* 0.085 g./ml., can be seen from Table I to be preponderantly monomeric since this table reports no appreciable band which can be attributed to a stretching of a hydrogen-bonded OH group. The very weak and broad absorption observed, however, for 0.01-g./ml. solutions at about 3500 cm.$^{-1}$ seems to be due to traces of dimeric OH groups in equilibrium with the great excess of monomeric phenol OH groups. The *ca.* 0.08-g./ml. solutions, on the other hand, showed a strong hydrogen-bonded OH stretching band and only a medium, free OH stretching band; hence these solutions are mainly nonmonomeric. They had to be used, however, since the bands in the 670–400-cm.$^{-1}$ region are relatively weak and the absorption of the solvent in this vicinity makes it very difficult to work with a cell thickness of over 0.5 mm.

The results reported in Table I for normal phenol dissolved in carbon tetrachloride agree generally well with those reported in the literature, *e.g.*, by Green.[2] However, the O–H stretching frequency of 3620 cm.$^{-1}$ reported in Table I seems to be more accurate than the value of 3612 cm.$^{-1}$ reported earlier.[2]

No real band was observed at about 1220 cm.$^{-1}$ for a dilute carbon tetrachloride solution of normal phenol; the strong 1220-cm.$^{-1}$ band reported for it by Green[2] seems thus to be either a misprint or a mistake. Evans[6] and Jakobsen[4] also did not observe such a band for dissolved phenol, neither is such an absorption shown by phenol vapor.[4,6]

The 608-cm.$^{-1}$ frequency, given in Table I for a solution of normal phenol in carbon tetrachloride, is somewhat lower than the corresponding values given by Green[2] (617 cm.$^{-1}$) and Jakobsen[4] (616 cm.$^{-1}$). The respective value for the phenol vapor is, however,[2] 591 cm.$^{-1}$. The 536-cm.$^{-1}$ frequency, on the other hand, is appreciably higher than the 526-cm.$^{-1}$ value reported by Green[2] although it is quite near to the 530-cm.$^{-1}$ frequency reported by Evans.[6]

The 400- and 320-cm.$^{-1}$ values for a cyclohexane solution of normal phenol agree, on one hand, with the 404- and 398-cm.$^{-1}$ frequencies reported by Evans[6] for dissolved and vaporized phenol, respectively, and on the other with the ~300-cm.$^{-1}$ value estimated for phenol solution and the 306-cm.$^{-1}$ frequency observed for phenol vapor.[6]

(10) S. Pinchas, D. Samuel, and B. L. Silver, *Spectrochim. Acta*, **20**, 179 (1964).

The bands reported in Table I at 272, 252, and 226 cm.$^{-1}$ seem to have been unobserved before (although Jakobsen[4] reports a very strong and broad absorption for the vapor phase, below 300 cm.$^{-1}$).

Discussion

As is apparent from Table I the isotopic exchange of O^{16} for O^{18} in phenol brings about a decrease of 10 cm.$^{-1}$ in the stretching frequency of the free OH group. This value compares very well with the value calculated for this shift on the assumption that this stretching affects practically only the OH group (this being a very close approximation to reality since this frequency is quite isolated from the other bond stretchings of the phenol molecule).

With Hooke's law holding, ν_i, the O^{18}–H stretching frequency is then equal to $\nu(\mu/\mu_i)^{1/2}$ where ν is the O^{16}–H stretching frequency of monomeric normal phenol (3620 cm.$^{-1}$) and μ and μ_i are the reduced masses of O^{16}–H and O^{18}–H, respectively. This gives $\nu_i = 3620 \times (304/306)^{1/2} = 3608$ cm.$^{-1}$, and a shift of 12 cm.$^{-1}$ as compared with the observed value of 10 ± 2 cm.$^{-1}$.

When the graphically integrated absorption intensity of the phenolic O^{18}–H stretching band, between the 3500- and 3700-cm.$^{-1}$ limits, was compared with the corresponding value for the O^{16}–H band, it was observed that the former is lower by about 24% for a carbon tetrachloride solution and by *ca.* 18% for a cyclohexane solution, as can be seen from Table II (which gives the results obtained from measurements made mainly in an 0.0414-cm. cell). The two results for the labeled phenol in carbon tetrachloride which were made in two different cells are not fully comparable since the (original) nominal cell thickness in each case might have changed by the time the measurements were carried out.

The fact that in the case of O^{18}-phenol also, as in many cases of $X{=}O^{18}$ compounds[11,12] the integrated absorption intensity of the XO^{18} stretching band is, unexpectedly, appreciably different from the intensity of the corresponding XO^{16} band, is especially interesting since this shows that this phenomenon is not limited to multiple-bonded XO groups only, as thought previously,[12] but is shared by single-bonded XO groups as well.

This phenomenon is even more unexpected in this case, as a result of the very small difference between the stretching frequencies of the isotopic OH groups which amounts only to 0.3% of their values as compared with a difference of about 20% in the corresponding integrated absorption intensities.

The value for the integrated absorption intensity of the OH band of monomeric normal phenol (in CCl_4) calculated on the basis of its molar absorbancy index and its half-width by Forel, Leicknam, and Josien[13] (1350 ± 100) seems to be in error by a factor of 10 if natural logarithms were used for this calculation (230 × 17 × $\pi/2$ × 2.3 = 13,800). Our values for the molar absorbancy index and half-width of this band are, however, only a little different, being 185 ± 10 l. mole^{-1} cm.$^{-1}$ and 18 cm.$^{-1}$, respectively, as compared with 230 l. mole^{-1} cm.$^{-1}$ and 17 cm.$^{-1}$, reported by Forel, *et al.*[13]

Table II: The Relative Integrated Absorption Intensity of the Isotopic Phenolic O–H Stretching Bands

Material	Concn., g./l.	Solvent	Integrated intensity, l. mole^{-1} cm.$^{-2}$
Normal	4.90	CCl_4	5390
Normal	6.12	CCl_4	5220
		Mean	5300 ± 100
Labeled	5.06	CCl_4	4050 ± 200
Labeled[a]	4.03	CCl_4	4400
Normal	6.44	C_6H_{12}	5540
Normal	6.66	C_6H_{12}	5540
		Mean	5540 ± 100
Labeled	5.85	C_6H_{12}	4700
Labeled	8.55	C_6H_{12}	4300
		Mean	4500 ± 200

[a] In a 1.02-mm. cell.

The normal phenol band which appears at 1472 cm.$^{-1}$ appears for the labeled phenol as a doublet band at about 1480 and 1455 cm.$^{-1}$. This doublet absorption seems to be the result of a Fermi resonance between the 1472 cm.$^{-1}$ b_1 ring stretching (which by itself should be practically unaffected by the O^{18} labeling) and the 1250 + 224 cm.$^{-1}$ combination of the labeled phenol which, originally, has probably also a frequency of about 1470 cm.$^{-1}$.

The frequency of the 1344-cm.$^{-1}$ band and the 1333-cm.$^{-1}$ shoulder (observed by Green[2] at 1322 cm.$^{-1}$, but reported by Evans[6] at 1332 cm.$^{-1}$ and by Table I at 1333 cm.$^{-1}$) of normal phenol is practically unchanged in the case of the O^{18}-phenol (1342 and 1330 cm.$^{-1}$). This proves that Green's interpretation[2] of the 1344 and 1333-cm.$^{-1}$ absorptions as due to a Fermi resonance between a $\nu_{C-C} \sim 1333$ cm.$^{-1}$ fundamental and a 502 + 825 cm.$^{-1}$ combination (according

(11) I. Laulicht, S. Pinchas, D. Sadeh, and D. Samuel, *J. Chem. Phys.*, **41**, 789 (1964).

(12) J. Bernstein, M. Halmann, S. Pinchas, and D. Samuel, *J. Chem. Soc.*, 821 (1964).

(13) M. T. Forel, J. P. Leicknam, and M. L. Josien, *J. chim. phys.*, **57**, 1103 (1960).

to Table I this must be the 510 + 827 cm.$^{-1}$ combination), is improbable since in the O^{18}-phenol case the lower bands appear at 506 and 841 cm.$^{-1}$, respectively. Their sum is therefore higher by 10 cm.$^{-1}$ than the sum of the O^{16}-phenol frequencies while the ν_{C-C} frequency is probably the same in both cases. Hence, were Green's assumption right, the Fermi resonance in the O^{18}-phenol case would have been much weaker than in the O^{16}-phenol case and the resulting doublet would then have been moved to about 1350 and 1335 cm.$^{-1}$, instead of appearing at 1342 and 1330 cm.$^{-1}$, respectively, as observed. On the other hand, these results support the view of Evans[6] who attributes a partial in-plane O–H bending character to the 1344-cm.$^{-1}$ vibration, since according to this view one would expect a small decrease in this frequency as a result of the O^{18} labeling, as found. It is, however, difficult to accept his assignment of the 1333-cm.$^{-1}$ shoulder to the 814 + 530 cm. combination (according to Table I, 812 + 536 cm.$^{-1}$) since this would mean a decrease of about 16 cm.$^{-1}$ in the parallel frequency of $C_6H_5O^{18}H$ (which shows the lower bands at 802 and 530 cm.$^{-1}$, correspondingly) while the observed decrease amounts only to 3 cm.$^{-1}$. It might be, on the other hand, that the 1333-cm.$^{-1}$ shoulder belongs to the 1000 + 320 cm.$^{-1}$ combination while in the case of $C_6H_5O^{18}H$ it moves to 1330 cm.$^{-1}$ since it then belongs to the corresponding 1000 + 315 cm.$^{-1}$ combination.

The decrease of about 11 cm.$^{-1}$ observed for the frequency of the 1313-cm.$^{-1}$ band as a result of O^{18} labeling shows that its assignment to the ν_3 in-plane C–H deformation[2] is wrong since this deformation is, no doubt, insensitive to this labeling. The alternative assignment of this band as a 416 + 883 cm.$^{-1}$ combination[6] is also improbable since, as seen from Table I, the frequency of both of these bands is not decreased by the O^{18} labeling so this combination cannot result in the 1313–1302-cm.$^{-1}$ absorption. This band probably belongs to the 812 + 510 cm.$^{-1}$ combination of normal phenol, which corresponds to the 802 + 506 cm.$^{-1}$ combination of $C_6H_5O^{18}H$. The ν_3 C–H deformation absorption seems to be masked by the 1256-cm.$^{-1}$ band.

Evans' assignment of the band at about 1180 cm.$^{-1}$ as an in-plane bending of the monomeric OH group[6] with a ring stretching character seems to be borne out by the fact that its frequency is decreased only by about 2 cm.$^{-1}$ in the case of the O^{18}-phenol. A pure O–H bending[2] would be expected to show a somewhat higher isotopic shift (~5 cm.$^{-1}$).

The very weak 1133-cm.$^{-1}$ band of labeled phenol, which is absent from the spectrum of normal phenol, is probably due to the overtone of the O^{18}-phenol band at 574 cm.$^{-1}$. Its 1112-cm.$^{-1}$ shoulder seems to belong to the 604 + 506 cm.$^{-1}$ combination (which, in the case of normal phenol, might have merged together with the 1152-cm.$^{-1}$ band since it is then a little higher: 608 + 510 cm.$^{-1}$).

The O^{18}-phenol shoulder at 1085 cm.$^{-1}$ may be due to the 574 + 506 cm.$^{-1}$ combination.

It can be seen from Table I that all the dilute solutions of both normal and labeled phenol show a weak, yet distinct, absorption at about 1048 cm.$^{-1}$ (although no such band seems to have been reported in the literature), besides the absorption at about 1027 cm.$^{-1}$. These absorptions, in the case of the normal phenol, seem to be the result of a Fermi resonance between the a_1 ν_{18a} in-plane C–H bending[2] at about 1035 cm.$^{-1}$ and the 536 + 510 cm.$^{-1}$ combination. Since the combination originally has a higher frequency than that of the fundamental, the resulting higher band (at 1052 cm.$^{-1}$) has a higher combination character than the lower band and hence is only very weak for a carbon tetrachloride solution. In the case of a cyclohexane solution the C–H fundamental seems to be somewhat higher in frequency than the original combination; hence, now the higher band is more a C–H bending fundamental (the situation for the vapor phase appears to be analogous) and is therefore stronger than the lower band.

The corresponding combination band of the labeled phenol is appreciably lower than that of normal phenol since its constituent frequencies are now 530 + 506 cm.$^{-1}$. Therefore, even for a carbon tetrachloride solution the 1048-cm.$^{-1}$ band is mainly a C–H fundamental and, as such, is stronger than the lower shoulder at about 1028 cm.$^{-1}$.

The band which appears in the spectrum of a carbon tetrachloride solution of labeled phenol only, at 918 cm.$^{-1}$, is probably due to the 506 + 416 cm.$^{-1}$ combination. Such a combination seems to be responsible also for the 910-cm.$^{-1}$ band observed for both of the isotopic phenols in cyclohexane solutions while the 950-cm.$^{-1}$ band of labeled phenol in cyclohexane might be due to the 574 + 389 cm.$^{-1}$ combination.

That the normal phenol 827-cm.$^{-1}$ band, assigned to the out-of-plane ν_{10a} C–H bending,[2] seems to be replaced in the case of O^{18}-phenol by the 841-cm.$^{-1}$ absorption (its 823-cm.$^{-1}$ neighbor, being so very weak, is probably due to the *ca.* 26% content of normal phenol present in the labeled phenol sample), is not so astonishing if it is remembered that toluene shows this band at 843 cm.$^{-1}$, aniline at 833 cm.$^{-1}$, and $C_6H_5O^{16}D$ at[2] 821 cm.$^{-1}$; *i.e.*, this band is quite sensitive to the identity of the X group.

The O^{18}-phenol weak band at 716 cm.$^{-1}$ can be

Table III: The Assignment of the Main Bands ($cm.^{-1}$) of Phenolic Solutions

Normal phenol				
Present work[a]	Lit.	O^{18}-Phenol	Present assignment	Previous assignment[b]
3620	3612[c]	3610	OH stretching	
3500	...	3500	Dimeric OH stretching	
3076, 3046	3076, 3046[c]	3077, 3047	CH stretchings	
3024	3023[c]	3022		
1598	1596[c]	1598	Ring stretchings	
1502	1502[d]	1500		
1472	1472[c]			
		1480	~1470 ring stretching;	
		1455	224 + 1250	
		1412	574 + 841	
1344	1344[c]	1342	Ring stretching with δ OH character[d]	b_1 fundamental;
...	1322[c]	...		502 + 825
1333	1332[d]		320 + 1000	530 + 814[d]
		1330	315 + 1000	
1313	1313[c]		510 + 812	In-plane CH deformation
		1302	506 + 802	
1256	1255[c]	1250	a_1 (7a) X-sensitive[c]	
1182	1182[c]	1180	Monomeric OH in-plane bending with ring stretching character[d]	COH bending
1152	1153[c]	1155	b_1 CH bending	
1072	1071[c]	1071		
1044[e]	...	1046[e]	a_1 ν_{18a} CH bending[c]; 510 + 536 or	
1027[e]	1024[c]	1026[e]	506 + 530 (for $C_6H_5O^{18}H$)	ν_{18a}
884	884[c]	884	b_2 out-of-plane CH bending	
827[e]	825[c]	841[e]	a_2 out-of-plane CH bending	
812[e]	810[c]	802[e]	a_1 (ν_{12}) X-sensitive[c]	
751[e]	752[c]	751[e]	b_2 out-of-plane CH bending	
688[e]	688[c]	688[e]	b_2 out-of-plane ring deformation	
608	617[c]	604	b_1 (6b) ring deformation[c]	
...	...	574	253 + 315	
536	530[d]	530	a_1 (6a) X-sensitive[c]	
510	508[d]	506	b_2 (16b) X-sensitive[c]	
400[e]	404[d]	389[e]	b_1 in-plane monomeric C–OH bending	
320[e]	~300[d]	315[e]	Out-of-plane monomeric OH bending	
272, 252[e]	...	277, 253[e]	Out-of-plane monomeric C–OH bendings	
235, 226[e]	...	233, 224[c]		

[a] Unless stated to the contrary, the solvent was CCl_4. [b] Given for $C_6H_5O^{16}H$, only when different from the present assignment and, unless indicated otherwise, according to Green.[2] [c] Reference 2. [d] Reference 6. [e] In cyclohexane.

due to the 315 + 416 $cm.^{-1}$ combination while the small decrease (4 $cm.^{-1}$) observed in the 608-$cm.^{-1}$ absorption frequency as a result of O^{18} labeling appears to indicate some participation of the C–OH bond in the b_1 ring deformation (6b) responsible for it.[2]

It can be seen from Table I that the 536-$cm.^{-1}$ band of normal phenol moves to 530 $cm.^{-1}$ in the case of the O^{18}-labeled phenol. This finally proves its assignment[2,4-6] as an X-sensitive, a_1 in-plane ring deformation (6a). The weak band observed for the relatively concentrated normal phenol solution at 458 $cm.^{-1}$ seems to be the dimeric phenol counterpart of the solid normal phenol band observed at 455 $cm.^{-1}$ and attributed to the hydrogen-bonded C–OH in-plane bending vibration.[5,6] Similarly, the 415–416-$cm.^{-1}$ band of both of the isotopic phenol solutions appears to be identical with that observed for the liquid and solid normal phenol at about 410 and 415 $cm.^{-1}$, respectively, and assigned to an out-of-plane ring deformation.[5,6]

The decrease of the 400-$cm.^{-1}$ band of monomeric normal phenol, to 389 $cm.^{-1}$ in the case of O^{18}-phenol proves the correctness of its assignment to the *hydrogen bond free* C–OH group b_1 in-plane bending.[2,4,6]

The band observed for monomeric normal phenol at 320 $cm.^{-1}$ and for monomeric O^{18}-phenol at 315 $cm.^{-1}$ is clearly due to the free O–H out-of-plane bending vibration which rises, however, up to about 700 $cm.^{-1}$ when this group is intermolecularly hydrogen bonded,

as, *e.g.*, in the solid state.[6] This band was found for the vapor phase of normal phenol at about[6] 306 cm.$^{-1}$.

Both the monomeric normal phenol absorption at 235 cm.$^{-1}$ and that of monomeric O^{18}-phenol at 233 cm.$^{-1}$ seem to be related to the solid normal phenol band observed[5] at about 244 cm.$^{-1}$ and the corresponding Raman band at about 240 cm.$^{-1}$ found for liquid normal phenol.[2,4,6] This band was assigned to a b_2, out-of-plane, C–X bending[5,6] vibration and the somewhat lower frequency observed for it in the case of O^{18}-phenol is in accordance with this assignment. The bands at about 272, 252, and 226 cm.$^{-1}$ might be the result of a splitting of this mode of vibration as a result of the lower symmetry of the phenol molecule, as compared with C_6H_5X compounds, on one hand, and rotational isomerism of the OH group on the other.

Table III summarizes the assignments of the main bands of phenolic solutions.

Experimental

O^{18}-Phenol was prepared by reaction of a solution of aniline (14 g.) in a mixture of dry ethanol (30 ml.) and alcoholic hydrogen chloride (100 ml.; 16% w./v. HCl) with isoamyl nitrite (*ca.* 19 g.) at 10° until a clear solution was obtained. Dry ether was added to precipitate the diazonium salt which was filtered off and, while still wet with ether, carefully transferred to an emulsion of O^{18}-labeled water (5 ml. of 75 atom % O^{18}) in ether (30 ml.). The suspension was refluxed gently (*ca.* 50°) until no further evolution of nitrogen was observed. The two layers were introduced into a separating funnel and separated, the water layer being extracted twice with dry ether, and the combined ether extracts were dried with $MgSO_4$. After removing the solvent, the residue was fractionally distilled twice at atmospheric pressure. The fraction (b.p. 180–182°; 5.1 g.) which remained solid at room temperature was retained.

The isotopic analysis of O^{18}-phenol by mass spectrometry presents many problems due to the difficulty in converting phenol to carbon dioxide[14] or water[15] in a clean reaction. A modification of the method mentioned by Oae[16] was used in this work and bromine was added carefully to a solution of the phenol in water. The precipitated 2,4,6-tribromophenol was filtered off, dried, and converted to carbon dioxide by heating it with a mixture of mercuric chloride and mercuric cyanide to 500° for 3 hr.[17] The phenol prepared as described above was found to contain 73.6 atom % O^{18}.

Normal phenol was a pure commercial product.

The instrument used for the infrared absorption measurements in the 4000–650-cm.$^{-1}$ region was a Beckman IR-7 spectrophotometer equipped with the linear absorbance attachment. For the region of 650–400 cm.$^{-1}$ a Perkin-Elmer Model 12C spectrophotometer containing a potassium bromide prism was used. The 400–220-cm.$^{-1}$ bands were scanned with the same instrument containing a cesium iodide prism.

The calibration of the IR-7 spectrophotometer was checked and, after correction, this calibration seems to be exact within ±1 cm.$^{-1}$ for slow scanning of sharp bands in all the region below 3630 cm.$^{-1}$. The absolute wave number accuracy of the Perkin-Elmer instrument seems to be well within 3 cm.$^{-1}$ for most of the measured bands.

The integrated absorption intensity measurements were made under the following conditions: speed, 8 cm.$^{-1}$/min.; period, 8; slit schedule, standard; ordinate scale, 0–1 (absorbance); scale, 40 cm.$^{-1}$/in. Under these conditions the noise was negligible. The estimation of the integrated intensity was done by (a) cutting the graph paper between the solution *vs.* solvent curve and the solvent *vs.* solvent curve; (b) weighing the cut piece of paper; and (c) comparing its weight with that of a square of known dimensions of the same paper (in absorbance and reciprocal centimeters).

The half-width of the monomeric normal phenol O–H band was estimated from an absorbance *vs.* wave number curve, run in duplicate with a scale of 20 cm.$^{-1}$/in. Each of the labeled phenol spectra was measured in the same cell that was used for the measurement of the corresponding normal phenol spectrum.

Acknowledgment. The authors wish to acknowledge the loan of a Beckman IR-7 spectrophotometer by the National Heart Institute, National Institutes of Health, and the technical assistance of Mr. J. Goldberg with the measurements.

(14) D. Rittenberg and L. Ponticorvo, *Intern. J. Appl. Radiation Isotopes*, **1**, 208 (1956).

(15) H. Dahn, H. Moll, and R. Menasse, *Helv. Chim. Acta*, **42**, 1225 (1959).

(16) S. Oae, T. Fukumoto, and R. Kiritani, *Bull. Chem. Soc. Japan*, **36**, 345 (1963).

(17) M. Anbar and S. Guttman, *Intern. J. Appl. Radiation Isotopes*, **3**, 233 (1959); see also D. Samuel, *J. Chem. Soc.*, 1318 (1960).

Evolution of Amine Cations Adsorbed on Montmorillonite with Dehydration of the Mineral

by Jean Chaussidon and Raoul Calvet

Station Centrale d'Agronomie, Centre National de la Recherche Agronomique, Versailles (S-et-O), France
(Received December 29, 1964)

Aliphatic and aromatic amine saturated montmorillonites are dehydrated by heating at temperatures up to 250°. Under these conditions the organic products undergo various transformations of which the first step is a break of the C–N link. An analysis of the reaction products shows that they consist of a mixture of hydrocarbons in the case of aliphatic amines and of phenols corresponding to the amines in the case of aromatic amines.

Introduction

The complexity of the dehydration mechanism of montmorillonite is well known. Fripiat, *et al.*,[1] have shown the impossibility of dehydrating thoroughly a montmorillonite without dehydroxylating the mineral. The residual water, probably chemisorbed on the clay surface around specific sites constituted by the exchangeable cations, may be expected to possess special properties. Among them, Mortland, *et al.*,[2] Chaussidon, *et al.*,[3] and Calvet, *et al.*,[4] have shown the occurrence of catalytic phenomena during dehydration, which appear as a proton transfer towards adsorbed ions or molecules. For instance, in the case of NH_3 sorption, the infrared spectrum exhibits a band due to NH_4^+, and in the case of $Co(NH_3)_6^{3+}$ the same result is obtained, moreover, with a rapid decomposition of the complex ion. Mortland, *et al.*,[2] have stressed the weak value of the dissociation heat of the residual water. Ducros, *et al.*,[5-7] have observed the great mobility of the protons of adsorbed water by n.m.r.

As a consequence of these studies, the quoted authors were led to ascribe proton-transfer phenomena to a high degree of residual water dissociation. At this stage two questions arise. (1) Is it possible to show any reactivity of the OH^- anion resulting from water dissociation? (2) Is it possible to extend the previous results to other kinds of nitrogen compounds? In order to answer these questions, the evolution of adsorbed aliphatic and aromatic amines during dehydration of the clay has been studied.

Experimental

The clay used in this study was the fraction $<2\ \mu$ of montmorillonite from Camp Berteau (Morocco) saturated with the following amine cations: aliphatic: methyl-, ethyl-, propyl-, butyl-, diethyl-, and triethylamine; aromatic: aniline, and *o*-, *m*- and *p*-toluidine. Clay samples were dehydrated by heating and studied by infrared spectroscopy. Reaction products were either trapped to −195° or extracted by benzene and studied by gas chromatography, thin layer chromatography, and visible spectroscopy of characteristic derivatives.

Results

A. Aliphatic Amines. (1) Infrared Spectra. When thermal treatment was applied, one observed a progressive weakening of bands due to amine cations and the development of two bands, one at 1430 cm.$^{-1}$ and the other at 3280 cm.$^{-1}$ characteristic of NH_4^+ clay.

(1) J. J. Fripiat, J. Chaussidon, and R. Touillaux, *J. Phys. Chem.*, **64**, 1234 (1960).

(2) M. M. Mortland, J. J. Fripiat, J. Chaussidon, and J. Uytterhoeven, *ibid.*, **67**, 26 (1963).

(3) J. Chaussidon, R. Calvet, J. Helsen, and J. J. Fripiat. *Nature*, **196**, 161 (1962).

(4) R. Calvet, J. Chaussidon, P. Cloos, C. de Kimpe, J. J. Fripiat, M. C. Gastuche, J. Helsen, A. Jelli, A. Leonard, G. Poncelet, and J. Uytterhoeven, *Bull. Groupe Franc. Argiles*, **14**, 59 (1964).

(5) P. Ducros and M. Dupont, *Compt. rend.*, **254**, 1409 (1962).

(6) P. Ducros and M. Dupont, *Bull. Groupe Franc. Argiles*, **14**, 99 (1964).

(7) P. Ducros, *ibid.*, **14**, 143 (1964).

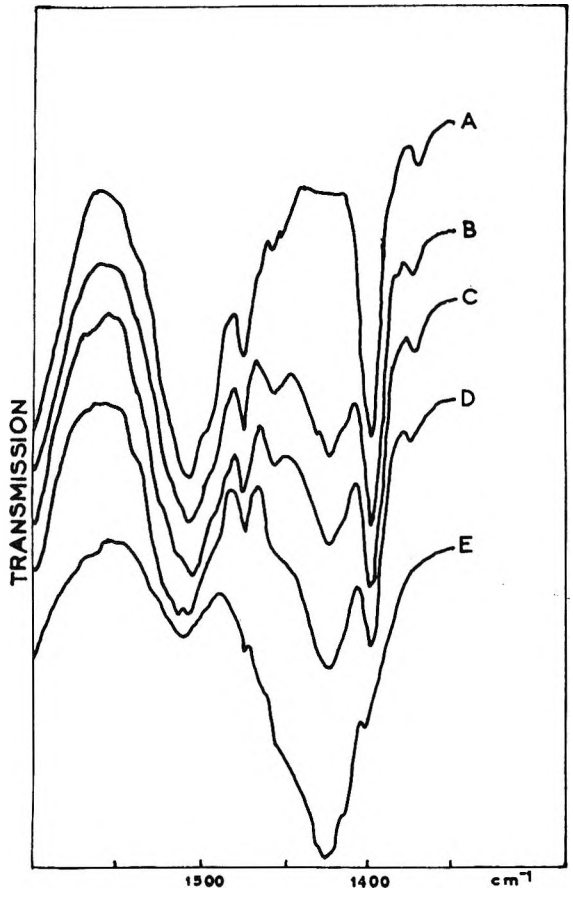

Figure 1. Infrared spectra of ethylamine clay. Samples heated at: A, 20°; B, 100°; C, 150°; D, 200°; E, 250°.

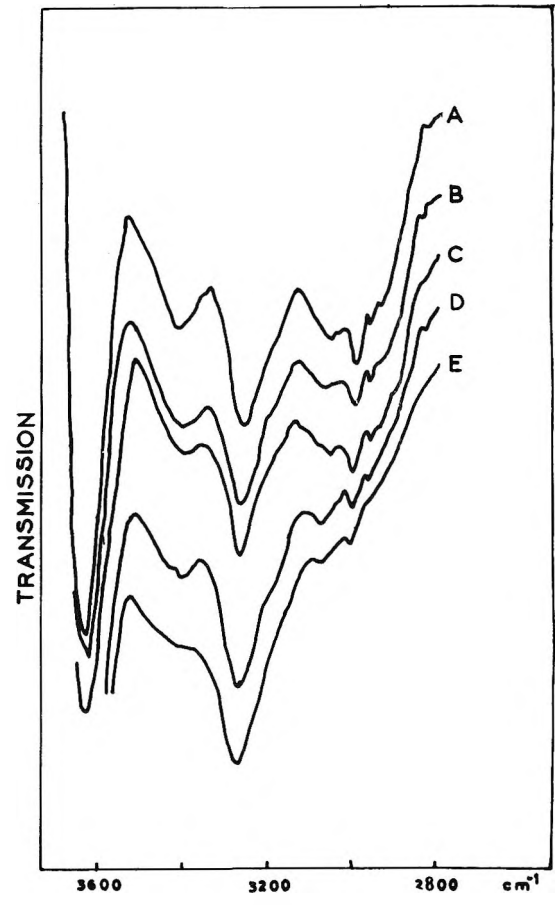

Figure 2. Infrared spectra of ethylamine clay. Samples heated at: A, 20°; B, 100°; C, 150°; D, 200°; E, 250°.

After heating at 250°, the evolution was achieved, and the spectrum corresponded to a mere NH_4^+ clay. Figures 1 and 2 show various intermediate states for ethylamine-saturated clay.

(2) *Gas Chromatography.* Reaction products are a mixture of saturated and ethylenic hydrocarbons. The qualitative composition of this mixture is practically the same whatever may be the nature of the adsorbed amine. The percentages of detected gas may change largely from one sample to another, especially for ethylene, propane, and propylene. Accurate determinations were possible up to 1,3-butadiene. C_6 hydrocarbons were detected but not analyzed.

B. Aromatic Amines. It was not possible to determine any gaseous product. Reaction products condensed in the cooled trap exhibited properties of phenolic compounds. These compounds were found also in the clay. They were analyzed by infrared spectroscopy and by chemical techniques as described previously.

(1) *Infrared Spectra.* For samples dried at room temperature no decomposition occurred. When the clays were heated at 150° for 6 hr., new bands developed. It is noteworthy that C–H out-of-plane vibrations were not modified throughout the heating process.

Figures 3–5 show spectral evolution of *o*-toluidine-saturated clay.

Three observations may be made from Figures 3–5: (a) the aromatic structure is maintained as well as the type of substitution; (b) bands at 1430 and 3280 cm.$^{-1}$ due to NH_4^+ clay appear in the spectra; (c) similar compounds are formed whatever may be the initial amine. They can be characterized by two bands in the 1200–1400-cm.$^{-1}$ region and one band in the 3380–3390-cm.$^{-1}$ region.

This last point needs some discussion. The high frequency band may be due either to an OH group or an NH group (stretching mode). In the clay samples investigated nitrogen can only be engaged in the forms NH_3^+ or NH_4^+, and it has been recognized that

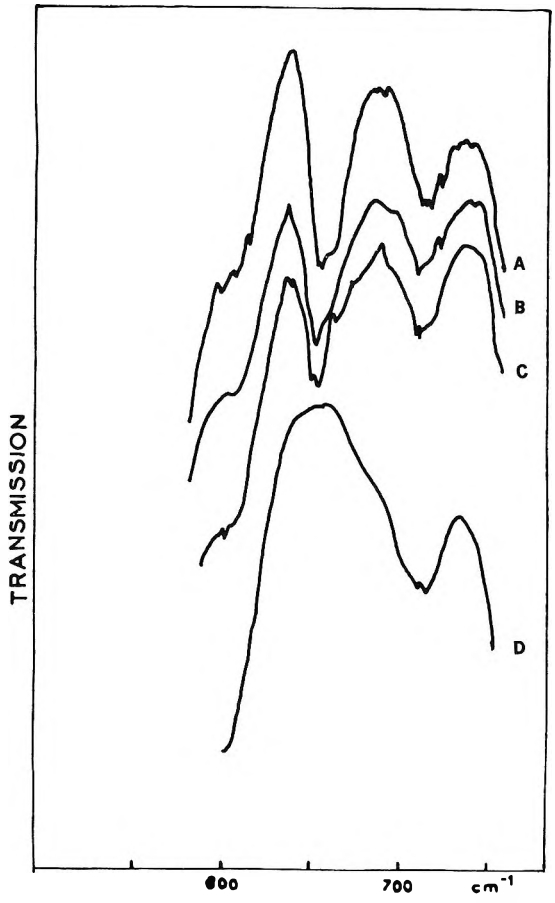

Figure 3. Infrared spectra of *o*-toluidine clay. Samples heated at: A, 20°; B, 100° (for 4 hr.); C, 100° (for 7 hr.); D, 250° (for 2 hr.).

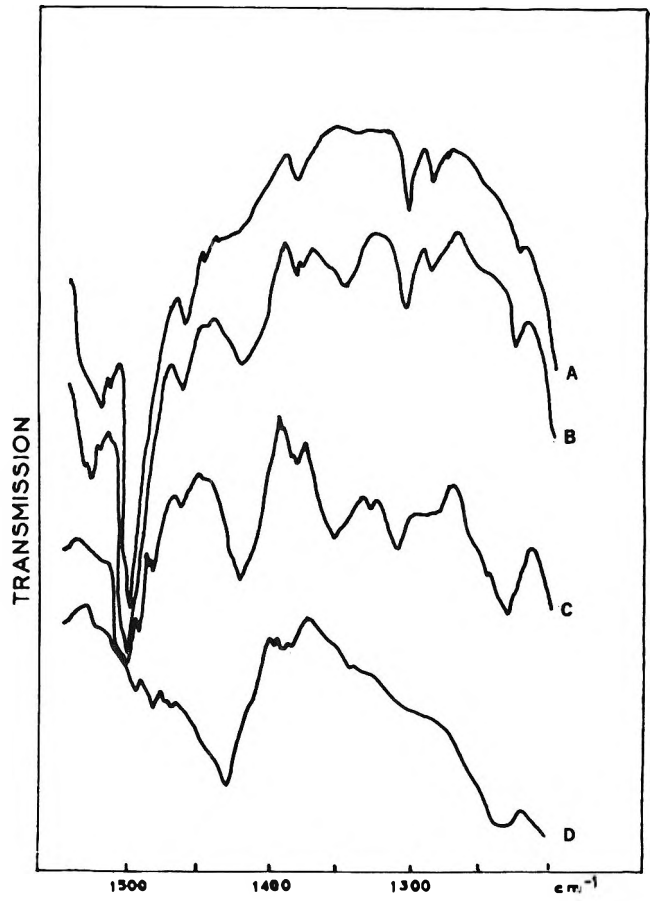

Figure 4. Infrared spectra of *o*-toluidine clay. Samples heated at: A, 20°; B, 100° (for 4 hr.); C, 100° (for 7 hr.); D, 250° (for 2 hr.).

the upper frequency for these groups on the clay is 3300 cm.$^{-1}$. This leads one to assume that the 3380-cm.$^{-1}$ band is due to OH groups, the low frequency of which implies evident H bonding. The two bands in the 1200–1400-cm.$^{-1}$ region are more difficult to interpret. It may be observed that compounds such as phenol or *o*-, *m*-, and *p*-cresols exhibit the same bands which are attributed to a complex C–OH deformation.

(*2*) *Chemical Analysis.* All the methods showed that the reaction product was constituted by the phenol corresponding to the adsorbed amine, that is, phenol for aniline and *o*-, *m*-, and *p*-cresol for *o*-, *m*-, and *p*-toluidine.

In the case of high temperature experiments (for instance, heating at 250° for 24 hr.) the formation of condensed products cannot be precluded.

Discussion

According to the results presented by Mortland, *et al.*,[2] Chaussidon, *et al.*,[3] and Calvet, *et al.*,[4] it has been recognized that protons due to a highly dissociated state of residual water can react with physically adsorbed NH_3 or $Co(NH_3)_6^{3+}$ balancing the clay exchange capacity, to give NH_4^+ ions.

Experiments reported in this paper allow us to ascribe to these protons the same properties toward adsorbed aliphatic or aromatic amines. This was proved by the steady transformation of amine cation into NH_4^+ which under experimental conditions exhibited two bands at 1430 and 3280 cm.$^{-1}$. Moreover, X-ray diffraction data indicated a collapse of the clay during thermal treatment. For the samples dried at room temperature a rational basal spacing of 13.8 Å. was observed under a vacuum; under the same conditions, heated samples showed a smaller spacing which was no more rational. This indicated a mixed-layer system, one of the components being the 10-Å. NH_4^+ clay.

In addition to these results it is possible to give an interpretation of the role played by OH^- ions. Let

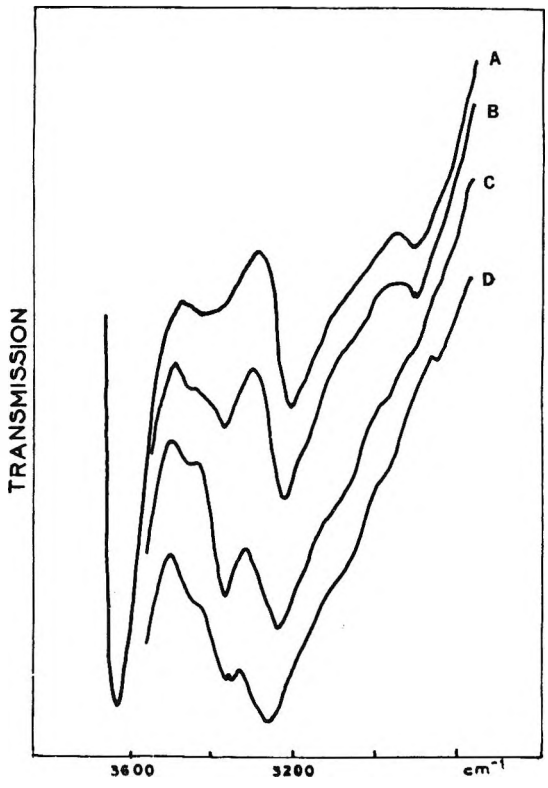

Figure 5. Infrared spectra of *o*-toluidine clay. Samples heated at A, 20°; B, 100° (for 4 hr.); C, 100° (for 7 hr.); D, 250° (for 2 hr.).

$]\text{–}ANH_3^+$ represent an adsorbed amine. One can write schematically

$$]\text{–}ANH_3^+ + H^+ + OH^- \rightarrow]\text{–}NH_4^+ + AOH$$

AOH is either an alcohol or a phenol.

It was not possible to detect any alcohol when dehydrating a clay saturated with an aliphatic amine. This is not surprising because it is well known that clay is a very efficient dehydration catalyst for alcohols, leading to hydrocarbons through complex cracking and reforming reactions. It was only possible to check the formation of hydrocarbons, which agrees implicitly with the proposed scheme.

It is difficult to correlate quantitative data with the nature of the amine because a simultaneous break of the C–N link and of C–C links is possible.

With aromatic amines the AOH compound must be phenolic. It may be expected in this case that a part of this reaction product will still be detectable after heating, this being due to the higher stability of this kind of product. Once again, experimental facts agree with the hypothesis. Chemical analyses show that phenolic compounds corresponding to adsorbed amines are formed. This is also observed by infrared spectroscopy and probably means that, in the transformations encountered in the investigated systems, only the C–N link is broken, without any visible alteration of the aromatic ring.

Such reactions may explain some special features of the evolution of fresh organic matter in the soil and represent in part a possible explanation for the genesis of oil and natural gas.

Some Electrochemical Aspects of Germanium Dissolution.

Simultaneous Chemical and Electrochemical Oxidation

by Walter E. Reid, Jr.

Electrochemistry Section, National Bureau of Standards, Washington, D. C. *(Received December 30, 1964)*

The dissolution of germanium by oxidation–reduction agents was investigated for both unpolarized and polarized specimens. The rate of the chemical oxidation process is expressed directly as a corrosion current, i_c, proportional to the oxidation–reduction potential, $E°$, above a certain minimum value, E_m, and obeys the relation $i_c = k(E° - E_m)$. The electrode potential, V_E, for this case can be correlated with i_c and with $E°$. A mathematical expression is obtained relating $E°$ with i_c and i_a, the respective rates of the chemical and electrochemical oxidation rates. This relation $E° = 0.21(2i_c/i_a + 1) \log i_a$ enables the interrelation of these quantities to be better understood and indicates the reasons for "current multiplication." The enhancement of the chemical corrosion current by anodic polarization is due to an increase in the number of surface sites and the enhancement of the anodic process by chemical corrosion is due to the partially oxidized state of the surface. The techniques used give a general method for determining fairly accurately the standard electrode potentials of oxidation–reduction couples not easily measured by conventional means. For Ge the values are: $E°_{Ge-Ge^{+2}} = 0.24$ v.; $E°_{Ge^{+2}-Ge^{+4}} = 0.00$ v.

Certain aspects of the behavior of the germanium anode in the presence of oxidizing reagents have been studied extensively.[1-3] The effects of simultaneous anodic and chemical dissociation for varying current densities and oxidizing agents of different oxidation–reduction potentials have not been thoroughly investigated, although some studies of this nature have been made by Beck and Gerischer.[4-6] A fairly extensive investigation of the chemical corrosion of Ge and Si has been made by Turner.[7]

The anodic and chemical dissolution behavior of a p-type Ge anode was examined in the presence of oxidizing agents of varying $E°$ values for a range of current densities to determine the interdependence of these variables in the dissolution process. As a part of this investigation the mechanism of current increase brought about by oxidizing agents, so-called "current multiplication," was also investigated.

I. The Chemical Oxidation Reaction. If we place two dissimilar metals in contact or mix two solutions containing oxidizing materials of different standard electrode potentials ($E°$), we observe a transfer of electrons from the higher to the lower energy state. With a metal in contact with an oxidizing solution the process becomes expressable as a corrosion current or rate which will vary with the concentration of oxidizing material provided the reaction products are soluble in the solution. Charge transfer occurs directly across the metal–solution interface, and for a clean surface is controlled only by the rate of transport of oxidizing species to the metal surface and the activation energy of the process. For a series of similar oxidizing agents of differing $E°$, the corrosion rate will be a linear function of the $E°$ values at constant temperature, stirring speed, and concentration, as will be discussed below.

(1) D. R. Turner, "The Electrochemistry of Semiconductors," P. J. Holmes, Ed., Academic Press Inc., New York, N. Y., 1962.

(2) J. F. Dewald, "Semiconductors," N. B. Hannay, Ed., Reinhold Publishing Corp., New York, N. Y., 1959.

(3) E. A. Efimov and I. G. Erusalimchik, "Electrochemistry of Germanium and Silicon," Sigma Press, Washington, D. C., 1963 (English Translation).

(4) F. Beck and H. Gerischer, *Z. Elektrochem.*, **63**, 943 (1959).

(5) F. Beck and H. Gerischer, *ibid.*, **63**, 500 (1959).

(6) H. Gerischer and F. Beck, *Z. physik. Chem.* (Frankfurt), **24**, 378 (1960).

(7) D. R. Turner, *J. Electrochem. Soc.*, **107**, 810 (1960).

The intercept of the resulting straight line in the plot of E° *vs.* i_c will be the minimum standard oxidizing potential, E_m, required to oxidize the metal. If the metal has only two stable valence states, the intercept will give the E° of the lower valence state in general, since stepwise electron removal must occur,[8] and the initial electron removal usually involves the higher energy requirements.

Experimental Procedure

A p-type Ge specimen of resistivity 2.3 ohm cm. was used in almost all of the experiments; however, n-type Ge was found to give identical results in several of the corrosion experiments. A definite area (5 cm.^{2}) of the Ge specimen was exposed to the oxidizing solution under examination, and the weight loss after a fixed time was determined. This weight loss was converted to a corrosion current density by means of Faraday's law: i_c = (wt. loss/t)($\mathfrak{F}$/equiv. wt.)($1/A$). The corrosion current for each oxidizing solution was determined at least three times. If the experimental work was interrupted for several days, it was found necessary to remove the thick oxide film found on the specimen with CP-4 etchant; otherwise, the corrosion rates were abnormally low. Since the corrosion current varied linearly with the concentration of the oxidizing ion (Figure 1), the experiments were performed for short time intervals (~15 min.) so that the concentration would not change drastically. The initial concentration of the oxidizing agent was 0.1 N in all cases. All experiments were performed in a 400-ml. Pyrex tall-form beaker containing 100 ml. of solution. A Fisher magnetic stirrer, Model 14-1511-1, was used with a 27 × 6 mm. Teflon-coated stirring bar. The stirrer was operated at its minimum speed. The stirring rate was such that at these concentrations the maximum possible corrosion rate or limiting current was about 27 ma./cm.^{2} as determined from the corrosion of a Cu specimen. It was found for Cu that a series of oxidizing agents with $E^\circ > \sim 0.60$ v. gave an i_c value essentially constant at 27 ma./cm.^{2} indicating diffusion control. Below this E° value the Cu was not dissolved. This value of 27 ma./cm.^{2} was taken as the maximum possible corrosion rate for the experimental conditions described. The following solutions were used for the corrosion studies of Ge

0.1 N VO^{2+} in 1 M H_2SO_4; E° = 0.30 v. (hydrogen scale[9])

0.1 N $K_3Fe(CN)_6$ in 0.1 N H_2SO_4; E° = 0.56 v.

0.1 N VO_2^+ in 1 M H_2SO_4; E° = 0.92 v. (this investigation)

0.1 N Ce^{4+} in 1 M H_2SO_4; E° = 1.43 v.

The $K_3Fe(CN)_6$ solution was used immediately after preparation as it decomposed slowly upon standing. The experiments with this solution were kept as brief as possible, as a white precipitate, believed to be a germanium ferrocyanide compound, was slowly formed on the Ge specimen, and thus in the electrochemical oxidation studies a slight increase in potential was occasionally required to maintain a constant current. In similar experiments involving copper, an analogous compound was formed very readily.

It is noted that the VO_2^+–VO^{2+} couple (E° = 0.92 v.) is reduced to the VO^{2+}–VO^+ couple (E° = 0.30 v.). The corrosion current of the latter is assumed to be sufficiently small for the conditions used so as not to affect seriously the value obtained for the corrosion current of the former. The short exposure times and the dependence of i_c upon concentration justify this assumption.

All potential measurements were made with the Hg|Hg_2SO_4|1 M H_2SO_4 reference electrode (E = 0.67 v.) and are expressed relative to the normal hydrogen electrode. The junction potential was assumed to be less than the experimental error and was neglected. Measurements made of the potential of Ge in the 1 M H_2SO_4 with and without stirring indicated no significant change (<0.003 v.) due to stirring. The Ge was cleaned by anodic dissolution immediately before these measurements were made.

All experiments were performed at room temperature and in a normally lighted laboratory room. Although the effect of light was not examined extensively, preliminary experiments gave identical results for the corrosion rates in a normally lighted and unlighted room.

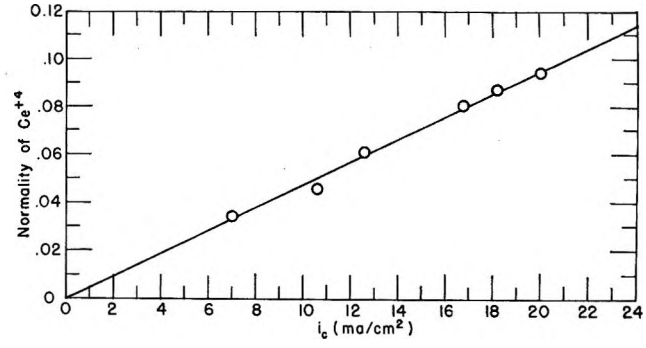

Figure 1. Dependence of corrosion current on concentration of oxidation–reduction agent.

(8) K. J. Vetter, Transactions of the Symposium on Electrode Processes, Philadelphia, Pa., May 1959, p. 65.
(9) See ref. 1, p. 192.

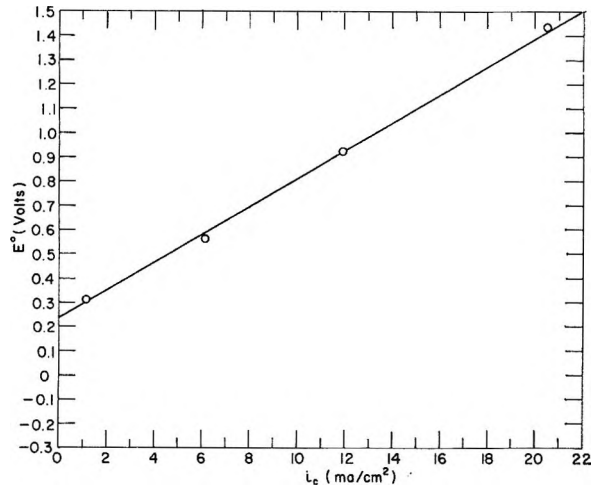

Figure 2. Rate of chemical corrosion of germanium by oxidizing agents.

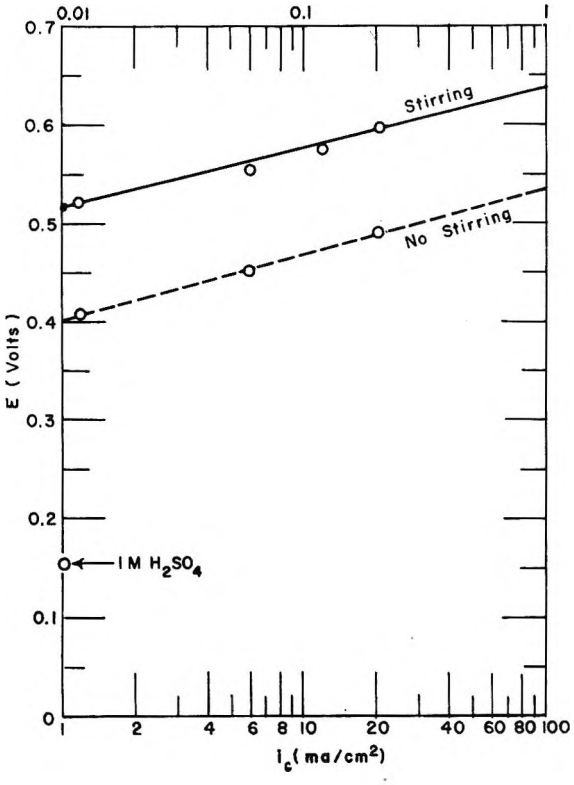

Figure 3. Electrode potential of Ge during chemical corrosion. (The scale at the top of the figure applies to the unstirred solutions.)

The solutions used were not deaerated since the corrosion rate of Ge in 1 *M* H_2SO_4 was insignificant compared to the lowest rate observed in this study.

Experimental Results and Discussion

The experimental curve for the corrosion currents of Ge when exposed to solutions of various oxidizing agents is given in Figure 2 where the corrosion current densities (i_c) are plotted against $E°$ of the oxidizing agents. The intercept at $i_c = 0$ gives the minimum oxidizing potential, E_m, required to oxidize the metalloid and yields the relation

$$i_c = k(E° - E_m) \quad (1)$$

If now we measure the potential of the Ge in the various oxidizing solutions, we obtain the values shown in Figure 3. The potential of Ge in 1 *M* H_2SO_4 is included. In all cases the potential is shifted in the anodic direction from that found in 1 *M* H_2SO_4. The Ge potential in the stirred solutions obeys approximately the relation $E_{Ge} = 0.52 + 0.06 \log i_c$, where i_c is expressed as milliamperes per square centimeter. The dashed line in Figure 3 results when the potential of the Ge specimen in unstirred solutions of the same composition, as given by the points on the solid line, are plotted directly below these points. The slopes of the two lines are the same, within experimental error, and indicate that the potential of the Ge is primarily a function of the corrosion current density. The experimental values for i_c in the unstirred solutions were not measured with high precision in the lower part of this range but they were found to be of the proper order of magnitude. These potential values are reasonably reproducible (±0.02 v.). The fact that these values differ by two orders of magnitude is attributable to the specific experimental conditions.

These data are best interpreted in terms of the following model. The introduction of an oxidizing agent produces an increase in the number of partially oxidized Ge atoms on the surface of the specimen. This is due to the stepwise oxidation of the Ge which requires the removal of four electrons per atom upon going into solution as H_2GeO_3. The increase in the formation of positively charged Ge surface atoms, as indicated by an increase in potential, varies as the logarithm of the corrosion current, and increasing the corrosion current by a factor of 20 results in a potential change of only about +0.08 v. Therefore, most of the initial change of the electrode potential of Ge results from the oxidation of the Ge surface by an oxidizing agent with $E°$ only slightly above E_m.

This model was tested using copper as the metal specimen. In this case the shift of potential (+) was smaller in magnitude. For the same experimental conditions the shift in rest potential when changing from 1 *M* H_2SO_4 to 0.1 *N* Ce^{4+} in 1 *M* H_2SO_4 was approximately 0.48 v. for Ge and 0.12 v. for Cu. In each case the i_c values were of the same order of magnitude. Although the mechanism of the dissolution process itself was not investigated in detail, it is reasonable to as-

sume it is analogous to and only slightly more complex than the mechanism of the anodic dissolution process. The experimental procedure was such that electron removal by the oxidizing agent was rate controlling. Some intermediate slow step between this process and the appearance in solution of the dissolved ion, occurring immediately after electron removal, best explains the potential behavior observed and the difference in the potential change for Ge and Cu.

Even though the basic natures of semiconductors and metals differ profoundly, the indicated model appears to be satisfactory from an electrochemical point of view.

For a sufficiently concentrated solution and in the absence of polarization, concentration gradients at the interface, and surface contamination, one may expect changes in the Ge electrode potential to correspond to changes in the Ge surface potential, Ψ_s. This was pointed out by Dewald[2] and substantiated by Brattain and Boddy,[10] who showed that

$$\Psi_s - RT/\mathfrak{F} \ln \lambda = V_E + \text{constant} \qquad (2)$$

where Ψ_s = surface potential, $\lambda = p_i/p_0$ where p_i and p_0 refer, respectively, to the actual and intrinsic hole densities at equilibrium, and V_E is the electrode potential.

Although this equation is deduced for an equilibrium situation, it is desirable to show that it applies to the nonequilibrium conditions used here, since this would strengthen the model used.

One may reasonably assume that the electrochemical potential of electrons in the Ge was initially the same in all cases since the same Ge specimen was used throughout this investigation. When this specimen is placed in an oxidizing solution, there is a shift in the Fermi level as the system attempts to reach equilibrium and charge flows from one phase to the other. The field which develops is insufficient to prevent charge transfer, and the specimen thus corrodes at a rate determined by the experimental conditions. If E° of the oxidizing couple is varied, then the shift in the Fermi level of the Ge specimen would be linearly dependent on this E° value, since $i_c = k(E^\circ - E_m)$ for $E_m = 0.24$ v. This shift in the Fermi level of the Ge specimen as E° is varied, as indicated by the change in the electrode potential of the Ge specimen, permits the substitution $\lambda = k'(E^\circ - E_m)$ since the value of λ characterizes the initial Fermi level for the Ge specimen and $E^\circ - E_m$ characterizes the Fermi level for the steady-state corrosion process. Recalling that $i_c = k(E^\circ - E_m)$ one may substitute $\lambda = k''i_c$ to obtain $V_E = V_k + RT/\mathfrak{F} \ln i_c$, where V_k is a constant, as found experimentally above. One has also that $\Psi_s = V_{k'} + RT/\mathfrak{F} \ln i_c$.

Capacitance values expected in the present case would be at least as high as the integral capacitance for copper electrodes (30 μf./cm.^{2}).[11] Since the potential shift of Ge is about four times that of Cu for the conditions mentioned previously, the charge on the Ge would be on the order of four times greater. By using 7.5×10^{14}/cm.^{2} as the average number of surface atoms, the average number of positive charges associated with each surface atom is estimated to be about 0.5.

The shift of potential in the presence of the oxidizing agent ($E^\circ > 0.24$ v.) is in the anodic direction; however, an increase in pH of the electrolyte causes a shift in the direction of cathodic potentials.[10b,12] In the present investigation the rate of corrosion increases linearly with increasing concentration of oxidizing agent (Figure 1) in agreement with the observations of Harvey and Gatos[12] for oxygen. The explanation proposed for the potential shift in ref. 10b and 12 involves OH^- ions and/or water molecules adsorbed on the surface. From available data (~1961), Carasso and Faktor[13] showed that the normal variation of Ge potential with pH could be expected to obey the Nernst equation. As shown elsewhere,[5,14] the dissolution process in acidic solution would involve essentially, per electron equivalent, the reaction, $0.25Ge + H_2O \rightarrow 0.25Ge(OH)_4 + H^+ + e$. For the unpolarized Ge electrode, in the absence of oxidizing agents, this could be expected to be the potential-determining reaction; however, this reaction occurs simultaneously with the formation of the Ge^{2+}–Ge^{4+} oxidation–reduction couple.[14b] The capacitance minima method of Boddy and Brattain[10b] gives the proper thermodynamic dependence of the Ge^0–Ge^{4+} couple on pH in the range 4.5–11.5 which supports the conclusion[14b] that the effect of the Ge^{2+}–Ge^{4+} oxidation–reduction couple on the potential is normally fairly small. An increase in the concentration of dissolved germanium by anodic dissolution such that the Ge^{2+}:Ge^{4+} ratio could be changed by oxidizing agents would greatly disturb the electrode potential. In the absence of oxidizing agents the cathodic shift of electrode potential due to a pH increase therefore appears to be due primarily to the above reaction and would obey the Nernst equation.

The above discussion of oxidizing agents applies only for oxidizing ions for which one electron is trans-

(10) (a) W. H. Brattain and P. J. Boddy, *J. Electrochem. Soc.*, **109**, 574 (1962); (b) P. J. Boddy and W. H. Brattain, *ibid.*, **110**, 570 (1963).

(11) R. J. Brodd and N. Hackerman, *ibid.*, **104**, 704 (1957).

(12) W. W. Harvey and H. C. Gatos, *ibid.*, **107**, 65 (1960).

(13) J. Carasso and M. Faktor, ref. 1, p. 205.

(14) (a) P. J. Boddy, *J. Electrochem. Soc.*, **111**, 1136 (1964); (b) W. E. Reid, Jr., *J. Phys. Chem.*, in press.

ferred in the reduction process. It is also restricted to those cases where the surface of the Ge is available to the oxidizing agent. When I_2 in KI solution (E° = 0.54 v.) was examined, an abnormally low rate of corrosion was observed with an induction period similar to the reaction of O_2 with Ge in water.[12] In view of the strong adsorption of I^- on Ge[15] it appears that the Ge is effectively shielded from I_2 attack. The presence of an oxide film on Ge has been found to explain best the initial behavior of Ge with O_2 in water.[16] In support of these conclusions is cited a recent investigation in this laboratory[17] of the oxidation (O_2) of Ag in NaCl at 900° which indicated that the very low oxidation rates were due primarily to adsorption of Cl^- ions.

II. The Electrochemical Oxidation Reaction. A brief discussion of certain fundamental aspects of electrochemical dissolution is helpful before considering the simultaneous processes. If electrons are removed by external means from a conductor which is in equilibrium with the solution in contact with it, the equilibrium shifts temporarily and is then restored by the most convenient means. This involves the transfer of electrons to the conductor from the solution or the removal of positively charged ions from the conductor. The latter process will occur if the potential of the conductor is sufficiently high to remove electrons from the surface atoms and no species capable of being oxidized at or below this potential are present in the solution.

If then we speak of a dynamic process in which the rate of removal of electrons is fixed, the potential of the conductor at which electrochemical dissolution is occurring is always higher than the reversible potential due to the slowness of some step in the anodic process.

For p-type Ge anodes the anode potential becomes large at moderate currents and for n-type Ge it becomes abnormally large.[1] Since holes are consumed by the anode process,[18] the low rate of diffusion of holes to the surface, especially in n-type Ge, has been identified with the slow step in the anode process which results in unusually high anode potentials at moderate current densities.[2]

If the slow rate of diffusion of holes is responsible for the large potentials at the Ge anode then there should exist a large hole gradient (space-charge region) near the Ge anode interface. The hole current would decrease if this hole gradient were decreased. The presence of an oxidizing agent at the Ge anode interface would decrease this gradient by hole injection.[4] However, as shown below and elsewhere,[4] although the gradient is decreased, the hole current is actually increased with more current flowing at the same applied anode potential.

This argument states that if holes are consumed by the anodic process, then the injection of holes by oxidizing agents will increase the rate of this process. It is contradictory, however, in that this process would decrease the hole gradient within the space-charge region with an accompanying decrease in the rate of arrival of holes from the bulk of the Ge. The rate of the dissolution process would be expected to remain about the same. If the gradient remained unaffected by the hole injection process, then a current increase would be expected.

A more adequate explanation for the relatively high anodic potentials observed in the normal anode dissolution process would include the rate of removal of electrons from the Ge anode surface atoms.

An important consequence of the relatively large polarization values of p-type Ge (see Figure 5) is that the potential drop within the Helmholtz layer may be fairly small. In view of the fact that a Ge specimen is essentially homogeneous in chemical composition up to the anode surface, the electron removal from the surface atoms themselves must be the primary factor in the slowness of the over-all process. The correctness of this conclusion was indicated by making the p-type Ge specimen anodic in a 0.1 N Ce^{3+} solution. At the highest current density attainable with the apparatus used (5 amp./cm.^{2}) the potential of the Ge surface was insufficient to oxidize the cerous ions (E° = 1.43 v.). An investigation of the behavior of n-type Ge specimens under similar conditions was not made.

III. Simultaneous Chemical and Electrochemical Oxidation. When a Ge specimen is made anodic in a solution containing an oxidizing material, it is unreasonable to expect the two reactions (chemical and electrochemical oxidation) to occur independently since the driving force responsible for each reaction is varying in opposite directions, *i.e.*, by increasing the anode potential the rate of electrochemical oxidation is increased while a sufficiently high potential may cause oxidation of the oxidizing agent so that as this potential is approached the driving force for the chemical oxidation will decrease. For a metal anode, the anodic corrosion current density, i_a, increases logarithmically with an increase in anode potential, *i.e.*, it obeys the Tafel relation if charge transfer is the slow step. The current density of the chemical oxidation at a polarized Ge anode would be expected to have the form of eq. 1

(15) W. W. Harvey, W. J. LaFleur, and H. C. Gatos, *J. Electrochem. Soc.*, **109**, 155 (1962).

(16) W. W. Harvey and H. C. Gatos, *ibid.*, **105**, 654 (1958).

(17) K. H. Stern and W. E. Reid, Jr., *J. Phys. Chem.*, **68**, 3757 (1964).

(18) W. H. Brattain and C. G. B. Garrett, *Bell System Tech. J.*, **34**, 129 (1955).

$$i_c \propto (E^\circ - E_{m'}) \quad (3)$$

where $E_{m'}$ is the minimum standard electrode potential below which Ge will not be chemically oxidized *when the Ge anode is polarized* and the other symbols are as previously designated. This expression states simply that the chemical corrosion current density is proportional to the driving force of the reaction.

The electrochemical oxidation which is occurring simultaneously must also be considered. This reaction would be expected to increase the rate of the chemical oxidation (compare Turner[19]) and *vice versa* since the chemical oxidation would leave the surface atoms in varying stages of oxidation so that the electrochemical reaction could proceed at a lower applied anode potential. Similarly chemical oxidation is enhanced since oxidizable surface sites are made available more rapidly than they would be if formed by the chemical oxidation alone, and the chemical corrosion current density will be a function of the anodic current density provided the limiting transport rate of the oxidizing ions is greater than the chemical-corrosion rate. The rate of the chemical corrosion reaction, i_c, is thus proportional to the rate of the electrochemical reaction, i_a, and also the driving force of the chemical corrosion reaction. We must then modify relation 3 to have the more precise form

$$i_a[k(E^\circ - E_{m'})] = i_c \quad (4)$$

From an experimental viewpoint the most convenient way to study these two reactions is to determine the weight loss of the anode after a fixed time at a constant current density in a known volume of standardized solution of an oxidizing agent. This enables a rapid determination to be made of the amount of corrosion due to each of the two reactions. This requires a slight rearrangement of eq. 4.

The relation $i_a/(i_c + i_a) = f_a$ yields $1/f_a - 1 = i_c/i_a$ which enables eq. 4 to be written in the form

$$E^\circ - E_{m'} = k'(1/f_a - 1) \quad (5)$$

where $k' = 1/k$.

The constant k' can then be readily evaluated from the slope of the curves obtained at constant f_a, the fraction of the process due to electrochemical reaction.

Experimental

The cell and materials used were the same as described in the preceding section. In the constant-current experiments a small beaker was used as the cathode compartment, and this was connected to the cell with a siphon. After an appropriate time at constant current density (~15 min.), the weight loss of the Ge specimen was determined to within 0.1 mg. and the value f_a was calculated from the data obtained, assuming $\mathfrak{F}$ = 96,487 coulombs/equiv. and the equivalent weight of Ge = 18.15 g./equiv. To ensure that all reactions were quantitative, an analysis was made of the unreacted oxidizing agent remaining after one of the experiments; it was found that the number of equivalents of Ge dissolved equals the number of equivalents dissolved electrochemically plus the number of equivalents of Ge dissolved chemically.

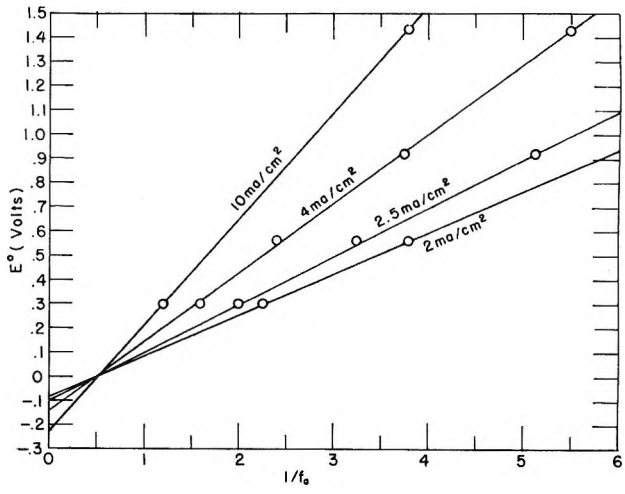

Figure 4. Dependence of f_a^{-1} on E° at various current densities.

The data obtained are shown in Figure 4. Each point represents the average of two or more individual experiments.

The polarization curves presented in Figure 5 were obtained by means of a conventional potentiostat. Although each point represents the average of two to six determinations, no high accuracy is claimed for these data.

Discussion

The quantity $E_{m'}$ for the unpolarized Ge specimen is 0.24 v.; for the polarized anode, however, $E_{m'}$ will not be a constant but will vary in exactly the same manner as the polarized electrode, as shown below.

Writing eq. 5 in the form

$$E^\circ = k'(1/f_a - 1) + E_{m'} \quad (6)$$

enables k' to be evaluated from the slope of E° *vs.* $1/f_a$ at constant current density. The resulting slopes *vs.* log i_a gives $k' = 0.02 + 0.42 \log i_a$ with a maximum uncertainty of ± 0.02 in the first constant and ± 0.03 in the second. Equation 6 then becomes

$$E^\circ = (0.02 + 0.42 \log i_a)(1/f_a - 1) + E_{m'} \quad (7)$$

(19) D. R. Turner, *J. Electrochem. Soc.*, 108, 561 (1961).

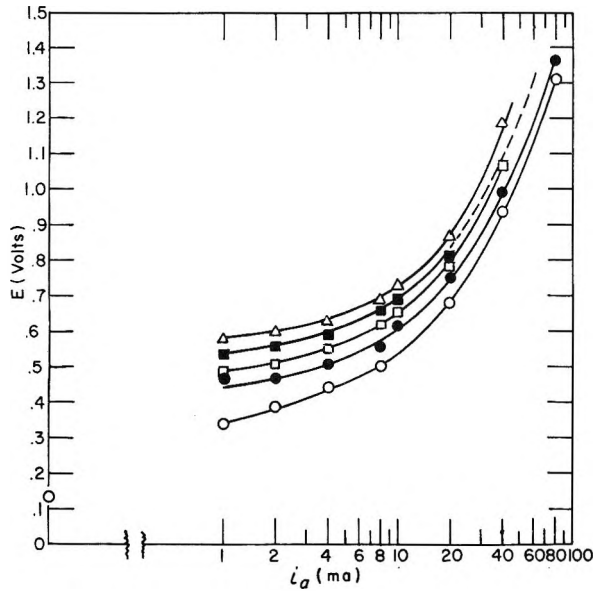

Figure 5. Potential shift in polarization curves caused by oxidation-reduction agents: ○, 1 *M* H_2SO_4; ●, VO^{2+}; □, $K_3Fe(CN)_6$; ■, VO_2^+; △, Ce^{4+}. The corresponding potential for the unpolarized Ge specimen in 1 *M* H_2SO_4 is indicated on the ordinate. The exposed surface area was 5 cm.² in each case.

Evaluating at the point $E^\circ = 0$, $1/f_a = {}^1/_2$ gives

$$(0.02 + 0.42 \log i_a)({}^1/_2) = E_{m'}$$

$$E_{m'} = 0.01 + 0.21 \log i_a \approx 0.21 \log i_a \quad (8)$$

$$\text{and } E^\circ \approx 0.21(2/f_a - 1) \log i_a \quad (9)$$

Equation 9 can be partially derived from a consideration of all possible charge-transfer steps involved in both oxidation processes assuming that the rate of the anodic process is proportional to $e^{k(V-V_0)}$, as predicted by the absolute reaction rate theory, and that the rate of the chemical process is proportional to $E^\circ - E_{m'}$. However, a number of additional simplifying assumptions have to be made without sufficient supporting data. The empirical derivation alone is preferred in view of the present state of knowledge of this system.

The above relations and the data in Figure 4 yield certain fundamental electrochemical information. The point $1/f_a = 1$ on any of the current density lines gives the actual electrode potential of the Ge anode for these experimental conditions in the absence of what may be considered to be "space-charge" polarization (see Dewald[2]). The value of this potential at any current density is given approximately by $E_{m'} = 0 + 0.21 \log i_a$. It is obvious that even for very large current densities this potential is always reasonably low for p-type Ge. The data in Figure 5, by contrast, show that the observable electrode potential measured with a reference electrode is fairly high.

Values of $1/f_a < 1$ indicate that the oxidation–reduction agent present is being oxidized anodically. For example, if the oxidation–reduction agent has an E° of -0.10 v., a current density of <2.5 ma./cm.² would be necessary to oxidize it quantitatively; at higher current densities a fraction of the anode process would involve anodic oxidation of Ge. For an oxidizing agent with $E^\circ = +0.30$ v. the Ge would not be chemically attacked at current densities >20 ma./cm.².

It must be borne in mind that the current-density curves are extrapolated below E° values of 0.30 v. and the Ge is not attacked chemically by oxidizing agents with $E^\circ \leq 0.24$ v.

The intersection of all current-density curves at $1/f_a = {}^1/_2$ and $E^\circ = 0$ gives the E° of the couple Ge^{2+}–Ge^{4+}. This interpretation is based on the following. Since all the current-density lines have a common point of intersection, this point is independent of current density and is a characteristic property of the Ge anode. The value of f_a at this point is 2, which means that the oxidation of a Ge atom to the tetravalent state (formation of H_2GeO_3) is accomplished by the electrochemical removal of only two electrons. Bearing in mind that the current-density curve at $E^\circ = 0$ is an extrapolated value and that above $E^\circ = 0.24$ v. the surface of the Ge specimen is partially oxidized, one must conclude that the electrochemical process occurring at $E^\circ = 0$ is the oxidation process $Ge^{2+} \rightarrow Ge^{4+} + 2e$. This potential is identical with the conventional value obtainable at zero ionic strength since concentration effects would cause only a change in the slopes of the current-density curves.

The correctness of identifying these two potential values with the corresponding oxidation processes is borne out by the good agreement between the calculated thermodynamic and actual experimental values of E° for electrode processes occurring on metals such as Au and Pt.[20]

Half-wave potentials previously reported for the two Ge couples[21] support the E° values found in this investigation.

The technique described above appears to be perfectly general and should be useful for the determination of standard electrode potentials of other materials unmeasurable by conventional means.

The corrosion of Ge is also a useful means of establishing or checking the E° values of oxidation–reduction

(20) A. Hickling, *Trans. Faraday Soc.*, **41**, 333 (1945); **42**, 518 (1946).

(21) D. A. Everest, *J. Chem. Soc.*, 660 (1953).

couples when other means give unreliable values. The value of the VO_2^+–VO^{2+} couple, for example, was found to be 0.92 v. in the present investigation. Values obtained for this couple for other environmental conditions by conventional methods are discussed elsewhere.[22,23] E° values obtained by means of this technique are found to be within 20 mv. of previously reported values and could be improved with more elaborate experimental procedures.

Current Multiplication and Related Phenomena

It has been shown above that the corrosion current is enhanced by polarization and that this enhancement is entirely due to kinetic reasons. Similarly, it is well established that the electrochemical reaction is also increased by simultaneous chemical corrosion.[4] The present investigation gives additional insight into the fundamental cause of this. A saturation current is observed with n-type Ge, and current-multiplication studies have usually been made with this type of Ge specimen because the effects are easily detected.

The experiments of Uhlir[24] show a current increase when changing from a Ge–metal interface to a Ge–solution interface. Similarly, current increases are caused by light.[18] It is also observed when Ge is dissolved anodically in KI solutions at low current densities.[25] Since the saturation current is due to the depletion of holes at the anode surface and the diffusion rate through the bulk Ge is fixed, then current multiplication can only result from hole injection or surface generation.[18] One can, however, discuss the surface processes in a different way and arrive at equally satisfactory results with slightly broader applicability. For example, the diffusion of holes through bulk Ge and the movement of a hole onto a surface atom of Ge may not occur with equal ease. If the latter is the slow step in the over-all anodic process, one must decide between hole transfer and electron transfer, and although both occur simultaneously, the driving force for each may differ considerably. Since electron removal is more easily visualized and is more fundamental, the oxidation process will be considered in these terms.

The electrical work required to oxidize a surface Ge atom is lowered considerably by oxidizing agents because the removal of surface electrons by oxidizing agents permits the anodic process to occur at much lower applied potentials, as shown in Figure 5. This process constitutes one of the better known examples of "current multiplication."

The observation that iodide ions produce an increase in the normal saturation current for n-type Ge[25] indicates that electron removal is facilitated in some way by iodide ion adsorption. Available evidence indicates that the iodide, a nonoxidizing anion, may be covalently bonded to the Ge surface.[12,15] This in turn implies that an electron is displaced either completely or partially from the iodide ion or a surface germanium atom in the process. Assuming that the electron is displaced from the germanium atom, equivalent to partial oxidation, and further that the rate of iodide adsorption is fast compared to the normal anodic dissolution process (*i.e.*, the current density is fairly low) then a current increase would result.

The experiments of Uhlir[24] may be interpreted to show that the principal effect of light on the saturation current is associated with internal rather than surface processes.[2]

The current increases associated with all of these processes can best be explained in terms of the following general situation.

When the Ge anode is polarized, there results near the interface a hole gradient, the space-charge region, which extends up to the Helmholtz region. This gradient is highly dependent upon the bulk properties of the Ge anode.[2] In order to increase the potential drop across the Helmholtz region, the hole gradient must be increased. The potential drop across the space-charge region may thus become quite large to change the potential drop across the Helmholtz region even a small amount. The net result is that a large potential applied to the Ge anode may result in only a small increase in the anodic current. The hole gradient and the corresponding anodic potential can be reduced considerably if the electrical work required to remove electrons from the surface atoms is decreased by some means. Thus even a small reduction in the electrical work required to remove electrons from the surface atoms may cause a relatively large increase in current at the same applied potential. Appropriate evidence has been presented to show that, in the case of oxidizing agents, this reduction of electrical work in the removal of electrons from the surface atoms is the primary reason for the decrease of the anodic potential at constant current. The data presented are interpreted further to show that the oxidizing agent acts to remove the surface (dangling bond) electrons[1] of a surface Ge atom and thereby enables the remaining electrons of the surface atom shared with other Ge atoms to be removed electrochemically at a lower applied potential.

The synergetic process described provides a reason-

(22) C. D. Coryell and D. M. Yost, *J. Am. Chem. Soc.*, **55**, 1909 (1933).

(23) J. E. Carpenter, *ibid.*, **56**, 1847 (1934).

(24) A. Uhlir, Jr., *Bell System Tech. J.*, **35**, 333 (1956).

(25) E. A. Efimov and I. G. Erusalimchik, *Dokl. Akad. Nauk SSSR*, **128**, 124 (1959).

able mechanism for those cases of current increase considered.

Summary

The behavior of oxidation–reduction agents was investigated for both an unpolarized and a polarized Ge specimen. The rate of the chemical oxidation process is directly proportional to the oxidation–reduction potential, E°, above a certain minimum value, E_m. The electrode potential, V_E, can be correlated with the corrosion current and the values of E°, relating the surface charge, Ψ_s, to the corrosion current.

The polarized Ge anode in the presence of oxidation–reduction agents gives an increase in both the chemical and electrochemical oxidation rates. The relation between these is deduced and verified. Reasons for this increase are explained on a kinetic basis and a general explanation for current increases is presented for Ge anodes.

The technique used gives a general method for determining fairly accurately the standard electrode potentials of various oxidation–reduction couples not easily measured by conventional means.

Further Studies on the Decarboxylation of Picolinic Acid in Polar Solvents

by Louis Watts Clark

Department of Chemistry, Western Carolina College, Cullowhee, North Carolina *(Received January 4, 1965)*

Kinetic data are reported for the decarboxylation of picolinic acid in 12 polar solvents. Results of this research combined with data previously reported yielded 32 sets of activation parameters. Analysis of the data favored the picolinic acid molecule (instead of the zwitterion) as the entity involved in the formation of the intermediate complex.

Two mechanisms have been proposed for the decarboxylation of picolinic acid in polar solvents, namely, either that the reacting entity is the zwitterion[1] (I) or

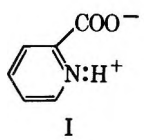

I

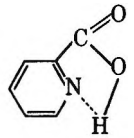

II

the chelated molecule[2] (II).

In order to try to distinguish between the two possibilities, Cantwell and Brown studied the decarboxylation of picolinic acid and several methyl-substituted picolinic acids in *p*-dimethoxybenzene[3] and the decarboxylation of picolinic acid in several polar solvents[4] but failed to eliminate either of the proposed mechanisms.

Subsequent studies on the decarboxylation of picolinic acid in the molten state and in several additional polar solvents indicated that the reaction was bimolecular.[5] However, in order to be able to establish the correct mechanism of the reaction beyond dispute, it was realized that more kinetic data were needed. With this in view, further kinetic studies were carried out in this laboratory on the decarboxylation of picolinic acid in 12 additional solvents. The results of this investigation are reported herein.

(1) B. R. Brown, *Quart. Rev.* (London), **5**, 131 (1951).

(2) M. R. F. Ashworth, R. P. Daffern, and D. L. Hammick, *J. Chem. Soc.*, 809 (1939).

(3) N. H. Cantwell and E. V. Brown, *J. Am. Chem. Soc.*, **74**, 5967 (1952).

(4) N. H. Cantwell and E. V. Brown, *ibid.*, **75**, 4466 (1953).

(5) L. W. Clark, *J. Phys. Chem.*, **66**, 125 (1962).

Experimental

Reagents. The picolinic acid used in this research was 99.5% assay. Reagent grade or highest purity solvents were used and were freshly distilled at atmospheric pressure immediately before use.

Apparatus and Technique. The apparatus and technique used in studying the decarboxylation of picolinic acid in solution (involving measuring the volume of CO_2 evolved with time) has been described previously.[6] The thermometer used to determine the temperature of the thermostat, as well as the buret in which the CO_2 was collected, was calibrated by the U. S. Bureau of Standards. The use of a completely transistorized temperature-control unit made it possible to keep the temperature of the oil bath constant to $\pm 0.005°$ during the course of an experiment. The temperature of the water surrounding the buret was controlled to within $\pm 0.05°$ using a water circulator, electric heater, mercury thermoregulator, and electronic relay. In each experiment a 0.2212-g. sample of picolinic acid (the amount required to furnish 40.0 cc. of CO_2 at STP on complete reaction, calculated on the basis of the actual molar volume of CO_2 at STP, 22,267 cc.) was weighed quantitatively into a fragile glass capsule and was introduced in the usual manner into the reaction flask containing approximately 60 ml. of solvent previously saturated with dry CO_2 gas.

Results

The decarboxylation of picolinic acid in the 12 solvents studied was first order throughout practically the entire course of the reaction. Reactions in each solvent were carried out two or three times at three different temperatures over about a 20° range. The average values of the apparent first-order rate constants, obtained from the slopes of the experimental logarithmic plots, are shown in Table I. Average deviations were generally of the order of 1% in each case. The activation parameters of the absolute reaction rate equation[7]

$$k = \frac{\kappa T}{h} e^{\Delta S^*/R} e^{-\Delta H^*/RT}$$

based upon the data in Table I, are shown in Table II, along with corresponding data for other solvents obtained previously by the same author.[5]

Table I: Apparent First-Order Rate Constants for the Decarboxylation of Picolinic Acid in Various Polar Solvents

Solvent	Temp., °C. (cor.)	$k \times 10^4$, sec.$^{-1}$
Diphenyl oxide	180.05	2.82
	190.33	7.57
	200.19	18.7
1,4-Butanediol	171.23	1.52
	180.65	3.82
	191.13	10.36
5-Chloro-*o*-toluidine	171.08	1.34
	181.00	3.60
	191.21	9.52
2,4-Dimethylbenzophenone	171.10	1.57
	181.08	3.20
	191.52	8.49
N-Ethylaniline	170.82	1.89
	180.60	4.89
	190.45	12.3
t-Butyl-*o*-thiocresol	171.68	1.13
	181.32	4.99
	191.49	14.4
Isopropylphenol	171.47	1.29
	182.37	4.02
	185.13	5.31
	191.61	10.7
o-Nitrotoluene	170.44	1.24
	180.85	3.26
	190.68	8.25
Quinoline	172.81	1.16
	182.85	2.52
	192.72	5.97
Octanoic acid	172.81	2.0
	182.06	4.276
	192.72	10.39
Triethyl phosphate	171.04	2.56
	181.20	7.285
	191.62	17.75
1,3-Butanediol	170.47	1.40
	180.70	3.72
	190.33	10.0

Discussion

The data in Tables II–IV indicate that the enthalpy of activation for the decarboxylation of picolinic acid is not affected strongly by the acidity or basicity of the solvent. There are some exceptions to this statement, however. The largest value of ΔH^* observed (43.7 kcal./mole) occurs in the most basic solvent (tributylamine), whereas some of the lowest values (32.0 and 32.7 kcal./mole, respectively) occur in the neutral ethers (*p*-dimethoxybenzene and *p*-bromoanisole). Nevertheless, the lowest value (31.4 kcal./mole) occurs in a fairly basic medium, aniline. (In view of the fact that Cantwell and Brown studied this particular reaction over a temperature range of only 8.5° the accuracy of this reported value may be questioned.[4]) The value of ΔH^* for the reaction in the *nonpolar* solvent *p*-cymene is fairly high (39.3 kcal./mole), with a ΔS^* value of +12.8 e.u./mole. If these values are compared with

(6) L. W. Clark, *J. Phys. Chem.*, **60**, 1150 (1956).

(7) S. Glasstone, K. J. Laidler, and H. Eyring, "The Theory of Rate Processes," McGraw-Hill Book Co., Inc., New York, N. Y., 1941, p. 14.

Table II: Activation Parameters for the Decarboxylation of Picolinic Acid in Various Polar Solvents (Data of Clark)

Solvent	ΔH^*, cal./mole	ΔS^*, e.u./mole
p-Dimethoxybenzene[a]	32.0	−4.6
β-Chlorophenetole[a]	33.1	−2.0
Quinoline	33.8	−1.67
Octanoic acid	34.3	+0.5
Nitrobenzene[a]	34.4	+0.5
p-Cresol[a]	35.8	+4.5
Phenetole[a]	35.9	+3.4
N-Ethylaniline	38.1	+9.5
1,4-Butanediol	38.3	+10.2
2,4-Dimethylbenzophenone	38.5	+9.3
o-Nitrotoluene	38.6	+9.65
Diphenyl oxide	38.7	+9.76
5-Chloro-*o*-toluidine	39.1	+10.9
Molten picolinic acid[a]	39.8	+13.2
Triethyl phosphate	40.32	+14.86
Isopropylphenol	41.2	+15.5
1,3-Butanediol	41.8	+17.0
t-Butyl-*o*-thiocresol	41.9	+17.7

[a] See ref. 5.

corresponding values for the decarboxylation of *molten* picolinic acid (39.8 kcal./mole and +13.2 e.u./mole, respectively), it would appear that *p*-cymene is acting as an *inert solvent*, the transition complex in the solvent being identical with that in the molten flux.

Table III: Activation Parameters for the Decarboxylation of Methyl-Substituted Picolinic Acids in *p*-Dimethoxybenzene[a] (Data of Cantwell and Brown)

Reactant	ΔH^*, kcal./mole	ΔS^*, e.u./mole
4-Methylpicolinic acid	33.7	−0.35
6-Methylpicolinic acid	34.1	−0.05
4,6-Dimethylpicolinic acid	37.8	+8.20
5-Methylpicolinic acid	39.1	+10.30

[a] See ref. 3.

It will be seen in Tables II and IV that the values of the activation parameters for the reaction in quinoline obtained by Clark are not in agreement with those obtained by Cantwell and Brown. Again, inasmuch as Cantwell and Brown studied the reaction in quinoline[4] over a temperature range of only 9° whereas Clark's results are based upon a 21° range,[5] Clark's values are probably more reliable.

The data in Tables II–IV are shown graphically in line I of Figure 1. The 14 black circles represent the data of Cantwell and Brown (from Tables III and IV), and the 18 white circles those of the author (from Table II). Although there is some scattering, it is evident that all 32 points conform very closely to the line. This is all the more striking in view of the fact that entirely different techniques were utilized by the different investigators in obtaining the two sets of data.

Table IV: Activation Parameters for the Decarboxylation of Picolinic Acid in Various Polar Solvents[a] (Data of Cantwell and Brown)

Solvent	ΔH^*, kcal./mole	ΔS^*, e.u./mole
p-Bromoanisole	32.7	−2.5
Nitrobenzene	34.2	+1.0
p-Dibromobenzene	34.7	+1.9
p-Nitrotoluene	35.2	+3.0
p-Cymene	39.3	+12.8
Aniline	31.4	−6.11
p-Nitroaniline	36.0	+4.2
N,N-Diethylaniline	36.8	+6.7
Quinoline	36.9	+6.1
Tributylamine	43.7	+21.4

[a] See ref. 4.

Petersen, *et al.*,[8] have critically analyzed the problem of the validity of an observed linear enthalpy–entropy of activation relationship. They have shown that such an observed relationship is probably invalid (hence, fortuitous and the result of experimental error) if the range of ΔH^* values is less than twice the maximum possible error in ΔH^*. Applying their mathematical interpretation to the present data we find that the range of ΔH^* values (from 31.4 to 43.7 kcal./mole) is 12.3 kcal./mole, whereas the maximum possible error in ΔH^* (assuming a maximum fractional error in the rate

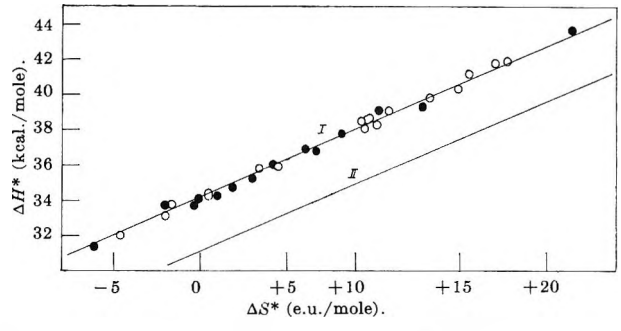

Figure 1. Line I: enthalpy–entropy of activation plot for the decarboxylation of picolinic acid and its derivatives in the molten state and in solution: ●, data of Cantwell and Brown; ○, data of Clark. Line II: projection of the isokinetic temperature line for the decarboxylation of malonic acid and oxamic acid and their derivatives in the molten state and in solution (from ref. 8).

(8) R. C. Petersen, J. H. Markgraf, and S. D. Ross, *J. Am. Chem. Soc.*, **83**, 3819 (1961).

constants to 0.05) turns out to be 2.0 kcal./mole. On this basis the range of ΔH^* values is thus more than three times as great as twice the maximum possible error in ΔH^*. Therefore, according to Petersen, *et al.*, line I of Figure 1 is probably a valid relationship and not due to experimental error.

If a given reaction series affords a set of linearly related activation parameters, the slope of the line produced by the parameters is known as the isokinetic temperature of the reaction series. All the reactions conforming to the line occur at the same rate at the isokinetic temperature.[9] The slope of line I of Figure 1 is found to be 422°K. or 149°C.

It is interesting to note that lines I and II in Figure 1 are parallel. Line II is an extension of the isokinetic temperature line obtained previously for the decarboxylation of malonic acid and its derivatives as well as oxamic acid and its derivatives in the molten state and in a variety of polar solvents.[10] It is worth noting that this was based upon 56 sets of parameters derived from more than 500 kinetic experiments carried out over a period of about 8 years.

For a given reaction a change in structure of reactant often results in the formation of a new isokinetic temperature line parallel to the original line.[9] Leffler has attributed this discontinuous structure effect to the existence of two potential energy minima in either the ground state or the transition state.[9]

One of the properties of an isokinetic series is that all the reactions in the series take place by the same mechanism.[9] Evidently, for the same kind of reaction, if a new reaction series is observed yielding an isokinetic temperature line parallel to the original line, the two series of reactions probably take place by the same or similar mechanisms. On this basis it may be inferred that the mechanism of the decarboxylation of picolinic acid in polar solvents is the same as, or similar to, that of malonic acid and oxamic acid and their derivatives.

Yankwich and his collaborators have proposed that the mechanism of the decarboxylation of malonic acid in polar solvents involves the formation of an activated complex between *un-ionized* malonic acid and solvent.[11] Considerable evidence has been accumulated in recent years in support of this proposal.[10] If it develops that this is the correct mechanism of the malonic acid reaction, the results of the present research strongly favor the un-ionized form of picolinic acid, rather than the zwitterion, as the entity involved in the decarboxylation reaction.

The intercept of the isokinetic temperature line on the zero (entropy of activation) axis yields ΔF^*_0, the free energy of activation for all the reactions at the isokinetic temperature. This value of ΔF^*_0 can be substituted in the absolute reaction rate equation[7]

$$k = \frac{\kappa T}{h} e^{-\Delta F^*/RT}$$

enabling the rate of reaction at the isokinetic temperature to be calculated. On this basis it is found that, for line I, ΔF^*_0 is 34,100 cal., and k_{149} is 0.00002 sec.$^{-1}$, whereas, for line II, ΔF^*_0 is 31,000 cal., and k_{149} is 0.00078 sec.$^{-1}$. At 149°, therefore, the decarboxylation of malonic acid, etc., takes place 40 times as fast as that of picolinic acid. These results are consistent with the relative electronegativities of the oxygen and nitrogen atoms. (The cleavage of the C–C bond in the decarboxylation reaction is facilitated by electron-attracting groups in the α- and β-positions. The greater the electronegativity of the group, the weaker will be the bond.)

Acknowledgment. Acknowledgment is made to the donors of the Petroleum Research Fund, administered by the American Chemical Society, for support of this research.

(9) J. E. Leffler, *J. Org. Chem.*, **20**, 1202 (1955).

(10) L. W. Clark, *J. Phys. Chem.*, **68**, 3048 (1964).

(11) G. Fraenkel, R. L. Belford, and P. E. Yankwich, *J. Am. Chem. Soc.*, **76**, 15 (1954).

A Study of Proton Fluctuation in Protein. Experimental Study of the Kirkwood–Shumaker Theory

by Shiro Takashima

Electromedical Division, Moore School of Electrical Engineering, University of Pennsylvania, Philadelphia, Pennsylvania *(Received January 11, 1965)*

Experimental verification of the Kirkwood–Shumaker proton fluctuation theory was attempted by studying the pH dependence of the dielectric increment of proteins. According to the theory, the fluctuation of protons along the polar groups such as carboxyl, imidazole, and amino groups would give rise to an induced dipole moment. The magnitude of the induced moment is sufficiently large to account for the electric polarization of proteins. It is predicted by their theory that (1) the pH–dipole moment profile of protein solutions has three maxima near pH 4, 6.5, and 10 if the electrostatic interaction between protons is neglected and (2) the dipole moment would exhibit a monotonous decrease with increasing pH if a correction is made for the electrostatic interaction. It was observed that the pH–dipole moment profile of ovalbumin and bovine serum albumin (BSA) showed a monotonous increase with increasing pH. It assumes nearly a constant value above a certain pH. The disagreement between the experimental curve and the theory is obvious, and it was concluded that the Kirkwood–Shumaker theory is not sufficient to explain the dipole moment of ovalbumin and bovine albumin. The ion fluctuation moment is recalculated on the basis of the thermodynamic fluctuation theory. The agreement between the theory and the experimental results is improved. Not only the magnitude of dipole moment but also the pH dependence is similar to the experimental results.

Introduction

The interpretation of the dielectric polarization of aqueous solutions of macromolecules such as proteins had been based on a concept of permanent dipole moment.[1] It became, however, obvious that the polarization of counterions played an important part in the electric polarization of aqueous solutions of macromolecules.[2–4] A theory of proton fluctuation on the surface of the protein molecule was first introduced by Kirkwood and Shumaker.[5] They assumed that the deviation of protons from a symmetric distribution would give rise to a sufficiently large induced dipole moment. Since the number of basic sites usually exceeds the number of bound protons, there would be a sufficient opportunity for the protons to fluctuate and to give rise to a nonvanishing square dipole moment ($\Delta\mu^2$). They concluded by comparing their theory with the experimental values[1] that the dipole moment induced by proton fluctuation would be sufficiently large that the permanent dipole was not necessarily the major component of the dipole moment of some proteins. Kirkwood and Shumaker estimated, on a theoretical basis, the proton fluctuation dipole moment at various pH values. They found that the magnitude of the moment strongly depended on the pH of the solution and that only those groups with pK values nearly equal to the pH of the solution make the major contribution to the induced dipole. This is easily understood since the terms $[H^+]/K$ and $K/[H^+]$ in the denominator in eq. 7 have sharp minima when $[H^+]$ is equal to K. The theoretical curves for ovalbumin and bovine serum

(1) J. L. Oncley, "Amino Acids, Proteins and Peptides," E. T. Cohn and T. T. Edsall, Ed., Reinhold Publishing Corp., New York, N. Y., 1945.

(2) C. T. O'Konski, *J. Phys. Chem.*, **64**, 605 (1960).

(3) H. P. Schwan, *Advan. Biol. Med. Phys.*, **5**, 729 (1957).

(4) G. Schwarz, *J. Phys. Chem.*, **66**, 2636 (1962).

(5) J. G. Kirkwood and J. B. Shumaker, *Proc. Natl. Acad. Sci. U. S.*, **38**, 855 (1952).

albumin are shown in Figures 1 and 2. Although the comparison of experimental and theoretical values at one pH would offer a test of the theory, more satisfactory evaluation of the theory would be to obtain the pH–dipole moment profile and fit the curve into the theoretical curve. The thorough evaluation of the theory by obtaining the pH–dipole moment profile has not been done because of the experimental difficulties in low and high pH regions. With the improvement of instruments and the technique of correction for electrode polarization, however, it is now possible to carry out these measurements with considerable reliability. A systematic determination of dielectric increment of ovalbumin and bovine serum albumin was conducted over a wide pH range, and a more rigorous comparison between the theory and experiment was made.

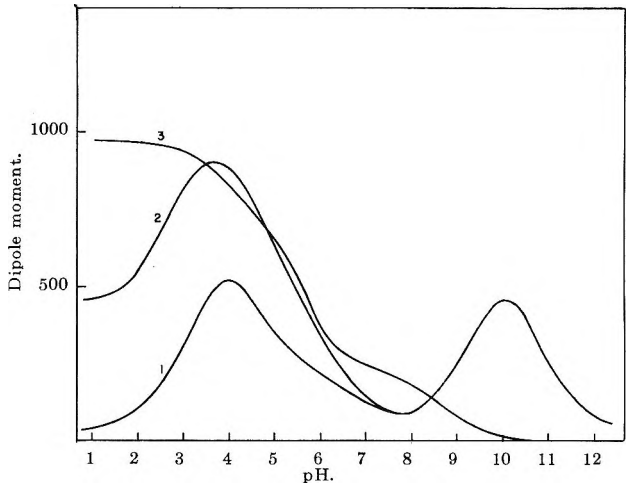

Figure 1. The theoretical values of the dipole moment of ovalbumin: curve 1, the dipole moment associated with proton fluctuation ($\Delta\mu$) without the correction for the electrostatic interaction; curve 2, $\langle\mu^2\rangle^{1/2}$ ($= (\langle\mu\rangle^2 + \Delta\mu^2)^{1/2}$) without the correction for electrostatic interaction; curve 3, $\langle\mu^2\rangle^{1/2}$ with the correction.

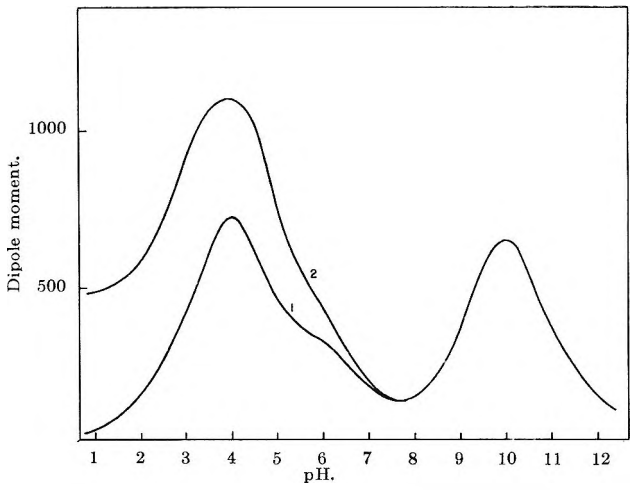

Figure 2. The theoretical values of the dipole moment of bovine albumin: curve 1, $\Delta\mu$ without the correction for the electrostatic interaction; curve 2, $\langle\mu^2\rangle^{1/2}$ without the correction.

Method of Calculation

The Kirkwood–Shumaker theory is essentially based on the fluctuation theory. If the fixed charges are distributed symmetrically, the protein molecule would not have a permanent dipole moment. Fluctuation of protons, however, may give rise to an induced dipole moment. According to the calculation of Kirkwood and Shumaker, the magnitude of the proton fluctuation moment can be sufficiently large to account for the experimental values of dipole moment of proteins.

The dielectric polarization of protein solution is represented by the equation

$$P = \frac{4\pi N}{3}\left(\alpha_i + \frac{\langle\mu_i^2\rangle}{3RT}\right) \tag{1}$$

where α_i is the polarizability at optical wave length and $\langle\mu_i^2\rangle$ is the mean-square dipole moment. $\langle\mu_i^2\rangle$ consists of two components, namely

$$\langle\mu_i^2\rangle = \langle\mu\rangle^2 + \Delta\mu^2 \tag{2}$$

where $\langle\mu\rangle^2$ is square-mean dipole moment and $\Delta\mu$ is the square fluctuation moment. The term $\Delta\mu^2$ can be expressed by the equation

$$\Delta\mu^2 = \langle(\mu - \langle\mu\rangle)^2\rangle \tag{3}$$

By introducing a proton occupation parameter x_i, the following equation is obtained

$$\Delta\mu^2 = e^2\Sigma[\langle x_i x_k\rangle - \langle x_i\rangle\langle x_k\rangle]R_iR_k \tag{4}$$

where $\langle x_i\rangle$ and $\langle x_k\rangle$ are the most probable values of fluctuating parameters x_i and x_k. This equation is equivalent to

$$\Delta\mu^2 = e^2\Sigma\langle(x_i - \langle x_i\rangle)(x_k - \langle x_k\rangle)\rangle R_iR_k \tag{5}$$

This is a second fluctuation moment of the parameter x_i and x_k. The second moments are usually very small when $i \neq k$, and the effective second moment can be given by the equation

$$\Delta\mu^2 = e^2\Sigma\langle(x_i - \langle x_i\rangle)^2\rangle R_i^2 \tag{6}$$

By calculating $\langle x_i^2\rangle$ and $\langle x_i\rangle^2$, they reached the following final expression for the induced dipole moment.

$$\Delta\mu^2 = e^2f^2b_0^2\sum_\alpha \frac{\nu_\alpha}{2 + K_\alpha/[\mathrm{H}^+] + [\mathrm{H}^+]/K_\alpha} \tag{7}$$

where

$$f^2 = \frac{\sigma^{4/3}}{4} \frac{(\sigma^2 + 2)\sqrt{\sigma^2 - 1} + \sigma^2(\sigma^2 + 4) \text{ sec.}^{-1} \sigma}{\sigma^2\sqrt{\sigma^2 - 1} + \sigma^4 \text{ sec.}^{-1} \sigma} \quad (8)$$

and

$$\sigma = a/b \qquad b_0 = (ab^2)^{1/3}$$

where σ is the axial ratio and b_0 is the radius of the equivalent sphere and ν_α is the equivalent titrated groups of the type α in the molecule.

The ion fluctuation moment is calculated by using eq. 7 for ovalbumin and bovine serum albumin. In eq. 7, the correction for the electrostatic interaction between protons is neglected. The correction was carried out numerically by Kirkwood and Shumaker for ovalbumin. (The method of this calculation is not described in their original article, and the author could not apply the method to bovine albumin.) The results of their calculation are all illustrated in Figures 1 and 2. The mean-square dipole moment $\langle\mu^2\rangle$ is given by eq. 2. The experimental value should be compared with the magnitude of $\langle\mu^2\rangle$ instead of $\Delta\mu^2$. In order to do so, the square-mean moment must be calculated independently and added to $\Delta\mu^2$. The magnitude of the square-mean moment can be calculated by the equation

$$\langle\mu\rangle^2 = \mu_0^2 + \sum_\alpha \frac{e^2 f^2 b_0^2}{1 + K_\alpha[\text{H}^+]} \quad (9)$$

The vectorial summation of all the terms would be

$$\langle\mu^2\rangle = \mu_0^2 + \sum_\alpha \frac{e^2 f^2 b_0^2}{1 + K_\alpha[\text{H}^+]} + \sum_\alpha \frac{e^2 f^2 b_0^2 \nu_\alpha}{2 + K_\alpha[\text{H}^+] + [\text{H}^+]K_\alpha} \quad (10)$$

The term $\Sigma e^2 f^2 b_0^2/(1 + K_\alpha/[\text{H}^+])$ has a considerable value at very acidic pH region, but it decreases rapidly with increasing pH. The magnitude of μ_0 may be small compared with the second term of eq. 9 and omitted from the calculation.

The following data are used for the calculation of the dipole moment. The titration data are reproduced in Table I. The amino acid data of ovalbumin are taken from the article by Tristram,[6] and those of bovine albumin are taken from Tanford, Swanson, and Shore.[7]

Dielectric increments are obtained by the formula

$$\Delta\epsilon = \frac{\epsilon_0 - \epsilon_\infty}{g} \quad (11)$$

where ϵ_0 and ϵ_∞ are the low-frequency and high-frequency dielectric constants, respectively. The molar dielectric increment is equivalent to P in eq. 1, and the dipole moment therefore can be expressed by the following equation ignoring the polarizability at optical wave length.

$$\langle\mu^2\rangle = \frac{9kT}{4\pi N}\Delta\epsilon M \quad (12)$$

Table I: Titratable Amino Acid Composition of Ovalbumin and Bovine Albumin

	pK	Ovalbumin	BSA
Free carboxyl	4.0	51	99
Imidazole	6.9	7	16
Amino group	9.8	29	57
Tyrosine	10.1	9	19

Methods

A Boonton Radio R-x Meter was used to measure the dielectric constant of protein solutions. The accuracy of the capacity reading is

$$\pm(0.5 + 0.0002f^2)\% \pm 0.1 \ \mu\mu\text{f.} \quad (13)$$

and is only slightly dependent on the frequency. Since the total capacity of the cell with protein solution used in this experiment is about 18 $\mu\mu$f., the reading error is approximately 0.15 $\mu\mu$f. Since the total dielectric increment of a protein solution is about 2 $\mu\mu$f., the error is about 15%, which is not very serious for the determination of the specific dielectric increment.

The correction for the inductance was made according to the equation[8]

$$C_s = \frac{C(1 + \omega^2 LC) + LR^2}{(1 + \omega^2 LC)^2 + (\omega L/R)^2} \quad (14)$$

Usually the inductance correction was negligible. The dielectric constant was calculated by the equation

$$\epsilon_s = \left[\frac{C_s - C_{\text{air}}}{C_{\text{H}_2\text{O}} - C_{\text{air}}}(\epsilon_{\text{H}_2\text{O}} - 1)\right] + 1 \quad (15)$$

This equation includes a minor correction term for the capacity of water.

Although the random error of each capacity reading was rather small, a systematic error due to electrode polarization in the lower frequency range was considerable in low and high pH regions where the conductivity of the solution was much higher. To eliminate elec-

(6) G. R. Tristram, *Advan. Protein Chem.*, 5, 84 (1949).

(7) C. Tanford, S. Swanson, and W. Shore, *J. Am. Chem. Soc.*, 77, 6414 (1955).

(8) H. P. Schwan, "Physical Techniques in Biological Research," Vol. 6, Academic Press, New York, N. Y., 1963, Chapter 6.

trode polarization, the electrodes were very carefully plated with platinum black to increase the surface capacity. Since the dielectric dispersion of proteins appeared in the neighborhood of 1 Mc., no further correction was necessary if the conductivity of the solution was sufficiently low. Accordingly, electrode polarization was not a serious problem in the isoionic pH region.

Dilute HCl or NaOH were used to change pH of the solution, and the addition of acid and alkali caused considerable conductivity increase. Further correction for electrode polarization was, therefore, necessary in these cases.

Various methods for the correction of electrode polarization have been described.[8] The total measured capacity can be expressed as

$$C = C_s + \frac{1}{C_p R^2 \omega^2} \qquad (16)$$

where C_s is the capacity of solution, ω is the angular frequency, R is the resistivity, and C_p is the electrode polarization. The effect of electrode polarization is, therefore, inversely proportional to C_p, and this means that the larger the electrode polarization, the smaller the second term of the equation. The electrodes were, therefore, plated with platinum black as often as possible to keep the electrode capacity as large as possible. Very clean platinum electrodes were plated with platinum black at 10 ma. for 10 min. By doing this, the effect of electrode polarization was effectively lowered, making measurements possible between pH 3 and 10, which was sufficient for the study of the Kirkwood-Shumaker theory.

Ovalbumin and bovine serum albumin were purchased from Sigma Chemical Corp. and were found to have specific dielectric increments of 0.22 for ovalbumin and 0.37 for BSA. The value for ovalbumin was slightly higher than that obtained by Oncley, *et al.*[9] (0.17). However, it was demonstrated[10] that the dielectric increment of ovalbumin was considerably dependent on the method of purification and the history of the solution; therefore, the difference might be due to the same reasons.

Results

Dielectric dispersion curves of ovalbumin at pH 7, 4.3, and 3.2 are shown in Figure 3. The low-frequency plateau at pH 7.0 can be easily obtained, and no further correction is necessary. At pH 3.2, the conductivity is higher, and this makes the effect of electrode polarization larger. The rise of the dielectric constant in the low-frequency region is undoubtedly due to electrode polarization. Fortunately, the low-frequency plateau begins to appear before electrode polarization is very serious; hence, one can extrapolate the line through the measured points at higher frequencies, as shown by the broken line.

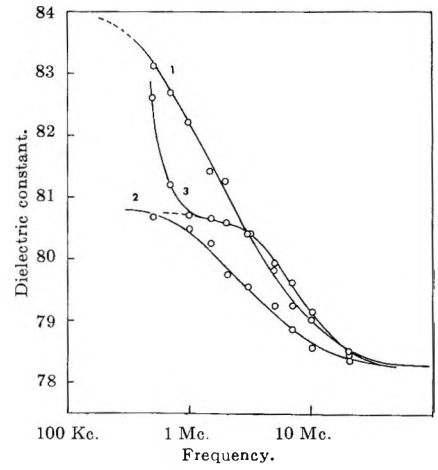

Figure 3. Dielectric dispersion of ovalbumin at pH 7 (curve 1), 4.3 (curve 2), and 3.2 (curve 3).

Figure 4 illustrates the dipole moment of ovalbumin between pH 3 and 10. The dipole moment increases from pH 3 to 5 monotonically and approaches a constant value. The dissimilarity between theoretical curves and the experimental curve is very obvious (see Figure 1).

Figure 5 illustrates the dielectric dispersion of BSA at pH 7.0 and 4.5. It has been known that BSA undergoes a structural transformation at pH 5.0 and assumes

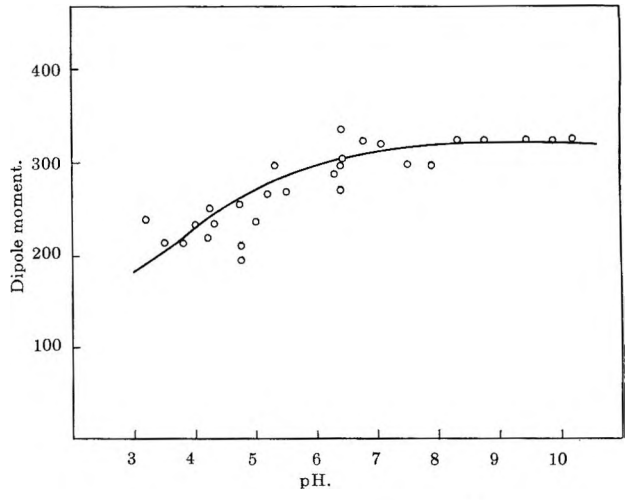

Figure 4. Dipole moment of ovalbumin at various pH values. The ordinate is in Debye units.

(9) J. L. Oncley, J. D. Ferry, and J. Shack, *Ann. N. Y. Acad. Sci.*, **40**, 371 (1940).

(10) S. Takashima, *J. Polymer Sci.*, **A1**, 2791 (1963).

a disordered configuration. The dielectric dispersion at pH 4.5 is very different from that at pH 7.0. The dispersion curve is shifted to a lower frequency region, and the dielectric increment obviously assumes a larger value indicating the transition of the structure from highly ordered to less ordered configurations. The transitions will change the shape parameter in eq. 7, and the correction must be made for this structural change. We do not, however, have sufficient information about the structure of denatured proteins so that the data below pH 4.5 cannot be used for the evaluation of the theory.

Figure 6 shows the dipole moment of bovine serum albumin between pH 4.5 and 10. The points below pH 4.5 are omitted, but the broken line indicates the rise of the curve. In spite of the complication due to structural change, the dipole moment–pH profile of bovine albumin is still similar to that of ovalbumin, and the curve likewise does not fit the theory.

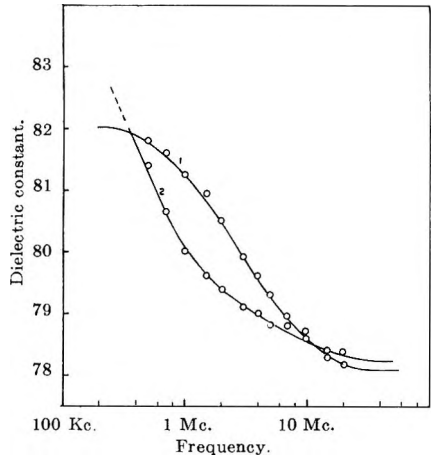

Figure 5. Dielectric dispersion of bovine albumin at pH 7 (curve 1) and 4.5 (curve 2).

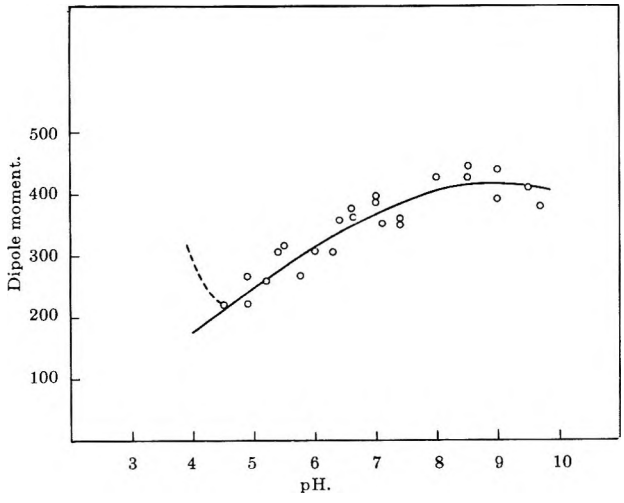

Figure 6. Dipole moment of bovine albumin at various pH values. The ordinate is in Debye units.

Discussion

As mentioned, the dipole moment–pH profile of ovalbumin and bovine albumin do not agree with the theoretical curves based on the Kirkwood–Shumaker theory. BSA is known to undergo structural change below pH 5.0[11]; hence, the increase of dielectric increment of this protein below pH 5.0, undoubtedly due to the structural change, must be disregarded.

Taking the structural complication into account, it is obvious that the dipole moment has an entirely different pH dependence from what was predicted by the theory. Although the agreement between the experimental result and the theory in its present form is very poor, one may be able to obtain a different equation by adopting different methods of calculation. As was pointed out earlier, the Kirkwood–Shumaker theory is based on the calculation of the second fluctuation moment. If we make an assumption that the fluctuation of the proton in a weak electric field is not much more than the magnitude of thermodynamic fluctuation, the problem reduces to the calculation of the second moment of thermodynamic fluctuation. Conversely, the problem reduces to whether the fluctuation of the proton, the magnitude of which is not much more than that of thermodynamic fluctuation, can produce a large dipole moment or not. This calculation can be done without much trouble once we known the distribution function for the parameter x_i. According to Kirkwood–Shumaker, the proton occupation number can be expressed by the equation

$$\langle x_i \rangle = x_i e^{(F - F_i)/kT} \tag{17}$$

where F is the free energy of the average proton configuration and F_i is the free energy of instantaneous proton configuration; if this distribution function is combined with the formula

$$\langle x_i \rangle = \frac{1}{1 + K_i/[\mathrm{H}^+]} \tag{18}$$

the second moment is obtained by the derivatives[11]

$$\langle (x_i - \langle x_i \rangle)^2 \rangle = kT \frac{\partial \langle x_i \rangle}{\partial \lambda_i} \tag{19}$$

where $\lambda_i = [\mathrm{H}^+]/K_i$. Hence

$$\langle (x_i - \langle x_i \rangle)^2 \rangle = kT \sum_i \left[\frac{K_i}{[\mathrm{H}^+](1 + K_i/[\mathrm{H}^+])} \right]^2 \tag{20}$$

(11) T. Hill, "Statistical Mechanics," McGraw-Hill Book Co., Inc., New York, N. Y., 1956, p. 97.

The induced dipole moment associated with the proton fluctuation is finally

$$\Delta\mu^2 = kT\sum_i \sigma_i \left[\frac{K_i}{[H^+](1 + K_i/[H^+])}\right]^2 e^2 b_0^2 f^2 \quad (21)$$

The symbols have the same meaning as before except for σ_i which is now the charge density per unit area. The theoretical values are calculated by this equation, and the results are shown in Figure 7. The agreement between the theoretical values and the experimental results is greatly improved. The calculated dipole moment has the same order of magnitude as that of the observed. Moreover, this equation predicts a pH dependence of dipole moment which is in fair agreement with the experimental observation. Although this is a rough calculation, it indeed indicates that a small fluctuation of a proton can give rise to a large dipole moment in protein. It is interesting to note that protons do not have to move from one end of the molecule to the other, but a slight shift from the equilibrium position is enough to produce a considerable dipole moment.

It must be remembered that the preceding calculation is a rough estimation of the fluctuation moment and is by no means conclusive. As a matter of fact, there are experimental results which support the permanent dipole theory, and the possibility of the existence of a permanent dipole should not be ruled out.

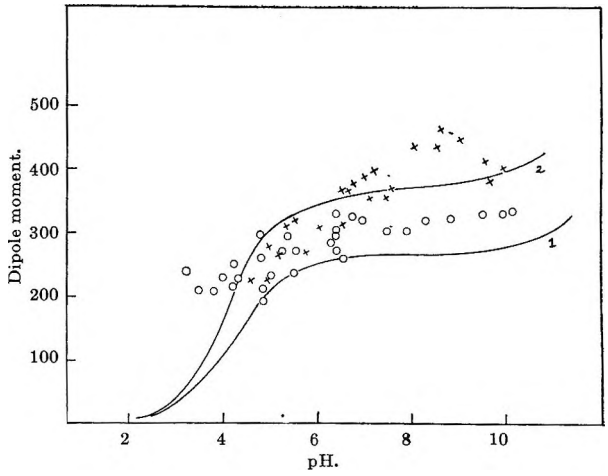

Figure 7. pH dependence of dipole moment of ovalbumin and BSA. Curves 1 and 2 are theoretical curves calculated by eq. 21 for ovalbumin and BSA. The open circles and the crosses are experimental values for ovalbumin and BSA, respectively.

Acknowledgments. The author is indebted to Prof. H. P. Schwan for his stimulating discussion and advice. This work was supported by Public Health Service Grant GM-12083-01.

Rates of Mercapto Proton Exchange for 2-Mercaptoethanol in Aqueous Solution[1a,b]

by Maurice M. Kreevoy,[1c] Dale S. Sappenfield, and William Schwabacher

School of Chemistry, University of Minnesota, Minneapolis, Minnesota 55455 *(Received January 11, 1965)*

The rate of exchange of the mercapto proton of 2-mercaptoethanol with aqueous solutions has been studied by an n.m.r. line-broadening technique in acetic acid–sodium acetate buffers and also in perchloric acid. It was concluded that the exchange is catalyzed by bases but not by acids, even up to 11 *M* $HClO_4$. Presumably, the mechanism of catalysis is abstraction of a proton from the mercaptan by the base. At room temperature the rate constant for catalysis by acetate ion is $\sim 2 \times 10^3$ l. mole^{-1} sec.$^{-1}$ in the limit of low mercaptan concentration and somewhat lower at substantial mercaptan concentration. The rate constant for the uncatalyzed reaction (and/or the water-catalyzed reaction) is ~ 32 sec.$^{-1}$.

Recently developed techniques based on n.m.r. line broadening permit the measurement of rates with half-times in the range 10^{-1} to 10^{-3} sec.[2] They are particularly effective in measuring proton-exchange rates. Such a technique has now been applied to the exchange rate of the mercapto proton of 2-mercaptoethanol in aqueous solution at room temperature. The reaction is so sensitive to catalysis by bases that rates had to be measured in somewhat acidic solutions (pH 4 to 5.5).

Experimental

2-Mercaptoethanol (Eastman grade, Distillation Products Industries) was redistilled and had b.p. 153–154°, $n^{25.5}$D 1.4987 (lit.[3] b.p. 157–158°, n^{20}D 1.4996). Acids and bases, and sodium chloride solutions, were made up from analytical reagent grade materials and were standardized in the usual way. The pH of several solutions was measured with a pH meter, and values in reasonable agreement with those calculated from dissociation constants were obtained.

The n.m.r. spectra were obtained with a Varian Model 4300B high resolution spectrometer (modified so as to be equivalent to Model HR-60) operating at 56.442 Mc. Typical spectra were produced with a radiofrequency attenuation of 80 db. below 0.5 w. The sweep rate was typically 1 cycle sec.$^{-2}$, so that the width at half-height being measured was several millimeters. These widths were measured with a ruler; sometimes with the aid of a bow divider. It was shown that reducing the sweep rate by a factor of 5 did not materially alter the results.

Relative frequencies were first established by the side-band technique, using a Hewlett-Packard counter to determine the side-band frequencies. Once the frequency separation of the two aqueous solution triplets was known, most subsequent spectra were calibrated by assuming that this frequency separation remained constant.

Values of intensity ratios and unbroadened peak widths were obtained by averaging measurements made on from 6 to 16 spectra. Between 12 and 16 spectra were initially obtained. Widths at half-height were measured on the broadened as well as the unbroadened peak, and those spectra were rejected

(1) (a) This research was supported, in part, by the U. S. Army Medical Research and Development Command through Contract DA-49-193-MD-2027. Reproduction in whole or in part is permitted for any purpose of the United States Government; (b) taken, in part, from the Ph.D. thesis of D. S. Sappenfield, University of Minnesota, 1962; (c) Sloan Foundation Fellow, 1960–1964; National Science Foundation Senior Postdoctoral Fellow, 1962–1963.

(2) (a) A. Lowenstein and T. M. Connor, *Ber. Bunsenges. physik. Chem.*, **67**, 280 (1963); (b) H. Strehlow, "Investigation of Rates and Mechanisms of Reactions," Part II, 2nd Ed., S. L. Friess, E. S. Lewis, and A. Weissberger, Ed., Interscience Publishing Division, John Wiley and Sons, Inc., New York, N. Y., 1963, p. 865.

(3) G. M. Bennett, *J. Chem. Soc.*, 2139 (1922).

in which the product of the height and the width at half-height for the broadened and the unbroadened peak differed by more than 10%. Certain other spectra were rejected because their general appearance was unsatisfactory.

Results

In fairly concentrated carbon tetrachloride solution, the n.m.r. spectrum of 2-mercaptoethanol consists of a triplet of weight 1, τ = 8.49 p.p.m.[4] (SH); a quadruplet of weight 2, τ = 7.36 p.p.m. (SCH_2); a triplet of weight 2, τ = 6.34 p.p.m. (OCH_2); and a singlet of weight 1, τ = 5.85 p.p.m. (OH). Both the low intensity triplet and the quartet show second-order splitting. In neutral or basic aqueous solution both the low intensity triplet and the singlet disappear, presumably by exchange with the water. The rest of the spectrum takes on the appearance of a slightly distorted A_2X_2 system. As the aqueous solution is made more acidic, however, beginning at about pH 5.5, the high-field triplet broadens, until, at about pH 4, it is hardly distinguishable as a triplet. This broadening is most notable in the central line of the triplet because it is substantially sharper than the others to start with. The appearance of the spectrum then remains roughly the same up to 11 *M* $HClO_4$. The high-field band does not sharpen, and the SH signal does not become distinguishable. The low-field triplet does not change systematically with pH. Representative spectra are shown in Figures 1 and 2.

These changes can be qualitatively understood if there is an uncatalyzed or water-catalyzed exchange of the mercapto proton and also a base-catalyzed exchange but no acid catalyzed exchange. The hydroxyl proton exchanges very rapidly in all of these solutions.[2,5] Coupling with the mercapto proton would double each line of the triplet if its exchange were slow by comparison with the inverse of the coupling constant. If they are comparable, the lines of the triplet are broadened.[2]

Following this interpretation eq. 1 was used to determine the half-time for mercapto proton exchange. Equation 1 is a rearranged version of eq. 7 in the work of Takeda and Stejskal.[6]

$$\frac{1}{\tau} = \frac{4(I/I_0 - 1)/T_2\delta\omega + (I/I_0)T_2\delta\omega}{8(1 - I/I_0)/\delta\omega} \qquad (1)$$

where $\tau \equiv$ the mean lifetime of a mercapto proton, $I \equiv$ the height of the broadened peak, $I_0 \equiv$ the height of the unbroadened peak, $1/T_2 \equiv$ the width at half-height of the unbroadened peak, and $\delta\omega \equiv$ the separation, in sec.$^{-1}$, of the two peaks that would be observed in the absence of exchange. In the limiting case, as I/I_0 approaches unity, eq. 1 simplifies to eq. 2. Although

$$\frac{1}{\tau} = \frac{(I/I_0)T_2(\delta\omega)^2}{8(1 - I/I_0)} \qquad (2)$$

eq. 1 was actually used throughout in the present work, values derived from eq. 2 would not be very

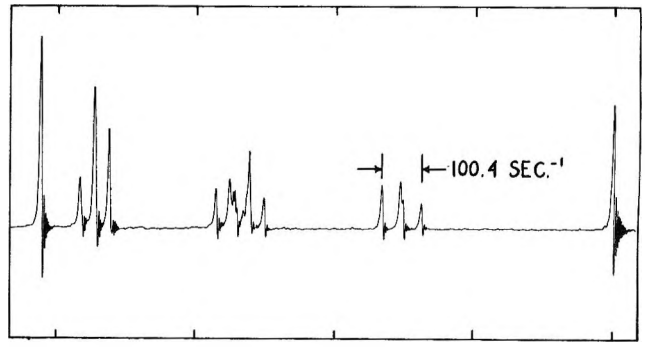

Figure 1. N.m.r. spectrum of a 20% solution of 2-mercaptoethanol in carbon tetrachloride.

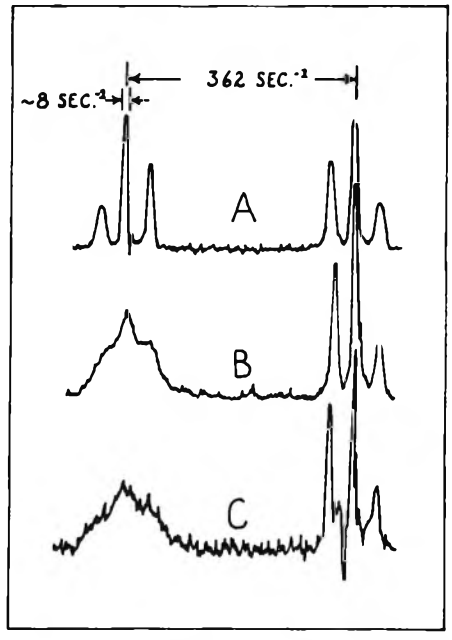

Figure 2. N.m.r. spectra of 2.4 *M* aqueous solutions of 2-mercaptoethanol: A, in neutral water; B, in 5×10^{-4} *M* perchloric acid; C, in 11 *M* perchloric acid. The multiplet separation and the width at half-height of a typical unbroadened peak are shown. The spectrum in relatively concentrated perchloric acid has a poorer signal to noise ratio than the others owing to the absorption of energy by the solvent.

(4) G. V. D. Tiers, *J. Phys. Chem.*, **62**, 1151 (1958).

(5) J. D. Roberts, "Nuclear Magnetic Resonance," McGraw-Hill Book Co., Inc., New York, N. Y., 1959, pp. 64–66.

(6) M. Takeda and E. O. Stejskal, *J. Am. Chem. Soc.*, **82**, 25 (1960).

different. Table I shows the values of $1/\tau$ obtained in a variety of acetic acid–sodium acetate buffers. In all of these determinations the ionic strength was maintained at 0.22 M by addition of appropriate quantities of sodium chloride. The temperature in the probe could not be controlled, but it was measured on a number of occasions and consistently found to be between 25 and 30°. The reproducibility of $1/\tau$, as judged from repetitive determinations, shown in Table I, would seem to be about ±10%, and a good part of this scatter is probably due to temperature variations. With an activation energy of 10 kcal. mole^{-1} a temperature change of 3° would change $1/\tau$ by 18%.

Since $1/\tau$ has the significance of a pseudo-first-order rate constant, eq. 3 expresses quantitatively the idea that there is an uncatalyzed (and/or water-catalyzed) exchange and also the possibility of a base-catalyzed exchange for any base present in solution. The bases

$$1/\tau = k_1 + \sum_{B} k_B(B) \qquad (3)$$

actually present in the solutions studied are the alcohol end of the substrate, acetate ion, thiolate ion, hydroxide ion, and alcoholate ion. The last three are derived from the mercaptan end of the substrate, the water, and alcohol end of the substrate, respectively, on equilibrating with the acetate ion.

The acetate ion catalytic coefficient, k_{OAc^-}, was obtained as the slope of plots of $1/\tau$ as a function of acetate concentration at constant buffer ratio and constant ionic strength for substrate concentrations, 2.4 and 1.3 M. The buffer ratio, $(OAc^-)/(HOAc)$, was 1.06 at the higher mercaptan concentration and 0.71 at the lower. At 2.4 M mercaptan, four values of $1/\tau$ were obtained for acetate concentrations ranging from 2.0×10^{-3} to 2.2×10^{-1} M. They gave a slope, k_{OAc^-}, of 1.2×10^3 l. mole^{-1} sec.$^{-1}$ with 50% confidence limits of $\pm 0.1 \times 10^3$ and 90% confidence limits of $\pm 0.3 \times 10^3$ l. mole^{-1} sec.$^{-1}$. The intercept, which is the quantity, $k_1 - k_{OAc^-}(OAc^-) + \sum_{B} k_B(B)$, has the value, 81 sec.$^{-1}$, with 50% confidence limits of ±4 sec.$^{-1}$. At 1.3 M mercaptan, six values of $1/\tau$ gave a slope, k_{OAc^-}, of 1.9×10^3 l. mole^{-1} sec.$^{-1}$ and an intercept, $k_1 - k_{OAc^-}(OAc^-) + \sum_{B} k_B(B)$, of 70 sec.$^{-1}$, with similar confidence limits. These values, and their uncertainties, were all obtained by the method of least squares.[7] The best estimate of k_{OAc^-} in infinitely dilute solutions would seem to be about 2×10^3 l. mole^{-1} sec.$^{-1}$.

For each substrate concentration the uncatalyzed rate, k_1, was obtained by plotting $\{1/\tau - k_{OAc^-}(OAc^-)\}$ as a function of the buffer ratio. These plots are satisfactorily linear. The intercept, k_1, is 34 ± 4 sec.$^{-1}$ at 1.3 M substrate and 31 ± 6 sec.$^{-1}$ at 2.4 M substrate. The values and the uncertainties (which are 50% confidence limits) were obtained by the method of least squares[7] from 10 values of $1/\tau$ at 1.3 M mercaptan and 7 values of $1/\tau$ at 2.4 M mercaptan. In the same way, but much less reliably, k_1, 25 sec.$^{-1}$, can be obtained from the two pieces of data available for 0.5 M mercaptan. These values do not suffer badly from whatever uncertainty exists in k_{OAc^-} because most of the solutions having low buffer ratios, which are most important in determining these intercepts, also have low acetate concentrations, $\sim 3 \times 10^{-3}$ M. Thus, the $k_{OAc^-}(OAc^-)$ term subtracted from $1/\tau$ is ~5 sec.$^{-1}$, fairly small by comparison with k_1. If it is assumed that the spectra in strong perchloric acid are near the coalescence point, which seems reasonable from their appearance (Figure 2, B and C), a value of 30–40 sec.$^{-1}$ is obtained for $1/\tau$.[8] This must be identified with k_1, as no basic species are present. Thus, k_1 seems to have a value of ~32 sec.$^{-1}$, fairly independent of the medium.

After k_1 and the acetate term have been accounted

Table I: Exchange Rates in Acetic Acid–Sodium Acetate Buffers at Room Temperature

(RSH), M	10^3(OAc$^-$), M	10^3(HOAc), M	$1/\tau$, sec.$^{-1}$
0.5	2.7	3.2	53
0.5	10.0	1.0	353
0.9	2.7	3.2	71
1.3	87	123	223
1.3	43	61	149
1.3	17	24	125
1.3	2.6	3.7	78
1.3	2.6	3.7	67
1.3	2.6	3.7	63
1.3	2.6	11.5	45
1.3	2.6	5.8	65
1.3	2.6	0.12	153
1.3	2.6	0.12	154
2.4	2.0	5.8	38
2.4	2.0	2.9	55
2.4	2.0	1.9	75
2.4	2.0	0.58	171
2.4	216	204	340
2.4	83	79	162
2.4	22	21	127

(7) C. A. Bennett and N. L. Franklin, "Statistical Analysis in Chemistry and the Chemical Industry," John Wiley and Sons, Inc., New York, N. Y., 1954, pp. 36–40, 231.

(8) J. A. Pople, W. G. Schneider, and H. J. Bernstein, "High-resolution Nuclear Magnetic Resonance," McGraw-Hill Book Co., Inc., New York, N. Y., 1959, p. 223.

for, the remaining terms under the summation in eq. 3 are the hydroxide term, which can be written k_{OH}-K_W-$(OAc^-)/K_{HOAc}(HOAc)$, the intramolecular alkoxide term, which can be written k'_{RO}-$K_{ROH}(OAc^-)/K_{HOAc}$-(HOAc), the intermolecular alkoxide term, which can be written k_{RO}-$K_{ROH}(OAc^-)(S)/K_{HOAc}(HOAc)$, and the mercaptide term, which can be written k_{RS}-K_{RSH}-$(OAc^-)(S)/K_{HOAc}(HOAc)$. (In these terms K_W is the autoprotolysis constant of water, K_{BH} is the acid dissociation constant of BH, and S is the substrate.) All of these terms are directly proportional to the buffer ratio, giving rise to the linear plots of $\{1/\tau - k_{OAc^-}$-$(OAc^-)\}$ *vs.* buffer ratio at constant substrate concentration noted in the previous paragraph. If the constants involved were all invariant under changes in substrate concentration, the slopes of these plots would either be constant (if the intermolecular alcoholate term and the mercaptide term were negligible) or would increase monotonically with the substrate. The actual slopes are 25 sec.$^{-1}$ at 0.5 *M* substrate, 42 sec.$^{-1}$ at 0.9 *M* substrate, 51 ± 3 sec.$^{-1}$ at 1.3 *M* substrate, and 41 ± 4 sec.$^{-1}$ at 2.4 *M* substrate. The latter two were obtained from the least-squares analysis mentioned in the previous paragraph, and the uncertainties are 50% confidence limits. They are considerably more reliable than the others. For 1.3 and 2.4 *M* substrate the measured values of k_{OAc^-} were used. For both 0.5 and 0.9 *M* substrate a value of k_{OAc^-} had to be assumed and 2.0×10^3 l. mole^{-1} sec.$^{-1}$ was used. For 0.9 *M* substrate a value of k_1 also had to be assumed, and 32 sec.$^{-1}$ was used. From these results, it is plainly impossible to sort out the contributions of the various bases other than acetate ion. The results probably show the influence of the uncertainty in k_{OAc^-}, and it is likely that the various k_B are not invariant under changes in substrate concentration, as k_{OAc^-} seems not to be.

It is possible to examine the results at 1.3 *M* mercaptan and 2.4 *M* mercaptan for internal consistency. The intercepts, *I*, of the plots, mentioned above, of $1/\tau$ *vs.* the acetate concentration at constant buffer ratio are given by eq. 4. From the known values of *I*, the buffer ratios, and k_1, *Z* is readily obtained. It

$$I = k_1 + Z(OAc^-)/(HOAc) \quad (4)$$

$$Z \equiv \{k_{OH}\text{-}K_W + k'_{RO}\text{-}K_{ROH} + k_{RO}\text{-}K_{ROH}(S) + k_{RS}\text{-}K_{RSH}(S)\}/K_{HOAc}$$

should be identical with the *slopes* cited in the previous paragraph. At 1.3 *M* substrate, with buffer ratio 0.71, *I* was 70 sec.$^{-1}$, from which *Z* is 54 sec.$^{-1}$. At 2.4 *M* mercaptan, with buffer ratio 1.06 and *I* 81 sec.$^{-1}$, *Z* is 46 sec.$^{-1}$. These values are in excellent agreement with those obtained by the other method. They confirm the conclusion that at least one and perhaps several of the terms in *Z* must contribute substantially to the observed rates.

Discussion

The general base catalysis and the absence of detectable acid catalysis strongly suggests that proton abstraction by base is the predominant exchange mechanism. If this interpretation can be accepted, k_{OAc^-}, 2×10^3, is the rate constant for the abstraction of a proton from the mercaptan by acetate ion. From the acid dissociation constants of 2-mercaptoethanol, 3.7×10^{-10},[9] and acetic acid, 1.75×10^{-5},[10] the equilibrium constant, 2.1×10^{-5}, for the reaction of the mercaptan with acetate ion can readily be calculated. From this the value, 10^8 l. mole^{-1} sec.$^{-1}$ is obtained for the rate constant of the reverse reaction, that of acetic acid with mercaptide ion. This is probably about two powers of ten below the diffusion rate for these two species.[11]

The simplest interpretation of k_1 is that this is the rate constant for the abstraction of a proton by water from the mercaptan. The rate constant of the reverse reaction, that of the proton with the mercaptide ion, then becomes 9×10^{10} l. mole^{-1} sec.$^{-1}$. This seems rather large, even for a diffusion-controlled reaction.[11,12] An alternative is to suppose that a significant part of k_1 is due to internal proton transfer to give the zwitterion, $H_2O^+CH_2CH_2S^-$.

The lack of an acid-catalyzed exchange bespeaks the very feeble basicity of the mercapto group.[13]

Eigen and Maass seem to have measured the rates of proton abstraction from 2-mercaptoethanol by a variety of bases[11,12] and obtained results analogous to those presented here. Unfortunately, the numerical values of their rate constants do not seem to have been published. Sheinblatt and Luz[14] have observed both acid- and base-catalyzed proton exchange in liquid 2-mercaptoethanol, but this medium is so different from dilute aqueous solution that their results are not directly comparable with ours.

Acknowledgment. Part of this work was done while M. M. Kreevoy was a guest in the Physical Chemistry Laboratory, Oxford. He wishes to thank Professor

(9) M. M. Kreevoy, E. T. Harper, R. E. Duvall, H. S. Wilgus, III, and L. T. Ditsch, *J. Am. Chem. Soc.*, **82**, 4899 (1960).

(10) G. Kortum, W. Vogel, and K. Andrussow, "Dissociation Constants of Organic Acids in Aqueous Solution," Butterworth and Co. Ltd., London, 1961, p. 241.

(11) M. Eigen, *Pure Appl. Chem.*, **6**, 97 (1963).

(12) M. Eigen, *Angew. Chem.*, **75**, 489 (1963).

(13) E. M. Arnett, C. Y. Wu, J. N. Anderson, and R. D. Bushick, *J. Am. Chem. Soc.*, **84**, 1674 (1962).

(14) Unpublished results.

Sir Cyril Hinshelwood and Mr. R. P. Bell of that laboratory for their hospitality. He also wishes to thank Dr. A. Loewenstein, of the Technion, Haifa, for a very useful consultation on this work.

The Mercury-Photosensitized Decomposition of Isopentane

by Robert R. Kuntz

Department of Chemistry, University of Missouri, Columbia, Missouri *(Received January 14, 1965)*

The $Hg(^3P_1)$-sensitized decomposition of isopentane has been studied at 25° and 10 cm. pressure, and the hydrogen atom reactions have been studied by means of added trimethylethylene. The average value for the disproportionation/combination ratio of the various isopentyl radicals is 2.5. Rate constant ratios for H atom reactions with isopentane and trimethylethylene compare favorably with liquid phase results. The product distribution is similar to that observed in the liquid phase.

Introduction

The mercury($^3P_1$)-sensitized decomposition of a number of alkanes has been studied in detail. These studies have indicated the primary interaction between $Hg(^3P_1)$ and alkane molecules results in hydrogen atoms and free radicals: $Hg^* + RH \rightarrow R + H + Hg$. A mechanism has been proposed for this process in the vapor phase.[1] The liquid phase decomposition gives evidence of more than one primary process,[2] but the behavior of the final products of this interaction is the same. Recently, the mercury-photosensitized decompositions of some alkanes have been studied in the liquid phase, and values for the disproportionation/combination ratio of the alkyl radicals measured.[2] This series of studies was initiated in order to compare rate constant data for free radicals in the vapor phase with those observed in the liquid phase photolysis and radiolysis studies.

Experimental

Pure grade isopentane from the Phillips Petroleum Co. was used in all cases. All olefin and polar impurities were removed by the peak isolation technique on 0.64-cm. × 2.75-m. β-β-oxydipropionitrile column. Trimethylethylene of stated 99% purity was obtained from Matheson Coleman and Bell and used without further purification. Hydrocarbon samples were degassed by the freeze–thaw technique and stored over P_2O_5. The reaction vessel was constructed of Vycor tubing 30 × 250 mm. connected through a graded seal to a mercury cutoff which doubled as a manometer. The light source was a Hanovia low pressure, mercury resonance lamp. The reaction vessel was mounted 50 cm. from the resonance lamp in order to reduce the intensity such that low conversion experiments might be carefully timed. A manual shutter allowed the lamp to be warmed up prior to exposure.

Products not condensable at liquid air temperature were pumped directly into the chromatograph inlet by a Toepler pump. This gas consisted, within analytical error, entirely of hydrogen. The hydrogen was analyzed by the change in thermal conductivity of a nitrogen stream passing through a silica gel column after sample injection. Results obtainable in this manner were reproducible to ±3%.

All experiments were done at 10 cm. isopentane pressure and 25°. The hydrogen was removed at intervals such that never more than 0.3% of the excited

(1) Y. Rousseau, O. P. Strausz, and H. E. Gunning, *J. Chem. Phys.*, 39, 962 (1963).

(2) R. R. Kuntz and G. J. Mains, *J. Am. Chem. Soc.*, 85, 2219 (1963).

mercury atoms was quenched by hydrogen. In experiments with added olefin, the concentration was kept below 0.7% so no more than 3% of the excited mercury atoms was quenched by olefin.

Results

In Figure 1, the rate of hydrogen production is plotted against illumination time. Samples were taken at various intervals with the lowest conversions being about 0.05%. The rate of hydrogen production fell rapidly from an extrapolated value of 5.08×10^{-9} mole/sec. Gas chromatographic analysis of the liquid products indicates two products in the olefin region and three products in the dimer region. The predominant olefin was identified by retention time to be trimethylethylene. While dimer products were not identified, their relative retention times and peak areas closely resemble those observed on a similar column in the mercury-sensitized decomposition of liquid phase isopentane.[3]

In a few experiments, trimethylethylene was added to determine the reactivity of H atoms with this predominant olefin. Results are shown in Figure 2.

Discussion

The mechanism proposed for the decomposition of isopentane is similar to that proposed for other alkanes.[4,5]

$$\mathrm{Hg} + h\nu \longrightarrow \mathrm{Hg}^* \qquad (1)$$

$$\mathrm{Hg}^* + \mathrm{RH} \longrightarrow \mathrm{R} + \mathrm{H} + \mathrm{Hg} \qquad (2)$$

$$\mathrm{H} + \mathrm{RH} \longrightarrow \mathrm{H_2} + \mathrm{R} \qquad (3)$$

$$\mathrm{R} + \mathrm{R} \longrightarrow \mathrm{RH} + \mathrm{R}(-\mathrm{H}) \qquad (4)$$

$$\mathrm{R} + \mathrm{R} \longrightarrow \mathrm{R_2} \qquad (5)$$

As olefin accumulates in the system, reactions 6 and 7 become important.

$$\mathrm{H} + \mathrm{R}(-\mathrm{H}) \longrightarrow \mathrm{R} \qquad (6)$$

$$\mathrm{H} + \mathrm{R}(-\mathrm{H}) \longrightarrow \mathrm{H_2} + \mathrm{R}(-2\mathrm{H}) \qquad (7)$$

If one is to accept the results of Holroyd and Klein[6] as a true indication of radicals produced in reaction 2, these radicals will be 75% $CH_3\dot{C}(CH_3)CH_2CH_3$ and 24% $CH_3CH(CH_3)\dot{C}HCH_3$. Reaction 3 will give these same radicals owing to the greater reactivity of tertiary and secondary CH bonds. Addition of H atoms to trimethylethylene will also produce these radicals. Depletion of the olefin formed in reaction 4 by H atom abstraction, reaction 7, will lead to an olefin radical. This radical will disappear by reactions 8–10.

$$\mathrm{R}(-2\mathrm{H}) + \mathrm{RH} \longrightarrow \mathrm{R}(-\mathrm{H}) + \mathrm{R} \qquad (8)$$

$$\mathrm{R}(-2\mathrm{H}) + \mathrm{R} \longrightarrow 2\mathrm{R}(-\mathrm{H}) \qquad (9)$$

$$\mathrm{R}(-2\mathrm{H}) + \mathrm{R} \longrightarrow \mathrm{RR}(-2\mathrm{H}) \qquad (10)$$

The relative importance of these reactions cannot be properly assessed from the present data. The disappearance of an olefin by reaction 7, however, always leads to the production of another olefin, and the total olefin concentration is not depleted by this reaction. As a first approximation, then, the rate of depletion of olefin by reaction 7 is compensated for by reactions 8–10, and these latter reactions will not significantly affect the H atom reaction kinetics.

Under conditions of constant light intensity and low concentrations of products, the initial rate of quenching of Hg* by isopentane is a constant K equal to the initial

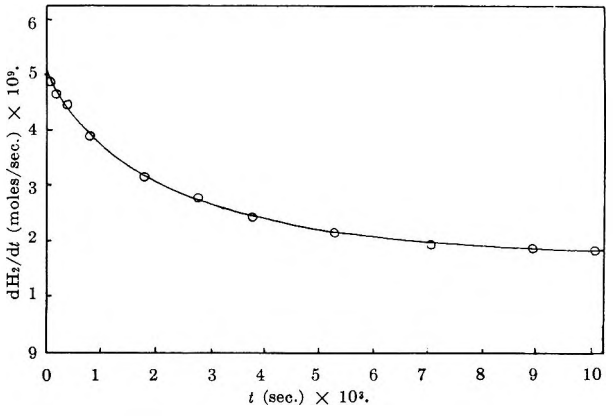

Figure 1. Hydrogen production as a function of photolysis time.

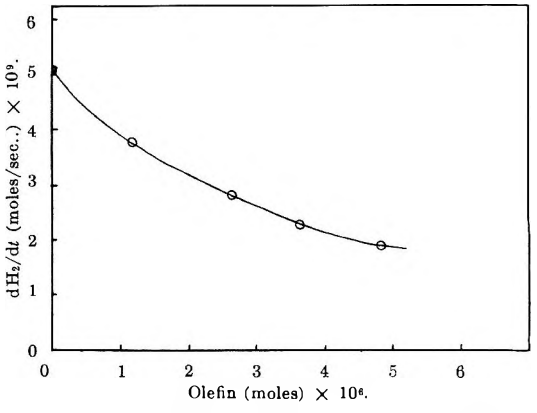

Figure 2. Effect of trimethylethylene on H_2 production.

(3) R. Kuntz, Ph.D. Thesis, Carnegie Institute of Technology, 1962.

(4) R. A. Back, *Trans. Faraday Soc.*, **54**, 512 (1958).

(5) R. J. Cvetanović, W. E. Falconer, and K. R. Jennings, *J. Chem. Phys.*, **35**, 1225 (1961).

(6) R. A. Holroyd and G. W. Klein, *J. Phys. Chem.*, **67**, 2273 (1963).

rate of hydrogen production.[7] From this reaction scheme, it can be shown that

$$\frac{dH_2}{dt} = \frac{k_3[RH] + k_7[S]}{k_3[RH] + (k_6 + k_7)[S]}K \qquad (I)$$

where [S] is the olefin concentration. The initial conditions [S] = 0 and $t = 0$ give

$$\left(\frac{d^2H_2}{dt^2}\right)_{t=0} = \frac{-Kk_6}{k_3[RH]}\frac{d[S]}{dt} \qquad (II)$$

where the left-hand side of eq. II is the initial slope of the curve in Figure 1. The decrease in the rate of hydrogen production from the initial to the plateau value, $(5.08 - 1.80) \times 10^{-9}$ mole/sec. $= 3.28 \times 10^{-9}$ mole/sec., must be attributed to the removal of H atoms by reaction 6. Since olefin is formed by reactions 4, 8, 9, and 10 and destroyed by reactions 6 and 7, the rate of olefin production must be at least as great as the rate of hydrogen loss, the difference depending on the importance of reaction 7. Using 3.28×10^{-9} mole/sec. for $d[S]/dt$, we obtain a value of 470 as an upper limit for k_6/k_3. The error limits on this value are quite high since its validity is determined by experimental error in the low conversion points of Figure 1. If we consider reaction 7 to be unimportant, then it may be shown that

$$\frac{d[S]}{dt} = \frac{dH_2}{dt} - \left(\frac{dH_2}{dt}\right)_{\text{steady state}} \qquad (III)$$

A graphical integration of Figure 1 gives [S] as a function of time. This is shown in Figure 3 along with an experimental determination of the isopentenes at the steady state by gas chromatographic analysis. This lower value indicates that at least some of the olefin has become distributed into higher molecular weight products *via* reactions 7 and 10. Rearrangement of eq. I gives

$$\frac{K}{dH_2/dt} = 1 + \frac{k_6[S]}{k_3[RH]} \qquad (IV)$$

and k_6/k_3 may now be evaluated for each experimental point. The average value calculated in this manner is 170.

The value k_4/k_5 may be estimated in a similar manner. Since the material balance requires

$$\frac{d[S]}{dt} + \frac{d[R_2]}{dt} = 5.08 \times 10^{-9} \text{ mole/sec.} \qquad (V)$$

initially and $d[S]/dt = 3.28 \times 10^{-9}$ mole/sec., then $d[R_2]/dt = 1.80 \times 10^{-9}$ mole/sec. or $k_4/k_5 = 1.82$ and $k_4/(k_4 + k_5) = 0.645$ or 65% of the radicals produced disproportionately. The actual values must be somewhat higher than this because of the aforementioned limitations on this determination of $d[S]/dt$. Nevertheless, these values are in agreement with the respective values of 2.6 and 73% observed in the liquid phase.[2]

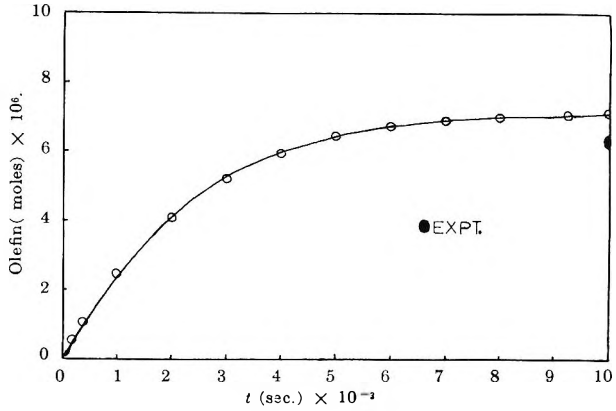

Figure 3. Olefin concentration as a function of photolysis time.

Figure 2 shows the effect of adding trimethylethylene. Rearrangement of eq. I gives

$$(K - dH_2/dt)\frac{[RH]}{[S]} = A\left(\frac{dH_2}{dt}\right) - BK \qquad (VI)$$

where $A = (k_6 + k_7)/k_3$, $B = k_7/k_3$, and [S] is the concentration of added trimethylethylene. A plot of the left-hand side of eq. VI *vs.* dH_2/dt is shown in Figure 4. Values extracted from the plot are $A = 21.2$ and $B = 19.3$. Thus, $k_7/k_3 = 19.3$ and the abstraction of hydrogen from trimethylethylene is 19 times faster than that from isopentane. $k_7/(k_6 + k_7) = B/A = 0.091$ or about 9% of the H atoms reacting with trimethylethylene abstract hydrogen. Similarly, $k_7/k_6 = A/(A - B) = 0.0985$ which is in good agreement with the vaule of 0.085 found by Hardwick[8] in the liquid phase. $A - B = k_6/k_3 = 193$ which corresponds to the measurements $170 \cong k_6/k_3 < 470$. Since almost all of the radicals produced in the system are secondary and tertiary, it is not surprising that the measured values in the mercury-sensitized system correspond to the experiments with added trimethylethylene.

The total rate of H atom reaction with trimethylethylene $(k_6 + k_7)$ was measured by Allen, Melville, and Robb[9] to be 7.35×10^{11} cc./mole sec. at 18°. Correcting this value to 25° with an approximate

(7) The nomenclature of Back[4] will be used throughout this discussion.

(8) T. J. Hardwick, *J. Phys. Chem.*, **66**, 291 (1962).

(9) P. E. M. Allen, H. W. Melville, and J. C. Robb, *Proc. Roy. Soc.* (London), **A218**, 311 (1953).

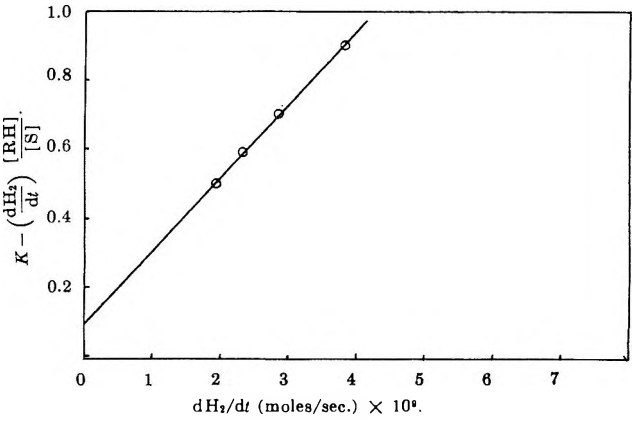

Figure 4. Plot of eq. IV.

activation energy of 2 kcal. gives 7.94×10^{11} cc./mole sec. Therefore, $k_3 = (7.94 \times 10^{11})A = 3.75 \times 10^9$ cc./mole sec. This value is somewhat lower than 9.6×10^9, which would be predicted from the group additive approach of Hardwick,[10] but compares favorably with the value of 2.74×10^9 found for the hydrogen atom abstraction from a similar alkane, isobutane.[11]

The measured decrease in hydrogen production resulting from H atom reaction with olefin is low by a factor of 0.0985 since this fraction of H atoms abstracts from rather than adds to the scavenger. With this correction, the initial rate of olefin production is given by (1.1) $(3.28 \times 10^{-9}$ mole/sec.) $= 3.61 \times 10^{-9}$ mole/sec. and k_4/k_5 becomes $3.61/1.47 = 2.45$, in good agreement with the liquid phase value of 2.6.

Owing to the approximation concerning the reactivity of H atoms with olefins produced in reactions 8–10 and the difficulty of differentiating between reactions of the two predominant isopentyl radicals, the calculated rate constant ratios must be regarded as approximate. The good agreement between the average disproportionation/combination ratio for these two isopentyl radicals from this technique and from the measured olefin and dimer production in the liquid phase, mercury-sensitized decomposition of isopentane, however, adds confidence to the other values which were calculated here.

Acknowledgment. Acknowledgment is made to the donors of the Petroleum Research Fund, administered by the American Chemical Society, for partial support of this research.

(10) T. J. Hardwick, *J. Phys. Chem.*, **65**, 10 (1961).
(11) K. Yang, *ibid.*, **67**, 562 (1963).

On the Polymorphic Modifications of Phthalocyanines

by Jacques M. Assour

RCA Laboratories, Princeton, New Jersey 08540 *(Received January 15, 1965)*

X-Ray powder diffraction patterns, infrared absorption spectra, and electron spin resonance data show undisputable evidence for the existence of only two phthalocyanine crystalline modifications defined as α and β. Experimental results for the alleged γ-polymorph strongly suggest that the α- and γ-phases differ only in particle size.

I. Introduction

For years phthalocyanines have been investigated by the dyestuff and pigment industries to determine their tinctorial and color strength, dispersibility and solubility in organic solvents, crystallization, and flocculation of pigments.[1] A striking result obtained from these investigations is the capability of the molecular phthalocyanines to exist in at least three alleged polymorphic forms—α, β, and γ. Recently, in our laboratories we have been engaged in the study of the electronic properties of phthalocyanines and their potential use in the field of molecular electronics. Detailed investigations of the electronic properties of the phthalocyanine complexes are dependent on the accurate knowledge of the molecular and crystal structures. The dependence on crystallography becomes more significant if the organic complex is known to exist in more than one crystalline modification, a result which might give rise to different physical and electrical properties. Wihksne and Newkirk,[2] and Eley and Parfitt[3] have already reported on the sharp difference between the electrical conductivities of the α- and β-phthalocyanine polymorphs. Recent electron spin resonance experiments have also shown[4] an increased perturbation on the energy levels of the cobalt atom when the cobalt phthalocyanine molecule is embedded in the α- or β-lattice. Although the subject of phthalocyanine polymorphs has been considered by several workers, the investigations reported in the literature were mainly confined to the identification of only two crystalline phases. In the present paper, we report our experimental results on the identification of the alleged third crystalline form defined as the γ-phase.

II. Earlier Identification of the Phthalocyanine Polymorphs

According to the nomenclature[5] first reported by Andrews and co-workers,[6] the β-crystalline modification is the most stable phase since it does not undergo a polymorphic transition when stored in organic solvents, while the α and γ are metastable polymorphs. β-Phthalocyanines are the only polymorphs prepared by sublimation at about 550°, and well-defined monoclinic single crystals can be easily grown. Experimentally, we have found that the α-phase is completely converted to the β-phase when heat-treated above 300°.

The molecular orientation and crystal structure of the β-modification have been thoroughly studied by Robertson.[7] Detailed X-ray analyses of the α- and γ-phthalocyanines have not been performed because it has not been possible to grow single crystals of these polymorphs. However, Robinson and Klein[8] have determined the lattice constants of α-CuPc from the X-ray diffraction pattern of a polycrystalline specimen.

(1) For a detailed discussion of these properties see F. H. Moser and A. L. Thomas, "Phthalocyanine Compounds," Reinhold Publishing Corp., New York, N. Y., 1963.

(2) K. Wihksne and A. E. Newkirk, *J. Chem. Phys.*, **34**, 2184 (1961).

(3) D. D. Eley and G. D. Parfitt, *Trans. Faraday Soc.*, **51**, 1529 (1955).

(4) J. M. Assour and W. K. Kahn, *J. Am. Chem. Soc.*, **87**, 207 (1965).

(5) Unfortunately, this nomenclature has not been adopted universally and several workers have switched the α- and β-notation.

(6) D. B. Andrews, *et al.*, Fiat Final Report No. 1313 PB 85172, Feb. 1, 1948.

(7) J. M. Robertson, *J. Chem. Soc.*, 615 (1935); 1195 (1936); 219 (1937).

(8) M. T. Robinson and G. E. Klein, *J. Am. Chem. Soc.*, **74**, 6294 (1952).

According to their interpretation, the crystal structure of α-CuPc is presumably tetragonal.

The work by Susich[9] on the identification of organic dyestuffs by X-ray powder diffraction has attracted several workers in the field, and X-ray powder patterns for both the α- and β-phthalocyanines were measured by Tarantino and co-workers,[10] Ebert and Gottlieb,[11] Karasek and Decius,[12] and Shigemitsu.[13] A single X-ray powder diffraction pattern for the alleged γ-crystalline modification has been reported by Eastes.[14] Thus, identification of the phthalocyanine polymorphs was invariably achieved by comparing their characteristic X-ray powder patterns.

A second well-established and more sensitive method for differentiating between the phthalocyanine polymorphs has been the application of infrared spectroscopy.[15] Indeed, nicely resolved spectra for the α- and β-phthalocyanine derivatives were measured by Ebert and Gottlieb,[11] Kendall,[15] and Sidorov and Kotlyar.[16] The distinct spectral differences between the frequencies and intensities of the infrared absorption bands observed for both polymorphs enable one to identify each crystalline phase quite readily. To our knowledge, no infrared spectrum has been reported for the γ-phthalocyanine.

III. Experimental Methods

The investigations reported here were carried out primarily with copper phthalocyanine (CuPc) because experimental results for this complex, with which we can compare our data, are readily available in the literature. These studies, however, were also extended to other phthalocyanine derivatives such as H_2Pc, CoPc, NiPc, and ZnPc. The phthalocyanine compounds were synthesized by the method of Barrett and co-workers.[17] The products were purified chemically to remove excess acid and organic impurities. The resultant powder was then sublimed in a nitrogen atmosphere at $T = 500°$. The sublimation process which lasted for 4 days yielded large single crystals in the shape of thin needles. The crystal structure was identified by X-ray measurements and agreed with the monoclinic structure determined by Robertson.[7] The α-CuPc polymorph was prepared by dissolving the β-phase crystallites in 98% sulfuric acid. The solution was then poured slowly into crushed ice, stirred well in order to maintain the temperature constant, causing the α-CuPc phase to precipitate. The product was separated by centrifugation, digested several times with NH_4OH and CH_3OH, and dried under vacuum. The γ-CuPc complex was prepared according to the method described by Eastes.[14] β-CuPc powder was slurried in aqueous sulfuric acid of 60% concentration for a period of 4 hr. The precipitate was then extracted by centrifugation, washed thoroughly to remove excess acid, and dried under vacuum.

1. X-Ray Diffraction Patterns. Powder diffraction patterns were recorded by a Norelco X-ray diffractometer employing nickel-filtered copper radiation. Samples in the form of fine powder were packed into a 1 × 2-cm. aluminum groove. The entire scan from 5 to 50° was swept using a 1° divergence slit and a receiving slit of 0.015 cm. The diffractometer traces were also supplemented with X-ray powder photographs recorded by a Philips powder camera.

2. Infrared Spectra. Infrared spectra were measured with a Perkin-Elmer double-beam spectrophotometer Model 221. A standard infrared spectrum of a polystyrene thin film was employed for calibration, and the errors found were less than ± 2 cm.$^{-1}$. Samples of α- and β-CuPc were prepared and measured in the form of KBr pellets and evaporated thin films on NaCl disks. Samples of the γ-CuPc phase were prepared by suspending the powder in Nujol and Fluorolube, respectively. The infrared spectra were measured at room temperature.

3. Electron Micrographs. Thin films of α- and γ-CuPc were prepared by dispersing fine powder in a 1% solution of collodion. Micrographs of the phthalocyanine crystallites were taken with an RCA electron microscope Model 3B at 28,700 direct magnification. The photographs shown in Figure 1 were enlarged four times.

IV. Experimental Results and Discussion

Micrographs of the α- and γ-CuPc crystallites are shown in Figure 1. The γ-form particles have an apparent shape of an elongated flat plate, and those of the α-form have a rod-like structure. The scale of 0.5 μ affords a direct comparison between the average size of the primary crystallites.[18] The average length of each α-particle is of the order of 0.1 μ or less, whereas

(9) G. Susich, *Anal. Chem.*, 22, 425 (1950).

(10) F. R. Tarantino, D. H. Stubbs, T. F. Cooke, and L. A. Melsheimer, *Am. Ink Maker*, 29, 35 (1951).

(11) A. A. Ebert, Jr., and H. B. Gottlieb, *J. Am. Chem. Soc.*, 74, 2806 (1952).

(12) F. W. Karasek and J. C. Decius, *ibid.*, 74, 4716 (1952).

(13) M. Shigemitsu, *Bull. Chem. Soc. Japan*, 32, 607 (1959).

(14) J. W. Eastes, U. S. Patent 2,770,620 (1956).

(15) D. N. Kendall, *Anal. Chem.*, 25, 382 (1953).

(16) A. N. Sidorov and I. P. Kotlyar, *Opt. i Spektroskopiya*, 11, 92 (1961).

(17) P. A. Barrett, C. E. Dent, and R. P. Linstead, *J. Chem. Soc.*, 1719 (1936).

(18) It should be noted that the collodion solution used to disperse the fine powder of each phase may alter the size of the agglomerates, but it should have no effect on the size of the primary particles.

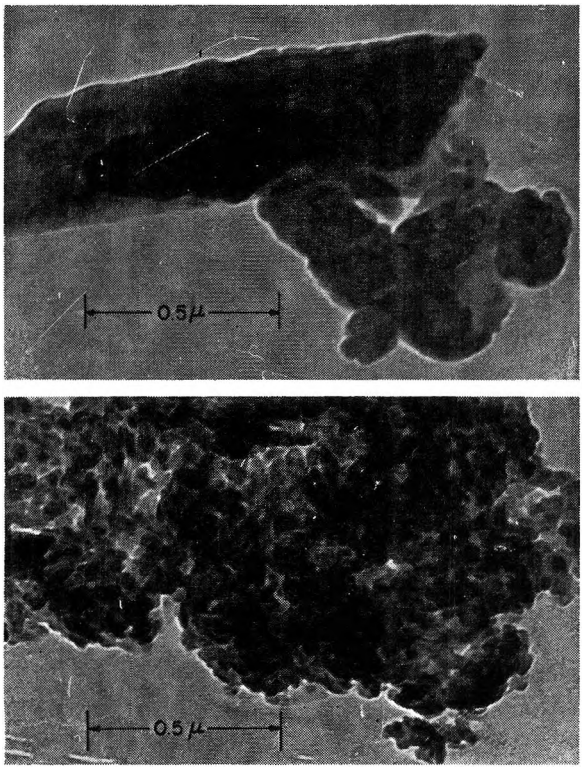

Figure 1. Micrographs of γ-CuPc (top) and α-CuPc (bottom).

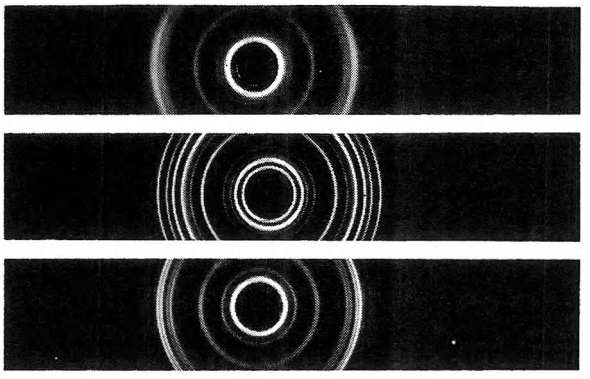

Figure 2. X-Ray powder diffraction photographs of α-CuPc (top), β-CuPc (middle), and γ-CuPc (bottom).

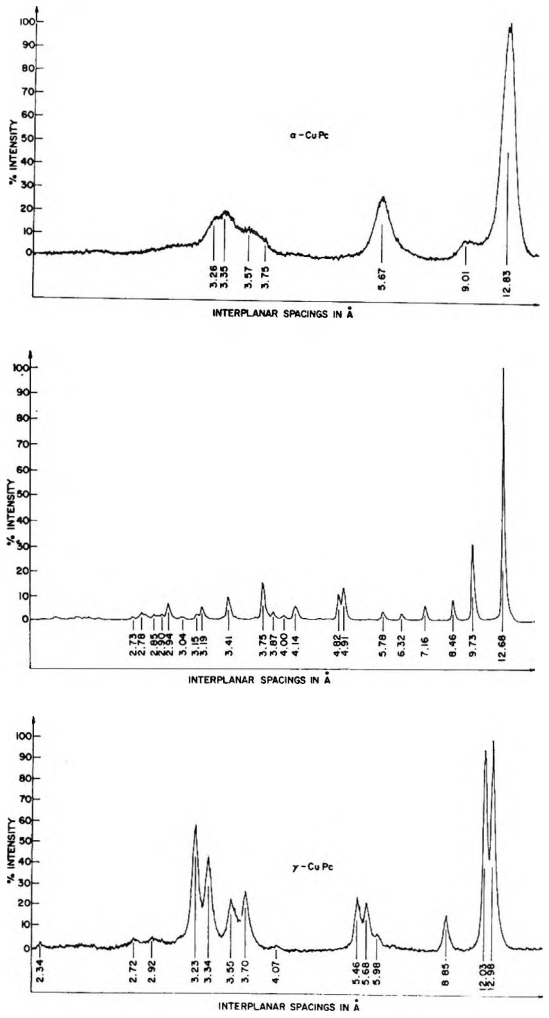

Figure 3. X-ray powder diffraction of copper phthalocyanine polymorphs.

the average size of the γ-particle is approximately 1 μ. For X-ray powder measurements the particle size of the α-polymorph is too small to yield sharp diffraction maxima. Crystallites with average diameter in the range of 10^{-5} to 10^{-6} cm.$^{-1}$ will invariably give rise to a powder pattern whose lines are diffused into broad diffraction bands which are difficult to characterize accurately. This effect has severely limited the application of X-ray powder diffraction in identifying two similar crystalline modifications. On the other hand, crystallites of the γ-polymorph have the proper size to produce well-resolved diffraction maxima. The above two effects are clearly illustrated in Figures 2 and 3.

The X-ray powder diffraction patterns for three crystalline modifications, prepared in our laboratories, are shown in Figures 2 and 3. Before we compare our data with the experimental results reported previously, it is of interest to summarize briefly the characteristic features of the powder diffraction patterns published thus far. For example, in four out of the five patterns recorded[8,10-13] for the α-phase, only one diffraction line of maximum intensity was observed at an interplanar spacing of approximately 12.8 Å. in the region from 11 to 14 Å. In the fifth diffraction pattern,[8] this line is split into two almost equally intense peaks. The interplanar spacing (d_{hkl}) corresponding to this line differs in each pattern by as much as 0.36 Å. ($\sim$3%). Furthermore, by comparing the diffraction lines recorded in the middle-angle region, we find that the interplanar spacings in all the α-patterns are in

poor agreement. Another striking feature of the CuPc diffraction patterns is apparent from the pattern of the alleged γ-polymorph[14]; the two lines of maximum intensity at 11.95 and 13.5 Å. occur in the same region as the broad intense line at 12.8 Å. observed in the α-phase, and the lower interplanar spacings for γ-CuPc can be easily correlated to those of the α-CuPc. Since X-ray diffraction patterns are characteristic of the atomic arrangement in a given crystal, the discrepancies noted previously for the interplanar spacings clearly demonstrate the uncertainties in the interpretation of the experimental results obtained for the phthalocyanine polymorphs.

The powder patterns (Figures 2 and 3) recorded for our samples have the general features described above; *i.e.*, the α-pattern has a single intense broad line at 12.83 Å. and is in agreement with the patterns reported by Tarantino and co-workers,[10] Ebert and Gottlieb,[11] and Shigemitsu.[13] The pattern of the alleged γ-CuPc has the same splittings as those observed by Eastes[14] for the γ-phase and by Robinson and Klein[8] for the α-phase although the interplanar spacings are different. The major differences in the d_{hkl} values occur in the region from 11 to 14 Å., but they do not exceed 4%. The causes which might give rise to these errors can be numerable; however, if one assumes that all the samples investigated by several workers were "pure" phthalocyanines and contained each only one polymorph, the errors amounting to 4% in the region of low Bragg angle diffraction might occur in powder diffraction experiments since in this region absorption effects become significant. Other factors which are known to contribute to the above discrepancies are sample purity, particle size effects, preferred orientation, crystal texture, and experimental techniques.

The distinct characteristics of both the α- and β-powder diffraction patterns strongly indicate that these two complexes have indeed two different crystalline structures. The existence of these two phthalocyanine crystalline modifications has been also confirmed by infrared spectroscopy and electron spin resonance experiments to be discussed below. Eastes,[14] on the other hand, presumably identified the alleged γ-CuPc polymorph by comparing his X-ray powder pattern with the α- and β-complexes. Unfortunately, Eastes failed to report in detail his experimental procedures. More importantly, the fact that the diffraction patterns of both the α- and γ-phases have basically the same characteristics and apparently differ only in the degree of resolution leads us to conclude that these differences are insufficient to identify the γ-phase unequivocally. Therefore, the identification of the alleged γ-copper crystalline modification which is based on one X-ray powder pattern is questionable.

Although, as mentioned earlier, Robinson and Klein[8] have interpreted the crystal structure of α-CuPc as tetragonal, our X-ray powder data on the same polymorph imply a preferred orthorhombic structure. It is also interesting to note that the occurrence of 6 molecules/unit cell for an orthogonal crystal structure is rare. Several tetragonal structures of the analogous tetraphenylporphine chelates, which are known to exist in more than one polymorph,[19] have only 2 or 4 molecules/unit cell. A definite identification of the crystal structure of the α-polymorph must therefore await a careful X-ray analysis similar to that performed by Robertson[7] on the β-phase.

The average size of the primary crystallites of the α- and γ-phases, which is believed to be responsible for the difference in the X-ray patterns, was found to be critically dependent on the method of pigment preparation. Since the α-polymorph is usually prepared by pouring the concentrated sulfuric acid solution of phthalocyanine on crushed ice, it is believed that the sudden contact at low temperature considerably limits the growth of the nuclei of the crude pigments, and particles 0.1 μ long are invariably obtained. On the other hand, when the sulfuric acid solution was poured into water which was maintained at room temperature, different-size particles were obtained which gave rise to a distorted powder diffraction pattern. The γ-phase, however, is prepared at room temperature with a 60% sulfuric acid solution. This method apparently provides favorable conditions necessary for the increased growth of the primary particles to sizes exceeding 1 μ. Several strictly controlled methods for the preparation of different phthalocyanine pigments have been discussed by Andrews and co-workers.[6]

There are two other important reasons to question the identification of the γ-crystalline modification. The first is apparent from the interpretation of the infrared spectra shown in Figure 4. For the sake of this discussion we have adopted the notation of Sidorov and Kotlyar.[16] The vibrational bands are numbered progressively according to their frequencies in increasing order. The vibrational frequencies and intensities of the bands observed for both the α- and β-copper complexes are in excellent agreement with those reported by Sidorov and Kotlyar. Identical spectra for these complexes were recorded with samples in the form of KBr pellets and evaporated thin films. Furthermore, after heat treating a thin film of α-copper

(19) E. B. Fleisher, C. K. Miller, and L. E. Webb, *J. Am. Chem. Soc.*, 86, 2342 (1964).

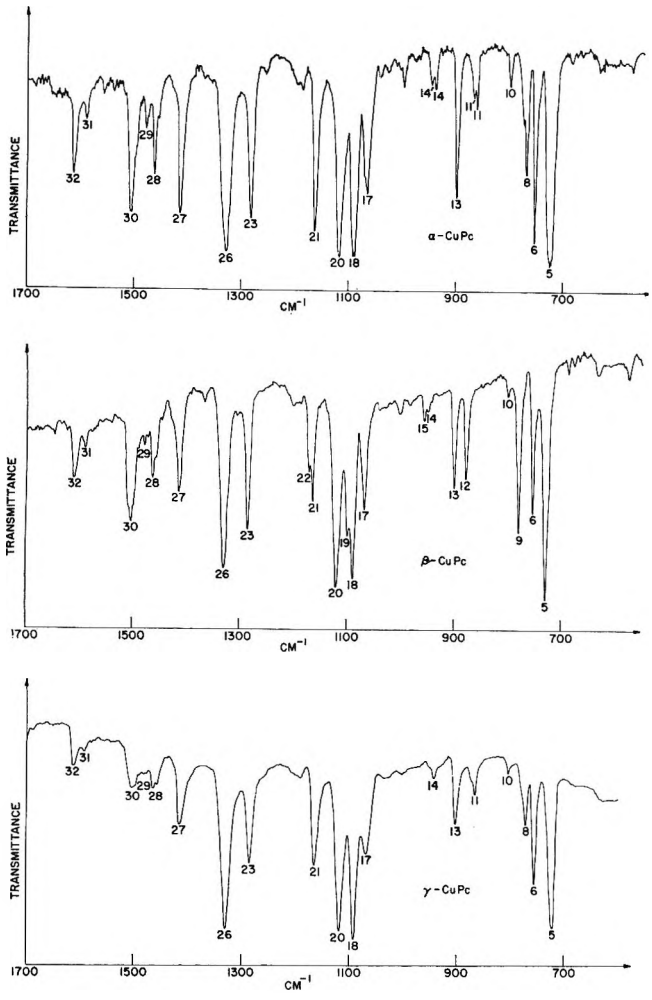

Figure 4. Infrared absorption of copper phthalocyanine polymorphs: top, α-CuPc (KBr); middle, β-CuPc (thin film); bottom, γ-CuPc (Nujol and Fluorolube).

phthalocyanine at 300°, the β-polymorph was obtained as shown by an infrared spectrum. The dissimilarity of the vibrational frequencies in both the α- and β-phases reveals not only their polymorphic character, but it also provides a reliable method for identifying these organic complexes.

Since little is known of the polymorphic transition of the γ-phase under the influence of high pressures or elevated temperatures, we have measured the infrared spectrum of the γ-phase in the form of Nujol mulls. However, since Nujol has two strong bands in the region 1350 to 1500 cm.$^{-1}$, we have measured the phthalocyanine bands in this region in Fluorolube. The spectrum of the γ-phase, shown in Figure 4, was found to be identical with that of the α-phase, and no variations between the vibrational bands were detected. Since the dissimilarity of the infrared vibrations observed in both the α- and β-phases can be attributed to different packing, together with different intramolecular linkages, based on the infrared spectra, one can conclude that both the α- and γ-phases have the same structure.

A second reason to dispute the identification of the γ-polymorph can be established by referring to the electron spin resonance (e.s.r.) study[4] of cobalt phthalocyanine. The remarkable feature of the e.s.r. data is the sensitivity of the spin-Hamiltonian parameters of the square-bonded cobalt phthalocyanine to the change in crystal structure and molecular environment. E.s.r. spectra of α- and β-polymorphs, which were prepared according to the known techniques and identified by X-ray diffraction and infrared spectroscopy, clearly revealed the existence of two crystalline modifications. More significantly, we have observed the transition from the α-phase to the β-phase through e.s.r. experiments. On the other hand, samples prepared according to the method of Eastes[14] for the γ-polymorph yielded e.s.r. spectra which were identified as those of the α-polymorph. Several attempts to measure the e.s.r. of the alleged γ-polymorph were unsuccessful; in each attempt the e.s.r. spectrum was typical of the α-polymorph.

Summary

The experimental results for the identification of three alleged copper phthalocyanine polymorphs show undisputable evidence for the existence of only two crystalline modifications defined as α and β. Data for the alleged γ-copper polymorph are insufficient to allow unequivocal identification of this crystalline phase. Our results suggest that the X-ray spectral differences for the α- and γ-phases can be attributed to differences in the average size of the primary particles. The determination of the crystal structure and molecular orientation of the α-polymorph must await a careful X-ray analysis.

Acknowledgment. The author wishes to acknowledge the assistance of Mr. L. Korsakoff, Dr. D. Ross, and Mr. S. Bennet. The help extended to us by the members of the X-ray department is gratefully acknowledged.

The Measurement of Small Surface Areas by the B.E.T. Adsorption Method[1]

by P. Chènebault

Département de Métallurgie, Service de Chimie des Solides, Section des Combustibles Ceramiques, Chemin des Martyrs, Grenoble, Isère, France

and A. Schürenkämper

Service de Métallurgie, Euratom, CCR Ispra *(Received January 18, 1965)*

It is possible to measure surface areas of the order of a few square centimeters by using a mixture of natural xenon and ^{133}Xe as the adsorbate. The vapor tension of xenon at the temperature of liquid nitrogen is equal to 2.15×10^{-3} mm. The surface measured for glass is equal to the geometrical surface of the samples. In the case of sintered uranium dioxide samples of different densities, the lower the density, the greater the surface area.

Introduction

An important technological problem arising from the use of sintered uranium dioxide as a nuclear fuel is the migration and escape of krypton and xenon which are formed *in situ* as the result of fission.[2]

One mechanism governing the escape of these gases from UO_2 is volume diffusion. However, direct measurements of fission gas escape give only an apparent diffusion coefficient D' which is related to the volume diffusion coefficient D by the equation

$$D' = {}^1/_9\left(\frac{S}{V}\right)^2 D \qquad (1)$$

where S is the specific surface area and V is the true volume of the sample. There is usually a large scatter in the results of such measurements and it is suspected that this may result from variations in S; thus it is desirable to know the actual specific surface of each microsample, the geometrical area of which is about 0.25 cm.^{2}. This paper describes a method for measuring small surface areas with a sensitivity near 0.1 cm.^{2}.

I. Choice of the Conditions of Measurement

The method used is based on the application of the B.E.T. equation[3] to the isothermal adsorption of xenon. This equation

$$\frac{p}{V_a(p_0 - p)} = \frac{1}{CV_m} + \frac{C - 1}{CV_m}\left(\frac{p}{p_0}\right) \qquad (2)$$

where p is adsorbate pressure, p_0 is adsorbate vapor pressure, V_a is adsorbed volume, V_m is monomolecular layer volume, and C is a constant related to heats of adsorption and liquefaction, is applicable in the range of relative pressures (p/p_0) from 0.05 to 0.35 and experimental conditions must be chosen to meet this requirement. A further limitation is that the surface area to be measured is small, so that the total volume of adsorbed gas is small. For measuring the gas volume adsorbed on a surface of 1 cm.^{2}, it is necessary to use an adsorbate whose pressure is approximately 10^{-3} torr at the adsorption temperature and to reproducibly measure pressure variations of 10^{-4} torr.

Pressure Measurement. Pressures are measured by the γ-activity of a radioactive isotope of the gas or vapor chosen as the adsorbate. The number of γ-photons emitted per second is proportional to the number of molecules present; thus, it is also directly proportional to the pressure. If the radioactive properties of the adsorbate are suitable (half-life not too short, specific activity high enough) pressure measurements with a precision of 1% are quite feasible in the range 10^{-4} torr.

(1) Work performed under contract No. 031.60.10 RDF between European Atomic Energy Community and the Commissariat à l'Energie Atomique.

(2) (a) A. H. Booth and G. T. Rymer, CRDC-720, August 1958; (b) W. B. Cottrell, *et al.*, ORNL-2935, September 1960.

(3) S. Brunauer, P. H. Emmett, and E. Teller, *J. Am. Chem. Soc.*, **60**, 309 (1938).

It should be noted that what is actually determined by this method is the partial pressure of a radioactive isotope which, if isotopic effects are negligible, is equal to the partial pressure of the adsorbate.

Choice of the Adsorbate. Adsorption measurements at 24° have been conducted with mercury and with bromonaphthalene activated in a neutron flux. Adsorption was followed by the γ-activity of the isotopes ^{203}Hg and ^{82}Br. The quantity of mercury adsorbed on the surface of glass or UO_2 at pressures lower than 2×10^{-3} torr represented only about 1% of the quantity necessary for the formation of a monomolecular layer; thus mercury vapor could not be used as an adsorbate. Tests using bromonaphthalene indicated a chemical reaction with UO_2. Bromonaphthalene is partially decomposed under neutron irradiation, and it is likely that the bromine formed reacts with UO_2.

On the other hand, adsorption isotherms at 77.5°K. with a mixture of natural xenon and xenon-133 were found to be type II of Brunauer.[3] Techniques and results relative to the xenon method are described in the following sections.

II. Description of the Adsorption Apparatus

Figure 1 shows a sketch of the apparatus used for surface area measurement; it includes a vacuum system capable of obtaining a pressure 5×10^{-6} torr, connections for introducing both natural xenon and xenon-133, a McLeod gauge, a γ-counting system, an adsorption section (volume V_1) with a measuring bulb (volume V_2), a mercury trap, and a xenon trap.

The xenon trap contains a few activated charcoal particles able to adsorb (at liquid nitrogen temperature) the total quantity of xenon in the adsorption section of the apparatus. This trap allows one to introduce or withdraw a given quantity of xenon from the adsorption section as required.

The measuring bulb (Figure 1) was designed so that the surface on which adsorption occurs is not sensitive to variations of the liquid nitrogen level. Automatic regulation controls that level to ±2 mm.

III. Procedure

Preparation of the Adsorbate. A quartz bulb furnished with a fragile extension (see Figure 1) containing a 50-mg. uranium chip is sealed under high vacuum. After a 120-hr. irradiation in a neutron flux of 5×10^{12} n. cm.$^{-2}$ sec.$^{-1}$ and after a decay time of some days, the uranium is melted by high frequency induction, the sample itself being used as the susceptor, to release the fission gases; the only radioactive isotope present in a measurable quantity is ^{133}Xe. The bulb is put in the measuring apparatus, where it can be broken

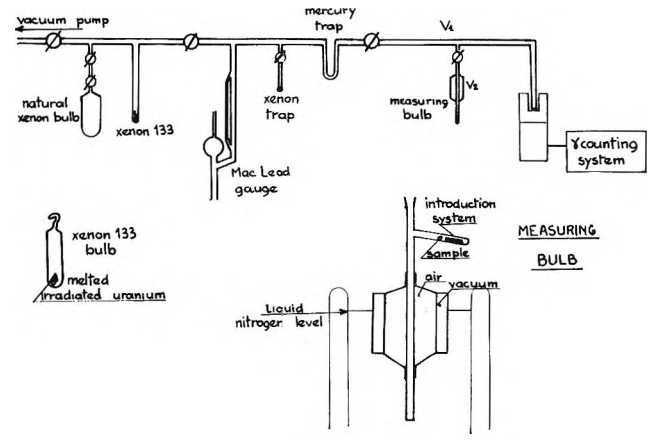

Figure 1. Apparatus for surface area measurements.

with a magnetic hammer and the ^{133}Xe mixed with the natural xenon. The activity of ^{133}Xe can be adjusted at such a level that the mixture can be used during the second and third weeks after irradiation.

In operation, the apparatus is first carefully degassed, then natural xenon (99.94% Xe supplied by the Air Liquide Co.) is introduced at about 5×10^{-3} torr and the pressure is read with the McLeod gauge. The bulb containing ^{133}Xe is then broken and pressure is calibrated in terms of the activity recorded by the counting system. The quantity of ^{133}Xe is sufficiently small that the pressure measured by the McLeod gauge does not change.

The volume of the apparatus is about 700 cm.^{3} at 5×10^{-3} torr; this corresponds to 4.2×10^{-3} cm.^{3} (NTP) of gas, a quantity capable of covering 250 cm.^{2} with a monomolecular layer.

Introduction of a Mercury Trap. The vapor pressure of mercury is 2×10^{-3} torr at 24°. The partial pressure of mercury vapor in the apparatus is therefore of the same order of magnitude as the partial pressure of xenon. When the measuring bulb is cooled with liquid nitrogen, mercury in the McLeod gauge evaporates and condenses on the walls of the measuring bulb. A trap cooled to −80° is therefore placed between the McLeod gauge and the adsorption section.

During cooling of this trap, the counting device immediately records a 5–15% increase in the quantity of xenon in the adsorption section of the apparatus. This increase results from the equilibration of pressure on both sides of the trap and moreover it is possible for the xenon to be entrained by the mercury.

Measurement of Adsorbed Volume. The calibration of pressure *vs.* activity having been effected, and the mercury trap cooled to −80°, a quantity V_1 of the natural xenon–xenon-133 gas mixture is introduced into the adsorption section. The bulb is then cooled to

liquid nitrogen temperature and the adsorption is followed until an equilibrium pressure, p, is obtained, as indicated by the activity recorder. After successive introductions of the gas mixture, a series of equilibrium states is obtained which allows the adsorption isotherm of xenon on the measuring bulb to be determined.

Then the sample is introduced and the adsorption isotherm for the bulb plus sample is determined in the same way. The adsorption isotherm for the sample alone is given by the difference between the two experiments. Before plotting isotherms, the phenomenon of thermal transpiration must be accounted for. Values of the corrected pressure (p^*) given by Podgurski and Davis[4] have been used.

IV. Results

Adsorption Isotherms—Values of p_0. Adsorption isotherms for the glass bulb and for a sample of sintered UO_2 were determined by plotting the adsorbed volume V_a as a function of the equilibrium xenon pressure p^* after correction for the thermal transpiration effect as shown in Figures 2 and 3. The isotherms show no hysteresis effects, but for a sample with a density of

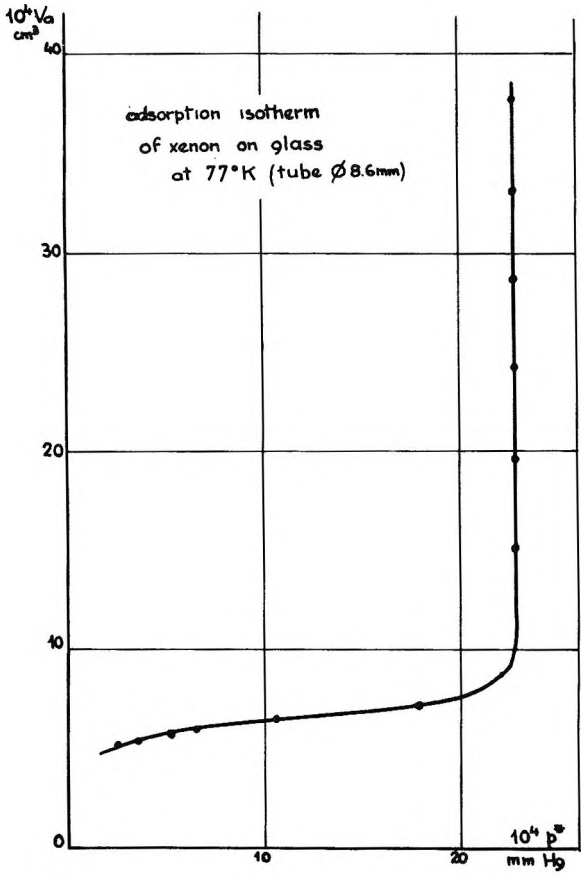

Figure 2.

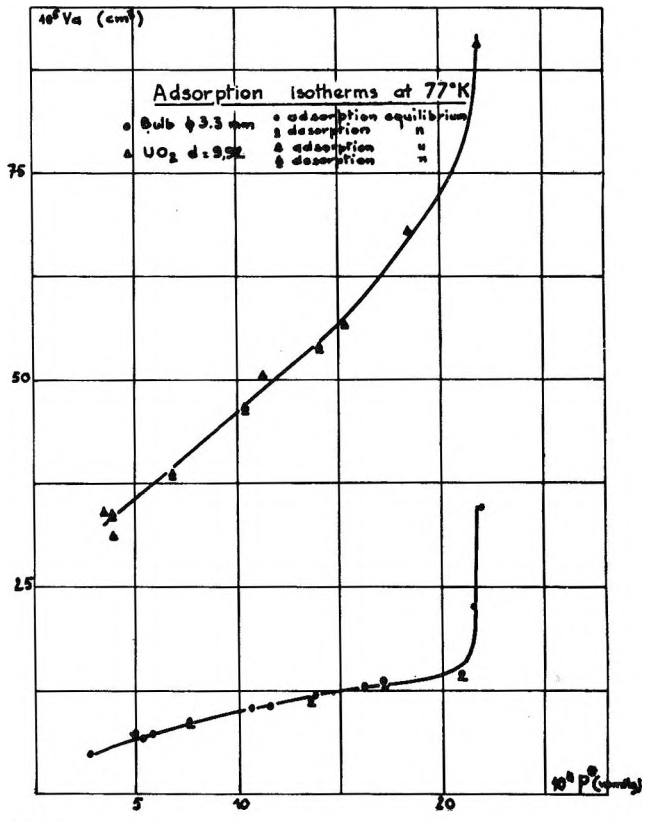

Figure 3.

9.92 g./cc. (theoretical density of UO_2 is 10.96) there is an important amount of open porosity (about 5% by volume) and equilibrium is slowly obtained; in this case it is difficult to distinguish between a false equilibrium and a hysteresis effect. The values obtained for p_0 (vapor tension of xenon at liquid nitrogen temperature) are slightly different in the curves of Figures 2 and 3; this could result from a variation of the liquid nitrogen temperature.

The value of p_0 has been determined by a series of measurements made with measuring bulbs having an internal diameter of 3.2 or 3.3 mm. and also with a 20-cm. long glass tube of 3.3-mm. internal diameter; this diameter was selected in order to have similar thermal transpiration correction factors each time. The agreement between results obtained with the tube and with the bulbs is good and gives confidence in the thermal transpiration correction factor applied to the measuring bulbs. The result of these measurements is $p_0 = 2.15 \pm 0.1 \times 10^{-3}$ torr.

Adsorption Measurements. Figure 4 shows results of four different measurements with the same glass

(4) H. H. Podgurski and F. N. Davis, *J. Phys. Chem.*, **65**, 1343 (1961).

Table I: Results of Surface Area Measurements on Glass and UO_2

	C	V_m (NTP), cm.³	Surface area, cm.²	Geometric surface area, cm.²	S, cm.²/g.	Ratio of surface area to geometric surface area
Measuring bulb	24	5.95×10^{-6}	4	~4.1		1
Measuring bulb + glass sample about 1 cm.²	21.5	7.17×10^{-6}	4.8	~5.1		1
Measuring UO_2: 9.92 g./cc., fragment 68 mg.	100	2.16×10^{-4}	14.5	<0.5	213	>29
Measuring UO_2: 10 g./cc., fragment 25 mg.	100	1.54×10^{-5}	1.0	<0.5	41	>2.1
Measuring UO_2: 10.2 g./cc., cylinder 70 mg.	13	3.08×10^{-6}	2.2	0.27	32	8.3
Measuring UO_2: 10.5 g./cc., parallelopiped 167 mg.	22	0.6×10^{-6}	0.4	0.4	2.4	1

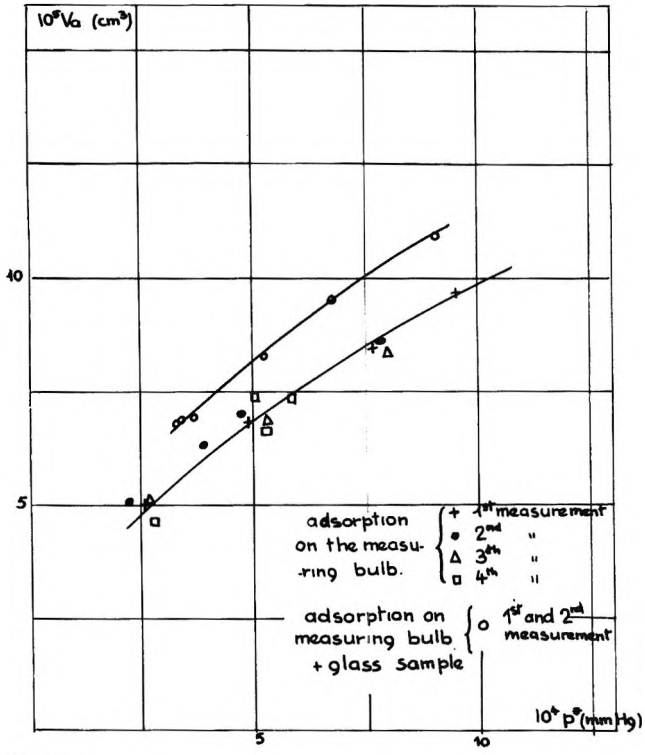

Figure 4.

bulb and of two measurements with a glass sample having a geometric surface area of about 1 cm.².

For each sample of UO_2 the adsorption was determined as the difference between the gas volume adsorbed on the "bulb + UO_2" and on the "bulb" alone. Results are shown in Figure 5.

Calculation of Surface Area. The parameter $p^*/V_a(p_0 - p^*)$ was plotted as a function of p^*/p_0 to obtain values for the monomolecular layer volume, V_m, and the constant C in the B.E.T. equation (2). Taking the value for the atomic cross section of xenon at liquid nitrogen temperature as $\sigma = 25$ Å.² (the mean value proposed in the literature[5]), the surface area is given by the relation $S = 6.7 \times 10^4 V_m$, when S is expressed as cm.² and V_m as cm.³ (NTP).

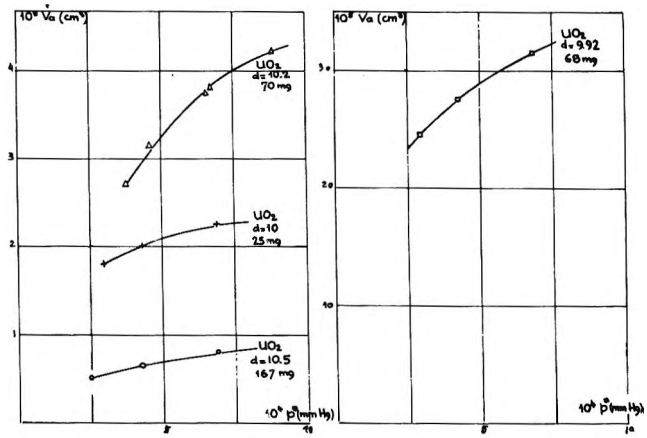

Figure 5.

Figures 6, 7, and 8 show the B.E.T. curves obtained for the xenon adsorption on glass (bulb and sample) and on uranium dioxide samples. Table I summarizes the values of C and V_m and the surface areas S calculated from these curves.

V. Discussion of Results

Precision and Sensitivity of the Measurements. Apart from any systematic error caused by calibration of the McLeod gauge, pressures measured from the activity of ^{133}Xe are known with a precision of $\pm 1\%$. The volumes V_1 and V_2 calibrated with mercury are known with the same precision. This results in a total uncertainty of about $\pm 7\%$ for the value of the first adsorbed volume.

B.E.T. curves used for determining the surface area (Figures 6–8) are obtained from the difference between two adsorption curves. Not enough results are available to have a statistical analysis of the resulting errors. Also, unknown experimental variations may result from variations in bulb surface area during an experiment (by dust accumulation, for example) from temperature uncertainties resulting from the low rate

(5) W. A. Cannon, *Nature*, **197**, 1000 (1963).

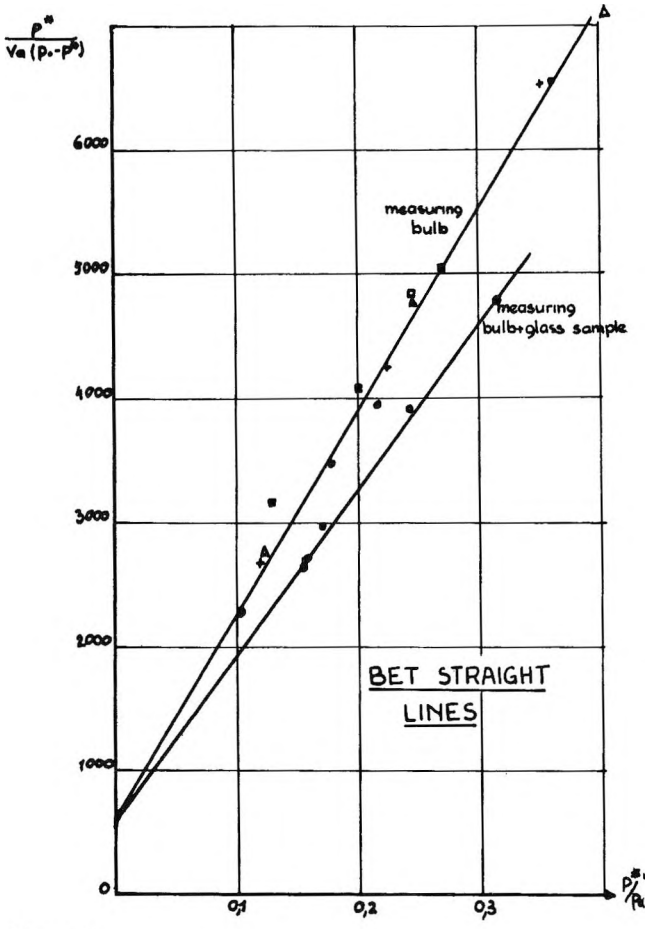

Figure 6.

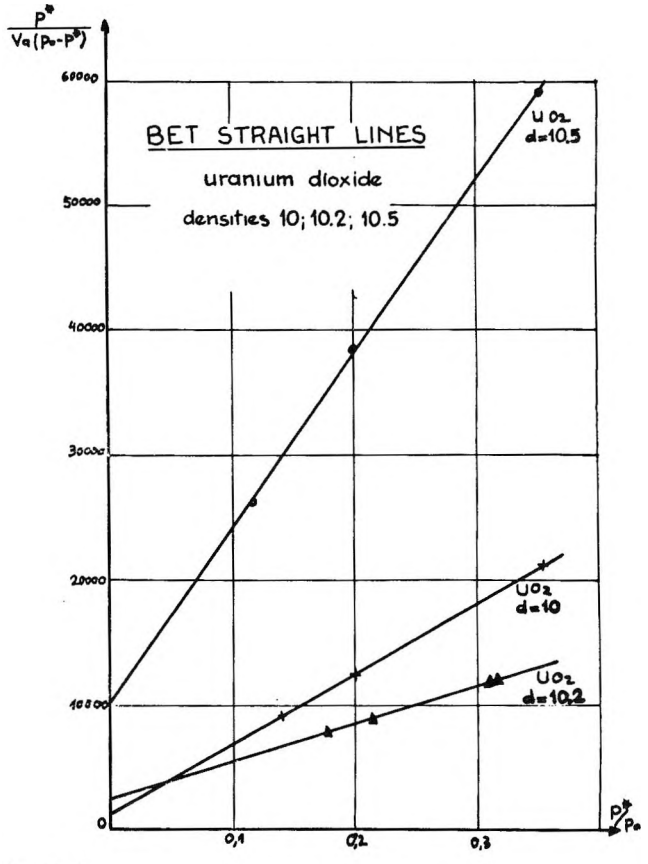

Figure 7.

of thermal equilibration under the experimental conditions used[6] or from variations in p_0 resulting from changes in the liquid nitrogen temperature.

However, the starting and final (desorbed) volumes of xenon always were found equal within ±3%, the experimental B.E.T. curves (Figures 6, 7, and 8) are linear, distinctly different adsorption curves were found for the bulb alone and the bulb plus a sample of known surface area of about 0.4 cm.², and the measured and geometrical surface areas of fully dense UO_2 and glass samples agree within ±0.1 cm.². As a result we believe that the reported measurements are reliable within about ±10% for a 1-cm.² sample.

Results

The values obtained from the measuring bulb and for the glass sample show that the B.E.T. surface area obtained is practically equal to the geometrical surface area. However, for UO_2 we find that the surface area is much larger than the geometrical area for low density samples. This presumably results from the presence of open porosity in the sintered UO_2. The

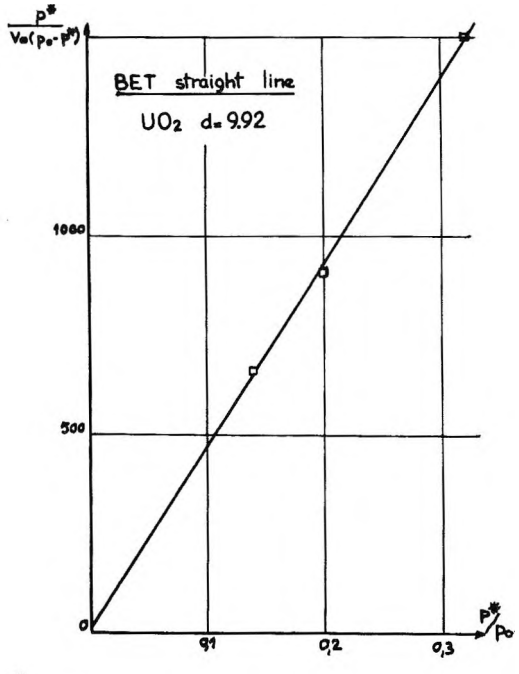

Figure 8.

(6) C. Moreau, Rapport CEA No. 1678, 1960.

values obtained for the constant C in the B.E.T. equation are larger for the lower density UO_2 samples. This may indicate that heat of adsorption for the first layer of xenon is higher when densities are low, which is in agreement with Smith's results[7] for krypton adsorption on UO_2.

Conclusions

It is possible to measure small surface areas of about 1 cm.^{2} with a precision of ± 0.1 cm.^{2} using a mixture of natural xenon and xenon-133. The xenon vapor pressure at liquid nitrogen temperature was found to be 2.15×10^{-3} torr after a thermal transpiration correction.

The surface area measured for glass samples is equal to the geometrical surface area. For sintered UO_2, the B.E.T. surface area is much larger than the geometrical surface area, and the ratio between these increases as the density decreases. The described technique makes it possible for one to measure the surface areas of high activity samples (irradiated UO_2 for instance).

Acknowledgment. The authors thank Miss Y. Carteret (CEN Saclay) very much for her kind collaboration. They are grateful for the critical comments of their colleagues of their laboratory (CEN Grenoble).

(7) T. Smith, NAA-SR-53, October 1960, p. 19.

Fluorine Bomb Calorimetry. XI. The Enthalpy of Formation of Yttrium Trifluoride[1]

by Edgars Rudzitis, Harold M. Feder, and Ward N. Hubbard

Chemical Engineering Division, Argonne National Laboratory, Argonne, Illinois *(Received January 19, 1965)*

The energy of formation of yttrium trifluoride was measured by direct combination of the elements in a bomb calorimeter. The standard enthalpy and Gibbs free energy of formation at 298.15°K. were determined to be -410.7 ± 0.8 and -393.6 ± 1.0 kcal. mole^{-1}, respectively.

This work, which is part of a series of fluorine bomb calorimetric studies, was prompted by the unavailability of thermochemical data on YF_3, an important intermediate in the production of metallic yttrium. The combustion method employed was developed earlier.[2] An yttrium metal sample was suspended in a fluorine-filled combustion bomb and ignited electrically. The interior surfaces of the bomb were protected by a tamped liner of YF_3. Extensive experimentation showed that adequate combustion of yttrium in fluorine could be achieved only if the temperature of the burning metal was well in excess of its melting point (1509°) and high enough to volatilize the reaction product YF_3 (b.p. ~2300°).

Experimental

Materials. (*a*) *Y.* An yttrium ingot (Lunex Co., nuclear grade) was rolled to a sheet approximately 1 mm. thick. Chemical and spectrochemical analysis showed the following significant impurities (in p.p.m.): Ta, 2500; O, 1390; C, 188; H, 42. If the impurities are assumed to be present as the chemical species, Ta, Y_2O_3, YC_2, and YH_2, the calculated content of elemental yttrium in the sample is 99.37 mole %.

(1) Work performed at Argonne National Laboratory, operated by the University of Chicago under the auspices of the U. S. Atomic Energy Commission, Contract No. W-31-109-eng-38.

(2) E. Rudzitis, H. M. Feder, and W. N. Hubbard, *J. Phys. Chem.*, **68**, 2978 (1964).

(*b*) F_2. The fluorine used was purified by distillation. Its impurity content was approximately 0.01%.

(*c*) YF_3. The material was prepared by the reaction of Y_2O_3 and HF in a fluidized bed[3] and contained approximately 0.1% oxygen. It was further purified by autoclaving with a mixture of anhydrous hydrogen fluoride and chlorine trifluoride at 250°. This treatment reduced the oxygen content to below the limit of detection.

Procedures. The apparatus and experimental procedures used in this work were analogous to those described for combustions of magnesium in fluorine.[2] The calorimetric samples were preconditioned by exposure to fluorine. The bomb was initially charged with 8 atm. of F_2. After combustion, the unburned metal residue was determined by the hydrogen evolution method.[4] The well-crystallized reaction product of the combustion, YF_3, was identified by its X-ray diffraction pattern.

Results

All combustion experiments attempted for the series were acceptable; the results are summarized in Table I. Energy quantities are expressed in terms of the defined calorie equal to (exactly) 4.184 absolute joules. The entries in the table are: (1) the mass of yttrium sample burned (percentage of introduced sample), (2) the observed increase in the calorimeter temperature corrected for the heat exchanged between the calorimeter and its surroundings, (3) the energy equivalent of the calorimeter multiplied by the negative of the corrected temperature increase, (4) the energy equivalent of the initial and final contents of the bomb, each multiplied by its appropriate portion of the corrected temperature increase (the sum of items 3 and 4 is the total evolved heat corrected to the isothermal bomb process at 25°), (5) the net correction of the bomb gas to the standard state, (6) the electrical energy input for the ignition, (7) the net impurity correction, and (8) the energy change per gram of yttrium for the reaction $Y(c) + {}^3/_2F_2(g) \rightarrow YF_3(c)$ with the reactants and products in their respective standard states at 25°.

For the calculation of item 1, the mass of sample introduced was corrected for unburned yttrium and for the increase in weight owing to preconditioning. The latter corrections were based on the assumption that YF_3 was the product formed. The weight increases were 0.69, 0.47, 0.43, 0.57, 0.46, 0.52, and 0.52 mg. for the seven experiments as listed. Item 3 was calculated using a value of ε(calor.) of 3433.45 cal. deg.$^{-1}$. This was the result of a series of six benzoic acid calibration experiments. The standard deviation of the mean was 0.79 cal. deg.$^{-1}$. (The same value was used for the magnesium studies[2] because magnesium and yttrium combustions were carried out alternately in a continuous series.) For calculation of item 4 the following values were used: C_p: Y,[5] 6.34; Ni,[5] 6.23; NiF_2,[6] 15.31 cal. mole^{-1} deg.$^{-1}$; C_v: F_2,[7] 5.50 cal. mole^{-1} deg.$^{-1}$. The heat capacity of YF_3 was estimated to be 22.2 cal. mole^{-1} deg.$^{-1}$ by the application of Kopp's law to the related structures[8] of YF_3 and CeF_3. The following auxiliary values were used: C_p: CeF_3,[9] 22.34; Ce,[5] 6.44 cal. mole^{-1} deg.$^{-1}$. The contents of the bomb were 0.2 g. of NiF_2, 196.8 g. of Ni and the varying amounts of YF_3 of 244.6, 228.2, 231.9, 222.4, 206.5, 193.0, and 182.5 g. for the seven experiments listed. The volume of the empty bomb was 0.354 l. The corrections to the standard states were applied in the usual manner.[10] Item 7 was obtained by calculating the thermal effects of the reaction of impurities with fluorine and subtracting the thermal effect which would result if an equal mass of yttrium reacted with fluorine. The following $\Delta H_f^\circ{}_{298}$ values were used (in kcal. mole^{-1}): YF_3,[11] −410.7; TaF_5,[12] −455.0; Y_2O_3,[13] −455.5; YC_2,[14] −52; CF_4,[15] −220.4; HF,[15] −64.8. The uncertainty in the impurity corrections was estimated to be ±2 cal./g. of sample.

Item 8 was calculated by summation of items 3 through 7 and division by item 1. The following standard thermal data in kcal. mole^{-1} were derived for the formation of YF_3(c) according to eq. 1: $\Delta E_f^\circ = -409.8 \pm 0.8$; $\Delta H_f^\circ = -410.7 \pm 0.8$; $\Delta G_f^\circ = -393.6 \pm 1.0$. The uncertainties in ΔE_f° and ΔH_f° equal twice the combined standard deviations arising from

(3) I. E. Knudsen and N. M. Levitz, ANL-6011, May 1959.

(4) E. Rudzitis, H. M. Feder, and W. N. Hubbard, *J. Phys. Chem.*, **67**, 2388 (1963).

(5) R. Hultgren, R. L. Orr, P. D. Anderson, K. K. Kelley, "Selected Values of Thermodynamic Properties of Metals and Alloys," John Wiley and Sons, Inc., New York, N. Y., 1963.

(6) E. Catalano and J. W. Stout, *J. Chem. Phys.*, **23**, 1284 (1955).

(7) W. H. Evans, T. R. Munson, and D. D. Wagman, *J. Res. Natl. Bur. Std.*, **55**, 147 (1955).

(8) A. Zalkin and D. H. Templeton, *J. Am. Chem. Soc.*, **75**, 2453 (1953).

(9) E. F. Westrum, Jr., and A. F. Beale, Jr., *J. Phys. Chem.*, **65**, 353 (1961).

(10) W. N. Hubbard in "Experimental Thermochemistry," Vol. II, H. A. Skinner, Ed., Interscience Publishers Ltd., London, 1961, Chapter 6.

(11) This work.

(12) E. Greenberg, C. A. Natke, and W. N. Hubbard, *J. Phys. Chem.*, **69**, 2089 (1965).

(13) E. J. Huber, Jr., E. L. Head, and C. E. Holley, Jr., *ibid.*, **61**, 497 (1957).

(14) Estimated.

(15) G. T. Armstrong, Chemical Propulsion Information Agency Publication No. 44 (U), Vol. I, Johns Hopkins University, Silver Spring, Md., 1964, p. 59.

Table I: Results of Yttrium Combustion Experiments[a]

	Expt. no. 1	2	3	4	5	6	7
1. Mass, g.	1.3332$_2$	1.0415$_1$	0.8387$_8$	1.0800$_3$	0.9187$_5$	0.8188$_0$	1.0861$_8$
(%)	(99.82)	(99.53)	(97.63)	(99.80)	(99.78)	(99.74)	(99.83)
2. Δt_c,[b] deg.	1.75540	1.36663	1.09937	1.42287	1.21214	1.07710	1.43267
3. ε(calor.)$(-\Delta t_c)$, cal.	−6027.1	−4692.3	−3774.6	−4885.4	−4161.8	−3698.2	−4919.1
4. ΔE(cont.),[c] cal.	−102.5	−76.4	−62.0	−75.2	−51.3	−54.4	−70.2
5. ΔE(gas), cal.	−0.7	−0.5	−0.4	−0.5	−0.4	−0.4	−0.5
6. ΔE(ignition), cal.	−0.1						
7. ΔE(impurities), cal.	−30.4	−23.8	−19.1	−24.6	−21.0	−18.7	−24.8
8. $\Delta E_c°/M$, cal. g.$^{-1}$	−4620.9	−4601.9	−4597.1	−4616.2	−4608.9	−4606.2	−4616.6

Mean $\Delta E_c°/M$ = −4609.7
Std. dev. of mean, ±3.2 cal. g.$^{-1}$ or 0.07%.

[a] The symbols are explained in ref. 10. [b] $\Delta t_c = t^f - t^i - \Delta t_{cor}$. [c] $\Delta E(\text{cont.}) = [\varepsilon^f(\text{cont.}) - \varepsilon^i(\text{cont.})](25 - t^i) + \varepsilon^f(\text{cont.})(-\Delta t_c)$.

the scatter of $\Delta E_c°/M$ values, the impurity correction, and the calibration data. The uncertainty in $\Delta G_f°$ includes the estimated additional uncertainty in the $\Delta S_f°$ value. The atomic weight of yttrium was taken at 88.905 g. (g.-atom)$^{-1}$. The entropies $S°_{298}$ were taken to be: Y,[16] 10.63; F_2,[17] 48.5; YF_3, 26.2 cal. deg.$^{-1}$ mole^{-1}. The latter value was an estimate based on $S°_{298}$ (CeF_3) = 27.54 cal. deg.$^{-1}$,[9] and Latimer's rule.[18] The present results are the only known thermochemical data on the formation of YF_3, except for an estimate by Brewer, *et al.*,[19] of $\Delta H_f°(YF_3)$ = −397 ± 7 kcal. mole^{-1}.

Acknowledgments. The authors wish to acknowledge the help of F. J. Karasek for fabricating yttrium metal into sheets and L. Ross for valuable discussions. Thanks are due to R. Terry and E. Van Deventer for checking the manuscript and calculations.

(16) L. D. Jennings, R. E. Miller, and F. H. Spedding, *J. Chem. Phys.*, **33**, 1849 (1960).

(17) K. K. Kelley and E. G. King, U. S. Bureau of Mines Bulletin 592, U. S. Government Printing Office, Washington, D. C., 1961.

(18) G. N. Lewis, M. Randall, K. S. Pitzer, and L. Brewer, "Thermodynamics," 2nd Ed., McGraw-Hill Book Co., Inc., New York, N. Y., 1961, p. 518.

(19) L. Brewer, L. A. Bromley, P. W. Gilles, and N. L. Lofgren, "Chemistry and Metallurgy of Miscellaneous Material, Thermodynamics," L. L. Quill, Ed., McGraw-Hill Book Co., Inc., New York, N. Y., 1950.

Fluorine Bomb Calorimetry. XII. The Enthalpy of Formation of Ruthenium Pentafluoride[1,2]

by Howard A. Porte, Elliott Greenberg,[3] and Ward N. Hubbard

Chemical Engineering Division, Argonne National Laboratory, Argonne, Illinois *(Received February 23, 1965)*

The energy of formation of ruthenium pentafluoride was measured by direct combination of the elements in a combustion bomb calorimeter. The standard enthalpy of formation, $\Delta Hf^{\circ}_{298.15}$, was calculated to be $-213.4_1 \pm 0.3_5$ kcal. mole^{-1}.

Introduction

Higher fluorides of transition metals have been the object of considerable recent experimental and theoretical interest.[4] Properties of these materials, with few exceptions, are known only qualitatively. This investigation is part of a continuing program[5] to obtain precise thermochemical data by fluorine bomb calorimetry, and deals with the enthalpy of formation of ruthenium pentafluoride.

RuF_5 was first prepared by Ruff and Vidic[6] by passing fluorine over finely divided ruthenium. This reaction probably constitutes the easiest method for making the compound. In the pure form at room temperature, RuF_5 is a pale green solid with a vapor pressure of about 0.1 mm.[7] RuF_5 reacts with moisture immediately to form HF, RuO_4, and lower oxides. Because of the reactivity of RuF_5 and the great difficulties experienced in handling it, the compound has not been studied extensively. Even the melting point and boiling point are in doubt.[7,8]

Experimental

Calorimetric System. The calorimeter, laboratory designation ANL-R1, and combustion bomb, laboratory designation Ni-5, have already been described.[9,10] The system was calibrated with benzoic acid (National Bureau of Standards Samples 39h and 39i) whose certified energy of combustion was 26.434 ± 0.003 abs. kjoules g.$^{-1}$ under prescribed conditions. Nine experiments, some preceding and some following the ruthenium combustions, yielded an average value for ε(calor.), the energy equivalent of the calorimetric system, of 3545.1_1 cal. deg.$^{-1}$, with a standard deviation of the mean of 0.4 cal. deg.$^{-1}$.

Materials. Specially fabricated high-purity ruthenium, in the form of 3-mm. diameter rod and 0.1-mm. foil, was generously donated by Mr. R. Vines of The International Nickel Co., to whom thanks are due. The impurities in the samples are summarized in Table III and will be discussed in a later section. Purified fluorine (99.94%) was prepared by distillation of commercial fluorine in a low-temperature still.[9,11] Because of the unavailability of ruthenium wire, high-purity molybdenum wire,[12] 0.1 mm. in diameter, was used as fuse material.

Combustion Technique. The sample arrangement, ignition, and combustion technique were essentially

(1) This work was performed under the auspices of the U. S. Atomic Energy Commission.

(2) Presented in part at the 18th Calorimetry Conference in Bartlesville, Okla., Oct. 1963.

(3) To whom inquiries concerning this paper should be addressed.

(4) B. Weinstock, *Chem. Eng. News*, **42**, No. 38. 86 (1964).

(5) E. Greenberg, C. A. Natke, W. N. Hubbard, *J. Phys. Chem.*, **69**, 2089 (1965); see also previous papers in this series.

(6) O. Ruff and E. Vidic, *Z. anorg. allgem. Chem.*, **143**, 163 (1925).

(7) J. H. Holloway and R. D. Peacock, *J. Chem. Soc.*, 527 (1963).

(8) H. A. Bernhardt, R. L. Farrar, Jr., R. A. Gustison, and S. S. Kirslis, "The Preparation of Ruthenium Pentafluoride and the Determination of Its Melting Point and Vapor Pressure," U. S. Atomic Energy Commission Report AECD-2390 (1948). (Available from Office of Technical Services, U. S. Department of Commerce, Washington 25, D. C.)

(9) E. Greenberg, J. L. Settle, H. M. Feder, and W. N. Hubbard, *J. Phys. Chem.*, **65**, 1168 (1961).

(10) E. Greenberg, J. L. Settle, and W. N. Hubbard, *ibid.*, **66**, 1345 (1962).

(11) L. Stein, E. Rudzitis, and J. L. Settle, "Purification of Fluorine by Distillation," Argonne National Laboratory, ANL-6364 (1961). (Available from Office of Technical Services, U. S. Department of Commerce, Washington 25, D. C.)

(12) J. L. Settle, H. M. Feder, and W. N. Hubbard, *J. Phys. Chem.*, **65**, 1337 (1961).

the same as described[9] for the combustion of zirconium in fluorine. The sample consisted of a 0.5-cm.^{2} piece of foil inserted in a slot in the end of a 3.5-cm. length of rod. The bomb was evacuated overnight with an oil diffusion pump in order to eliminate traces of moisture and was then charged with 3900 mm. of pure fluorine. A sample exposed to fluorine under these conditions showed no significant change in weight. The calorimetric measurements were made in the usual manner.

Post-Combustion Examinations. After one of the calorimetric experiments, the gas in the bomb was condensed into a liquid nitrogen cold trap, fluorine and other permanent gases were pumped off, and the condensable gases were evaporated into an infrared absorption cell equipped with silver chloride windows. No absorption was observed in the infrared region of the spectrum. This was taken to indicate that ruthenium hexafluoride was not present since it shows a strong absorption peak[13] at 735 cm.$^{-1}$. The sensitivity of this absorption peak was such as to fix the possible RuF_6 concentration at less than 0.1% of the total ruthenium combustion product.

Immediately after the bomb was opened (in an inert-atmosphere glove box), the only visible combustion product was a uniform green solid which was determined to be ruthenium pentafluoride by comparison of its X-ray powder diffraction pattern with that reported by Holloway, Peacock, and Small.[14] No lines due to RuF_3, RuO_2, Ru, or ruthenium oxyfluorides were detected. However, X-ray diffraction analysis might have failed to detect small amounts of these possible contaminants or lower fluorides formed during combustion. More sensitive experiments were carried out in which weighed samples were heated *in vacuo* in order to evaporate away the relatively volatile RuF_5 product. Such experiments were made difficult by the fact that in handling RuF_5 it reacts readily to yield nonvolatile hydrolysis products. In the most successful experiments a nonvolatile residue of 0.4% was obtained. Thus, at least 99.6% of the combustion product was RuF_5. We believe that the 0.4% nonvolatile residue was a hydrolysis product formed in handling the RuF_5 rather than a lower fluoride of ruthenium formed during combustion.

The combined evidence of the post-combustion examinations has been interpreted to mean that the reaction studied was

$$Ru(c) + {}^5/_2F_2(g) \longrightarrow RuF_5(c) \qquad (1)$$

The amounts of unburned ruthenium and molybdenum were determined as follows. The interior of the bomb was washed with water, and the unburned stub of ruthenium rod was scrubbed with a brush to remove the adhering insoluble hydrolysis products, dried, and weighed. The difficulty in effecting a quantitative separation and determining the mass of unburned ruthenium is reflected in the precision of the results. The remnants of the molybdenum fuse wire were isolated and weighed separately.

Results

The results of six combustion experiments, expressed in terms of the defined calorie equal to (exactly) 4.184 absolute joules, are summarized in Table I. The corrections to standard states were applied in accordance with the procedure illustrated for the combustion of molybdenum in fluorine.[15] The entries in the table are identical with those previously used and explained.[10]

For the calculation of items 5 and 7, the auxiliary data shown in Table II were used. The contents of the bomb included 78.17 g. of nickel and 0.17 g. of Teflon. The internal volume of the empty bomb was 0.318 l. The value of -3868.4 cal. g.$^{-1}$ for the energy of combustion of molybdenum[12] was used for the calculation of item 8.

For the calculation of item 9, the data shown in Table III were used. Except for oxygen, which was assumed to be present as RuO_2, all of the impurities in the sample were assumed to be present uncombined. The corrections for hydrogen and nitrogen are negligible and the assumptions made regarding their presence in the sample are therefore not critical. The net correction made for all impurities was 2.19 ± 0.09 cal. g.$^{-1}$ of ruthenium sample burned.

The remaining corrections to standard states were all negligible. $\Delta Ec^\circ/M$ is just the sum of items 4 through 9 divided by the mass of sample burned.

The energy of formation ($\Delta Ef^\circ = \Delta Ec^\circ$) and enthalpy of formation (ΔHf°) of ruthenium pentafluoride at 25°, in accordance with reaction 1, were calculated to be $-211.9_3 \pm 0.3_5$ and $-213.4_1 \pm 0.3_5$ kcal. mole^{-1}, respectively. The atomic weight[16] of ruthenium was taken as 101.07. The uncertainties given are uncertainty intervals[17] equal to twice the combined standard deviations arising from known sources. The uncertainty in the results is due primarily to the un-

(13) H. H. Claassen, H. Selig, J. G. Malm, C. L. Chernick, and B. Weinstock, *J. Am. Chem. Soc.*, **83**, 2390 (1961).

(14) J. H. Holloway, R. D. Peacock, and R. W. H. Small, *J. Chem. Soc.*, 644 (1964).

(15) W. N. Hubbard in "Experimental Thermochemistry," Vol. II, H. A. Skinner, Ed., Interscience Publishers, Ltd., London, 1962, Chapter 6.

(16) A. E. Cameron and E. Wichers, *J. Am. Chem. Soc.*, **84**, 4175 (1962).

(17) F. D. Rossini in "Experimental Thermochemistry," F. D. Rossini, Ed., Interscience Publishers, Inc., New York, N. Y., 1956, Chapter 14.

Table I: Results of Combustion Experiments

1.	Combustion no.	1	2	3	4	7	8
2.	m', g.	2.21286	2.36557	2.30688	2.63436	2.24629	2.27021
3.	Δt_c, deg.	1.31456	1.39981	1.36703	1.56054	1.32878	1.34577
4.	$\mathcal{E}$(calor.)$(-\Delta t_c)$, cal.	−4660.26	−4962.48	−4846.27	−5532.29	−4710.67	−4770.90
5.	$\Delta E_{\text{contents}}$, cal.	−11.36	−12.26	−11.99	−13.76	−11.66	−11.80
6.	$\Delta E_{\text{ignition}}$, cal.	0.58	0.45	0.58	0.49	0.49	0.45
7.	ΔE_{gas}, cal.	−0.42	−0.59	−0.59	−0.60	−0.59	−0.58
8.	$\Delta E_{\text{Mo fuse}}$, cal.	14.58	15.78	15.32	17.60	16.29	14.82
9.	$\Delta E_{\text{impurities}}$, cal.	4.85	5.18	5.05	5.77	4.92	4.97
10.	$\Delta Ec^\circ/M$, cal. g.$^{-1}$	−2102.27	−2094.18	−2097.16	−2096.44	−2092.88	−2098.06

Mean $\Delta Ec^\circ/M$ = −2096.8 cal. g.$^{-1}$
Std. dev. of mean = ±1.3 cal. g.$^{-1}$

Table II: Auxiliary Data for Calculation of Items 5 and 7 in Table I

Substance	c_p, cal. deg.$^{-1}$ g.$^{-1}$	ρ, g. cc.$^{-1}$
Ni	0.1061[a]	8.907[b]
Teflon	0.28[c]	2.24[c]
Ru	0.0569[a]	12.1[d]
RuF_5	0.16[e]	3.92[f]
F_2(g)	[g,h]	

[a] R. Hultgren, R. L. Orr, P. D. Anderson, and K. K. Kelley, "Selected Values of Thermodynamic Properties of Metals and Alloys," John Wiley and Sons, Inc., New York, N. Y., 1963, pp. 198, 243. [b] H. E. Swanson and E. Tatge, "Standard X-Ray Diffraction Powder Patterns," Vol. I, National Bureau of Standards Circular 539, U. S. Government Printing Office, Washington, D. C., 1953, p. 13. [c] W. D. Good, D. W. Scott, and G. Waddington, *J. Phys. Chem.*, **60**, 1080 (1956). [d] Experimental determination. [e] A. Glassner, "The Thermochemical Properties of the Oxides, Fluorides, and Chlorides to 2500°K.," Argonne National Laboratory, ANL-5750 (1957). (Available from U. S. Government Printing Office, Washington, D. C.). [f] See ref. 14. [g] C_v = 5.50 cal. deg.$^{-1}$ mole^{-1}; W. H. Evans, T. R. Munson, and D. D. Wagman, *J. Res. Natl. Bur. Std.*, **55**, 147 (1955). [h] μ_{298} = 0.000803 atm.$^{-1}$ and $(\partial E/\partial P)_{298}$ = −1.781 cal. atm.$^{-1}$ mole^{-1}; see J. O. Hirschfelder, C. F. Curtiss, and R. B. Bird, "Molecular Theory of Gases and Liquids," John Wiley and Sons, Inc., New York, N. Y., 1954, and D. White, J. H. Hu, and H. L. Johnston, *J. Chem. Phys.*, 21, 1149 (1953).

Table III: Data for Calculation of Item 9 in Table I

Impurity	Impurity concn., p.p.m.	Assumed combustion product of impurity	ΔHf°_{298} of combustion product, kcal. mole^{-1}	Impurity correction, cal. g.$^{-1}$ of Ru
C[a]	135	CF_4(g)	−221[b]	2.19
O[a]	400	O_2(g)	0[c]	−1.49
H[a]	0.5	HF(g)	−64.8[b]	0.03
N[a]	0.7	N_2(g)	0	0.00
Fe	750	FeF_3(c)	−235[d]	1.57
Os	100	OsF_6(g)	−215[e]	−0.09
Rh	50	RhF_3(c)	−175[f]	−0.02
Ni	20	NiF_2(c)	−159.5[c]	0.01
Pd	10	PdF_2(c)	−112[d]	−0.01
Mo	2	MoF_6(g)	−372.4[g]	0.00

[a] Chemical analysis by Chemical Research Services, Inc., Addison, Ill.; all others are spectrochemical data reported by The International Nickel Co. [b] These values have been tentatively adopted by the National Bureau of Standards, Washington, D. C., for the revised edition of NBS Circular 500. [c] ΔHf°_{298} (RuO_2) = −52.5 kcal. mole^{-1}; see "Selected Values of Chemical Thermodynamic Properties," National Bureau of Standards Circular 500, U. S. Government Printing Office, Washington, D. C., 1952. [d] L. Brewer, L. A. Bromley, P. W. Gilles, and N. L. Lofgren, "The Chemistry and Metallurgy of Miscellaneous Materials: Thermodynamics," L. L. Quill, Ed., McGraw-Hill Book Co., Inc., New York, N. Y., 1950, pp. 76–192. [e] Estimated. [f] See footnote *e* of Table II. [g] See ref. 12.

certainties in the impurity corrections and in determining the mass of unburned ruthenium. The only previous value for the enthalpy of formation of RuF_5 is an estimate[18] of −300 kcal. mole^{-1}.

Acknowledgment. We wish to thank C. A. Natke and R. Terry for making the calorimetric measurements, R. V. Schablaske for X-ray diffraction analyses, and H. M. Feder for his continued interest and suggestions during this research.

(18) See footnote *e* of Table II.

The Enthalpy of Formation and Entropy of Aluminum(I) Fluoride(g)

by Hon Chung Ko, Michael A. Greenbaum, Jay A. Blauer, and Milton Farber

Maremont Corporation, Rocket Power, Inc., Research Laboratories, Pasadena, California
(Received January 19, 1965)

From a study of the reaction $2Al(l) + AlF_3(g) \rightarrow 3AlF(g)$ between 1199 and 1348°K. by means of the transpiration technique, a ΔH_r at 1273°K. of 93.35 ± 1.78 kcal. and a ΔS_r at 1273°K. of 62.15 ± 1.37 cal./(deg. mole) were obtained. Extrapolation to 298°K. by means of published thermal functions coupled with the use of published thermodynamic data for Al and AlF_3 yields values of −60.65 ± 0.59 kcal./mole and 51.93 ± 0.46 cal./(deg. mole) for the ΔH_{f298} and $S°_{298}$ for AlF(g), respectively.

Introduction

Experimental data for the thermodynamic properties of AlF are comparatively scarce, and large uncertainties and differences exist between the reported values. The heat of formation of AlF(g) at 298° was calculated in 1950 by Irmann[1] who employed the Born–Haber cycle to arrive at a value of −50 ± 5 kcal./mole. In 1948, Campbell, Gross, Kent, and Levi[2] employed the reaction of AlF_3 with Al to measure the heat of formation of AlF(g) and obtained a value of −49 kcal./mole. Gross, Hayman, and Levi in 1954[3] reported a value of −59.2 kcal./mole for ΔH_f of AlF(g) based on a new experimentally determined heat of formation of AlF_3 combined with thus previously measured values for the AlF_3–Al reaction.[2]

Spectrographic measurements were used by Barrow, Johns, and Smith in 1956[4] to evaluate the entropy of AlF(g). The reported value was 51.4 e.u. Using spectroscopic data, Barrow obtained a heat of formation of −62.4 kcal./mole for AlF(g). In 1959, Witt and Barrow[5] used a torsion effusion technique and spectroscopic data to determine the heat of sublimation of AlF_3 and heat of formation of AlF(g). The reported value for ΔH_f of AlF(g) was −60.97 ± 0.41 kcal./mole.

Owing to this uncertainty in the thermodynamic properties for AlF(g) an experimental study was undertaken to obtain reliable values for these properties. Accordingly, a study of the reaction

$$2Al(l) + AlF_3(g) \longrightarrow 3AlF(g) \qquad (1)$$

was undertaken employing the transpiration technique.

Experimental

The experimental apparatus consisted of three basic parts: the furnace, the reaction and generation cells, and the chamber for the entire apparatus. The furnace, a two-part tungsten coil resistance furnace, has been described in detail in an earlier publication.[6] The two-part furnace was employed to permit independent variations of the AlF_3 temperature and thus its pressure. The reaction apparatus (Figure 1) consisted of a graphite generator cell for $AlF_3(c)$, an aluminum oxide reaction cell to contain the molten Al, and an aluminum oxide connecting tube. This generator and reaction cells were contained with graphite sleeves to ensure uniform temperature and to prevent condensation of materials on the cells. For weighing purposes, the graphite sleeves were removed. The inlet tube for the carrier gas (into the AlF_3 generator cell) and the outlet tube from the reaction cell were also constructed of aluminum oxide.

The entire furnace assembly and cell assembly were placed inside a vacuum chamber (Figure 2) consisting of a 15.24-cm. i.d., 45.72 cm. long Pyrex pipe with two 5.08-cm. i.d. side arms. A vacuum gauge was connected to one side arm, and the other was con-

(1) F. Irmann, *Helv. Chim. Acta*, **33**, 1449 (1950).

(2) P. Gross, C. S. Campbell, P. J. C. Kent, and D. L. Levi, *Discussions Faraday Soc.*, **4**, 206 (1948).

(3) P. Gross, C. Hayman, and D. L. Levi, *Trans. Faraday Soc.*, **50**, 477 (1954).

(4) R. F. Barrow, J. W. C. Johns, and F. J. Smith, *ibid.*, **52**, 913 (1956).

(5) W. P. Witt and R. F. Barrow, *ibid.*, **55**, 730 (1959).

(6) M. A. Greenbaum, *et al.*, *J. Phys. Chem.*, **67**, 703 (1963).

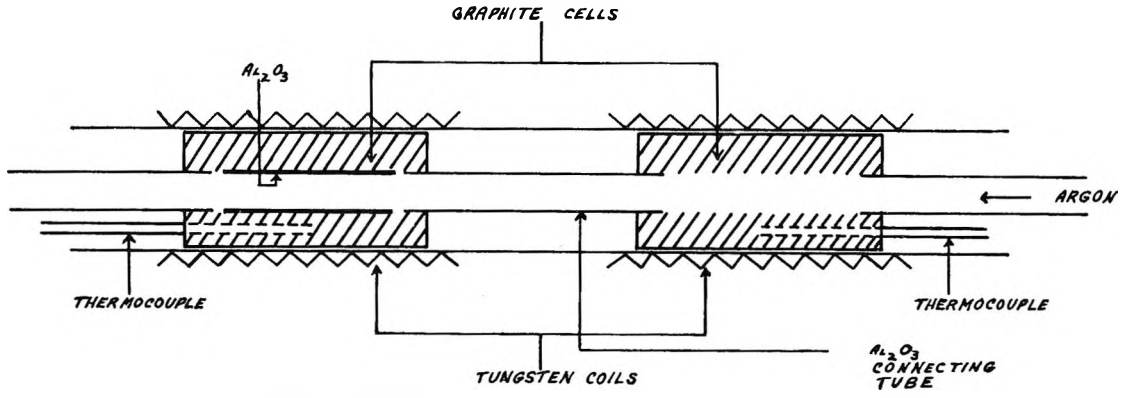

Figure 1. Cell assembly for transpiration experiment.

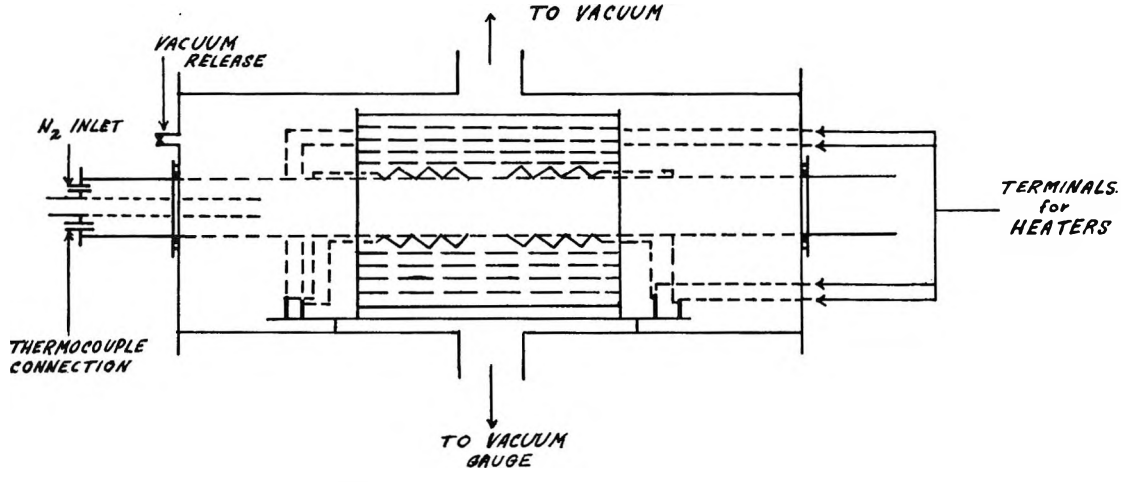

Figure 2. Complete experimental apparatus for the transpiration studies.

nected to the pumps. Both ends of the Pyrex pipe were closed each with a 0.635 cm. thick brass plate with holes permitting the 61-cm. alumina tube going through both ends. O-rings and small plates were used to ensure vacuum-tight fitness between the brass plates and the alumina tube. A valve was connected to one of the brass plates as the vacuum release. Heater terminals on the stainless steel base plate were connected to the other brass plate with copper wires. The vacuum system was necessary to protect the tungsten coils from oxidation during heating.

The furnace tube was constructed of aluminum oxide, and during runs nitrogen gas was passed through this tube around the outside of the graphite sleeves to prevent rapid oxidation of the graphite by air at the elevated temperatures. This was accomplished as indicated in Figure 2.

Each section of the two-part furnace was controlled separately by means of variable transformers. Temperature measurements were accomplished by means of calibrated chromel–alumel thermocouples inserted into holes in the graphite sleeves enclosing the generator and reaction cells. The thermocouples were used in conjunction with a Leeds and Northrup K-3 potentiometer and d.c. null detector. Temperatures were controlled to ± 1–$2°$, and the absolute temperatures as reported are good to $\pm 1°$ as established by means of a calibration of inside cell temperatures *vs.* measured sleeve temperatures.

High purity aluminum wire (>99.5% purity) obtained from the Kern Chemical Co. and aluminum fluoride obtained from City Chemical Co. and further purified by vacuum sublimation were employed in all experiments. Prepurified nitrogen was used as a blanket for the cell assembly, and argon was employed as the carrier gas for the AlF_3. A precisely calibrated flowmeter was employed to control the flow rate of the argon.

Experimental studies were carried out at reaction temperatures between 1199 and 1348°K. at a total pressure of 1 atm. using argon as the carrier gas. Generator and reaction cells were weighed with AlF_3

and Al before and after each run. Fresh samples of materials were used for each run, and quantities in large excess of those consumed were always employed. Studies of the effects of flow rate and pressure of $AlF_3(g)$ were carried out. No reaction was found to occur between AlF_3 and graphite or between graphite and Al_2O_3 under the conditions employed in the present study.

Because of the limitations of reaction temperature range and generation temperature of $AlF_3(g)$, it was necessary to work, at times, where the reaction zone was nearly 70° cooler than the AlF_3 generation temperature. Blank runs were carried out during which $AlF_3(g)$ was passed over an empty reaction vessel. In no instances was any AlF_3 found to have condensed on the vessel.

Treatment of Data. The vapor pressures of AlF(g) and $AlF_3(g)$ were calculated from the experimentally determined weight losses of Al and $AlF_3(c)$ according to the following equation, based on the assumption that the perfect gas law holds in the equilibrium zone

$$p = \frac{nRT}{V_t} \tag{2}$$

where p is the partial vapor pressure, n is the number of moles of species, R is the gas constant, T is the temperature of reaction, and V_t is the volume of gas transpired. Since V_t is related to the initial flow of gas V_0 at the temperature T_0 at which the flow is measured, eq. 2 can be written as

$$p = \frac{nRT_0}{V_0} \tag{3}$$

where T_0 is referred to room temperature. The vapor pressure of Al(l) in the temperature range investigated is less than that of AlF(g) and $AlF_3(g)$ by a factor of 10^4. Vapor pressures of AlF(g) and $AlF_3(g)$ were calculated according to the equations

$$p_{AlF} = \frac{{}^3/_2 n_{Al} RT_0}{V_0} \tag{4}$$

$$p_{AlF_3} = \frac{(n_{AlF_3} - {}^1/_2 n_{Al})RT_0}{V_0} \tag{5}$$

The equilibrium constant at a given temperature was calculated from the expression

$$K = \frac{(p_{AlF})^3}{p_{AlF_3}} \tag{6}$$

Results and Discussion

Although preliminary calculations based on an estimated value for $AlF_2(g)$[7] and an average value of those reported for AlF(g) indicated that at 1 atm. pressure and temperatures between 1200 and 1400°K. no $AlF_2(g)$ would be formed, a study of the pressure dependence of the equilibrium constant for the assumed reaction (eq. 1) was carried out at one temperature. The results of this study are presented in Table I and indicate by inspection that within the experimental accuracy only AlF(g) is formed during the reaction of liquid aluminum and gaseous aluminum fluoride. It should be pointed out that the AlF_3 generation temperature is not generally the same as the reaction temperature as indicated by the two temperature columns. This was further confirmed by plotting log P_{AlF} against log P_{AlF_3}. A straight line with slope of 0.35 ± 0.05 was obtained when this was done. The theoretical value for the slope based on eq. 1 is 0.33. The value expected from the formation of $AlF_2(g)$ according to eq. 7 is 0.67.

$$Al(l) + 2AlF_3(g) \longrightarrow 3AlF_2(g) \tag{7}$$

As has been demonstrated previously[8,9] by studies in these laboratories, the equilibrium constant for a reaction studied by the transpiration procedure is markedly affected by the flow rate of the carrier gas. In some instances there is a range of flow rates (generally fairly narrow) where the measured equilibrium constant does not change. A study of the equilibrium constant as a function of flow rate was carried out at 1273°K., and the results are summarized in Table II. Based on the results of this study, it appears that there does exist a small range of flow rates (3–9 cc./min.) within which the measured equilibrium constant does not change. All experimental studies were accordingly carried out at approximately 5–6 cc./min. which falls within this range. At the highest and lowest temperatures studied, two flow rate measurements (at 3 and 9 cc./min.) were made to ensure that departure from the equilibrium zone was not occurring. Results here also indicated no effect of the flow rate on the equilibrium constant within experimental error.

Having established an equilibrium flow rate zone and showing the absence of formation of $AlF_2(g)$ (the only other reaction which could be reasonably expected), experimental determinations of the equilibrium constant as a function of temperature were carried out over the region 1199–1348°K. Ten points were studied in this region, and the experimental results are presented in Table III, together with the calculated vapor pres-

(7) "JANAF Thermochemical Tables," USAF Contract AF 33(616)-6149, Advanced Research Projects Agency, Washington 25, D. C.

(8) M. Farber, *J. Chem. Phys.*, **36**, 661 (1962).

(9) J. Blauer and M. Farber, *ibid.*, **39**, 158 (1963).

Table I: Pressure Study

Reaction temp., °K.	Wt. loss of Al, mg./hr.	Generation temp., °K.	Wt. loss of AlF_3, mg./hr.	Partial press. of AlF, atm.	Partial press. of AlF_3, atm.	K
1199	3.06	1199	10.6	1.26×10^{-2}	5.2×10^{-3}	3.83×10^{-4}
1199	3.75	1223	15.1	1.54×10^{-2}	8.2×10^{-3}	4.47×10^{-4}
1199	4.33	1248	23.6	1.78×10^{-2}	1.4×10^{-2}	3.99×10^{-4}
1199	5.16	1273	31.3	2.12×10^{-2}	2.1×10^{-2}	4.65×10^{-4}
1199	4.85	1273	32.9	1.99×10^{-2}	2.2×10^{-2}	3.55×10^{-4}
1199	4.50	1263	26.6	1.85×10^{-2}	1.7×10^{-2}	3.68×10^{-4}

Table II: Flow Rate Study at 1273°K.

Flow rate, cc./min.	Wt. loss of Al, mg./hr.	Wt. loss of AlF_3, mg./hr.	K
3	5.3	18	4.02×10^{-3}
5.5	8.4	23.2	4.49×10^{-3}
9.3	15.7	49.5	4.28×10^{-3}

sures of AlF and AlF_3. The equilibrium constants as calculated according to eq. 6 are also included in Table III. It should be pointed out again that the temperature column refers only to reaction temperatures, not to the AlF_3 generation temperature.

A plot of the experimental data in Table III in the form log K *vs.* $1/T$ is presented in Figure 3. A least-squares analysis of the data yields a value for the slope of the line of 93.35 ± 1.78 kcal./mole which corresponds to the ΔH_r at the average temperature of 1273°K. Similarly a value of ΔS_{r1273} of 62.15 ± 1.37 cal./(deg. mole) is obtained from the intercept of the curve. Employing the available thermodynamic values and thermal functions for $AlF_3(g)$ and Al(l)[8] and the calculated thermal functions for AlF(g), the $\Delta H_f°_{298}$ and $S°_{298}$ for AlF(g) were found to be −60.65 ± 0.59 kcal./mole and 51.93 ± 0.46 cal./(deg. mole), respectively. A third-law calculation for $H_f°_{298}$ yields a value of −61.36 ± 0.14 kcal./mole, in excellent agreement with the second-law value. The slight trend in the third-law data obtained might tend to indicate a small systematic error in the work. This is, however, at most very small. The stated uncertainty in the third-law value reflects only the statistical uncertainty. In any event, the preferred second-law value has a stated uncertainty four times as great as that of the third-law value.

Sublimation of $AlF_3(c)$. The sublimation pressures of the AlF_3 employed in these studies were determined in the temperature range of 10.27–1184°K. by means of gravimetric effusion. These data are shown plotted in Figure 4 in the form described by the van't Hoff equation. These data were obtained from cells having orifice areas differing by a factor of 12. An analysis of variance of the data showed that within experimental error the orifice size had no effect upon the measured pressures. The following equation describes the experimental data and was obtained by the method of least squares

$$\log P(\text{atm.}) = 9.727 - \frac{14{,}974}{T} \qquad (8)$$

The results of the investigation indicate values for the heat and entropy of sublimation at an average temperature of 1105°K. of 68.5 ± 1.0 kcal./mole and 44.5 ± 1.0 cal./(deg. mole), respectively. Extrapola-

Table III: Experimental Data from Transpiration Studies of the Reaction $2Al(l) + AlF_3(g) = 3AlF(g)$

Reaction temp., °K.	Wt. loss of Al, mg./hr.	Flow of argon, cc./min.	Wt. loss of AlF_3, mg./hr.	p_{AlF}, atm.	p_{AlF_3}, atm.	$K = \frac{(p_{AlF})^3}{p_{AlF_3}}$
1199	4.6	5.5	26.55	1.89×10^{-2}	1.71×10^{-2}	3.96×10^{-4}
1211	4.8	5.5	22.6	1.97×10^{-2}	1.33×10^{-2}	5.75×10^{-4}
1223	6.2	5.5	30.9	2.54×10^{-2}	1.88×10^{-2}	8.71×10^{-4}
1248	7.1	5.5	26.3	2.92×10^{-2}	1.34×10^{-2}	1.84×10^{-3}
1261	7.3	5.5	23.5	3.01×10^{-2}	1.07×10^{-2}	2.54×10^{-3}
1273	8.35	5.5	23.2	3.43×10^{-2}	0.90×10^{-2}	4.49×10^{-3}
1298	9.5	5.5	23.3	3.90×10^{-2}	0.75×10^{-2}	7.89×10^{-3}
1310	10.5	5.5	23.6	4.32×10^{-2}	0.64×10^{-2}	1.27×10^{-2}
1323	13.6	5.5	34.9	5.59×10^{-2}	1.21×10^{-2}	1.44×10^{-2}
1348	12.2	5.5	23.65	5.02×10^{-2}	0.44×10^{-2}	2.88×10^{-2}

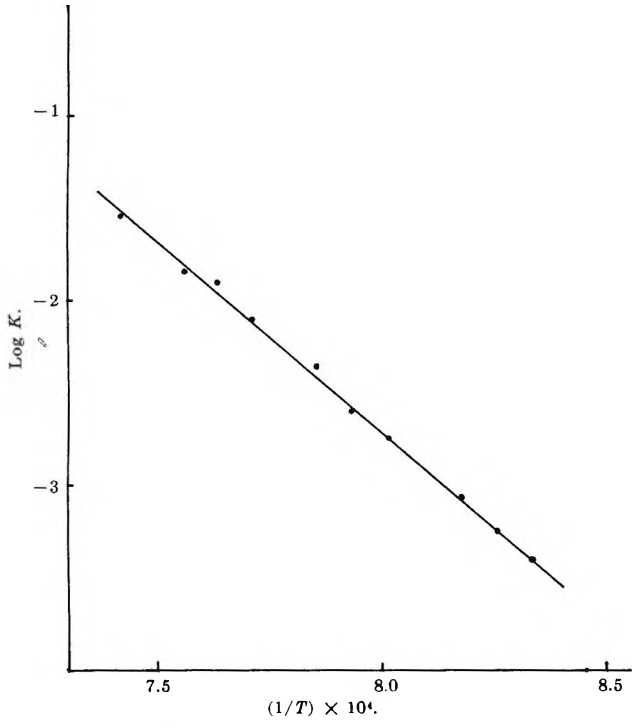

Figure 3. Equilibrium constant for the reaction 2Al(l) + AlF_3(g) = 3AlF(g) as a function of temperature.

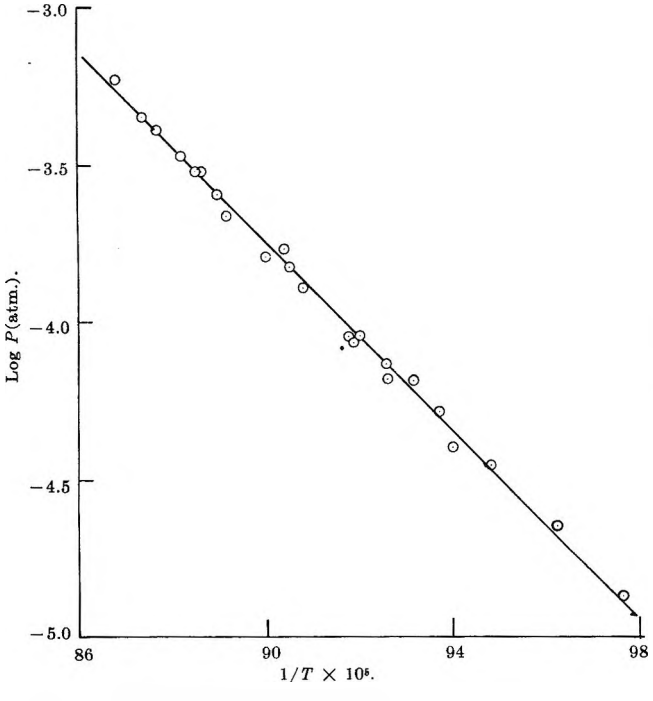

Figure 4. Vapor pressure of AlF_3(c) as a function of temperature.

tions with estimated values of the heat capacities[7] of the species involved yield 71.7 ± 1 kcal./mole and 50.1 ± 1 cal./(deg. mole), respectively, for the corresponding values at 298°K. This heat of sublimation is in excellent agreement with the value of 71.5 kcal./mole obtained by averaging the third-law values of several investigators.

Krause, *et al.*,[10] have given some indication that some dimer of AlF_3 may be present. Unless considerably more dimer were present than reported by Krause, the van't Hoff plot should not exhibit significant curvature over the temperature range studied assuming that the molal heats of sublimation of monomer and dimer were not identical. However, a significant departure of the measured entropy of the simple diatomic molecule AlF would be noted even should the molal heats of sublimation of monomer and dimer be identical considering the large difference to be expected in entropies between monomer and dimer. A detailed discussion of this matter as it applies to $BeCl_2$ has been presented previously.[11] An examination of Figure 4 shows that no curvature is distinguishable within experimental error in our data. Consequently, it was assumed in the analysis that only monomer was present.

It should be pointed out that the vapor pressures of AlF_3 calculated from eq. 8 do not correspond exactly with those calculated for the experimental runs. This is not surprising since no attempt was being made to measure accurately AlF_3 vapor pressure during the runs. Small variations in temperature of the AlF_3 generator as well as nonequilibrium flow conditions for AlF_3 vapor pressures (even though equilibrium flow rates for reaction were established) could account for the differences. This situation is not uncommon in transpiration reaction studies and in no way bears

Table IV: Calculated Thermodynamic Data for the Reaction 2Al(l) + AlF_3(g) = 3AlF(g)

T, °K.	ΔF_r, kcal./mole	$\Delta H_r°$, kcal./mole
1199	18.671	91.750
1211	17.955	91.705
1223	17.125	91.557
1248	15.619	91.348
1261	14.974	91.403
1273	13.678	91.771
1298	12.491	90.916
1310	11.372	90.407
1324	11.152	90.916
1348	9.499	90.568
		Av. 91.239 ± 0.43

(10) R. F. Krause, Jr., A. C. Victor, and T. B. Douglas, National Bureau of Standards Report No. 7796, 1963.

(11) M. A. Greenbaum, R. E. Yates, and M. Farber, *J. Phys. Chem.*, 67, 1802 (1963).

Table V: Summary of Thermodynamic Data for the Reaction $2Al(l) + AlF_3(g) = 3AlF(g)$

	Second-law treatment	Third-law values
$\Delta H_r°_{1273}$	93.35 ± 1.78 kcal.	91.234 ± 0.43 kcal.
$\Delta S_r°_{1273}$	62.15 ± 1.37 cal./deg.	
$\Delta H_f°_{1273}(AlF(g))$	−65.70 ± 0.59 kcal./mole	−66.41 ± 0.14 kcal./mole
$\Delta H_f°_{298}(AlF(g))$	−60.65 ± 0.59 kcal./mole	−61.36 ± 0.14 kcal./mole
$S°_{1273}(AlF(g))$	64.16 ± 0.46 cal./(deg. mole)	
$S°_{298}(AlF(g))$	51.93 ± 0.46 cal./(deg. mole)	51.40 cal./(deg. mole)

on the validity of the measured equilibrium constants which have been shown to be highly consistent.

The values obtained in this study of the reaction of liquid aluminum and gaseous aluminum fluoride by means of a transpiration technique are in excellent agreement with the values reported by Gross[3] in 1954 based on an experimental determination of ΔH_f of $AlF_3(g)$ and by Witt and Barrow[5] in 1959 by means of an effusion technique coupled with optical spectroscopy. The excellent agreement of the second- and third-law values lends credence to the reliability of the presently reported thermodynamic values for AlF(g).

The Use of Nonlinear Estimation Techniques in Simple Molecular Orbital Calculations[1a]

by Thomas H. Brown[1b]

IBM Watson Laboratory, Columbia University, New York, New York

and Robert L. Taylor

Union Carbide Corporation, Computer Center, New York, New York *(Received January 19, 1965)*

Nonlinear estimation techniques have been applied to simple π-electron molecular orbital calculations which seek to have self-consistent Coulomb integrals and charge densities. Having analytic expressions for the various derivatives involved allows one to use the Newton–Raphson–Gauss estimation procedure, rather than iteration by substitution, as is customarily done. The present procedure converges very rapidly to the self-consistent solution, in contrast with the slow convergence or even divergence of the previous method.

Nonlinear estimation techniques can be of considerable value when applied to problems in molecular quantum mechanics which seek a self-consistent solution.[2a] In this report we demonstrate the usefulness of this method when applied to simple molecular orbital calculations.

In recent years a number of refinements have been made to the simple Hückel molecular orbital procedure.[2b] Usually an attempt has been made to maintain a number of simplifying assumptions of the Hückel technique while introducing a certain amount of sophis-

(1) (a) This research was initiated when both authors were employed by the Union Carbide Corp.; (b) author to whom correspondence should be addressed.

(2) (a) A general discussion of these applications will be available elsewhere; T. H. Brown and R. L. Taylor, to be published; (b) see for example, A. Streitwieser, Jr., "Molecular Orbital Theory for Organic Chemists," John Wiley and Sons, Inc., New York, N. Y., 1961.

tication into the calculations. The self-consistency procedures suggested by Wheland and Mann[3] and by Muller, Pickett, and Mulliken[4] represent one such approach. A simplified version of this procedure has been used extensively by Streitwieser and co-workers[2a,5,6] among others. It is this latter approach which we shall use as an example in this report.

Streitwieser, in what he has called the "ω-technique," considers the proposition that atoms having unequal charge densities should have unequal Coulomb integrals, contrary to the simple Hückel theory. Specifically, in the ω-technique it is assumed that the various Coulomb integrals have the form shown in eq. 1.

$$\alpha_t = \alpha_0 + \omega(Q_t - q_t)\beta_0 \tag{1}$$

Making the usual simplifications, we may write the difference from the normal value of the Coulomb integral for atom i, δ_t, as in eq. 2, where Q_t is the core charge on

$$\delta_t = \omega(Q_t - q_t) \tag{2}$$

the atom in question, and q_t is the computed electron charge density on the same atom. It is thus assumed that the difference in a Coulomb integral is directly proportional to the net charge density, ω being the constant of proportionality. Several values for ω have been suggested in the literature, some having been chosen to give a "best fit" to experiment.[2a]

The computational aspect of the ω-technique, wherein its serious disadvantages lie, is basically iteration by simple substitution.[2a,5] An appropriate value for ω and a fixed set of β-values are first chosen; then an initial set of charge densities $q_t^{(0)}$ is guessed and used to determine the $\delta_t^{(0)}$ *via* eq. 2. The secular equation is solved, and a set of charge densities, $q_t^{(1)}$, is computed from the eigenvectors by eq. 3. If the $q_t^{(1)}$ do not agree

$$q_t = \sum_j n_j C_{tj}^2 \tag{3}$$

with the $q_i^{(0)}$, a new set of $\delta_t^{(1)}$ are computed from eq. 2, and the process is continued. The problem is said to converge when the charges computed from the eigenvectors by eq. 3 are identical with those used to determine the secular equation *via* eq. 2, that is, when $q_t^{(k+1)} = q_i^{(k)}$, for all i. The disadvantages of this technique are (1) that convergence is frequently not attained and (2) that, when convergence is attained, it may be reached very slowly. A discussion of the divergence of such procedures can be found elsewhere.[7]

We consider the problem of self-consistency from the standpoint of nonlinear estimation.[8] The end result will involve the same model for self-consistency as used in the ω-technique (eq. 1 and 2) but will utilize a superior computational technique.

Specifically, we wish to determine a set of δ_t-values which minimize a particular expression in the least-squares sense.[9] Here the δ_t-values have the same significance as in the previous method. We now consider two expressions for determining the charge density at atom i. The first of these is eq. 3, while the second is obtained by rearranging eq. 2, *i.e.*

$$q_t = Q_t - \frac{\delta_t}{\omega} \tag{4}$$

By subtracting eq. 4 from eq. 3, we obtain the quantities Y_t given in eq. 5. It is clear that the condition $Y_t = 0$,

$$Y_t = \sum_j n_j C_{tj}^2 - Q_t + \frac{\delta_t}{\omega} \tag{5}$$

for all i, represents the same criterion of self-consistency as is used in the ω-technique. We have thus reduced the problem of self-consistency to a nonlinear estimation problem, *i.e.*, finding a set of δ_t-values which minimize the magnitude of the Y_t-values.

At this point a variety of estimation procedures is available. We choose to make use of analytic expressions, which have been discussed in another context, for the derivatives, $\partial Y_t/\partial\delta_j$.[10] These are based upon general expressions for the derivatives of eigenvalues and eigenvectors with respect to arbitrary molecular integrals appearing in the secular equations. As we shall see, the present problem is sufficiently linear that the use of these derivatives coupled with a straightforward application of the Newton–Raphson–Gauss estimation procedure provides a rapid method of obtaining a self-consistent solution; that is, for example, the first refinement of $\boldsymbol{\delta}^{(0)}$, where $\boldsymbol{\delta}$ is the vector of δ_t-values, is given by

(3) G. W. Wheland and D. E. Mann, *J. Chem. Phys.*, **17**, 264 (1949).

(4) N. Muller, L. W. Pickett, and R. S. Mulliken, *J. Am. Chem. Soc.*, **76**, 4770 (1954).

(5) A. Streitwieser, Jr., and P. M. Nair, *Tetrahedron*, **5**, 149 (1959).

(6) A. Streitwieser, Jr., *J. Am. Chem. Soc.*, **82**, 4123 (1960); A. Streitwieser, Jr., J. I. Brauman, and J. B. Bush, *Tetrahedron*, **19**, Suppl. 2, 379 (1963).

(7) See for example, (a) P. O. Löwdin, *J. Mol. Spectry.*, **10**, 12 (1963); (b) L. R. Turner, *Ann. N. Y. Acad. Sci.*, **86**, 817 (1960).

(8) We use the term nonlinear estimation to refer to the general procedure whereby various linear least-square methods are used to approximate the solution of a nonlinear problem. In general, the procedures are iterative, continuing until convergence is reached in the least-square sense. See, for example, ref. 7b; G. E. P. Box, *Ann. N. Y. Acad. Sci.*, **86**, 792 (1960); and H. O. Hartley, *Technometrics*, **3**, 269 (1961).

(9) Wheland and Mann in their calculation of fulvene (ref. 3) give results obtained by a procedure which is somewhat similar to one iteration of the technique proposed here. Their method is similar in that it also considers the interrelations between charge densities and Coulomb integrals and utilizes atom polarizabilities which are similar to the derivatives Z_{ij} used here. (See ref. 10.) We would like to thank a referee for clarifying their calculation.

(10) T. H. Brown and R. L. Taylor, *J. Chem. Phys.*, to be published.

$$\delta^{(1)} = \delta^{(0)} - (\mathbf{Z}^{\dagger}\mathbf{Z})^{-1}\mathbf{Z}^{\dagger}\mathbf{Y} \quad (6)$$

where $Z_{ij} = \partial Y_i/\partial\delta_j$. Thus, having chosen a value for ω and a fixed set of β-values, we proceed as follows.

(1) An initial set of Coulomb integrals, $\delta_i^{(0)}$, is chosen; these for the purposes of comparison can be chosen to reproduce the Hückel charge densities *via* eq. 4. (2) The secular equation is solved for the coefficients of the atomic orbitals, C_{ij}. (3) The $Y_i^{(0)}$ are computed, and, if they are not sufficiently small, the derivatives $\partial Y_i/\partial\delta_j$ are computed. (4) Values for $\delta_i^{(1)}$ are obtained by using the Newton–Raphson–Gauss procedure. (Note that at this point, if we wish to introduce further sophistication, it is possible by modification of the Newton–Raphson–Gauss procedure to guarantee that the $Y^{2(1)}$ will not be larger than the $Y^{2(0)}$ in the least-squares sense, where $Y^2 = \sum_j Y_i^2$. In actual practice this precaution seems unnecessary.) (5) The procedure then continues from step 2 until a set of values for $Y_i^{(k)}$ is obtained that are sufficiently small. (In general two iterations are generally sufficient to reduce all of the Y_i-values to the order of 10^{-6} to 10^{-7}.)

The technique as described above has been used successfully on a wide variety of examples, including all of the divergent cases given in ref. 5, *i.e.*, the benzyl cation, etc. The superiority of the present method is best shown by some comparisons. We consider first α-protonated pyrrole. This is a four-atom problem with four electrons and a net charge of 1+. For simplicity, we set all resonance integrals equal; *i.e.*, $\beta_{C-N} = \beta_{C-C} = \beta_0$. Using $\omega = 1.2$, the ω-technique diverges, as is shown for four iterations in Table I, whereas the technique described herein converges rapidly and without difficulty to a self-consistent answer. See Table II. (Since the y_i-values are the quantities being iterated, the charge densities at each iteration are ambiguous. Values of the charge densities as computed by both eq. 3 and eq. 4 are therefore included in Table II.) For the case of $\omega = 1.0$, the ω-technique again diverges; in addition, though the correct charge densities are 1.3120, 0.8153, 0.9829, and 0.8897, starting the ω-technique, with such sets of charge densities as 1.310, 0.817, 0.985, 0.888, and 1.314, 0.813, 0.981, 0.892, still produces divergence. In other words, divergence in the ω-technique cannot be blamed on an extraordinarily bad initial guess. An initial bad guess does not affect the method described here for the problem discussed. The same solution is reached in two additional steps when the initial charges are chosen to be the ridiculous values of 5001, 5001, −4999, and −4999. This is equivalent to saying that the problem converges in approximately the same number of iterations, no matter whether the initial charges are chosen 1.0, 1.0, 1.0, and 1.0, or the unrealistic values of 0.0, 0.0, 2.0, and 2.0.

Table I: ω-Technique, α-Protonated Pyrrole, $\omega = 1.2$

Iteration	q_1	q_2	q_3	q_4
0	1.000	1.000	1.000	1.000
1	1.598	0.626	1.037	0.739
2	1.036	1.003	0.859	1.102
3	1.603	0.630	1.140	0.627
4	0.993	1.013	0.761	1.233
		All diverge		

Table II: α-Protonated Pyrrole, Y^2-Technique, $\omega = 1.2$

Iteration	Eq.	q_1	q_2	q_3	q_4
0	4	1.0000	1.0000	1.0000	1.0000
	3	1.5980	0.6256	1.0369	0.7395
1	4	1.3815	0.7798	0.9737	0.8651
	3	1.3029	0.8267	0.9670	0.9033
2	4	1.3415	0.8015	0.9760	0.8810
	3	1.3415	0.8015	0.9760	0.8810

Table III: ω-Technique, Butadiene Cation, $\omega = 1.4$[a]

Iteration	q_1	q_2
0	0.652	0.848
1	0.729	0.771
2	0.669	0.831
3	0.716	0.784
4	0.679	0.821
..	...	...
..	...	...
..	...	...
..	...	...
10	0.691	0.809
11	0.698	0.802
∞	0.695[b]	0.805[b]

[a] From ref. 5. [b] An estimate given in ref. 5.

Table IV: Y^2-Technique, Butadiene Cation, $\omega = 1.4$

Iteration	Eq.	q_1	q_2
0	4	0.6520	0.8480
	3	0.7287	0.7713
1	4	0.6947	0.8053
	3	0.6950	0.8050
2	4	0.6949	0.8051
	3	0.6948	0.8051

We lastly wish to compare the two techniques on a problem for which the ω-technique converges. We choose an example given by Streitwieser and Nair,[5] the butadiene cation. The two methods are compared in Tables III and IV, where the initial charge densities are the same. The superiority of the present method is clear; the ω-technique still produces sizable variations in the third significant figure, even after 11 iterations, whereas the Y^2-technique gives a reasonable answer in only one iteration. It should be pointed out that it is not fair to make a direct comparison of the number of iterations the two methods take. The iterations of the Y^2-technique are more complex than those of the ω-technique; nonetheless, there is an appreciable saving in time with the present technique, in addition to its obvious advantage of succeeding where the ω-technique fails.

Acknowledgment. The authors wish to thank Dr. M. Karplus, Dr. V. Schomaker, and Dr. E. B. Whipple for several helpful discussions.

Kinetics of Uranyl Ion Hydrolysis and Polymerization[1]

by M. P. Whittaker, E. M. Eyring, and E. Dibble[2]

Department of Chemistry, University of Utah, Salt Lake City, Utah *(Received January 20, 1965)*

Temperature jump relaxation times have been observed in acidic, aqueous solutions of uranyl ion that have been identified with the equilibrium $2UO_2^{2+} + 2H_2O \underset{k_{-2}}{\overset{k_2}{\rightleftharpoons}} (UO_2)_2(OH)_2^{2+} + 2H^+$. The rate constant k_2 at 25° is found to have the value 116 M^{-1} sec.$^{-1}$. This result is compared with the dimerization of chromate and vanadate ions.

Recently a number of workers have reported equilibrium constants for the hydrolysis and polymerization of uranyl ion in aqueous solution.[3-6] In principle, such data permit the determination of rate constants for several over-all reactions using relaxation methods. A similar kinetic study of aqueous boric acid polymerization has been reported.[7]

The hydrolysis mechanism and equilibrium constants or uranyl ion in aqueous nitrate media proposed by Baes and Meyer[4] and also those proposed by Dunsmore, Hietanen, and Sillén[5] were used as a basis for explaining relaxation times observed with a Joule heating-type temperature jump apparatus. The hydrolytic species and their corresponding equilibrium constants reported by Rush and Johnson[6] were the basis for our calculations of rate constants in aqueous perchlorate medium. The calculated rate constants were essentially the same regardless of which set of equilibrium constants was used in their calculation provided that the reaction responsible for the observed relaxation time was assumed to be the formation of dimer, $(UO_2)_2(OH)^{3+}$ or $(UO_2)_2(OH)_2^{2+}$ depending upon the hydrolysis scheme, from monomer.

Experimental

For our experiments with uranyl nitrate, samples of

(1) This research was supported in part by an equipment grant from the University of Utah research fund and by Grant AM-06231 from the National Institute of Arthritis and Metabolic Diseases of the U. S. Public Health Service.

(2) National Science Foundation Undergraduate research participant.

(3) R. M. Rush, J. S. Johnson, and K. A. Kraus, *Inorg. Chem.*, 1, 378 (1962).

(4) C. F. Baes, Jr., and N. J. Meyer, *ibid.*, 1, 780 (1962).

(5) H. S. Dunsmore, S. Hietanen, and L. G. Sillén, *Acta Chem. Scand.*, 17, 2644 (1963).

(6) R. M. Rush and J. S. Johnson, *J. Phys. Chem.*, 67, 821 (1963).

(7) J. L. Anderson, E. M. Eyring, and M. P. Whittaker, *ibid.*, 68, 1128 (1964).

Mallinckrodt analytical reagent grade uranyl nitrate were weighed out directly and dissolved in distilled, demineralized, boiled water. The pH of the sample was adjusted with Wasco reagent grade NaOH and determined with a Radiometer TTT-1 titrimeter. The ionic strength μ of each sample was made 0.5 M by the addition of Merck reagent grade KNO_3. Mallinckrodt methyl orange was used in those experiments involving an acid–base indicator.

A stock solution of uranyl perchlorate was prepared by dissolving G. F. Smith Chemical Co. hydrated uranyl perchlorate in distilled water. The concentration of the stock solution was determined by reducing the UO_2^{2+} to U^{4+} by means of a Jones reductor packed with reagent grade granulated lead and titrating the resulting U^{4+} back to UO_2^{2+} with standard dichromate solution. The ionic strength was adjusted to 0.5 M with $NaClO_4$.

A single-beam temperature jump apparatus of the type described by Hammes and Steinfeld[8] was used to perturb the uranyl equilibria. The temperature jump from 15 to approximately 25° was effected in a few microseconds by discharging a 0.1-μf. capacitor charged to 30 kv. through the 1-ml. sample volume having a resistance of 50 ohms. A temperature jump of this magnitude typically effects a change of less than 10% in the equilibrium concentrations. The oscilloscope trace for each experiment, depicting change in optical absorbance as a function of time, was recorded photographically, and the relaxation times were obtained from the exponential curves by looking for linearity in semilogarithmic plots of vertical deflection *vs.* time. Three sets of experiments were carried out at pH 3.0: uranyl nitrate with indicator, uranyl perchlorate with indicator, and uranyl perchlorate without indicator. The analyzing wave length of light passing through the cell was 520 mμ for the first two sets of experiments and 410 mμ for the last. As is apparent from Figure 1, pH 3 is the optimum for these experiments since at this pH we are justified in making the approximation that only monomer and dimer are present. A second relaxation time was not resolved at higher pH or higher concentrations of uranyl nitrate so that it was only possible to determine rate constants for the monomer–dimer equilibrium as will be shown.

Calculations

The derivation of relaxation times in terms of rate constants and equilibrium concentrations which follows is for uranyl nitrate concentrations using the equilibrium constants proposed by Baes and Meyer.[4] The derivation for uranyl perchlorate is similar, the major difference being that Rush and Johnson[6] did not include the

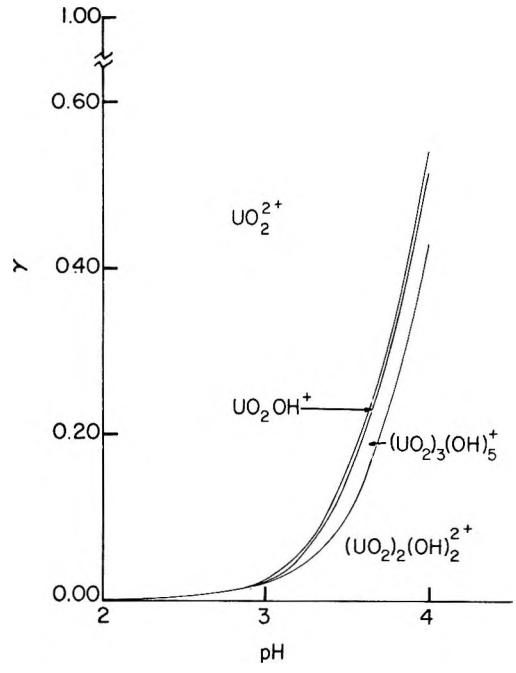

Figure 1. Distribution of uranium(VI) between different ions in 0.5 M ionic strength medium (adjusted with KNO_3) when total uranyl nitrate concentration is $c_0 = 0.01$ M. At a given pH, the fraction γ of uranium(VI) present as a given ion is represented by the length of a vertical line segment falling between curves.

$(UO_2)(OH)^+$ species in their hydrolysis mechanism; consequently, the perchlorate derivation is somewhat simplified.

According to Baes and Meyer, the uranyl equilibria with their corresponding equilibrium constants at 25° are

$$UO_2^{2+} + H_2O \underset{k_{-1}}{\overset{k_1}{\rightleftharpoons}} UO_2OH^+ + H^+$$

$$K_1 = 2 \times 10^{-6} \quad (1)$$

$$2UO_2^{2+} + 2H_2O \underset{k_{-2}}{\overset{k_2}{\rightleftharpoons}} (UO_2)_2(OH)_2^{2+} + 2H^+$$

$$K_2 = 1.2 \times 10^{-6} \quad (2)$$

$$3UO_2^{2+} + 5H_2O \underset{k_{-3}}{\overset{k_3}{\rightleftharpoons}} (UO_2)_3(OH)_5^+ + 5H^+$$

$$K_3 = 6 \times 10^{-17} \quad (3)$$

The observed relaxation times τ can be expressed as a function of the desired rate constants and known equilibrium concentrations and constants by a systematic method proposed by Castellan.[9] To save space

(8) G. G. Hammes and J. I. Steinfeld, *J. Am. Chem. Soc.*, **84**, 4639 (1962).

(9) G. W. Castellan, *Ber. Bunsenges.*, **67**, 898 (1963).

we will use the following: $H \equiv H^+$, $A \equiv UO_2(OH)^+$, $B \equiv UO_2^{2+}$, $C \equiv (UO_2)_2(OH)_2^{2+}$, and $E \equiv (UO_2)_3(OH)_5^+$, with a bar over the symbol denoting an equilibrium concentration. At pH 3 the calculated concentration of B in our sample solutions was always about 500 times that of A. We then assumed that the dimerization $2B \rightarrow C + 2H$ was more important than $2A \rightarrow C$. In fact, when the latter reaction was incorporated in our presumed mechanism, the calculated rate constants were much less satisfactory than those reported below. When the dimerization $B + A \rightarrow C + H$ is substituted for $2B \rightarrow C + 2H$ in the presumed mechanism, one obtains somewhat less constant specific rates, hence our preference for the incorporation of $2B \rightarrow C + 2H$ in the mechanism

$$B \underset{k_{1-}}{\overset{k_1}{\rightleftharpoons}} A + H \qquad r_1 = k_1\bar{B} = k_{-1}\bar{A}\bar{H} \tag{4}$$

$$2B \underset{k_{-2}}{\overset{k_2}{\rightleftharpoons}} C + 2H \qquad r_2 = k_2\bar{B}^2 = k_{-2}\bar{H}^2\bar{C} \tag{5}$$

$$B + C \underset{k_{-3}}{\overset{k_3}{\rightleftharpoons}} E + 3H \qquad r_3 + k_3\bar{B}\bar{C} = k_{-3}\bar{E}\bar{H}^3 \tag{6}$$

$$g_{11} = \frac{1}{\bar{B}} + \frac{1}{\bar{A}} + \frac{1}{\bar{H}} \qquad g_{12} = \frac{2}{\bar{B}} + \frac{2}{\bar{H}} \tag{7}$$

$$g_{22} = \frac{4}{\bar{B}} + \frac{1}{\bar{C}} + \frac{4}{\bar{H}} \qquad g_{13} = \frac{1}{\bar{B}} + \frac{3}{\bar{H}} \tag{8}$$

$$g_{33} = \frac{1}{\bar{B}} + \frac{1}{\bar{C}} + \frac{1}{\bar{E}} + \frac{9}{\bar{H}} \qquad g_{23} = \frac{2}{\bar{B}} - \frac{1}{\bar{C}} + \frac{6}{\bar{H}} \tag{9}$$

whence

$$\begin{vmatrix} r_1g_{11} - \lambda & r_1g_{12} & r_1g_{13} \\ r_2g_{21} & r_2g_{22} - \lambda & r_2g_{23} \\ r_3g_{31} & r_3g_{32} & r_3g_{33} - \lambda \end{vmatrix} = 0 \tag{10}$$

where $\lambda = \tau^{-1}$. Making the safe assumption that the relaxation times of the second and third equilibria are both much longer than that of the first protolytic equilibrium and making the much less certain assumption also discussed below that the relaxation time of the third equilibrium is much longer than that of the second, we have

$$\tau_1 \ll \tau_2 \ll \tau_3 \tag{11}$$

whence

$$r_1g_{11} \gg r_2g_{22} \gg r_3g_{33} \tag{12}$$

Taking r_2 and r_3 to be zero and evaluating the determinant of eq. 10, we obtain

$$(r_1g_{11} - \lambda)(-\lambda)(-\lambda) = 0 \tag{13}$$

$$\lambda_1 = \frac{1}{\tau_1} = r_1g_{11} \tag{14}$$

and

$$k_1 = \frac{1}{\tau_1g_{11}\bar{B}} \tag{15}$$

To obtain k_2 we divide row one of eq. 10 by r_1; *i.e.*, we let $r_1 \rightarrow \infty$ and also assume $r_3 = 0$. We then have

$$\begin{vmatrix} g_{11} & g_{12} & g_{13} \\ r_2g_{21} & r_2g_{22} - \lambda & r_2g_{23} \\ 0 & 0 & -\lambda \end{vmatrix} = 0 \tag{16}$$

Expanding the third row by minors, dividing both sides by $-\lambda$, and evaluating the resulting two-by-two determinant, we find

$$\lambda = \frac{r_2D_2}{D_1} = \frac{1}{\tau_2} \tag{17}$$

where

$$D_1 = g_{11}$$

$$D_2 = \begin{vmatrix} g_{11} & g_{12} \\ g_{21} & g_{22} \end{vmatrix}$$

$$k_2 = \frac{D_1}{D_2\bar{B}^2\tau_2} \tag{18}$$

To determine k_3 we divide the first row of eq. 10 by r_1 and the second row by r_2; *i.e.*, we let both r_1 and $r_2 \rightarrow \infty$ and obtain

$$\begin{vmatrix} g_{11} & g_{12} & g_{13} \\ g_{21} & g_{22} & g_{23} \\ r_3g_{31} & r_3g_{32} & r_3g_{33} - \lambda \end{vmatrix} = 0 \tag{19}$$

Equation 19 can be rewritten as

$$\begin{vmatrix} g_{11} & g_{12} & g_{13} \\ g_{21} & g_{22} & g_{23} \\ r_3g_{31} & r_3g_{32} & r_3g_{33} \end{vmatrix} - \lambda \begin{vmatrix} g_{11} & g_{12} \\ g_{21} & g_{22} \end{vmatrix} = 0 \tag{20}$$

or $r_3D_3 - \lambda D_2 = 0$ from which it follows that

$$k_3 = \frac{D_2}{\tau_3\bar{B}\bar{C}D_3} \tag{21}$$

Results and Discussion

In addition to the hydrolytic species present in solution, there are various other complexes involving the combination of the particular anions present with the uranyl ion. Unlike many hydrolyzing systems, the behavior of the uranyl system varies markedly in different ionic media, which indicates that the anions present are also involved in the formation of the hydrolytic species themselves. Therefore, there are

several sets of equilibria governing the concentrations of species present in solution which are of potential importance in the determination of the observed relaxation time. We are able to show that only one reaction describing the behavior of species in these solutions can give the experimental relaxation times observed.

The metal ligand complex reactions are all of the form

$$ML \underset{k_R}{\overset{k_D}{\rightleftharpoons}} M + L \qquad (22)$$

The expression for the relaxation time of a reaction of this type is

$$1/\tau = k_R(\bar{M} + \bar{L} + K) \qquad (23)$$

Hence, a reaction of this type should be strongly dependent upon the concentration of the ligand. As is evident from Table I, no such dependence is observed. The fact that the rate constant is independent of the type of ligand present (see Table II) further supports the neglect of equilibrium 22.

Table I: Temperature Jump Relaxation Data on Aqueous Uranyl Nitrate Solutions, pH 3 and Total Uranyl Concentration $c_0 = 0.05\ M$, Illustrating Independence of Anionic Ligand Concentration

$[NO_3^-]$, M	τ, msec.
0.1	1.18
0.2	1.07
0.3	1.12
0.4	1.15

Table II: Temperature Jump Relaxation Data on Aqueous Uranyl Solutions, pH 3.0 and Ionic Strength $\mu = 0.5\ M$, Yielding the Dimerization Specific Rate

c_0[a], M	τ[b], msec.	k_2,[c] M^{-1} sec.$^{-1}$	τ,[d] msec.	k_2,[c] M^{-1} sec.$^{-1}$	τ,[e] sec.	k_2,[c] M^{-1} sec.$^{-1}$
0.07	0.70	91			0.62	112
0.05	1.09	101			1.00	118
0.03	2.26	108	2.24	108	2.25	114
0.02	3.36	117	3.41	115	3.40	128
0.01	6.91	110	6.10	125	7.40	107
Mean k_2		105 ± 8		116 ± 6		116 ± 6

[a] Total concentration of uranyl in ion moles per liter; where methyl orange was used, its total concentration was $3 \times 10^{-5}\ M$. [b] Experimental relaxation time determined for uranyl perchlorate solutions containing indicator. [c] Rate constant calculated from experimental τ and eq. 18. [d] Experimental relaxation time for uranyl perchlorate solutions without indicator. [e] Experimental relaxation time for uranyl nitrate solutions with indicator.

There is a large accumulation of data on relaxation times and rate constants of protolytic reactions in aqueous media[10] that suggests that k_{-1} of eq. 1 should be over $10^{10}\ M^{-1}$ sec.$^{-1}$ as estimated from Debye's equation.[11] From eq. 15 and this estimated value of k_{-1} it follows at once that at pH 3.0 and a uranyl nitrate concentration of .07 M the relaxation time of equilibrium 1 would be about 10 nanosec., which is far too short for measurement with our temperature jump apparatus. The possibility of equilibrium 3 contributing to the observed relaxation time can be eliminated since the experimental data were obtained at a pH where there is essentially no formation of the trimer. The only reaction that could possibly give the experimental relaxation times observed is then equilibrium 2, the formation of the dimer. The values for the specific rate k_2 are given in Table II. The mean value is $k_2 = 116 \pm 6\ M^{-1}$ sec.$^{-1}$. Since the equilibrium, $(UO_2)_2(OH)_2^{2+} \rightleftharpoons (UO_2)_2(OH)^{3+} + OH^-$, between the dimeric species postulated by different authors[4-6] would be attained far too rapidly for direct observation by the temperature jump method, an unequivocal choice between these two dimeric structures on the basis of our kinetic data is not possible. We have used the equilibrium constants of Baes and Meyer[4] and Rush and Johnson[6] in the above kinetic calculations, and, since these authors do not postulate significant equilibrium concentrations of $(UO_2)_2(OH)^{3+}$, we have not included this species in eq. 2. We have repeated the kinetic calculations using the equilibrium constants of Dunsmore, *et al.*,[5] and replacing eq. 2 by $2UO_2^{2+} + H_2O \rightleftharpoons (UO_2)_2(OH)^{3+} + H^+$ and have obtained an average specific rate $k_2 = 142\ M^{-1}$ sec.$^{-1}$ at pH 3.0 that is somewhat less precise for our range of uranyl concentrations but is clearly in good agreement with the results of Table II. When the pH was raised to 3.5 and 4.0, a second relaxation time was not resolvable so that a determination of k_3 was not effected.

It has been proposed[12] that the formation of the dimeric species is accomplished by the bridging of OH^- groups between two plane-square or plane-pentagon coordinated uranyl groups with H_2O supplying the additional coordinating ligands. If the anions present are involved in the formation of the dimeric species, our data indicate that they replace solvating water

(10) M. Eigen and L. DeMaeyer, "Technique of Organic Chemistry," Vol. VIII, Part II, S. L. Friess, E. S. Lewis, and A. Weissberger, Ed., Interscience Publishers, Inc., New York, N. Y., 1963, Chapter 18.

(11) P. Debye, *Trans. Electrochem. Soc.*, **82**, 265 (1942).

(12) H. T. Evans, Jr., *Science*, **141**, 154 (1963).

molecules without affecting the over-all rate of the dimerization.

It is also interesting to compare k_2 for the dimerization of uranyl ion with similar results for dimerization of chromate and vanadate ions in aqueous solution. Swinehart and Castellan[13] found a specific rate $k_{23} = 1.8 \pm 0.3\ M^{-1}$ sec.$^{-1}$ for the dimerization

$$2HCrO_4^- \underset{}{\overset{k_{23}}{\rightleftharpoons}} Cr_2O_7^{2-} + H_2O \qquad (24)$$

in good agreement with an earlier estimate.[14] In the case of the dimerization of vanadate ion in dilute aqueous solution at pH 10

$$2VO_2(OH)_3^{2-} + H_2O \overset{k_{12}}{\rightleftharpoons} (VO_2)_2(OH)_5^{3-} + OH^- \qquad (25)$$

a specific rate $k_{12} = 2.5 \times 10^2\ M^{-1}$ sec.$^{-1}$ has been determined by the temperature jump method.[15] While there are undoubtedly marked differences in the structures of the three different dimers, it is interesting that the dimerization specific rates in the three cases of uranyl, chromate, and vanadate ions are of roughly the same magnitude in much the same way that specific rates of proton abstraction from an organic acid[16]

$$HA - OH^- \overset{k_2}{\rightleftharpoons} A^- + H_2O \qquad (26)$$

have values k_2 in the rather restricted range 10^7 to $10^{10}\ M^{-1}$ sec.$^{-1}$ even when quite strong intramolecular hydrogen bonding is present in the acid HA.

(13) J. H. Swinehart and G. W. Castellan, *Inorg. Chem.*, **3**, 278 (1964).

(14) G. Schwarzenbach and J. Meier, *J. Inorg. Nucl. Chem.*, **8**, 302 (1958).

(15) J. Asay and E. M. Eyring, in preparation.

(16) J. L. Haslam, E. M. Eyring, W. W. Epstein, G. A. Christiansen, and M. H. Miles, *J. Am. Chem. Soc.*, **87**, 1 (1965).

The Photolysis of Mercury Divinyl

by A. G. Sherwood and H. E. Gunning

Department of Chemistry, University of Alberta, Edmonton, Alberta, Canada *(Received January 21, 1965)*

Mercury divinyl was photolyzed in the gas phase at 50.00° in a static system. The reaction products were 1,3-butadiene, ethylene, and acetylene, as well as traces of C_6 compounds. Runs were done with various additives (CO_2, N_2, hydrocarbons) as well as at various light intensities. A mechanism is proposed which involves, as the primary reaction, the decomposition of the substrate molecule into two vinyl radicals and a mercury atom. The main reaction consuming substrate is $C_2H_3\cdot + Hg(C_2H_3)_2 \rightarrow C_4H_6 + C_2H_3\cdot + Hg$. The chain-ending reactions are the disproportionation and combination of vinyl radicals.

Introduction

This study was undertaken as part of an investigation of the reactions of unsaturated free radicals. Vinyl radicals are of special interest because of their role in the polymerization of acetylene and vinyl monomers. LeRoy and Steacie[1] suggested that the mercury-photosensitized polymerization of acetylene was a free-radical reaction in which vinyl radicals and substituted vinyl radicals played an important part.

Tickner and LeRoy[2] produced vinyl radicals by the sodium flame reaction with vinyl iodide and observed products attributable to disproportionation and combination reactions. Their interpretation of the results was hampered, however, by a lack of knowledge of the

(1) D. J. LeRoy and E. W. R. Steacie, *J. Chem. Phys.*, **12**, 117 (1944).

(2) A. W. Tickner and D. J. LeRoy, *ibid.*, **19**, 1247 (1951).

nature of the reaction of vinyl radicals with the substrate and by the formation of nonvolatile products.

Trotman-Dickenson and Verbeke[3] studied the pyrolysis of mercury divinyl (MDV) in a toluene carrier flow system at temperatures between 502 and 642°. Their observations were interpreted in terms of the formation, in the primary reaction, of vinyl radicals which abstract hydrogen from the toluene to give ethylene. Acetylene and 1,3-butadiene were also found, which indicated that disproportionation and combination reactions were also occurring. A value of 48.3 kcal./mole was determined for the dissociation energy of the first vinyl–mercury bond.

This paper presents the results of an investigation of the photolysis of MDV as a possible source of vinyl radicals.

Experimental

Since the substrate has a vapor pressure of less than 2 torr at room temperature, the photolyses were carried out with the reaction cell immersed in a 50° water bath. No decomposition was observed when blank runs were carried out under these conditions. The quartz reaction cell was 10 cm. long and 5 cm. in diameter and was connected by a graded seal to a mercury cutoff which served both as a manometer and as a valve. Distilled water was circulated through the bath at 50.00 ± 0.05°.

The light source was a Hanovia Type SH medium-pressure mercury arc. The light was roughly collimated and passed through a 2-mm. Vycor 7910 filter and into the cell through quartz windows in the sides of the bath. MDV absorbs at wave lengths shorter than about 2600 Å. and has an absorption maximum at about 2300 Å. The absorbed light thus lies between 2200 Å. (the lower transmission limit of the filter) and 2600 Å.

The runs were carried out as follows. A sample of MDV was removed from the storage bulb, distilled through a trap at −45°, and collected at −78°. This procedure removed any less volatile material and any ethylene, acetylene, or butadiene which may have been present. Sufficient freshly distilled MDV was then condensed into the cell to give a pressure of 3.60 torr at 50°. The cell was allowed to equilibrate for 1 hr., and the lamp for 0.5 hr. before each run.

After the run, the contents of the cell were separated into fractions by distillation and analyzed by g.c. The C_2 and C_4 fractions were analyzed on an alumina column, modified with 2.5% silicone rubber. Some runs were done with added CO_2, in which case the added gas was removed by reaction with solid NaOH before g.c. analysis of the fraction.

The intensity of the absorbed radiation was varied by inserting, between the lamp and the cell, aluminum screens calibrated with a Cary Model 14 spectrophotometer.

After each run, the cell was cut from the system, washed in hot nitric–sulfuric acid mixture, rinsed with distilled water, dried, and resealed to the system. The position of the cell was made reproducible by means of a jig.

The MDV was prepared from vinylmagnesium chloride, obtained in tetrahydrofuran solution from Peninsular Inc. The procedure was that of Reynolds, *et al.*[4] Phillips research grade isobutane, nominally 99.97% pure, was degassed and used without further purification. Matheson Bone Dry grade CO_2 was distilled through a trap at −130° before use. The acetylene was also obtained from Matheson. It contained acetone which was removed by distillation through a −130° trap. The only remaining impurity was 0.01% ethylene which was considered negligible.

Results

The main products of the reaction were 1,3-butadiene, ethylene, and acetylene. Traces of propane and propylene were also found, as well as C_6 and C_8 compounds in amounts too small for more precise identification.

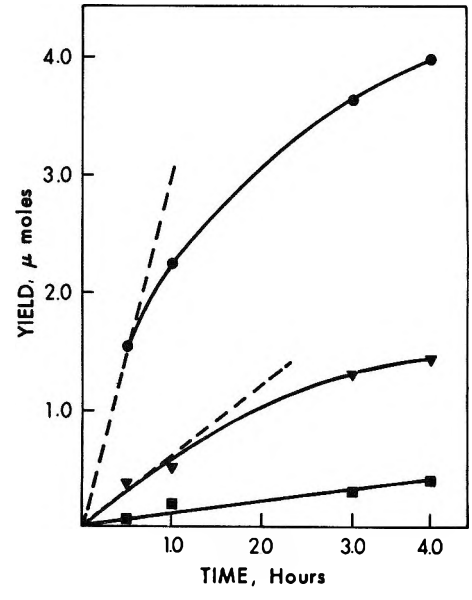

Figure 1. Yield of products *vs.* time. MDV pressure 3.52 ± 0.03 torr; temperature 50.00°; ●, C_4H_6; ▼, C_2H_4 (×10); ■, C_2H_2 (×10).

(3) A. F. Trotman-Dickenson and G. J. O. Verbeke, *J. Chem. Soc.*, 2580 (1961).

(4) G. F. Reynolds, R. E. Dessey, and H. H. Jaffe, *J. Org. Chem.*, **23**, 1217 (1958).

The yields of the main products at different exposure times are shown in Figure 1, which clearly indicates the leveling off of yields for longer runs.

The effect on product yields of added CO_2 is seen in Figure 2. These results are for 2-hr. runs.

Figure 3 shows the effect on the product yields of added 2,3-dimethylbutane (DMB) and of isobutane. With both addends, acetylene and butadiene are suppressed while the yield of ethylene is increased to approximately 1 μmole. Runs were done with added cyclopentane which had qualitatively the same effect.

Product yields were determined as a function of exposure time at three lower light intensities. The results are shown in Table I. These data were plotted and estimates made of the initial rates of formation of C_2H_4 and C_4H_6. The values are given in Table II. Z is the factor by which the light intensity is attenuated by the insertion of the wire screen.

Table I: Yield of Products as a Function of Time for Various Values of Z[a]

Z	Exposure, hr.	Yield (μmoles) C_2H_2	C_2H_4	C_4H_6
0.324	1.13	0.009	0.032	1.33
0.324	2.09	0.012	0.052	1.99
0.324	3.53	0.018	0.075	2.56
0.324	6.00	0.023	0.110	3.07
0.119	1.00	Trace	Trace	0.69
0.119	2.00	0.008	0.030	1.17
0.119	4.00	0.014	0.048	1.63
0.119	8.00	0.016	0.063	2.21
0.0385	3.00	0.006	0.025	0.97
0.0385	5.00	0.010	0.031	1.24
0.0385	8.00	0.008	0.040	1.66
0.0385	12.00	0.012	0.066	1.98

[a] Substrate pressure 3.55 torr; temperature 50°.

Table II: Rate of Formation of Products as a Function of Light Intensity[a]

Z	C_4H_6 Rate, μmoles/hr.	C_4H_6 R/Z	C_2H_4 Rate, μmoles/hr.	C_2H_4 R/Z	$R_{C_4H_6}/R_{C_2H_4}$
1.000	3.0	3.0	0.060	0.06	50
0.324	1.2	3.7	0.030	0.09	40
0.118	0.67	5.7	0.015	0.13	45
0.034	0.32	8.4	0.0075	0.20	43

[a] MDV pressure 3.55 torr; temperature 50°.

The results of 2-hr. runs done with added acetylene are given in Table III. No benzene could be detected in runs with less than 8.2 torr of added acetylene.

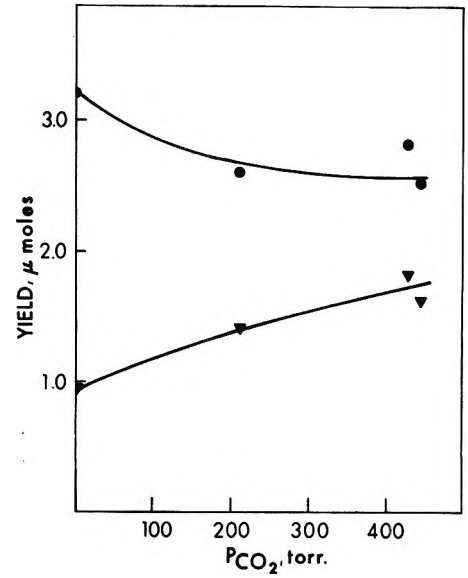

Figure 2. Yields of products *vs.* CO_2 pressure; MDV pressure 3.52 ± 0.03 torr; temperature 50.00°; ●, C_4H_6; ▼, C_2H_4 (×10).

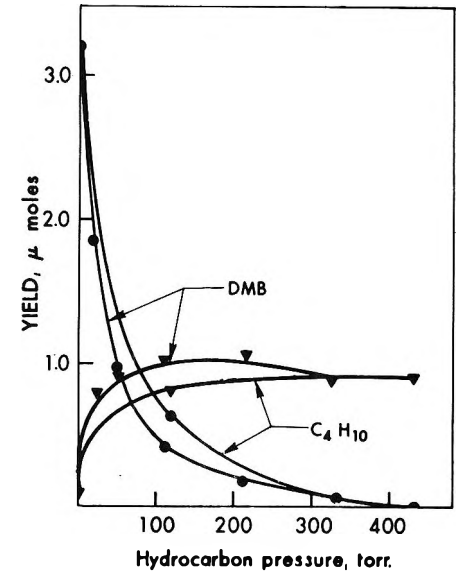

Figure 3. Yield of products *vs.* pressure of added hydrocarbon; MDV pressure 3.52 ± 0.03 torr; temperature 50.00°; ●, C_4H_6; ▼, C_2H_4.

Some runs were done at lower substrate pressures at room temperature with a higher lamp intensity. The results are shown in Figure 4. At long exposure times the yields of ethylene and of acetylene are seen to level off as before, while the yield of butadiene attains a maximum and then declines.

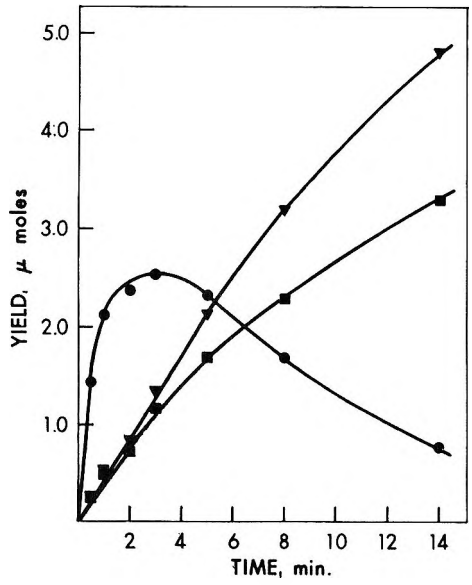

Figure 4. Yield of products *vs.* time. MDV pressure 1.62 torr; temperature 22 ± 1°; ●, C_4H_6; ▼, C_2H_4 (×10); ■, C_2H_2 (×10).

Table III: Yield of Products as a Function of Pressure of Added Acetylene[a]

C_2H_2 added, μmoles	C_2H_2 added, torr	C_2H_2 recovered, μmoles	C_2H_4, μmoles	C_4H_6, μmoles	C_6H_6, μmoles
0	0	0.020	0.095	3.2	0
0.98	0.10	0.88	0.096	3.1	0
10.6	1.14	10.5	0.089	3.0	0
76.5	8.2	75.8	0.134	2.8	n.d.[b]
1200	112	n.d.[b]	0.27	n.d.[b]	0.4

[a] Runs (2-hr.) at 50°; MDV pressure 3.55 torr. [b] n.d. = not determined.

Discussion

With absorption at λ = 2200–2600 Å. sufficient energy is available[3] for the dissociation of MDV into two vinyl radicals

$$Hg(C_2H_3)_2 + h\nu \longrightarrow Hg + 2C_2H_3\cdot \qquad (1)$$

The absence of any significant depressing effect on the rate by addition of large pressures of CO_2 (Figure 2) suggests that excited molecules do not play an important role in the reaction.

The main products of the reaction suggest combination and disproportionation reactions of vinyl radicals.

$$2C_2H_3\cdot \longrightarrow C_4H_6 \qquad (2)$$

$$\longrightarrow C_2H_2 + C_2H_4 \qquad (3)$$

The decrease in the product rates with reaction time (Figures 1, 4) indicates consumption of products in secondary reactions. Even in the shortest runs, however, the yield of acetylene was less than that of ethylene. Thus, ethylene is probably formed by an additional reaction to (3).

The runs with added DMB and *i*-C_4H_{10} (Figure 3) were done to determine the primary rate of formation of vinyl radicals. With sufficient added RH all vinyl radicals should be scavenged as C_2H_4

$$C_2H_3\cdot + RH \longrightarrow C_2H_4 + R\cdot \qquad (4)$$

If (1)–(3) constitute the total sequence for the photolysis of pure MDV, added RH should depress the rates for acetylene and butadiene and increase the ethylene rate. With all vinyl radicals disappearing *via* (4), the rates should obey the relation

$$R_{C_2H_4} = 2R^0_{C_2H_4} + 2R^0_{C_4H_6} \qquad (a)$$

where $R_{C_2H_4}$ is the limiting rate for ethylene at high RH pressures, and the R^0 terms refer to the rates of formation of the products in the absence of RH. This relation takes into account the consumption of two vinyl radicals in the formation of each molecule of ethylene and each molecule of butadiene. It ignores the acetylene discrepancy.

From Figure 3 it can be seen that the formation of butadiene is completely suppressed at high RH pressures, while $R_{C_2H_4}$ is only about one-sixth of the value predicted by eq. a. This indicates that the number of vinyl radicals consumed in the formation of products is considerably greater than the number formed in the primary process. A chain reaction such as (5) would be consistent with this observation

$$C_2H_3\cdot + Hg(C_2H_3)_2 \longrightarrow C_4H_6 + Hg + C_2H_3\cdot \qquad (5)$$

This reaction may occur in two steps—the addition of the vinyl radical to the substrate to give an excited radical, which decomposes into butadiene, a mercury atom, and a vinyl radical

$$CH_2{=}CH\cdot + CH_2{=}CH{-}Hg{-}CH{=}CH_2 \longrightarrow \left[CH_2{=}CH{-}\underset{\displaystyle CH_2\cdot}{CH}{-}Hg{-}CH{=}CH_2\right]^* \qquad (5a)$$

$$\downarrow$$

$$CH_2{=}CH{-}CH{=}CH_2 + Hg + C_2H_3\cdot$$

The decomposition of the intermediate radical is facilitated by the high heat of formation of butadiene and by the weakness of the Hg–C bond.

A similar displacement reaction has been found to occur in the mercury-photosensitized decomposition of

vinyl chloride. Gunning and co-workers[5] found that vinyl radicals react with vinyl chloride to give an intermediate radical which decomposes to yield butadiene.

$$C_2H_3\cdot + C_2H_3Cl \longrightarrow [C_4H_6Cl]^* \longrightarrow C_4H_6 + Cl\cdot \quad (5b)$$

The runs at reduced light intensity (Table I) were done to test for reaction 5. Since, according to the mechanism, the butadiene is formed largely by a reaction unimolecular in vinyl radicals, while the ethylene is formed by a bimolecular reaction of vinyl radicals, the ratio of the rates of formation of the two compounds should depend upon the light intensity. As can be seen from the sixth column of Table II, this ratio is, within experimental error, constant. This would suggest that the ethylene, as well as the butadiene, is formed largely by reactions unimolecular in vinyl radicals. Such a reaction is suggested even more clearly by the data for ethylene alone. If ethylene were formed only by (3), a steady-state treatment of the mechanism would lead to the expression

$$(C_2H_3\cdot)^2 = \frac{2I_a}{k_2 + k_3} \quad (b)$$

where I_a is the intensity of the absorbed light. The rate of formation of ethylene would be given by the expression

$$R_{C_2H_4} = k_3(C_2H_3\cdot)^2 = \frac{2k_3I_a}{k_2 + k_3} \quad (c)$$

Thus, if reaction 3 were the only mode of formation of ethylene, the ratio $R_{C_2H_4}/Z$ would be independent of the light intensity. As can be seen from Table II, this ratio increases with decreasing light intensity.

The same type of argument may be used to show that reaction 2 is not the sole mode of formation of butadiene. This is indicated by the dependence on the light intensity of the ratio $R_{C_4H_6}/Z$ (Table II). The reaction forming the additional ethylene may be hydrogen abstraction by vinyl radicals from the substrate

$$C_2H_3\cdot + MDV \longrightarrow C_2H_4 + \cdot CH{=}CH{-}Hg{-}CH{=}CH_2 \quad (6)$$

With this reaction included in the mechanism, the expression for the steady state in vinyl radicals becomes

$$2I_a = (k_2 + k_3)(C_2H_3\cdot) + k_6(C_2H_3\cdot)(MDV) \quad (d)$$

This expression is equivalent to expression a if we assume that the second term is negligible, *i.e.*, that the consumption of vinyl radicals by the disproportionation and combination reactions is greater than their consumption by reaction 6 at this intensity. We may then write an expression for the rate of formation of butadiene

$$R_{C_4H_6} = \frac{2k_2}{k_2 + k_3}I_a + k_5(MDV)\left(\frac{2}{k_2 + k_3}\right)^{1/2} I_a^{1/2} \quad (e)$$

where I_a is the intensity of absorbed light. The attenuation factor of the screen, Z, is equal to I_a/I_a^0, where I_a^0 is the intensity of absorbed light in the absence of a screen. Substituting ZI_a^0 for I_a in eq. e and rearranging gives

$$\frac{R_{C_4H_6}}{Z} = \frac{2k_2I_a^0}{k_2 + k_3} + k_5(MDV)\left(\frac{2I_a^0}{k_2 + k_3}\right)^{1/2} Z^{-1/2} \quad (f)$$

This equation predicts that the ratio $R_{C_4H_6}/Z$ will be a linear function of $Z^{-1/2}$. A graph of this expression is shown in Figure 5. It is, within experimental error, linear.

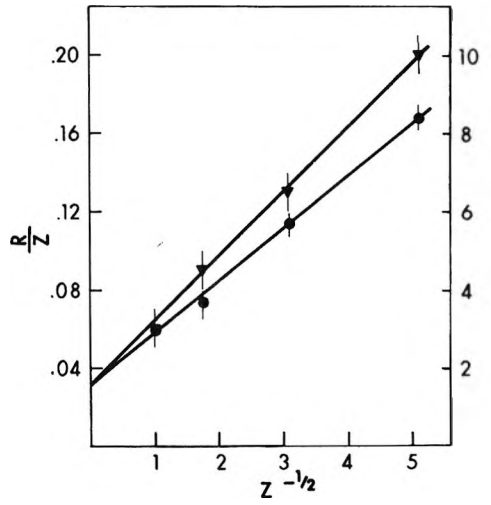

Figure 5. Photolyses of mercury divinyl: $R_{C_4H_6}/Z$ *vs.* $Z^{-1/2}$ (●) and $R_{C_2H_4}/Z$ *vs.* $Z^{-1/2}$ (▼).

The following similar expression involving the rate of formation of ethylene may also be derived

$$\frac{R_{C_2H_4}}{Z} = \frac{2k_3I_a^0}{k_2 + k_3} + k_6(MDV)\left(\frac{2I_a^0}{k_2 + k_3}\right)^{1/2} Z^{-1/2} \quad (g)$$

In Figure 5 it can be seen that a linear relation again obtains.

The ratio of intercepts for eq. e and f yields the ratio, k_2/k_3 which, from Figure 5, is 50 ± 30. Similarly, the ratio of slopes gives $k_5/k_6 = 50 \pm 20$.

(5) M. G. Bellas, J. K. S. Wan, W. F. Allen, O. P. Strausz, and H. E. Gunning, *J. Phys. Chem.*, **68**, 2170 (1964).

Although the occurrence of reaction 6 is consistent with the formation of more ethylene than acetylene, some consideration must be given to the fate of the mercury-containing radical produced. The most probable reaction is disproportionation with vinyl radicals to give additional ethylene

$$C_2H_3\cdot + \cdot C_2H_2\text{–}Hg\text{–}C_2H_3 \longrightarrow C_2H_4 + C_2H\text{–}Hg\text{–}C_2H_3 \quad (7)$$

Introduction of this step into the kinetic scheme merely introduces a factor of 2 into the second term on the right-hand side of eq. g. This also increases the calculated value of k_5/k_6 by a factor of 2. Disproportionation with vinyl radicals would not account for the formation of more ethylene than acetylene while the combination reaction would not affect eq. g.

As an alternative to (6), the possibility must be considered that ethylene is formed by the reaction of vinyl radicals with the intermediate radical arising in reaction 5a, *i.e.*

$$C_2H_3\cdot + C_4H_6\text{–}Hg\text{–}C_2H_3 \longrightarrow C_2H_4 + C_4H_5\text{–}Hg\text{–}C_2H_3 \quad (8)$$

Substitution of (8) for (6) in the mechanism and application of the steady-state treatment indicates that the ratio $R_{C_2H_4}/Z$ should be independent of light intensity. The observed dependence of the ratio on light intensity shows that, although (8) may occur, it is not an important source of ethylene in this system.

The acetylene discrepancy cannot be explained by the reaction of vinyl radicals with acetylene. The results shown in Table III indicate that this reaction is slow compared with the reaction of vinyl radicals with the substrate. When sufficient pressures of acetylene are added to the reaction system, some benzene is formed. This observation supports the suggestion[6] that vinyl radicals are the precursors of the benzene formed in the mercury-photosensitized polymerization of acetylene.

The data of Table III and Figure 4 show that, under conditions of high light intensity and low substrate pressure, when the consumption of MDV becomes significant, the butadiene yield actually reaches a maximum as the reaction proceeds and then falls steadily. The decline in the rates of formation of acetylene and ethylene is much less. Part of the decrease in the butadiene rate must be ascribed to reduced light absorption with the consumption of the substrate. Secondary reactions of vinyl radicals with butadiene would also be important. These results indicate, however, that a significant amount of the butadiene is consumed by direct photolysis. Thus, Srinivasan[7] and Haller and Srinivasan[8] studied the photolysis of butadiene at these wave lengths and found among the products 1,2-butadiene, ethylene, acetylene, vinylacetylene, and hydrogen, as well as polymer. Photolysis of butadiene in the MDV system is therefore a plausible reason why ethylene and acetylene continue to form even after the yield of butadiene has started to decrease (Figure 4).

It should also be noticed from Figure 4 that under conditions of high light intensity and low substrate pressure, *i.e.*, under conditions favoring radical–radical reactions, the difference between the yields of ethylene and acetylene is less than at lower light intensity and higher substrate pressure (Figure 1). This observation is also consistent with the mechanism.

The present study provides evidence that the photolysis of MDV is in fact a chain decomposition of the substrate. Free vinyl radicals are the chain carriers while the chain-terminating steps are the disproportionation and combination reactions of vinyl radicals.

Acknowledgments. The authors wish to express their appreciation to Dr. W. F. Allen for helpful discussions. The financial support of the National Research Council of Canada under Grant No. T-162 is gratefully acknowledged.

(6) J. K. Cashion and D. J. LeRoy, *Can. J. Chem.*, **32**, 906 (1954).
(7) R. Srinivasan, *J. Am. Chem. Soc.*, **82**, 5063 (1960).
(8) R. Haller and R. Srinivasan, *J. Chem. Phys.*, **40**, 1992 (1964).

Critical Opalescence of Binary Liquid Mixtures. The Debye Molecular Interaction Range

by B. Chu

Chemistry Department, The University of Kansas, Lawrence, Kansas *(Received January 22, 1965)*

Critical opalescence of two binary liquid mixtures, *n*-heptane–perfluorocyclic oxide and carbon tetrachloride–perfluorocyclic oxide, is investigated. The results indicate that the molecular interaction range of Debye, discussed in terms of the solubility parameter theory of Hildebrand and Scatchard, is an appropriate parameter for the averaged intermolecular pair potential.

It has been shown that the angular dissymmetry of critical opalescence in one- and two-component systems provides a measure of molecular interactions between the molecules. In particular, according to the Debye theory of critical opalescence,[1-3] the temperature dependence of the persistence length of fluctuations near the critical point is related to the second moment of the intermolecular pair potential called the "range of molecular forces" (or sometimes referred to as the Debye *l*-parameter[4]). A number of experimental light- and X-ray-scattering studies of critical opalescence have furnished values for the range of molecular forces which are consistent with the theory.[4-13] Debye has also shown that, for one-component systems, an extension of the range of investigation to large values of s/λ [$s = 2 \sin(\theta/2)$, λ = wave length] by means of X-rays may provide additional information concerning the intermolecular pair potential.[3] Deviations from the straight-line behavior in plots of reciprocal scattered intensity *vs.* $(s/\lambda)^2$ for two-component systems were indeed observed.[14-16] Unfortunately, the interpretation of deviations for two-component systems is not exactly known.[17] Furthermore, the scattering behavior at small values of s/λ remains an open question since the correlation function of Ornstein and Zernike[18] does not agree with scattering experiments of critical binary liquid mixtures very near the critical point. Reviews have been presented elsewhere.[19-21]

The purpose of this article is to show that the molecular interaction range of Debye, discussed in terms of the solubility parameter theory of Hildebrand[22] and Scatchard,[23] is an appropriate parameter for the averaged intermolecular pair potential even though the tem-

(1) P. Debye in "Non-Crystalline Solids," V. D. Frechette, Ed., John Wiley and Sons, Inc., New York, N. Y., 1960, p. 1.

(2) P. Debye, *J. Chem. Phys.*, **31**, 680 (1959).

(3) P. Debye in "Electromagnetic Scattering," M. Kerker, Ed., The Macmillan Co., New York, N. Y., 1963, p. 393.

(4) R. Pancirov and H. Brumberger, *J. Am. Chem. Soc.*, **86**, 3562 (1964).

(5) B. Zimm, *J. Phys. Colloid Chem.*, **54**, 1306 (1950).

(6) P. Debye, H. Coll, and D. Woermann, *J. Chem. Phys.*, **32**, 939, 1746 (1960).

(7) P. Debye, B. Chu, and D. Woermann, *ibid.*, **36**, 851 (1962).

(8) P. Debye, B. Chu, and H. Kaufmann, *ibid.*, **36**, 3378 (1962).

(9) P. Debye, D. Woermann, and B. Chu, *J. Polymer Sci.*, **A1**, 255 (1963).

(10) B. Chu, *J. Phys. Chem.*, **67**, 1969 (1963).

(11) B. Chu, *J. Chem. Phys.*, **41**, 226 (1964).

(12) J. E. Thomas and P. W. Schmidt, *ibid.*, **39**, 2506 (1963).

(13) J. E. Thomas and P. W. Schmidt, *J. Am. Chem. Soc.*, **86**, 3554 (1964).

(14) B. Chu, *J. Chem. Phys.*, **42**, 426 (1965).

(15) P. Debye, D. Caulfield, and J. Bashaw, *ibid.*, **41**, 3051 (1964).

(16) B. Chu, *ibid.*, **42**, 2293 (1965).

(17) Measurements on one-component systems over large ranges of s/λ are in progress.

(18) F. Zernike, *Koninkl. Ned. Akad. Wetenschap., Proc.*, **17**, 793 (1916); *Arch. néerl. sci.*, [III] **A4**, 74 (1917); L. S. Ornstein and F. Zernike, *Physik. Z.*, **19**, 134 (1918); **27**, 761 (1926).

(19) M. Fixman, *Advan. Chem. Phys.*, **6**, 175 (1964).

(20) M. E. Fisher, *J. Math. Phys.*, **5**, 944 (1964).

(21) B. Chu, *J. Am. Chem. Soc.*, **86**, 3557 (1964).

(22) J. H. Hildebrand and R. L. Scott: (a) "The Solubility of Nonelectrolytes," 3rd Ed., Reinhold Publishing Corp., New York, N. Y., 1950; (b) "Regular Solutions," Prentice-Hall, Inc., Englewood Cliffs, N. J., 1962.

(23) J. Scatchard, *Chem. Rev.*, **8**, 321 (1931).

perature dependence of the persistence length of fluctuations near the critical point may be interpreted in a different quantitative form at very small temperature distances from the critical solution temperature.

The systems perfluorocyclic oxide ($C_8F_{16}O$)–*n*-heptane (*n*-C_7H_{16}) and perfluorocyclic oxide ($C_8F_{16}O$)–carbon tetrachloride (CCl_4) are investigated because of their strong deviation in the calculated solubility parameter differences, $\delta_2 - \delta_1$, when compared with the corresponding observed values.

Experimental

Materials. The materials used were purified by preparative gas chromatography on an Aerograph Model A-700 Autoprep vapor fractometer.

n-Heptane (n-C_7H_{16}). An SE-30 column was used. The details have been described elsewhere.[21]

Perfluorocyclic Oxide ($C_8F_{16}O$). This material was the major constituent in "Fluorochemical FC-75" manufactured by the Minnesota Mining and Manufacturing Co. A 6.1-m. long × 0.95-cm. o.d. column packed with 20% tricresyl phosphate on 60/80 Chromosorb W, operated at 100° and 40 p.s.i.g., was used. Flow rates of helium carrier gas were around 200 cc./min. The injection volume was limited to 0.1 cc. each time, and a short cut in the main peak was collected under helium.

The purified perfluorocyclic oxide was then analyzed with a 6.1-m. long × 0.95-cm. o.d. column packed with 20% QF-1 on 45/60 Chromosorb W. Two overlapping main peaks were resolved on an injection volume of 5 μl. Therefore, the perfluorocyclic oxide which we have purified could be a mixture of two extremely close-boiling liquids, possibly in the form of isomers.

Carbon Tetrachloride (CCl_4). Fisher Certified Reagent grade CCl_4 exhibited only one peak when subjected to chromatographic analysis using either an SE-30 column or a QF-1 column, so this liquid was not further purified.

Procedure. Detailed descriptions of the light-scattering photometer,[11,24] preparation of solutions, phase separation temperature determinations, and attenuation corrections due to critical opalescence are discussed elsewhere.[11,21]

The critical solution concentrations (ϕ_{2c}) were taken from the literature. In our case, we have arbitrarily taken perfluorocyclic oxide as the second component. ϕ_{2c} (*n*-C_7H_{16}–$C_8F_{16}O$) = 40.7 vol. % $C_8F_{16}O$.[25] ϕ_{2c} (CCl_4–$C_8F_{16}O$) = 37.8 vol. % $C_8F_{16}O$.[25] The phase separation temperature, T_p, for the system *n*-C_7H_{16}–$C_8F_{16}O$ is 322.4°K., and T_p(CCl_4–$C_8F_{16}O$) = 326°K., while T_p(*n*-C_7H_{16}–$C_8F_{16}O$) = 320°K. and T_p(CCl_4–$C_8F_{16}O$) = 321°K. from the literature.[25] Our observed phase separation temperature for the system *n*-C_7H_{16}–$C_8F_{16}O$ agrees to within 0.03° even after the liquids have been dried in aluminum oxide. Thus, it is conjectured that the disagreement of our phase separation temperatures with the literature may arise from the difference in the isomeric compositions of perfluorocyclic oxide. The presence of isomers could effect both T_p and ϕ_{2c}. In addition, the Debye theory is no longer as rigorous because the mixture contains more than two components. However, this discrepancy becomes less important when we discuss the Debye *l*-parameter in a qualitative way.

Refractive indices of the two critical liquid mixtures at different wave lengths (λ_0 364, 436, and 575 mμ) were calculated from an empirical mixture rule[10] with the aid of known dispersion curves and densities.[25,26] The calculated corresponding wave lengths in the medium are λ 271, 325, and 428 mμ for *n*-C_7H_{16}–$C_8F_{16}O$ and λ —, 313, and 413 mμ for CCl_4–$C_8F_{16}O$, respectively.

Results and Discussion

The treatment of data according to the Debye theory is described elsewhere.[8,11,21]

At small temperature distances above the critical solution temperature, T_c, only attenuation corrections are important. If we neglect the density-scattering term, we than have the following equation for the relative scattered intensity I^*[8,11]

$$\frac{1}{I^*} = F(T)\left(\frac{T_c}{T}\right)\left[\frac{\Delta T}{T_c} + \frac{8\pi^2}{3} l^2 \frac{\sin^2\frac{\theta}{2}}{\lambda^2}\right] = A + B\sin^2\left(\frac{\theta}{2}\right)$$

where T is the temperature in °K., $\Delta T = T - T_c$, λ is the wave length of light in the medium, and l is the molecular interaction range. $F(T)$ may be an exponential correction factor, the form of which is unimportant so long as it is not dependent on scattering angles. Figure 1 shows a typical set of intensity curves in a plot of $1/I^*$ *vs.* $\sin^2(\theta/2)$ at fixed temperature distances above T_c. Such a plot is sometimes referred to as an OZD plot. The periodic character in the low relative intensity lines, where the temperature distances are large, comes from limits of error of the photometer and is an experimental effect. Figure 2 shows a plot of A/B *vs.* T, where $A/B = (3\lambda^2/8\pi^2 l^2 T_c)(T - T_c)$ with T_c =

(24) B. Chu, *Rev. Sci. Instr.*, **35**, 1201 (1964).

(25) B. G. Kyle and T. M. Reed, III, *J. Am. Chem. Soc.*, **80**, 6170 (1958).

(26) G. D. Oliver, S. Blumkin, and C. W. Cunningham, *ibid.*, **73**, 5722 (1951) ($C_8F_{16}O$); J. Timmermans, "Physico-Chemical Constants of Pure Organic Compounds," Elsevier Publishing Co., New York, N. Y., 1959 (*n*-C_7H_{16}, CCl_4).

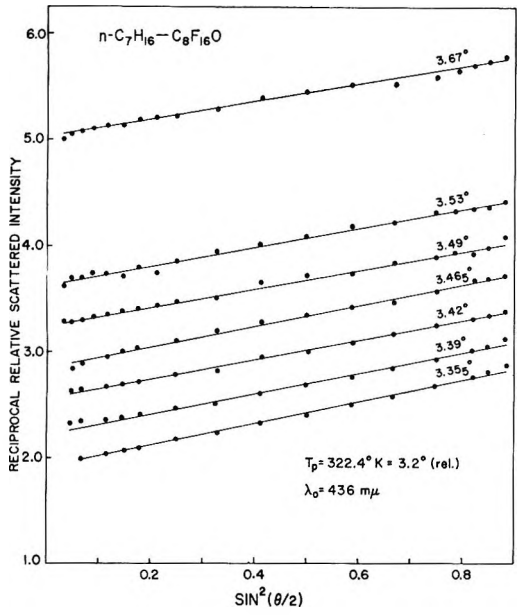

Figure 1. Plot of reciprocal relative scattered intensity *vs.* $\sin^2(\theta/2)$.

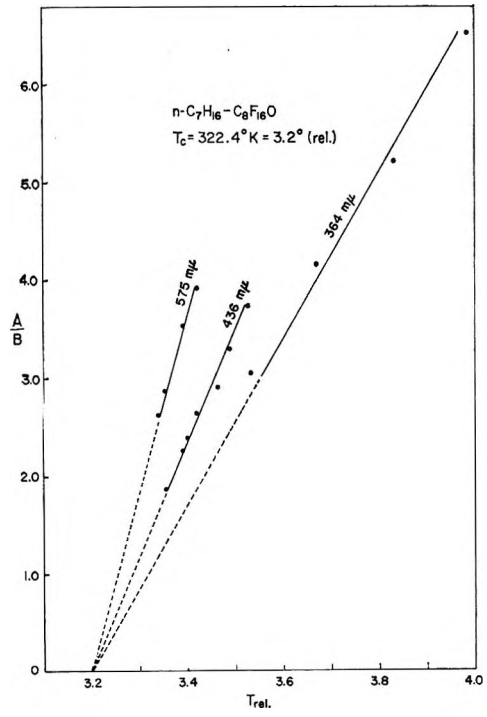

Figure 2. Plot of A/B *vs.* temperature. $A/B = (3\lambda^2/8\pi^2 l^2 T_c)(T - T_c)$ with T_c = −intercept/slope of the resulting straight line.

−intercept/slope of the resulting straight line. $l = 10.4 \pm 0.5$ Å. for the system n-C_7H_{16}–$C_8F_{16}O$ and $l = 12.0 \pm 0.5$ Å. for the system CCl_4–$C_8F_{16}O$. It should be noted that at intermediate temperature distances (say, $T - T_c$ ranging from 0.05 to 1°) and for systems which exhibit large differences in the index of refraction of the two components, the scattered intensity due to concentration fluctuations is the dominating term. In addition, we are not concerned with the scattering behavior at very small values of s/λ and at very small temperature distances (say $T - T_c < 0.01°$). However, since A/B *vs.* T extrapolates close to T_c, it implies that the extrapolation from straight lines in an OZD plot is justified at intermediate temperature distances. In other words, the "curvatures" at very small values of s/λ and at this intermediate temperature range in such an OZD plot have to be negligibly small.[27] The classical theory of Debye indeed provides an excellent representation of experimental facts in the intermediate temperature distances over large ranges of s/λ.

It is interesting to observe the similarities between the Debye l-parameter and the solubility parameter of Hildebrand and Scatchard. The details have been discussed elsewhere.[21] Tables I and II summarize the additional pertinent properties of liquids which we need for a comparison between the two parameters. We have freely estimated the δ-values of alcohols and oxides without justifying the questionable nature of their use. This is again permissible as long as we are concerned with only the qualitative aspects of the parameters. For the same reason, some of the δ-values are calculated at 25°, and their temperature dependence is ignored. We further assume that these values are appropriate for solutions. However, systems with water[4,28] or coiling molecules[7,29] as one of their two com-

Table I: Observed (or Estimated) Molal Volume and Solubility Parameter at 25°

Liquids	Formula	$\bar{V}_{298}$, cm.³	δ, cal.$^{1/2}$/cm.$^{3/2}$
Isooctane	C_8H_{18}	166	6.9[a]
Isopentane	C_5H_{12}	117	6.8[a]
Perfluorocyclic oxide	$C_8F_{16}O$	236	8.2[b]
Perfluorotributylamine	$(C_4H_9)_3N$	360	5.9[a]

[a] See ref. 22. [b] $\delta = [(\Delta H^v - RT)/V]^{1/2}$ from ref. 22. ΔH^v from J. W. Sargent and J. D. Lazerte, "Fluorocarbon Gases and Volatile Liquids—Properties and Applications," presented at the Symposium on Electrical Insulating Gases, Pittsburgh, Pa., 1962; care should be exercised on the general use of δ-values for polar substances.

(27) B. Chu and W. P. Kao, *J. Chem. Phys.*, **42**, 2608 (1965).
(28) B. Chu and W. P. Kao, *Can. J. Chem.*, in press.
(29) P. Debye, B. Chu, and D. Woermann, *J. Chem. Phys.*, **36**, 1803 (1962).

Table II: Observed and Calculated Molecular Interaction Range and Solubility Parameter

System	$\lvert\delta_2 - \delta_1\rvert_{obsd}$	$\lvert\delta_2 - \delta_1\rvert_{calcd}$[a]	l^2_{obsd}, Å.^{2}	l^2_{calcd},[b] Å.^{2}
i-C_5H_{12}–$(C_4F_9)_3N$	0.9	2.16	196[c]	1.78×10^3
i-C_8C_{16}–n-C_7F_{16}	1.01	2.48	159[d]	1.40×10^3
n-C_7H_{16}–$C_8F_{16}O$	0.8	2.58	108	4.04×10^3
CCl_4–$C_8F_{16}O$	0.4	2.74	144	1.46×10^4

[a] See ref. 22b, p. 143.

$$RT_c = \frac{2X_1X_2V_1^2V_2^2}{(X_1V_1 + X_2V_2)^4}(\delta_1 - \delta_2)^2$$

where T_c and X are critical solution temperature and mole fraction, V is the molal volume, and δ is the solubility parameter defined as $(\Delta E^v/V)^{1/2}$. [b] See ref. 21, p. 3561.

$$l^2_{calcd} = 3\frac{\delta_1^2\sigma_{11}^2 + \delta_2^2\sigma_{22}^2 - \delta_1\delta_2\dfrac{(\sigma_1 + \sigma_2)^2}{2.29}}{(\delta_1 - \delta_2)^2}$$

where σ_{ii} is a "collision" diameter between two i molecules and is taken to be the cube root of molar volume, δ is the solubility parameter, and $\sigma_{12} \cong [(\sigma_1 + \sigma_2)/2](1/1.07)$ (footnote 33, ref. 21). [c] See ref. 15. [d] B. Chu, unpublished results.

ponents have intentionally been omitted because of the crude hard-core attractive tail model. An almost linear proportionality exists between the ratios of observed and calculated values of the two parameters as was shown in a linear plot of $(\delta_2 - \delta_1)^2_{calcd}/(\delta_2 - \delta_1)^2_{obsd}$ *vs.* l^2_{calcd}/l^2_{obsd} over somewhat shorter ranges.[21] We have now demonstrated that this near linearity persists over large ranges. Figure 3 shows a log–log plot of $(\delta_2 - \delta_1)^2_{calcd}/(\delta_2 - \delta_1)^2_{obsd}$ *vs.* l^2_{calcd}/l^2_{obsd}. A log–log plot is used because of the large range of values of $(\delta_2 - \delta_1)^2_{calcd}/(\delta_2 - \delta_1)^2_{obsd}$ and l^2_{calcd}/l^2_{obsd}. It should be noted that the correlation does not occur between the solubility parameters and the Debye molecular interaction ranges, but between the ratios of experimental and calculated values of these parameters. The reason for this correlation could probably be attributed to the fact that both theories were based on essentially the same physical approximations,[30] and, therefore, deviations between theoretical and experimental values of both parameters would be expected to be in the same direction. The agreement between the systems i-C_8H_{18}–n-C_7F_{16} and i-C_5H_{12}–$(C_4F_9)_3N$, measured by two separate research groups, is also very encouraging. In addition, for ordinary binary liquid mixtures, the molecular interaction range of Debye may be estimated from Figure 3 if the solubility parameters are known. The angular dissymmetry of critical opalescence is undoubtedly related to the molecular interactions, and the Debye l-parameter is an appropriate measure of the average intermolecular pair potential.

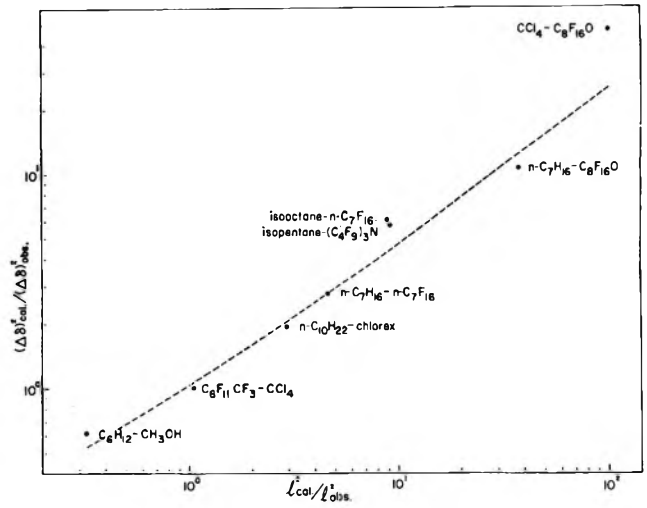

Figure 3. Plot of $(\delta_1 - \delta_2)^2_{calcd}/(\delta_1 - \delta_2)^2_{obsd}$ *vs.* l^2_{calcd}/l^2_{obsd}. Results from Table II and ref. 21.

Acknowledgments. This work was supported by the National Science Foundation and the U. S. Army Research Office (Durham). The author wishes to thank M. Pallesen for performing part of the measurements.

(30) One of the approximations for the computation of l^2_{calcd} comes from arbitrarily equating $l^2_{calcd} \cong l^2_{obsd}$ for the system perfluoromethylcyclohexane–carbon tetrachloride. This rather poor assumption which hides our ignorance in the σ_{12}-term (see footnote 33 of ref. 21), is not a consequence of the Debye theory.

Diffusion in Dilute Hydrochloric Acid–Water Solutions

by J. A. Harpst, E. Holt, and P. A. Lyons

Department of Chemistry, Yale University, New Haven, Connecticut *(Received January 22, 1965)*

Diffusion coefficients for dilute aqueous HCl solutions have been measured at 25° using a conductometric technique. The applicability of the Onsager–Fuoss transport theory has been confirmed for the case of a negative electrophoretic correction. Limitations of the method used are reviewed. The diffusion data can be used to predict precisely the activity coefficient of HCl in dilute aqueous solutions.

Introduction

There have been extensive studies of diffusion in dilute electrolyte solutions, in particular 1–1 electrolyte solutions. For this latter class, there is abundant evidence that diffusive flow is correctly predicted by the theory of Onsager and Fuoss. This work is reviewed in standard treatises.[1]

In very dilute solutions the definitive work was performed by Harned and associates using a conductometric technique. The Lucite cells used in these studies were not suitable for use with acids. It has been shown by one of the authors that these cells appear to adsorb protons. However, it was possible to devise a satisfactory all-glass cell for weak electrolyte studies.[2] Modifications of this design were used for the present work on strong acids.

Prior to this study there had been no accurate diffusion data reported for strong acids which were of value for a comparison with theory. The most reliable measurements have used the stirred diaphragm cell procedure. The nature of these experiments precludes the possibility of obtaining data in very dilute solutions. For example, the excellent diaphragm cell data of Stokes for HCl–H_2O extend only to 0.05 *M*.[3]

A major point of interest in the comparison of diffusion results with theory is the validity of the "electrophoretic effect" which, for the 1–1 salts which have been studied, is quite small and positive. Since many possible experimental errors in the conductometric procedure (due to such random factors as vibration, poor temperature control, etc.) tend to give high values for the diffusion coefficient, it might be argued that the agreement of experiment with theory was fortuitous. Because of the great difference in the ionic mobilities of H^+ and Cl^-, it develops that the over-all electrophoretic effect is somewhat larger than for 1–1 salts and, more importantly, it is negative. This means that diffusion data for dilute aqueous HCl solutions should provide a cleaner, single test for the theory than any system yet studied. In addition, this work was an obvious and necessary prelude to studies on multicomponent systems, such as MCl–HCl–H_2O and HCl–mixed solvent, which were being considered in this laboratory.

Experimental

Materials. Baker's Analyzed reagent grade HCl was diluted with distilled water and used without further purification. The conductance of the water used was monitored to ensure that solvent corrections at all times were negligible.

Baker's Analyzed reagent grade KCl, used in the calibration of auxiliary cells, was recrystallized twice from water, dried in a vacuum oven at 145°, and stored in a desiccator.

Equipment and Procedure. The cells used for this work consisted of three thin-walled pieces of glass tubing bonded to rectangular plate-glass end plates. One end plate was provided with three holes into which the tubes just fit. Slits to accommodate 1 × 4 mm. platinum electrodes were cut into opposite sides of the tubing in pairs at precisely one-sixth of the distance from the top and bottom of the cylindrical compartment in which the restricted diffusion would take place.

(1) See, for example, H. S. Harned and B. B. Owen, "The Physical Chemistry of Electrolytic Solutions," 3rd Ed., Reinhold Publishing Corp., New York, N. Y., 1958, pp. 245–252; R. A. Robinson and R. H. Stokes, "Electrolyte Solutions," Butterworth and Co. Ltd., London, 1955, pp. 293–308.

(2) E. Holt, Ph.D. Thesis, Yale University, 1961.

(3) R. H. Stokes, *J. Am. Chem. Soc.*, 72, 2243 (1950).

The apparatus was assembled with Bondmaster No. M-648-T air-drying epoxy cement, using No. CH-23 curing agent. After several days of cure, the sliding surface of the bored end plate was ground flat (and to the proper final height) by the use of a diamond wheel in a milling machine head and then lapped.

Cell 1 had tubes which provided a diffusion compartment 72 mm. high, 13 mm. in inside diameter, and 1 mm. in wall thickness. This cell was fragile and after several months hairline cracks appeared near the electrode inserts. Neither the use of soft glass tubing to match the coefficient of thermal expansion of Pt nor considerable care to keep the cell always at 25 ± 3° prevented this from occurring. In cell 2 the corresponding dimensions were 72, 13, and 2 mm. The heavier wall tubing used in the latter cell delayed the onset of disintegration for just over 6 months. This type of unit, though simple, is not recommended as a permanent laboratory accessory and, in fact, has since been supplanted here by an inevitably more elaborate, rugged, all-glass device.

With only minor differences, the procedure followed is the same as outlined by Harned and Nuttall.[4] Their paper should be consulted to get a detailed account of the introduction of samples, measurement of conductances at the upper and lower electrode pairs, and the computation of the diffusion coefficient.

Successful results in this work required very light platinization (~5 ma. current for about 1 min. was satisfactory). After the measurements were complete —about 5 days—the cell was removed from the bath, shaken, inverted for a few hours, and returned to the bath for overnight equilibration. The cell constants of the electrode pairs were then determined. Following this, the concentrations in the cells were determined by removing measured amounts of the cell contents, diluting appropriately, and measuring the resistance of the latter solutions in auxiliary conductance cells which had been calibrated.[5]

To verify the conductometric results at higher concentrations, the Gouy interferometric procedure was used. The general procedure for this method has been well described,[6] and slight modifications employed in this laboratory have been noted before.[7] A specially designed Tiselius cell with a 50-mm. channel length along the optic axis was employed since the refractive increment across the boundary was so small.

Results and Discussion

Calculations of differential diffusion coefficients were made from the equation

$$D = -\frac{a}{\pi^2}\frac{\Delta \ln (K_B - K_T - \Delta K)}{\Delta t} \qquad (1)$$

where a is the length of the closed cell compartment, K_B and K_T are the conductances at the bottom and top electrode pairs at time t, and $\Delta K = K_B^\infty - K_T^\infty$ corrects for the difference between the cell constants. Because of the possibility of a slight drift in cell constants, ΔK is usually treated as a parameter which may be precisely evaluated by an iterative procedure.[8]

The calculated results are listed in Table I together with quantities pertinent to the comparison with theory. Despite the fact that a precision of 0.1% has been obtained by this method for KCl solutions, in the present work on HCl the results appear to have an uncertainty of about 0.2–0.3%. The criterion for acceptability of the reported conductometric results was that values of D, computed in a given experiment from various pairings of the K and Δt values, should have an average deviation from the mean of ±0.2% or less.

Table I

c, mole/l.	q[a]	$D' \times 10^5$[b]	Δ'[c]	Δ''[d]	$D_{OF} \times 10^5$[e]	$D \times 10^5$[f]	$\Delta \times 10^5$[g]
0.0	1.0	3.337			3.337		
0.0063	0.9643	3.218	−0.0236	0.0068	3.202	3.217	−0.001
0.0113	0.9563	3.191	−0.0306	0.0098	3.171	3.173	−0.018
0.0144	0.9529	3.180	−0.0338	0.0113	3.158	3.160	−0.020
0.0154	0.9520	3.176	−0.0349	0.0117	3.154	3.147	−0.029
0.0188	0.9492	3.167	−0.0379	0.0132	3.144	3.133	−0.034
0.0199	0.9485	3.165	−0.0388	0.0136	3.141	3.149	−0.016
0.0216	0.9473	3.161	−0.0402	0.0143	3.136	3.136	−0.025
0.0247	0.9456	3.155	−0.0426	0.0154	3.130	3.129	−0.026
0.0286	0.9438	3.149	−0.0451	0.0166	3.122	3.122	−0.027
0.034[h]	0.9419	3.143	−0.0483	0.0181	3.114	3.11	−0.033
0.05[i]					3.10	3.07	

[a] $q = (1 + c(\partial \ln y_\pm/\partial c))$. [b] $D' = D_0(1 + c(\partial \ln y_\pm/\partial c))$; $D_0 = 3.337 \times 10^{-5}$. [c] $\Delta' = 2000RT(\Delta M'/c)$. [d] $\Delta'' = 2000 \times RT(\Delta M''/c)$. [e] D_{OF} is the value predicted by eq. 2. [f] D is the experimental value. [g] $\Delta = D - D'$. [h] Gouy result. [i] Stirred diaphragm result of Stokes.[3]

With this criterion it was not possible to extend the range of measurement in either direction beyond the concentration range listed. Thus this method would appear to be unsatisfactory for studying diffusion in multicomponent systems of HX–MX–H_2O at high concentrations at constant total molality. Many of

(4) H. S. Harned and R. L. Nuttall, *J. Am. Chem. Soc.*, **69**, 736 (1947).

(5) J. E. Lind, Jr., J. J. Zwolenik, and R. M. Fuoss, *ibid.*, **81**, 1557 (1959).

(6) L. G. Longsworth, *ibid.*, **69**, 2510 (1947); L. J. Gosting, E. Hanson, G. Kegeles, and M. S. Morris, *Rev. Sci. Instr.*, **20**, 209 (1949).

(7) P. A. Lyons and C. L. Sandquist, *J. Am. Chem. Soc.*, **75**, 3896 (1953).

(8) H. S. Harned and D. M. French, *Ann. N. Y. Acad. Sci.*, **46**, 267 (1945).

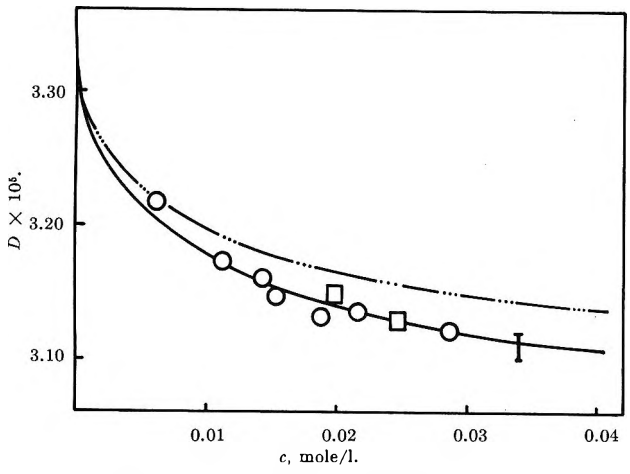

Figure 1. Comparison of diffusion coefficients for HCl–H_2O with Onsager–Fuoss theory: ———, complete Onsager–Fuoss theory; —·····—, theory without electrophoretic terms; I, Gouy method; □, cell 1; ○, cell 2.

the difficulties encountered in this diffusion study are much the same as those which Stokes has described in his elegant study of conductance in HCl solutions.[9]

Fortunately, the conductometric data appear to be internally self-consistent. A short theoretical extrapolation indicates agreement with the optical value. It is interesting that a continued extrapolation agrees with Stokes' lowest value within the accuracy of his experiment.

In Figure 1, the data are compared with the Onsager–Fuoss theory; the agreement is very good. For convenience, the values of electrophoretic contribution have been tabulated in Table I. They are obtained by subtracting from the measured value of D the quantity $D' = D_0(1 + c(\partial \ln y_\pm/\partial c))$ as suggested by Guggenheim.[10] This quantity Δ (column 8, Table I) may be compared with the sum of columns 4 and 5 (after multiplication by q).

The Onsager–Fuoss equation for strong electrolytes is often written

$$D = 2000RT\frac{\bar{M}}{c}\left(1 + c\frac{\partial \ln y_\pm}{\partial c}\right) \qquad (2)$$

where

$$\frac{\bar{M}}{c} = 1.0741 \times 10^{-20}\frac{\lambda_1^0\lambda_2^0}{\nu_1|z_1|\Lambda^0} + \frac{\Delta\bar{M}'}{c} + \frac{\Delta\bar{M}''}{c} \qquad (3)$$

In eq. 3, the first- and second-order electrophoretic terms are given by

$$-\Delta\bar{M}' = \frac{(|z_2|\lambda_1^0 - |z_1|\lambda_2^0)^2}{2(\Lambda^0)^2|z_1z_2|}\frac{3.132 \times 10^{-19}}{\eta_0(\epsilon T)^{1/2}}\frac{c\sqrt{\Gamma}}{(1 + Ka)} \qquad (4)$$

and

$$\Delta\bar{M}'' = \frac{(z_2^2\lambda_1^0 + z_1^2\lambda_2^0)^2}{(\Lambda^0)^2}\frac{9.304 \times 10^{-13}c^2}{\eta_0(\epsilon T)^2}\phi(Ka) \qquad (5)$$

$\phi(Ka) = [e^{2Ka}E_i(2Ka)/(1 + Ka)^2]$ has been tabulated conveniently in Table 5-3-2 of the Harned and Owen treatise.[1]

Since the ionic mobilities of H^+ and Cl^- differ so much, the negative electrophoretic term, $\Delta\bar{M}'$, is larger than $\Delta\bar{M}''$; at 0.01 M it is three times as great. Thus, in contrast to the case for 1–1 salts, for this system the theory predicts a negative electrophoretic contribution, a direction opposite to that which might occur due to errors of the type mentioned earlier.

As has been pointed out by Harned[11] and associates, precise activity coefficients may be evaluated from electrolyte diffusion data in dilute solutions. These HCl data can be treated in the same way, giving at $c = 0.01$, as an example, $y_\pm = 0.903$ as compared with 0.9048 obtained from e.m.f. studies. The fit is of course better at lower concentrations.

The agreement of theory and experiment for this system, coupled with substantial confirmation for salt systems in which the pertinent effect has a different sign, suggests that either the complete theory is valid or we are dealing with interesting and repeated coincidence.

Acknowledgment. This work was supported in part by an Atomic Energy Commission Grant, AT(30-1)-1375. For helpful discussions we are grateful to H. S. Harned.

(9) R. H. Stokes, *J. Phys. Chem.*, **65**, 1242 (1961).
(10) E. D. Guggenheim, *Trans. Faraday Soc.*, **50**, 1048 (1954).
(11) H. S. Harned, *Proc. Natl. Acad. Sci. U. S.*, **40**, 551 (1954).

Diffusion of Potassium Chloride in Methanol–Water Solutions

by M. V. Kulkarni and P. A. Lyons

Department of Chemistry, Yale University, New Haven, Connecticut *(Received January 22, 1965)*

Diffusion coefficients for dilute KCl solutions in a mixed solvent of methanol and water have been measured at 25°. Methanol concentrations were 10, 20, and 38.6% by weight. Theory based on pseudo-binary behavior correctly predicts the results over the entire range of concentrations in 10% methanol solutions, is valid at the lowest concentrations for the 20% methanol data, and yields values about 1% below experiments for the 38.6% methanol case. The diffusion data may be used to compute precisely the salt activity coefficients for the 10 and 20% data and these data are compared with some experimental values and with results deriving from accepted electrochemical theory. The success of this procedure suggests that this method may be used to estimate activities in mixed solvents which are presently experimentally inaccessible.

Introduction

Although a great deal of transport data have been amassed for electrolytes in aqueous solutions and in mixed solvents, relatively little is known about pure diffusion in mixed solvents.[1] In dilute solutions there are no precise results, yet there are several questions for which such measurements would provide answers.

First, would diffusion in very dilute mixed solvent solutions mimic the analogous behavior in simple binary systems; when would it become necessary to deal with these systems as ternary systems? Beyond this, would the concentration dependence follow the classical Onsager–Fuoss theory? Finally, could diffusion data obtained for such mixed solvent systems be used for the practical computation of the electrolyte chemical potential?

The potassium chloride–methanol–water system was the obvious choice for this initial study for several reasons. Accurate transference numbers are available for K^+ and Cl^- in these mixtures and they are nearly equal. The cell lubrication problem for these solutions is not as serious as for other mixed solvent choices (dioxane–water for an example). Diffusion data for aqueous KCl solutions conform to theory over a greater range of concentrations than for any electrolyte yet studied.

Experimental

Procedure. Because of the nature of the system and the low concentrations of KCl involved the natural choice of experimental technique was the conductometric method. The procedure followed has been described.[2] In this method a cell is placed on a heavy brass platform in an air thermostat which, in turn, is submerged in a water bath. By appropriate manipulation, a small quantity of electrolyte is introduced into the bottom of a cell which previously had been filled with solvent. After introduction of the electrolyte, the cell contents are isolated and, after a period of time sufficient to develop restricted diffusion, the further flow of electrolyte is followed by measuring the conductivity at positions one-sixth of the distance from the top and bottom of the cell.

The all-glass cell used in this work was patterned after one used earlier in this laboratory for studying diffusion in partially dissociated electrolytes.[3] For the current experiments it was desirable to collect data over a rather long period of time. As a consequence, the height of the new cell was 6 cm. (the previous height was 3.6 cm.). The resulting unit was a glass rectangular parallelepiped 1.0 × 3.0 × 6.0 cm. in dimension with platinum electrodes 1 mm. thick and 30 mm.

(1) H. S. Harned and B. B. Owen, "The Physical Chemistry of Electrolytic Solutions," 3rd Ed., Reinhold Publishing Corp., New York, N. Y., 1958; R. A. Robinson and R. H. Stokes, "Electrolyte Solutions," Butterworth and Co., Ltd., London, 1955.

(2) H. S. Harned and R. L. Nuttall, *J. Am. Chem. Soc.*, 69, 736 (1947).

(3) E. Holt, Ph.D. Thesis, Yale University, 1961.

long inserted in the cell walls 1 cm. from the top and bottom of the cell.

This new cell was found to perform very well, so a second cell of the same general design with three chambers (1.0 × 2.0 × 6.0 cm.) was made. While both cells were assembled and bonded in the same way—Shell Epon VIII epoxy cement cured at 200°F.—the cement in the second cell was softened by 38.6% methanol–water solutions, whereas the first cell was not perceptibly affected. The second cell was also more strained; a number of cracks appeared in this cell after several months of use. Although none of these cracks interfered with the function of the cell, it seems that the single chamber cell is a safer design even if it does result in stretching out the data collection a bit. A great advantage of both cells is their large electrode areas, 0.3 and 0.2 cm.^{2} for the single and triple units, respectively. For this conductometric experiment, the normal computational procedure employs a correction for the inequality of the cell constants of the top and bottom electrode pairs.[2] In earlier work this quantity, which can have an appreciable effect on the derived results, was estimated by an iterative process which minimized the temporal drift in the computed diffusion coefficients. Since larger electrodes can be more easily matched, it is not surprising that the correction for the new cells is very small. With the improved electrode design it is possible to evaluate the correction directly by measuring the cell constant for each pair; no longer is the correction employed as a parameter to minimize drift in the data.

Sliding surfaces of the cell were lubricated with Apiezon M which had been extracted with methanol for about 1 week. Concentrations of the final (infinite time) cell contents were obtained by measuring the conductances of those solutions in an auxiliary cell. A relation between the resistance of the solutions and the square root of the concentration was established through a series of measurements on carefully prepared solutions of known composition.

All experiments were carried out at 25°. The outer water bath was controlled at 25 ± 0.01°. Within the air thermostat the control was much better; no fluctuations could be observed with a Beckmann thermometer immersed in water in that unit.

Reagents. Fisher certified reagent grade methanol was used without purification. Deionized distilled water with a specific conductance less than 10^{-6} was used. Both liquids were deaerated before the preparation of the solvent mixtures. KCl precipitated from a saturated solution by passage of HCl through the solution was dried for several days in a vacuum desiccator, placed in a platinum dish, dried under vacuum at 100° for 1 hr., and fused at 800° under vacuum.[4]

Results and Discussion

Diffusion coefficients were computed at various concentrations using the equation

$$D = -\frac{a^2}{\pi^2}\frac{\Delta \ln (K_B - K_T - \Delta K)}{\Delta t} \quad (1)$$

where a is the total height of the diffusion chamber, K_B and K_T are conductances of the bottom and top electrode pairs, Δt is the time interval corresponding to $\Delta \ln (K_B - K_T - \Delta K)$, and $\Delta K = K_B^\infty - K_T^\infty$, as measured after shaking the cell at the end of the run.

These diffusion data will be compared with values predicted by the Onsager–Fuoss theory, which leads to the expression[1]

$$D = (\nu_1 + \nu_2)1000RT\left(1 + c\frac{\partial \ln y_\pm}{\partial c}\right) \times \left(1.0741 \times 10^{-20}\frac{\lambda_1^0\lambda_2^0}{\nu_1|z_1|\Lambda^0} + \frac{\Delta\bar{M}'}{c} + \frac{\Delta\bar{M}''}{c}\right) \quad (2)$$

where ν, λ, Λ^0, z, and $y_\pm$ have their accepted electrochemical meanings, and the electrophoretic terms, $\Delta\bar{M}'$ and $\Delta\bar{M}''$, are given by the equations

$$-\Delta\bar{M}' = \frac{(|z_2|\lambda_1^0 - |z_1|\lambda_2^0)^2}{\Lambda^{02}|z_1z_2|(\nu_1 + \nu_2)}\frac{3.132 \times 10^{-19}}{\eta_0(\epsilon T)^{1/2}}\frac{c\sqrt{\Gamma}}{(1 + \kappa a)} \quad (3)$$

and

$$\Delta\bar{M}'' = \frac{(z_2^2\lambda_1^0 + z_1^2\lambda_2^0)^2}{\Lambda^{02}}\frac{9.304 \times 10^{-13}}{\eta_0(\epsilon T)^2}c^2\varphi(\kappa a) \quad (4)$$

ϵ is the dielectric constant, η_0 is the solvent viscosity, Γ is the ional concentration, and $\varphi(\kappa a)$ is defined and tabulated in ref. 1. The equation used to fit the thermodynamic term $(1 + \partial \ln y_\pm/\partial \ln c)$ is developed later (eq. 12).

In Table I are listed the experimental values for the diffusion coefficients and those supplementary data needed for a comparison with theory. The results are also plotted in Figure 1. It is apparent that the agreement with theory is excellent for the 10% methanol data and surprisingly good for the 20% data. At 38.6% methanol, the results are about 1% higher than theory in the range of concentrations covered.

While in some cases the conductometric method can yield data with an apparent precision of ±0.1%, the results reported here for 10 and 20% methanol are no more reliable than ±0.2% and an uncertainty of ±0.3%

(4) T. Shedlovsky, *J. Am. Chem. Soc.*, **54**, 1411 (1932).

Table I

c_1, mole/l.	$D \times 10^5$, cm.^{2} sec.$^{-1}$	$D \times 10^5$ calcd., cm.^{2} sec.$^{-1}$
	10% CH_3OH	
0.00211	1.559	1.557
0.00273	1.549	1.552
0.00395	1.545	1.545
0.00425	1.542	1.543
0.00529	1.533	1.538
0.00943	1.521	1.523
0.01250	1.513	1.516
0.01382	1.513	1.513
0.02108	1.505	1.502
0.02905	1.491	1.490
	20% CH_3OH	
0.01476	1.251	1.248
0.01587	1.249	1.246
0.01863	1.249	1.243
0.02102	1.246	1.239
	38.61% CH_3OH	
0.00240	1.026	1.017
0.00302	1.027	1.014
0.00757	1.005	0.996
0.01050	1.008	0.989
0.01513	0.9992	0.978

Methanol, wt. %	10.00%	20.00%	38.61%
$\eta_0 \times 10^3$, poises[a]	12.40	14.80	17.00
ϵ[b]	74.1	69.2	60.2
S_f	0.5587	0.6184	0.7622
A'	1.186	1.227	1.314
$\lambda^0_{K^+}$[c]	60.1	50.0	39.7
$\lambda^0_{Cl^-}$[c]	59.8	49.4	39.4

a for KCl = 3.5 Å.

[a] C. Carr and J. A. Riddick, *Ind. Eng. Chem.*, **43**, 692 (1951). [b] See ref. 1. [c] R. Kay, Mellon Institute, private communication.

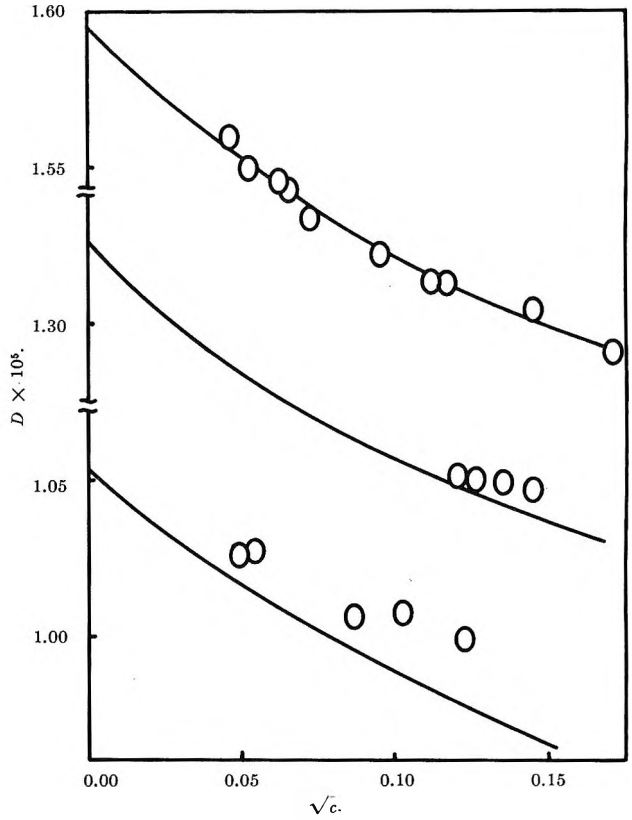

Figure 1. Diffusion of potassium chloride in different methanol–water mixtures: top curve, 10% CH_3OH; middle curve, 20% CH_3OH; lower curve, 38.61% CH_3OH.

is associated with the 38.6% methanol values. Since our cells did give diffusion values for very dilute aqueous KCl solutions within 0.05% of the theoretical value, it is assumed that for this mixed solvent system distillation losses attendant upon filling the cell and analyzing the final cell contents tended to scatter the results because of imprecision in both the diffusion coefficients and the concentrations.

In any event, the 10% methanol data agree with simple binary theory over the entire concentration range covered. The 20% data just meet theory at the lowest concentrations and the 38.6% data are about 1% above theory. Significantly, in the work-up of the data for all methanol concentrations there was no systematic variation in the values of D computed from various pairings of time. The time invariance of D and ΔK will be shown to be consistent with first-order departure from pseudo-binary behavior.

Of course, the agreement with theory does not require identical interaction of ions with either methanol or water. This is obviously not the case. The conductance data and transference numbers which are used to compute the limiting values of the diffusion coefficients already admit of differences in specific interactions. Where results agree with theory it can only be stated that the variation with concentration of the diffusion coefficient follows the same rule as a very dilute aqueous solution of a 1–1 electrolyte.

It may be of some interest to consider in a rough approximation how results such as these might be expected to depart from pseudo-binary behavior. Calling the concentrations of KCl and methanol c_1 and c_2, respectively, in moles per liter, and assuming as is reasonable that a preferential coupling of ions with water would result in a lowered concentration of methanol as a result of salt flow into a given volume element, and if the initial concentration of methanol in the mixed solvent were c_2^0, moles per liter, then where n = the net number of moles of water transported by KCl, the methanol concentration in the solvent at any

level in the cell would be $c_2 \cong c_2^0 - nc_1$. The apparent diffusion coefficient measured for this system by the Harned method is related to the flow of salt, J_1, by Fick's second law

$$-\frac{\partial}{\partial x}(J_1) = \frac{\partial c_1}{\partial t} = D_{app}\frac{\partial^2 c_1}{\partial x^2} \tag{5}$$

Following Fujita and Gosting,[5] we may also write

$$\frac{\partial c_1}{\partial t} = D_{11}\frac{\partial^2 c_1}{\partial x^2} + D_{12}\frac{\partial^2 c_2}{\partial x^2} \tag{6}$$

Using the approximation $c_2 \cong c_2^0 - nc_1$, and comparing (5) and (6), we find D_{app} is given approximately by the difference, $D_{11} - nD_{12}$.

In this first-order estimate, the pseudo-binary diffusion coefficient would approach the Onsager–Fuoss value for D under circumstances where nD_{12} was very small. Since we expect D_{12} to be both small and negative and also that n, the net water transport, is small, we expect the deviation to be small and positive. Additionally, since n should increase with methanol concentration, the deviation should increase also. Finally, the pseudo-binary constant should appear to be a time invariant quantity $\cong (D_{11} - nD_{12})$ for higher methanol concentrations. All of these features are consistent with the observed data. (Unfortunately, the positive deviation cannot be considered to be particularly decisive since this is the direction of departure from theory for 1–1 electrolytes in simple aqueous solutions.)

It is appropriate to consider how well activity coefficients for the salt can be computed from the diffusion data for this mixed solvent system.

The theoretical value for the diffusion coefficient may be written in a simple form

$$D = \nu 1000RT\left(\frac{\bar{M}}{c}\right)\left(1 + c\frac{\partial \ln y_\pm}{\partial c}\right) \tag{7}$$

where $(\bar{M}/c)$ is the combined mobility term.

Calling

$$\frac{D}{\nu 1000RT(\bar{M}/c)} - 1 = D' = c\frac{\partial \ln y_\pm}{\partial c} \tag{8}$$

gives[6]

$$\ln y_\pm = \int_0^c \frac{D'}{c}dc = \int_0^{c^{1/2}} \frac{2D'}{c^{1/2}}dc^{1/2} \tag{9}$$

At the limit

$$\lim_{c\to 0}\left[\frac{D'}{\sqrt{c}} = \frac{\partial \ln y_\pm}{2\partial c^{1/2}} = \frac{2.3026}{2}\frac{\partial \log y_\pm}{\partial c^{1/2}}\right] = \frac{-2.3026S_f}{2} \tag{10}$$

where the Debye–Hückel limiting slope

$$S_f = \frac{1}{\nu}(\Sigma \nu_i z_i^2)^{3/2}\frac{1.290 \times 10^6}{(\epsilon T)^{3/2}} \tag{11}$$

A graphical integration of the plot of $D'/c^{1/2}$ *vs.* $c^{1/2}$ yields log $y_\pm$. These values can then be compared with experimental values. For convenience, values of $y_\pm$ obtained from the diffusion data, from limited experimental data, and from a Debye–Hückel fit of the data are presented at round concentrations in Table II. (See also Figure 2.)

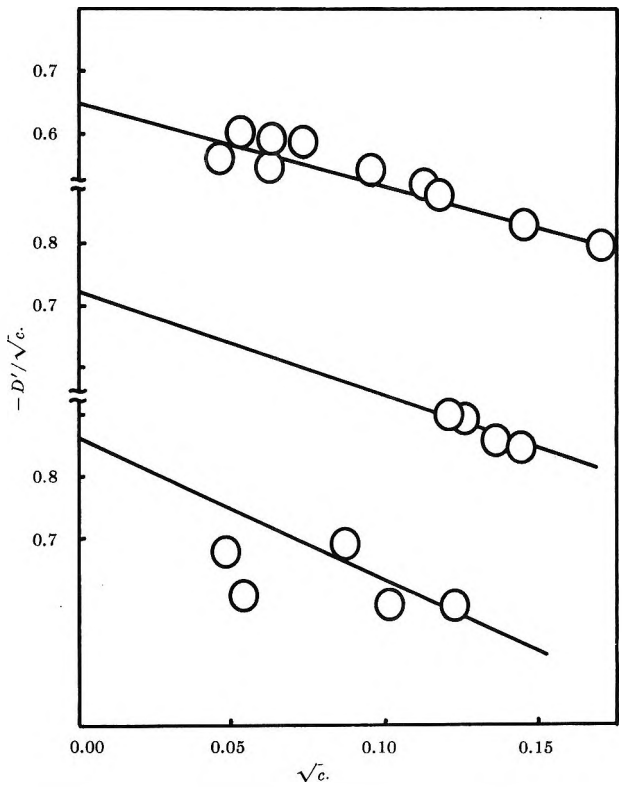

Figure 2. Plots for computing activity coefficients from eq. 9: top curve, 10% CH_3OH; middle curve, 20% CH_3OH; lower curve, 38.61% CH_3OH.

For the above comparison the experimental activity data were fit to an equation of the form

$$\log y_\pm = \frac{-S_f\sqrt{c}}{1 + A'\sqrt{c}} + B'c \tag{12}$$

The value of A' in methanol–water mixtures was estimated using the approximate relation

$$\frac{A'(\text{water})}{A'(\text{mixture})} = \left(\frac{\epsilon_{\text{mixture}}}{\epsilon_{\text{water}}}\right)^{1/2} \tag{13}$$

(5) H. Fujita and L. J. Gosting, *J. Am. Chem. Soc.*, **78**, 1099 (1956).
(6) H. S. Harned, *Proc. Natl. Acad. Sci. U. S.*, **40**, 551 (1954).

Table II

% methanol	c_1	$y_\pm$ from equation	$y_\pm$ from Harned rule[a]	$y_\pm$ from e.m.f.[b]	$y_\pm$ from Figure 2
10	0.001	0.962	0.959	...	0.962
10	0.010	0.892	0.892	...	0.891
10	0.020	0.856	0.857	0.857	0.856
10	0.030	0.832	...	...	0.831
10	0.050	0.797	0.803	0.794	...
20	0.001	0.957	0.960	...	0.957
20	0.010	0.881	0.883	...	0.881
20	0.020	0.843	0.849	0.849	0.844
20	0.030	0.817	...	...	0.820
20	0.050	0.786	0.791	0.776	...
38.61	0.001	0.948	0.951	...	0.955
38.61	0.010	0.857	0.858	...	0.879
38.61	0.020	0.813	0.812	0.812	0.840
38.61	0.030	0.782	...	...	0.821
38.61	0.050	0.741	0.737	0.717	...

[a] Values of $y_\pm$ were obtained from $\gamma_\pm$. See H. S. Harned, *J. Phys. Chem.*, **66**, 589 (1962). [b] Revised values (see ref. *a*). G. Akerlof, *J. Am. Chem. Soc.*, **52**, 2353 (1930).

A choice of $B' = 0.02$ for both 10% methanol and 20% methanol fits the data over the entire range of concentrations (c up to 0.03 and 0.02, respectively).

An interesting method proposed by Harned for estimating log $y_\pm$ may also be tested.[7] His rule empirically relates the activity coefficients of two different electrolytes in the same solvent. The rule is

$$\log \frac{\gamma_1}{\gamma_2} = Bm \qquad (14)$$

where γ is the activity coefficient on the molal scale, m is the molality, and B is a constant which can be evaluated from the activity data for both electrolytes in pure water.

Values of B for the KCl–HCl system are tabulated for concentrations above 0.01 m.[7] Since precise e.m.f. data exist for hydrochloric acid–methanol–water mixtures, $\gamma_\pm$ and then $y_\pm$ may be computed for potassium chloride–methanol–water solutions. Values of these are included also in Table II. The agreement is very good.

In sum, these measurements show that KCl solutions in 10 and 20% methanol–water mixtures behave as pseudo-binary systems as confirmed by the close agreement with the Onsager–Fuoss theory for binary solutions. As a consequence, the salt activity coefficient can be determined from diffusion data at low KCl concentrations. The results presented here are the first experimental values for solutions of electrolytes in mixed solvents below 0.02 m. They also refer unambiguously to the infinitely dilute solution as the reference state. In addition, the results support the utility of the Harned rule. However, it has not been shown that either this diffusion technique or the Harned rule can be used successfully at higher concentrations than those for which activity coefficients could be computed with a modified Debye–Hückel equation of the form of Guggenheim with judiciously selected constants.

Acknowledgment. This work was supported by Atomic Energy Commission Contract No. AT(30-1)-1375.

(7) See footnote *a* in Table II.

Diffusion in Dilute Aqueous Acetic Acid Solutions

by E. L. Holt and P. A. Lyons

Department of Chemistry, Yale University, New Haven, Connecticut *(Received January 22, 1965)*

Diffusion coefficients have been measured at 25° for dilute aqueous acetic acid solutions in the concentration region from about 0.001 to 0.1 *M* using the conductometric technique. A new all-glass cell design for these measurements is described. At the higher concentrations, the data overlap results previously obtained from an interferometric procedure. The results display the general trend to be expected for this dissociating system; there is a rapid increase in the diffusion coefficient as the less mobile molecules are converted to more rapidly moving pairs of oppositely charged ions. The data are somewhat higher than predicted with accepted theory; this discrepancy is reviewed.

Introduction

Diffusive flow in a binary system may be described by a single diffusion coefficient despite the fact that a component may dissociate.[1] In dilute aqueous weak-electrolyte solutions, this diffusion coefficient may be computed if the mobilities of the species in equilibrium are known, assuming the rate of equilibration to be rapid compared with the rate of flow. A general theory dealing with this problem has been developed[2] from which relations proposed for particular cases may be retrieved.[3,4]

For the equilibrium system, $HOAc \rightleftarrows H^+ + OAc^-$, the ionic mobilities can be computed from available conductivity data.[5] The mobility of the undissociated species can be determined at low concentrations by an appropriate extrapolation of diffusion data obtained at concentrations where the degree of dissociation is negligible.[6]

Precise data are available for the system under discussion only as low as about 0.03 *M*,[6] at which concentration the degree of dissociation is only about 2.5%. This work was undertaken to discover how well the diffusion of acetic acid would conform to expectation when the degree of dissociation was greater.

Experimental

Procedure. Conventional optical techniques cannot readily be used for the precise study of diffusion in very dilute solutions. As a consequence, it was decided to use a conductometric method for this work.[7,8] Several preliminary experiments using previously constructed Lucite cells were unsuccessful. Although this type of cell works well with salt solutions, the evidence was strong that Lucite might be adsorbing protons. An all-glass cell of the same type as used by Harned[8] was constructed. In the new design, the diffusion channel was a parallelepiped with dimensions 10 × 30 × 36 mm. Platinum electrodes 1 × 30 mm. were sandwiched into positions one-sixth of the way from the top and bottom of the cell. The necessary pieces of Pittsburgh plate glass were machined with a diamond wheel, assembled with the electrodes on a jig, and the entire cell was bonded with Shell Epon cement. The curing temperature was 200°F. All sliding surfaces were lubricated with Vaseline (these sliding surfaces were ground and lapped but not polished).

The cell was placed in a Lucite air thermostat, which itself was suspended in a large water thermostat. A tripod holder for the cell fit reproducibly into locaters on a 100-lb. brass block which served to minimize temperature changes or mechanical disturbances. The

(1) L. Onsager, *Ann. N. Y. Acad. Sci.*, **46**, 241 (1945).

(2) W. H. Stockmayer, *J. Chem. Phys.*, **33**, 1291 (1960).

(3) H. S. Harned and R. M. Hudson, *J. Am. Chem. Soc.*, **73**, 3781 (1951).

(4) G. T. A. Müller and R. H. Stokes, *Trans. Faraday Soc.*, **53**, 642 (1957).

(5) D. A. MacInnes and T. Shedlovsky, *J. Am. Chem. Soc.*, **54**, 1429 (1932).

(6) V. Vitagliano and P. A. Lyons, *ibid.*, **78**, 4538 (1956).

(7) H. S. Harned and D. M. French, *Ann. N. Y. Acad. Sci.*, **46**, 267 (1945).

(8) H. S. Harned and R. L. Nuttall, *J. Am. Chem. Soc.*, **71**, 1460 (1949).

bath was supported by correctly loaded Lord mounts which were isolated from the basement floor slab by Isomode pads. A slow-speed stirring motor was wall-mounted.

Resistance measurements were made with a Leeds and Northrup Jones bridge, calibrated by the method of Dike.[9] A 1-kc. signal, after amplification, entered the bridge at 0.75 v. Previously described procedures were used to introduce correct amounts of solute into the cell.[8] Resistances were measured about 48 hr. after the introduction of the solute. About nine readings a day were taken for about 3 days, at which time the cell was removed from the thermostat, shaken, and returned to the bath. On the next day, resistance measurements were made on the homogeneous solutions to provide a ratio of cell constants for the electrode pairs. Once again the cell was removed. A 5-ml. aliquot of the contents, diluted to 15 ml., was placed in an auxiliary calibrated conductance cell. The average concentration of the homogeneous solution was computed from the resistance of the sample using the data of MacInnes and Shedlovsky.[5]

Materials. Baker's Analyzed Reagent glacial acetic acid was used. Titration of the sample used gave a purity of 99.8%. The acid was used without further treatment. Baker's Analyzed Reagent potassium chloride was recrystallized twice from water and dried in a vacuum oven at 145°.

Analysis of Experimental Data. The solution of Fick's second law for restricted diffusion in a cell of length a may be written as a Fourier series at each electrode-pair position, $^1/_6\ a$ and $^5/_6\ a$. In the method employed here, the changes in concentration of the component are followed by measurement of the resistances due to only ionic species. Therefore, multiplying each side of the series solution by α, the degree of dissociation at a given electrode pair, we obtain

$$\alpha c = \alpha \sum_{n=0}^{\infty} A_n e^{-n^2\pi^2 Dt/a^2} \cos \frac{n\pi}{6} \qquad (1)$$

and a similar series in $\cos(n5\pi/6)$. Taking differences and neglecting terms in the series beyond the first gives

$$\begin{aligned}(\alpha_B C_B - \alpha_T C_T) &= A_1 e^{-\pi^2 Dt/a^2}\left[\alpha_B \cos\frac{\pi}{6} - \alpha_T \cos\frac{5\pi}{6}\right] \\ &= A' e^{-\pi^2 Dt/a^2}[\alpha_B + \alpha_T] \\ &\propto (K_B - K_T) \end{aligned} \qquad (2)$$

Dropping terms beyond the first requires a long wait for meaningful readings. A negligible error for this system can be assumed only if the approximation is applied to readings taken after about 48 hr. (A cell with electrode positions at $a/4$ and $3a/4$ is being constructed. For this geometry the second term in the series expansion goes to zero, permitting readings to be taken earlier. Whether this design will yield substantially more reliable data over a longer interval remains to be seen.)

In the usual method, ΔK, a correction for non-equivalence of cell constants, is introduced giving for the right side of eq. 2 a quantity equal to $(K_B - K_T + \Delta K)$. In the present procedure it will be convenient to define a correction, measured and/or computed, equal to the ratio of the infinite time cell constants, $r = k_B^\infty/k_T^\infty$. Equation 2 then becomes

$$[rK_B - K_T] = A'' e^{-\pi^2 Dt/a^2}[\alpha_B + \alpha_T] \qquad (3)$$

Taking differences corresponding to various times gives

$$\left\{\frac{\Delta \ln [rK_B - K_T] - \Delta \ln [\alpha_B + \alpha_T]}{\Delta t}\right\}\frac{a^2}{\pi^2} = -D \qquad (4)$$

Equation 4 differs from the analogous expression for strong electrolytes only by a correction term, $\Delta \ln [\alpha_B + \alpha_T]$, which must be known as a function of concentration. To evaluate this term we start with the relations for the degree of dissociation

$$\alpha = \frac{\Lambda}{\Lambda_E} \qquad (5)$$

and the equilibrium constant

$$\frac{\alpha^2 c}{1 - \alpha} = K' \qquad (6)$$

where Λ_E is the hypothetical equivalent conductance of the completely dissociated weak electrolyte at concentration c, and

$$\Lambda = \frac{10^3 kK}{c} \qquad (7)$$

k is the cell constant and K the conductance. The magnitude of the correction term is not significantly altered by the assumption, implicit in (6) and (7), that $y_\pm$ and y_μ, the activity coefficients for the dissociated and undissociated species, respectively, are unity.

In terms of the above definitions α becomes

$$\alpha = \frac{\Lambda_E K'}{\Lambda_E K' + 10^3 kK} \qquad (8)$$

Hence the correction term may be written

$$(\alpha_B + \alpha_T) = b\left[\frac{1}{b + 10^3 rK_B} + \frac{1}{b + 10^3 K_T}\right] \qquad (9)$$

(9) P. H. Dike, *Rev. Sci. Instr.*, 2, 379 (1931).

where

$$b = \frac{\Lambda_E K'}{k_T} \tag{10}$$

k_T need not be known with great accuracy since b is less than 10^2K, b as a multiplier in (9) disappears when differences in logarithms are taken, and finally since the entire correction term is very small compared with $\ln [rK_B - K_T]$.

Introducing (9) into (4) and using logarithms gives the working equation

$$\left\{ \frac{\Delta \ln [rK_B - K_T] - \Delta \ln \left[\frac{1}{b + 10^3 rK_B} + \frac{1}{b + 10^3 K_T} \right]}{\Delta t} \right\} \frac{a^2}{\pi^2} = -D \tag{11}$$

Results and Discussion

Diffusion coefficients and auxiliary data of interest are listed in Table I. The accuracy of these data is not as good as that obtained in experiments on strong electrolytes. Without much more work with the conductometric technique on weak acid systems, we are reluctant to assume accuracy better than ±0.5%. The data are plotted in Figure 1; the internal self-consistency of the data is good. Where the two methods overlap, the conductometric and optical data agree well within the suggested experimental error.

Table I

$c \times 10^3$, M	$(\alpha c)^{1/2} \times 10^2$	$D_{theory} \times 10^5$	$D_{obsd} \times 10^5$
0.945	1.104	1.252	1.291
2.13	1.369	1.235	1.284
6.72	1.848	1.220	1.250
7.68	1.913	1.219	1.251
16.3	2.323	1.213	1.239
22.3	2.518	1.211	1.213
36.6	2.860	1.209	1.221
42.8[a]	2.956	1.206	1.212
55.5	3.182	1.204	1.207
97.1[a]	3.648	1.200	1.200

[a] These data obtained by the Gouy method.[6]

Figure 1 includes for comparison values for the diffusion coefficient computed according to the relation used by Müller and Stokes

$$D = \frac{\alpha D_i + 2(1 - \alpha) D_m}{2 - \alpha} \tag{12}$$

which can be rearranged into the form used by Harned and Hudson. D_i and D_m are the diffusion coefficients

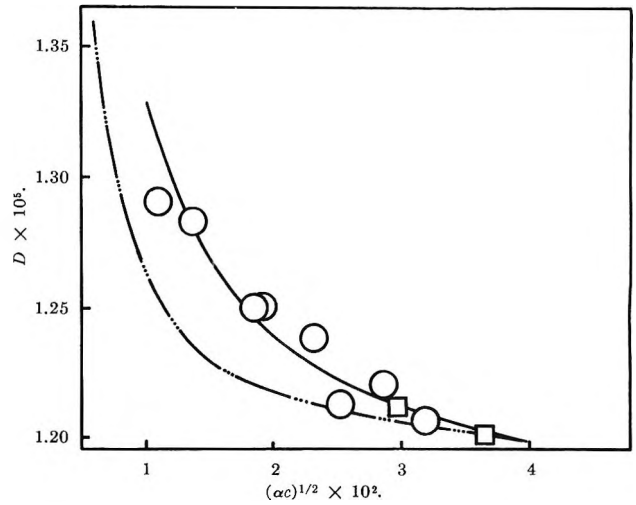

Figure 1. Comparison of diffusion coefficients for aqueous acetic acid solutions with theory and with eq. 16: ———, eq. 16; —···—, theory; □, Gouy method.

of the ionized and undissociated forms of the acid. This expression can be obtained from the general statement of Stockmayer, assuming rapid ionic recombination, ideality of both the molecular and the ionized forms of the solute, and no coupling of flows except between the oppositely charged H^+ and OAc^- ions.

The value of D_m was obtained by a linear extrapolation of data obtained by the Gouy optical technique at higher concentrations, for which $\alpha \cong 0$. A plot of $D \times 10^5/(1 + \partial \ln y/\partial \ln c)\ \eta_0/\eta$ *vs.* $\eta - \eta_0/\eta$ is linear up to $c = 3$. This same behavior is characteristic of many nonelectrolyte systems. If this extrapolation is valid, the value of D_m in the range of concentrations up to $c = 0.05$ may be taken as $D_m \times 10^5 = 1.201 - 0.055c$ and varies only from 1.201 to 1.198 in the interval of interest in this discussion.

Values of D_i have been determined from the Nernst equation

$$D_i = \frac{2RT\lambda_1\lambda_2}{F^2(\lambda_1 + \lambda_2)} \tag{13}$$

We have replaced the ionic mobilities by their conductances which, at low concentrations were estimated from the Onsager conductance theory.

As is apparent from Figure 1, general variation of the diffusion data with concentration is what is expected, increasing rapidly with dissociation into more rapidly moving pairs of oppositely charged ions as the concentration decreases. Unfortunately, the comparison leaves much to be desired. At about 0.001 M, the experiment is more than 3% higher than would be predicted by eq. 12. Although the discrepancy is not

enormous, it is, in fact, quite large considering that only about 10% of the acetic acid is dissociated at that concentration.

It is interesting to observe that the data agree, within experimental error, with values which would be predicted if it were assumed that the diffusion coefficient reflected simply the number-average frictional coefficient of the Gibbs component, acetic acid. Thus

$$D = \frac{RT}{Nf_{av}}\left(1 + \frac{\mathrm{d} \ln y_G}{\mathrm{d} \ln c_G}\right) \tag{14}$$

where $(1 + \alpha)f_{av} = \{\alpha f_{H^+} + \alpha f_{OAc^-} + (1 - \alpha)f_m\}$ and y_G is the activity coefficient of acetic acid at total concentration c_G. This may be simply rearranged to give

$$D = \frac{(1 + \alpha)\lambda_{H^+}\lambda_{OAc^-}D_m}{(1 - \alpha)\lambda_{H^+}\lambda_{OAc^-} + \frac{F^2}{RT}\alpha D_m(\lambda_{H^+} + \lambda_{OAc^-})} \times \left(1 + \frac{\mathrm{d} \ln y_G}{\mathrm{d} \ln c_G}\right) \tag{15}$$

or

$$D = \frac{(1 + \alpha)D_m D_i}{(1 - \alpha)D_i + 2\alpha D_m}\left(1 + \frac{\mathrm{d} \ln y_G}{\mathrm{d} \ln c_G}\right) \tag{16}$$

The thermodynamic term $(1 + (\mathrm{d} \ln y/\mathrm{d} \ln c)$ has been evaluated[6] from the experimental data of Hansen, Miller, and Christian.[10] A comparison of these values with the experimental results is evident in Table I and in Figure 1. Although this very good agreement is interesting, it is nonetheless disconcerting since it is generally agreed, and for excellent reasons, that eq. 12 not eq. 16 should predict the correct values.[2-4] Conflict with correct theory might possibly arise from the data used in the computation—conductances, degrees of dissociation, and mobilities of the undissociated species—or from incorrect experimental data. Careful examination fails to disclose any evident sources of error. The electrochemical data, conductances, and degrees of dissociation are probably the most reliable quantities which appear in the analysis of data. The linear extrapolation of diffusion data to get mobilities of the undissociated molecule is in keeping with general nonelectrolyte behavior. In addition, the extrapolated value is in excellent correspondence with conductometric data at low values of α.

Although the experimental data are not as precise as analogous data reported for strong electrolytes, they agree well with optical data in a region of overlap. In the absence of reasons to dismiss either theory or experiment, we must conclude that this initial study in dilute weak electrolyte solutions has demonstrated our lack of understanding of all the details of diffusive flow in such systems.

Acknowledgments. This work was supported in part by an Atomic Energy Commission grant (AT-30-1-1375). We were fortunate to have enlightening comments on this weak electrolyte problem from H. S. Harned, L. Onsager, W. H. Stockmayer, and R. H. Stokes.

(10) L. S. Hansen, F. A. Miller, and S. D. Christian, *J. Phys. Chem.*, 59, 391 (1955).

Radiation-Induced Reactions in *n*-Hexadecane[1]

by R. Salovey and W. E. Falconer

Bell Telephone Laboratories, Inc., Murray Hill, New Jersey *(Received January 22, 1965)*

The effects of irradiation of *n*-hexadecane are apparently independent of source and dose rate, the major effect being C–H rupture resulting in dimerization by cross linking to form isomers of dotriacontane and hydrogen. Chromatographic analyses of products indicate that scission of the paraffin chain is suppressed in the irradiation of *solid* *n*-hexadecane relative to irradiation in the liquid state. Mass spectrometric studies of gases evolved following irradiation and molecular weight measurements by vapor pressure depression are consistent with this observation. Increased chain scission in irradiated polyethylene melts may explain the reduction in gel measured under such conditions. From the distribution of isomeric dimers on irradiation of pure *n*-hexadecane we conclude that the main sites of cross linking are nonterminal. That is, cross linking occurs at random and there is no need to postulate radical-center mobility. However, irradiated solid *n*-hexadecane containing 5% *n*-octadecane end links to form linear dotriacontane to the extent of about 2% of total dimer.

Recent studies on the irradiation of hydrocarbon polymers have led to diverse views concerning the effect of state on the relative importance of the cross-linking reaction. Less crystalline polyethylenes cross link more readily than more ordered materials.[2] On the other hand, gel formation is greater for highly crystalline polyethylene as compared to a supercooled melt of the same material several degrees below the melting point.[3] The authors suggest[4] a marked increase of chain mobility and cross-linking efficiency in the crystalline state at temperatures exceeding 100°. Further, preferential cross linking at folds and radical center mobility were inferred from studies on irradiated polyethylene single crystal aggregates.[5] It was suggested that cross linking between chains in the crystal lattice was improbable.

An extrapolation from *n*-hexane radiolysis at 77°K. to polyethylene at room temperature[6] does not distinguish between state and temperature effects.[3] Moreover, a more justifiable comparison with polyethylene should involve *n*-paraffins having a lower end-group concentration. The present study of the product distribution in irradiated *n*-hexadecane, both in the solid and liquid states over a narrow temperature interval near 10°, concerns experiments which bear on the effect of physical state on radiation-induced reactions.

Experimental

n-Hexadecane (0.5-ml. samples, Humphrey Chemical Co. petroleum-derived product, olefin-free grade, minimum purity 99%) was placed in thin-walled (0.5 mm.) Pyrex glass tubes, outgassed at 10^{-6} torr for several hours, and then sealed. Solutions of *n*-hexadecane containing about 5% *n*-octadecane (Humphrey Chemical Co., petroleum derived, 99% purity) were similarly prepared. Materials were irradiated with 1-Mev. electrons at 2.5 Mrads min.$^{-1}$ to total doses between 1.1 and 20 Mrads,[7] or with Co^{60} γ-rays at 0.5 Mrad hr.$^{-1}$ to a total dose of 2.5 Mrads. For a 2.5-Mrad dose, conversion was $<1\%$. Irradiations were performed either at 19° on a hollow copper block thermostated by circulating water, at 4° on the same block cooled by circulating ice water, at −80° on powdered

(1) Presented at the Metropolitan Regional Meeting of the American Chemical Society, Feb. 1, 1965, Hoboken, N. J.

(2) (a) E. J. Lawton, J. S. Balwit, and R. S. Powell, *J. Polymer Sci.*, **32**, 257 (1958); (b) R. Salovey, *ibid.*, **B2**, 833 (1964).

(3) R. Kitamaru, L. Mandelkern, and J. Fatou, *ibid.*, **B2**, 511 (1964).

(4) R. Kitamaru and L. Mandelkern, *J. Am. Chem. Soc.*, **86**, 3529 (1964).

(5) R. Salovey and D. C. Bassett, *J. Appl. Phys.*, **35**, 3216 (1964).

(6) L. Kevan and W. F. Libby, *J. Chem. Phys.*, **39**, 1288 (1963).

(7) R. Salovey and W. Rosenzweig, *J. Polymer Sci.*, **A1**, 2145 (1963).

solid carbon dioxide, or at −196° in liquid nitrogen. Hexadecane was solid except at the highest irradiation temperature, 19°.

An F and M Model 700 gas chromatograph with linear programming, dual column compensation, and flame-ionization detection was used to analyze the irradiated samples. Columns were 4 ft. long, 0.25 in. i.d., stainless steel packed with a mixture of 10% GE SE-30 silicone gum rubber and 60–80 mesh Celite. Aliquots of each irradiated sample were analyzed isothermally at 265° to estimate higher molecular weight products. To estimate lower molecular weight products, further aliquots were analyzed with linear programming from 100 to 225° at 11° min.$^{-1}$ and to 300° at 5.6° min.$^{-1}$. Retention times were reproducible to ±2%; peak areas for duplicate analyses to ±5% for small peaks and ±3% for the major products.

Differences in yields between γ- and electron irradiation may reflect uncertainties in absolute dosimetry. That is, electron doses have been calibrated in terms of energy deposited per incident 1-Mev. electron.[7] However, for irradiations in glass tubes the electrons striking the sample are not monoenergetic. Measurements of doses deposited under such conditions indicate that absolute G values in Table I for electron irradiation may be as much as 20% too high. Thus for electron bombardment, irradiation yields are internally consistent but may be too high. Since γ-radiation has greater range, similar uncertainties in absolute dosimetry do not arise.

Table I: Dimer and Hydrogen Yields in Irradiated *n*-Hexadecane

Material	Irradiation temp., °C.	Electron irradiation G_{dimer}	Electron irradiation $G_{hydrogen}$	γ-Irradiation G^{γ}_{dimer}
Liquid hexadecane	19	2.60	4.1	1.59
Solid hexadecane	4	2.30	3.0	
Solid hexadecane	−80	2.01		1.50
Solid hexadecane	−196	1.23		0.99
Liquid hexadecane containing *n*-$C_{18}H_{38}$	19	2.47		
Solid hexadecane containing *n*-$C_{18}H_{38}$	4	1.95		

Number-average molecular weights of hexadecane irradiated at 4° and at 19° were determined with a Mechrolab Model 301 vapor pressure osmometer. In addition, gases evolved from samples irradiated under comparable conditions were measured by mass spectrometry.[8]

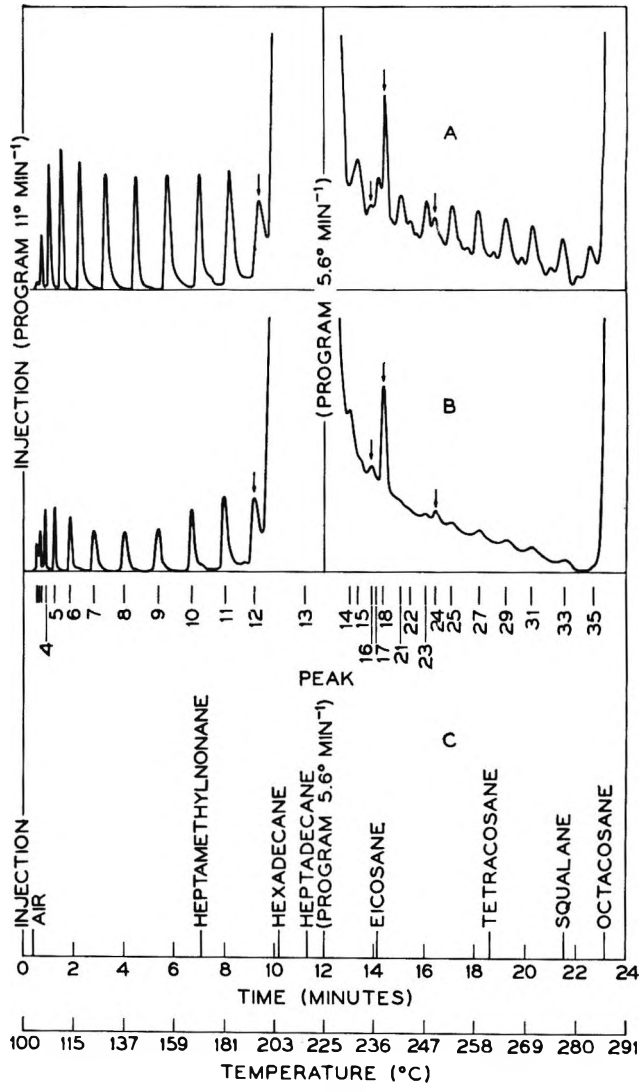

Figure 1. Temperature-programmed chromatograms of irradiated *n*-hexadecane: A, liquid phase irradiation, 2.3 Mrads at 19°; B, solid phase irradiation, 2.3 Mrads at 4°; C, elution pattern of standard normal paraffins, heptamethylnonane and squalane.

Results

Typical chromatograms for electron-irradiated liquid hexadecane at 19° and solid hexadecane at 4° are shown using programmed column temperatures in Figure 1 and for isothermal analysis in Figure 2. Standards are included for comparison in each case. Impurity peaks are denoted by arrows. Elution is in order of boiling point and, for the isothermal analyses, the logarithm of the retention time is an approximately linear function of boiling point. Therefore, highly branched compounds are eluted before more nearly

(8) Gollob Analytical Service, Inc., Berkeley Heights, N. J.

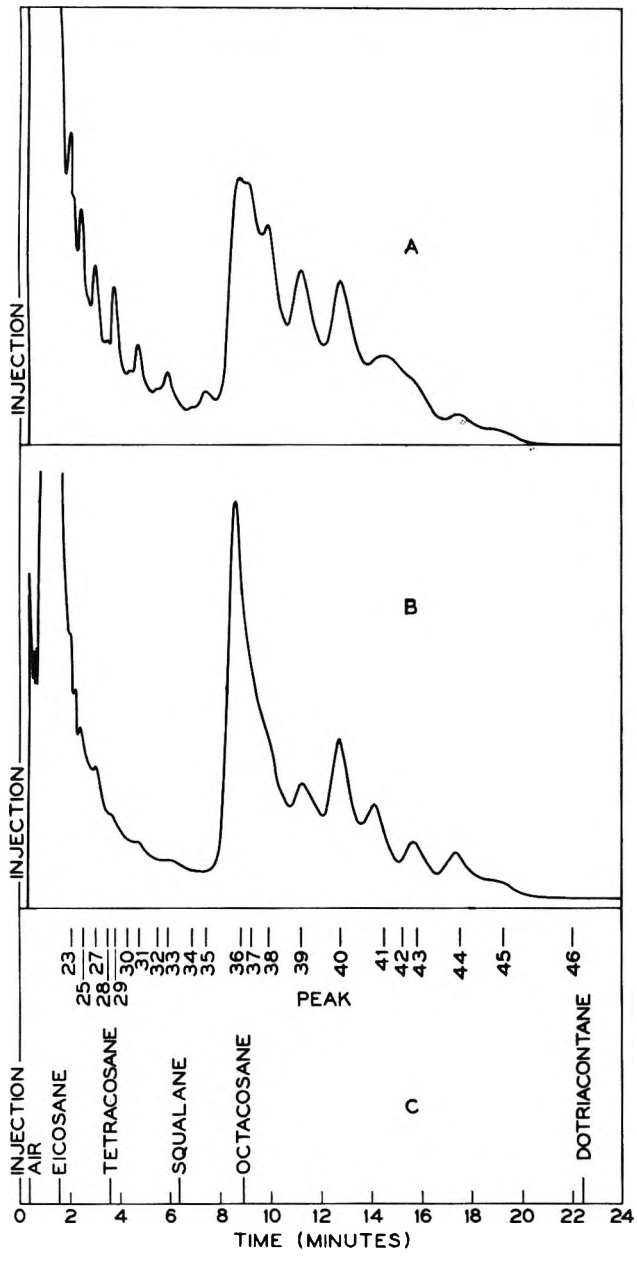

Figure 2. Isothermal chromatograms of irradiated *n*-hexadecane: A, liquid phase irradiation, 2.3 Mrads at 19°; B, solid phase irradiation, 2.3 Mrads at 4°; C, elution pattern of standard normal paraffins and squalane.

linear isomers of identical molecular weight, or even before linear compounds of lower molecular weight. Thus squalane (hexamethyltetracosane) elutes before *n*-octacosane.

Average G values, the number of molecules formed for 100 e.v. of energy absorbed, of the higher molecular weight radiation products (designated as dimers) are given in Table I for various irradiation conditions. Dimer yields were determined by comparing the areas of appropriate peaks with standards. The yield of dimer following γ-irradiation of *n*-hexadecane at several temperatures is also tabulated ($G^{\gamma}_{\text{dimer}}$). G values for lower molecular weight irradiation products decrease somewhat with decreasing temperature, although the decrease is less than that for dimer (Table I). Corresponding average values (over 1–20 Mrads) for hydrogen yields are included for liquid and solid hexadecane. In addition to hydrogen, relatively small amounts of methane and C_2–C_4 hydrocarbons were present in the gaseous product fraction. These total less than 7 mole % compared to hydrogen in the irradiated liquid and less than 4% in the solid.

Results of number-average molecular weight determinations following irradiation of solid and liquid hexadecane correspond to a dimer yield of about 3 for the solid at 4° and 18 Mrads, but variable number-average molecular weights were found for the liquid. The latter were sensitive to outgassing and could even be lower than the unirradiated control.

Discussion

The irradiation behavior in condensed states of normal paraffins with low chain-end concentrations should be analogous to that of polyethylene. Irradiation studies of lower paraffins,[9] including recent detailed studies of *n*-hexane in the solid state at 77°K.[6] and over a wide temperature range as liquid and solid,[10] were therefore extended to *n*-hexadecane, whose melting point (18°) makes it a convenient polyethylene prototype for examining the effect of physical state on radiation chemistry near room temperature.

Electron or γ-irradiation of paraffins yields vibrationally excited species *via* processes of ionization and electronic excitation.[11] Radical-scavenging techniques provide evidence for the direct participation of ionic[12] and excited molecule[13] processes in the reaction mechanism of hydrocarbon irradiations. Ion-fragmentation and hydride-transfer reactions are particularly important, at least in the gas phase. However, higher molecular weight products of hydrocarbon radiolysis arise largely from thermal free radicals[14] and recent

(9) A. V. Topchiev, "Radiolysis of Hydrocarbons," Elsevier Publishing Co., Amsterdam, 1964.

(10) H. Widmer and T. Gäumann, *Helv. Chim. Acta*, **46**, 944 (1963).

(11) A. Chapiro, "Radiation Chemistry of Polymeric Systems," Interscience Publishers, Inc., New York, N. Y., 1962.

(12) P. J. Ausloos and S. G. Lias, *J. Chem. Phys.*, **36**, 3163 (1962); R. P. Borkowski and P. J. Ausloos, *ibid.*, **39**, 818 (1963).

(13) W. H. T. Davison, *Chem. Ind.* (London), 662 (1957).

(14) H. A. Dewhurst, *J. Phys. Chem.*, **62**, 15 (1958); A. J. Swallow, "Radiation Chemistry of Organic Compounds," Pergamon Press, Inc., New York, N. Y., 1960.

results[10] are in accord with such a mechanism. Moreover, free-radical concentrations measured directly in irradiated polyethylene approximately correspond to the extent of cross linking.[15] Therefore, we have chosen to discuss many of the irradiation reactions in hexadecane in terms of a free-radical mechanism. The products observed and their change in distribution with conditions can be described by five primary reactions of the vibrationally excited molecule formed by irradiation of *n*-hexadecane.

$$n\text{-hexadecane} \xrightarrow{\sim} n\text{-hexadecane}^* \quad (1)$$

$$n\text{-hexadecane}^* \longrightarrow \text{primary hexadecyl}\cdot + \text{H}\cdot \quad (2)$$

$$n\text{-hexadecane}^* \longrightarrow \text{secondary hexadecyl}\cdot + \text{H}\cdot \quad (3)$$

$$n\text{-hexadecane}^* \longrightarrow \text{hexadecene} + \text{H}_2 \quad (4)$$

$$n\text{-hexadecane}^* \longrightarrow 2 \text{ smaller alkyl radicals}\cdot \quad (5)$$

$$n\text{-hexadecane}^* + \text{M} \longrightarrow n\text{-hexadecane} + \text{M} \quad (6)$$

The radicals and hydrogen atoms formed in reactions 2, 3, and 5 will undergo further reactions either with the parent hydrocarbon or with themselves.

$$\text{alkyl}\cdot + n\text{-hexadecane} \longrightarrow \text{paraffin} + \text{hexadecyl}\cdot \quad (7)$$

$$\text{H}\cdot + n\text{-hexadecane} \longrightarrow \text{H}_2 + \text{hexadecyl}\cdot \quad (8)$$

$$\text{H}\cdot + \text{H}\cdot + \text{M} \longrightarrow \text{H}_2 + \text{M} \quad (9)$$

$$\text{H}\cdot + \text{hexadecyl}\cdot \longrightarrow n\text{-hexadecane} \quad (10a)$$

$$\longrightarrow \text{H}_2 + \text{hexadecene} \quad (10b)$$

$$\text{H}\cdot + \text{alkyl}\cdot \longrightarrow \text{paraffin} \quad (11a)$$

$$\longrightarrow \text{H}_2 + \text{olefin} \quad (11b)$$

$$\text{alkyl}\cdot + \text{alkyl}\cdot \longrightarrow \text{paraffin} \quad (12a)$$

$$\longrightarrow \text{paraffin} + \text{olefin} \quad (12b)$$

$$\text{alkyl}\cdot + \text{hexadecyl}\cdot \longrightarrow \text{paraffin} \quad (13a)$$

$$\longrightarrow \text{paraffin} + \text{hexadecene} \quad (13b)$$

$$\longrightarrow \text{olefin} + n\text{-hexadecane} \quad (13c)$$

$$\text{hexadecyl}\cdot + \text{hexadecyl}\cdot \longrightarrow \text{dotriacontane} \quad (14a)$$

$$\longrightarrow n\text{-hexadecane} + \text{hexadecene} \quad (14b)$$

According to Topchiev,[9] primary carbon–hydrogen bond rupture is about half as probable as that for a secondary carbon–hydrogen bond in irradiated liquid or solid *n*-hexane. If the same ratio holds for *n*-hexadecane, with a much lower end-group concentration, reaction 2 will occur only 10% as often as reaction 3, and the majority of radicals formed by C–H rupture will be the various secondary hexadecyl isomers. The abstraction reactions 7 and 8 which may occur *via* either thermal or "hot" radicals are a further source of hexadecyl radicals. For thermalized species these reactions have activation energies[9,16] of 5–10 kcal. mole^{-1} and will be relatively unimportant in the solid at low temperature, and slow even at room temperature. The probability of reaction 7 decreases as the size of the alkyl radical increases, probably because only small species such as hydrogen atoms and methyl radicals can possess appreciable excess kinetic energy on formation, and it is the "hot" radicals which are responsible for much of the abstraction process. Secondary hexadecyl radicals will be formed preferentially in reactions 7 and 8, both on a statistical basis and because the secondary C–H bond is about 5 kcal. mole^{-1} weaker than a primary C–H bond in normal paraffins.[17] Thus the hexadecyl radicals occurring in the reaction scheme are largely a mixture of secondary isomers.

In the present experiments, conversions have purposely been kept low so that properties intrinsic to the undamaged material are observed. The results permit an evaluation of the relative importance of many of the above reactions under varying conditions of state and temperature. Chromatographic peaks are numbered in order of elution to permit direct comparison between programmed (Figure 1) and isothermal (Figure 2) analyses. Peak 13 in Figure 1 corresponds to the parent hydrocarbon *n*-hexadecane. Other peaks were not identified specifically because standards were not available for comparison of retention times and product yields were too small to permit mass spectrographic examination of trapped components. Some peaks are undoubtedly mixtures, with unresolved fine structure.

On this basis, observed products have been divided into three groups.

(1) Peaks 1–12, which elute before *n*-hexadecane, are scission products from further reactions of alkyl radicals produced in reaction 5. Topchiev[9] reports that CH_3–CH_2 rupture is only one-fifth as probable as CH_2–CH_2 rupture, but that all internal C–C bonds have a similar chance of rupture. Therefore almost all of the radicals formed in reaction 5 will be ethyl through tetradecyl and, because of their size, will not tend to abstract from the parent (reaction 7). They will combine and disproportionate with hydrogen atoms, with each other, and with hexadecyl radicals. Those

(15) M. G. Ormerod, *Polymer*, **4**, 451 (1963).

(16) A. F. Trotman-Dickenson, "Free Radicals," Methuen and Co. Ltd., London, 1959.

(17) G. C. Fettis and J. H. Knox, *Progr. Reaction Kinetics*, **2**, 1 (1964); T. L. Cottrell, "The Strengths of Chemical Bonds," 2nd Ed., Butterworth and Co. (Publishers) Ltd., London, 1958.

products with more than four but less than 15 carbon atoms will in general be sufficiently volatile to elute in this region. Both for electron and γ-irradiations about twice as much material was detected in this range for *n*-hexadecane irradiated as a liquid than as a solid. This may not be ascribed to the 15° difference in irradiation temperature, as temperature effects between 4 and −196° are relatively minor.[17] The reduction in light product yield in the solid would be caused by cage recombination of chain fragments in the crystalline solid resulting in a net suppression of main chain scission.

The various hexadecenes resulting from the dehydrogenation of *n*-hexadecane either molecularly (reaction 4) or by a radical mechanism (reactions 10b, 13b, and 14b) probably elute under the large parent peak 13.

(2) Peaks 14–35 are products of intermediate volatility, eluting after the parent hydrocarbon. These arise predominantly from the combination of radicals generated by scission (reaction 5) with various hexadecyl radicals (reaction 13a). In this region of the chromatograms, differences between solid and liquid irradiations are very pronounced, as was observed for *n*-hexane.[10] Hexadecane irradiated in the solid state yields a much smaller amount of intermediate products than the irradiated liquid. This difference may be explained by a net suppression of reaction 5 associated with enhanced cage recombination in the solid.

(3) Peaks 36–46 are believed to be mixed dimers, the main products of hydrocarbon irradiation,[9] resulting from the combination of hexadecyl radicals, reaction 14a. Since long-branched combination products of hexadecyl radicals will be difficult to resolve chromatographically and will be the first of the dotriacontane isomers to elute, a large, somewhat broadened peak containing unresolved dimers is anticipated at the onset of the dotriacontane region. Peaks 36 and above have therefore been identified with C_{32} paraffins.

No products with elution times greater than that of *n*-dotriacontane were observed. Although yields of dimer are comparable for solid and liquid hexadecane, the distribution of isomers is different. This may result from the fewer number of isomers possible by cross linking hexadecyl radicals aligned in the crystal lattice.

The probability of combination of two primary hexadecyl radicals would be of the order of 1–2% if radical encounters were random, but could be ten times this high if orientation effects restricted the interactions of primary radicals with secondary radicals. Normal dotriacontane which would result from the combination of primary hexadecyl radicals was not observed in the liquid, and only traces were found in the pure solid (~0.2% of the total dimer; the limit of detection is ~0.1%). However, for *n*-hexadecane containing about 5% *n*-octadecane a similar over-all product pattern was observed in both solid and liquid states, except that on irradiation in the solid state the yield of linear dimer increased to 2% of the total dimer. This may be explained on a crystallographic basis. That is, pure solid *n*-hexadecane assumes a triclinic modification, whereas following the addition of other paraffins the crystal habit is orthorhombic.[18] Since the environments of chain ends differ in these modifications, differences in end linking on irradiation may be anticipated.

Changes in the observed product pattern demonstrate the important influence of physical state on the number and distribution of radiation products. Chromatographic analyses are consistent with increased efficiency of main-chain scission in the irradiated liquid as compared to crystalline *n*-hexadecane. Mass spectrometric analyses of volatile radiation products from irradiated liquid and solid *n*-hexadecane indicate an evolution of more than twice the amount of C_1–C_4 hydrocarbons and about 30% more hydrogen following liquid irradiations. In addition, molecular weight measurements on irradiated liquid hexadecane are complicated by the presence of volatile scission products.

The presence of a substantial yield of product in the C_1–C_{15} range indicates that disproportionation processes occur both in solid and liquid phase irradiations although they are reduced in the solid. Recent results[19] indicate that disproportionation relative to combination is at least as important in condensed phases as in the gas phase.[20] In fact, Dixon, *et al.*,[21] found that disproportionation increased relative to combination with decreasing temperature for ethyl radicals in gas, liquid, and solid phases and in a number of solvents. All reactions from 10a through 14b should therefore contribute to the final products, the b reactions being responsible, together with molecular elimination, for most of the lower molecular weight products. The small change in yield of these products with temperature is consistent with low or zero activation energy reactions.

(18) A. Müller and K. Lonsdale, *Acta Cryst.*, **1**, 129 (1948).

(19) R. A. Holroyd and G. W. Klein, *J. Am. Chem. Soc.*, **84**, 4000 (1962); J. W. Falconer and M. Burton, *J. Phys. Chem.*, **67**, 1743 (1963); C. E. Klots and R. H. Johnsen, *Can. J. Chem.*, **41**, 2702 (1963).

(20) R. A. Holroyd and G. W. Klein, *J. Phys. Chem.*, **67**, 2273 (1963); J. G. Calvert, *Ann. Rev. Phys. Chem.*, **11**, 41 (1960); J. A. Kerr and A. F. Trotman-Dickenson, *Progr. Reaction Kinetics*, **1**, 105 (1961).

(21) P. S. Dixon, A. P. Stefani, and M. Szwarc, *J. Am. Chem. Soc.*, **85**, 2551 (1963).

Enhanced chain scission in irradiated liquid *n*-hexadecane relative to the crystalline solid may be pertinent to the behavior of polyethylene on irradiation. In extrapolating from hexadecane to polyethylene, G_{dimer} is equated to $G_{cross\ linking}$ and segmental mobility is assumed comparable in polyethylene and hexadecane near their respective melting points. It has been reported[22] that in the room-temperature irradiation of solid polyethylene, the radiation yield of hydrogen equaled the sum of cross linking and unsaturation. However, the yield of hydrogen exceeded the sum of cross linking and unsaturation for molten polyethylene irradiated at 142°.[22] This material-balance discrepancy would be eliminated if chain degradation were enhanced in the melt. Correcting for scission, the calculated value for the cross-linking yield would be increased. Similarly, the observation of increased radiation-induced gelation in crystalline polyethylene at 133°, compared to the supercooled melt at the same temperature,[3] may result from relatively greater chain scission in the latter.

Since dimer yields are quite close for electron-irradiated liquid and solid hexadecane at similar temperatures, while other radiolytic products are enhanced for the liquid, it follows that the formation and coupling of hexadecyl radicals to form dimer proceeds independently of chain fragmentation. This is consistent with two separate processes, C–C rupture and C–H rupture. Products from the former are suppressed by cage recombination in the solid crystalline state, whereas the yield of dotriacontane from the combination of hexadecyl radicals is little affected by change of state.

An increase in combination and disproportionation reactions of hydrogen atoms with trapped radicals is expected with decreasing temperature because of the 6–9 kcal. mole^{-1} greater activation energy for the abstraction process.[23] The reduced importance of reaction 8 relative to reaction 10 is probably a principal factor in the reduction of dimer yield with decreasing irradiation temperature (Table I). Enhanced collisional deactivation (reaction 6), at lower temperatures, would also be expected to reduce all product yields.

Similarly in polyethylene, cross-linking yields decrease with irradiation temperature to −80°.[11] Since the onset of segmental mobility in paraffins would occur at lower temperatures than in polyethylene, it is expected that G_{dimer} will decrease at lower irradiation temperatures in hexadecane. The small decrease in dimer yield with temperature indicates that differences in the irradiation of solid hexadecane at 4° and liquid hexadecane at 19°, such as hydrogen evolution and product distribution, may be properly assigned to an effect of physical state.

Since the total doses absorbed from energetic electron beams were varied between 1 and 20 Mrads, the dose dependence of radiation yields can be examined. For both liquid and solid hexadecane there is a small decrease in dimer yield with dose, whereas hydrogen yields do not evidence any clear trends with dose. Since olefinic products of irradiation can react with radicals or behave as electron traps, it is not surprising to find some dose dependence, even at low conversions. Since dimer yields for irradiation with 1-Mev. electrons at 2.5 Mrads min.$^{-1}$ are very close to those for γ-irradiation at 0.5 Mrad hr.$^{-1}$, the effects of the detailed nature of the ionizing radiation and the dose rate are minor.

Conclusions

The effects of irradiation of *n*-hexadecane are apparently independent of source and dose rate, the major effect being C–H rupture resulting in dimerization by cross linking to form isomers of dotriacontane and hydrogen. Chromatographic analyses of products indicate that scission of the paraffin chain is suppressed in the irradiation of *solid* *n*-hexadecane relative to irradiation in the liquid state. Mass spectrometric studies of gases evolved following irradiation and molecular weight measurements by vapor pressure depression are consistent with this observation. Increased chain scission in irradiated polyethylene melts may explain the reduction in gel measured under such conditions. From the distribution of isomeric dimers on irradiation of pure *n*-hexadecane we conclude that the main sites of cross linking are nonterminal. That is, cross linking occurs at random and there is no need to postulate radical-center mobility. However, irradiated solid *n*-hexadecane containing 5% *n*-octadecane end links to form linear dotriacontane to the extent of about 2% of total dimer.

Acknowledgment. We thank Dr. D. C. Bassett and Mrs. A. M. Hunt for helpful discussions on crystallographic aspects of the irradiation of paraffins and W. A. Sunder for experimental assistance.

(22) M. B. Fallgatter and M. Dole, *J. Phys. Chem.*, 68, 1988 (1964).
(23) K. Yang, *ibid.*, 67, 562 (1963).

Surface-Active Agents and Interfacial Transfer in Gas–Liquid Chromatography. A New Tool for Measuring Interfacial Resistance

by M. R. James, J. C. Giddings, and H. Eyring

Department of Chemistry, University of Utah, Salt Lake City, Utah (*Received January 25, 1965*)

It is found that the addition of cetyl alcohol to a chromatographic column, in which water is the liquid phase, greatly increases the width of a number of solute zones. By using a glass bead column where the major effects can be described by independent chromatographic theory (as shown here), one can isolate the influence of interfacial resistance. This provides a new means for measuring the latter. The advantages and disadvantages of this technique are discussed.

In recent years gas chromatography has evolved as an important tool for measuring physical properties. Physical data, like chemical analyses, are usually achieved with greater speed in this way than through conventional methods. Equilibrium properties (partition coefficients, adsorption isotherms), in particular, can be obtained with speed and accuracy.[1] The measurement of dynamic properties comprises a less developed field. So far, this has been confined to the measurement of diffusion coefficients.[2,3] However, it appears from the results obtained here that interfacial resistance of solute–solvent systems can also be measured by means of gas chromatography. The advantages and disadvantages, along with experimental results on a cetyl alcohol–water system, will be discussed here.

Theory

The commonly used measure of zone dispersion in chromatography is the theoretical plate height, defined by $H = d\sigma^2/dz$, where σ is the standard deviation of the concentration profile and z the distance of migration. Theory and experiment have shown that H is composed of many terms, accounting for longitudinal diffusion and nonequilibrium (mass-transfer) effects within the column.[4] The finite rate of crossing the interface between gas and liquid in gas–liquid chromatography leads to a plate height contribution of $C_k v$, where v is the downstream flow velocity and C_k is a nonequilibrium term given by[5]

$$C_k = \frac{8(1 - R)^2}{\alpha \bar{c}} \frac{V_g}{A_l} \qquad (1)$$

where α is the accommodation coefficient, $\bar{c}$ the mean molecular velocity, R the ratio of zone velocity to gas velocity, and V_g/A_l the ratio of gas volume to gas liquid interfacial area.

The procedure for obtaining α involves the measurement of the chromatographic parameter, C_k. The isolation of these various plate height terms has occupied considerable attention.[6] The coated glass bead column, as used here, has the advantage that all terms except C_k can be calculated independently with reasonable accuracy,[7] and C_k can be obtained by subtraction. For instance, the dominant term, C_l, in a column without surface-active agent is caused by the finite diffusion time in the liquid held at the contact point between beads. The precise geometry of these liquid units leads to an equation in which all parameters can be

(1) S. Kenworthy, J. Miller, and D. E. Martire, *J. Chem. Educ.*, **40**, 541 (1963).

(2) J. C. Giddings and S. L. Seager, *J. Chem. Phys.*, **33**, 1579 (1960).

(3) J. C. Giddings and S. L. Seager, *Ind. Eng. Chem., Fundamentals*, **1**, 277 (1962).

(4) J. C. Giddings, *Anal. Chem.*, **35**, 439 (1963).

(5) M. R. James, J. C. Giddings, and H. Eyring, *J. Phys. Chem.*, **68**, 1725 (1964).

(6) J. C. Giddings and P. D. Schettler, *Anal. Chem.*, **36**, 1483 (1964).

(7) J. C. Giddings, K. L. Mallik, and M. Eikelberger, *ibid.*, **34**, 1026 (1962).

obtained without recourse to chromatographic experiments, *i.e.*[7]

$$C_l = \frac{R(1 - R)d_p^2}{120D_l}\left(\frac{\%\rho_g}{3m\rho_l}\right)^{1/2} \quad (2)$$

where d_p is the average bead diameter, D_l is liquid diffusivity, % is the percentage of liquid loading referred to the weight of glass beads, ρ_g is glass density, ρ_l is liquid density, and m is the average number of contact points per bead. The fact that the experimental plate heights measured here agree well with an equation in which this is the dominant term confirms the essential correctness of this equation.

Experimental

Apparatus. Three columns packed with glass beads initially loaded with (1) water, (2) water and acetone, and (3) water, acetone, and cetyl alcohol were used in the experiments. They were of lengths 199.7, 196.0, and 200.0 cm., respectively. Because of the relatively high vapor pressure of water, helium carrier gas was bubbled through water and run through two presaturation columns before entering the chromatographic column. The presaturation columns consisted of a 10-m. tube filled with Chromosorb P (a ground firebrick) with 60% liquid load of water followed by a 2-m. column of beads also wet with water. The columns were placed in a water bath maintained at 2 ± 0.03°. A Carle microthermal conductivity detector was employed, with the detector block being maintained at room temperature. Short-term temperature fluctuations of the detector block were minimized by insulation. Because of condensation of water vapor in the inlet tubing of the detector, it was necessary to warm it slightly by means of a small heating tape. Samples were injected directly into the chromatographic column by means of a 10-μl. Hamilton syringe. Helium was metered through two pressure gauges and a 10-cm. segment of fine capillary tubing. The helium stream was split just prior to entering the chromatographic column to give approximately equal flow in the reference and sample sides of the detector. Volume flow of carrier gas was measured by means of soap bubble flow meters.

Surface-Active Agent. The surface-active agent not only should be effective in reducing the rate of absorption of solutes but also should be one that can be spread in a monomolecular film on the water without much change in the distribution of water on the beads. Experiments dealing with film formation on glass surfaces[8] show that cationic agents yield surfaces nonwettable to water. Such wetting agents would therefore not be suitable.

The effects of surface-active agents on the evaporation of water[9] and on the absorption of various gases[10] and vapors[11] have demonstrated the effectiveness of straight-chain saturated paraffinic alcohols. Of these, cetyl alcohol appears to be most effective.[12] Cetyl alcohol was found to have no effect on the wettability of the glass and also to possess desirable spreading qualities, and it was therefore selected for this work.

Coating Procedure. The glass beads were cleaned by refluxing them for 30 min. in H_2SO_4 containing a small amount of HNO_3 and leaving them overnight in aqua regia. They were then washed with water and dried with oxygen. All tubing was washed with reagent grade acetone and ether and dried with oxygen.

The beads were then weighed into an airtight flask, and water was added as the liquid phase. The wet beads were packed into the column with the system closed to the atmosphere to minimize evaporation. Cetyl alcohol was added to one group of beads by dissolving it in sufficient acetone to make it soluble in the binary acetone–water system. Enough cetyl alcohol was added to give a monomolecular covering plus 10% based on the surface area of the beads and 20.5 Å.^{2} as the effective cross section of a cetyl alcohol molecule.[13] In order to make sure that the additional broadening of the chromatographic zone was due to the surface-active agent rather than impurities in the acetone, a reference column was packed with essentially the same amount of water and acetone. In those cases where acetone was employed, it was, before use, evaporated off (after the column had reached the bath temperature) by passing carrier gas through the system until no further recorder drift was observed.

Materials. Stainless steel beverage tubing of 0.64-cm. o.d. and 0.05-cm. wall thickness was used. The glass beads were screened in the diameter range 0.12–0.10 cm. and found by visual examination to be of good spherical quality. Water, distilled twice from a basic permanganate solution, was used in both washing the equipment and serving as the liquid phase. Commercial grade cetyl alcohol was employed, and the following compounds were used as the chromatographic solutes: acetone, methyl acetate (MeAc), acrolein, dimethoxymethane (DMOM), and acetonitrile.

(8) G. J. Kahan, *J. Colloid Sci.*, **6**, 571 (1951).

(9) V. K. LaMer and L. A. G. Aylmore, *Proc. Natl. Acad. Sci. U. S.*, **48**, 316 (1962).

(10) F. Goodridge and D. J. Bricknell, *Trans. Inst. Chem. Engrs.* (London), **40**, 54 (1962).

(11) I. Langmuir and D. B. Langmuir, *J. Phys. Chem.*, **31**, 1719 (1927).

(12) L. H. Udani and K. F. Gordon, *A.I.Ch.E. J.*, **5**, 510 (1959).

(13) J. Adam, "Physics and Chemistry of Surfaces," 3rd Ed., Oxford University Press, London, 1941, p. 25.

Procedure. Liquid samples ranging from 0.1 to 0.4 μl. were injected into the columns. Variation of sample size in this range was found to have no effect on peak symmetry or width, thus ensuring linearity. Detector response was measured by a Leeds and Northrup Speedomax H strip chart recorder with a chart speed of 2 in./min. Results were obtained at two flow rates, 0.84 and 0.97 cc./sec. At these flow rates longitudinal diffusion in the gas phase (the B/v term of eq. 4) contributes less than 8% of the total plate height.

Results

An example of the effect of cetyl alcohol on the broadening of an acetone peak is shown in Figure 1. The additional spreading due to a surface-active agent in this typical case is very pronounced and thus convenient to work with. (Peak heights and centers were adjusted in the figure so as to coincide for the two cases.) The plate heights of chromatographic peaks obtained from each of the five samples in the three columns were determined both experimentally and theoretically. For the experimental values, the number of theoretical plates, N, was obtained by means of the standard equation[14]

$$N = 5.54\frac{y^2}{W_{1/2}^2} \quad (3)$$

where y is the distance on the chart from the point of injection to the peak maximum and $W_{1/2}$ is the peak width at half-height, as illustrated for one peak in Figure 1. The plate height is related to N by $H = L/N$, where L is the length of the column. Values of the plate height determined in this manner, $H_{W1/2}$, are given in Table I. Although the peaks obtained in the absence of the surface-active agent were quite symmetrical, with a ratio of the back to front width at half-height, b/f, of less than 1.25 in all cases, this did not hold true in the column containing the cetyl alcohol. Here, the ratio ranged from 1.3 to 1.7. In an attempt to take this asymmetry into consideration, assuming the tail is spurious, values of twice the front width at half-height, $2f$, were determined and used in place of $W_{1/2}$ in eq. 3. Values of the plate height determined in this manner, H_{2f}, are also listed in Table I.

Theoretical values of the plate height, H_{theor}, were calculated from the full equation[4,7]

$$H_{theor} = \frac{2\gamma D_g}{v} + \frac{R(1-R)d_p^2}{120D_l}\left(\frac{\%\rho_g}{3m\rho_l}\right)^{1/2} v + \frac{\omega d_p^2}{D_g} v = B/v + C_l v + C_g v \quad (4)$$

The obstructive factor γ was taken as 0.60[15] while a particle diameter, d_p, of 0.11 cm. was used. The glass to liquid density ratio, ρ_g/ρ_l, was determined to be 3.0, and the number of contact points per bead, m, was assumed to be 6.25.[7] The percentage of liquid load, %, was determined by assuming that when the liquid is added to the dry beads it distributes itself equally over the surface of the beads and the screw cap flask. Values of % so calculated were 0.40 ± 0.02% for each of the three columns. Loss of water during the period of use of the column was determined to be slight by the change in the retention times of the samples. Correction for this loss from one series of runs to another was made, however. Values of R and the geometrical factor[16] $\omega \cong 0.6 - 0.2R$ were obtained for each sample from the relationship

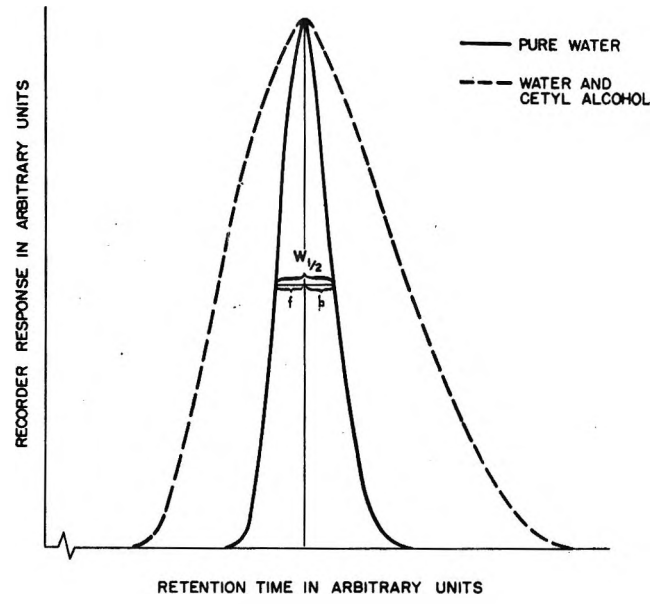

Figure 1. Chromatographic peaks for acetone with and without surface-active agent in the liquid phase.

$$R = \frac{V_g}{V_R + (V_g - V_A)} \quad (5)$$

where V_R and V_A are retention volumes of sample and air, respectively, and V_g is the free gas volume of the column. Equation 5 was used in preference to the usual equation, $R = V_A/V_R$, in order to take into consideration recorder and other instrumental time constants. The gaseous diffusion coefficient, D_g, was determined for each sample from the Hirschfelder

(14) A. B. Littlewood, "Gas Chromatography," D. H. Desty, Ed., Butterworth and Co. Ltd., London, 1958, p. 23.

(15) J. H. Knox and L. McLaren, *Anal. Chem.*, **36**, 1477 (1964).

(16) J. C. Giddings, *ibid.*, **34**, 1186 (1962).

Table I: Summary of Data

	H_2O column				H_2O + cetyl alcohol column						
Sample	Flow velocity, cm./sec.	$H_{W1/2}$, cm.	H_{2f}, cm.	H_{theor}, cm.	Flow velocity, cm./sec.	$H_{W1/2}$, cm.	H_{2f}, cm.	H_{theor}, cm.	$H_{2f} - H_{theor}$, cm.	C_k, sec.	α
MeAc	9.95	3.76	3.27	3.68	9.98	26.8	17.2	3.41	13.8	1.39	1.9×10^{-6}
	8.65	3.36	2.98	3.12	8.63	23.2	16.2	2.98	13.3	1.54	
Acetone	9.98	1.57	1.36	1.28	9.98	16.4	12.9	1.17	11.7	1.17	2.4×10^{-6}
	8.70	1.32	1.29	1.13	8.63	14.6	11.0	1.02	10	1.16	
DMOM	9.95	4.90	4.05	4.51	9.95	46.5	25.8	4.51	21.3	2.14	1.2×10^{-6}
	8.65	4.41	3.73	3.92	8.57	43.6	24.9	3.90	21.0	2.45	
Acrolein	9.95	3.92	3.49	3.59	9.95	27.7	17.3	3.18	14.2	1.42	1.8×10^{-6}
	8.70	3.72	3.06	3.15	8.59	21.8	14.5	2.74	11.7	1.36	
Acetonitrile	10.0	1.02	0.94	0.86	10.0	7.63	5.39	0.76	4.63	0.46	5.0×10^{-6}
	8.65	0.92	0.87	0.76	8.59	6.45	4.98	0.67	4.31	0.50	

equation[17] in the modified form given by Wilke and Lee.[18] Liquid diffusion coefficients, D_L, were obtained from the Wilke–Chang equation.[19] The mean flow velocity was determined from the measured volume flow and the column void space.

Values of H_{theor} obtained from eq. 5 are given in Table I. Deviation between H_{theor} and H_{2f} is less than 20% for all samples in the two columns which did not contain the surface-active agent. Assuming the same accuracy in determining the contribution of $B/v + C_l v + C_g v$ to plate height in the presence of cetyl alcohol, values of C_k may be determined from the difference $C_k v = H_{2f} - H_{theor}$, where H_{theor} is given by eq. 4. Values of $H_{2f} - H_{theor}$ and C_k are listed in Table I. The contribution of the H_{theor} terms to H_{2f} is less than 20% in every case.

By using eq. 1, values of the accommodation coefficient, α, may be obtained. As a first approximation, it is assumed that the liquid surface area is the same as the surface area of the beads. Determination of A_l values on this basis is justified in the present case by the small relative error from this source. These values, along with calculated values of V_g, R, C_k, and $\bar{c} = [(8kT)/(\pi m_2)]^{1/2}$ were then used to determine α. Average values of α obtained from the two values of C_k are listed in Table I. They lie roughly in the same range as those determined by classical methods for slightly soluble gases.

Langmuir and Langmuir,[11] departing also from the usual case of slightly soluble gases, studied the evaporation of saturated aqueous solutions of ether. They found that in the presence of a monomolecular film of various surface-active agents the rate of evaporation of ether was cut down to less than one-tenth of its former value. It was their conclusion that for most of the systems studied the additional resistance was due to the film stopping the surface currents which stir the liquid, rather than an impermeability of the film. One exception to this was observed on using cetyl alcohol as the surface-active agent. Here, the additional resistance could not be completely accounted for by their theory, and they credited it to the comparative impermeability of the alcohol film. This is confirmed by our measurement of a significant interfacial resistance in the presence of cetyl alcohol. This additional resistance is shown to be independent of surface mixing currents of the type discussed by Langmuir and Langmuir. Proof of this resides in the fact that without a surface-active agent our experimental values agree with theoretical where the latter is based on a stationary liquid hypothesis.

In earlier work by Giddings, Mallik, and Eikelberger,[7] experimental and theoretical values of C_l, without surface-active agents, were compared for different bead sizes and different liquid loads. For a bead size of $d_p = 0.0540$ cm. and a liquid load of 0.395%, the ratios of experimental C_l to theoretical C_l were in the neighborhood of 1.6. Comparison of this work with the present case, in which $\% \simeq 0.40$ and $d_p = 0.11$, is of interest in evaluating the theoretical expression for C_l, eq. 2. Theoretical values were determined as before, and average experimental values were obtained from $H_{2f} - B/v - C_g v$ with the latter two terms calculated as in eq. 4. These values and their ratios are given in Table II. The agreement is better than in the previous work with the ratios of experimental to theoretical C_l values lying within the limits of 0.93–1.16.

(17) J. O. Hirschfelder, R. B. Bird, and E. L. Spotz, *Trans. ASME* 71, 921 (1949).

(18) C. R. Wilke and C. Y. Lee, *Ind. Eng. Chem.*, 47, 1253 (1955).

(19) C. R. Wilke and P. Chang, *A.I.Ch.E. J.*, 5, 510 (1959).

Table II: Comparison of Theoretical and Experimental C_l

	H_2O column		
Sample	C_l (exptl.)	C_l (theor.)	$\frac{C_l \text{ (exptl.)}}{C_l \text{ (theor.)}}$
MeAc	0.310	0.334	0.93
Acetone	0.117	0.103	1.14
DMOM	0.396	0.426	0.92
Acrolein	0.328	0.338	0.97
Acetonitrile	0.073	0.063	1.16

The values of α given in Table I vary by only a factor of 4. Such uniformity is difficult to explain on the basis of structural or chemical differences between solutes when one considers the wide range represented. The uniform magnitude of the α-values is perhaps due to an effect arising in the surface film with only a weak dependence on solute. One possible explanation is to consider the undisturbed film as essentially impermeable to solute molecules. On this basis a solute molecule will pass through the interface only when there is a momentary fracture or "hole" in the film. In this case, the size of the solute molecule rather than any structural differences will be the important factor. Since the solute molecules used in this study are comparable in size, one would expect them to give similar values of α, as observed. Further studies using a wider range of solute–solvent systems, as well as a variety of surface-active agents, would be useful in determining the exact nature of this effect.

Gas–Liquid Chromatography as a Tool for Measuring α

The potential of gas–liquid chromatography (g.l.c.) as compared with the classical methods of measuring α is not yet entirely clear. It appears that g.l.c. might be complementary to the established methods, as will be discussed. The success of any method depends on making interfacial resistance the rate-controlling (or at least a rate-influencing) step in place of dominance by diffusion through the gas or liquid phase. In g.l.c. this is done automatically since, owing to the finely divided space, all diffusion paths are relatively short. Nonetheless, one cannot, at this point, measure C_k values of less than $\sim 10^{-3}$ sec. Under favorable circumstances (small glass beads) this means that the method will not yield α unless $\alpha < 10^{-3}$, roughly the same limitation applying to other methods.

G.l.c. appears to differ from the classical methods in the kind of solute–solvent systems that can be successfully studied. The classical methods are best suited to slightly soluble gases in order to minimize the influence of gaseous diffusion. G.l.c. behaves in just the opposite way; low solubility leads to a high relative migration rate, R, and thus tends to render C_k of eq. 1 negligible so that it can no longer be measured. Solutes with high solubility can be measured much more effectively. Not only does C_k approach a maximum as R approaches zero, but also the chief competitor, liquid phase diffusion, goes to zero at this limit as shown in eq. 2. This difference in tractable ranges of solubility is one aspect of g.l.c. which complements existing methods.

G.l.c. is probably more suitable for the study of viscous solvents than the methods making use of a flowing liquid. One encounters here, as with any other method, slower liquid diffusion and thus more competition from this source. This can be partially avoided by adjusting liquid load and temperature to make R near zero. On the other hand, g.l.c. is probably not suitable for solvents composed of light molecules at fairly high temperature because of their volatility and subsequent loss from the column. One can use presaturation, as in the procedure reported here, but this works only to a point since gas decompression resulting from the inevitable pressure gradient (which maintains flow) leads to undersaturation.

The accuracy of the g.l.c. method relative to others depends very much on the particular system under study and the approach used. Previous work on interfacial mass transfer has been done with both dynamic and static systems. The dynamic methods make use of moving liquid in wetted-wall columns,[20] wetted spheres,[21] laminar liquid jets,[22] rotating drums,[23] rotating endless belts,[24] etc. Accuracy depends upon how well the flow field in the vicinity of the interface is known, the degree to which end effects have been minimized, and the accuracy of the analysis of the extremely small concentrations of gas which are absorbed.[24] A static method has been developed which incorporates the use of an interferometer. It is claimed to eliminate convection difficulties, but it still requires various corrections.[25]

The lower limit to which accommodation coefficients may be determined by any of these methods is in the neighborhood of 10^{-3}. Accuracy, on the other hand, is much less certain. Presumably, these errors are

(20) R. E. Emmert and R. L. Pigford, *Chem. Eng. Progr.*, **50**, 87 (1954).

(21) J. F. Davidson and E. J. Cullen, *Trans. Inst. Chem. Engrs.* (London), **35**, 51 (1957).

(22) P. Raimondi and H. L. Toor, *A.I.Ch.E. J.*, **5**, 86 (1959).

(23) P. V. Dankwerts and A. M. Kennedy, *Chem. Eng. Sci.*, **8**, 201 (1958).

(24) T. S. Govindan and J. A. Quinn, *A.I.Ch.E. J.*, **10**, 35 (1964).

(25) E. A. Harvey and W. Smith, *Chem. Eng. Sci.*, **10**, 274 (1959).

fairly large owing to the experimental problems, but it is difficult to evaluate these errors.[26]

A number of errors also exist in the present g.l.c. method. Some of these could be reduced quite easily while others are more intractable. Some error is encountered in using the total surface area of the glass beads in the theoretical equation. Owing to accumulation around the contact points, the actual liquid area is less by a calculable amount; this error, however, partially compensates for the area of liquid on the tube wall. These sources of error could be greatly reduced. Another source of error, and perhaps the main one here, is that the somewhat asymmetric peaks must be adjusted to a theory dealing with symmetrical "Gaussian" peaks. The discrepancy between $H_{W1/2}$ and H_{2f} in Table I reflects this difficulty. If one takes the mean between these two extremes it is rarely more than 30% from either. (We have used H_{2f}, feeling that this is more reasonable, but the error may nonetheless be up to 30%.) This error could undoubtedly be reduced to <5% by using smaller glass beads or a longer column. It will also be improved by present studies which are concerned with the origin of asymmetry (mostly tailing) in chromatography.[27]

Finally, some error is encountered by assuming that the plate height is an additive sum of C_l and C_k terms (plus some others). This is not strictly true. However liquid geometry is well enough understood that a numerical correction could be established using the nonequilibrium theory of chromatography.[4]

There is no reason why α-values cannot be measured using the more conventional porous (diatomaceous earth) solids of g.l.c. One would have more difficulty in determining surface area, however, and could not rely as heavily on theory (because of the complex pore space). At this point, therefore, glass beads coated with solvent would appear to provide the best medium for g.l.c. studies.

Acknowledgment. The help of Dr. S. J. Hawkes in setting up the experimental program is gratefully acknowledged. This work was supported by the U. S. Atomic Energy Commission under Contract No. AT (11-1)-1144 and by the National Science Foundation, Grant No. GP-153.

(26) L. J. Delaney and L. C. Eagleton, *A.I.Ch.E. J.*, **8**, 418 (1962).
(27) J. C. Giddings, *Anal. Chem.*, **35**, 1999 (1963).

The Effect of Solubilization by Surfactants on the Kinetics of Alkaline Decomposition of Indoaniline Dyes

by L. K. J. Tong, R. L. Reeves, and R. W. Andrus

Research Laboratories, Eastman Kodak Company, Rochester, New York 14650 *(Received January 26, 1965)*

The kinetics of alkaline decomposition of anionic indoaniline dyes have been studied over a wide range of concentrations of anionic, cationic, and nonionic solubilizing agents. The results are interpreted in terms of a model involving partitioning of the dye between the aqueous phase and micelles of the solubilizing agent. From the kinetic data alone, the partition coefficient, K, and the rate constant for reaction of the solubilized dye, k_m, can be calculated in the case of the nonionic and anionic solubilizing agents. The critical micelle concentrations (c.m.c.) can be estimated from the sharp break that occurs in a plot of rate constant against concentration of the anionic and nonionic agents. The model fails for the cationic agent, and the data indicate that a 1:1 complex forms between the anionic dye and cationic agent at concentrations well below the c.m.c. The data indicate that both electrostatic and geometric factors may be important in determining the degree of solubilization and the reactivity of the solubilized substrate.

In reaction systems where the components themselves have colloidal properties or where colloids are added deliberately to alter the reaction, the kinetics are sensitive to the state of dispersion of the reactants. The kinetics may be interpreted if the colloidal properties of the system are known, or conversely, knowledge of the colloidal properties of a system may be gained from kinetic measurements. We have made such measurements in solutions of anionic, cationic, and nonionic surfactants and have evaluated critical micelle concentrations (c.m.c.), solubilization constants, and rate constants for the solubilized substrates. The derived values of the c.m.c. agree with values determined independently. The alkaline hydrolysis of the anionic indoaniline dyes,[1,2] I and II, was chosen as a model system because the high extinction coefficients permitted their use at very low concentration without perturbation of the colloidal properties of the medium. These dyes offered the additional advantages of water solubility, differing degrees of solubilization, and a reaction free from side reactions. The model is similar to the one used in an earlier publication on the effect of solubilizing agents on the kinetics of formation of indoaniline dyes.[3] We assume that: (1) the dyes are solubilized in surfactant micelles, a well-known phenomenon[4]; (2) the dyes are distributed between the aqueous and the micellar phases with a constant "distribution coefficient"; and (3) the rate constant for solubilized dye is different, in general, from that of the free dye.

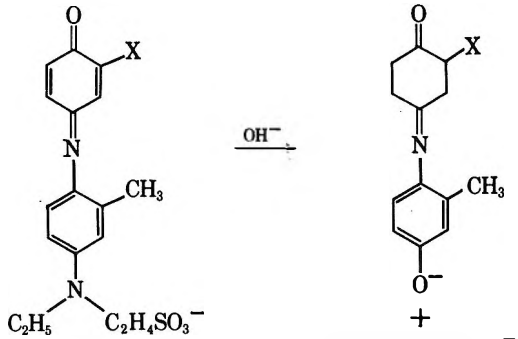

I, X = $-CONHC_6H_5$
II, X = $-CONH_2$

The effects of solubilizing agents on equilibria and

(1) (a) R. Möhlau, *Ber.*, **16**, 2843 (1883); (b) *ibid.*, **18**, 2913 (1885).

(2) S. Hünig and W. Daum, *Ann.*, **595**, 131 (1955).

(3) L. K. J. Tong and M. C. Glesmann, *J. Am. Chem. Soc.*, **79**, 4306 (1957).

(4) M. E. L. McBain and E. Hutchinson, "Solubilization and Related Phenomena," Academic Press Inc., New York, N. Y., 1955.

the kinetics of reaction of ionic and nonionic organic substrates have been reported.[5,6] The results have been interpreted in terms of solubilization of the substrates in micelles.

We have tried here to determine the "distribution coefficients" and the rate constants of the solubilized and free dyes by means of kinetic measurements alone.

Treatment of Data

The spectrophotometric method of following dye decomposition in the presence of solubilizing agents gives only the over-all rates. We assume that these rates can be expressed according to the equation

$$-(V_a + V_m)\frac{d\bar{C}}{dt} = k_a V_a C_a + k_m V_m C_m \qquad (1)$$

where V_m = the volume of the micelles ≈ volume or weight of solubilizing agent added (corrected for the concentration of free molecules when necessary), V_a = the volume of aqueous buffer, C_m = the concentration of dyes in (or on) the micelles (solubilized dye), C_a = the concentration of dyes in the aqueous region (free dye), k_m = the pseudo-first-order rate constant of solubilized dye, k_a = the pseudo-first-order rate constant of unsolubilized dye, and $\bar{C}$ = the average concentration of dye related through the equation

$$(V_a + V_m)\bar{C} = V_a C_a + V_m C_m$$

We also assume that the dye distribution has a constant coefficient

$$\frac{C_m}{C_a} = K \qquad (2)$$

Then the combination of eq. 1 and 2 leads to eq. 3, where k is the measured pseudo-first-order rate constant.

$$k = \frac{-d \ln \bar{C}}{dt} = \frac{k_a - k_m}{1 + K(V_m/V_a)} + k_m \qquad (3)$$

Under special conditions we obtain two equations having applications here.

(a) When $k_a >> k_m$ and $K >> V_a/V_m$

$$k \cong \frac{k_a}{K}\left(\frac{V_a}{V_m}\right) + k_m \qquad (3a)$$

(b) When $k_m = 0$ and the value of K is comparable to V_a/V_m

$$k \cong \frac{k_a}{1 + KV_m/V_a} \qquad (3b)$$

Results and Discussion

To use equations 3, 3a, and 3b we must be able to evaluate V_m, the volume of micelles in the system. As an approximation, we shall use for V_m the volume (in milliliters) or weight (in grams) of solubilizing agents added in making up the solutions, and, when necessary, we shall correct for the concentration of unassociated solubilizing agents by assuming this to be the critical micelle concentration (c.m.c.).

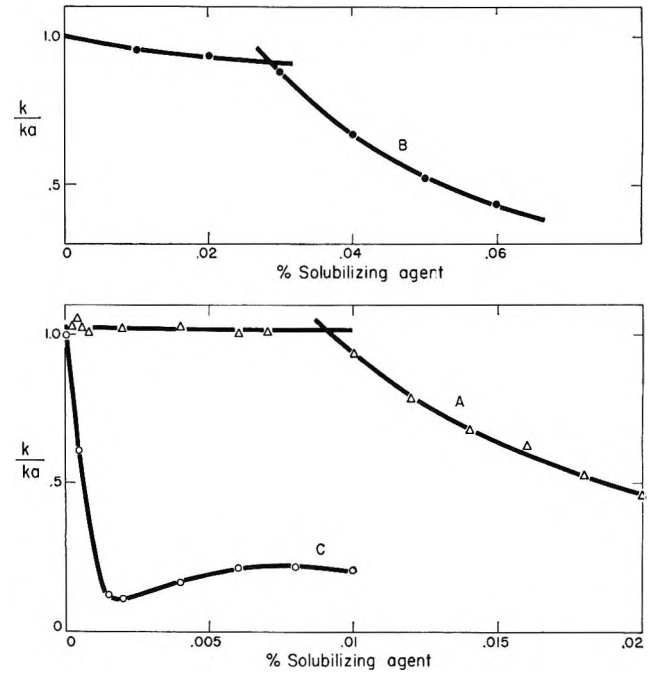

Figure 1. The effect of solubilizing agents on the rates of deamination of dye I at concentrations near the c.m.c.: curve A, Triton X-100; curve B, sodium lauryl sulfate; curve C, Aerosol SE; temperature, 25°; pH 10.1; μ 0.2.

The derivation of eq. 3 is based on the assumption that the effect of solubilizing agent on the rate of decomposition involves the solubilization of the dyes in micelles; therefore, it predicts that no change is to be observed below the c.m.c. and an abrupt change in rate will occur at this concentration. The concentration of dye used here is sufficiently low that it will not alter the c.m.c. values, which were determined in its absence. As shown in Figure 1, the expected results were observed for dye I with the two solubilizing agents: Triton X-100 (nonionic) and sodium lauryl sulfate (anionic). However, Aerosol SE (cationic) has an entirely different effect on the same dye. Curve C of Figure 1 shows a steep negative slope at the initial addition of solubilizing agent, suggesting strong interaction

(5) (a) E. F. J. Duynstee and E. Grunwald, *J. Am. Chem. Soc.*, **81**, 4540 (1959); (b) *ibid.*, **81**, 4542 (1959).

(6) (a) M. J. A. Behme and E. H. Cordes, *ibid.*, **87**, 260 (1965); (b) M. J. A. Behme, J. G. Fullington, R. Noel, and E. H. Cordes, *ibid.*, **87**, 266 (1965).

between the dye and Aerosol SE, perhaps formation of a stable complex. The interpretation can be made quantitative upon further consideration of the situation. Referring to Figure 1, (1) curve B shows a break at 0.03% sodium lauryl sulfate; the published[7] c.m.c. at the ionic strength used here (0.20) is 0.035%. (2) Curve A shows a break at 0.009% Triton X-100; we determined the c.m.c. to be 0.008% by an independent method. (3) The tangent of curve C at zero Aerosol SE has a value of $k/k_a = 0.1$ (the minimum of the curve) at 10^{-3}%. Aerosol SE, with a molecular weight of 549, is in equimolar ratio with the dye (1.25×10^{-5} M) at 0.69×10^{-3}%. This strongly suggests that the initial rapid decrease in rate, which occurs at concentrations of Aerosol SE well below the c.m.c. of 0.003%,[8] is associated with the formation of a 1:1 complex between the anionic dye and the cationic solubilizing agent. The complex is considerably more stable toward nucleophilic attack by hydroxide ion than is the free dye. The fact that little change in rate occurs as the concentration of solubilizing agent is increased above the c.m.c. indicates that the rate of deamination of the solubilized dye is nearly the same as that of the complex. It is therefore concluded that the method of analysis just outlined cannot be applied to mixtures of dyes and solubilizing agents having opposite charges.

At higher concentrations of solubilizing agents, the results were analyzed graphically from the plots of k *vs.* V_a/V_m according to eq. 3 or one of the simplified forms. The data are plotted in Figures 2 and 3. The derived constants k_m and K, when obtainable, are listed in Table I. As pointed out earlier, the results for dye I in the presence of Aerosol SE cannot be simply interpreted; however, k_m can still be obtained by empirical extrapolation, but it should then be interpreted as the reactivity of the solubilized complex. The slope in this case has no simple interpretation. Qualitatively, the linear relationship between the rate and V_a/V_m for dye I (Figure 2) corresponds to the case where $K >> V_a/V_m$ and $k_a >> k_m$ (eq. 3a) and shows that this dye is strongly solubilized by sodium lauryl sulfate and Triton X-100. In contrast, the curvilinear relationship shown in Figure 3 for dye II corresponds to the case given by eq. 3b, where K is comparable to V_a/V_m, and shows that this dye is only weakly solubilized. The solid line in Figure 3 was calculated using eq. 3b and the constants given in Table I. It is significant that the distribution coefficient for dye II is the same for both the nonionic and the anionic solubilizing agents, whereas dye I is more strongly solubilized by the nonionic agent.

In the absence of solubilizing agent, there is a slight dependence of rate on the concentration of dye I. At 5 $\times 10^{-5}$ M, at which most of the experiments were carried out, the mean rate constant at pH 10.1 is 1.5×10^{-3} sec.$^{-1}$, whereas the rate constant extrapolated to zero dye concentration is 1.9×10^{-3} sec.$^{-1}$. The latter value was used in the calculation of K by eq. 3 because in the presence of solubilizing agent the concen-

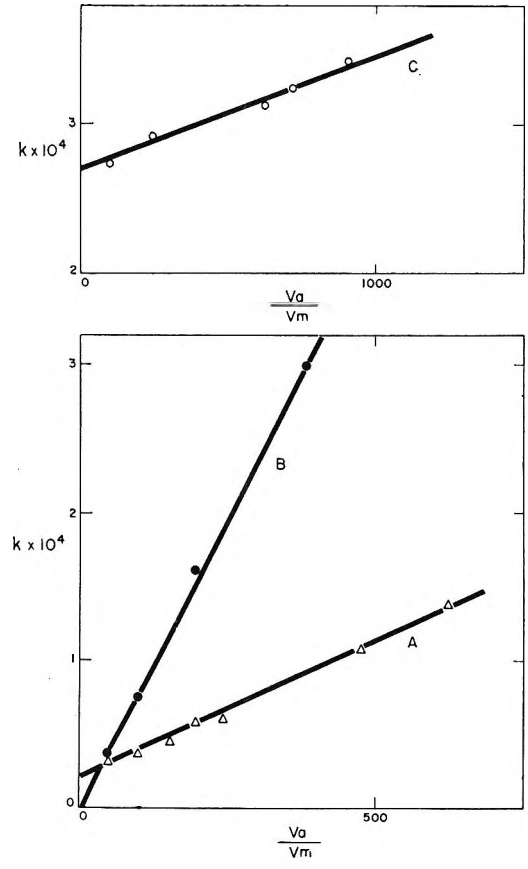

Figure 2. Plots of rate constants for deamination of dye I against V_a/V_m at concentrations of solubilizing agents much greater than the c.m.c.: curve A, Triton X-100; curve B, sodium lauryl sulfate; curve c, Aerosol SE.

Table I: Reaction Rate Constants of Solubilized Dyes and Distribution Constants

Solubilizing agent	Dye	k_m	K
Sodium lauryl sulfate	I	$<0.02 \times 10^{-4}$	4.6×10^3
Triton X-100	I	0.10×10^{-4}	20×10^3
Aerosol SE	I	2.7×10^{-4}[a]	...
Triton X-100	II	0 (assumed)	2.1×10^2
SLS	II	0 (assumed)	2.1×10^2

[a] Rate constant for solubilized complex.

(7) K. Aoki and J. Hori, *Bull. Chem. Soc. Japan*, **29**, 104 (1956).

(8) C. M. Judson, A. A. Lerew, J. K. Dixon, and D. J. Salley, *J. Phys. Chem.*, **57**, 916 (1953).

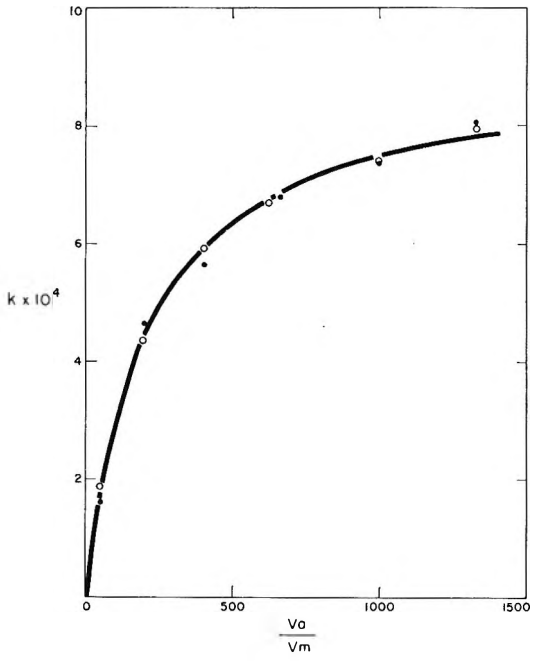

Figure 3. Plot of the rate constant for deamination of dye II against V_a/V_m at concentrations of solubilizing agents much greater than the c.m.c.: open circles, Triton X-100; closed circles, sodium lauryl sulfate; solid curve calculated from eq. 3b.

tration of free dye is very low and the extrapolated value is more appropriate. For dye II, there is no measurable dependence of the rate on dye concentration up to 5×10^{-5} *M*; the rate constant was found to be 9×10^{-4} sec.$^{-1}$. The decrease in rate with concentration is suspected to be due to aggregation of dye. This would be expected to be more pronounced for dye I than for dye II, since the former is more hydrophobic because of the extra benzene ring. The difference is also borne out by the fact that the distribution coefficient, *K*, in Triton X-100 is 100 times larger for dye I than for dye II. The fact that *K* for dye I is smaller in the anionic than in the nonionic solubilizing agent might suggest that electrostatic repulsion from the similar charges on the dye and the solubilizing agent is an important factor in determining the solubilization. The equal values of *K* for dye II in the same two solubilizing agents, however, indicate that relative charge types may not be as important as geometric factors.

It is interesting that the rate constants of the solubilized dye I fall in the same order as would be expected when the electrostatic interaction between the micelles and the attacking OH^- is considered. This observation is in agreement with that reported by Duynstee and Grunwald on the rates and equilibria of alkaline fading of triphenylmethane dyes.

The reaction site in the indoaniline dyes studied here is near the hydrophilic SO_3^- group, which is most probably oriented toward the aqueous solution and therefore quite accessible to the OH^- attack. For other substrates, where the reaction site is farther from the hydrophilic portion of the molecule, solubilization may provide greater protection to nucleophilic attack by anions by making the reaction site very inaccessible. Indeed, we have found that solubilization greatly reduces the rates of alkaline bleaching of indoaniline dyes similar to I and II but derived from substituted α-naphthols.[9] In these cases, the hydroxide ion attacks at the central >C=N— bond.[10]

Experimental

Materials. 2-Carbamyl-N-[2-methyl-4-(N-ethyl-N-β-sulfoethylamino)phenyl]-1,4-benzoquinoneimine (II) and the 2-(N-phenylcarbamyl) analog (I) were prepared by oxidative coupling of purified 2-methyl-4-(N-ethyl-N-β-sulfoethylamino)aniline with salicylamide and salicylanilide, respectively,[9] at pH 8–9. A large excess of the phenol was used to ensure good yields of the dye. The pH of the reaction solution was lowered to 7 as soon as the dye was formed and the solution was extracted with ethyl acetate to remove excess phenol. The aqueous solution of dye was saturated with salt, the dye was extracted into *n*-butyl alcohol, and the butanol solution was evaporated to dryness. The crude dye was purified by countercurrent distribution in a Craig apparatus having a capacity of 100 ml. of each phase per tube. The contents of several tubes at the center of the final distribution were evaporated separately at room temperature and the absorptivities of each fraction were determined. The sample having the highest absorptivity was used for the rate measurements. The major impurities in the preparation beside inorganic salts were colored materials having partition coefficients similar to, but greater than, those for the desired dyes. Solvents were therefore selected for the distributions that gave partition coefficients for the desired dyes of less than 1 in order to effect the greatest separation from other colored materials. In each case, the lower phase was water. Dye II was distributed through 17 stages, *n*-butyl alcohol being used as the upper phase.

Anal. Calcd. for $C_{18}H_{20}N_3NaO_5S \cdot H_2O$: C, 50.2; H, 5.1; N, 9.8. Found: C, 50.5; H, 5.4; N, 8.6.

Dye I was distributed through 30 stages, a 1:4 volume ratio of *n*-butyl alcohol–ethyl acetate being used as the upper phase.

(9) R. L. Reeves and L. K. J. Tong, *J. Am. Chem. Soc.*, **84**, 2050 (1962).

(10) R. L. Reeves and L. K. J. Tong, *J. Org. Chem.*, **30**, 237 (1965).

Anal. Calcd. for $C_{24}H_{24}KN_3O_5S \cdot H_2O$: C, 55.2; H, 5.0; N, 8.0. Found: C, 55.1; H, 5.4; N, 7.7.

Sodium lauryl sulfate and Aerosol SE (γ-stearamidopropyl-2-hydroxyethyldimethylammonium chloride) were commercial products that were purified further by recrystallization. The Triton X-100 (Rohm and Haas) was used without further purification.

Isolation and Identification of the Reaction Product. A solution of dye II, prepared at pH 8, was made basic to pH 11. The color changed from blue-green to purple within a few minutes. After 10 min., the pH was lowered to 7 and the product and excess salicylamide were extracted into ethyl acetate. The extract was dried, concentrated, and chromatographed on silica gel. The eluate (ethyl acetate) was concentrated and rechromatographed on Florisil. The salicylamide was eluted with acetone and the dye with methanol. The dye eluate (blue, ionic form) was treated with just enough acetic acid in methanol to neutralize it and was rechromatographed on silica gel. The final product was recrystallized from methanol, m.p. 195.5–196°.

Anal. Calcd. for $C_{14}H_{12}N_2O_3$: C, 65.6; H, 4.7. Found: C, 65.5; H, 4.6.

Separate experiments on dilute solutions showed that the deamination was quantitative.

Kinetic Measurements. In all runs a stock buffer solution containing 0.1 *M* sodium carbonate and 0.1 *M* bicarbonate was used. The pH was adjusted to 10.1 when necessary prior to a run. For the runs, the buffer was diluted in half by adding aliquots of freshly prepared stock solution of dye in water, and of solubilizing agent in water, and water to the desired volume. The rates were measured at 25° by following the decrease in absorbance of the substrate dye. The product dyes had low absorptivities at the analytical wave lengths. Plots of log $(A - A_\infty)$ *vs.* time were linear throughout each run. It was found that rates measured on different days were less precise than when a series was measured in a single day. However, the different series had good agreement when multiplied by correction factors for each series. Where possible, all the rate runs needed for a given experiment were carried out in one day, using common stock solutions.

Critical Micelle Concentration of Triton X-100. Twenty solutions of 1×10^{-4} *M* Rhodamine 6G dye in 0.1 *M* carbonate buffer (pH 10.1) containing concentrations of Triton X-100 from zero to 0.02% were prepared. The optical densities at 526 mμ were determined on a Beckman DU spectrophotometer and were plotted against concentration of solubilizing agent. At concentrations below the c.m.c., a straight line of positive slope was obtained. A second straight line of negative slope was obtained at concentrations above the c.m.c. The lines intersected at 0.008% Triton X-100, which was taken as the c.m.c.

The Reactivity of the Cyclic Polyenes toward Free Radicals. IV. Cyclohexadiene-1,3 and the Isopropyl Radical

by D. G. L. James and R. D. Suart

Department of Chemistry, University of British Columbia, Vancouver 8, British Columbia, Canada
(Received January 27, 1965)

A kinetic study of addition and metathesis between the isopropyl radical and cyclohexadiene-1,3 reveals that a significant fraction of the initial products of each reaction is consumed by disproportionation with the isopropyl radical to give propane. The fractions involved are 8 ± 3% of the initial adduct radicals and 34 ± 4% of the initial products of metathesis. Neglect of the propane formed from the latter source leads to significant errors in the calculation of the rate constants and Arrhenius parameters for both addition and metathesis, but neglect of the propane formed by the disproportionation of the initial adduct radicals does not lead to significant errors in any of these quantities. The rate constants for addition (k_7) and metathesis (k_6) between the isopropyl radical and cyclohexadiene-1,3 are given by: $k_7/k_2^{1/2} = 10^{(-7.0 \pm 0.2)} \exp(-5.8 \pm 0.4)10^3/RT$ cm.$^{3/2}$/molecule$^{1/2}$ sec.$^{1/2}$, and $k_6/k_2^{1/2} = 10^{(-6.8 \pm 0.4)} \exp(-7.1 \pm 0.6)10^3/RT$ cm.$^{3/2}$/molecule$^{1/2}$ sec.$^{1/2}$, where k_2 is the rate constant for the dimerization of isopropyl radicals. The significance of these results is discussed in conjunction with the value of the rate constant for metathesis between the isopropyl radical and cyclohexadiene-1,4.

Introduction

Metathesis between the isopropyl radical and cyclohexadiene-1,4 yields the cyclohexadienyl radical. If

the isopropyl radical is present in large excess the cyclohexadienyl radical is consumed by two reactions of combination and one of disproportionation. The

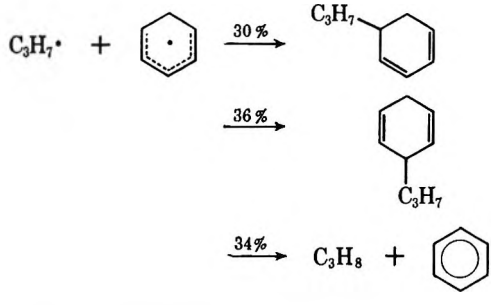

relative rates of these reactions were measured in a recent kinetic study of the photolysis of a gaseous mixture of diisopropyl ketone and cyclohexadiene-1,4 under carefully controlled conditions.[1] This system is not complicated by side reactions as the addition of the isopropyl radical to cyclohexadiene-1,4 proceeds too slowly to be detected.

The standard free energy at 95°[2] of cyclohexadiene-1,3 lies only 0.58 kcal./mole below that of cyclohexadiene-1,4, and both species possess activated methylene groups. The cyclohexadienyl radical should therefore be almost as easily formed from cyclohexadiene-1,3 as from cyclohexadiene-1,4 by metathesis with the

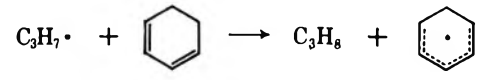

isopropyl radical. Accordingly, a gaseous mixture of diisopropyl ketone and cyclohexadiene-1,3 was illuminated with 3130-Å. radiation in this investigation. Conditions were again controlled to maintain the isopropyl radical in great excess over the cyclohexadienyl

(1) D. G. L. James and R. D. Suart, *J. Am. Chem. Soc.*, 86, 5424 (1964).

(2) R. B. Bates, R. H. Carnighan, and C. E. Staples, *ibid.*, 85, 3030, 3032 (1963).

Table I: Addition and Metathesis between the Isopropyl Radical and Cyclohexadiene-1,3[a]

Temp., °K.	Concn., molecules/ml. 10^{-17}[D]	Concn., molecules/ml. 10^{-17}[B]	$10^{-12}R$, molecules/ml. sec. CO	C_3H_8	C_3H_6	M'[b]	$10^{12}U_0$ (ml./molecule sec.)$^{1/2}$	$10^{13}U$ (ml./molecule sec.)$^{1/2}$	$10^{13}k_6/k_2^{1/2}$ (ml./molecule sec.)$^{1/2}$	$10^{13}V_0$ (ml./molecule sec.)$^{1/2}$	$10^{13}(V_0 + 0.342U)$ (ml./molecule sec.)$^{1/2}$	$10^{13}k_7/k_2^{1/2}$ (ml./molecule sec.)$^{1/2}$
315.3	3.14	1.53	33.9	11.2	10.00	0.841	17	13	(7)[c]	85	89	95
323.2	2.97	0.867	30.5	10.9	9.22	0.879	49	37	(29)[c]	107	120	127
329.5	3.08	1.47	33.0	11.4	8.62	0.795	51	38	30	119	132	141
340.0	2.71	1.01	34.6	11.9	9.37	0.811	62	46	35	162	178	190
349.2	2.46	1.07	28.8	9.9	7.13	0.771	74	55	43	176	195	207
363.2	3.59	1.08	38.1	12.7	8.68	0.725	128	95	77	251	283	302
374.4	2.84	0.628	39.4	13.9	9.25	0.757	180	134	107	382	428	456
384.2	2.84	0.427	34.6	12.6	8.60	0.794	226	168	136	434	491	522
394.7	2.54	0.277	38.7	14.3	10.70	0.846	271	202	166	502	571	608
399.9	2.49	0.260	35.4	12.9	9.45	0.825	290	216	173	590	664	708
406.1	2.48	0.292	35.6	13.2	8.93	0.804	330	246	202	609	693	738

[a] Reaction time = 300 sec. [b] $M' = R_{C_3H_8} - R_{C_6H_6} + R_{C_3H_6}/0.58/R_{CO}$, where $R_7 - R_{7d} = (1 - M')R_{CO}$. [c] The values in parentheses were excluded on statistical grounds.

radical, so that the consumption of the cyclohexadienyl radical should repeat the pattern described above.

Addition of the isopropyl radical to cyclohexadiene-1,3 was also observed in this system. Previous kinetic

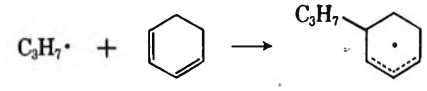

studies of radical addition to cyclohexadiene-1,3 have been carried out with the methyl,[3] ethyl,[4] and polyacrylonitrile[5] radicals; the radical homopolymerization[6-8] and copolymerization[5,9] of cyclohexadiene-1,3 have also been described. In each of these systems the addition of the radical to cyclohexadiene-1,3 was shown to occur much more rapidly than the corresponding addition to cyclohexadiene-1,4. Cyclohexadiene-1,3 is also the more reactive isomer towards the formation of a 1:1 adduct with ethyl azodicarboxylate, but this reaction occurs by a concerted addition–abstraction process whose rate is unchanged by the presence of hydroquinone, an effective scavenger of free radicals.[10]

The stereochemistry of free-radical addition to cyclohexadiene-1,3 has received little study apart from the identification of the *trans*-1,4 structure of polycyclohexadiene formed by the action of high-energy radiation upon a canal complex of cyclohexadiene-1,3 and thiourea.[11] The initial addition of a radical to the delocalized four-carbon electronic system of cyclohexadiene-1,3 is likely to occur at one of the terminal atoms of the system, as the allylic structure confers the greatest possible stability upon the radical adduct. The pattern of initial addition at the terminal atom of the delocalized system has been confirmed with 2,3-dimethyl butadiene-1,3[12,13] and 2,5-dimethyl hexadiene-2,4,[13,14] although the steric conditions differ greatly at the terminal atoms of these systems. This pattern has therefore been adopted in reaction 7 of the mechanism given below.

Experimental

Isopropyl radicals were generated in the presence of cyclohexadiene-1,3 by the illumination of a gaseous mixture of diisopropyl ketone and cyclohexadiene-1,3 with 3130-Å. radiation. The experimental conditions were chosen so that the isopropyl radical should always be present in great excess over the $C_6H_7\cdot$ and $C_9H_{15}\cdot$ radicals, and are listed in Table I.

The materials, diisopropyl ketone from the K and K Laboratories and cyclohexadiene-1,3 from the Columbia Organic Chemical Co., were purified by gas chromatography, using the 12-ft. Apiezon J column of the

(3) J. Gresser, A. Rajbenbach, and M. Szwarc, *J. Am. Chem. Soc.*, **83**, 3005 (1961).

(4) A. C. R. Brown and D. G. L. James, *Proc. Chem. Soc.*, 81 (1962).

(5) E. S. Ferdinandi, W. P. Garby, and D. G. L. James, *Can. J. Chem.*, **42**, 2568 (1964).

(6) S. F. Naumova and L. G. Tsykalo, *Vysokomolekul. Soedin.*, **3**, 1031 (1961).

(7) P. S. Shantarovich and I. A. Shlyapnikova, *ibid.*, **3**, 1364 (1961).

(8) B. V. Erofeev, S. F. Naumova, and L. G. Tsykalo, *Dokl. Akad. Nauk SSSR*, **147**, 106 (1962).

(9) G. Lefebvre and F. Dawans, *J. Polymer Sci.*, **A2**, 3277 (1964).

(10) (a) B. Franzus and J. H. Surridge, *J. Org. Chem.*, **27**, 1951 (1962); (b) B. Franzus, *ibid.*, **28**, 2954 (1963).

(11) J. F. Brown, Jr., and D. M. White, *J. Am. Chem. Soc.*, **82**, 5671 (1960).

(12) C. S. Hsia Chen and E. F. Hosterman, *J. Org. Chem.*, **28**, 1585 (1963).

(13) A. A. Oswald, K. Griesbaum, and B. E. Hudson, Jr., *ibid.*, **28**, 1262 (1963).

(14) A. A. Oswald, B. E. Hudson, Jr., G. Rodgers, and F. Noel, *ibid.*, **27**, 2439 (1962).

Beckman Megachrom instrument at 95 and 75°, respectively. The resultant diisopropyl ketone was essentially pure, but the cyclohexadiene-1,3 still contained somewhat less than 1% of benzene; this was not important as benzene is unreactive and was not directly estimated in this investigation. The apparatus and method differ from the description given in an earlier paper[1] in a few details.

The analysis followed the pattern of fractionation into CO, C_3, and residual samples, supplemented by gas chromatography. A C_6 hydrocarbon fraction could be separated from the other products and analyzed for diisopropyl and benzene as described previously.[1] The kinetic analysis requires precise values for the rates of formation of both diisopropyl and benzene, but greater precision was obtained if these rates were calculated from the rates of formation of propene and of reaction 6, respectively, as described in the next section. The residual fraction therefore nominally included the C_6 hydrocarbons in addition to the C_9H_{14}, C_9H_{16}, and $C_{12}H_{22}$ groups of isomers. This fraction was analyzed for its content of these isomers with the 150-ft. polyethylene glycol column of the Perkin-Elmer Model 226 chromatograph. The column was first held at room temperature for 10 min. to allow the passage of the C_6 hydrocarbons and the diisopropyl ketone, and subsequently held at 120° for the separation of the C_9H_{14}, C_9H_{16}, and $C_{12}H_{22}$ groups of isomers. The identification and estimation of these isomers will be discussed in the next section.

The Kinetic Analysis

The photolysis of diisopropyl ketone vapor by 3130-Å. radiation under the specified conditions conforms to the established mechanism (1–5). A recent study[1]

$$C_3H_7COC_3H_7 + h\nu \longrightarrow 2C_3H_7\cdot + CO \quad (1)$$

$$2C_3H_7\cdot \longrightarrow C_6H_{14} \quad (2)$$

$$2C_3H_7\cdot \longrightarrow C_3H_8 + C_3H_6 \quad (3)$$

$$C_3H_7\cdot + C_3H_7COC_3H_7 \longrightarrow C_3H_8 + \cdot C_3H_6COC_3H_7 \quad (4)$$

$$C_3H_7\cdot + \cdot C_3H_6COC_3H_7 \longrightarrow C_6H_{13}COC_3H_7 \quad (5)$$

of this photolysis gave $M = (R_{C_3H_8} + R_{C_6H_{14}})/R_{CO} = 0.99 \pm 0.05$, confirming the simple mechanism, and $R_{C_3H_8}/R_{C_6H_{14}} = k_3/k_2 = 0.58 \pm 0.04$, in good agreement with the literature value.[15]

Values of $k_4/k_2^{1/2}$ were obtained from the equation

$$k_4/k_2^{1/2} = (R_{C_3H_8} - R_{C_3H_6})/[D]R_{C_6H_{14}}^{1/2}$$

where [D] is the concentration of the ketone and R_Z is the rate of formation of the product Z; they were in good agreement with the published results,[15] and have been employed in this study.

If a gaseous mixture of diisopropyl ketone and cyclohexadiene-1,3 is photolyzed by 3130-Å. radiation under the conditions specified above, then the participation of the following reactions must be considered, in addition to reactions 1–5.

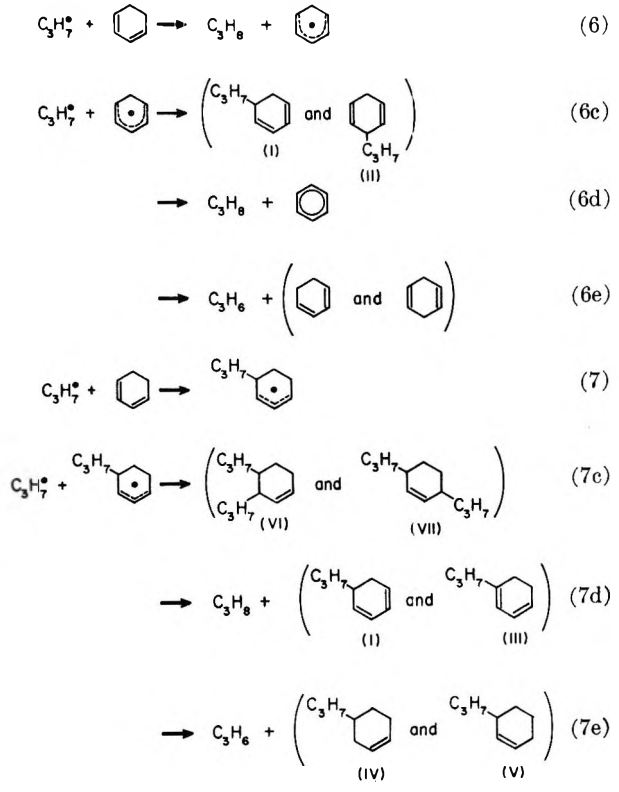

It is important to establish that the cyclohexadienyl radical formed by reaction 6 is removed from the system exclusively by reaction with the isopropyl radical. A quantitative study of the interaction of the cyclohexadienyl and isopropyl radicals under closely similar conditions of concentration, temperature, and pressure has been performed previously[1] by the photolysis of a gaseous mixture of diisopropyl ketone and cyclohexadiene-1,4. No cyclohexadiene-1,3 was found among the products, although even small traces could have been detected. This was shown to furnish convincing evidence that cyclohexadienyl radicals were not removed either by mutual interaction or by reaction 6e; they were consumed exclusively by reactions 6c and 6d. In the present system no cyclohexadiene-1,4 could be detected among the products, thereby confirming that the cyclohexadienyl radical did not react significantly with any radical other than the isopropyl radical, and that reaction 6e was negligible.

The combination and disproportionation reactions 6c and 6d therefore remain as the only significant re-

(15) C. A. Heller and A. S. Gordon, *J. Phys. Chem.*, **60**, 1315 (1956).

actions of the cyclohexadienyl radical; the products I and II from combination and the benzene from disproportionation were separated and measured by gas chromatography in the previous study[1] giving the ratios: $k_{6d}/k_{6c} = 0.52 \pm 0.09$ and $k_{6c}^{I}/k_{6c}^{II} = 0.85 \pm 0.09$. In the present system the products I and II could be identified and estimated by gas chromatography, but the amount of benzene formed in reaction 6d was much less than the residual benzene in the reactant cyclohexadiene-1,3, and for greater precision the rate of formation of benzene was estimated by the relationship

$$R_{C_6H_6} = R_6 k_{6d}/(k_{6c} + k_{6d}) = 0.342R_6 \qquad (8)$$

R_6 can be calculated from eq. 11.

Addition of the isopropyl radical to cyclohexadiene-1,3 yields the radical $C_9H_{15}\cdot$; we have made the reasonable assumption that this radical will resemble the cyclohexadienyl radical by reacting exclusively with the isopropyl radical. The relevant reactions are then 7c–e.

The disproportionation reaction (7d) yields the product I, which is also formed by the combination reaction (6c). Appropriately, the corresponding ratio of the peak areas $A(I)/A(II)$ exceeds the value of 0.85 ± 0.09 found for the system (isopropyl + cyclohexadiene-1,4) where the addition reaction is negligible. Comparison of the observed value of $A(I)/A(II)$ with 0.85 allows the estimation of the rate of formation of product I by reaction 7d. We have equated this rate with the rate of formation of propane by reaction 7d; this is completely accurate only if product III gives a chromatographic peak which augments the area of the peak due to product I, or if product III is formed in a negligible amount. A very small peak appears just before the peaks of I and II; it cannot be definitely assigned and may be due to one or more of the products III–V. The formation of product III involves the abstraction of a hydrogen atom from a position which is well shielded by the isopropyl group, and therefore k_{7d}^{III} is likely to be much smaller than k_{7d}^{I}. We conclude that the rate of formation of propane by reaction 7d may be estimated from the areas of the peaks due to I and II by means of the expression

$$\frac{R_{7d}}{R_6} = \frac{k_{6c}}{k_{6c} + k_{6d}} \frac{A(I) - (k_{6c}^{I}/k_{6c}^{II})A(II)}{(1 + k_{6c}^{I}/k_{6c}^{II})A(II)} = \frac{A(I) - 0.85A(II)}{2.81A(II)} = H \qquad (9)$$

R_{7d} can be estimated with reasonable precision by this procedure and is found to change the values of both $k_6/k_2^{1/2}$ and $k_7/k_2^{1/2}$ by amounts which are not significant in relation to the limits of error at the 5% probability level; the corresponding changes in the energies of activation and the pre-exponential factors also fail to be significant.

Reaction 6e has been shown to be negligible for the cyclohexadienyl radical, and it is very probable that reaction 7e is negligible for the $C_9H_{15}\cdot$ radical. The only chromatographic peak which could reasonably be assigned to products IV and V is the particularly small one mentioned above. This leaves reaction 3 as the only significant source of propene. The rate of formation of diisopropyl can therefore be estimated by the equation[1] $R_{C_6H_{14}} = (k_2/k_3)R_{C_3H_6}$, where $k_3/k_2 = 0.58 \pm 0.04$. This method gave results which were consistent with, but more precise than, those obtained from the direct estimation of diisopropyl by the separation and analysis of the C_6 fraction.

The combination reaction (7c) should yield four products, as VI and VII each represents a pair of geometrical isomers. Three peaks of roughly equal area were found on the chromatogram at appropriate retention times; perhaps one of the possible stereoisomers is not formed, or else the column fails to resolve one of the pairs.

The respective fractions, F and G, of the $C_6H_7\cdot$ and $C_9H_{15}\cdot$ radicals suffering disproportionation are

$$F = \frac{k_{6d}}{k_{6c} + k_{6d}} = 0.34_2; \quad G = \frac{k_{7d}}{k_{7c} + k_{7d}}$$

The kinetic analysis requires a procedure for the estimation of R_6, R_7, and G from accessible data.

Propene is formed only in reaction 3, propane only in reactions 3, 4, 6, 6d, and 7d. Moreover, $R_{6d} = FR_6$, $R_{7d} = GR_7 = HR_6$, $R_6 = k_6[B](R_{C_6H_{14}}/k_2)^{1/2}$, $R_7 = k_7[B](R_{C_6H_{14}}/k_2)^{1/2}$, and $R_{C_6H_{14}} = R_{C_3H_6}/0.58$. In these equations B denotes cyclohexadiene-1,3, and it is likely that H varies with temperature, whereas F and G do not.

The evaluation of $k_6/k_2^{1/2}$ and $k_7/k_2^{1/2}$ is based upon the equations

$$R_{C_3H_8} = R_3 + R_4 + R_6 + R_{6d} + R_{7d} \qquad (10)$$

$$R_6 = \frac{[R_{C_3H_8} - R_{C_3H_6} - [D]R_{C_6H_{14}}^{1/2}(k_4/k_2^{1/2})]}{(1 + F + H)} \qquad (11)$$

$$R_7 = [R_{CO} + R_{6d} + R_{7d}] - [R_{C_3H_8} + R_{C_6H_{14}}]$$
$$= [R_{CO} + (F + H)R_6] - [R_{C_3H_8} + R_{C_6H_{14}}] \qquad (12)$$

R_6 and R_7 can be evaluated if H is known. The value of H is determined by the reaction conditions, and it is known for a particular experiment only if $A(I)$ and $A(II)$ have been measured. Then we can make use of the expressions

$$\frac{k_6}{k_2^{1/2}} = \frac{1}{1+F+H}\left[\frac{R_{C_3H_8} - R_{C_3H_6}}{[B](R_{C_3H_6}/0.58)^{1/2}} - \frac{[D]}{[B]}\frac{k_4}{k_2^{1/2}}\right] \quad (13)$$

$$\frac{k_7}{k_2^{1/2}} = \frac{R_{CO} - \frac{R_{C_3H_6}}{0.58} - \frac{R_{C_3H_8} + (F+H)R_{C_3H_8}}{1+F+H}}{[B](R_{C_3H_6}/0.58)^{1/2}} - \frac{F+H}{1+F+H}\frac{[D]}{[B]}\frac{k_4}{k_2^{1/2}} \quad (14)$$

Alternatively, these rate constants may be calculated using the value of the parameter G, which is independent of reaction conditions. This parameter can be evaluated from the results of those experiments for which H has been measured. Rearrangement of the expression for R_7 gives the equation

$$\frac{1-G}{G} = \frac{R_{CO} + FR_6 - R_{C_3H_8} - R_{C_3H_6}/0.58}{HR_6} \quad (15)$$

which yields the value $G = 0.08 \pm 0.03$, independent of temperature. Let U and V_0 be defined by the equations

$$U = \frac{1}{1+F}\left[\frac{R_{C_3H_8} - R_{C_3H_6}}{[B](R_{C_3H_6}/0.58)^{1/2}} - \frac{[D]}{[B]}\frac{k_4}{k_2^{1/2}}\right]$$

$$V_0 = \frac{R_{CO} - R_{C_3H_8} - R_{C_3H_6}/0.58}{[B](R_{C_3H_6}/0.58)^{1/2}}$$

It is easily shown that

$$\frac{k_6}{k_2^{1/2}} = \frac{(1+F)(1-G)U - GV_0}{1+F-G} = 0.979U - 0.064V_0 \quad (16)$$

$$\frac{k_7}{k_2^{1/2}} = \frac{(1+F)(V_0 - FU)}{1+F-G} = 1.064V_0 + 0.364U \quad (17)$$

Results and Discussion

The kinetic results obtained for addition and metathesis between the isopropyl radical and cyclohexadiene-1,3 are given in Figure 1 and in Tables I and II. The importance of reactions 7d and 6d in the reaction scheme can be judged by comparison of the last six columns of the tables. The effect of neglecting the propane formed in 7d can be found by placing $G = 0$ in eq. 16 and 17, when $k_6/k_2^{1/2} \rightarrow U$, and $k_7/k_2^{1/2} \rightarrow V_0 + 0.342U$; the corresponding values are given in Table I. Statistical analysis reveals that the neglect of reaction 7d leads to no significant change in the values of the rate constants at 100° or in the Arrhenius parameters; the pairs of values are compared in Table II. The effect of neglecting both reactions 6d and 7d

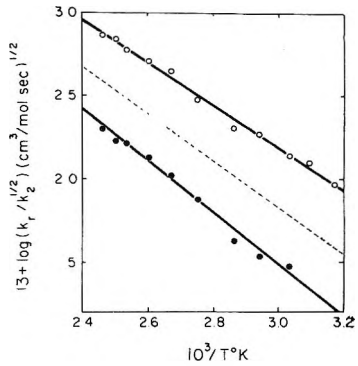

Figure 1. Reactions of the isopropyl radical with cyclohexadiene-1,3. Addition: $k_r = k_7$, $E_7 - {}^1/_2E_2 = 5.8 \pm 0.4$ kcal./mole; metathesis: $k_r = k_6$, $E_6 - {}^1/_2E_2 = 7.1 \pm 0.7$ kcal./mole. The broken line represents metathesis between the isopropyl radical and cyclohexadiene-1,4.

can be found by placing $F = G = 0$ in eq. 16 and 17 when $k_6/k_2^{1/2} \rightarrow U_0$ and $k_7/k_2^{1/2} \rightarrow V_0$, where $U_0 = (1+F)U = 1.342U$. Table I shows that this approximation involves much larger errors in the rate constants, and the corresponding Arrhenius parameters deviate significantly from the more accurate values of Table II. We conclude that eq. 16 and 17 are adequate to yield accurate values of rate constants and Arrhenius parameters from the experimental data of this investigation.

Cyclohexadiene-1,3 is significantly more reactive towards the isopropyl radical in addition than in metathesis; the ratio of the rate constants is 4.3 ± 1.5 at 100°. This difference in reactivity is due to a difference in the energies of activation of 1.3 ± 1.1 kcal./mole.

High intrinsic reactivity for cyclohexadiene-1,3 in radical polymerization is implicit in the value of 1.76 for the Alfrey–Price parameter Q.[5] It is not surprising, therefore, that high polymer is formed both by the radical homopolymerization of cyclohexadiene-1,3 in the solid state as a canal complex with thiourea at room temperature[11] and by the radical copolymerization of cyclohexadiene-1,3 with acrylonitrile in the liquid state at 60°.[5] In contrast, attempts to homopolymerize cyclohexadiene-1,3 under homogeneous free-radical conditions have not succeeded in forming polymer with a higher degree of polymerization than 12.[9] Clearly some process of structural chain termination is able to compete with the process of propagation far more efficiently in the third system than in the other two. One referee has suggested that this competing process is mutual combination, and its unusual relative efficiency in the third system is due to an exceptional slowness of homopropagation associated with the de-

Table II: Reactions of the Isopropyl Radical with Cyclohexadiene-1,3 and Cyclohexadiene-1,4[a]

Substrate	Reaction	No. of experiments	C	B	$13 + \log A_r/A_2^{1/2}$	$E_r - {}^1/_2E_2$, kcal./mole	$13 + \log k_r/k_2^{1/2}$[b]
Cyclohexadiene-1,3	Addition	11	6.024	1.276	6.0 ± 0.2	5.8 ± 0.4	2.61 ± 0.06
Cyclohexadiene-1,3	*Addition*	*11*	*6.016*	*1.283*	*6.0 ± 0.2*	*5.9 ± 0.3*	*2.58 ± 0.06*
Cyclohexadiene-1,3	Metathesis	9	6.156	1.557	6.2 ± 0.4	7.1 ± 0.7	1.98 ± 0.09
Cyclohexadiene-1,3	*Metathesis*	*9*	*6.136*	*1.514*	*6.1 ± 0.4*	*6.9 ± 0.6*	*2.08 ± 0.08*
Cyclohexadiene-1,4	Metathesis	14	6.044	1.407	6.0 ± 0.6	6.5 ± 1.0	2.27 ± 0.13

[a] The values in italics were calculated without correcting for the propane formed in reaction 7d; B and C are the coefficients of the straight lines, $13 + \log k_r/k_2^{1/2} = C - 10^3B/T$, fitted to the experimental results; k_r represents k_6 and k_7, respectively, for metathesis and addition; limits of error are given at the 5% probability level. [b] At 100°.

localized cyclohexenyl structure of the propagating radical species. This explanation must be reconciled with the formation of high copolymer with a molar composition close to 1:1 from mixtures of cyclohexadiene-1,3 and acrylonitrile covering a wide range of composition.[5] In such systems the corresponding copropagation process between a radical terminated by a cyclohexenyl unit and a molecule of acrylonitrile cannot be exceptionally slow, or inhibition would result; no doubt this copropagation process is promoted by a favorable polar effect, but so is the corresponding cross-termination process.

Degradative chain transfer to monomer may be considered as an alternative or complementary process for efficient structural termination in the homogeneous homopolymerization of cyclohexadiene-1,3. The cyclohexadienyl radical formed is highly delocalized and therefore unlikely to reinitiate by addition to cyclohexadiene-1,3. Degradative chain transfer competes with propagation for the same reactant species, and these processes are therefore analogs of reactions 6 and 7 in which a substituted cyclohexenyl radical has replaced the isopropyl radical. As the difference $E_6 - E_7$ is small, we may reasonably predict that the corresponding difference $E_f - E_p$ is also small, and that the ratio k_7/k_6 will provide a measure of the order of magnitude of k_p/k_f, the ratio of the rate constants of propagation and degradative chain transfer. The low degree of homopolymerization is then consistent with the low value of k_p/k_f given above.

Mutual termination of polymer radicals is eliminated from the mechanism of the emulsion homopolymerization of cyclohexadiene-1,3, and therefore the competition between the propagation and degradative chain transfer processes for polymer radicals can be assessed directly in an emulsion system. We have polymerized cyclohexadiene-1,3 (4.3 g.) in water (7.7 g.) containing sodium stearate (0.21 g.) and potassium persulfate (0.0064 g.) for 200 min. at 50°. A degree of polymerization of 6 was estimated for the homopolymer obtained (0.007 g.) using a Mechrolab Model 301A osmometer with benzene as the solvent. This value is of the same order of magnitude as those obtained for homogeneous homopolymerization under comparable conditions,[9] and we conclude that degradative chain transfer is the principal cause of the low degree of polymerization of cyclohexadiene-1,3 obtained under homogeneous conditions.

The rate constant of metathesis with the isopropyl radical at 100° is significantly higher for cyclohexadiene-1,4 than for cyclohexadiene-1,3, but the limits of error do not allow the identification of any significant variation among the Arrhenius parameters. Energetic and steric factors may be expected to combine to make cyclohexadiene-1,3 the less reactive isomer. First, it has the lower standard enthalpy of formation[2]; secondly, its methylene groups are adjacent, so that an unfavorable steric factor may be imposed by the mutual crowding of the methylene groups.

The results of ref. 1 and of this investigation indicate that a comparative kinetic study of the reactions of a series of simple primary, secondary, and tertiary alkyl radicals with the cyclohexadiene isomers should prove rewarding; such a study is in progress and will be described elsewhere.

Acknowledgment. We wish to thank the National Research Council of Canada for the financial support of this work, and for a studentship to R. D. S.

Studies on Spreading, Collapse, and Temperature and Compression Rate Effects on Monolayers of α,ω-Dicarboxylic Acids[1a]

by Peter M. Jeffers[1b] and Jerome Daen

Department of Chemistry, Lehigh University, Bethlehem, Pennsylvania *(Received January 28, 1965)*

Monolayers of α,ω-dicarboxylic acids with 12, 14, 16, 20, and 24 methylene groups were studied under conditions of varying compression rate and temperature on both acidified distilled water and concentrated ammonium sulfate solution substrates. The surface pressure isotherms indicated that both carboxyls are bound to the substrate and that there is some buckling of the hydrocarbon chain. Measurements of surface potentials and the temperature dependence of the equilibrium spreading pressure support this conclusion. Acidified ammonium sulfate substrates stabilized the films, reduced solution, and caused an increase in the surface potential and collapse pressures; collapse areas, however, were essentially unaltered. Equilibrium spreading pressure measurements indicated that most portions of the spread monolayer isotherms refer to nonequilibrium states; this fact explains the π–A dependence on compression rate. A collapse mechanism involving a "rolling-over" process is proposed.

Introduction

The saturated, long-chain α,ω-dicarboxylic acids, an interesting series of monolayer-forming materials, have not been extensively studied in the past. Adam and Jessop[2a] reported that the dicarboxylic acids formed rather unstable gaseous films which contracted under low pressure to condensed films collapsing at 8 to 12 Å.^{2}/molecule. Dervichian[2b] presented pressure–area isotherms for the dicarboxylic acids with 16 and 20 methylene groups (for convenience, diacids 16 and 20), which indicated that the films collapsed at 60 to 70 Å.^{2}/molecule under a pressure of 7 to 10 dynes/cm. Some data on diacid monolayers have been given by Hotta and Isemura.[3]

The present paper will extend the results previously reported from this laboratory.[4] Surface pressures and potentials for diacids 12, 14, 16, 20, and 24 will be presented for substrates of both acidified distilled water and concentrated ammonium sulfate solutions. Equilibrium spreading pressures will also be reported for several of the homologs. Compression rate effects and film collapse processes observed with the diacids will be interpreted in terms of the equilibrium pressures and a discussion of the monolayer collapse will be presented.

Experimental

Surface pressures were measured with an automatically recording null-type Wilhelmy surface balance and a surface tray machined from solid Teflon. Surface potentials were determined with an Ra^{226} ionizing air electrode,[5] a fiber-type calomel electrode, and a Keithley Model 620 electrometer. Though surface pressures were measured at 100% relative humidity, the existence of extensive parallel electrical leakage paths under saturated conditions required that surface potentials be investigated at ambient room humidity. The pressures were measured to ± 0.05 dyne/cm.; surface potentials were read to a precision of ± 3 mv., and surface areas were estimated to within 1%. Isotherms of

(1) (a) Partially supported by a grant from the U. S. Army Research Office (Durham); (b) National Science Foundation Cooperative Fellow, 1961–1964.

(2) (a) N. K. Adam and G. Jessop, *Proc. Roy. Soc.* (London), **A112**, 376 (1926); (b) D. G. Dervichian and M. Joly, *J. Phys. Radium*, **10**, 375 (1939).

(3) H. Hotta and T. Isemura, *Bull. Chem. Soc. Japan*, **25**, 101 (1952).

(4) P. M. Jeffers and J. Daen, Proceedings of the Fourth International Congress on Surface Activity, Brussels, 1964, in press.

(5) J. H. Schulman, L. Nanis, and M. Baruch, NONR226(64), June 1, 1960.

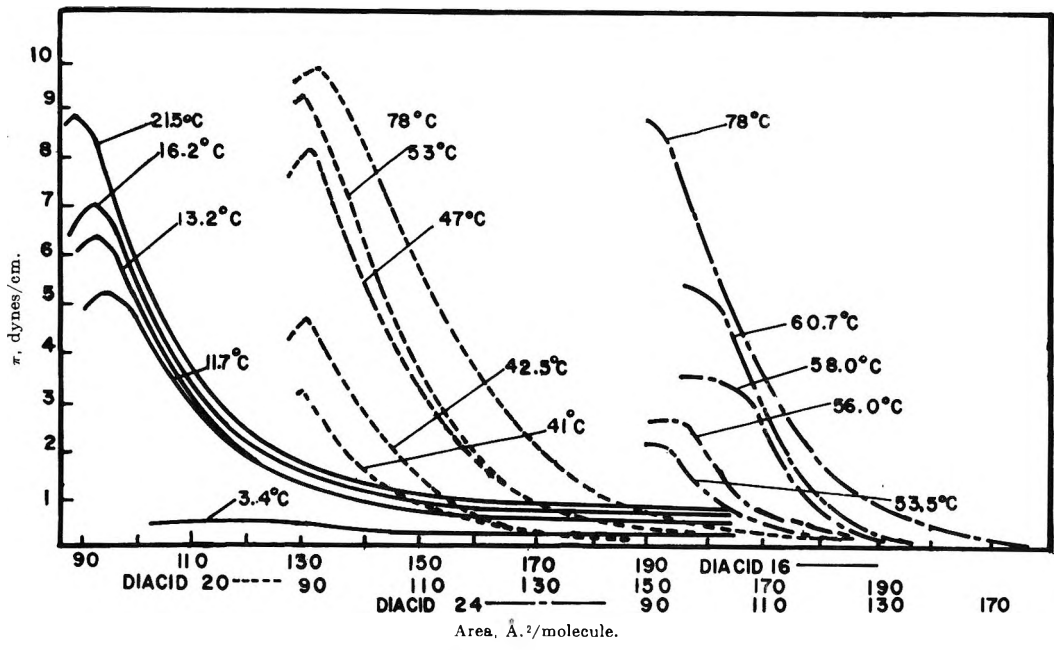

Figure 1. Force–area isotherms for various diacids on acidified distilled water at a compression rate of 21.8 Å.²/molecule min.

stearic acid obtained with this apparatus reproduced those reported by Gaines.[6]

Equilibrium spreading pressures were found by sprinkling finely powdered, crystalline diacid on a fixed area of 100 cm.² and measuring the resulting surface pressures with the Wilhelmy balance.

The dicarboxylic acids were synthesized by Kolbe electrolysis and were spread from chloroform solutions of *ca.* 0.4 mg./ml. concentration. Distilled water was acidified to pH 2.0 with sulfuric acid. Reagent grade ammonium sulfate was used without purification to prepare substrate solutions having a salt concentration of 30–40% by weight; these also were acidified with sulfuric acid. Details of the experimental techniques and material preparation have been given elsewhere.[4,7]

Results

Pressure–area isotherms for films of diacid 16, 20, and 24 on acidified water substrates are presented in Figure 1. That the diacids formed liquid- or vapor-expanded films was indicated by the isotherms and the film compressibilities. With rising temperature, the films expanded smoothly and collapse pressures increased over a 15 to 20° temperature span, from 1–2 dynes/cm. to about 10 dynes/cm.; collapse areas were sensibly independent of temperature.

No monolayer appeared to form below a temperature characteristic of each diacid. Diacid 32 did not seem to spread even at 90°. For diacid 24 a monolayer could be spread observably only above 53°, while the corresponding temperature for diacid 20 was 41°. At 3.4°, diacid 16 appeared to be just above its apparent characteristic spreading temperature and, in passing, it may be remarked that at this temperature diacid 14 formed a well-expanded film.

Figure 2 illustrates the isotherms obtained for diacid 16 on acidified distilled water at various compression rates. Generally, it was observed that all diacids exhibit a comparatively large decrease in collapse pressure and a slight increase in collapse area with decreasing compression rate.

Both the surface potential ΔV and the apparent dipole moment μ measured for diacid 16 on the acidic substrate are displayed in Figure 3. As with the pressure–area isotherm, the surface potential rose smoothly from 200 Å.²/molecule to collapse and was free from sharp breaks except at collapse. Collapse points on both the pressure and the surface potential isotherms were coincident. Within experimental error the surface moment–area curve was linear from 200 Å.²/molecule to collapse. It may be noted that the pressure increased by a factor of about 10, the surface potential rose by a factor of 2.5, and the surface moment changed by 30% between 200 and 90 Å.²/molecule.

Hotta and Isemura's values[3] for μ of 410, 350, and

(6) G. L. Gaines, *J. Colloid Sci.*, **15**, 321 (1960).

(7) P. M. Jeffers, Ph.D. Thesis, Lehigh University, Bethlehem, Pa., 1964.

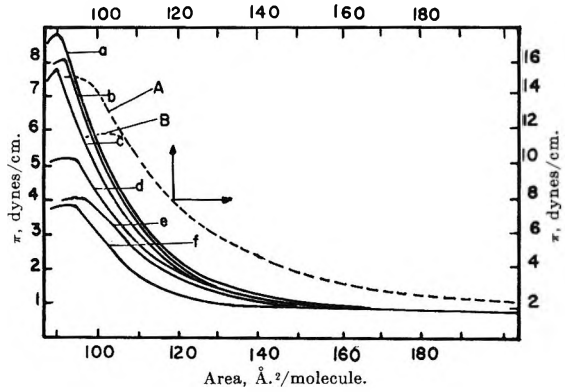

Figure 2. Compression rate effects on π–A isotherms. Acidified distilled water substrate, diacid 16 at 22° (in Å.²/molecule min.): a, 21.8; b, 10.9; c, 7.27; d, 2.91; e, 0.727; and f, 0.242. Acidified ammonium sulfate substrate, diacid 12 at 26° (in Å.²/molecule min.): A, 10.9; B, 2.9.

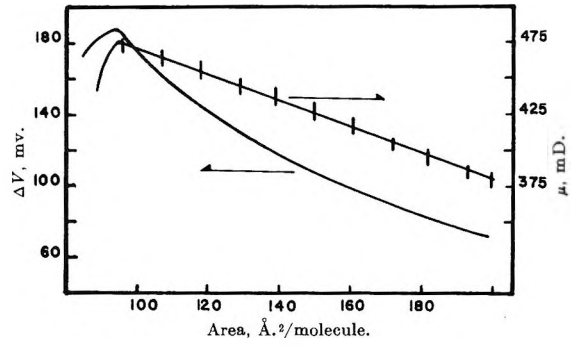

Figure 3. Surface potential and moment of diacid 16 at 22° and a compression rate of 10.9 Å.²/molecule min.

320 mD. at 100, 200, and 300 Å.²/molecule for diacid 16 are within about 10% of the present measurements. These authors reported diacid 16 as forming a gaseous film, in agreement with the present work, but did not present any isotherms in their paper, thus preventing further comparisons.

With diacids 12 and 14 at room temperature and with diacid 16 at temperatures above 60°, there was extensive film loss from the surface. Films were spread on concentrated ammonium sulfate solutions (as, *e.g.*, Brooks and Alexander[8]) to clarify whether solution or vaporization was the major responsible factor. Loss from diacid 12 and 14 films was essentially eliminated, confirming the hypothesis of solution of these smaller molecules into the water substrate. Moreover, on the salt substrate all of the diacid films were stable to much higher pressures with π attaining values of 20 dynes/cm. in some cases. Solubility was reduced so dramatically that diacid 10 which was completely soluble when spread on water at 25° formed a film on ammonium sulfate which, when compressed at a rate of 10.9 Å.²/molecule min., collapsed at 16 dynes/cm., and at an apparent area of 40 Å.²/molecule. Partial but far from complete solution of the film is inferred from this small collapse area.

The behavior of diacid 12 on ammonium sulfate solutions at room temperature and at two different compression rates is shown in Figure 2. Again, the trends noted on distilled water are evident, though on the salt substrate compression rate changes do not appear to displace the curves from each other. Isotherms for other diacids at various temperatures are presented in Figure 4. In these instances, the effect of temperature was the same as that for water substrates. As before, diacids 20 and 24 apparently would not spread below certain temperatures, but the initial spreading temperature was appreciably depressed on ammonium sulfate. At 25°, diacid 20 spread and was stable to 5 dynes/cm., while diacid 24 collapsed only at 6 dynes/cm. at 51°.

Surface potential–area isotherms for diacids 12, 16, and 20 on ammonium sulfate are displayed in Figure 5. The curves for diacids 12 and 16 were very similar and almost coincide within experimental limits; the shapes of the isotherms for diacid 16 on pure water and on salt are identical. For the diacid 16 film on ammonium sulfate, the curve, however, is displaced by 20 to 30 mv.

Measured values of equilibrium spreading pressure for diacids 10, 12, 14, and 16 may be found in Table I.

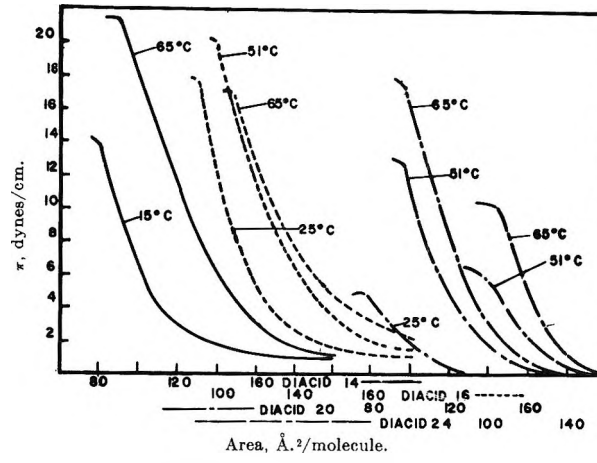

Figure 4. Force–area isotherms for various diacids on acidified ammonium sulfate at a compression rate of 10.9 Å.²/molecule min.

(8) J. H. Brooks and A. E. Alexander, Proceedings of the Third International Congress on Surface Activity, Cologne, 1960, Vol. II p. 196.

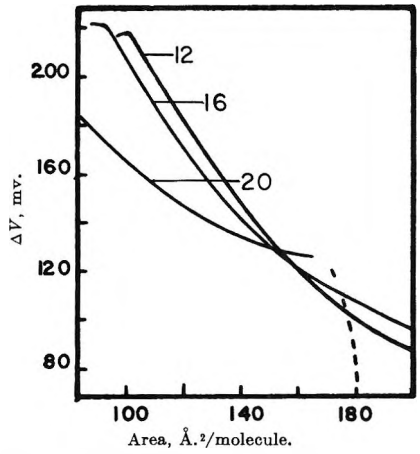

Figure 5. Surface potentials of various diacids on ammonium sulfate at 25° and 10.9 Å.²/molecule min.

Although the three smaller diacids were lost rapidly from spread films by solution into the substrate, the presence of excess surface crystal ensured the determination of acceptable equilibrium pressures. The recorded pressures were reached within 1 to 10 min. after the diacid crystals were applied to the surface and remained essentially constant thereafter.

Table I: Equilibrium Spreading Pressures (dynes/cm.)

Di-acid	Temperature, °C. 1°	20°	25°	31°	50°	60°
10	0.3	1.7	2.3	2.7	7.0	...
12	...	0.5	0.6, 5.5[a]	1.0	4.4	11.0[a]
14	...	...	0.07	0.25	2.0	...
16	...	...	0.04	0.12	0.4	6[a]
24	...	...	...	...	...	Small[a]

[a] Film on $(NH_4)_2SO_4$ substrate; all others on acidified distilled water.

To test equilibrium attainment with a diacid 10 film at 25°, the surface area was increased, then decreased by an amount sufficient to change the surface pressure momentarily by 0.5 dyne/cm. After the area increase, the pressure rose immediately to its original value, as expected, since spreading of diacid 10 was quite rapid and the reservoir of diacid crystal on the surface was sufficient to saturate the additional uncovered area. A slight decrease in pressure with time occurred shortly after the film was compressed; the original value of equilibrium pressure was not quite reached during the 15–30-min. observation period, this experiment meaning that the recorded equilibrium pressure values may be low by no more than 0.3 dyne/cm.

It can be seen that the equilibrium spreading pressures were considerably higher on the salt solution than on water. Spreading rates, as determined visually, for the diacids decreased with increasing chain length in agreement with Brooks and Alexander's findings for the fatty alcohols.[8]

Discussion

That no monolayer can be compressed indefinitely is well known; there are a number of different usages, however, of the term "collapse" appearing in the literature.[9–13]

It seems appropriate to term as collapse any process involving the transfer of molecules from the monolayer to any bulk phase. This definition would include solution, evaporation, and the formation of bulk crystals, but would not include reorientation within the film if unimolecular character were maintained. Under this definition, such processes as the "low pressure reversible collapse" discussed by MacRitchie would not be called a collapse since the protein molecules as a whole appear to remain anchored to the water surface, but collapse would include both the evaporation and solution found by Brooks and Alexander[10] in the fatty alcohol series. The distinction concerning collapse and reorientation evidently will be most significant in monolayers of macromolecular materials.

In this work, the diacid monolayers underwent collapse into a solid phase in addition to any accompanying dissolution or evaporation from the surface. Both solution and evaporation would depend on surface pressure, but only crystal formation would lead to the sharp break and rapid decrease in pressure observed with the diacids. Since the diacids melt only above 120°, the collapse was to a form of solid rather than to a liquid lens, although hydration of the carboxyls may have caused a different crystal structure from that usually found. It is known that the crystalline structure of fatty alcohols is influenced by the presence of water.[10]

The large collapse areas observed with all of the diacids under the various experimental conditions imply a horizontal configuration with both carboxyl groups

(9) N. K. Adam, *Proc. Roy. Soc.* (London), **A101**, 452 (1922).

(10) J. H. Brooks and A. E. Alexander, "Evaporation Retardation by Monolayers," V. K. La Mer, Ed., Academic Press, Inc., New York, N. Y., 1962, p. 245.

(11) F. MacRitchie, *J. Colloid Sci.*, **18**, 555 (1963).

(12) R. J. Goldacre, "Surface Phenomena in Chemistry and Biology," J. F. Danielli, K. G. A. Pankhurst, and A. C. Riddiford, Ed., Pergamon Press, New York, N. Y., 1958, p. 278.

(13) A. W. Adamson, "Physical Chemistry of Surfaces," Interscience Publishers, Inc., New York, N. Y., 1960.

anchored to the surface and with little vertical bowing of the hydrocarbon chain before collapse. Moreover, the maximum value of μ for diacid 16 is 475 mD.

Now, the surface potential for stearic acid at 22 Å.^{2}/molecule is 400 mv. and this corresponds to a surface moment of 230 mD. Thus, the apparent diacid dipole moment is just slightly greater than twice the value for stearic acid. Recognizing that the major contribution to the surface moment is that of the carboxyl groups, the diacid surface potentials are rather direct proof that each carboxyl in the diacid is anchored to the surface.

Additional perspective on these conclusions may be drawn from the energetics of the bulk-to-monolayer spreading process. In Table II are summarized thermodynamic quantities computed from the spreading pressure data already presented. As a result of the very low equilibrium spreading pressures and their small temperature coefficients, it is difficult to compute highly accurate values. It proved necessary to estimate areas for the lower molecular weight diacid equilibrium monolayers by extrapolation from isotherms for the larger diacids whose spread monolayers were essentially insoluble. These factors limit the reliability of the estimated energies and entropies to about $\pm 30\%$.

The heat of spreading was calculated using the Clausius–Clapeyron equation in the two-dimensional form proposed by Cary and Rideal[14] and discussed by Alexander and Goodrich[15]; free energies and enthalpies of equilibrium spreading were calculated following Harkins, Young, and Boyd.[16] For comparison, corresponding quantities for several monofunctional materials measured by Boyd[17] are included.

When, for example, entropies or latent heats of equilibrium spreading for the diacids are compared with corresponding properties of the monoacids, the interesting and significant fact emerges that the former are approximately twice as large as the latter. On the basis of moles of carboxyl group spread, one may say that the entropy change for the diacids is roughly that of the monofunctional acid. In other words, these thermodynamic results support the conclusion that both polar groups are bound to the substrate.

Table II: Estimated Energies and Entropies of Spreading for Several Diacids

Material	T, °C.	Q_s, kcal./mole	G_s, kcal./mole	H_s, kcal./mole	S_s, kcal./mole
Diacid 10	30	13	−0.47	12	42
Diacid 12	30	12	−0.36	12	40
Diacid 14	35	8.9	−0.18	8.7	29
Tridecylic	0	5.20	−0.38	4.82	19.0
acid[17]	30	7.52	−1.25	6.28	24.8
Myristic	5	6.39	−0.16	6.23	23.0
acid[17]	30	8.49	−0.89	7.60	28.0
Pentadecylic	15	4.69	−0.50	4.19	16.3
acid[17]	30	5.13	−0.77	4.36	16.9
Palmitic	15	5.01	−0.23	4.78	17.4
acid[17]	30	5.61	−0.52	5.09	18.5

It is somewhat surprising that the collapse areas do not show greater variation with chain length, since with a horizontal orientation the chain length might be expected to be an important determinant of the limiting area. Relatively slight flexibility of the extended hydrocarbon chain in the film is, of course, sufficient to account for this observation. The most obvious effect in passing from one member of the diacid series of the next is the relation of chain length to the temperature range of monolayer expansion. Thus the chain length effects are quite similar to those usually found in monofunctional homologous series.

When it is recalled that stearic acid is stable to 40–60 dynes/cm. depending on compression rate, the diacid collapse pressure of less than 10 dynes/cm. may appear unusual. However, the difference in orientation must not be forgotten. With the upright hydrocarbon chain in stearic acid films, 40 dynes/cm. is equivalent to about 140 atm. in three-dimensional pressure, while, assuming a film thickness of 6 Å. for the horizontal diacids, 10 dynes/cm. corresponds to 165 atm.

The strong dependence of the isotherms on compression rate indicates that the diacid monolayers are not equilibrium systems but are in fact metastable. Equilibrium spreading pressures for the diacids are indeed seen to be very low, so that most pressures attained on compression of the spread monolayers are above equilibrium values. Consistent with Cary and Rideal's statement[14] that the film-to-crystal transformation is frequently very slow, the diacid isotherms were very reproducible at a given compression rate. As a result, the films can perhaps be best described as quasi-equilibrium systems.

The measurements of equilibrium spreading pressures suggest that the initial spreading temperatures found for the diacid monolayer may, under the present experimental conditions, coincide with the temperature where the equilibrium spreading coefficient of the solid

(14) A. Cary and E. K. Rideal, *Proc. Roy. Soc.* (London), **A109**, 318 (1925).

(15) A. E. Alexander and F. C. Goodrich, *J. Colloid Sci.*, **19**, 468 (1964).

(16) W. C. Harkins, F. F. Young, and G. E. Boyd, *J. Chem. Phys.*, **8**, 954 (1940).

(17) G. E. Boyd, *J. Phys. Chem.*, **62**, 536 (1958).

crystal becomes positive. Such an observation is in agreement with Cary and Rideal's statement[14] that films of behenic acid, which contract spontaneously at room temperature, become stable at temperatures above that where the equilibrium spreading pressure becomes positive.

In this connection, the work of Fernandez, Aenlla, and Trillo,[18] who recently studied monolayers of diacid 20, a naturally occurring cork acid, at areas between 10,000 and 30,000 Å.^{2}/molecule, is pertinent. The fact that these workers could spread diacid 20 films at 15°, while the present investigation indicated condensed films of diacid 20 to form only above 41°, may be explained by the very dilute nature of the former system, the pressures measured being on the order of 0.002 dyne/cm. Under such conditions one would expect the decay toward the equilibrium state to be extremely slow. Thus, it appears that the characteristic temperatures observed in the experiments described here may very well be functions of the experimental conditions as are other monolayer phenomena. In other words, in such situations one must recognize the metastability when interpreting the observations.

With stearic acid, aggregates in the form of long wrinkles become visible upon collapse,[19] and similar visible aggregates are formed upon collapse of protein films.[14] With the diacids there was no visible evidence of this sort. It is likely that many tiny collapse sites were formed scattered over the entire surface; collapse proceeded into microcrystals rather than into a long, "folded" structure illustrated by stearic acid.

For the diacids on water there was no tendency for collapsed films to respread. Several films were compressed just past the collapse point, then were expanded immediately and subsequently left undisturbed. After 4 hr., recompression showed the films to have collapsed further rather than to have respread. On concentrated ammonium sulfate, a film of diacid 20 was compressed at 5° until collapse began; at this instant the film was expanded. Immediate recompression showed that the film had respread almost completely during the expansion. The equilibrium spreading pressures were considerably higher on ammonium sulfate than on water, and with expansion of the diacid 20 film, the surface pressure fell below the equilibrium spreading pressure so that re-expansion should have occurred as observed.

The stabilization of diacid films on ammonium sulfate, in addition to suppressing the solution process, is in accord with the results of Pankratov,[20] who noted both an expansion of the film and an increase in the surface potential with hexadecanol and ethyl palmitate monolayers on salt solutions.

The increased equilibrium spreading pressures on ammonium sulfate are consistent with greater stability of the spread monolayers, since the films spread on ammonium sulfate are less removed from equilibrium than are films on distilled water. The pressure–area isotherms and the compressibilities indicate the diacid films to be liquid-like around the region of collapse. In this vicinity, one would expect the monolayer to be composed of many small randomly oriented and distributed but somewhat internally ordered regions. The collapse sequence may then involve the reorganization of the small ordered regions to "microcrystals" with the initial stage involving only the rolling of one chain of molecules up onto the back of an adjacent chain, much as a layer of pencils would buckle under lateral compression perpendicular to their axes. Enough energy must be supplied by mechanical compression to tear the carboxyls from the water surface to initiate collapse. Once begun, the energy of crystallization is probably sufficient to carry the process to the point of equilibrium between monolayer and crystal. This scheme is similar to that discussed by Ries and Kimball[21] for stearic acid. However, since the diacid monolayer is much thinner than a stearic acid film, a shorter translation of the molecules pushed out of the surface is involved with the diacids. Although the equilibrium spreading pressure (and thus the theoretical limit of compression) decreases with increasing chain length,[8] Ries and Kimball found the collapse pressure, under dynamic conditions, for *n*-hexatricontanoic acid to be 58 dynes/cm., 16 dynes/cm. greater than the collapse pressure for stearic acid. The low collapse pressures found with the diacids are consistent with this idea. This and the high stability of the diacid bulk crystal, as evidenced by very low equilibrium spreading pressures and low temperature coefficient of the spreading pressure, are probably responsible for the relative instability of the diacid films.

No points of first-order phase change were observed. Moreover, since no measureable pressure was observed above about 170 Å.^{2}/molecule even at high temperatures, the surface vapor pressure of the diacid 20 and 24 liquid-expanded films must be less than 0.05 dyne/cm.

(18) S. G. Fernandez, E. O. Aenlla, and J. M. Trillo, *Kolloid-Z.*, **197**, 151 (1964).

(19) W. Rabinovitch, R. F. Robertson, and S. G. Mason, *Can. J. Chem.*, **38**, 1881 (1960).

(20) A. Pankratov, *Acta Physicochim. URSS.*, **10**, 45 (1939).

(21) H. E. Ries and W. A. Kimball, Proceedings of the Second International Congress on Surface Activity, Vol. I, Academic Press, New York, N. Y., 1957, p. 75.

Thermodynamic Quantities in the Exchange of Lithium with Cesium Ion on Cross-Linked Polymethacrylate Ion Exchangers[1]

by S. Lindenbaum and G. E. Boyd

Oak Ridge National Laboratory, Oak Ridge, Tennessee 37831 *(Received January 28, 1965)*

Calorimetric measurements showed that heat was absorbed in the selective uptake of lithium ion from dilute aqueous solutions in an exchange reaction with cesium ion on cross-linked polymethacrylic acid (PMA) ion exchangers. The standard entropies of exchange, $\Delta S°$, observed with nominal 1 and 15% divinylbenzene cross-linked preparations were 1.8 and 6.2 e.u., respectively. The magnitude of $T\Delta S°$ showed that it was the increase in entropy which caused the standard free energy of exchange to be negative. The increase in $\Delta S°$ was attributed to a decrease in the hydration of Li^+ ion in the exchange reaction. It was proposed that the alkali metal cation affinity sequence $Li^+ > Na^+ > K^+ > Rb^+ > Cs^+$ for PMA exchangers resulted from "site-binding" of the lightest members.

One of the central problems in the understanding of the ionic selectivity exhibited by synthetic organic ion exchangers is that concerned with the nature of the binding of ions by the ionogenic groups in these materials. In our previous study[2] of the free energy, enthalpy, and entropy of exchange of Na^+ with H^+, Li^+, K^+, and Cs^+ ions in cross-linked polystyrene sulfonate exchangers it was found that the preferential uptake of these cations from dilute aqueous solutions was accompanied by the evolution of heat and by a decrease in entropy. The magnitude of the standard free energy decrease, $-\Delta F°$, was determined by the difference between the lowering of the enthalpy, $\Delta H°$, and the decrease in $\Delta S°$. Therefore, the ionic selectivity was governed by the lowering of the energy of the exchanger.

The affinity sequence of the alkali metal cations in their exchange reactions in aqueous solutions at 25° on cross-linked polymethacrylic acid (PMA) exchangers is known[3] to be the reverse of that with polystyrene sulfonates where $Cs^+ > Rb^+ > K^+ > Na^+ > Li^+$. It has seemed probable that the cause for this inversion was related to the type of binding of these cations with the carboxylate groups of the exchanger. Accordingly, the relative signs and magnitudes of $\Delta H°$ and $\Delta S°$ for the reactions are of interest. Measurements of selectivity coefficients, $D_{M^+}^{K^+}$, for the exchange of potassium with lithium and with sodium ion on cross-linked PMA exchangers have been reported.[4] A strong dependence of $D_{M^+}^{K^+}$ on cross linking and on the mole fraction of potassium, x_{K^+}, in the exchanger was found, and reversals in the strength of ionic binding were observed in the K^+–Li^+ exchange for $x_{K^+} > 0.45$ with all but the most lightly cross-linked preparation. Potassium–lithium selectivity coefficients measured at 4° with four differently cross-linked PMA exchangers were found not to differ from the values determined at 25° indicating that $\Delta H°$ was nearly zero. This latter result is unexpected, and, therefore, we have made calorimetric measurements of the heats of exchange of Cs^+ with Li^+ ion as a function of x_{Li^+} for nominal 1 and 15% divinylbenzene (DVB) cross-linked PMA exchangers. Equilibrium selectivity coefficients also were determined, and the derived $\Delta S°$ values showed that it was the increase in entropy which determined the selective uptake of Li^+ ion.

(1) Presented before the Division of Colloid and Surface Chemistry, 149th National Meeting of the American Chemical Society, Detroit, Mich., April 1965. Research sponsored by the U. S. Atomic Energy Commission under contract with Union Carbide Corp.

(2) G. E. Boyd, F. Vaslow, and S. Lindenbaum, *J. Phys. Chem.*, **68**, 590 (1964).

(3) J. I. Bregman, *Ann. N. Y. Acad. Sci.*, **57**[3], 126 (1953).

(4) H. P. Gregor, M. J. Hamilton, R. J. Oza, and F. Bernstein, *J. Phys. Chem.*, **60**, 263 (1956).

Experimental

Calorimetric Measurements. The calorimeter used in the heat of exchange measurements was identical in many respects with that previously employed.[2,5] Temperature changes were followed with two 2000-ohm thermistors possessing a temperature coefficient of -3.9%/deg. placed on opposite arms of a Wheatstone bridge. The other two arms of the bridge were decade resistance boxes. The unbalanced current from the bridge was amplified with a d.c. breaker amplifier (Beckman Model 14) and recorded as a function of time on a 100-mv. Leeds and Northrup Speedomax recorder. The temperature sensitivity of the calorimeter was approximately 15×10^{-6}°. The electrical energy input to the calorimeter heater used in the calibration was determined by voltage drop and current measurements with a Type K-3 Leeds and Northrup potentiometer. The length of the heating period was controlled by an electrical timer which was activated simultaneously with the heater current. The overall performance of the calorimeter system was checked from time to time by measurements of the heat of solution of KCl(c). Values in good agreement with those reported by Somsen, Coops, and Tolk[6] were obtained.

The measurements of the heats of the exchange reaction of Li^+ with Cs^+ ion were performed with *ca.* 10 mequiv. of the wet, swollen PMA exchanger initially in either the Li or the Cs form contained in the sample pipet. The calorimeter was filled with 500 ml. of aqueous 0.1 *N* LiOH or CsOH solution, or with mixtures of these electrolytes. The exchange reaction was rapid and appeared to reach completion in fewer than 4 min. after initiation as judged by the temperature history of the calorimeter.

At the conclusion of the calorimeter experiment, an aliquot of the equilibrium aqueous phase was taken. The exchanger was separated from the solution by filtration, rinsed with ethanol, and eluted with HCl solution to remove all Li^+ and/or Cs^+ ions. The eluate and equilibrium aqueous phases were analyzed for lithium and cesium by flame spectrophotometry.[7] The number of equivalents of cation involved in the exchange reaction, the composition of the equilibrium exchanger, and the selectivity coefficient for the exchange reaction were computed from these measurements.

Materials. Spherical polymethacrylic acid type cation-exchanger preparations nominally cross linked with 1 and 15% divinylbenzene (DVB) were used.[8] Total exchange capacities were measured after pretreatment of the "as received" acid forms to remove unreacted monomers and impurities. Values of 11.13 and 7.72 mequiv./g. of dry H form, respectively, were found. To minimize hydrolysis problems the exchanger always was weighed in the H form and converted to the Li or Cs form in the calorimeter pipet by adding an excess of LiOH or CsOH and adjusting the final concentration of the supernatant solution to 0.1 *N*. In the course of these operations, the swelling of the Cs form was observed to be distinctly greater than that of the Li form.[9]

The LiOH and CsOH solutions were prepared by treating the corresponding chloride salt solutions with silver oxide, filtering, and diluting to volume.

Results and Discussion

Heats and Free Energies of Partial Exchange. The dependence of the differential heats of exchange, $\Delta\bar{H}$, of Li^+ with Cs^+ ion for the nominal 1 and 15% DVB cross-linked PMA exchangers on the equivalent fraction of Li^+ ion in the exchanger is shown in Figures 1 and 2. Heat was absorbed over the entire range of compositions in the more lightly cross-linked preparation, whereas heat was evolved for the uptake of small amounts of lithium ion by the Cs form of the 15% DVB exchanger. A marked dependence of $\Delta\bar{H}$ on x_{Li^+} was exhibited by both preparations, and with the highly cross-linked exchanger the reaction was strongly endothermic when only microamounts of Cs^+ ion remained (*i.e.*, $x_{Li^+} = 1.0$).

The compositional dependence of the selectivity coefficient, $D_{Cs^+}^{Li^+}$, for the exchange reaction is shown in Figure 3 where it may be noted that a selectivity reversal occurred with both preparations when x_{Li^+} exceeded *ca.* 0.70 to 0.75. Thus, small quantities of Cs^+ ion were taken up preferentially by the homoionic Li forms.

Standard Heats, Free Energies, and Entropies of Exchange. The measurements shown in Figures 1–3 were employed to estimate the standard enthalpies, $\Delta H°$, free energies, $\Delta F°$, and entropies, $\Delta S°$, of ion exchange for the hypothetical reaction

(5) G. E. Boyd and F. Vaslow, *J. Chem. Eng. Data*, **7**, 237 (1962).

(6) G. Somsen, J. Coops, and M. W. Tolk, *Rec. trav. chim.*, **82**, 231 (1963).

(7) The authors are indebted to T. C. Rains of the ORNL Analytical Chemistry Division for these determinations which were performed with a precision in the Li^+/Cs^+ ratio of better than 1%.

(8) These materials were supplied through the generosity of the Rohm & Haas Co., Philadelphia, Pa., by Dr. R. Kunin.

(9) Measurements on a nominal 6% DVB cross-linked PMA exchanger by H. P. Gregor, M. J. Hamilton, J. Becher, and F. Bernstein, *J. Phys. Chem.*, **59**, 874 (1955), have shown the volume of the K form to be greater than either the Li form or Na form which swelled to the same extent approximately in dilute aqueous base solutions.

CsR (a = 1, equil. with 0.1 N CsOH) +
LiOH (aq., a = 1) $\rightleftarrows$
LiR (a = 1, equil. with 0.1 N LiOH) +
CsOH (aq., a = 1) + nH$_2$O (a_w = 1)

The integral heat of exchange is given by

$$\Delta H = \int_0^1 (\partial \Delta H / \partial x_{Li^+}) dx_{Li^+}$$

and it was evaluated by graphical integrations of the differential heats given in Figures 1 and 2.

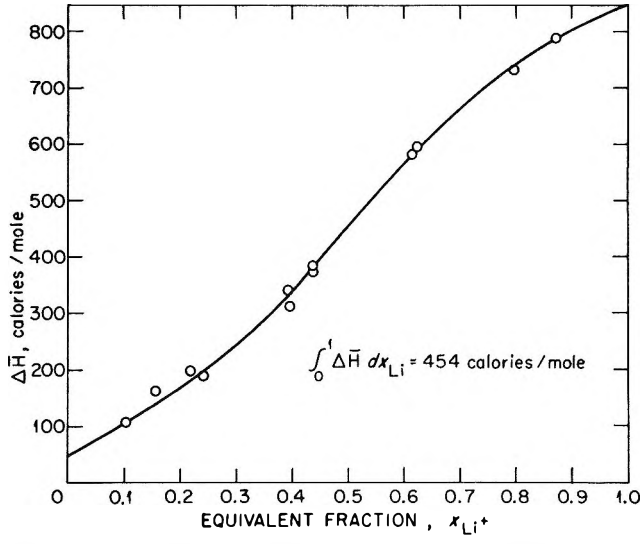

Figure 1. Differential heats of exchange of Li$^+$ with Cs$^+$ ion in nominal 1% DVB cross-linked PMA ion exchanger. Open circles indicate midpoints of chords for heats of partial exchange.

Standard heats, $\Delta H°$, for the Li$^+$–Cs$^+$ exchange reaction were derived by correcting the ΔH values by the appropriate difference in the relative apparent molal heat contents, ϕ_L, of the two 0.1 N aqueous solutions. Corrections for heats of swelling and for the heat of mixing of electrolyte at μ = 0.1 in the actual exchange reaction were assumed to be negligibly small.

Standard free energies, $\Delta F°$, were computed from the corrected selectivity coefficients, D_0, with the formula

$$-\Delta F° = 2.3RT \int_0^1 \log D_0 dx_{Li^+}$$

The required values of D_0 were obtained by correcting the observed $D_{Cs^+}^{Li^+}$ by the activity coefficient ratio, $\gamma_\pm^2$(CsOH)/$\gamma_\pm^2$(LiOH), for the aqueous 0.1 N electrolyte mixture. The thermodynamic quantities are summarized in Table I.

The primary observation to be drawn from the entries in Table I is that the selectivity shown by the

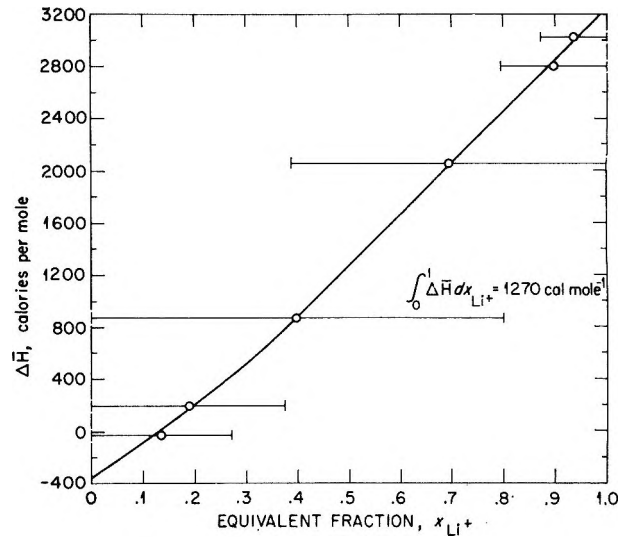

Figure 2. Differential heats of exchange of Li$^+$ and Cs$^+$ ion in nominal 15% DVB cross-linked PMA exchanger. Open circles indicate midpoints of chords for heats of partial exchange.

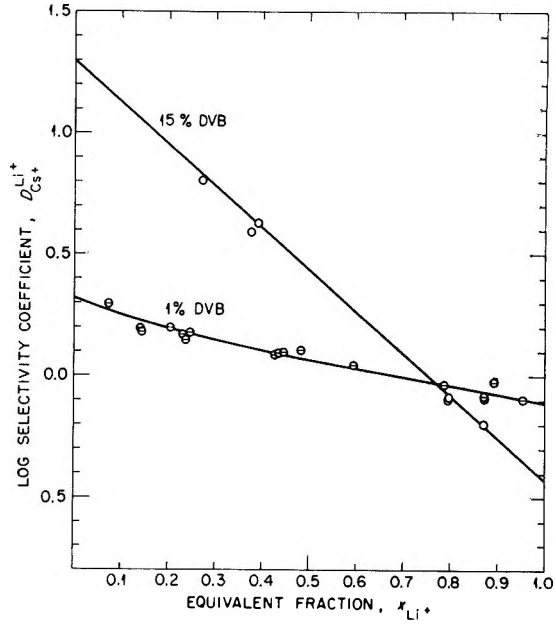

Figure 3. Selectivity coefficients for the exchange of Li$^+$ with Cs$^+$ ion in cross-linked PMA ion exchangers.

PMA exchangers for Li$^+$ ion was determined by the entropy rather than the energy change. The uptake of Li$^+$ ion is accompanied by an increase in the energy, but this is over-balanced by the entropy increase to give a free energy decrease. This interplay of thermodynamic quantities may be contrasted with that for the reaction of Li$^+$and Cs$^+$ ions on cross-linked polystyrenesulfonic acid (PSSA) exchangers. The uptake of the

Table I: Thermodynamic Quantities for the Exchange at 298.2°K. of Li^+ with Cs^+ Ion in Cross-Linked Polymethacrylate Ion Exchangers

Cross-linking % DVB	ΔH, cal. mole^{-1}	$\Delta\phi_L$, cal. mole^{-1}	$\Delta H°$, cal. mole^{-1}	$\Delta F°$, cal. mole^{-1}	$\Delta S°$, e.u.
1.0	454	−50	404	−134	1.8
15	1270	−50	1220	−621	6.2

preferred cesium ion by the Li form of a nominal 16% DVB cross-linked PSSA preparation is accompanied by a strong lowering of the energy of the exchanger ($\Delta H°$ = −2890 cal. mole^{-1}) and by an entropy decrease ($\Delta S°$ = −6.9 e.u.).[2] The enthalpy decrease, however, is larger than $T\Delta S°$, and $\Delta F°$ is negative.

Nature of the Ionic Binding in PMA Exchangers. It will be of interest to speculate briefly on possible causes for the entropy increase in the exchange of Li^+ for Cs^+ ion in cross-linked PMA exchangers. The type of ionic binding cannot be the same as with PSSA exchangers where the alkali metal cations appear to retain their primary hydrations and to interact electrostatically with the structurally bound sulfonate anions.[2] To account for the preference of Li^+ ions it appears necessary to assume that a specific association exists between them and the carboxylate groups of the exchanger or that "site-binding" of Li^+ occurs. The evidence that interaction of alkali metal and alkaline earth metal ions with anionic polyelectrolytes takes place with the release of water molecules from the solvated participating species has been reviewed recently, and dilatometric measurements with linear polymethacrylate have shown that a volume increase of *ca.* 3 ml. equiv.$^{-1}$ occurs in the system when tetramethylammonium counterions are replaced by Li^+ or Na^+ ions.[10] If water is released in "site-binding," an appreciable positive contribution to $\Delta S°$ also would be expected.[11]

The positive $\Delta S°$ values found in this research therefore may be taken as supporting evidence for "site binding" of Li^+ ion by PMA exchangers.[12] The question whether or not the carboxyl group replaces water and enters the first coordination sphere of the ion cannot be decided from the evidence available. It is possible that the interaction displaces only the more loosely bound water in the outer coordination layer and that an ion association involving a water molecule as an intermediary between Li^+ and COO^- occurs. This latter hypothesis ("localized hydrolysis" mechanism) has been employed by Robinson and Harned[13] to account for the reversal in the sequence of activity coefficient values for aqueous solutions of the alkali metal salts when the anion is a proton acceptor (*i.e.*, formate, acetate, fluoride, etc.). The greater ability of carboxylate compared with sulfonate groups to "complex" with the "smaller" alkali metals has been cited[14] also to explain the reversal in concentrated aqueous lithium salt solutions in the order of elution of these cations from a polymethacrylic acid exchanger.

(10) U. P. Strauss and Y. P. Leung, *J. Am. Chem. Soc.*, 87, 1476 (1965).

(11) The increase in entropy for the release of water by crystalline hydrates is 9.4 e.u.; *cf.*, W. M. Latimer, "Oxidation Potentials," Prentice-Hall, New York, N. Y., 1952, p. 364.

(12) The deswelling of the exchanger on going from its Cs form to its Li form gives a positive contribution to $\Delta S°$ because of an increase in the configurational entropy of the molecular network. An estimate of the deswelling entropy with the Flory–Rehner theory for uncharged, cross-linked polymers indicates the contribution is only 0.1–0.2 e.u., however.

(13) R. A. Robinson and H. S. Harned, *Chem. Rev.*, 28, 419 (1941).

(14) D. C. Whitney and R. M. Diamond, *Inorg. Chem.*, 2, 1284 (1963).

A Thermodynamic Calculation of the Ionic Strength Dependence of Ion-Exchange Reaction Selectivity Coefficients[1]

by G. E. Boyd and S. Lindenbaum

Oak Ridge National Laboratory, Oak Ridge, Tennessee 37831 *(Received February 12, 1965)*

Ion-exchange reaction selectivity coefficients for synthetic organic exchangers are known to be determined by the nature of the ionogenic groups, by the exchange capacity and cross linking and by the ionic composition of the copolymer. Additionally, it is required by thermodynamics that the ionic selectivity vary with the ionic strength, μ, of the external aqueous electrolyte if the swelling of the exchanger varies with μ and its ionic composition. Selectivity coefficients measured for the uptake of Br^- ion by the fluoride and chloride salt forms of a lightly cross-linked, strong-base anion exchanger showed increases of approximately 50 and 11%, respectively, when μ increased from 0 to 0.2 and 0.35 *m*. Thermodynamic calculations of the ionic strength dependence of the bromide–chloride selectivity coefficient were made based on the assumption that the exchanger was a three-component system. Satisfactory agreement with experiment was found up to $\mu = 0.2$; above this concentration, invasion of the exchanger by aqueous electrolyte occurred, and the assumption of a ternary mixture was invalidated.

It is generally recognized that the ionic selectivity shown by organic ion exchangers at constant temperature is dependent on the nature of the ionogenic groups, on the exchange capacity and cross linking, and on the ionic composition of the copolymer. However, the fact that the selectivity is also dependent on the ionic strength, μ, of the aqueous electrolyte mixture with which the exchanger is in equilibrium does not seem to have been observed. For example, in an earlier study[2,3] of the exchange of potassium with hydrogen and with lithium ions in variously cross-linked polystyrene sulfonate type cation exchangers it has been reported that there was no change in the selectivity coefficient with a 2% divinylbenzene (DVB) copolymer as μ increased from 10^{-3} to 1.0 *m* and that with 10 and 23% DVB resins the selectivity remained constant for increases in μ from 10^{-3} to 0.1 *m* but *decreased* when $\mu = 1.0$ *m*. In careful measurements on the sodium–hydrogen ion exchange with Dowex-50, Argersinger and Davidson[4] have reported equilibrium constants of 1.66, 1.68, and 1.73 for $\mu = 0.1$, 0.3, and 1.0 *M*, respectively. However, these authors quote an average value of 1.69 for the equilibrium constant, which, in our opinion, incorrectly ignores the trend in their data.

Ion-exchange equilibrium selectivity coefficients, D_1^2, for the exchange of ion 2 in aqueous solution with ion 1 in the exchanger may be estimated with the Gibbs–Donnan equation, and we have found[5,6] that the calculated variation of log D_1^2 with cross linking and with ionic composition at 25° was in satisfactory agreement with experiment. This same equation may be employed to compute the variation of the selectivity coefficient with the ionic strength of the external mixed electrolyte solution. The form in which it may be utilized for this latter purpose is

$$\log D/D^0 = P(\bar{v}_1 - \bar{v}_2)/2.3RT + 0.05551I_R - 2 \log (\gamma_1/\gamma_2)_w \quad (1)$$

(1) Presented before the Division of Physical Chemistry, 149th National Meeting of the American Chemical Society, Detroit, Mich., April 4–9, 1965. Research sponsored by the U. S. Atomic Energy Commission under contract with the Union Carbide Corp.

(2) H. P. Gregor and J. I. Bregman, *J. Colloid Sci.*, **6**, 323 (1951).

(3) J. I. Bregman, *Ann. N. Y. Acad. Sci.*, **57**[3], 126 (1953).

(4) W. J. Argersinger, Jr., and A. W. Davidson, *J. Phys. Chem.*, **56**, 92 (1952).

(5) G. E. Myers and G. E. Boyd, *J. Phys. Chem.*, **60**, 521 (1956).

(6) G. E. Boyd, S. Lindenbaum, and G. E. Myers, *ibid.*, **65**, 577 (1961).

where D^0 is the coefficient for the exchange reaction at $\mu = 0$ and the other symbols are as defined earlier.[6] The second term on the right-hand side of eq. 1 is frequently the dominant one. It measures the contribution of the activity coefficient ratio of ions 1 and 2 in the exchanger ("ionic interaction free energy"), and it can be calculated with the equation

$$[\partial \log (\gamma_1/\gamma_2)_r/\partial \log a_w]_{x_2} = 0.05551(\partial x_w/\partial x_2)_{a_w} \quad (2)$$

which follows from an application of the Cauchy cross-differentiation identity to the Gibbs equation for the change of the free energy of a ternary system with composition. The assumption must be made, as in previous uses of eq. 1 and 2, that the exchanger may be treated as a ternary aqueous electrolyte mixture (resinate 1, resinate 2, and water); this assumption implies that the invasion of the exchanger by electrolyte from the aqueous phase is always sufficiently small to be neglected. In eq. 2, x_w is the weight swelling[7] of the exchanger, x_2 is the equivalent fraction of ion 2 in the exchanger, and a_w is the water activity. The quantity, I_R, in eq. 1 is defined by

$$I_R = \int_0^{\log a_w} (\partial x_w/\partial x_2)_{a_w} d \log a_w \quad (3)$$

and is evaluated with experimental measurements of the variation of x_w with x_2 and a_w. Because x_w varies with a_w which in turn is determined by the ionic strength, it follows that the selectivity coefficient must vary with μ.

The object of this paper is to report measurements of the ionic strength dependence of D_1[2] with a lightly cross-linked, strong-base anion exchanger and to present the results of thermodynamic calculations which will be compared with the experimental selectivity coefficients for the Br^-/Cl^- ion-exchange equilibrium. (Br^- will be taken as ion 2 and Cl^- as ion 1.)

Experimental

Weight swelling measurements taken in isopiestic vapor equilibrations[6] with the pure and mixed chloride and bromide ion salt forms of a weakly cross-linked (nominal 0.5% DVB), strong-base anion exchanger (Dowex-2) were employed in the calculations of the ionic strength dependence of $D_{Cl^-}^{Br^-}$. Determinations of x_w for very small values of $-\log a_w$ (*i.e.*, high water activities) were made by immersing the exchanger in dilute aqueous sodium chloride–sodium bromide mixtures and then separating it from the aqueous phase following a carefully standardized centrifugation technique.[8,9] The data in Figure 1 reveal that the exchanger was not fully swollen until μ was less than 0.001 M. The chloride form (*i.e.*, $x_{Br^-} = 0.0$) showed the greatest, and the bromide form the least swelling at constant electrolyte concentration.

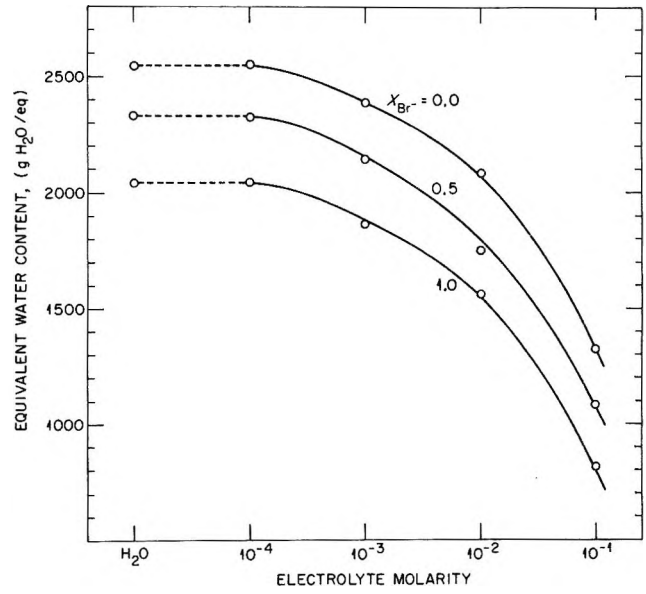

Figure 1. Variation of the weight swelling of weakly cross-linked Dowex-2 with concentration of external aqueous NaCl + NaBr mixtures: top curve, homoionic Cl form; bottom curve, homoionic Br form.

Independent measurements of the swelling of the chloride form were performed with a procedure which did not require a separation of the exchanger from the aqueous electrolyte. In this new method,[10] a predetermined number of milliequivalents of exchanger were placed in a glass column and were brought to equilibrium with the desired electrolyte containing very small known concentrations of high molecular weight, linear Dowex-1 Cl form by passing solution through the bed. The liquid level was brought to the top of the bed, and the column plus contents were weighed. The bed was rinsed with distilled water, and the concentration of linear polyelectrolyte, which did not invade the exchanger, was estimated from optical density measurements at 262 and 268 mμ, respectively. These measurements of the amount of linear polyelectrolyte in the bed permitted a calculation of the

(7) The weight swelling is a measure of the water content and is expressed in units of grams of water per equivalent of ion-exchange groups.

(8) K. W. Pepper, D. Reichenberg, and D. K. Hale, *J. Chem. Soc.*, 3129 (1952).

(9) H. P. Gregor, M. Held, and J. Bellen, *Anal. Chem.*, **23**, 620 (1951).

(10) An analogous method has been used by G. D. Manalo, R. Turse, and W. Rieman, III, *Anal. Chim. Acta*, **21**, 383 (1959), to determine the interstitial volume in ion-exchange columns.

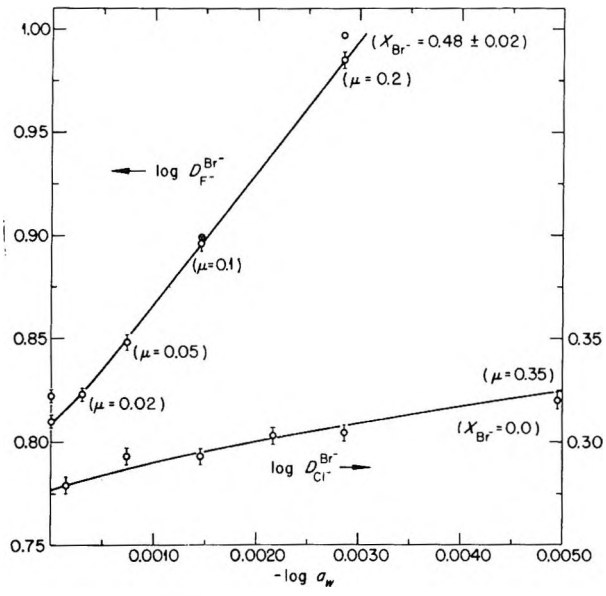

Figure 2. Concentration dependence of the selectivity coefficients for the exchange of Br^- with F^- and Cl^- on Dowex-2X0.5.

weight of interstitial water which was subtracted from the gross weight of the bed to give the weight of water in the exchanger plus the weight of the exchanger. The latter was known from the dry capacity (3.66 mequiv./g. of Cl form) and the total milliequivalents in the bed; hence, the weight of water per equivalent of exchanger could be derived. Excellent agreement with the x_w value for pure water determined by the centrifuge method was obtained; with the electrolyte solutions, however, the linear polyelectrolyte method gave values consistently larger by about 10%.

The bromide–chloride and bromide–fluoride ion selectivity coefficient measurements shown in Figure 2 were performed in batch- and in column-type experiments, respectively. In the former, the uptake of microquantities of bromide ion from KCl solutions of various ionic strengths was measured with 35.9-hr. ^{82}Br tracer. After equilibration at 25° the exchanger was separated from the solution by filtration and quickly rinsed with ethanol to remove the remaining interstitial and surface-occluded aqueous electrolyte. The exchanger then was eluted with 2 M $NaNO_3$ solution, and assays of the amounts of Cl^- and Br^- ions in the equilibrium solution and in the eluate were performed. An estimate of the propagation of experimental errors indicated that the selectivity coefficients were reliable to slightly better than ±1%.

In the measurements of $D_{F^-}^{Br^-}$, anion exchanger in the Cl form was placed in a 10-mm. i.d. glass column to form a bed approximately 10 cm. deep and eluted with 2 M $NaNO_3$. The eluate was titrated for Cl^- ion from which the total milliequivalents of exchanger (*ca.* 3 mequiv.) were computed. Next, a mixed aqueous NaF + NaBr solution of predetermined ionic strength was passed through the column until the F^- and Br^- influent and effluent concentrations were identical. Analyses for F^- were made with the PbClF method; Br^- ion was determined by micropotentiometric titration with $AgNO_3$. After equilibration, the interstitial solution was drained from the bed which was then eluted with 2 M $NaNO_3$. This eluate was analyzed for Br^- ion content, and the amount of F^- ion in the exchanger was found by difference from the total milliequivalents present. An error analysis indicated the selectivity coefficient values to be reliable to ±1%.

Several features in Figure 2 require additional comment. The quantity $-\log a_w$ is plotted on the abscissa rather than μ for reasons of convenience and ease in extrapolation to obtain log D^0 (*cf.* eq. 1). The relationship used to estimate $-\log a_w$ was that which defines the molal osmotic coefficient, ϕ, $-\log a_w = 0.007824\nu m\phi$, where ν is the number of ions given by 1 mole of electrolyte, and m is the molality. The required values of ϕ below $m = 0.1$ were derived with an empirical equation due to Guggenheim[11]; values at higher concentrations were taken from available tables.

A significant dependence of $D_{F^-}^{Br^-}$ on μ is shown in Figure 2 where the selectivity coefficient may be seen to increase by nearly 50% from 6.45 in pure water to 9.66 when $\mu = 0.2$. The increase in $D_{Cl^-}^{Br^-}$ is smaller but nonetheless amounts to 11% when $\mu = 0.35$. These results emphasize the danger in the usual procedure where the exchanger is rinsed with pure water following an equilibration with an electrolyte mixture. Errors much larger than those in the analyses can be introduced in this way.

The increase in D with μ shown in Figure 2 can be assigned almost entirely to the exchanger. The contribution of the aqueous activity coefficient ratio (eq. 1) to this increase has been estimated for the KCl + KBr mixtures from published data by McCoy and Wallace.[12] The correction term to log $D_{Cl^-}^{Br^-}$, $-2 \log (\gamma_{KCl}/\gamma_{KBr})$, amounts to only 1.8% when $\mu = 1.0$. The observed increases in the selectivity coefficients with $-\log a_w$ must be related, therefore, to the decrease in the swelling of the exchanger as μ increases.

Measurements of the invasion of the homoionic chloride form of the exchanger by aqueous KCl solu-

(11) E. A. Guggenheim and J. C. Turgeon, *Trans. Faraday Soc.*, **51**, 747 (1955).

(12) W. H. McCoy and W. E. Wallace, *J. Am. Chem. Soc.*, **78**, 1830 (1956).

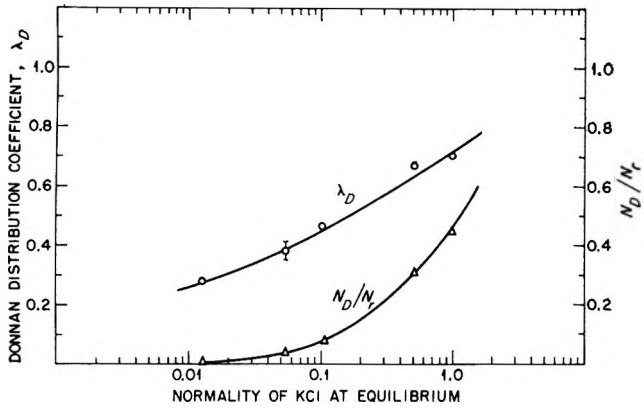

Figure 3. Invasion of the Cl form of Dowex-2X0.5 by aqueous KCl solutions: upper curve, molar Donnan distribution coefficients; lower curve, ratio of concentration of KCl in exchanger to resinate concentration.

tions also were made (Figure 3). A cylindrical bed of resin contained in a glass column was brought to equilibrium successively with varying predetermined concentrations of KCl between 0.01 and 1.0 N. The bed was washed with pure water, and the wash collected. The KCl in the exchanger and in the interstitial space was determined by a micropotentiometric titration of Cl^-. The K^+ ion in the exchanger was found by subtracting from the total KCl the amount of KCl in the interstitial volume. This latter was derived from the amount of water determined by the linear polyelectrolyte method previously mentioned and the influent (equilibrium) KCl concentration. The concentration of K^+ ion, $(N_{K^+})_r$, inside the exchanger was computed from its water and KCl content. The data are plotted in Figure 3 in terms of the Donnan distribution coefficient, λ_D, defined by $\lambda_D = (N_{K^+})_r/(N_{K^+})_w$. The ratio of the normality of KCl inside the exchanger to the normality of resin chloride, N_D/N_r, also is plotted. This latter ratio shows that, when the external KCl normality exceeds 0.1, the concentration of invading KCl becomes greater than 10% of the concentration of resin chloride.

Results and Discussion

Computations of log $D_{Cl^-}^{Br^-}$ were performed with eq. 1–3 using the experimentally measured variation of the weight swelling, x_w, with x_{Br^-} and water activity, a_w. The first term on the right-hand side of eq. 1 was negligibly small relative to the second term because the swelling pressure (strain energy) in a lightly cross-linked exchanger is very nearly zero. Thus, the contribution of the first term to log $D_{Cl^-}^{Br^-}$ is but -0.00024 when $x_{Br^-} = 0.0$ and -0.00012 when $x_{Br^-} = 1.0$. Estimates of the third term in eq. 1, which is small relative to the second term, were made empirically because data on activity coefficients in aqueous NaCl + NaBr mixtures do not exist. A method outlined by Robinson and Stokes[13] which makes use of γ-values for binary electrolyte solutions and tabulated empirical constants[11] was followed.

The curves in Figure 4 indicate that a satisfactory agreement between the experimentally measured and calculated values of $D_{Cl^-}^{Br^-}$ was observed up to an ionic strength of *ca.* 0.2 m. At higher μ-values the experimental selectivity coefficients fell below the calculated curves, and are not shown. The reason for this is believed to reside in the breakdown of the assumption, basic to the calculation, that the ion exchanger could be treated as a ternary aqueous electrolyte mixture. As shown in Figure 3, a significant penetration of the exchanger by aqueous electrolyte solution occurred when $\mu > 0.2$ m. At higher concentrations, five rather than three components will be present in the exchanger, and agreement with experiment cannot be expected.

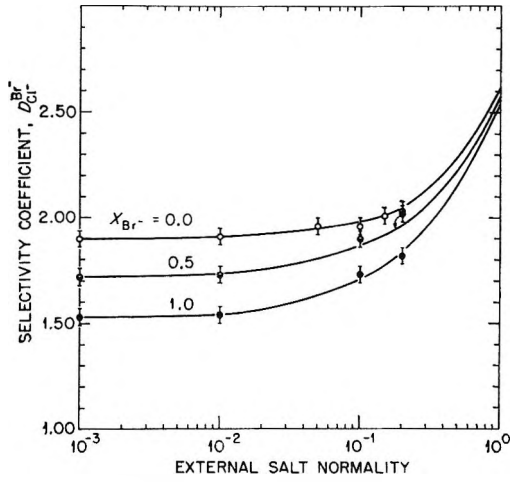

Figure 4. Variation of the bromide–chloride ion-exchange equilibrium selectivity coefficient with external electrolyte concentration: upper curve for pure NaCl solution; lower curve for pure NaBr solution.

Two observations will be made in conclusion.

(a) Although the selectivity coefficient was observed to increase with the ionic strength of the aqueous solution in this work, there is nothing in the thermodynamics that requires this behavior. Usually the quantity, $(\partial x_w/\partial x_2)_{a_w}$, in eq. 2 is negative (*i.e.*, swelling decreases with the uptake of increasing amounts of the preferred ion); however, systems are known where a

(13) R. A. Robinson and R. H. Stokes, "Electrolyte Solutions," Butterworth and Co. Ltd., London, 1955, p. 468.

positive value occurs over a range in $-\log a_w$. In this latter circumstance, the selectivity coefficient must decrease with increasing μ.

(b) For a given exchanger at constant composition, the selectivity coefficient will depend on the identity of the common cation (or anion) in the external electrolyte mixture. For example, with Dowex-2X0.5 at $x_{Br^-} = 0.0$, the value of $D_{Cl^-}^{Br^-}$ at a fixed μ will be slightly greater when Li^+ is the common ion than when this is Cs^+.

Studies on Solutions of High Dielectric Constant. VII.[1] Cationic Transport Numbers of Potassium Bromide in N-Methylacetamide at Different Temperatures

by Ram Gopal and Om Narain Bhatnagar[2]

Department of Chemistry, Lucknow University, Lucknow, U. P., India *(Received February 3, 1965)*

The cationic transport numbers of potassium bromide in N-methylacetamide (NMA) have been determined at different temperatures and concentrations, and the data have been used to calculate the ionic mobilities in this solvent from the available electrolytic conductance. The values of the ionic mobilities at 40°, thus obtained, compare well with those obtained by Dawson and co-workers from the usual indirect method. An estimation of the ionic solvation appears to indicate appreciable ion–solvent interaction in NMA.

Introduction

There has been a good deal of research activity during the past few years in the field of liquids of high dielectric constant, other than water and liquid hydrogen cyanide, and appreciable experimental data, especially on the conductance of electrolytes in these solvents, have been reported. The question of dividing the electrolytic conductance at infinite dilution, λ_0, into separate ionic mobilities in most of these solvents, remains unsolved because of the lack of experimental data on the transport number of ions. In order to make this useful data available to workers in this field, studies were undertaken in this laboratory, and the cationic transport numbers of potassium chloride in formamide at different temperatures have already been reported.[3] The cationic transport numbers of potassium bromide in N-methylacetamide at different temperatures are reported in the present communication.

Experimental

Potassium bromide was chosen, in place of the usual potassium chloride, as the more appropriate electrolyte because of its higher solubility as compared to that of KCl and hence the determination of the transport numbers at several significantly different concentrations is possible with KBr. A.R. grade potassium bromide, recrystallized from conductivity water and thoroughly dried, was used in making solutions. NMA of specific conductivity 10^{-5} mho was dried over freshly ignited quicklime and twice distilled under reduced pressure. The distillate was fractionally crystallized and distilled again under reduced pressure. The process was re-

(1) Work supported by the Council of Scientific and Industrial Research, India.

(2) Junior Research Fellow, Council of Scientific and Industrial Research.

(3) R. Gopal and O. N. Bhatnagar, *J. Phys. Chem.*, 68, 3892 (1964).

peated until its conductivity fell to about 7–8 × 10^{-7} mho. The sample melted at about 29°. It was stored in dark-colored bottles in a drybox.[4]

The transport-number cell was similar to that used previously for solutions in formamide.[3] The distance between the electrodes was now reduced to overcome the current-reducing effect of the highly viscous NMA without increasing, unduly, the voltage in the circuit. The cathode of the cell was a silver bromide electrode which was prepared as follows.

A silver wire about 90 cm. long and 0.5 mm. in diameter was wound on a stout silver rod and the whole was made the anode, and a platinum wire was the cathode of an electrolytic cell containing a potassium bromide solution. A current of 10–15 ma. was passed for 4–5 hr. The anode was taken out, washed thoroughly with conductivity water, dried, and subsequently used in the transport-number cell as the cathode, the anode being a long silver wire of approximately the same dimensions as the cathode, wound in the form of a spiral of about 2.5 mm. in diameter and 2.5 cm. in length.

Solutions of desired concentrations were prepared in freshly distilled and purified samples of NMA, and all solvent transfers were done in the nitrogen drybox. The rest of the experimental procedure was the same as described previously,[3] including the precautions for carrying out the experiments in a moisture-free atmosphere. The experimental results are summarized in Table I.

Table I: Transport Numbers of K^+ in Solutions of KBr in NMA at Different Temperatures and Concentrations

Concn.,	Transport no., t_+			
M	35°	40°	45°	50°
0.00	0.3839	0.3900	0.3950	0.3990 (from the graph)
0.10	0.3642	0.3707	0.3782	0.3845
0.15	0.3606	0.3692	0.3767	0.3797
0.20	0.3594	0.3668	0.3730	0.3801
0.25	0.3572	0.3638	0.3694	0.3784
0.30	0.3545	0.3614	0.3678	0.3760

From the values of the transport numbers, t_+, at different temperatures and concentrations, given in Table I, the values of the limiting transport numbers, t_+^0, of K^+ at different temperatures were obtained by the usual graphical method using the well-known Longsworth procedure as described previously.[3] The values of the limiting equivalent conductance, λ_0, of KBr at different temperatures, needed to calculate the Longsworth function, $t_+^{0\prime}$, were those given by French and Glover[5] and by Dawson and co-workers.[6] The required values of the dielectric constant of NMA have been taken as 169.7, 165.5, 157.5, and 151.8 at 35, 40, 45, and 50°, respectively.[7] The values of the limiting transport numbers, t_+^0, at different temperatures are also given in Table I.

Discussion

From Table I it may be seen that the variation of the transport number, t_+, with temperature and concentration follows the same pattern of behavior as that in formamide solutions,[3] *i.e.*, it increases with increase in temperature and decreases with increase in concentration. As in formamide, the effect of temperature is consistent with the Kohlrausch's law that the faster the ion, the smaller the temperature coefficient of its mobility so that the slower moving ion K^+ has a positive temperature coefficient and t_+ increases almost linearly with temperature. The reverse will be the case with the faster bromide ion. The difference in the activation energies of transport of the two ions K^+ and Br^-, from the Eyring–Slater theory of reaction rates,[8] is about 850 cal. It appears that the ion–solvent interaction in formamide and in NMA is of the same nature.

Ionic Mobilities. Although the ionic mobilities in NMA have been obtained by Dawson and co-workers by the indirect method, *i.e.*, by assuming that the mobilities of octadecyltrimethylammonium and octadecyl sulfate ions are equal,[9] it will be instructive to calculate their values from t_+^0 data directly, *i.e.*, from the experimental transport numbers t_+^0 of K^+ at different temperatures, and then following the usual ionic mobility additivity rule of Kohlrausch, applicable at infinite dilution, for the other ions. The conductance data at infinite dilution of different electrolytes in this solvent have been reported by different workers[5,6] and can be used to calculate mobilities of various ions. Table II summarizes the values of the ionic mobilities thus obtained at different temperatures.

(4) O. D. Bonner, C. F. Jordon, and K. W. Bunzl [*J. Phys. Chem.*, 68, 2450 (1964)] have described a sample of NMA with a melting point of 30.55° and in which electrolytes are reported to be virtually insoluble. Actually, electrolytes are extremely slow to dissolve in this solvent and it is likely that the observations of Bonner and co-workers about virtual insolubility of electrolytes are due to this difficulty.

(5) C. M. French and K. H. Glover, *Trans. Faraday Soc.*, 51, 1427 (1955).

(6) L. R. Dawson, P. G. Sears, and R. H. Graves, *J. Am. Chem. Soc.*, 77, 1986 (1955).

(7) Obtained graphically from the data of G. R. Leader and G. F. Gormley [*ibid.*, 73, 5731 (1951)] and of S. J. Bass, W. I. Nathan, R. M. Meighan, and R. H. Cole [*J. Phys. Chem.*, 68, 509 (1964)].

(8) R. W. Allgood, D. J. Le Roy, and A. R. Gordon, *J. Chem. Phys.*, 8, 418 (1940).

(9) L. R. Dawson, *et al.*, *J. Am. Chem. Soc.*, 79, 3004 (1957); *J. Phys. Chem.*, 67, 278 (1963).

Table II: Ionic Mobilities of Some Ions at Different Temperatures

Ion	Ionic mobility 35°	40°	45°	50°
H^+	...	9.18	...	...
Li^+	5.65	6.63	7.88	8.16
Na^+	7.19	8.13	9.30	10.26
K^+	7.28	8.23	9.46	10.46
Cs^+	8.33	9.63	10.76	11.76
NH_4^+	...	9.52	...	...
$0.5Ba^{2+}$		10.03		
$0.5Sr^{2+}$		10.26		
$0.5Ca^{2+}$		10.25		
$0.5Mg^{2+}$		9.41		
Et_4N^+	10.33	...	13.24	...
Cl^-	10.60	11.47	13.12	14.24
Br^-	11.72	12.87	14.47	15.74
I^-	13.42	14.67	16.59	16.74
Picrate	10.93	11.96	13.51	...
ClO_4^-		16.83		
CNS^-		16.25		
BrO_3^-		13.69		
$C_{18}H_{37}SO_4^-$		7.24		

The values of the ionic mobilities given in Table II should be the best values for the present, and they very nearly correspond to those reported by Dawson, *et. al.*[9] (at 40° only). The values increase with rise in temperature as in other solvents, the increase being roughly 2% per degree in most cases, and is approximately the same as in water. It may be noticed that Na^+ and K^+ have similar mobilities in contrast with the corresponding values in water in which the predominant structure (tetrahedral) breaking effect of K^+ enhances its mobility abnormally. Apparently no such effect is possible in this solvent as there is no such structure present here. Solvation only appears to play a significant role as the smaller ions have lower mobilities. This aspect has been examined in the succeeding paragraphs.

Solvation Numbers of Some Ions in NMA. Once the ionic mobilities are satisfactorily known, they may be used to calculate the solvation numbers of ions. Unfortunately, this can be done only at 40° as all the required data are known only at this temperature. The original method of Robinson and Stokes[10] has been improved upon by Nightingale[11] whose method has been used here, although both the methods give almost the same solvation number for an ion. The curve obtained, by plotting the radius, r_s, given by $r_s = 0.82|z|/\lambda_0\eta_0$ (terms used have their usual significance) of tetraalkylammonium ions against the respective crystal radius, r_c, of the ion concerned, is given in Figure 1. Out of the four ions whose λ_0^+ data are available, tetramethylammonium ion is an exception as in water due to solvation. The other three ions appear to lie on a straight line from which, on extrapolation, the actual radii, r_{HX}, in solution, of other smaller ions, can be read off, on the ordinate axis, from the knowledge of the corresponding r_s values. The positions of some ions are indicated on the curve. Of course, for tetraalkylammonium ions r_{HX} and r_c are the same because the ions, except for $(CH_3)_4N^+$, are unsolvated. Although the nature of the curve beyond the region $r_c \approx 4$–5 Å. is a little uncertain, it will be a fairly reasonable guess that 1:1 correspondence between r_s and r_{HX} (*i.e.*, correction factor unity) occurs in the 7–9-Å. region; *i.e.*, an ion of this or of a larger radius in solution, whether due to solvation or its own large size, will obey Stokes' law in NMA. The value 7–9 Å. may not have an exact significance. It is obvious, however, that Stokes' law will be applicable in this solvent only to particles of a much larger size as compared to those in water where the cor-

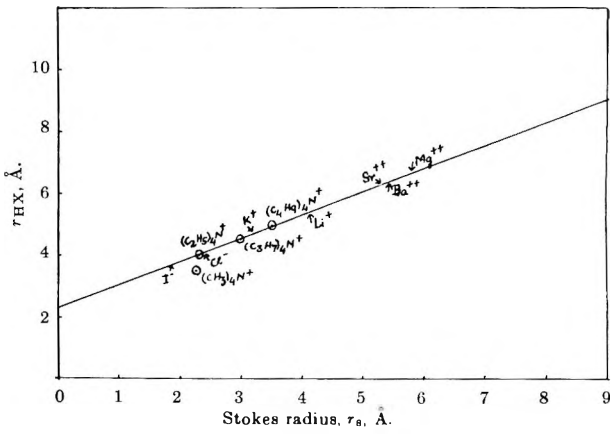

Figure 1.

Table III

Ion	Solvation no.	Ion	Solvation no.	Ion	Solvation no.
Li^+	5.1	Cl^-	2.1	Ba^{2+}	9.0
Na^+[a]	3.5	Br^-	1.7	Sr^{2+}	8.6
K^+	3.3	I^-	1.5	Ca^{2+}	8.6
Cs^+	2.6	CNS^-	1.3	Mg^{2+}	10.3
NH_4^+	2.7	NO_3^-	1.5		

[a] L. R. Dawson, *et al.* [*J. Am. Chem. Soc.*, **79**, 4654 (1957)] expect the solvation number of Na^+ in NMA to be 3–4 from diffusion coefficient measurements.

(10) R. A. Robinson and R. H. Stokes, "Electrolyte Solutions," Butterworth and Co. (Publishers) Ltd., London, 1959, pp. 124–126.

(11) E. R. Nightingale, Jr., *J. Phys. Chem.*, **63**, 1381 (1959).

rection factor becomes unity in the $r_s \approx 5$-Å. region.[11] This increase in the range of inapplicability of Stokes' law in NMA is obviously due to the larger size of the molecule of NMA.[12,13] So the appropriate calculations described elsewhere[10,11] lead to solvation numbers of some ions given in Table III.

It is clear from Table III that, roughly, the larger the crystal radius of an ion, the smaller the solvation and hence the common cations are more solvated than the anions. It appears that the solvation of K^+, Cs^+, Cl^-, Br^-, and I^- is larger in NMA than in water where the structure breaking of the solvent near these ions results in a net lower hydration. However, in view of the large association in NMA, leading to molecular chain formation,[12,13] these conclusions, based on the modified Stokes' law, may be doubtful. Further studies can only clarify the position.

(12) R.-Y. Lin and W. Dannhauser, *J. Phys. Chem.*, 67, 1805 (1963).
(13) R. M. Meighan, *et al.*, *ibid.*, 68, 503, 509 (1964).

Isotopic Exchange in Nitrogen Gas Induced by γ-Radiation[1]

by D. H. Dawes[2] and R. A. Back

Division of Pure Chemistry, National Research Council Laboratories, Ottawa, Canada
(Received February 8, 1965)

Isotopic exchange in nitrogen gas induced by γ-rays has been studied at pressures from 100 to 400 torr, at dose rates of about 10^5 and 10^6 r./hr., and at ambient temperatures. A value of $G_{exchange} = 7.3 \pm 0.5$ molecules/100 e.v. was found, independent of pressure, dose rate, and conversion. The effects of O_2, NO, N_2O, C_3H_6, Ne, Xe, and an electric field were also examined. A mechanism for the exchange is postulated which involves the random combination of nitrogen atoms formed by neutralization of ions and by dissociative excitation, together with a nonatomic process. It is suggested that the latter may be the exchange of atoms in the N_4^+ ion.

Isotopic exchange in gaseous nitrogen induced by ionizing radiation had, until recently,[3] apparently not been studied. Recent experiments in this laboratory indicated that the atomic exchange reaction in nitrogen is extremely slow at ordinary temperatures.[4] The mass spectrum of nitrogen is very simple (about 98% N_2^+ at 50 e.v.) and ion–molecule reactions of N_2^+ appear to be limited to the formation of N_4^+, so that a relatively simple radiolytic exchange mechanism might be expected which could be related in a simple way to primary processes in the radiolysis.

During the course of our own studies of this system, a note by Anbar and Perlstein appeared,[3] reporting some measurements of isotopic exchange in nitrogen gas induced by γ-rays and X-rays. Similar but more extensive experiments using γ-radiation are described in the present paper, and rather different conclusions are reached about the mechanism of the exchange.

Experimental

Nitrogen gas, about equimolar in $N^{14}N^{14}$ and $N^{15}N^{15}$, with about 4% $N^{14}N^{15}$, was irradiated in sealed vessels made from Pyrex tubing (8-mm. o.d.), of about 3-cc. volume, equipped with break-seals and thoroughly baked out under vacuum at 250° before use. Samples

(1) Issued as National Research Council No. 8496.
(2) National Research Council Postdoctoral Fellow, 1962–1964.
(3) M. Anbar and P. Perlstein, *J. Phys. Chem.*, 68, 1234 (1964).
(4) R. A. Back and J Y. P. Mui, *ibid.*, 66, 1362 (1962).

were prepared in a conventional mercury-free vacuum line evacuated by an oil diffusion pump guarded by a liquid nitrogen trap. Liquid helium was used to transfer nitrogen and other gases by condensation. Gases were thoroughly mixed by convection in a small spherical bulb before admission to the sample tubes. Vessels were sealed with the contents at the desired pressure, which was measured by a quartz spiral gauge accurate to about ±1 torr. Samples were usually prepared in batches of about half a dozen, retaining one as a blank and irradiating the others for various times.

Most of the samples were irradiated in a Gammacell 200 (Atomic Energy of Canada Ltd.) Co^{60} source with a nominal exposure dose rate of about 10^6 rads/hr.; a similar source, of about 10 times lower intensity, was used in some experiments.[5] Times of irradiation varied from about 10 to 250 hr. Temperature was about 35 and 27° in the high and low intensity sources, respectively.

After irradiation, samples were analyzed with a mass spectrometer, measuring the ratios of the peaks corresponding to masses 28, 29, and 30 as accurately as possible.[6] With samples containing NO, N_2O, or propylene, these adducts were removed by condensation at −196° to minimize their interference with the mass spectra.

Nitrogen gas with an N^{15} content of 95.5% was obtained from Merck Sharp and Dohme of Canada Ltd. Isotopically natural nitrogen was obtained from two sources, Linde (M.S.C. grade) and Airco (Research grade), both sealed in Pyrex flasks, and was used without further purification. Analysis by gas chromatography showed impurity concentrations within the specified tolerances, with two exceptions; the Linde nitrogen appeared to contain about 100 p.p.m. of argon, while the Airco gas showed similar amounts of hydrogen. The two types of nitrogen gave indistinguishable results.

Nitric oxide containing 96.6 atom % N^{15} was obtained from Bio-Rad Laboratories. Isotopically natural nitric oxide was obtained from Matheson. Both these gases were subjected to simple bulb-to-bulb distillation to remove traces of N_2 and N_2O. Nitrous oxide (Matheson), propylene (Phillips research grade), and neon and xenon (Linde, M.S.C. grade) were all used without purification. Air, admitted through a liquid nitrogen trap, was the source of oxygen, which thus contained about 5% argon.

Results

Treatment of Experimental Data. Within the accuracy of the mass spectrometric analysis, the percentage of $N^{14}N^{15}$ increased linearly with time of irradiation in all experiments. Values of R_{29}, the rate of formation of $N^{14}N^{15}$, were obtained from the least-squares slopes of plots of $N^{14}N^{15}$ *vs.* time of irradiation, usually for sets of about five samples of identical composition and pressure, irradiated for various times (including zero).

It is intuitively obvious that R_{29} would be a maximum for an equimolar mixture of $N^{14}N^{14}$ and $N^{15}N^{15}$, with $N^{14}N^{15} = 0$. It may be shown by a simple statistical treatment that

$$R_{29}/R^0_{29} = [4X^2Z + (Z - X)Y^2 - 4XZ^2]/(X - Z) \quad (1)$$

where X, Y, and Z represent mole fractions of $N^{14}N^{14}$, $N^{14}N^{15}$, and $N^{15}N^{15}$, respectively. The right-hand side of eq. 1 becomes indeterminate but approaches unity when $X = Z = 0.5$ and $Y = 0$, so that R^0_{29} corresponds to the maximum rate of formation of $N^{14}N^{15}$ from the equimolar mixture. In practice, approximately, $X = Z = 0.48$ and $Y = 0.04$, and all data except where noted otherwise were normalized using eq. 1, so that the ratio R_{29}/R^0_{29} was in most cases close to 0.92.

Ion current measurements in a small cylindrical Pyrex vessel, similar in size and shape to the radiolysis vessels, showed that the energy absorbed was not exactly a linear function of pressure. A small correction was made for this nonlinearity, so that the corrected values of R^0_{29} correspond to energy absorption proportional to pressure. Thus, if $G_{exchange}$ were independent of pressure, R^0_{29}, expressed as per cent of total N_2 per hour, would also be independent.

Finally, all values of R^0_{29} were corrected for decay of the γ-sources, assuming a linear dependence on radiation intensity.

Experiments with Pure Nitrogen. A number of experiments, about 40 samples in all, was made with pressures from 100 to 400 torr, irradiation times from about 10 to 160 hr., with both high and low intensity γ-ray sources and with both Linde and Airco nitrogen. All these data, after corrections were applied for the difference in radiation intensity in the two sources, for decay, for pressure, and for slight differences in composition, were plotted together on a single graph (Figure 1). Within the accuracy of the measurement of per cent $N^{14}N^{15}$, which was about ±1 p.p.h. or 0.04% of the total nitrogen, the data fell on a single linear plot of the change in per cent $N^{14}N^{15}$ *vs.* time, showing no

(5) We are grateful to Atomic Energy of Canada Ltd., Commercial Products Division, Ottawa, for the use of the high-intensity Gammacell and to Dr. A. G. Davies and Mr. C. Smith for assistance in carrying out the irradiations.

(6) We wish to thank Mr. R. Pilon for making these analyses.

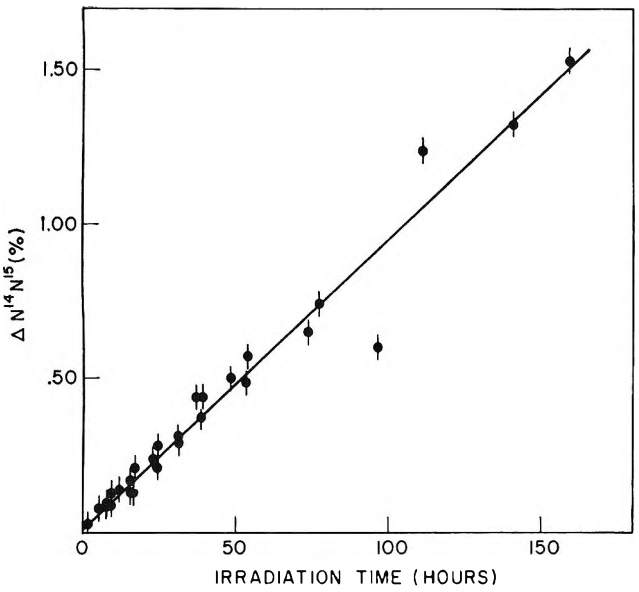

Figure 1. Radiation-induced change in the concentration of $N^{14}N^{15}$, expressed as a percentage of the total nitrogen. Radiation times have been normalized to take into account differences in dose rate and in composition of the gas. Vertical bars represent an uncertainty of ±0.04% or 1 p.p.h. in the $N^{14}N^{15}$ concentration.

significant trends with pressure, radiation intensity, or source of nitrogen. Least-squares treatment yielded a slope corresponding to $R^0_{29} = 1.029 \times 10^{-2}$% $N^{14}N^{15}$/hr. for the high intensity radiation source.

Dosimetry. The energy absorbed in the nitrogen gas was estimated by measurement of the saturation ion current in a cylindrical Pyrex ion chamber, with graphite coatings for electrodes, closely resembling the radiolysis vessels in size, shape, and wall thickness. Assuming a value of W, the average energy absorbed per ion pair, of 34.7 e.v.,[7] a value of G^0_{29} (corresponding to R^0_{29}) of 3.65 molecules of $N^{14}N^{15}$/100 e.v. was obtained. Finally, to obtain G for exchange (hereafter G_{ex}) as usually defined, this value must be multiplied by 2 to take into account the exchange of isotopically similar atoms. Thus, we find G_{ex} for pure nitrogen is 2 × 3.65 = 7.30 molecules/100 e.v. An uncertainty of ±0.5 may be rather arbitrarily attached to this value.

The Effect of Oxygen. Sets of samples containing about 0.01, 0.1, 0.4, and 2% O_2 were irradiated, and the results are shown in Table I. G(exchange) with 0.01% O_2 was indistinguishable within the experimental accuracy from its value with pure nitrogen, and, since analysis by gas chromatography showed $O_2 < 0.01$% in the nitrogen, it would seem that the experiments were not affected by oxygen impurity.

Experiments with Added Nitric Oxide. Two types of experiments were done. In the first, $N^{15}O$ was added to isotopically normal N_2. No detectable amounts of $N^{15}N^{15}$ were formed. Yields of $N^{14}N^{15}$ are shown in Table II, corrected in this case for the 3.4% $N^{14}O$ present and for the $N^{14}N^{15}$ originally present in the nitrogen; the yields are thus normalized to correspond to a mixture of pure $N^{14}N^{14}$ with pure $N^{15}O$.

Table I: The Effect of Oxygen

% O_2 added	G_{ex} Molecules/100 e.v.	G_{ex} Relative to pure N_2, %
0.00	7.30	100
0.01	7.45	102
0.10	6.50	89
0.39	6.20	85
2.40	4.30	59

Table II: $N^{14}H^{15}$ Production from $N^{15}O + N^{14}N^{14}$

% $N^{15}O$	G^0_{29}, molecules/100 e.v.
1.3	2.45
1.4	2.61
3.8	2.65
6.6	2.57
	Av. 2.57

In the second type of experiment, 1.1% nitric oxide, approximately equimolar in $N^{15}O$ and $N^{14}O$, was added to the usual $N^{14}N^{14}$–$N^{15}N^{15}$ mixture. G^0_{29} was reduced to 2.85.

Experiments with Added Nitrous Oxide. Again, two types of experiment were done. In the first, $N^{14}{}_2O$ was added to $N^{15}N^{15}$, and in Table III is shown G^0_{28},

Table III: Experiments with Added Nitrous Oxide

$N^{14}N^{14}O + N^{15}N^{15}$

% N_2O	G^0_{28}
0.0	0.00
1.4	2.56
3.6	1.99

$N^{14}N^{14}O + N^{14}N^{14}$–$N^{15}N^{15}$ mixture

% N_2O	G_{ex} Molecules/100 e.v.	G_{ex} Relative to pure N_2, %
0.0	7.30	100
1.6	5.26	72
3.3	4.48	61

(7) R. J. Weiss and W. Bernstein, *Radiation Res.*, **6**, 603 (1957).

the yield of $N^{14}N^{14}$, for two pressures of nitrous oxide. These data are corrected for $N^{14}N^{15}O$ impurity in the $N^{14}{}_2O$.

In the second type of experiment, $N^{14}{}_2O$ was added to the usual $N^{14}N^{14}$–$N^{15}N^{15}$ mixture. $G^0{}_{29}$, normalized in the usual way, is shown in Table III.

The Effect of Added Propylene. In one series of samples, 1.7% propylene was added to the usual $N^{14}N^{14}$–$N^{15}N^{15}$ mixture. G(exchange) was reduced to 3.58, 49% of its value in pure nitrogen.

The Effect of Inert Gases. Four series of samples, two each with neon and xenon added to the usual nitrogen mixture, were irradiated. The results are summarized in Table IV.

Table IV: Nitrogen–Rare Gas Mixtures

Compn.	G_{ex} (based on energy absorbed by N_2) Molecules/100 e.v.	Relative to pure N_2, %
Pure N_2	7.30	100
N_2 + 46% Ne	11.23	154
N_2 + 52% Ne	9.43	129
N_2 + 42% Xe	2.85	39
N_2 + 51% Xe	2.48	34

The Effect of an Electric Field. Several experiments were made with pure nitrogen in a cylindrical Pyrex vessel with graphite coatings for electrodes, similar to one described previously,[8] but smaller, 1.1 cm. in diameter, 15 cm. long, with a volume of about 26 cc., to study the effect of an electric field and to permit direct comparison of ion current and chemical yield in the same vessel. Pressure of nitrogen was 178 torr, and the high-intensity γ-source was used. The following results were observed. (a) With no field applied, the rate of exchange was about 20% higher than in the usual radiolysis vessels. (b) The saturation ion current measured at the end of a 65-hr. irradiation was 35% higher than that measured initially. (c) The rate of exchange with 1000 v. between the electrodes, giving an average X/p of 10.2 v. cm.$^{-1}$ torr^{-1}, was about 10% higher than in the experiment in the same vessel with no field applied.

The most probable explanation of these observations is that nitrogen atoms or ions reacted with the graphite electrodes, forming a product (perhaps cyanogen) which reduced W, thereby increasing the ion current. At the same time, the exchange process seems to have been enhanced. Uncertainties arising from these complications render unreliable the direct measure of an ion pair yield and obscure any effect of the applied field. About all that can be said is that an electric field does not grossly affect the exchange process.

Discussion

Pure Nitrogen. The present results are in fair agreement with those of Anbar and Perlstein.[3] Our G_{ex} of 7.3 ± 0.5 may be compared with their value of 9.5 ± 0.25, and we confirm the absence of dependence on pressure and dose rate within our more limited range of these variables. In the absence of more detailed knowledge of the dosimetry methods of Anbar and Perlstein, the reason for our lower G value is not obvious.

Anbar and Perlstein suggested that radiation-induced exchange in nitrogen gas proceeded through the production and subsequent random combination of nitrogen atoms

$$N^{14}N^{14},\ N^{15}N^{15} \overset{\gamma\text{-rays}}{\sim\!\!\sim\!\!\rightarrow} 2N^{14} + 2N^{15} \quad (2)$$

$$N^{14} + N^{15} \longrightarrow N^{14}N^{15} \quad (3)$$

$$N^{14} + N^{14} \longrightarrow N^{14}N^{14} \quad (4)$$

$$N^{15} + N^{15} \longrightarrow N^{15}N^{15} \quad (5)$$

For $G_{ex} = 7.3$, $G_N = 14.6$ is required by this mechanism since two atoms are needed for each $N^{14}N^{15}$ molecule formed (the inefficiency arising from reactions 4 and 5 has already been taken into account in the definition of G_{ex}). One source of nitrogen atoms is undoubtedly ionization followed by dissociative neutralization

$$N_2 \overset{\gamma\text{-rays}}{\sim\!\!\sim\!\!\rightarrow} N_2^+ + e^- \quad (6)$$

$$N_2^+ + e^- \longrightarrow N_2^* \longrightarrow 2N \quad (7)$$

Taking W, the average energy per ion pair,[7] as 34.7, then $G_{N_2^+} = 2.88$ and G_N(from ionization + neutralization) = 5.76. The formation of $N^+ + N$, estimated to be 2% from the mass spectrum of nitrogen, is ignored throughout.

Anbar and Perlstein suggested that the rest of the nitrogen atoms required ($G = 8.84$ for our G_{ex} of 7.30, or $G = 13.24$ for their $G_{ex} = 9.5$) came from excitation of nitrogen molecules followed by collision-induced dissociation. This mechanism seems to us an extremely unlikely one in several respects. Its most serious flaw is that there is simply not enough energy available to produce enough nitrogen atoms by an excitation mechanism. Ionization must use up at least 2.88 × 15.56 = 44.8 e.v. out of each 100 e.v. absorbed. A wastage of energy in "sub-dissociation" electrons (electrons left after a collision with insufficient energy to dissociate nitrogen) of about 9.76 × 2.88 × 0.5 = 14.1 e.v. may be roughly estimated. This leaves a maximum of

(8) R. A. Back, T. W. Woodward, and K. A. McLauchlan, *Can. J. Chem.*, **40**, 1380 (1962).

about 41 e.v. available for excitation, or enough to dissociate 41/9.76 = 4.2 molecules of N_2/100 e.v. absorbed, or G_N = 8.4. This is an absolute maximum since it allows for no wastage of energy through excitation or ionization involving energies about the bare thresholds for these processes or for excitation to states below the dissociation energy. Taking these factors into account, a more realistic estimate of G_N(excitation) would range between 6 and 3, well below the 8.84 required by our G_{ex} = 7.3 or the 13.24 required for G_{ex} = 9.5 reported by Anbar and Perlstein.

Thus, it appears that simple atom combination does not provide an adequate mechanism for radiolytic exchange in nitrogen. One obvious way to account for additional exchange is the atomic exchange reaction

$$N^{14} + N^{15}N^{15} \longrightarrow N^{14}N^{15} + N^{15} \qquad (8)$$

This was ruled out by Anbar and Perlstein because G_{ex} did not show the dependence on N_2 pressure and radiation intensity expected of an atomic chain mechanism and because "nitrogen atoms ... were shown (by Back and Mui) not to undergo isotopic exchange with nitrogen molecules."[3] The latter reasoning apparently takes no account of the higher pressures and lower atom concentrations in the radiolysis system which favor reaction 8 relative to the combination reactions 3–5; a quantitative consideration of these factors, however, supports the conclusion that reaction 8 did not occur. Back and Mui[4] observed no exchange at 1000° and were able to establish an upper limit for k_8 at 1000° of 4×10^8 cc. mole^{-1} sec.$^{-1}$ and a reasonable lower limit for the activation energy of 14 kcal./mole. These data lead to an upper limit of $k_8 \leqq 64$ cc. mole^{-1} sec.$^{-1}$ at 60°, the highest temperature used by Anbar and Perlstein. Assuming a rate of production of nitrogen atoms equal to the rate of exchange for a radiation intensity of about 10^6 rads/hr., or 10^{-2}%/hr., and termolecular combination of atoms with a rate constant[9] of 5.7×10^{15} cc.^{2} mole^{-2} sec.$^{-1}$, a steady-state atom concentration of 2.2×10^{-12} mole/cc. may be estimated, and thence an upper limit for the rate of reaction 8, of 5×10^{-5}%/hr., some 200 times slower than the observed rate of exchange. The upper limit for k_8 estimated by Back and Mui was a generous one, and the activation energy is not likely to be less than 14 kcal. The present experiments and most of those of Anbar and Perlstein were done at temperatures considerably lower than 60°. Homogeneous combination of atoms was assumed in the calculations; this gives an upper limit for the atom concentration, which would be reduced if wall combination were occurring, making reaction 8 even less likely. All these facts, combined with the lack of pressure or intensity dependence observed by Anbar and Perlstein and confirmed by us in a limited way, would seem to rule out reaction 8 as an effective exchange process in the present system. There remains a possibility that translationally hot nitrogen atoms, generated in reaction 7 or by direct dissociative excitation, could have reacted *via* reaction 8 in a limited, nonchain process. While rather unlikely, this is difficult to rule out entirely.

The most likely cause of the high value of G_{ex} in pure nitrogen appears to be the reaction

$$N_2^+ + N_2 \longrightarrow N_4^+ \qquad (9)$$

This reaction is well established by mass spectrometry[10] and by ionic-drift techniques,[11] and there is little doubt that at the pressures of the present experiments, N_2^+ was completely converted to N_4^+. There have been no suggestions about the structure of N_4^+ although a rather loose $N_2^+ \cdot N_2$ complex has been tacitly implied. If a more intimate association occurred, however, in which N_2^+ and N_2 could effectively exchange atoms (perhaps through a four-membered ring), then, on neutralization, atomic exchange would be effected with the usual 50% efficiency, *e.g.*

$$(N^{14}N^{14})^+ + N^{15}N^{15} \longrightarrow \begin{bmatrix} N^{15}\text{–}N^{15} \\ | \quad | \\ N^{14}\text{–}N^{14} \end{bmatrix}^+ \xrightarrow{+e^-}$$

$$N^{14}N^{15} + N^{14} + N^{15} \qquad (10)$$

This would lead to an additional molecule of $N^{14}N^{15}$ for every two ion pairs, or $G^0_{29} = 1.44$ and $G_{ex} = 2.88$ (taking into account the regeneration of $N^{14}N^{14}$ and $N^{15}N^{15}$). The atoms produced in reaction 10 would also contribute to exchange through random combination as before.

There is one difficulty with this mechanism. If atoms were exchanged within the N_4^+ structure, then any redissociation into $N_2^+ + N_2$ before neutralization would give rise to additional exchange. An ionic chain mechanism would result, with dependence on intensity and pressure, contrary to observations. In ionic-drift experiments in nitrogen,[11] it was thought that N_2^+ and N_4^+ were in facile equilibrium, and, from the effect of field strength and of temperature, an exothermicity of about 12 kcal. was estimated for reaction 9. If one assumes for the reverse of reaction 9 a "normal" unimolecular frequency factor of 10^{14} sec.$^{-1}$, half-lives for N_4^+ with respect to decomposition

(9) J. T. Herron, J. L. Franklin, P. Bradt, and V. H. Dibeler, *J. Chem. Phys.*, **30**, 879 (1959).

(10) P. F. Knewstubb and A. W. Tickner, *ibid.*, **37**, 2941 (1962).

(11) R. N. Varney, *ibid.*, **31**, 1314 (1959).

of 3×10^{-8}, 5×10^{-5}, and 0.1 sec. may be calculated, corresponding to activation energies of 10, 15, and 20 kcal. The unimolecular rate constant, however, is probably considerably lower than its high-pressure limit, and, in fact, the decomposition may well be closer to a bimolecular process. If one assumes a "normal" bimolecular pre-exponential factor of 10^{11} l. mole^{-1} sec.$^{-1}$, then at 60°, with a nitrogen concentration equivalent to 300 torr at 25°, half-lives for N_4^+ of 2×10^{-3}, 3, and 6×10^3 sec. may be estimated for activation energies of 10, 15, and 20 kcal., respectively. Ion current measurements with an intermittent collecting field[12] indicated an actual ion half-life with respect to neutralization of about 10^{-2} sec. in our radiolysis vessels at 300 torr pressure with the low-intensity γ-source. It is fairly obvious in view of the uncertainties in the activation energy and the pressure dependence that the calculations can neither confirm nor deny the decomposition of N_4^+ before neutralization in the present system, and the suggested mechanism is at least not impossible.

It was hoped that experiments with an electric field applied would cast some light on the stability of N_4^+ and its role in the exchange. The value of X/p of 10.2 v. cm.$^{-1}$ torr^{-1} corresponds to an ion "temperature" (as defined by Varney[11]) of about 170°, so that decomposition of N_4^+ should have been considerably enhanced. A 10% increase in G_{ex} was observed with the field applied, but, as was pointed out earlier, complications in the applied-field experiments made their interpretation very uncertain.

If N_4^+ were, in fact, redissociating appreciably, there would still be the alternative that exchange occurred not in N_4^+, but in the excited N_4 species formed on neutralization. This would again be a non-chain process and would contribute an additional $G_{ex} = 2.88$, as before. The present data do not distinguish clearly between this alternative and the original suggestion although it will be seen that some evidence supports the latter.

Our suggested mechanism for isotopic exchange in pure nitrogen is summarized in Table V. For $G_{ex} = 7.3$, it is seen that G_N(by excitation) = 3.08 is required. For $G_{ex} = 9.5$, as reported by Anbar and Perlstein, G_N(by excitation) = 7.48 would be needed, which, while still rather unlikely, is not impossibly high. It will be seen that the mechanism outlined in Table V accounts reasonably well for the effects of added gases.

The Effect of Oxygen. The addition of 2.4% oxygen reduced G_{ex} from 7.3 to 4.3. This is most simply explained by negative ion formation

$$O_2 + e^- + M \longrightarrow O_2^- + M \qquad (11)$$

If the consequent modification of the neutralization of N_4^+ eliminated formation of atoms by reaction 10, G_{ex} would be reduced by 2.88, close to the observed reduction of 3.0. One might also expect removal of nitrogen atoms, formed by excitation, by the reaction

$$N + O_2 \longrightarrow NO + O \qquad (12)$$

and this probably did occur. However, the reaction

$$N + NO \longrightarrow N_2 + O \qquad (13)$$

is about 10^6 times faster (at 60°) than reaction 12,[13,14] so that NO formed in (12) would rapidly react *via* (13), with the resulting exchange being indistinguishable from random combination of atoms.

Table V: Isotopic Exchange in Pure Nitrogen

Mechanism	Yields of intermediates	G_{ex} Molecules/ 100 e.v.	G_{ex} % of total
Random combination of atoms formed by the neutralization of N_2^+ or N_4^+	$G_N = 5.76$	2.88	39
Random combination of atoms formed by dissociative excitation	$G_N = 3.08$	1.54	21
Exchange in N_4^+ or in neutral excited N_4	$G_{N_4^+ \text{ or } N_4^*} = 2.88$	2.88	39
	Total = 7.30		

This explanation of the effect of oxygen requires that the exchange *via* N_4^+ be unaffected by oxygen, which perhaps lends support to the exchange occurring in N_4^+ rather than N_4^*.

Experiments with Added Nitric Oxide. If the exchange in nitrogen were due entirely to random combination of atoms and if NO acted only by removing atoms *via* reaction 13, it is easily seen that G^0_{29} from the $N^{15}O$–$N^{14}N^{14}$ system should have been four times that in pure N_2, or 14.6, while in the $N^{14}O$–$N^{15}O$ + $N^{14}N^{14}$–$N^{15}N^{15}$ system, G^0_{29} should have been twice that in pure N_2, or 7.3. The observed values of 2.57 and 2.85 show that the atom combination mechanism is inadequate and/or the action of NO is more complex.

The value of $G^0_{29} = 2.57$ observed in the $N^{15}O$–$N^{14}N^{14}$ system may be taken as an upper limit for G_N *in the*

(12) R. A. Back, D. H. Dawes, and C. J. Wood, to be published.

(13) M. A. A. Clyne and B. A. Thrush, *Proc. Roy. Soc.* (London), **A261**, 259 (1961).

(14) J. T. Herron, *J. Chem. Phys.*, **35**, 1138 (1961).

presence of NO (it is an upper limit because $N^{14}N^{15}$ could have arisen by some reaction other than (13) although this seems unlikely). Thus, out of an estimated yield of atoms of 8.84 in pure nitrogen (Table V), only 29% was still generated in the presence of NO. This approximately fits a mechanism in which NO interfered with the neutralization step of reaction 10, preventing atom formation by this means but left the dissociative excitation process unaffected. There is a difficulty with this explanation in that no $N^{15}N^{15}$ was produced, which implies that no free N^{15} atoms were formed by dissociation or reaction of $N^{15}O$ since these would have rapidly reacted by reaction 13 to give N^{15}-N^{15}. Charge transfer, followed by neutralization of NO^+, seems incompatible with this observation, and perhaps this is evidence for the participation of an ion–molecule reaction.

In the $N^{14}O$–$N^{15}O$ + $N^{14}N^{14}$–$N^{15}N^{15}$ system, G^0_{29} = 2.85, and from the $N^{15}O$–$N^{14}N^{14}$ experiments, it may be estimated that $N^{14}N^{15}$ equivalent to $G^0_{29} = 0.5 \times 2.57 = 1.29$ arose from the same reactions with NO that gave $N^{14}N^{15}$ in the latter system. Thus "normal" exchange in the nitrogen to the extent of $G^0_{29} = 2.85 - 1.29 = 1.56$ or $G_{ex} = 3.12$ was occurring in the presence of NO. This is convincing evidence that the purely atomic mechanism is inadequate as reaction 13 is very efficient[10] and should have completely eliminated nitrogen atoms from the system. The observed G_{ex} = 3.12 in the presence of NO corresponds fairly closely to the 2.88 estimated for the N_4^+ exchange process, and this seems the most likely explanation. This also requires that exchange occurs within the N_4^+ species and therefore that its formation should be rapid enough so that no charge transfer or other reaction of N_2^+ with NO could interfere. This is not an unreasonable requirement.

The suggested mechanism for exchange in nitrogen in the presence of NO may now be summarized

$$N_2 \xrightarrow{\text{ionization}} N_2^+ + e^- \quad (6)$$

$$N_2 \xrightarrow{\text{excitation}} 2N \quad (14)$$

$$N_2^+ + N_2 \longrightarrow N_4^+ \text{ (which exchanges internally)} \quad (9)$$

$$N_4^+ + NO + e^- \longrightarrow 2N_2 \text{(from } N_4^+\text{) (no N, no further exchange, and no decomposition of NO)} \quad (15)$$

$$N + NO \longrightarrow N_2 + O \quad (13)$$

Reaction 15 probably proceeds through several steps, whose mechanism is uncertain.

Experiments with Added Nitrous Oxide. Recently[15] it has been suggested that added N_2O acted as a quantitative scavenger of electrons in the radiolysis of propane

$$N_2O + e^- \longrightarrow N_2 + O^- \quad (16)$$

and reduced product yields by modifying the ion neutralization processes. Its action in the present system appears to be very similar, with one or two minor complications.

In the $N^{14}{}_2O$ + $N^{15}N^{15}$ system, G^0_{28} rather surprisingly decreased with rising N_2O concentration (Table III). The values observed could be extrapolated back reasonably well to a value of 2.88 (G_{e^-}) at zero concentration of N_2O, as one would expect from reaction 16. The cause of the decrease in G^0_{28} with rising N_2O concentration is not obvious, but the stabilization of an N_2O^- intermediate by association with another N_2O molecule is one possibility.

In the $N^{14}{}_2O$ + $N^{14}N^{14}$–$N^{15}N^{15}$ experiments, G_{ex} fell to 4.48 at the highest N_2O concentration. This is close to the value of 4.42 expected if N_2O interfered only with the neutralization step of reaction 10, preventing formation of nitrogen atoms by its presence in the neutralization process. Nitrous oxide is thus seen to resemble oxygen in its effect on the nitrogen exchange.

The Effect of Added Propylene. The persistence of isotopic exchange to the extent of G_{ex} = 3.58 in the presence of propylene at a concentration which should have removed nitrogen atoms completely[16] confirms again the occurrence of a nonatomic exchange process. To a fair approximation, this process corresponds to the postulated exchange *via* N_4^+, with G_{ex} = 2.88.

The Effect of Rare Gases. The experiments with neon and xenon showed the general behavior expected from a consideration of the pertinent ionization and excitation potentials, shown in Table VI.

Table VI: Ionization and Excitation Potentials of N_2, Ne, and Xe

Gas	Min. I.P., e.v.	Min. E.P., e.v.
N_2	15.56	6.1
Ne	21.56	16.6
Xe	12.13	8

The net transfer of energy from nitrogen to xenon indicated by the reduction in G_{ex} was about 60 to 65% efficient. This could represent completely efficient

(15) G. R. A. Johnson and J. M. Warman, *Nature*, **203**, 73 (1694).
(16) G. S. Trick and C. A. Winkler, *Can. J. Chem.*, **30**, 915 (1952).

charge transfer from N_4^+ and complete quenching of dissociative excitation by energy transfer (note that the minimum E.P. for Xe is less than 9.76, the dissociation energy of N_2), leaving only exchange *via* the N_4^+ mechanism. More probably, the net effect arose from a more complex summation of the various energy- and charge-transfer processes that are possible.

The neon–nitrogen system is perhaps simpler since both Ne^+ and Ne excited to its lowest excitation level of 16.6 e.v. would be capable of ionizing or dissociating nitrogen, and no reverse transfers from nitrogen to neon should be possible. The energy absorbed by the neon, based on stopping powers relative to air of 0.969 and 0.664 for nitrogen and neon, respectively,[17] and taking averages of G_{ex} and per cent Ne for the two experiments (Table IV), was 124% efficient (relative to energy absorbed in nitrogen) in causing exchange in the nitrogen. The higher efficiency is probably due to increased ionization of nitrogen relative to excitation, which occurred because the minimum E.P. of neon exceeds the I.P. of nitrogen. This enhances the exchange reaction because, by our proposed mechanism, ionization is three times as efficient as excitation in causing exchange.

Summary

The present results show clearly that another exchange process in addition to the random combination of atoms must be operative in the γ-ray-induced isotopic exchange in nitrogen gas. The mechanism we have suggested accounts fairly well for the experimental facts, both for pure nitrogen and for mixtures with various additives, although the role of N_4^+ must be regarded for the moment as speculative. Further experiments are planned to test this and other aspects of the proposed mechanism.

(17) G. G. Meisels, *J. Chem. Phys.*, **41**, 51 (1964).

Kinetics of the Decomposition of Hydrogen Oxalate Ion in Glycerine Solution

by M. A. Haleem and Peter E. Yankwich

Noyes Laboratory of Chemistry, University of Illinois, Urbana, Illinois *(Received February 11, 1965)*

The decomposition of hydrogen oxalate ion in 96% glycerine solution has been studied between 88 and 121° over a limited range of degree of decomposition; the reaction is first order with respect to the ion, with observed Arrhenius parameters: $E = 24.7 \pm 0.3$ kcal. mole^{-1}, and log A (sec.$^{-1}$) $= 9.5 \pm 0.2$. The similarity of free acid-monoanion activation parameter shifts in this system and those found for malonic acid in water is shown. The observations support (but not conclusively) the notion that all four decompositions proceed *via* intramolecular hydrogen transfer.

Introduction

Some years ago, Brown,[1] in a review of the decarboxylation of oxalic acid, remarked, "Further work on this dibasic acid is required, as nothing is known of the stability of its univalent anion, $HO_2C{\cdot}CO_2^-$"; the view is still valid. This report concerns a brief investigation of the kinetics of the decomposition of hydrogen oxalate ion, undertaken to provide information useful to the planning of later isotope effects work parallel to earlier studies on malonic acid[2,3] and hydrogen malonate ion.[4,5]

(1) B. R. Brown, *Quart. Rev.* (London), **5**, 131 (1951).

(2) P. E. Yankwich and R. L. Belford, *J. Am. Chem. Soc.*, **75**, 4178 (1953); **76**, 3067 (1954).

(3) P. E. Yankwich and R. M. Ikeda, *ibid.*, **81**, 5054 (1959); **82**, 1891 (1960).

Experimental

Reagents. Fisher "Certified" analytical reagent oxalic acid and 96% glycerine were used; the anhydrous oxalic acid was heated to 110° for 1 hr. before being stored over magnesium perchlorate *in vacuo*, while the glycerine was used as received. Baker's analyzed carbonate-free sodium hydroxide and freshly boiled deionized water were used for partial neutralization of the oxalic acid.

Apparatus and Procedure. The flow system used in the study of the kinetics of the decomposition of the free acid[6] was employed in these experiments. Glycerine (50 ml.) was placed in the reactor and 40.00 or 60.00 mg. of sodium hydroxide dissolved in 0.50 ml. of water was added. Exactly 90.00 mg. of oxalic acid was weighed into a small glass dish which was set onto the end of a movable probe inside the reaction vessel. The reaction was started in the closed system by tipping the oxalic acid into the solvent (solution being assisted by agitation of the reactor), and quenched by the addition of 50 ml. of cold aqueous 0.10 *M* sulfuric acid. The reaction vessel was then lifted out of the thermostat and dry tank nitrogen was used to sweep the carbon dioxide product into the traps of the gas-handling system.

The carbon dioxide product in the traps was purified carefully by distillation, then estimated manometrically. Each kinetics run thus yielded just one α (degree of decomposition)–t (time) data pair. Experiments at half-neutralization were carried out at 88.0, 100.0, 112.0, and 121.0°; experiments at three-fourths neutralization[7] were carried out only at 100.0°. As a convenience, run times were limited to 4 hr. or less; as a result, only the first few per cent decomposition was observed, except at the highest temperature, and late-occurring anomalies in the reaction would have been missed.

Results

The values of the apparent first-order rate constant (k_1) obtained from least-squares analysis of all data pairs are shown in Table I, as is other information concerning the experiments at each temperature. In Table II we compare the various activation parameters for the decompositions of oxalic acid[6] and hydrogen oxalate ion in 96% glycerine, with those calculated from the data of Hall[8] for the decarboxylation of malonic acid and hydrogen malonate ion in aqueous solutions.

Table I: Rate of Decomposition of Hydrogen Oxalate Ion in 96% Glycerine Solution

Run temp., °C.	No. of data pairs	α_{max}	Av., $k_1 \times 10^5$, sec.$^{-1}$
88.0	7	0.0497	0.341 ± 0.004
100.0	5	0.0361	1.00 ± 0.04
	10	0.0391	0.92 ± 0.02[a]
112.0	8	0.124	2.83 ± 0.05
121.0	8	0.295	6.17 ± 0.14

[a] Three-fourths neutralization of oxalic acid; other results are for half-neutralization.

Table II: Comparison of Activation Parameters

Compd.	E, kcal./mole	Log A (sec.$^{-1}$)	ΔH^*, kcal./mole	ΔS^*, cal./mole deg.	ΔF^*, kcal./mole	$k_1 \times 10^5$, sec.$^{-1}$[a]
Malonic acid[b]	30.8	13.4	30.0	+0.1	29.9	124
Hydrogen malonate ion[b]	28.5	11.0	27.7	−10.8	32.2	8.4
Oxalic acid[c]	28.4 ± 0.2[d]	12.3 ± 0.1[d]	27.6 ± 0.2[d]	−4.9 ± 0.4[d]	29.6 ± 0.3[d]	197
Hydrogen oxalate ion	24.7 ± 0.3[d]	9.5 ± 0.2[d]	23.9 ± 0.3[d]	−17.7 ± 0.8[d]	31.2 ± 0.4[d]	25.8

[a] At 140°. [b] Reference 8. [c] Reference 6. [d] Errors are all standard deviations evaluated by a least-squares procedure.

Discussion

The decomposition of hydrogen oxalate ion is kinetically first order, within ±0.1 (estimated), over the range of decomposition investigated. Though the agreement between the two results at 100.0° is not so close as one would wish, it is clear that, as expected, the oxalate ion is stable to decomposition under the reaction conditions.

(4) P. E. Yankwich and H. S. Weber, *J. Am. Chem. Soc.*, 77, 4513 (1955); 78, 564 (1956).

(5) P. E. Yankwich and R. M. Ikeda, unpublished experiments.

(6) M. A. Haleem and P. E. Yankwich, *J. Phys. Chem.*, 69, 1729 (1965).

(7) In later calculations it is assumed that 40.00 mg. of sodium hydroxide results in the production of 0.9992 mmole of $HO_2CCO_2^-$ and 0.0004 mmole of $^-O_2CCO_2^-$ from the original 0.9996 mmole of oxalic acid; where 60.00 mg. of sodium hydroxide was employed, the calculated quantities of these ions are 0.4992 and 0.5004 mmoles, respectively. Because sodium hydroxide picks up water rapidly, these numbers are probably in error in the third figure by ±3.

(8) G. A. Hall, *J. Am. Chem. Soc.*, 71, 2691 (1949).

It is unfortunate that the only data available for comparison with the results obtained in this study are for the monoanion of a different dicarboxylic acid in a different solvent. However, the voluminous work of Clark on the decompositions of oxalic acid[9] and malonic acid[10] in many different solvents provides support for the view that the relative inertness of glycerine toward oxalic acid is similar to that of water toward malonic acid. Although the character of water is such that one would not feel secure in a like statement about the respective monoanions, the results in Table II suggest that there are similar relationships between the acid monoanion comparisons for the two acids.

For both of the free acids it has been proposed that the mechanism of decarboxylation involves intramolecular hydrogen transfer.[11-14] Carbon isotope effect studies on hydrogen malonate ion[4,5] support the intuitive conclusion that carbon dioxide originates from the COOH group and not from the CO_2^- group in decarboxylation in both quinoline and dioxane; presumably, the situations in glycerine and water would not be the reverse. If the monoanion decarboxylations involve intramolecular hydrogen transfer, the entropies of activation should be more negative than in the cases of the free-acid decompositions, but the other activation parameters should be little changed. Unfortunately, a similar shift in entropy of activation would be predicted were a bimolecular solvent-bridging step effective for the monoanions; thus, the results at hand do not permit elucidation of this aspect of the mechanism. To us, however, the intramolecular mechanism seems definitely the more reasonable.

Carbon isotope effect studies designed to shed additional light on this reaction are in progress in this laboratory.

Acknowledgment. This research was supported by the U. S. Atomic Energy Commission.

(9) A lead reference is L. W. Clark, *J. Phys. Chem.*, **67**, 1355 (1963).

(10) A lead reference is L. W. Clark, *ibid.*, **65**, 2271 (1961).

(11) A. Dinglinger and E. Schröer, *Z. physik. Chem.*, **A179**, 401 (1937).

(12) J. A. King, *J. Am. Chem. Soc.*, **69**, 2738 (1947).

(13) F. H. Westheimer and W. A. Jones, *ibid.*, **63**, 3283 (1941).

(14) K. J. Pedersen, *ibid.*, **51**, 2098 (1929); **60**, 595 (1938).

Electromotive Force Studies in Aqueous Solutions at Elevated Temperatures. VI. The Thermodynamic Properties of HCl–NaCl Mixtures[1]

by M. H. Lietzke, H. B. Hupf,[2] and R. W. Stoughton

Department of Chemistry, University of Tennessee, Knoxville, Tennessee, and Chemistry Division, Oak Ridge National Laboratory, Oak Ridge, Tennessee *(Received February 12, 1965)*

The activity coefficient of HCl in HCl–NaCl mixtures has been studied to 175°. At constant temperature and ionic strength the logarithm of the activity coefficient of HCl in the mixtures varies linearly with the molality of NaCl. The activity coefficient of NaCl in the mixtures was calculated by using the parameters describing this variation and those for the variation of the activity coefficient of NaCl with ionic strength in pure NaCl solutions. The activity coefficient behavior observed in the HCl–NaCl mixtures is compared with that observed in the previously studied HBr–KBr mixtures.

In a previous paper[3] in this series the original e.m.f. data obtained in HCl solutions[4,5] were used to recalculate the thermodynamic properties of these solutions in a manner consistent with the assumption that over the temperature range studied (25–225°) the value of ΔC_p is a constant. This assumption permitted all of the data to be used simultaneously in estimating both the standard potential of the Ag, AgCl electrode as a function of temperature and the parameters describing the activity coefficient of HCl as a function of temperature and ionic strength. In the present work these data have been combined with measurements of the e.m.f. of the cell, $Pt–H_2(p)|HCl(m_2), NaCl(m_3)|AgCl, Ag$, and of the osmotic coefficient of NaCl[6] to calculate the thermodynamic properties of both HCl and NaCl in HCl–NaCl mixtures. In addition, the original e.m.f. data in the HBr–KBr system[7] were used to recalculate the thermodynamic properties of HBr–KBr mixtures in a manner consistent with the present calculations on HCl–NaCl mixtures, so that a direct comparison of these two systems could be made.

Experimental

The experimental apparatus and the preparation of electrodes and solutions were the same as described previously.[4,8] The e.m.f. measurements were carried out in the temperature range 25–175° in solutions of total ionic strength 0.4 and 1.0 in which the ratio of HCl to NaCl was varied. The e.m.f. values taken at the same temperature were reproducible to *ca.* ±0.5 mv. In general, they were more reproducible in the solutions containing a higher fraction of HCl. No drift of e.m.f. with time was observed.

Results and Discussion

In treating the results, the hydrogen pressure was calculated by subtracting the vapor pressure of the solution from the observed total pressure, while the vapor pressure of the solution was obtained by taking the vapor pressure of pure water at the temperature of measurement from the steam tables[9] and correcting

(1) Research sponsored by the U. S. Atomic Energy Commission under contract with the Union Carbide Corp.

(2) This paper is based in part on a thesis by H. B. Hupf presented to the Department of Chemistry of the University of Tennessee in partial fulfillment of the requirements for the M.S. degree, March 1965.

(3) M. H. Lietzke and R. W. Stoughton, *J. Phys. Chem.*, **68**, 3043 (1964).

(4) R. S. Greeley, W. T. Smith, Jr., R. W. Stoughton, and M. H. Lietzke, *ibid.*, **64**, 652 (1960).

(5) R. S. Greeley, W. T. Smith, Jr., M. H. Lietzke, and R. W. Stoughton, *ibid.*, **64**, 1445 (1960).

(6) E. R. Gardner, P. T. Jones, and H. J. de Nordwall, *Trans. Faraday Soc.*, **59**, 1994 (1963).

(7) M. H. Lietzke and R. W. Stoughton, *J. Phys. Chem.*, **67**, 2573 (1963).

(8) M. B. Towns, R. S. Greeley, and M. H. Lietzke, *ibid.*, **64**, 1861 (1960).

(9) E. Schmitt, Ed., "VDI-Wasserdampftafeln," 4th Ed., Springer-Verlag, Berlin, 1956, pp. 15–20.

Table I: Values of the E.m.f. in Volts for the Cell, Pt–$H_2(p)$|HCl(m_2), NaCl(m_3)|AgCl, Ag, and Deviations[a] of the E.m.f. Values Calculated from Smoothed Activity Coefficients

		t, °C.					
m_2	m_3	25	60	90	125	150	175
0.0102	0.3903	0.3782	...	...	0.3488	0.3334	...
		0			+7	−2	
0.0309	0.3795	0.3490	0.3404	...	...	0.2913	0.2723
		−1	−6			−13	−11
0.1015	0.2975	0.3191	0.3077	0.2932	0.2709	0.2513	0.2294
		0	0	+5	+11	+8	+7
0.2051	0.1986	...	0.2874	0.2710	0.2458	0.2246	...
			+1	+3	0	−4	
0.0302	0.9628	0.3266	0.3158	0.3032	0.2818	0.2650	0.2460
		+1	−2	+8	−3	−1	−1
0.0971	0.8877	0.2961	0.2822	0.2660	0.2421	0.2223	0.2010
		−4	−4	−1	−2	−5	−4
0.2484	0.7467	0.2723	0.2552	0.2360	0.2100	0.1891	0.1660
		+8	+2	−2	+3	+8	+11
0.4824	0.4950	...	0.2357	0.2150	0.1870	...	...
			−3	−8	−5		

[a] The deviations are given below each e.m.f. as observed e.m.f. values less the values calculated from smoothed activity coefficients. Thus, a positive deviation indicates that the e.m.f. reported here is algebraically larger.

for the presence of NaCl and HCl in solution by Raoult's law. Each e.m.f. value was corrected to 1.00 atm. of hydrogen pressure by subtracting $(RT/2\mathfrak{F})$ ln f_{H_2}, where the hydrogen fugacity f_{H_2} was taken equal to the hydrogen pressure. The solubility of AgCl was neglected, and the ionic strength was taken to be equal to the sum of the HCl and NaCl molalities. The corrected e.m.f. values E at each ionic strength were plotted as a function of temperature and the values corrected to the round values of the temperature, 25, 60, 90, 125, and 150°. The temperature of measurement was never more than 1° from the corresponding round temperature. These corrected values are given in Table I.

The activity coefficient $\gamma_\pm$ of HCl at each temperature and set of concentrations in the mixtures was evaluated by using the Nernst equation and previous values[3] of the standard potential E° of the Ag, AgCl electrode.

$$E = E^\circ - \frac{RT}{\mathfrak{F}} \ln [m_2(m_2 + m_3)] - \frac{2RT}{\mathfrak{F}} \ln \gamma_\pm \quad (1)$$

In this equation m_2 and m_3 are the molalities of HCl and NaCl, respectively, while T is the absolute temperature, R the gas constant, and $\mathfrak{F}$ the Faraday.

A plot of ln $\gamma_\pm$ *vs.* ionic strength fraction of NaCl was made at each temperature and at the total ionic strengths 0.4 and 1.0. Also included in these plots were the values for pure HCl[3] at all temperatures and for 0.01 m HCl in NaCl[10] at 25 and 60°. (The values at 60° were obtained by extrapolations of data from 0 to 50°.) In all cases the plots were linear within experimental error in conformity with Harned's rule.

Expressions for $\gamma_\pm$ of HCl and NaCl in the Mixtures. The activity coefficients of HCl were smoothed as to HCl and NaCl concentrations and temperature and those of NaCl were evaluated as follows. As shown previously,[7] the excess free energy of the solution G^e, *i.e.*, excess over the molality and Debye–Hückel terms, may be expressed as

$$\frac{1}{2}\frac{G^e}{RT} = \sum_{ij} B_{ij}\frac{n_i n_j}{w} + \sum_{ijk} C_{ijk}\frac{n_i n_j n_k}{w^2} \quad (2)$$

where n represents the numbers of moles of each solute, w is the number of kilograms of water, and the sums are taken over each solute i, j, k = 2 (for HCl) to 3 (for NaCl). B and C are interaction coefficients to be determined from the data.

(10) H. S. Harned and B. B. Owen, "The Physical Chemistry of Electrolytic Solutions," 3rd Ed., Reinhold Publishing Corp., New York, N. Y., 1958, Appendix A, p. 748.

Then for either solute component

$$\ln \gamma_q^{e} = \frac{1}{2}\frac{\partial}{\partial n_q}\left(\frac{G_q^{e}}{RT}\right) = 2\sum_i B_{iq}m_i + 3\sum_{ij} C_{ijq}m_i m_j \quad (3)$$

where $q = 2$ or 3. The coefficient 2 of the first sum results from the fact that $\partial n_q^2/\partial n_q = 2n_q$ and from the fact that since $B_{23}n_2n_3$ is indistinguishable from $B_{32}\cdot n_3n_2$ they may be combined; the coefficient 3 in the second sum results from similar reasoning. (In eq. 3 the second sum is a double sum over i and j.) Thus, for HCl

$$\ln \gamma_2^{e} = 2B_{22}m_2 + 2B_{23}m_3 + 3C_{222}m_2^2 + 6C_{223}m_2m_3 + 3C_{233}m_3^2 = 2I[B_{22} + (B_{23} - B_{22})x_3] + 3I^2[C_{222} + 2(C_{223} - C_{222})x_3 + (C_{222} + C_{233} - 2C_{223})x_3^2] \quad (4)$$

where the coefficient in parentheses of the x_3^2 term is zero according to Harned's rule (*i.e.*, that $\ln \gamma_2$ varies linearly with x_3), which the data have been shown to obey. Here x represents ionic strength fraction, while the ionic strength $I = m_2 + m_3$. If Harned's rule is assumed to hold for HCl then $\ln \gamma_2^{e}$ and $\ln \gamma_3^{e}$ become

$$\ln \gamma_2^{e} = 2I[B_{22} + (B_{23} - B_{22})x_3] + 3I^2[C_{222} + 2(C_{223} - C_{222})x_3] \quad (5)$$

and

$$\ln \gamma_3^{e} = 2I[B_{33} + (B_{23} - B_{33})]x_2 + 3I^2[C_{333} + 2(C_{233} - C_{333})x_2 + (C_{333} + C_{223} - 2C_{233})x_2^2] \quad (6)$$

and hence the total $\ln \gamma_q$ is given by adding the Debye–Hückel term to eq. 5 or 6. The Debye–Hückel term was assumed to be identical for HCl and NaCl with the denominator parameter set equal to 1.5 at each temperature. Hence, at each temperature

$$\ln \gamma_q = \ln \gamma_q^{e} - s\rho^{1/2}\sqrt{I}/(1 + 1.5\sqrt{I}) \quad (7)$$

where s is the limiting slope and ρ is the density of water which corrects the ionic strength to a volume basis, as required by the Debye–Hückel theory.

In the study of HBr–KBr mixtures[7] the activity coefficients of HBr were smoothed as to temperature using expressions of the type

$$B_{iq} = B'_{iq} + B''_{iq}/T \text{ and } C_{ijq} = C'_{ijq} + C''_{ijq}/T \quad (8)$$

in eq. 5. These parameters gave temperature-independent excess free enthalpies and entropies. In the present work on HCl–NaCl mixtures these same expressions were first used to smooth the activity coefficients of HCl as to temperature. The resulting fit was about the same as that obtained in the case of HBr. In an effort to secure a better fit, an attempt was made to express both the B and C coefficients with equations of the type

$$B_{iq} = B'_{iq} + B''_{iq}/T + B'''_{iq}\log T \quad (9)$$

and

$$C_{ijq} = C'_{ijq} + C''_{ijq}/T + C'''_{ijq}\log T \quad (9')$$

where the parameters B', B'', B''', C', C'', and C''' were to be determined by the method of least squares. Convergence difficulties were encountered, however, when eq. 9 and 9′ were used in eq. 5 to fit the activity coefficients of HCl, probably because the parameters in the expression for C_{ijq} were too strongly correlated. When C_{ijq} was expressed as in eq. 10 with only two

$$C_{ijq} = C'_{ijq} + C''_{ijq}/T \quad (10)$$

parameters and eq. 9 and 10 were used in eq. 5, then no difficulties were encountered in the least-squares determination. Moreover, the least-squares fit of the data was much better when eq. 9 and 10 were used (variance of fit of 2.0×10^{-5}) than when the expressions given in eq. 8, with two fewer parameters, were used (variance of fit of 4.3×10^{-5}). Equation 9 gives rise to excess enthalpies varying linearly with temperature and excess entropies varying linearly with $\ln T$, while eq. 10 is again consistent with temperature-independent values. In the ionic strength range studied (to 1.0 m) the contribution of the B terms is much more important than that of the C terms (hence, the difficulty in determining as many parameters in the C coefficients).

The values of B'_{22}, B''_{22}, B'''_{22}, B'_{23}, B''_{23}, B'''_{23}, C'_{222}, C''_{222}, C'_{223}, and C''_{223} were obtained directly by the least-squares fit, while the values of C'_{233} and C''_{233} were obtained by the application of Harned's rule: $C_{222} + C_{233} - 2C_{223} = 0$. The additional parameters needed for calculating γ_3^{e} by eq. 6, namely, the parameters in the coefficients B_{33} and C_{333} (for pure NaCl solutions), were evaluated by the method of least squares using osmotic coefficient data[6] on NaCl solutions. In this fit it was possible to express both B_{33} and C_{333} with equations of the type given by eq. 9 and 9′, presumably because data over a wider range of concentrations (to 3 m) were available.

The parameters for calculating the various B and C coefficients are given in Table II. Activity coefficients of HCl and NaCl in the mixtures ($I = 0.4$ and 1.0) calculated using these parameters are shown as the solid lines in Figures 1 and 2. The values of the activity coefficient of HCl calculated from the observed e.m.f. values are shown as data points in Figure 1. The activity coefficient of HCl in the mixtures varies more rapidly with temperature, the smaller the ionic

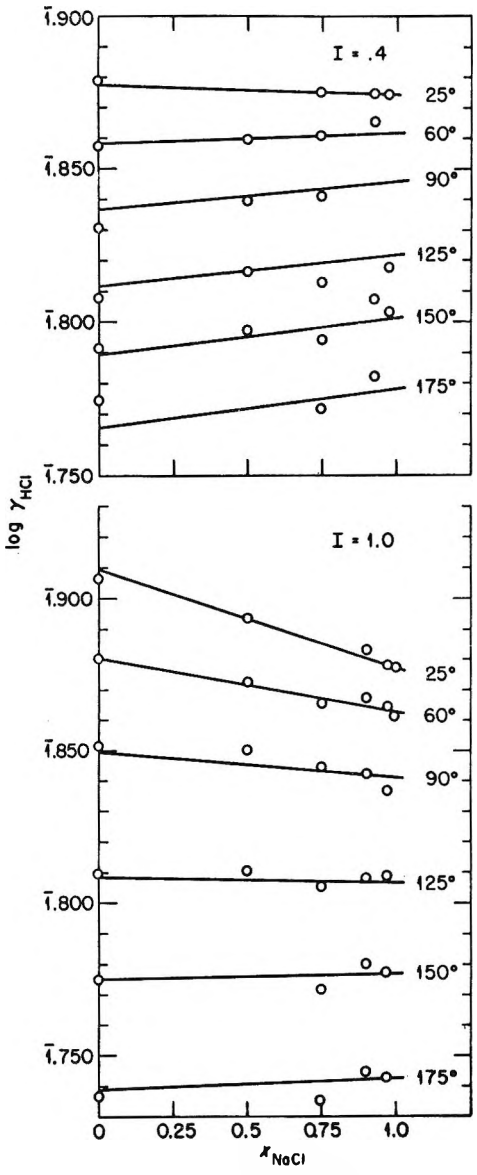

Figure 1. Log γ_{HCl} *vs.* X_{NaCl} in HCl–NaCl mixtures.

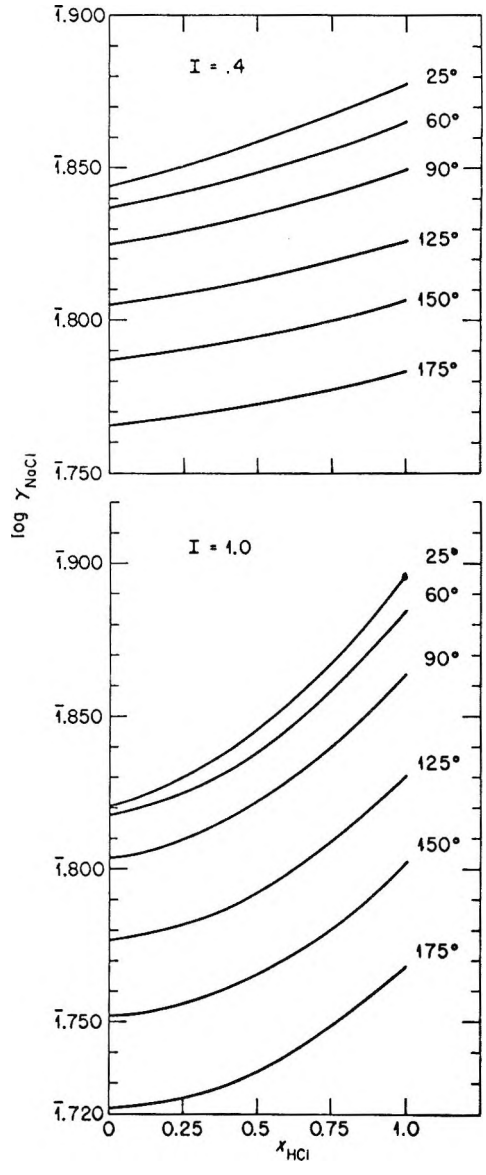

Figure 2. Log γ_{NaCl} *vs.* X_{HCl} in HCl–NaCl mixtures.

Table II: Parameters of the B and C Coefficients (eq. 9 and 10) for the HCl–NaCl System over the Range 25 to 175°

$B'_{22} = 1.86790$	$B''_{22} = -59.3857$	$B'''_{22} = -0.65366$
$B'_{23} = 2.72578$	$B''_{23} = -121.853$	$B'''_{23} = -0.91431$
$B'_{33} = 2.89603$	$B''_{33} = -151.120$	$B'''_{33} = -0.96167$
$C'_{222} = 0.0258302$	$C''_{222} = -6.73533$	
$C'_{223} = 0.0132623$	$C''_{223} = -4.90705$	
$C'_{233} = 0.0006944$	$C''_{233} = -3.07877$	
$C'_{333} = -0.091257$	$C''_{333} = 5.33016$	$C'''_{333} = 0.030096$

strength fraction of NaCl. This general behavior is consistent with previous observations[10,11] over a smaller temperature range. As can be seen, the activity coefficient of NaCl in the mixtures does not obey Harned's rule.

Values of the e.m.f. E were calculated, using the previously determined $E°$ values and the B and C values for the smoothed activity coefficients (Table II), for each experimental point. The algebraic difference between the observed E values and those calculated are given below the observed E values in Table I.

It is interesting to compare the values of log γ_2 and log γ_3 obtained in the present study with values computed from the parameters reported by Harned.[12]

(11) M. H. Lietzke and R. W. Stoughton, *J. Tenn. Acad. Sci.*, **39**, 30 (1964).

(12) H. S. Harned, *J. Phys. Chem.*, **63**, 1299 (1959).

The comparison can be made only at $I = 1.0$ at 25° since Harned's values span the range $I = 1.0$ to 3.0 at temperatures of 0 to 50°. The results are shown in Table III.

Table III: A Comparison of the Values of Log γ_2 and Log γ_3 Obtained in the Present Study with Those Reported by Harned at $I = 1.0$ and 25°

	Log γ_2	
X_3[a]	Present study	Harned
0.25	$\bar{1}.9010$	$\bar{1}.9000$
0.50	$\bar{1}.8932$	$\bar{1}.8921$
0.75	$\bar{1}.8852$	$\bar{1}.8843$
	Log γ_3	
X_2[a]	Present study	Harned
0.25	$\bar{1}.8300$	$\bar{1}.8310$
0.50	$\bar{1}.8457$	$\bar{1}.8452$
0.75	$\bar{1}.8675$	$\bar{1}.8595$

[a] Fraction of either component 2 or 3 in the mixture.

The agreement between the two sets of values of log γ_2 is very good (within about 0.1%). Similar agreement between the values of log γ_3 is observed at the two lower fractions (X_2) of HCl. The values of log γ_3 at $X_2 = 0.75$ differ by about 1%; this may be due in part to the fact that a different set of values of osmotic coefficients of NaCl over a wide range of temperatures (25 to 200°) was used in evaluating the activity coefficient of pure NaCl solutions.

The relationship between the B and C coefficients as defined by eq. 9 and 10 and the α-coefficient of Harned's rule as well as the expressions for the partial molal free energy $\bar{G}_q$, the partial molal enthalpy $\bar{H}_q$, and the partial molal entropy $\bar{S}_q$ for component q may be calculated using the expressions previously reported[10] in the study of HBr–KBr mixtures.

When the activity coefficients of HBr in the HBr–KBr system were refitted using eq. 9 and 10 in eq. 5, then the parameters shown in Table IV were obtained. These parameters provide a significantly better fit of the activity coefficients than did the expressions in eq. 8, the parameters of which were given in the earlier paper.[7] (When eq. 8 was used, the variance of fit was 2.1×10^{-4}, while the use of eq. 9 and 10 gave a variance of fit of only 2.1×10^{-5}.) The effect is most pronounced when log γ_{KBr} is calculated and plotted *vs.* the fraction of HBr in the mixture at $I = 1.0$. The newer plots are much more nearly linear than were the plots previously given.

Table IV: Parameters of the B and C Coefficients (eq. 9 and 10) for the HBr–KBr System over the Range 25 to 100°

$B'_{22} = 3.95636$	$B''_{22} = -185.972$	$B'''_{22} = -1.31428$
$B'_{23} = 2.57573$	$B''_{23} = -103.558$	$B'''_{23} = -0.888431$
B'_{33}[a] $= 0.0689068$	$B''_{33} = -21.21950$	
$C'_{222} = 0.00216642$	$C''_{222} = -1.87841$	
$C'_{223} = 0.0141473$	$C''_{223} = -5.03595$	
$C'_{233} = 0.02612818$	$C''_{233} = -8.19349$	
$C'_{333} = -0.00133241$	$C''_{333} = 0.715351$	

[a] The osmotic coefficients of KBr were not refitted. Hence, these parameters are for the B expression given in eq. 8.

When the two systems are compared, it is seen that plots of log γ_{acid} *vs.* fraction of salt in the mixtures are linear at all temperatures at both $I = 0.4$ and 1.0 in conformity with Harned's rule. In the HBr–KBr system these plots have a negative slope at all temperatures, whereas the corresponding plots in the HCl–NaCl system have a negative slope at $I = 0.4$ at 25° and a positive slope at the higher temperatures. At $I = 1.0$ the plot of log γ_{HCl} decreases at 25, 60, and 90°, becomes almost flat at 125°, then increases at 150 and 175°. In the HCl–NaCl system the plots of log γ_{NaCl} *vs.* the fraction of HCl in the mixtures are concave upward at all temperatures at both $I = 0.4$ and 1.0, the curvature becoming more pronounced at the higher ionic strength. In the HBr–KBr mixtures the plots of log γ_{KBr} *vs.* the fraction of HBr at $I = 0.4$ are almost linear at 25, 60, and 90°; osmotic coefficient data are not available on KBr solutions above 100°. At $I = 1.0$ the 25° plot is almost linear, while at the higher temperatures the curves are concave downward.

Acknowledgment. The authors wish to express their sincere appreciation to R. W. Whitfield and W. D. Armstrong for their assistance in making the e.m.f. measurements.

Halogen Complexes. III. The Association of 2,4,6-Trimethylpyridine and Trifluoroiodomethane

by David Walter Larsen and A. L. Allred[1]

Department of Chemistry and Materials Research Center, Northwestern University, Evanston, Illinois
(Received February 12, 1965)

The 1:1 complex formed between trifluoroiodomethane and 2,4,6-trimethylpyridine in cyclopentane solution was studied by n.m.r. spectroscopy, and the enthalpy and entropy of formation were found to be -5.0 ± 0.1 kcal./mole and -12.6 ± 0.4 e.u., respectively.

Introduction

In earlier papers in the series,[2,3] the complexes of iodine with various Lewis bases in solution were studied by n.m.r. spectroscopy, and average lifetimes for the complexes and thermodynamic constants were determined. The purpose of the present investigation is to contrast the behavior of the pseudo-halogen, trifluoroiodomethane, toward 2,4,6-trimethylpyridine with that of iodine.

Experimental

Reagents. Trichlorofluoromethane, obtained from the K and K Laboratories, Inc., was used without further purification and at concentrations no greater than 1% by weight. Trifluoroiodomethane, prepared[4] by reacting silver trifluoroacetate with iodine, was distilled and stored under Dry Ice. Cyclopentane was dried over sodium and distilled. 2,4,6-Trimethylpyridine was distilled shortly before use.

N.m.r. Samples and Measurements. The n.m.r. samples were prepared by introducing weighed amounts of base, solvent, and trichlorofluoromethane (internal reference) into 5-mm. o.d. Pyrex tubes equipped with ground glass joints. The sample tubes were then connected to a vacuum line and measured amounts of trifluoroiodomethane were distilled into the tubes. The tubes were then degassed and sealed.

The fluorine n.m.r. spectra were observed using a Varian Associates, Inc., HR spectrometer, operating at 56.4 Mc./sec. Chemical shifts were measured by the side-band technique with a standard deviation of approximately 0.008 p.p.m. The samples were thermostated[5] to within $\pm 0.5°$.

Results and Discussion

Chemical shifts were observed for solutions containing initially before complex formation, 0.04 mole fraction of trifluoroiodomethane, 0.01 mole fraction of trichlorofluoromethane, and from 0 to 0.48 mole fraction of 2,4,6-trimethypyridine in the solvent cyclopentane.

Values of concentrations and chemical shifts in the temperature range -30 to 40° are presented in Table I.

Table I: Values of Chemical Shifts for Trifluoroiodomethane and 2,4,6-Trimethylpyridine in Cyclopentane Relative to Internal Trichlorofluoromethane

CF_3I initial mole fraction	2,4,6-Trimethylpyridine, initial mole fraction	Chemical shift, c.p.s. (Temp., °C.)					
		−30	−16	−3	11	25	40
0.040	0	265.1	264.5	264.5	265.8	266.3	265.3
0.040	0.096	656.1	609.2	561.1	508.2	463.4	424.6
0.040	0.336	732.4	712.1	687.5	655.3	621.2	581.9
0.040	0.480	734.1	719.6	698.6	673.6	640.2	610.0

Values of K_N and the association shift were determined by a previously described[6] reiterative method and

(1) Alfred P. Sloan Research Fellow.

(2) D. W. Larsen and A. L. Allred, *J. Am. Chem. Soc.*, 87, 1216 (1965).

(3) D. W. Larsen and A. L. Allred, *ibid.*, 87, 1219 (1965).

(4) W. Fronk, Thesis, Northwestern University, 1959.

(5) J. Palmer, Thesis, Northwestern University, 1960.

are presented in Table II. From a least-squares plot of log K_N *vs.* $1/T$, the values of 5.0 ± 0.1 kcal./mole and −12.6 ± 0.4 e.u. are obtained for the enthalpy and entropy changes, respectively, accompanying complex formation.

Table II: Values of K_N and Association Shifts for Trifluoroiodomethane and 2,4,6-Trimethylpyridine in Cyclopentane Solution

Temp., °C.	K_N, $\frac{1}{\text{mole fraction}}$	Association shift, c.p.s.
−30	61 ± 6	488
−16	35 ± 1.8	485
−3	22 ± 1.1	478
11	13 ± 0.5	476
25	9.0 ± 0.5	466
40	6.4 ± 0.2	463

It is evident that the trifluoroiodomethane–2,4,6-trimethylpyridine complex is much less stable than corresponding 1:1 complexes of iodine with aza aromatics. For the association of iodine and 2,4,6-trimethylpyridine in chloroform at 28°, K is reported[7] to be 52 l./mole. The change of enthalpy accompanying formation in heptane of the pyridine–iodine complex is −7.8 ± 0.2 kcal./mole.[8] Reported values of the equilibrium constant for the pyridine–iodine complex vary: K_c = 200 l./mole in heptane at 25° (by interpolation),[8] K_c = 100 l./mole in carbon tetrachloride at 25°,[9] K_c = 43.74 l./mole in chloroform at 28°,[7] K_c = 107 ± 27 l./mole at 26° in cyclohexane, in carbon tetrachloride, and in *n*-heptane.[10]

No line broadening was observed for the CF_3I solutions at temperatures as low as −30°. Thus the exchange of the trifluoroiodomethane–2,4,6-trimethylpyridine complex is rapid and the average lifetime of the complex is small with respect to the inverse of the association shift, or $\tau_c < 3 \times 10^{-4}$ sec.

Acknowledgments. D. W. L. expresses appreciation for a Woodrow Wilson Fellowship, a fellowship from the Lubrizol Corporation, and a predoctoral fellowship from the Division of General Medical Sciences, U. S. Public Health Service. We thank the Northwestern University Computing Center for providing computor time. The research upon which this report is based was partially supported by the Advanced Research Projects Agency of the Department of Defense, through the Northwestern University Materials Research Center.

(6) C. J. Creswell and A. L. Allred, *J. Phys. Chem.*, **66**, 1469 (1962).
(7) J. N. Chadhuri and S. Basu, *Trans. Faraday Soc.*, **55**, 898 (1959).
(8) C. Reid and R. S. Mulliken, *J. Am. Chem. Soc.*, **76**, 3869 (1954).
(9) A. I. Popov and R. H. Rygg, *ibid.*, **79**, 4622 (1957).
(10) A. G. Maki and E. K. Plyler, *J. Phys. Chem.*, **66**, 766 (1962).

Kinetics of the Decarboxylation of Phenylmalonic Acid

by George A. Hall, Jr., and E. S. Hanrahan

Department of Chemistry, West Virginia University, Morgantown, West Virginia
(Received February 15, 1965)

The kinetics of the decarboxylation of phenylmalonic acid and its monosodium salt have been studied in water as a function of pH and in dioxane–water mixtures as a function of solvent composition. In water, the reaction follows first-order kinetics. The reaction rate is a maximum at a pH of 3.4. The location of the maximum and the variation of rate with pH are explained by resolving the data into individual rate constants for the simultaneous decomposition of the undissociated acid and the monoanion. The monoanion decomposes 3–4 times as fast as the undissociated acid. In dioxane–water mixtures, first-order kinetics were observed in all cases except for the decomposition of the monosodium salt in solutions containing 90% or more dioxane. The rate of decomposition of the free acid reaches a maximum in the region 60–80% dioxane. The rate of decomposition of the monoanion increases with dioxane content. Activation parameters are consistent with a proposed mechanism which postulates an intramolecular hydrogen bond in the transition state.

Introduction

In previous studies[1,2] it has been shown that the decarboxylation of malonic acids can be analyzed in terms of individual rates of simultaneous decarboxylation of the undissociated acid and its monoanion. The undissociated species of malonic acid decomposes nearly 10 times as fast as the monoanion,[1] while the monoanion of dibromomalonic acid decarboxylates at such a rapid rate that it completely masks any decarboxylation of the undissociated acid.[2] We are interested in extending these studies to other substituted malonic acids.

The decarboxylation of phenylmalonic acid has been studied before,[3–9] but, except for the work of Gelles, no attempt was made to analyze the over-all reaction rate in terms of the individual ionic species or to obtain data in nonaqueous media.

Experimental

Phenylmalonic acid (m.p. 151–152°) was prepared by saponification of the commercially available diethyl ester.[10] Sodium hydrogen phenylmalonate (m.p. 184–188°) was prepared by half-neutralization of the acid.[11] Purities were checked periodically by titration with standard NaOH. Dioxane was purified by the method of Fieser[12] and stored under nitrogen. The dioxane purity was determined by the analysis[13] of time–temperature cooling curves to be not less than 99.67 mole %. All other chemicals were reagent grade, used without further purification.

Buffer solutions were prepared from stock solutions of disodium citrate and hydrochloric acid, with KCl added as necessary to bring the total ionic strength to 4.00. The pH was measured with a Beckman Model G pH meter, calibrated against standard buffer solutions. The dioxane–water mixtures were prepared by

(1) G. A. Hall, Jr., *J. Am. Chem. Soc.*, **71**, 2691 (1949).

(2) R. E. Cunningham, Ph.D. Dissertation, West Virginia University, 1955.

(3) A. L. Bernoulli and H. Jakubowicz, *Helv. Chim. Acta*, **4**, 1018 (1921).

(4) A. L. Bernoulli and W. Wege, *ibid.*, **2**, 511 (1919).

(5) A. Fry and M. Calvin, *J. Phys. Chem.*, **56**, 901 (1952).

(6) E. Gelles, *J. Am. Chem. Soc.*, **75**, 6199 (1953).

(7) E. Gelles and K. S. Pitzer, *ibid.*, **77**, 1974 (1955).

(8) H. Jakubowicz, *Z. anorg. Chem.*, **121**, 113 (1922).

(9) K. S. Pitzer and E. Gelles, *J. Am. Chem. Soc.*, **75**, 5132 (1953).

(10) S. Basterfield and L. A. Hamilton, *Trans. Roy. Soc. Can.*, **III27**, 125 (1933).

(11) S. Basterfield and J. W. Tomecko, *Can. J. Res.*, **8**, 447 (1933).

(12) L. F. Fieser, "Experiments in Organic Chemistry, Part II," D. C. Heath and Co., New York, N. Y., 1941, pp. 368, 369.

(13) B. J. Mair, A. R. Glasgow, and F. D. Rossini, *J. Res. Natl. Bur. Std.*, **26**, 591 (1941).

transferring dioxane to a tared flask using pressurized nitrogen, followed by dilution with the calculated amount of water. All solutions were saturated with carbon dioxide prior to use. All reactions were carried out in an oil bath thermostated to 0.1°. Concentrations of acid and monoanion varied from 0.025 to 0.150 *M*.

The rate constants were evaluated by measuring the volume of CO_2 evolved during the course of the reaction. The CO_2 was collected in a 100-ml. mercury-filled gas buret equipped with a leveling tube.[2] Adjustment of mercury levels was made with the assistance of a cathetometer. Volume readings were taken to the nearest 0.05 ml., and all volumes were corrected to STP. In most experiments, the total volume of CO_2 evolved was calculated from the known weight of acid and did not differ significantly from the measured total volume obtained by allowing several reactions to proceed to completion.

Dissociation constants of phenylmalonic acid in aqueous solution were calculated from data obtained by potentiometric titration with standard NaOH. The values obtained are given in Table I and are in good agreement with previously published results.[6,11] Dissociation constants in dioxane–water mixtures were determined by the method of Trivich and Verhoek,[14] using thymol blue indicator. Corrections for the dissociation of HCl in dioxane–water mixtures were taken from the data of Owen and Waters.[15] Results are given in Table II.

Table I: Concentration Dissociation Constants of Phenylmalonic Acid

Acid concn., *M*	Ionic strength (added salt)	K_1	K_2
0.025	0.000	3.2×10^{-3}	3.8×10^{-6}
0.025	4.000	2.0×10^{-2}	1.7×10^{-5}
0.100	0 000	3.2×10^{-3}	4.2×10^{-6}
0.100	4.000	1.6×10^{-2}	1.9×10^{-5}

Table II: Dissociation Constant in Dioxane–Water Mixtures (K_1)

Acid concn., *M*	% dioxane 20	40	60	80
0.025	1.3×10^{-3}	3.3×10^{-4}	5.0×10^{-5}	...
0.050	1.7×10^{-3}	3.8×10^{-4}	5.3×10^{-5}	6.9×10^{-7}
0.100	2.0×10^{-3}	5.6×10^{-4}	5.8×10^{-5}	5.2×10^{-7}
0.150	2.4×10^{-3}	6.2×10^{-4}	6.1×10^{-5}	5.4×10^{-7}

Results and Discussion

The decarboxylation follows first-order kinetics except for the decomposition of the sodium hydrogen salt in solutions containing 90% or more dioxane. This deviation from first-order kinetics may be due to decreased solubility of the sodium salt.

Rate measurements in aqueous solution are summarized in Table III and Figure 1. The rate reaches a maximum at pH 3.0–3.4 and decreases rapidly above pH 4.5. In aqueous solution, there are three species of phenylmalonic acid, and undissociated

Table III: Decarboxylation of Phenylmalonic Acid in Aqueous Solution

pH	Initial acid concn., *M*	$k_{obsd} \times 10^5$ sec.$^{-1}$ 55°	65°	Exptl. activation energy, E_x, kcal./mole
0.25	0.100	1.10	3.75	27.2
0.85	0.100	1.45	5.35	28.6
1.75	0.100	2.75	9.95	28.1
1.95	0.025	3.20	...	...
2.25	0.100	3.85	14.8	29.6
2.45	0.100	4.15	16.0	29.8
2.70	0.025	5.10	17.6	27.2
3.05	0.100	5.30	17.6	26.6
3.40	0.100	5.30	18.2	27.2
3.55	0.100	5.05	17.8	27.8
3.55	0.025	5.05	18.7	29.0
3.85	0.100	4.70	17.1	28.6
4.25	0.100	3.55	13.2	28.9
4.25	0.025	3.65	14.1	29.8
4.85	0.100	2.05	7.85	29.5

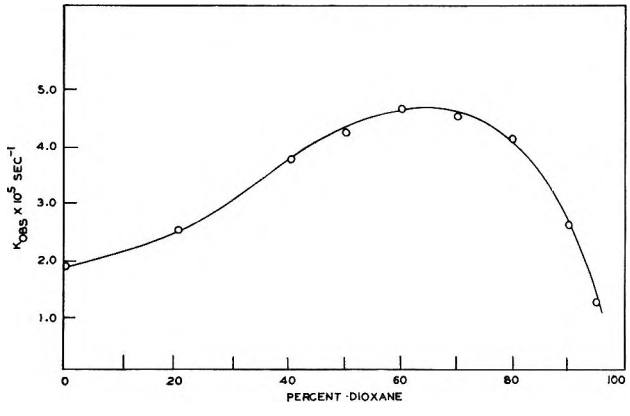

Figure 1. Decomposition of phenylmalonic acid in aqueous buffer solutions, ionic strength 4.00, at 55°.

(14) D. Trivich and F. H. Verhoek, *J. Am. Chem. Soc.*, **65**, 1919 (1943).

(15) B. B. Owen and G. W. Waters, *ibid.*, **60**, 2371 (1938).

acid, the monoanion, and the dianion. Decarboxylation may take place preferentially through one or two of these species, or all species may decompose simultaneously. In the present work, a sample of disodium phenylmalonate did not show any appreciable decomposition in boiling water over a 24-hr. period. The disodium salt is therefore regarded as stable under the conditions of this study.

If both the monoanion and the undissociated acid species are decomposing simultaneously, and in a manner which conforms to the first-order rate law, the over-all rate of reaction can be represented by

$$\text{rate} = k_{\text{obsd}}(c) = k_1(c - x) + k_2(x) \qquad (1)$$

or

$$k_{\text{obsd}} = k_1 + (k_2 - k_1)(x/c) \qquad (2)$$

where k_{obsd} is the first-order rate constant calculated from the data, k_1 is the rate constant for decomposition of the undissociated acid species, and k_2 is the first-order rate constant for decarboxylation of the monoanion. The stoichiometric total acid concentration (all species) is c, and x is the concentration of monoanion in solution. If either the undissociated acid or monoanion is stable, eq. 1 and 2 can be simplified by taking k_1 or k_2 as zero. Equation 2 indicates that a plot of k_{obsd} *vs.* x/c should show a straight line relationship, with the intercept ($x = 0$) equal to k_1 and the slope equal to $(k_2 - k_1)$. This relationship is illustrated in Figure 2. Applying eq. 2 to the data of Table III, using the method of least squares, indicates that both undissociated acid and monoanion are decomposing but at different rates. At 55°, $k_1 = 0.90 \times 10^{-5}$ sec.$^{-1}$ and $k_2 = 5.40 \times 10^{-5}$ sec.$^{-1}$; at 65°, $k_1 = 3.65 \times 10^{-5}$ sec.$^{-1}$ and $k_2 = 19.3 \times 10^{-5}$ sec.$^{-1}$. Phenylmalonic acid represents an intermediate between the extremes of malonic acid,[1] where $k_1 \approx 10\ k_2$, and dibromomalonic acid,[2] where $k_2 >> k_1$.

Tables IV and V and Figure 3 summarize the results of measurements of the decomposition of the acid and monosodium salt, respectively, in dioxane–water mixtures. The observed rate of decomposition of the acid passes through a maximum in the region 50–80% dioxane. The rate of decomposition of the monosodium salt increases with increasing dioxane content. The slight concentration effect observed at low dioxane concentrations can be explained by considering the changes in degree of dissociation with changes in concentration.

In order to apply eq. 2 to these data, the acid dissociation constants must be known at all dioxane concentrations. The data of Table II indicate, however, that the degree of dissociation in solutions containing more than 60% dioxane is less than 1%. In this

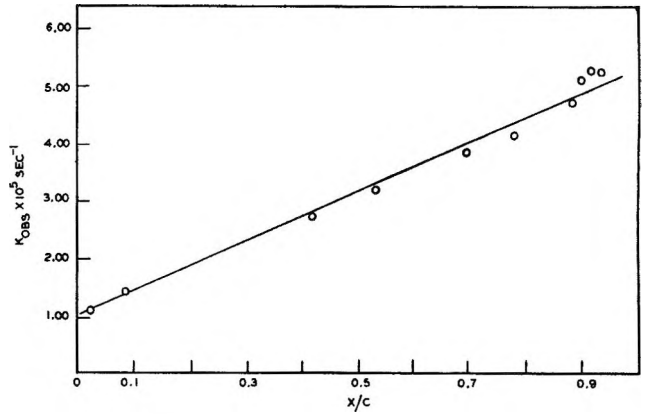

Figure 2. The observed rate constant for the decomposition of phenylmalonic acid *vs.* x/c, the degree of primary dissociation of the acid in water, ionic strength 4.00, 55°.

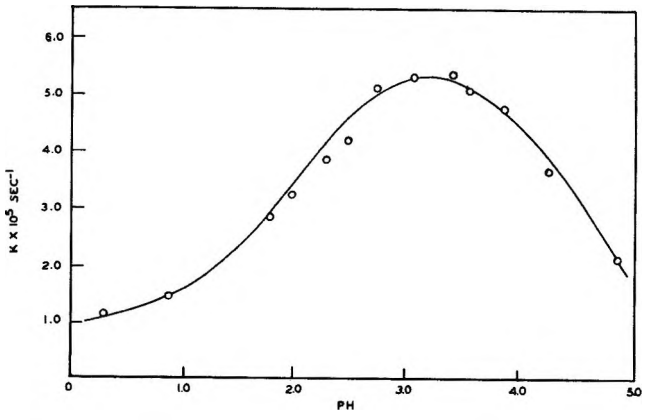

Figure 3. Decomposition of 0.150 *M* phenylmalonic acid in dioxane–water mixtures at 55°.

situation, k_{obsd} is equal to k_1. Measurements with the monosodium salt, however, give a direct determination of k_2. Since k_2 can always be determined directly, the maximum uncertainty is in the values of k_1 in solutions of low dioxane content. Indirect evidence of the magnitude of this uncertainty is obtained by comparing values of k_2 calculated from eq. 2 with values determined directly. This comparison is shown in Table VI. As expected, the maximum divergence occurs in the region (40% dioxane) where dissociation is small but still appreciable and where uncertainty in the determination of the dissociation constants will have maximum influence. The results for 0 and 20% dioxane provide experimental verification of the relationship expressed in eq. 2.

The rate constants observed in the present study are in satisfactory agreement with the previous work of Gelles[6] and others.[3,4,8] Changes in reaction rate with solvent composition do not show any systematic

Table IV: $k_{obsd} \times 10^5$ Sec.$^{-1}$ for the Decarboxylation of Phenylmalonic Acid in Dioxane–Water Mixtures

Acid concn., M	Temp., °C.	% dioxane 0	20	40	50	60	70	80	90	95
0.025	55	2.45	2.90	3.95	4.40	4.75	4.60	...	...	...
0.050	55	2.23	2.80	3.90	...	...	...	...	...	...
0.100	55	2.00	2.60	...	...	...	...	...	...	...
0.150	55	1.90	2.60	3.80	4.25	4.70	4.55	4.15	2.70	1.30
0.025	65	8.10	8.45	11.4	...	13.2	...	...	7.50	...
0.150	65	6.70	8.20	11.3	...	13.5	...	11.2	7.60	4.00
Activation energy, E_x, kcal./mole		27.9	25.9	23.4	...	23.1	...	22.0	23.3	24.6

Table V: Decomposition of Sodium Hydrogen Phenylmalonate in Dioxane–Water Mixtures

% dioxane	$k_2 \times 10^5$ sec.$^{-1}$ 45°	55°	65°	Activation energy, kcal./mole
0	...	4.20	14.9	28.0
20	1.75	6.65	25.5	28.6
40	3.25	12.0	44.0	27.4
60	7.05	24.0	...	25.4
80	14.1	45.0	...	24.2

Table VI: Comparison of Observed and Calculated Rate Constants for Decarboxylation of the Monoanion of Phenylmalonic Acid

% dioxane	$k_2 \times 10^5$ sec.$^{-1}$ 55° a	55° b	65° a	65° b
0	6.8	4.2	13.8	14.9
20	6.6	6.7	21.0	25.5
40	6.8	12.0	18.0	44.0

[a] Calculated from eq. 2. [b] Observed, Table V.

variation, as is usually the case in mixed solvent systems.[16]

Activation energies calculated from the Arrhenius equation are shown in Tables III–V. The activation parameters ΔF_a, ΔS_a, and ΔH_a were calculated from the experimental rate constants and activation energies by means of the following[17] equations and are listed in Table VII.

$$k = \frac{(kT)}{h} \exp(-\Delta F_a/RT) \quad (3)$$

$$\Delta H_a = E_x - RT \quad (4)$$

$$\Delta S_a = (\Delta H_a - \Delta F_a)/T \quad (5)$$

The uncertainty in the activation energies was estimated[18] to be 4.5 kcal./mole for k_1 (aqueous), 1.2 kcal./mole for k_2 (aqueous), and 1.5 kcal./mole for both k_1 and k_2 in dioxane–water mixtures. In view of the uncertainty in E_x and hence ΔH_a, the individual variations in ΔS_a are not regarded as significant, even though trends are apparent.

Table VII: Activation Parameters for Decarboxylation of Acid (1) and Monoanion (2) in Dioxane–Water Mixtures

% dioxane	Exptl. activation energy, E_x, kcal./mole (1)	(2)	ΔH_a, kcal./mole (1)	(2)	ΔF_a, kcal./mole (1)	(2)	ΔS_a, cal./deg. mole (1)	(2)
0	24.6	28.0	23.9	27.4	26.7	25.8	−8.2	4.9
20	22.6	28.6	21.9	28.0	26.3	25.6	−13.3	7.3
40	21.9	27.4	21.8	26.8	26.0	25.2	−14.1	4.9
60	21.8	25.4	21.1	24.8	25.8	24.7	−13.8	0.3
80	22.0	24.2	21.3	23.6	25.9	24.3	−14.1	−2.1
90	23.0	...	22.3	...	26.1	...	−11.1	...
95	24.0	...	23.3	...	26.6	...	−9.7	...

It is, however, interesting to compare the entropies of activation of malonic, dibromomalonic, and phenyl-

Table VIII: Comparison of Entropies of Activation of Substituted Malonic Acids

Acid	Water H_2A	Water HA^-	80% dioxane H_2A	80% dioxane HA^-
Malonic	−2	+1	−9	−2
Dibromomalonic	...	+15	...	+4
Phenylmalonic	−8	+5	−14	−2

(16) J. E. Leffler and E. Grunwald, "Rates and Equilibria of Organic Reactions," John Wiley and Sons, Inc., New York, N. Y., 1963, pp. 397–402.

(17) A. A. Frost and R. G. Pearson, "Kinetics and Mechanism," 2nd Ed., John Wiley and Sons, Inc., New York, N. Y., 1961, pp. 98, 99.

(18) S. W. Benson, "The Foundations of Chemical Kinetics," McGraw-Hill Book Co., Inc., New York, N. Y., 1960, p. 91.

malonic acids as shown in Table VII. A negative value for the entropy of activation indicates a greater degree of ordering in the transition state than in the initial state. Table VIII shows that, for both malonic and phenylmalonic acids, in 100% water and in 80% dioxane, the undissociated acid species has a more negative entropy of activation than the monoanion species.

These data are consistent with a proposed mechanism[19] of decarboxylation which postulates the formation of an intramolecular hydrogen bond in the transition state. The reasoning is as follows. (1) An acid which has an intramolecular hydrogen bond in the initial state will have a correspondingly less negative entropy of activation. (2) Intramolecular hydrogen bonding will be energetically favored in the monoanion as compared with the undissociated acid. (3) The monoanion should therefore have a lower (less negative) entropy of activation than the undissociated species.

Considering only the activation entropies of the monoanions, the same reasoning can be applied to a comparison of the two solvents. The data indicate that an intramolecular hydrogen bond is more probable in water than in 80% dioxane. Dodd, Miller, and Wynne-Jones[20] have carried out infrared spectroscopic studies which indicate that the acid maleate ion contains an intramolecular hydrogen bond which is stable in water, but not in dioxane. The situation is apparently similar with malonic acids.

(19) B. R. Brown, *Quart. Rev.* (London), **5**, 141 (1951).

(20) R. E. Dodd, R. E. Miller, and W. F. K. Wynne-Jones, *J. Chem. Soc.*, 2790 (1961).

The Partial Volumes of 1-Butanol in Dilute Aqueous Solutions at 30°

by William H. Pasfield

Department of Chemistry, St. John's University, New York, New York *(Received February 18, 1965)*

A dilatometer is described which has been designed for the determination of the partial specific volumes of liquids over small concentration ranges. The partial specific volume of 1-butanol was determined with this apparatus and was found to depend on the mole fraction of 1-butanol, X_2, in the following way: $\bar{v}_2 = 1.17403 - 2.165X_2 + 152.2X_2^{2.16}$.

Introduction

The partial volume of electrolytes in aqueous solution have been the subject of a number of rather precise studies.[1] Not only are limiting values at infinite dilution known for the more common electrolytes, but, what is perhaps more important, it has been established with reasonable certainty that at low concentrations the partial volume varies linearly with the square root of the electrolyte concentration.

Unfortunately, our knowledge of the partial volumes of nonelectrolytes is substantially less complete than this. In particular, no quantitative information about the limiting behavior of the partial volume of even the most common liquid nonelectrolytes seems to be available. Precise density measurements of aqueous solutions of such liquids are available, but, because of the spacing of these data (very few measurements at less than 1% solute by weight), they do not lend themselves to the calculation of partial volume in this limiting region. For example, Nakanishi,[2] in an

(1) See, for example, H. S. Harned and B. B. Owen, "The Physical Chemistry of Electrolytic Solutions," 3rd Ed., Reinhold Publishing Corp., New York, N. Y., 1958, Chapter 8.

(2) K. Nakanishi, *Bull. Chem. Soc. Japan*, **33**, 793 (1960).

interesting paper has calculated the partial specific volumes of the four butyl alcohols at 20° from five place density measurements. While he was able to determine the concentrations at which the partial specific volumes of three of the alcohols attain their minimum values, he could give no numerical information about the limiting behavior of any of them.

The neglect of liquid nonelectrolytes can be attributed in large measure to the experimental difficulties encountered in obtaining accurate density values at accurately known high dilutions. The difficulties arise from the hygroscopic and/or volatile nature of liquids of this type, both of these characteristics contributing markedly to the uncertainty in concentration particularly at high dilutions. It was felt that these difficulties could be circumvented and that, indeed, liquids would be even more amenable to study than solids if a dilatometric method were used. This paper describes the dilatometer which was designed for use with liquid solutes over small concentration ranges and reports the results of measurements made with it on dilute aqueous solutions of 1-butanol.

Experimental

Materials. 1-Butanol was first dried over CaO, then fractionally distilled twice, once at atmospheric pressure and finally at a pressure sufficiently reduced to keep the boiling temperature between 40 and 45°. The final product was stored under vacuum. Purity was determined by gas phase chromatography and density measurements at 25 and 30°. The water content was estimated from g.p.c. to be of the order of 0.01%. The presence of a second trace impurity was detected in preliminary experiments when it was noted that a 2-ml. portion of the alcohol dissolved incompletely when added to a solution whose mole fraction in 1-butanol was greater than about 0.013. A second 2-ml. portion added to the same solution behaved in exactly the same way indicating that the effect was due to an impurity and not to just a slowing down in the rate of solution. The amount of this residue was reduced when the purification procedure was modified to include a final low temperature distillation. Surprisingly enough, the inclusion of this final step had no measurable effect on the density of the final product. d^{25}_4 and d^{30}_4 were found to be 0.80584 and 0.80191. The value at 25° falls within the range of values reported in the literature; however, it is slightly higher than what is probably the most reliable value of 0.80572 reported by Jones and Christian.[3] The value at 30° is slightly lower than Timmermans and Martin's[4] value of 0.80206.

The water used in this work was obtained from an all-glass still and was boiled just prior to use to remove dissolved air.

Temperature Control. The dilatometric measurements were carried out in a thermostat whose temperature was kept constant to within 0.001°. The thermostat was a conventional glass-jar type bath with the following essential modifications. Heat was supplied from a 250-w. infrared drying lamp mounted outside the bath. Adsorption of heat was effected by the presence of approximately 10 mg. of nigrocene black dye dissolved in the bath water. A mercury-in-glass thermorelay was located in the bath directly in the path of the incident light and about 5 cm. from the wall of the jar. Provided room temperature did not change by more than 1–2°, variation in the bath temperature over a period of from 4 to 5 days could not be detected with a Beckmann thermometer and was therefore assumed to be no greater than 0.001°. In addition to the effect of seasonal changes in room temperature, small changes in the operating temperature of the bath were caused by gradual precipitation of the dye. For the entire study the average operating temperature was 30.0°.

Apparatus. The dilatometer, shown in Figure 1 as it would appear in the middle of an experiment, was designed to measure the increase in volume accompanying the consecutive addition to some solvent of five portions of liquid solute. At 30° with the mercury reservoir filled to the reference mark (A) the volume of the flask with the pipet in place was 592.36 ± 0.01 ml. The capacities of the bulbs in the pipet (E) (each about 2 ml.) were determined to within ±0.0001 ml. using mercury. In this operation the pipet was sealed to a stopcock which in turn was sealed to a mercury syphon of 0.5-mm. tubing. The fact that the four determinations made were in good agreement was taken as evidence that gradual replacement of mercury in the bore of the stopcock with stopcock grease was not a serious source of error. Finally, the volume per unit length of the 0.5-mm. capillary tubing connecting the bulbs was determined so that the necessity of stopping the mercury level exactly at a reference mark could be avoided.

In a typical experiment freshly boiled distilled water was added to the flask which was then stoppered and placed in the thermostat. As its contents cooled, additional water was drawn into the flask from a small funnel attached at B. Agitation was effected by means of the Teflon encapsulated magnetic stirring bar (C). The pipet reservoir (D), initially containing

(3) G. Jones and S. M. Christian, *J. Am. Chem. Soc.*, **61**, 82 (1939).
(4) J. Timmermans and F. Martin, *J. chim. phys.*, **25**, 411 (1928)

mercury, was filled with 1-butanol by drawing the mercury into the pipet (E) to a point well above the top reference mark. (When the pipet was loaded for the first time, it was, of course, necessary to flush the reservoir once to remove the entrapped air.) The 1-butanol was sealed into the pipet by drawing a thread of mercury into the delivery tip (F). The pipet was then positioned in the flask, and the whole apparatus was replaced in the thermostat. After about 15 min. stopcock G was opened to permit the mercury level in the pipet to drop into the capillary tubing above the first bulb. The mercury remaining in the delivery tip was then carefully expelled into the flask by allowing some mercury to flow from H to D. Finally, the liquid level in the calibrated 0.5-mm. capillary tubing was adjusted to near its reference mark (J) by opening K and adjusting the level of mercury in the container at the arm of the syphon outside the thermostat. As a final test for thermal equilibrium K was closed and the liquid level at J was observed for change over a 15-min. period. The liquid level at J and the mercury levels in the pipet and near A were then measured (relative to their respective reference marks) with a cathetometer to the nearest 0.1 mm.

Before adding a portion of 1-butanol, L was closed to prevent loss of liquid from the flask, and K was opened to permit mercury to be displaced from the reservoir into the external container. Addition of 1-butanol was accomplished by opening G and allowing an amount of mercury to drain from the pipet sufficient to bring the level into the capillary tubing between the first and second bulbs. After about 15 min. L was opened, and the liquid level was again brought as near as possible to J. K was closed, and the liquid level was observed for change as before. Final measurement of the mercury level in the pipet and the liquid level were then made. Subsequent additions were carried out in an identical fashion.

The initial liquid content of the flask was calculated from the calibrated volume of the flask corrected for the initial displacement of the mercury level from A, and for the mercury expelled into the flask from the delivery tip. The weight of 1-butanol added was calculated from the known volume of the bulbs in the pipet (corrected for any small displacement in the mercury levels from the reference marks) and the density of 1-butanol. The volume increase of the solution was calculated from the weight of mercury expelled from the flask (corrected for small differences in the liquid level).

In a number of instances experiments were run consecutively; that is, the final solution from one experiment was used as the initial solution for the next.

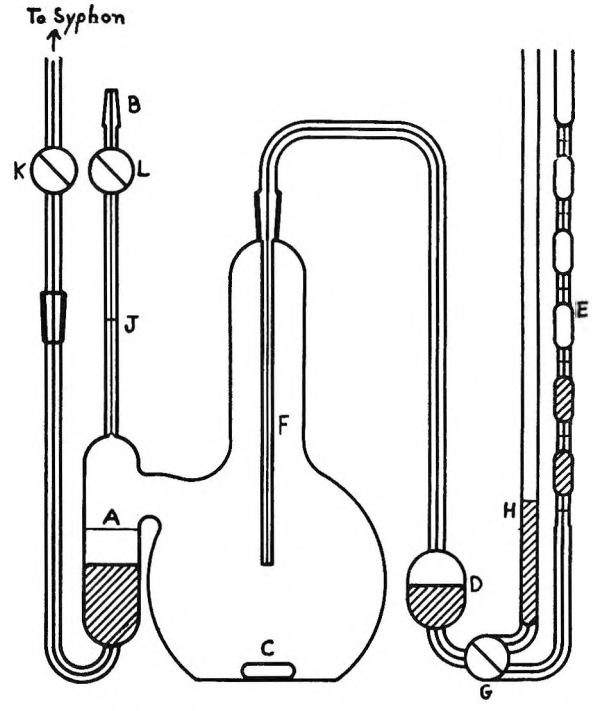

Figure 1. Apparatus.

It was from experiments of this type that density values were calculated.

Calculations

Calculation of partial specific volumes from the measured finite increments was accomplished by one of two methods depending on the range of concentrations covered. When 1-butanol was added to water it was found that $\Delta V/g'$ decreased linearly with an increase in g'. Here, g' is the total weight of 1-butanol added to the initial solution and ΔV is the accompanying volume change. In this case the appropriate linear equation was determined by the method of least squares and then differentiated to obtain the equation for the partial specific volume, $\bar{v}_2$. Finally, g' was replaced by Δg_2 (g. of 1-butanol added/1000 g. of H_2O) to give what will be referred to as a primary equation.

When the starting solution contained more than about 3 g. of 1-butanol, the dependence of $\Delta V/g'$ was no longer linear, and consequently a second-order term had to be included. The obvious extension of the procedure just described to this situation proved to be unsatisfactory since the resulting primary equations for consecutive experiments failed to meet at their common point. Without exception the value of $\bar{v}_2$ at this point calculated from the first of a pair of such experiments was substantially lower than the value calculated from the second. This discrepancy arose

in part from the fact that each individual addition and its attendant volume change was not being given equal weight in the determination of the constants in the empirical equation. Since the data used in the least-squares analysis just described consisted of the accumulated increments, the value of the first individual increment contributed to the values of all of the others while the value of the last individual increment was given a weight of $^1/_5$ in the determination of the value of the final accumulated increment. This unsymmetrical weighting clearly favored the first individual increments and would have been an acceptable treatment if one were interested in evaluating $\bar{v}_2$ under the initial conditions of the experiment. In order to arrive at an empirical expression which would give the best values for all possible increments in a given range the following method was devised.

It was assumed that within a given range the partial specific volume can be represented by an equation of the form

$$\bar{v}_2 = b_0 + b_1 g' + b_2 g'^2 \quad (1)$$

Integrating this equation between the limits g'_i and g'_j, then dividing both sides by $g'_i - g'_j$ we find that

$$\frac{\Delta V}{\Delta g'} = b_0 + {}^1/_2 b_1 (g'_i + g'_j) + {}^1/_3 b_2 (g'^2_i + g'_i g'_j + g'^2_j) \quad (2)$$

The constants b_0, b_1, and b_2 were evaluated by fitting all possible values $\Delta V/\Delta g'$ from a single experiment to eq. 2 by the method of least squares. Thus, for a typical experiment in which five incremental additions were made, a total of 15 values of $\Delta V/\Delta g'$ were used.

Equation 2 gives the value of $\Delta V/\Delta g'$ between *any* two points g_i and g_j lying within the appropriate range. This equation is valid for all values of g_i and g_j (within the range), and if we let g_i approach g_j, we obtain eq. 1 as the limit. Finally, as in the previous case a primary equation was obtained by changing the independent variable from g' to Δg_2.

Results

Table I gives the range in g. of 1-BuOH/1000 g. of H_2O, the initial volume, V^0, in ml./1000 g. of H_2O, as well as the constants for the primary equations. The last column gives the uncertainty of the equations as estimated from the expression

$$0.674\left(\frac{\Sigma r^2}{N-k}\right)^{1/2}$$

The agreement among these equations was better than that among equations which were arrived at using cumulative increments only (*i.e.*, with g'_i in eq. 2 equal to zero). Despite this improvement, however, the agreement was not as good as the uncertainty values would seem to suggest. A plot of the primary equations showed that except for the linear region the best agreement among the curves was obtained by rejecting the end portions of each curve.

Table I: Ranges and Empirical Constants of Primary Equation

Expt. no.	Range, g. of BuOH/1000 g. of H_2O	Volume, V^0, ml./1000 g. of H_2O	a_0	$10^4 a_1$	$10^5 a_2$	Uncertainty $\times 10^5$
5-80	0.00–14.45	1004.340	1.17420	−5.358	...	2.8
5-84	14.51–29.26	1021.320	1.16747	−5.235	1.122	1.6
5-85	29.26–44.28	1038.459	1.16253	−3.452	1.118	3.0
5-88	0.00–14.51	1004.340	1.17426	−5.220	...	3.4
5-89	14.51–28.28	1021.326	1.16777	−5.157	0.979	7.3
5-91	44.29–59.57	1055.954	1.15926	−1.206	0.666	0.9
5-92	33.92–49.00	...	1.16136	−3.150	0.939	2.0
5-94	35.46–50.57	...	1.16117	−3.884	1.625	2.3
5-109	46.44–61.75	...	1.15956	−2.615	1.748	0.7
5-111	8.59–23.26	1014.404	1.17037	−6.055	1.279	8.5
5-112	23.26–38.17	1031.524	1.16449	−4.737	1.370	2.5
5-118	0.00–14.50	1004.340	1.17400	−4.957	...	1.3

From the data in Table I values of the partial specific volume of 1-butanol were calculated at intervals of 0.001 mole fraction. Any value which fell near the extremes of the range of its primary equation was rejected. The remaining values were averaged to give the results shown in the first column of Table II.

Essentially the same procedure was followed to obtain the values for the densities of aqueous 1-butanol

Table II: Partial Volumes and Densities

X_2	$\bar{v}_2$ (obsd.), ml./g.	$\bar{v}_2$ (calcd.), ml./g.	d^{30}_4, g./ml.	$\bar{v}_1$, ml./g.
0.000	1.17415	1.17403	(0.995678)	(1.004340)
0.001	1.17201	1.17192	0.994993	1.004345
0.002	1.16987	1.16993	0.994321	1.004358
0.003	1.16786	1.16808	0.993662	1.004380
0.004	1.16653	1.16638	0.993012	1.004401
0.005	1.16484	1.16484	0.992377	1.004432
0.006	1.16351	1.16352	0.991752	1.004463
0.007	1.16227	1.16225	0.991136	1.004496
0.008	1.16125	1.16121	0.990527	1.004531
0.009	1.16049	1.16035	0.989930	1.004555
0.010	1.15969	1.15967	0.989342	1.004584
0.011	1.15897	1.15917	0.988753	1.004620
0.012	1.15885	1.15880	0.988124	1.004681
0.013	1.15852	1.15873	0.987606	1.004637
0.014	1.15897	1.15879	0.987037	1.004613
0.015	1.16001	...	0.986474	1.004545

solutions. The values reported are actually relative densities calculated by means of the expression

$$d = \frac{V^0 d^0 + \Delta g_2}{V^0 + a_0 \Delta g_2 + {}^1/_2 a_1 \Delta g_2^2 + {}^1/_3 a_2 \Delta g_2^3} \quad (3)$$

Values calculated from experiment 5–85 were in severe disagreement with other values in the same range and as a consequence were rejected.

Finally, from the values of $\bar{v}_2$ and $d^{30}{}_4$ the partial specific volume of water, $\bar{v}_1$, was determined.

For all but a few values the precision in $\bar{v}_2$ is estimated to be ± 0.0001 ml./g. Values of $\bar{v}_2$ at mole fractions greater than about 0.013 may be in error by as much as ± 0.0003 ml./g. owing to the incomplete dissolving of sample referred to earlier.

In contrast, the precision of the density values varies from ± 0.000001 g./ml. at the lowest mole fractions to at worst ± 0.00001 g./ml. for the last four values. This progressive decrease in precision is, of course, not unexpected since, in order to cover this concentration range, four consecutive experiments were needed, for each of which a d^0 and a V^0 had to be determined.

In general, the precision of the $\bar{v}_1$ values parallels the precision of the density values.

Because of the manner in which the partial volumes and densities were measured, it would be difficult to determine rigorously the effect on these quantities of impurities in the sample of 1-butanol. However, if we neglect changes in the partial specific volumes which occur in the concentration range covered by a single experiment, then the magnitude of this error can be determined rather easily. If we let $\bar{v}_2$ and $\bar{v}_2'$ equal the measured and true values for 1-butanol, respectively, then

$$\bar{v}_2 = (1 - x)\bar{v}_2' + x\bar{v}_3 \quad (4)$$

where x and $\bar{v}_3$ are, respectively, the weight fraction and partial specific volume of the impurity. It follows immediately that

$$\bar{v}_2 - \bar{v}_2' = (\bar{v}_3 - \bar{v}_2')x \quad (5)$$

A reasonable estimate of the amount of impurity in the 1-butanol would be 0.05% and, assuming that $\bar{v}_2' - \bar{v}_3$ is 2×10^{-1} ml./g., then the error due to impurities is of the order 5×10^{-5} ml./g. Since the amount of impurity is small, its presence in solution will have a negligible effect on the partial specific volumes of the other components. As a result 5×10^{-5} ml./g. represents the magnitude of this error throughout the entire concentration range studied.

Similarly, if we let d and d' be the measured and true value of the density, respectively, then for a single experiment

$$d - d' = \frac{g_f}{V_f} - \frac{g_f}{V_f - x\Delta g_2(\bar{v}_3 - \bar{v}_2)} \quad (6)$$

where $g_f = 1000 + \Delta g_2$ and $V_f = V^0 + \Delta V$. From this we find

$$d - d' \approx -\frac{\Delta g_2}{V_f}(\bar{v}_3 - \bar{v}_2)x \quad (7)$$

Since g_2/V_f is about 10^{-3}, then for the situation mentioned previously $d - d'$ is about equal to 10^{-7} for a single experiment and will certainly be less than 10^{-6} for any density value reported. Thus, it can be concluded that uncertainties in the reported partial volumes and densities caused by impurities are no larger than the uncertainties in the measurements themselves.

The constants in the linear limiting equation for $\bar{v}_2$ were evaluated from experiments 5-80, 5-88, and 5-118. According to the data, the limiting behavior of $\bar{v}_2$ can best be represented by the equation

$$\bar{v}_2 = 1.17415 - 2.15X_2 \quad (8)$$

The uncertainty in the limiting value of v_2 is ± 0.00010 ml./g. and the uncertainty in the slope is ± 0.07.

Three experiments covered the regions in which $\bar{v}_2$ attains its minimum value. The minimum value and the mole fraction at which the minimum occurs were calculated from the corresponding primary equations and are shown in Table III. Since the first derivatives of the primary equations were used to evaluate the concentration at the minimum, these figures are particularly sensitive to the reliability of the primary equations. For this reason there would seem to be ample justification for giving little weight to the middle figure, since the uncertainty in that primary equation is substantially higher than it is in the other two.

Table III: Value and Position of $\bar{v}_2$ (min.)

Expt. no.	Mole fraction	$\bar{v}_2$ (min.)
5-91	0.0126	1.15872
5-94	0.0114	1.15885
5-109	0.0129	1.15858

Interestingly enough, values for $\bar{v}_2$ for concentrations up to $X_2 = 0.014$ can be calculated (Table II, column 3) with good precision from the expression

$$\bar{v}_2 = 1.17403 - 2.165X_2 + 152.2X_2^{2.16} \quad (9)$$

It will be noted that the limiting linear form of this equation is in excellent agreement with the limiting linear equation obtained by direct measurement. An analogous equation with weight fraction as the independent variable

$$\bar{v}_2 = 1.17409 - 0.5343W_2 + 8.282W_2^{2.20} \quad (10)$$

represents the data with nearly the same reliability. Both equations, however, predict values of the mole fraction at the minimum which are slightly high, 0.0131 and 0.0134 for eq. 9 and 10, respectively. Equation 9 is, therefore, perhaps the better of the two.

Acknowledgment. The author wishes to express his appreciation to St. John's University for its support of this research in the form of a St. John's University summer research stipend.

On the Effect of the Double-Impact Collision on Dissociation Rate Constants

by H. Shin

Department of Chemistry, University of Nevada, Reno, Nevada *(Received February 19, 1965)*

The effect of the double-impact collision on the dissociation rate constant of the collision system RA + B, where RA is a molecule and B is an incident particle, is studied by calculating the probability of the momentum transfer between the collision partners. When the masses of the system satisfy $m_B/m_R = (m_A/m_R + 1)/(m_R/m_A - 1)$, the exact analysis of the impact process between A of RA and B and, in turn, the explicit formulation of the transition probability are found to be possible. Relatively few energetic particles which just missed the second impact with the molecules predominantly control the magnitude of the rate constant.

Introduction

In a recent paper[1] we have developed an idealized model of the colinear collision between a hydrocarbon RH and a hydrogen atom H to formulate the classical probability of free-radical formation. In this model we have assumed that the mass of R, m_R, is much greater than that of H, m_H, so that the position of R is practically unchanged during the collision between two hydrogen atoms, that H is attached to R through an inextensible string, and that the interaction is impulsive. Although the model is not realistic, it has revealed some important features of the radical-formation reaction. In this collision system, the bound H atom can suffer at most two impacts by the incident H atom. Therefore, when RH is hit twice by H, the momenta of the two hydrogen atoms are unchanged.

In collision theories, the rate expressions are commonly discussed without properly considering the effect of the impact multiplicity,[2-4] which invariably brings considerable mathematical difficulties. In the collision between a polyatomic molecule and an inert heat-bath molecule (usually a monatomic molecule), the molecule may suffer many impacts before it produces a small fragment(s) if the mass of the fragment is much smaller than that of the heat-bath molecule. On the other hand, if the magnitudes of the masses are reversed, the fragment can most likely be hit only once by the incident particle before it dissociates.

(1) H. Shin, *J. Phys. Chem.*, 68, 3410 (1964).

(2) T. A. Bak and J. L. Lebowitz, *Discussions Faraday Soc.*, 33, 189 (1962); S. E. Nielsen and T. A. Bak, *J. Chem. Phys.*, 41, 665 (1964).

(3) E. W. Montroll and K. E. Shuler, *Advan. Chem. Phys.*, 1, 361 (1958).

(4) I. Prigogine and T. A. Bak, *J. Chem. Phys.*, 31, 1368 (1959).

Therefore, in the former case, it is necessary to include all possible impacts to formulate the correct rate expression. If all impacts are not taken into account in the formulation, the resulting rate expression may give values which are much lower than the experimental values.

In the present paper we consider the dissociation of RA by the collision with B, where R can be either a radical or atom, A is an atom (=H, D, ...), and B is an incident atom. When the masses of R, A, and B satisfy certain relations, RA can suffer either one or two impacts by B but not more than two. In such cases we can solve the collision process of the three-body problem analytically. The purpose of this paper is to study the effect of the two-impact collision between A and B on the values of the rate constants for the dissociation of RA. Although the study of the collision process with more than two impacts will give more detailed information about the effect, we feel that the analytical solution of the two-impact process will suffice to draw some conclusions about the importance of the impact multiplicity in collision theories.

Method

The model is the same as the one considered in ref. 1 except in the present case the mass ratio m_R/m_A is not infinite, and m_A and m_B are not in general identical. The exceptions make the present method different from ref. 1 although the same potential energy surface can be used. To present a more complete account, the main features of the earlier model will be briefly recapitulated. We use the notations and terminologies shown in ref. 1 whenever possible.

Consider the collision system of RA + B, where A is hit impulsively along its line of oscillation by the incident particle, B. The linear collision coordinate is shown in Figure 1. The atom A oscillates between $r_1 = 0$, the closest approach A can make toward R, and $r_1 = l$. The number of impacts between A and B is dependent on the initial phase of A, *i.e.*, the position of A when B reaches $r_1 = l$ from right, on the magnitudes of their momenta, and on the masses of R, A, and B. There are assumed to be three regions in which the potential energies are

$$V = \begin{cases} \infty & r_1 < 0 \\ V_0 & 0 < r_1 < l \\ 0 & r_1 > l, \end{cases}$$

where V_0 is a critical bond energy. The molecule RA is assumed to dissociate instantaneously for $V > V_0$.

Since the present system is a three-body collision problem, we cannot use the method shown in ref. 1 to calculate the transition probability which is needed in the formulation of the rate constant. It is therefore necessary to introduce a new coordinate system in which the motion of the collision partners can be ex-

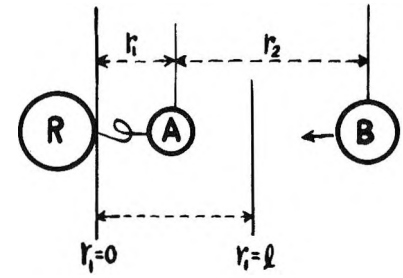

Figure 1. Collision coordinates for RA + B. At the moment of the first impact B always moves leftward, while A moves either rightward or leftward.

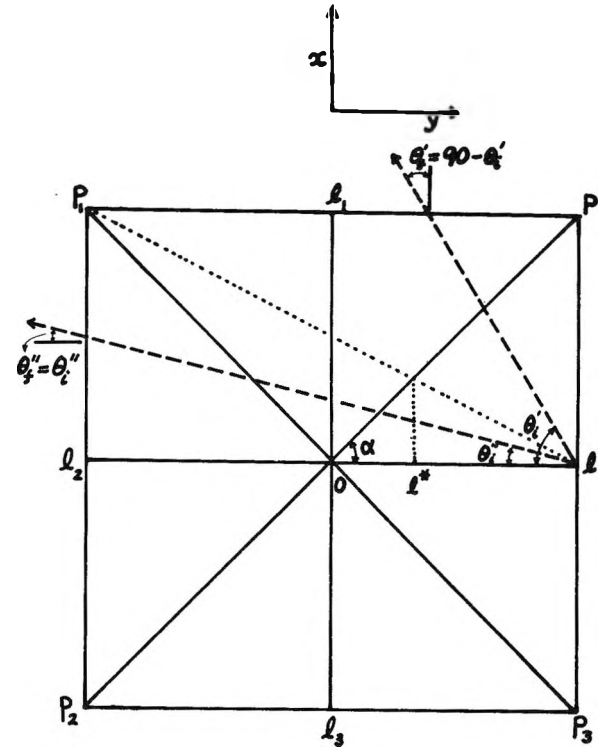

Figure 2. The kinematic diagram for $\alpha = 45°$. ΔOPl is the original potential energy surface. Others are the images of ΔOPl generated through the axis OP, OP_1, OP_2, or OP_3. $\overline{Ol^*}/\overline{l^*l} = 1/2$. For the rightward motion of A at the moment of impact, if $\dot{x} > \dot{y}/2$, the system involves only one impact irrespective of the position of $\overline{Ol}$. However, if $\dot{x} < \dot{y}/2$, only A which is in the range $2\overline{Ol}(\dot{x}/\dot{y})$ suffers only one impact irrespective of the position in $\overline{Ol}$. If $\dot{y} > \dot{x} > \dot{y}/2$, only A in the range $2\overline{Ol}(\dot{x}/\dot{y}) - \overline{Ol}$ suffers one impact. When we divide the sum of these ranges of $2\overline{Ol}$, we obtain eq. 6.

pressed rectilinearly throughout the potential energy surface.

By drawing the axes of the collision coordinates at an appropriate angle, we can diagonalize the internal kinetic energy of the collision system. The potential energy surface constructed by this procedure then gives information about the distribution of vibrational and relative translational energy in the system. The most effective coordinate system with this feature may be expressed in terms of the original coordinates r_1 and r_2[5,6]

$$y = \left(\frac{m_R}{m_R + m_A}\right) r_1 + r_2 \tag{1}$$

$$x = \left[\frac{m_R m_A (m_R + m_A + m_B)}{m_B}\right]^{1/2} \left(\frac{1}{m_R + m_A}\right) r_1 \tag{2}$$

i.e., y is the distance between B and the center of gravity of RA and x is proportional to the amplitude of vibration of RA. The total kinetic energy in the new coordinate system is, in terms of the corresponding momenta $\dot{x}$ and $\dot{y}$

$$\text{K.E.} = \frac{1}{2}\left[\frac{(m_R + m_A)m_B}{m_R + m_A + m_B}\right]^{-1} (\dot{x}^2 + \dot{y}^2) \tag{3}$$

The motion of RA + B is therefore equivalent to the rectilinear motion of a single particle of the mass $M = m_B(m_R + m_A)/(m_R + m_A + m_B)$ in the x,y-plane as shown in ΔOPl of Figure 2 (the kinematic diagram for $\alpha = 45°$). In this figure the angle α is determined from

$$\tan \alpha = \left[\frac{(m_R + m_A + m_B)m_A}{m_R m_B}\right]^{1/2} \tag{4}$$

The kinematic diagram for $\alpha = 45°$ is shown in Figure 2. The rectilinear motion of the configuration point in ΔOPl which perfectly reflects at both OP and Ol can also be extended to the images of ΔOPl, which are generated through the axis OP. It should be noted that OP is the impact line for the A–B collision, and Ol is the reflecting line for A; *i.e.*, A reaches $r_1 = 0$ and reverses its direction of motion rightward. The initial angle of inclination θ_i between the motion of the configuration point and the line perpendicular to Pl is determined from the relation $\tan \theta_i = \dot{x}_i/\dot{y}_i$. Similarly, the final angle of inclination θ_f is determined from the relation $\tan \theta_f = \dot{x}_f/\dot{y}_f$. In the latter case, however, θ_f can appear in one of the following two ways depending on the initial angle, θ_i, and the initial position of the configuration point on Pl; they are the angle between the motion of the configuration point and the line perpendicular to Pl_1(or P_1l_1) and the angle between the motion of the configuration point and the line perpendicular to P_1l_2. As will be shown, these two possibilities correspond to the one-impact and the two-impact collisions, respectively. It is important to note that the kinetic energy of relative motion E_T of B and RA and the vibrational energy E_V of RA are related to the above angles by $|\tan \theta|_i = (E_V^i/E_T^i)^{1/2}$ and $|\tan \theta_f| = (E_V^f/E_T^f)^{1/2}$, respectively.[6]

In Figure 2, the final value of the velocity (or momentum) ratio $\dot{x}_f/\dot{y}_f = \tan \theta_f$ is equal to $\dot{y}_i/\dot{x}_i = \cot \theta_i$ if the configuration point crosses only one impact line, *i.e.*, OP. On the other hand, if it crosses two impact lines, *i.e.*, OP and OP_1, $\dot{x}_f/\dot{y}_f = \tan \theta_f$ is equal to $\dot{x}_i/\dot{y}_i = \tan \theta_i$. Therefore, in the former case the momenta of the x- and y-component are interchanged, while in the latter case there is no interchange. This simple but important property makes the exact solution of the three-body collision between RA and B possible. In this paper we only consider the $\alpha = 45°$ case. For the formulation of the rate constant we first calculate the transition probability of interchange $\dot{x} \rightarrow \dot{y}$ per collision.

Transition Probability

When $\alpha = 45°$, from eq. 4, we obtain

$$\frac{m_B}{m_R} = \frac{\dfrac{m_A}{m_R} + 1}{\dfrac{m_R}{m_A} - 1} \tag{5}$$

Therefore, if the masses of the collision system satisfy this expression, the three-body (RA + B) collision process can be completely analyzed using Figure 2. It is important to note that, if $m_R >> m_A$, this expression represents a two-body collision problem with $m_B = m_A$, which is equivalent to the origin of the plot of m_A/m_R *vs.* m_B/m_R.

The kinematic diagram of the present case, *i.e.*, Figure 2, is essentially identical with that of the two-body collision case.[1] Therefore, it can be readily shown from ref. 1 that the transition probability for the interchange $\dot{x} \rightarrow \dot{y}$ per collision between A and B is

$$P(\dot{x},\dot{y}) = \begin{cases} 1 & \infty > \dfrac{\dot{x}}{\dot{y}} > 1 \\ \dfrac{\dot{x}}{\dot{y}} & 1 > \dfrac{\dot{x}}{\dot{y}} > 0 \end{cases} \tag{6}$$

Here, in the $1 > \dot{x}/\dot{y} > 0$ region, some molecules are hit twice by the incident particles. The fractional $P(\dot{x},\dot{y})$

(5) D. W. Jepsen and J. O. Hirschfelder, *J. Chem. Phys.*, **30**, 1032 (1959).

(6) R. J. Rubin, *ibid.*, **40**, 1069 (1964).

value in this region results from the effect of the two-impact collision.

Rate Constant and Discussion

The rate constant for the dissociation of RA can be obtained by integrating the product of the transition kernel $z(\dot{y})P(\dot{x},\dot{y})$ and the equilibrium fraction of A, which appears in terms of the x-component of the configuration point, over all possible values of $\dot{y}$ and over values of $\dot{x} > (2MV_0)^{1/2}$. The collision frequency $z(\dot{y})$ may be written

$$z(\dot{y}) = \frac{c}{M}\left(\frac{2}{\pi MkT}\right)^{1/2}\dot{y}e^{-\dot{y}^2/2MkT} \tag{7}$$

where c is the concentration of B along the line of motion of each A atom. The total number of collisions per unit time suffered by an A atom is

$$Z = \int_0^\infty z(\dot{y})\mathrm{d}\dot{y} = c\left(\frac{2kT}{\pi M}\right)^{1/2} \tag{8}$$

The rate constant may then be expressed as

$$\kappa = \frac{1}{MkT}\int_{(2MV_0)^{1/2}}^\infty \dot{x}e^{-\dot{x}^2/2MkT}\mathrm{d}\dot{x}\int_0^\infty z(\dot{y})P(\dot{x},\dot{y})\mathrm{d}\dot{y} \tag{9}$$

When we substitute eq. 6 into eq. 9

$$\kappa = \frac{1}{MkT}\int_{(2MV_0)^{1/2}}^\infty \dot{x}e^{-\dot{x}^2/2MkT}\mathrm{d}\dot{x} \times \left[\int_0^{\dot{x}} z(\dot{y})\mathrm{d}\dot{y} + \dot{x}\int_{\dot{x}}^\infty \frac{z(\dot{y})}{\dot{y}}\mathrm{d}\dot{y}\right] \tag{10}$$

With eq. 7, eq. 10 can be solved in terms of the error function $\phi'(\beta)$, where $\beta = (V_0/kT)^{1/2}$. Although for small β-values the error function becomes particularly simple, we consider the solutions with large β-values. In such a case the error function may be written

$$1 - \phi'(\beta) = \frac{e^{-\beta^2}}{\pi^{1/2}\beta}\sum_{r=0}^{n}\frac{(-1)^r(2r)!}{2^{2r}r!\beta^{2r}} \qquad r < \beta^2$$

With this approximate expression we integrate eq. 10 to obtain

$$\kappa = Ze^{-V_0/kT}\left[\left(\frac{\pi V_0}{kT}\right)^{1/2} + 1 - {}^1/_2\, e^{-V_0/kT} + \frac{\pi}{2}\phi(\beta)\right] - ZEi\left(-\frac{2V_0}{kT}\right)\sum_{r=0}^{n}\frac{(2r)!}{2^{r+1}(r!)^2} - Ze^{-V_0/kT}\sum_{r=0}^{n}\sum_{l=0}^{r-1}\frac{(-1)^{r+l+1}(2r)!(r-l-1)!}{2^{2r-l+1}(r!)^2\beta^{2(r-l)}} \tag{11}$$

where $-Ei(-x) = \int_x^\infty e^{-v}\mathrm{d}v$, the exponential integral.

An insight into the impact multiplicity is gained by formulating κ for the one-impact collision case. If we consider only one impact, which corresponds to $P(\dot{x},\dot{y}) = 1$ regardless of the relative magnitudes of $\dot{x}$ and $\dot{y}$, the rate constant is simply

$$\kappa^* = Ze^{-V_0/kT} \tag{12}$$

Since the second and third terms in the right-hand side of eq. 11 are significantly smaller than the first

$$\kappa \simeq Z\left[\left(\frac{\pi V_0}{kT}\right)^{1/2} + 1 - {}^1/_2\, e^{-V_0/kT} + \frac{\pi}{2}\phi(\beta)\right]e^{-V_0/kT} \tag{13}$$

from which we see immediately the dependence of κ on the transition kernel in the momentum ratio range, $1 > \dot{x}/\dot{y} > 0$, by comparing with eq. 12. The term $(\pi V_0/kT)^{1/2}$ is the leading factor obtained by including the collisions in this momentum ratio range. Physically, $\dot{x}$ should be excited to $\dot{y}$ to cross the potential barrier of V_0. Therefore, in this model, the conditions for the dissociation of RA are that the incident particle with an energy greater than that of the vibrational energy of A must hit the latter only once and that A is not too close to the origin $r_1 = 0$. If $r_1 \simeq 0$ (or $x \simeq 0$), the collision process will predominantly involve two impacts; this situation results in the difficulty of the excitation of RA.

As $V_0/kT \longrightarrow \infty$, eq. 11 simplifies to

$$\kappa \sim \kappa_\infty = Z\left(\frac{\pi V_0}{kT}\right)^{1/2}e^{-V_0/kT} \tag{14}$$

which shows that only the incident particles which reached the momentum ratio range $1 > \dot{x}/\dot{y} > 0$ but barely missed two impacts contribute to the limiting value. By comparing eq. 11 and 12, we then obtain

$$\frac{\kappa}{\kappa^*} \sim \left(\frac{\pi V_0}{kT}\right)^{1/2} \qquad \frac{V_0}{kT} \longrightarrow \infty$$

i.e., the inclusion of the contribution of the impacts from the $1 > \dot{x}/\dot{y} > 0$ region increases κ, in the asymptotic limit, by a factor of $(\pi V_0/kT)^{1/2}$, which is much greater than unity.

From the above results it can be said that the most energetic incident particles, which correspond to the motion of the configuration points with small θ_i values, dominate the over-all magnitude of κ. Thus, in the present collision model, the rate may be small at the most probable energy of the incident particles but can be large at the high energies in the "tail" of the Boltzmann distribution curve.

Acknowledgment. The author wishes to thank M. P. Hanson for making several helpful suggestions.

Effects of pH and Divalent Cations on the Transport of Univalent Cations across a Weak-Acid Membrane[1]

by H. G. Spencer and T. M. Ellison

Department of Chemistry, Clemson University, Clemson, South Carolina *(Received February 23, 1965)*

Interdiffusion fluxes of univalent cations across an interpolymer membrane containing a poly(carboxylic acid) were measured with a variety of compositions of the external solutions. Significant changes in the barrier properties of the membrane to the fluxes of the univalent cations are attributed to the specific association of the ionic sites with H^+ ions and divalent cations. The results were analyzed in terms of a simple flux equation which relates the fluxes to the total univalent cation concentration in the membrane and to the diffusion coefficients in the different membrane structures.

Introduction

The ion-exchange properties of weak-acid membranes are strongly dependent on the nature of the adjacent solutions. The apparent capacity, swelling, sorption of electrolyte, and diffusion coefficients are affected by the pH, the concentration of electrolyte, and the nature of the counterions of the external solution.[2] Divalent cations accumulate appreciably in interpolymer membranes containing poly(carboxylic acids)[3] and the complexity constants of the cations with these systems are apparently greater than with the corresponding dicarboxylic acids.[4] The present work is an investigation of the effects that the pH and the presence of complexing ions have on the membrane structure and interdiffusion fluxes of univalent cations in an interpolymer membrane containing a poly(carboxylic acid).

Experimental

Materials. The membranes were composed of poly(vinyl methyl ether–maleic acid), PVM–MA, dispersed in a matrix of poly(vinyl alcohol), PVA. The PVM–MA was provided in the anhydride form by the General Aniline and Film Corp. The high viscosity PVA (Elvanol, Grade 72–60) was provided by E. I. du Pont de Nemours and Co., Inc. Alkaline hydrolysis of the poly(vinyl acetate) was greater than 99%. The ion selectivity and the mechanical and electrical properties of these membranes have been reported.[5]

The membranes were prepared by dissolving the appropriate dry weights of the polymers, 10% PVM–MA + 90% PVA, in deionized water, mixing thoroughly, filtering, and casting on a glass plate in a drybox. After drying at room temperature for 2 to 3 days, the membranes were stripped from the glass and rendered insoluble by baking in a drying oven at 100° for 24 hr. The membranes were soaked in 1 *M* HCl for 24 hr. and washed in deionized water until a negative chloride test was obtained. The dry thickness was determined with a micrometer caliper which could be read with an accuracy of $\pm 2\ \mu$. The membranes were uniform within this accuracy.

The salts were analytical grade reagents used without further purification, and the water was distilled and deionized with a mixed-bed ion-exchange column.

Conductivity. The conductivities of the membranes in equilibrium with various solutions were determined in a cell in which a membrane separated two solution compartments containing platinized platinum elec-

(1) Preliminary report presented at the 147th National Meeting of the American Chemical Society, Philadelphia, Pa., April 1964.

(2) F. Helfferich, "Ion Exchange," McGraw-Hill Book Co., Inc., New York, N. Y., 1962, pp. 79, 137, 279, 350.

(3) H. P. Gregor and D. M. Wetstone, *Discussions Faraday Soc.*, **21**, 162 (1956).

(4) (a) H. P. Gregor, L. B. Luttinger, and E. M. Loebl, *J. Phys. Chem.*, **59**, 34, 366 (1955); (b) H. Morawetz, A. M. Kotliar, and H. Mark, *ibid.*, **58**, 619 (1954).

(5) H. G. Spencer and O. L. Hunt, *J. Appl. Polymer Sci.*, **6**, 656 (1962).

trodes. The membrane conductivity, κ, was calculated using the equation

$$\kappa = L/[A(R - R_0)] \quad (1)$$

where L is the membrane thickness in centimeters, A is the membrane cross section, 2.14 cm.^{2}, and $R - R_0$ is the difference between the resistances of the cell, in ohms, with and without the membrane. The resistance was measured at 30.00 ± 0.05° using an Industrial Instruments Inc. conductivity bridge, Model RC16B2 at 1000 c.p.s. The uncertainty in the resistance was ±0.1 ohm, which by eq. 1 makes the uncertainty in the membrane conductivity ±7% or less, depending on the magnitude of the difference in resistance, $R - R_0$. Resistance values for membranes from the same sheet, 25 μ thick, were within the uncertainty limit. The cell solutions contained 0.1000 M univalent metal chloride, and the effects of the divalent cations were determined by also making the solutions 0.0025 M in divalent metal chloride. The addition of the divalent metal chloride had a negligible effect on the cell resistance measured without the membrane barrier.

Osmotic Flow Rates. Osmotic flow rates were determined using a simple osmometer described by Gregor, *et al.*[6] Prior to the flow rate determination, the membrane was equilibrated in a solution 0.1000 M in KCl and 0.0025 M in the divalent metal chloride. The osmometer containing the membrane was brought to the experimental temperature, 30°, in deionized water and then transferred to a vigorously stirred 1.00 M sucrose solution. A previous study[5] had shown membranes of this type to be impermeable to sucrose. The flow rates, Q, were calculated from the equation

$$Q = (\Delta V)L/At \quad (2)$$

where (ΔV) is the volume change in microliters in t hours, L is the membrane thickness, 4.5 × 10^{-3} cm., and A is the membrane cross section, 2.63 cm.^{2}.

Concentrations of Ions in the Membrane. Procedures for determining the ionic concentrations are the same as those reported by Gregor and Wetstone.[3] Two samples weighing 2.33 and 2.17 g., respectively (K form, dried under vacuum at 50°), in sheets of various sizes and 69 ± 5 μ thick were equilibrated in solutions that were 0.1000 m in KCl plus 0.0025 m in the divalent metal chloride. Equilibrium was established by subjecting the samples to four 250-ml. portions of the solution each for 24 hr. at 30°. The pH of the initial portion was adjusted to approximately 10.5 and the subsequent portions to 5.5. No change in concentration was observed in the final portion. After equilibration, the samples were blotted with paper tissue and weighed to obtain "wet weights." They were then dried at 55° until a constant weight was obtained (several days) and weighed to obtain dry weights. The difference in the two weights was taken as the weight of pore water. Each sample was eluted with 300 ml. of 1.0 M HCl for 24 hr. The cations were not detected in subsequent elutions. The K^+ ion in the eluent was analyzed by flame photometry employing a Baird Atomic, Inc., Model KY-1 instrument. No interference was observed from Mg^{2+}, Ca^{2+}, or Cu^{2+} ions. Mg^{2+} and Ca^{2+} ion concentrations were determined by EDTA titration using Calmagite as the indicator.[7] Cu^{2+} was determined colorimetrically using a Bausch and Lomb Spectronic 20 instrument. The blue color produced upon the addition of a 50% solution of pyridine in water to a copper sample obeyed Beer's law over the concentration range of interest.

The concentration ratio, $\bar{C}_{Na}/\bar{C}_K$, for Na^+ and K^+ ions were determined by equilibrating the membrane in 0.0500 m NaCl and 0.0500 m KCl. The ratio for $N(CH_3)_4^+$ and K^+ ions was determined by equilibrating one sample in 0.1000 m KCl and the second in 0.0500 m KCl and 0.0500 m $N(CH_3)_4Cl$. The $N(CH_3)_4^+$ ion concentration in the membrane was taken as the difference between the K^+ concentration in the two samples. The membrane capacity at a pH of 5.5 was determined from the sample equilibrated in KCl. The membrane concentrations reported are average values for at least three determinations and were reproducible to within ±0.03 m.

Transport of Ions across the Membrane. A two-compartment Plexiglass cell similar to the one used by McKelvey, Spiegler, and Wyllie[8] was used to measure the transport rates. The compartments, each with a volume of 270 cc., were separated by a membrane with an area of 5.13 cm.^{2}. The solutions in the compartments were stirred at 375 ± 25 r.p.m. and were maintained at 30.00 ± 0.05°. The system 0.1000 M KCl–membrane–0.1000 M $N(CH_3)_4Cl$ was used to determine the interdiffusion rates of K^+ and $N(CH_3)_4^+$ ions. The solutions remained in the cell overnight, and then fresh solutions were introduced and stirred for 30 min. prior to each run. Fresh solutions were again introduced to commence the run. Samples (0.2 ml.) were taken periodically from the $N(CH_3)_4Cl$ side and analyzed for K^+ by the flame photometric method. A similar procedure was used with other combinations of cations. The effects of pH on the K^+–$N(CH_3)_4^+$ ion interdiffusion were determined in the same way, except the pH

(6) H. P. Gregor, H. Jacobson, R. C. Shain, and D. M. Wetstone, *J. Phys. Chem.*, **61**, 141 (1957).

(7) F. Lindstrom and H. Diehl, *Anal. Chem.*, **32**, 1123 (1960).

(8) J. G. McKelvey, K. S. Spiegler, and M. R. J. Wyllie, *J. Electrochem. Soc.*, **104**, 387 (1957).

Table I: Properties of Membranes in Equilibrium with Various External Solutions and Osmotic Flow Rates

External soln. concn.		Metal ion concn. in membrane				Osmotic flow rate, Q, μl. cm.$^{-1}$ hr.$^{-1}$
KCl, M	MCl_2, M	K^+, $\bar{m}$[a]	M^{2+}, $\bar{m}$	Total, mequiv./g. of water	Water content, wt. %	
0.1000	0	1.24	...	1.24	43.0	0.152
0.1000	0 (pH 2.1)	0.113	...	0.113	...	...
0.1000	2.5×10^{-3} (M = Mg)	0.427	0.257	0.94	47.0	0.0798
0.1000	2.5×10^{-3} (M = Ca)	0.400	0.395	1.19	43.5	0.0766
0.1000	2.5×10^{-3} (M = Cu)	0.117	0.979	2.08	38.0	0.0590

[a] ± 0.003 $\bar{m}$.

of both sides of the cell was adjusted to the desired value by adding HCl. The effects of complexing ions on the univalent cation interdiffusion were also determined in the same way, but both sides of the cell were brought to 0.0025 M in the divalent metal chloride. Except for the experiments concerned with the effects of pH, all solutions were at a pH of 5.5 ± 0.5. The accuracy for the K^+ and Na^+ concentrations was within $\pm 1 \times 10^{-4}$ M. The resulting range for the experimental fluxes was within 6% of the values reported. All interdiffusion measurements were made on membranes cut from the same sheet and were reproducible within the 6%. The membrane thickness was 30 μ.

Results

Exchange and Osmotic Flow Properties. The equilibrium exchange properties and the osmotic flow rates are tabulated in Table I. The total concentration of the metal ions (weight normality) and the K^+ ion concentration (molality) vary appreciably with the pH and the divalent metal ion of the external solution. The K^+ ion concentration is reduced by both lower pH and greater accumulation of the divalent metal ion in the membrane. The changes in swelling caused by the external conditions are indicated by the water content and the osmotic flow rate. The osmotic flow rate of the membrane converted to the acid form was 0.0816 μl. cm.$^{-1}$ hr.$^{-1}$; thus, the decrease in pH of the external solution reduces osmotic flow rate, as does the accumulation of divalent metal ions. The variation of the water content is neither so orderly nor so large as the flow rate variation, which indicates that the fraction of the water which is mobile differs in these membrane structures.

Conductivity. The results of the conductivity measurements are listed in Table II. Using the equation[9]

$$\bar{D}_i = \frac{RT10^3\kappa\bar{l}_i}{|Z_i|F^2\bar{C}_i} \qquad (3)$$

the self-diffusion coefficients, $\bar{D}_i$, were calculated. In

Table II: Conductivities and Calculated Diffusion Coefficients

Divalent cation, 2.5×10^{-3} M	Conductivity, $\kappa \times 10^4$, ohm.$^{-1}$ cm.$^{-1}$			Diffusion coeff., $\bar{D}_i \times 10^5$, cm.^{2}/sec.		
	KCl	NaCl	$N(CH_3)_4Cl$	K^+	Na^+	$N(CH_3)_4^+$
None	3.89	3.34	0.935	8.49	7.29	2.04
Mg	1.38	1.30	0.324	8.74	8.24	2.06
Ca	1.37	0.898	0.308	9.27	6.07	2.08
Cu	0.139	0.105	0.050	3.21	2.43	1.16

eq. 3, R is the gas constant, T is the temperature in degrees Kelvin, F is the Faraday constant, $\bar{l}_i$ is the transport number of the ith ion in the membrane, $\bar{C}_i$ is the normality of the ith ion in the pore liquid. The values of $\bar{D}_i$ in Table II were calculated with the assumptions that $\bar{l}_i = 1$ for the univalent cation, i, and that $\bar{C}_i$ for i = Na^+ and $N(CH_3)_4^+$ is equal to the measured concentration of the K^+ ion. The assumption that $\bar{l}_i = 1$ is reasonable for the system containing no divalent cations, as these values were estimated previously from concentration potentials.[5] This assumption may be poor for the systems containing divalent cations which may permit appreciable transport of current by either the divalent cations or sorbed anions. However, no flux of the divalent cations could be detected. The assumption that $\bar{C}_i$ is independent of i for the three univalent cations is based on determination of the ratio of $\bar{C}_{Na}/\bar{C}_K = 1.04$ and $\bar{C}_{N(CH_3)_4}/\bar{C}_K = 1.25$ for a membrane equilibrated with a solution containing equal concentrations of the two salts. Because these ratios are near unity and likely change in the presence of the divalent cations, the above assumption was made for the purposes of estimating values of $\bar{D}_i$.

Interdiffusion. A theory of interdiffusion outlined by Helfferich,[10] based on the model that the membrane

(9) K. S. Spiegler and C. D. Coryell, *J. Phys. Chem.*, **57**, 687 (1953).

(10) F. Helfferich, "Ion Exchange," McGraw-Hill Book Co., Inc., New York, N. Y., 1962, Chapter 8.

is a quasi-homogeneous phase in which the anion groups are fixed, is useful in understanding the results in weak-acid membranes. A number of assumptions is necessary in order to derive an integrated form of the flux equations: (1) the flux is completely controlled by the membrane; (2) the concentration of the fixed groups, the activity coefficients, and the diffusion coefficients are constant across the membrane; (3) convection and the presence of coions are disregarded; (4) electric current is absent; (5) the diffusing ions i and j do not associate with fixed or mobile ionic species; and (6) stationary-state or constant-flux conditions are maintained. The equation obtained for the interdiffusion fluxes of univalent ions i and j is

$$\bar{J}_i = \bar{J}_j = \left[\frac{\bar{D}_i\bar{D}_j}{\bar{D}_i - \bar{D}_j} \ln \frac{\bar{D}_i}{\bar{D}_j}\right] \frac{\bar{C}}{L} \qquad (4)$$

where $\bar{C}$ is the total counterion concentration and L is the thickness of the membrane. Equation 4 describes interdiffusion across strong-acid membranes. A modification of eq. 4 is necessary in order to use it with weak-acid membranes. It is assumed that only the univalent metal ions are mobile; thus, it is only the sum of their concentrations, $\bar{C}'$, which should appear in the equation. The modified equation is

$$\bar{J}_i = \bar{J}_j = \left[\frac{\bar{D}_i\bar{D}_j}{\bar{D}_i - \bar{D}_j} \ln \frac{\bar{D}_i}{\bar{D}_j}\right] \frac{\bar{C}'}{L} \qquad (5)$$

Since $\bar{C}'$ depends on the nature of the external solution, $\bar{J}_i$ will change with any modification of the external solution which alters $\bar{C}'$.

The experimental and calculated interdiffusion fluxes for the system K^+–$N(CH_3)_4^+$ are listed in Table III. The values for the Na^+–$N(CH_3)_4^+$ system were identical with the K^+–$N(CH_3)_4^+$ system within the experimental reliability. The result for the Na^+–K^+ system without added divalent cation salts was $J_K = J_{Na} = 21.8 \times 10^{-9}$ equiv. cm.$^{-2}$ sec.$^{-1}$, or about $2 \times \bar{J}_i$ for the first two systems. Equation 5 predicts that $\bar{J}_K$ is influenced most by the ion with the smallest value of $\bar{D}_i$. Since the results of the conductivity experiments (Table II) indicate that $\bar{D}_K \cong \bar{D}_{Na} > \bar{D}_{N(CH_3)_4}$, eq. 5 predicts that $\bar{J}_i$ should be approximately equal in the first two systems and larger in the last one. Only qualitative agreement should be expected since $\bar{C}'$ is likely not constant in the three systems. The column of calculated fluxes in Table III was calculated using eq. 5 and substituting the K^+ ion concentration determined from the equilibrium experiment (Table I) for $\bar{C}'$ and using $\bar{D}_i$ values from Table II. The agreement between calculated and measured $\bar{J}_i$ values is only qualitative.

Table III: Experimental and Calculated Interdiffusion Fluxes for the System 0.1000 *M* KCl–Membrane–0.1000 *M* $N(CH_3)_4Cl$ in the Presence of Divalent Cations

Divalent cation salt, 2.5×10^{-4} *M*	Interdiffusion flux, $\bar{J}_K$, equiv. cm.$^{-2}$ sec.$^{-1}$ $\times 10^9$	
	Exptl.	Calcd.
None	10.3	15.8
None (pH 2.1)	1.61	...
$MgCl_2$	7.43	5.54
$CaCl_2$	5.82	5.35
$CuCl_2$	1.62	0.72

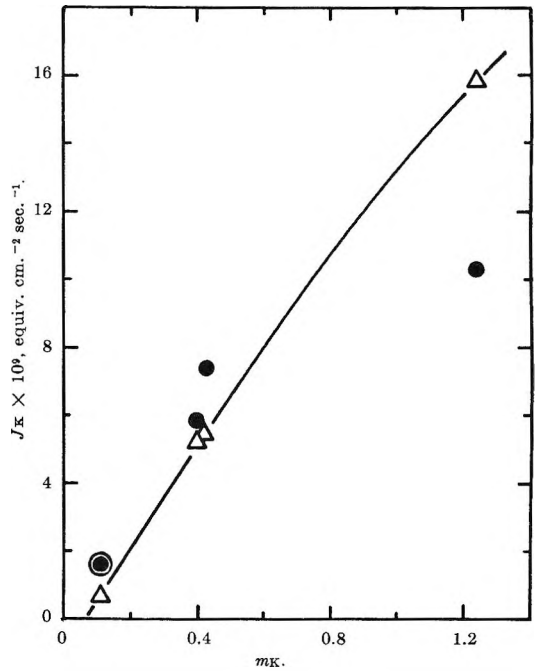

Figure 1. Interdiffusion flux for the system K^+–$N(CH_3)_4^+$ as a function of the K^+ ion concentration in the membrane: ●, measured flux; △, calculated flux.

From Table III, it is evident that $\bar{J}_i$ decreases as the pH decreases and as the accumulation of divalent cation increases; *i.e.*, $\bar{J}_i$ decreases as $\bar{C}'$ decreases, which is predicted by eq. 5. The decrease in $\bar{D}_i$ in the presence of Cu^{2+} ions also reduces $\bar{J}_i$ in that system. Figure 1 shows the dependence of $\bar{J}_K$ on the concentration of the K^+ ion in the membrane, and Figure 2 shows the dependence of $\bar{J}_K$ on the pH of the external solution. It is noteworthy that $\bar{J}_K$ has the same value in the system at pH 2.1 and in the system containing divalent copper and that the equilibrium concentration of the K^+ ion is nearly equal in these two systems. Note the encircled point in Figure 1. This result, in terms of the modified equation, indicates that the values of $\bar{D}_i$ do not differ greatly in the two systems.

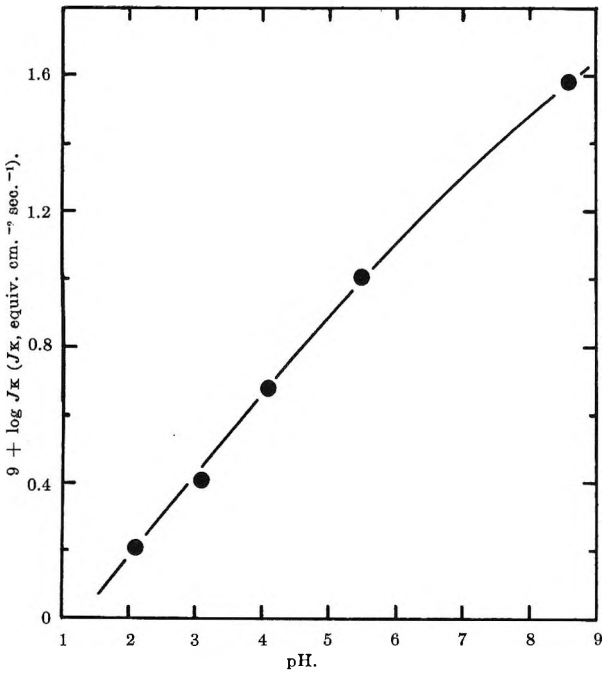

Figure 2. Interdiffusion flux for the system K^+–$N(CH_3)_4^+$ as a function of the pH of the external solutions.

The H^+–K^+ and H^+–Na^+ systems were also investigated, and the results are listed in Table IV. In these systems the fluxes of the coion, Cl^-, cannot be disregarded and are in fact appreciable. The fluxes of the divalent cations are detectable, but the Cl^- ion flux is primarily responsible for maintaining electroneutrality in these systems in which $\bar{J}_H > \bar{J}_K$ and $\bar{J}_H > \bar{J}_{Na}$. Equation 5 cannot be used even in a qualitative way in these systems where the Donnan exclusion of coions is not effective and the H^+ ions associate with the carboxylic acid groups of the membrane.

The fluxes of K^+ ion in systems of the type, 0.1000 *M* KCl–membrane–0.0333 *M* MCl_2 are presented in Table V. Equation 4 or 5 modified to include the difference in valence of the two counterions cannot adequately provide descriptions of these systems since the sorption experiments indicate that neither $\bar{C}$ nor $\bar{C}'$ is constant across the membrane.

Discussion

The values of the fluxes of the univalent counterions vary over a 10- to 20-fold range for this weak-acid membrane depending upon the nature of the external solutions. The specific association of the weak-acid groups with H^+ ions and divalent metal ions provides a means of significantly altering the barrier properties of the membrane to univalent cations. The oversimplified theory provides a semiquantitative description of the causes of these changes in barrier properties in some experiments but fails to describe adequately the systems when either anion penetration or variable internal total concentrations of univalent cations occur.

Table IV: Experimental Interdiffusion Fluxes for the Systems 0.1000 *M* HCl–Membrane–0.1000 *M* KCl or NaCl in the Presence of Divalent Cation Salts

Divalent cation salt, 2.5×10^{-3} *M*	Flux, equiv. cm.$^{-2}$ sec.$^{-1}$ × 10^9					
	$\bar{J}_H$	$\bar{J}_K$	$\bar{J}_H - \bar{J}_K$	$\bar{J}_H$	$\bar{J}_{Na}$	$\bar{J}_H - \bar{J}_{Na}$
None	4.57	3.60	0.97	4.73	3.75	0.98
$MgCl_2$	4.57	3.60	0.97	...	...	...
$CaCl_2$	4.90	3.27	1.63	5.23	2.78	2.45
$CuCl_2$	5.23	3.92	1.31	4.25	2.12	2.13

Table V: Fluxes of K^+ and Na^+ ions in Systems 0.1000 *M* MCl–Membrane–0.0333 *M* MCl_2

Divalent metal ion	J_K × 10^9, equiv. cm.$^{-2}$ sec.$^{-1}$	
	K^+–M^{2+}	Na^+–M^{2+}
Mg	3.14	1.85
Ca	2.58	2.77
Cu	1.10	0.92

Acknowledgment. Support by the National Institutes of Health under Grant RG 8774 is gratefully acknowledged.

Ionic Association of Potassium and Cesium Chlorides in Ethanol–Water Mixtures from Conductance Measurements at 25°[1]

by James L. Hawes[2] and Robert L. Kay[3]

Metcalf Research Laboratory, Brown University, Providence 12, Rhode Island, and Mellon Institute, Pittsburgh, Pennsylvania 15213 *(Received February 23, 1965)*

A special conductance cell was designed for the precise measurement of the conductance of the alkali halides in nonaqueous solvents. The cell contains guarded electrodes sealed in the center of a 2-l. flask in such a way that the solution being measured can be continually stirred. An automatic salt-dispensing device eliminates any chance of atmospheric contamination during a measurement. The characteristics of the cell are described and compared to standard conductance cells. The Fuoss–Onsager conductance theory indicated significant ion pair association for KCl and CsCl in solvents of dielectric constant less than 43 and 55, respectively. Log K_A was linear in the reciprocal dielectric constant for both salts, and points for KCl in liquid SO_2 and liquid NH_3 are close to the line. The slopes of these lines gave $\mathring{a}_K = 3.0$ for KCl and 3.5 for CsCl which agree well with the sum of the ionic radii and fairly well with the $\mathring{a}_J$ obtained from the conductance equation. These results are in almost complete contrast with the behavior of these salts in dioxane–water mixtures. Numerous reasons are considered for the dependence of the association constant on the nature of the nonaqueous component of the solvent mixture. The lower association of KCl when compared to CsCl is attributed to the higher solvation energy of the potassium ion.

Introduction

The effects of the nature of the ions and of the solvent on the association constant for the formation of electrostatic ion pairs have been studied by a number of workers. Atkinson and co-workers[4] have investigated the effect of dielectric constant on the association of ions of higher charge. The effect of ionic shape has been demonstrated most aptly by Lind and Fuoss.[5] The list of investigations of the effect of dielectric constant on the association of electrolytes is too long to include here. Most of the work that has been published has dealt with the alkylammonium salts in solvents or solvent mixtures in the dielectric range below 30. We chose the alkali halides for this investigation owing to the large variations in size and solvation energy which were available. The use of ethanol–water mixtures permitted measurements to be made at any solvent composition including both pure components and permitted a comparison to be made with known data for KCl[6] and CsCl[7] in dioxane–water mixtures. In these aqueous mixtures the assumption is generally made that only water participates in solvation, and, consequently, at the same dielectric constant the degree of association of any salt should be independent of the organic component of the mixture.

Measurement of conductances in the ethanol-rich mixtures presented certain difficulties owing to the slow rate of solution of the alkali halides. For this reason, a cell was constructed in which there were no unstirred areas and in which the solution could be stirred vigor-

(1) Presented in part at the 139th National Meeting of the American Chemical Society, St. Louis, Mo., 1961.

(2) Adapted from a Ph.D. Thesis submitted to Brown University, 1962.

(3) Mellon Institute, Pittsburgh, Pa. All experimental work performed at Brown University.

(4) G. Atkinson and C. J. Hallada, *J. Am. Chem. Soc.*, **84**, 721 (1962).

(5) J. E. Lind, Jr., and R. M. Fuoss, *J. Phys. Chem.*, **66**, 1749 (1962).

(6) J. E. Lind, Jr., and R. M. Fuoss, *ibid.*, **65**, 999 (1961).

(7) J. Justice and R. M. Fuoss, *ibid.*, **67**, 1707 (1963).

ously while a measurement was being made. A guarded electrode best fitted these requirements since the electrodes could be placed in the center of the solution flask. The use of guarded electrodes was an interesting research in itself since they have not been used for precision conductance measurements. Since the salts took a matter of hours to dissolve at times, the cell was fitted with a cup-dropping device whereby the salt samples could be added one at a time without opening the cell and contaminating the contents with CO_2 and O_2. Considerable care was exercised in the measurement of all quantities involved, and a precision of 0.01% is claimed with considerable confidence.

Experimental

Conductance Cell. The conductance cell, shown in Figure 1, consisted of a 2-l. round flask into which the electrodes were inserted by ring seals placed slightly off center. The neck of the flask was fitted with a 34/45 standard taper joint onto which the dispensing device, to be described, was fitted. A detailed drawing of the electrode containing the guard ring is shown in Figure 2. The metal parts are shown in black, glass is cross-hatched, and insulators are clear. The center lead consists of 12-gauge copper wire and is well insulated from the surrounding 0.95-cm. brass tubing

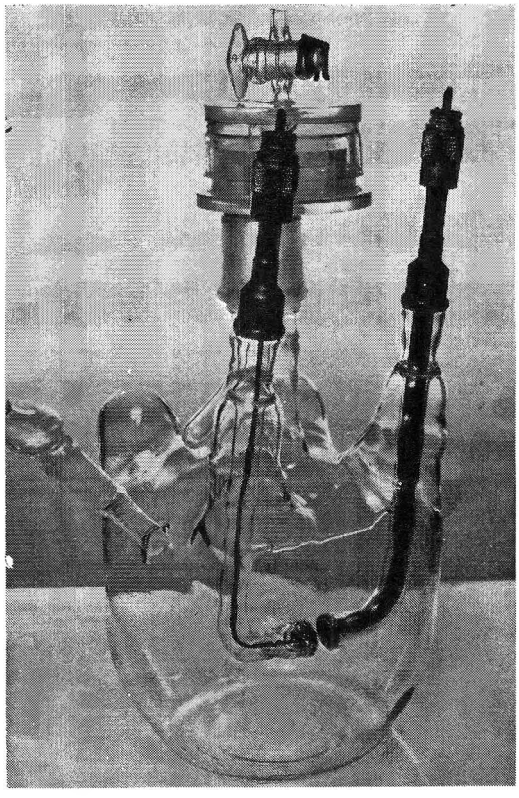

Figure 1. The conductance cell.

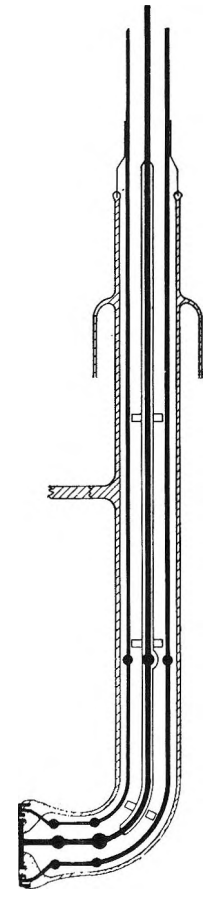

Figure 2. Details of the guarded electrode.

by polyethylene tubing and Teflon spacers. This brass tube is connected to copper braid at the bend which in turn is connected to the guard ring electrode by six 0.8-mm. platinum wires. Both the guard ring and the center electrodes are constructed of 0.15 mm. thick platinum and have diameters of 10 and 16 mm., respectively. The 1-mm. gap between these two electrodes is filled with 7070 glass, and both electrodes are backed with a thick layer of 7070 glass for mechanical strength. As shown in the drawing, the edges of the electrodes are turned back and sealed into 7070 glass, a Pyrex-type glass which wets platinum readily. This 7070 glass is connected to Pyrex glass a short distance from the electrode seal. At the top of the electrode assembly, above the ring seal, the brass tube is soldered to a Housekeeper seal and then to the outside of an Amphenol-type CPH cable connector, the central terminal of which is connected to the central copper cable from the center electrode. A second electrode assembly containing the high voltage electrode (diameter 16 mm.) was sealed into the flask so that a 10-mm. separation existed between the high and low voltage electrodes. It is of similar construction to the

guarded electrode shown in Figure 2 with two exceptions. There is no guard ring, and the central wire to the electrode is not electrically shielded. For rigidity the two electrode assemblies were joined by a 2-mm. glass rod after they had been sealed into the flask.

The primary purpose of a guarded electrode system is to surround the current lines to the center electrode by a fringe field that is carried to ground and therefore balanced by one arm of a Wagner ground. In a well-guarded electrode the current lines to the center electrode are parallel and completely independent of the environment. Complete guarding is obtained only as the width of the guard ring is made large compared to the separation between the two electrodes and compared to the gap width between the center electrode and guard ring.[8] Considering the electrode dimensions, it can be seen that both dimensional requirements are far from being met. The first ratio is 0.2, and the second is about 2. Technical problems in constructing this type of electrode did not permit a reduction in the gap width. Since electrolytic conductance is strongly dependent on the temperature, the total current passing through the cell must be kept small so that no significant heating occurs. Increasing the relative size of the guard ring reduces the current available at the measuring electrode and consequently reduces the sensitivity of the conductance measurement. For this reason the design of a guarded electrode system for the purpose of measuring conductance must compromise the effectiveness of the shielding in order to maintain a sufficient sensitivity. Although guarded electrodes have not been used for precise conductance measurements, they have been used extensively in the field of dielectrics where the conductivity and resultant heating of the sample is not, in general, large enough to be a problem.

Since the field arriving at the center electrode is contained by the guard field, it is not necessary to place the electrodes in a special chamber in order to obtain a cell constant independent of the solution level. In practice, by keeping the solution level slightly above the neck of the flask, it is easy to control the total volume of the solution to within 25 ml. The removal of 200 ml. of solution, which corresponds to a drop in the solution level of 1 cm., changed the measured resistance by only 0.01%. During a measurement the solution was continually stirred by a magnetic stirrer, but, in contrast to previous experience,[6] no detrimental effect of stirring could be detected. On the other hand, stirring added greatly to the precision of the measurements since it eliminated the effects of small temperature fluctuations and minimized the effect of electrode contamination.[9] During the course of the measurements one of the electrodes developed a small leak which would have made the standard type of cell useless. However, owing to the rapid stirring in the large chamber, it was possible to maintain conductivity water at a specific conductance below 10^{-7} ohm^{-1} cm.$^{-1}$ for several hours.

The frequency dependence of the resistance measurements was determined for aqueous solutions at frequencies ranging from 0.5 to 6 kHz. using unplatinized electrodes. At resistances below 20,000 ohms the measured resistances were found to be linear functions of the reciprocal of the frequency and to increase with decreasing frequency as is typical of electrode polarization. The extrapolated value at $1/f = 0$ was assumed to be the correct value. The effect was small even for unplatinized electrodes since the difference between the resistance at 5 kHz. and the extrapolated value amount to 0.01% at 1000 ohms and only 0.004% at 13,000 ohms. All conductances recorded here were carried out using lightly platinized electrodes which reduced the frequency dependence by a factor of 5 in aqueous and ethanol solutions. In the ethanol–water mixtures no detectable frequency dependence was observed over the frequency range 0.5 to 5 kHz.

The current through the guard ring electrode was found to be three times that carried by the center electrode although both electrode areas are of comparable size. The effect of electrode polarization at the guard electrode was found to be more than three times that occurring at the center electrode, indicating that the elimination of the sharp edges on the center electrode, and thereby points of high current density, can effectively reduce electrode polarization. Such points of high current density are also eliminated in the Shedlovsky-type pipet cell[10] and could account, in part, for the excellent results obtained with that type of cell. No Parker effect could be detected, indicating that the brass tube effectively shielded the lead to the center electrode from all capacitance–resistance bypaths.

At the very high resistances encountered in measuring solvents, a different frequency effect was observed. The resistance increased with increasing frequency which is opposite in direction to the Parker effect. At intermediate resistances (greater than 0.5 megohm) it was possible to get first a decrease due to polarization and then an increase in the resistance as the frequency increased. The same effect in erlenmeyer cells at much lower resistances has been reported by Nichol

(8) A. von Hippel, "Dielectric Materials and Applications," John Wiley and Sons, Inc., New York, N. Y., 1954, p. 48.

(9) J. E. Prue, *J. Phys. Chem.*, **67**, 1152 (1963).

(10) T. Shedlovsky, *J. Am. Chem. Soc.*, **54**, 1411 (1932).

and Fuoss.[11] This effect, we believe, results from a change in shape of the field depending upon the degree of polarization of the glass wall of the cell. This interpretation would indicate that the low frequency value, corrected for any electrode polarization, is the correct value. The effect is being studied further in a new cell which contains a more efficiently guarded electrode. All solvent resistances reported here were measured with the cell shunted by a 50K General Radio Type 510 resistor.

The cell constant for the cell was obtained by measuring the conductance of seven aqueous KCl solutions equally spaced over the concentration range 10^{-3} to 7×10^{-3} M. As a standard, the weighted average conductance function for KCl in aqueous solution at 25°, as given by Lind, Zwolenik, and Fuoss,[12] was used. The resulting cell constant was 0.6623 cm.$^{-1}$ with a standard deviation of 0.005% for each run at seven concentrations but with a maximum deviation of any given run from the average value of 0.04%. Thus, the precision in any one determination over a wide concentration range is entirely satisfactory, but the uncertainty in the absolute value of the cell constant is somewhat higher than one would expect for a rigidly placed set of electrodes. The fluctuations from one run to another appeared to be random over a period of 3 years. The most reasonable explanation of these fluctuations is mechanical deformation since a change in the electrode separation of only 0.01 mm. could account for the total variation. Considering the independent suspension of the electrodes, this much deformation is not at all surprising. This cell was designed for the determination of the concentration dependence of conductance, and small variations in the cell constant from one run to another will only affect the value of Λ_0.

Conductance Bridge. The standard Leeds and Northrup Dike–Jones conductance bridge was used for all resistance measurements, but, owing to the presence of the guarded electrode, two modifications were necessary. The sizable current to ground through the guard electrode required the addition of external resistors and capacitors to the opposite side of the Wagner ground. The requirement for balance using a guarded electrode is that the potential at both the center electrode and its guard electrode must be brought to ground potential. Normally, in the Dike–Jones bridge one electrode is not brought to ground potential but rather is above or below ground by the potential drop across the lead from the bridge to the cell, and an ordinary lead resistance correction can be made. In our guarded cell this correction creates a problem because three times as much current is carried by the guard electrode as is carried by the center electrode. Both electrodes could be brought to the same potential by a careful matching of lead resistances, but the problem was avoided by altering the bridge so that the potential lead from the detector was connected directly to the cell terminals. The cable connector at the cell terminal facilitated this change. Owing to these changes and the fact that the guard ring carries three times as much current as the center electrode, the resistance of the cell is given by $R = r + L_1 - 4L_2$, where r is the corrected resistances of the variable resistors of the bridge, L_1 is the resistance of the lead from these variable resistors to the center electrode of the guarded electrode, and L_2 is the resistance of the lead from the bridge to the high voltage electrode. Both L_1 and L_2 were measured directly.

The signal generator was a Hewlett-Packard Model 200 CD oscillator. Amplification of the off-balance signal was provided by a Rohde and Schwarz Type UBM tunable amplifier, the output of which was detected in the form of Lessajous figures on a Hewlett-Packard Model 120AR oscilloscope.

Salt-Dispensing Device. The solution of the alkali halides in aqueous solvent mixtures containing appreciable amounts of ethanol is an extremely slow process. For this reason, the first solvent mixtures used were equilibrated more or less with the atmosphere in order to keep the solvent conductance constant during a run ($\kappa_0 = 1.0$–1.5×10^{-6} ohm^{-1} cm.$^{-1}$). However, it was found that such solvents resulted in cell constants that were slightly concentration dependent whereas solvents of conductance 0.1×10^{-6} or less gave cell constants that were independent of concentration to 0.005%. It is difficult to correct a solvent conductance for changes in ionic strength, and consequently all measurements recorded here were carried out in a closed system with solvents of as low conductance as possible.

Salt samples were introduced into the solvent in the closed system by means of the dispensing device shown in Figure 3. It consists of a 55/50 standard taper joint sealed into the two Lucite plates E and D with epoxy resin. The joint is lubricated with Apiezon M permitting the top section to rotate relative to the bottom. Into the bottom plate D is sealed a 35/45 standard taper joint which is lubricated with Apiezon M and which fits onto the top of the conductance cell. Pin B is sealed into plate E and fits into a hole in disk C, which in turn is free to move around pin A. Disk C also contains the openings F into which eight salt cups

(11) J. C. Nichol and R. M. Fuoss, *J. Phys. Chem.*, 58, 696 (1954).

(12) J. E. Lind, Jr., J. J. Zwolenik, and R. M. Fuoss, *J. Am. Chem. Soc.*, 81, 1557 (1959).

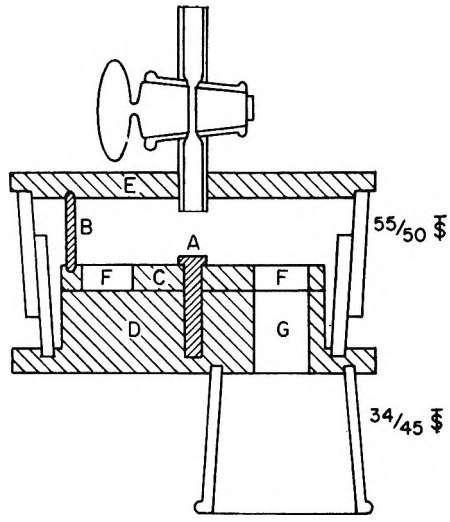

Figure 3. Salt cup dispensing device.

can be placed. By movement of the top plate E relative to D, cups containing salt can be brought in line with opening G and dropped in succession into the solvent. The stopcock at the top is used to flush the whole system with purified nitrogen after the solvent and salt cups are in place. When the dispensing device is not in use, a tube of Ascarite is placed in the 35/45 joint so as to avoid the buildup of CO_2 in the crevices.

The cups used to contain the salt samples were made of Pyrex glass and measured 12 mm. in height and 9 mm. in diameter. The cups were selected to weigh just over 1 g. Since the largest salt samples used weighed about $^1/_3$ g., it was not necessary to change the 1-g. weight in the Mettler microbalance. In blank runs it was demonstrated that the addition of eight cups to the solvent increased the solvent conductance by no more than 10^{-9} ohm^{-1} cm.$^{-1}$.

Procedure. Reagent grade *potassium chloride* was recrystallized twice from HCl-saturated conductivity water and once from an ethanol-water mixture. After a preliminary drying, the salt was ground to a fine powder and dried under vacuum for 6 hr. at 250°.

Cesium chloride was purified by the method of Jander and Busch[13] in which cesium and rubidium are precipitated from the potassium by silicomolybdic acid followed by a preferential precipitation of cesium chloride by antimony trichloride. Molybdenum trioxide was purified by sublimation in a stream of hydrogen chloride gas at about 150°. The sublimation product, molybdenyl chloride, was dissolved in dilute hydrochloric acid, and this solution was used to prepare the precipitating solution of silicomolybdic acid according to the procedure outlined by Jander and Busch. The cesium silicomolybdate was decomposed in a stream of warm hydrogen chloride gas, and after taking up the pure white residue in a small portion of dilute HCl, the silicic acid was filtered off. The cesium was precipitated by the addition of antimony trichloride dissolved in 5 *N* HCl. After decomposition of the cesium antimony chloride in a stream of HCl gas at 500°, the nonvolatile residue of cesium chloride was dissolved in a minimum amount of distilled water and precipitated by the addition of distilled acetone. The partially dried and finely ground salt was heated to 300° under high vacuum for 3 hr.

Conductivity water, of a specific conductance of 10^{-7} ohm^{-1} cm.$^{-1}$ or lower was prepared by passing distilled water through an Amberlite MB-1 mixed-bed, ion-exchange column. To avoid hydrolysis products from the resin, the first liter of water passed through the column was discarded if the column was not in continual use.

U.S.P. 95% *ethanol* was refluxed under nitrogen for 24 hr. with freshly ignited calcium oxide to reduce the water content to less than 0.5%. A middle cut was distilled into freshly prepared magnesium ethoxide and refluxed under purified nitrogen for 24 hr. The ethanol was finally distilled in a 65-cm. silvered, vacuum-jacketed Stedman column to give a 60% overall yield. The final product had a specific conductance that ranged between 1 and 2 $\times$ 10^{-8} ohm^{-1} cm.$^{-1}$ with a density of 0.78506 g./ml. This method of purification closely parallels that used by Graham, Kell, and Gordon,[14] and the conductance and density compare favorably with their values of 0.7 $\times$ 10^{-8} and 0.78504, respectively.

All solutions were made up by weight and corrected to vacuum using 1.98, 3.97, and 7.7 g./ml., respectively, for the densities of KCl, CsCl, and the Mettler weights. The salt samples were weighed in the Pyrex cups on a Mettler microbalance and the solutions on a kilogram equi-arm balance. All weights of both balances were calibrated in terms of the Mettler 10-g. weight. The molecular weights of potassium and cesium chloride were taken to be 74.557 and 168.367, respectively. Solution and solvent densities were determined by measuring the loss in weight of a 55-ml. glass ball suspended in the thermostated liquid on a 0.005-cm. tungsten wire. The densities, d, of the dilute solutions were assumed to follow the linear relationship $d = d_0 + A\bar{m}$ where d_0 is the density of the solvent mixture and $\bar{m}$ is the concentration in moles/kg. of solution. The constant A was obtained from

(13) G. Jander and F. Busch, *Z. anorg. Chem.*, **194**, 38 (1930).

(14) J. R. Graham, G. S. Kell, and A. R. Gordon, *J. Am. Chem. Soc.*, **79**, 2352 (1957).

density measurements on the most concentrated solution studied and was found to have the value 0.042 for all the KCl solutions and 0.12 for all the CsCl solutions with the exception of pure ethanol, in which case it was equal to 0.16. The temperature of the oil bath was controlled at 25 ± 0.001° by a mercury-in-glass thermoregulator, the actual temperature being determined by a repeatedly calibrated platinum resistance thermometer and a Mueller bridge.

The procedure followed in making a conductance run started with a cleaning of the conductance cell with fuming nitric acid followed by a thorough rinsing with conductivity water. A Teflon stirring bar was added and the dry weight obtained. The cell was then thoroughly purged with purified nitrogen after which the solvents were added in a closed system under nitrogen pressure. After weighing the cell and solvent the dispensing device, with the stopcock open and containing the weighted salt cups, was added to the cell and the whole system purged with purified nitrogen for 15 min. The stirring bar was rotated by a magnet situated in the bath below the cell and activated by an external motor through a flexible cable.

Results

The properties of the various solvent mixtures used are given in Table I. The weight per cent ethanol in the mixtures, w, was obtained from the measured solvent densities by interpolation of known density data.[15] Literature values[16] were used for the viscosity, η, in poise, and Åkerlöf's[17] values for the dielectric constants, ϵ, of the solvent mixtures. The specific conductances of the solvents, κ_0, in ohm^{-1} cm.$^{-1}$, are included in Table I and can be seen to be extremely small. In the worst case (lowest concentration, 38% ethanol–water) the solvent conductance correction amounted to only 0.3%.

Table I: Properties of Ethanol–Water Mixtures

w	d_0	ϵ	$10^2\eta$	$10^7\kappa_0$
38.37	0.93484	55.5	2.360	1.7
39.91	0.93170	55.1	2.375	0.8
60.25	0.88634	43.3	2.224	0.8
79.29	0.84084	33.1	1.762	0.6
87.92	0.81898	29.0	1.488	0.2
40.38	0.93073	54.9	2.379	0.7
60.13	0.88670	43.3	2.230	0.5
73.90	0.85405	35.7	1.919	0.4
84.33	0.82822	30.7	1.602	0.2
91.25	0.81013	27.5	1.382	0.2
93.24	0.80468	26.8	1.317	0.2
100	0.78506	24.3	1.084	0.2

The measured conductances are given in Table II for KCl and in Table III for CsCl. Here C is the molar concentration and Λ is the molar conductance in cm.^{2} ohm^{-1} mole^{-1}.

Table II: Conductance of KCl in Ethanol–Water Mixtures at 25°

10^4C	Λ	$\Delta\Lambda$	10^4C	Λ	$\Delta\Lambda$
38.37% ethanol			39.91% ethanol		
13.919	55.895	−0.001	11.465	54.889	−0.014
33.003	54.870	−0.007	26.392	54.010	+0.001
49.813	54.240	+0.002	42.677	53.325	+0.008
65.339	53.763	+0.007	57.379	52.826	+0.010
84.366	53.260	+0.002	73.941	52.345	+0.004
98.849	52.933	+0.004	90.101	51.942	+0.002
114.869	52.603	+0.001	105.059	51.609	−0.002
133.883	52.249	−0.007	123.484	51.241	−0.008
60.25% ethanol			79.29% ethanol		
12.619	44.421	+0.001	15.643	39.919	+0.007
22.922	43.577	+0.002	25.226	38.737	−0.006
34.755	42.828	−0.003	34.614	37.820	−0.008
48.560	42.125	−0.005	45.546	36.938	−0.002
58.271	41.711	+0.003	55.479	36.255	+0.003
70.644	41.235	+0.002	67.130	35.558	+0.009
82.477	40.832	+0.002	77.250	35.019	+0.005
105.032	40.164	+0.002	91.853	34.330	−0.008

87.92% ethanol		
10^4C	Λ	$\Delta\Lambda$
13.088	39.600	+0.007
20.203	38.315	−0.006
28.457	37.137	−0.007
37.421	36.093	−0.002
45.376	35.308	+0.004
54.811	34.501	+0.008
65.151	33.734	+0.005
74.543	33.115	−0.008

The data were analyzed by the Fuoss–Onsager conductance theory[18,19] in the form

$$\Lambda = \Lambda_0 - SC^{1/2} + EC \log C + JC \qquad (1)$$

in those cases where association was negligible (KCl in less than 60% ethanol) and in the form

$$\Lambda = \Lambda_0 - S(C\gamma)^{1/2} + EC\gamma \log C\gamma + JC\gamma - K_A C\gamma\Lambda f^2 \qquad (2)$$

(15) N. S. Osborne, E. C. McKelvey, and H. W. Bearce, *J. Wash. Acad. Sci.*, **2**, 95 (1912).

(16) "International Critical Tables," Vol. 5, McGraw-Hill Book Co., Inc., New York, N. Y., 1929, p. 22.

(17) G. Åkerlöf, *J. Am. Chem. Soc.*, **54**, 4125 (1932).

(18) R. M. Fuoss and L. Onsager, *J. Phys. Chem.*, **61**, 668 (1957).

(19) R. M. Fuoss and F. Accascina, "Electrolytic Conductance," Interscience Publishers, Inc., New York, N. Y., 1959.

Table III: Conductance of CsCl in Ethanol–Water Mixtures at 25°

10^4C	Λ	$\Delta\Lambda$	10^4C	Λ	$\Delta\Lambda$
40.38% ethanol			60.13% ethanol		
8.784	56.075	+0.002	8.202	45.712	+0.001
17.503	55.377	+0.002	15.678	44.867	−0.001
26.008	54.862	+0.002	25.113	44.057	−0.001
33.708	54.460	−0.006	34.370	43.408	−0.004
42.169	54.090	+0.004	41.382	42.989	+0.003
49.935	53.778	+0.002	50.040	42.522	+0.004
60.127	53.413	+0.002	59.605	42.057	−0.002
69.348	53.111	−0.003	69.035	41.652	−0.001
73.90% ethanol			84.33% ethanol		
8.490	42.023	+0.004	7.558	41.174	+0.006
18.286	40.529	−0.005	16.151	39.191	−0.010
27.023	39.536	−0.002	24.226	37.830	−0.004
35.098	38.774	+0.000	31.373	36.847	+0.001
43.445	38.094	+0.002	38.021	36.059	+0.004
51.767	37.498	+0.005	44.964	35.334	+0.005
60.923	36.912	+0.001	53.468	34.553	+0.003
69.934	36.394	−0.004	63.430	33.752	−0.006
91.25% ethanol			93.24% ethanol		
6.932	41.282	+0.008	7.087	41.200	+0.009
12.159	39.514	−0.008	13.403	38.968	−0.009
19.390	37.692	−0.009	19.427	37.380	−0.009
26.153	36.357	−0.002	25.822	36.027	−0.003
33.681	35.137	+0.006	32.663	34.833	+0.007
40.674	34.177	+0.009	40.293	33.709	+0.009
48.010	33.301	+0.004	48.656	32.665	+0.006
56.381	32.429	−0.009	58.249	31.642	−0.010
100% ethanol					
9.534	39.687	+0.000			
16.479	36.887	+0.001			
23.088	34.936	−0.002			
30.324	33.270	+0.001			
38.442	31.777	+0.000			

for associated electrolytes. Here all symbols have their usual significance.[19] Owing to the small ions involved here, the viscosity term $F\Lambda_0C$ was considered to be negligibly small. A Fortran computer program was used for all calculations. This program is identical in all essentials with that used for the IBM 650 computer which has been described in detail elsewhere.[20] In all solvent mixtures the upper concentration limit was well below the concentration at which $\kappa a = 0.2$. The measurements were of such high precision that no significant difference was obtained if Λ was weighted by C or unweighted.[20] All the results recorded here are for unweighted Λ. The results of the analysis are given in Table IV where the constants of eq. 1 and 2 are included along with the parameters and the literature data for KCl in pure water[20] and pure ethanol.[14,20] Included in the table are the standard deviations of the unknowns. It can be seen that these standard deviations are low enough that association constants as small as 3 could be detected with considerable precision. The mixtures containing less than 60% ethanol gave negative value for K_A for KCl when analyzed by eq. 2. Conversely, when the ethanol-rich mixtures were analyzed by eq. 1, exceedingly low values of $\mathring{a}_J$, the size parameter obtained from the coefficient J, were obtained as expected. The difference between the measured conductances and those calculated from the parameters and constants in Table IV are included in Tables II and III.

In order to be sure that small changes in the cell constant from run to run were not affecting the values of $\mathring{a}_J$ and K_A, 1% was added to each conductance and the data recalculated. This increase in Λ was found to change only Λ_0, the change in $\mathring{a}$ and K_A being only a fraction of the standard deviation in each case. The results are more sensitive to errors in the dielectric constant, but again the change in the parameters attributable to a 1% error on the dielectric constant was only slightly more than one standard deviation.

Discussion

The performance of the conductance cell with the guarded electrode was, in general, very satisfactory. The rapid stirring of the solution actually being measured greatly reduced the problems of temperature regulation and those resulting from contamination of the solution by impurities on the cell walls. In particular, the salt cup dispensing device, the use of which is not restricted to the cell described here, eliminated the problem of a changing solvent conductance during salt additions and permitted the measurements to be made on a completely closed system. This device would be particularly useful for measurements with toxic or extremely volatile solvents.

Good use could be found for the excellent frequency characteristics of guarded electrodes if they could be constructed with relative ease, with better guarding than was obtained here and with sufficient rigidity so as to ensure a constant geometry. It should be mentioned at this point that an ideal bridge for this cell would be the Cole–Gross type[21] modified for precision resistance[22] rather than capacitance measurements.

(20) R. L. Kay, *J. Am. Chem. Soc.*, 82, 2099 (1960). A copy of this program and of the Fortran card deck can be obtained by contacting one of the authors (R. L. K.). One change has been made in that, besides C and Λ, the program will accept the weight of salt, the solution resistances, and the other data required for the computation of C and Λ.

(21) R. H. Cole and P. M. Gross, *Rev. Sci. Instr.*, 20, 252 (1949).

(22) J. G. Janz and G. D. E. McIntyre, *J. Electrochem. Soc.*, 108, 272 (1961).

Table IV: Conductance Parameters and Constants

w	Λ_0	$\mathring{a}_J$	K_A	S	E	J
			KCl			
0.0[a]	149.94[a]	3.11[a]	...	95	59	200
38.37	57.822 ± 0.004	2.71 ± 0.01	...	49.5	70.9	144.7
39.91	56.645 ± 0.006	2.64 ± 0.02	...	49.2	70.9	140.9
60.25	46.768 ± 0.006	2.99 ± 0.06	3.0 ± 0.2	58.8	120.2	250.5
79.29	44.05 ± 0.02	3.03 ± 0.08	11.6 ± 0.7	84.0	252.4	505.3
87.92	44.59 ± 0.02	3.25 ± 0.06	23.5 ± 0.9	105.1	377.4	789.0
100.0	45.42 ± 0.02[b]	4.6 ± 0.2[b]	95 ± 3[b]	150	634	1700
			CsCl			
40.38	57.690 ± 0.007	3.9 ± 0.3	3.0 ± 0.4	49.71	73.46	209.9
60.13	47.725 ± 0.005	3.8 ± 0.1	8.4 ± 0.3	59.25	123.41	316.0
73.90	44.849 ± 0.008	3.53 ± 0.07	18.0 ± 0.4	75.18	206.05	469.5
84.33	44.90 ± 0.01	3.58 ± 0.07	38.5 ± 0.7	95.89	322.28	726.1
91.25	45.99 ± 0.02	3.72 ± 0.08	68 ± 1	116.75	457.86	1045.5
93.24	46.39 ± 0.02	3.76 ± 0.08	80 ± 1	123.36	497.36	1144.0
100.0	48.33 ± 0.01	4.20 ± 0.03	158.1 ± 0.6	153.70	685.53	1704.0

[a] See ref. 20. [b] See ref. 14 and 20.

The closely coupled transformer arms of this bridge automatically reflect any current to ground equally across both arms of the bridge, thereby eliminating any need for a Wagner ground. Consequently, only one point must be brought to ground potential for complete balance of the bridge. It has been demonstrated that the bridge is capable of measurements of the highest precision using commercial components.[22]

An inspection of Tables II and III shows that the Fuoss–Onsager theory as expressed in eq. 1 and 2 is capable of fitting the conductance data with considerable precision. $\Delta\Lambda$ is less than 0.03% in all cases, and the standard deviation of the individual points in the worst case was found to be 0.01 conductance unit, indicating an excellent fit. However, we estimate the precision of our measurements to be 0.01%, indicating that $\Delta\Lambda$ is somewhat higher than is to be expected from random errors. A careful inspection of Tables II and III does show that, although the $\Delta\Lambda$-values are small, the deviations follow the same pattern in each set of results.

Both KCl and CsCl show considerable association in these solvent mixtures. At present, the criteria generally accepted as good evidence that an electrolyte is associated in any solvent are that analysis by eq. 1 gives low values of $\mathring{a}_J$ and poor precision, whereas an analysis by eq. 2 gives higher values of $\mathring{a}_J$, positive values of K_A of greater magnitude than the standard deviation, and a considerably better fit of the data. This latter point is necessary since it is generally easier to fit the data with three parameters than with two. When the data for the two salts, with the exception of those for KCl in the two water-rich mixtures, were analyzed by eq. 1, the fit was poor, the standard deviation of the individual points was as much as 10 times greater than that obtained with eq. 2, and $\mathring{a}_J$ was significantly smaller than that obtained from eq. 2. The association constants of 3.0 found in two systems as shown in Table IV should be accepted with some reservation since this amount of association results from a decrease in Λ of only 0.5 unit at 5×10^{-3} M, and small errors in the theory could account for deviations of this magnitude. Although the low $\mathring{a}_J$ values for KCl in the two water-rich mixtures could be an indication of a significant amount of association, neither the theory nor the model on which it is based is in the state of refinement required for a calculation of such extremely small association constants.

In Figure 4, log K_A values for KCl and CsCl in ethanol–water mixtures are plotted as a function of the reciprocal dielectric constant with the size of all the circles in the plot indicating the magnitude of the standard deviation. A very good straight line is obtained for CsCl over the whole range of mixtures studied including the point for pure ethanol. These results are compared in Figure 4 with those of Pedersen and Amis[23] after their association constants had been recomputed on the basis of the Fuoss–Onsager equation (2). Negative values were obtained in the case of the 58 and 43% ethanol mixtures, but for 80 and 100% ethanol the K_A obtained agree well with our values as

(23) L. G. Pedersen and E. S. Amis, *Z. physik. Chem.* (Frankfurt), **36**, 199 (1963).

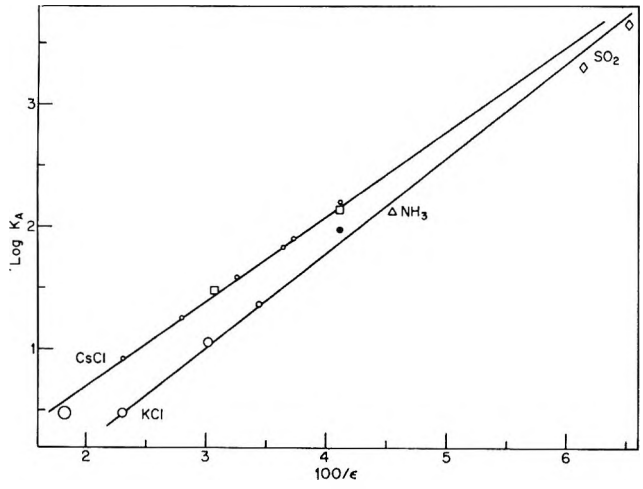

Figure 4. Dependence of log association constant for KCl and CsCl on the reciprocal dielectric constant: open circles, this research; closed circles, KCl in anhydrous ethanol (ref. 14); squares, CsCl in ethanol–water (ref. 23).

is shown in Figure 4. Their values of Λ_0 for CsCl in the 80, 58, and 43% ethanol mixtures agree well with our own as can be demonstrated on a large-scale plot, but their value of 47.2 ± 0.1 for CsCl in pure ethanol is in poor agreement with our value of 48.33 ± 0.01.

Although the data for KCl in ethanol–water mixtures are not as extensive, it is clearly shown in Figure 4 that log K_A is linear in the reciprocal dielectric constant, with K_A for KCl in pure ethanol[14,20] somewhat high. It is of interest to note on this plot that the association constants for KCl in liquid ammonia[20,24] (measured at −34° but corrected to 25°) and in liquid SO_2[25] (measured at 0.12 and −8.93° but corrected to 25°) fall very close to the same straight line.

The linearity of the plots in Figure 4 suggests that the association constants conform to the simple coulombic expression

$$K_A = K_A^0 \exp(e^2/\mathring{a}_K \epsilon k T) \qquad (3)$$

The lines in Figure 4 were drawn with $\mathring{a}_K$ set equal to the sum of the crystallographic radii, that is, with $\mathring{a}_K$ equal to 3.14 and 3.50 for KCl and CsCl, respectively. By changing $\mathring{a}_K$ to 3.2 it would be possible to put the points for liquid SO_2 on the line. However, we prefer the lines as drawn since the fit is quite satisfactory considering the assumptions involved, and this might be considered a good example of ideal behavior as far as the change of K_A with ϵ is concerned. It would be entirely premature at this time to propose that KCl and CsCl form contact ion pairs in these mixtures owing to the fact $\mathring{a}_K$ and the sum of the crystallographic radii agree.

It should also be pointed out that the values of a_J for the ethanol–water mixtures obtained from eq. 2 and reported in Table IV agree fairly well with the corresponding values of $\mathring{a}_K$. This observation has been made before by Fuoss in the case of tetrabutylammonium bromide in three different solvent mixtures.[26] a_J for KCl in the two water-rich mixtures are definitely low due to association. It can be seen that the agreement between a_J and a_K is poor for pure ethanol, liquid NH_3, and liquid SO_2, and it is impossible to manipulate the data to obtain coincidence. It was hoped that equating a_J and a_K would be possible in most systems since the predictive possibilities would be most useful, but, as we shall see, it is the exception instead of the general rule. An example can be given here. If the lines in Figure 4 are extrapolated, association constants of 1.1, 0.4, and 1.5 are obtained for KCl in 38% ethanol–water, KCl in pure water, and CsCl in pure water, respectively. If the data are analyzed with these values of K_A in eq. 2, $\mathring{a}_J$ values of 3.9, 4.1, and 5.2 are obtained, respectively. It can be seen in Table IV that these values are substantially higher than both a_K and a_J obtained for the ethanol-rich mixtures. Association constants for salts in solvents of relatively high dielectric constant, obtained by extrapolation of log K_A plots, must be considered to be of questionable value.

Figure 4 clearly illustrates the fact that CsCl, in spite of its greater size, is more associated than KCl in ethanol–water mixtures. This is in agreement with the order found by Kay[20] for the alkali halides in various hydrogen-bonded solvents; namely, association increases Li < Na < K < Rb < Cs. Fuoss and co-workers[27] have found the same order for many of the alkali halides in dioxane–water mixtures, and Parfitt and Smith[28] have reported KNO_3 more associated than $LiNO_3$ in ethanol.

The pre-exponential factor K_A^0 of eq. 3 was found to be 0.049 for KCl and 0.204 for CsCl. K_A^0 contains

(24) V. F. Hnizda and C. A. Kraus, *J. Am. Chem. Soc.*, 71, 1565 (1949).

(25) N. N. Lichtin and H. P. Leftin, *J. Phys. Chem.*, 60, 160 (1956). These authors used the earlier Fuoss–Shedlovsky procedure to obtain association constants of 13.5 × 10^3 and 9.2 × 10^3 at 0.12 and −8.93°, respectively. When analyzed by the Fuoss–Onsager equation (2), the data at the higher temperature gave a negative a_J and a poor fit, but the data at the lower temperature gave a fair fit and a K_A = (9.4 ± 0.3) × 10^3, a good check on the results of the Fuoss–Shedlovsky analysis. This should be the case since at this low dielectric constant (ϵ 16) the concentration of free ions is small, and any theory should predict their conductance accurately enough. Consequently, the points in Figure 4 correspond to the K_A computed by the Fuoss–Shedlovsky treatment corrected to 25°.

(26) R. M. Fuoss, *Proc. Natl. Acad. Sci.*, 45, 807 (1959).

(27) T. L. Fabry and R. M. Fuoss, *J. Phys. Chem.*, 68, 971 (1964).

(28) G. D. Parfitt and A. L. Smith, *Trans. Faraday Soc.*, 59, 257 1963).

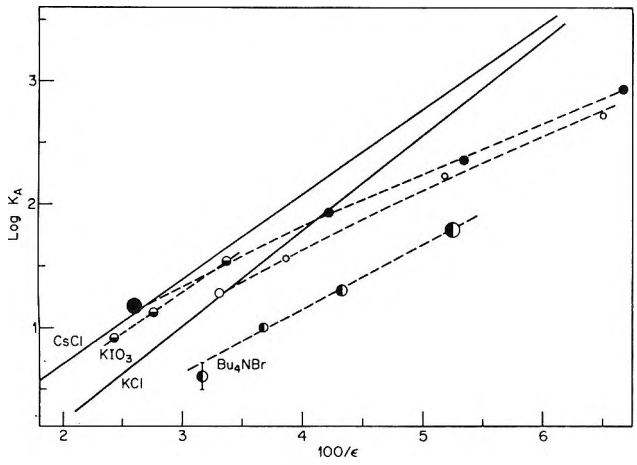

Figure 5. A comparison of association constants for various salts in ethanol–water mixtures (solid lines) and dioxane–water mixtures (dashed lines): ○, KCl (ref. 6); ●, CsCl (ref. 7); ◒, KIO_3 (ref. 33); ◐, tetrabutylammonium bromide (ref. 31).

the contribution to association for all factors except the long-range coulombic interaction, and in particular it is determined to a large extent by the difference in the solvent interaction with the free ions and with the ion pairs. It is the large solvation energy of potassium as compared to that for cesium ion which accounts for the lower K_A^0 and lower association of KCl. The Denison and Ramsey[29] equation obviously does not hold for these systems since that theory sets K_A^0 equal to unity. The Fuoss[30] evaluation predicts K_A^0 to be proportional to $\mathring{a}_K^3$ and neglects all differences in solvation energy of the free ions and ion pairs: $K_A^0 = 4\pi N_0 \mathring{a}_K^3/3000$ predicts a K_A^0 for KCl of 0.079 and for CsCl of 0.108. Thus, the prediction is too high for KCl and too low for CsCl by 50 and 100%, respectively. The assumption as to no solvation energy would tend to make these predictions too high and could therefore explain the result for KCl but not for CsCl.

In Figure 5 our association constants for the ethanol–water mixtures as represented by the solid lines are compared with those obtained by Fuoss and coworkers[6,7] for dioxane–water mixtures as given by the dashed lines through the open and closed circles. As can be seen, the arrangement is poor, the K_A values for KCl and CsCl in dioxane–water mixtures are lower than our results for the same salts in ethanol–water mixtures, and only appear to converge with our results as the percentage of water becomes large. The best straight line through the dioxane–water data gives the considerably higher $\mathring{a}_K$ values of 5.2 and 5.9 for KCl and CsCl, respectively. Also, $\mathring{a}_J$ was found to increase to unreasonably high values as the percentage of dioxane increased.

Some additional data are available for salts in dioxane–water mixtures, but, with one exception, they do not cover the dielectric constant range studied here or involve salts that are so slightly associated that precise association constants could not be obtained directly from the conductance data without further assumptions. The one exception is the data of Mercier and Kraus[31] for tetrabutylammonium bromide (Bu_4NBr) that have been recalculated[32] on the basis of eq. 2 and are included in Figure 5. The points lie on a good straight line with approximately the same slope as that obtained for CsCl and KCl. However, this slope is reasonable for a salt with such a large cation since $\mathring{a}_K$ is found to be 5.1. The results for KIO_3 in dioxane–water recalculated from the data of Boch[33] are included in Figure 5 to establish the fact that KIO_3 is more associated than KCl in dioxane–water mixtures. A value of 3.8 was obtained for $\mathring{a}_K$. In general, oxy anions have been found to be more associated[20,34] than can be explained by their relatively large size.

Attempts have been made to explain low association constants by appealing to specific solvent affects. Ramsey[35] has attributed low association constants for quaternary ammonium salts in ethylene chloride and 1,2-dichloropropane to the fact that the influence of the electrostatic field of the ions can produce more *gauche* (polar) form in the solvent than is present in the pure liquid. The increased dielectric constant would then account for the smaller association constants. Hyne[36] applied the same reasoning to dioxane–water mixtures by assuming that the electrostatic charge of anions could increase the amount of the boat-form dioxane and thereby increase the dielectric constant. However, in order to bring the association constants for CsCl and KCl in dioxane–water mixtures into coincidence with those for ethanol–water mixtures, it would be necessary to increase the dielectric constants by over 25% for the mixtures of lower dielectric constant. An increase in the dielectric constant of this

(29) J. T. Denison and J. B. Ramsey, *J. Am. Chem. Soc.*, **77**, 2615 (1955).

(30) R. M. Fuoss, *ibid.*, **80**, 5059 (1958).

(31) P. L. Mercier and C. A. Kraus, *Proc. Natl. Acad. Sci. U. S.*, **41**, 1033 (1955).

(32) The results obtained from our computer program differ only slightly from those obtained by a graphical method as quoted in ref. 19, p. 237.

(33) E. Boch, *Can. J. Chem.*, **37**, 1888 (1959).

(34) R. L. Kay in "Electrolytes," B. Pesce, Ed., Pergamon Press Inc., New York, N. Y. 1962, p. 119.

(35) H. K. Bodenseh and J. B. Ramsey, *J. Phys. Chem.*, **67**, 140 (1963).

(36) J. B. Hyne, *J. Am. Chem. Soc.*, **85**, 304 (1963).

magnitude seems unlikely particularly when the fact is taken into account that the dielectric constant of these mixtures is determined to a considerable extent by the amount of hydrogen bonding present, and the presence of ions should tend to reduce the amount of hydrogen bonding. Furthermore, there is direct evidence from high-resolution chemical-shift measurements[37] that the state of dioxane is unchanged by the addition of electrolytes.

At this point the association constants themselves should be questioned in that they could be artifacts resulting from the theory used to obtain eq. 1 and 2. If this is the case, the errors introduced must be different in the case of ethanol–water mixtures than in the case of dioxane–water mixtures. One way this could come about has been demonstrated by Kay and Dye,[38] who showed that the electrophoretic contribution to conductance can be obtained independent of the relaxation effect from the concentration dependence of transference numbers. Their calculations show that the Fuoss–Onsager equation evaluates the electrophoretic effect correctly for water and methanol solutions but not for ethanol solutions. They were able to show that the assigned association constants of 27 and 44 for LiCl and NaCl, respectively, in anhydrous ethanol were the result of an incorrect evaluation of the electrophoretic effect. Using the electrophoretic term evaluated from transference numbers and the Fuoss–Onsager[18] relaxation terms, they were able to fit the conductance data for these salts without invoking any assumption as to association. This method cannot be applied to KCl and CsCl directly owing to the lack of sufficient concentration dependence for the transference numbers, but it is reasonable to assume that the association constants reported here for these salts in pure ethanol are too high. Values between 50 and 70 for KCl and between 110 and 130 for CsCl would be more reasonable. If this corrected K_A for KCl in anhydrous ethanol is used in Figure 4 the points for ethanol, liquid NH_3, and liquid SO_2 lie on a very good straight line with the same slope but somewhat different intercept than the present line. However, the correction is not of sufficient magnitude to bring the ethanol–water data into coincidence with dioxane–water data. Furthermore, this electrophoretic effect correction would also apply to dioxane–water mixtures although it will be much lower in magnitude owing to their higher viscosity when compared with ethanol–water mixtures. At dielectric constants below 20, the degree of association is so large that small errors in the theory should have little effect.

Atkinson[4] has found the same effect for higher valence electrolytes as is reported here for the alkali halides. Both manganese sulfate and manganese *m*-benzenedisulfonate are more associated in methanol–water mixtures than in dioxane–water mixtures at the same dielectric constant. Atkinson and Kor[39] have explained this dependence on the specific organic component of the mixture by means of ultrasonic absorption measurements. Three absorption maxima were observed for these salts in each solvent mixture, and they invoked a three-step equilibrium[40] for the ion pair association process. In this mechanism an unspecified but decreasing number of solvent molecules separate the ions in each equilibrium step, so that the last state is a contact ion pair. The ratio of the over-all association constant for any salt in two solvent mixtures (here methanol–water and dioxane–water) at the same dielectric constant can be shown to be given by

$$\frac{K_A^M}{K_A^D} = \frac{1 + K_2^M + K_2^M K_3^M}{1 + K_2^D + K_2^D K_3^D}$$

where the superscripts identify the organic component of the solvent mixture, and the numbered subscripts indicate the equilibrium step. The first step can be considered to involve the approach of two completely solvated ions whereas the third step involves the formation of a contact ion pair. From the shift of the ultrasonic absorption maxima with concentration, it is possible to evaluate K_2 and K_3 for both solvent mixtures. Atkinson and Kor show that, although $K_2^M < K_2^D$ for $MnSO_4$, the over-all equilibrium constant ratio is determined by the fact that $K_3^M >> K_3^D$. Thus, it would appear that the $MnSO_4$ ion pair prefers to be separated by at least one solvent molecule to a greater extent in dioxane–water mixtures than when in a methanol–water mixture of the same dielectric constant.

We believe that the low K_A values for KCl in dioxane–water can be explained in the same way by an appeal to a multistep mechanism for association. However, measurements of a more specific nature than conductance are required for the detection of the individual states. If the sensitivity can be increased, it could be

(37) A. Fratiello and D. C. Douglas, *J. Chem. Phys.*, **39**, 2017 (1963).

(38) R. L. Kay and J. L. Dye, *Proc. Natl. Acad. Sci. U. S.*, **49**, 5 (1963).

(39) G. Atkinson and S. K. Kor, *J. Phys. Chem.*, **69**, 128 (1965).

(40) M. Eigen and K. Tamm, *Z. Elektrochem.*, **66**, 93, 107 (1962).

(41) B. P. Fabricand, S. S. Goldberg, R. Leifer, and S. G. Ungar, *Mol. Phys.*, **7**, 425 (1964).

(42) H. G. Hertz and M. D. Zeidler, *Ber. Bunsenges. physik. Chem.*, **67**, 774 (1963).

done by ultrasonic absorption measurements. Possibly spin-lattice relaxation[41,42] measurements could detect the specific solvent effects.

Acknowledgment. This work was supported by the U. S. Atomic Energy Commission under Contract AT(30-1)-2727 and by a grant from the Research Corp.

Hydrophobic Bonding and Micelle Stability[1]

by Douglas C. Poland and Harold A. Scheraga

Department of Chemistry, Cornell University, Ithaca, New York *(Received February 26, 1965)*

The problem of micelle stability is that of explaining why the free energy per molecule has an extremum at some large degree of aggregation (*i.e.*, forming micelles) instead of at low degrees of aggregation (dimer, trimer, etc.). Three components of the free energy for a solution of similar, spherical, nonionic micelles are considered, *viz.*, external, internal, and solvent contributions. The external contribution to the free energy arises from the translational and rotational motion of the micelle. The internal contribution to the free energy arises from the freedom of motion of the hydrocarbon tails within the micelle; two alternative treatments of this contribution, a free-volume one and a lattice one, are presented. The solvent contribution to the free energy is taken from the recent theory of hydrophobic bonding developed by Némethy and Scheraga.[2] In order to obtain a stable micelle it is necessary not only that the free energy per molecule be a minimum at some large degree of aggregation but also that the free energy at the minimum be smaller than that of the monomer. These conditions on the free energy function yield implicit expressions for the variation of the most probable micelle size with temperature and concentration. It is argued that the internal contribution to the free energy is essential in order to obtain an extremum in the free energy function, *i.e.*, in order to account for micelle stability; if this contribution is not introduced, then dimers, trimers, etc., would be the preferred species. Comparison of the theory with experimental data from the literature provides confirmation of predictions of the theory of hydrophobic bonding[2] and of the predicted dependence of the free energy contributions on micelle size. For example, the dependence of micelle size on concentration and temperature is accounted for; in particular, a predicted linear dependence of the cube root of the micelle size on the reciprocal of the absolute temperature, for long chains, is verified.

Introduction

Molecules having an aliphatic hydrocarbon tail with about seven or more carbon atoms and either a polar or ionic head differ from ordinary solutes in that they form large stable aggregates (of the order of many tens of molecules) rather than dimers, trimers, etc., as the solute concentration is increased in the range of solubility. Since a quantitative treatment of the interaction of hydrocarbon portions of molecules in water (hydrophobic bonding) has recently been developed[2]

(1) This work was supported by a research grant (HE-01662) from the National Heart Institute of the National Institutes of Health, U. S. Public Health Service, and by a research grant (GB-2238) from the National Science Foundation.

(2) G. Némethy and H. A. Scheraga, *J. Phys. Chem.*, **66**, 1773 (1962); **67**, 2888 (1963).

and since an understanding of these interactions is essential in accounting for the stability of micelles, it appeared worthwhile to consider the micelle problem in light of this new information.

It will be shown here that three factors must be taken into consideration in order to account for the existence of large stable micelles. These are (1) the loss of translational and rotational entropy of the aggregate relative to the monomer, (2) solvent effects, in that they play a role in hydrophobic bonding between the nonpolar parts of the monomer molecules within the micelle, and (3) the freedom possessed by the nonpolar parts of the monomer molecules within the micelle. We will consider micelles formed from monomer molecules having uncharged polar heads; it is assumed that the polar head serves only to solubilize the monomers and the micelle in water and does not contribute to the free energy of the micelle.

Statistical Mechanical Formulation

The Model. We will consider a system in which only one species is present in solution. Thus, if N monomer units are added to the solution, *all* of them will be considered to be in the form of spherical aggregates of s molecules each (an s-type micelle). In a *very schematic* way, we are envisaging a micelle as represented in Figure 1, with polar heads on the surface and the nonpolar portions in the interior partially coiled up (with some freedom of internal motion) and interacting with each other by means of hydrophobic bonds. The free energy of formation of these bonds will be taken from the theory developed by Némethy and Scheraga.[2] We seek the most probable value of s.

If the partition function for a single s-type micelle is $Q(s)$, then the partition function for the solution, according to the above model, is

$$Z = \frac{Q(s)^{N/s}}{\left(\frac{N}{s}\right)!} \tag{1}$$

where s can be any value from 1 on up. Of course, there will actually be a distribution of micelle sizes, and eq. 1 should really be replaced by a product of partition functions for all-size micelles, summing over all possible ways to distribute N monomers among the different size micelles. However, we use eq. 1, rather than a more rigorous expression, in order to simplify the mathematics; we justify this approximation by stating that we are interested in the first-order effects which will lead to a minimum in the free energy of the system at a given (large) value of s and will pay no attention to the second-order effects which will lead to an approximately Gaussian distribution of micelle sizes around the most probable value of s.

The free energy of the solution is obtained directly from eq. 1 as

$$F(N,s) = -kT \ln Z \tag{2}$$

Using Stirling's approximation this becomes

$$\frac{-F(N,s)}{NkT} = \frac{1}{s} \ln \frac{seQ(s)}{N} \tag{3}$$

which is the most convenient form for the calculation of the negative of the free energy per mole of solute, divided by RT. The problem of accounting for micelle stability is that of demonstrating how this free energy function can have a maximum value at some large value of s.

The Form of $Q(s)$. We will assume that $Q(s)$ can be written as the product of three partition functions representing contributions from the external energy levels of the micelle itself, from the interaction of the micelle with the solvent, and from the internal energy levels of the micelle, respectively.

$$Q(s) = Q(s)_{\text{external}} Q(s)_{\text{solvent}} Q(s)_{\text{internal}} \tag{4}$$

Then eq. 3 can be written

$$\frac{-F(N,s)}{NkT} = \frac{1}{s} \ln \frac{seQ(s)_{\text{ext}}}{N} + \frac{1}{s} \ln Q(s)_{\text{solv}} + \frac{1}{s} \ln Q(s)_{\text{int}} \tag{5}$$

The External Partition Function. $Q(s)_{\text{ext}}$ will be taken as the product of the classical partition functions for the translation and rotation of the micelle as a whole.

$$Q(s)_{\text{ext}} = Q(s)_{\text{trans}} Q(s)_{\text{rot}} \tag{6}$$

with

$$Q(s)_{\text{trans}} = \left(\frac{2\pi s m_0 kT}{h^2}\right)^{3/2} V_f = \frac{s^{3/2} V_f}{\Lambda^3} \tag{7}$$

and

$$Q(s)_{\text{rot}} = \frac{\pi^{1/2}}{\sigma} \left(\frac{8\pi^2 IkT}{h^2}\right)^{3/2} \tag{8}$$

where m_0 is the mass of a monomer unit, V_f is the free volume, Λ is $(2\pi m_0 kT/h^2)^{-1/2}$, σ is the symmetry number, and I is the moment of inertia (assuming $I \sim I_x \sim I_y \sim I_z$). A more complete discussion of the use of the classical gas phase partition functions for molecules in solution has been given by Steinberg and Scheraga[3-5]; as shown previously,[3] the use of a gas

phase partition function is valid since the solvent effects are taken into account in $Q(s)_{solv}$.

The moment of inertia of a sphere (*i.e.*, the micelle) is

$$I = \frac{2}{5}MR^2 \tag{9}$$

with

$$M = sm_0 \tag{10}$$

and

$$R = \left(\frac{3v_0}{4\pi}\right)^{1/3} s^{1/3} \tag{11}$$

where v_0 is the volume of a monomer, giving

$$I = \left(\frac{2}{5}\right)\left(\frac{3}{4\pi}\right)^{2/3} (v_0)^{2/3} m_0 s^{5/3} \tag{12}$$

Assuming $\sigma = 1$ (see ref. 3 for discussion of this), we have

$$Q(s)_{ext} = \left[\frac{3\pi^4(32/5)^{3/2} v_0 m_0^3 (kT)^3}{4h^6}\right] V_f s^4 \tag{13}$$

We will assume that v_0 and m_0 are both linear in n, where n is the number of CH_2 groups in the aliphatic chain. Taking the volume of a CH_2 group as 21 Å.^{3} from Courteauld's space-filling models and the mass as 14, this linearity may be expressed as

$$v_0 = 21n \tag{14}$$

and

$$m_0 = 14n \tag{15}$$

in appropriate units. Thus

$$\frac{1}{s} \ln \frac{seQ(s)_{ext}}{N} = \frac{1}{s}(a + b \ln s) \tag{16}$$

where

$$a = 4 \ln n + 3 \ln T - \ln (\text{concentration}) + \ln f_x + 0.062 \tag{17}$$

and

$$b = 5 \tag{18}$$

The concentration is the ratio of N/V, expressed in moles of monomer per liter, where it has been assumed that

$$V_f = f_x V \tag{19}$$

with f_x being a small fraction,[5] of the order of 10^{-2}. It should be noted that eq. 17 is the only part of the theory in which the concentration will appear in the partition function.

If eq. 16 were the only contribution to the free energy in eq. 5, then, of course, the monomer would be the most probable species; *i.e.*, $s = 1$ is the most probable value since the negative free energy of the system decreases as s increases (eq. 16). Thus, in order to account for stable micelles, we must include also the other terms of eq. 5.

The Solvent Interaction Partition Function. Before writing an expression for $Q(s)_{solv}$, let us consider the effect on the micelle–solvent interaction of inserting polar heads on the micelle surface. (See Figure 1.)

Since portions of some of the hydrocarbon tails are exposed to the solvent near the micelle surface, only a fraction $\theta(s)_{H\Phi}$ of the total hydrocarbon surface is involved in hydrophobic bonding. We assume that $\theta(s)_{H\Phi}$ is given by

$$\theta(s)_{H\Phi} = \frac{\left(\begin{matrix}\text{total hydrocarbon}\\ \text{surface}\end{matrix}\right) - \left(\begin{matrix}\text{exposed hydrocarbon}\\ \text{surface}\end{matrix}\right)}{(\text{total hydrocarbon surface})} \tag{20}$$

Now

$$(\text{total hydrocarbon surface}) = sa_t \tag{21}$$

where a_t is the surface area of the hydrocarbon tail of a monomer. For a spherical micelle

$$(\text{exposed hydrocarbon surface}) = 4\pi R^2 - s(a_h)h \tag{22}$$

where a_h is the area of the polar head, and $(a_h)h$ is the effective area covered by a polar head on the surface of a micelle. Thus, h is a measure of how much of the neighboring water structure is disrupted by a polar head; h would be expected to be a small number close to unity. The radius of the micelle, R, is given by eq. 11. Hence

$$\theta(s)_{H\Phi} = 1 - \frac{4\pi\left(\frac{3v_0}{4\pi}\right)^{2/3}}{s^{1/3}a_t} + \left(\frac{a_h}{a_t}\right)h \tag{23}$$

(3) I. Z. Steinberg and H. A. Scheraga, *J. Biol. Chem.*, **238**, 172 (1963).

(4) This footnote calls attention to an error in the treatment in ref. 3. While it is correct to integrate over solute coordinates separately from solvent coordinates since the average solute–solvent interaction is the same regardless of solute configuration, not all the volume is available since solvent is present. Thus, over most of the volume $U_{ik}(MN) = \infty$, or the Boltzmann factor is zero, and one cannot count that element of volume. Thus, in eq. 7 of ref. 3, the total volume V should be replaced by a free volume, V_f, where[5] $V_f \sim (10^{-2}$ to $10^{-3})V$. This introduces an entropy loss of $R \ln (10^{-2}$ to $10^{-3}) = -9.2$ to -13.8 e.u., which does not invalidate the authors' conclusions.

(5) A. Bondi, *J. Phys. Chem.*, **58**, 929 (1954).

Since eq. 23 was derived for an aggregate of monomers, it should be applied only for large values of s.

Reich[6] has offered the hypothesis that the size of the most stable micelle is that for which the micelle surface is completely covered by polar heads (so that the nonpolar tails realize a complete degree of hydrophobic bonding). Let us examine this hypothesis. According to Reich, the most probable micelle size would occur when $\theta(s)_{H\Phi} = 1$ or, according to eq. 23, when

$$s^{1/3}_{\text{max coverage}} = \frac{4\pi\left(\frac{3v_0}{4\pi}\right)^{2/3}}{(a_h)h} \tag{24}$$

For a tail of 16 carbon atoms and a head about the size of a carboxyl group

$$s^{1/3}_{\text{max coverage}} \simeq \frac{16.2}{h} \tag{25}$$

If $h = 1$, *i.e.*, if the polar head does not disturb the water structure around the neighboring CH_2 groups on the surface, then $\theta(s)_{H\Phi}$ will equal unity when

$$s_{\text{max coverage}} \simeq 16.2^3 = 4250 \tag{26}$$

This is a rather large number. Hence, the Reich hypothesis does not seem to be a realistic one for explaining micelle stability. In addition, the Reich hypothesis would require that there be a single most probable size, independent of concentration or temperature, contrary to the findings of this discussion and of experiment (see Discussion section).

A way to demonstrate the difficulty with the Reich hypothesis is to compare the value of s in eq. 26 with the size of a micelle (s_c) having a radius R equal to the fully extended length, L_0, of the hydrocarbon tail.[7] Now

$$s_c v_0 = \frac{4\pi L_0^3}{3} \tag{27}$$

Thus

$$s_c = \frac{4\pi L_0^3}{3v_0} \tag{28}$$

which, for a tail of 16 carbon atoms, gives

$$s_c \simeq 253 \tag{29}$$

In order that

$$s_{\text{max coverage}} = s_c \tag{30}$$

h must be equal to about 2.6. This is not impossible, but present thinking would not allow a nonionic head to destroy that much water structure around adjacent nonpolar groups (for example, in polypeptides[2,8] the backbone CH group which is flanked by NH and CO groups is considered to take part in hydrophobic bonding). Thus, we shall abandon the Reich hypothesis and derive an expression for $Q(s)_{\text{solv}}$ for incorporation into eq. 5.

If $\Delta F_{H\Phi}$ is the free energy of formation of a hydrophobic bond per monomer, we have then

$$Q(s)_{\text{solv}} = e^{-s\Delta F_{H\Phi}\theta(s)_{H\Phi}/RT} \tag{31}$$

giving

$$\frac{1}{s}\ln Q(s)_{\text{solv}} = -\frac{\Delta F_{H\Phi}}{RT}\theta(s)_{H\Phi} \tag{32}$$

$\theta(s)_{H\Phi}$ is given by eq. 23, which can be simplified somewhat. From the above discussion we are not depending on complete surface coverage by polar heads as an explanation of micelle stability. Hence, we drop the small term a_h/a_t. Equation 23 then has the form $(1 - \text{constant}/s^{1/3})$ where the constant is approximately 1. Thus

$$\theta(s)_{H\Phi} = 1 - 1/s^{1/3} \tag{33}$$

Substituting eq. 33 into eq. 32, we obtain

$$\frac{1}{s}\ln Q(s)_{\text{solv}} = -\frac{\Delta F_{H\Phi}}{RT}\left(1 - \frac{1}{s^{1/3}}\right) = c\left(1 - \frac{1}{s^{1/3}}\right) \tag{34}$$

Since $\Delta F_{H\Phi}$ is negative, c is a positive number.

In the Discussion section, it is shown that $Q(s)_{\text{ext}}$ and $Q(s)_{\text{solv}}$ are not sufficient to account for stable micelles at large values of s. Hence, we consider next the last term of eq. 5.

The Internal Partition Function. $Q(s)_{\text{int}}$ corresponds to the internal freedom of the micelle arising from the motions of the hydrocarbon tails. A monomer molecule in a micelle will make two large contributions to the internal free energy of the micelle and therefore to $Q(s)_{\text{int}}$. These are (1) the motion of the monomer molecule as a whole within the micelle and (2) internal rotation (including complex vibrations and torsional oscillations) in the hydrocarbon tails. In the formulation of Némethy and Scheraga,[2] the term $\Delta F_{H\Phi}$ (which already appeared in $Q(s)_{\text{solv}}$) includes contribution 2 as well as contributions from the van der Waals interaction between nonpolar groups and changes in the water structure when nonpolar groups associate. Thus, we have to discuss contribution 1[9-11] in order to obtain an expression for $Q(s)_{\text{int}}$.

(6) I. Reich, *J. Phys. Chem.*, **60**, 257 (1956).

(7) For values of R greater than L_0, some polar heads would have to be *inside* the micelle, or the micelle would have to be hollow.

(8) M. Bixon, H. A. Scheraga, and S. Lifson, *Biopolymers*, **1**, 419 (1963).

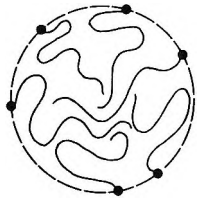

Figure 1. *A very schematic* representation of the cross section of a spherical micelle. The polar heads are shown on the surface.

The physical picture of a micelle is that of a spherical aggregate of hydrocarbon tails; the polar heads are on the surface, with the tails more or less coiled and entangled inside (Figure 1). In considering the internal motion of the monomer in the micelle, one can take either of two points of view. In the first, we can take a free-volume approach and treat the motion as translation; in the second, we can consider the micelle as a lattice and compute the permutation of the monomers over sites on the lattice. We will consider both approaches and show that they both lead to the same type of dependence of $Q(s)_{\text{int}}$ on s.

In the first approach we follow Hoeve and Benson[12] and assume that the translational motion of the monomers within the micelle can be treated in terms of a free-volume expression. Hence, $Q(s)_{\text{int}}$ becomes a translational partition function, $Q(s)_{\text{int trans}}$, for the monomer in the micelle.

$$Q(s)_{\text{int trans}} = \frac{1}{s!}\left(\frac{V_f}{\Lambda^3}\right)^s = \left(\frac{eV_f}{s\Lambda^3}\right)^s \tag{35}$$

where the symbols are defined in connection with eq. 7; the last expression on the right-hand side of eq. 35 is obtained by application of Stirling's approximation. As before, V_f is given by eq. 19, where now

$$V = V_{\text{shell}}\frac{(s-1)}{s} \tag{36}$$

where V_{shell} is the volume of the outer shell to which the polar heads are restricted, and the factor $(s-1)/s$ reflects the fact that the volume occupied by a given molecule is not available to itself for translational motion.

$$V_{\text{shell}} = 4\pi R^2 L = 4\pi\left(\frac{3v_0}{4\pi}\right)^{2/3} s^{2/3} L \tag{37}$$

where L is the thickness of the shell (a not-very-well-defined quantity). This gives

$$\frac{1}{s}\ln Q(s)_{\text{int trans}} = A' + \ln\left(\frac{1}{s^{1/3}} - \frac{1}{s^{4/3}}\right) \tag{38}$$

with

$$A' = \ln\frac{ef_x(4\pi)\left(\frac{3v_0}{4\pi}\right)^{2/3}L}{\Lambda^3} \tag{39}$$

In the second approach we consider the surface of the micelle as a lattice of sites where a polar head can reside. Then, if there are S equivalent sites, we have, in place of $Q(s)_{\text{int trans}}$ of eq. 35, a partition function for permutations over the sites on the lattice.

$$Q(s)_{\text{int permut}} = \frac{S!}{(S-s)!s!}p^s \tag{40}$$

where p is the partition function for each site, and S is given by

$$S \sim \frac{(\text{surface of micelle}) - \begin{pmatrix}\text{surface area of one}\\ \text{monomer unit in}\\ \text{the micelle surface}\end{pmatrix}}{(\text{area of a polar head})} \tag{41}$$

with

$$\begin{pmatrix}\text{surface area of one}\\ \text{monomer unit in the}\\ \text{micelle surface}\end{pmatrix} = \frac{(\text{surface of micelle})}{s} \tag{42}$$

giving

$$S = B\left(s^{2/3} - \frac{1}{s^{1/3}}\right) \tag{43}$$

If the proportionality constant in eq. 41 is unity, then a consideration of molecular dimensions indicates that $B \sim 16$ for our example of a chain of 16 carbon atoms and a carboxyl head. Using Stirling's approximation

$$\frac{1}{s}\ln Q(s)_{\text{int permut}} = B\left(\frac{1}{s^{1/3}} - \frac{1}{s^{4/3}}\right)\times$$
$$\ln\frac{\left(\frac{1}{s^{1/3}} - \frac{1}{s^{4/3}}\right)}{\left(\frac{1}{s^{1/3}} - \frac{1}{s^{4/3}}\right) - \frac{1}{B}} + \left[\left(\ln\frac{1}{s^{1/3}} - \frac{1}{s^{4/3}}\right) - \frac{1}{B}\right] + \ln pB \tag{44}$$

Since $1 < s_m << 4000$, we have $1/s^{1/3} >> 1/B$ (for $B \sim 16$). Hence, eq. 44 becomes

(9) In experimental work[10,11] to test the theory of Némethy and Scheraga,[2] a question has arisen concerning the correctness of the inclusion of the term ΔF_{rot} which pertains to restrictions on internal rotation on forming a hydrophobic bond. This point, then, remains open. It should be pointed out that ΔF_{rot} is a very small part of $\Delta F_{H\Phi}$, so that the values[2] of $\Delta F_{H\Phi}$ are still valid.

(10) E. E. Schrier, M. Pottle, and H. A. Scheraga, *J. Am. Chem. Soc.*, **86**, 3444 (1964).

(11) H. Schneider, G. C. Kresheck, and H. A. Scheraga, *J. Phys. Chem.*, **69**, 1310 (1965).

(12) C. A. J. Hoeve and G. C. Benson, *ibid.*, **61**, 1149 (1957).

$$\frac{1}{s} \ln Q(s)_{\text{int permut}} \approx A'' + \ln\left(\frac{1}{s^{1/3}} - \frac{1}{s^{4/3}}\right) \quad (45)$$

In summary, as far as $Q(s)_{\text{int}}$ is concerned, in the free-volume approach, one treats the interior of the micelle like a very imperfect gas whose molecules undergo translational motion in a limited space, while in the lattice approach the interior is treated like an imperfect crystal. Both approaches (eq. 38 and 45) give the same dependence on s. This function has a maximum at $s = 4$; hence, it alone cannot account for micelle formation. Also, this function is not applicable for the case of small s since "internal" freedom has no meaning for small s. Further, it may be noted that $(1/s) \ln Q(s)$ of eq. 38 and 45 decreases with increasing s for $s > 4$. This behavior arises because the free volume of the shell is proportional to $s^{2/3}$ while the number of polar heads in the shell is s; *i.e.*, the concentration, $s/s^{2/3}$, increases as s increases, and the negative of the free energy per molecule decreases.

Thus, we may use eq. 38 for $Q(s)_{\text{int}}$.

$$\frac{1}{s} \ln Q(s)_{\text{int}} = A + \ln\left(\frac{1}{s^{1/3}} - \frac{1}{s^{4/3}}\right) \quad (46)$$

where

$$A = A' + \ln \frac{q(m)}{q(1)} \quad (47)$$

with A' being given by eq. 39; $q(m)$ is the average partition function for complex vibrations and internal rotation of a monomer molecule in a micelle, and $q(1)$ represents the same quantities for the free monomer. Since A is the least certain of the parameters introduced in this discussion, it will be treated as an unknown parameter. We may take cognizance of the fact that $(1/s)^{4/3}$ is very small compared to $(1/s)^{1/3}$ for moderate values of s and rewrite eq. 46, for $s > 10$, as

$$\frac{1}{s} \ln Q(s)_{\text{int}} = A - \frac{1}{3} \ln s \quad (48)$$

It should be mentioned that we have not considered the dependence of the number of allowed isomers of internal rotation (for each monomer) on micelle size. This may possibly be a very important effect, for, as the micelle grows in size, a monomer unit must, on the average, take up a more elongated conformation to fulfill the geometric packing requirements of the micelle. Thus, in analogy with the stretching of rubber, the conformational entropy of a monomer in a micelle would decrease as the micelle size increases; this would probably lead to a limitation on micelle size (rather than to phase separation). However, it is not clear to what extent hydrocarbons of moderate length are flexible chains. Until the nature of the potential function for internal rotation in hydrocarbon chains is better known,[13] we shall leave this as an important, unanswered question.

The Necessary Conditions for Micelle Formation

The Free Energy Function. Substituting eq. 16, 34, and 48 into eq. 5, we obtain an expression for the free energy of 1 l. of solution of N monomer molecules as a function of micelle size.

$$\frac{-F(N,s)}{NkT} = \frac{1}{s}(a + b \ln s) + c\left(1 - \frac{1}{s^{1/3}}\right) + A - \frac{1}{3} \ln s \quad (49)$$

where the physical significance of the constants is as follows: a = (external free energy per micelle)/RT (given by eq. 17); $b = 5$ (eq. 18); $c = -\Delta F_{H\Phi}/RT$ (eq. 34); A = (internal free energy per monomer molecule)/RT (which is treated as an unknown parameter).

In order to obtain a stable micelle, the free energy function in eq. 49 must have a maximum at a large value of s. In order to obtain some physical insight as to how $-F(N,s)/NkT$ can exhibit a maximum, let us consider the various terms on the right-hand side of eq. 49. These are each plotted in Figure 2 as a function of s. Curve A represents the external free energy (essentially the translational and rotational entropy) which decreases rapidly as s increases. Curve B is the free energy due to solvent effects (*i.e.*, hydrophobic bonding), while curve C represents the internal free energy of the micelle. The free energy scales for the three curves are arbitrary; the figure is intended to illustrate only the dependence on s. The main point of interest is that, for large-sized aggregates, say above $s = 50$, all three components depend very little on s, and the combination of the three curves to produce a maximum at some large value of s depends very sensitively on the shapes of the curves; the conditions for the occurrence of this maximum will be discussed in the subsequent paragraphs. Figure 3 is a schematic representation of the sum of the three components of Figure 2, *i.e.*, $-F(N,s)/NkT$, at various concentrations; the sharpness of the maximum has been exaggerated for illustrative purposes. Concentration contributes to $-F(N,s)/NkT$ through the external partition function, whose influence can be seen from curve A of Figure 2 and eq. 16 and 17. At very low concentration, the term $-\ln$ (concentration), which is part of the a term of eq. 17, becomes very large and favors

(13) R. A. Scott and H. A. Scheraga, *J. Chem. Phys.*, 42, 2209 (1965).

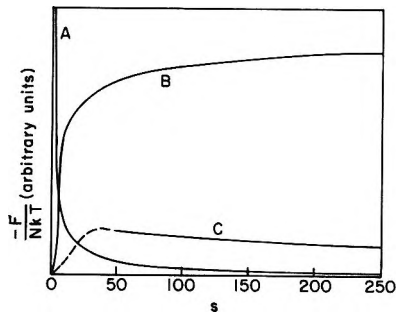

Figure 2. Schematic illustrative curves, showing the contributions to $-F(N,s)/NkT$ of eq. 49. Curve A is the external free energy; curve B is the solvent-interaction free energy; and curve C is the internal free energy (the dashed part of curve C was not computed but was inserted since the function must approach zero as s decreases). The free energy scale is arbitrary.

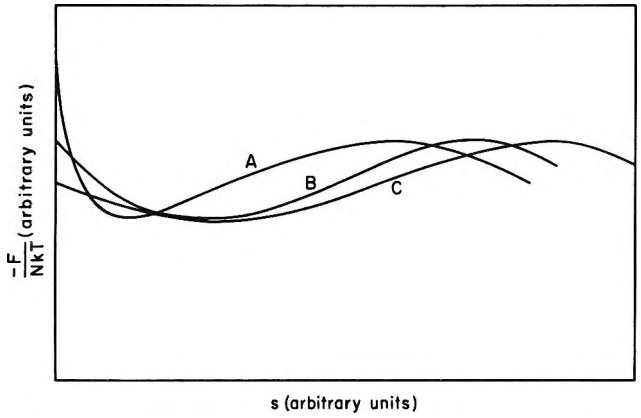

Figure 3. Schematic representation of $-F(N,s)/NkT$ as a function of s for three concentrations, illustrating the formation of micelles as the concentration is increased. Curve A is for a low concentration, where monomer is the most probable species; curve B is for the critical concentration, where monomer and micelle are equally probable; and curve C is for a high concentration where the micelle is the most probable species.

the monomer; this situation is shown in curve A of Figure 3. As the concentration increases, the contribution of the external free energy decreases, and the free energy of the monomer approaches that of the large aggregates; at the critical concentration, curve B of Figure 3, the free energies of monomer and micelle are equal. At still larger concentration, curve C, the negative free energy of the micelle becomes larger than that of the monomer.

With these qualitative ideas in mind, let us examine quantitatively the conditions for the existence of a stable micelle. If there is to be an extremum in $-F(N,s)/NkT$, the following equation must hold.

$$\left(-\frac{1}{NkT}\right)\left(\frac{\partial F(N,s)}{\partial s}\right) = 0 \tag{50}$$

Equation 50 cannot be solved explicitly to find the value of s_m which makes the free energy an extremum. Hence, it is convenient to perform the differentiation and solve for c, *i.e.*, to express the existence of an extremum as a condition on c, *i.e.*, on the magnitude of the hydrophobic bond strength.

Condition 1

$$c = \frac{3(a + b \ln s_m - b)}{s_m^{2/3}} + s_m^{1/3} \tag{51}$$

The second condition for micelle formation is that the extremum be a maximum

$$\left(-\frac{1}{NkT}\right)\left(\frac{\partial^2 F(N,s)}{\partial s^2}\right)_{s=s_m} < 0 \tag{52}$$

Again, this cannot be solved explicitly and is best stated as a condition on c

Condition 2

$$c < \frac{3}{2} s_m^{1/3} + \frac{9}{2} b s_m^{-2/3} \tag{53}$$

The third and final condition for micelle formation is that

$$-F(N,1) < -F(N,s_m) \tag{54}$$

or

$$a < \frac{1}{s_m}(a + b \ln s_m) + c\left(1 - \frac{1}{s_m^{1/3}}\right) + A - \frac{1}{3}\ln s_m \tag{55}$$

There is no term A on the left-hand side of eq. 55 since it cannot arise for a monomer. Equation 55 thus provides a third condition on c

Condition 3

$$c > \frac{s_m^{1/3}(a + {}^1/_3 \ln s_m) - \dfrac{(a + b \ln s_m)}{s_m^{2/3}}}{(s_m^{1/3} - 1)} - \left(\frac{s_m^{1/3}}{s_m^{1/3} - 1}\right)A \tag{56}$$

Equations 51, 53, and 56 provide three conditions on c, in which c must be equal to, less than, and greater than certain quantities, respectively. These conditions, then, determine the characteristic features of micelle formation. It may be noticed that, of these conditions, only eq. 56 contains the unknown parameter A. We now discuss the implications of these conditions.

The Critical Micelle Concentration. Condition 3 (eq. 56), which expresses the requirement that the

hydrophobic bond strength must be large enough, may be looked upon as a necessary but not sufficient condition for micelle formation; *e.g.*, instead of leading to micelle formation, a large value of c might lead to precipitation. For large values of s_m eq. 56 becomes

$$c > a + \frac{\ln s_m}{3} - A \qquad (57)$$

Substituting for a from eq. 17, we obtain

$$c > 4 \ln n + 3 \ln T - \ln (\text{concentration}) + \frac{\ln s_m}{3} + \text{constant} \qquad (58)$$

Since A is essentially an entropy which is neither that of an imperfect gas nor that of an imperfect crystal, but something in between, its dependence on n and T would be expected to be small; it is, therefore, absorbed in the constant in eq. 58. The critical micelle concentration, c.m.c., is the concentration at which the inequality of eq. 54 becomes an equality, *i.e.*, where the free energies of the monomer and the micelle are equal. Hence, eq. 58 (or, equivalently, eq. 56) must be an equality, *i.e.*

$$-\ln \text{c.m.c.} = c - 4 \ln n - 3 \ln T - \frac{\ln s_m}{3} - \text{constant} \qquad (59)$$

Assuming that

$$c = -\frac{n\Delta F_{H\Phi}(CH_2)}{RT} \qquad (60)$$

where $\Delta F_{H\Phi}(CH_2)$ is the free energy of formation of a hydrophobic bond, per CH_2 group, eq. 59 becomes

$$-\ln \text{c.m.c.} \approx -n\frac{\Delta F_{H\Phi}(CH_2)}{RT} - 4 \ln n - 3 \ln T - \frac{\ln s_m}{3} - \text{constant} \qquad (61)$$

Ignoring the small dependence of $\ln s_m$ on n, we obtain

$$-\left(\frac{\partial \ln \text{c.m.c.}}{\partial n}\right)_T = \frac{-\Delta F_{H\Phi}(CH_2)}{RT} - \frac{4}{n} \qquad (62)$$

We have thus obtained some useful information from condition 3. It may be noticed that condition 3 contains the unknown parameter A. In order to obtain further information, specifically to see how we obtain micelle formation rather than precipitation (by having made c large enough according to condition 3), we must examine conditions 1 and 2.

The Value of c as a Criterion for Micelle Formation. We now consider conditions 1 and 2 (eq. 51 and 53).

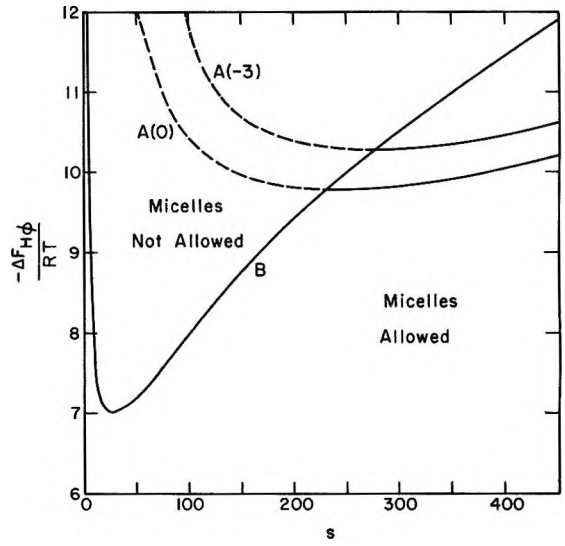

Figure 4. Illustration of conditions for micelle formation. Curves A(0) and A(−3) represent condition 1 at concentrations of 1.0 and 10^{-3} M, respectively. Curve B represents condition 2.

These are most easily discussed by referring to graphical representations. Figure 4 shows these conditions for $n = 16$, plotted as c *vs.* s. Condition 1 is represented by curves A(0) and A(−3) at concentrations of 10^0 M and 10^{-3} M, respectively; condition 2 is represented by curve B. Condition 1 implies that, for a given concentration, micelles will be formed when the values of c and s lie on the appropriate curve (A(0), A(−3), or a similar one); condition 2 implies that micelles will form only for c and s values which lie *below* curve B. Combining these two conditions, we see that micelles can exist only in the region where curves A are represented by solid lines, and not by dashed lines. Further, we see that a specification of n, T, and concentration fixes the value of a (eq. 17); hence, since b is a constant (eq. 18), conditions 1 and 2 by themselves serve to fix the value of s_m once c is specified. The only use served by condition 3 is to tell us whether the chosen value of the concentration is, or is not, above the c.m.c.

It can be seen from Figure 4 that condition 2 (curve B) places a great restriction on the magnitude of c (*i.e.*, on how large the hydrophobic bond strength must be); also, it does not allow small micelles to form. If c were too large, then one would have the usual case of small polymer association (dimers, trimers, etc.) or phase separation; condition 2 states that c cannot be too large in order to obtain micelles.

Since c must be rather small, according to condition 2, then A must be large in order to be able simultaneously to fulfill condition 3 (see eq. 57 and the Discussion section).

Figure 4 makes plausible the facts that, in a solution of long-chain hydrocarbon molecules with polar heads, one observes monomers and large micelles but no small aggregates. The area of Figure 4 which is of most interest, as far as micelles are concerned, is that part of a given A curve which lies to the right of its intersection with the B curve. This detail is shown at greater magnification in Figure 5 for four concentrations (10^0, 10^{-1}, 10^{-2}, and 10^{-3} M), the corresponding curves being labeled A(0), A(−1), A(−2), and A(−3), respectively.

With the aid of Figure 5, let us consider what happens as the concentration is increased. Suppose the value of A is such that, according to eq. 61, the c.m.c. is 10^{-3} M, and, further, suppose, for illustrative purposes, that 10^{-1} M is the saturation concentration. From Figure 5, it can be seen that the value of s_m at the c.m.c. (point a) is about 275. If we increase the concentration, c must remain constant. Hence, we move to the right along the horizontal line of constant c. At 10^{-2} M, the system is at point b, and $s_m \sim 385$; when the concentration is increased to 10^{-1} M (point c), precipitation occurs with $s_m \sim 425$. Figure 6 shows a plot of the concentration dependence of s_m; it can be seen that, as the concentration is increased, the most probable micelle size increases up to the saturation concentration.

We may also consider the effect of temperature on micelle size. Suppose the concentration is 10^{-3} M and the temperature (and, therefore, c) is altered. Now, condition 1 (curves A of Figure 5) is only very slightly dependent on T for large s (about a 0.1% variation); condition 2 leads to no temperature dependence.

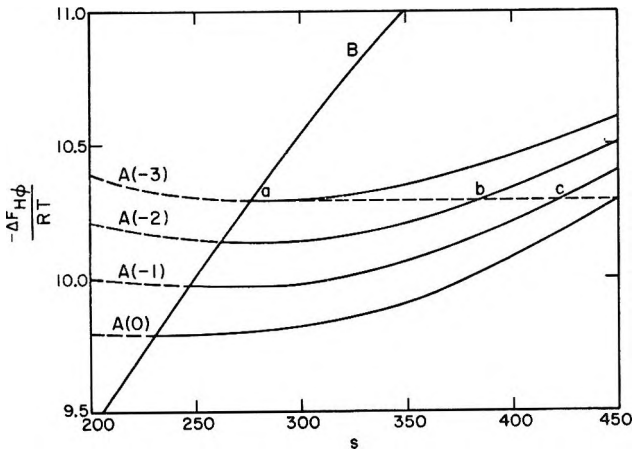

Figure 5. Magnified portion of Figure 4 illustrating conditions for micelle formation. Curves A(0) to A(−3) correspond to 10^0, 10^{-1}, 10^{-2}, and 10^{-3} M, respectively.

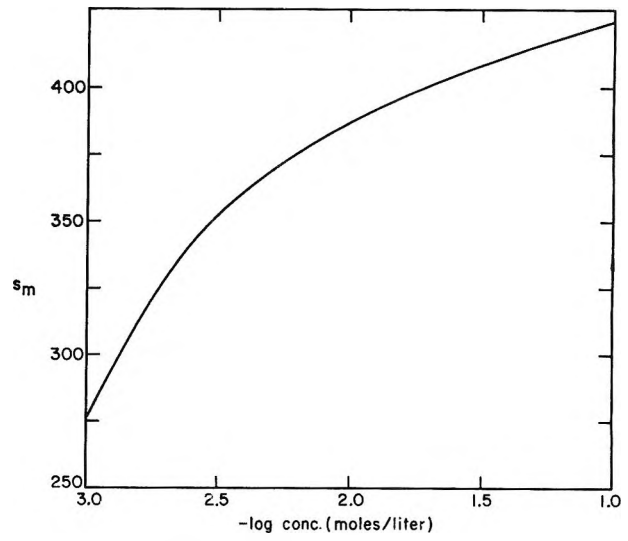

Figure 6. Illustration of the variation of the most probable micelle size with concentration.

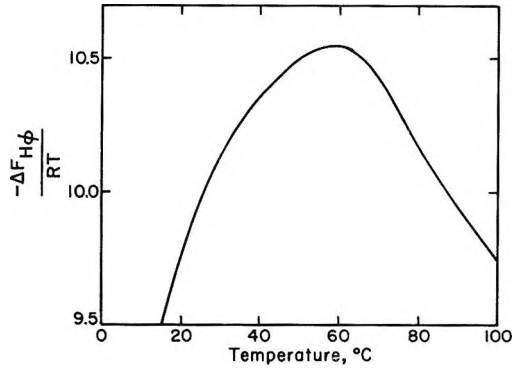

Figure 7. Illustrative variation of $-\Delta F_{H\Phi}/RT$ with temperature.[2]

The temperature dependence of c is that of $-\Delta F_{H\Phi}/RT$ where $\Delta F_{H\Phi}$ is given by

$$\Delta F_{H\Phi} = a' + b'T + c'T^2 \qquad (63)$$

and a', b', and c' pertain to a particular pair of nonpolar groups. The primes are used here to distinguish a', b', and c' from the parameters a, b, and c of the micelle theory. Taking these constants proportional to those for an alanine–alanine hydrophobic bond,[2] we may obtain the temperature dependence of c, which is plotted in Figure 7; the well-known maximum in the c *vs.* T curve is observed; *i.e.*, the hydrophobic bonds get stronger and then weaker, with increasing temperature. Now, if 10^{-3} M is the c.m.c. at low temperature (point a in Figure 8), it will be greater than the c.m.c. if the temperature is raised; however, at some still higher temperature (point b in Figure 8), it will again become the c.m.c. because of the behavior of c in

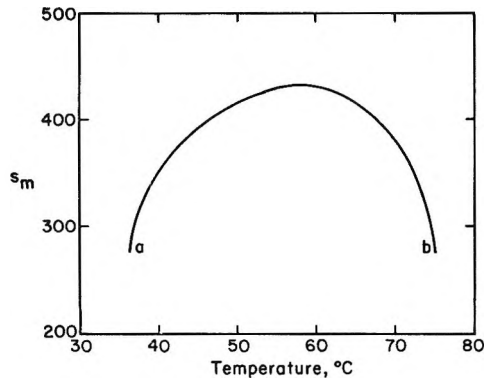

Figure 8. Illustration of the variation of the most probable micelle size with temperature. It should be noted that the concentration is constant (10^{-3} M) and equal to the c.m.c. only at points a and b.

Figure 7. The temperature dependence of the c.m.c. is given by eq. 61, the ln T term not contributing much. The variation of the most probable micelle size with temperature at a fixed concentration of 10^{-3} M is given in Figure 8, using the information of Figure 5. The curve ends abruptly at low and high temperatures (points a and b of Figure 8); at temperatures below point a and above point b, there are no micelles, and the turbidity vanishes.

Discussion

General Solute Association. We address ourselves here to the important point that the function $-F(N,s)/NkT$ cannot exhibit a maximum at a large value of s unless the term $Q(s)_{int}$ is introduced; for this purpose, we consider the association of any solute and ask why micelle-forming solutes are unique.

Suppose we have a solute whose free energy of association has only the first two contributions of eq. 5, *i.e.*, the external free energy of eq. 16 and an interaction free energy depending only on the number of solute–solute interactions (and, therefore, given by an equation of the type of eq. 34, where c is replaced by a free energy of interaction, $\Delta F_{interact}$). Thus, for this simple picture of association, we would have

$$\frac{-F(N,s)}{NkT} = \frac{1}{s}(a + b \ln s) + \frac{\Delta F_{interact}}{RT}\left(1 - \frac{1}{s^{1/3}}\right) \quad (64)$$

In order that large aggregates are stable, eq. 52 and 54 must hold (as well as eq. 50). These two conditions lead to the result that

$$\frac{9}{2}\frac{b}{s_m^{2/3}} > \frac{\Delta F_{interact}}{RT} > \left(\frac{s_m^{1/3}}{s_m^{1/3} - \frac{2}{3}}\right)\left(a - \frac{b}{s_m}\right) \sim a \quad (65)$$

Equation 65 demands that $\Delta F_{interact}/RT$ be greater than a but simultaneously less than $9b/2s_m^{2/3}$. Since, in general, a will be greater than $9b/2s_m^{2/3}$, it will not be possible to satisfy eq. 65. Hence, large aggregates of ordinary solutes will not arise; instead, there will be the usual case of limited association (*i.e.*, exponentially decreasing concentrations of dimer, trimer, etc.).

In order to obtain stable micelles, it is not sufficient to offset the loss of translational and rotational entropy by a large free energy of association. We require, in addition, a large negative internal free energy (largely an entropy) that is not proportional to the number of solute–solute contacts. The loose nature of hydrophobic bonds[14] provides this high degree of internal freedom in the micelle; the decrease of this internal freedom with increasing micelle size accounts for the stability of large aggregates.

Comparison with Experiment. Recent papers by Corkill, *et al.*,[15,16] report the size and heat of formation of micelles of the nonionic alkylhexaoxyethylene compounds [$RO(CH_2CH_2O)_6H$]; since R is $CH_3(CH_2)_{n-1}$, the general formula of these compounds is C_nE_6. These compounds are not similar to the model of a monomer discussed here since the polar "head," E_6, is composed of 19 chain atoms. Thus, any comparison can be only semiquantitative. The authors find an excess turbidity as concentration is increased above the c.m.c., indicating an increase in the most probable micelle size, as predicted. It may be noted that a dependence of micelle size on concentration means that $Q(s)_{ext}$ must be an important part of $Q(s)$ since the concentration appears only in the a term (eq. 16 and 17). Corkill, *et al.*, also find that the most probable size increases with temperature, but, since none of their measurements was made above 60°, they do not observe any decrease in micelle size at very high temperature as we predict. For C_8E_6 the critical concentration is 4.45×10^{-3} g./ml. at 18° where $s_m = 30$. This is much smaller than we predict, presumably owing to the presence of the very large polar part of the molecule (70%); *i.e.*, although C_8E_6 has 20 CH_2 groups (most of which are in the E_6 portion), it probably is more analogous to a similar compound whose hydrocarbon tail contains only 8 CH_2 groups. As the length of the

(14) It is interesting to point out that this same "loose" nature of hydrophobic bonds, allowing large amounts of internal freedom, provides an entropy contribution when a dimer is formed from *very large* monomers (*i.e.*, proteins) and enables the dimer to overcome the large loss of translational entropy when two large monomers associate.[3]

(15) R. R. Balmbra, J. S. Clunie, J. M. Corkill, and J. F. Goodman, *Trans. Faraday Soc.*, **60**, 979 (1964).

(16) J. M. Corkill, J. F. Goodman, and J. R. Tate, *ibid.*, **60**, 996 (1964).

alkyl tail is increased, micelle sizes become very large because of a linear increase in c, as can be inferred from Figure 4.

We may examine the temperature dependence of s_m. In this respect, the data of Corkill, *et al.*, pertain to a range of concentrations where the micelle size no longer depends on concentration, and our numerical example (see Figure 8) applies to a constant concentration; thus, the only quantity which depends on temperature is the hydrophobic parameter $c = -\Delta F_{H\Phi}/RT$. Considering the logarithmic change of s_m for C_8E_6, the data of Corkill, *et al.*, give

$$\left(\frac{\partial \log s_m}{\partial T}\right)_{40°} = 0.015 \qquad (66)$$

while for our numerical example (see Figure 8) we obtain

$$\left(\frac{\partial \log s_m}{\partial T}\right)_{40°} = 0.013 \qquad (67)$$

Thus, the trend is well predicted, for the short hydrocarbon chain.

In the case of the longer chains, the dependence of $\Delta F_{H\Phi}$ on temperature does not account for the dependence of s_m on temperature. We suggest that this is due to increased burial of the E_6 portion of the molecule in the micelle as the micelle size becomes large. This burial would probably manifest itself by a large positive contribution to the free energy, as discussed elsewhere,[17] because of the removal of the oxyethylene oxygens from the dipolar influence of water. In this case, c would be given by

$$-c = \frac{\Delta F_{H\Phi}}{RT} + \frac{\Delta H_{burial}}{RT} \qquad (68)$$

Since $\Delta F_{H\Phi}$ is given by eq. 63, eq. 68 becomes

$$-c = \frac{a' + \Delta H_{burial}}{RT} + \frac{b'}{R} + \frac{c'T}{R} \qquad (69)$$

If ΔH_{burial} is large, the last two terms on the right-hand side of eq. 69 do not contribute much, and the dependence of c on temperature will be essentially as $1/T$. Now, from condition 1 (eq. 51), c becomes equal to $s_m^{1/3}$ for large values of s_m; hence, $-s_m^{1/3}$ should vary as $1/T$ for large values of s_m. The term $s^{1/3}$ in eq. 51 is the ratio of two terms, *i.e.*, $s/s^{2/3}$, where the s in the numerator and the $s^{2/3}$ in the denominator come, respectively, from the terms $(1/3)$ ln s and $(1 - 1/s^{1/3})$ in eq. 49. Thus, if $s_m^{1/3}$ were to be found to vary linearly with $1/T$, we would have evidence for the validity of the partition functions $Q(s)_{solv}$ and $Q(s)_{int}$. The data of Corkill, *et al.*, plotted in Figure 9, indicate

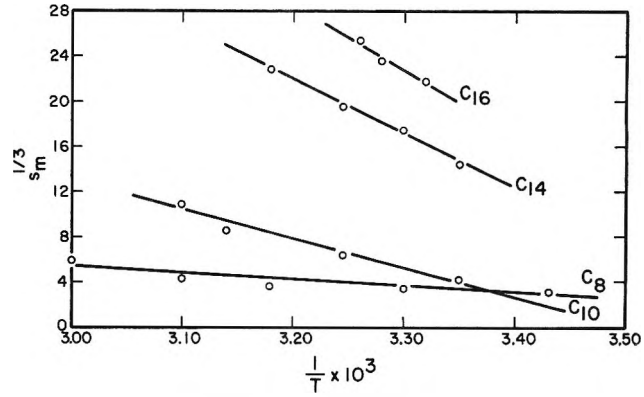

Figure 9. Variation of the most probable micelle size with temperature for C_nE_6 micelles. The data are for those of ref. 15 and 16.

that the large micelles seem to obey this relation. The increase in the negative slope with increasing chain length is some measure of the increasing degree of burial of oxygen groups, indicating that the E_6 "shell" becomes more tightly packed as the micelle size increases with increasing chain length.

Another comparison that can be made is the dependence of the critical concentration on temperature. From eq. 59, log c.m.c. depends on c and on an unknown constant; the temperature dependence of c is given by eq. 63, and we ignore the ln T term. Inserting the experimental value of the critical concentration for C_8E_6 into eq. 59 at 30° to fix the unknown constant, the data of Table I are obtained for the calculated dependence of the critical concentration on temperature, the constant being taken independent of T. Again the correct trend is predicted.

Table I: Dependence of the C.m.c. on Temperature

− Log c.m.c. (exptl.)	t, °C.	− Log c.m.c. (calcd.)	t, °C.
2.35	18	2.34	20
2.46	30	2.46	30
2.55	40	2.56	40

The heats of formation of C_nE_6 micelles are positive, which, of course, supports the notion that hydrophobic bonding makes essentially the main contribution to ΔH. The temperature dependence of ΔH is shown in Table II, where the values have been made to agree at 30° by setting $\Delta H_{exptl} = \Delta H_{H\Phi}$ at 30°. It can be

(17) D. C. Poland and H. A. Scheraga, *Biopolymers*, paper I, in press.

seen that the positive experimental value of ΔH and its decrease with increasing temperature are as predicted by the theory of hydrophobic bonding.[2]

Table II: Temperature Dependence of Heat of Formation of C_nE_6 Micelles

	ΔH, kcal./mole	
t, °C.	Calcd. from eq. 63	Obsd.[15,16] for C_8E_6
10	7.0	
20	5.6	
25	4.9	4.8
30	4.3	4.3 (interpolated from the data at 25 and 40°)
40	2.8	3.5
50	1.4	

There is a glaring discrepancy between theory and experiment when the dependence of ΔH on chain length is considered. The value of ΔH per molecule becomes more negative (less positive) as chain length increases. Corkill, *et al.*, suggest an increase in negative cohesive energy (van der Waals' interaction) between hydrocarbon tails as a possible explanation. The theory of Némethy and Scheraga,[2] as already mentioned, includes the effect of cohesive energy between hydrocarbon portions, but the effect of solvent structure (leading to the positive enthalpy of hydrocarbon association) should parallel that of chain length at the same rate as the number of $CH_2 \cdots CH_2$ interactions increases; thus, the increase in the positive ΔH should parallel the increase in chain length, and the value of ΔH per molecule should become more positive as the chain length increases. In this respect, the theory of Némethy and Scheraga[2] has been quantitatively confirmed for the dependence of the free energy of dimerization of carboxylic acids as a function of chain length[10] and for a similar chain-length dependence of the enthalpy of binding of carboxylic acids to polystyrene in water.[11] The effect of the polar chain in the weird type of monomer studied by Corkill, *et al.*, is perhaps the cause of this observed discrepancy.

This explanation is rendered plausible by the following consideration. There is an increase of only two chain atoms between the compounds C_8E_6 and $C_{10}E_6$. Since E_6 has 19 chain atoms, the fraction of the molecule that is E_6 is relatively little changed; also the decrease in the per cent of E_6 in the molecule is counterbalanced by the increase in C_n. Now, the experimental value of s_m at 25° is about 35 for C_8E_6 and 73 for $C_{10}E_6$ (both at the critical concentration). Further, $R \sim s_m^{1/3}$ (eq. 11), and the surface area is $\sim s_m^{2/3}$. Since there are s_m polar E_6 heads in a micelle, the surface area per E_6 group is $\sim s_m^{2/3}/s_m \sim s_m^{-1/3}$. Thus, since s_m is greater for $C_{10}E_6$ than for C_8E_6, it follows that the relative amount of E_6 on the surface is lower for $C_{10}E_6$. Specifically

$$\frac{\text{surface area of } C_{10}E_6 \text{ per } E_6}{\text{surface area of } C_8E_6 \text{ per } E_6} \simeq \left(\frac{73}{35}\right)^{-1/3} = 0.78 \quad (70)$$

while the ratio of the experimental ΔH values of micelle formation is

$$\frac{\Delta H(C_{10}E_6)}{\Delta H(C_8E_6)} = 0.75 \quad (71)$$

Thus, some sort of surface effect, involving the E_6 portion of the molecule, might account for the trend in ΔH with chain length. More data on simpler systems are required before this question can be resolved.

This treatment has been extended to micelles formed from monomer molecules having charged head groups; in this case an electrostatic free energy and a free energy arising from the solvation of the charged head groups have been introduced.[18]

(18) D. C. Poland and H. A. Scheraga, *J. Colloid Sci.*, submitted.

The Entropy of Iodine Monochloride. Heat Capacity from 17 to 322°K. Vapor Pressure. Heats of Fusion and Vaporization[1]

by G. V. Calder and W. F. Giauque

Low Temperature Laboratory, Departments of Chemistry and Chemical Engineering, University of California, Berkeley, California (*Received March 1, 1965*)

The heat capacity of ICl has been measured from 17 to 322°K. The melting point and heat of fusion were found to be 300.53° and 2773 ± 2 cal./mole, respectively. The entropy of ICl(s) = 23.41 gibbs/mole, and its free energy of formation from the elements is $\Delta F^\circ = -3363 \pm 25$ cal./mole, each at 298.15°K. Values of C_p°, S°, $(F^\circ - H^\circ_0)/T$, and $(H^\circ - H^\circ_0)/T$ have been tabulated. The total vapor pressure and the partial pressures of ICl and Cl_2 have been measured over stoichiometric liquid ICl, and the data have been used to calculate the partial pressure of ICl over the solid and liquid from 250 to 330°K. $\Delta H^\circ_0 = 13{,}273$ cal./mole for the vaporization process. A simple and accurate experimental method has been described for determining the equilibrium composition of the vapor over solutions with more than one volatile component. Equilibrium is preserved by extremely slow sampling through a capillary, with condensation in a liquid nitrogen cooled, evacuated collection vessel. The data of McMorris and Yost for the reaction NO + ICl = NOCl + $^1/_2I_2(g)$ have been reconsidered and give $\Delta H^\circ_0 = -5375 \pm 15$ cal./mole and $\Delta F^\circ_{298.15°K.} = -1216 \pm 15$ cal./mole. Also the data of Beeson and Yost for the reaction NOCl = NO + $^1/_2Cl_2$ have been re-examined and give $\Delta H^\circ_0 = 8630 \pm 10$ cal./mole and $\Delta F^\circ_{298.15°K.} = 4897 \pm 10$ cal./mole. Corrosion tests run on Hastelloy C alloy in liquid ICl showed essentially complete resistance at ordinary temperatures.

The thermodynamic properties of the iodine–chlorine system are not very accurately known. The situation is complicated by the presence of Cl_2 and I_2 gases in equilibrium with the several solid phases including ICl and ICl_3 as was first shown by the work of Stortenbeker.[2,3] Stortenbeker's substantial investigations covered the freezing point curves and eutectic data, with some approximate values of vapor composition. A summary of the more important references to and properties of ICl is given by Greenwood[4] in a review of the properties of interhalogen compounds. The present work contributes the entropies of solid and liquid iodine monochloride, the partial pressure of ICl over stoichiometric ICl, and additional information which will help in the ultimate evaluation of the thermodynamics of this system.

Iodine monochloride has two crystalline forms designated α and β with melting points at about 27.3 and 13.9°, respectively. The unstable β is not very difficult to obtain temporarily, in small amount, and it was observed during the course of preparatory work. We had hoped to obtain the heat capacity of both forms to supply one of the few cases that illustrate the approach to zero entropy at 0°K. by each of the crystalline forms. However, in this we were unsuccessful, and it appears that either the unstable β form cannot be supercooled very far, or at least the chance of avoiding one or more centers of spontaneous recrystallization is very small in an amount of the order of 100 cm.^{3}.

The X-ray structural determinations[5,6] show that

(1) This work was supported in part by the National Science Foundation.

(2) W. Stortenbeker, *Rec. trav. chim.*, **7**, 152 (1888).

(3) W. Stortenbeker, *Z. physik. Chem.*, **3**, 11 (1889); **10**, 183 (1892).

(4) N. N. Greenwood, *Rev. Pure Appl. Chem.*, **1**, 84 (1951).

(5) H. K. Boswijk, J. van der Heide, A. Vos, and E. H. Wiebenga, *Acta Cryst.*, **9**, 274 (1956), for the α form.

(6) G. B. Carpenter and S. M. Richards, *ibid.*, **15**, 360 (1962), for the β form.

both forms consist of similarly ordered chain arrangements that should approach zero entropy at 0°K. The staggered chains have the atomic order Cl–I–I–Cl–I–I with Cl branches on alternate iodine atoms in each structure, so that the conversion of β to α would appear to be a rather simple process, unfavorable to supercooling.

Apparatus. Most of the calorimetric apparatus was that used by Giauque and Egan,[7] including the standard copper–constantan thermocouple W-25, except that the gold calorimeter could not be used with corrosive iodine monochloride. Corrosion measurements were made on a sheet of Hastelloy Type C alloy,[8] which is largely nickel, containing Mo (15.80), Cr (15.58), Fe (6.15), W (3.75), Co (1.61), Mn (0.53), Si (0.52), V (0.25), C (0.05), P (0.01), and S (0.004), where values in parentheses are percentages. The sheet, which had a surface area of 23.1 cm.^{2}, was cleaned and immersed in ICl at 28 to 30° for various times. As expected, the first immersion showed a very small loss in weight followed by essentially complete resistance to ICl. The sheet was cleaned with pure acetone and dried in an oven at 110° for 10 min. before each weighing. The results are given in Table I.

Table I: Corrosion Test of Hastelloy C with ICl

Time, hr.	Wt., g.
0	7.5596
2	7.5589
8	7.5590
24	7.5589
242	7.5587

After the calorimeter was constructed it was treated with liquid ICl for 34 days, followed by washings with aqueous KI solution and distilled water before use.

A 1:3 mixture of Kel-F 200 wax with Kel-F 210 grease[9] was used in stopcocks and ground-glass joints. A 5.4123-g. sample of Kel-F 200 increased to 5.4189 g. after immersion in ICl at 30° for 3 hr. The small increase in weight was taken to indicate a slight solubility of ICl in the Kel-F which would have little effect considering the limited exposed surface in ground-joint use.

The cylindrical calorimeter had a 4.0-cm. o.d. and an 11.0-cm. wall 0.1 cm. thick. It was 11.6 cm. in overall length owing to the rounded ends. There were no vanes in the calorimeter for heat conduction since Hastelloy has a poor thermal conductivity. The effectiveness of the calorimeter would have been considerably improved by the addition of a soldered copper tube encasing the cylindrical walls to provide better heat distribution. The poor heat conductivity made thermal equilibrium periods two or three times as long as those in a gold or copper calorimeter. The volume of the calorimeter was 144 cm.^{3}. A Hastelloy C tube of 0.254-cm. o.d., 0.17-cm. i.d., and 165-cm. length was attached to the calorimeter. All fabrication was by heliarc welding. A Hastelloy fitting at the top of the tube matched standard taper ground-glass fittings to a vacuum system and to a glass weight buret for introducing the sample. The weight buret also had a standard taper fitting to a long Hastelloy capillary tube, 0.159-cm. o.d. and 0.129-cm. i.d., which could be inserted into the upper end of the calorimeter. After the sample had been transferred into the calorimeter, the inlet capillary was removed and washed with CCl_4 to enable quantitative analysis of the small amount of ICl which had adhered.

The high-resistance thermometer–heater was wound from No. 40 Au wire, which contained 0.1% Ag, in a manner similar to that described by Murch and Giauque,[10] except that type BT 3477 Formvar[11] varnish was used. At turn 280 from the bottom a single turn of No. 30 double silk covered copper wire was laid down and soldered into the continuous 503 turns of the thermometer. The total thermometer resistance was 287.3 ohms at 0°.

The previously standardized thermocouple, W-25, was compared to the triple (13.95°K.) and boiling (20.37°K.) points of hydrogen and the triple (63.14°K.) and boiling (77.33°K.) points of nitrogen. It was found to have values 0.10 and 0.12° high at the triple and boiling points, respectively, for hydrogen, and agreed exactly at the triple and boiling points of nitrogen. Appropriate corrections were applied. The temperature 0°C. was taken as 273.15°K. and 1 defined calorie was taken as 4.1840 absolute joules.

Preparation of Iodine Monochloride. Iodine monochloride was made by direct combination of Mallinckrodt iodine with chlorine. The iodine was stated to contain only 0.005% of Cl + Br and 0.01% of non-volatile material. The commercial grade 99.5% chlorine was purified by distillation in a low-temperature, vacuum-jacketed, silvered fractionating column, 180 cm. long, with a reflux ratio of 130:1 maintained by means of a capillary take-off tube and condensation in liquid nitrogen. The column was packed with glass

(7) W. F. Giauque and C. J. Egan, *J. Chem. Phys.*, **5**, 45 (1937).
(8) Union Carbide Stellite Co., Kokomo, Ind.
(9) Minnesota Mining and Manufacturing Co., St. Paul, Minn.
(10) L. E. Murch and W. F. Giauque, *J. Phys. Chem.*, **66**, 2052 (1962).
(11) Westinghouse Inc., Benolite Dept., Manor, Pa.

helices. The column condenser was cooled to about 195°K., with solid carbon dioxide in methylene chloride, which maintained a chlorine pressure of about 65 torr.

The direct combination was accomplished in a bath at 195°K. as recommended in *Inorganic Syntheses.*[12] A weighed amount of iodine was cooled to 195°K. and evacuated to 10^{-4} torr. A small excess of Cl_2 was added, and the excess was evaluated by a second weighing and matched by the final addition of the stoichiometric amount of iodine. An ICl sample weighing 1352 g. was made. The sample was purified by five successive fractional recrystallizations in a closed system. The amount was reduced to 600 g. as the temperature rose from 24.66° to near the melting point. Melting point measurements made later in the calorimeter indicated a liquid-soluble, solid-insoluble impurity of 0.010 mole %.

Analysis for the Cl:I mole ratio was performed by weighing approximately 2-g. samples of solid ICl in weighing bottles and then converting completely to the silver halide for reweighing. Conversion to the sodium halides was accomplished by immersing the weighing bottles in a filtered dilute solution of $NaBH_4$, kept at 0° to control the reaction rate with the solid ICl. Additional $NaBH_4$ was added slowly as needed to complete the reaction. A blank test showed that no halide was present in the sodium borohydride. Four samples gave the Cl:I mole ratio as 1.0014, 0.9985, 0.9997, and 0.9997, average 0.9998 ± 0.0012. It would have been more accurate to convert the ICl to I_3^- by means of aqueous KI solution followed by weight titration with aqueous $Na_2S_2O_3$ solution as was done in later measurements. However, we believe the recrystallization ensured a 1:1 ratio.

The sample placed in the calorimeter weighed 442.6630 g. (*in vacuo*) after correction for the amount adhering to the capillary used to introduce it. The molecular weight was taken as 162.3574; thus, the amount of sample was 2.72647 moles.

The Heat Capacity of Iodine Monochloride. The heat capacity measurements involved no unusual problems, except that the previously mentioned poor thermal conductivity of the Hastelloy calorimeter increased the length of the equilibrium periods after energy additions and, thus, increased the corrections for heat leak. The data are given in Table II. The measurements were continuous in the sense that intervals were not left between runs. The temperature increments can be inferred roughly from the separation of the mean temperatures. The correction for vaporization into the limited gas space was trivial because of the low vapor pressure.

Melting Point of Iodine Monochloride. The melting point of α-ICl was measured as a fraction, f, of the sample melted. A plot of T *vs.* $1/f$ gives a good straight line with the intercept of $1/f = 0$ at 300.53°K. The slope of the line indicates a liquid-soluble, solid-insoluble impurity of 0.010 mole %. This impurity is undoubtedly something other than nonstoichiometric chlorine or iodine since dissociation products of ICl

Table II: Heat Capacity of Iodine Monochloride[a,b]

T_{av}, °K.	C_{measd}	T_{av}, °K.	C_{measd}
17.71	1.91	134.23	10.66
19.24	2.18	142.55	10.55[c]
21.37	2.57	151.94	11.08
23.42	2.96	161.94	11.14
25.18	3.31	171.19	11.43
27.57	3.67	180.48	11.58
30.41	4.16	190.23	11.71
33.50	4.65	200.06	11.84
37.26	5.20	209.53	12.01
41.52	5.79	218.32	12.13
46.06	6.31	226.99	12.28
50.27	6.74	236.28	12.43
55.18	7.19	245.53	12.55
62.00	7.71	255.88	12.50[c]
69.06	8.26	266.91	12.60[d]
75.95	8.64	277.50	12.95[d]
82.27	8.93	287.22	13.13[d]
88.49	9.19	295.04	13.74[d]
95.62	9.45	Liquid	
102.46	9.72	303.68	24.63
109.66	9.96	310.45	24.69
117.60	10.20	317.76	24.61
125.82	10.53		

[a] 0°C. = 273.15°K., molecular weight = 162.3574, C in gibbs/mole, 1 gibbs = 1 defined cal./defined deg. [b] 442.6630 g. (*in vacuo*) = 2.72647 moles in calorimeter. [c] Measurements not used in drawing the smoothed curve. [d] ΔT values of last four runs on solid were 10.303, 9.620, 8.477, and 6.362° in order of increasing T.

Table III: Melting Point of Iodine Monochloride[a]

Fraction melted, f	Resistance thermometer T, °K.	Thermocouple T, °K.
0.089	300.446	300.44
0.195	300.491	300.51
0.351	300.506	300.51
0.507	300.514	300.50
(∞)	(300.527)	...

Accepted value = 300.53 ± 0.05°K.

[a] 0°C. = 273.15°K.

(12) *Inorg. Syn.*, **1**, 165 (1939).

should not give a straight line for T *vs.* $1/f$. No impurity eutectic melting was observed during the heat capacity measurements. The melting point details are given in Table III, where it may be noted that the relative temperature values as given by the gold resistance thermometer are precise to a much higher accuracy than can be claimed with respect to absolute temperature.

Table IV: Thermodynamic Properties of Iodine Monochloride[a,b]

T	$C_p°$	$S°$	$-(F° - H°_0)/T$	$(H° - H°_0)/T$
15	1.368	0.592	0.170	0.422
20	2.333	1.125	0.337	0.788
25	3.284	1.744	0.554	1.190
30	4.101	2.415	0.807	1.608
35	4.885	3.106	1.085	2.021
40	5.599	3.806	1.383	2.423
45	6.216	4.502	1.690	2.812
50	6.723	5.182	2.007	3.175
55	7.180	5.845	2.320	3.525
60	7.579	6.488	2.646	3.842
65	7.970	7.112	2.966	4.146
70	8.312	7.716	3.283	4.433
80	8.830	8.863	3.910	4.953
90	9.243	9.926	4.520	5.406
100	9.619	10.921	5.111	5.810
110	9.980	11.854	5.682	6.172
120	10.287	12.737	6.234	6.503
130	10.556	13.570	6.766	6.804
140	10.785	14.362	7.281	7.081
150	10.990	15.113	7.778	7.335
160	11.193	15.829	8.259	7.570
170	11.417	16.514	8.725	7.789
180	11.584	17.172	9.176	7.996
190	11.716	17.802	9.613	8.189
200	11.840	18.406	10.038	8.368
210	11.976	18.987	10.451	8.536
220	12.154	19.548	10.852	8.696
230	12.336	20.092	11.241	8.851
240	12.485	20.620	11.621	8.999
250	12.614	21.133	11.992	9.141
260	12.740	21.630	12.353	9.277
270	12.856	22.113	12.705	9.408
273.15	12.895	22.263	12.815	9.448
280	12.980	22.583	13.050	9.533
290	13.102	23.041	13.386	9.654
298.15	13.200	23.405	13.655	9.750
300	13.223	23.487	13.716	9.771
300.53	13.229	23.510	13.733	9.777
		Liquid		
300.53	24.588	32.738	13.733	19.005
310	24.695	33.503	14.325	19.178
320	24.561	34.285	14.937	19.348
322	24.501	34.439	15.058	19.381

[a] Solid was α crystalline form. [b] Units are gibbs/mole.

Heat of Fusion. As usual, the heat of fusion was measured by starting heat input somewhat below the melting point and ending somewhat above. Correction was made for any premelting which had occurred before each run started. During the measurement of a heat of fusion the last portion of the solid will be at the bottom of the calorimeter. To avoid excessive superheating of the liquid near the top of the calorimeter, heat was introduced by means of the lower section of the heater. However, a very small current was permitted to flow through the upper section so that a continuous record of its resistance and, thus, small change in the temperature were obtained. This was needed in order to evaluate the heat leak from this portion of the calorimeter surface during energy input. This procedure was especially indicated in the Hastelloy calorimeter because of the poor thermal conductivity. The $\int C_p dT$ corrections were made using the C_p values as listed in Table IV. The details are given in Table V.

Table V: Heat of Fusion of Iodine Monochloride[a]

	Run I	Run II	Run III
T_1, °K.	298.00	297.63	297.66
T_2, °K.	305.88	304.89	304.89
Total heat	2933.9	2916.0	2917.3
Premelting	3.5	2.9	3.1
$\int C_p(s)dT$	−33.5	−38.4	−38.0
$\int C_p(l)dT$	−131.8	−107.4	−107.4
ΔH_m	2772	2773	2775

Average value = 2773 ± 2 cal./mole.

[a] Units are cal./mole, m.p. = 300.53°K., 0°C. = 273.15°K.

The above data have been used to calculate the thermodynamic properties of solid and liquid ICl. The low temperature extrapolation of heat capacity was made on a C_p/T *vs.* T^2 plot. The results have been given in Table IV.

The Vapor Pressure of Iodine Monochloride. The vapor pressure of ICl was measured accurately over a short region above the melting point. Measurements were made with a mercury manometer using a series of capillaries and mixing bulbs with nitrogen gas as a buffer to protect the mercury. The series consisted of six mixing bulbs each with a volume of 12 cc. Before each measurement a stopcock in the line to the calorimeter was closed, and all the bulbs were evacuated. The three bulbs next to the manometer were then filled with the balancing pressure of nitrogen, and the three next to the calorimeter were opened to the

ICl. This not only prevented any remote possibility of diffusion of nitrogen into the ICl but also was designed to sweep any trace of inert gas out of the calorimeter. Since liquid ICl cannot evaporate at constant composition, the preceding procedure also ensured that only minor amounts were evaporated, and the composition should have remained at the stoichiometric ratio. To prevent condensation in the connecting lines, it was necessary to cover the apparatus with a plastic tent and raise the temperature sufficiently above that of the room. Thus, it was not practicable to extend the measurements to higher temperatures with this arrangement. A Société Genévoise cathetometer with a precision of 0.002 cm. was used as a comparison instrument with a standard meter bar. The usual corrections for capillary depression, temperature of the mercury and the meter bar, and the standard acceleration of gravity, 980.665 from the local 979.973 cm./sec.^{2}, were made. The observations are given in Table VI, where they are compared with the results of Cornog and Bauer[13,14] by means of an equation based on their results and derived by Greenwood.[4] Cornog and Bauer passed electrolytically generated hydrogen and oxygen over ICl. The amount corresponding to the partial pressure was obtained by absorption in soda lime and weighing. They made the incorrect assumption that the gas consisted only of undissociated ICl. While their data are probably the best previously available, their results over the liquid should have become increasingly low as they continued to remove a gas containing an appreciable excess of Cl_2, thus increasing the proportion of iodine in the remaining solution. Their lower values in Table VI are consistent with this.

Table VI: Vapor Pressure of Liquid Iodine Monochloride

T, °K.,	303.16	304.05	306.39
P, torr,	39.31	41.83	48.90 (this research)
P, torr,	38.90	40.83	46.29 (Cornog and Bauer[13])

Assuming that I_2 and ICl crystallize from their solutions as pure phases, Stortenbeker's[3] phase diagram and data indicate the following situations.

Below the I_2–ICl eutectic temperature, which Stortenbeker has given as 7.9°, a dynamic method should produce $I_2 + Cl_2$ in such small amounts that the I_2 could not condense as a solid, and the small pressures of I_2 and Cl_2 should be equal. This statement is based on a calculation using the free energy equation for the dissociation of ICl gas to be given later. Thus, within the limits of accuracy of the measurements of Cornog and Bauer, their total pressure below 7.9° should correspond to the partial pressure of ICl. However, their experimental sequence is not given, and it is possible that measurements at higher temperatures caused the accumulation of a considerable amount of iodine before the measurements below the eutectic were made. The results have been compared on both bases in Table VII. The partial pressure of ICl is taken from data to be given in a later section. The sublimation pressure of solid iodine is taken from Shirley and Giauque,[15] who combined their low temperature calorimetric data with the highly accurate vapor pressure measurements of Baxter, Hickey, and Holmes[16] and tables of $(F^\circ - H^\circ_0)T$ for $I_2(g)$ based on band spectra.

Table VII: Vapor Pressure of Solid Iodine Monochloride. Comparison with Data of Cornog and Bauer[13,14]

t, °C.	Total P, mm. (Cornog and Bauer)	Partial P, ICl (this research)	P, $I_2(s)$[a]	P, ICl + $I_2(s)$ (this research)
−15	1.2	0.939	0.006	0.945
−10	2.0	1.509	0.011	1.520
−7	3.1	2.380	0.018	2.398
0	4.6	3.689	0.031	3.720
5	6.8	5.623	0.050	5.673

[a] The correct P_{I_2} has been given; however, Cornog and Bauer, in effect, would have obtained $1.563P_{I_2}$ since they divided all weights by the molecular weight of ICl.

The reason for the higher pressures obtained by Cornog and Bauer is not apparent since the technique is somewhat similar to that used so accurately by Baxter, Hickey, and Holmes for I_2. If solid solutions are formed instead of pure phases, the pressures should be lower rather than higher than those calculated. Bauer[13] states that the data are averages with a maximum spread of 0.4 mm., and it seems probable that some undetected error must have entered. We see no reason why careful dynamic experiments on pure solid ICl in the range near 0° should not yield accurate values of P_{ICl} and ΔH°_0.

Between the eutectic temperature and the melting point of ICl, the vapor pressure measured by Cornog and Bauer should be determined by solid ICl in equilibrium with a liquid in which I_2 is saturated with ICl.

(13) J. Cornog and E. E. Bauer, *J. Am. Chem. Soc.*, 64, 2620 (1942).

(14) E. E. Bauer, Thesis, State University of Iowa, May 1942.

(15) D. A. Shirley and W. F. Giauque, *J. Am. Chem. Soc.*, 81, 4778 (1959).

(16) G. P. Baxter, C. H. Hickey, and W. C. Holmes, *ibid.*, 29, 127 (1907).

At the eutectic the pressure should be essentially that of ICl alone, and, as will be shown, the pressure of Cl_2 should gradually increase until it contributes about 5% of the total pressure at the melting point. There are insufficient data to calculate this sequence, but it is evident that the data of Cornog and Bauer are too high near the eutectic but do indicate the contribution of the Cl_2 to the total pressure, approximately, near the melting point.

Above the melting point, about the only statement which can be made is that a dynamic method will give pressures which will be increasingly lowered as evaporation proceeds; the iodine concentration of the liquid increases and the Cl_2 pressure is suppressed, an effect which has been noted in Table VI and which is accurately shown in Table VIII, to be given later.

Use of dP/dT as a measure of the heat of vaporization, as has been done by Cornog and Bauer and others, is not valid since the gas and liquid change in composition during vaporization. Thus, the heats of vaporization and sublimation given by Cornog and Bauer[13] are in error. This is shown by their value of the heat of fusion of ICl, obtained by difference as 1850 cal./mole, whereas the calorimetric result previously given is 2773 ± 2 cal./mole.

It should also be noted that dynamic measurements such as those of Cornog and Bauer assume a knowledge of the molecular constitution of the vapor. They absorbed weighed amounts of vapor and divided the weight by the molecular weight of ICl. As we shall show, the vapor is rich in chlorine, and the true vapor pressure cannot be computed from the dynamic results without an evaluation of the amounts of such species as Cl_2 and ICl_3, if present.

The Heat of Vaporization of Iodine Monochloride. Stortenbeker[2] has shown that the vapor in equilibrium with a liquid with the stoichiometric composition ICl contains a small amount of Cl_2. He made a rather inaccurate determination of the proportions in a series of experiments at 30° that varied from 0.8 to 7.6%, average 4.3% Cl_2.

The ICl-Cl_2 mixture in equilibrium with the liquid must contain an extremely small pressure of I_2, and essentially all of the I_2, corresponding to the Cl_2 formed, should remain in the residual liquid during the vaporization process. Thus, as vaporization continues, the proportions of ICl and Cl_2 in the vapor and the heat of vaporization should change. However, a series of such measurements, extrapolated back to the start of the first increment removed, should correspond to the heat of vaporization of equilibrium vapor from stoichiometric ICl liquid plus the heat of solution of the retained I_2.

The vapor pressure of ICl is almost the same as that of CH_3NO_2, and Jones and Giauque[17] found that the heat of vaporization of this substance could be readily measured by condensing it in a bulb cooled by liquid air, with the flow rate controlled by means of a capillary. A similar expedient was tried in the present case, but the exit tube always plugged with solid I_2 despite attempts to have most of the pressure drop in an outside capillary system which could be heated locally.

It was then decided to utilize the $(F^\circ - H^\circ_0)/T$ data based on the third law of thermodynamics along with the corresponding data, based on the band spectrum of ICl gas, to calculate the heat of the process of evaporating stoichiometric ICl liquid to give pure ICl gas. For this purpose it was necessary to determine the partial pressure of ICl over its liquid.

A 250-cc. glass bulb containing 183.0423 g. of ICl was immersed in a water thermostat held at 30.45°. The liquid was stirred gently by means of a magnetic stirrer as samples of vapor were withdrawn very slowly for analysis. The flow rate was controlled by means of a very fine capillary which started at the surface of the thermostat and was electrically heated throughout its entire length to prevent condensation of iodine. There was no appreciable pressure drop in the apparatus at thermostat temperature.

When the preceding arrangement was first tried, the observations were somewhat erratic, and it appeared that the heater used to prevent the deposition of I_2 in the capillary had heated some of the gas near the capillary entrance. The results indicated that some Cl_2 was diffusing back into the ICl. The addition of a train of two 0.07-mm. capillaries, each 1 cm. long and separated by a 1-cc. bulb just below the water surface of the thermostat, increased the gas flow rate sufficiently in the temperature gradient to prevent any back diffusion, while introducing a trivial pressure drop, and there was no further difficulty. The samples were condensed in bulbs cooled with liquid nitrogen or sometimes ice and weighed. Aqueous KI solution was then sucked into the air-free bulbs to convert all of the halogen to I_3^-. Titration with sodium thiosulfate in a weight buret evaluated the total halogen collected, and this with the weight enabled the Cl:I ratio in the gas to be calculated accurately. The results fall very accurately on a smooth curve through the experimental increments, and the interpolation on a weight basis due to the loss of the analysis in run III should cause no error.

(17) W. M. Jones and W. F. Giauque, *J. Am. Chem. Soc.*, 69, 983 (1947).

Table VIII: Composition of Vapor Evaporated from Liquid Iodine Chloride at 303.60°K.

Run	Wt. removed, g.	G.-atom of halogen removed	G.-atom of Cl removed	G.-atom of I removed	Atom ratio, r = Cl/I, in sample, av.	Halogen in remaining liq., moles	Excess I in remaining liq., g.-atom	r at end of run, from smooth curve
0	0				1.1048[a]	1.12741[b]	0	
1	4.8495	0.061418	0.032200	0.029218	1.1021	1.09670	0.002982	1.0991
2	5.4626	0.069045	0.036079	0.032966	1.0944	1.06218	0.006095	1.0899
3	5.0481	0.063633	0.033102	0.030531	1.0840[c]	1.03036	0.008666	1.0784
4	5.6222	0.070623	0.036524	0.034099	1.0711	0.99505	0.011091	1.0618
5	5.8026	0.072525	0.037191	0.035334	1.0526	0.95879	0.012948	1.0437

[a] Limiting value of r = Cl/I, over pure ICl, obtained by extrapolation. [b] Starting weight = 183.0423 g. = 1.12741 moles of ICl in a 250-cc. flask. [c] Analysis lost. Data accurately interpolated on weight basis for continuity.

Let $n_{Cl} + n_I = n$ = total gram-atoms of halogen in a collected sample.

$$35.453n_{Cl} + 126.904n_I = \text{weight of sample}$$

from which

$$n_{Cl} = \frac{126.904n - \text{weight}}{91.451} \quad (1)$$

$$n_I = \frac{\text{weight} - 35.453n}{91.451} \quad (2)$$

$$\frac{n_{Cl}}{n_I} = \frac{126.904n - \text{weight}}{\text{weight} - 35.453n} = \text{ratio } r \quad (3)$$

To obtain the partial pressures we have the relations

$$P = P_{ICl} + P_{Cl_2} + P_{I_2} \quad (4)$$

and

$$r = \frac{P_{ICl} + 2P_{Cl_2}}{P_{ICl} + 2P_{I_2}} \quad (5)$$

Combining eq. 4 and 5

$$P_{ICl} = \frac{2P}{r+1} - 2P_{I_2} \quad (6)$$

It will be shown later that P_{I_2} is trivial under the conditions of experiment; thus, the measured values of P and r at 303.60°K. determine the partial pressure of ICl.

The above equations accept the result of Stortenbeker[2] that ICl_3 is unstable in the gas phase. However, the evidence that ICl_3 molecules do not constitute a portion of the saturated vapor is not conclusive, and it is desirable to show that our result is accurate even if ICl_3 is present.

Assume

$$P = P_{ICl} + P_{Cl_2} + P_{ICl_3} + P_{I_2} \quad (7)$$

Then

$$r = \frac{P_{ICl} + 2P_{Cl_2} + 3P_{ICl_3}}{P_{ICl} + P_{ICl_3} + 2P_{I_2}} \quad (8)$$

Eliminating P_{ICl_3} from eq. 7 and 8

$$P_{ICl} = \frac{(3-r)}{2}P + \frac{(r-1)}{2}P_{Cl_2} - \frac{(r+3)}{2}P_{I_2} \quad (9)$$

If we make $P_{Cl_2} = 0$ as the most severe deviation from our assumption and introduce the experimental r = 1.1048, $P_{ICl} = 0.948P - 2.05P_{I_2}$, if all excess chlorine in the vapor is in ICl_3, instead of $P_{ICl} = 0.950P - 2.00\,P_{I_2}$ if all the excess chlorine is present as Cl_2.

The difference is trivial; thus, if a small fraction or all of the excess chlorine is present in the vapor as ICl_3, it will not appreciably affect the accuracy of our measured value of the ICl partial pressure.

The observations and results are given in Table VIII. Each removal of some 0.03 mole of halogen required about 24 hr. so that any lack of equilibrium between the liquid and gas phases is highly improbable.

In the last column of Table VIII values of r corresponding to the end of each run have been read from a smooth curve through the increments. These values have not been used in the present work but could be used in obtaining rather good estimates of the changing pressure of Cl_2 as a function of iodine concentration.

From the vapor pressure data in Table VI, the total pressure over stoichiometric liquid ICl at 303.60°K. is 40.54 torr. Combining this with the limiting value of r = 1.1048, P_{ICl} = 38.52 torr and P_{Cl_2} = 2.02 torr.

For the process

$$ICl(s)(l) = ICl(g) \quad (10)$$

$$\Delta F^\circ/T = R \ln (760/P) = \Delta(F^\circ - H^\circ_0)/T + \Delta H^\circ_0/T \quad (11)$$

Combining the $(F^\circ - H^\circ_0)/T$ data in Table IV with the $(F^\circ - H^\circ_0)/T$ data for ICl gas given by Evans, Munson, and Wagman,[18] we find for process 10

$$4.5758 \log (760/38.52) = -37.794 + \Delta H^\circ_0/303.60$$

from which $\Delta H^\circ_0 = 13{,}273$ cal./mole and $\Delta F^\circ_{298.15^\circ K.} = 1995$ cal./mole. Also

$$\Delta H^\circ_{298.15^\circ K.} = 298.15[\Delta(H^\circ - H^\circ_0)/298.15] + 13{,}273 \quad (12)$$

and using the same thermodynamic tables $\Delta H^\circ_{298.15^\circ K.} = -2.090 \times 298.15 + 13{,}273 = 12{,}650$ cal./mole for the solid. For the heat of vaporization of the liquid, which can easily be supercooled to 298.15°K.

$$\mathrm{ICl(l)} = \mathrm{ICl(g)} \quad (10)$$

$$\Delta H^\circ_{298.15^\circ K.} = \Delta H_{sub,198.15^\circ K.} - \Delta H_{m,300.53^\circ K.} + \Delta C_{p,fusion(300.53 - 298.15^\circ K.)} = 12{,}650 - 2773 + 11.360 \times 2.38 = 9904 \text{ cal./mole} \quad (13)$$

$$\Delta F^\circ_{298.15^\circ K.} = 1974 \text{ cal./mole}$$

The partial pressure of ICl(g) over solid and liquid ICl is obtained by substituting the several values of $\Delta(F^\circ - H^\circ_0)/T$ in eq. 11. A range of values is given in Table IX.

Table IX: The Partial Pressure of ICl over Stoichiometric ICl

T, °K.	P, torr	T, °K.	P, torr
250	0.42	300	29.96
260	1.12	300.53[a]	31.13
270	2.74	Liquid	
273.15	3.69	303.60	38.52
280	6.55	310	59.33
290	11.44	320	112.4
298.15	26.27	330	204.3

[a] Melting point.

The Equilibrium Decomposition of ICl. We have also re-examined the several data which have been used to obtain the free energy of the reaction

$$\mathrm{ICl(g)} = {}^1/_2\mathrm{Cl_2} + {}^1/_2\mathrm{I_2(g)} \quad (14)$$

McMorris and Yost[19] combined the reactions

$$\mathrm{NOCl} = \mathrm{NO} + {}^1/_2\mathrm{Cl_2} \quad (15)$$

and

$$\mathrm{NO} + \mathrm{ICl(g)} = \mathrm{NOCl} + {}^1/_2\mathrm{I_2(g)} \quad (16)$$

to give the net reaction (14).

Also, McMorris and Yost attempted to obtain the equilibrium in reaction 14 directly by assuming that they could use results of Gire,[20] who had studied the decomposition pressure of $BaPtCl_6$.

McMorris and Yost placed $BaPtCl_6$ with weighed amounts of solid I_2 in a reaction vessel of known volume and studied the total pressure at various temperatures on the assumption that $BaPtCl_6$ would give fixed and known partial pressures of Cl_2 corresponding to each temperature. This type of technique can fail badly if the decomposition produces microscopic particles of the solid product—in this case Pt. If a system has the mechanism for transporting material from microscopic particles, which have a high and variable free energy, to macroscopic phases, stable equilibrium may be obtained. In the preceding case the results scattered widely and can be given no weight.

In using the combination of reactions 15 and 16, McMorris and Yost made measurements on reaction 16 and at first combined these results with those given by Dixon[21] for reaction 15. Later, Beeson and Yost[22] remeasured the dissociation of NOCl in a very careful series of experiments, which included corrections for gas imperfection. Their interpretation of their data was handicapped by lack of accurate spectroscopic information and interpretation on NOCl, and the then necessary use of the slope of a log K *vs.* $1/T$ plot, a method which is correct in principle but lacking in discrimination and sensitivity and which often has led to incorrect results when small systematic errors have temperature trends. They gave the heat for reaction 15 as $\Delta H_{298^\circ K.} = 9030 \pm 100$ cal./mole. We find in a re-examination of their excellent experimental data, by the much more powerful point by point method, $\Delta H_{298^\circ K.} = 9211 \pm 10$ cal./mole.

The $(F^\circ - H^\circ_0)/T$ data for Cl_2 were obtained from Evans, Munson, and Wagman[18] and that for NOCl and NO from the "JANAF Thermochemical Tables."[23] A summary of the present analysis of the data for the three runs given by Beeson and Yost is given in Table X.

The seven observations of McMorris and Yost[19] for reaction 16 cover the range 410–452°K., and the equilibrium constant, K, at 452°K. has decreased to one-fifth of its value at 410°K. The reaction was described as "rapid and readily reversible." Values of $(H^\circ - H^\circ_0)/T$ and $(F^\circ - H^\circ_0)/T$ for ICl were taken

(18) W. H. Evans, T. R. Munson, and D. D. Wagman, *J. Res. Natl. Bur. Std.*, **55**, 147 (1955).

(19) J. McMorris and D. M. Yost, *J. Am. Chem. Soc.*, **54**, 2247 (1932).

(20) G. Gire, *Ann. chim.*, **4**, 186 (1925).

(21) J. K. Dixon, *Z. physik. Chem. Bodenstein Festband*, 679 (1931).

(22) C. M. Beeson and D. M. Yost, *J. Chem. Phys.*, **7**, 44 (1939).

(23) "JANAF Thermochemical Tables," Thermal Research Laboratory, Dow Chemical Co., Midland, Mich., NOCl, June 30, 1961; NO, June 30, 1963.

Table X: Analysis of Data of Beeson and Yost

$$NOCl = NO + {}^1/_2Cl_2{}^a$$

Run	Temp. range, T, °K.	No. of measurements	$\Delta H°_0$, mean av.	Dev. from mean
III	372–462	10	8628	±20
IV	373–472	11	8635	±11
V	373–491	13	8628	±8

Accepted $\Delta H°_0 = 8630 \pm 10$ cal./mole

$\Delta H°_{298.15°K.} = \Delta H°_0 + \Delta(H°_{298.15°K} - H°_0) = 8630 + 581 = 9211 \pm 10$ cal./mole

$\Delta F°_{298.15°K.} = 4897 \pm 10$ cal./mole

[a] Cal./mole of NOCl.

from Evans, Munson, and Wagman.[18] The values of $\Delta H°_0$ show a small trend at the three higher temperatures, and, on account of the considerable decrease in the value of K, we have accepted the four lower values which give $\Delta H°_0 = -5375 \pm 15$ (actual average ±13) cal./mole, $\Delta H°_{298.15°K.} = -5141 \pm 15$ cal./mole, and $\Delta F°_{298.15} = -1216 \pm 15$ cal./mole. Combining the data for reactions 15 and 16, $\Delta H°_0 = 3255 \pm 25$ cal./mole, $\Delta H°_{298.15°K.} = 3277 \pm 25$ cal./mole, $\Delta F°_{298.15°K.} = 3682 \pm 25$ cal./mole.

Evans, Munson, and Wagman[18] summarize the data and references for the spectroscopic dissociation limits of Cl_2, I_2, and ICl

$$I = {}^1/_2I_2 \qquad \Delta H°_0 = -28{,}540 \text{ cal./g. atom}$$

$$Cl = {}^1/_2Cl_2 \qquad \Delta H°_0 = -17{,}770 \text{ cal./g.-atom}$$

$$ICl = I + Cl \qquad \Delta H°_0 = 49{,}640 \text{ cal./mole}$$

from which

$$ICl(g) = {}^1/_2I_2(g) + {}^1/_2Cl_2 \qquad \Delta H°_0 = 3330 \text{ cal./mole}$$

McMorris and Yost[19] used a similar method to derive an earlier value $\Delta H°_0 = 3280$ cal./mole; however, while the extent of agreement is interesting, we believe that the value $\Delta H°_0 = 3255$ cal./mole, derived from the combined equilibrium measurements of McMorris and Yost[19] and Beeson and Yost,[22] should be accepted at full weight.

In order to check on our assumption that the partial pressure of I_2 over stoichiometric ICl is trivial, $\Delta F_{303.60°K.}$ is found to be 3689 cal./mole.

$$\frac{-R}{2} \ln K^2 = \frac{3689}{303.60} \qquad K^2 = \frac{[Cl_2][I_2]}{[ICl]^2} = 4.886 \times 10^{-6}$$

$[Cl_2] = 2.02$ torr and $[ICl] = 38.52$ torr at 303.60°K., from which the partial pressure of $I_2 = 3.59 \times 10^{-3}$ torr. The correction to the partial pressure of ICl derived from eq. 6 is less than 0.01 torr, and no readjustment of the calculations is necessary.

At this point it is of interest to make some very approximate calculations as to the extent of the dissociation in liquid ICl at 303.60°K.

Using the heat of fusion of I_2[24] as 3740 cal./mole at its melting point, 386.8°K., and estimating the ΔC_p of fusion as 1.5 cal./mole on the basis of those for Cl_2 (2.75) and Br_2 (2.0), we may write

$$I_2(s) = I_2(l) \tag{17}$$

$$\Delta H_m = 3160 + 1.5T \text{ cal./mole} \tag{18}$$

$$\frac{d \ln P_{(l)}/P_{(s)}}{dT} = \frac{-\Delta H_m}{RT^2} \tag{19}$$

from which $P_{I_2(l)} = 2.570 P_{I_2(s)}$ for supercooled liquid iodine at 303.60°K. From Shirley and Giauque,[15] $P_{I_2(s)} = 0.4843$ torr at 303.60°K., from which $P_{I_2(l)} = 1.245$ torr at 303.60°K.

Making the approximate assumption that Raoult's law holds for the whole range of composition in the halogen mixture $N_{I_2} \times 1.245 = 3.59 \times 10^{-3}$ torr and $N_{I_2} = 0.00288$ in liquid ICl at 303.60°K.

If we now assume an equal molal concentration of Cl_2, and combine this with the measured partial pressure of $Cl_2 = 2.02$ torr, a Raoult's law calculation gives $2.02/0.00288 = 701$ torr as the vapor pressure of liquid chlorine at 303.60°K. This is at least some eightfold too low and suggests that the dissolved chlorine is held largely as ICl_3, which is not improbable since ICl_3 exists as a solid when the concentration of Cl_2 is increased sufficiently.

We do not care to carry this kind of speculation further since the ideal of accurately determinable concentrations of specific molecular aggregates in liquids is usually unattainable. In the present case one must ask the question as to whether some of the chain structure in solid ICl does not persist into the liquid to complicate the ideal use of mole fractions. Moreover, the long-known electrical conductivity of ICl indicates some ionization. The evidence is summarized by Greenwood,[4] who quotes evidence by Fialkov and Kaganskaya[25] for the reaction $2ICl = I^+ + ICl_2^-$. Chlorine formed at the anode and iodine at the cathode would form ICl_3 and I_2, respectively.

The high heat capacity of liquid ICl is undoubtedly due to the increasing dissociation with increasing tem-

(24) "Selected Values of Thermodynamic Properties," U. S. National Bureau of Standards, Circular 500, U. S. Government Printing Office, Washington, D. C., 1952.

(25) Y. A. Fialkov and K. Y. Kaganskaya, *J. Gen. Chem. USSR*, 18, 289 (1948).

perature. The heat capacities of solid Cl_2 and ICl at their melting points are 13.27 and 13.23 gibbs/mole, respectively, whereas the corresponding values for the liquids are 16.03 and 24.59 gibbs/mole. Several additional useful relationships are given. Combining eq. 10 and 14

$$ICl(s) = {}^1/_2Cl_2 + {}^1/_2I_2(g) \quad (20)$$

$$\Delta H^\circ_0 = 16{,}528 \pm 25 \text{ cal./mole}$$

$$\Delta F^\circ_{298.15^\circ K.} = 5677 \pm 25 \text{ cal./mole}$$

and combining eq. 20 and 21

$$I_2(g) = I_2(s)^{15} \quad (21)$$

$$\Delta H^\circ_0 = -15{,}658 \text{ cal./mole}$$

$$\Delta F^\circ_{298.15^\circ K.} = -4628 \text{ cal./mole}$$

we find

$$ICl(s) = {}^1/_2Cl_2 + {}^1/_2I_2(s) \quad (22)$$

$$\Delta H^\circ_0 = 8699 \pm 25 \text{ cal./mole}$$

$$\Delta F^\circ_{298.15^\circ K.} = 3363 \pm 25 \text{ cal./mole}$$

and

$$ICl(l) = {}^1/_2Cl_2 + {}^1/_2I_2(s) \quad (23)$$

$$\Delta F^\circ_{298.15^\circ K.} = 3342 \pm 25 \text{ cal./mole}$$

Acknowledgment. We thank J. P. Chan, J. A. Duisman, and P. R. Siemens for assistance with the calorimetric measurements.

Surface Effects in the Uninhibited and the Inhibited Pyrolyses of Isomeric Hexanes. IV. 2,3-Dimethylbutane (Diisopropyl)

by J. Chrysochoos[1a] and W. A. Bryce[1b]

Department of Chemistry, University of British Columbia, Vancouver 8, British Columbia, Canada
(Received March 2, 1965)

The rates of pyrolysis of diisopropyl decrease with increasing S/V ratio in the pressure range 10–100 mm. at 500–520°. Hydrogen is formed in significant amounts and its main source is assumed to be the isopropyl radicals. The chain length of the decomposition is sufficiently large because the termination reaction, $CH_3 + CH_3 \rightarrow C_2H_6$, participates very slightly by contributing less than 0.2% to the total amount of the products. Nitric oxide inhibits the decomposition to about 75% and affects the product distribution slightly. The simultaneous increase in the yields of C_3H_6 and CH_4 with increasing NO pressure can be accounted for by the reactions $i\text{-}C_3H_7 + NO \rightarrow C_3H_6 + HNO$; $CH_3 + HNO \rightarrow CH_4 + NO$. The inhibitor appears to function in both phases.

Introduction

Very few investigations have been done so far concerning the uninhibited and the fully inhibited decomposition of higher hydrocarbons. Peard, *et al.*,[2] have investigated the nitric oxide inhibited decomposition of diisopropyl but their interests were focused on the apparent chain lengths. The nature of inhibition, by nitric oxide, in the decomposition of organic compounds has not been clarified completely as yet in spite of the great deal of investigations made. In the early theories of Hobbs and Hinshelwood[3,4] on the thermal decomposition of ethane and propane, nitric oxide was assumed to function by capturing the chain propagating radical, reducing inevitably the rate of the decomposition. Recently, the inhibitor has been associated with both initiation and termination processes.[5–8]

The inhibitor was also assumed to capture β- or μ-radicals and to be regenerated from the bound states (βI) and (μI).[9] The rate expressions so derived were in good agreement with experimental results obtained by others.[10] The phenomenon of inhibition was considered in all above theories as a fully homogeneous process.

Voevodsky[11] assumed that inhibition is fully heterogeneous. Surface effects have been found in the case of isopentane,[12] *n*-hexane, 2-methylpentane, and 3-methylpentane.[13]

A thorough investigation of the isomeric hexanes with respect to the effect of S/V ratio and NO on both reaction rates and product distribution has been carried out. The details of the decomposition of diisopropyl are described here.

Experimental

The diisopropyl used was research grade (99.91%) obtained from the Phillips Petroleum Co., Bartlesville, Okla. It was subjected to repeated trap-to-trap

(1) (a) Department of Chemistry, Harvard University, Cambridge, Mass. 02138. (b) The premature death of Professor Bryce has deprived kineticists of an able scientist and his colleagues of a trusted friend.

(2) M. G. Peard, F. J. Stubbs, and C. N. Hinshelwood, *Proc. Roy. Soc.* (London), **A214**, 339 (1952).

(3) J. E. Hobbs and C. N. Hinshelwood, *ibid.*, **A167**, 439 (1938).

(4) J. E. Hobbs and C. N. Hinshelwood, *ibid.*, **A167**, 447 (1938).

(5) B. W. Wojciechowski and K. J. Laidler, *Can. J. Chem.*, **38**, 1027 (1960).

(6) K. J. Laidler, N. H. Sagert, and B. W. Wojciechowski, *Proc. Roy. Soc.* (London), **A276**, 254 (1962).

(7) N. H. Sagert and K. J. Laidler, *Can. J. Chem.*, **41**, 838 (1963).

(8) N. H. Sagert and K. J. Laidler, *ibid.*, **41**, 848 (1963).

(9) T. Ree, K. Yang, and H. Eyring, *Trans. Faraday Soc.*, **58**, 2375 (1962).

(10) F. J. Stubbs and C. N. Hinshelwood, *Proc. Roy. Soc.* (London), **A200**, 458 (1950).

(11) V. V. Voevodsky, *Trans. Faraday Soc.*, **55**, 65 (1959).

(12) W. A. Bryce and J. Chrysochoos, *ibid.*, **59**, 1842 (1963).

(13) Parts I–III, J. Chrysochoos and W. A. Bryce, *Can. J. Chem.*, in press.

distillation at −196 and −78°. No impurities could be detected by conventional gas chromatographic techniques. The nitric oxide (99%), supplied by the Matheson Company, East Rutherford, N. J., was further purified by repeated trap-to-trap distillations. The absence of NO_2 in the purified NO was confirmed by infrared spectroscopy.

The pyrolyses were done in a conventional static system. For all of the inhibited and some of the uninhibited pyrolyses, a 300-ml. quartz reaction vessel, held in an insulated brass block furnace, was used in which the temperature could be controlled to within 1° at 500°. Packing of the vessel was done with fire-polished quartz tubes.

For some of the uninhibited pyrolyses, two 160-ml. quartz reaction vessels, one packed with fire-polished quartz and the other unpacked, were placed in a well-insulated double furnace. The increase in pressure due to decomposition was recorded for each vessel under otherwise identical conditions with a sensitive pressure transducer (9 mm. recorder response per mm. of mercury pressure).

Manometric initial rates were obtained throughout the study after establishing a 0.93:1 correspondence between the initial rates so obtained and those found from the disappearance of diisopropyl by direct analysis.

Results

Analytical balances were obtained by gas chromatographic techniques supplemented by infrared analyses. Two typical sets of results are given in Tables I and II.

Table I: Analytical Results (mole %) for the Decomposition of Diisopropyl (T = 520°; $\Delta P/P_i$ = 0.20)

Products	P_i = 100 mm.	P_i = 80 mm.	P_i = 60 mm.
CH_4	11.0	8.9	9.5
C_3H_8	1.0	0.9	0.4
C_3H_6	6.4	7.1	6.7
i-C_4H_8	2.0 ?	0.9	1.0
2-Methylbutene-2	8.0	11.0	10.6
H_2	5.0	4.5	4.0
C_2H_6	Trace (0.1)	Trace	Trace
C_2H_4	Trace	Trace	Trace
Diisopropyl	66.0	66.0	67.5
Total	99.4	99.3	99.7

The effect of an 11-fold increase in the S/V ratio on the reaction rates and the product distribution is less marked than in the case of the less-branched isomeric hexanes.[13] The reaction rates are slightly lower in the packed vessel and this reduction in rate due to the packing, which is approximately 25–30% for diisopropyl pressures around 10 mm., becomes vanishingly small at diisopropyl pressures around 100 mm. (Figure 1). The increased S/V ratio affects very slightly the ratio C_3H_6/C_3H_8 but it has no definite effect on the ratios C_3H_6/i-C_4H_8 and H_2/CH_4. Some results are given in Table III.

Table II: Analytical Results (mole %) for Various NO Pressures in the Inhibited Decomposition of Diisopropyl (T = 520°; $\Delta P/P_i$ = 0.25; P_i = 100 mm.)

Products	NO pressure, mm. 0	5	10	15
CH_4	13.0	14.0	14.0	15.0
C_3H_8	1.3	1.2	1.3	1.1
C_3H_6	6.6	7.5	8.2	7.8
i-C_4H_8	0.3	0.4	0.8	0.8
2-Methylbutene-2	7.0	6.2	6.4	7.7
H_2	4.5	4.3	4.7	4.6
Diisopropyl	67.0	66.0	63.5	61.0
Total	99.7	99.6	98.9	98.0

Activation energies and frequency factors were calculated from the Arrhenius equation using rate con-

Table III: Variation of the Product Distribution with Diisopropyl Pressure in the Packed and the Unpacked Vessels (T = 520°; $\Delta P/P_i$ = 0.20)

Press., mm.	C_3H_6/C_3H_8 Unpacked	C_3H_6/C_3H_8 Packed	C_3H_6/i-C_4H_8 Unpacked	C_3H_6/i-C_4H_8 Packed	H_2/CH_4 Unpacked	H_2/CH_4 Packed
50	...	...	...	...	0.47	0.48
60	5.4	4.9	9.6	9.4	0.48	0.50
70	5.8	5.2	9.2	9.0	0.48	0.50
80	5.4	4.9	8.2	9.1	0.48	0.46
90	4.0	3.7	...	...	0.48	0.47
100	5.0	4.7	9.2	9.0	0.46	0.45
120	4.4	4.1	8.6	8.0	...	...

Table IV: Variation of Activation Energy and Frequency Factors with Initial Pressure of Diisopropyl

P_i, mm.	E_A, kcal./mole	A, sec.$^{-1}$
0–30	51.5 ± 2.5	1.7×10^{11}
30–50	51.0 ± 5	4.2×10^{11}
50–80	48.0 ± 5	1.4×10^{10}
80–100	48.0 ± 4	1.1×10^{10}
100–130	47.5 ± 5	1.1×10^{10}
130–150	47.5 ± 5	6.4×10^{9}

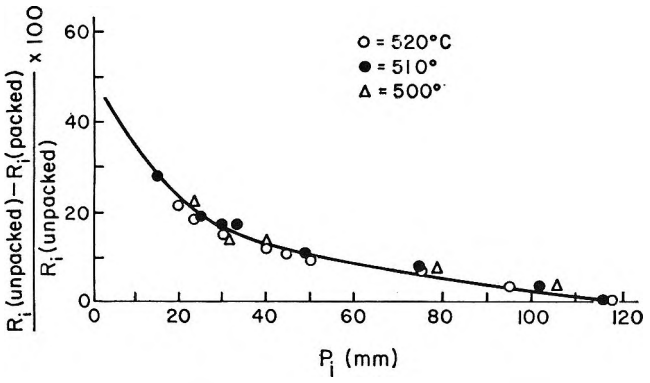

Figure 1. Percentage reduction in rate due to packing for various initial pressures of diisopropyl.

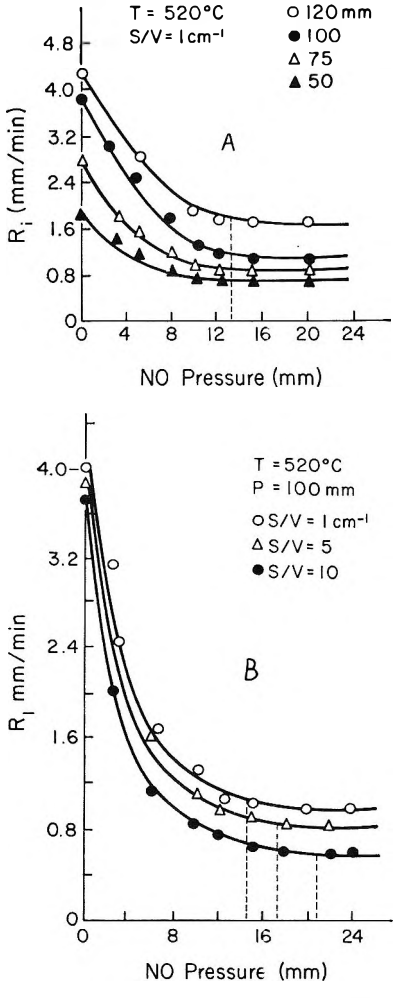

Figure 2. Dependence of the initial rate on NO pressure in (A) the unpacked and (B) the packed vessels for diisopropyl.

stants obtained at 490, 500, 510, and 520°. Average values of six determinations are given in Table IV.

Nitric oxide reduces the rate of decomposition of

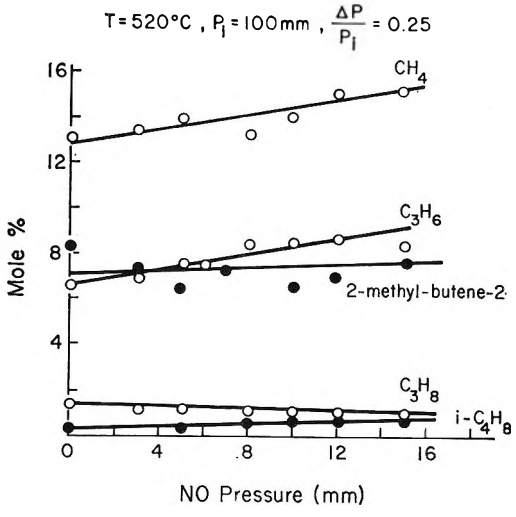

Figure 3. Variation of the product distribution with NO pressure for diisopropyl.

diisopropyl to approximately 75%. The reduction in rate is more gradual than in the case of the less-branched isomeric hexanes.[13] The nitric oxide pressure required for maximum inhibition is approximately the same, namely 12–14 mm., for the diisopropyl pressure ranging from 50 to 120 mm. (Figure 2a) and shifts to slightly higher values for higher S/V ratios (Figure 2b). Nitric oxide affects the product distribution slightly. The yields of CH_4 and C_3H_6 increase and the yield of C_3H_8 decreases very slightly with increasing NO pressure. So far as the yield of 2-methylbutene-2 is concerned, there is too much scatter in the results to decide whether it decreases or not with increasing NO pressure (Figure 3).

The S/V ratio has little effect on the product distribution. A higher S/V ratio appears to favor slightly the formation of C_3H_8 in both the uninhibited and the inhibited pyrolyses (Figure 4).

Discussion

The products of the uninhibited pyrolysis of diisopropyl can be accounted for by the mechanism

$$(CH_3)_2CHCH(CH_3)_2 \longrightarrow CH_3 + (CH_3)_2CHCHCH_3 \quad (1a)$$

$$\longrightarrow 2(i\text{-}C_3H_7) \quad (1b)$$

$$CH_3 + (CH_3)_2CHCH(CH_3)_2 \longrightarrow CH_4 + (CH_3)_2CCH(CH_3)_2 \quad (2a)$$

$$\longrightarrow CH_4 + (CH_3)_2CHCH(CH_3)CH_2 \quad (2b)$$

$$i\text{-}C_3H_7 + (CH_3)_2CHCH(CH_3)_2 \longrightarrow C_3H_8 + \text{diisopropyl radicals} \quad (3a, 3b)$$

$$H + (CH_3)_2CHCH(CH_3)_2 \longrightarrow H_2 + \text{diisopropyl radicals} \quad (4a, 4b)$$

diisopropyl radicals $\longrightarrow$

$$CH_3 + (CH_3)_2C{=}CHCH_3 \quad (5)$$

$$\longrightarrow i\text{-}C_3H_7 + C_3H_6 \quad (6)$$

$$(CH_3)_2CHCHCH_3 \longrightarrow CH_3 + (CH_3)_2C{=}CH_2 \quad (7)$$

$$\longrightarrow C_2H_5 + C_3H_6 \quad (8)$$

$$i\text{-}C_3H_7 \longrightarrow H + C_3H_6 \quad (9)$$

$$\longrightarrow CH_3 + C_2H_4 \quad (10)$$

$$CH_3 + CH_3 \longrightarrow C_2H_6 \quad (11)$$

Ethane and ethylene were found only in traces. This indicates that reaction 11 participates to a very slight extent. In other words, the chain length of the decomposition should be large, as it is revealed from the ratio CH_4/C_2H_6 obtained from Table I. The ratio increases with increasing diisopropyl pressure. The yield of i-C_4H_8 which is directly related to the initiation process, reactions 1a and 7, is very low, confirming the conclusion that the chain length is large and it accounts for the decomposition products almost completely.

The relative probabilities of reactions 7 and 8 have been discussed by Kossiakoff and Rice.[14] By using a very rough approximation, they predicted that $k_8 = 4k_7$. From the study of the decomposition of isomeric pentanes it was found[15] that reaction 8 is about twice as fast as reaction 7. The amount of i-C_4H_8 formed is about 0.5% (Tables I and II). Therefore, about 1% of propylene is expected to be produced through reaction 8. The total amount of propylene is about 7% (Table I), so approximately 6% of it is expected to be formed through reactions 6 and 9. If reaction 9 is the only source of H atoms and if the chain is long enough to neglect any loss of H atoms through recombination or any contribution from the initiation processes to the products, then the yield of H_2 will be proportional to the concentration of H atoms. From reactions 6 and 9 it is obvious that the formation of one H atom will be accompanied by the formation of two C_3H_6 molecules provided that reaction 10 participates very slightly as it is further discussed. Therefore, one might expect that the ratio H_2/C_3H_6 will be approximately $^1/_2$.

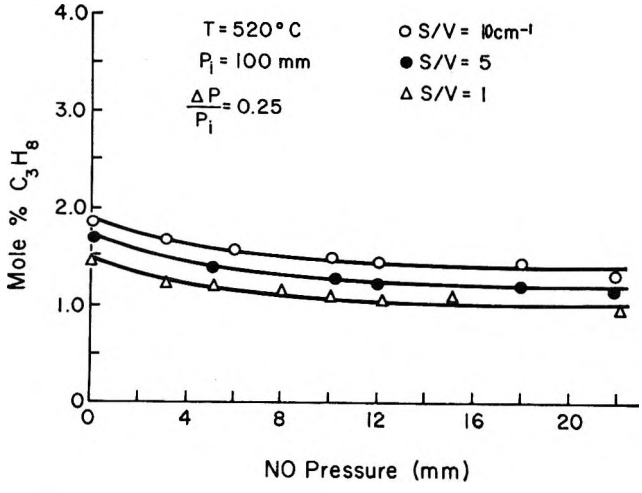

Figure 4. Variation of the C_3H_8 yield with NO pressure and S/V ratio for diisopropyl.

The yield of H_2 is less than 6% (Table I) but its correspondence to the yield of C_3H_6 is not 1:2. Therefore, some other radicals like $(CH_3)_2CHCHCH_3$ and C_2H_5 may participate in the formation of H atoms to a minor extent.

Methyl and isopropyl radicals are the main chain-propagating radicals. The yield of C_3H_8, however, is very small. Therefore reactions 3a and 3b participate to a lesser extent. Isopropyl radicals undergo further decomposition

$$i\text{-}C_3H_7 \longrightarrow H + C_3H_6 \quad (9)$$

$$\longrightarrow CH_3 + C_2H_4 \quad (10)$$

It was found that at about 500° and up[16]

$$k_{10}/k_9 \leq 0.07; \quad k_9 \geq 14k_{10}$$

Since the only source of C_2H_4 is reaction 10 the ratio C_2H_4/C_3H_6 will be approximately 0.07 from reactions 9 and 10. However, reaction 9 is not the only source for the formation of propylene but it yields about half of the amount of C_3H_6 formed, the other half being formed through reaction 6. According to the discussion above 6% of C_3H_6 is formed through reactions 6 and 9 and therefore about 3% of C_3H_6 is formed through reaction 9. Thus from the ratio $C_2H_4/C_3H_6 \simeq 0.07$ we expect that the yield of C_2H_4, if any, will be about 0.2%.

The energy of activation appears to be low. It can be mainly attributed to the low D(C–C) value for diisopropyl[17]

$$D(CH_3)_2CH{-}CH(CH_3)_2 = 66.5 \text{ kcal.}$$

(14) A. Kossiakoff and F. O. Rice, *J. Am. Chem. Soc.*, **65**, 590 (1943).

(15) J. Chrysochoos, M.Sc. Thesis, University of British Columbia, 1962.

(16) W. M. Jackson and J. R. McNesby, *J. Chem. Phys.*, **36**, 2272 (1962).

(17) M. Szwarc, *Chem. Rev.*, **47**, 75 (1950).

and the long chain length. Both kinetic parameters are decreasing with increasing diisopropyl pressure tending to more or less constant values at higher diisopropyl pressures. This can be attributed to the participation of the propagation process to a higher extent as the diisopropyl pressure increases. At very low pressures the activation energy is governed predominantly by the activation energy of the initiation process.

The surface-to-volume ratio has no effect on the propagation processes. The ratios $C_3H_6/i\text{-}C_4H_8$ and H_2/CH_4 are not affected by an increase in S/V ratio. The spontaneous decomposition of large radicals is too rapid to be affected by the surface. However, as the required activation energy for a process is increasing, the effect of the surface becomes more significant. Chemisorbed molecules on the walls of the reaction vessel would require less energy to dissociate than a molecule in the gas phase because of the weakening of the various bonds due to the chemisorption.

The termination processes are also affected by the surface. Radicals chemisorbed on the walls of the reaction vessel have more chance for recombination than in the gas phase. Therefore the effect of the surface on the thermal decomposition of organic compounds can be expressed as

$$\text{net effect} = \text{effect on initiation} - \text{effect on termination}$$

In the case of diisopropyl, the second term predominates so that a reduction in the rates is observed for the packed vessel. Similar effects were found in the less branched isomeric hexanes[13] while in the case of isopentane an increase in the rates was observed[12] for the packed vessel. In the latter case a relatively low temperature was used, 490°. One might expect that the effect of surface on the initiation processes will gain significance at lower temperatures because both the rate of decomposition and the rate of desorption from the walls of the reaction vessel will decrease with decreasing temperature. Therefore, the effect of S/V ratio on the initiation processes might be more marked. However, this explanation cannot be considered as completely unambiguous.

The nitric oxide required for maximum inhibition appears to be independent of the partial pressure of diisopropyl. If the role of NO is (at least in part) heterogeneous, the NO pressure required for maximum inhibition must be related to the conditions of the decomposition more than to the hydrocarbon itself. In such a case, NO may function by suppressing the heterogeneous initiation, thus causing a reduction in the rate. An equilibrium established between adsorbed and desorbed NO molecules will depend on the number of active sites of the surface. If the limiting rate of the decomposition, which is not affected by NO any more, is related to such an equilibrium, then the NO pressure required for maximum inhibition will depend partially on the S/V ratio. A slight shift to higher values has been observed in this NO pressure for increased S/V ratio as can be seen in Figure 2b.

Nitric oxide functions also homogeneously, as is revealed by its effect on the product distribution. The simultaneous increase in the yield of C_3H_6 and slight decrease in the yield of C_3H_8 with increasing NO pressure can be attributed to the set of competitive reactions

$$i\text{-}C_3H_7 + NO \longrightarrow C_3H_6 + HNO \qquad (12)$$

$$i\text{-}C_3H_7 + RH \longrightarrow C_3H_8 + R \qquad (3a, 3b)$$

Reaction 12 is exothermic by about 4 kcal./mole based on the values $D(H\text{–}NO) = 48.6$ kcal./mole[18,19] and $D(i\text{-}C_3H_6\text{–}H) = 45$ kcal/mole.[20]

The role of HNO is not known, but its relatively high stability[21] indicates that it may participate in such reactions as

$$CH_3 + HNO \longrightarrow CH_4 + NO \qquad (13)$$

which may account for the increase in the yield of CH_4 with increasing NO pressure.

At higher S/V ratios, more NO molecules will be kept adsorbed on the surface after an equilibrium is established between adsorption and desorption. Therefore, reactions 3a and 3b will gain somewhat over reaction 12. No effect of the surface is observed on the yield of C_3H_6 because it may be very small compared to the total yield of C_3H_6. However, some effect of the surface on the yield of C_3H_8 is observed since such an effect is comparable to the total yield of C_3H_8. The formation of C_3H_8 is favored slightly by increased S/V ratio.

Nitric oxide was recovered completely for pressures up to 5 mm., but some consumption up to 20% was found for higher NO pressures. This indicates that NO may also participate in such reactions as

$$R + NO \longrightarrow RNO \longrightarrow \text{oxime} \longrightarrow \text{further decompositions} \qquad (14)$$

(18) M. A. A. Clyne and B. A. Thrush, *Trans. Faraday Soc.*, **57**, 1305 (1961).

(19) M. A. A. Clyne and B. A. Thrush, *Discussions Faraday Soc.*, **33**, 139 (1962).

(20) M. Szwarc, *ibid.*, **10**, 143 (1951).

(21) F. W. Dalby, *Can. J. Phys.*, **36**, 1336 (1958).

Nitrogen-containing products were not detected, perhaps because of the analytical method used. However, in a system of CH_3 and NO, products like HCN, H_2O, NH_3, CO, N_2, CO_2, and CH_3CN were detected by mass spectrometry.[22]

Acknowledgment. We are grateful to the National Research Council and to the Petroleum Research Fund of the American Chemical Society for financial support. We are also greatly indebted to Dr. G. B. Porter for many valuable discussions.

(22) W. A. Bryce and K. U. Ingold, *J. Chem. Phys.*, **23**, 1968 (1955).

NOTES

Structure of Aluminum Cations in Aqueous Solutions

by J. J. Fripiat, F. Van Cauwelaert, and H. Bosmans

Laboratoire de Chimie Minérale, Institut Agronomique de l'Université de Louvain, Héverlé-Louvain, Belgium
(Received November 30, 1964)

Structural data on polynuclear complexes in solution may be obtained from potentiometric and spectroscopic methods. Theoretical treatment developed by Sillén leads to the calculation of average condensation degrees $\bar{p}$ and $\bar{q}$ for A_pB_q complexes.[1] Moreover, if parallel curves $Z(\log [A])_B$ are obtained, Sillén has shown that these complexes have the structure $B(A_tB)_n$ where t and n may be derived according to different hypotheses.[2,3] Z is the average number of OH^- bound to aluminum. (See Figure 1.)

The attenuated total reflectance technique developed by Fahrenfort[4,5] makes possible observation of the infrared spectrum of an ion in solution since the strong absorption bands due to the solvent are weakened materially. The method has been applied already by Katlafsky and Keller[6] to several inorganic and organic salts. Unfortunately, the concentration ranges in which the potentiometric and the spectroscopic methods are applicable do not overlap. Observing the infrared spectra of hydration shells of polynuclear aluminum cations requires concentrations not lower than 0.5 F, while titration techniques cannot be successfully applied to concentrations in aluminum cations higher than 0.05 F. Spectroscopic data obtained in 2, 1, and 0.5 F Al^{3+} solutions, however, did not show any noticeable modifications in vibration frequencies but indicated a progressive decrease of the band intensities. It will be therefore tentatively assumed that conclusions deduced from spectroscopy in the concentration 0.5 F may be extrapolated to more dilute solutions.

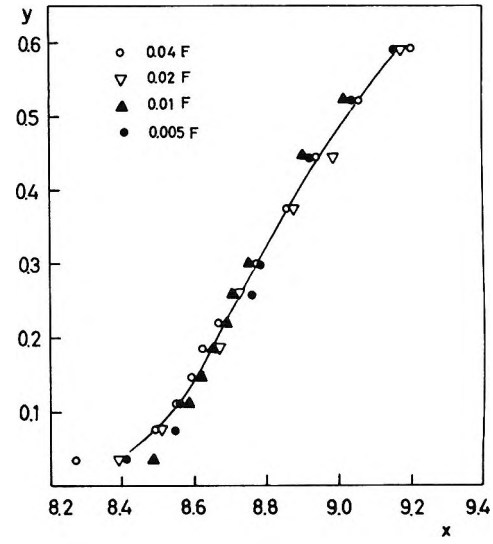

Figure 1. The best theoretical curve Y of X overlapping the experimental points y and x. $y = Z/t$ and $x = -t \log h + \log B$, Z being the average number of OH^- bound to aluminum, B, the total concentration in Al, h, the free concentration in H^+, in accordance with Sillén symbols.

(1) L. G. Sillén, *Acta Chem. Scand.*, **15**, 1981 (1961).
(2) L. G. Sillén, *ibid.*, **8**, 299 (1954).
(3) L. G. Sillén, *ibid.*, **8**, 318 (1954).
(4) J. Fahrenfort, *Spectrochim. Acta*, **17**, 698 (1961).
(5) J. Fahrenfort and W. M. Visser, *ibid.*, **18**, 1103 (1962).
(6) B. Katlafsky and R. Keller, *Anal. Chem.*, **35**, 1665 (1963).

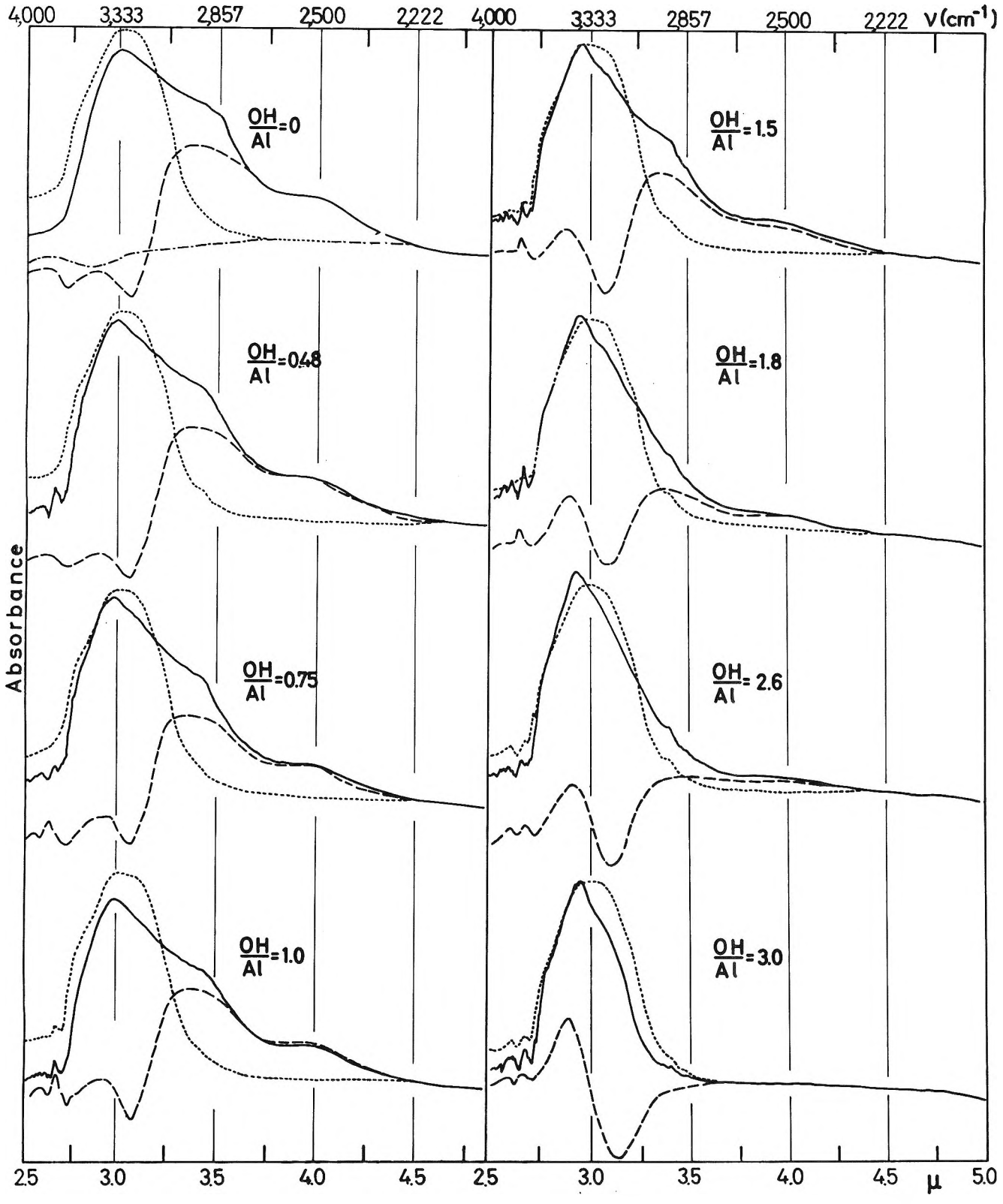

Figure 2. Infrared spectra observed upon progressive neutralization of 1.75 *F* $AlBr_3$ solutions at 30°: OH/Al, hydroxyls added to aluminum present in solution; ···, reference spectrum of water; —, spectrum obtained with a single A.T.R. unit; ---, differential spectrum observed with two A.T.R. units, one of these filled with water and placed in the reference beam; —, differential tracing observed with two A.T.R. units filled with water.

Potentiometric Titrations

Titration curves were performed at 30 and 40° by mixing suitable volumes of $Al(NO_3)_3$ and NaOH solutions in 2 F $NaNO_3$. The pH values were obtained after 48 hr. or more to ensure that equilibrium conditions had been reached. The concentration range between 1.25×10^{-3} and 4×10^{-2} F was covered within six different dilutions of $Al(NO_3)_3$. The average condensation degrees $\bar{p}$ and $\bar{q}$ showed a variation from 4 to 7 with increasing Z. Since parallel curves were obtained, Sillén's $B(A_tB)_n$ treatment may be applied. Hypothesis III $C^{2,3}$ was found to give the best fit between experimental and theoretical data for $t = 2.7$ and $k_0 = 0.008$ at 30° and $k_0 = 0.001$ at 40°. This hypothesis applies for an unlimited polymerization mechanism for the formation of $Al[(OH)_8Al_3]_n^{4+}$ complexes as

$$4Al^{3+} + 8H_2O \rightleftharpoons Al_4(OH)_8^{4+} + 8H^+$$

$$7Al^{3+} + 16H_2O \rightleftharpoons Al_7(OH)_{16}^{5+} + 16H^+$$

More details will be published elsewhere. Calculations by Brosset, Biedermann, and Sillén[7] on data published previously by Brosset[8] had suggested the formation of $Al_6(OH)_{15}^{3+}$ to be the most likely.

Infrared Spectra

Infrared spectra were recorded from 2 to 4.5 μ by using one or two Connecticut Instrument A.T.R. units fitted with KRS5 prisms and the Beckman IR4 equipped with a CaF_2 monochromator. $AlBr_3$, $AlCl_3$, and $Al(NO_3)_3$ solutions in the concentration range from 0.75 to 1.755 F were compared at several neutralization degrees obtained by adding NaOH.

The operation was performed either with a single A.T.R. unit containing one of these solutions or with a second one containing the solvent and placed in the reference beam. The results obtained with $AlBr_3$ solutions are reported in Figure 2. The spectra recorded with only one A.T.R. unit showed an important broadening of the OH stretching band and the formation of low frequency, diffuse side bands. In the spectra recorded by using two A.T.R. units, three absorption bands at 3480 cm.$^{-1}$ (2.88 μ), 2965 cm.$^{-1}$ (3.375 μ), and 2530 cm.$^{-1}$ (3.95 μ) are clearly observed. On progressive neutralization, the intensity of the 3480-cm.$^{-1}$ band increases while the 2965- and 2530-cm.$^{-1}$ bands fade correspondingly.

It was verified experimentally that the nature of the anion did not influence noticeably either the positions nor the intensities of these bands. For OH:Al ratios higher than 2, the width of the OH stretching band observed with one A.T.R. unit was narrower than the corresponding band for water. According to Hornig and Busing,[9] this effect arises from the influence of alkali and halogen ions on the structure of water and especially on the low frequency H_2O Raman band observed at 3225 cm.$^{-1}$.

Discussion

In hexahydrated octahedral aluminum cations, Jackson[10] considers the electrical charge as being equally distributed on the six water molecules. Consequently, each hydrogen atom brings an electrical positive charge of 0.25. In hydronium this charge is 0.33 so that the hydrated aluminum cation might be described as a hexahydronium cation in which the ligands are octahedrally coordinated. In hydrated polynuclear structures a similar situation exists as shown schematically in Figure 3. Additional water molecules belonging to a secondary hydration shell are probably strongly hydrogen bonded to each "hydronium." At least three different OH stretching vibrations should characterize such a structure, corresponding with the three kinds of OH (a, b, c) indicated in Figure 3. The high-frequency band observed at 3480 cm.$^{-1}$ (2.88 μ) is probably due to the OH directly bound to the aluminum (a species) since (1) the complex OH stretching band of Bayerite appears between 2.83 and 2.90 μ with a maximum located around 2.86 μ and (2) the intensity of this band reinforces on increasing OH:Al ratios.

The medium-frequency band observed at 2965 cm.$^{-1}$ is attributed to the $O-H^{+0.25}$ stretching vibration (b species) for two reasons: (1) the intensity of this band decreases with the progress of the neutralization and (2) the stretching (ν_3, E) of H_3O^+ appears in solution at 2900 cm.$^{-1}$ according to Falcq and Giguère.[11]

The low-frequency band at 2530 cm.$^{-1}$ would then be attributed to the c species, *i.e.*, the water molecules strongly hydrogen bonded to hydronium. According to the plots of OH stretching frequency shifts with respect to $O-H\cdots O$ oxygen distance as proposed by Lippincott and Schroeder[12] or by Nakamoto, Margosches, and Rundle,[13] a band at 2530 cm.$^{-1}$ should

(7) C. Brosset, G. Biedermann, and L. G. Sillén, *Acta Chem. Scand.*, **8**, 1917 (1954).

(8) C. Brosset, *ibid.*, **6**, 910 (1952).

(9) W. R. Busing and D. F. Hornig, *J. Phys. Chem.*, **65**, 284 (1961).

(10) M. L. Jackson, Transactions of the 7th Congress of the International Soil Science Society, Vol. 2, 1961, p. 445.

(11) M. Falcq and P. A. Giguère, *Can. J. Chem.*, **35**, 1195 (1957).

(12) E. R. Lippincott and R. Schroeder, *J. Am. Chem. Soc.*, **73**, 1122 (1951).

(13) K. Nakamoto, M. Margoshes, and R. E. Rundle, *ibid.*, **77**, 6480 (1955).

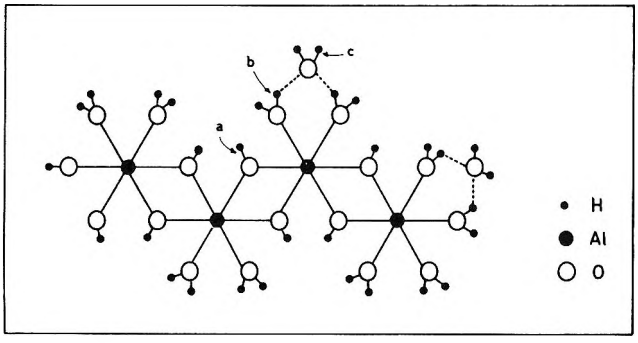

Figure 3. Schematic structure of $Al_4(OH)_8^{4+}$ hydrated.

correspond to an oxygen–oxygen bond length in the range of 2.57 to 2.60 Å. As reported by Pimentel and McClellan,[14] such values have been observed by Luzatti[15,16] in crystalline $HNO_3 \cdot 3H_2O$.

In summary, it is proposed that the observed frequencies may be attributed to the following: 3840 cm.$^{-1}$ to OH^- bond to aluminum, a species; 2965 cm.$^{-1}$ to $O\text{-}H^{+0.25}$ of hydronium, b species; 2530 cm.$^{-1}$ to hydrogen-bonded water, c species.

(14) G. C. Pimentel and A. L. McClellan, "The Hydrogen Bond," W. H. Freeman and Co., San Francisco, Calif., 1960.

(15) V. Luzatti, *Acta Cryst.*, **4**, 239 (1951).

(16) V. Luzatti, *ibid.*, **6**, 152 (1953).

Infrared Spectrum of $HBBr_2(g)$[1]

by Satish K. Wason and Richard F. Porter

Department of Chemistry, Cornell University, Ithaca, New York
(Received February 15, 1965)

In several recent publications infrared spectra of gaseous HBF_2[2,3] and $HBCl_2$[4-7] have been reported. Vibrational frequency assignments have been given for both molecules.[8] In this note, we report our observations and interpretation of the infrared spectrum of $HBBr_2(g)$. Samples of $HBBr_2(g)$ were prepared by the reaction of BBr_3 with boroxine. The apparatus and procedure for the preparation of solid boroxine from a high temperature reaction of $H_2O(g)$ and boron has been described.[3] A preparation time of about 2 hr. was required for an ample quantity of boroxine. The sample was condensed in a 150-ml. reaction vessel and diborane, which is produced by the partial decomposition of the solid, was removed before the addition of BBr_3. Boron tribromide vapor was then introduced into the reaction vessel at a pressure of 30 torr. When the reaction vessel was maintained at room temperature, the main product was B_2H_5Br as noted from a mass spectral analysis. When the reaction vessel was heated to 100°, $HBBr_2$ was obtained in high yield. The compound was identified from its mass spectrum which shows a strong $HBBr^+$ peak. Fractionation of volatile B_2H_5Br and B_2H_6 in a −78° trap left a mixture of $HBBr_2$ and BBr_3. The mixture could not be separated by ordinary fractional distillation. Deuterated products were obtained by repeating the reaction with deuterated boroxine. Infrared bands due only to $HBBr_2$ could be determined by comparison of the spectra of the more volatile and less volatile fractions.

Spectral data for $HBBr_2$ and $DBBr_2$ obtained with a Perkin-Elmer Model 521 grating infrared spectrophotometer are given in Table I. Three of the possible six infrared active bands are observed. One or two bands probably lie below our spectral cutoff at 400 cm.$^{-1}$. The bands at 2620 and 1965 cm.$^{-1}$ are readily

Table I: Infrared Spectra and Frequency Assignments for $HBBr_2$ and $DBBr_2$

Frequency, cm.$^{-1}$[a] $HBBr_2$	$DBBr_2$	Intensity[b]	Assignment	Symmetry type	Description
2620		m	ν_1	A_1	B–H stretch
	1960	m	ν_1	A_1	B–D stretch
1050		m	ν_4 (^{10}B)	B_1	^{10}B–Br asymmetric stretch
1040		s	ν_4 (^{11}B)	B_1	^{11}B–Br asymmetric stretch
	903	m	ν_4 (^{10}B)	B_1	^{10}B–Br asymmetric stretch
	872	s	ν_4 (^{11}B)	B_1	^{11}B–Br asymmetric stretch
798		m	ν_5 (^{10}B)	B_1	^{10}B–H in-plane bend
775		s	ν_5 (^{11}B)	B_1	^{11}B–H in-plane bend
	658	m,w	ν_5	B_1	B–D in-plane bend

[a] Band centers measured from band contour. [b] s = strong, m = medium, w = weak.

(1) Work supported by Army Research Office (Durham) and the Advanced Research Projects Agency.

(2) (a) T. D. Coyle, J. J. Ritter, and T. C. Farrar, *Proc. Chem. Soc.*, 25 (1964); (b) L. Lynds and C. D. Bass, *Bull. Am. Phys. Soc.*, [6] **9**, 661 (1964).

(3) R. F. Porter and S. K. Wason, *J. Phys. Chem.*, **69**, 2208 (1965).

(4) L. Lynds and C. D. Bass, *Inorg. Chem.*, **3**, 1063 (1964).

(5) D. Brieux de Mandirola and J. F. Westerkamp, *Spectrochim. Acta.*, **20**, 1633 (1964).

(6) L. Lynds and C. D. Bass, *J. Chem. Phys.*, **40**, 1590 (1964).

(7) C. D. Bass, L. Lynds, T. Wolfram, and R. E. DeWames, *J. Chem. Phys.*, **40**, 3611 (1964).

(8) (a) For HBF_2 see ref. 2b and 3; (b) for $HBCl_2$ see ref. 4, 5, and 7.

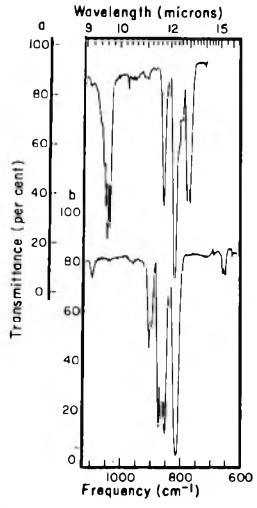

Figure 1. Portion of the infrared spectra of $HBBr_2$ (upper curve) and $DBBr_2$ (lower curve). Bands at 820 and 856 cm.$^{-1}$ are due to BBr_3: slit width ~2 cm.$^{-1}$.

attributed to B–H and B–D stretching vibrations, respectively. In the low-frequency range (Figure 1), two strong bands of about equal intensities are observed for $HBBr_2$ and one strong band and one weak band are observed for $DBBr_2$. The band at 872 cm.$^{-1}$ in $DBBr_2$ lies close to the B–Br asymmetric stretching vibration in BBr_3[9] and is assigned to ν_4. The assignment of ν_4 in $HBBr_2$ was complicated since the choice of either the 1040- or 775-cm.$^{-1}$ band would necessitate either an unusually large deuterium isotope shift (168 cm.$^{-1}$) or an isotope shift in the direction opposite to that normally expected. A plausible explanation is that the two strong bands in $HBBr_2$ are ν_4 and ν_5 (the in-plane B–H bend) but are split by strong Fermi resonance while the two bands in $DBBr_2$ do not coincide favorably for such an interaction. This explanation is also consistent with the observed variation in relative band intensities for the two molecules. For the B_1 symmetry type, the product rule[10] gives

$$\frac{(\nu_4\nu_5)_H}{(\nu_4\nu_5)_D} = \left\{\left(\frac{m_D}{m_H}\right)\left(\frac{M_{HBBr_2}}{M_{DBBr_2}}\right)\left(\frac{I_{Z(H)}}{I_{Z(D)}}\right)\right\}^{1/2}$$

where m_H and m_D are the masses of H and D atoms, M is the molecular weight of $HBBr_2$ or $DBBr_2$, and I_Z is the moment of inertia about an axis perpendicular to the plane of the molecule. From the moments of inertia for $HBBr_2$ and $DBBr_2$ reported by Lynds and Bass,[11] we calculate for the ^{11}B molecule a value of 1.399 for the product of frequency ratios. From Table I, the observed value is 1.404. Unfortunately, the spectral data do not permit an unambiguous distinction between ν_4 and ν_5 in $HBBr_2$ and it is possible that these two assignments in Table I could be reversed.

(9) L. P. Lindeman and M. K. Wilson, *J. Chem. Phys.*, **24**, 242 (1956).

(10) G. Herzberg, "Infrared and Raman Spectra of Polyatomic Molecules," D. Van Nostrand Co., Inc., New York, N. Y., 1945, p. 231.

(11) L. Lynds and C. D. Bass, *J. Chem. Phys.*, **41**, 3165 (1964).

Graphitic Acid of Pyrolytic Carbon and Its Heat Treatment

by Eitaro Matuyama

Faculty of Engineering, Yamaguchi University, Ube, Japan
(Received December 14, 1964)

We have previously reported[1] the crystallographic change of several lamellar compounds of natural graphite by heat treatment. In these compounds, the original graphite structure was restored as soon as most of the foreign atoms were driven off from the layers. The graphitic acid (graphite oxide) was an exception; it required 1800° to be completely restored.

In recent years, pyrolytic carbon (pyrographite)[2] has attracted considerable interest as a material for high temperature applications or as a material having unusually high anisotropic physical properties. Using this material we have prepared graphitic acid and have performed X-ray studies as a supplement to the previous work. This modification of carbon is usually formed by the thermal decomposition of a hydrocarbon vapor at 1600–2500°. The basal layer planes are highly oriented parallel to the substrate, but the successive hexagonal layers are randomly displaced laterally to each other, *i.e.*, turbostratic. In the as-deposited material, the crystallite dimension is of the order of 100 Å. As the grains grow when heat-treated at higher temperatures, the two-dimensional ordering gradually transforms to the three-dimensional one. In the present experiment, the carbon was prepared as follows. Benzene vapor diluted with an inert carrier gas was pyrolyzed at 1600° on a carbon rod 8 mm. in diameter, and the deposited carbon shell was heated at 2000° under vacuum for 30 min.

Figure 1 shows the logarithmic plot of intensity of the diffracted X-rays as a function of the Bragg angle for Co Kα radiation. The lowest curve designated "original" is for the pyrolytic carbon obtained in this way. The (0002) and (0004) lines having a sym-

(1) E. Matuyama, *J. Phys. Chem.*, **58**, 215 (1954).

(2) C. A. Klein, *J. Appl. Phys.*, **33**, 3338 (1962).

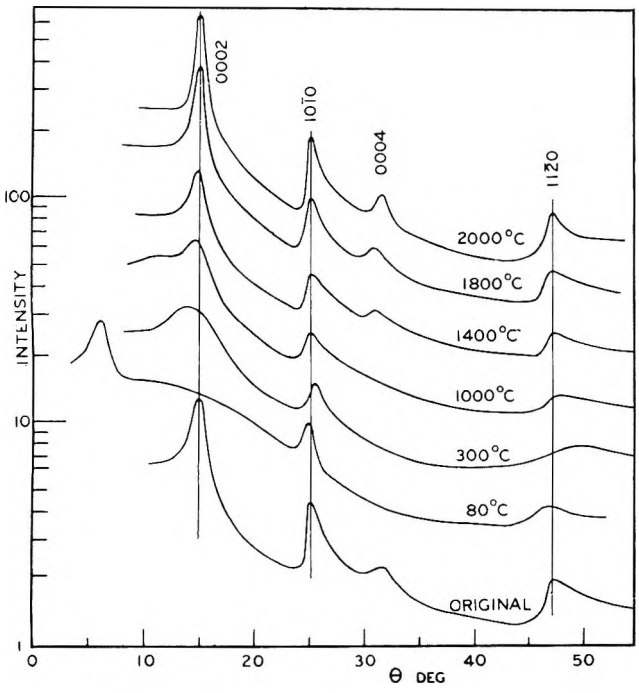

Figure 1. Successive change of the X-ray diffractions. The intensity as a function of the Bragg angle for Co $K\alpha$ radiation.

metrical shape are the three-dimensional reflections from the layer planes. The (10$\bar{1}$0) and (11$\bar{2}$0) lines which are distinctly asymmetrical are the reflections from the planes perpendicular to the layers, often indexed (10) and (11).[3] This curve is similar to the diffractometer curve published recently by Guentert.[4] He used a pyrolysis temperature of 2100°. This temperature is higher than that of our experiment; hence, his lines are slightly narrower than the present curve. Graphitic acid was prepared by treating the pyrolytic carbon with Staudenmaier's reagent[5,6] which is a mixture of nitric acid, sulfuric acid, and potassium perchlorate. The treatment was carried out as described in the previous report. The chemical composition of the resulting sample depended on many experimental conditions, especially on the amount of water introduced. However, the X-ray patterns were similar except for a difference in the diffraction angle of the (0002) line. The curve of the sample dried at 80° is shown in the figure. On the curve designated "80°C" only three peaks appear corresponding, respectively, to the (0002), (10$\bar{1}$0), and (11$\bar{2}$0) lines as in the sample prepared from the natural graphite; however, their widths are too large by nearly a factor of 3. The shift of the (0002) line indicates an increase of the interlayer spacing by 2.5 times. The swelling is nearly equal to that of the sample prepared from natural graphite. The spacing as well as the mass decreased with temperature. The first stage was due to the loss of water and continued until 100°. The second state starting at 150° was an exothermic decomposition which accelerated the decrease and finally resulted in an explosion at about 200° if the heating rate was not carefully controlled. In this temperature range most of the inclusions were driven off; hence, the diffraction pattern showed a rapid and complicated change. The observed splitting of the (0002) peak presumably originated from temporal overlapping of the intermediate states. The observed distortion was slowly removed when the sample was heated to higher temperatures, and at 1800° the original state was almost restored.

The diffraction patterns of the successive stages are shown in the figure in which the temperatures of the heat treating are designated on the respective curves. At each temperature, the sample was kept for 30 min. in a stream of nitrogen gas and then evacuated at temperatures above 300°. At 300°, the (0002) peak is already in the correct position, but the line width is remarkably wide. This would seem that the hexagonal layers are wavy or indicate a combination of lattices having different interlayer spacings. The breadth decreased slowly with the temperature. At 300°, the (10$\bar{1}$0) and (11$\bar{2}$0) lines are also broader than at 80°, and, in addition, they are shifted to the high-angle side which corresponds to a contraction of the layer planes by 0.55%. A slightly larger value of 0.75% was obtained in the previous experiment. The discrepancy may be partially attributed to errors due to the large line width of the pyrolytic carbon. As can be seen in the figure, the line shift decreases slowly with the temperature. We have assumed buckled layers to account for these shifts. A small line shift on the opposite side is shown on the "80°C" curve. This indicates expansion of the layer planes. Such trends can be understood if we assume the effect of layer puckering has been overcome by increased interatomic distance caused by the bonding of foreign atoms between the layers.

In pyrolytic carbon as well as the natural graphite, complete curing of the buckled layers occurs at a much lower temperature than that required for the construction of the layer lattice as in the graphitizing process. The former is effected by heat treating at

(3) B. E. Warren, *Phys. Rev.*, **59**, 693 (1941).

(4) O. J. Guentert, *J. Chem. Phys.*, **37**, 884 (1962).

(5) U. Hofmann and E. König, *Z. anorg. allgem. Chem.*, **234**, 311 (1937).

(6) A. R. Ubbelohde and F. A. Lewis, "Graphite and its Crystal Compounds," Clarendon Press, Oxford, 1960, p. 151.

1800°; the latter requires a temperature between 2000 and 3000°. This situation seems to be similar in some respects to graphite damaged by neutron irradiation in which complete recovery occurs when the annealing temperature approaches 2000°.[7-9]

(7) M. Burton and T. J. Neubert, *J. Appl. Phys.*, 27, 557 (1956).
(8) A. Herpin, *J. phys. radium*, 24, 499 (1963).
(9) E. A. Kellett and H. P. Rooksby, *G.E.C. Journal*, 31, 28 (1964).

The Heat of Formation of Lanthanum Oxide[1]

by George C. Fitzgibbon, Charles E. Holley, Jr.,

University of California, Los Alamos Scientific Laboratory, Los Alamos, New Mexico

and Ingemar Wadsö

Thermochemistry Laboratory, University of Lund, Lund, Sweden
(Received December 23, 1964)

Values of the heats of solution of lanthanum metal and lanthanum oxide are presented as determined in calorimeters previously described,[2,3] and, in conjunction with the heat of formation of liquid water from its elements,[4] are used to determine the heat of formation of La_2O_3.

Experimental

The calorimeter used in Los Alamos is an isothermal solution calorimeter whose environmental temperature may be kept constant at any setting between 23 and 33° to within 0.001° in an 800-l. thermostatically controlled bath. The vacuum-jacketed, silver-bodied, platinum-lined calorimeter reaction vessel has a volume of ~450 cc., a thermal leak modulus of 0.005/min., and a heat capacity of 420 cal.

Within the reaction chamber are a heater, a thermistor, a Pyrex rod to which is attached a platinum stirrer, and a glass sample bulb. The heater consists of a 15.24-cm. length of 0.64-cm. o.d. platinum tubing, the lower end gold soldered, the upper end sealed to glass tubing which extends through the calorimeter lid and carries the heater leads. The platinum tubing contains 23 ohms of bifilarly wound, helically coiled, silk-covered manganin wire with leads to measure the voltage drop, located at the solution level. A Fenwall 2300-ohm thermistor is used as the sensing element to measure temperature differences up to 1.6° to within 0.0001°. A Brown recorder was modified to an automatic changing multiscale self-balancing Wheatstone bridge, whose arm position is an indication of the resistance of the thermistor.

The energy equivalent is determined by passing a current from a precision voltage-regulated supply through the calorimeter heater and a 0.1-ohm standard resistor in series and measuring the voltage drops using a Rubicon Type B potentiometer and a Rubicon reflecting galvanometer. The input time is read directly from an electronic decade counter whose time base is derived from a 100-kc. crystal-controlled oscillator, accurate and stable to 0.01%.

The lanthanum metal was obtained from the Ames Laboratory, Ames, Iowa, in the form of a small ingot, through the courtesy of Prof. F. H. Spedding. It was prepared before each run by filing the surfaces to a shiny luster before cutting off several small pieces. The sample size was chosen to give a temperature rise of ~1°. The composition of the sample, calculated from an analysis, is: La, 98.810; Mg, 0.005; Ca, 0.010; Fe, 0.050; LaN, 0.164; La_2O_3, 0.146; LaC_2, 0.047; LaH_2, 0.768.

The hydrated sesquioxide was obtained from the Michigan Chemical Co. It was treated by heating in an induction furnace, under vacuum, to 1200° in an alundum crucible for about 1 hr. It was then transferred to a drybox for weighing and sealing in a sample bulb. The oxide sample used in Lund was further treated before use by heating in air at 1050° for about 30 min. in a platinum crucible. It was then stored under dry N_2 for about 1 hr. before being put into a calorimetric ampoule. The composition of the oxide sample, calculated from an analysis, is: La_2O_3, 99.882; SiO_2, 0.002; BaO, 0.006; CaO, 0.040; Fe_2O_3, 0.070.

The heats of solution of this lanthanum metal and oxide were determined in 1.00 *M* HCl saturated with hydrogen. The average duration of a run was 10 min. from the breaking of the sample bulb until equilibrium was reached in the after period. Weights are given *in vacuo*. The defined calorie (4.1840 absolute joules) is used in expressing the results. The atomic weight used for lanthanum is 138.91. The sample sizes of metal and oxide were adjusted so that the final solution in both cases had approximately the same composition, *i.e.*, *ca.* 0.0065 *M* in $LaCl_3$ and with enough excess of HCl that its concentration changed only

(1) Work done in part under the auspices of the U. S. Atomic Energy Commission.
(2) G. C. Fitzgibbon, D. Pavone, E. J. Huber, Jr., and C. E. Holley, Jr., Los Alamos Scientific Laboratory Report, LA-3031 (1964).
(3) S. Sunner and I. Wadsö, *Acta Chem. Scand.*, 13, 97 (1959).
(4) "Selected Values of Chemical Thermodynamic Properties," National Bureau of Standards Circular 500, U. S. Government Printing Office, Washington, D. C., 1952.

slightly. The results of the experiments on lanthanum metal are shown in Tables I and II.

Table I: Heat of Solution of Lanthanum Metal—Los Alamos Results

Mass of La, g.	Mass of solvent, g.	Energy equiv., cal./ arbitrary unit	Temp. rise, arbitrary unit	Energy from La, cal./g.	Dev., cal./g.
0.36589	399.41	17.003	26.122	1204.2	0.3
0.36587	399.38	17.046	26.060	1204.2	0.3
0.36640	399.95	17.009	26.150	1204.2	0.3
0.36633	399.88	17.056	26.076	1204.4	0.5
0.36665	400.23	17.001	26.159	1203.2	0.7
0.36678	400.37	17.030	26.120	1203.2	0.7
			Av.	1203.9	0.5
			Correction for H_2O evap.	5.0	
			Heat of solution of La metal	1208.9	
			2 × std. dev. of the mean		0.4

Table II: Heat of Solution of Lanthanum Metal—Lund Results[a]

Mass of La, g.	Temp. rise, arbitrary unit	Energy from La, cal./g.	Dev., cal./g.
0.09326	12.504	1206.4	1.2
0.09119	12.212	1205.0	0.2
0.09759	13.064	1204.5	0.7
0.09658	12.921	1203.8	1.4
0.09400	12.600	1206.1	0.9
	Av.	1205.2	0.9
	Correction for H_2O evap.	3.8	
	Heat of solution of La metal	1209.0	
	2 × std. dev. of the mean		1.0

[a] Mass of solvent = 101.50 g.; energy equivalent (mean value) = cal./arbitrary unit.

The uncertainty in the heat for the evaporation of the H_2O by the escaping H_2 is taken as 10% or 0.07 kcal./mole. Heats of alloy formation are ignored. The value of the correction for the impurities, with its uncertainty, is -0.69 ± 0.30 kcal./mole. The corrected value for the heat of solution of La metal in 1 *M* HCl at 298° is thus -168.62 ± 0.32 kcal./mole from the Los Alamos results and -168.63 ± 0.32 kcal./mole from the Lund results.

These values are both in good agreement with the value -168.77 ± 0.20 reported by Spedding and Flynn.[5]

The heats of solution of the lanthanum oxide were also determined in 1 *M* HCl saturated with H_2 with the amounts of oxide and acid adjusted so that the final composition of the solution was approximately the same as for the metal solutions. The results are shown in Tables III and IV.

Table III: The Heat of Solution of Lanthanum Oxide—Los Alamos Results

Mass of La_2O_3, g.	Mass of solvent, g.	Energy equiv., cal./ arbitrary unit	Temp. rise, arbitrary unit	Energy from La_2O_3, cal./g.	Dev., cal./g.
0.43030	400.50	16.752	8.940	348.08	0.03
0.43000	400.22	16.789	8.914	348.04	0.01
0.43020	400.40	16.749	8.929	347.65	0.40
0.43080	400.97	16.721	8.975	348.38	0.33
0.42920	399.48	16.690	8.941	347.71	0.34
0.42955	399.80	16.720	8.951	348.44	0.39
				Av. 348.05	0.25
			2 × std. dev. of the mean		0.26

Table IV: Heat of Solution of Lanthanum Oxide—Lund Results[a]

Mass of La_2O_3, g.	Temp. rise, arbitrary unit	Energy from La_2O_3, cal./g.	Dev., cal./g.
0.10031	3.947	347.44	0.21
0.10086	3.975	348.00	0.35
0.10054	3.961	347.88	0.23
0.10009	3.938	347.41	0.24
0.10037	3.950	347.50	0.15
	Av.	347.65	0.24
	2 × std. dev. of the mean		0.26

[a] Mass of solvent = 101.50 g.; energy equivalent (mean value) = 8.830 cal./arbitrary unit.

The correction for impurities was made on the assumption that the oxide had the composition given earlier and that the SiO_2 was inert. The possibility of the formation of mixed oxides was ignored. The correction for impurities amounts to 0.02 kcal./mole giving a corrected value for the heat of solution of hexagonal lanthanum oxide in 1 *M* HCl of -113.38 ± 0.09 kcal./mole from the Los Alamos results and -113.25 ± 0.09 kcal./mole from the Lund results. Both values are in good agreement with the value of -113.38 ± 0.37 kcal./mole reported by Montgomery[6] for somewhat different concentrations.

(5) F. H. Spedding and J. P. Flynn, *J. Am. Chem. Soc.*, **76**, 1476 (1954).

(6) R. L. Montgomery, U. S. Department of the Interior, Bureau of Mines, Report of Investigations No. 5445, Pittsburgh, Pa., 1959.

Comparison of Results

The results from the two laboratories are summarized in Table V. In addition, results are also shown for the heat of solution of Tris, which has been proposed for use as a comparison material for solution calorimeters.[7] It appears that the two calorimeters give results which agree with each other, within the precision of the measurements, on these three rather diverse materials.

Table V: Comparison of Heat of Solution Results Obtained at Los Alamos and at Lund

	Heat of solution, cal./g. (uncor.)		Difference (L.A. − Lund), %
	Los Alamos	Lund	
La metal	1203.9 ± 0.4	1205.2 ± 1.0	−0.11
La_2O_3	348.05 ± 0.26	347.65 ± 0.26	+0.11
Tris	7116 ± 8	7107 ± 4	+0.13

Table VI: The Heat of Formation of La_2O_3 at 298°K.

Reaction	ΔH, kcal./mole	
	Los Alamos	Lund
1. $2La(s) + 6HCl(aq) \rightarrow 2LaCl_3(aq) + 3H_2(g)$	337.24 ± 0.64	337.26 ± 0.64
2. $La_2O_3(s) + 6HCl(aq) \rightarrow 2LaCl_3(aq) + 3H_2O(l)$	113.38 ± 0.09	113.25 ± 0.09
3. $3H_2(g) + 1.5O_2(g) \rightarrow 3H_2O(l)$	204.96 ± 0.03	204.96 ± 0.03
4. $2La(s) + 1.5O_2(g) \rightarrow La_2O_3(s)$	428.82 ± 0.64	428.97 ± 0.64

$\Delta H = \Delta H_1 + \Delta H_3 - \Delta H_2$

The Heat of Formation of La_2O_3. The calculation of the heat of formation of lanthanum oxide is shown in Table VI. These values agree with each other within the estimated uncertainties and they both agree with the combustion value, −428.57 ± 0.19 kcal./mole, obtained by Huber and Holley.[8] The weighted average of these three sets of measurements is −428.6 ± 0.2 kcal./mole. The heat of formation of hexagonal La_2O_3 can now be regarded as having been determined to within rather narrow limits (about 0.1%) by two independent methods.

Acknowledgment. Grateful acknowledgment is extended to Mr. Dan Pavone for his preparation of the oxide samples.

(7) R. J. Irving and I. Wadsö, *Acta Chem. Scand.*, **18**, 195 (1964).

(8) E. J. Huber, Jr., and C. E. Holley, Jr., *J. Am. Chem. Soc.*, **75**, 3594 (1953).

Viscosity of Glass-Forming Solvent Mixtures at Low Temperatures

by Hina Greenspan and Ernst Fischer

Photochemical Laboratory, The Weizmann Institute of Science, Rehovoth, Israel *(Received December 23, 1964)*

The viscosity of solvent mixtures has a pronounced effect on bimolecular reactions, such as photosensitized reactions[1] and second-order triplet decay.[2] In monomolecular reactions, such as photoinduced molecular rearrangements, the role of high viscosities is less pronounced but still marked. Thus, it was observed that the internal rearrangement of merocyanines, after their formation by irradiation of the corresponding spiropyrans, is slowed down sharply in hydrocarbon glasses,[3] apparently by the combined effect of low temperature and high viscosity. Similarly, the thermal tautomerization of 1-phenylazo-2-naphthol following photoisomerization was found[4] to be slowed down by cooling their solutions in hydrocarbon mixtures to −185° or in plastic films to about −100°.

The macroscopic viscosity is clearly not identical with the "microscopic" one at the molecular level. However, one may expect a rough parallelism between the two, at least in chemically similar media. It was therefore interesting to get an idea of the viscosities of these glasses at temperatures down to that of liquid nitrogen—if not directly, then at least by extrapolation from temperatures at which the viscosity is already high, though still measurable.

Experimental

Since the ordinary viscosimetric methods cannot easily be applied at very high viscosities, a penetrometric method was employed in which one measured the penetration rate of a 3-mm. glass rod, carrying a weight of up to 400 g., into the solvent mixtures at various temperatures. This is described schematically in Figure 1, where the weight is an iron core, released at a suitable moment by switching off an external electromagnet. In the apparatus described, the solvents are distilled in a high vacuum system[5] into the

(1) S. Malkin and E. Fischer, *J. Phys. Chem.*, **68**, 1153 (1964).

(2) (a) G. Porter and F. Wilkinson, *Proc. Roy. Soc.* (London), **A264**, 1 (1961); (b) G. Oster and Y. Nishijima, *Fortschr. Hochpolym. Forsch.*, **3**, 313 (1964).

(3) (a) R. Heiligman-Rim, Y. Hirshberg, and E. Fischer, *J. Phys. Chem.*, **66**, 2470 (1962); (b) T. Bercovici and E. Fischer, to be published.

(4) G. Gabor and E. Fischer, to be published.

(5) Y. Hirshberg and E. Fischer, *Rev. Sci. Instr.*, **30**, 197 (1959).

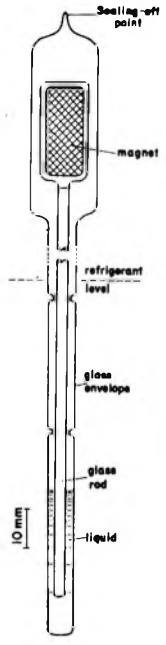

Figure 1. Sealed-type penetrometer.

tube, which is then sealed off. At temperatures down to $-160°$ the tubes were placed in a transparent dewar vessel cooled by a stream of thermostated cold air.[5] This made possible visual inspection of the behavior of the solvent mixtures during the measurements. For experiments at still lower temperatures, the tube was surrounded by a copper block immersed in the neck of a 2-l. dewar flask containing liquid air boiling at a controlled rate. Comparative experiments were also performed in open tubes, in which case the weight forcing the rod into the liquid could be changed between 30 and 400 g., corresponding to pressures of 0.4–5.3 kg./cm.^{2}. These experiments showed that the rate of penetration is proportional to the weight.

In a typical experiment the tube is cooled down to the required temperature and kept at the latter for at least 10 min. to ensure temperature equilibration. The glass rod, which under these conditions is already in the liquid, is then released, allowed to travel 20 mm., and the time required for another 10, 20, and 25 mm. of penetration is measured by a stopwatch.

The method is based on a combination of several effects and thus is not suitable for absolute measurements. However, it is possible to estimate relative viscosity values if we make the plausible assumption that equal rates of penetration mean equal viscosities and that rates of penetration are proportional to viscosities. By applying the method to glycerol, whose viscosity has been determined in a similar range,[6] the relative scale of experimental values can be converted into an absolute one.

The falling-sphere method can be used to measure viscosities high enough to just overlap with the lowest ones still measurable by the above penetration method. The two methods thus supplement each other.

Results

It was found that within a narrow (40- to 50-fold) range of viscosity the logarithm of the latter, or rather of the penetration rate R, is a linear function of the inverse absolute temperature T: $\ln R = A + B/T$, where A and B are constants. This makes it possible to plot the results in a linear form and to extrapolate them with some degree of certainty to temperatures above and below the range measured. The results are summarized in Figure 2, in which the intersections

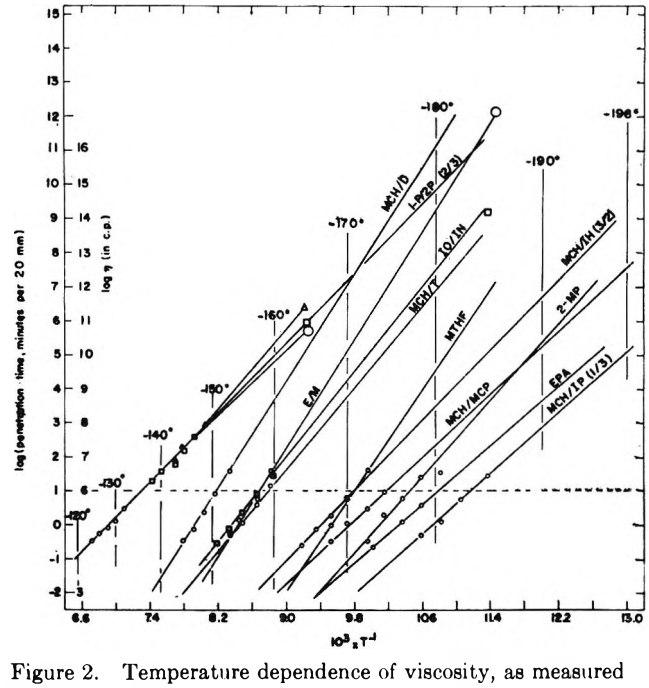

Figure 2. Temperature dependence of viscosity, as measured with the sealed-type penetrometer (30-g. weight). In 1-P–2-P the range was extended by using either the falling-sphere method (circles) or the penetrometric method with a 400-g. weight (triangles).

of the experimental lines with any horizontal line give the temperature at which the various mixtures have a given viscosity, while intersections with vertical lines show relative viscosities at any one temperature. The constant B may be used to calculate critical increments E by taking[7] $B = E/R$ and thereby making possible comparison with the results of previous

(6) G. Tamman and W. Hesse, *Z. anorg. allgem. Chem.*, 156, 245 (1926).

(7) W. J. Moore, "Physical Chemistry," 3rd Ed., Prentice-Hall, Englewood Cliffs, N. J., 1962, p. 723.

authors. The values of E thus calculated from the observed temperature dependence of R for various mixtures are summarized in Table I, together with the

Table I: Temperature T of Equal Viscosity (20-mm. Penetration during 10 min., 30-g. Weight), Critical Increments E, and Approximate Extrapolated Values of the Viscosity η at $-180°$ for Various Glass-Forming Solvents and Solvent Mixtures

Solvent[a]	T, °C.	E, kcal./mole	η, cp.
Glycerol	−33	27.5	...
1-P–2-P (2:3)	−143	12.0	6×10^{14}
E–M	−158	18.0	2×10^{14}
E–M + 4.5% water	−151.5	15.5	...
E–M + 9% water	−146.5	14.5	...
IO–IN	−158	14.5	3×10^{12}
MCH–D	−151	18.0	1×10^{16}
MVH–T	−159.5	13.5	7×10^{11}
MCH–IH (3:2)	−171	12.0	3×10^{8}
MCH–MCP	−174.5	11.0	2×10^{7}
MCH–IP	−177	13.0	...
MCH–IP (1:3)	−183.5	10.0	1×10^{5}
2-MP	−177	13.0	7×10^{6}
2-MTHF	−171	17.0	4×10^{9}
EPA	−180	10.0	9×10^{6}

[a] 1:1 mixtures unless indicated otherwise. Solvent designation: 1-P, 1-propanol; 2-P, 2-propanol; E, ethanol; M, methanol; IO, isooctane; IN, isononane; MCH, methylcyclohexane; D, a mixture of *cis*- and *trans*-decalin (1:1), f.p. −64.5°; T, toluene; IH, mixture of isohexanes; MCP, methylcyclopentane; IP, isopentane; 2MP, 2-methylpentane; 2-MTHF, 2-methyltetrahydrofuran; EPA, a mixture of ether, isopentane, and ethanol (5:5:2).

temperature at which the penetration rate of the glass rod is 20 mm./10 min., under the present experimental conditions. With glycerol this temperature was found to be about −33°, where its viscosity is known[6] to be about 10^6 cp. The ordinate scale inside the frame of Figure 2 was set up accordingly.

By using heavier weights, the range of measurement could be extended to correspondingly higher viscosities, at lower temperatures, as seen in Figure 2, curve 1-P–2-P. The same curve also shows the results obtained with the falling-sphere method at somewhat lower viscosities.

Table I shows that the viscosity of mixtures increases with the percentage of the higher-melting component (water in alcohol–water, MCH in IP–MCH). (See Table I for abbreviations of solvent names.)

Viscosities in the presence and in the absence of air (*i.e.*, measured in thoroughly degassed liquids) were essentially identical.

There was no clear-cut influence of the direction from which the temperature of measurement was approached (*i.e.*, from above or from below), except in mixtures tending to manifest phase separation. Such a tendency was observed in mixtures of MCH with decalin and with toluene, even when these were distilled into the measuring tube from a sodium–potassium alloy[5] to ensure complete absence of hydroxylic contaminants. Phase separation is apparently aided by the friction between the glass rod and the tube walls and manifests itself by "colloid" colors, turbidity, or downright precipitation. The rather peculiar behavior exhibited by these mixtures merits a somewhat more detailed description.

Gradual cooling of a MCH–D mixture down to about −150° and subsequent measurement of the viscosity does not result in any visible changes in appearance. However, when the liquid is then warmed to about −85°, gradual precipitation occurs, and eventually the system is transformed into a white slurry. The precooling to −150° is essential for the subsequent precipitation at higher temperatures and apparently helps in the formation of nuclei. Further warming of the slurry, to about −70°, clears up the system.

In a MCH–T mixture the situation is more complex. Cooling to about −120° has no visible effect. At about −156° a bluish color gradually develops; the solution then becomes more and more opaque, and eventually a white mass precipitates. A somewhat similar phenomenon has been described in a water–glycerol mixture.[8] Subsequent warming clears up the system completely at about −150° but at about −135° results in slow crystallization which eventually seems to involve the whole system. The latter clears up again only upon further warming to about −95°. Rapid cooling from room temperature to −168° causes only a blue coloration. Warming to −156° results in the phenomena already described. In this case, too, precooling (to at least −145°) seems to be essential for subsequent precipitation, the rate of the latter increasing with decreasing temperature of precooling.

The results were even more startling with the much-used EPA (a mixture of ether, isopentane, and ethanol) which forms excellent glasses when quenched in liquid air. If it is cooled gradually, crystallization takes place in the range −150 to −160°, depending on the rate of cooling. Before that, the viscosity is low and not measurable in the present setup. The solid mass resulting from this crystallization "melts" at around

(8) D. Keilin and E. F. Hartree, *Nature*, **164**, 254 (1949); **165**, 504 (1950).

$-135°$. The viscosities given in Figure 2 and Table I were measured by first quenching the EPA in liquid air and then warming it up to the temperatures of measurement. Results of measurements taking a long time may be too high because of slow phase separation.

In all three of the systems mentioned, precipitation also occurs on recooling the liquids after clearing-up has taken place at the temperatures indicated. This behavior is analogous to that normally observed in systems undergoing crystallization.[9]

Discussion

An examination of the existing data on the relationship between viscosity and temperature for several liquids reveals that an Arrhenius-type equation holds for many hydrocarbons[10] and alcohols,[11] the critical increments being in the range of 2–4 kcal./mole.

The values of 10–20 kcal./mole observed by us are very much higher, both for hydrocarbons and for alcohols, recalling somewhat similar earlier results.[6,12–14] The question remains open whether, over a wide range of viscosities, the slope of the log η *vs.* $1/T$ curve either increases continuously with the viscosity[12,13] or else there exist several regions in each of which the slope is approximately constant.[6,14]

The data collected in Table I and Figure 2 do not show any clear correlation between the value of E and the chemical nature of the solvent. It therefore seems unjustified to assume that the high E values observed are due to intramolecular hydrogen bonding.[12]

The possible temperature dependence of the E values themselves at viscosities beyond those measured in the present investigation makes extrapolations to much higher viscosities (Figure 2) rather uncertain, and it is clearly desirable to measure such viscosities directly, despite the experimental difficulties involved.[12] The extrapolation in Figure 2, leading *inter alia* to the values of η given in the last column of Table I, should be viewed with this uncertainty in mind. These extrapolations were carried down to temperatures where many of the glasses crack since these data may still be useful for luminescence and energy-transfer investigations not involving accurate absorption measurements.

In mixtures with one common component, the temperature at which a certain viscosity is reached decreases with the melting point of the second component (*e.g.*, D > T > IH > MCP > IP in mixtures with MCH).

The three mixtures exhibiting phase separation seem to constitute metastable systems at low temperatures because of the dissimilarity of the components. These solvent mixtures could nevertheless be used extensively in this laboratory and elsewhere (EPA) for low-temperature photochemical and spectrophotometric investigations because either nucleation or phase separation is very slow under many conditions.

Concerning correlation with molecular phenomena, the macroscopic viscosity indicated by the above results is at best only a rough indication of microscopic viscosity. It is therefore interesting to note the fact that molecular rearrangements following irradiation could be slowed down to a similar extent[3] by cooling to $-160°$ in MCH–D and to $-180°$ in MCH–IH. As may be seen in Figure 2, these two mixtures have about the same viscosity at the respective temperatures. The data presented in this figure make it possible to plan similar comparative experiments with other systems.

Acknowledgment. The authors gratefully acknowledge helpful discussions with Dr. B. Perlmutter-Hayman and a research grant from the U. S. National Bureau of Standards, which served to finance the work described here.

(9) A. Findlay, A. N. Campbell, and N. O. Smith, "The Phase Rule," 9th Ed., Dover Publications, Inc., New York, N. Y., 1951, p. 45.

(10) H. A. Kierstead and J. Turkevich, *J. Chem. Phys.*, **12**, 24 (1944).

(11) "Landolt-Börnstein Tabellen," Main Vol., Part I, 5th Ed., J. Springer, Berlin, 1923, p. 151.

(12) G. S. Parks, L. E. Barton, M. E. Spaght, and J. W. Richardson, *Physics*, **5**, 193 (1934).

(13) E. Kanda, A. Otsubo, and T. Haseda, *Sci. Rept. Res. Inst. Tohoku Univ.*, **A2**, 9 (1950).

(14) J. W. Hilpern, G. Porter, and L. J. Stief, *Proc. Roy. Soc.* (London), **A277**, 437 (1964).

Diffusion of Chloroacetic Acid in Water

by C. W. Garland, S. Tong,

Department of Chemistry, Massachusetts Institute of Technology, Cambridge, Massachusetts 02139

and W. H. Stockmayer

Department of Chemistry, Dartmouth College, Hanover, New Hampshire 03755 *(Received December 23, 1964)*

The interactions of aqueous solute molecules and ions with the surrounding solvent have recently received much attention,[1] thanks largely to the biological im-

(1) H. S. Frank and W-Y. Wen, *Discussions Faraday Soc.*, **24**, 133 (1957); W. Kauzmann, *Advan. Protein Chem.*, **14**, 1 (1959); G. Nemethy and H. A. Scheraga, *J. Chem. Phys.*, **36**, 3382, 3401 (1962).

portance of the subject. Among the transport properties which reflect the ordering or disordering influence of solutes on water structure are viscosity[2,3] and diffusion.[4] As a contribution to this question we have made some measurements by the porous-frit method[5] of the isothermal diffusion at 25° in the system chloroacetic acid–water. From these results, the limiting diffusivity at infinite dilution of the uncharged molecular species $ClCH_2COOH$ is evaluated and then compared to that of the chloroacetate anion.

The unglazed Selas porcelain frits used in this work were the same ones used for our measurements[6] of diffusion in the systems mercuric chloride–water and cadmium iodide–water and were calibrated with aqueous KCl solutions. Eastman Chemicals Pure grade chloroacetic acid was used without further purification, and the concentrations of the solutions were determined by titration with standard NaOH solution. As shown elsewhere,[7] the diffusion coefficient obtained by the frit method is very close to the differential diffusion coefficient D at the concentration of the solution *outside* the frit. The experimental values of D are given in Table I.

Table I: Diffusion Coefficients of Aqueous Chloroacetic Acid Solutions at 25°

Frit[a]	c, M	$D \times 10^5$ cm.² sec.⁻¹	η/η_0	α	$D'_m \times 10^5$ cm.² sec.⁻¹
C	2.67	6.55	1.52[b]	0.021	9.84
C	1.84	7.89	1.31	0.027	10.11
A	1.42	8.44	1.24	0.030	10.31
C	1.20	8.76	1.20	0.033	10.34
A	0.918	9.28	1.15	0.038	10.50
C	0.829	9.45	1.14	0.040	10.52
C	0.588	9.82	1.09	0.047	10.46
C	0.422	10.25	1.07	0.055	10.68
C	0.237	10.86	1.04	0.073	10.93

[a] See ref. 6. [b] Values in this column are taken from H. M. Dawson and C. K. Reiman, *J. Chem. Soc.*, **107**, 1426 (1915).

An apparent diffusion coefficient D'_m for the neutral molecular species can be calculated from the expression[4,8]

$$(1 - \alpha)D'_m + \alpha D^0_i/2 = D(\eta/\eta_0)(1 - \alpha/2) \quad (1)$$

in which D is the experimental diffusion coefficient, α is the fraction ionized, and D^0_i is the limiting diffusivity of the completely ionized acid. The value of D^0_i can be found from the Nernst equation

$$D^0_i = 2\frac{RT}{F^2}\frac{\lambda^0_{H^+}\lambda^0_{ClCH_2COO^-}}{\lambda^0_{H^+} + \lambda^0_{ClCH_2COO^-}} = 20.04 \times 10^{-5} \text{ cm.}^2 \text{ sec.}^{-1} \quad (2)$$

with the ionic mobilities $\lambda^0_{H^+} = 349.8$ and $\lambda^0_{ClCH_2COO^-} = 42.20$ listed by Robinson and Stokes.[9] The viscosity ratio η/η_0 in eq. 1 is a frequently used but essentially empirical factor which has the useful practical effect of reducing the dependence of the obtained values of D'_m on solute concentration. The fraction ionized, α, was calculated from an ionization constant, K, equal to 1.36×10^{-3} for chloroacetic acid.[10] The values of η/η_0, α, and D'_m are all given in Table I.

Minor corrections which have been deliberately omitted from Table I include the effect of activity coefficients of the ionic species on the degree of dissociation and the interionic electrophoretic effect on the mobilities of these ions. Inclusion of these corrections produces a change of less than 0.3% in the values of D'_m. This is considerably smaller than the uncertainty of our measurements, which we consider to be of the order of 1%.[6]

A plot of D'_m against concentration (Figure 1) is essentially linear over the entire concentration range

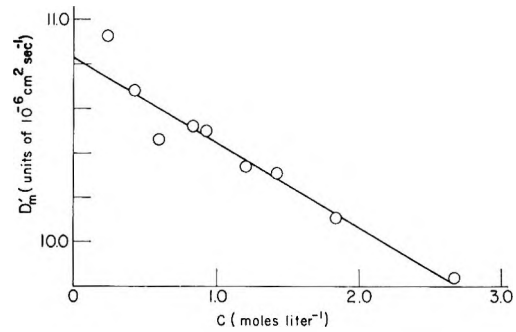

Figure 1. The apparent diffusion coefficient D'_m for the neutral chloroacetic acid molecular species as a function of the over-all concentration c.

(2) W. M. Cox and J. H. Wolfenden, *Proc. Roy. Soc.* (London), **A145**, 475 (1934).

(3) R. W. Gurney, "Ionic Processes in Solution." McGraw-Hill Book Co., Inc., New York, N. Y., 1953, pp. 159–171.

(4) G. T. A. Muller and R. H. Stokes, *Trans. Faraday Soc.*, **53**, 642 (1957).

(5) F. T. Wall, P. F. Grieger, and C. W. Childers, *J. Am. Chem. Soc.*, **74**, 3562 (1952).

(6) C. W. Garland, S. Tong, and W. H. Stockmayer, *J. Phys. Chem.*, **69**, 1718 (1965).

(7) F. T. Wall and R. C. Wendt, *ibid.*, **62**, 1581 (1958).

(8) H. S. Harned and R. M. Hudson, *J. Am. Chem. Soc.*, **73**, 3781, 5880 (1951).

(9) R. A. Robinson and R. H. Stokes, "Electrolytic Solutions," 2nd Ed., Academic Press, New York, N. Y., 1959, p. 463.

(10) D. J. G. Ives and J. H. Pryor, *J. Chem. Soc.*, 2104 (1955).

(11) Professor P. A. Lyons of Yale University has informed us that his unpublished measurements on chloroacetic acid by the Gouy method agree with our results to within a few per cent over the concentration range where the two sets of data overlap and give essentially the same extrapolated value of D^0_m.

studied, and the limiting diffusion coefficient D^0_m of the neutral $ClCH_2COOH$ molecule[11] is found by extrapolation to be $(10.8 \pm 0.1) \times 10^{-6}$ cm.^{2} sec.$^{-1}$. For comparison, the diffusion coefficient of the chloroacetate ion at 25° is $D^0 = \lambda^0 RT/F^2 = 11.2 \times 10^{-6}$ cm.^{2} sec.$^{-1}$.

The preceding values and those for a few other pairs of molecular and ionic species are listed in Table II. There it may be noted that the halogenated system is rather different from those of the lower fatty acids, in which the anions are appreciably slower than the neutral species. Thus, the order-producing effect of the carboxylate charged group[2,3] is reduced, probably by the electron-withdrawing action of the chlorine atom; when still larger polar substituent groups are introduced, as in citric acid, the neutral molecule is much the slower. The sluggishness of argon as compared to potassium and chloride ions is, of course, well known and is presumptive evidence for the "iceberg" concept.[1] Some new diffusion data for the paraffin hydrocarbons (footnote *g* of Table II) show the structure-producing effects of these neutral species.

Table II: Diffusivities[a] of Some Ions and Related Neutral Species in Water at 25°

Solutes	$D \times 10^6$ cm.^{2} sec.$^{-1}$
CH_3COOH, CH_3COO^-	12.0,[b] 10.9[c]
CH_3CH_2COOH, $CH_3CH_2COO^-$	11.1,[d] 9.5[c]
n-C_3H_7COOH, butyrate ion	10.7,[d] 8.7[e]
n-C_4H_9COOH, valerate ion	9.0,[d] 8.3[e]
$ClCH_2COOH$, $ClCH_2COO^-$	10.8, 11.2[c]
Citric acid, citrate ion	6.6,[f] 8.1[f]
C_2H_6, $CH_3NH_3^+$	15.2,[g] 15.6[c]
C_3H_8, $CH_3CH_2NH_3^+$, $CH_3NH_2^+CH_3$	12.1,[g] 13.0,[e] 13.8[e]
n-C_4H_{10}, n-$C_3H_7NH_3^+$, $NH_2CH_2CH_2NH_3^+$	9.8,[g] 11.2,[e] 12.0[e]
Ar, K^+, Cl^-	14.6,[h] 19.6,[c] 20.3[c]

[a] All ionic diffusivities have been computed from the electrical mobilities as found in the references given. [b] Recalculated from the data of V. Vitagliano and P. A. Lyons, *J. Am. Chem. Soc.*, **78**, 4538 (1956). [c] See ref. 9. [d] A. F. H. Ward and L. H. Brooks, *Trans. Faraday Soc.*, **48**, 1124 (1952). [e] "International Critical Tables," Vol. VI, McGraw-Hill Book Co., Inc., New York, N. Y., 1929, p. 259 ff. [f] See ref. 4. [g] P. A. Witherspoon, Abstracts of Research, 8th Annual Report on Research, Petroleum Research Fund, administered by the American Chemical Society, 1964, p. 52. [h] R. E. Smith, E. T. Friess, and M. F. Morales, *J. Phys. Chem.*, **59**, 382 (1955).

On Obtaining the Kinetic Parameters of the Glass Transition

by Stuart M. Ellerstein

Textile Research Institute, Princeton, New Jersey
(Received January 18, 1965)

A method is proposed whereby one may obtain the kinetic parameters associated with the glass transition directly from calorimetric data.

Consider a glass-forming polymer which has been cooled from a temperature well above its glass transition region to a temperature somewhat below in a quasi-static manner. Subsequent reheating of the sample would give a heat capacity curve which is markedly dependent upon the heating rate.[1-3] This is illustrated schematically in Figure 1.

Since we have started at the same temperature, T_i, and presumably put in the same total energy by the time T_f is reached, it may be seen that

$$\text{area (I)} + \text{area (IV)} + \text{area (V)} = \text{area (II)} + \text{area (III)} + \text{area (IV)} + \text{area (V)} \quad (1)$$

and therefore

$$\text{area (I)} = \text{area (II)} + \text{area (III)} \quad (2)$$

A general consideration of relaxation processes usually assumes that the internal energy of a system obeys a first-order rate law (if one is not too far away from equilibrium).[4] Thus we assume that

$$\frac{dU}{dT} = -\frac{U - U'}{q\tau} \quad (3)$$

where U is the instantaneous value of the internal energy associated with the process under consideration (here the molecular modes contributing to the glass transition), U' is the corresponding quasi-static value of the internal energy, dU/dT is the ordinate displacement (vertical dashed line) between the experimental curve 2 and the extrapolated low-temperature base line at an arbitrary temperature T, q is the constant heating rate dT/dt, and τ is the relaxation time (here

(1) R. O. Davies and G. O. Jones, *Advan. Phys.*, 2, 370 (1953).

(2) B. Wunderlich, D. M. Bodily, and M. H. Kaplan, *J. Appl. Phys.*, **35**, 95 (1964).

(3) M. V. Vol'kenstein and O. B. Ptitsyn, *Sov. Phys.-Tech. Phys.*, 1 2138 (1957).

(4) K. F. Herzfeld and T. A. Litovitz, "Absorption and Dispersion of Ultrasonic Waves," Academic Press, New York, N. Y., 1959, Chapter II.

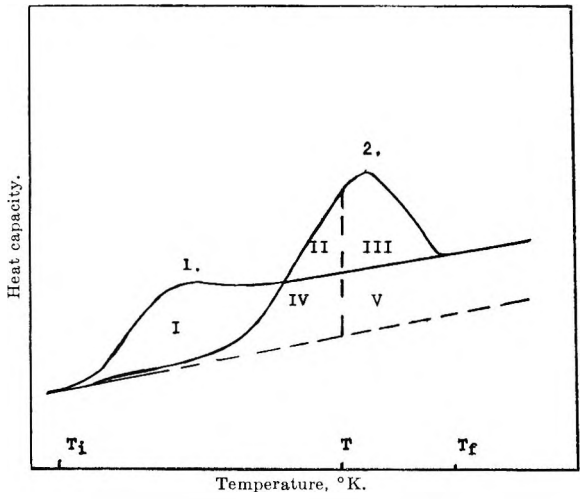

Figure 1. Schematic diagram of heat capacity *vs.* absolute temperature; curve 1, quasi-static heating; curve 2, rapid heating; both performed after quasi-static cooling.

considered to be of the Frenkel[5] type, *i.e.*, $\tau = \tau_0 \exp(E^*/RT)$.

Referring again to Figure 1, it may be seen that

$$U = \text{area (II)} + \text{area (IV)} \quad (4)$$

$$U' = \text{area (I)} + \text{area (IV)} \quad (5)$$

Therefore, substituting eq. 4 and 5 in eq. 3, and making use of eq. 2, one obtains

$$\frac{dU}{dT} = \frac{\text{area (III)}}{q\tau} \quad (6)$$

The kinetic parameters (activation energy and pre-exponential factor) may be obtained by a method analogous to one previously used for interpreting thermoanalytical data.[6,7] Expressing eq. 6 logarithmically and then taking finite differences of both sides of the resulting equation, one obtains

$$\frac{\Delta \log \frac{dU}{dT}}{\Delta \log \text{area (III)}} = \frac{-E^*}{2.303R} \frac{\Delta(1/T)}{\Delta \log \text{area (III)}} + 1 \quad (7)$$

Plotting $[\Delta \log dU/dT]/[\Delta \log \text{area (III)}]$ *vs.* $[\Delta (1/T)]/[\Delta \log \text{area (III)}]$ will result in a linear curve of slope $[-E^*/2.303R]$ and an intercept of unity, if the rate law is indeed first order. (Another method which is based on the experimental quantities being evaluated only at the peak temperature may also be used,[8,9] but this has distinct disadvantages.)

In these laboratories we are currently studying the glass transition using the Perkin-Elmer differential scanning calorimeter DSC-1. The thermogram so obtained yields measurable quantities which are commensurate with those of eq. 6. Thus it is seen that one is enabled to get the kinetic parameters directly by dynamic differential calorimetry.

Acknowledgment. The author wishes to express his gratitude to the TRI postdoctoral fellowship program of Textile Research Institute for supporting this work. Thanks are also given to Dr. J. H. Dillon for his most valuable discussion of the manuscript.

(5) J. Frenkel, "Kinetic Theory of Liquids," Dover Publications, New York, N. Y., 1955, Chapter IV.

(6) H. J. Borchardt and F. Daniels, *J. Am. Chem. Soc.*, **79**, 41 (1957).

(7) B. S. Freeman and B. Carroll, *J. Phys. Chem.*, **62**, 394 (1958).

(8) H. L. Friedman, presented at the 145th National Meeting of the American Chemical Society, New York, N. Y., Sept. 1963.

(9) R. M. Fuoss, I. O. Salyer, and H. S. Wilson, *J. Polymer Sci.*, **A2**, 3147 (1964).

Adsorption of Gases on Alkali Fluorides

by Yung-Fang Yu Yao

Scientific Laboratory, Ford Motor Company, Dearborn, Michigan
(Received January 22, 1965)

The adsorption of krypton on various surfaces and its application to surface area measurements have been treated quite extensively in the literature[1-4]; in general, one can evaluate the monolayer capacity from either the conventional B.E.T. plots or the volume adsorbed at the end of the vertical rise in an isotherm exhibiting vertical steps. In this laboratory, the adsorption of krypton has been used to measure the surface areas of several metal oxides and alkali fluorides micro single crystals. This note is to report some anomalies found for the adsorption of Kr and O_2 on NaF and LiF (100) faces.

The NaF crystals were precipitated out by adding an aqueous solution of NaF (B and A reagent grade) to absolute methanol very slowly with continuous stirring. The LiF crystals were prepared by adding an aqueous solution of NH_4F dropwise into a hot aqueous LiBr solution with continuous stirring. The LiF precipitate was further washed with triple-distilled water. The crystals appeared to be cubic under the microscope. They were outgassed at 450° to a final pres-

(1) R. A. Beebe, J. B. Beckwith, and J. M. Honig, *J. Am. Chem. Soc.*, **67**, 1554 (1945).

(2) B. B. Fisher and W. G. McMillan, *J. Chem. Phys.*, **28**, 549, 555, 562 (1958).

(3) G. L. Gaines, Jr., and P. Cannon, *J. Phys. Chem.*, **64**, 997 (1960).

(4) P. J. Malden and J. D. F. Marsh, *ibid.*, **63**, 1309 (1959).

sure of $\sim 1 \times 10^{-5}$ mm. Some sintering did occur during the first few hours of outgassing. All the adsorption measurements reported here were made on surfaces which have apparently reached their maximum sintering.

The adsorption of N_2, O_2, and Kr on these crystals at -183 and $-195°$ were determined using conventional volumetric adsorption apparatus. A cathetometer readable to 0.05 mm. was used for measuring the N_2 and O_2 pressures. In the case of Kr, a microscope coupled with a microscope slide readable to 0.001 mm. was used. In between runs the sample was degassed at 25° to $<1 \times 10^{-6}$ mm. overnight. Each experiment was repeated at least once and the reproducibility was good.

The isotherms of N_2, O_2, and Kr on NaF and LiF are shown in Figure 1. The vapor pressures of N_2 and O_2 measured directly at the bath temperatures were used. For Kr the pressure obtained by extrapolating the vapor pressures of liquid Kr to the bath temperatures were used as p_0. It is seen that N_2 gives the typical type-II isotherms. O_2 and Kr adsorption showed much less initial adsorption followed by a sharp rise and a leveling off at values approaching that of the B.E.T. V_m of N_2. Such steps in adsorption isotherms have been reported for inert gases on graphite or halides by many workers previously,[5] but they usually occur at much lower relative pressures (<0.1) than those of the present case. The fact that the vertical rise in the oxygen isotherm occurs at a higher relative pressure on the NaF surface than on the LiF surface suggests that the vertical rise expected for the Kr isotherm on NaF may not be nonexistent but may occur at a still higher relative pressure. Unfortunately, due to the fact that the relative pressures of krypton are calculated based on extrapolated vapor pressure of the liquid, points beyond relative pressure of 0.65 could not be measured experimentally without causing condensation on the walls.

Considerable controversy has been reported in the literature[5] on the possible experimental artifacts which may be responsible for the discontinuities in the isotherms at very low relative pressures. The following facts found in the present results tend to substantiate the conclusion that the vertical steps are reality rather than artifacts. (1) The similar vertical steps that were found for both O_2 and Kr despite the difference in the magnitude of their absolute pressures rules against the possibility of instrumental error. Furthermore, dosers of different sizes and different sections of the mercury manometer have been used not only for different gases but also for the same adsorbates, and there was no instrumental effect observed. (2) The relatively coarse,

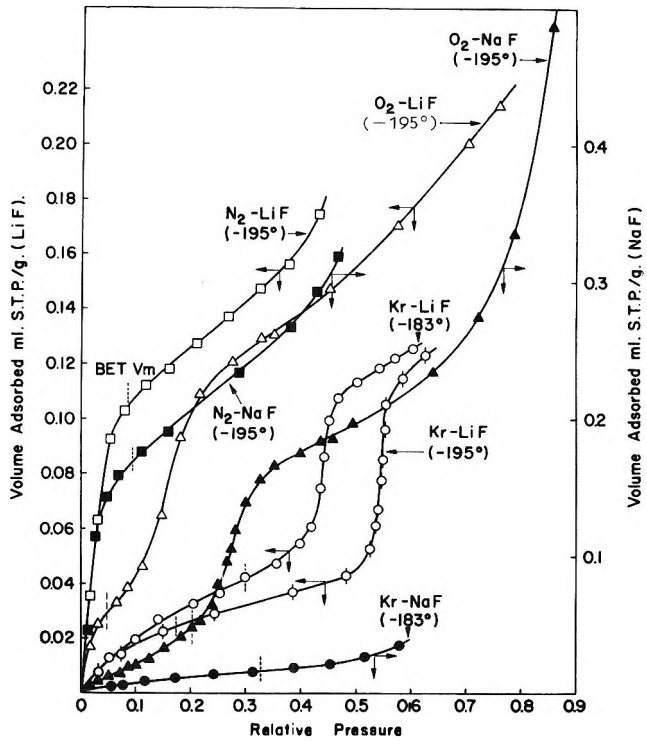

Figure 1. Adsorption isotherms.

nonporous crystals were held in the annular space between two short concentric tubes and the gas was led to the sample through two arms of a U-tube of diameter approximately equal to the width of the annular space. So, diffusion would not be a problem as that suspected for Fe_2O_3 powders.[5] (3) Apparent equilibrium was reached within 10 min. in all cases. However, more than 1 hr. for the first point of Kr adsorption and about 30 min. for the rest were allowed to ensure equilibrium. Corrin and Rutkowski[6] reported that adsorption of Kr on calcium halophosphate was very slow at relative pressures below 0.005 above which equilibrium was obtained within 5 min. The pressures reported here, particularly where the vertical steps occur, are so high that such difficulty in attaining equilibrium encountered at very low pressures is not expected. In the case of O_2 on NaF, four isotherms up to relative pressure of 0.7–0.9 were determined at $-195°$. In two of the experiments, 9 or 10 points were taken at relative pressures of 0.05–0.30, and about 5 or 6 points for the higher pressure range. In the other two experiments, only 3 or 4 points were taken up to relative pressure of 0.3, and 8–10 points at higher pressures. All four isotherms

(5) See for example, D. M. Young and A. D. Crowell, "Physical Adsorption of Gases," Butterworth and Co. (Publishers) Ltd., London, 1962, pp. 120–132.

(6) M. L. Corrin and C. P. Rutkowski, *J. Phys. Chem.*, **58**, 1089 (1954).

thus obtained coincide and no discrepancy was reported.

Upon application of the B.E.T. equation to the Kr and O_2 adsorption results, straight lines were obtained to the point where a vertical step begins. B.E.T. V_m terms and the corresponding surface areas can be evaluated from the straight lines. The results based on molecular areas of N_2 16.0 Å.^{2}, O_2 14.1 Å.^{2}, and Kr 19.5 Å.^{2} are shown in Table I. It is shown that the surface areas obtained from B.E.T. V_m of N_2 and from the amount of gas adsorbed at the end of the vertical rise found in the Kr and O_2 isotherm are of the same order of magnitude. A deviation of 10–20% is not unexpected in this case because: (1) the estimation of the end of the vertical step can only be approximate, (2) the liquid density molecular area of O_2 is used which may not be correct in this case, and (3) some second or higher layer may be included in the end-of-step points for Kr and O_2. On the other hand, the usual B.E.T. plots of the Kr and O_2 adsorption would give surface areas of only 0.125–0.5 of the nitrogen value. Gaines and Cannon[3] suggested that in using gas adsorption to determine surface area, the molecular cross-sectional area, σ, used should be adjusted according to the strength of the adsorption energy. For weak adsorption of Kr, the ratio of σ based on liquid density to σ in the monolayer varies from 0.68 to 0.85. However, this is not sufficient to make the surface areas calculated from B.E.T. V_m of Kr and O_2 to be comparable to that derived from B.E.T. V_m of N_2. Estimation of particle size based on the electromicrographs of LiF crystals give a value of 0.35 m.^{2}/g. Even though this number is less reliable due to the usual difficulty of getting true average samples, the inherent overemphasis of large particles, particularly in this case where the crystals tend to stack together, would favor a surface area greater than 0.35, *i.e.*, closer to the N_2 value than to the value derived from the B.E.T. plot of Kr or O_2 isotherms. It is the purpose of this communication to point out these anomalies and to re-emphasize the fact that one should not take gas adsorption and B.E.T. equations for surface area measurements as routine unless (1) at least two different types of adsorbates have been used on the same surface for comparison and (2) the adsorption measurements have been carried to as high relative pressure as feasible at least once to ascertain that there is no anomalous behavior.

Table I: Surface Areas in m.^{2}/g.

	LiF	NaF
N_2 (B.E.T., −195°)	0.457 (c = 95)	0.742 (c = 84)
O_2 (B.E.T., −195°)	0.137 (c = 16)	0.179 (c = 31)
O_2 (End-of-step, −195°)	0.418	0.607
Kr (B.E.T., −195°)	0.127 (c = 16)	...
Kr (B.E.T., −183°)	0.222 (c = 9)	0.090 (c = 7)
Kr (End-of-step, −195°)	0.571	...
Kr (End-of-step, −183°)	0.561	...

This type of adsorption with sharp-rising steps in isotherms at a relatively high relative pressure range has not been reported in the literature and the nature of the adsorbed state is by no means known. However, based on the following points it would seem that the usual model of mobile adsorption on an energetically uniform surface for step isotherms is also valid here. (1) The surface is essentially uniform, (100) faces with small fraction of heterogeneities due to edges, corners, etc. (2) The energies of interaction between Kr (and O_2) and the surfaces of the fluorides are low. This is shown by the low B.E.T. c values listed in Table I. Therefore, the quadrupole moments of diatomic molecules, especially the high moment of N_2, plays an important role in determining the shape of the isotherms. (3) Hill[7] derived the following relations for the critical conditions of a mobile monolayer with lateral interaction: $\theta_c = 1/3$ and $x_cC = 0.0869$, where θ_c and x_c are the critical fraction of surface coverage and critical relative pressure, respectively, and C is the analog of the B.E.T. c constant. It can be seen from Figure 1 that the θ_c terms for Kr and O_2 are of the right order of magnitude (*ca.* one-third of a monolayer). The average x_c for Kr on LiF is 0.35 which leads to the prediction that the heat of adsorption would be less than the heat of vaporization. The isoteric heats of ad-

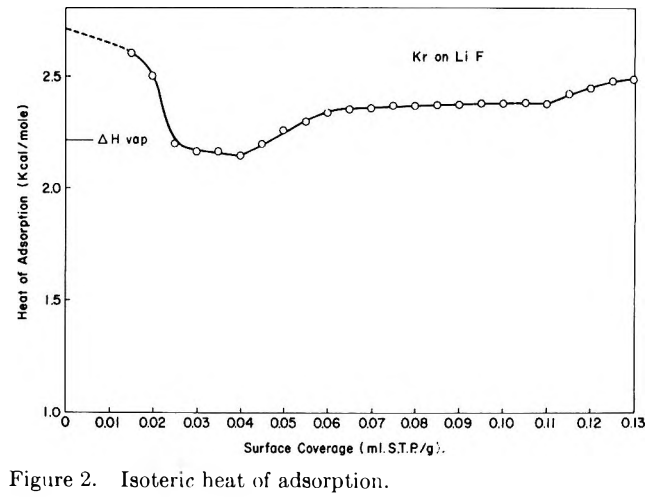

Figure 2. Isoteric heat of adsorption.

(7) T. L. Hill, *J. Chem. Phys.*, 14, 441 (1946).

sorption of Kr on LiF calculated from the isotherms at −183 and −195° are shown in Figure 2. The ΔH_v value is the heat of vaporization of liquid krypton at its normal boiling point.[8] If one takes the initial higher heat as due to some surface heterogeneities and the latter part of that including contributions of lateral interactions, then the minimum in the heat curve probably corresponds to the adsorption of individual molecules on the surface. This confirms the above prediction.

Acknowledgment. The author is grateful to Dr. J. T. Kummer of this laboratory for many helpful discussions during the course of this work.

(8) "Selected Values of Chemical Thermodynamic Properties," National Bureau of Standard Circular 500, U. S. Government Printing Office, Washington, D. C.

The Photochemistry of $\Delta^{2,5}$-Bicyclo[2.2.1]heptadiene[1]

by B. C. Roquitte[2]

Division of Pure Chemistry, National Research Council, Ottawa, Canada *(Received January 25, 1965)*

Theoretical calculation[3] indicates that there is interaction between the two isolated double bonds in the lowest excited state of $\Delta^{2,5}$-bicyclo[2.2.1]heptadiene, BCHD[2.2.1]; recent experimental observation that BCHD in ether solution upon irradiation with ultraviolet light causes isomerization to quadricyclene lends support to this view.[4] It is quite likely that the excited

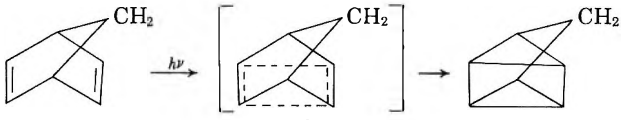

excited state

species involved in the liquid phase photolysis may be stabilized by collision to give a product which could be entirely different from that of the gas phase photolysis, or an altogether different excited species may be present in the gas phase.

This work was undertaken in order to gain better understanding of the excited state involved in the photodecomposition of BCHD, in particular, the behavior of such an excited species in the gas phase. Preliminary work indicated a difference between the behavior of the excited species in the liquid and that in the gas phase, depending upon the amount of excess energy present.[5]

Experimental

In order to avoid the mercury-photosensitized decomposition of BCHD, a mercury-free vacuum system which employed a two-stage oil diffusion pump backed by a mechanical pump was used. The reaction system, consisting of a cylindrical quartz cell 10 cm. long and 180 cc. in volume, connected to a piston-type circulating pump used for mixing reagent gases, and a diaphram gauge used as a null-type manometer, was enclosed in an air thermostat controlled to ±1°. The light source was a mercury resonance lamp used previously in this laboratory,[6] operated at a current of 60 ma. to obtain maximum intensity. A Corning 7910 filter was used in conjunction with the lamp to eliminate the 1849 radiation, so that the actinic light consisted mainly of 2537-Å. radiation. Two runs were made using no filter to investigate the effect of wave length on the product distribution. The light intensity was varied by interposing a wire-gauze screen between the light source and the reaction cell, and the relative intensity was measured with a 935 phototube connected to a sensitive galvanometer. Spectrograde acetone (Eastman Kodak Co.) was used as a gas phase actinometer.

BCHD[2.2.1] purchased commercially from Chemical Intermediate and Research Laboratories, Ohio, was fractionated and a middle fraction further purified by gas chromatography. The purified sample on analysis by gas chromatography was estimated to be 99.9% pure and was degassed and stored under vacuum. The standard sample of cyclopentadiene (used for the calibration of the gas chromatograph) was synthesized from dicyclopentadiene (Eastman Kodak Co.). Nitric oxide (Matheson 98%) was purified by bulb-to-bulb distillation from −160 to −196°. Oxygen, helium, and hydrogen (all Matheson C.P. grade) were used directly from the cylinder. Sulfur hexafluoride (Matheson 98.7%) was subjected to bulb-to-bulb distillation before use. Ethyl ether (Mallinckrodt) and cyclohexane (Phillips research grade) were distilled under vacuum, and only middle fractions were used. After irradiation, the reaction mixture was condensed out of

(1) Issued as National Research Council No. 8520. Presented at the 47th Canadian Institute of Chemistry Conference, Kingston, Ontario, June 1–3, 1964.

(2) Radiation Research Laboratories, Mellon Institute, Pittsburgh 13, Pa.

(3) C. P. Wilcox, Jr., S. Winstein, and W. G. McMillan, *J. Am. Chem. Soc.*, **82**, 5450 (1959); R. B. Hermann, *J. Org. Chem.*, **27**, 441 (1962); B. C. Roquitte, unpublished data.

(4) W. G. Dauben and R. L. Cargil, *Tetrahedron*, **5**, 197 (1961).

(5) B. C. Roquitte, *J. Am. Chem. Soc.*, **85**, 3700 (1963).

(6) R. A. Back and D. Van Der Auwera, *Can. J. Chem.*, **40**, 2339 (1962).

the reaction zone into an ampoule and sealed off under vacuum. When noncondensible gas was added, the contents of the reaction cell after photolysis were passed through two traps at −196° (when SF_6 was used, trap temperature was −130°) and noncondensibles discarded. The condensible portion was then transferred into the ampoule and sealed off. The products from the ampoule were introduced into the inlet system of an F & M temperature-programmed gas chromatograph Model 720 by means of a special crushing device. A silicon grease column (7.9 m., 25% by weight on Celite) was used for quantitative analysis of the products. In addition, a Reoplex column (18% by weight on Celite) and a Ucon fluid column (18% by weight on Celite) were used for the identification of the products. Each product was confirmed by mass spectrometric analysis. The identity of cyclopentadiene was also confirmed by ultraviolet absorption[7] [λ_{max} 4000 Å. (ϵ 3000)]; the infrared spectrum of product cyclopentadiene was also found to be identical with that reported.[8] Toluene was identified in the gas chromatograph by its retention time.

Results

The photolysis of BCHD with 2537-Å. radiation in a mercury-free system at temperatures of 27 and 57° and initial pressures from 4 to 31 mm., in the presence and absence of added gas, gave acetylene and cyclopentadiene in equal amounts; toluene was detected as a minor product. In most of the experiments, the conversion was approximately 0.1%; at higher conversion, cycloheptatriene was also a product. Since cyclopentadiene absorbs 2537-Å. radiation, at higher conversion complications arose from its secondary decomposition. The results of the photolysis of BCHD are given in Table I. In order to examine the effect of inert gas on the decomposition, a variety of gases was added, and the results are tabulated in Table II, which also includes the results of the photolysis in ether and cyclohexane solution.

Table I: Photolysis of BCHD under Various Conditions[a]

Initial concn., moles/l. × 10^4	$\phi_{C_2H_2}$	$\phi_{C_6H_8}$	ϕ_{tol}	Relative intensity, %
		27°		
1.07	0.40	0.40	...	100
2.29	0.50	0.51	0.058	100
2.65	0.50	0.53	0.054	39
3.42	0.49	0.50	0.051	100
6.24	0.50	0.50	0.052	100
6.27	0.54	0.50	...	39
9.28	0.49	0.50	0.059	100
16.81	0.49	0.49	0.055	39
		57°		
3.94	0.48	0.49	0.050	100
2.26	0.54	0.52	0.055	100

[a] $I_0 = 4.21 \times 10^{13}$ quanta/cc. sec.

Table II: Effect of Added Gas on the Photolysis of BCHD at 27°[a]

$\phi_{C_2H_2}$	$\phi_{C_6H_8}$	ϕ_{tol}	Added gas, mm.
0.52	0.51	0.056	H_2, 100
0.50	0.49	0.048	H_2, 300
0.42	0.41	0.050	H_2, 690
0.42	0.41	0.050	He, 650
...	0.49	0.055	NO, 10
...	0.42	0.051	NO, 600
0.41	0.42	0.053	O_2, 612
...	0.48	0.053	SF_6, 44
...	0.39	0.051	SF_6, 400
0.12	0.14	0.042	Ether sol.
0.11	0.13	0.052	Cyclohexane sol.

[a] Initial concentration 6.84×10^{-4} *M*. $I_0 = 4.21 \times 10^{13}$ quanta/cc. sec.

The yields of the products, cyclopentadiene and acetylene, are plotted as functions of time in Figure 1. From the linearity of the plots, it may be concluded that there was no change in the rate of formation of either of the products over the range of conversion used in this study. At higher conversion, the rate of production of cyclopentadiene decreased because of secondary decomposition.

Discussion

The ultraviolet absorption spectrum of BCHD has not been studied in detail. Qualitatively, the absorption begins at about 2700 Å. and exhibits a shoulder at 2300 Å. and several bands with fine structure between 2260 and 1990 Å.[3] At 2537 Å., the absorption was found to obey Beer's law accurately in the pressure range 4–31 mm.

The fact that photolysis of BCHD with 2537-Å. radiation produced acetylene and cyclopentadiene in equal amounts and a small amount of toluene suggests that in the gas phase BCHD exhibits no less than two primary processes

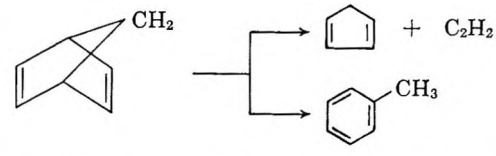

(7) L. W. Pickett, E. Paddock, and E. Sackter, *J. Am. Chem. Soc.*, **63**, 1073 (1941).

(8) J. Thiec and J. Wiemann, *Bull. Soc. Chim. France*, 207 (1958).

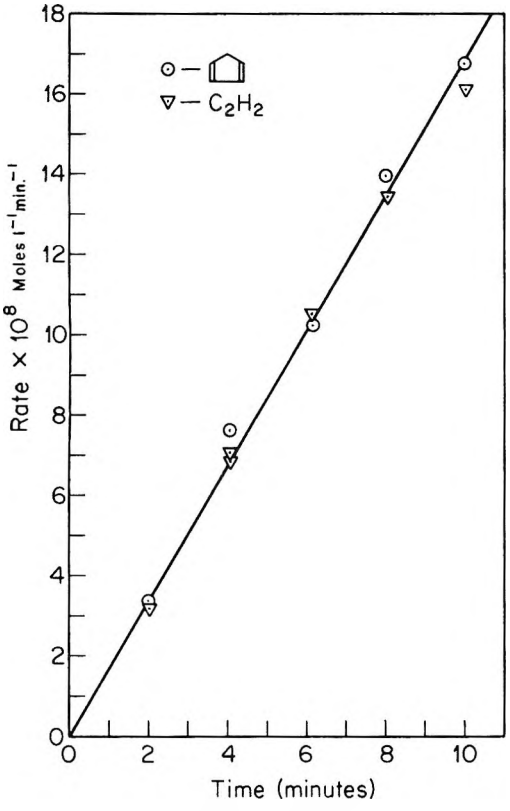

Figure 1. Variation of rate of formation of cyclopentadiene and acetylene with time.

Since we were unable to observe any emission visually, it is assumed that the molecules of BCHD do not dissipate energy by fluorescence at wave lengths ~3600–7000 Å. Over a range of pressure the total quantum yield (Tables I and II) for decomposition was 0.55 ± 0.02; thus, it seems likely that 45% of the excited molecules were internally converted to the ground state. While the photodecomposition of BCHD presumably proceeds *via* some excited state, the almost negligible effect of added gas and temperature and the independence of the quantum yields on the pressure indicate that any such excited species had too short a life to suffer collisional deactivation under our experimental conditions. In view of the energy (112 kcal.) per quanta of 2537-Å. radiation, this is not at all surprising. This is also consistent with the fact that in the liquid phase (Table II), where one would expect very many more collisions among the molecules, the quantum yields ($\Phi_{C_2H_2}$ and $\Phi_{C_6H_6}$) were lowered by a factor of 4. It is not clear why the quantum yield for the production of toluene was not affected, unless it originates from a different electronic excited state altogether. It is to be noted that nitric oxide behaved as an inert gas in this system, which suggests that the decomposition did not involve monoradicals. In addition, since oxygen had no effect on the product yields, it might be concluded that long-lived triplets were not involved in the photochemistry of BCHD. The decomposition probably proceeds through the intermediate formation of highly reactive biradicals I and II. The decomposition of bi-

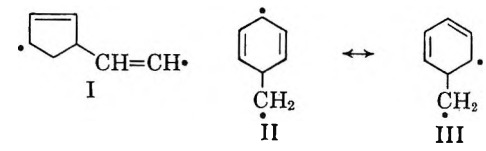

radical I could give cyclopentadiene and acetylene, while biradical II could rearrange to give biradical III and finally toluene. The rearrangement of a biradical of the above type is known in terpene chemistry.[9,10]

Acknowledgment. The author is grateful to Drs. K. O. Kutschke and R. A. Back for their interest in this work.

(9) H. Pines and J. Ryer, *J. Am. Chem. Soc.*, **77**, 4370 (1955).
(10) R. L. Burwell, Jr., *ibid.*, **73**, 4461 (1951).

γ-Radiolysis of Ammonium Perchlorate[1a,b]

by George Odian,[1c] Terese Acker, and Thomas Pletzke

Radiation Applications Inc., Long Island City, New York 10111, and Department of Chemical Engineering, Columbia University, New York, New York 10027 *(Received February 1, 1965)*

Although the radiolysis of various alkali and alkaline earth perchlorates has been extensively studied,[2,3] that of ammonium perchlorate has received little attention. Freeman and co-workers,[4] in one of the few reports on the chemical products of ammonium perchlorate radiolysis, have found chloride, chlorate, nitrite, and nitrate to be present. We wish here to describe the results of our studies on solid ammonium perchlorate radiolysis.

(1) (a) Presented in part at the 148th National Meeting of the American Chemical Society, Chicago, Ill., Sept. 1964. (b) The authors wish to acknowledge gratefully the support of this work by the Air Force Office of Scientific Research, Propulsion Division, under Contract AF 49(638)-1125. (c) To whom inquiries should be addressed: Department of Chemical Engineering, Columbia University, New York, N. Y. 10027.

(2) (a) L. A. Prince and E. R. Johnson, *J. Phys. Chem.*, **69**, 359, 377 (1965); (b) L. A. Prince, Ph.D. Thesis, Stevens Institute of Technology, 1963.

(3) H. G. Heal, *Can. J. Chem.*, **31**, 91, 1153 (1953); **37**, 979 (1959).

(4) (a) E. S. Freeman and D. A. Anderson, *J. Phys. Chem.*, **63**, 1344 (1959); **65**, 1662 (1961); (b) J. S. Hyde and E. S. Freeman, *ibid.*, **65**, 1636 (1961); (c) E. S. Freeman, D. A. Anderson, and J. J. Campisi, *ibid.*, **64**, 1727 (1960).

Reagent grade ammonium perchlorate (Matheson Coleman and Bell) was recrystallized twice from deionized water, dried, and then irradiated in stoppered test tubes with cobalt-60 at 10–15° at a dose rate of 0.36 Mrad/hr. No precautions were taken to exclude air from the specimens prior to radiolysis. The irradiated ammonium perchlorate was dissolved in water and analyses were performed for chlorate, chlorine dioxide, chlorite, hypochlorite, chlorine, chloride, and the total of nitrite plus nitrate. All of the analytical procedures were checked out with known mixtures of the various chemical species and it was ascertained that interferences were not present.

Chlorine dioxide, chlorite, hypochlorite, and chlorine were analyzed by their oxidation of iodide ion to iodine in a manner similar to that of Johnson and Prince.[2] The iodine was determined spectrophotometrically at 350 mμ. In basic media (pH 8–9), ClO^- and Cl_2 would be reduced to Cl^-, ClO_2 to ClO_2^-, while ClO_2^- would be unaffected. On acidification to pH 1–2, ClO_2^- (both ClO_2^- formed from NH_4ClO_4 radiolysis and that from the reduction of ClO_2 in basic media) would also be reduced (to Cl^-) in addition to the ClO_2, ClO^-, and Cl_2. Since no additional oxidation of iodide was observed on acidification, it was concluded that both ClO_2 and ClO_2^- are not products of ammonium perchlorate radiolysis. Thus, the basic oxidation of iodide ion was due to ClO^- plus Cl_2. The yields of these two species were separated by performing the iodide oxidation analysis with and without prior flash-boiling. Flash-boiling resulted in the expulsion of Cl_2 from the solution of irradiated ammonium perchlorate and was accomplished by heating the solution to boiling.

The oxidizing power of the solution of irradiated ammonium perchlorate toward ferrous ion in acidic media was also observed in a procedure similar to that of Johnson and Prince.[2] The ferric ion was determined spectrophotometrically at 305 mμ. In addition to the ClO^- and Cl_2, ClO_3^- is also reduced (to Cl^-) by ferrous ion. Thus, the ClO_3^- yield is obtained by the difference between the iodide and ferrous oxidations.

Chloride ion was determined by a modification of the Volhard procedure utilized by Burns and Muraca.[5] An excess of silver nitrate was added to the sample and the excess silver ion was back-titrated with thiocyanate ion. The yield must be corrected to take into account the fact that hypochlorite also reacts with silver ion (yielding AgCl and O_2).

The sum of nitrite plus nitrate was determined by a modification of the procedure used by Norwitz[6] in the analysis of nitrate. This involved the reduction of both nitrate and nitrite to nitric oxide by ferrous ion (in concentrated sulfuric acid solution) followed by the formation of $Fe(NO)^{2+}$ whose absorption at 525 mμ was then determined.

As indicated above, ClO_2 and ClO_2^- were found not to be products of ammonium perchlorate radiolysis in any appreciable amount. The same was observed for NO_3^- plus NO_2^-. ClO_3^-, ClO^-, Cl_2, and Cl^- were found to be the major products of the radiolysis of ammonium perchlorate and the results are shown in Figure 1. The initial G values were calculated and

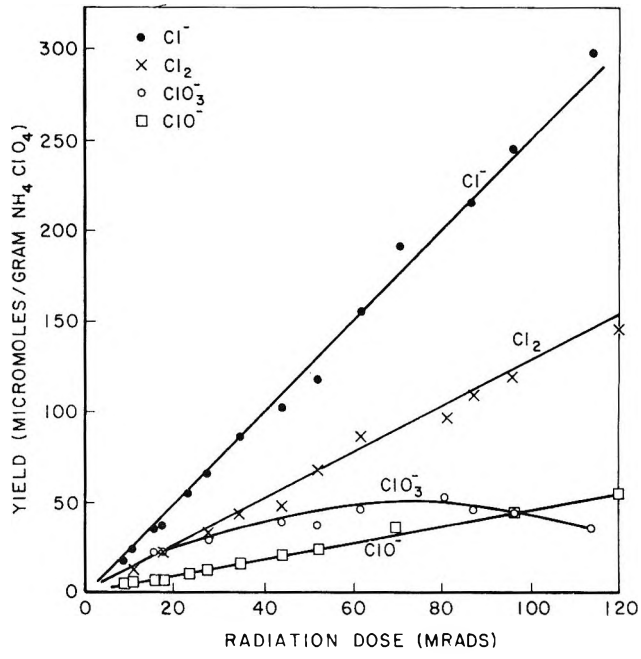

Figure 1. Yields in ammonium perchlorate radiolysis.

are given in Table I. It can be seen from Figure 1 that all yields except that of ClO_3^- were essentially independent of dose over the range studied. The ClO_3^- yield, however, was observed to fall off and decrease at the higher doses. This probably indicates that the ClO_3^- is undergoing radiolytic decomposition. This is very similar to the results of Heal[3] on the radiolysis of potassium perchlorate although Johnson and Prince[2] did not observe the effect.

The ammonium perchlorate radiolysis differs markedly in two respects from those of the metal perchlorates studied by Johnson and Prince. The

(5) E. A. Burns and R. F. Muraca, *Anal. Chim. Acta*, **23**, 136 (1960).
(6) G. Norwitz, *Anal. Chem.*, **34**, 227 (1962).

radiolytic decomposition of ammonium perchlorate is greater than that of the alkali or alkaline earth perchlorates by a factor of *ca.* 2–5 (depending on the particular metal perchlorate considered). Another difference is that Cl_2, while a major product (G = 1.2) of ammonium perchlorate radiolysis, is not reported at all in the radiolysis of the metal perchlorates.

The "crystal free volume" (the difference between the volume per mole of crystal derived from the X-ray density and the volume per mole of constituent ions[7]) has been successfully used to correlate the radiolytic yields of the metal perchlorates[2] and also the alkali metal bromates.[7] The radiolytic yields in those two groups of compounds had been found to increase with increasing free volume. However, the increased radiolytic yield of ammonium perchlorate relative to the metal perchlorates could not be correlated with the free volume nor with other properties of the cation such as the radius or the radius:charge ratio. It is thought that the anomalous results in the case of ammonium perchlorate may be due to participation of the ammonium ion in the decomposition reaction. As part of the effort to search for changes in the oxidation state of nitrogen in irradiated ammonium perchlorate, analyses were performed for nitrite plus nitrate. The negligible yields observed for nitrite–nitrate also precluded the presence of a variety of nitrogen compounds such as NO_2, NO, N_2O_3 since these would have showed up in the nitrite–nitrate analyses. The only nitrogen compounds which would not have been analyzed by the procedure are molecular nitrogen and possibly also N_2O. Further work is required before the high radiolytic yields in ammonium perchlorate can be understood.

Table I: Ammonium Perchlorate Radiolysis

Product	G value[a]
ClO_3^-	1.3
ClO_2	<0.02
ClO_2^-	<0.02
ClO^-	0.45
Cl_2	1.2
Cl^-	2.5
$NO_3^- + NO_2^-$	<0.05

[a] G = the number of ions or molecules formed per 100 e.v.

(7) G. E. Boyd, E. W. Graham, and Q. V. Larson, *J. Phys. Chem.*, **66**, 300 (1962).

Reciprocal Relations among Transport Coefficients

by Fred M. Snell

Department of Biophysics, State University of New York at Buffalo, Buffalo, New York 14214
(Received February 1, 1965)

Rayleigh,[1,2] in his original development of the dissipation function, considers forces proportional to velocities, absolute or relative, and first demonstrates reciprocal relations among the coefficients involved in the equations of motion.

Onsager[3,4] has given validity to reciprocal relations among transport coefficients and other phenomenological coefficients based upon microscopic reversibility. Statistical validity is derived from fluctuation theory.[5,6] Spiegler[7] has derived the reciprocal relations among transport coefficients from mechanical considerations. It may be shown that in systems assumed to be in mechanical equilibrium and in which only conservative forces operate, the reciprocal relations among transport coefficients follow from macroscopic thermodynamic reasoning alone. In such systems we have

$$m_i \frac{d\vec{v}_i}{dt} = -\text{grad } \mu_i + \sum_{j \neq i} \xi_{ij} c_j (\vec{v}_j - \vec{v}_i) + \sum_k \vec{F}_{ik} \quad (i = 1, 2 \ldots)$$

in which m_i is the molecular mass of species i, $\vec{v}_i$ is its mean molecular velocity, μ_i its chemical potential, c the concentration, and $\vec{F}_{ik}$ terms are the various conceivable body forces acting on i. The coefficient ξ_{ij} is the mean mole frictional coefficient of species j acting on species i. We consider only those forces derivable from a potential, and furthermore exclude those which are odd functions of time (eliminating magnetic and Coriolis forces unless their time average vanishes), whereupon they may be included in grad μ_i. Mechanical equilibrium then states that $d\vec{v}_i/dt = 0$ with reference to a laboratory coordinate frame of reference. Thus it follows that

(1) Lord Rayleigh, *Proc. Math. Soc.* (London), **4**, 363 (1873).
(2) Lord Rayleigh, "Theory of Sound," Vol. I, MacMillan and Co., Ltd., 2nd Ed., 1894, p. 102.
(3) L. Onsager, *Phys. Rev.*, **37**, 405 (1931).
(4) L. Onsager, *ibid.*, **38**, 2265 (1931).
(5) L. Onsager and S. Machlup, *ibid.*, **91**, 1505 (1953).
(6) S. Machlup and L. Onsager, *ibid.*, **91**, 1512 (1953).
(7) K. Spiegler, *Trans. Faraday Soc.*, **54**, 1409 (1958).

$$c_i \text{ grad } \bar{\mu}_i = \sum_{j \neq i} c_i \xi_{ij} \vec{J}_j - \sum_{j \neq i} \vec{J}_i \xi_{ij} c_j$$

where $\vec{J}_i = c_i \vec{v}_i$, and $\bar{\mu}_i$ is now the total chemical potential. In matrix notation this equation, summed over all i becomes

$$C^T \text{ grad } \mu = C^T \Xi J - J^T \Xi C$$

In that the left-hand side vanishes in every region to which thermodynamics apply as a result of the Gibbs–Duhem relation, the right-hand side must likewise vanish. The right-hand side can vanish if and only if $\Xi = \Xi^T$ thus showing that the $\xi_{ij} = \xi_{ji}$ for all ij.

Acknowledgment. The author acknowledges support by U. S. Public Health Service Grant GM06730.

Electronic Spectra of the Ga_2, In_2, and Tl_2 Molecules

by Dorothy S. Ginter,[1a] Marshall L. Ginter, and K. Keith Innes[1b]

Vanderbilt University, Nashville, Tennessee
(Received February 1, 1965)

Any group III metal, when heated to 2000° in a carbon-tube furnace, is vaporized to the extent that a visible band spectrum is emitted. Recently, we have published the results of a study of the case of aluminum.[2] There, rotational analysis and the observation of intensity alternation showed the emitter to be the Al_2 molecule, and it was mentioned that the Ga_2, In_2, and Tl_2 molecules also had been identified. As might be expected for the heavier molecules, the results were by no means as definitive as those for Al_2. However, since we are not aware of any other spectra that have been shown to arise from any one of the three heavier molecules, we offer here a summary of our observations.

It may be useful at the outset to indicate the nature of the evidence for the identifications. All emission spectra found have the general appearances of diatomic band spectra, appear in similar wave length regions, and show vibrational frequencies lower than that of the lower state of the Al_2 molecule. Moreover, the indium spectrum is the same whether obtained in a pure graphite, a pure molybdenum, or an Alundum tube, so that the emitter must be the homonuclear diatomic molecule, In_2. The other identifications follow by analogy.

Experimental

The various spectra were obtained using a graphite resistance tube (King) furnace and were photographed in the first and second orders of a 3.4-m. Ebert spectrograph (reciprocal dispersions 2.4 and 1 Å./mm., respectively). For absorption spectra, a xenon lamp served as the source of continuum.

When indium metal[3] was heated in a graphite tube, a previously unreported emission spectrum was observed in the 5000–6000-Å. region. Prominent bands are listed in Table I. For temperatures greater than 1300°, the spectrum could be photographed in the second order on Kodak 103a-F plates in about 90 min. The intensity of this spectrum (as well as of those discussed below) was unaffected by the introduction of helium or argon but was drastically reduced in hydrogen (InH being formed preferentially). Similar experiments were performed using either an extruded molybdenum or an Alundum tube inside the graphite heating element, in order to exclude carbon. Spectra obtained with and without the liner tubes were identical in structure and intensities. Thus, on a purely empirical basis, the emitter of the spectrum can be identified as In_x.

When gallium metal was heated to about 1500° in the King furnace, a new system of emission bands between 4600 and 5500 Å. (Table II) could be photographed in the first order in about 25 min. using 103a-F plates. The intensity of this spectrum was much lower than that of the In_x spectrum. Though much rotational fine structure was observed, it was only partially resolved and band heads were poorly defined.

Indium and gallium were heated together to about 1300° in either the graphite heating element or the molybdenum liner. One group of new emission features was found at 4824 Å. Since the features could be found only when both metals were present, they were taken as consistent with an emitter of formula Ga_yIn_z.

Thallium metal, on account of its toxicity, was heated only in a molybdenum tube which was long enough to extend through the furnace and carry its own vacuum system. A new emission spectrum was observed near 6300 Å. while a number of new complex absorption bands were observed below 4500 Å.

(1) (a) Monsanto Fellow, 1960–1961; Woodrow Wilson Fellow, 1958–1959; (b) to whom communications should be sent.

(2) D. S. Ginter, M. L. Ginter, and K. K. Innes, *Astrophys. J.*, 139, 365 (1964).

(3) Although higher purity indium was occasionally used, for most of the experiments the indium used was quoted at 99.9% purity. Analysis by Accurate Metal Laboratories, Chicago, Ill., was consistent with the quotation. The only impurity that analyzed at more than 0.01% was lead.

Table I: Prominent Band Heads of the In_2 Spectrum[a]

λ_{air}, Å.	ν_{vac}, cm.$^{-1}$	Remarks
	Emission bands	
R 5107.8	19,572.3	Line
V 5132.6	19,478.0	Line
V 5144.4	19,433.1	Line
V 5153.4	19,399.4	Line
V 5156.5	19,387.4	Double line
V 5162.6 (2)	19,364.5	Line
V 5172.4 (2)	19,328.0	Line
V 5182.6 (2)	19,289.8	Line
V 5193.4 (2)	19,250.4	Line
V 5204.6	19,208.5	Overlapped
V 5216.4 (2)	19,165.0	Line
V 5229.0 (2)	19,118.9	Line
V 5242.6 (2)	19,069.3	Line
V 5256.5 (2)	19,018.6	Line
V 5269.0 (2)	18,973.5	
V 5279.5	18,936.0	
V 5318.4 (1)	18,797.4	
V 5321.0 (4)	18,788.1	
5335.5	18,737.1	Atomic line (?)
V 5351.7 (4)	18,680.4	
R 5378.1 (3)	18,588.9	
V 5387.6 (3)	18,556.0	
V 5391.0	18,544.4	
R 5393.8 (3)	18,534.5	
V 5409.6 (3)	18,480.6	
R 5411.4	18,474.4	
R 5419.8	18,445.8	
V 5436.6 (3)	18,388.6	Line
R 5445.8	18,357.8	
R 5451.2 (3)	18,339.5	
R 5462.1 (3)	18,302.9	
V 5467.7 (4)	18,284.2	
V 5483.4 (2)	18,231.8	
V 5488.6 (4)	18,214.4	Line
V 5492.0 (4)	18,203.3	Line
V?5504.6 (3)	18,161.7	Line
5507.9 (4)	18,150.2	Long-λ edge measured
5509.8 (5)	18,144.5	Line
V 5510.5 (4)	18,142.2	
R 5515.4 (5)	18,125.9	Line
5516.9 (5)	18,121.1	Line b
5520.1 (4)	18,110.7	Line
V 5520.8 (4)	18,108.3	
5523.5 (5)	18,099.4	Long-λ edge measured
5526.2 (5)	18,090.6	Long-λ edge measured
5526.8 (5)	18,088.6	Long-λ edge measured
5532.6 (4)	18,069.8	Line
R 5535.7 (3)	18,059.4	
R 5550.6 (3)	18,011.1	
V?5551.4 (2)	18,008.5	
R 5595.0 (2)	17,868.2	
R 5603.6	17,840.6	
R 5640.0 (3)	17,725.5	
R 5648.6	17,698.5	
R 5685.6 (3)	17,583.5	
R 5693.3 (3)	17,559.7	
	Absorption bands[b]	
R 3588.5 (4)	27,859	
3595	27,808	Broad intensity maximum
R 3617.2 (5)	27,638	
R 3628.2 (5)	27,554	
3658	27,328	Broad intensity maximum
R 3673.2 (5)	27,216	
V 3680.2 (3)	27,165	
R 3685.7 (4)	27,124	
R 3693.2 (3)	27,069	
V 3720.4 (4)	26,871	
V 3737.6 (4)	26,747	
R 3746.7 (4)	26,683	
R?3782.1 (4)	26,432	

[a] The following symbols are used: R, degraded to longer wave lengths; V, degraded to shorter wave lengths; M, no detectable degrading; 0....5, a rough, visual intensity scale for the most distinct bands; s, sharp; d, diffuse; b, broad; and v, very. [b] In addition to these bands there is much badly over lapped fine structure at wave lengths greater than 4025 Å.

Results and Discussion

A. Indium. Over 100 band-like emission features were measured between 5000 and 5950 Å. The more prominent of these have been listed, with attempted descriptions, in Table I. The long wave length portion of the spectrum is overlapped slightly by the emission spectrum of the InH molecule. However, the InH emission spectrum has been studied separately[4] so that we have been able to eliminate InH features from Table I.

Since convincing, complete vibrational analyses have not been found for any one of the several band types we restrict discussion to the most characteristic vibrational intervals. These are most easily recognized for those red-degraded bands which exhibit rotational structure and are free of overlapping bands of other types between 5500 and 5800 Å. The best-defined heads are at 18,011, 17,868, 17,726, and 17,584 cm.$^{-1}$, and at 17,841 and 17,699 cm.$^{-1}$. An interval of 142 cm.$^{-1}$ is strongly suggested by these numbers, and the less well-defined heads that can be fitted into a resulting Deslandres table indicate that 142 cm.$^{-1}$ applies to the lower electronic state. If so, the upper-state frequency is smaller, probably about 115 cm.$^{-1}$.

(4) M. L. Ginter, *J. Mol. Spectry.*, 11, 301 (1963).

Table II: Prominent Band Heads of the Ga_2 Emission Spectrum[a]

λ_{air}, Å.	ν_{vac}, cm.$^{-1}$[b]	Remarks
R 4648.4	21,506.9	Fine structure (?)
R 4684.2	21,342.2	
R 4719.2	21,184.4	vb
R 4767.4	20,969.7	s
R 4804.2	20,809.2	Double head and fine structure
R 4852.5	20,602.1	Double head and fine structure
R 4892.2	20,435.1	Double head (?)
M 4932.0	20,270.7	Fine structure
R 4942.5	20,227.1	s
R 4971.5	20,109.3	Fine structure (?)
R 4975.5	20,092.7	
R 4993.2	20,021.7	Fine structure
R 5013.5	19,940	Fine structure
V 5065.7	19,735	
R 5068.8	19,723	
V 5117.3	19,536	
V 5120.7	19,523	
V 5143.9	19,435	

[a] The symbols are those used in Table I. [b] When the sixth significant figure is lowered a half space, the measurement is estimated to be correct to ±0.7 cm.$^{-1}$.

Both of these differences are found for bands of other types in this extensive spectrum but the other systems do not stand in any obvious relation to the red-degraded system.[5]

Wajnkranc[6] had earlier noted absorption by indium vapor at shorter wave lengths and this is summarized and supplemented in Table I. Although the fine structure appears sharp, the bands show only a few obvious heads and are therefore even less susceptible to analysis than are the emission bands.

Rotational analysis of single-headed bands at 17,868 and 17,584 cm.$^{-1}$ was attempted but line numberings and combination differences could not be made unique. Successful rotational analysis must await sharper fine structure.

Both vibrational and rotational structure, however, suggest a diatomic emitter which, on the basis of the experiments described, must be the In_2 molecule. The vibrational frequency is reasonable by comparison with the value, 350 cm.$^{-1}$, known for the lower state of Al_2. Since the detailed vibrational and rotational analyses have been inconclusive, the electronic states involved remain undetermined.

B. Gallium. The observed spectrum consists primarily of red-degraded bands between 4600 and 5500 Å. At wave lengths longer than 5200 Å., GaH emission bands[7] are superimposed. The most clearly defined of the new band heads are listed in Table II. If one considers only those red-degraded bands which are most prominent (*e.g.*, those comparable features at 20,435 and 20,602 cm.$^{-1}$), frequency differences seem clustered about 165 cm.$^{-1}$, but are notable for lack of constancy. Attempts to arrange less prominent bands in the same vibrational scheme suggest that 165 cm.$^{-1}$ is an upper-state frequency. Yet even this is not certain. Since the frequency falls between the values found for Al_2 and In_2, it seems reasonable to assign it to the Ga_2 molecule.[8]

Unlike indium, which occurs predominantly in one isotopic form, gallium occurs naturally as a mixture of two isotopes, in the ratio 3:2. Other things being equal we should expect for Ga_2 three bands (intensities 12:9:4) for each band of In_2. We believe that this is the reason that our vibrational analysis of the spectrum of Ga_2 is even more fragmentary than for that of the heavier molecule.

As indicated in Table II many bands exhibit rotational structure, but we have made no progress in its analysis. Again the electronic states cannot be identified.

C. Indium–Gallium. The strongest of the line-like features near 4824 Å. show a constant second difference of frequencies which could be characteristic of either a vibrational sequence or a rotational branch. Under vacuum the observations are (cm.$^{-1}$) 20,760.5, 20,761.7, 20,763.8, 20,767.2, 20,771.6, and 20,776.7. Regardless of which interpretation is adopted, no molecular constants specific to *one* electronic state can be derived. The sequence interpretation seems most likely for Ga_yIn_z but it is conceivable that the emitter is a nonlinear molecule such as GaInH in which case the features could arise from rotational subbands of a single band.

D. Thallium. The weak *emission* bands are all degraded to the red and fall naturally into a Deslandres table with upper- and lower-state vibrational frequencies of 88 and 136 cm.$^{-1}$, respectively. These are slightly lower than those suggested for In_2. Their magnitudes and the method of excitation indicate that the emitter is the Tl_2 molecule. Unambiguous analyses have not been found for the strong *absorption* bands of Table III.[5] (Again the table contains only bands not attributable to TlH.[9])

(5) Complete lists of observed bands and possible vibrational schemes for all spectra summarized in this note may be found in the Ph.D. thesis of D. S. Ginter, Vanderbilt University, 1965.

(6) R. Wajnkranc, *Z. Physik*, **104**, 122 (1936–1937).

(7) M. L. Ginter and K. K. Innes, *J. Mol. Spectry.*, **7**, 64 (1961).

(8) Some confirmation of the identification is found in mass spectroscopic work on species effusing from a graphite furnace containing gallium metal at 1600°K. There, it was found that Ga_2 is the most abundant molecular species by more than an order of magnitude: W. A. Chupka, J. Berkowitz, C. F. Giese, and M. G. Inghram, *J. Phys. Chem.*, **62**, 611 (1958).

Table III: Prominent Features of the Tl_2 Spectrum[a]

λ_{air}, Å.	ν_{vac}, cm.$^{-1}$	Remarks
	Emission bands	
R 6250.2 (0)	15,995	
R 6283.6 (1)	15,910	
R 6318.6 (1)	15,822	
R 6337.4 (0)	15,775	
R 6373.8 (1)	15,685	
R 6391 (0)	15,642	
R 6426.6 (0)	15,556	
R 6481.2 (0)	15,425	
R 6535.4 (0)	15,297	
	Absorption bands	
4237		Broad intensity maximum
V 4254.1 (5)	23,500.1	
R 4289.6 (5)	23,305.4	
V 4292.7 (5)	23,288.8	s
R 4293.7 (5)	23,283.5	s
V 4297.9 (4)	23,260.6	Overlapped
V 4315.7 (5)	23,164.7	s
V 4321.0 (5)	23,136.2	
V 4353.0 (3)	22,966.2	s
4402		Broad intensity maximum

[a] The symbols are those used in Table I.

It may be noted that the small differences in the apparent frequencies of In_2 and Tl_2 are similar to those for Ag_2 and Au_2.[10,11]

Conclusion

It has been argued that most bands listed in this note are emitted by the homonuclear diatomic molecules Ga_2, In_2, and Tl_2. The longest wave length, red-degraded bands are for each molecule the source of the least ambiguous vibrational analysis. Apparent dissimilarities in the series at the shorter wave lengths may arise from the expected differences in coupling of motions and in selection rules between lighter and heavier members of the series. For the lighter members of the series, electron configurations should be analogous to those discussed already for Al_2.[2]

Acknowledgments. This research was sponsored by the Naval Ordnance Laboratory (White Oak, Md.), the U. S. Army Ballistic Missile Agency (Huntsville, Ala.), and the Chemistry Office of the Advanced Research Projects Agency [monitored by the U. S. Army Research Office (Durham, N. C.)].

(9) H. Neuhaus and V. Muld, *Z. Physik*, **153**, 412 (1959); T. Larsson and H. Neuhaus, *Arkiv Fysik*, **23**, 461 (1963).

(10) B. Kleman and S. Lindkvist, *ibid.*, **9**, 385 (1955).

(11) B. Kleman, S. Lindkvist, and L. E. Selin, *ibid.*, **8**, 505 (1954).

The Continuous Absorption Spectrum of Iodine Monochloride[1]

by E. B. Nebeker and C. J. Pings

Division of Chemistry and Chemical Engineering, California Institute of Technology, Pasadena, California
(Received February 2, 1965)

Seery and Britton[2] presented values of the extinction coefficient for iodine monochloride between 220 and 600 mμ. Since this information has only recently become available, we were previously compelled to make these measurements. Although our data agree with Seery and Britton's results in most regions of the spectra, we want to point out that their data do not agree with Binder's[3] and ours in the spectral region of 290 to 370 mμ. In addition, we have quantitatively compared our data to the presently existing literature values of the extinction coefficient of iodine monochloride.[2-4]

Experimental

Chemicals. Iodine monochloride was prepared by combining iodine with chlorine in a vacuum system. Baker and Adamson 99.8% purity iodine was employed. The chlorine used was stated to be 99.9% pure by the Matheson Co. We checked this analysis by examining the absorption spectrum in the ultraviolet, visible, and infrared regions.

Measurements. A Cary Model 14 recording spectrophotometer with a 10-cm. quartz optical cell was used in all the measurements. Kel-F wax was used to lubricate the stopcock and tapered joint of the cell. All measurements were made at room temperature, 25 ± 1°.

Five measurements were made, three with an excess of iodine and two with an excess of chlorine. The concentration of iodine monochloride was determined from a previous knowledge[3] of the extinction coefficient of iodine monochloride at the point of maximum absorbancy in the ultraviolet region of the spectrum. This extinction coefficient agrees exactly with that of Seery and Britton to four significant figures. In order to correct the iodine monochloride spectrum for the absorbancy of chlorine in the runs in which chlorine was

(1) Work supported by Directorate of Chemical Sciences of the Air Force Office of Scientific Research under Contract No. AF 49(638)-1273.

(2) D. J. Seery and D. Britton, *J. Phys. Chem.*, **68**, 2263 (1964).

(3) J. L. Binder, *Phys. Rev.*, **54**, 114 (1938).

(4) G. E. Gibson and H. C. Ramsperger, *ibid.*, **30**, 598 (1927).

in excess, the total pressure of the optical cell was measured with a silicone oil manometer and a cathetometer. After the excess chlorine was accounted for, the data of the five runs agreed very well throughout the spectrum. For example, the maximum in the visible region was 116.5 (mole-cm./l.)$^{-1}$ with a variance of 0.9 (mole-cm./l.)$^{-2}$. Our results are the arithmetic average of the data of the five runs.

Results

In Figure 1 our results have been compared to the data of Seery and Britton,[2] Binder[3] at 18°, and Gibson and Ramsperger.[4] A line has been passed through our data and Binder's. Our data are not reported at

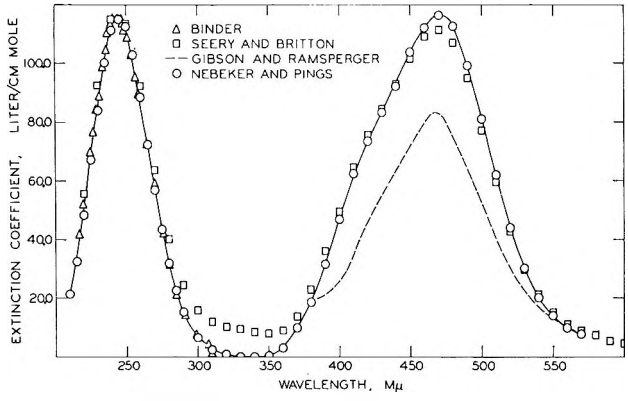

Figure 1. Decadic extinction coefficients of iodine monochloride.

wave lengths greater than 576 mμ because this is the convergence limit, above which the absorption spectrum is discrete.[5] In the ultraviolet region, our measurements fall on the same curve as those of Binder, with Seery and Britton's results deviating slightly from this curve. However, in the region between 290 and 370 mμ, the measurements of Binder and ourselves differ greatly from those of Seery and Britton. Also, since their data in the visible region are slightly displaced toward shorter wave lengths, we suspect that their instrument may not have been accurately calibrated. We calibrated the Cary Model 14 spectrophotometer wave length scale by independent measurements and found the accuracy to be well within the 4-Å. tolerance specification of the instrument. Nevertheless, our data agree fairly well with those of Seery and Britton in the visible region, differing by 4% at the maximum. Seery and Britton also noticed that their data did not agree with that of Gibson and Ramsperger.[4] However, Gibson and Ramsperger may not have reported true extinction coefficients.

(5) O. Darbyshire, *Phys. Rev.*, **40**, 366 (1932).

Difluoroacetylene[1]

by Julian Heicklen and Vester Knight

Aerospace Corporation, El Segundo, California
(Received February 25, 1965)

We wish to report the preparation and purification of difluoroacetylene. The preparation of this compound has not been previously reported except in two patents.[2] In the first, Gochenour claimed a method of preparation for all of the perfluorinated alkynes though he presents no evidence that he ever prepared C_2F_2. In the second patent, difluoromaleic anhydride was thermally decomposed at 500–1000°. The reported products of the reaction were FC≡CCOF, C_2F_2, CO_2, and CO, and the polymers of the fluorinated compounds. The presence of C_2F_2 was inferred by distilling the condensed products of the pyrolysis directly into a mass spectrometer and noting that the peak at *m/e* 62 was prominent. While such evidence is highly suggestive, the C_2F_2 was never isolated.

We prepared C_2F_2 from the photolysis of C_2F_4. Four different experiments were performed. A sample at 20 mm. pressure was photolyzed in a quartz cell with a Hanovia spiral low-pressure mercury resonance lamp or a Hanovia Type-SH U-shaped medium-pressure mercury lamp. In both cases, runs were made with and without a Corning 9-54 filter. This filter removed radiation below 2200 Å. With the low-pressure resonance lamp, the reaction cell remained cold, whereas with the medium-pressure lamp, the cell became hot, probably reaching temperatures between 100 and 200°.

In all the experiments, *c*-C_3F_6 was produced owing to double-bond cleavage followed by addition of CF_2 radicals to C_2F_4.[3,4] Additional products were found only in the experiments with the medium-pressure lamp when no filters were used. Under these conditions, the only additional products were C_2F_2, the polymer of C_2F_4, and perhaps in some experiments a trace of some C_4 fluorocarbons, even when photolysis was sufficiently long to exhaust the C_2F_4 monomer. (We did not analyze for CF_4, so it might also have been present.) The room-temperature mercury-sensitized photolysis of C_2F_4 at 2537 Å. does not break C–F

(1) This work was supported by the U. S. Air Force under Contract No. AF 04(695)-269.

(2) (a) C. I. Gochenour, U. S. Patent 2,546,997 (1951); (b) W. J. Middleton, U. S. Patent 2,831,835 (1958).

(3) B. Atkinson, *J. Chem. Soc.*, 2684 (1952).

(4) J. P. Heicklen, V. Knight, and S. A. Greene, *J. Chem. Phys.*, **42**, 221 (1965).

bonds.[3,4] Apparently, the medium-pressure lamp emits radiation below 2200 Å. which can cleave the C–F bond. The mechanism that explains the results with 2537-Å. radiation is[3,4]

$$Hg + h\nu(2537\ Å.) \longrightarrow Hg^* \quad (1)$$

$$Hg^* + C_2F_4 \longrightarrow Hg + 2CF_2 \quad (2)$$

$$CF_2 + C_2F_4 \longrightarrow c\text{-}C_3F_6 \quad (3)$$

$$2CF_2 \longrightarrow C_2F_4 \quad (4)$$

When higher-energy radiation is also present, then

$$C_2F_4 + h\nu(<2200\ Å.) \longrightarrow C_2F_3 + F \quad (5)$$

$$F + C_2F_4 \longrightarrow C_2F_5 \quad (6)$$

$$(C_2F_4)_nF + C_2F_4 \longrightarrow (C_2F_4)_{n+1}F \quad (7)$$

$$(C_2F_4)_nF + (C_2F_4)_mF \longrightarrow (C_2F_4)_{m+n}F_2 \quad (8)$$

$$2C_2F_3 \longrightarrow C_2F_4 + C_2F_2 \quad (9)$$

Reactions 6–8 are known to occur with the chlorine atom as the initiator.[5] Perhaps the C_2F_3 radicals can also combine to form C_4F_6. Such a reaction apparently is not favored but could account for the trace amounts of C_4 fluorocarbons observed in some experiments.

The reacted mixture was analyzed on a Beckman GC-2A gas chromatograph by the method of Greene and Wachi.[6] They had found that in some of their work a small peak appeared just after C_2F_4, which could only be assigned to C_2F_2. This assignment must be correct for two reasons. First, the peak has a retention time that lies in the C_2 or possibly the C_3 region. Since other C_2 and C_3 perfluorocarbon retention times were known, this assignment is the only one that remains except for the unlikely possibility of perfluorocyclopropene. Second, we have since verified that the light hydrocarbons have retention times on our column similar to the corresponding fluorocarbons. The peak assigned to C_2F_2 has nearly the same retention time as C_2H_2.

During the gas chromatographic analysis, the peak believed to be C_2F_2 was isolated and trapped in liquid nitrogen. Then, this product was purified by again passing it through the column and retrapping it. The infrared spectrum of the purified product was observed in a Perkin-Elmer 21 spectrometer. With a sample at only a few tenths of a millimeter pressure, a very intense peak was observed at 1149 cm.$^{-1}$ and one at least 10 times weaker at 1370 cm.$^{-1}$. The ratios of the intensities of the two bands did not appear constant. This spectrum corresponds to no known perfluorinated carbon compound and can be associated with C_2F_2. Difluoroacetylene has only two infrared active fundamentals. The asymmetric bend would be below 700 cm.$^{-1}$ and thus would not have been detected. The asymmetric C–F stretch should be extremely intense and lie between 1000 and 1400 cm.$^{-1}$. The band at 1149 cm.$^{-1}$ was surely this fundamental. The 1370-cm.$^{-1}$ band might have been an overtone, or, more likely, it might have been associated with a higher polymer, perhaps the dimer. If the ratio of the two band intensities does indeed vary, as the data seem to indicate, then two different molecules must be involved. The monomer is quite unstable at room temperature and rapidly polymerizes; thus, it would not be surprising if some dimer had been present even though the infrared spectrum was taken within a couple of hours after purification.

If the 1370-cm.$^{-1}$ band is ruled out as a fundamental, then the spectrum must have been that of C_2F_2, for it is the only perfluorinated carbon compound with only one infrared active stretching vibration.

(5) D. Marsh and J. P. Heicklen, Southwest Regional Meeting of the American Chemical Society, Dec. 1964; also Aerospace Report No. TDR-469(5240-20)-11, March 1965.

(6) S. A. Greene and F. M. Wachi, *Anal. Chem.*, **35**, 928 (1963).

COMMUNICATIONS TO THE EDITOR

Isotopic Equilibrium Separation Factors in the Hydrogen Solubility Process in Platinum–Palladium Alloys

Sir: The studies on platinum–palladium alloys have been greatly extended during the past few years. It has been pointed out[1] that using an alloy of appropriate palladium–platinum ratio, the respective separate equilibrium solubilities of hydrogen and deuterium may be as high as 15:1 (25°). A separation factor

(1) T. B. Flanagan, *J. Phys. Chem.*, **67**, 203 (1963).

of 10 to 15 has been obtained by means of electrochemical experiments.[1] It is of interest to determine if this large separation factor represents an equilibrium factor, the magnitude of which would be quite unusual at room temperature. It was decided therefore to carry out new measurements by direct gas–metal equilibration techniques.

In view of obtaining a fast isotopic equilibration, a highly dispersed material was employed. A 10 mole % platinum–palladium alloy was deposited on porous sintered α-alumina granules, following a procedure previously used for the deposition of pure palladium.[2] X-Ray examination and hydrogen sorption isotherms compared with those obtained by others on bulk alloys[3] (where the nature of the alloy is not in doubt) and on dispersed alloys[4] showed that platinum and palladium were present on the carrier as a homogeneous alloy: in our isotherm on Pt–Pd preparation, the plateau of the two-phase $\alpha \rightleftarrows \beta$ region has completely disappeared, which is a proof that an alloy is obtained.

The separation factor α was measured at −78, 20, and 82° under atmospheric total pressure, using both a chromatographic technique with 75% deuterium-enriched hydrogen and single-stage equilibrations of hydrogen of natural abundance (130 p.p.m. of deuterium as 260 p.p.m. of (HD)/(HD + D_2)) with subsequent mass spectrometric analysis.[2]

The following equilibria have to be considered

$$H_2(\text{gas}) + D(\text{soln.}) \rightleftharpoons HD(\text{gas}) + H(\text{soln.}) \qquad K_1 = 2\alpha_1 \quad (1)$$

which takes place almost exclusively for a low deuterium abundance

$$HD(\text{gas}) + D(\text{soln.}) \rightleftharpoons D_2(\text{gas}) + H(\text{soln.}) \qquad K_2 = \alpha_2/2 \quad (2)$$

which prevails for very high deuterium content

$$H_2(\text{gas}) + 2D(\text{soln.}) \rightleftharpoons D_2(\text{gas}) + 2H(\text{soln.}) \qquad K_3 = \alpha_1\alpha_2 \quad (3)$$

$$H_2(\text{gas}) + D_2(\text{gas}) \rightleftharpoons 2HD(\text{gas}) \qquad K_4 = K_1/K_2 = 4\alpha_1/\alpha_2 \quad (4)$$

$$H_2(\text{gas}) \rightleftharpoons 2H(\text{soln.}) \qquad K_5 \quad (5)$$

$$D_2(\text{gas}) \rightleftharpoons 2D(\text{soln.}) \qquad K_6 \quad (6)$$

The K's represent the equilibrium constants; α_1 and α_2 are the isotopic separation factors, defined as [D/H](gas)/[D/H](soln.), for low concentration range and high concentration range, respectively. Equilibrium 3 may be written as (1) + (2) or as (5) − (6). Equilibrium 4 may be written as (1) − (2).

Our single-stage equilibration, with hydrogen of natural abundance, gives accurate knowledge of equilibrium 1 and its dependence on temperature. The established law, $\log \alpha_1 = 77.5/T + 0.0175$ (very similar to the law with pure palladium[2]), allows the calculation of $-\Delta H_1$ (1 atm.) = 350 cal./mole for the enthalpy of exchange reaction 1, exothermic in the reverse direction, and of $-\Delta G_1$ (1 atm., 20°) = $RT \ln K_1 = RT \ln 2\alpha_1$ = 794 cal. for the change in free energy. The separation factor is not dependent on the deuterium concentration in the low concentration range.

Our chromatographic measurements with a gas rich in D_2 give to the first approximation the knowledge of equilibrium 2 in the same range of temperature: α_2 seems to be slightly greater than α_1, and ΔH_2 greater than ΔH_1, as we can expect from the known data concerning K_4 dependence on temperature. However, our measurements of (2) were not precise enough to make this assessment a definite one.

The possibility was considered for the α values given above of having been altered by some hydrogen surface adsorption.[4] However, the shape of our solubility isotherms on palladium and on Pd–Pt alloy corresponds well with those published for bulk alloys, where only solubility of hydrogen occurs.[3] It is notably different from those published for dispersed alloys, where both solubility and adsorption of hydrogen occur.[4] This rules out an appreciable surface adsorption; this assessment is also supported by the fact that a mixture of separate palladium and platinum metals in the same 9:1 proportion, but unalloyed, deposited on the same alumina, exhibited quite the same isotherm as palladium alone, without supplementary adsorption. This absence of surface adsorption leads to the conclusion that the values reported above for α are those related exclusively to the solubility process.

In a later and more detailed publication,[5] a comparison between thermodynamic values (1 atm., 20°) for equilibrium 3 will be given, as obtained by the following ways: (a) experiments concerning (1) and (2); (b) accurate experiments concerning equilibrium 1 and the known data published for equilibrium 4; (c) published values[6] concerning equilibria 5 and 6 referred to various Pt–Pd alloys. We hope that this study

(2) F. Botter, J. Menes, S. Tistchenko, and G. Dirian, CEA Report 2545, Saclay (1964).

(3) A. W. Carson, T. B. Flanagan, and F. A. Lewis, *Trans. Faraday Soc.*, **56**, 1332 (1960).

(4) A. I. Stetsenko and J. P. Tverdovskii, *Zh. Fiz. Khim.*, **26**, 647 (1952).

(5) F. Botter, J. Menes, and P. Charpin, to be published in *J. chim. phys.*

(6) A. Maeland and T. B. Flanagan, *J. Phys. Chem.*, **68**, 1419 (1964).

will provide a better understanding of the nature of the alloys "Pd–Pt"[7] and "Pt, Pd–H, D" and a possible explanation for the considerable discrepancy between α_1 (20°, 1 atm.) = 1.95 obtained here and the solubility ratio of each isotope considered individually under the same conditions (pressure, temperature, 10% Pt alloy). The same effect is observed with pure palladium, where the isotopic solubility ratio at 20° under atmospheric pressure is 1.08,[1] while the observed separation factor is 2.0.[2]

On the other hand, in the electrochemical experiments mentioned above,[1] the over-all separation factor might be the product of a solubility separation factor and of a high kinetic factor arising from the cathodic process; we have examples of this,[8] mainly in acid solutions like those used in these experiments.

Acknowledgments. We wish to thank Mrs. J. Menes for her experimental contribution, Mrs. P. Charpin for X-ray studies, Miss N. Repellin for establishing the solubility isotherms, and Mr. G. Dirian for fruitful discussions. Most of the isotopic analyses have been carried out in the Section of Mass Spectrometry at Saclay.

(7) F. A. Lewis, *Platinum Metal Rev.*, 5, 21 (1961).

(8) H. London, Ed., "Separation of Isotopes," George Newnes Ltd., London, 1961.

SERVICE DES ISOTOPES STABLES
CENTRE D'ETUDES NUCLÉAIRES DE SACLAY
FRANCE
F. BOTTER

RECEIVED DECEMBER 18, 1964

The Electron Spin Resonance Associated with Photochromism in 2,2′-Dimethylbianthrone

Sir: The electron spin resonance (e.s.r.) spectrum of solutions of the 2,2′-dimethyl-$\Delta^{10,10'}$-bianthrone negative ion in 2-methyltetrahydrofuran have been obtained and compared with the e.s.r. spectrum observed during low temperature photolysis of solutions of the parent, 2,2′-dimethyl-$\Delta^{10,10'}$-bianthrone (I).

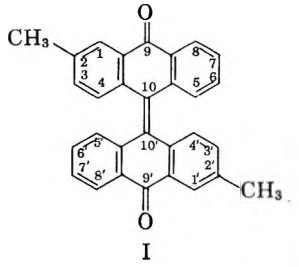

I

The negative ion of I was produced by two different methods, by reaction with potassium *t*-butoxide and by reaction with stannous chloride. Both techniques gave the same e.s.r. spectrum but resulted in vastly different visual appearance. The solution obtained from the stannous chloride reaction remained a yellow of approximately the same hue as the solution of the parent bianthrone while the portion treated with potassium *t*-butoxide gave a blood-red solution. The spectrum obtained consisted of a major heptet of lines (intensities 1, 6, 15, 20, 15, 6, 1), each of which showed further splitting into a quintet. The splitting of the major heptet of lines was 2.83 gauss and the minor splitting was 0.79 gauss. The pattern was centered at g 2.0028.

The major heptet of lines can result from a set of six protons giving nearly equivalent hyperfine interaction and the remaining five-line minor interaction results from four equivalent protons. The observation that hyperconjugation in the ethyl radical[1] gives nearly the same splitting for the β-protons as for the α-protons lends credulity to the interpretation that the major heptet arises from three ring protons and the three methyl protons with nearly equal interactions while the minor interaction is a result of four ring protons.

A tentative assignment of the major heptet to interaction with positions 4, 5, and 7 ring protons, together with the three 2-methyl protons and the minor splitting arising through interaction with protons on carbons 1, 3, 6, and 8, is indicated.

The spectrum observed is comparable to that obtained by Wasserman[2] for the $\Delta^{10,10'}$-bianthrone thermochromic form if one assumes that, instead of the assignment suggested, the major splittings of the $\Delta^{10,10'}$-bianthrone resulted from the protons in the 2, 4, 5, and 7 positions, rather than the 1, 3, 6, and 8 positions.

The spectrum obtained from photolysis of I at −100° and observed at −195° shows the same major features as the negative ion spectrum, but it is less fully resolved due to dipolar broadening in the glassy solid. The observed major splitting of the photolytically produced species is approximately 3 gauss, but due to the greatly reduced resolution and larger modulations involved in this measurement this is probably equivalent to the measured 2.83 gauss in the room temperature liquid. The signal intensity observed at −195° is not directly related to the visually estimated production of the green form but seems to maximize before maximum (visual) conversion.

The above observations indicate that the observed resonance signal does not arise from a biradical of the

(1) R. Fessenden and R. Schuler, *J. Chem. Phys.*, 39, 2147 (1963).

(2) E. Wasserman, *J. Am. Chem. Soc.*, 81, 5006 (1959).

structure proposed by Wasserman.[2] Furthermore, it appears that the e.s.r. signal may not arise from the major colored species but may be associated with parallel reactions of the parent material or subsequent reactions of the colored modifications. The spectra of the negative ion and of the low-temperature photolytic species both indicate structures in which the unpaired spin is effectively localized in one half of the molecule and are probably skewed conformations.

AIR FORCE MATERIALS LABORATORY
WRIGHT-PATTERSON AIR FORCE BASE, OHIO
LARRY A. HARRAH

DEPARTMENT OF CHEMISTRY
UNIVERSITY OF HOUSTON
HOUSTON, TEXAS
RALPH BECKER

RECEIVED MAY 14, 1965

A Suggested Mechanism for the Hydrogen–Fluorine Reaction

Sir: Two recent papers by Levy and Copeland[1,2] report experimental studies of the rate of reaction of hydrogen and fluorine. These authors were not able to devise a mechanism to explain their data quantitatively, although they did discuss their results in a qualitative manner. It is the purpose of this communication to suggest a mechanism which quantitatively accounts for the results of Levy and Copeland; it is hoped that this will provide a useful working hypothesis for planning future work.

In their first paper,[1] Levy and Copeland investigated the reaction of hydrogen–fluorine mixtures diluted with nitrogen in a flow system at 110°. They found the reaction rate to be proportional to fluorine concentration and independent of hydrogen concentration. This result can be explained by the reactions

$$F + H_2 \xrightarrow{k_1} HF + H \quad (1)$$

$$H + F_2 \xrightarrow{k_2} \alpha HF^* + (1 - \alpha)HF + F \quad (2)$$

$$HF^* + F_2 \xrightarrow{k_3} HF + 2F \quad (3)$$

$$HF^* + M_{(4)} \xrightarrow{k_4} HF + M_{(4)} \quad (4)$$

$$2F + M_{(5)} \xrightarrow{k_5} F_2 + M_{(5)} \text{ (or perhaps } 2HF \text{ for } M_{(5)} = H_2) \quad (5)$$

The first two reactions—both exothermic—are analogous to steps occurring in the hydrogen–bromine and hydrogen–chlorine reactions. In the case of the reaction $H + Cl_2 \rightarrow HCl + Cl$ nearly 25% of the product HCl is vibrationally excited.[3] It seems reasonable to expect the same phenomenon in reaction 2, and HF* represents hydrogen fluoride molecules excited to the fourth vibrational level and above. These molecules are energetic enough to dissociate fluorine *via* reaction 3, although de-excitation *via* reaction 4 seems more likely. In the reaction between hydrogen atoms and chlorine, 1.3% of the HCl is excited to the fourth level or above. This would seem a conservative estimate for reaction 2, since the heat of reaction is larger relative to the size of the vibrational quantum. Thus we might expect $\alpha \sim 0.013$–0.02.

By applying the steady-state approximation to the hydrogen and fluorine atom concentrations and also the concentration of vibrationally excited HF*, the following rate expression for the kinetics is easily obtained

$$\frac{d[HF]}{dt} = \frac{2\alpha k_1^2 k_3 [H_2]^2 [F_2]}{k_5 [M_{(5)}](k_3[F_2] + k_4[M_{(4)}])}$$

This corresponds to the observed kinetics provided $k_4[M_{(4)}] \gg k_3[F_2]$ and provided the inert collision partners $M_{(4)}$ and $M_{(5)}$ are both preferentially hydrogen.

The condition $k_4[M_{(4)}] \gg k_3[F_2]$ is almost certainly satisfied in Levy and Copeland's experiments, since their fluorine concentrations were always low (mole fraction less than 0.05). Furthermore, reaction 4, a vibrational relaxation, is expected to be very fast, whereas reaction 3 may have a very low steric factor.

The assumption that $M_{(4)}$ is preferentially hydrogen is also reasonable. Reaction 4 is a vibrational de-excitation, and light molecules seem to be especially effective in robbing diatomic molecules of excess vibrational energy. Thus Millikan and White's[4] correlation predicts that hydrogen should be thirty times as effective as nitrogen and over forty times as effective as fluorine in relaxing HF from the first vibrational level. In addition, the fundamental vibrational frequencies of HF and H_2 differ by only about 6%, so that there is the possibility of de-excitation by transfer of vibrational quanta from HF to H_2.

On the other hand, there is no *a priori* reason to expect that $M_{(5)}$ is preferentially hydrogen; hydrogen does not seem to be especially effective in recombining other halogens.[5] It is possible to provide an *ad hoc* explanation by postulating an intermediate with a few kilocalories of stability, so that recombination occurs stepwise

$$F + H_2 + M \rightleftharpoons H_2F + M$$
$$H_2F + F \longrightarrow \text{products}$$

(1) J. B. Levy and B. K. W. Copeland, *J. Phys. Chem.*, **67**, 2156 (1963).

(2) J. B. Levy and B. K. W. Copeland, *ibid.*, **69**, 408 (1965).

(3) J. T. Airey, R. R. Getty, J. C. Polanyi, and D. R. Snelling, *J. Chem. Phys.*, **41**, 3255 (1964).

(4) R. C. Millikan and D. R. White, *ibid.*, **39**, 3209 (1963).

(5) D. L. Bunker and N. Davidson, *J. Am. Chem. Soc.*, **80**, 5086 (1958).

Such a scheme has been proposed[5] to explain the remarkable efficiency of iodine molecules in recombining iodine atoms.

One further fact seems to support this mechanism. We might expect that hydrogen fluoride would be especially effective in deactivating HF* by transfer of vibrational quanta, for example

$$HF^*_{(v=4)} + HF_{(v=0)} \longrightarrow HF_{(v=3)} + HF_{(v=1)}$$

Thus we should anticipate strong inhibition by the reaction product. The data in Levy and Copeland's first paper are generally for a small extent of reaction and frequently with a large excess of hydrogen, so it is not possible to draw conclusions as to possible inhibition by HF. However, the first figure of their second paper shows two stoichiometric runs carried past 60% completion. These two runs suggest very strong product inhibition. Indeed, they fit this mechanism very nicely by assuming $k_{4,HF} \sim 10k_{4,H_2}$.

In summary, the mechanism proposed here provides a quantitative explanation of the kinetics of the reaction between hydrogen and fluorine. The most unique feature of the scheme is the assumption of an energy transfer chain branching step. The most questionable feature is the assumption that hydrogen is especially effective in recombining fluorine atoms.

Acknowledgment. The author wishes to thank Frank E. Belles for helpful suggestions, especially as to the role of hydrogen in reactions 4 and 5.

LEWIS RESEARCH CENTER
NATIONAL AERONAUTICS AND SPACE ADMINISTRATION
CLEVELAND, OHIO 44135

RICHARD S. BROKAW

RECEIVED JUNE 1, 1965

Remarks on the Hydration of Tricalcium Silicate

Sir: Recently, Greenberg and Chang[1] reported measurements on the hydration of C_3S ($3CaO \cdot SiO_2$) that according to the summary of the paper concerned, "substantiated the solution theory of hydration."

It is the purpose of this note to show that Greenberg and Chang's data can be combined with phenomena reported by other research workers into a much more coherent picture of C_3S hydration than that offered by these authors.

It is not quite clear from the paper what exactly is understood by the "solution theory of hydration." As long as it is meant to represent no more than dissolution of calcium and silicate ions from the C_3S, hydrolysis of these ions, and precipitation in the form of one hydrate (either throughout the solution or on the C_3S particles), it is apparent that no more than one peak in the concentration of any species can be understood. A number of subsequent peaks, as reported by Greenberg and Chang for the silicic acid concentration (see Figure 3 of their paper), is incomprehensible on the basis of such a solution theory alone. Greenberg and Chang, for instance, interpret the peak in silicic acid concentration, occurring in suspensions of 1.25 g. of C_3S/l. after about 35 min., as follows: "some time (40 min.) elapses before the silicic acid concentration is sufficient to cause rapid crystallization"; they disregard the silicic acid *decrease* up to about 20 min. hydration showing that the silicic acid concentration peak after about 35 min. is in reality the second peak, the first being situated shortly after addition of the C_3S to water.

As far as the present authors can see, the only way of understanding these data is to assume either recrystallization of calcium silicate hydrates or a changing reactivity of the C_3S (or both). Conversion of a first formed hydrate (F.H.) into a second one (S.H.) has been found by Kantro, *et al.*,[2] on the basis of analyses of the hydrates formed and of surface area measurements; the present authors reported[3] the influence of amorphous silica on C_3S hydration, both in suspensions and in pastes, to be consistent with the following mechanism: the F.H. adheres firmly to the C_3S surfaces and strongly retards its hydration, the S.H. does so to a much lesser extent; conversion of F.H. into S.H. is accelerated by the presence of S.H. nuclei and is accompanied by an increasing reactivity of C_3S.

This mechanism explains Greenberg and Chang's data, notably the silicic acid concentration data referred to, much more substantially than the simple solution theory as outlined above. It should be noted that some electron microscopical evidence for the ultimate conversion of S.H. has been adduced[3] which together with the formation of F.H. and the conversion of F.H. into S.H. might be correlated with the three concentration peaks recorded by Greenberg and Chang in suspensions of 1.25 g. of C_3S/l. The shift of the second silicic acid concentration peak toward later hydration times in C_3S suspensions of higher solid content (5 g./l.) is readily understood from this mechanism, since lower calcium and hydroxyl ion concentrations in the water phase during the early stages of the reaction seem to

(1) S. A. Greenberg and T. N. Chang, *J Phys. Chem.*, 69, 553 (1965).

(2) D. L. Kantro, S. Brunauer, and C. H. Weise, *ibid.*, 66, 1804 (1962).

(3) H. N. Stein and J. M. Stevels, *J. Appl. Chem.* (London), 14, 338 (1964).

accelerate S.H. nucleus formation and consequently F.H. conversion.[3]

Greenberg and Chang's chief argument for a "solution theory," the complete dissolution of C_3S in very dilute suspensions (0.25 g./l.), may be understood from the point of view mentioned: at such concentrations as pertain in the water phase of very dilute C_3S suspensions during the first minutes of the hydration, any F.H. layer retarding the dissolution of C_3S is expected to be converted soon. In view of this more complicated mechanism, it is not surprising that Greenberg and Chang's data do not fit either a simple dissolution equation or an equation based on diffusion through a hydrate layer as the rate-determining step.

It is of course not intended to regard these remarks as a conclusive proof for the mechanism proposed by the present authors; it will, however, be noted that it is consistent with all data available at present including Greenberg and Chang's data.

TECHNOLOGICAL UNIVERSITY
EINDHOVEN, NETHERLANDS
H. N. STEIN
J. M. STEVELS

RECEIVED MAY 21, 1965

Solvent Shifts in Charge-Transfer Complex Spectra

Sir: Mulliken's[1] description of donor–acceptor complexes is generally accepted. The following expressions represent the wave functions for the ground and excited states of a complex

$$\psi_N \approx a\psi_0\,(D, A) + b\psi_1\,(D^+\text{–}A^-)$$
$$\psi_E \approx a^*\psi_1\,(D^+\text{–}A^-) - b^*\psi_0\,(D, A)$$

where $a^2 >> b^2$ and $a^{*2} >> b^{*2}$.

Since the excited state of the complex is considerably more polar than the ground state, it has been predicted,[2] despite the Franck–Condon constraints, that increasing solvent polarity should favor stabilization of the excited state, thereby reducing the energy requirements for charge-transfer electronic transitions. Scattered efforts[3] have failed to confirm the validity of these predictions, using dielectric constants as a measure of solvent polarity.

It is the purpose of this paper to report the results of our studies on aromatic hydrocarbon–TCNE complexes. In order to avoid potential difficulties in this initial study, polar donors were excluded. This was also considered desirable in view of Davis and Symons'[4] recent attempt to interpret solvent shifts as a function of solvent interaction with donor and acceptor species.

Table I: Absorption Maxima[a] of Charge-Transfer Transitions in Various Solvents

	CH_3OH	CH_3CN	*n*-Hexane	CH_2Cl_2	CCl_4
D[b]	33.6	37.5	1.9	9.1	2.2
n_D[c]	1.331	1.344	1.375	1.424	1.463
Toluene–TCNE	263	262	251	246	244
o-Xylene–TCNE	244	243	236	233	231
Mesitylene–TCNE	228	227	220	217	216
HMB–TCNE	194	192	190	184	185
Naphthalene–TCNE	208	200	187	182	182
Fluorene–TCNE	192	192	181	175	177

[a] Wave number, cm.$^{-1}$ × 10^{-2}. [b] Dielectric constant at 20°. [c] Index of refraction at 20°.

Spectroscopic data were obtained on a Cary Model 11 spectrophotometer equipped with a four-place digital voltmeter and wave length maxima were determined to a precision of ±1 mμ. Data for the frequency maxima of the charge-transfer bands are given in Table I, which also contains values for dielectric constants and refractive indices.

Since the donors and ground state complexes are nonpolar, it may be expected that the excited state of the complexes should experience the major coulombic interactions with polar solvents. In the absence of electronic excitation, the solvent molecules are randomly oriented with respect to solute. The interval of an electronic transition to a Franck–Condon state does not allow sufficient time for effective orientation of the permanent dipoles of the solvent. Therefore, stabilizing interactions must be attributed to the polarizability of the solvent molecules. Our data are consistent with this view. No correlations between solvent dielectric constants and the position of ν_{max} can be discerned. As can be seen in Table I, ν_{max} decreases with increasing values of refractive index (within experimental error). Since the index of refraction is related to polarizability, we suggest that this solvent property can provide a useful basis for predicting solvent spectra shifts of donor–acceptor complexes having nonpolar ground states.

(1) R. S. Mulliken, *J. chim. phys.*, 20 (1963).

(2) (a) J. N. Murrell, *Quart. Rev.* (London), **15**, 191 (1961); (b) S. F. Mason, *ibid.*, **15**, 287 (1961).

(3) (a) G. Briegleb, "Electronen Donator-Acceptor Komplexe," Springer-Verlag, Berlin, 1961, p. 38; (b) R. Foster and D. L. Hammick, *J. Chem. Soc.*, 2685 (1954).

(4) K. M. C. Davis and M. C. R. Symons, *ibid.*, 2079 (1965).

AIR FORCE MATERIALS LABORATORY
RESEARCH & TECHNOLOGY DIVISION
WRIGHT-PATTERSON AIR FORCE BASE, OHIO
H. M. ROSENBERG
D. HALE

RECEIVED MAY 14, 1965